HANDBOOK OF HYDROTHERMAL TECHNOLOGY

A Technology for Crystal Growth and Materials Processing

by

K. Byrappa
University of Mysore
Manasagangotri
Mysore, India

and

Masahiro Yoshimura
Tokyo Institute of Technology
Yokohama, Japan

DropBooks

NOYES PUBLICATIONS
Park Ridge, New Jersey, U.S.A.

WILLIAM ANDREW PUBLISHING, LLC
Norwich, New York, U.S.A.

Copyright © 2001 by Noyes Publications
No part of this book may be reproduced or utilized in any form or by any means, electronic or mechanical, including photocopying, recording or by any information storage and retrieval system, without permission in writing from the Publisher.
Library of Congress Catalog Card Number: 00-021998
ISBN: 0-8155-1445-X
Printed in the United States

Published in the United States of America by
Noyes Publications / William Andrew Publishing, LLC
13 Eaton Avenue
Norwich, NY 13815
1-800-932-7045
www.knovel.com

10 9 8 7 6 5 4 3 2 1

Library of Congress Cataloging-in-Publication Data

Byrappa, K.
Handbook of Hydrothermal Technology / by K. Byrappa and Masahiro Yoshimura.
p. cm.
Includes bibliographical references and index.
ISBN 0-8155-1445-X
1. Crystallization. 2. Crystal growth. I. Title
QD921.B97 2001
548'.5--dc21 00-021998
CIP

To

Sunitha and Akiko

DropBooks

NOTICE

To the best of our knowledge the information in this publication is accurate; however the Publisher does not assume any responsibility or liability for the accuracy or completeness of, or consequences arising from, such information. This book is intended for informational purposes only. Mention of trade names or commercial products does not constitute endorsement or recommendation for use by the Publisher. Final determination of the suitability of any information or product for use contemplated by any user, and the manner of that use, is the sole responsibility of the user. We recommend that anyone intending to rely on any recommendation of materials or procedures mentioned in this publication should satisfy himself as to such suitability, and that he can meet all applicable safety and health standards.

MATERIALS SCIENCE AND PROCESS TECHNOLOGY SERIES

Series Editors

Gary E. McGuire, Microelectronics Center of North Carolina
Stephen M. Rossnagel, IBM Thomas J. Watson Research Center
Rointan F. Bunshah, University of California, Los Angeles (1927–1999), founding editor

Electronic Materials and Process Technology

CHARACTERIZATION OF SEMICONDUCTOR MATERIALS, Volume 1: edited by Gary E. McGuire

CHEMICAL VAPOR DEPOSITION FOR MICROELECTRONICS: by Arthur Sherman

CHEMICAL VAPOR DEPOSITION OF TUNGSTEN AND TUNGSTEN SILICIDES: by John E. J. Schmitz

CHEMISTRY OF SUPERCONDUCTOR MATERIALS: edited by Terrell A. Vanderah

CONTACTS TO SEMICONDUCTORS: edited by Leonard J. Brillson

DIAMOND CHEMICAL VAPOR DEPOSITION: by Huimin Liu and David S. Dandy

DIAMOND FILMS AND COATINGS: edited by Robert F. Davis

DIFFUSION PHENOMENA IN THIN FILMS AND MICROELECTRONIC MATERIALS: edited by Devendra Gupta and Paul S. Ho

ELECTROCHEMISTRY OF SEMICONDUCTORS AND ELECTRONICS: edited by John McHardy and Frank Ludwig

ELECTRODEPOSITION: by Jack W. Dini

HANDBOOK OF CARBON, GRAPHITE, DIAMONDS AND FULLERENES: by Hugh O. Pierson

DropBooks

HANDBOOK OF CHEMICAL VAPOR DEPOSITION, Second Edition: by Hugh O. Pierson

HANDBOOK OF COMPOUND SEMICONDUCTORS: edited by Paul H. Holloway and Gary E. McGuire

HANDBOOK OF CONTAMINATION CONTROL IN MICROELECTRONICS: edited by Donald L. Tolliver

HANDBOOK OF DEPOSITION TECHNOLOGIES FOR FILMS AND COATINGS, *Second Edition:* edited by Rointan F. Bunshah

HANDBOOK OF HARD COATINGS: edited by Rointan F. Bunshah

HANDBOOK OF ION BEAM PROCESSING TECHNOLOGY: edited by Jerome J. Cuomo, Stephen M. Rossnagel, and Harold R. Kaufman

HANDBOOK OF MAGNETO-OPTICAL DATA RECORDING: edited by Terry McDaniel and Randall H. Victora

HANDBOOK OF MULTILEVEL METALLIZATION FOR INTEGRATED CIRCUITS: edited by Syd R. Wilson, Clarence J. Tracy, and John L. Freeman, Jr.

HANDBOOK OF PLASMA PROCESSING TECHNOLOGY: edited by Stephen M. Rossnagel, Jerome J. Cuomo, and William D. Westwood

HANDBOOK OF POLYMER COATINGS FOR ELECTRONICS, *Second Edition:* by James Licari and Laura A. Hughes

HANDBOOK OF REFRACTORY CARBIDES AND NITRIDES: by Hugh O. Pierson

HANDBOOK OF SEMICONDUCTOR SILICON TECHNOLOGY: edited by William C. O'Mara, Robert B. Herring, and Lee P. Hunt

HANDBOOK OF SEMICONDUCTOR WAFER CLEANING TECHNOLOGY: edited by Werner Kern

HANDBOOK OF SPUTTER DEPOSITION TECHNOLOGY: by Kiyotaka Wasa and Shigeru Hayakawa

HANDBOOK OF THIN FILM DEPOSITION PROCESSES AND TECHNIQUES: edited by Klaus K. Schuegraf

HANDBOOK OF VACUUM ARC SCIENCE AND TECHNOLOGY: edited by Raymond L. Boxman, Philip J. Martin, and David M. Sanders

HANDBOOK OF VLSI MICROLITHOGRAPHY: edited by William B. Glendinning and John N. Helbert

HIGH DENSITY PLASMA SOURCES: edited by Oleg A. Popov

HYBRID MICROCIRCUIT TECHNOLOGY HANDBOOK, *Second Edition:* by James J. Licari and Leonard R. Enlow

IONIZED-CLUSTER BEAM DEPOSITION AND EPITAXY: by Toshinori Takagi

MOLECULAR BEAM EPITAXY: edited by Robin F. C. Farrow

SEMICONDUCTOR MATERIALS AND PROCESS TECHNOLOGY HANDBOOK: edited by Gary E. McGuire

ULTRA-FINE PARTICLES: edited by Chikara Hayashi, R. Ueda and A. Tasaki

WIDE BANDGAP SEMICONDUCTORS: edited by Stephen J. Pearton

Ceramic and Other Materials—Processing and Technology

ADVANCED CERAMIC PROCESSING AND TECHNOLOGY, Volume 1: edited by Jon G. P. Binner

CEMENTED TUNGSTEN CARBIDES: by Gopal S. Upadhyaya

CERAMIC CUTTING TOOLS: edited by E. Dow Whitney

CERAMIC FILMS AND COATINGS: edited by John B. Wachtman and Richard A. Haber

CORROSION OF GLASS, CERAMICS AND CERAMIC SUPERCONDUCTORS: edited by David E. Clark and Bruce K. Zoitos

FIBER REINFORCED CERAMIC COMPOSITES: edited by K. S. Mazdiyasni

FRICTION AND WEAR TRANSITIONS OF MATERIALS: by Peter J. Blau

HANDBOOK OF CERAMIC GRINDING AND POLISHING: edited by Ioan D. Marinescu, Hans K. Tonshoff, and Ichiro Inasaki

HANDBOOK OF HYDROTHERMAL TECHNOLOGY: edited by K. Byrappa and Masahiro Yoshimura

HANDBOOK OF INDUSTRIAL REFRACTORIES TECHNOLOGY: by Stephen C. Carniglia and Gordon L. Barna

SHOCK WAVES FOR INDUSTRIAL APPLICATIONS: edited by Lawrence E. Murr

SOL-GEL TECHNOLOGY FOR THIN FILMS, FIBERS, PREFORMS, ELECTRONICS AND SPECIALTY SHAPES: edited by Lisa C. Klein

SOL-GEL SILICA: by Larry L. Hench

SPECIAL MELTING AND PROCESSING TECHNOLOGIES: edited by G. K. Bhat

SUPERCRITICAL FLUID CLEANING: edited by John McHardy and Samuel P. Sawan

Other Related Titles

HANDBOOK OF PHYSICAL VAPOR DEPOSITION (PVD) PROCESSING: by Donald M. Mattox

Preface

The term *hydrothermal* is purely of geological origin. It was first used by the British geologist, Sir Roderick Murchison (1792–1871), to describe the action of water at elevated temperature and pressure in bringing about changes in the earth's crust, and leading to the formation of various rocks and minerals. Geologists carried out the earliest work on the hydrothermal technique in the 19th century in order to understand the genesis of rocks and minerals by simulating the natural conditions existing under the earth crust. However, materials scientists popularized the technique, particularly during 1940s. Schafhautl who obtained quartz crystals upon freshly precipitated silicic acid in a papin's digestor carried out the first hydrothermal synthesis in 1845. Subsequently, hydrothermal synthesis of a wide variety of minerals was carried out, especially in Europe.

The largest-known single crystal formed in nature (beryl crystal of >1000 kg) and some of the largest quantities of single crystals created in one experimental run (quartz crystals of >1000 kg) are both of hydrothermal origin.

The first successful commercial application of hydrothermal technology began with mineral extraction or ore beneficiation in the 19th century. With the beginning of the synthesis of large single crystals of quartz by Nacken (1946) and zeolites by Barrer (1948), the commercial importance of the hydrothermal technique for the synthesis of inorganic compounds was realized

DropBooks

The general acceptance of plate tectonics theory some 2 ½ decades ago garnered much interest in geochemical processes at plate boundaries which led to the discovery of hydrothermal activity in the deep sea directly on the Galapagos Spreading Center in 1977 and a large number of other spectacular submarine hydrothermal systems of global significance to ocean chemistry and geochemistry. In fact, this discovery has led to a new thinking in marine biology, geochemistry and in economic geology, and has spawned an entirely new term, viz., hydrothermal ecosystems, which means water-containing terrestrial, subterranean, and submarine high temperature environments, which are the sites of investigations for many palaeobiologists and biologists looking for primitive forms of life. It is strongly believed that the roots of life on earth can be found in hydrothermal ecosystems. These ecosystems may also serve as an analog for the possible origin of life on Mars, where a similar environment might have existed or still exists.

Earth is a blue planet of the universe where water is an essential component. Circulation of water and other components such as entropy (energy) are driven by water vapor and heat (either external or internal). Water has a very important role in the formation of material or transformation of materials in nature, and hydrothermal circulation has always been assisted by bacterial activity.

From mid-1970s, exploration of the advantages of hydrothermal reactions, other than the hydrometallurgical and crystal growth aspects, began in Japan, particularly with reference to the ceramic powder processing. A team of researchers from the Tokyo Institute of Technology, Japan, did pioneering work in ceramic processing such as powder preparation, reaction sintering, hot isostatic processing, and so on.

In the last decade, the hydrothermal technique has offered several new advantages like homogeneous precipitation using metal chelates under hydrothermal conditions, decomposition of hazardous and/or refractory chemical substances, monomerization of high polymers like polyethylene terephthalate, and a host of other environmental engineering and chemical engineering issues dealing with recycling of rubbers and plastics (instead of burning), and so on. The solvation properties of supercritical solvents are being extensively used for detoxifying organic and pharmaceutical wastes and also to replace toxic solvents commonly used for chemical synthesis. Similarly, it is used to remove caffeine and other food-related compounds selectively. In fact, the food and nutrition experts in recent years are using

a new term, *hydrothermal cooking*. These unique properties take the hydrothermal technique altogether in a new direction for the 21st century and one can forecast a slow emergence of a new branch of science and technology for sustained human development. We have collected a more-or-less complete list of publications in hydrothermal technology and provided the statistical data to show the growing popularity of the technique (Figures 1.10–1.12). The main disadvantage of the hydrothermal system, as believed earlier, is the black-box nature of the apparatus, because one cannot observe directly the crystallization processes. However, in the recent years, remarkable progress has been made in this area through the entry of physical chemists, and the modeling of the hydrothermal reactions and the study of kinetics of the hydrothermal processes, which have contributed greatly to the understanding of the hydrothermal technique. One can understand the hydrothermal chemistry of the solutions more or less precisely, which provides a solid base for designing hydrothermal synthesis and processing at much lower pressure and temperature conditions. The hydrothermal technique exhibits a great degree of flexibility, which is being rightly exploited by a large scientific community with diversified interests. Hydrothermal processing has become a most powerful tool, in the last decade, for transforming various inorganic compounds and treating raw materials for technological applications.

DropBooks

Today, the hydrothermal technique has found its place in several branches of science and technology, and this has led to the appearance of several related techniques, with strong roots to the hydrothermal technique, involving materials scientists, earth scientists, materials engineers, metallurgists, physicists, chemists, biologists, and others. Thus, the importance of hydrothermal technology from geology to technology has been realized. In view of such a rapid growth of the hydrothermal technique, it is becoming imperative to have a highly specialized book on this topic. There are thousands of articles and reviews published on the various aspects of science of hydrothermal research but, so far, the most comprehensive works on this topic were limited to reviews and edited books, and there is not even a single monograph or book available.

The first author, Dr. K. Byrappa, edited a book entitled *Hydrothermal Growth of Crystals* in 1990 for Pergamon Press, Oxford, UK. During early 1995, the authors conceived an idea of writing this handbook and began collecting old records from various sources. The writing of this handbook started in 1997. In this handbook, we have dealt with all the

aspects of hydrothermal research covering historical development, natural hydrothermal systems, instrumentation, physical chemistry of hydrothermal growth of crystals, growth of some selected crystals like quartz, berlinite, KTP, calcite, and hydrothermal synthesis of a host of inorganic compounds like zeolites, complex coordinated compounds (silicates, germanates, phosphates, tungstates, molybdates, etc) and simple oxides, native elements, and the hydrothermal processing of materials with an emphasis on future trends of hydrothermal technology in the 21st century.

Many publications on hydrothermal research, especially in the Russian journals, were not easily accessible to us. Our Russian colleagues in the field of hydrothermal research extended great cooperation in this regard. Especially, the help rendered by Dr. L. N. Demianets, Dr. V. I. Popolitov and Dr. O. V. Dimitrova is highly appreciated. The authors are very grateful for the help and encouragement extended by the senior people in this field like Prof. Shigeyuki Sōmiya (Professor Emeritus), Prof. N. Yamasaki (Tohoku University, Japan), late Dr. Bob Laudise (AT & T Bell Labs.), Prof. Rustom Roy (Penn State University), Prof. C. N. R. Rao (Director, JNCASR), Prof. R. Chidambaram (Chairman, Atomic Energy Commission, India), Dr. B. P. Radhakrishna (former Director, Dept. of Mines & Geology), late Prof. J. A. Rabenau (Max-Planck Institute of Physics, Stuttgart), Prof. Ichiro Sunagawa, Prof. J. A. Pask, Prof. Paul Hagenmuller, Prof. H. L. Barnes, late Prof. Saito Shinroku, and Prof. Toshiyuki Sata. Both Prof. Sōmiya and Prof. Yamasaki spent several hours with the authors and provided fruitful discussion. Their suggestions and comments have been included in this book. We would like to extend our special thanks to the most active hydrothermal researchers of the present day, like Prof. S. Hirano, Prof. M. Hosaka, Prof. K. Yanagisawa, Prof. T. Moriyoshi (Director, RIST, Takamatsu), Prof. S. Komarneni, Prof. R. E. Riman, Dr. Don Palmer, Dr. Dave Wesolowski, Dr. S. Taki, Prof. K. Arai, Prof. T. B. Brill, Prof. T. M. Seeward, Prof. Yuri Gogosti, Prof. K. Bowen, Prof. David A Payne, Prof. Fred F. Lange, and Prof. Fathi Habashi, who have helped us by providing their results and data for inclusion in this book. Our colleagues at the Tokyo Institute of Technology, like Prof. Masato Kakihana, Prof. Nabuo Ishizawa, Prof. Eiichi Yasuda, Prof. Akira Sawaoka, Prof. Masatomo Yashima, Prof. Yasuo Tanabe, Prof. Masanori Abe, Prof. Kazunari Domen, and Prof. Kiyoshi Okada, extended great cooperation in our task. Other Japanese friends, like Dr. Yasuro Ikuma, Prof. Tsugio Sato, Prof. Koji Kajiyoshi, Dr. Atsuo Ito, Dr. E. H. Ishida, Prof. Zenbee Nakagawa,

Prof. Yusuke Moriyoshi, Prof. Yasumichi Matsumoto, Prof. Tadashi Ohachi (Doshisha University, Kyoto), Dr. Kohei Soga (Tokyo University), Prof. Toshio Yamaguchi and a host of other friends in the field of hydrothermal research, have helped us extensively in completing this great work. We would like to express our sincere thanks to our friends and colleagues from India (late Prof. M. N. Vishwanathiah, late Prof. B. V. Govindarajulu, Prof. J. A. K. Tareen, Prof. D. D. Bhawalkar, Dr. Krishan Lal, Dr. R. V. Anantha Murthy, Prof. A. B. Kulkarni, Prof. T. R. N. Kutty, Prof. P. N. Satish, Dr. B. Basavalingu, Prof. H. L. Bhat, Dr. K. M. Lokanath Rai, and Dr. M. A. Shankara), Russia (Prof. V. S. Balitsky, Prof. V. A. Kuznetsov, Prof. D. Yu Pushcharovsky, Dr. Oleg Karpov, Dr. G. I. Dorokhova, and Dr. E. Strelkhova), Korea (Prof. Choy Jin-ho and Prof. Z. H. Lee), Spain (Prof. Rafael Rodriguez Clemente, and Prof. Salvador Gali), Poland (Prof. Keshra Sangwal), and China (Prof. Shen-tai Song, Prof. Y-T. Qian, and Prof. S. Feng), who were a great source of inspiration and help while writing this book. Here, it is extremely difficult to list all the names of the students, post-docs and research associates from our groups who have helped us greatly. Among them, the help rendered by Mr. B. V. Suresh Kumar, Mrs. B. Nirmala, Mr. J. R. Paramesha, Mr. Dinesh, Dr. W. Suchanek, and Dr. S. Srikanta Swamy is greatly appreciated. Miss S. Vidya, secretary of Prof. K. Byrappa, typed the manuscript. Mr. Murruli of Microsystems, Mysore, did the scanning of drawings, figures and photographs. The manuscript was read and corrected for typographical errors and English usage by Dr. K. T. Sunitha, Chair, Dept. of English, Univ. of Mysore, India (wife of Prof. K. Byrappa), and Miss Shobha M. Gowda, Lecturer in English, University of Mysore (currently in the McGill University, Montreal, Canada). Mrs. Hiroko Yoshioka, Mrs. Fujiko Mori, and Mrs. Keiko Kato, who are the secretaries of Prof. Yoshimura, have greatly assisted the authors in the preparation of this manuscript. We are highly obliged to all our family members—Dr. Sunitha Byrappa, Shayan and Nayan (Prof. Byrappa's family members), Mrs. Akiko Yoshimura, Sayaka, Ayumi, and Hirono (Prof. Yoshimura's family members) for their great patience and cooperation with us during these 3½ years of book writing.

We would like to acknowledge the financial support received from Japan Society for Promotion of Science (JSPS), New Energy and Industrial Technology Development Organization (NEDO), Japan, and Research Institute of Solvothermal Technology (RIST), Kagawa, Japan, Dept. of Atomic Energy, Govt. of India, and University of Mysore, India.

DropBooks

Finally we would like to express our deep gratitude to Mr. George Narita of Noyes Publications, William Andrew Publishing, for bringing out this book. It is also an added pleasure to acknowledge the role played by the staff of Noyes Publications, especially Mary Bourke and Brent Beckley, and the staff of Write One, New York, for composition. If we have omitted any important topic or any other names of the friends, or citation of the important references in this book, it is not intentional. We have tried our best to cover as much as we could of the hydrothermal research based on the most exhaustive up-to-date literature search. Hopefully, this book will be a most valuable textbook and reference for the students and researchers in the field of hydrothermal technology, both at the beginners' and advanced levels.

September 2000

K. Byrappa
M. Yoshimura

Contents

1 Hydrothermal Technology—Principles and Applications 1

1.1 INTRODUCTION 1

1.2 DEFINITION 7

1.3 MINERALIZERS 9

1.4 NATURAL HYDROTHERMAL SYSTEMS 9

1.5 THE BEHAVIOR OF VOLATILES AND OTHER INCOMPATIBLE COMPONENTS UNDER HYDROTHERMAL CONDITIONS 13

1.5.1 Water 14

1.5.2 Fluorine and Chlorine 14

1.5.3 Boron 14

1.5.4 Phosphorus 15

1.5.5 Behavior of Alkalis 15

1.5.6 Crystallization Temperatures 16

1.6 SUBMARINE HYDROTHERMAL SYSTEMS 19

1.7 HYDROTHERMAL CRYSTAL GROWTH AND MATERIALS PROCESSING 27

1.8 STATISTICS OF PUBLICATIONS AND RESEARCH IN HYDROTHERMAL TECHNOLOGY 32

DropBooks

1.9 HYDROTHERMAL MATERIALS PROCESSING 39
REFERENCES 43

2 History of Hydrothermal Technology 53
2.1 INTRODUCTION 53
REFERENCES 78

3 Apparatus 82
3.1 INTRODUCTION 82
3.2 SELECTION OF AUTOCLAVE AND AUTOCLAVE MATERIALS 84
3.3 LINERS 90
3.4 TEMPERATURE AND PRESSURE MEASUREMENTS 97
3.5 AUTOCLAVES AND AUTOCLAVE DESIGNS 101
3.5.1 Conventional Autoclave Designs 101
3.5.2 Novel Autoclaves 118
3.6 SAFETY AND MAINTENANCE OF AUTOCLAVES 149
REFERENCES 151

4 Physical Chemistry of Hydrothermal Growth of Crystals 161
4.1 INTRODUCTION 161
4.1.1 Physico-Chemical and Hydrodynamic Principles of the Hydrothermal Growth of Crystals 162
4.2 BASIC PRINCIPLES OF PHASE FORMATION UNDER HYDROTHERMAL CONDITIONS 166
4.3 SOLUTIONS, SOLUBILITY AND KINETICS OF CRYSTALLIZATION 170
4.4 THERMODYNAMIC PRINCIPLES OF SOLUBILITY 174

4.5 KINETICS OF CRYSTALLIZATION UNDER HYDROTHERMAL CONDITIONS 182
4.5.1 Experimental Investigations of Solubility 186
REFERENCES 191

5 Hydrothermal Growth of Some Selected Crystals 198
5.1 QUARTZ 198
5.2 GROWTH OF HIGH-QUALITY (AND DISLOCATION FREE) QUARTZ CRYSTALS 207
5.2.1 Growth Rate 208
5.2.2 Seed Effect 209
5.2.3 Nutrient Effect 211
5.2.4 Solubility 213
5.2.5 Defects Observed in Synthetic α-quartz Single Crystals 215
5.2.6 Processing of α-quartz for High Frequency Devices 219
5.3 BERLINITE 223
5.3.1 Crystal Chemical Significance of the Growth of $AlPO_4$ Crystals 225
5.3.2 Solubility of Berlinite 226
5.3.3 Crystal Growth 231
5.3.4 Morphology 236
5.3.5 Thermal Behavior 243
5.3.6 Piezoelectric Properties of Berlinite 244
5.4 GALLIUM PHOSPHATE, $GaPO_4$ 247
5.4.1 Crystal Growth of Gallium Phosphate 248
5.4.2 Morphology 253
5.4.3 Dielectric Properties of Gallium Phosphate 254
5.5 POTASSIUM TITANYL PHOSPHATE (KTP) 256
5.5.1 Crystal Growth of KTP 259
5.5.2 Solubility of KTP 264
5.5.3 Morphology 268
5.6 POTASSIUM TITANYL ARSENATE 269

DroopBooks

5.7 CALCITE 273
5.7.1 Crystal Growth 279
5.7.2 Hydrothermal Hot Pressing of Calcite 284
5.7.3 Growth of Related Carbonates 285
5.8 HYDROXYAPATITE (HAp) 287
5.8.1 Crystal Structure of Apatite 291
5.8.2 Phase Equilibria 291
5.8.3 Crystal Growth 295
REFERENCES 300

6 Hydrothermal Synthesis and Growth of Zeolites 315
6.1 INTRODUCTION 315
6.2 MINERALOGY OF ZEOLITES 316
6.3 CRYSTAL CHEMISTRY OF ZEOLITES 318
6.4 COMPARISON BETWEEN NATURAL AND SYNTHETIC ZEOLITES 327
6.5 SYNTHESIS OF ZEOLITES 331
6.5.1 Molar Composition 338
6.5.2 The Aging of Hydrogel 340
6.5.3 Water in Zeolite Synthesis 348
6.5.4 Temperature and Time 349
6.5.5 Alkalinity (pH) 350
6.5.6 Structure Directing and Composition Determining Species (Templating) 352
6.5.7 Nucleation 354
6.6 CRYSTAL GROWTH 364
6.7 ALUMINOPHOSPHATE ZEOLITES 377
6.8 GROWTH OF ZEOLITE THIN FILMS AND CRYSTALS AT INORGANIC/ORGANIC INTERFACES (PREPARATION OF ZEOLITE-BASED COMPOSITES) 383
6.9 APPLICATIONS OF ZEOLITES 391
6.10 OXIDATIVE CATALYSIS ON ZEOLITES 398
REFERENCES 404

7 Hydrothermal Synthesis and Growth of Coordinated Complex Crystals (Part I) 415

7.1 INTRODUCTION 415

7.2 CRYSTAL CHEMICAL BACKGROUND 416

7.3 RARE EARTH SILICATES 426

7.4 PHASE FORMATION OF RARE EARTH SILICATES (IN AQUEOUS SOLVENTS) 426

7.5 CRYSTAL CHEMICAL SIGNIFICANCE OF PHASE FORMATION 436

7.5.1 Phase Formation in Surplus R_2O_3 451

7.5.2 Silicates 451

7.5.3 Phase Formation in the Rare Earth Silicate Systems in the High Silica Region 454

7.6 DEGREE OF SILIFICATION 457

7.7 PROPERTIES OF RARE EARTH SILICATES 459

7.8 SODIUM ZIRCONIUM SILICATES 461

7.9 GROWTH OF SELECTED SILICATES 467

7.9.1 Bismuth Silicate, $Bi_{12}SiO_{20}$ 471

7.9.2 Beryl, $Be_3Al_2(SiO_3)_6$ 475

7.9.3 Tourmaline 483

7.9.4 Nepheline 484

7.9.5 Zincosilicates 486

7.10 HYDROTHERMAL GROWTH OF LITHIUM SILICATES 495

7.11 HYDROTHERMAL GROWTH OF GERMANATES 497

7.11.1 Rare Earth Germanates 499

7.11.2 Zirconium Germanates 511

7.11.3 Zincogermanates 515

7.12 PROPERTIES OF GERMANATES 516

7.13 HYDROTHERMAL GROWTH OF PHOSPHATES 519

7.13.1 Structural Chemistry of Rare Earth Phosphates 522

7.13.2 Hydrothermal Growth of Rare Earth Phosphates 523

DropBooks

7.13.3 Structure Types of Rare Earth Phosphates 533
7.14 HYDROTHERMAL GROWTH OF MIXED VALENT METAL PHOSPHATES 533
7.15 PROPERTIES OF RARE EARTH AND MIXED VALENT METAL PHOSPHATES 555
7.16 HYDROTHERMAL SYNTHESIS OF VANADATES 561
7.16.1 Growth of $R = MVO_4$ (R = Nd, Eu; M = Y, Gd) 562
7.16.2 Growth of Mixed Valent Vanadates 570
7.17 HYDROTHERMAL SYNTHESIS OF BORATES 572
7.17.1 Hydrothermal Growth of Selected Borates 576
REFERENCES 597

8 Hydrothermal Synthesis and Crystal Growth of Fluorides, Sulfides, Tungstates, Molybdates, and Related Compounds 618
8.1 INTRODUCTION 618
8.2 FLUORIDES 618
8.2.1 Hydrothermal Synthesis of Rare Earth Fluorides 619
8.2.2 Spectroscopic Properties of Rare Earth Fluorides 623
8.3 HYDROTHERMAL SYNTHESIS OF TRANSITION METAL FLUORIDES 626
8.4 HYDROTHERMAL SYNTHESIS OF FLUOROCARBONATES AND FLUOROPHOSPHATES 629
8.5 OXYFLUORINATED COMPOUNDS 631
8.6 PHYSICAL PROPERTIES OF TRANSITION METAL FLUORIDES AND FLUORO-CARBONATES/FLUOROPHOS-PHATES/OXYFLUORIDES 633

8.7 HYDROTHERMAL SYNTHESIS OF TUNGSTATES 636
8.8 HYDROTHERMAL SYNTHESIS OF MOLYBDATES 646
8.9 HYDROTHERMAL SYNTHESIS OF TITANATES 650
8.9.1 Crystal Chemistry of Titanates 651
8.9.2 Hydrothermal Synthesis of Selected Titanates 655
8.10 HYDROTHERMAL GROWTH OF LITHIUM METAGALLATE CRYSTALS 663
8.11 HYDROTHERMAL SYNTHESIS OF SULPHIDES 665
8.11.1 Hydrothermal Synthesis of Sulphides of Univalent Metals 666
8.11.2 Hydrothermal Synthesis of Divalent Metal Sulphides 666
8.11.3 Hydrothermal Synthesis of Complex Sulphides 672
8.11.4 Hydrothermal Synthesis of Chalcohalides 672
8.12 HYDROTHERMAL SYNTHESIS OF SELENIDES, TELLURIDES, NIOBATES AND TANTALATES 674
8.13 HYDROTHERMAL SYNTHESIS OF ARSENATES 680
REFERENCES 682

9 Hydrothermal Synthesis of Native Elements and Simple Oxides 691
9.1 INTRODUCTION 691
9.2 HYDROTHERMAL SYNTHESIS OF NATIVE ELEMENTS 691
9.3 HYDROTHERMAL SYNTHESIS OF HYDROXIDES 700

DropBooks

9.4 HYDROTHERMAL SYNTHESIS OF SELECTED OXIDES 702
9.4.1 Cu_2O (Cuprite) 702
9.4.2 BeO (Bromelite) 703
9.4.3 Zinc Oxide 703
9.4.4 Hydrothermal Growth of Corundum 707
9.4.5 Hydrothermal Growth of Oxides of Ti, Zr and Hf 712
9.5 HYDROTHERMAL GROWTH OF TELLURIUM DIOXIDE 714
9.6 HYDROTHERMAL SYNTHESIS OF TiO_2 AND RELATED OXIDE POWDERS 717
9.7 HYDROTHERMAL SYNTHESIS OF MIXED OXIDES 729
9.7.1 Hydrothermal Synthesis of Aluminates 729
9.7.2 Hydrothermal Synthesis of Antimonites and Antimonates 731
9.7.3 Hydrothermal Synthesis of Garnets 734
9.7.4 Hydrothermal Synthesis of Ferrite 736
9.7.5 Hydrothermal Synthesis of Complex Oxides 739
REFERENCES 743

10 Hydrothermal Processing of Materials 754
10.1 INTRODUCTION 754
10.2 HYDROTHERMAL PREPARATION OF ADVANCED CERAMICS 755
10.2.1 Hydrothermal Preparation of Simple Oxide Ceramics 758
10.2.2 Hydrothermal Preparation of Perovskite Type of Mixed Oxide Ceramics 762
10.2.3 Hydrothermal Processing of Bioceramics 773
10.2.4 Hydrothermal Preparation of Thin Films 777
10.2.5 Hydrothermal Processing of Composites 785

10.3 HYDROTHERMAL PROCESSING OF WHISKER CRYSTALS 793

10.4 RELATED METHODS OF HYDROTHERMAL PROCESSING OF MATERIALS 801

10.4.1 Hydrothermal Hot Pressing (HHP) and Hot Isostatic Pressing (HIP) 802

10.4.2 Hydrothermal Reaction Sintering of Processing Materials 804

10.4.3 Microwave Hydrothermal Processing 808

10.4.4 Hydrothermal Treatment/Recycling/Alteration ... 813

10.5 HYDROTHERMAL TECHNOLOGY FOR THE 21ST CENTURY 815

10.5.1 Thermodynamic Principles of Advanced Materials Processing 818

REFERENCES 829

Index 846

DropBooks

1

Hydrothermal Technology—Principles and Applications

1.1 INTRODUCTION

The hydrothermal technique has been most popular, garnering interest from scientists and technologists of different disciplines, particularly in the last fifteen years. The term *hydrothermal* is purely of geological origin. It was first used by the British Geologist, Sir Roderick Murchison (1792–1871), to describe the action of water at elevated temperature and pressure in bringing about changes in the earth's crust leading to the formation of various rocks and minerals.[1] A majority of the minerals formed in the postmagmatic and metasomatic stages in the presence of water at elevated pressure and temperature conditions are said to be "of hydrothermal origin." This covers a vast number of mineral species including ore deposits. It is well known that the largest single crystal formed in nature (beryl crystal of >1000 gm) and some of the largest quantities of single crystals created by man in one experimental run (quartz crystals of several 100's of gm) are both of hydrothermal origin.

An understanding of the mineral formation in nature under elevated pressure and temperature conditions in the presence of water led to the development of the hydrothermal technique. It was successfully adopted by Schafthaul (1845) to obtain quartz crystals upon transformation of freshly precipitated silicic acid in Papin's digestor.[2] Thus, the hydrothermal technique became a very popular means to simulate the natural conditions existing under the earth's crust and synthesizing them in the laboratory. These studies dealing with laboratory simulations have helped the earth scientists to determine complex geological processes of the formation of rocks, minerals, and ore deposits. As the subject became more and more popular among geologists, new branches of geology emerged as "Experimental Mineralogy" and "Experimental Petrology."

The first successful commercial application of hydrothermal technology began with mineral extraction or ore beneficiation in the previous century. The use of sodium hydroxide to leach bauxite was invented in 1892 by Karl Josef Bayer (1871–1908) as a process for obtaining pure aluminum hydroxide which can be converted to pure Al_2O_3 suitable for processing to metal.[3] Even today, over 90 million tons of bauxite ore is treated annually by this process.[4] Similarly, ilmenite, wolframite, cassiterite, laterites, a host of uranium ores, sulphides of gold, copper, nickel, zinc, arsenic, antimony, and so on, are treated by this process to extract the metal. The principle involved is quite simple, very effective, and inexpensive, as shown below, for example.

DropBooks

$$Al(OH)_3 + OH^- \rightarrow [AlO(OH)_2]^- + H_2O$$

$$AlOOH + OH^- \rightarrow [AlO(OH)_2]$$

The above process is easy to achieve and the leaching can be carried out in a few minutes at about 330°C and 25,000 kPa.[5]

Further importance of the hydrothermal technique for the synthesis of inorganic compounds in a commercial way was realized soon after the synthesis of large single crystals of quartz by Nacken (1946) and zeolites by Barrer (1948) during late 1930s and 1940s, respectively.[6][7] The sudden demand for the large size quartz crystals during World War II forced many laboratories in Europe and North America to grow large size crystals. Subsequently, the first synthesis of zeolite that did not have a natural counterpart was carried out by Barrer in (1948) and this opened altogether a new field of science, viz., molecular sieve technology.[8] The

success in the growth of quartz crystals has provided further stimuli for hydrothermal crystal growth.[9]

Today, the hydrothermal technique has found its place in several branches of science and technology, and this has led to the appearance of several related techniques with strong roots attached to the hydrothermal technique. So we have hydrothermal synthesis, hydrothermal growth, hydrothermal alteration, hydrothermal treatment, hydrothermal metamorphism, hydrothermal dehydration, hydrothermal decomposition, hydrothermal extraction, hydrothermal sintering, hydrothermal reaction sintering, hydrothermal phase equilibria, hydrothermal electrochemical reaction, and so on, which involve materials scientists, earth scientists, materials engineers, metallurgists, physicists, chemists, biologists, and others. Although the technique has attained its present high status, it has passed through several ups and downs owing to the lack of proper knowledge pertaining to the actual principles involved in the process. Hence, the success of the hydrothermal technique can be largely attributed to the rapid advances in the apparatus involved (new apparatus designed and fabricated) in hydrothermal research, and also to the entry of a large number of physical chemists, who have contributed greatly to the understanding of hydrothermal chemistry.[10] Further, the modeling and intelligent engineering of the hydrothermal processes have also greatly enhanced our knowledge in the field of hydrothermal research.[11][12]

In recent years, with the increasing awareness of both environmental safety and the need for optimal energy utilization, there is a case for the development of nonhazardous materials. These materials should not only be compatible with human life but also with other living forms or species. Also, processing methods such as fabrication, manipulation, treatment, reuse, and recycling of waste materials should be environmentally friendly. In this respect, the hydrothermal technique occupies a unique place in modern science and technology. The rapid development in the field of hydrothermal research in the last fifteen years, or so, motivated the present authors to bring out this handbook covering almost all aspects of hydrothermal research. Although there is a growing interest among scientists from various branches of science, at the moment there are no books or monographs available in the field of hydrothermal technology. Most of the major works, even by the pioneers in this field, have been confined to reviews and edited books. Table 1.1 lists important reviews and edited books in the field of hydrothermal research.

Table 1.1. List of the Books and Reviews in the Field of Hydrothermal Research

BOOKS

Sl. No.	Author	Title	Publishers
1.	Labachev, A. N. (ed.)	*Hydrodrothermal Synthesis of Crystals*	Nauka, Moscow (1971)
2.	Ulmer, G. C. (ed.)	*Research Techniques for High Pressure and High Temperature*	Springer-Verlag, New York (1971)
3.	Labachev, A. N. (ed.)	*Crystallization Processes under Hydrothermal Conditions*	Consultants Bureau, New York (1973)
4.	Ikornikova, N. Yu	*Hydrothermal Synthesis of Crystals in Chloride Systems*	Nauka, Moscow (1975)
5.	Kuzmina, I. P. and Khaidukov, N. M.	*Crystal Growth from High Temperature Aqueous Solutions*	Nauka, Moscow (1977)
6.	Demianets, L. N., Labachev, A. N., & Emelechenko, G. A.	*Germanates of Rare Earth Elements*	Nauka, Moscow (1980)
7.	David T. Rickard Frans E. Wickman (ed.)	*Chemistry and Geochemistry of Solutions at High Temperature and Pressure*	Pergamon, New York (1981)
8.	Somiya. S. (ed.)	*Proc. 1st Int. Symp. Hydrothermal Reactions*	Japan (1982)
9.	Litvin, B. N. and Popolotov, V. I.	*Hydrothermal Synthesis Inorganic Compounds*	Nauka, Moscow (1984)
10.	Popolitov, V. I. and Litvin, B. N.	*Growth of Single Crystals under Hydrothermal Conditions*	Nauka, Moscow (1986)
11.	Ulmer, G. C. and Barnes, H. L. (eds.)	*Hydrothermal Experimental Techniques*	John Wiley & Sons, New York (1987)
12.	Nesterov, P. V. (ed.)	*Progress in Science and Technology, Crystal Chemistry of Germanates of Tetravalent Metals*	Moscow, VINITI (1989)
13.		*Hydrothermal Reactions ISHR - 89*	Nauka, Moscow (1989)

DropBooks

Table 1.1. *(Cont'd.)*

BOOKS *(Cont'd.)*

Sl. No.	Author	Title	Publishers
14.	Occelli, M. L. & Robson, H. E. (eds)	*Zeolite Synthesis*	ACS Symp. Series 398 Am. Chem. Soc., Washington, DC (1989)
15.	Somiya, S. (ed.)	*Hydrothermal Reactions for Engineering*	Elsevier, Applied Sci. (1989)
16.	Byrappa, K. (ed.)	*Hydrothermal Growth of Crystal*	Pergamon, Oxford (1991)
17.	Cuney, M. & Cathelineau, M. (eds.)	*Proc. 4th Int. Symp. Hydrothermal Reactions*	Nancy France (1993)
18.		*Proc. 1st Int. Conf. Solvothermal Reactions*	Japan, (Dec. 6-8 1996)
19.		*Proc. 2nd Int. Conf. Solvothermal Reactions*	Japan, (Dec.18-20 1996)
20.	Palmer, D. A. & Wesoloski, D. J.	*Proc. 5th Symp. Hydrothermal Reactions*	Gatlinburg, USA (1997)
21.		*Proc. 3rd Int. Conf. Solvothermal Reactions*	Bordeaux, France (1999)

REVIEWS

Sl. No.	Author	Title	Publishers
1.	Morey, G. W.	*Hydrothermal Synthesis*	*J. Am. Ceram. Soc.* (1953)
2.	Roy, R. & Tuttle	*Investigation under Hydrothermal Conditions*	*Phy. Chem. Earth* 1:138 (1955)
3.	Ballman, A. A. Laudies, R. A.	*Solution Growth*	In: *Art and Science of Growing Crystals* (Gilmann, J. J., ed.) Wiley, New York (1963)

Table 1.1. *(Cont'd.)*

REVIEWS *(Cont'd.)*

Sl. No.	Author	Title	Publishers
4.	Laudise, R. A.	*Hydrothermal Growth of Crystals*	In: *The Growth of Single Crystals*, Prentice-Hall, New York (1970)
5.	Kuznetsov, V. A. & Lobachev, A. N.	*Hydrothermal Method for the Growth of Crystals*	*Sov. Phys. Crystallogr.* 70:775-804 (1973)
6.	Nassau, K.	*Synthetic Emerald: The Confusing History and The Current Technology*	*J. Crystal Growth* 35:211-222 (1976)
7.	Rabenau, A.	*The Role of Hydrothermal Synthesis in Preparative*	*Angew. Chem. Int Engl. Ed.* 24:1026–1040 *Chemistry* (1985)
8.	Laudise, R. A.	*Hydrothermal Crystal Growth - Some Recent Results*	In: *Advanced Crystal Growth*, Prentice Hall, New York (1987)
9.	Komareni, S. Fregeau, E. Breval, E. &. Roy, R.	*Hydrothermal Preparation of Ultrafine Ferrites & their Sintering.*	*J. Am. Ceram. Soc*, (1988)
10.	Somiya, S.	*Hydrothermal Reactions in Inorganic Systems*	In: *Advance Materials Frontiers* in *Mat. Sci. & Eng.* (Somiya, S.: ed.); *Trans. Mat. Res. Soc. Jpn.*, Vol. 19B, Elsevier Science, B.V. (1994)
11.	Yoshimura, M. & Suda, H.	*Hydrothermal Processing of Hydroxyapatite: Past, Present & Future.*	In: *Hydroxyapatite and Related Compounds*, Brown, P. W. & Constantz, B. (eds.) p. 45–72, CRC Press (1994)
12.	Byrappa, K.	*Hydrothermal Growth of Crystals*	In: *Handbook of Crystal Growth, Vol. 2a*, (D. T. J. Hurle, ed.), Elsevier Science B.V. (1994)
13.	Leco catalogue	Leco corporation	Tem-Press division USA (1999)

DropBooks

1.2 DEFINITION

In spite of the fact that the hydrothermal technique has made tremendous progress, there is no unanimity about its definition. The term *hydrothermal* usually refers to any heterogeneous reaction in the presence of aqueous solvents or mineralizers under high pressure and temperature conditions to dissolve and recrystallize (recover) materials that are relatively insoluble under ordinary conditions. Morey and Niggli (1913) defined hydrothermal synthesis as "…in the hydrothermal method the components are subjected to the action of water, at temperatures generally near though often considerably above the critical temperature of water (~370°C) in closed bombs, and therefore, under the corresponding high pressures developed by such solutions."[13] According to Laudise (1970), hydrothermal growth means growth from aqueous solution at ambient or near-ambient conditions.[14] Rabenau (1985) defined hydrothermal synthesis as the heterogeneous reactions in aqueous media above 100°C and 1 bar.[15] Lobachev (1973) defined it as a group of methods in which crystallization is carried out from superheated aqueous solutions at high pressures.[16] Roy (1994) declares that hydrothermal synthesis involves water as a catalyst and occasionally as a component of solid phases in the synthesis at elevated temperature (>100°C) and pressure (greater than a few atmospheres).[17] Byrappa (1992) defines hydrothermal synthesis as any heterogenous reaction in an aqueous media carried out above room temperature and at pressure greater than 1 atm.[18] Yoshimura (1994) proposed the following definition: reactions occurring under the conditions of high-temperature–high-pressure (>100°C, >1 atm) in aqueous solutions in a closed system.[19]

The above definitions hold good for materials synthesis, metal leaching and treatment of waste materials. However, there is no definite lower limit for the pressure and temperature conditions. The majority of the authors fix the hydrothermal synthesis, for example, at above 100°C temperature and above 1 atm. But, with the vast number of publications under mild hydrothermal conditions in recent years, we propose to define hydrothermal reaction as "any heterogenous chemical reaction in the presence of a solvent (whether aqueous or nonaqueous) above room temperature and at pressure greater than 1 atm in a closed system." In addition to this non-unanimity, there is also a lot of confusion with regard to the very usage of the term *hydrothermal*. For example, chemists prefer to use a broader term, viz., *solvothermal*, meaning any chemical reaction

in the presence of a solvent in supercritical or near supercritical conditions.[20] However, this term has been introduced recently, and in fact, the early work in this direction was carried out by geologists using CO_2.[21] Japan has already organized two International Conferences and one International Workshop on Solvothermal Reactions.[22]–[24] The third International Conference on Solvothermal Reactions was held in July 1999 in Bourdeaux, France. Similarly, there are several other terms like *glycothermal*, *alcothermal*, *ammonothermal*, and so on, depending upon the type of solvent used in such chemical reactions. However, the purpose behind using these different solvents in the chemical reactions is essentially to bring down the pressure-temperature conditions. In this context, Yoshimura has proposed a new term, *soft solution processing*, for processes in which the pressure and temperature conditions reach near or just above ambient conditions.[25] Though this term has a broader meaning, it covers only a portion of the hydrothermal research and refers mainly to any solution processing at or near the ambient conditions. Thus, in the present book, the authors retain a broader term, *hydrothermal*, throughout the text and use other terms only when such occasion arises.

As mentioned above, under hydrothermal conditions, the reactants which are otherwise difficult to dissolve go into solution as complexes under the action of mineralizers or solvents, Hence, one can expect the conditions of chemical transport reactions. Therefore, some workers even define hydrothermal reactions as special cases of chemical transport reactions. Owing to the specific physical properties, particularly the high solvation power, high compressibility, and mass transport of these solvents, one can also expect the occurrence of different types of reactions like:

i. Synthesis of new phases or stabilization of new complexes.

ii. Crystal growth of several inorganic compounds.

iii. Preparation of finely divided materials and microcrystallites with well-defined size and morphology for specific applications.

iv. Leaching of ores in metal extraction.

v. Decomposition, alteration, corrosion, etching.

ProjoBooks

1.3 MINERALIZERS

In any hydrothermal system or reaction confined to any one of the processes described in Sec. 1 of this chapter, the role played by the solvent under the action of temperature and pressure is very important. It has been interpreted in various ways by many workers. Recently Yoshimura and Suda (1994) have described these processes to understand the action of solvent, for example, water on solid substances under elevated pressure and temperature conditions.[19] This process is represented in Table 1.2.

Through proper interpretation of the above listed processes, one can easily develop a required hydrothermal process corresponding to the material synthesis or crystal growth or materials process using a suitable solvent to increase the solubility of the desired compound. Water is the most important solvent and it was popularly used as a hydrothermal mineralizer in all the earlier experiments. However, several compounds do not show high solubility for water even at supercritical temperature, and hence the size of the crystals or minerals obtained in all the early hydrothermal experiments of the 19th century did not exceed thousandths or hundredths of a millimeter. Therefore, the search for other suitable mineralizers began in the 19th century itself. A variety of aqueous and nonaqueous solutions were tried to suit the preparation of a particular compound. The selection of the mineralizers and their role in hydrothermal systems with suitable examples are discussed in great detail in Ch. 3. The knowledge acquired through the use of several new mineralizers has helped to implement this hydrothermal technique as an effective one in preparative chemistry. Table 1.3 shows the use of hydrothermal processing in various fields of materials synthesis, crystal growth, and materials processing.[19] Before going into the details of this, it is appropriate to discuss the natural hydrothermal systems.

1.4 NATURAL HYDROTHERMAL SYSTEMS

The beginning of hydrothermal research is firmly associated with the study of the natural systems by earth scientists, who were interested in understanding the genesis of various rocks, minerals and ore deposits through laboratory simulations of the conditions existing in the earth's crust. Therefore, it is appropriate to discuss briefly the research on natural hydrothermal systems and its contribution to the development of this field to its present status. Starting from the earliest experiment by Schafthaul in

1845 on the synthesis of quartz,[2] over 130 mineral species were synthesized by the end of 19th century, and the experiments were carried out on various geological phenomena ranging from the origin of ore deposits to the origin of meteorites. Today, it is being popularly used by geologists to solve several existing problems in petrology, geochemistry, mineralogy, ore genesis, and palaeontology. The impetus for the experimental investigations during the 19th century was provided not only by a desire to explain geological phenomena, but also by greatly improved equipment and techniques fostered by industrial revolution. Such investigations helped in unraveling the hitherto unknown natural geological processes of mineral formation. On the other hand, it helped in finding uses for the artificially synthesized single crystals like ruby, emerald, sapphire, quartz, and diamond, in the gemstone industry.

Table 1.2. Action of Hydrothermal Fluid (High-Temperature–High-Pressure Aqueous Solution/Vapor) on Solid State Materials

Classified	Action	Application
1. Transfer Medium	Transfer of Kinetic Energy, Heat and Pressure Forming, etc.	Erosion, Machining Abrasion, HIP
2. Adsorbate	Adsorption/Desorption at the Surface	Dispersion, Surface Diffusion, Catalyst, Crystallization, Sintering, Ion Exchange, etc.
3. Solvent	Dissolution/Precipitation	Synthesis, Growth, Purification, Extraction, Modification, Degradation, Etching, Corrosion, etc.
4. Reactant	Reaction	Formation/Decomposition (hydrates, hydroxides, oxides) corrosion, etc.

DropBooks

Table 1.3. Development of Hydrothermal Processing

1. Crystal Synthesis and Growth	:	Oxide, Sulfide,Fluoride...(1978 ~)
2. Controlled Fine Crystals Composition, Size, Shape	:	PZT, ZrO_2, $BaTiO_3$, HAp, ferrite (1978 ~)
3. Crystallized Thin/Thick Films	:	$BaTiO_3$, $SrTiO_3$, $LiNbO_3$ (1989 ~)
4. Etching, Corrosion	:	Oxide, Nitride, Carbide
5. Polishing, Machining	:	Oxide, Nitride, Carbide
6. Combined with Electrical, Photo-, Radio- & Mechano-Processing	:	Synthesis, Modification, Coating
7. Organic and Biomaterials 8. Non-aqueous Solution 9. Continuous system	:	Hydrolysis, Extraction Polymerization, Synthesis, Decomposition, Wet Combustion

In order to understand the formation of several ore deposits including that of nobel metals, it is necessary to discern the physico-chemical conditions which govern the transport and precipitation mechanisms of these metals in hydrothermal solutions. Several thermodynamic models have been proposed to explain these mechanisms in nature. Relatively much is known, for example, about the hydrothermal chemistry of gold.[27][28] Similarly, the behavior of common rock-forming minerals in a variety of electrolytic solutions has been studied in detail. Here, the authors present only the salient features of these works to provide the background for the hydrothermal technique since the main theme of this handbook is on crystal growth and materials processing. Besides, a quantitative model of the transport and deposition mechanisms is still impeded by a dearth of reliable high temperature and pressure, experimentally based, thermodynamic data. However, there is some remarkable progress made in this direction, thanks to the advances in the thermodynamic modeling, the direct sampling and analyses of the natural geothermal systems, their extinct analogues, epithermal ore deposits, and other geologic environments, primarily by analyses of fluid inclusions.[29] Therefore, an understanding of the mineral-water reaction kinetics is essential to quantifying the behavior of natural and engineered earth systems. Although, several studies have been carried out on the behavior of most

hydrothermal systems, the predictions based upon rates from deionized water are unlikely to be representative of processes occurring in complex fluids of natural systems which contain numerous dissolved ions. These constituents have both significant rate-inhibiting and enhancing effects on behavior, even when present in very small quantity.[30][31]

In nature, the most common minerals in soils and rocks are generally in contact with water at a wide pH range. In extreme cases, the pH can be nearly 2 in the presence of sulfides, which oxidizes to give H_2SO_4, and as high as 10 in the presence of alkaline salts like Na_2CO_3. Here, the authors briefly discuss the gold deposition in hydrothermal ore solutions. In this case, the major role is played by the chloride and sulphur-containing ligands.[32][33] The dominant gold complexing ligands are usually sulphide species. The stability constants for gold(I) chloride complexes (for example, at 250°C) are up to twenty orders of magnitude smaller than those of Au(I) hydrosulphide complexes and, therefore, the latter predominates in nature.[36] Despite this observation, the stability constants for Au(I) hydrosulphide complexes under high temperature and pressure environments are not yet well defined. This is particularly true for the low pH region where no satisfactory data are available.

DropBooks

Benning and Seward[35] have proposed three sets of experimental conditions of pH range for gold deposition in nature:

$$Au_{(s)} + H_2S + + H_2O + H_2\,(gas) \qquad pH \approx 4$$

$$Au_{(s)} + H_2S + NaHS + H_2O + H_2\,(gas) \qquad pH \approx \text{neutral}$$

$$Au_{(s)} + H_2S + H_3PO_4 + H_2O + H_2\,(gas) \qquad pH < 4$$

The solubility of gold increases with increasing temperature, pH, and total dissolved sulphur. At near neutral pH, an inverse correlation between solubility and pressure has been observed, whereas in acid pH solutions, above 150°C, increase in pressure increases the solubility. The equilibrium constants for the uncharged complex, AuHS show that this species plays an important role in the transport and deposition of gold in ore depositing environments, which are characterized by low pH fluids.

Recently some thermodynamic modeling in the chloride systems Au-NaCl-H_2O and Au-NaCl-CO_2-H_2O shows that the gold solubility decreases in the presence of CO_2 due to decreasing dielectric permeability of CO_2 bearing solution.[36] This model has been experimentally verified at 350°C and 50 MPa in 1 M KCl + 0.1 M HCl solutions in the presence of 3M CO_2 and without CO_2. It was found that the gold concentration in

chloride CO_2-bearing solutions is one order lower in magnitude than in systems without CO_2. Similarly, the silver bearing systems show distinct influence of CO_2 in comparison with gold system. CO_2 has negative solubility effect on gold and silver crystallization and CO_2 acts as a nonpolar component of crustal fluids in the crystallization of many ore deposits.[37] Thus, the recent hydrothermal solution speciation (solvation to ion pairing and complexing) study has greatly contributed to the knowledge and better understanding of various geological problems.

1.5 THE BEHAVIOR OF VOLATILES AND OTHER INCOMPATIBLE COMPONENTS UNDER HYDROTHERMAL CONDITIONS

The physical and thermodynamic properties of silicate melts depend upon melt structure. The structure of a melt is determined by both its composition and the ambient conditions and, with the notable exception of liquid immiscibility, may vary continuously with changes in these parameters. The structures of crystalline silicates vary only within restricted limits. As a result, variation in mineral-melt equilibria caused by changes in either compositions or external parameters may very well reflect the change in properties of the melt phase to a greater extent than those of the crystalline silicates.

The behavior of P_2O_5 is complex. Phosphorus pentoxide (P_2O_5) depolymerizes pure SiO_2 melts by entering the network as a fourfold coordinated cation, but polymerizes melts in which an additional metal cation, other than silicon, is present. The effect of this polymerization is apparent in the widening of the granite-ferrobasalt two-liquid solvus. In this complex system, P_2O_5 acts to increase phase separation by further enrichment of the high charge density cations Ti, Fe, Mg, and Ca, in the ferrobasaltic liquid. Phosphorus pentoxide (P_2O_5) also produces an increase in the ferrobasalt-granite REE liquid distribution coefficients. These distribution coefficients are close to 4 in P_2O_5-free melts, but close to 15 in P_2O_5-bearing melts.

Several attempts to understand the internal evolution of highly fractionated pegmatites focused on the roles of H_2O and other components, especially rare alkalis, B, P, F, are being carried out from time to time. Such studies yield a great amount of data on the role of these volatiles under hydrothermal conditions and also distinguish rare earth pegmatites

from other rocks.[38][39] These volatiles exert a significant control on fluid properties, solidus and liquidus temperatures.

1.5.1 Water

Water is an important constituent of any hydrothermal system. It exhibits unique properties, especially under supercritical conditions. These properties have been exploited appropriately in the recent years to disintegrate toxic organics, and recycle or treat waste materials. In nature, also, water plays an important role in the formation of various rocks and minerals and in the creation of life (origin of life). As a component of granitic melts, H_2O depresses solidus and liquidus temperatures,[40][41] lowers melt viscosities,[42]-[45] and promotes coarse grain size.[46]

1.5.2 Fluorine and Chlorine

Fluorine, as H_2O lowers solidus and liquidus temperatures, enhances cation diffusivities, and decreases melt viscosities.[47]-[49] One important difference between F and H_2O is that the DCF vapor/melt is L1 in metaluminous and peraluminous granitic bulk compositions.[50][51] Fluorine decreases the solubility of the melt[52][53] so that, at equal H_2O content of volatile-undersaturated magma at the same pressure and temperature, H_2O is higher in F-bearing melts than in F-absent melt. Metal-fluoride complexing in aqueous vapor may be important in rare-metal transport and formation of hydrothermal ores.[54][55]

DropBooks

1.5.3 Boron

The pronounced effects of boron in hydrous silicate melt are well known. Boron lowers the solidus, and it increases the solubility of H_2O in silicate melts. Lewis acid-base properties suggest that the solubility of H_2O/mole B_2O_3 in melts should increase with increasing boron content because of changes in B-O coordination. Boron also decreases the viscosity of silicate melts presumably through melt depolymerization caused by the synergistic network-modifying effects of boron and water.[56]

In silicate melts, boron forms two common oxyanions: trigonal planar BO_3^{3-} and tetrahedral BO_4^{5-}. The [BO_4^{5-}/BO_3^{3-}] ratio increases with melt alkalinity,[57][58] and boron content.[59] Although boron exhibits strong interaction with silicate melt, non-ideal mixing between borate and

silicate melt components is reflected by stable liquid-liquid or metastable glass-glass immiscibility over a wide range of bulk compositions in an hydrous silicate system.[60] The miscibility gap between metal-rich borate and essentially pure silica liquids increases with increasing field strength of added metal cations, with a consequent rise in the consolute temperature. Limited experimental evidence also indicates that the solubilities of other high charge-density cations (e.g., Group IV and Group V elements) are significantly higher in borosilicate melts than in simple aluminosilicate melts.[61]

As in fluorine-bearing systems, the addition of boron to silicate melts leads to an expansion of the liquidus field of quartz.[62] This behavior may reflect removal of cations from coordination with SiO_4^{4-} of the melt framework, resulting in higher SiO_2 through increased polymerization of SiO_4^{4-} tetrahedra.[63] Among Group I cations, boron has a tendency to depress the activities of the higher field-strength ions. The increased solubility of H_2O in borosilicate melts corresponds to a lower H_2O that may stem from direct hydrolysis of borate oxyanions.

1.5.4 Phosphorus

Phosphorus exhibits limited solubility in silicate melt,[64][65] hence the addition of phosphorus promotes phosphate-silicate liquid immiscibility. The phase equilibria data in the systems: SiO_2-P_2O_5, P_2O_5-M_xO_y, and P_2O_5-M_xO_y-SiO_2 show that phosphorus has an affinity for H, and it increases the solubility of H_2O in silicate melts, possibly by: $P = O + H_2O \rightarrow (HO)\text{-}P\text{-}(OH)$.[68] Although experimental evidence of the interaction of phosphorus with other Group I elements is lacking, the common pegmatite assemblage $LiAlPO_4$ (OH,F) + $NaAlSi_3O_8$ [rather than $NaAlPO_4$(OH,F) + $LiAlSi_2O_6$ + H_2O] suggests that P is more compatible with the smaller, more acidic cations of Group I.

1.5.5 Behavior of Alkalis

The zonation of rare element pegmatites is manifested largely by heterogeneous distributions of alkali aluminosilicates. Theoretical and experimental investigations of the interactions of Group I elements with aluminosilicate melts provide a basis for understanding the zonation of alkali aluminosilicates in pegmatites.

Both De Jong and Brown (1980), and Navrotsky, et al. (1985), proposed that the smaller alkalis Li and Na should exhibit a greater tendency to destabilize silicate melts than K, Rb, and Cs.[53][60]

A number of salient pegmatite characteristics can be explained by the effects of high concentrations of boron, fluorine, and phosphorus on phase equilibria in hydrous aluminosilicate melts.

1.5.6 Crystallization Temperatures

Comparatively high concentrations of B, P, F, and Group I elements serve to depress pegmatite magma liquid to approximately 650°C (within the stability fields of petalite or spodumene), and solidus to < 500°C. The low liquidus temperatures permit rare-element pegmatite magmas to migrate to metamorphic conditions of the anadalusite-cordierite/staurolite facies.[69][70] The physical migration of magma may be facilitated also by the lower melt viscosities of the H_2O-, B-, and F-rich pegmatite system. Because of the low temperature interval of crystallization, however, rare element pegmatite magmas may experience rapid increases in melt viscosity with only slight cooling, as glass transition temperatures are approached (e.g., as in the macusanite analogue). As a result of increased kinetic barriers to crystallization, internal disequilibrium may prevail (an important and poorly defined parameter in pegmatite crystallization is the rate of cooling, but evidence from wall-rock studies indicates that rare element pegmatite magmas are hosted by rocks at temperature < 500°C (e.g., Morgan, 1986).[71] Common textural features of rare element pegmatites, such as graphic intergrowths and radial or banded fabrics, can be interpreted as disequilibrium phenomena in supercooled liquids or glasses.[72] Experiments with dry macusanite, however, present alternative possibilities. In these experiments, pegmatitic fabrics, mineral assemblages, and zonation have been generated at or near equilibrium conditions with high concentrations of B, P, and F but low water content.

DropBooks

Numerous experimental investigations of aqueous systems at high temperature and pressure have been undertaken using conductivity, potentiometric, spectrophotometric, solubility, PVT and calorimetric, neutron diffraction, EXAFS, and other related methods. These studies yield a vast amount of information on cation-oxygen pairing and their increased or decreased distances with varying temperature. Likewise, the anion-water distances, for example, as in the case of iodide-oxygen (water) bond lengths, indicate that the solvation shell expands slightly with increasing

temperature. Similarly, molecular dynamics simulation studies on the alkali metals hydration in high temperature water up to 380°C have been carried out recently, demonstrating a small expansion of the first hydration shell around chloride with increasing temperature.[73] More or less complete data is available on the formation of simple, neutral ion pairs for dilute alkali metal halide solutions at high-pressure/temperature conditions. However, the understanding of the formation of polynuclear species is still not been clearly understood. Some workers have studied the ion pairing and cluster formation in a 1M NaCl solution at 380°C and near critical pressure.[74] These studies indicate the presence of simple monocationic ions and ion pairs together with triple ions such as Na_2Cl^- and $NaCl_2^-$ as well as the $Na_2Cl_2^-$ and more complicated polynuclear species. Similar studies on other solutions are available in the literature. All these studies have greatly contributed to the understanding of the geochemical system wherein the metal-complexing by other ligands is the most important aspect. However, there is a major lack of overall experimental data pertaining to the metal complex equilibria in supercritical aqueous systems as well as in binary solvent systems such as H_2O-CO_2. Such data are of enormous importance to the understanding of geochemistry of element transport by hydrothermal fluids active in the earth's crust.

In the last couple of years, a new concept, viz., *geothermal reactor*, introduced by Japanese workers is slowly catching the attention of hydrothermal engineers.[75][76] The principles of geothermal reactors include the direct use of geothermal energy as a heat source or driving force for chemical reactions. It helps to produce hydrothermal synthesis of minerals and a host of inorganic materials, extraction of useful chemical elements contained in crustal materials such as basalt, and use them as raw materials for hydrothermal synthesis. Thus, the concept of geothermal reactor leads to the construction of a high temperature and pressure autoclave underground. This has several advantages over the conventional autoclave technology.

Figure 1.1 shows the schematic sketch of a typical geothermal reactor for mineral synthesis.[76] The major advantages of the geothermal reactor are:

1. Synthesis of ceramic materials by hydrothermal reaction is possible without using fuel or electricity as main energy source.
2. The system does not discharge the used heat.

3. Outer tube with a slit in the bottom must be strong enough to keep the inner space of the tube against the pressure by the wall of formation, but inner double tube does not need the strength against the inner pressure as usual autoclaves.
4. Area of the plant is small because of the vertical long reactor in the ground.
5. It is highly useful to study the alteration of various rocks occurring in the earth crust in the presence of fluids of various compositions. Such studies have been carried out for granite and basalts.[75]

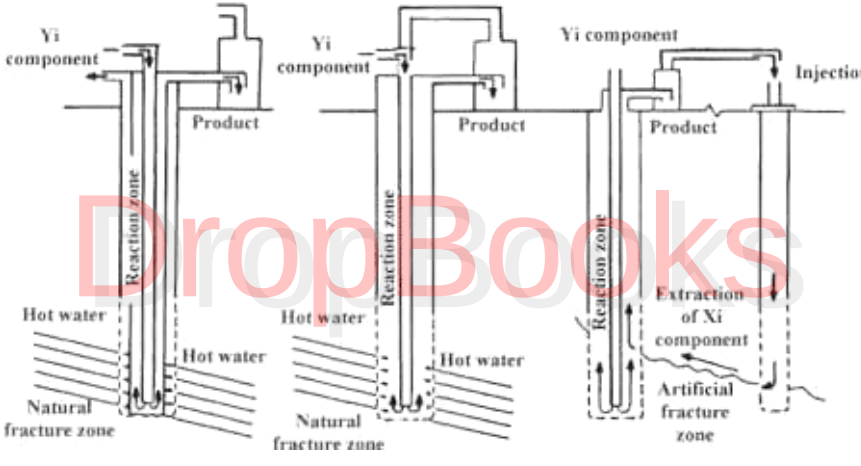

Figure 1.1. Geothermal reactors for mineral synthesis.[76]

The main disadvantage of the geothermal reactor is that the flow characteristics of high temperature slurry accompanied with the chemical reaction must be well understood for controlling the reaction. The volumetric capacity of the geothermal reactor is very large compared to that of usual autoclave, and the operation must be continuous. The merit of the geothermal reactor and its cost of operation can be realized only if the target material is to be developed in large quantity.

1.6 SUBMARINE HYDROTHERMAL SYSTEMS

The general acceptance of plate tectonics theory some 2½ decades ago has garnered much interest in geochemical processes at plate boundaries which has led to the discovery of hydrothermal activity in the deep sea directly on the Galapagos Spreading Centre in 1977,[77] and a large number of other spectacular submarine hydrothermal systems (like Red Sea Rift Valley, Juan de Fuca Ridge-North Pacific Ocean; 21°N East Pacific Rise, Kamchatka, Kurile Islands, Atlanti's II Deep in Red Sea, Lake Kivu, and so on) of global significance to ocean chemistry and geochemistry.[78] In fact, this discovery has led to a new thinking in marine biology and geochemistry, and in economic geology and has spawned an entirely new term, viz., *hydrothermal ecosystems,* which means water-containing terrestrial, subterranean, and submarine high temperature environments which are the sites of investigations for many palaeobiologists and biologists looking for primitive forms of life. It is strongly believed that the roots of life on earth can be found in hydrothermal ecosystems. These ecosystems may also serve as an analogue for the possible origin of life on Mars, where a similar environment might have existed or still exist. The conditions at the hydrothermal ecosystems mimic, to some extent, the conditions on early earth because of the presence of both heat and water. These conditions were abundant at around 3.5 Ga, when there was much greater vulcanism and a higher ambient temperature on earth. Dick Henley (1996) describes the geochemical activity of the hydrothermal ecosystems as biotic factory.[79] According to Everett Shock (1992), life thrives in submarine hydrothermal conditions because they have a (geologically supplied) source of chemical disequilibrium which brings in redox reactions.[80] Further, he states that life originated at warmer temperatures. This was also supported by simple experiments on organic synthesis under hydrothermal conditions. These higher temperatures would mix various elements and supply the energy for the formation of simple compounds. Abundant mineral deposits at hydrothermal ecosystems imply that they provide a fossil record of their biological inheritance. Often the minerals deposited are precious metals such as gold, silver, copper, and zinc. These are common outpourings from hydrothermal vents. Thermal waters usually contain high concentrations of dissolved components which are deposited when the hot spring discharge gases are released and the temperatures fall, leading to the deposition of mostly calcium carbonate, silica, iron and manganese

oxides. Thus, any living organisms that once existed in the vents become fossilized at the very site it lived in. All these theories proposed that the life existed some 3.5 billion years ago.

The spectacular nature of the submarine hydrothermal ecosystem with features such as *black smokers*, *white smokers*, and peculiar ecosystems that are independent of sunlight as a source of reducing power, has focused much interest on hydrothermal processes for the explanation of an array of geochemical processes and phenomena.[81] The submarine hydrothermal systems reveal that most primitive organisms found in modern environments are thermophiles (for example, *archea*). Many scientists believe in a "redox neutral" in the primitive atmosphere. The most important aspect is the possibility that the iron vapor and reduced carbon liberated from impacting objects like meteorites would leave the ocean reducing for a long period. In addition, those submarine hydrothermal systems are the only environments where primitive life would have been protected against postulated meteoritic impacts and partial vaporization of the ocean. The presence of supercritical fluids like H_2O, CO_2, or CH_4, are the main constituents of any hydrothermal system. They serve as excellent solvents of organic compounds and would probably be of great potential for several of the chemical reactions eventually leading to the origin of life. Further, the pressure and temperature gradients existing in natural hydrothermal systems have a dramatic effect on the properties of the hydrothermal fluids. This is known from the current experimental data on many electrolytic solutions and some nonaqueous solutions.[82]

DropBooks

The submarine hydrothermal systems operate today in much the same manner as they are believed to have functioned in the pre-Cambrian period. They provide a wide range of closely linked gradients in both physical and chemical conditions obviously having a direct link with magmatic heat. Thus, the biological communities (biotic family) occupying vast and relatively stable soft bottom habitats of the sea are characterized by low population densities, high species diversity, and low biomass, compared to those inhabiting the unstable conditions of submarine hydrothermal ecosystems which exhibit high densities and biomass, low species diversity, rapid growth rates and high metabolic rates.

Despite such an understanding of the hydrothermal ecosystem, there are many unclear aspects like period of formation and depth. As mentioned earlier, the available evidences indicate that the ancient

ocean was a chemically reducing environment, probably warm or hot (> 30°C to > 100°C),[83] shallow (maximum depth of 1000–2000 m), and considerably more active, tectonically and hydrothermally, than it is today.[84] The model proposed by Abbott and Hoffman (1984) suggests that, at the time of formation of the ocean (4.2 Ga.), it is likely that the whole earth was covered with water and that hydrothermal activity was at least five times greater than at present.[85] The overall rate of sea floor spreading and subduction has declined steadily over the evolution of the earth. Figure 1.2 shows the geological and geochemical features of hydrothermal circulation of seawater through the oceanic crust at mid-ocean ridges.[86] Rona et al. (1983) have found two types of vents occurring along spreading ridge crests of the East Pacific Rise and Juan de Fuca Ridge in the Pacific.[87] The fluids emanating from these vents are enriched with magmatically derived elements and complexes. Depending upon the degree of mixing, we can expect a variety of chemical components in different quantities which serve as the primary energy sources for the extensive microbial communities as represented in Figs. 1.3 and 1.4. All the biologically important trace elements are also known to be associated with submarine hydrothermal vents. However, the actual reactions involved in the production of various chemical components are not clearly known. It is well known that both H_2 and CO are common gases associated with volcanic activity. The major source of H_2 is believed to be the oxidation of magnetite to hematite, while CO is believed to originate within the magma from C-O-H-S equilibrium.[88] Similarly, the concentration of CH_4 and helium gases has been discussed in the submarine hydrothermal vents. Oxygen and other electron acceptors (NO^{3-}, SO_4^{2-} and PO_4^{3-}) and a variety of many unknown chemical components have allowed for the abundant growth of a diverse microorganisms in the modern oceans.

In order to prove the above theories and discoveries, several workers have proposed the thermodynamics of strecker synthesis in hydrothermal systems and also the hydrothermal synthesis of several amino acids under laboratory conditions. Schulte and Shock (1995) and Shock (1995) have worked out the strecker synthesis to produce biomolecules (amino and hydroxy acids) from starting compounds (ketones, aldehydes, HCN and ammonia).[88][89] They have evaluated their work quantitatively using thermodynamic data and parameters for the revised Helgeson-Kirkham-Flowers (HKF) equation of state. Although there is an overwhelming thermodynamic drive to form biomolecules through streckers

synthesis under hydrothermal conditions, the availability and concentration of starting components limit the efficiency and productivity of strecker reactions. Some representative reactions for strecker synthesis are given below:[89]

$$\underset{\text{aldehyde / ketone}}{RCHO} + NH_3 + HCN = \underset{\text{amino nitrile}}{RCH(NH_2)CN} + H_2O$$

$$\underset{\text{amino nitrile}}{RCH\,(NH_2)CN} + H_2O = \underset{\text{amino amide}}{RCH(NH_2)CO(NH_2)}$$

$$\underset{\text{aldehyde/ketone}}{RCHO} + HCN + H_2O = \underset{\text{amino acid}}{RCH(NH_2)COOH}$$

There are several reports on the laboratory hydrothermal synthesis of amino acids to justify the origin of life on the earth. It is appropriate to mention that the organic synthesis on the whole is not new and, in fact, it began in the previous century. However, the organic synthesis under hydrothermal conditions with reference to the origin of life began in a systematic way only during 1980s, after the discovery of hydrothermal activity in the deep sea on a Galapagos spreading rich in thermophile organisms (Fig. 1.5 a and b) during 1977. The reader can get additional information from the works of Fox and Windsor (1970); Marshall (1987); Shock (1990, 1992); Hennet et al. (1992).[90]-[94] These workers have synthesized amino acids in a temperature range of 150°C to 275°C from aqueous solutions containing KCN, NH_3, HCHO, CO_2, H_2, O_2, NaCN, NH_4HCO_3. Miller (1953)[95] and Amend and Shock (1988) in Ref. 97 have shown that the autotrophic synthesis of all twenty protein-forming amino acids was energetically favored in hot (100°C), moderately reduced, submarine hydrothermal solutions relative to the synthesis in cold (18°C), oxidized, surface sea water.[95] Although the above studies do not support the challenge raised by several others over the life in submarine hydrothermal ecosystems, these studies definitely have set a new trend in hydrothermal research.

This field of research is growing very fast and a large number of publications are coming on diversified aspects of submarine hydrothermal ecosystems. The reader can refer to some of the most important reviews for further studies.[95]-[97]

PrintBooks

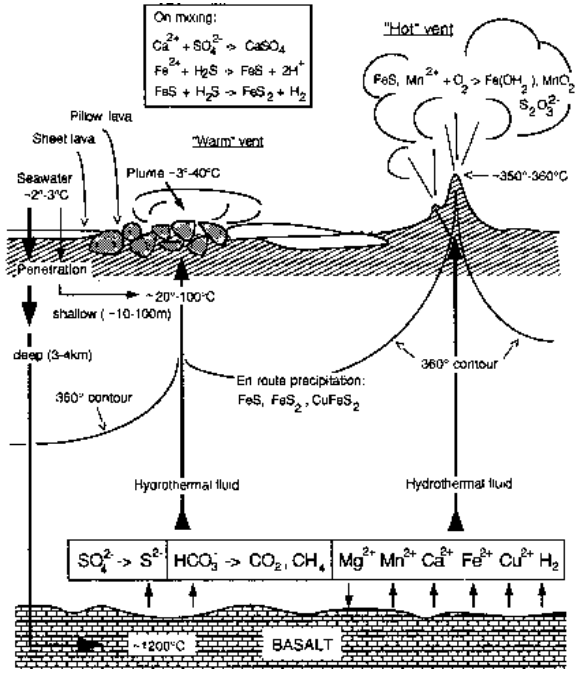

Figure 1.2. Major processes during the hydrothermal circulation of seawater through the oceanic crust at mid-ocean ridges. *(Courtesy H. W. Jannasch)*

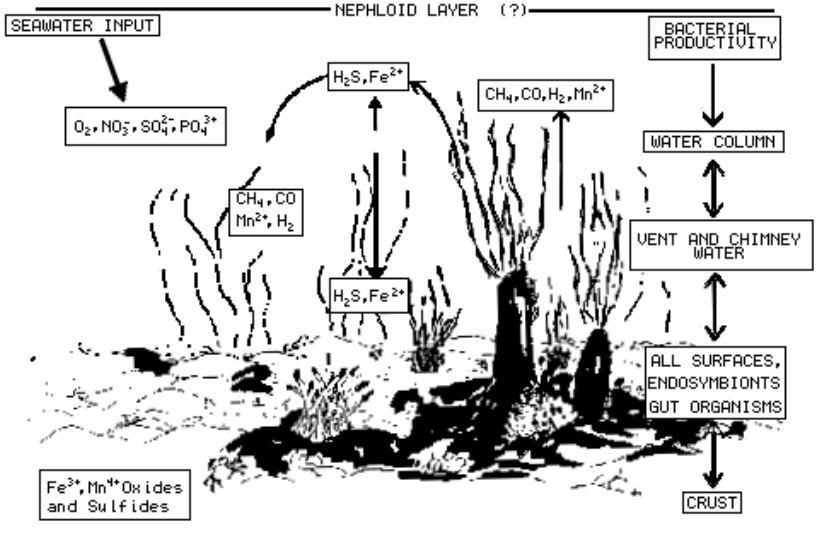

Figure 1.3. Microbial community.[81]

Plate 1. The Pompei worm *Alvinella* at 9°N on the East Pacific Rise. The densely-packed tubes form the wall of a chimney. One worm has emerged: to the upper right, the tips of the tentacles of several others can be seen at the tube openings.

Plate 2. A dead vent field on the Galapagos Rise near Rose Garden. Partially dissolved shells of vesicomyid clams fill the extinguished vent opening. But there are a few survivors - mussels filter-feeding for ambient suspended particles.

Plate 3. Barnacles encrust the edge of a vent opening at the Mariana back-arc spreading center. Alvinoconchid snails live in the openings where temperatures were measured at 10-25°C. Bresiliid shrimp and bythograeid crabs scavenge off the surfaces of rock and other animals. The cloudiness of the water is caused by suspended bacteria.

Plate 4. The tip of a chimney at the Mariana vent emitting 250°C effluent. Animals avoid this hot spot, but are able to live only a few centimeters below it, where the temperature is only 25°C. Alvinoconchid snails, bresiliid shrimp, bythogracid crabs and limpets can be seen.

DropBooks

Figure 1.4. Microbial community. Photos are reproduced from Ref. 97.

Plate 1. The Rose Garden vent on the Galapagos Rise in 1979. Vestimentiferan tube-worms and mussels dominate. Bresiliid shrimp and archacogastropod limpets walk on them.

Plate 2. Bresiliid shrimp at a Mid-Atlantic Ridge vent.

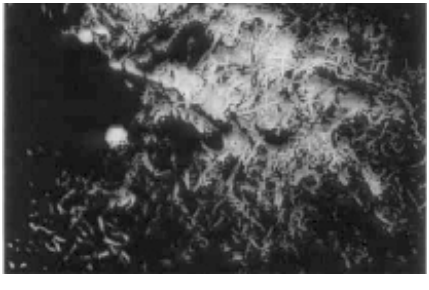

Plate 3. Serpulid polychacies and a dandelion in the near-field at the Rose Garden. Most of the serpulids are retracted into their tubes, but the tentacles of several are spread for capturing food particles from the water.

Plate 4. Spaghetti worms cover pillow lava at the periphery of Rose Garden.

(a)

Figure 1.5. Hydrothermal activity in the deep sea (a, b). Plates are reproduced from Ref. 97.

Plate 5. The huge thicket of vestimentiferan tube-worms at the main vent fissure at Rose Garden in December, 1979. Mussels live among the worms, principally at the base of the tubes.

Plate 6. The population of vestimentiferans has been drastically reduced, and mussels have proliferated to form a great pile over the fissure opening.

Plate 7. The rift valley on the East Pacific Rise at 9°N in April 1991. A recent lava flow has blanketed the valley. Wide-scale venting has encouraged bacterial growth, but there are not yet any animals grazing on the mats.

Plate 8. The same general area in December, 1993, a little over two and a half years later, showing vigorous colonization by vestimentiferans. The bacterial mats have disappeared.

DropBooks

(b)

Figure 1.5. *(Cont'd.)*

1.7 HYDROTHERMAL CRYSTAL GROWTH AND MATERIALS PROCESSING

After the successful application of the hydrothermal technique in hydrometallurgy in the previous century, the other important application of this method began with the artificial production of bulk single crystals of quartz and also with the synthesis of zeolites during late 1930s and 1940s. The hydrothermal method of crystal growth has several advantages. It is very important for its technological efficiency in developing bigger, purer, and dislocation-free single crystals. The method has been widely accepted since 1960s and practically all inorganic species, starting from native elements to the most complex oxides, silicates, germanates, phosphates, chalcogenides, carbonates, and so on, have been obtained by this method. The technique is being employed on a large scale to prepare piezoelectric, magnetic, optic, ceramic and a host of other materials both as single crystals and polycrystalline materials. In the recent years, several new advantages of the hydrothermal technique have been described by many workers and they are discussed in Chs. 5 to 10 in great detail. The hydrothermal technique, in contrast to other conventional techniques, offers several advantages:

i. Compounds with elements in oxidation states that are difficult to obtain, especially important for transitional metal compounds, can be obtained in a closed system by the hydrothermal method [e.g., ferromagnetic chromium (IV) oxide].

ii. The hydrothermal method is also useful for the so-called low temperature phases, e.g., α-quartz, α-berlinite, and others.

iii. For the synthesis of metastable compounds, such as subiodides of tellurium, Te_2I, the hydrothermal method is unique.

Commercial production of quartz and zeolites began during 1940s, but it was during 1940s and 1950s that the study of hydrothermal phase equilibria became quite popular owing to the appearance of new designs in autoclaves, particularly the Tuttle cold-cone sealed autoclaves which became popular as test tube type autoclaves.[98] The main advantage of the phase equilibria studies under hydrothermal conditions is that it is a closed system; one can study the influence of temperature, pressure

and compositional variations individually. These studies helped to understand the phase formations in many inorganic systems, which had direct bearings on the natural systems as well. They also helped in the crystallization of several new phases which do not have the natural analogues. Moreover, these studies laid a firm foundation for the growth of some most complex inorganic single crystals which did not have analogues in nature. During 1960s, there was a question about the search and growth of hitherto unknown compounds of photo-semiconductors, ferromagnets, lasers, piezo- and ferrielectrics, so the hydrothermal method gained greater attention. This also led to the studies concerning the solubility, solvent-solute interaction, kinetics, and thermodynamic aspects of crystal growth. A large number of groups appeared in Europe, Asia and North America, and also the number of crystals obtained by hydrothermal method increased exponentially. Further, the studies concerning the phase equilibria paved a way for the emergence of a new technology, viz., *ceramics processing technology*.[99]

From mid-1970s, exploration of the advantages of hydrothermal reactions other than the hydrometallurgical and crystal growth aspects began in Japan, particularly with reference to the ceramic powder processing. A team of researchers from the Tokyo Institute of Technology, Japan, did pioneering work in ceramic processing such as powder preparation, reaction sintering, hot isostatic processing, and so on. The powder prepared by the hydrothermal technique is not agglomerated, but is fine-grained, highly pure, with controlled morphology, has a narrow size distribution, and consists of single crystals. The technique has several advantages like high reaction rate of powders, good dispersion in liquid, almost pollution free, does not require very expensive and highly sophisticated equipment, energy saving processing, and many times it produces new phases. These aspects are discussed in the subsequent chapters of this book.

PrepBooks

In the last decade, the hydrothermal technique has offered several new advantages like new homogeneous precipitation using metal chelates under hydrothermal conditions, decomposition of hazardous and/or refractory chemical substances, monomerization of high polymers like polyethylene terephthalate, and a host of other environmental engineering and chemical engineering issues dealing with recycling of rubbers and plastics instead of burning, and so on. The solvation properties of supercritical solvents are being extensively used for detoxifying organic and pharmaceutical wastes and also for replacing toxic solvents commonly

used for chemical synthesis. Similarly, it is used to remove caffeine and other food-related compounds selectively. In fact, a new term, *hydrothermal cooking,* is being used by the food and nutrition experts in recent years.[100] These unique properties take the hydrothermal technique altogether in a new direction towards the 21st century and one can forecast a slow emergence of a new branch of science and technology for sustained human development. An understanding of the structure, dynamics and reactivity of water and other aqueous electrolyte solutions with the advancement in instrumentation like neutron diffraction, x-ray, Raman and NMR spectroscopic approaches, have greatly contributed to the emergence of this new branch of science and technology employing hydrothermal techniques. As is well known, water is environmentally the safest material and the cheapest of all solvents. It can act as a mineralizer or a catalyst under elevated pressure-temperature conditions. The thermodynamic and transport properties of supercritical water are remarkably different from those of ambient water. The solubility of nonpolar species increases, whereas that of ionic and polar compounds decrease. As a result of the drop of the polarity of water, the molecular mobility increases due to a decrease in the solvent viscosity (η). Drastic changes of ionic hydration are brought about by the decrease in the dielectric constant (ε) and density (ρ). Table 1.4 gives the values of dielectric constant, density and viscosity of water varying with temperature and pressure in comparison with the ambient values of 78.3, 0.997 g cm^{-3}, and 0.890 mPa, respectively.[101] The temperature dependence of the saturation vapor pressure is illustrated up to the critical point in Fig. 1.6.[101] Below 150–200°C, the saturation vapor pressure is relatively low. Above this temperature, however, the vapor pressure rises rather sharply. Such anamolous properties of water with pressure-temperature variations are associated with the hydrogen bonding, which has attracted the attention of solution chemists. Thus recent advances in hydrothermal solution chemistry have paved a new path to materials processing techniques with minimum energy consumption in comparison with larger energy consumption to create melt, vapor, gas or plasma. Figure 1.7 shows free energy vs. temperature diagram in a single component system. Similarly, Fig. 1.8 shows the pressure-temperature range for material preparation or processing. A portion of the hydrothermal field falls within the biocompatability range, which can be further supported with the recent findings in the field of submarine hydrothermal or biohydrothermal research.

Table 1.4. Values of ε_r, ρ (g cm^{-3}), and η (mPa s) of Water at High Temperatures and High Pressures*

p/MPa	Parameter	t/°C					
		200	250	300	350	400	450
10	ε_r	35.1	27.4	20.4	1.2	1.2	1.1
	ρ	0.871	0.806	0.715	0.045	0.038	0.034
	η	0.136	0.108	0.087	0.022	0.025	0.027
20	ε_r	35.3	28.0	21.2	14.1	1.6	1.4
	ρ	0.878	0.816	0.733	0.600	0.101	0.079
	η	0.139	0.110	0.091	0.070	0.026	0.028
30	ε_r	35.9	28.4	22.0	15.7	5.9	2.1
	ρ	0.885	0.826	0.751	0.646	0.357	0.148
	η	0.141	0.113	0.094	0.076	0.044	0.031
40	ε_r	36.3	28.9	22.6	16.7	10.5	3.8
	ρ	0.891	0.835	0.765	0.672	0.523	0.271
	η	0.114	0.115	0.097	0.080	0.062	0.039
50	ε_r	36.6	29.3	23.1	17.6	12.2	6.6
	ρ	0.897	0.843	0.777	0.693	0.278	0.402
	η	0.146	0.118	0.099	0.083	0.068	0.051
60	ε_r	37.0	29.7	23.6	18.2	13.3	8.5
	ρ	0.903	0.850	0.788	0.711	0.612	0.480
	η	0.148	0.120	0.101	0.086	0.073	0.059
70	ε_r	37.3	30.0	24.0	18.8	14.2	9.9
	ρ	0.909	0.857	0.798	0.726	0.638	0.528
	η	0.150	0.122	0.104	0.089	0.077	0.065

* Cited from IAPWS Release on the Values of Temperature, Pressure and Density of Ordinary and Heavy Water Substances at their Respective Critical Points, 1992.

DropBooks

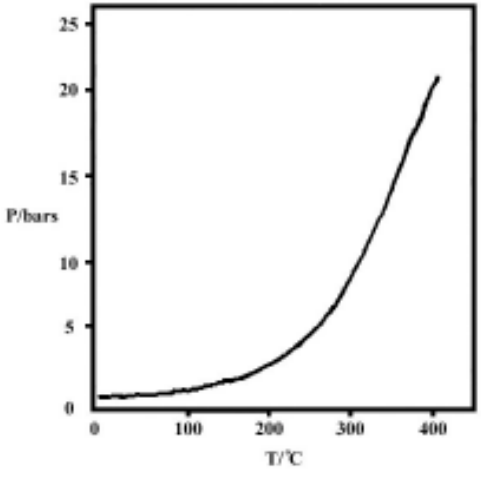

Figure 1.6. Temperature dependence of saturation vapor pressure.

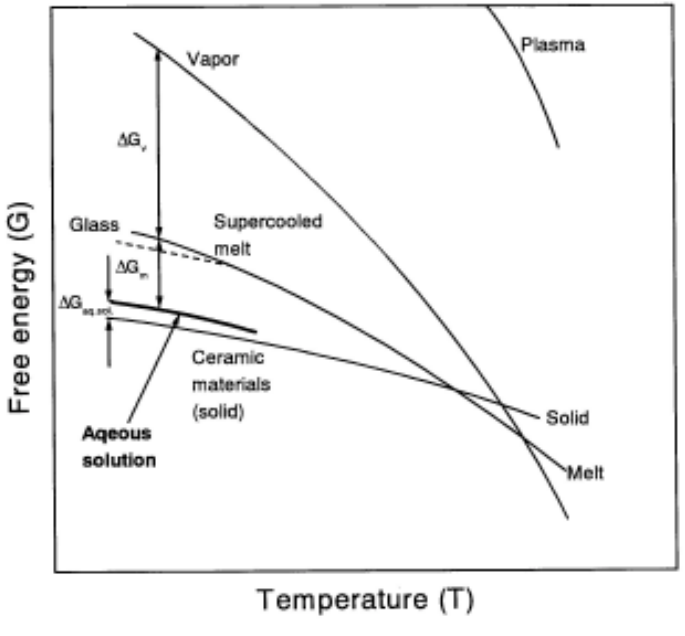

Figure 1.7. Schematic energy diagram (G-T) in a single component system.

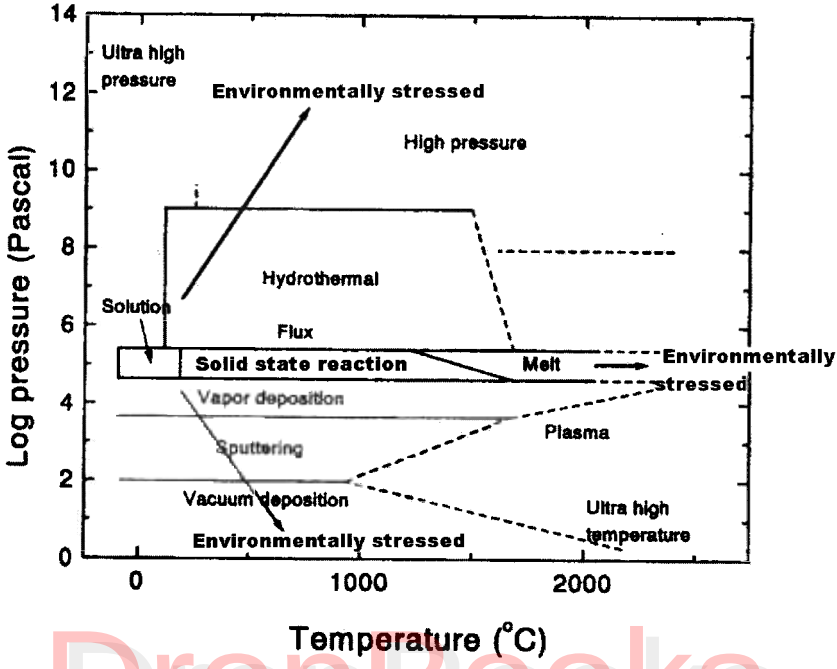

DropBooks

Figure 1.8. Pressure-temperature range for material preparation.

1.8 STATISTICS OF PUBLICATIONS AND RESEARCH IN HYDROTHERMAL TECHNOLOGY

The statistical data on the hydrothermal research give a picture about its developments. Throughout the course of its evolution from geoscientists to modern technologists, the hydrothermal technique has captured the attention of scientists and technologists from different branches of science. Today it is a highly interdisciplinary subject and the technique is popularly used by geologists, biologists, physicists, chemists, ceramists, hydrometallurgists, materials scientists, engineers and so on. Figure 1.9 shows various branches of science either emerging out from the hydrothermal technique or closely linked up with the hydrothermal technique. One could firmly say that this family tree will keep expanding its branches and the roots in the years to come.

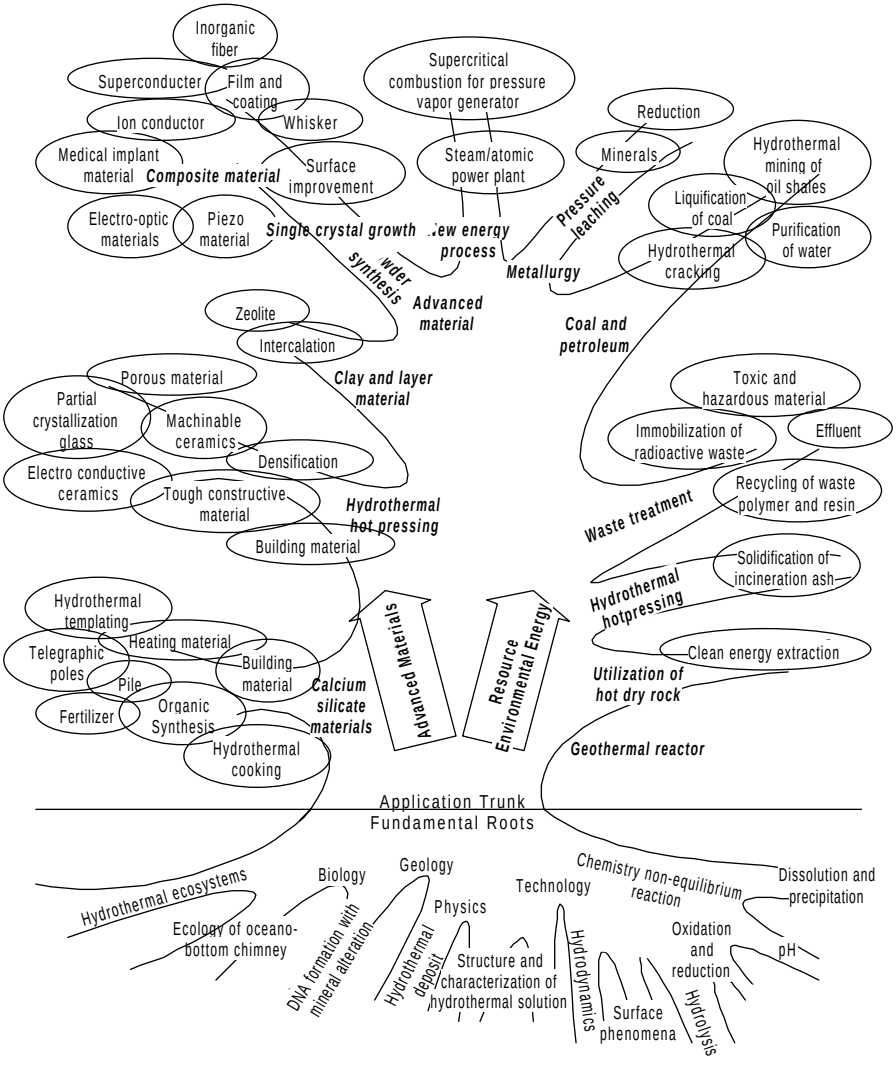

Figure 1.9. Tree showing the interdisciplinary natureof hydrothermal technology. *(Figure courtesy of N. Yamasaki, modified by K. Byrappa.)*

In view of such a rapid growth of the hydrothermal technique, it is becoming imperative to have a highly specialized book on this topic. There are thousands of articles published on various aspects of hydrothermal research. In the initial days of the hydrothermal research, there was a dearth of diversified journals, thus much of the hydrothermal research data from the 19th century to the beginning of the second half of this century was published in essentially *Earth Science Journals*, *Chemistry Annals*, and *Bulletins*. Since then, success in the growth of large single crystals of quartz and, subsequently, a large number of other minerals and inorganic compounds, as well as the progress achieved in the instrument side in attaining higher pressure and temperature conditions, led to the slow diversity of the field. Today a large quantum of work on hydrothermal research is being published in more than one hundred journals, and the number is still growing. Owing to the limitation of space and with an intention to focus on the main theme of the book, we give below only the important journals which publish the work on hydrothermal research:

Journal of Crystal Growth
Journal of Materials Research
Journal of Materials Science
Journal of Materials Science Letters
Materials Research Bulletin
Materials Physics and Chemistry
Advanced Materials
Materials Science Forum
Materials Letters
Journal of Solid State Chemistry
European Journal of Solid State and Inorganic Chemistry
Progress in Crystal Growth and Characterization of Materials
Crystal Research and Technology
Crystallography (Russian Journal)
Izvestia Academy Nauk Inorganic Materials (Russian)
Solid State Communication
Doklady Academy Nauk (Russian)
Journal of American Ceramic Society
Chemistry of Materials

DropBooks

Journal of Applied Physics
Physics and Chemistry of Earth
Journal of American Chemical Society
American Mineralogist
Canadian Mineralogist
Geochimica Cosmochimica Acta
Zeolites
Journal of Ceramic Society of Japan
Bio-materials
Japanese Journal of Applied Physics
Ceramics Transactions
Materials Science and Engineering
Materials Science Research
Materials Technology
Journal of Microporous Materials

Although there are thousands of research publications on hydrothermal research, so far, the most comprehensive works are limited to the scale of only reviews and edited books and there is not even a single monograph available. In connection with the hydrothermal technique for crystal growth and materials processing, the books and reviews listed in Table 1.1 are very useful.

We have made a very sincere effort to collect a more-or-less complete list of publications related to the field of hydrothermal technology, especially with a higher reliability in the last decade. Therefore, it is interesting to discuss briefly the statistics of this field of research. Figure 1.10 shows the number of publications year-wise and this number is increasing sharply with the entry of scientists from other branches of science. As evident from Fig. 1.11, the preparative chemists and ceramists have dominated this field, particularly with the recent advances in the advanced materials and electronic ceramics. It is interesting to note that the hydrothermal technique of material synthesis, although began in the previous century, has gained its momentum during the postwar period. Prior to that, majority of the compounds synthesized under hydrothermal conditions were essentially the natural analogues, as the main thrust was on the study of the origin of rocks, minerals and ores through laboratory simulations.

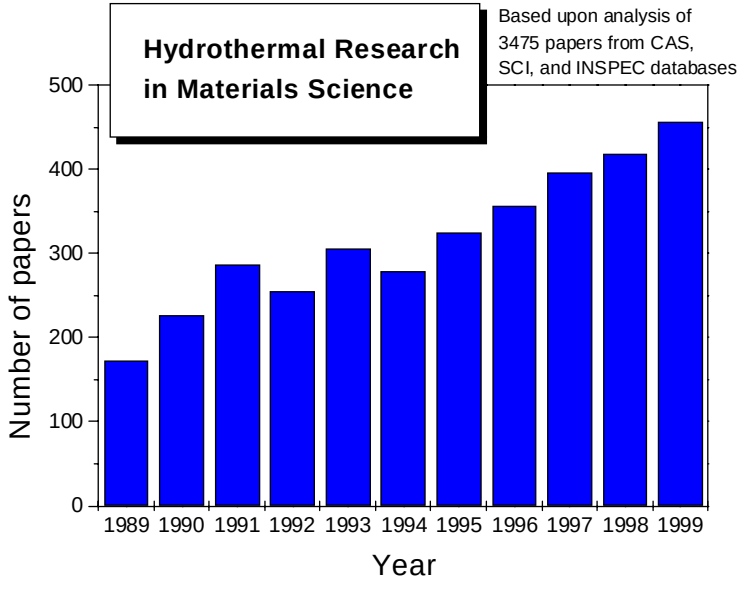

Figure 1.10. Number of publications year-wise.

DropBooks

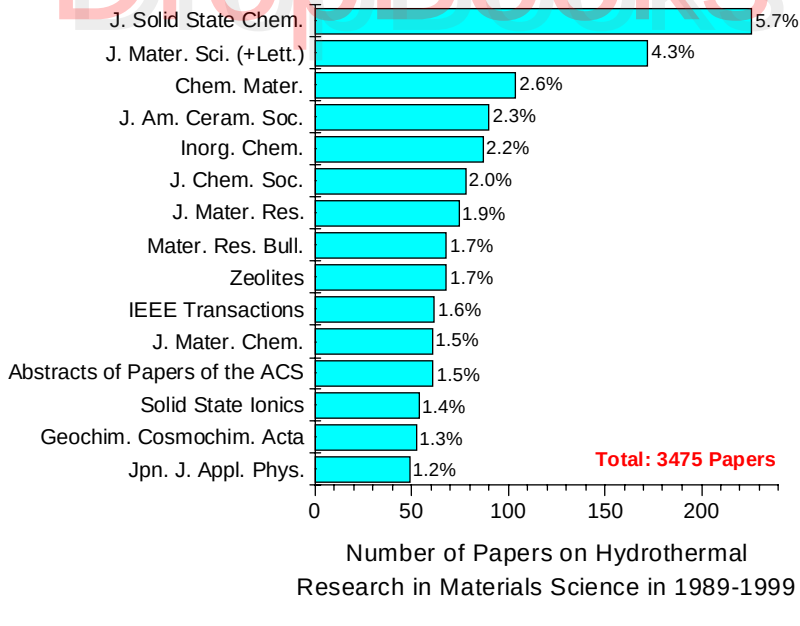

Figure 1.11. Number of papers on hydrothermal research in materials.

With the availability of the improved equipment and also with the knowledge on the preparative chemistry routes to synthesize many inorganic compounds, with or without natural analogues under hydrothermal conditions, the popularity of the technique grew fast. Today, the number of compounds without any natural analogue synthesized under hydrothermal conditions is more than the number of compounds with natural analogues synthesized. With the advent of new mineralizers, a wide variety of organic and inorganic compounds hitherto unknown are being prepared by hydrothermal technique. The technique is being popularly used for crystallization of materials, crystal growth, materials processing, thin film preparation, and so on. As evident from the synthesis of silicates, phosphates and oxides followed by the ceramics are very popular materials being obtained under hydrothermal conditions. The popularity of this field is probably connected with the better understanding of the hydrothermal solution chemistry and the effective use of several new mineralizers which have virtually changed the scenario, particularly with reference to the pressure and temperature conditions of synthesis of materials which were obtained under very high pressure and temperature conditions. For instance, rare earth tungstates, rare earth silicates and so on are being obtained under mild hydrothermal conditions.[102]

Hydrothermal research had its origin in Europe, and later spread its activity to North America during the early 20th century. The hydrothermal research in Asia began in the 1920s in Japan. Today, Japan has emerged as a leader in this field of research on par with the USA. However, the hydrothermal research is becoming quite popular in several other countries, particularly in the last three decades. The countries engaged in hydrothermal research are listed below in alphabetical order: Australia, Belgium, Brazil, Bulgaria, Chile, China, Canada, Denmark, France, Germany, Holland, Italy, India, Japan, Korea, Norway, Poland, Russia, Switzerland, Spain, Sweden, Taiwan, UK, Ukraine, USA. Amongst these countries over 75% of the hydrothermal research is going on in Japan and USA. Figure 1.12 shows the countries actively engaged in hydrothermal research.

The above statistical data on hydrothermal research clearly illustrate a growing popularity of the technique, covering various branches of science. The main disadvantage of the hydrothermal system, as believed earlier, is the black-box nature of the hydrothermal autoclave, because one can not make any direct observation of the crystallization processes. Though several attempts were made to observe the crystallization

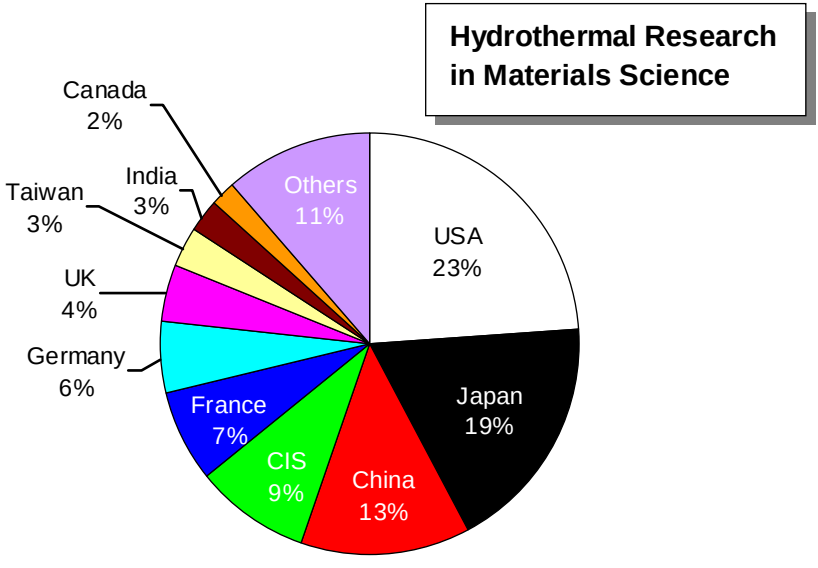

Figure 1.12. Number of papers on hydrothermal research in materials.

DropBooks

processes through special ruby windows for these autoclaves, not much success has been achieved because of the high pressure and temperature of the system. However, in recent years, remarkable progress was made in this area through the entry of physical chemists and the modeling of the hydrothermal reactions, and the study of kinetics of the hydrothermal processes have contributed greatly to understand the hydrothermal technique. One can now understand the hydrothermal chemistry of the solutions more or less precisely, which provides a solid base for hydrothermal synthesis and processing at much lower pressure and temperature conditions.[29][103] These developments are slowly removing the concept of the black box for the hydrothermal system, and one can make use of thick-walled silica autoclaves to carry out hydrothermal experiments up to a temperature of 300°C and pressure up to several hundreds of bars, to facilitate direct observation of the hydrothermal processes taking place in a given system. Already some groups in Russia, Japan and USA have begun work in this direction and numerous publications have appeared. These developments have given the hydrothermal technique an edge over other techniques for the preparation of pure materials as it is a closed system providing a more controlled diffusion. Besides, the role of pressure

together with temperature helps enhanced molecular arrangements including those of organic molecules as supported by the synthesis of organic amino acids and other life forming complexes, and also the natural submarine hydrothermal ecosystems. Thus the hydrothermal technique exhibits a great degree of flexibility or adaptability which is being rightly exploited by a large scientific community with diversified interests.

1.9 HYDROTHERMAL MATERIALS PROCESSING

Hydrothermal materials processing is becoming a popular field of research, particularly after the successful development of ceramic processing technology during 1970s. Further there is a growing interest to enhance the hydrothermal reaction kinetics using microwave, acousto-wave simulations, mechanical mixing, and electrochemical reactions. These processes have made the hydrothermal technique more attractive to ceramists and preparative chemists because of the enhanced kinetics. The duration of the experiments is reduced by two orders of magnitude, at least, which makes the technique more economic. The microwave hydrothermal technique is especially handy for the synthesis of PZT and other oxide ceramics. Added to this, the crystal size, morphology and level of agglomeration of the different ceramic oxides can be controlled through careful selection of ratio of starting materials, pH, time, and temperature. Submicron size powders of TiO_2, ZrO_2, Fe_2O_3, $KNbO_3$, $BaTiO_3$, $PbTiO_3$ and their solid solutions have been prepared by this way. This has made the technique a more valuable one in the low temperature production of fine ceramic powders, clays, and zeolites.[17][104][105]

Similarly, ultrasonic energy, sonochemical simulation is used to prepare novel materials and accelerate the chemical reactions. In this way, hydrothermal reactions can be carried out at very rapid rates, and several new phases and high temperature phases can be obtained in minutes.

Hydrothermal epitaxy began during 1970s in connection with the development of magneto-optic and magnetic bubble domain devices, especially thin and highly crystallized magnetic films of yttrium iron garnets and their solid solutions on gadolinium gallium garnet substrates.[106][107] It did not capture the attention of specialists owing to the higher experimental pressure and temperature conditions involved ($T > 500°C$, $P > 1$ kb). However, in the last five years, the work in this direction has been revived. With the use of electrochemical reactions

under hydrothermal conditions, it has become possible to grow highly pure and dislocation free crystalline thin films of various perovskite type oxides like $BaTiO_3$, $SrTiO_3$, $CaTiO_3$, and so on, under much lower pressure (< 100 bars) and temperature (100–200°C) conditions over a variety of substrates.[108]-[110] The method offers a high success rate and there are efforts to obtain functionally gradient materials through hydrothermal electrochemistry. With an increase in the demand for the composites, the hydrothermal technique offers an excellent facility for coating of various compounds on metals, and ceramics. For example, the coating of HAp or bone like apatite layers on chemically treated Ti metals, organic polymers and other metals has emerged out as a promising field.[111]-[113] This is discussed in detail in Ch. 10.

The hydrothermal technique has become very useful for the production of whiskers, which are finding extensive applications in modern technology. For example, whiskers of HAp are being produced under mild hydrothermal conditions. Although, the crystal growth of whiskers with controlled morphology is not a new field, it was already on the verge of extinction during the last decade. A few years ago, some reports on the growth of whiskers which are biocompatible under mild hydrothermal conditions appeared, giving a fresh lease on life to this field of research concerning whiskers crystal growth.[114][115] Amongst the popular whiskers crystal growth, the most popular one is the biocompatible HApwhiskers of nanometer size and this can be prepared at temperatures < 200°C, and pressure < 2 MPa within a few hours. Whiskers prepared by the hydrothermal method have a more controlled and better morphology, uniformity in size and purity in composition compared to the HAp whiskers produced by other methods. The whiskers obtained by other methods usually contained contaminants like carbonates, heterogeneity in shape and size. The hydrothermally prepared whiskers are finding promising applications mostly as reinforcements in composites, and thermal insulation. They are highly biocompatible, as they contain nontoxic species, such as Ca, P, OH^-, and are noncarcinogenic, chemically inert both outside and inside the living bodies. This is discussed in greater detail in Ch. 10.

The hydrothermal hot-pressing technique is becoming a very simple and most effective processing technique for the preparation of solid bodies from inorganic powders under mild hydrothermal conditions.[116][117] This technique is especially useful for the solidification of thermally decomposable powders such as carbonates, sulphates and nitrates at high temperatures. The solidification process is thought to be similar to liquid-phase sintering under pressure. In this technique, the starting powder containing water is continuously compressed from the

PrepBooks

outside of an autoclave under hydrothermal conditions. The powder is then treated at autogeneous pressure, while it is compressed at much higher pressure than the vapor pressure inside the autoclave. The water still remaining in the compacts after the hydrothermal hot pressing can be easily drained out by drying in air. By this means, porous ceramics can be easily prepared. This technique becomes handy for the solidification of radioactive wastes[119] and sludge ashes.[120]

Corrosion is a major problem in industries and power stations. Corrosion afflicts all metals, alloys and even advanced ceramics. The commonly observed problems of corrosion include exfoliation, stress-corrosion cracking, intergranular corrosion, and dealloying. From the perspective of engineering, the prediction, monitoring, and mitigating the corrosion problem is highly cumbersome. Once the attack is initiated, it makes localized corrosion a major problem in industries, power plants and reactors. In this respect, the supercritical solvents oxidation, particularly of water can be of great help to solve many of the problems associated with corrosion and erosion. In these systems, the toxic and corrosive ions are treated and made to form a solid crystalline coating of the metal surfaces as oxides or as oxychlorides. Several aqueous and nonaqueous solvents have been tried on a variety of metals, alloys, and ceramics, which greatly contribute toward solving the major industrial corrosion problem. The reader can get additional information from the works in Refs. 121–127.

Hydrothermal processing has become a most powerful tool, in the last decade, to transform various inorganic compounds and also to treat the raw materials for technological applications. The hydrothermally treated raw materials become very highly reactive as a function of solvent used in the preparation of advanced materials. One can find an extensive literature data available on this topic covering a wide range of oxides and hydroxides, carbosils, and so on. Similarly, the hydrothermal transformation, for example, montmorillonite and other variety of clays into the most useful zeolites with larger pore volumes, is a subject of great interest, because of its efficiency and economy.[105] In the last couple of years, the hydrothermal technique has been widely employed for metal intercalated nanocomposites preparation. Several variety of clay minerals which have two-dimensional layer structures[128] like montmorillonite, beidellite, hectorite, saponite, nontronite, etc., are attractive materials, because of their properties like cation exchange and swelling-shrinking in the interlayers. They readily produce pillared clays upon hydrothermal treat-

ment. The preparation of pillared clays involves essentially the cation exchange with hydroxy polymeric cations followed by dehydration and dehydroxylation of the polymeric species to prop the layers apart with ceramic oxide pillars in the interlayers.[129] These pillared layers are successfully intercalated with transitional metals. Likewise, the hydrothermal technique is very useful for stabilizing the metastable phases. Also, for example, the water rich natural phyllosilicates, which have lower thermal stability can be made more stable chemically and thermally through replacement of $(OH)^-$ groups by oxygen atoms.[130] By these means, several phyllosiloxides have been prepared by many workers.[131]

All the above information on hydrothermal technology provides enough support for the growing popularity of this technique for materials synthesis, crystal growth, and materials processing.

The scope of this book has been restricted to recent developments under each one of the applications described above with the exception of the natural hydrothermal systems which are not within the perview of the present handbook. Although we have given the historical aspects of the technique in Ch. 2, the emphasis has been focused mainly on the crystal growth and materials processing through the ages.

DropBooks

This chapter clearly reveals the fact that the hydrothermal technique is drawing the attention of scientists from different branches of natural science. The future of this technique lies in this kind of multidisciplinary approach. More and more new findings and applications in this field are not only contributing to the scientific knowledge of the hydrothermal technique, but are also posing new problems. The role of organics in hydrothermal systems for example, has to be studied more seriously, which would definitely twist the geological thinking to a greater extent. It is well known that the organics in hydrothermal systems not only lead to the formation of new phases or new structures, and stability of metastable phases, but can also bring down the pressure and temperature conditions of crystallization. In nature, we can expect a very wide range of chemical components including hydrocarbons, which greatly contribute to the crystallization of rocks, minerals, and ore deposits. The role of these organics in the earth's crust has not been understood properly by geoscientists in the context of thermodynamics, and kinetics of crystallization. It is expected that such studies will definitely propose much lower temperature and pressure conditions of crystallization for various rock bodies, and add many more new questions to experimental petrology.

Thus, the future of hydrothermal research (both crystal growth and materials processing) is not towards higher pressure and temperature conditions, but definitely towards the lowering of the pressure and temperature conditions, which will facilitate *in situ* observation. This will also provide new stimuli for the fabrication of simpler (may be even silica and composites based) and larger autoclaves. As the design and fabrication of the autoclaves becomes simpler and easier, the cost will automatically go down, thereby making them more attractive to specialists. In the last fifteen years, as we see from the statistics discussed earlier in this chapter, more new applications for hydrothermal technique are being reported continuously. It is predicted that it will merge with soft solution chemistry and soft solution processing by being more compatible with biosphere. It will come out as an important tool for the development of advanced materials with limited resources and energy consumption. These materials are less hazardous to living species, also environmentally friendly without firing or sintering at ultrahigh temperatures, or melting or plasma or vaporizing. Because the energy consumed in attaining the melt or vapor or plasma conditions is very high, it proves to be environmentally unfriendly. Hence, the future of hydrothermal technology lies in promoting the lower pressure and temperature conditions for crystal growth and materials processing. We have made an attempt to expose the reader to the above mentioned aspects of hydrothermal growth and materials processing in the forthcoming chapters.

REFERENCES

1. Sir Roderick Murchison (1840s), (cited by S. Somiya)
2. Schafthaul, K. F. E., *Gelehrte Anzeigen Bayer. Akad*., 20:557, 569, 575, 592 (1845)
3. Goranson, R. W., Solubility of Water in Granite Magmas, *Amer. J. Sci*., 22: 481–502 (1931)
4. Habashi, F., Recent Advances in Pressure Leaching Technology, in: *Proc. First Intl. Conf. Solvothermal Reactions,* 13–16, Takamatsu, Jpn. (Dec. 5–7, 1994)
5. Habashi, F., *A Textbook of Hydrometallurgy*, Libraire Universitaire du Quebec, Quebec, Canada (1993)
6. Nacken, R., Artificial Quartz Crystals, etc., *U.S. Office of Technical Services Report*, PB-18–748 and 28–897 (1946)

7. Barrer, R. M., Syntheses and Reactions of Mordenite, *J. Chem. Soc*., 2158 (1948)
8. Barrer. R. M., Some Features of Ion Exchange in Crystals, in: *Molecular Sieves, Soc. Chem. Ind.*, pp. 1258–1266 (1962)
9. Nacken, R., Hydrothermal Synthese als Grundlage fur Zuchtung Von Quarz-Kristallen, *Chem. Z.*, 74:745–749 (1950)
10. Byrappa, K., Hydrothermal Growth of Crystals, in: *Handbook of Crystal Growth*, (D. T. J. Hurle, ed.), pp. 465–562, Elsevier Science B.V., England (1994)
11. Lencka, M. M., Anderko, A., and Riman, R. E., Hydrothermal Precipitation of Lead Zirconate Titanate Solid Solutions: Thermodynamic Modeling and Experimental Synthesis, *J. Am. Ceram. Soc*., 78:2609–2618 (1995)
12. Eckert, J. O., Jr., Hung-Houston, C. C., Gersten, B. L., Lencka, M. M. and Riman, R. E., Kinetics and Mechanisms of Hydrothermal Synthesis of Barium Titanate, *J. Am. Ceram. Soc*., 79:2929–2939 (1996)
13. Morey, G. W. and Niggli, P., The Hydrothermal Formation of Silicates, A Review., *J. Am. Chem. Soc*., 35:1086–1130 (1913)
14. Laudise, R. A., *The Growth of Single Crystals*, pp. 278–281, Prentice-Hall, Englewood Cliffs, NJ (1970)
15. Rabenau, A., The Role of Hydrothermal Synthesis in Preparative Chemistry, *Angew. Chem.*, (English Ed.), 24:1026–1040 (1985)
16. Lobachev, A. N., (ed.), *Crystallization Processes under Hydrothermal Conditions*, pp. 1–255, Consultants Bureau, New York (1973)
17. Roy, R., Acceleration the Kinetics of Low-Temperature Inorganic Syntheses., *J. Solid State Chem*., 111:11–17 (1994)
18. Byrappa, K. (ed.), *Hydrothermal Growth of Crystals*, pp. 1–365, Pergamon Press, Oxford, UK (1992)
19. Yoshimura, M. and Suda, H., Hydrothermal Processing of Hydroxyapatite: Past, Present, and Future, in: *Hydroxyapatite and Related Materials* (P. W. Brown and B. Constanz, eds.), pp. 45–72, CRC Press, Inc (1994)
20. Roy, R., Fifty-year Perspective on Hydrothermal Research, in: *Proc. Workshop on Solvothermal and Hydrothermal Reacts*., pp. 1.1–1.20, Sun Mess Kogawa (Jan. 22–24, 1996)
21. Tamma, G., *The State of Aggregation*, D. Van Nostrand Company (1925)
22. *Proc. 1st International Conference, Solvothermal Reactions*, pp. 1–223, Takamatsu, Jpn. (Dec. 5–7, 1994)
23. *Proc. Workshop on Solvothermal and Hydrothermal Reactions*, pp. 1–133, Sun messe Kagawa, Jpn. (Jan. 22–24, 1996)
24. *Proc. 2nd Intl. Conf. Solvothermal Reactions*, pp. 1–242, Takamatsu, Jpn. (Dec. 18–20, 1996)

DropBooks

25. Yoshimura, M., Why, and How about Advanced Inorganic Materials, *Eur. J. Solid State Inorg. Chem.* 32: I–IV (1995)

26. Litvin, B. N. and Tules, D. A., Apparatus for Hydrothermal Synthesis and Growth of Single Crystals, in: *Hydrothermal Synthesis of Crystals*, pp. 193–202, Nauka, Moscow (1968) (in Russian)

27. Seward, T. M., The Stability of Complexes of Silver in Hydrothermal Solutions up to 350°C, *Geochim. Cosmochim. Acta*, 40:1329–1341 (1976)

28. Seward, T. M., Metal Complex Formation in Aqueous Solutions at Elevated Temperatures and Pressures, in: *Chemistry and Geochemistry of Solutions at High Temperatures and Pressures*, (D. T. Rickard and F. E. Wichman, eds.), *Proc. Noble Symp.*, 13/14, pp. 113–132, Pergamon Press, New York (Sept. 1979)

29. Franck, E. U., Survey of Selected Non-Thermodynamic Properties and Chemical Phenomena of Fluids and Fluids Mixtures, in: *Chemistry and Geochemistry of Solutions at High Temperatures and Pressures*, (D. T. Rickard and F. E. Wichman, eds.), *Proc. Noble Symp.*, 13/14:65–88, Pergamon Press, New York (Sept. 1979)

30. Hurd, D. C., Factors Affecting the Solution Rate of Biogenic Opal in Seawater, *Earth Planetary Science Letters*, 15:411–417 (1972)

31. Dove, P. M. and Crerar, D. A., Kinetics of Quartz Dissolution in Electrolyte Solutions using a Hydrothermal Mixed Flow Reactor, *Geochim. Cosmochim. Acta*, 54:955–959 (1990)

32. Henley, R. W., Solubility of Gold in Hydrothermal Chloride Solutions, *Chem. Geol.*, 11:73–87 (1973)

33. Honma, H., Shikazono, N., and Nakata, M., Hydrothermal Synthesis of Gold, Electrum and Argentite, *Can. Min.*, 29:217–221 (1991)

34. Seward, T. M., Hydrothermal Solution Speciation (Solvation to Ion Pairing and Complexing), in: *Proc. 5th Int. Symp. Hydrothermal Reactions*, (D. A. Palmer and D. J. Wesolowski, eds.), pp. 7–9, Gatlinburg, USA (July 20–24, 1997)

35. Benning, L. G. and Seward, T. M., Hydrosulphide Complexing of Au^{1+} in Hydrothermal Solutions from 150–400°C and 500–1500 bar, *Geochimica et Cosmochimica Acta*, 60:1849–1871 (1996)

36. Kolonin, G. R., Palyanova, G. A., Shironosova, G. P., and Morgunov, K. G., The Effect of Carbon Dioxide on Internal Equilibria in the Fluid during the Formation of Hydrothermal Gold Deposits, *Geochemistry International*, 35:40–50 (1997)

37. Palyanova, G. A., Shironosova, G. P., Laptev, Lu. V. and Kolonin, G. R., Experimental Checking of CO_2 Influence on Gold and Silver Solubility in High–Temperature Complex Fluids, in: *Proc. 5th Int. Symp. Hydrothermal Reactions*, (D. A., Palmer and D. I. Wesolowski, eds), pp. 255–256, Gatlinburg, (July 20–24, 1997)

38. Jahns, R. H. and Burnham, C. W., Experimental Studies of Pegmatites Genesis: I.A. Model for the Derivation and Crystallization of Granitic Pegmatites, *Econ. Geol.*, 64:843–864 (1969)

39. Jahns, R. H., Internal Evolution of Pegmatite Bodies, in: *Granitic Pegmatites in Science and Industry* (P. Cerny, ed.), Mineral Assoc. Can. Short Course Handbook., 8:293–327 (1982)

40. Tuttle, O. F. and Bowen, N. L., Origin of Granite in The Light of Experimental Studies in The System $NaAlSi_3O_4$ – $KalSi_3O_4$ – SiO_4 – H_2O., *Geol. Soc. Amer. Mem.*, 74 (1958)

41. Luth. W. C., Jahns, R. H. and Tuttle, O. F., The Granite System at Pressures of 4 to 10 kbars., *J. Geophys*, 69:759–773 (1964)

42. Burnham, C. W., Water and Magmas: A Mixing Model, *Geochim. Cosmochim. Acta*., 39:1007–1084 (1975)

43. Burnham, C. W., Magmas and Hydrothermal Fluids, in: *Geochemistry of Hydrothermal Ore Deposits, 2nd ed*. (Barnes, ed.), pp. 71–136, John Wiley and Sons, New York (1979)

44. Shaw, H. R., Obsidian – H_2O Viscosities at 1000 and 2000 bars in the Temperature Range 700 to 900°C., *J. Geophys*., 68:6337–6343 (1963)

45. Shaw, H. R., Comments on Viscosity, Crystal Settling and Convection in Granitic Magmas, *Amer. J. Sci.*, 263:120–152 (1965)

46. Fenn, P. M., The Nucleation and Growth of Alkali Feldspars from Hydrous Melts., *Can. Mineral*, 15:135–161 (1977)

47. Wyllie, P. J. and Tuttle, O. F., Experimental Investigation of Silicate System Containing Two Volatile Components. Part II. The Effects of NH_3 and HF, in Addition of H_2O, on The Melting Temperatures of Albite and Granite, *Amer. J. Sci*., 259:128–143 (1961)

48. Manning, D. A. C., The Effect of Fluorine on Liquidus Phase Relationships in The System Qz – Ab – Or with Excess Water at 1 Kb., *Contrib. Mineral. Petrol*., 76:206–215 (1981)

49. Dingwell, D. B., The Structure and Properties of Fluorine-Rich Silicate Melts: Implications for Granite Petrogenesis (abstr.), in: *Granite – Related Mineral Deposits* (R. P. Toylor, and D. F. Strong, eds.), pp. 72–81, Can. Inst. Mining, Extended Abstr. of Conf., on Granite-Related Mineral Deposits, Halifax (1985)

50. Kogarko, L. N., Krigman, L. D., and Sharudilo, N. S., Experimental Investigations of The Effect of Alkalinity of Silicate Melts on The Separation of Fluorine into the Gas Phase, *Geochem. Int*., 8:782–790 (1968)

PrintBooks

51. Webster, J. D., Holloway, J. R. and Hervig, R. L., Phase Equilibra and Volatile Partitioning in a Be-, U- and F-Enriched Vitrophyre from Spor Mountain, *Utah. Geochim. Cosmochim, Acta*., 51:389–402 (1987)

52. Manning, D. A. C., Martin, J. S., Pichavant, M., and Henderson, C. M. B., The Effect of F, B and Li on Melt Structures in The Granite System: Different Mechanisms? in*: Progress in Experimental Petrology* (C. M. B. Henderson, ed.), *Nat. Env. Res. Council Publ. Ser*. D, 25: 36–41 (1984)

53. De Jong, B. H. W. S. and Brown, G. E. Jr., Polymerization of Silicate and Aluminate Tetrahedra in Glasses, Melts and Aqueous Solutions – II. The Network Modifying Effects of Mg^{+2}, K^+, Na^+, Li^+ ,OH^-, F^-, Cl^-, H_2O, CO_2 and H_3O^+ on Silicate Polymers, *Geochim. Cosmochim. Acta*., 44:1627–1642 (1980)

54. Bailey, J. C., Fluorine in Granitic Rocks and Melts: A Review, *Chem. Geol*., 19:1–42 (1977)

55. Cerny, P., Meintzer, R. E., and Anderson, A. J., Extreme Fractionation in Rare-element Granite Pegmatites: Selected Examples of Data and Mechanisms, *Can. Mineral*, 23:381–421 (1985)

56. London, D., Magmatic-Hydrothermal Transition in The Tanco Rare-element Pegmatite: Evidence from Fluid Inclusions and Phase Equilibrium Experiments, *Amer. Mineral., Jahns Mem. Issue*, 71:376–395 (1986)

57. Bray, P. J., NMR Studies of Borates. In Borate Glasses: Structure, Properties, Applications (L. D. Pye, V. D. Frenchette, and N. J. Kriedl, eds.), *Materials Sci. Res*., 1:321–351, Plenum Press, New York (1978)

58. Dell, W. J., Bray, P. J., and Xiao, S. Z., IIB NMR Studies and Structural Modeling of Na_2O-B_2O_3-SiO_2 Glasses of High Soda Content., *J. Non-Cryst. Solids*, 58:1–16 (1983)

59. Oestrike, R., Geisinger, K., Navrotsky, A., Turner, G. L., and Kirkpatrick, R. J., Structure and Thermochemistry of Glasses along the Join $NaAlSi_3O_8$-$NaBSi_3O_8$: The Effect of Boron (abstr.), *Geol. Soc. Amer. Abstr., Prog*., 18:709 (1986)

60. Navrotsky, A., Geisinger, K. L., McMillan, P., and Gibbs, G. V., The Tetrahedral Framework in Glasses and Melts—Inferences from Molecular, Thermodynamics and Physical Properties, *Phys. Chem. Min*., 11:284–298 (1985)

61. Mendel, J. E., The Storage and Disposal of Radioactive Waste as Glass in Canisters. PNL-2764, Pacific Northwest Laboratories, Richland, Washington (1978)

62. London, D., Internal Differentiation of Rare-Element Pegmatites: Effects of Boron, Phosphorus and Fluorine, *Geochimica et Cosmochimica*, Pergamon Journal Ltd., 51:403–420 (1987)

63. Hess, P. C., The Role of High Field Strength Cations in Silicate Melts, in: *Advances in Physical Geochemistry* (I. Kushiro, and I. Perchuk, eds.), Springer-Verlag, New York (1986)
64. Ryerson, F. J. and Hess, P. C., The Role of P_2O_5 in Silicate Melts, *Geochim. Cosmochim. Acta.*, 44:611–624 (1980)
65. Mysen, B. O., Ryerson, F., and Virgo, D., The Structural Role of Phosphorus in Silicate Melts, *Amer. Mineral*, 66:106–117 (1981)
66. Huffman, M., Navrotsky, A., and Pintchovski, F. S., Thermochemistry and Structure of Low Pressure Chemically Vapor Deposited and Bulk SiO_2-P_2O_5 and SiO_2-GeO_2 Glasses, *J. Electrochem. Soc*., 133:431–439 (1986)
67. Burnham, C., Wayne and Nekvasil, Hanna, Equilibrium Properties of Granite Pegmatite Magmas, *Amer. Mineral*, 71:239–263 (1986)
68. Wyllie, P. J. and Tuttle, O. F., Experimental Investigation of Silicate Systems Containing Two Volatile Components, Part III: The Effects of SO_3, P_2O_5, HCl and Li_2O, in Addition to H_2O, on the Melting Temperatures of Albite and Granite., *Amer. J. Sci*., 262:930–939 (1964)
69. Cerny, P., Petrogenesis of Granitic Pegmatites, in: *Granitic Pegmatites in Science and industry* (P. Cerny, ed.), Mineral. Assoc. Can. Short Course Handbook. 8:405–461 (1982)
70. London, D., Experimental Phase Equilibria in the System $LiAlSiO_4$-SiO_2-H_2O: A Petrogenetic Grid for Lithium-rich Pegmatites, *Amer. Mineral*, 69:995–1004 (1984)
71. Morgan, G. B., Alteration of Amphibolitic Wallrocks Around the Tanco Rare Element Pegmatite, *Manitoba. M.S. Thesis, Univ. Oklahoma*. VI (1986)
72. Fenn, P. M., On The Origin of Graphic Granite, *Amer. Mineral*, *Jahns Mem. Issue*, 71:325–330 (1986)
73. Quist, A. S. and Marshall, W. L., Electrical Conductances of Aqueous Sodium Chloride Solutions from 0 to 800°C and to Pressures to 4000 bars, *J. Phy. Chem*., 72:684–703 (1968)
74. Marshall, W. L. and Frantz, J. D., Electrical Conductance Measurements of Dilute, Aqueous Electrolytes at Temperatures to 800°C and to Pressures to 400 bars: Techniques and Interpretations, in: *Hydrothermal Experimental Techniques* (G. C. Ulmer, and H. L. Barnes, eds.), pp. 261–292, John Wiley and Sons, New York (1987)
75. Takahashi, H. and Nakatuka, K., Advanced Geothermal Energy Utilization for Geochemical Energy Utilization for Geochemical Reactor, in: *Proc. 1st Int. Conf. Solvothermal Reactions* (T. Moriyoshi, ed.), pp. 71–75, Takamatsu, Jpn. (Dec. 5–7, 1994)
76. Nakatsuka, K., Geothermal Reactor-Concept and Perspectives, in: *Proc. 2nd Int. Conf. Solvothermal Reactions* (T. Moriyoshi, ed.), p. 156, Takamatsu, Jpn. (Dec. 18–20, 1996)

DropBooks

77. Corliss, J. B., Metallogenesis at Oceanic Spreading Centres, *J. Geol. Soc. Lond.*, 136:621–626 (1979)

78. Fornari, D. J. and Embley, R. W., Tectonic and Volcanic Controls on Hydrothermal Processes at The Mid-Ocean Ridge: An Overview Based on Near-Bottom and Submersible Studies, in: *Seafloor Hydrothermal Systems Physical, Chemical, Biological and Geological Interactions* (S. E. Humphris, R. A. Zierenberg, L. S. Mullineause, and R. E. Thomson, eds.), pp. 1–46 (1995)

79. Henley, D., (cited by Gillings, A., Evolution of Hydrothermal Ecosystems on Earth [and Mars?]), *Bio Essays*, 18:515–517 (1996)

80. Shock, E. L., Chemical Environments of Submarine Hydrothermal Systems, *Origins of Life and Evolution of The Biosphere*, 22:67–107 (1992)

81. Baross, J. A. and Hoffman, S. E., Submarine Hydrothermal Vents and Associated Gradient Environments as Sites for the Origin and Evolution of Life, Origins of Life, 15:327–345 (1985)

82. Simoneit, B. R. T., Aqueous Organic Geochemistry at High Temperature / High Pressure, *Origins of Life and Evolution of the Biosphere*, 22:43–65 (1992)

83. Costa, U. R., Fyfe, W. S., Kerrich, R., and Nesbitt, M. W., Archean Hydrothermal Talc Evidence for High Ocean Temperatures, *Chemical Geol.*, 30:341–349 (1980)

84. Hoffinan, S. E. and Baross, J. A., Workshop on the Early Earth: The Interval from Accretion to the Older Archean, Lunar and Planetary Institute, Houston, 34, (1984)

85. Abbott, D. H. and Hoffman, S. E., Archean Plato Tectonics Revisited 1: Heat Flow, Spreading Rate and Age of Subducting Oceanic Lithosphere and their Effects on the Origin and Evolution of Continents, *Tectonics*, 3:429–448 (1984)

86. Jannasch, H. W., Microbial Interactions with Hydrothermal Fluids, in: *Seafloor Hydrothermal Systems*, (S. E. Humphris, R. A. Zierenberg, L. S. Mulineaux, and R. E. Thomson, eds.), pp. 273–296, American Geo-Physical Union, Washington (1995)

87. Rona, P. A., Bostrom, K., Laubier, L. and Smith, K. L., Jr. (eds.), *Hydrothermal Processes at Seafloor Centers*, NATO Conf. Series, Plenum Press, New York, p. 796 (1983)

88. Schulte, M. D. and Shock, E. L., Thermodynamics of Strecker Synthesis in Hydrothermal Systems, *Origins of Life and Evolution of the Biosphere*, 25:161–173 (1995)

89. Shock, E. L., Organic Acids in Hydrothermal Solutions: Standard Molar Thermodynamic Properties of Carboxylic Acids and Estimates of Dissociation Constants at High Temperatures and Pressures, *American Journal of Science*, 295:496–580 (1995)

90. Fox, S. W. and Windsor, C. R., Synthesis of Amino Acids by the Heating of Formaldehyde and Ammonia, *Science*, 170: 984–985 (1970)

91. Marshall, W. L., Possible Geochemical Production of Biological Precursors: Amino acids and other Amines (also Hydrocarbons) from Aqueous Ammonium Carbonate Solutions and Metal Carbides at 200°C–300°C (abstr.) *EOS*, 68:458 (1987)

92. Hennet, J. C., Holm, N. G. and Engel, M. H., Abiotic Synthesis of Amino Acids under Hydrothermal Conditions and The Origin of Life: a Perpetual Phenomenon?, *Naturwissenschaften*, 79 (1992)

93. Shock, E. L., Geochemical Constraints on the Origin of Organic Compounds in Hydrothermal Systems, *Origins of Life and Evolution of the Biosphere*, 20:331–367 (1990)

94. Shock, E. L., Chemical Environments of Submarine Hydrothermal Systems, *Origins of Life and Evolution of the Biosphere*, 22:66–107 (1992)

95. Miller, S. L., A Production of Amino Acids under Possible Primitive Earth Conditions, *Science*, 117:528–529 (1953)

96. Holm, N. G., Cairna-Smith, A. G., Daniel, R. M., Ferris, J. P., Hennet, R. J. C., Shock, E. L., Simoneit, B. R. T., and Yanagawa, H., *Origins of life and Evolution of the Biosphere*, 22:181–190 (1992)

97. Humphris, B. E., Zierenberg, R. A., Mullineaux, L. S. and Thomson, R. E., (eds.), in: *Seafloor Hydrothermal Systems, Physical, Chemical, Biological and Geological Interactions*, pp. 1–466, American Geophysical Union, Washington (1995)

98. Tuttle, O. F., A New Hydrothermal Quenching Apparatus, *Amer. J. Sci*., 246:628–635 (1948)

99. Somiya, S. (ed.), *Hydrothermal Preparation of Fine Powders, Advanced Ceramics III*, Elsevier Applied Science Publishers, UK (1990)

100. Tuitemwong, P. E. L. E., Fung, D. V. C. and Tuitemwong, K., Effect of Processing Temperature on Microbiological and Chemical Quality of Soy Milk Produced by Rapid Hydration Hydrothermal Cooking, *J. Food Process. Preserv*., 17:153–175 (1993)

101. IAPWS Release on the Values of Temperature, Pressure and Density of Ordinary and Heavy Water Substances at their Respective Critical Points, 1992; available from the IAPWS Secretary, Dr. Barry Dooley, Electric Power Research Institute, 3412 Hillview Avenue, Palo Alto, CA 94303, USA.

102. Byrappa, K., Crystallization Process in Some Phosphate Systems Under Hydrothermal Conditions, in: *Proc. 2nd Int. Conf. Solvothermal Reactions*, p. 84, Takamatsu, Jpn. (Dec. 18–20, 1996)

103. Lencka, M. M., Anderko, A., and Riman, R. E., Hydrothermal Precipitation of Lead Zirconate Titanate Solid Solutions: Thermodynamic Modeling and Experimental Synthesis, *J. Am. Ceram. Soc*., 78:2609–2618 (1995)

DropBooks

104. Komarneni, S., Roy, R., and Li, Q. H., Microwave-Hydrothermal Synthesis of Ceramic Powders, *Mater. Res. Bull*., 27:1393–1405 (1992)

105. Komarneni, S., Hussein, M. Z., Liu, C., Breval, E., and Malla, P. B., Microwave-Hydrothermal Processing of Metal Clusters Supported in and/or on Montmorillonite, *Eur. J. Solid State Inorg. Chem*., 32:837–849 (1995)

106. Kolb, E. D. and Laudise, R. A., Phase Equilibria of $Y_3Al_5O_{12}$, Hydrothermal Growth of $Gd_3Ga_5O_{12}$ and Hydrothermal Epitaxy of Magnetic Garnets, *J. Crystal Growth*, 29:29–39 (1975)

107. Van Hout, M. J. G., Verplanke, J. C., and Robertson, J. M., Hydrothermal Synthesis of Single Crystal Thin Films of Magnetic Garnets and Their Analysis, *Mat. Res. Bull*., 10:125–132 (1975)

108. Yoshimura, M., Yoo, S-E., Hayashi, M. and Ishizawa, N., Preparation of $BaTiO_3$ Thin Film by Hydrothermal Electrochemical Method, *Jpn. J. Appl. Phys*., 28:L2007–L2009 (1989)

109. Basca, R., Ravindranathan, P., and Dougherty, J. P., Electrochemical, Hydrothermal and Electro-Chemical-Hydrothermal Synthesis of Barium Titanate Thin Films on Titanium Substrates, *J. Mater. Res.*, 7:423–428 (1992)

110. Kajiyoshi, K., Hamaji, Y., Tomono, K., Kasanami, T. and Yoshimura, M., Microstructure of Strontium Titanate Thin Film Grown by the Hydrothermal-Electrochemical Method, *J. Am. Ceram. Soc*., 79:613–619 (1996)

111. Suchanek, W. and Yoshimura, M., Processing and Properties of Hydroxyapatite-based Biomaterials for use as Hard Tissue Replacement Implants, *J. Mat. Res*., 13:1–24 (1998)

112. Cho, W. S. and Yoshimura, M., Hydrothermal Synthesis of $PbTiO_3$ films, *J. Mater. Res*., 12:833–839 (1997)

113. Fujishiro, Y., Fujimoto, A., Sato, T., and Okuwaki, A., Coating of Hydroxyapatite on Titanium Plates Using Thermal Dissociation of Calcium-EDTA Chelate Complex in Phosphate Solutions under Hydrothermal Conditions, *J. Colloid Interface Sci*., 173:119–127 (1995)

114. Suchanek, W., Suda, H., Yashima, M., Kakihana, M. and Yoshimura, M., Biocompatible Whiskers with Controlled Morphology and Stoichiometry, *J. Mater. Res*., 10:512–529 (1995)

115. Suchanek, W., Yashima, M., Kakihana, M. and Yoshimura, M., Processing and Mechanical Properties of Hydroxyapatite Reinforced with Hydroxyapatite Whiskers, in*: Proc. of 2nd International Symposium on Apatite*, Japanese Association of Apatite Science, pp. 15–20 (1997)

116. Yanagisawa, K., Sasaki, M., Nishioka, M., Ioku, K. and Yamasaki, N., Preparation of Sintered Compacts of Anatase by Hydrothermal Hot-Pressing, *J. Mater. Sci. Letts*., 13:765–766 (1994)

117. Sato, K., Hashida, T., Takahashi, H. and Yamasaki, N., Development of High Strength Calcium Aluminate-Phosphate Cement by Hydrothermal Hot-Pressing, *J. Mater. Sci. Letts*., 16:1464–1468 (1997)

118. Yanagisawa, K., Ioku, K., and Yamasaki, N., Formation of Anatase Porous Ceramics by Hydrothermal Hot-Pressing of Amorphous Titania Spheres, *J. Am. Ceram. Soc*., 80:1303–1306 (1997)

119. Yamasaki, N., Yanagisawa, K., Nishioka, M. and Kanahara, A Hydrothermal Hot-Pressing Method: Apparatus and Application., *J., Material Science Letters*, 5:355–356 (1986)

120. Nishioka, M., Yanagisawa, K., and Yamasaki, N., Solidification of Sludge Ash by Hydrothermal Hot-Pressing., *Research J. Water Pollution Control Federation*, 62:926–927 (1991)

121. Heitz, E., in: *Advances in Corrosion Science and Technology* (M. Fontana, and R. Staehle, eds.), 4:149. Plenum Press, New York (1974)

122. Sakakibara, M., Saito, N., Nishihara, H., and Aramaki, K., Corrosion of Iron in an Hydrous Methanol, *Corrosion Science*, 34:391–409 (1993)

123. Gogotsi, G. Yu. and Yoshimura, M., Formation of Carbon Films on Carbides under Hydrothermal Conditions, *Nature*, 367:628–630 (Feb. 17, 1994)

124. Kelly, R. G., Small Scale Corrosion, *The Electrochemical Society Interface*, pp. 18–23, (Summer, 1997)

125. Sato, T., Tamura, K., and Okuwaki, A., Corrosion Behavior of Silicon Carbide Ceramics in Caustic Alkaline Solutions of High Temperature, *Br. Ceram. Trams. J.*, 91:181–182 (1992)

126. Habashi, F., (ed.), *Handbook of Extractive Metallurgy*, Vols. 1 to 4, p. 2500, Wiley-VCH, Germany (1997)

127. Lay, L., *Corrosion Resistance of Technical Ceramics*, Her Majesty's Stationery Office, London, UK (1984)

128. Yamanaka, S., Design and Synthesis of Functional Layered Nanocomposites, *Am. Ceram. Soc. Bull*., 70:1056–1058 (1991)

129. Malla, P. B., Revindranthan, P., Komarneni. S., and Roy, R., Intercalation of Copper Metal Clusters in Montmorillonite, *Nature*, 315:555–557 (1991)

130. Demazeau, G., Solvothermal Reactions: A New Opening in Materials Science Either for Basic Research or Industrial Applications, in: *Proc. 1st Intl. Conf. on Solvo-Thermal Reactions*, pp. 5–9, Takamatsu, Jpn. (Dec. 5–7, 1994)

131. Demazeau, G., The Solvothermal Synthesis: A Way to a New Chemistry, in: *Proc. Intl. Workshop on Soft and Solution Processing for Advanced Inorganic Materials*, (M. Yoshimura, ed.), pp. 4–12, Tokyo, Jpn. (Feb. 26–27, 1996)

DropBooks

2

History of Hydrothermal Technology

2.1 INTRODUCTION

In the ancient times, Romans used to celebrate the year-end and year-beginning in great festivities in honor of the God Janus, in whose honor the month January is named. The God Janus is a deity with two heads: one looking to the past and the other looking to the future (Fig. 2.1).[1] Here, we have made a sincere attempt to explore and review the early history of the hydrothermal technology that has an extremely promising future.

Figure 2.1. The God Janus.

As mentioned earlier, Sir Roderick Murchison, a British Geologist, was the first to use the term *hydrothermal* in the mid 19th century.[2] The first publication on hydrothermal research appeared in 1845 (Fig. 2.2). This reports successful synthesis of tiny quartz crystals upon transformation of freshly precipitated silicic acid in Papin's digestor by K. F. E. Schafthaul.[3] Following this, mineralogists, especially from France, Germany, and Italy, started synthesizing various other minerals. Although the size of the crystals or minerals they obtained did not exceed thousandths or hundredths of a millimeter, their main objective was to create or simulate, in the laboratory, the natural conditions existing in the earth's crust. If, in nature, minerals and mineral assemblages were formed at elevated temperature and pressure conditions in the presence of volatiles—mainly water, it will be quite impossible to simulate the natural conditions or processes responsible for the formation of rocks and minerals except under the *hydrothermal conditions*. Thus, the early interest in hydrothermal research was merely in the synthesis of a particular mineral or in obtaining compounds similar to natural minerals rather than to carry out any systematic investigation pertaining to phase relations or geochemistry of the earth's interior. Even the conditions under which they worked were, in general, simple and sometimes lacking precision. The minerals obtained by the earlier workers are chiefly those which are stable or at any rate, phanerostable, over a wide range of conditions, for example, quartz, and feldspar. As the resultant products obtained were very tiny, accurate chemical analysis or identification of the phase by optical microscopic methods was quite doubtful and many a times led to speculations. Besides, the experiments were carried out in glass tubes in which it was difficult to attain higher pressure-temperature conditions; also water was used in most cases as a solvent. Therefore, the crystals obtained were very small, and the purity of the crystals could not be studied satisfactorily. Most of the experiments during the 19th century under hydrothermal conditions, with some exceptions, were related to silicate synthesis. Therefore, the contribution from the glass tubes to the resultant product could not be precisely understood. After the introduction of steel autoclaves and suitable metal linings, attempts were initiated to reach higher pressure-temperature conditions to obtain other compounds and purer phases. However, no attention was paid to the chemistry of the solvent, the frequent appearance of the metastable phases, solubility relations, kinetics, phase equilibria and related phenomena. Thus, the frequent appearance of the metastable phases also complicated the earlier studies.

DropBooks

Bulletin der Königl. Akademie d. W.
1845 Nr. 12.

Gelehrte Anzeigen

München. herausgegeben von Mitgliedern 8. April.
Nro. 70. der k. bayer. Akademie der Wissenschaften. 1845.

Königl. Akademie der Wissenschaften.

Sitzung der mathematisch-physikalischen Classe am 8. Februar 1845.

1) Hr. Professor **Schafhäutl**:

Die neuesten geologischen Hypothesen und ihr Verhältniß zur Naturwissenschaft überhaupt.

(Fortsetzung.)

Anders verhält es sich bey der Geologie. Die Entwicklung der Erde, deren Geschichte der Geologe beschreiben will, ist längst vollendet; die Zeit der Bewegung und Veränderung ist längst verflossen, und er sieht nur die stummen Zeugen ehemaliger, seit unbestimmten Zeiten verübergegangener Bewegungen und Ereignisse übrigens. Primitive Gewißheit wird er also hier nie mehr erhalten; aber er kann durch Schlüsse auf zwey Wegen zu Hypothesen gelangen, über die Vorgänge längst verschwundener Tage, nämlich auf dem Cartesius'schen a priori oder dem Newtonischen a posteriori. Den ersten Weg, von allen übrigen Naturforschern seit Jahrhunderten verlassen, sind die meisten Geologen bisher treulich gewandelt; *) den zweyten müssen sie jedoch wandern, wenn es ihnen gelingen soll, künftig ein wirklich wissenschaftliches Gebäude zu schaffen. Der zweyte Weg a posteriori, der der Erfahrung ist schwieriger; aber, wie wir gesehen, der einzig naturwissenschaftliche.

Auf diesem Wege können wir zwar durch unmittelbare Beobachtung der Naturkörper in Ruhe nichts in Bezug auf ihre ehemalige Bewegung eruiren; aber den der Unveränderlichkeit der Naturgesetze stets auf ein gewisses Zusammenstimmen zu Gebote, das uns nahe mit eben der Sicherheit zum Ziele führen, als die unmittelbare Beobachtung des Vorgangs selbst. Newton hat diesen Weg betreten, als er sagte: „Ich erfinde die Ursachen nicht, aus welchen Phänomene folgen; ich ziehe sie aus den Phänomenen selbst, um die Ursachen zu finden." Aber gerade diese Beobachtungen, nach seinen Principien angestellt, haben den Werth dieses Weges mehr als klarer dargethan; denn diese Beobachtungen wurden von allen nachfolgenden Forschern als maßgebend in ihren respectiven Daten benutzt. Gleiches Zeugniß geben die geognostischen Beobachtungen in Norwegen, und der berühmte Leibniz (Goes Norvegiae 2. Lithg. p. p. 284.), der das Land nicht nach einem bloßen Vorurtheile beurtheilt hat, ich sich sogar genöthigt, über die durchaus verkehrten und falschen Ansichten einer durch Norwegen unternommenen Dilettantenreise, durch seine geologischen Forschungen in Afrika bekannt, zu erklären: „Berichte solcher Art dürfe man billigerweise über afrikanische Gegenden wegen setzen." Ja ich bin überzeugt, daß jenen Dilettanten unserer gegenwärtig vorherrschenden geognostischen Beobachtungen in ihr Nichts gerathen werden, sobald man die oft nur noch einem Zwitze ähnlichgewordenen Gegenden mit der Genauigkeit und in dem Umfange studirt haben wird, als dieß Wahrheit und Wissenschaft erfordern.

*) Ganz in diesem Sinne sagt der Vater der deutschen Geologie; „gerade der Dilettant gibt ein merkwürdiges Beyspiel, wie unbedeutend es sey, den Ursachen der Erscheinungen nachzuforschen, um nur die wirklich vorhandenen Thatsachen beobachten zu können." Aber gerade diese Beobachtungen, nach seinen Principien angestellt, haben den Werth dieses Weges mehr als klarer dargethan; denn diese Beobachtungen wurden von allen nachfolgenden Forschern als maßgebend in ihren respectiven Daten benutzt. Gleiches Zeugniß geben die geognostischen Beobachtungen in Norwegen, und der berühmte Leibniz (Goes Norvegiae 2. Lithg. p. p. 284.), der das Land nicht nach einem bloßen Vorurtheile beurtheilt hat, ich sich sogar genöthigt, über die durchaus verkehrten und falschen Ansichten einer durch Norwegen unternommenen Dilettantenreise, durch seine geologischen Forschungen in Afrika bekannt, zu erklären: „Berichte solcher Art dürfe man billigerweise über afrikanische Gegenden wegen setzen." Ja ich bin überzeugt, daß jenen Dilettanten unserer gegenwärtig vorherrschenden geognostischen Beobachtungen in ihr Nichts gerathen werden, sobald man die oft nur noch einem Zwitze ähnlichgewordenen Gegenden mit der Genauigkeit und in dem Umfange studirt haben wird, als dieß Wahrheit und Wissenschaft erfordern.

Figure 2.2. The first publication on the hydrothermal research. *(Courtesy of Prof. S. Somiya.)*

Most of the work on hydrothermal research during 19th century was confined only to Europe, especially to the Mineralogy, Petrology, and Geochemistry laboratories in Germany, France, Switzerland, and Italy. Bunsen (1845) carried out the hydrothermal experiments for the first time using thick walled glass tubes to contain high-temperature–high-pressure liquids and prepared strontium and barium carbonates.[4] Wohler (1848) recrystallized apophyllite by heating apophyllite in water solutions at 180–190°C under 10–12 atm pressure.[5] In fact, all the early hydrothermal experiments, until 1881, were carried out in simple glass tubes with sealed ends, of course, with an exception of one or two attempts with steel tubes. Even the term *hydrothermal bomb* was not used by earlier workers and they simply referred to them as autoclaves or tubes. The greatest contribution in the 19th century was by H. De Senarmont, the founder of hydrothermal synthesis in geoscience. He used glass tubes containing gel, SiO_2 and H_2O, HCl, or CO_2, enclosed in steel tubes, and heated at 200–300°C. The resultant product was a six-sided quartz prism with pyramidal termination.[6] When the solution contained $NaHCO_3$, CO_2 and some realgar, very little quartz was obtained. It was probably Daurree (1857), a French mineralogist, who first used a steel tube to synthesize quartz and wollastonite at about 400°C with water as a solvent. The most important aspect of his experiments was the pressure balance he introduced for the first time. The starting substances were taken in a sealed glass tube with water as a mineralizer, and this glass tube was placed inside a steel tube.[7] The space between the glass tube and steel tube was filled with water. He carried out a series of experiments with this design and a varied concentration of the starting materials to obtain several other minerals. Similarly, he conducted experiments on the recrystallization of felspars, micas, and pyroxenes.

Daurree's other significant contribution was his attempt to use natural hot spring water from Plombieres as a mineralizer and this led to the deposition of a small quantity of quartz in two days' time. In addition, he treated kaolin with Plombieres water under hydrothermal conditions and obtained felspar and a small amount of quartz. Here it is interesting to note that, after the discovery of hydrothermal activity in the deep sea on the Galapagos during the 1970s, active research is going on using the natural submarine hydrothermal vent fluid to study the origin of life (organic synthesis). This led to the establishment of the relation between the submarine hydrothermal activity and rich mineralization of a very wide spectrum from native elements to sulphides, oxides, and so on.[8]-[10] The

DropBooks

literature survey on the early hydrothermal research shows that several attempts were made to transform zeolite minerals and kaoline in the 19th century,[5]–[11] but it was only during 1940 that Barrer succeeded in synthesizing for the first time zeolite, that is, *analcime*, using the hydrothermal technique.[12] Although Deville St. Claire (1857) attempted to transform bauxite into corundum under hydrothermal conditions using NaOH as mineralizer, the experimental results were not definite. Perhaps he was the first one to use a mineralizer other than water.[13] In fact, many of the earlier workers, including von Chroustshoff, found that the glass tubes they were using were frequently attacked under hydrothermal conditions. However, they do not mention anything about precautions taken in this regard, as they were more concerned in obtaining a product corresponding to some natural minerals. During 1873, von Chroustshoff first proposed the gold lining of steel autoclaves to prevent corrosion. By introducing gold lining for the steel autoclaves, he could achieve a temperature of 350°C to synthesize tridymite phase of quartz and increased experimental duration.[15]

With the introduction of steel autoclaves along with noble metal linings, the tendency to reach higher pressure-temperature conditions than the usual 5 to 10 atm began. However, majority of the works up to 1880 remained pertaining to quartz, felspar, and related silicates. Thus, many of the earlier authors even define hydrothermal technique as the "one used in the synthesis of silicates." In 1880, Meunier carried out an experiment using water vapor passed over $AlCl_3$ and Mg contained in an open tube, heated to a low red heat and obtained mainly spinel. In some parts of the tube, he even observed tiny crystals of periclase and corundum.[15]

Followed by this work, Hannay (1880) claimed to have synthesized artificial diamond by the hydrothermal technique.[16] Similarly, Moissan (1893) also claimed to have synthesized diamond artificially as large as 0.5 mm from charcoal.[17] Though the success of these experiments was treated as dubious, they certainly provided a further stimulus for hydrothermal research, particularly the development of high-pressure techniques. It is interesting to note that the results of some of these earlier works were treated as dubious. This is probably in connection with the small size of their resultant products. The first ever large size crystals obtained by the earliest workers was that of hydrated potassium silicate, which was about 2–3 mm long, by Friedel and Sarasin (1881).[18] In this case, while growing orthoclase and felspar, hydrated potassium silicate was obtained as an additional phase containing surplus potassium silicate. Here it is

appropriate to quote one or two earlier experiments for the curiosity of the readers and to show their experimental conditions. Chroustshoff (1887) obtained quartz by heating a colloidal solution of SiO_2 to 250°C, almost every day for 6 months. He started his experiments with 4 tubes, 3 of which soon burst. Some crystals as large as 8 mm long and 3 mm wide, of type of vein quartz with $(10\bar{1}0)$, $(10\bar{1}1)$, $(01\bar{1}1)$ faces were crystallized. Perhaps this is the first systematic work on the growth of quartz. Although, the experimental duration was quite long, almost 6 months, he could obtain quartz crystals as large as 8 mm long and 3 mm wide.[19] In another experiment, Chroustshoff (1890) used a thick-walled evacuated glass tube of 25 cc volume, containing a mixture of colloidal SiO_2 solution, colloidal $Fe(OH)_3$, colloidal $Fe(OH)_2$, lime water, freshly precipitated $Mg(OH)_2$, and several drops of a NaOH-KOH solution which he heated for 3 months at 550°C. The resultant product contained, among other things, long, thick, dark-colored prismatic crystals of hornblende, 1 mm long, 0.5 mm thick, with (010), (110), (011) faces.[20] The most interesting point to be noticed here is that the experimenter obtained a mineral in 3 months under hydrothermal conditions having no bearing on its petrogenesis and no relation to any known equilibrium. Morey (1953) quotes this as a horrible experience of the experimenter.[21] Here, the reader should notice the duration of each experiment and the size and type of the minerals obtained. This is definitely related to the lack of knowledge in areas of solvent chemistry, kinetics, and solubility of the compound. Despite very low growth rates achieved in the 19th century, the earlier workers in hydrothermal research continued to synthesize a very wide range of mineral species. According to Morey and Niggli (1913), over 80 mineral species are supposed to have been synthesized during 19th century.[22] The list includes quartz, felspars, mica, leucite, nephelite, epidote, hornblende, pyroxene of minerals from the silicate group and several non-siliceous minerals like corundum (Al_2O_3), diaspore ($Al_2O_3 \cdot H_2O$), and brucite ($Mg(OH)_2$).

DropBooks

For the sake of convenience, the authors describe the further development of the hydrothermal research in coherence with the autoclave design, development, and pressure-temperature range. It is well known that the study of hydrothermal processes is merely the study of certain aqueous systems at high temperature, usually near to and often above the critical temperature of pure water, therefore considerable amount pressures are developed at these temperatures by water or aqueous solutions. The experimental difficulties of such a study are many, but are largely connected with the choice and control of working conditions and the

selection of a suitable autoclave to withstand the pressure at high temperatures over a long period of time. It was soon after Chroustshoff (1873) proposed the gold lining for the steel autoclaves that many earlier researchers began to work on new designs and new lining materials for autoclaves to obtain the most ideal conditions for the synthesis of several high temperature oxide minerals. Probably Friedel and Sarasin (1881) termed their hydrothermal autoclave as *hydrothermal bomb*, because of the high pressure working conditions in their experiments.[18] Obviously new metals and alloys available during that time were tested. For example, De Schulten (1882) even used a copper bomb to synthesize analcite by heating a mixture of sodium silicate, sodium aluminate, and lime water at 180°C for 18 hours.[23] Similarly, Sir Ramsay and Hunter (1882) used a cast iron bomb.[24] Bruhns (1889) used steel bombs lined with platinum, with a cover held down by bolts and made tight by means of a copper washer, which was protected by the action of the mineralizer on platinum.[25] Other contemporary workers used this design. Perhaps the simplest design of the autoclave, made of a nickeled gun-barrel or silver lined steel tube closed by a screw cap and copper washer, was developed by Doetler (1890). Using this type of autoclave, Doetler has done an extensive work by obtaining several mineral recrystallized species like chabazite, okenite, heulandite, analcite, natrolite, and so on.[26] However, in most of these works from 1870s to 1890s using the above mentioned type of autoclaves, experimental uncertainties were introduced owing to the lack of a perfectly tight closure, which resulted in the leakage of water, thereby causing variations in the pressure conditions (and hence the concentration) of water during the course of experiments. Friedel (1891) obtained corundum crystals by heating a solution of NaOH with excess of Al_2O_3 at a higher temperature at that time, 530–535°C.[27]

Towards the end of 19th century, Spezia from the Torino Academy of Science began his classical work on the seeded growth of quartz. His contribution to the field of hydrothermal research is remembered even today. Spezia (1896) found that plates of quartz kept at 27°C for several months with water under a pressure 1750–1850 atm did not lose its weight and also showed no etch figures. Thus, he concluded that pressure alone has no influence on the solubility of quartz.[28] Subsequently, Spezia studied the action of Na_2SiO_3 in the solubility of quartz with temperature. He found that when alkali was present in the system, SiO_2 separated out as quartz and the rhombohedral faces of the quartz were easily attacked, and on the other hand, on the same faces were the greatest

depositions of SiO_2 from Na_2SiO_3 solutions. The more rapid growth of the quartz crystals along the *c*-axis was explained.[29]

During the 19th century, much work was done on the geological side of hydrothermal research and the entire work was confined to Europe, particularly Germany, France, Italy, and Switzerland. It was only towards the turn of 19th century that the science of hydrothermal technology moved to North America, which was assisted by the American Industrial Revolution. Further, the establishment of the Geophysical Laboratory at the Carnegie Institute of Washington, USA, in 1907, probably marked the most important milestone in the history of hydrothermal technology. Although a great deal of research was carried out on hydrothermal technology in the 19th century, the facilities for large scale hydrothermal research before the end of the World War II were virtually nonexistent, except the Carnegie Institute of Washington, where Bowen began his hydrothermal research and later moved to the University of Chicago, Bridgman's high pressure laboratory at Harvard University during 1940s and 1950s, Kennedy's at the University of Chicago, and Tuttle's at Penn State University. This situation dramatically changed with the development of the test tube type pressure vessel by Tuttle in which high pressures up to 5 kbar could be maintained at temperatures of 750°C for a long period of time. However, before going into the contributions of these great personalities, we shall discuss the early contributions during the turn of the 19th century and the beginning of 20th century. As mentioned earlier, the entire activity on hydrothermal research was concentrated in Europe and there was no activity in North America or Asia, including Japan, China, India, and Taiwan, which are included today in the top ten countries actively engaged in hydrothermal research. Perhaps the first North American published work on hydrothermal research was by Barus (1898), who essentially worked on the impregnation of glass with water to such an extent that it melted below 200°C. He used steel bombs for these experiments.[30] Subsequently, Allen (1906) obtained very fine quartz crystals by heating a solution of $MgCl_2 \cdot 6NH_4Cl$ and Na_2SiO_3 for 3 days at 400–450°C. Also, large crystals of 2 mm long, often barrel shaped with short rhombohedral terminal faces, were obtained. Allen used steel bombs closed by a Cu disc held in place by a screw on steel cap, used either $MgCl_2 \cdot 6NH_4Cl$ solutions or a mixture of $MgCl_2$ solution with $NaHCO_3$, and either amorphous SiO_2 or Na_2SiO_3, heated for 3 to 6 days at 375–475°C to obtain magnetite, quartz, fosterite, etc.[31] However, the early American hydrothermal research was carried out using the autoclaves of

DropBooks

European designs. Around the turn of the century, it was again the German workers who were active in the field of new designs, especially Tammann and Boeke from Tottingen who carried out extensive studies with reference to many carbonate and silicate reactions in the newly designed bombs at higher pressure and temperature conditions with CO_2 pressure.[32] Perhaps this is the beginning of the solvothermal research, although the term *solvothermal* was introduced by French chemists in 1971.[33] The autoclaves used by Tammann and Boeke were all heavy steel vessels 10" diameter, 18" long, with soft metal gaskets which formed the seal when compressed by a set of radially deployed screws and nuts. The heating was internal with a resistance furnace.

With the establishment of the geophysical laboratory in Carnegie Institute of Washington, USA, Bowen established a fine hydrothermal research laboratory. Obviously, all the major contributions to the field of hydrothermal research from USA in the early 20th century are solely from this laboratory and have received worldwide recognition. Bowen took up a systematic study of the phase equilibria in high temperature silicate systems and, around the 1920s, he framed the most important petrologic principle, viz. *Bowen's Reaction Principle,* shown in Fig. 2.3.[34]

These ideas of Bowen have been, without question, one of the rare landmarks in the history of petrology. The main opposition for this principle was that the extrapolation of experimental phase equilibrium results was based on the data he obtained from systems made from relatively few and chemically pure components to natural systems. Subsequently, Bowen continued his research in this field, worked on several complex systems, and revised his earlier proposed reaction series slightly. While Bowen was working on the petrologic problems, Morey, Niggli, and Fenner were actively studying the silicate systems with water as one of the components. Morey first designed a simple, gasketed, sealed steel autoclave of 25 to 100 ml volume in the year 1913. It became very popular because of its simplicity and ease to handle. Later, the autoclave that bore his name was widely used for working up to the temperature of 450°C and 2 kbar pressure.[35] The details of the design and construction are discussed in Ch. 3. The first American autoclave designs were those of Adams and Smyth, again from Geophysical Laboratory of Carnegie Institute of Washington in 1923,[36] which later led to the modified versions by Goranson in 1931.[37] Figure 2.4 shows the schematic diagram of the autoclave design of Adams and Smyth. Before the development of these autoclaves, hydrothermal research was confined only to lower pressure and temperature limits because the externally heated

vessels failed as a result of creep and oxidation of the alloy used. On the other hand, the pressure vessels designed by Adams and Smyth were internally heated and externally cooled by circulating water. These developments in the 1920s are regarded as important milestones in hydrothermal research. They set a new trend in search of new alloys, and extended pressure and temperature limits. Using this set up, Goranson (1931) carried out a systematic study pertaining to the solubility of water in a liquid having the composition of the Stone Mountain Granite, and this investigation was considered as the most outstanding advancement in the application of hydrothermal laboratory studies to petrologic problems. The driving forces for the volcanic activity were related to the crystallization of hydrous silicate liquids.[37]

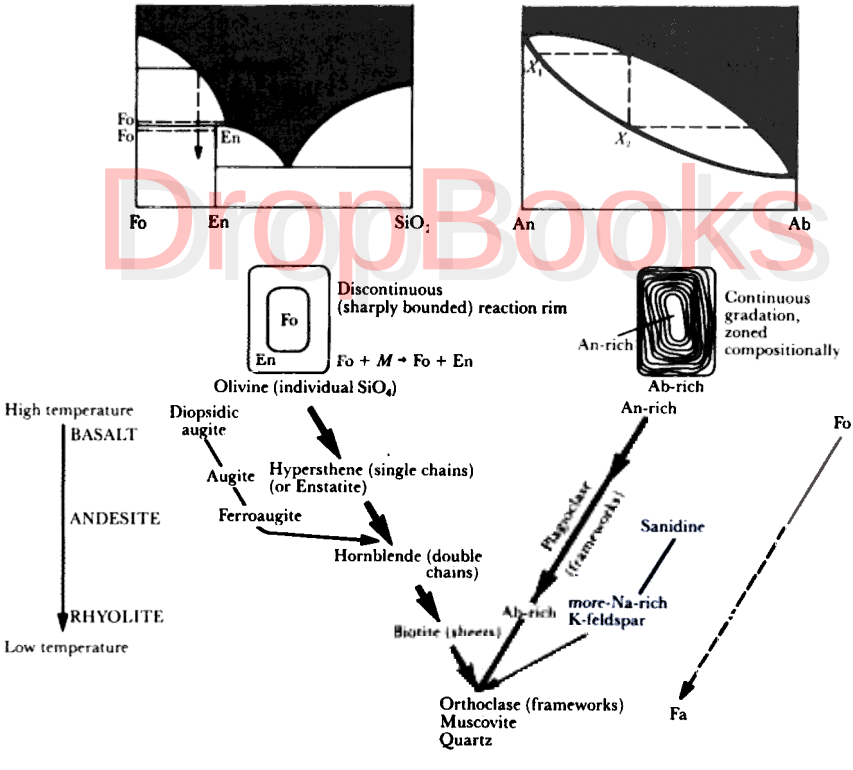

Figure 2.3. Bowen's Reaction Principle.[34]

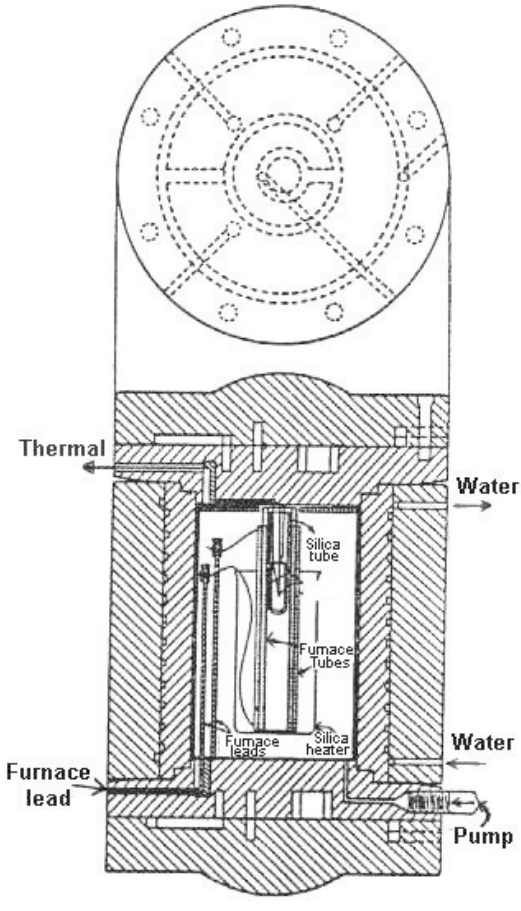

Figure 2.4. Schematic diagram of the autoclave design of Adams and Smyth.[36]

During this time, hydrothermal research began in Eastern Europe and Asia on a small scale, and much later in China and India—maybe after the Second World War. Here the reader should observe that the hydrometallurgy was quite an established field of research in many countries in Europe, North America, Eastern Europe, and Asia, particularly after the discovery of bauxite leaching by Karl Josef Bayer (1871–1908).[38] While writing the history of hydrothermal technology, the authors paid more attention to crystal growth and materials science rather than metallurgy or metal extraction. Therefore, historical references are not made for hydrometallurgical processes. As the authors of this monograph are from Japan and India, a brief history of the hydrothermal

research in these two countries is given. Today, Japan is the second most active country in the world for hydrothermal research next to the USA, and India stands in the 9th position next to Taiwan, with respect to the hydrothermal research in Materials Science (Fig. 1.12). If the hydrothermal research in geological science is also included, India's position goes up to the 7th place (based on the statistics prepared from Chemical Abstracts, Science Citation Index and INSPEC data bases from 1989 to 1997). More details on the statistics can be obtained from Ch. 1. According to Prof. Shigeyuki Somiya,[39] in Japan the hydrothermal work was first initiated in 1926 by Dr. Tominosuke Katsurai, and the work was related to hydrometallurgy. He worked on the soda treatment of aluminum ore through hydrothermal extraction. Following this, Prof. Shoichiro Nagai reported the synthesis of calcium silicate in 1931.[40] Perhaps this was the beginning of hydrothermal synthesis in Japan. Before going into the further developments which took place during the World War period, let us discuss briefly the progress achieved by the earliest workers of 20th century in the area of hydrothermal phase equilibrium studies.

Pioneers like Bridgman, Cohen, Morey, Niggli, Fenner, and Bowen in the early 20th century changed the scenario of hydrothermal research. They carried out an impressive amount of basic research along with their European counterparts, especially Tammann. Much of this early work was concerned with the setting up the pressure scale and testing. The results were predicted from thermodynamics. However, the total research effort was small and the study passed into a period of dormancy except for phase equilibria studies in some systems relevant to the natural systems. This was connected with the need for materials with a combination of high strength and corrosion resistance at high temperatures. Thus, the interest was again mostly geological, and the bulk of research is from the geological science side. It is fortunate for chemical science that most of the early geological workers appreciated the necessity for considering very simple chemical systems before there was any hope of understanding complexities of natural systems. Thus, the early work of Geophysical Laboratory of the Carnegie Institute of Washington was heavily biased towards pure chemistry.[41]

Here it is appropriate to discuss one or two important systems studied in early 20th century. Perhaps the first systematic and pioneering study of the hydrothermal system began with the publication of the work on the ternary system H_2O-K_2SiO_3-SiO_2 by Morey and Fenner (1917).[42]

PrepBooks

This work gives a more precise account of the pressure and temperature conditions throughout the experiment. Besides, nutrient materials were prepared from highly pure substances and consequently the composition of the charges used in each experiment was precisely known. The paper carried great significance to geological science as it demonstrated clearly the possibility of a complete solubility between anhydrous silicate phases and water, which in turn assisted in framing a mechanism for pegmatite crystallization in the presence of a volatile. Morey and Fenner (1917) studied this system from 200°C to >1000°C.[42] The work comprises of the determination of the composition and properties of the various stable solid phases which can coexist with solution and vapor within the above temperature range, of the composition of the solutions in equilibrium with the solid phases, of the change in composition of these solutions with temperature, and the approximate determination of the corresponding 3-phase pressures. Morey and Fenner used the famous Morey autoclave in all their work on phase equilibria studies in different systems. The isothermal polybaric saturation curves and the isobaric polythermal saturation curve at 1 atm pressure of H_2O vapor is shown in Fig. 2.5.

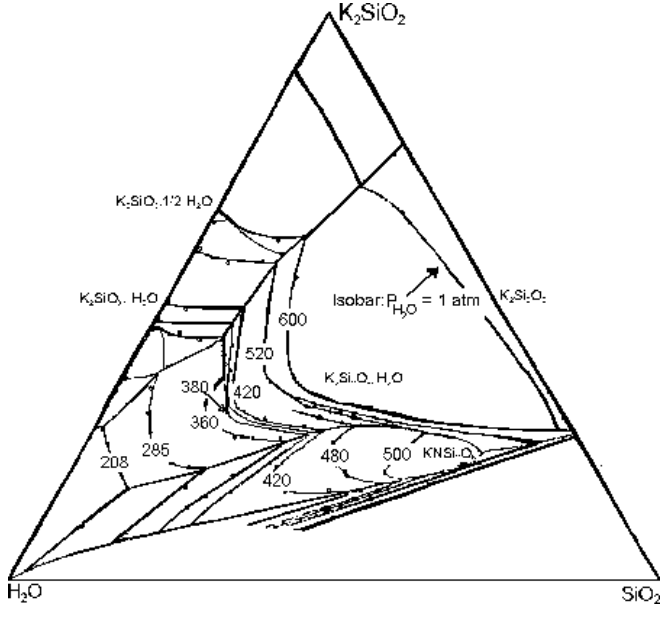

Figure 2.5. The isothermal polybaric saturation curves and the isobaric polythermal saturation curve at 1 atm pressure of H_2O vapor.[42]

The most significant aspect of this work is that a new trend can be observed here with reference to the theoretical relations governing the equilibrium in binary and ternary systems containing a volatile component, and a short discussion of the proper application of the term *solubility.* Besides Morey and his group, another group from the same laboratory led by Bowen was very active during that time. The study of the *p-v-t* relations of water became popular during the late 1920s. The works of van Nieuwenburg and Blumendahl (1932) followed by Keenan and Keyes are the most significant ones.[43][44] Later, Kennedy (1950) oriented his famous PVT data on water.[45] The Kennedy's diagram is shown in Fig. 2.6.

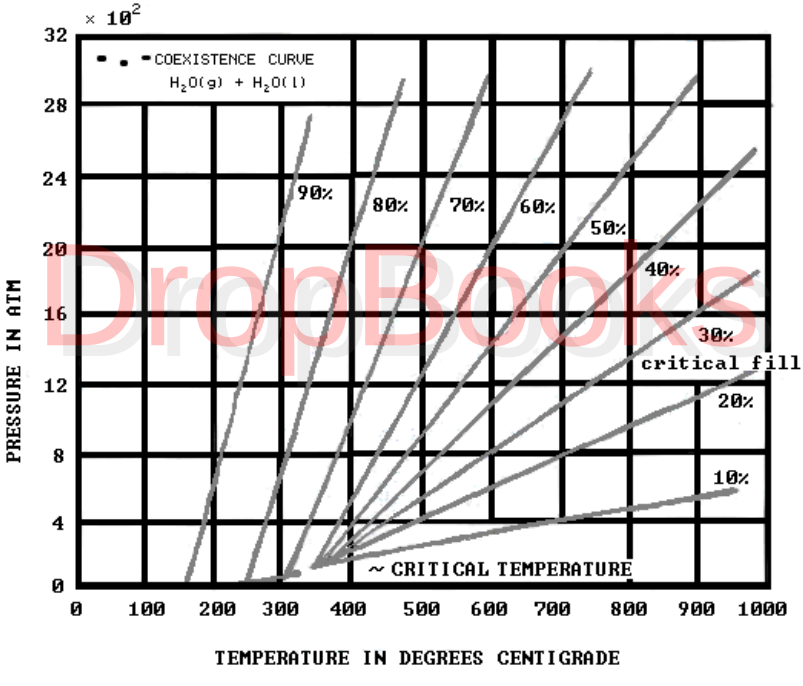

Figure 2.6. PVT diagram of water.[45]

Hitherto, the hydrothermal researchers were quite satisfied with the synthesis of inorganic compounds which resembles or which is similar to natural mineral. They did not bother much about the size of the crystals obtained. The growth rate was extremely low because of the lack of accurate knowledge on the proper solvent, and with such slow growth

rates, the hydrothermal research was less promising. Only a few number of people were engaged in this research studying the phase relations in various systems including that of water, and the interest was mainly on Geoscience. However, when Brazil imposed an embargo on the supply of high purity quartz which was a strategic material for the telecommunications purpose during the second world war, hydrothermal researchers began to think seriously about the growth rate of crystals. At that time, Brazil was the only country in the world for the source of electronic grade natural quartz, and even today, the situation is the same. Thus, the crisis owing to the shortage of pure quartz forced many researchers to jump into the field of hydrothermal research with a sole objective of growing large size single crystals of quartz. Many countries like the USA, UK, Germany, and the erstwhile Soviet Union were into the field and the success achieved was immense. Therefore, the period from the late 1930s to 1940s is referred to as the "golden period" in the hydrothermal research, not only because of the enhanced research activity, but also because of the many new discoveries with reference to autoclave designs and other important technological materials.

The authors feel that it is highly appropriate to discuss briefly the historical contribution made by the German hydrothermal researchers with reference to the increased growth rate and growth of large size single crystals of quartz. In contrast to the slow rate of growth achieved by the earliest workers like De Senarmont and Spezia, the captured German reports show that Nacken, using natural alpha-quartz as seed crystals and vitreous silica as the nutrient, had grown quartz crystals in an isothermal system and had succeeded in obtaining large single crystals of quartz from a small seed.[46] Prof. Richard Nacken (1884 to 1971) worked on the synthesis of various minerals from 1916 onwards, but left this field. In 1927 or 1928, he started working only on the hydrothermal growth of quartz crystals. On Nacken's work, Sawyer writes (cited by Bertaut and Pauthenet, 1957) that, "...Nacken made quartz crystals of 1" diameter by using hydrothermal method and the conditions are given as…" followed by some biographical data. Similarly, Nacken's emphasis on the quartz growth has also been documented by Sawyer. Almost at the same time, Nacken made emerald single crystals by the hydrothermal method and also beryl or corundum crystals for watch bearings. He prepared a large number of synthetic emeralds by using a trace of chromium to produce the color and could obtain hexagonal prisms of emerald weighing about 0.2 gm in a few days.[47] However, much of the work carried out by Nacken during late

1930s and 1940s remained as intelligence reports since he could not publish much.[48] During 1950, Nacken published his work on quartz that remains a classic even today.[49] Figure 2.7 shows a photograph of the quartz crystals obtained by Nacken.[49] As mentioned earlier, Doetler was the first one to use closed nickeled gun-barrel autoclaves, way back in 1890. It attained its prominence during World War II when several laboratories from many countries began working on the growth of large size crystals of quartz. This is also partly connected to the availability of alloys containing Mo and other important metals, which provided better strength to the alloys. Many countries attempted to grow large single crystals of quartz using old cannon barrels with closed ends during early 1940s. In this regard, the contributions of Lobachev and Shtenberg are important. By the mid 1940s, many laboratories, particularly from the USA, Germany, Russia, and the UK, were actively engaged in the growth of large quartz crystals. At this time, Tuttle (1948) designed a cone-in-cone seal for a small vessel with no threads to seize. However, the Tuttle apparatus could not achieve high pressure and temperature conditions, and it did not become very popular.[50]

DropBooks

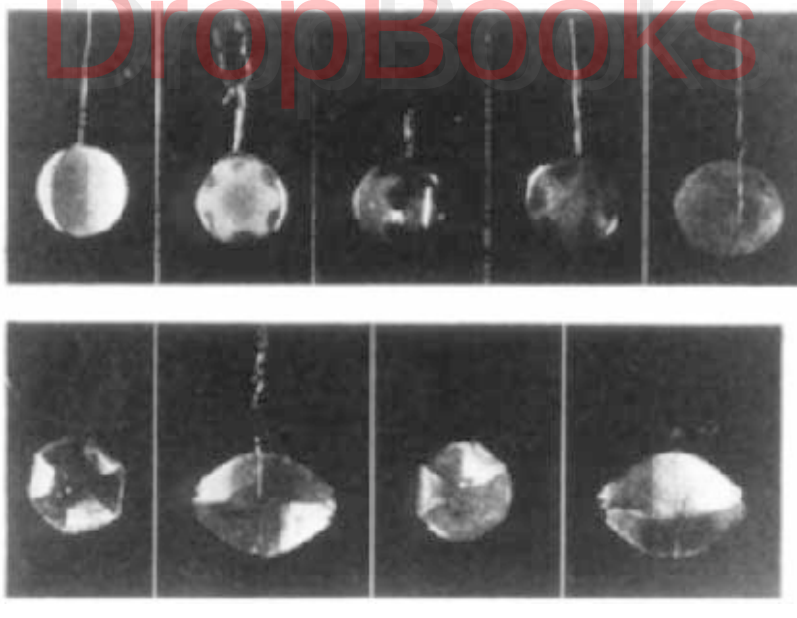

Figure 2.7. Photographs of the quartz crystals obtained by Nacken.[49]

Later, Rustom Roy modified another vessel that had been designed by Tuttle but never exploited. It proved to be much simpler and highly versatile. This modification by Roy is popularly known as the "test-tube bomb," which is made up of Hastelloy; Rene 41; Stellite 25 or Udimet, with 1–1½" o.d. × 8" long, having a $^{3}/_{16}$"–¼" diameter hole drilled down to ½" of the bottom. It was threaded at one end and closed at the other.[51] A more detailed description of the design and construction of this autoclave is given separately in Ch. 3. The greatest advantage of this test-tube bomb was not only the ease of operation, but also a large number of such vessels could be served by one pressure source. This integrated system of several vessels, each with its own gauge with one pressure generator, became a standard hydrothermal laboratory apparatus. Figure 2.8 shows a picture of such an assembly of 10 autoclaves of test-tube type, with one pressure generator source, operating simultaneously.

Figure 2.8. Picture of an assembly of 10 autoclaves in the laboratory of K. Byrappa.

Many laboratories throughout the world have this apparatus for studies concerning phase equilibria, materials synthesis, crystal growth, particles preparation, materials processing, diamond synthesis, and so on. The recent modifications of these test-tube bombs have been extended further for higher pressure and temperature conditions. The credit goes to the pioneers of this apparatus, Tuttle, Roy, and Licastro, who could set up a Tem-Press Company to manufacture these autoclaves at Penn State University. Thus, during the 1950s, the trend in hydrothermal research was towards the development of new designs, again to attain higher pressure and temperature limits with the better alloys available. This also led to the study of phase relations in several systems within a broader pressure-temperature range. In this regard, the contribution of Kennedy (1950), Morey and Hesselgesser (1951), Tuttle and England (1955), and Della Roy and Rustom Roy (1956) are very important.[52]-[54] The SiO_2-H_2O system was studied in great detail. Followed by this, many other laboratories in Europe, North America, erstwhile Soviet Union, and Japan took up the study of phase equilibria in several simple and complicated systems.[55] These studies laid a firm foundation for the ceramists and physical chemists, after many years, to develop a new technology. At this time, Prof. Yamasaki, Prof. Kumitomi, Prof. Ohara, and Dr. Akitsu were doing an excellent work in hydrothermal research in Japan. Some of them were closely associated with the industries like Toyo Communication Co. Ltd. and Nippon Dempa Co. Ltd., which resulted in the successful growth of large size quartz single crystals. Though they started in a very small way during the postwar period, Japan is now the largest producer of commercial quartz in the world. Japan alone produces >50 % of the world's annual production, it has the largest autoclaves in the world.[56] Figure 2.9 shows the quartz crystals obtained by Walker during 1950s.[57]

DropBooks

Figure 2.10 shows the quartz crystals obtained at AT&T Bell Labs during the 1970s,[58] and Fig. 2.11 shows the growth of quartz crystals in the world's largest autoclave located at the Toyo Communication Co. Ltd., in Japan during the 1980s.[56] In one experimental run, about 4000 to 4500 kg of quartz is produced. The early success in producing commercial quartz crystals in Japan during the postwar period paved the way for several others in the field. Some prominent ones are Prof. T. Noda, Prof. Doimon, Prof. R. Kiyoora, and Dr. Y. Itoh. When the North American laboratories were concentrating mainly on the development of new designs of autoclaves, the study of phase equilibria, and commercial production of quartz, Japan concentrated essentially on the growth of quartz crystals, and achieved its goal in becoming the world's largest producer.

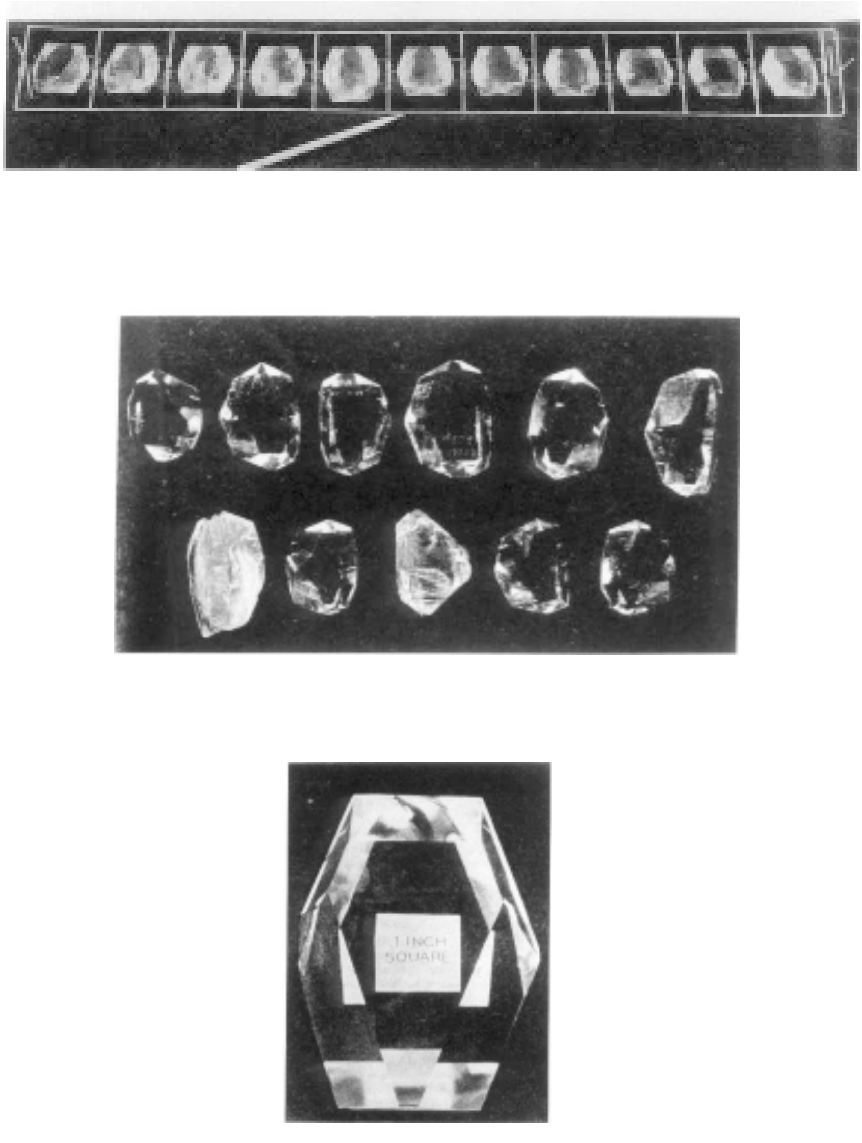

Figure 2.9. Quartz crystals obtained by Walker.[57]

DropBooks

Figure 2.10. Quartz crystals obtained at AT&T Bell Labs. *(Photo courtesy of R. A. Laudise.)*

Figure 2.11. Growth of quartz crystals in the world's largest autoclave. *(Photo courtesy of Dr. Taki.)*

The study of ternary and other more complex systems during the 1950s was very important, not only from the point of view of geological science, but also from the inorganic chemistry point of view, as several new compounds which were hitherto unknown or not found in nature could be crystallized. Some of the important systems studied under this category are: $MgO\text{-}SiO_2\text{-}H_2O$, $Al_2O_3\text{-}SiO_2\text{-}H_2O$, $BaO\text{-}Al_2O_3\text{-}H_2O$, $SrO\text{-}SiO_2\text{-}H_2O$, $K_2O\text{-}SiO_2\text{-}H_2O$, $Na_2O\text{-}SiO_2\text{-}H_2O$, $CaO\text{-}SiO_2\text{-}H_2O$, $CaO\text{-}Al_2O_3\text{-}H_2O$, $CaO\text{-}Al_2O_3\text{-}SiO_2\text{-}H_2O$, and so on. More accurate phase equilibria data were obtained for the earlier studied systems. At this time many laboratories in the erstwhile Soviet Union attained a special prominence and led to the rapid growth of this branch of science not only in terms of laboratories, but also in terms of research personnel.

At one time, in the erstwhile Soviet Union there were more than 1000 researchers in this field. During the 1960s, an intensive study of the hydrothermal process of synthesis and growth of single crystals which did not have the analogues in nature began. During the 1970s, there was a quest for the search and the growth of hitherto unknown compounds of photo-semiconductors, ferromagnets, lasers, piezo- and ferroelectrics and, in this regard, hydrothermal technology attracted a great attention. Many other nations, including China and India, got into the field of hydrothermal growth of crystals. Several established laboratories in the world began to study systematically various aspects of the hydrothermal growth of crystals such as the physicochemical principles, kinetics, designing new apparatus, growing new compounds, and so on. This marks a significant change in the trend of hydrothermal research. Specific aspects of the hydrothermal method as a modeling tool to understand the natural processes of mineral formation changed dramatically into an important method characteristic for inorganic chemistry. During the early 1980s, a new sealing for the autoclave was designed, that is, *Grey-Loc* sealing, which facilitates the construction of the very large size autoclaves with a volume of 5000 liters.[59] The world's largest autoclave is located in Japan works with such a Grey-Loc sealing mechanism. The details of the sealing mechanism is discussed in Ch. 3.

Towards the end of the 1970s, on the whole, the hydrothermal field experienced a declining trend for two reasons: there was no scope for further work on the growth of large size single crystals of quartz on the one hand, and on the other hand, large scale attempts to grow bigger crystals of other compounds investigated during the 1960s and 1970s failed. It was

PrepBooks

unanimously decided that the hydrothermal technique is not suitable for the growth of large crystals other than quartz. The focus at this time was on Czechrolskii, MOCVD, and MBE. This is largely connected to the general approach of the hydrothermal researchers to grow large single crystals without looking into the hydrothermal solvent chemistry and kinetics of the crystallization process. Although Franck started working on the study of the behavior of electrolytic solutions with temperature and pressure conditions way back in the 1950s,[60][61] it did not attract the hydrothermal researchers' attention immediately. They thought that the conditions under which Franck worked were confined to the lower pressure and temperature conditions, whereas the hydrothermal technique actually belonged to the higher pressure and temperature conditions at least until recently. In fact, Ballman and Laudise, in their famous article published in the book: *Art and Science of Growing Crystals* edited by Gilman, write that "crystal growth is more an art than science."[62] However, the Nobel Symposium organized by the Swedish Academy of Sciences, during September 17–21, 1979, on "The Chemistry and Geochemistry of Solutions at High Temperatures and Pressures" is remembered as an eye opener. The presence of pioneers in the field of hydrothermal physical chemistry like Franck, Seward, Helgeson, Pitzer, and so on, drew the attention of hydrothermal crystal growers and a new trend was set to look into the hydrothermal solvent chemistry and the physical chemistry of the hydrothermal systems.[63]-[66] Following this, Japan organized the first ever International Hydrothermal Symposium during April 1982, which was attended largely by specialists from different branches of science like physical chemistry, inorganic chemistry, solid state physics, materials scientists, organic chemists, hydrometallurgists, hydrothermal engineers, etc.[67] This is the dawn of modern hydrothermal research. Since then, new avenues in the field of hydrothermal research are being explored. The modeling of the hydrothermal systems, study of the hydrothermal crystallization mechanism, thermodynamics and kinetics of the reactions began. New designs of the reactors to suit the specific requirements of research into areas like crystal growth and materials processing were developed. Unfortunately, this period also marks the fall of the Russian domination in the field of hydrothermal research. Japan emerged as a leader in hydrothermal research on par with the US. The decade-wise evolution of the hydrothermal research with regard to its objective and apparatus used is given with appropriate remarks in Table 2.1.

Table 2.1. Evolution of Hydrothermal Technology with Time

Period	Focus	Equipment	Remarks
1850-1900	Mineral synthesis, imitation of natural conditions	Simple reactors, glass reactors, digestors	Lower growth rate, tiny particles, geological interest
1900-1940	Mineral synthesis, improvement in PT conditions, German domination	Morey autoclaves, flat closures	Lower growth rate, silicates, carbonates, Germany, Russia, France, USA, geological interest
1940-1950	Large size and large scale production of quartz, beginning of zeolites, clays, and micas	Test-tube type (cold-cone-sealed), welded closure modified Bridgman type	Cold-cone-seal type autoclaves made revolution, *PVT* diagrams systems
1950-1960	Phase diagrams for natural systems	Morey, Tuttle-Roy, welded closures, modified Bridgman	The dawn of modern hydro-thermal research
1960-1970	Synthesis of technological materials, new inorganic com-pounds without natural analogues	New designs from USSR, commercial-ization of the auto-claves, improved sealing, larger size of the autoclaves	Russian School dominated, Japanese labs appeared

DropBooks

Table 2.1. *(Cont'd.)*

Period	Focus	Equipment	Remarks
1970-1980	A variety of new materials synthesis, ceramic processing in a bigger way, advanced materials	New designs, improved PT conditions, Grey-Loc sealing, Large autoclaves	Appearance of many hydrothermal labs in several countries
1980-1990	Decline in interest on hydrothermal research. Importance of the technique in materials science, physical chemistry of hydrothermal solutions		Japan organized 1st Int. Conf. Hydrothermal Reactions. Beginning of the entry of physical chemists
>1990	Diversification of hydrothermal technique, age of solvo-thermal, physical chemistry of hydrothermal solutions	Design of new reactors to suit the specific applications: batch reactors, flow reactors, and so on.	Entry of organic chemists, environmental scientists, fall in Russian domination and beginning of the Japanese domination

Today, the hydrothermal technique is being applied widely by various specialists from different branches of science including organic chemistry, biochemistry, biotechnology, food and nutrition, environmental safety, and so on, as shown in Fig. 1.9. These developments in hydrothermal research form the main theme of this book.

REFERENCES

1. Habashi, F., (ed.) *A History of Metallurgy, Metallurgic Extractive*, Laval University, Quebec, Canada (1994)
2. Sir Roderick Murchison (1840s) (cited by S. Somiya, ed.), *Hydrothermal Reactions for Materials Science and Engineering*, Elsevier Applied Science, London (1989)
3. Schafthaul, K. F. E., *Gelehrte Anzeigen Bayer. Akad*., 20:557, 561, 569, 575, 593 (1845)
4. Bunsen, R., Bemerkungen Zu Cinigen Einwürten Gegen Mehrere Ansichten über die Chemisch-geologischon Erscheinungen in Island; *Ann.*, 65:70 (1848)
5. Wohler (1948) (cited by Bunsen, R.), *Ann.*, 65:80 (1848)
6. De Senarmont, H., *Ann. Chim. Phys*., 32:142–145 (1851)
7. Daurree, M., Sur le Metamorphisme et Recherches Experimentales sur Quelques-uns, *Ann. Mines*, 12:289–326 (1857)
8. Corliss, J. B., Metallogenesis at Oceanic Spreading Centres, *J. Geol. Soc. Lond.*, 136:621–626 (1979)
9. Corliss, J. B., Hot Springs and the Origin of Life, *Nature*, 347:624–625 (1990)
10. Holm, N. G. and Andersson, E. M., Abiotic Synthesis of Organic Compounds Under the Conditions of Submarine Hydrothermal Systems: A Perspective, *Planet. Space Sci*., 43:153–159 (1995)
11. Lamberg, J., Ueber Silicatumwandlungen, *Z. Deut. Geol. Ges.*, 28:519–621 (1876)
12. Barrer. R. M., Syntheses and Reactions of Mordenite, *J. Chem. Soc.*, 2158 (1948)
13. Deville, St. Claire, De la Pressance du vanadium clous un mineral alumine, *Ann. Chim. Phys*., 61:309–314 (1857)
14. Chroustshoff, K. von., *Ann. Chemist*., 3:281–286 (1873)
15. Meunier, S., Production et Cristallisation d'un Silicate Anhydre (enstatite) en Presence de la Vespeur d'eau á la Pression Ordinaire, *Compt. Rend*., 99:349–351 (1880)
16. Hannay, J. B., On the Artificial Formation of the Diamond, *Proc. Royal Soc. London*, 30:178–189 (1880)
17. Moissan, (cited by Edgar, A. D.), *Experimental Petrology, Basic Principles and Techniques*, p. 5, Clarendon Press, Oxford, U.K. (1973)
18. Friedel, C. and Sarasin, E., *Compt. Rend*, 92:1374–1378 (1881)
19. Chroustshoff, K. von, *Bull, Soc. Min.*, 10:31–36 (1887)
20. Chroustshoff, K. von, *Compt. Rend*., 122:677–679 (1890)

DropBooks

21. Morey, G. W., Hydrothermal Synthesis, *J. Amer. Ceram. Soc*., 36:279–285 (1953)
22. Morey, G. W. and Niggli, P., The Hydrothermal Formation of Silicates, A Review, *J. Am. Chem. Soc*., 35:1086–1130 (1913)
23. De Schulten, A., *Bull. Soc. Min*., 5:7–9 (1882)
24. Ramsay, W. and Hunter, *Rept. Brit. Assn.*, 1882:239–240 (1882)
25. Bruhns, W., Apparatus, A Steel Bomb, Lined with Platinum, *Neues Jahrb, Min. Geol.*, II:62–65 (1889)
26. Doetler, C., Recrystallization of Apophyllite, *Neues Jahrb. Min. Geol*., I:118–139 (1890)
27. Friedel, G., Hydrothermal Synthesis of Corundum, *Bull. Soc. Min*., 14:7–10 (1891)
28. Spezia, G., Sull accresimento del Quarzo, *Atti Accad. Sci. Torino*, 35:95–107 (1900)
29. Spezia, G., La Pressione e' Chimicamente Inattive Nella Solubilite e Riecostituzione del Quarzo, *Atti Accad. Sci. Torino*, 40:254–262 (1904–1905)
30. Barus, C., *Am. J. Sci.*, 6:270 (1898) (cited by Morey, G. W. and Niggli, P.), The Hydrothermal Formation of Silicates – A Review, *J. Am. Chem. Soc*., 35:1086–1130 (1913)
31. Allen, E. T., The Lime-Silica Series of Minerals by Day and Shepherd, *Am. J. Sci*., 22:297 (1906)
32. Tammann, G., *The States of Aggregation*, D. Van Nostrand Company (1925)
33. Demazeau, G., Marbeuf, A., Pouchard, M., and Hagenmuller, P., Sur une Serie de Compose's Oxygenes du Nickel Trivalent Derive's de la Perovskite, *J. Solid State Chem.* 3:582–589 (1971)
34. Bowen, N. L., The Behavior of Inclusions in Igneous Magmas, *J. Geol*., 30:513 (1922)
35. Morey, G. W., Neue Kristallisierte Silikate von Kalium und Natrium. Darstellung und Allgemeine Eigenschaften, *Z. Anorg. Chem*., 86:305–324 (1914)
36. Smyth, F. H., and Adams, The System Calcium-oxide Carbon-dioxide, *J. Amer. Chem. Soc*., 45:1172 (1923)
37. Goranson, R. W., Solubility of Water in Granite Magmas, *Amer. J. Sci.*, 22:481–502 (1931)
38. Bayer, K. J., (1887) (cited by Habashi, F.) *A Text book of Hydrometallurgy*, p. 10, Libraire Universitaire du Quebec, Canada (1993)

39. Katsurai (1926) (cited by S. Somiya, ed.) *Hydrothermal Reactions for Materials Science and Engineering,* Elsevier Applied Science, London (1989)
40. Nagai, S., (1931) (cited by S. Somiya ed.) *Hydrothermal Reactions for Materials Science and Engineering,* Elsevier Applied Science, London (1989)
41. Ellis, A. J., and Fyfe, W. S., Hydrothermal Chemistry, *Rev. Pure Appl. Chem.,* 7:261–316 (1957)
42. Morey, G. W. and Fenner, C. N., The Ternary System H_2O-K_2SiO_3-SiO_2, *J. Amer. Chem. Soc.,* 39:1173–1229 (1917)
43. Van Nieuwenburg, C. J. and Blumendahl, H. B., Isotherms of water from 350 to 480 and for pressures up to 600 kg/cm^2, *Rec. Trav. Chim.*, 51:707–714 (1932)
44. Keenan, J. H. and Keyes, F. G., *Thermodynamic Properties of Steam*, John Wiley and Sons (1936)
45. Kennedy, G. C., PVT Relations in Water at Elevated Temperatures and Pressures, *Amer. J. Sci.,* 248:540–564 (1950)
46. Nacken, R. Artificial Quartz Crystals, etc., U.S. Office of Technical Services Report PB-6948 (1946)
47. Nassau, K., Synthetic Emerald: The Confusing History and the Current Technologies, *J. Crystal Growth,* 35:211–222 (1976)
48. Nacken, R., Artificial Quartz Crystals, etc., U.S. Office of Technical Services Reports PB-18,748 and 28,897 (1946)
49. Nacken, R., Hydrothermal Synthese als Grundlage fur Zuchtung Von Quarz-Kristallen, *Chem. Z.,* 74:745–749 (1950)
50. Tuttle, O. F., A New Hydrothermal Quenching Apparatus, *Amer. J. Sci.,* 246:628–635 (1948)
51. Roy, R., Fifty-year Perspective on Hydrothermal Research, in: *Proc. Workshop on Solvothermal and Hydrothermal Reactions.,* pp. 1.1–1.20, Sun Messe Kogawa (Jan. 22–24, 1996)
52. Kennedy, G. C., A Portion of the System Silica-Water, *Econ. Geol.,* 45:629–623 (1950)
53. Morey, G. W. and Hesselgesser, J. M., The Solubility of Some Minerals in Superheated Steam at High Pressure, *Econ. Geol.,* 46:821–835 (1951)
54. Tuttle, O. F. and England, J. L., A Preliminary Report on the System SiO_2-H_2O., *Bull. Geol. Soc. Amer.,* 66:149–152 (1955)
55. Roy, D. M., and Roy, R., Synthesis and Stability of Minerals in the System MgO-Al_2O_3-SiO_2-H_2O, *Amer. Min*., 40:147–178 (1955)
56. Taki, S., Improvement of Growth Process and Characterization of Quartz Crystals, *Prog. Crystal Growth Charact.,* 23:313–339 (1991)

DropBooks

57. Walker, A. C., Hydrothermal Synthesis of Quartz Crystals, *Ind. Eng. Chem.*, 36:250–256 (1953)

58. Laudise, R. A., Personal Communication (1992)

59. Asahara, J., Nagai, K., and Harada, S., Synthetic Quartz Crystals by Large Autoclaves, in: *Proc. 1st Int. Symp. Hydrothermal Reactions* (S. Somiya, ed.), pp. 430–441, Gakujutsu Bunken Fukyu – Kai, Jpn (March 22–26, 1982)

60. Franck, E. U., Hochverdichteter Wasserdampf I. Ele - Ktrolyticshe Leitfahigkeit in KCl-H_2O Losungen bis 750°C, *Zeit. Physik. Chem.*, 8:92–106 (1956)

61. Franck, E. U., Experimental Investigation of Fluids at High Pressures and Elevated Temperatures, North American Treaty Organization (NATO) Advanced Study Institute, Series C, C41 (High Pressure Chemistry) (1978)

62. Ballman, A. A. and Laudise, R. A., Solution Growth, in: *Art and Science of Growing Crystals* (J. J. Gilman, ed.), p. 231, Wiley, New York (1963)

63. Franck, E. U., Survey of Selected Non-Thermodynamic Properties and Chemical Phenomena of Fluids and Fluids Mixtures, in: *Chemistry and Geochemistry of Solutions at High Temperatures and Pressures,* (D. T. Rickard and F. E. Wickman, eds.)*Proc. Noble Symp.,* 13/14:65–88, Pergamon Press, New York (Sept. 1979)

64. Seward, T. M., Metal Complex Formation in Aqueous Solutions at Elevated Temperatures and Pressures, in: *Chemistry and Geochemistry of Solutions at High Temperatures and Pressures* (D. T. Rickard and F. E. Wickman, eds.),*Proc. Noble Symp.*, 13/14:113–132, Pergamon Press, New York (Sept. 1979)

65. Helgeson, H. C., Prediction of The Thermodynamic Properties of Electrolytes at High Pressures and Temperatures, in: *Chemistry and Geochemistry of Solutions at High Temperatures and Pressures* (D. T. Rickard and F. E. Wickman, eds.) *Proc. Noble Symp.*, 13/14:133–178, Pergamon Press, New York (Sept. 1979)

66. Pitzer, K. S., Characteristics of Very Concentrated Aqueous Solutions, in: *Chemistry and Geochemistry of Solutions at High Temperatures and Pressures* (D. T. Rickard and F. E. Wickman, eds.), *Proc. Noble Symp.*, 13/14:249–272, Pergamon Press, New York (Sept. 1979)

67. *Proc. 1st Int. Symp. Hydrothermal Reactions* (S. Somiya, ed.), Gakujutsu Bunken Fukyu-Kai, Jpn (March 22–26, 1982)

3

Apparatus

3.1 INTRODUCTION

Advances in any scientific field of research depend largely on the equipment available. Crystal growth or materials processing under hydrothermal conditions requires a pressure vessel capable of containing highly corrosive solvent at high temperature and pressure. Experimental investigations under hydrothermal conditions require facilities that must operate routinely and reliably under extreme pressure-temperature conditions. Thus, the experimenter has to face a variety of difficulties, and often, peculiar problems pertaining to the design, procedure, and analysis.

DropBooks

Designing a suitable or ideal hydrothermal apparatus, popularly known as an autoclave, is the most difficult task, and perhaps impossible to define, because each project has different objectives and tolerances. In Ch. 2, we describe the historical development of hydrothermal technology closely associated with the development of the instrumentation. If we look into the historical development in the design and fabrication of autoclaves, the entire activity was concentrated in Europe alone during the 19th century. It was only after the American industrial revolution that activity slowly started spreading into the other parts of the world. Here, we discuss only the autoclaves or hydrothermal reactors used worldwide; they were all developed during the 20th century. There is a great variety of apparatus existing in hydrothermal technology. Most of the earlier workers had dealt with this aspect in their own way. Hence, we have made a thorough survey

of all the available literature and present it here in this section in a simple way to make the reader understand easily the problems of designing, fabrication, and maintenance.

The literature survey clearly indicates two schools of autoclave design: *1)* Western school and *2)* Russian school. The former is very important as it dominates most of the earliest designs and these later became the standard designs throughout the world. Most of these designs are relatively simple and quite old (designed prior to the 1970s), whereas, the Russian school had dominated this field from the 1970s and came out with many new designs. The Special Construction Bureau at the Institute of Crystallography, Academy of Sciences, Moscow, Russian Federation, has designed several new autoclaves to suit a specific task of either growing single crystals or studying physicochemical aspects such as solubility, PVT-behavior, and so on. Besides, several erstwhile Soviet hydrothermal laboratories have produced their own designs to suit their requirements and the type of crystal or material under investigation. Obviously, most of these autoclaves are only local and have not been adopted worldwide. Hence, for the benefit of the reader, we consider only the standard autoclaves used worldwide and some important designs from the Russian school. With the disintegration of the erstwhile Soviet Union, there is not much development in the field of design and fabrication of new autoclaves. The Japanese groups are coming out with new designs of autoclaves for applications in crystal growth and materials processing.

An ideal hydrothermal autoclave should have the following characteristics:

i. Inertness to acids, bases and oxidizing agents.

ii. Easy to assemble and dissemble.

iii. A sufficient length to obtain a desired temperature gradient.

iv. Leak-proof with unlimited capabilities to the required temperature and pressure.

v. Rugged enough to bear high pressure and temperature experiments for long duration, so that no machining or treatment is needed after each experimental run.

The most commonly used autoclaves in hydrothermal research are listed in Table 3.1.[1] The majority of these autoclaves are externally heated pressure vessels and their pressure-temperature range can not be

extended further due to lack of suitable refractory alloys. However, internally heated pressure vessels are now commercially available up to 10 kbar and 1400°C. The list given in the table does not include some of the recent designs and modifications or upgrades as their applications are restricted to specific studies.

Table 3.1. Autoclaves

Type	Characteristic data
Pyrex tube 5 mm i.d. 2 mm wall thickness	6 bar at 250°C
Quartz tube 5 mm i.d. 2 mm wall thickness	6 bar at 300°C
Flat plate seal, Morey type	400 bar at 400°C
Welded Walker-Buehler closure 2600 bar at 350°C	2 kbar at 480°C
Delta ring, unsupported area	2.3 kbar at 400°C
Modified Bridgman, unsupported area	3.7 kbar at 500°C
Full Bridgman, Unsupported area	3.7 kbar at 750°C
Cold-cone seal, Tuttle-Roy type	5 kbar at 750°C
Piston cylinder	40 kbar, 1000°C
Belt apparatus	100 kbar, > 1500°C
Opposed anvil	200 kbar, > 1500°C
Opposed diamond anvil	up to 500 kbar, >2000°C

DropBooks

3.2 SELECTION OF AUTOCLAVE AND AUTOCLAVE MATERIALS

When selecting a suitable autoclave, the first and foremost parameter is the experimental temperature and pressure conditions and the corrosion resistance in that pressure-temperature range in a given solvent or hydrothermal fluid. If the reaction is taking place directly in the vessel, the corrosion resistance is, of course, a prime factor in the choice of autoclave material. The most successful materials are corrosion resistant, high-strength alloys, such as 300 series (austenitic) stainless steel, iron, nickel, cobalt-based superalloys, and titanium and its alloys. Several workers have reviewed the properties of some alloys used commonly in the making of hydrothermal autoclaves.[2][3] Tables 3.2, 3.3, and 3.4 give

certain properties of these alloys. The critical property for a material used in a hydrothermal autoclave is its creep-rupture strength, a measure of the length of time until rupture of a stressed material occurs at a given temperature. Similarly, the ultimate tensile strength and yield strength are to be taken into account. In the 300 series of stainless steels, 316 has the greatest creep-rupture strength. The super alloys are usually much stronger than SS 316, even at higher temperatures. Pure titanium metal, though acid resistant, is weak and difficult to handle, but some of the titanium alloys have strengths comparable to stainless steels. Pure titanium, because of its superior corrosion resistance, can be used as an autoclave up to about 300°C or more. Its relatively low creep-strength becomes inadequate. For example, after 36 hrs at 300°C in 0.5 M HCl + 1.5 M NaCl mineralizer, titanium was slightly corroded/tarnished, but was distinctly corroded in 6 M HCl at 300°C. It is soluble even at room temperature in phosphoric acid, and is moderately resistant to acidic sulfate solutions.[4] Extra strength for alloys is required because the actual strengths of alloys under normal operating conditions are less than their strengths under ideal conditions owing to various corrosion processes that occur during hydrothermal reactions as well as to structural changes due to partial annealing of the alloy during conditions of prolonged high-temperature service. This is further complicated by the geometry of the vessel, because the effective stress is more intense in areas of high curvature. In addition, it is noted that the creep-rupture strengths decrease significantly with increasing temperature, thereby lowering the maximum permissible pressure of an experiment at higher temperature.

Alloys of either stainless steel or titanium have a tendency to form an impermeable oxide surface, which prevents continued oxidation. Thus, the corrosion resistance of an alloy depends upon the permeability, reactivity, and solubility of this oxide layer in the corrosive fluid. Obviously, a layer so permeable that solutions can penetrate and contact the unoxidized metal can react with the underlying metal. The corrosion can be crevice corrosion, stress corrosion cracking, and intergranular attack. The crevice corrosion can be prevented through proper agitation of the vessel, and polishing of the interior surface.

Intergranular corrosion can be prevented through the use of low-carbon stainless steel, or by alloying with small amounts of metals forming very stable carbides. Stress corrosion can be retarded through proper annealing of the alloy used for making autoclaves, and through the use of molybdenum containing austenitic steels.[3]

Table 3.2. Properties of Certain Alloys.[2] *(Courtesy of the Academic Press, Orlando, Florida.)*

	Resistance to aqueous OH	Rupture stress (atm) 1000 h, 800°C	Rupture stress (atm) 1000 h, 600°C
Low carbon steel	+		170
Tool steel	+		
4140 (similar to EN19)	+		170
Stainless type 340	—	270	1100
19-9-DL	?	680	2200
(Universal Cyclops Steel Co.)			
Croloy 15-15N	+	610	2260
Timken 17-22-A	+	-	-
Inconel X	?	1200	4500
Stellite	?	-	-
Udimet 500	?	2100	-
Silver	+ [b]		
Platinum	+ [b]		
Platinum-10% irridium	+ [b]		

Source: Data from Clauss (1969)

[a] Cr and Ni values in stainless steels are values < 2 wt %.

[b] Denotes the balance of metal in the alloy.

[c] A product of Allegheny Ludlum Steel Corporation, Pittsburgh, Pennsylvania.

[d] A product of Inco Alloys International, Inc., Huntington, West Virginia.

[e] A product of Cabot Corporation, Kokomo, Indiana.

DropBooks

Table 3.3. Compositions of High-Strength Alloys for Autoclaves

	Metal Content (wt %)												
	Cr	Ni	C	Mn	Mo	Si	Co	V	Al	Ti	Fe	Others	Note
Stainless Steel [a]													
304	19	9	0.1	2	-	1	-	-	-	-	ba[b]		
310	25	20	0.2	2	-	1	-	-	-	-	ba		
316	17	12	0.1	2	3	1	-	-	-	-	ba		
410	12	-	0.2	1	-	1	-	-	-	-	ba		
Titanium													
RMI-55	Commercially pure titanium												Alpha
Ti 6-4	—	—	0.1	—	—	—	—	4	6	ba	0.25		Alpha-beta phase
Ti 38644	6	—	0.05	—	4	—	—	8	3	ba	0.03	Zr-4	Beta phase
Ti 17	4	—	—	—	4	—	—	—	5	ba	—	Zr-2, Sn-2	Alpha-beta
Superalloys													
A-286	15	25	0.1	2	1	1	—	0.2	0.4	2	ba		Iron base
Waspalloy[c]	19	ba	0.1	1	4	0.7	13	—	1	3	2	Cu-0.5	Nickel base
Inconcl 702[d]	16	ba	0.1	1	—	0.7	—	—	3	0.5	2	Cu-0.5	Nickel base
Hastelloy B[e]	1.0	ba	0.05	1	28	1	2.5	0.4	—	—	5	—	Nickel base
Hastelloy C[e]	16	ba	0.1	1	16	1	2.5	0.4	—	—	5	W – 4	Nickel base
HS – 21	27	3	0.3	1	5	1	ba	—	—	—	2		Co base (stellite)

Source: Data from Clauss (1969)

[a] Cr and Ni values in stainless steels are values < 2 wt %.

[b] Denotes the balance of metal in the alloy.

[c] A product of Allegheny Ludlum Steel Corporation, Pittsburgh, Pennsylvania.

[d] A product of Inco Alloys International, Inc., Huntington, West Virginia.

[e] A product of Cabot Corporation, Kokomo, Indiana.

Table 3.4. High-Temperature Strength Properties of Autoclave Alloys[a]

Melt	Tensile Strength (°C)			Yield Strength (°C)			Creep Rupture Strength (hr)		Creep Strength (hr)		Thermal Expansion ($\times 10^6$)
	25	400	600	25	400	600	1,000	10,000	1,000	10,000	
Stainless Steels											
304	85	66	49	38	21	16	49	38	24	18	14
310	92	81	71	40	29	24	39	36	23	14	16
316	85	72	66	38	24	21	66	64	31	19	16
410	89	72	34	32	22	13	34	26	29	14	11
Carbon Steel											
0.3% C	64	57	25	36	25	16	19	12	—	10	12
Superalloys											
A-286	143	-	103	94	-	88	88	76	—	81	—
Waspalloy	180	-	170	115	-	100	85[b]	—	—	—	—
Inconel	141	-	105	85	-	75	65[c]	—	—	—	—
Hastelloy C	121	-	98	58	-	43	55[d]	—	—	—	—
HS-21	101	-	73	82	-	39	60[e]	—	—	—	—
Titanium Alloys											
RMI-55	65	30	20	55	18	10	20[f]	—	—	—	8
Ti 6-4	130	90	60	120	70	55	50	30	30	20	8
Ti 38644	170	150	120	160	130	90	140[g]	—	100	—	5
Ti 17[h]	—	—	—	(150–170)			—	—	—	—	—

DropBooks

Source: Data from Clauss (1969)

[a] Strength in 100 pounds per square inch (kpsi), yield strength is for 0.2 elongation, creep strength is for 1% elongation unless otherwise noted.

[b-c] For 1000 hr at 650°C.

[f] For 100 hr at 450°C.

[g] For 100 hr at 350°C and 0.2% elongation.

[h] Data from RMI Company, Niles, Ohio.

The hydrothermal experimenter should pay special attention to the systems containing hydrogen under hydrothermal conditions. Hydrogen at high temperature and/or pressures can have a disastrous effect on alloys used in the making of autoclaves. It reduces the strength of the autoclaves through any one of the following processes: hydrogen embrittlement, irreversible hydrogen damage, or metal-hydride formation. These problems could be overcome through careful selection of alloys containing small additives such as Ti, Mo, V, heating in H_2 free atmosphere, and using alloys with low thermodynamic activity.

The autoclave selection is usually done by considering the above discussed aspects accordingly, for the type of material or compound under investigation, the medium in which the reaction is taking place, and the experimental pressure-temperature conditions. Some crystals can be grown readily within the autoclave without any lining, liners, or cans. For example, the growth of quartz can be carried out in low carbon steel autoclaves. The low carbon steel is corrosion resistant in systems containing silica and NaOH, because, the relatively insoluble NaFe-silicate forms and protectively coats the ground vessel. In contrast, the growth of berlinite crystals requires a teflon lining or beakers because phosphorus is highly corrosive; it can even corrode platinum if used for a long time. Therefore, the corrosion resistance of any metal under hydrothermal condition is very important. For example, turbine engineers have long known that boiler water with pH > 7 is less corrosive than slightly acidic water, especially for alloys containing Si. Several conventional methods of studying corrosion are known. Usually low carbon steel is used in the fabrication of simple acid digestion bombs, Morey autoclaves, modified Bridgman autoclaves, and other related ones. Inconel, Udimet and Stellite are highly useful because of their high strength at high temperature. These alloys are used in the fabrication of cold cone-seal bombs employed in phase equilibria studies at pressures up to 5.4 kbar and temperatures up to 950°C. The recent TZM autoclaves are used at pressures up to 10 kbar.

Although the use of glass vessels began in the19th century, for low temperature and low pressure experiments thick glass vessels are still used. The quartz glass pressure vessel for hydrothermal studies was first used in 1964 by Speed and Filice (1964).[5] Recently, in 1991, Popolitov used a thick walled silica vessel with a teflon capping for experiments up to 200°C and < 500 bar pressure.[6] The construction details of various autoclaves will be given separately in the forthcoming section.

3.3 LINERS

In the majority of hydrothermal experiments, the mineralizer used is highly corrosive and it can attack the vessel, which is inimical to obtaining high purity crystals for devices. It requires a suitable lining for the inner wall of the autoclave or separate liners placed in the autoclave. Even in the case of quartz growth, where an acmite protective layer is found all along the inner wall of the autoclave, the purity of the substance is doubtful. Therefore, for the growth of high purity quartz, a silver lining for the autoclave is provided. Similarly, other metal linings are provided depending upon the solvent medium. For example, a copper lining is used in many of the borate systems. Copper partly dissolves in dilute bases at 400°C and copper crystals are deposited in the cooler region of the autoclave. Similarly, nickel lining can be used, but it is also readily attacked by the solvent. Hence, noble metal lining, liners, or capsules are used successfully for alkaline and neutral media. Titanium is much more corrosion resistant, but it is difficult to handle. Litvin and Tules (1971) have summarized the applicability of various liners[7] listed in Table 3.5.

The use of glass tube as a liner was first applied by De Senarmont as early as AD 1851 for the growth of carbonates, sulphates, and sulphides. Figure 3.1 shows the sealed glass tube used by De Senarmont.[8] The tubes were enclosed in water-filled fused gun barrels and heated up.

DropBooks

Daurree (1857) first introduced the pressure balance arrangement between the small glass tube containing the nutrient and the steel tube hosting this glass tube liner.[9] An improved version using pyrex glass and again water as a pressure transmitter was reported by Allen et al. (1912).[10] In fact, most of the earlier workers during the19th century, including von Chroustshoff, found that the glass tube they were using was much attacked under hydrothermal conditions, however, they did not mention anything about precautions taken to over come this effect, as the primary interest was only in synthesizing a product resembling some natural mineral. It was von Chroustshoff who first proposed the gold lining steel autoclaves to prevent corrosion. By doing so, he could attain a temperature of 350°C to synthesize tridymite phase of quartz and increased experimental duration. Subsequently, the use of steel autoclave and noble metal lining became very popular, and the tendency to reach higher pressure-temperature conditions also started. Bruhns (1889) used steel bombs with platinum lining and cover held down by bolts and made tight by means of a copper washer, which was protected from the action of the mineralizer by platinum.[11]

Table 3.5. Materials Used as Reactor Linings

Material	T (°C)	Solutions	Remarks
Titanium	550	chlorides hydroxides sulphates sulphides	Corrosion in NaOH solution > 25% in NH_4Cl solution > 10% (at 400°C)
Armco iron	450	hydroxides	Gradual oxidation producing magnetite
Silver	600	hydroxides	Gradual recrystallization and embrittlement, partial dissolution
Platinum	700	hydroxides chlorides sulphates	Blackening in chlorides in the presence of sulpher ions; partial dissolution in hydroxides
Teflon	300	chlorides hydroxides	Poor thermal conduction
Tantalum	500	chlorides	Begin to corrode in NH_4Cl solution 78%
Pyrex	300	chlorides	
Copper	450	hydroxides	Corrosion reduced in the presence of fluoride ions and organic compounds
Graphite	450	sulphates	Pyrolytic graphite most suitable for linings
Nickel	300	hydroxides	
Quartz	300	chlorides	
Gold	700	hydroxides sulphates	Partial dissolution in hydroxides

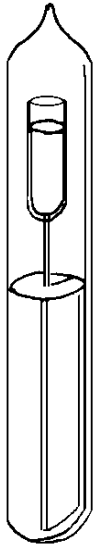

Figure 3.1. Sealed glass tube used by De Senarmont.[8]

DropBooks

Doetler (1890) used a nickeled gun barrel or a silver lined steel tube in his experiments.[12] The quartz glass tube liners of 15 mm-diameter can easily withstand the outside pressure of 3 kbar at 500°C. However, the internal pressure has to be kept a little below than that of the outside value. Rabenau and Rau (1973) have described this technique in detail.[13] For larger autoclaves, like the Morey flat and the modified Bridgman closures, noble metal, or other suitable metal lining is provided. The main difficulty in such a design is that the lining should be free of cracks, pinholes or ridges and it should be honed near to mirror finish. For Tuttle cold-cone seal autoclaves, capsules made of noble metals are used. The capsule tube charged with a desired amount of nutrient is clamped tightly at the top and is welded shut. During the experiment the capsule collapses but does not rupture. The vessel is then heated to the desired temperature at constant pressure. When the desired temperature is reached, the capsule expands to its original volume and is not subjected to tension and virtually no capsule failures occur. For some experiments, the capsule needs only to be pressed together, the capsule length being shorter for phase equilibria studies and longer where a temperature gradient for crystal growth is desired. In large diameter vessels, platinum liners are usually used. These liners have silver

caps to avoid platinum seizing. The liner is filled to a given percent and closed, and the space between the liner and the inner wall of the autoclave is filled to the same percent or slightly higher; this provides a pressure balance and the liner supports virtually no pressure. Pressure imbalance can cause rupture of the liner. For the growth of high purity crystals in solution in highly corrosive media, teflon beakers or liners are used. Similarly for special studies pertaining to reaction kinetics, solubility and materials processing under mild hydrothermal conditions or pressure-temperature conditions below 250 bars and 300°C, teflon is the most popularly used lining material. Several new autoclave designs with teflon lining or coating for such studies have been reported in literature. The teflon liner or beaker should sit exactly inside the autoclave without leaving any gap, pressure balancing technique can be used alternatively. A slightly higher pressure of nearly 1 to 2 percent of fill outside the teflon liner helps in the sealing of teflon liners as the cap and liner can not be welded. In addition, in some cases where the experiment is carried out for longer duration, effective sealing of the teflon liner can be obtained with a sharp ring-like mechanism on the liner as shown in Fig. 3.2. As the temperature rises, the teflon expands and hermitic sealing can be obtained. The greatest disadvantage with liners or cans is the difficulty associated with measuring of the actual temperature inside. Certainly temperature gradients are appreciably lower in the liners than in the autoclaves without liner. This difference becomes more prominent when teflon liners are used. The greatest disadvantages of teflon lining is that beyond 300°C, it can not be used because teflon dissociates, affecting the pH of unbuffered, near-neutral solutions.[14] This coating tends to tear and generally must be reapplied after one or two experiments. Despite all these difficulties, single crystal growth and materials processing using teflon are being carried out extensively at various laboratories.

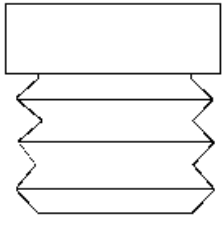

Figure 3.2. Sealing of the teflon liner.

Corrosion resistance can easily be improved at modest cost by coating the interior of the reaction vessels by painting, electroplating, or vapor deposition. As mentioned earlier, chromium and gold linings are often applied to stainless steel vessels to retard corrosion. Such linings are not permanent because of the intrinsic permeability of the thin linings along crystal boundaries or cracks that develop during temperature cycling owing to the differing thermal expansion of the lining and the vessel. When more acidic solutions are used, most of the alloys corrode readily and they must be provided with titanium lining, and high-strength titanium alloys, coated alloys, or other alternatives

Let us consider briefly the internal arrangement of liners in some typical hydrothermal crystal growth experiments. In the growth of quartz crystals, the liner has an assembly shown in Fig. 3.3.[15] The lower portion of the liner is filled with the required nutrient material. In the upper portion, a seed holder is placed and this is the growth zone (cooler zone). In between the growth zone and nutrient zone, a baffle having a definite percent of opening is placed at an appropriate position. The positioning of the baffle and the percent of opening together play an important role in the growth kinetics. This is the most popular liner assembly in hydrothermal crystal growth. In contrast to this, in the hydrothermal growth of berlinite, the internal assembly of the liner differs from that of quartz and is shown in Fig. 3.4. The liner material is usually teflon. As berlinite has a negative temperature coefficient of solubility, the nutrient material is placed in the upper portion (cooler zone) and the seed holder is placed at the lower portion (hotter zone). In between the two zones, a baffle with a desired percent of opening is placed in addition to the vertical positioning of these liners. There are several modifications, especially in the horizontally mounted autoclaves. Jumas, et al. (1985) proposed the liner internal assembly shown in Fig. 3.5[16] for the composite gradient method of growing berlinite crystals.

Ashby et al. (1970) proposed a variable-volume silver liner for high pressure hydrothermal crystal growth. The schematic diagram of the variable-volume silver liner is shown in Fig. 3.6.[17] Here, silver bellows segments are formed from dead-soft cup stock by hydraulic pressure applied internally. As the tube expands outward into a die, it is folded longitudinally. The intrinsic advantage of these liner lies in the fact that the percent fill in the liner may be adjusted without opening the liner. Thus, in practice the liner is charged with nutrient, a seed, and crystal growing medium. Such silver liners have been used by Ashby et al., successfully,

BrownBooks

hundreds of times up to 400°C for the hydrothermal growth of crystals. The authors also propose that a wide variety of metals including platinum and gold (liners) can be formed into bellows. Hence, internal assembly of the liner and the lining material are very important in crystal growth and materials processing.

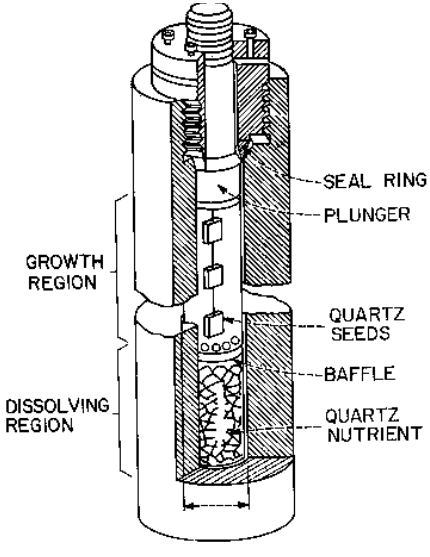

Figure 3.3. Growth of quartz crystals in the liner.[15] *(Courtesy of R. A. Laudise.)*

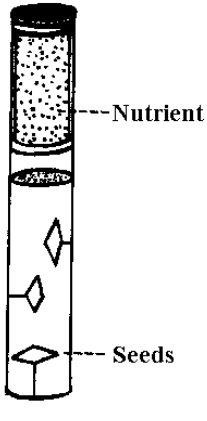

Figure 3.4. Hydrothermal growth of berlinite.

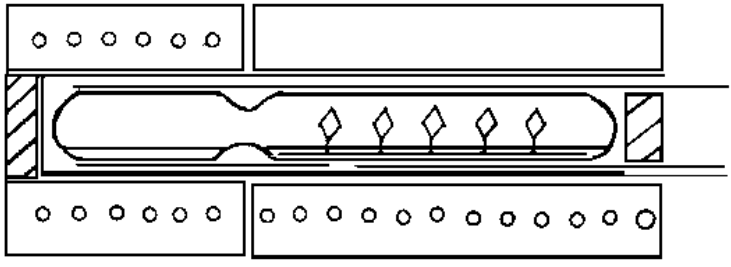

Figure 3.5. Liner internal assembly.[16]

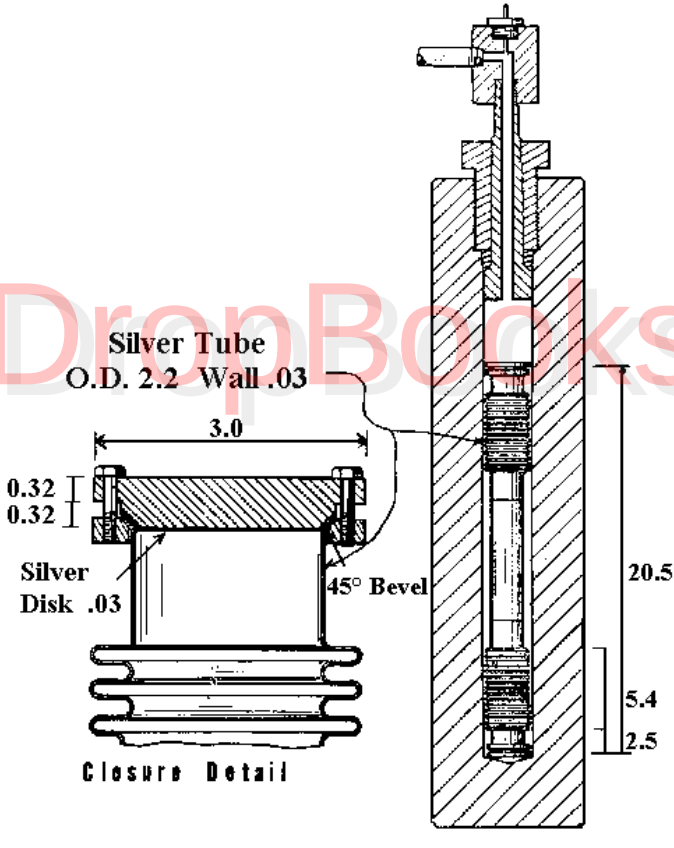

DropBooks

Figure 3.6. The schematic diagram of a high pressure autoclave with a variable-volume silver liner.[17]

3.4 TEMPERATURE AND PRESSURE MEASUREMENTS

Several modern electronic controllers are commercially available today to regulate temperature and pressure in hydrothermal experiments. Pressure vessels heated externally can be placed in a suitable isothermal zone or multiple heating zone furnaces controlled by thyristor-based controllers. Highly sophisticated temperature programmers-controllers are commercially available for programming the experimental temperature, temperature gradient, heating and cooling rates, etc. A variety of alloys are used for furnace windings to reach the desired temperatures in the hydrothermal range. The most common are nichrome and Kanthal. These are more durable and are less subject to damage if sheathed in magnesia insulation plus inconel or similar high-temperature alloys. The ratio of maximum voltage over the required amperage equals the necessary resistance of the furnace winding. The necessary resistance divided by the length of the winding provides the unit length with which the furnace should be constructed. Tables of resistance per unit length with for each of the available commercial heater wires are often supplied by the manufacturer. To control temperature gradients in the reaction vessel, the windings should be more closely spaced near the ends of the furnace, especially the end where more pressure tubing is connected to compensate for the higher heating fluxes from these areas.

The temperatures in hydrothermal experiments are measured using suitable thermocouples that are classified according to the pair of metals, as noble metal thermocouples, and base metal thermocouples. They are made of chromel and alumel or platinum and rhodium alloys owing to their stability and resistance to oxidation throughout the hydrothermal temperature range. Table 3.6 gives the list of some commonly used thermocouple wires and their temperature ranges.[18] Thermocouples are best inserted into holes drilled into the walls at both ends of the vessel to allow temperature gradients in the vessel to be monitored. Such external temperature measurements should be calibrated by inserting a thermocouple directly into a closed-bottom, hollow tube extending into the vessel. The thermocouple calibration is accomplished by measuring the elements at the melting points of reference materials. Table 3.7 shows the melting points of standards used for thermocouple calibration.[19]

Table 3.6. Some Common Thermocouple Wires and Their Temperature Ranges*

Wires	Temperature range (°C)	Maximum temperature (°C)
Chromel-Alumel (90% Ni-10% Cr) (95% Ni, 5% Al, SiMn)	-200 to 1200	1350
Pt-$Pt_{90}Rh_{10}$ Pt-$Pt_{87}Rh_{13}$ Pt-$Pt_{80}Rh_{20}$	0 to 1450	1700
Copper-Constantan (60 – 45% Cu, 40 – 55% Ni)	-200 to 350	600
Iron-Constantan	-200 to 750	1000

* Roeser, W.F., in: Temperature. Its measurement and Control in Science and Industry, p.180, Reinhold, New York (1941).

DropBooks

Table 3.7. Some Melting Point Standards for Thermocouple Calibration[a]

Material	Temperautre (°C)
Tin	231.9
Lead	327.4
Antimony	630.5
Sodium chloride	801.0
Silver[b]	960.8

[a] From Charles and Vidale. 1982.

[b] Calibration strongly impaired by minor amounts of dissolved oxygen.

A computer can be used to record the experimental temperatures uninterruptedly, and it requires an analogue-to-digital converter (ADC) to transform the thermocouple millivolt signal to a digital signal to be

processed and displayed by the computer. With a rack type system of 10–20 vessels, such a system can record run temperatures, in 1 second, of each vessel several times.

The pressure in hydrothermal experiments is measured by different means. In the initial experiments in a given system, standard calibrated bourdon gauges are used and are recalibrated at regular intervals against either a dead weight tester or master gauge. Pressure inside a vessel can be monitored through a pressure transducer to separate the corrosive contents of the vessel from the pressure gauge. It is useful to have a valve between the vessel and the transducer to act as a micropressure generator to check for hysteresis in the transducer and to isolate the vessel during evacuation at the start of the run. A stainless steel or titanium capillary tube is used for the connection with the pressure gauge because of its easy installation and the small volume of trapped fluid that it contains. For routine pressure measurements, Kennedy's PVT diagram and Bain's PVT data are used because of their simple procedure.[20][21] Whether heating or cooling, identical pressure values should be observed, and differences of a few tenths of a bar indicate either hysteresis in the pressure transducer, or that a gas consuming or evolving reaction is taking place. Automatic pressure controllers and recorders are also available commercially. For example, in the Tuttle cold-cone seal autoclaves unit (Tempress, Leco Corp. USA, Fig. 3.7 *a* and *b*), the required pressure is fixed in the gauge which will maintain the pressure at that level for fairly a long duration. However, pressure measurements with a temperature gradient have not been studied in detail, but it is certain that, under hydrothermal conditions, there can be no pressure gradient. Hence, the local temperature and local density anywhere in the system would determine the pressure of the entire system. With a computer, the experimental pressures can be continuously monitored by the EMF signal of a pressure transducer (i.e., strain gauge or manganin cell).

In addition to monitoring pressure and temperature, computers offer the potential to control run conditions. As an example, the computer could check the millivoltage signal from the thermocouple of each vessel and compare the signal to that of the desired temperature. The control action could be provided through on/off relays controlling power to the furnaces. Thus the computers can make the recording and controlling more handy in hydrothermal experiments in a rack like system.

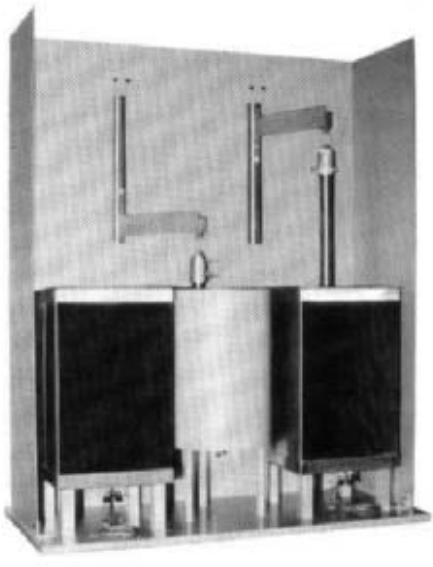

(a)

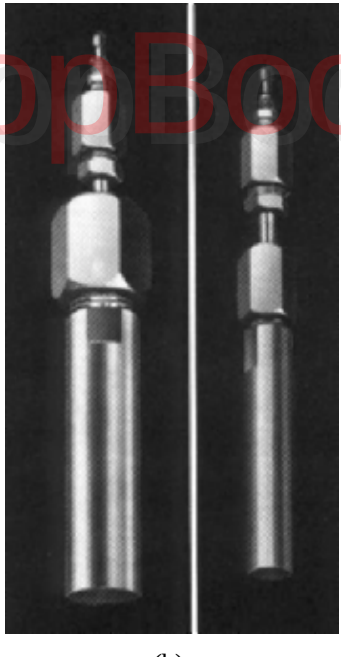

(b)

DropBooks

Figure 3.7 The Tuttle cone seal autoclave (*a* and *b*).

3.5 AUTOCLAVES AND AUTOCLAVE DESIGNS

This forms the most important aspect of hydrothermal research. The advances in the hydrothermal research go in parallel with the autoclave design. The earliest autoclaves were very simple in design and generally made up of glass; the availability of suitable metals and alloys was limited. Besides, the main objective was to synthesize some compound that resembled some natural mineral. Thus, the pressure-temperature range was rather low. It was only after the first successful application of stainless steel as the autoclave material[9] that the design and fabrication of autoclaves for higher pressure-temperature limits was actually initiated. Such efforts resulted in the attempts to grow diamond and corundam crystals during the1870s.[22][23] The actual impetus for the design of new autoclaves came during the 1940s with the development/discovery of several new alloys. The complexity in the designing of the autoclaves also began. Further, during the 1970s, the designing of autoclaves (using a suitable alloy) for specific purposes like the study of kinetics, solubility, direct or visual observation of the hydrothermal reactions, and so on began. With the entry of scientists from different branches of science into hydrothermal research, the diversity and adaptability of hydrothermal research began to make it a more interdisciplinary science than just the study of mineral or phase equilibria and crystal growth. The materials processing under hydrothermal conditions got a new impetus. All these developments resulted in the designing of a large number of new autoclaves, which are together grouped under novel designs. Byrappa (1994) has reviewed various autoclave designs in detail.[24] Here, it is extremely difficult to discuss the development of each and every autoclave design, as the number exceeds 100. However, a majority of them are only to suit a specific aspect of hydrothermal research and hence are not versatile. Therefore, for the sake of simplicity, we have discussed only the more universal autoclave designs under the two broad classes: *1)* conventional autoclave designs, and *2)* novel autoclave designs.

3.5.1 Conventional Autoclave Designs

These are the more universal designs commercially available for general hydrothermal research. The designing of the conventional autoclaves began in mid 19th century, and simple glass vessels were the earliest members of this category. Let us discuss some conventional autoclaves one by one.

Glass Vessels. The glass vessel in hydrothermal research has advantages of ease of observation and resistance to acid solutions (except HF acid). The disadvantages are the low pressure-temperature conditions and ease of attack by basic solutions. Hence, its use has been generally neglected in hydrothermal work, mainly because the early interest concerned materials requiring basic media and pressure-temperature conditions beyond the limits of glass. When the solvent and pressure-temperature conditions permit and the visual observation enables, glass vessels have much to their recommendation and should be used more frequently in hydrothermal work. Before the design of Morey autoclaves (1913), the hydrothermal vessels consisted of tubes loaded with solid and water and sealed either by welding both the ends of the tube or by means of a flat washer or screw. However, such vessels are very difficult to maintain and dangerous to operate. Croxall et al. (1979) from General Electric Company, UK, has successfully grown berlinite crystals using glass vessels.[25]

Sealed quartz-glass tubes were first tried successfully as pressure vessels in 1964 by Speed and Filice.[5] Quartz autoclaves are good for low pressure-temperature hydrothermal experiments in silica-saturated systems. These tubes provide an inexpensive means for making simultaneous runs along an isotherm with varying bulk composition, pH, partial gas pressure, etc., within a single heater. Figure 3.8 shows the cross sections of quartz glass tube. The lower half or charge chamber is made by nesting three close-fitting quartz glass tubes of 1.25 mm wall thickness and appropriate internal diameters and fusing the tubes together in vacuum. Quartz glass is the most suitable composition because of its strength at high temperatures, low thermal coefficient of expansion, and absence of possibly reactive components, whereas Vycor and Pyrex both contain 3% or more B_2O_3 in addition to significant quantities of Al_2O_3 and the alkalies, and Pyrex softens at about 600°C.[26] The authors[5] give the temperature and internal pressure of quartz glass tube failure in Table 3.8.

The use of quartz glass autoclaves, however, was not popular until recently because of the problems associated with higher pressure-temperature conditions. With the recent discovery of new mineralizers (mixed solvents, high molar acid solutions, organic solvents, etc.), there is a growing tendency for using the glass or thick-walled silica tubes in several hydrothermal experiments. The new mineralizers, and a better understanding of hydrothermal technology, have brought down the crystallization temperature with increased solubility for compounds hitherto obtained only

PrepBooks

at high pressure-temperature conditions. All these advances prompted Popolitov (1991) to develop and test a hydrothermal autoclave for visual examination.[6] The schematic diagram of the visual autoclave is given in Fig. 3.9. The apparatus consists of a cylindrical reactor made of transparent quartz glass with the following parameters: compression strength = 6556 kg/cm^2, tensile strength = 2734 kg/cm^2, bending strength = 1134 kg/cm^2, shock bending strength = 1.08 kg/cm^2. These data show that the quartz glass is a good material for a transparent reactor, provided that no shocks will occur during its operation. This condition requires certain precautions to be followed during charging, discharging, and sealing of the reactor.

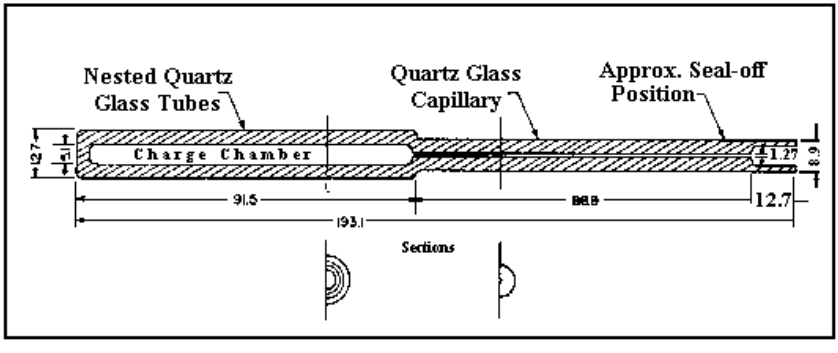

Figure 3.8. The cross sections of quartz glass tube.[5]

Table 3.8. Temperatures and Internal Pressures of Quartz Glass Tube Failure[5]

Tube	Charge	Temperature (°C)	Pressure (bars)
1	Saturated NaBr solution	543 ± 7	146 ± 4
2	Saturated NaCl solution	511 ± 13	345 ± 13
3	Saturated NaCl solution	493 ± 13	323 ± 12
4	H_2O	474 ± 5	414 ± 11

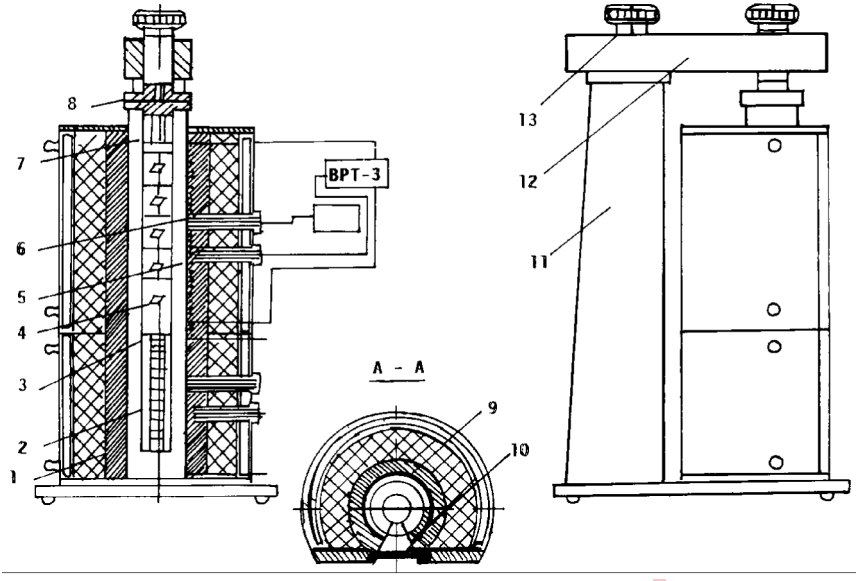

(1) Quartz reactor, (2) nutrient container, (3) baffle, (4) seed holder, (5) seeds, (6) teflon tube, (7) solid cylinder, (8) sealing disc, (9) heater, (10) thermocouple, (11) autoclave frame, (12) upper mount, (13) adjustable nuts.

DropBooks

Figure 3.9. The schematic diagram of the visual autoclave.[6]

The reactor has been fabricated in the following way: a cylindrical block of quartz glass of special purity having a diameter of 85–1000 mm was drilled using a diamond bore with the diameter 50 to 55 mm. Then the inner and outer walls were ground to the specified dimensions and polished. The hydrostatic pressure admissible for this reactor was not calculated before hand, but its strength was checked. To do so, the reactor was filled with water, sealed by a special valve, placed into a furnace, and heated. The growing pressure due to the heating was measured with a manometer. The reactor was heated until the pressure inside it achieved 100 atm but the reactor did bear this pressure. The external heating of steel autoclaves introduces stresses on its walls due to heating. By contrast, quartz glass has a very small coefficient of thermal expansion and hence

the stresses induced by temperature gradients are negligible. To make the quartz reactor tight, a valve, which meets the following requirements, should be used:

i. The valve must be self-sealing, i.e. stress in the seal must grow as the pressure increases, and no strong force that could damage the brittle reactor must be exerted on it when sealed.

ii. The sealing material must be plastic; if so, the initial stress needed for self-sealing is low and the reactor is safe.

iii. The valve must be chemically resistant with respect to the chemical agents or the solvents used.

The teflon ring is placed in an annular groove whose diameter is greater than that of the ring. Also, the ring's outer diameter will be greater than the inner diameter of the reactor block. Hence, stresses appear in the ring due to its deformation, and this is sufficient for the initial sealing.

The main advantage of quartz autoclaves is their high stability with respect to acid medium which permits us to use a condensed solution, i.e., the concentration of substance to be crystallized may be enhanced without increasing the temperature. In this case, a considerable gain can be obtained for the processes which run under lower temperature and pressure, which turns out to be cheaper and safer. The apparatus can also be used in alkali solutions and hydrofluoric acid media by providing a thin teflon coating to inner walls of the quartz glass. This quartz vessel can be used to synthesize and grow single crystals at temperatures up to 300°C and pressures up to 100 atm. The greatest advantage is the facility to observe all the processes taking place inside the autoclave including dissolution of the mixture, movement of the solution and growth of the crystal. By employing the appropriate thermocouple sheath, the temperature distribution in the autoclave can be measured accurately. It is convenient to study the physicochemical processes and hydrodynamics of the solution both in the homogeneous and binary phase "gas-liquid" reagents.

Steel Autoclaves. The success of the earliest experiments in the hydrothermal growth of minerals using very simple autoclaves during the 19th century provided an impetus for Morey at the Geophysical Laboratory of Carnegie Institute, Washington, to design a highly versatile autoclave to work in the medium pressure range.[27] This was further developed by him

and his co-workers to operate at 500 bar and 400°C.[28] Followed by this, several other designs appeared and today there are many designs to suit any particular aspect of hydrothermal crystallization. All the conventional autoclaves can be divided into four types and are popularly known as: *1)* flat-plate closures developed by Morey and co-workers; *2)* cold-cone seal closures designed by Tuttle[29] and popularized by Roy and co-workers; *3)* welded closures designed by Walker and Buehler;[30] and *4)* unsupported area closures developed by Bridgman and modified by several commercial autoclave vendors.[31] These autoclaves have been discussed by many authors.[1][2][32]

Flat Plate Closure Autoclave. This is popularly known as a *Morey autoclave* since Morey designed this simple gasketed, sealed steel autoclave of 25–100 ml capacity. It is widely used in hydrothermal research and the cross-section of a typical Morey-autoclave is shown in Fig. 3.10. The usual dimensions of a Morey autoclave are 10–20 cm length and 2.5 cm inner diameter. The problems encountered by Morey and co-workers in the initial experiments were alleviated in a later design by Morey (1913) in which the closure is made by a Bridgman unsupported area seal gasket made of copper or silver or teflon. Higher pressure-temperature conditions may be obtained with an inconel vessel. At low pressures, sealing is achieved by compression when the main nut or closure nut is tightened. The autoclave generates an autogeneous pressure depending on the degree of filling, the fluid, and the temperature. The autoclave is limited to ~ 450°C and 2 kbars in routine use. In the later versions, the pressure can be directly measured and adjusted during an experiment by providing an axial hole through the closure nut, but this caused, sometimes, compositional changes as the material was transported to the cooler region. A thermocouple is inserted in the well close to the sample and the vessel is placed inside a suitable furnace so that the entire Morey autoclave and closure lie within the element of the furnace. At the end of the run, the vessel is quenched in a jet of air followed by dipping in water and the closure seal is broken.

DropBooks

Cone Closure. By 1948, O. F. Tuttle at the Geophysical Laboratory had designed an ingenious cone-in-cone seal for a small vessel with no threads to seize. Although this “Tuttle apparatus” could go to much higher temperatures, and the pressure could be independently controlled by a drilled lower seat, it had very small volumes, and it did not catch on.

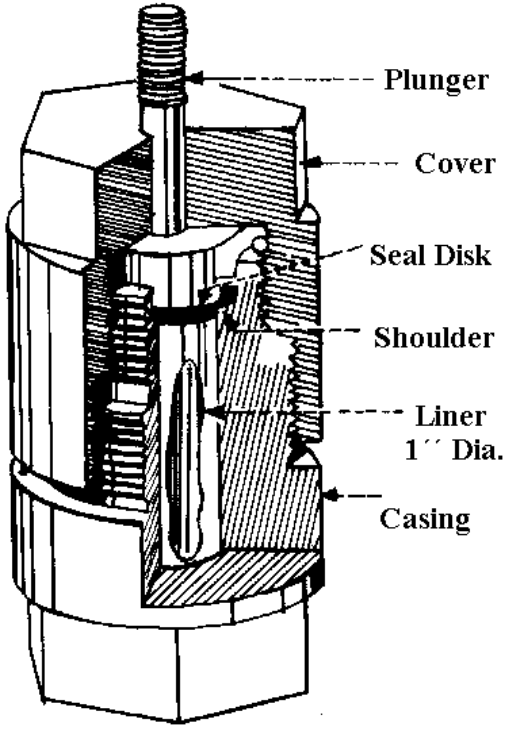

Figure 3.10. Cross-section of a typical Morey-Autoclave.[27]

These autoclaves are known as *cold-cone seal autoclaves,* and also as *Tuttle autoclaves,* Fig. 3.11.[33] A *Tuttle bomb* consists of a stainless steel, low carbon steel, or more exotic alloy such as inconel, udimett or stellite (Co alloy), test tube closed by a cone-in-cone seal. As with the Morey vessels, here also the entire vessel assembly is kept inside the furnace. The seal is closed by weights acting through heat resistant alloys above and below the vessels. The cone at the lower end of the support rod is machined to 59°, the cone or the vessel to 60°; this results in a ring seal. At pressures exceeding 2 kbar and temperatures above 800°C,

these cones have to be machined after each experiment. Pressure is transmitted to the sample through an axial hole in the lower support rod, and temperature is measured by placing a thermocouple in a well of the vessel within 3 mm of the sample. A vertical split furnace is mounted on a hinge allowing it to be swung clear of the vessel during loading or quenching. This vessel can be used up to 800°C at 4 kbar.

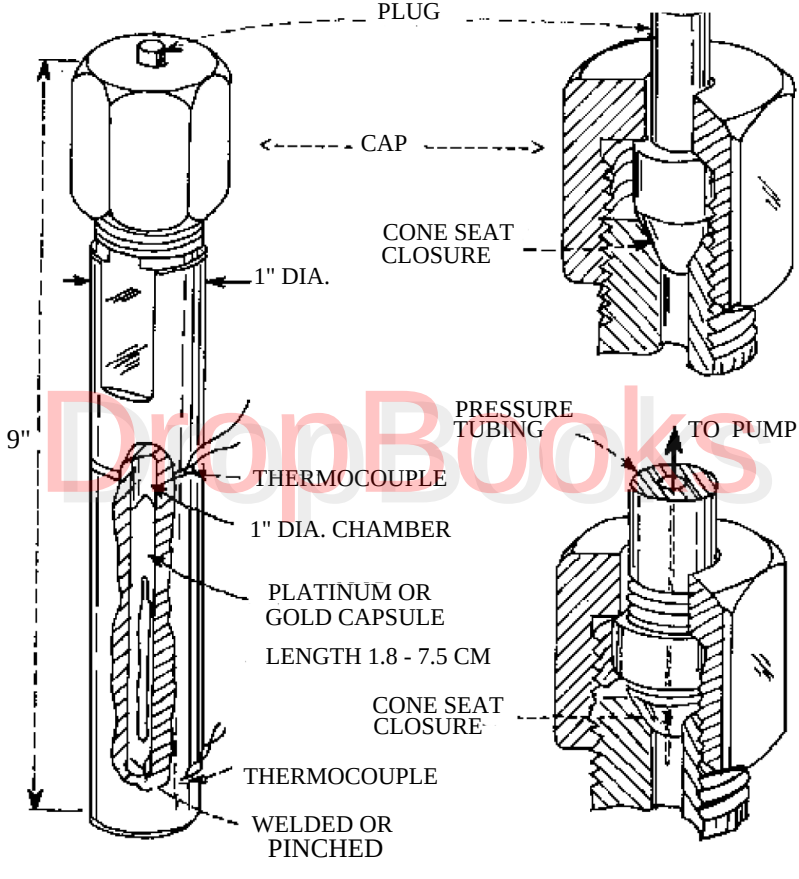

DropBooks

Figure 3.11. Tuttle autoclaves.[33]

In 1949, Tuttle described a modification to his earlier design, which is much easier to use. This consists of a longer vessel in which the open end and seal are outside the furnace; hence the term "cold-cone seal" (although in the real sense it is far from being cold). Pressure is transmitted to the sample, which is contained in a sealed capsule, through a hole in the closure. The capsules are normally made up of noble metals. These vessels may be operated closure up, closure down, or horizontally. The ratio of the vessel diameter to the hole diameter (wall diameter) determines the strength of the vessel. In most standard Tuttle vessels, this ratio is 4%. Using stellite 25, experiments can be carried out at 900°C and 1 kbar or 750°C and 3 kbar for long term use (from hours to weeks). Roy and Tuttle have actually made many hydrothermal experimental runs for several months in late 1950s. Moreover, the reaction could be "quenched" by lowering the furnace quickly and surrounding the bomb with a container of water.

Around 1950, Roy and Osborn[34] had also designed a simple universal pressure intensifier for compressing virtually all gases (H_2, N_2, CO_2, NH_3) or liquids like H_2O from the compressed gas tank pressures of about 100–200 bars to 5 kbars. And from 1950 onwards, "test tube racks" of hydrothermal vessels including such compressors were used worldwide for hydrothermal research, mainly in the geochemical community. Figure 3.12 shows the advertisement of Leco Company, Tem-press Research Bellefonte, Pennsylvania, which has been set up by Tuttle, Roy, and Licastro to make these key tools of hydrothermal research available worldwide. This continues to the present day, mainly due to the overriding convenience and simplicity.

Tuttle's original design underwent several improvements in closure design using new alloys which have extended the pressure-temperature range of cold seal vessels. Luth and Tuttle (1963)[35] described a modified Tuttle-type closure which permits vessels to go up to 8 inch length, 1.25 inch outer diameter, and 0.25 inch inner diameter to be used up to 10 kbar pressure and at temperatures as high as 750°C. Rene 41 (Ni based alloy) is used for this vessel. The most comprehensive reviews of design and operation of cold-seal equipment are given by Huebner in 1921, and Edgar in 1973.[36][37]

DropBooks

Figure 3.12. Advertisement of Leco Company, Tem-press Research, Bellefonte, Pennsylvania.

Similarly, Roy modified another vessel which had been designed by Tuttle but never exploited. It proved that Roy and Tuttle's improved version was much simpler and much more convenient than all others. This Roy modification is popularly known as the "test-tube bomb" and it is typically 1–1½" o.d. × 8" long superalloy (Hastealloy; Rene 41, Stellite 25 or Udimet) rod with a $\frac{3}{16}$ – ¼" diameter hole drilled down to ½" of the bottom. It was threaded at one end and the pressure seal was made there with a 59–60° cone seat against which the connector from the pressure pump was forced by a nut and thread.

This vessel made quantum advances on two fronts. First, it raised the temperature limit to ≈800°C with special steel, and 950°–1000°C with superalloys. Second, the connection to the pressure system of pumps and gauges meant that pressure and temperature were decoupled. Third, because of this simplicity, several vessels could be served by one pressure source. Hence an integrated system of several vessels, each with its own gauge with one pressure generator became a standard hydrothermal laboratory apparatus. By sealing the reactants from inside with gold or platinum tubes, one to four of which could be simply inserted into the "test tube," one could have a simple apparatus for maintaining a precise composition, with no contamination at any chosen pressure (up to 5 kbars) and temperature (up to 900°C) condition for periods which could extend from hours to weeks. We actually made many hydrothermal runs for several months in the late 1950s. Moreover, the reaction could be quenched by lowering the furnace quickly and surrounding the bomb with a container of water.

The advent of new materials, particularly molybdenum alloys, has extended the temperature capabilities of cold-seal vessels to about 1150°C at a pressure above 4 kbar (the so-called TZM vessels). The prospects of new refractory alloys extending up to this range are encouraging. These cold-seal vessels are safe, inexpensive, simple, and operationally routine.

All the above-described autoclaves are externally heated. In Morey and modified Bridgman type autoclaves, the pressure created inside the vessel is calculated through the PVT relation and in only a few cases an external pressure gauge is used. In the Tuttle cold-seal vessel, the pressure is built up by an external pump and the pressure medium is usually distilled water with a little glycol added to inhibit corrosion. For higher fluid pressure, a hydraulic intensifier or air-driven pump is used with argon or nitrogen as the pressure medium. Normally, several vessels run from a single pump, where each vessel is connected to a high-pressure line by a

valve and T-junction. The valve (two-way) isolates the vessels from the line. Each vessel is connected to a separate Bourdon gauge with a safety glass dial and blowout block. An auto-controller is normally used. The types of pressure tubing, valves, and fittings used depend on the operating pressures. Normally stainless steel alloy is used up to 13 kbar and recommended size is 1.4 inch outer diameter, $^{1}/_{16}$ inch inner diameter. Although there has been rather little evolution in the basic design of cold-seal pressure vessels, marked changes have occurred in controllers and pumps.

Welded Closure. This is a "work horse" vessel in most hydrothermal laboratories because the disposable liner permits a good deal of exploratory work to be done in systems where corrosion might ruin even a more complex vessel. It is a high-pressure vessel designed by Walker and Buehler (1950) with the temperature range up to 400°C and pressure of 3 kbar. The vessel consists of an inner liner welded at both ends and an outer tube of heavier construction. Figure 3.13 shows the construction of a welded closure.[30][38]

DropBooks

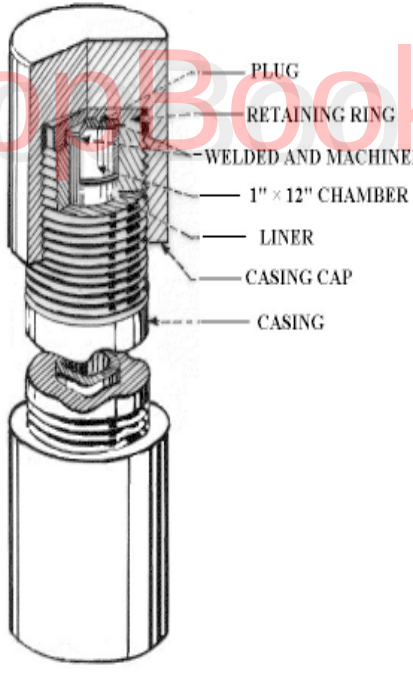

Figure 3.13. Construction of a welded closure.[30]

At the conclusion of an experiment, one end of the welded liner is sawn off to remove the charge. The liner is then driven out of the outer casing and discarded and a new liner is inserted. Thus, for a sequence of experiments, rather extensive machine shop services are needed. However, welded liners are still relatively inexpensive when compared with an entire vessel.

Modified Bridgman Autoclave. A further advancement in pressure-temperature capabilities, size, and design among the steel autoclaves is the modified Bridgman high-pressure autoclave. This is embodied in several commercially available autoclaves. Figure 3.14 shows a cross-section. The initial seal that closes the vessel is made by mechanically tightening the plunger against the deformable gasket (Fig. 3.15 shows a deformed copper ring) by the setscrews in the head. The unsupported area closure makes its seal. The force of the generated pressure acts upon the piston, moving it upward against the deformable gasket and creating a perfect sealing. Such vessels can be used quite successfully in the temperature and pressure range 500°C and 3.7 kbar. Construction materials such as stainless steel or inconel, etc., are chosen according to the requirements of the particular experimental conditions. For general applications, quartz is commonly grown under hydrothermal conditions directly in steel autoclaves. Autoclave attack is minimal because the common mineralizers react with iron to form sodium iron silicates, which adhere to the autoclave wall and inhibit further corrosion. The iron content in solution is so low that Fe in the grown quartz crystals is typically only a few ppm so that crystals of excellent acoustic quality and watch grade quality can be obtained.[15][38] However, almost all other hydrothermal crystals require growth in a low-carbon steel or mild steel liner or noble metal or copper liner. The pressure inside the liner is counterbalanced with pressure between the liner outer wall and inner wall of the autoclave. A required amount of the nutrient material and the solvent is introduced into the liner with a definite percent fill. Then the pressure inside the autoclave is calculated through PVT relations. The modified Bridgman vessels are commercially used for crystal growth and they are further modified to grow very large single crystals of industrial importance.[39] Sealing is the most important aspect in these autoclaves and it consumes much time and effort in the initial runs.

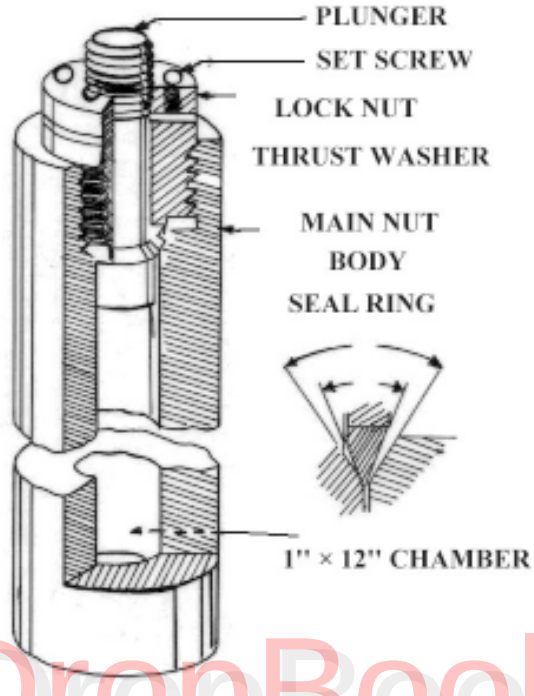

DropBooks

Figure 3.14. Modified Bridgman high-pressure autoclave.[15] *(Drawing courtesy of R. A. Laudise.)*

Figure 3.15. Deformed copper ring.

Most of the above closures, which are called *self-energized closures*, have sealing gaskets generally made of plastic materials and, most frequently, made of annealed copper. At temperatures below 300°C teflon can be used. If the closure is provided with a cooling system, rubber gaskets are used and sealing of such autoclaves does not require as much mechanical effort as with a copper gasket. In fact, much of the success in hydrothermal growth experiments is due to the equipment. A dramatic advance in upgrading the capacity of the autoclave (for example, as in the case of quartz growth) is the result of new sealing systems from the original flange type seals to the modified Bridgman seal which in turn has been superseded by Grey-Loc seals.[40] Large capacity autoclaves of 1000 to 5000 liters volume are in use in Japan with this type of sealing system. Table 3.9 shows the evolution of sealing with reference to the growth of quartz crystals.[41] In most hydrothermal experiments, corrosive solutions are used and special protective inserts are used nowadays to prevent contamination of the growth zone by corrosion products. A floating-type insert or variable-volume insert has been developed at the Institute of Crystallography, Moscow. Such an insert occupies only a part of the autoclave interior while the remaining space is filled with water. These inserts are usually made of carbon-free iron, copper, gold (for alkaline media), titanium, platinum various grades of glass, molten quartz (for acid media), teflon, etc.

Table 3.9. Historical Development of Large Autoclave[41]

Installation	1959	1963	1965	1973	1984
Sealing type	Flange	Modified-Bridgman		Grey-Loc	
Inside dia. (mm)	120	180	300	400	650
Depth (m)	2	3	5	8	14
Volume (l)	22	76	353	1005	4650
Output (kg)	7	25	120	450	3000

Laudise et al. (1994) have proposed pressure balance under hydrothermal conditions. The pressure-temperature relations in the can and in the space between the can and the autoclave system are critical.[42] The water fill is chosen so that the can is usually under compression when the autoclave is

heated to the desired temperature since the can is less likely to fail under compression. The goal is to have pressure balance at the operating temperature (or to have the can under slight compression). Unbalanced pressures result in can dimples, bubbles, and often ultimate failure. Dimples can restrict flow, crush crystals, and cause imperfections in crystals if they grow against the dimpled wall. To understand the balance strategy examination of H_2O and mineralizer solution, PVT data is essential. The authors have studied this while growing $K(TiO)PO_4$, a nonlinear optical material, in pressure balanced gold cans and suggest several strategies for pressure balance in order to avoid dimple formation. Figure 3.16 shows the minimized volume between the autoclave and noble metal lining. Usually autoclave bottoms are hemispherical and can bottoms are flat. A hemispherical metal "space filler" can be used to fill this volume. Similarly, a readily deformed region in the liner (a bellows, a soft metal section, or a thinner walled separate portion) is used where deformation will preferentially take place and will be of less importance. If the deformation is large during cooling, rapid cooling is advantageous as long as thermal shock does not crack large grown crystals. Such studies are very important in the self-energized closures.

All the above-discussed conventional autoclaves are externally heated ones. Though these autoclaves enjoy a great advantage of simplicity and convenience, they are limited with reference to temperature and pressure, by the high temperature strengths of alloys used. In contrast to this, another group/class of equipment in which the pressure vessel is cooled and the sample is heated internally had been designed by several workers. We shall discuss one or two such designs. In this category, one of the earliest designs was proposed in 1923 by Smyth and Adams[43] and was modified later in 1931 by Goranson[44] and again in 1950 by Yoder.[45] This type of vessel is capable of attaining experimental temperature as high as 1600°C and pressure >10 kbar. Thus, much of the later geochemical research has been carried out worldwide using such apparatus. Figure 3.17 shows the schematic diagram of the internally heated high pressure apparatus. It consists of a heavy-walled, heat-treated vessel of tool steel (usually 41–50 Cr-Mo) which contains the pressure, and an internal furnace and sample support. This vessel is admirably suited for the study of reactions by dynamic methods like differential thermal analyses at a series of pressures. In Yoder's modification, it is possible that a temperature of

PrepBooks

2000°C may be attained although no data have been recorded at temperatures above 1500°C. It can't be used directly with water as the pressure transmitting fluid, but by sealing charges containing water in platinum tube. Studies of such systems have also been made up to these temperatures (Goranson, 1931).[44] However, vessels of this type are both expensive and cumbersome for routine and small-scale hydrothermal research.

Similar to the above discussed high pressure autoclaves, there are many other designs, but most of them are for dry systems and also for growing crystals from flux in high pressure medium. For example, the belt apparatus, piston cylinder apparatus, opposed anvil or diamond anvil systems, or high-pressure autoclave system for flux growth.[46]–[50] However, this equipment is more useful for the geological sciences than for crystal growth or materials processing and hence we do not discuss these designs in this book.

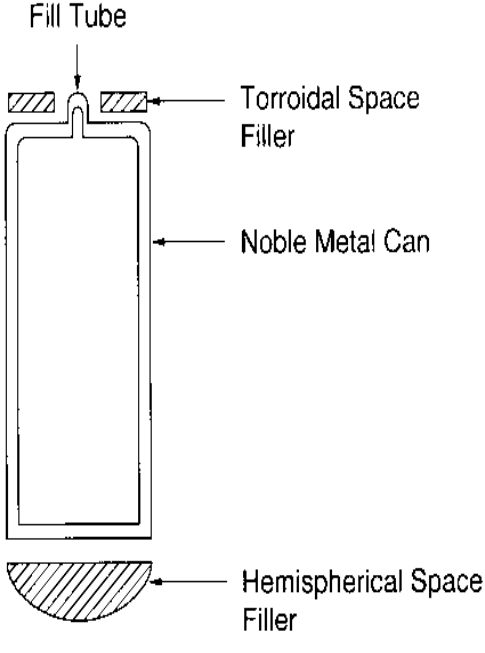

Figure 3.16. The minimized volume between the autoclave and noble metal lining.[42]

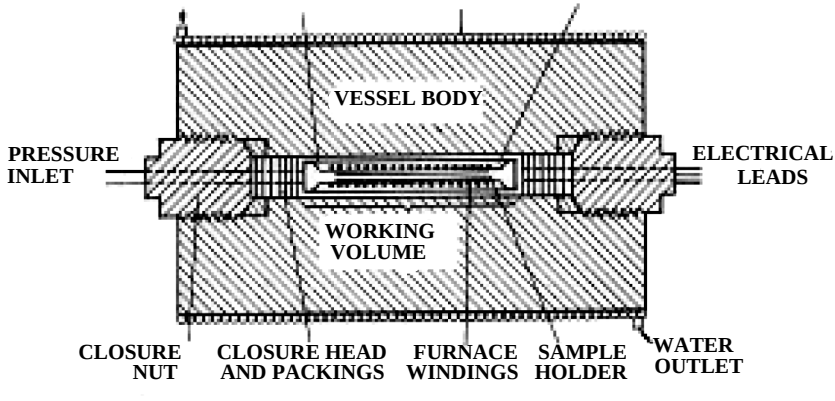

Figure 3.17. Schematic diagram of the internally heated high pressure apparatus.[37]

3.5.2 Novel Autoclaves

DropBooks

The novel designs of the autoclaves are for specific studies such as controlled growth, kinetics, solubility, PVT studies, hydrothermal-electrochemistry, conductivity of electrolytes, visual examination, hydrothermal hot pressing, microwave-plus-hydrothermal, sonar-plus-hydrothermal, and so on. The actual motive behind the designing of such novel equipment is that, in the the hydrothermal method, little information is available as to the processes taking place in the autoclave and also it is extremely difficult to observe these processes inside metal reactors, or autoclaves. Hence, several earlier workers called hydrothermal vessels/reactors "black boxes." Some of these novel designs have come from the Special Construction Bureau, Institute of Crystallography, Moscow, during the 1970s. It is very difficult to discuss each and every design in this book, as there are too many novel autoclave designs. Therefore, we shall restrict our discussion to only a few popular and unique designs.

Horizontal Autoclaves for Controlled Growth of Crystals. This autoclave is highly sensitive to the displacement of mass from the nutrient zone to the growth zone through the arrangement of a highly sensitive balance system. Figure 3.18 shows the fundamental arrangement. The main part of the unit is a horizontal autoclave mounted at the

center of gravity on the vertical axle. The autoclave freely swings in the furnace and the deflection of the axle from the vertical indicates a shift of the mass inside the autoclave from one side to the other. Special weighing scales make it possible to estimate the amount displaced material, and additional weights help to return the autoclave to a horizontal position.

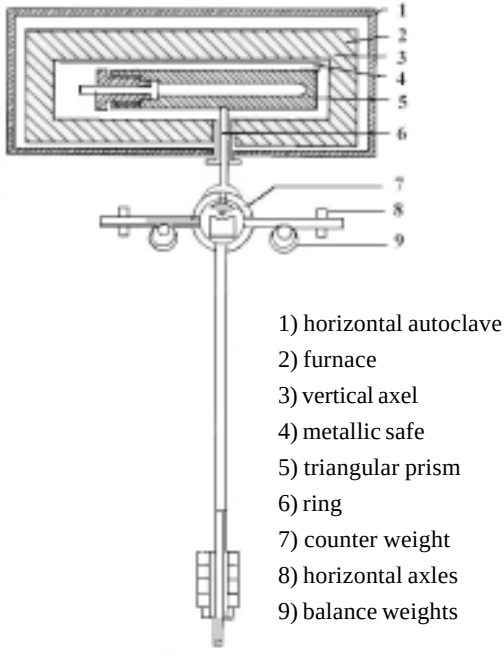

Figure 3.18. Fundamental arrangement of horizontal autoclaves.[51]

Thus, by carrying out experiments in the balance system, one can obtain continuous information regarding the motion of mass in the autoclave, and know when homogenization of the medium sets in. Also, information regarding whether recrystallization of the material is taking place, or at what velocity the recrystallization is proceeding can be obtained. If crystals are being grown on seeds with a pre-specified area, it would be possible to calculate the rate of growth of the crystals and to regulate this by varying the temperature difference between the dissolution and growth zones.

Shternberg (1968) designed and fabricated this autoclave.[51] He has also standardized this system to study the spontaneous crystallization of sphalerite, recrystallization of sodalite, solubility isochore of potassium niobate crystals, and so on.

Pendulum Apparatus. Mass transfer of material under hydrothermal conditions may be determined continuously or periodically from the motion of the center of gravity of a vertical autoclave mounted in the device shown schematically in Fig. 3.19.[51] The oscillations of the autoclave are recorded and counted by means of a photo-relay and pulse counter. Crystal growth can be monitored by observing the change in the oscillation period of the system. If the crystals are growing, the center of gravity of the autoclave will move upward and the oscillation period of the system will increase. The pendulum apparatus designed by Shternberg is highly useful for kinetic studies.

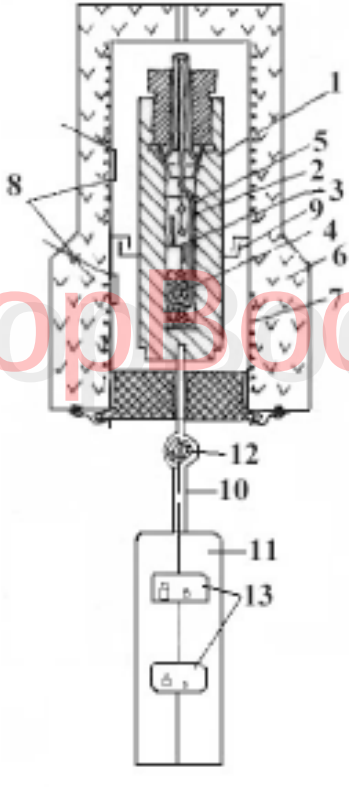

DropBooks

(1) Autoclave; (2) thermocouple; (3) baffle; (4) nutrient; (5) seed holder; (6) furnace; (7) electric winding; (8) two sets of thermocouples; (9) bellows-type barrier; (10) axle; (11) counter weight; (12) roller bearing; (13) two balance shelves.

Figure 3.19. Vertical autoclave mounted in the device.[51]

Hydrothermal Reaction Cell for Kinetic Studies. Recently, Clark et al. (1995) developed a large volume reaction cell for kinetic studies using energy-dispersive powder diffraction.[52][53] This apparatus offers a powerful method of measuring reaction rates for processes that involve crystalline materials. In addition, this helps to carry out multiphase quantitative analysis on a series of powder diffraction spectra collected during the course of a chemical reaction to determine the amount of each crystalline component as a function of time.[54] This has several advantages when a number of processes are occurring simultaneously as the powder method can determine the amount of each phase and the rate at which it takes place, in a mixture of phases. The hydrothermal cell consists of a stainless steel container with a teflon lining. The top of the cell is connected to a control mainfold, which contains a pressure bleed valve, a bursting disc assembly, and a pressure transducer which is used to measure the pressure inside the cell. The cell operates up to 40 bars at a maximum temperature of 230°C and is protected by a thin metal foil-bursting disc, which bursts at pressure beyond 65 bars. The sample holder is a cylinder with a volume of 30 cm^3. The cell wall thickness is 3 mm and is reduced to 1 mm at the beam entry and exit points. Figure 3.20 shows the schematic diagram of a hydrothermal reaction cell.

PVT Apparatus. Several designs have been made for PVT measurements in highly corrosive systems. These devices usually consist of standard pressure manometers. Kolb and Laudise (1982) have designed a PVT apparatus (Fig. 3.21) for highly corrosive fluids (e.g., berlinite systems).[55] Also, this has been used to measure the pressure in the H_2O-SiO_2-NaOH system. The pressure take-off is lined with platinum and connected to a water capillary of small capacity which goes to the pressure gauge. Several other designs have been proposed by the Special Construction Bureau, Institute of Crystallography, Moscow.

Apparatus for Solubility Determination. The solubility of substances under hydrothermal conditions is fundamental information concerning their crystal growth. Solubility measurements are usually carried out by the weight loss method. This approach is effective only for compounds having positive temperature coefficient of solubility. For compounds with negative solubility coefficient, the possibility of further weight loss of the specimen due to increased solubility during the quench, or even at room temperature, must be considered.[56] In such cases, solubility measurements are carried out in specially designed autoclaves. However, the solubility and phase equilibria studies are usually carried out in Tuttle

cold-cone sealed autoclaves or small autoclaves without a pressure gauge. Sometimes other available autoclaves are also used if the quenching can be carried out effectively. The quenching ensures maintenance of conditions in the autoclave corresponding to equilibrium conditions at test temperature. The Special Construction Bureau, Institute of Crystallography, Russian Academy of Sciences, Moscow, Russia, has designed several solubility measurement apparatuses consisting of single autoclave or multiple autoclaves (by creating a liquid thermostat). Figure 3.22 shows an assembly for studying solubility simultaneously in two autoclaves.[57]

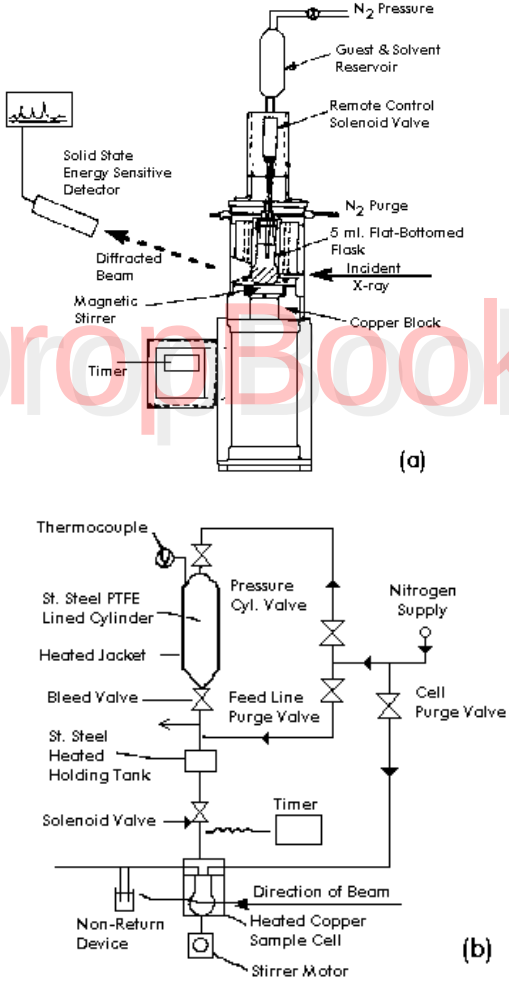

Figure 3.20. The schematic diagram of a hydrothermal reaction cell.[52][53]

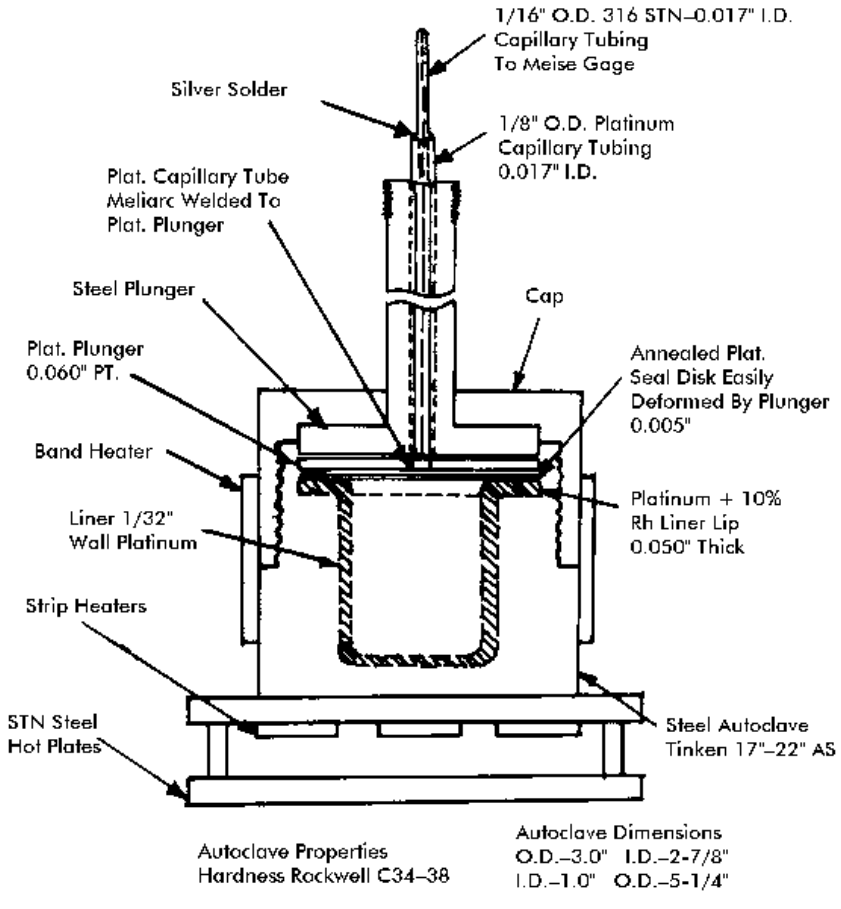

Figure 3.21. PVT apparatus.[55]

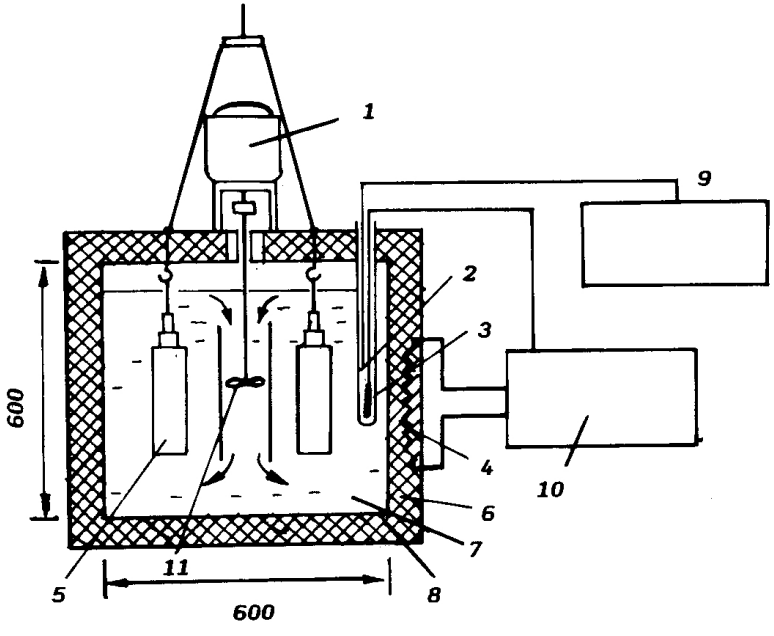

(1) Motor; (2) thermocouple; (3) sensor; (4) heater; (5) autoclave; (6) body of furnace; (7) salt solution; (8) thermal insulation; (9) potentiometer; (10) electronic regulator; (11) stirrer.

DropBooks

Figure 3.22. An assembly for studying solubility simultaneously in two autoclaves.[57]

More recently, Yanagisawa et al. (1993) designed an autoclave for solubility measurement.[58] This autoclave has relatively a simple design, but gives accurate solubility data under relatively mild hydrothermal conditions in which the vapor phase coexists with the liquid phase. The method basically consists of separation of the solid specimen from the solution under hydrothermal conditions in order to avoid regrowth or further weight loss during quenching. Figure 3.23 shows the schematic diagram of the autoclave designed for solubility measurements by Yanagisawa et al.[58] The autoclave was fabricated using stainless steel with a teflon liner. The chamber was separated into two parts by platinum mesh. A solution was transferred to the bottom of the chamber and crystals were placed on the platinum mesh. The position of the platinum mesh and the volume of the solution were selected so that the crystals did not have contact with the solution under hydrothermal conditions for

solubility measurements. The autoclave was connected to a rotation shaft in a hot air oven with an electric fan to minimize the temperature difference in the oven. The contents of the autoclave are agitated slowly, and this helps in establishing equilibrium. About three minutes are needed to complete the separation of the crystals from the solution, then it must be cooled to room temperature by an electric fan or cooling fan. The crystals are separated from the solution under the hydrothermal condition vapor phase during cooling. The solubility calculated from the weight loss of the crystals must be accurate as the crystals do not dissolve in water vapor, because this method totally hinders regrowth of crystals with a positive temperature coefficient of solubility, and redissolution of the crystals with a negative temperature coefficient. Using this autoclave, the authors have accurately determined the solubility of berlinite in phosphoric acid and calcinite in ammonium chloride solution and their results match well with the earlier published data.[58][61] Figure 3.24 *a* and *b* shows the solubility data for berlinite.

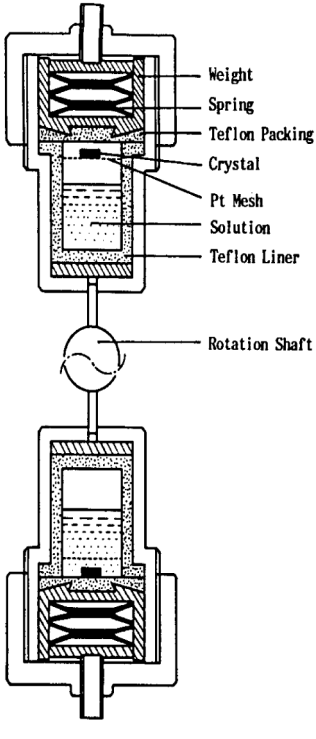

Figure 3.23. Schematic diagram of the autoclave designed for solubility measurements.[58]

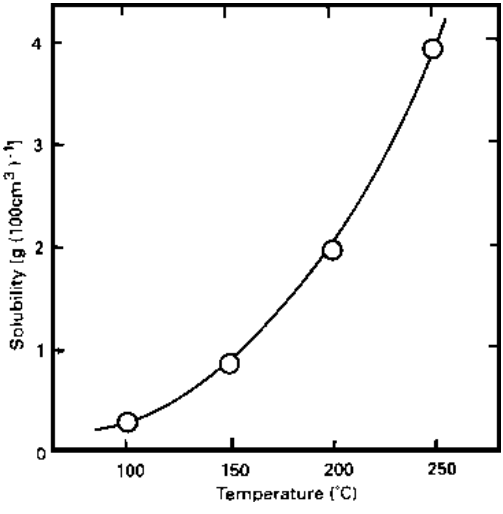

(a)

DropBooks

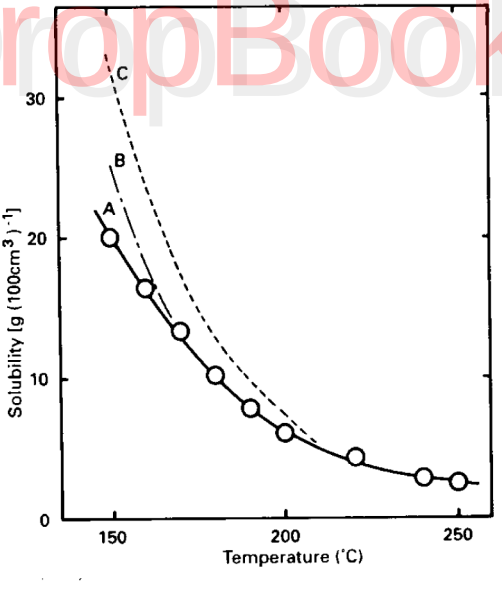

(b)

Figure 3.24. The solubility data for berlinite (*a* and *b*).[58][59]

Rocking Autoclaves. These are more versatile designs for carrying out a variety of hydrothermal experiments including measurements of mineral and gas solubilities, mineral phase stabilities, kinetics of mineral transformations, stable isotope fractionation factors, experiments involving crystal growth, and the formation of synthetic fluid inclusions. Some of these experiments are not only hazardous, but also have errors in applications and equipment failure. Figure 3.25 shows a schematic diagram of a rocking autoclave, which can be used for various types of studies.[62] These autoclaves are made of stainless steel or other useful alloys and contain usually the self-energized closures. There can be two types of rocking autoclaves: *1)* fixed-volume systems, and *2)* flexible-cell system. These systems are placed in a furnace that rotates on an axis 180°, approximately ten times each minute. The purpose of rocking the pressure vessel is for temperature stability and homogeneity as well as to mix the contents of the reaction cell, thereby accelerating chemical exchange between solids and fluids and attainment of equilibrium.[14] These rocking autoclaves provide an extremely reliable and effective means of conducting hydrothermal experiments under supercritical conditions.[63] A reader can get more information on the rocking autoclaves in Refs. 64 and 65.

Multi-Chamber Autoclave. Multi-chamber autoclaves are very useful in carrying out hydrothermal experiments with separately placed charge nutrients, and offer some advantages in the synthesis of special materials. The reaction products occur through ion diffusion. Yanagisawa et al. (1997) have designed and tested these multi-chamber autoclaves for the synthesis of xonotlite whiskers by ion diffusion. Figure 3.26 shows the schematic diagram of the multi-chamber autoclave.[66] It is made up of stainless steel with a total inner volume of 50 cm^3 and has two separate chambers each with volume 12.5 cm^3. The authors placed silica and calcium source at the bottom of each chamber, and poured decarbonated distilled water into the autoclave so as not to suspend the raw materials. The silica source was brought into contact with the calcium source via water, thus, ion species dissolved from the two sources diffuse into each other in the autoclave to produce xonotlite (hydrated calcium silicate). Platinum plates are placed in the autoclaves to collect the reaction products formed by ion diffusion. The design must have originated from the solution growth and gel growth techniques. This autoclave can work up to a temperature of 250°C and pressure usually < 100 bar. However, this design is very useful for the synthesis of some special compounds through ion diffusion.

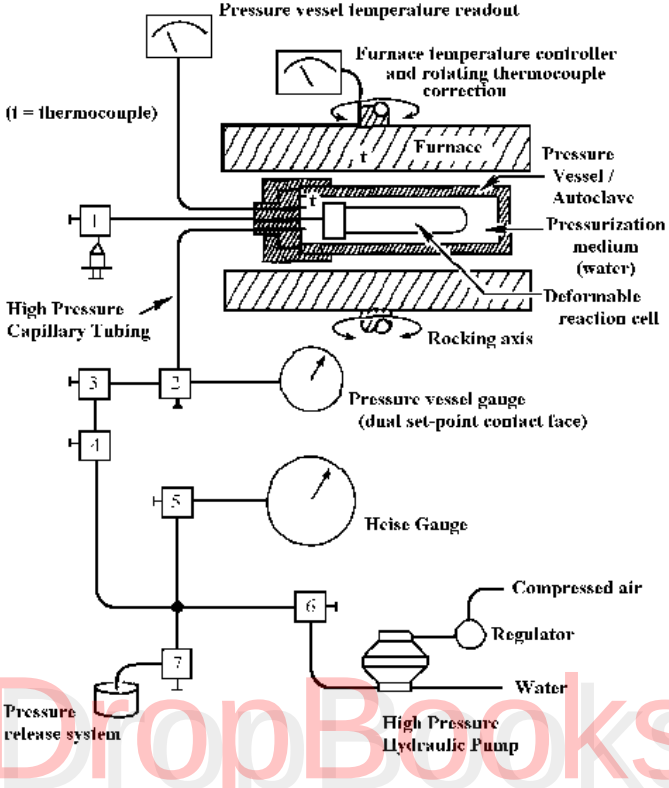

DropBooks

Figure 3.25. Schematic diagram of a rocking autoclave.[62]

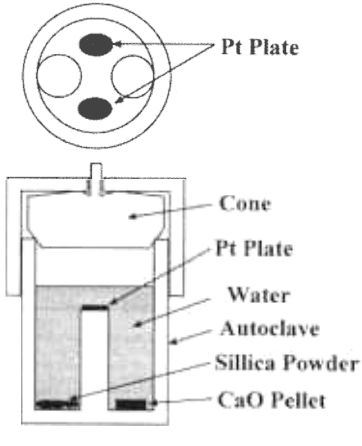

Figure 3.26. Schematic diagram of the multi-chamber autoclave.[66]

Autoclaves for Sampling of Hydrothermal Fluids. The "black box" nature of the hydrothermal system hinders the ready understanding of the hydrothermal crystallization processes taking place in a given set of conditions in an autoclave. This is one of the reasons for the slow raise in the popularity of hydrothermal research, especially in the previous century. The earliest autoclave designs did not have any provisions for the withdrawal of the sample or fluid from the autoclave during the experimental run. As the experiment progresses, the solvent-solute interaction yields several metastable and stable phases, accompanied by a continuous change in the characteristic properties of the media, for example, the pH, redox potential, and so on. It is possible to understand these changes only if we can withdraw the hydrothermal solution from the autoclave and subject it to several studies, or by introducing a desired gaseous pressure in the autoclave through an external pressure source. It is only in the last few decades, such provisions have been made in the autoclave designs, and they are commercially available. Figures 3.27, 3.28, 3.29 show the commercially available autoclaves with facilities to draw out the sample or fluid. These are popularly known as *Start Parr autoclaves* (Japan) (USA) and *Berghoff autoclaves*.[67][68] Also some Japanese manufacturers have come out with similar designs.[69][70] Several configurations of valves permit the sampling of fluids from hydrothermal vessels. The hydrothermal experiments using these autoclaves permit us periodic sampling at constant temperature and pressure, and total fluid chemical analysis. If mineral buffers are used to constrain the activity of pertinent aqueous species, these species should, if at all possible, be monitored directly to determine the system and provide a means to evaluate buffer reactivity and equilibria. Such studies have been carried out with excessively dissolved O_2, and the other with excessively dissolved H_2 and CH_4, to evaluate reaction progress and equilibria in the system Fe_3O_4-Fe_2O_3-S-C-NaCl-H_2O at 300°C, 500 bars. The dissolved concentrations of several redox-sensitive species were periodically monitored.[65]

It is important to measure the total weight of solution withdrawn from the vessel, including both liquid and vapor phases. Partitioning of water from the liquid to the vapor phase can significantly change the effective concentration of dissolved solutes from their initial room temperature values. For example, a solution of 1 M NaCl at room temperature would increase 10% in effective concentration to 1.1 M, in a vessel at 350°C, half-filled with liquid, because of the water partitioned out of the liquid into the gas phase. After each sample is taken, the salt and gas

concentrations must be recalculated for the effect of partitioning into the increased vapor volume, for the temperature of the next sample. As the whole procedure is highly complicated and cumbersome, the sampling studies are done only in some special cases, when required. This is

DropBooks

Figure 3.27. Commercially available autoclaves. *(Photo courtesy of Parr Instruments Co., Illinois, USA.)*

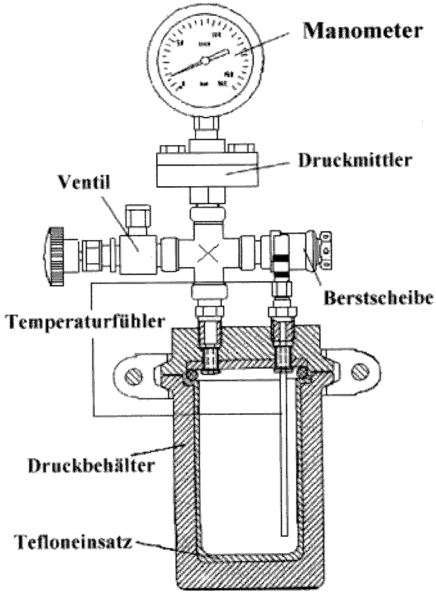

Figure 3.28. Commercially available autoclaves. *(Courtesy of M/S/ Toshin Kogyo Co. Ltd., Japan.)*

Figure 3.29. Commercially available autoclaves. *(Courtesy of M/S Toshin Kogyo Co. Ltd., Japan.)*

extremely useful in the solution speciation calculations to know the regular changes in the chemical equilibria, pH, and so on.

Hydrothermal Autoclaves for Electrical Conductance Measurements of Electrolyte Solutions. Although the electrical conductance of the dilute, aqueous electrolytes was highly desired in hydrothermal research in the early days, it was not popular among hydrothermal researchers owing to the lack of suitable autoclaves to work with such provisions under hydrothermal conditions. The electrical conductance measurements determine the extent of ionic behavior versus association of a dissolved aqueous electrolyte on the basis of conductance theory. It was not until early 1950s that Fogo et al. (1951, 1954) developed an apparatus and studied the conductivity of aqueous NaCl solutions at temperature up to 400°C and pressures to 300 bars. They were the first to obtain the values of ionization constants of NaCl as a function of density in the supercritical region.[71][72] Followed by this, Prof. E. U. Franck from Gottingen, presently at Karlsruhe, Germany, carried out the most pioneering research work from 1950s to date.[73]-[75] The other notable contributions are from T. M. Seward, from ETH, Zurich,[76][77] W. L. Marshall from Oak Ridge National Lab., USA,[78][79] Ryzhenko, Smolyakov, of Russia,[80][81] and Helgeson, of USA,[82][83] who not only popularized this field, but also designed some novel autoclaves for such studies. Figures 3.30 and 3.31 show the schematic diagrams of the interior of a conductance cell, and the conductance cell and electrodes developed by Quist and Marshall which are in use at the Oak Ridge National Lab., USA, for studies up to 800°C and pressures 4 kbar. Though this vessel was designed in 1956, initially by Franck in 1968, it was improved greatly by Quist and Marshall.[73][84] The cell assembly is made of 61 cm long platinum—25% iridium lined pressure vessel with a platinum-iridium wire running from one end of the vessel through a 30.5 cm long aluminium oxide tube to a platinum-iridium cylinder in the center. The wire passes out of the vessel through a Bakelite (a trademark of Union Carbide Corporation) insulator. The linings of the vessel and the small cylinder are both electrolytically coated with "platinum black" (a mixture of fine-grained platinum and platinum oxide) and both linings act as the two electrodes.[85]

Hydrothermal-Electrochemical. The hydrothermal-electrochemical method is an attractive technique for the synthesis of several complex oxide thin films, including the perovskite type. The method makes positive use of the reaction between species included in the electrolytic solution and the substrate being used as an electrode of the electrolytic cell

DropBooks

under hydrothermal conditions. For example, perovskite-type oxide, ABO_3, has to be synthesized on an electrode of B-site metal being oxidized anodically in an alkaline solution containing an A-site element at lower temperatures (typically, 100°–200°C) than those needed for conventional methods. Hawkins and Roy (1967) introduced electrodes into a hydrothermal bomb and studied the influence of an electric field on the synthesis of Kaolinite.[86] They showed a very substantial effect (> 100°C) of lowering the crystallization temperature of Kaolinite. Yoshimura popularized this concept by extending it to the synthesis of electroceramics, particularly perovskite-type oxides.[87]-[89] Basca et al. (1992) reported its advantages and disadvantages compared with a pure hydrothermal method,[90] and Bendale et al. (1993) investigated the thin film formation at lower temperature (29°–100°C).[91] Yoshimura's group has worked extensively on this and successfully prepared perovskite-type titanates such as $SrTiO_3$, $CaTiO_3$, and $BaTiO_3$ thin films up to several micrometers in thickness, almost linearly, at fairly lower temperatures (< 90°C). They have also studied the

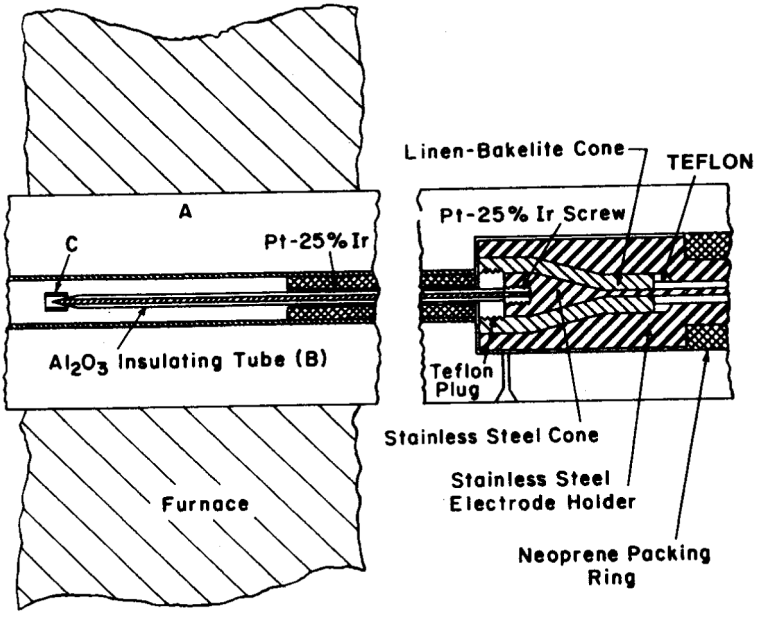

Figure 3.30. The schematic diagram of the interior of a conductance cell.[84] (Actual conductance cell is shown in Fig. 3.31.)

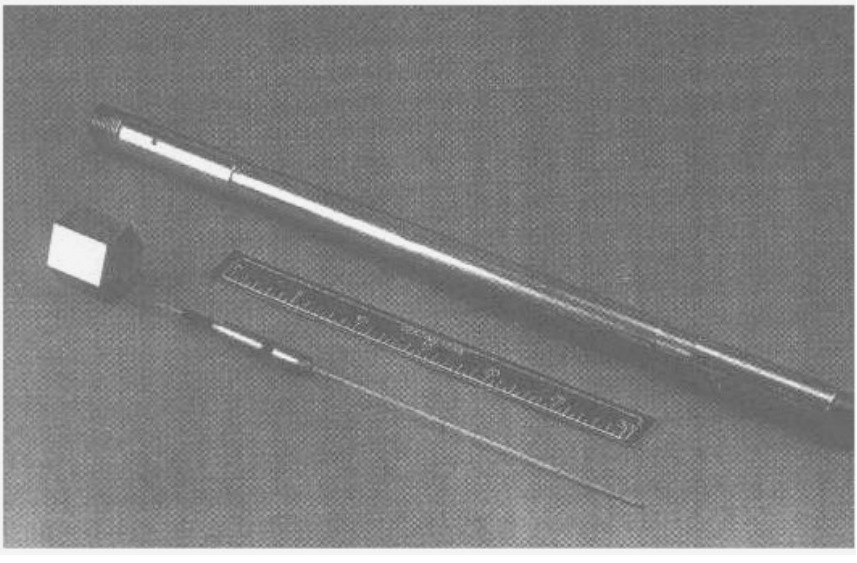

Figure 3.31. A conductance cell.[84] (Schematic is shown in Fig. 3.30.)

DropBooks

growing interface, the transport mechanism of the atoms across the growing film without concentration gradients.

Figure 3.32 shows the schematic diagram of the autoclave designed in Yoshimura's laboratory at the Tokyo Institute of Technology, Japan, for the hydrothermal-electrochemical reactions, using three-electrode technique of Bard et al. (1980).[92] This has a provision to measure potentials of electrodes in aqueous solutions in high temperatures and pressures on a thermodynamically meaningful scale, regardless of the electrolysis conditions.[93]-[95] The preprocessed Ti substrate and the platinum plate were suspended as the working electrode (anode) and the counter electrode (cathode), respectively, by 0.5 mm diameter wires of the same metal keeping an interval of 30 mm between them in the electrolytic cell containing 500 ml of the solution. The Ti electrode is kept at a desired potential until a prescribed quantity of electricity passes through it. The Ti electrode potential, the electrolysis current, and the quantity of electricity passed through the Ti electrode were recorded as functions of the electrolysis time to investigate the effect of oxygen evolution at the Ti electrode on the microstructure of the growing films, in a series of experiments. The pressure of the electrolytic cell was controlled at higher values than the

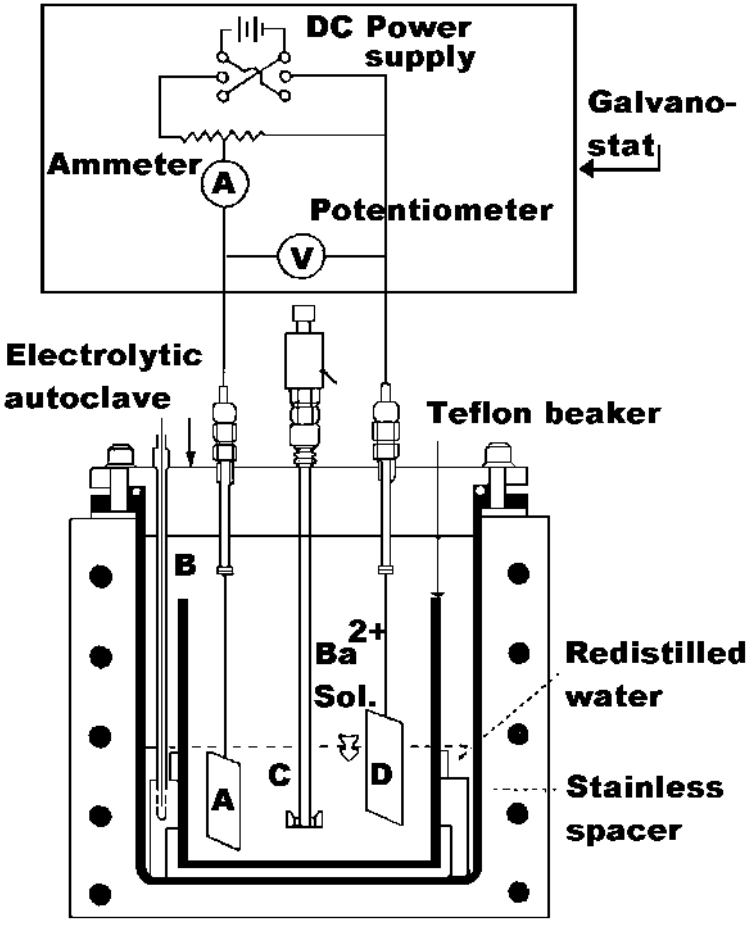

Figure 3.32. Schematic diagram of the autoclave designed by Yoshimura's laboratory.[87]

saturated vapor pressure. Similarly, the galvanostatic electrolysis can be used to control the rate of oxygen evolution.

Autoclave for Ammonothermal Synthesis. The first investigations on metal ammonia solutions were carried out by Weyl in 1864[96] and Seely in 1871.[97] It is well known that alkali and alkaline earth metals (except Be), as well as lanthanides like europium and ytterbium, dissolve in liquid ammonia under normal pressure. These interesting metal ammonia solutions have inspired many preparative chemists to synthesize mate-

rials in ammonia solution under hydrothermal conditions. The reaction products obtained in liquid ammonia under normal pressure are mostly microcrystalline or even amorphous. But this problem can be solved by working with supercritical ammonia as solvent and reactant at pressures up to 6 kbar and temperatures up to 520°C. Thus specially designed autoclaves are needed. As many of the compounds prepared by this method are sensitive to moisture and oxygen, special glove boxes have been constructed. Figure 3.33 shows the schematic diagram of the autoclave designed by Jacobs and Schmidt (1982) to work in the region of supercritical ammonia.[98] The autoclave is made up of a special alloy vacumelt ATS 340. Above 527°C, this alloy begins to flow. On the other hand, the workability of this alloy is quite difficult. The closing mechanism is a Bridgman-type closing, and the sealing rings are usually made up of copper or brass. Chalcogenides and polychalcogenides can also be synthesized by the reaction of the alkali metals with sulfur, selenium, or tellurium in ammonia under high pressure. Similarly some hydroxides and hydrosulfides

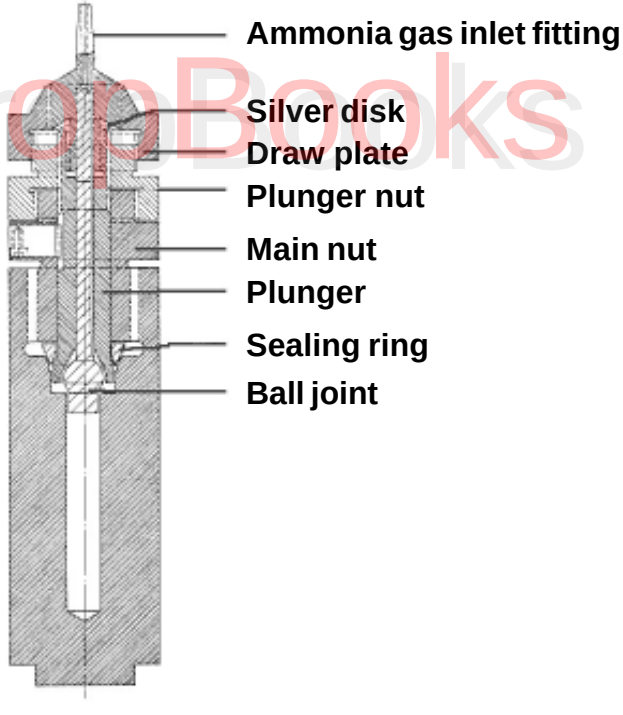

DropBooks

Figure 3.33. Schematic diagram of the autoclave designed by Jacobs and Schmidt.[98]

can be synthesized. Besides the synthesis, the ammonothermal technique has potential in the treatment or disintegration of organic compounds.

Microautoclave. Yamasaki et al. (1996) have developed a microautoclave lined with inconel-600 with reaction chamber volume of 18 ml for hydrothermal oxidation studies. The oxygen gas can be charged into the reaction chamber through the high-pressure value as an oxidant.[99] Figure 3.34 shows the schematic diagram of the microautoclave for using high-pressure gas. An Al_2O_3 stirring ball of diameter 9.0 mm was added to the autoclave and oxygen gas (2.0 MPa) was charged through the pressure valve as oxidant. This setup has been used by the designers to study the oxidation behavior of lead metal, and this autoclave is very effective for the treatment of lead. As the oxidation of sprayed liquid lead is carried out, usually at high temperature (250–400°C), by conventional processes, it results in vaporization of lead leading to an inevitable environmental

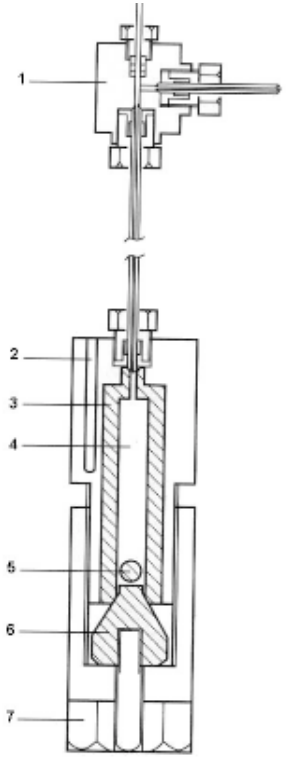

1) High pressure valve
2) Well for thermocouple
3) Liner
4) Chamber
5) Stirring ball
6) Cone
7) Binding nut

Figure 3.34. Schematic diagram of the microautoclave.[99]

pollution problem. In this connection, this novel equipment comes as a helping device.

Hydrothermal Autoclaves for Visual Examination. The hydrothermal process cannot be monitored by "looking" into a steel autoclave. Systematic errors appear in the analysis of the crystallization conditions because the post-factum information is difficult to interpret and is mainly based on consecutive approximations which are only sufficient if the crystal growth is reproducible. Nevertheless, in this case, it is difficult to point out a parameter that controls the entire process because the greater the number of non-measured parameters in the method, the more difficult it is to optimize the solution. In order to facilitate the direct observation and control of dissolution of solids, their synthesis, recrystallization, and growth on seeds, several hydrothermal autoclaves with quartz and sapphire windows have been designed both in the West and in Russia. However, their potential has not been fully exploited as the designs are highly complex, especially the earliest designs of Turlakov et al.[99] and Kuznetsov and Lobachev (1973) which are quite cumbersome to operate.[100][101] The objective of these earlier authors was to study the physicochemical properties of hydrothermal solutions, the states of crystalline substances in them, the solution chemistry, and so on, by direct observation. Their studies also included investigation of the convection currents in the autoclave. For this purpose, the walls of the autoclaves are drilled with two diametrically opposite holes, which are covered with transparent crystals, or windows made of quartz or sapphire. If the interior of the autoclave is illuminated through one such window, one can observe what is happening in the autoclave through the other. By replacing the eye with a camera, movie camera, or video camera, one can record the processes taking place inside the autoclave; and by using a spectrograph, the state of the solution can be investigated. Figure 3.35 shows the schematic diagram of the autoclave with transparent windows.[102] Several problems arose while using these autoclaves under moderate to higher pressures and temperatures due to the differential expansion of steel and sapphire, which can be partially overcome by machining the cap from a material with a coefficient of thermal expansion similar to that of the windows. For example, niobium has been successfully used to about 750°C in combination with sapphire windows.[103] The experiments showed that when the autoclave is not under higher pressure-temperature conditions, the structure could easily support an internal pressure up to 1 kb. However, it did not always remain sealed when subjected to high temperature and pressure

DropBooks

and to an active soda solution. The cause of leakage was either the cracking of sapphire windows or solution squeezing out through the sleeve sapphire seal. At temperatures >300°C, the surfaces of sapphire cylinders

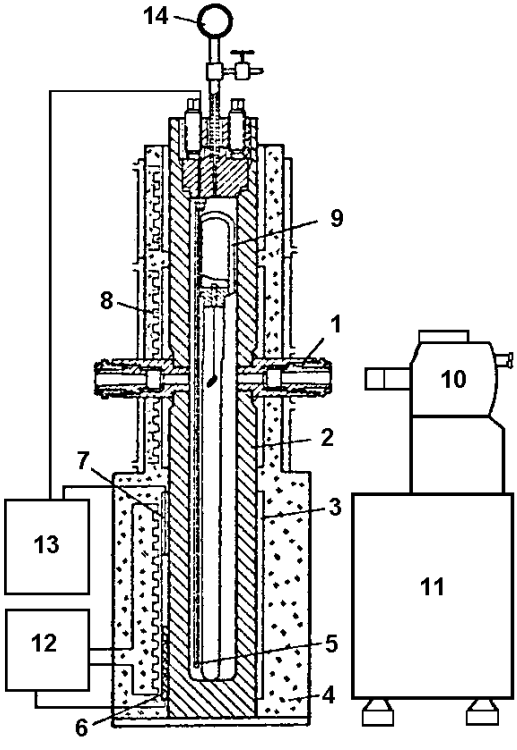

(1) Window; (2) body of autoclave; (3) copper casing; (4) thermal insulation; (5) measuring thermocouples; (6) resistance thermometer; (7) thermocouples; (8) heater; (9) seal; (10) camera; (11) device for automatic single frame filming; (12) three channels proportional regulator; (13) 12-point EPR-09-Rd apparatus; (14) pressure gauge.

Figure 3.35. Schematic diagram of the autoclave with transparent windows.[102]

in contact with the solution were etched and their transparency was impaired.

In recent years, several improvements have been made in the designs, and special provisions have been made to perform optical/ spectroscopic measurements. For example, the Laser Raman and other

vibrational spectroscopic cells have been fabricated in some of the recent autoclave designs.[104] It is worth mentioning here that the recent advances in the instrumentation, particularly to study the optical/vibrational spectroscopic measurements under hydrothermal conditions, have contributed greatly to understanding the nature or behavior of hydrothermal solutions during the crystallization process and the complexation processes taking place inside the autoclave. Thus, the hydrothermal autoclave is no longer a "black box." Further, such studies have greatly helped in reducing the pressure-temperature conditions of growth for a large variety of inorganic compounds. With the reduction in the pressure-temperature conditions of growth, one can use thick glass walled or thick silica glass autoclaves, which permit visual examination.

Hydrothermal Hot Pressing. Hydrothermal hot pressing (HHP) technology is a method by which hard solid bodies from powders can be produced in a short time and at a relatively low temperature (approximately 200–300°C) under saturated vapor pressure.[105] Using the hydrothermal hot pressing technique, one can obtain sintered compacts of pure oxides or inorganic powders which are not possible to obtain by other ordinary sintering processes due to the transformation. Silicate powders such as borosilicate and silica glass can easily form a solid body by hydrothermal hot pressing technology with compression at 20–30 MPa when the proper amount of water or alkaline solution is added as a mineralizer.

DropBooks

In this technique, a starting powder containing water is continuously compressed from outside an autoclave under hydrothermal conditions. The powder is hydrothermally treated at autogenous pressure while it is compressed at much higher pressure than the vapor pressure inside the autoclave. Figure 3.36 shows the schematic diagram of an autoclave for hydrothermal hot pressing. It is a cylinder made of steel with a cylindrical chamber 1 cm in diameter. The term *reaction pressure* means compressive pressure from outside the autoclave. The effective pressure for samples in the autoclave should be smaller than the reaction pressure because of vapor pressure in the autoclave. The piston had a space into which water from the starting sample was released by the hydrothermal hot-pressing treatment. The gland packing made of teflon between the piston and the push rod prevented leakage.

This technology has been used successfully for solidification of various industrial wastes such as sludge ash,[106] radioactive wastes,[107] and concrete wastes.[108] One of the advantages of hydrothermal hot-

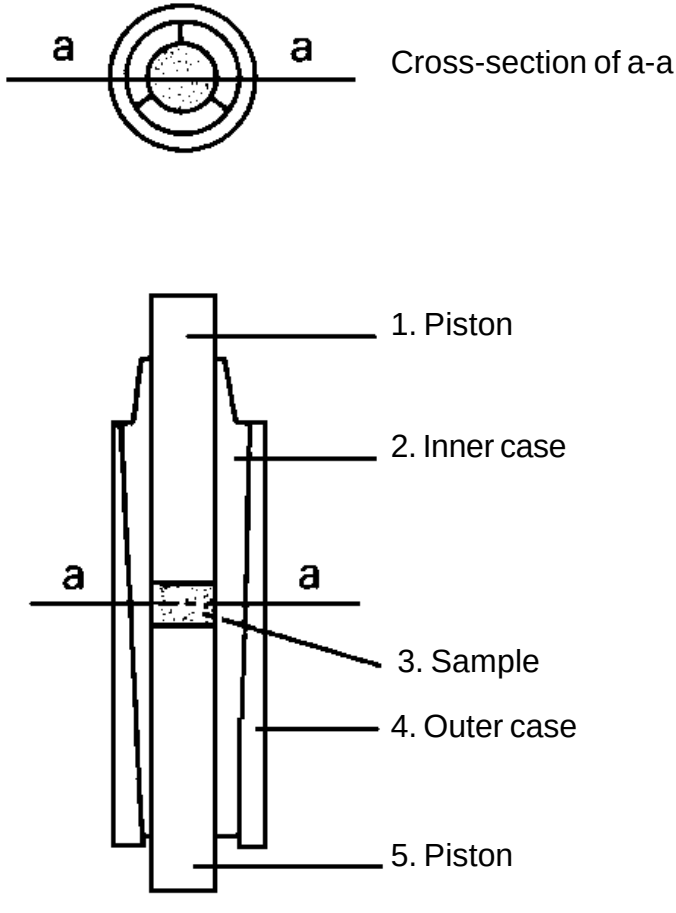

(a)

Figure 3.36. Schematic diagram of *(a)* die, and *(b)* autoclave for hydrothermal hot pressing.[107]

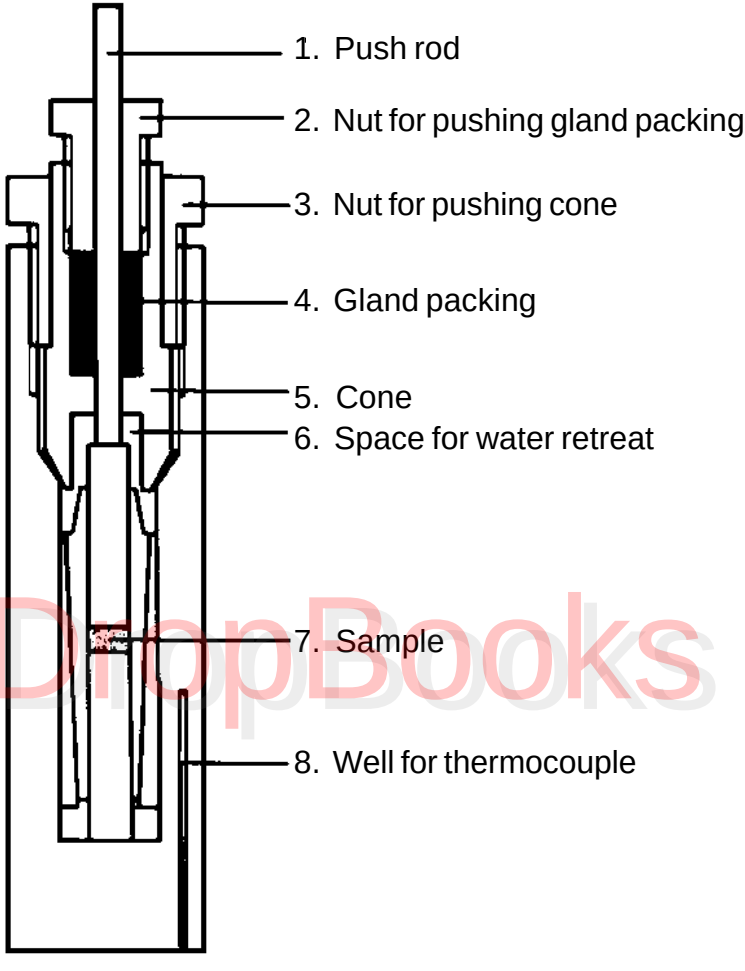

DropBooks

(b)

Figure 3.36. (*Cont'd.*)

pressing technology is that the hydrothermal reaction occurs in a closed system, which prevents the evaporation of volatile materials.[109]

Vertical Autoclaves Used in Hydrometallurgy. High-pressure hydrometallurgy has made considerable progress in the last decade owing to advances in autoclave designs, which are quite large and are on an industrial scale.[110] These autoclaves may be in the form of cylinders, vertically mounted or horizontally laid, spherical, or in the form of a long horizontal tube. The agitation in these autoclaves is accomplished with the injection of high-pressure steam.[111] These *steam agitated autoclaves* are used mainly for leaching bauxite by NaOH within the temperature range 140–150°C, and pressure 2500–3500 kPa. The vessels are usually fabricated from welded steel cylinders with spherical ends. Diameters vary from 1.5 to 2 m and heights from 6 to 12 m. Autoclaves of similar designs, but with acid resistant brick lining, are used for leaching oxidized ores, e.g., laterites by concentrated H_2SO_4 at 250°C and 4000 kPa. These autoclaves have undergone an enormous increase in size for processes treating pyrite and arsenopyrite concentrates, containing gold particles and other related sulfide ores. Some autoclaves, especially with spherical shape, have provisions for rotation at 8–15 rpm. In continuous operations, high-pressure membrane piston pumps are used for introducing pulps into autoclaves. Figure 3.37 shows schematic diagrams of representative autoclaves.[112] The reader can get more information in the works of Fathi Habashi.[110][111][113]

Flow Reactors. Under high-temperature and high pressure conditions, water has excellent properties similar to those which many organic liquids have at normal conditions. Much attention has been paid to the utilization of supercritical water as a reaction medium in which the decomposition of dangerous and toxic wastes, polymeric wastes or hazardous waste, the recovery of inorganic compounds, the preparation of new materials and so on, have been performed.[114][115] Hydrothermal flow reactors are the most suitable apparatus for such examination. A schematic diagram of a typical flow reactor is shown in Fig. 3.38. This consists basically of a sample solution reservoir, a liquid supply pump, a pressure transducer, digital temperature indicators, a spiral tubular reactor, a high-temperature thermostat, and a sampling vessel. To avoid the entry of air into the sample solution, the sample solution reservoir is filled with nitrogen gas. There are several versions of the flow-reactors and it is not possible to describe all the designs. Hence, we have shown only a representative one in Fig. 3.38. In recent years, large scale flow reactors are becoming very popular owing to the growing environmental awareness, and it is predicted

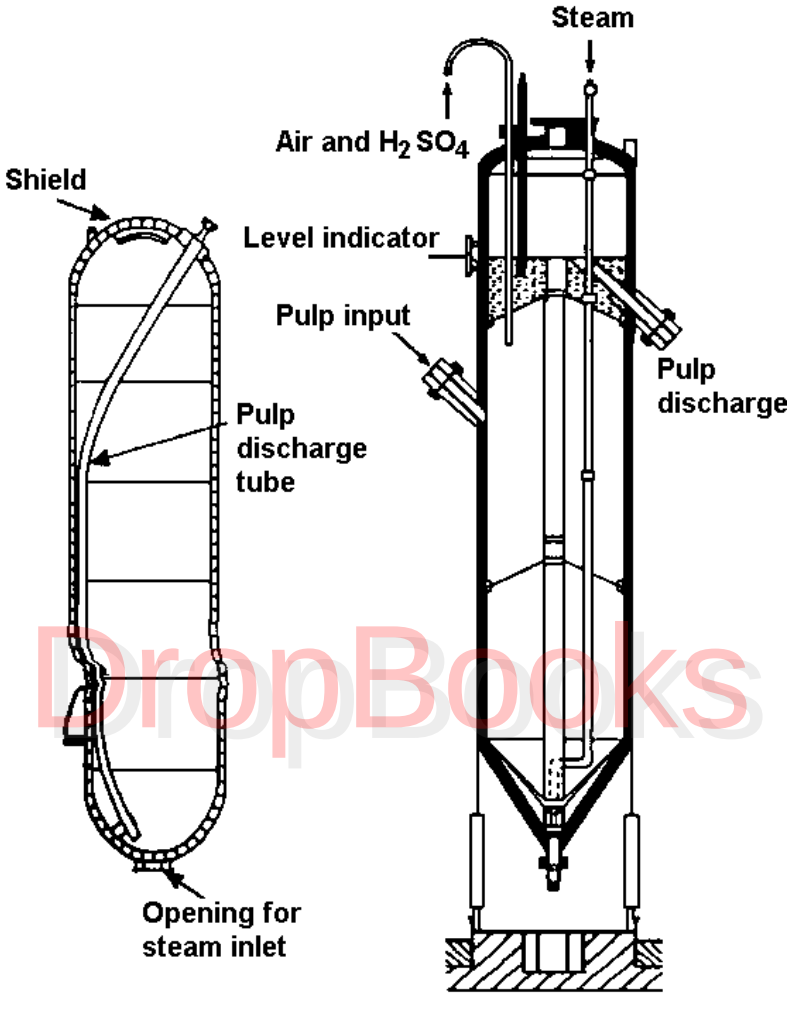

DropBooks

Figure 3.37. The schematic diagrams of autoclaves.[112]

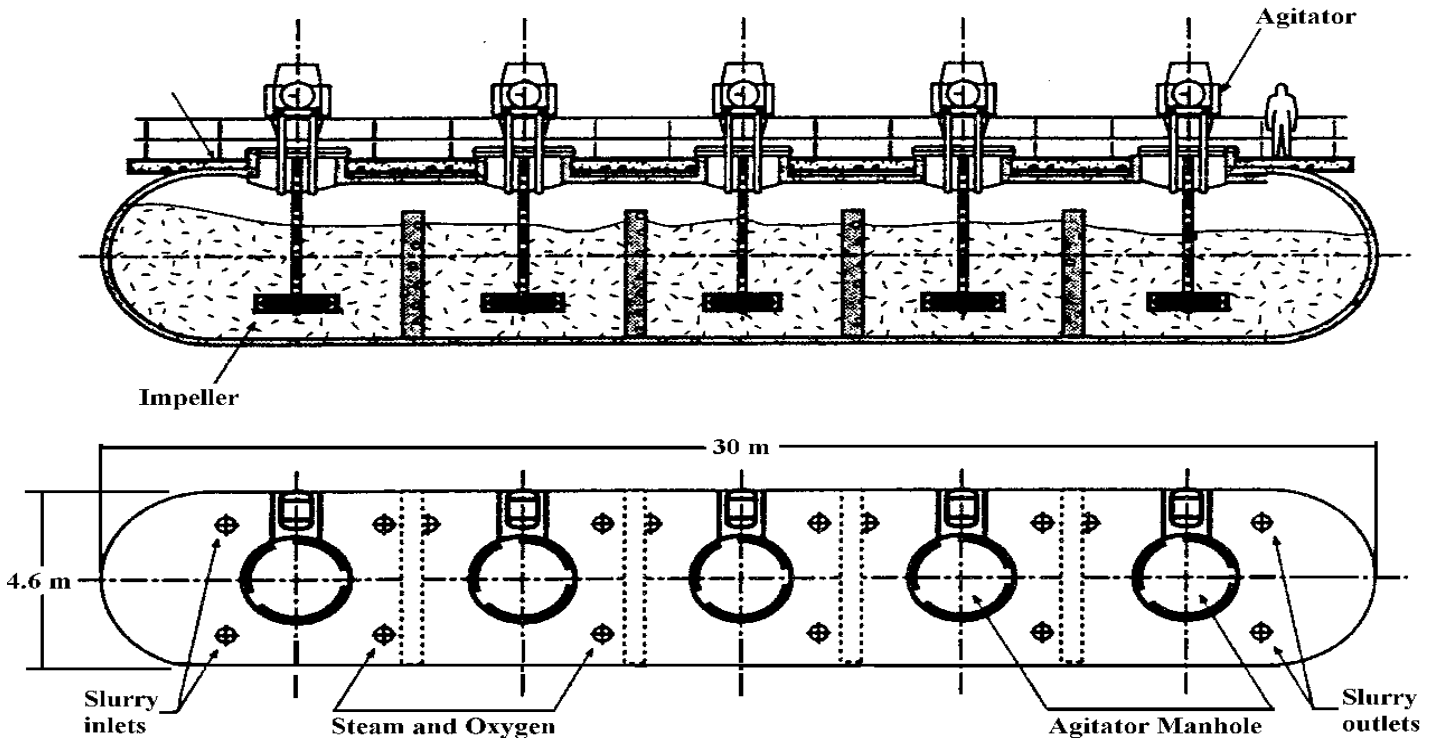

Figure 3.37. (*Cont'd.*)

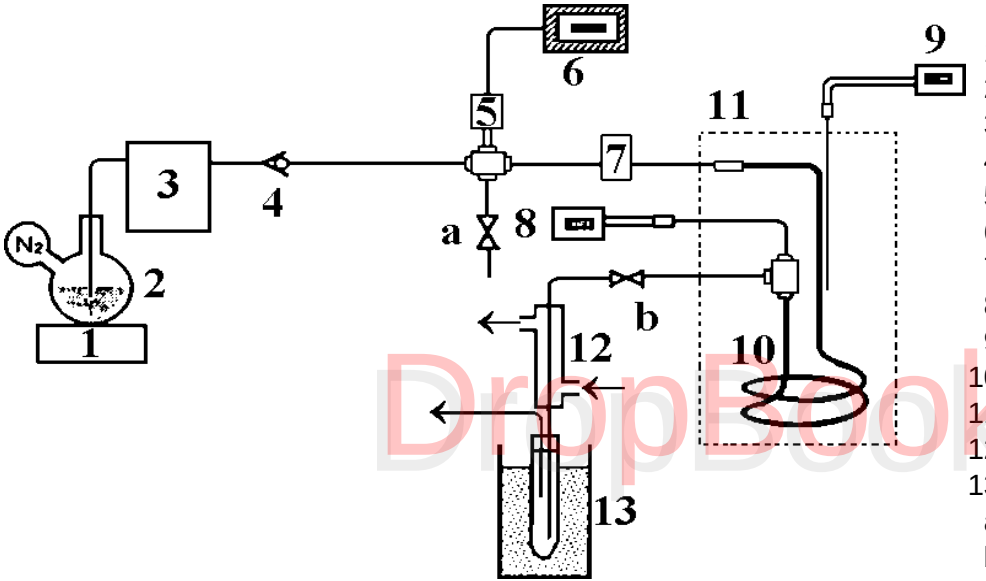

1. Magnetic stirrer
2. Reservoir
3. Liquid supply units
4. Check valve
5. Pressure transducer
6. Digital pressure-indicator
7. Relief valve
8. Digital temperature-indicator
9. Digital temperature-indicator
10. Spiral tubular reactor
11. High-temperature thermostat
12. Condenser
13. Sampling vessel
    a. Valve
    b. Valve

DropBooks

Figure 3.38. Schematic diagram of typical flow reactor.[114]

that there is a great future for this research in treating/recycling industrial waste.

Autoclaves for Accelerating the Kinetics of Hydrothermal Reactions. There is a growing interest in recent years in enhancing the hydrothermal reaction kinetics through superimposing electric fields or mechanical forces, or mechano-chemically including high uniaxial pressure with or without shear mechanical grinding, sonochemically (or acoustic wave stimulation, AWS), with microwave fields, and so on.[116] These techniques are being popularly used to synthesize a great variety of materials and also materials processing. Burns and Bredig[117] had established the remarkable effect that grinding calcite in a mortar converts it into aragonite. Dachille and Roy (1960) generalized the finding to many other phases such as PbO_2, MnF_2, etc., showing that mechano-chemical effects produce:[118]

a. High pressure phases stable above or even about 10–15 kbar at room temperature.

b. Enhanced kinetics by nearly two orders of magnitude in similar high-pressure solid state reactions, when shearing stresses are superimposed on pressures up to 100,000 atm.

It is obvious that the grinding and mechanical mixing and subsequent fracture generate fresh, highly reactive surfaces, and lead to substantial improvement in the reaction kinetics—especially in the conversion of highly stable oxides to make clays. This was made possible by a simple innovation in apparatus. In effect, the Morey autoclaves were converted into ball mills or rod mills.[119][120] The autoclave is rotated around its long axis inside the furnace. An increase in the rate of reaction by two or three orders of magnitude can be attained at a given pressure and temperature. It is not clear whether this should be ascribed to strain energy stored in the lattice or merely to breakage of bonds.

Boldyrev (1996), through his extensive work with mechano-chemical effects, concludes that for many reactions it is possible to increase the kinetics by about two orders of magnitude.[120]

During the early 1980s, a considerable number of publications have appeared in the field of sonochemical breakdown of liquid phases. Suslick (1990) gives an excellent review on this topic and shows that metallic phases may be melted and/or corroded in aqueous suspension at "room temperature."[121] The general understanding is that collapsing bubbles during cavitation could generate temperatures of the order of 5000

K and modest local pressures. Roy and his group attempted to synthesize novel materials or combination reactions, which could be accelerated at least by two orders of magnitude by using AWS. These AWS techniques have an interesting effect on size.[122] In another case, ultrasonic energy was used to accelerate the formation of hydroxylapatite.[123] Abu-Samra et al. (1975)[124] and Kingston and Jassie (1988)[125] reported that all inorganic mineral phases can be dissolved faster in (dilute) acids by several orders of magnitude when a microwave field is superimposed upon mild (< 200°C, 10–20 bars) hydrothermal conditions. This technique is used worldwide today for chemical analysis as well as for dissolving samples. Komarneni and Roy (1992, 1995), in a series of recent papers, have been applying hydrothermal-plus-microwave conditions for material synthesis, and their study enhances, by two orders of magnitude, the reaction kinetics of many reactions from the precipitation of metals from polyols to the synthesis of ferrites, phosphors, and so on.[126][127] There is also some advantage in morphology control and it sometimes leads to the crystallization of new phases like hydrate of Al_2O.[128] Recently Komarneni (1993) has reviewed the importance of this.[129] Figure 3.39 shows a schematic diagram of a typical hydrothermal-plus-microwave set up.[128] As the popularity of this technique is growing with the new results

DropBooks

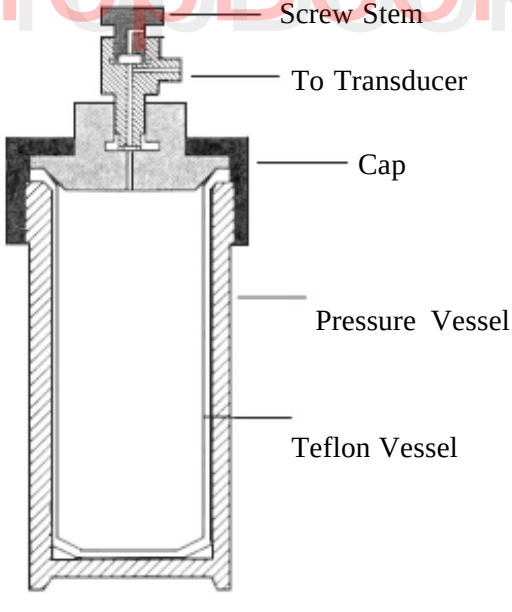

Figure 3.39. Schematic diagram of a typical hydrothermal-plus-microwave.[128]

poured into literature, there is already a commercial production of these autoclaves.

There are several other designs of hydrothermal autoclaves to suit a specific purpose. For example, Strubel (1975) has designed a teflon-lined autoclave with a stirrer.[130] Similarly, Shternberg (1971) has designed a double autoclave (exoclave) in order to avoid having a mechanical compression system for producing a desired pressure in the reaction chamber.[51] Also, this permits independent selection of temperature and pressure. The exoclave is designed for use at temperatures up to 700°C and pressures up to 3000 kPa/cm^2.

In recent years, high-pressure systems (about 40 kbar, temperatures up to 1500°C) have been used in the synthesis of new compounds. Cylindrical platinum cells of 4 mm diameter and 6 mm height serve as the reaction vessels. However, these high-pressure vessels are not very important for the growth of crystals and processing of materials.

3.6 SAFETY AND MAINTENANCE OF AUTOCLAVES

Safety is the prime factor in carrying out experiments under hydrothermal conditions. It is estimated that, for a 100 cm^3 vessel at 20 000 psi, the stored energy is about 20,000 joules. Hydrothermal solutions—either acidic or alkaline—at high temperatures are hazardous to human beings if the autoclave explode. Figure 3.40 *a* and *b* show stellite Tuttle cold-cone sealed autoclaves and stainless steel acid digestion bombs which ruptured at high pressure. Therefore, vessels should have rupture discs calibrated to burst above a given pressure. Such rupture discs are commercially available for various ranges of bursting pressure. Provision should be made for venting the live volatiles out in the event of rupture. A blow-down tank has to be commissioned in the case of a large-size hydrothermal laboratory. Proper shielding of the autoclave is needed to direct the corrosive volatiles away from the personnel. In the case of a large autoclave, the vessels are placed with proper shielding in a pit. For safety purposes, when hydrothermal autoclaves are operated simultaneously at a given temperature, a total static overpressure caused by a simultaneous rupture of all the operating autoclaves should not exceed 0.5 psi, which is determined by the strength of the walls and the dimension of the laboratory. In several laboratories, make-up pressure units are installed for safety.

The hydrothermal laboratory should have a well-equipped workshop for the proper maintenance of the autoclaves. After each run, the autoclave should be properly treated before using it for the next run. The contacts, especially at the sealing sections, should be kept sharp without any lint by polishing the surfaces at the contact after each run to avoid scratches. The gasket must remain flat in its seat without tilting. The autoclave threads should be maintained carefully and are always painted with pipe thread lubricant to reduce friction and prevent seizing of the autoclaves at high temperature. Some workers even place a light coating on the seal rings to ensure that they are properly sealed. Graphite grease or graphite in water medium and suspended molybdenum sulphide or copper

DropBooks

(a) (b)

Figure 3.40. (*a*) Stellite Tuttle cold-cone sealed autoclaves and (*b*) stainless steel acid digestion bombs which ruptured at high pressure.

lubricants are used. For runs above 200°C, graphite lubricant is more effective because the other lubricants may decompose.

With a new or recently remachined vessel, it is advisable first to clean out the residual cutting oil with an organic solvent and to heat distilled water in the vessel one or more times, until the odors of sulfur gases or organic species are no longer present. For vessels that have been used with H_2S, many cycles may be required. Once a vessel has contained reduced sulfur, it should not be used for sulfur-free experiments unless it

has been vacuum cleaned while hot. Such a degassed vessel previously used for reduced systems can then be heated, at about 350°C open to the atmosphere, to promote an oxide surface layer for corrosion protection. Proper precaution should be taken while sealing the vessel. In the case of cold-seal equipment, explosive vessel failure is of paramount concern. Such failure is likely to occur in the event of rapid quenching of the entire vessel and overheating of the furnace. In spite the simple, rapid quench it provides, immersing the vessel in water is to be avoided. Nowadays, numerous remote quenching designs have been developed.[131] Several authors have discussed, in detail, major hazards with hydrothermal autoclaves.[36][132]

Overheating of the furnace resulting from the malfunction of the control system is a common reason for vessel failure. Hence, furnaces should be properly shielded. Burns from hot vessels represent another major hazard with cold-seal laboratories. If it is necessary to handle a hot vessel, it should be done by grasping the relatively cool closure assembly wearing special insulated gloves.

Note that any vessel to be heated must never be filled completely with an aqueous solution. Fluids expand on heating and are capable of generating extreme pressures in a fluid-filled vessel even if heated only for a few degrees, pressures that can easily rupture an autoclave. It is critically important to calculate the thermal expansion of the aqueous phase and to allow at least 20% of total volume of the vessel for uncertainty or temperature overturn. An apprenticeship in an operating hydrothermal laboratory is strongly recommended to learn, to anticipate, and to cope with the dangers of such experiments. For those planning to set up a hydrothermal laboratory, it is advisable to visit other existing laboratories to review safety procedures as well as design. Therefore, autoclave maintenance and safety make hydrothermal experiments quite expensive.

REFERENCES

1. Rabenau, A., The Role of Hydrothermal Synthesis in Preparative Chemistry, *Angew.Chem.* (English Ed.), 24:1026–1040 (1985)
2. Laudise, R. A. and Nielsen, J. W., in: *Solid State Physics* (F. Seitz and D. Turnbull, eds.), Vol. XII, Academic, New York (1961)
3. Clauss, D., *Engineer's Guide to High-Temperature Materials*, pp. 612, McGraw-Hill, New York (1969)

4. Smithells, C. J., *Metals Reference Handbook*, 1:378, Plenum Press, New York (1967)
5. Speed, R., and Filice, A., Quartz Glass Pressure Vessels for Hydrothermal Studies, *Amer. Min.*, 49:1114–1119 (1964)
6. Popolitov, V. I., Hydrothermal Growth of Crystals Under Visual Examination, in: *Hydrothermal Growth of Crystals* (K. Byrappa, ed.), pp. 255–297, Pergamon Press, Oxford (1991)
7. Litvin, B. N., and Tules, D. A., Apparatus for Hydrothermal Synthesis and Growth of Monocrystals, in: *Crystallization Processes Under Hydrothermal Conditions* (A. N. Lobachev, ed.), p. 139, Studies in Soviet Science, Consultant Bureau, New York (1973)
8. De Senarmont, H., *Ann. Chim. Phis*., 32:129–132 (1851)
9. Daurree, M., Sur le Metamorphisme et Recherches Experimentales Sur Quelques-uns, *Ann. Mines*, 12:289–326 (1857)
10. Allen, E. T., Crenshaw, J. L., and Johnston, J., *Am. J. Sci. 4th Ser*., 33:167 (1912)
11. Bruhns, W., Apparatus, A Steel Bomb, Lined with Platinum, *Neues Jahrb. Min. Geol.*, II:62–65 (1889)
12. Doetler, C., Recrystallization of Apophyllite, *Neues Jahrb. Min. Geol*., I:118–139 (1890)
13. Rabenau, A., and Rau, H., Crystal Growth and Chemical Synthesis under Hydrothermal Conditions, *Philips Technical Review*, 30:14–21 (1969)
14. Barnes, H. L., Investigations in Hydrothermal Sulfide System, in: *Research Techniques for High Pressure and High Temperatures* (G. C. Ulmer, ed.), pp. 317–355, Springer-Verlag, New York (1971)
15. Laudise, R. A., What is Materials Chemistry? in: *Materials for Nonlinear Optics, Chemical Perspectives* (S. R. Marder, J. E. Sohn, and G. D. Stucky, eds), pp. 411–433, *Am. Chem. Soc.*, Washington, DC (1991)
16. Jumas, J. C., Goiffon, A., Capelle, B., Zarka, A., Doukhan, J. C., Schwartzel, J., Detaint, J., and Philippot, E., Crystal Growth of Berlinite, $AlPO_4$: Physical Characterization and Comparison with Quartz, *J. Crystal Growth*, 80:133–148 (1987)
17. Ashby, C. T., Berry, J. W., and Deutschman, A. J., A Variable-Volume Silver Liner for High Pressure Hydrothermal Crystal Growth, *Amer. Min*., 55:1800–1802 (1970)
18. Roeser, W. F., in: *Temperature: Its Measurement and Control in Science and Industry*, p. 180, Reinhold, New York (1941)
19. Charles, R. W., and Vidale, R., Temperature Calibration of a New Rapid Quench Vessel, *Amer. Min*., 67:175–179 (1982)
20. Kennedy, G. C., Pressure-Volume-Temperature Relations in Water at Elevated Temperatures and Pressures, *Am. J. Sci*., 248:540–564 (1950)

DropBooks

21. Bain, R. W., *Steam Tables*, pp. 146 , Edinburgh, Her Majesty's Stationary Office (1964)

22. Hannay, J. B., On The Artificial Formation of The Diamond, *Proc. Royal Society London*, 30:188–189 (1880)

23. Friedel, G., Hydrothermal Synthesis of Corundum, *Bull. Soc. Min*., 14:7–10 (1891)

24. Byrappa, K., Hydrothermal Growth of Crystals, in: *Handbook of Crystal Growth*, (D. T. J. Hurle, ed.), pp. 465–562, Elsevier Science B.V., England (1994)

25. Croxall, D. F., Christie, L. R. A., Isherwood. B. J., Todd, A. G., and Brich, J., The Growth and Assessment of Berlinite Single Crystals, *Proc. 2nd European Conference Crystal Growth*, Lancaster (1979)

26. Holser, W. T., Fugacity of H_2O at High Temperature and Pressure. *J. Phys. Chem*., 58:316–17; Corning Glass Works, Properties of Selected Commercial Glasses, *Bull*., Vol. 83 (1957)

27. Morey, G. W. and Niggli, P., The Hydrothermal Formation of Silicates, A Review., *J. Am. Chem. Soc.*, 35:1086–1130 (1913)

28. Morey, G. W. and Ingerson, E., The Pneumatolytic and Hydrothermal Alteration and Synthesis of Silicates, *Econ. Geol*., 32:607–761 (1937)

29. Tuttle, O. F., Two Pressure Vessels for Silicate-Water Systems, *Geol. Soc. Amer. Bull.*, 60:1727–1729 (1949)

30. Walker, A. C. and Buehler, E., Growth Large Quartz Crystals, *Ind. Eng. Chem.*, 42:1369–1375 (1950)

31. Laudise, R. A., Hydrothermal Synthesis and Crystal Growth—History, Status and Prospects, in: *Advanced Crystal Growth* (P. M. Dryburgh, B. Cockayne, & K. G. Barraclough, eds.), p. 267, Prentice-Hall, London (1987)

32. Laudise, R. A., Hydrothermal Growth, in: *Crystal Growth: An Introduction* (P. Hartman, ed.), p. 162–197, North-Holland Publ. Co., (1973)

33. Tuttle, O. F., A New Hydrothermal Quenching Apparatus, *Amer. J. Sci.*, 246:628–635 (1948)

34. Roy, R. and Osborn, E. F., Some Simple Aids in Hydrothermal Investigation of Mineral System, *Econ. Geol*., 47:717–721 (1952)

35. Luth, W. C., and Tuttle, O. F., Externally Heated Cold-Seal Pressure Vessels for Use to 10,000 Bars and 750°C, *Amer. Min.*, 48:1401–1403 (1963)

36. Huebner, J. S., Buffering Techniques for Hydrostatic Systems at Elevated Pressures, in: *Research Techniques for High Pressure and High Temperature* (G. C. Ulmer, ed.), pp. 123–177, Springer-Verlag, New York (1971)

37. Edgar, A. D., *Experimental Petrology: Basic Principles and Techniques*, p. 217, Clarendon Press, Oxford (1973)

38. Walker, A. C., Hydrothermal Synthesis of Quartz Crystals, *Ind. Eng. Chem.*, 36:250–256 (1953)

39. Laudise, R. A., *The Growth of Single Crystals*, pp. 278–281, Prentice-Hall, Englewood Cliffs, NJ (1970)
40. Asahara, J., Nagai, K., and Harada, S., Synthetic Quartz Crytals by Large Autoclaves, in: *Proc. 1st Intl. Symp. on Hydorthermal Reactions* (S. Somiya, ed.), pp. 430–441, Gakujutsu Bunken Fukyu-Kai, Jpn, (March 22–26, 1982)
41. Taki, S., Improvement of Growth Process and Characterization of Quartz Crystals, *Prog. Crystal Growth and Characterization.*, 23:313–339 (1991)
42. Laudise, R. A., Bridenbaugh, P. M., Iradi, T., Pressure balance under hydrothermal conditions, *J. Crystal Growth*, 140:51–56 (1994)
43. Smyth, F. H., and Adams, L. H., The System Calcium-Oxide-Carbon Dioxide, *J. Amer. Chem. Soc.*, 45:1172 (1923)
44. Goranson, R. W., Solubility of water in granite magmas, *Amer. J. Sci.* 22:481–502 (1931)
45. Yoder, H. S., High-low Quartz Inversion up to 10,000 kg/cm^3, *Trans. Amer. Geophys. Union*, 31:827–835 (1950)
46. Boyd, F. R., and England, J. L., The Quartz-Coesite Transition, *Geophys. Research*, 65:741–749 (1960)
47. Vodar, B., and Kieffer, J., in: Mechanical Behavior of Materials Under Pressure (A. Pugh, ed.), p. 1, Elesvier, Barking, Essex (1970)
48. Hall, H. T., *Rev. Scient. Instrum.*, 29:267 (1958)
49. Bassett, W. A., Shen, A. H. and Bucknum, M., A New Diamond Anvil Cell for Hydrothermal Studies to 2.5 Gpa and From -190 to 1200°C, *Rev. Sci. Instrum.*, 64:2340–2345 (1993)
50. Mroczkowski, S., Development of High-Pressure, High-Temperature Technique for Growing Single Crystals From The Flux , *J. Crystal Growth*, 24/25:683–687 (1974)
51. Shternberg, A. A., Controlling the Growth of Crystals in Autoclaves, in: *Crystallization Processes under Hydrothermal Conditions*, (A. N. Lobachev, ed.), pp. 225–240, Consultant Bureau, New York (1973)
52. Clark, S. M., Nield, A., Rathbone, T., Flaherty, J., Tang, C. C., Evans, J. S.O., Francis, R. J. and O'Hare, D., Development of Large Volume Reaction Cells for Kinetic Studies Using Energy-Dispersive Powder Diffraction, *Nucl. Inst. Methods Phys. Res.*, B97:98–101 (1995)
53. Evans, J. S. O., Francis, R. J., O'Hare, D., Price, S. J., Clark, S. M., Flaherty, J., Gordon, J., Nield, A., and Tang, C. C., An Apparatus for the Study of the Kinetics and Mechanism of Hydrothermal Reactions by *in situ* Energy Dispersive X-ray Diffraction, *Rev. Sci. Instrum.*, 66:2442–2445 (1995)
54. Clark, S. M., and Doorhyee, E., A Quantitative Kinetic Study of the I ↔ II Phase Transition of Ammonium Chloride, *J. Phys. Condensed Matter*, 4:8969–8974 (1992)

DropBooks

55. Kolb, E. D. and Laudise, R. A., Pressure-Volume-Temperature Behavior in The System H_2O-H_3PO_4-$AlPO_4$ and its Relationship to The Hydrothermal Growth of $AlPO_4$, *J. Crystal Growth*, 56:83–92 (1982)

56. Kolb, E. D., Barns, R. L., Laudise, R. A., and Grenier, J. C., Solubility, Crystal Growth and Perfection of Aluminum Orthophosphate, *J. Crystal Growth*, 50:404–418 (1980)

57. Ikornikova, N. Yu., Lobachev, A. N., Vasenin, A. R., Egrov, V. M., and Autoshin, A. V., Apparatus for Precision Research in Hydrothermal, in: *Crystallization Processes under Hydrothermal Conditions*, (A. N. Lobachev, ed.), p. 241, Consultant Bureau, New York (1973)

58. Yanagisawa, K., Xian-Pin, M., Nishioka, M., Ioku, K., and Yamasaki, N., Development of Solubility Measurement Method under Hydrothermal Conditions. *J. Mater. Sci. Letts*., 12:1800–1802 (1993)

59. Stanley, J. M., Hydrothermal Synthesis of Large Aluminium Phosphate Crystals, *Industr. Eng. Chem.*, 46:1684–1689 (1954)

60. Poignant, Marechal, L. Le., and Toudic, Y., Etude De La Solubilite Du Phosphate d'Alunimium ($AlPO_4$) Dans Des Solutions Hydrothermales d'Acide Orthophosphorique (H_3PO_4), *Mat. Res. Bull*., 14:603–612 (1979)

61. Kinloch, D. R., Belt, R. F., and Puttbach, R. C., Hydrothermal Growth of Calcite in Large Autoclaves, *J. Crytals Growth*, 24/25:610–613 (1974)

62. Yamasaki, N., Fujiki, M., Nishioka, M., Ioku, K., Yanagisawa, K., Kozai, N., and Muraoka, S., Hydrotheraml Decomposition of TBP and Fixation of its Decomposed Residue by Hydrothermal Hot Pressing Technique, in: *Proc. 3rd Intl. Symp. Adv. Nucl. Energy Res.—Global Environment and Nuclear Energy*, pp. 1–5 (1994)

63. Seyfried, W. E., Jr. and Janecky, D. R., Heavy Metal and Sulfur Transport During Subcritical and Supercritical Hydrothermal Alteration of Basalt: Influence of Fluid Pressure and Basalt Composition and Crystallinity, *Geochim. Cosmochim. Acta*, 49:2545–2560 (1985)

64. Bourcier, W. L. and Barnes, H. L., Rocking Autoclaves for Hydrothermal Experiments I. Fixed-Volume Systems, in: *Hydrothermal Experimental Techniques* (G. C. Ulmer, and H. L. Barnes, eds.), pp. 189–215, John Wiley and Sons, New York (1987)

65. Seyfried, W. E., Jr., Janecky, D. R., and Berndt, M. E., Rocking Autoclaves for Hydrothermal Experiments II, The Flexible Reaction-Cell System, in: *Hydrothermal Experimental Techniques* (G. C. Ulmer, and H. L. Barnes, eds.), pp. 216–239, John Wiley and Sons, New York (1987)

66. Yanagisawa, K., Feng, Q. and Yamasaki, N., Hydrothermal Synthesis of Xonotlite Whiskers by Ion Diffusion, *J. Mat. Sci. Letts*., 16:889–891 (1997)

67. Parr Autoclaves Co., U. S. A., Catalogue (1999)

68. Berghoff Autoclaves Ltd., Germany, Catalogue (1999)
69. Toshin Kogyo Co., Ltd., Jpn., Catalogue (1999)
70. Nitto Koatsu Co., Jpn., Catalogue (1999)
71. Fogo, J. K., Copeland, C. S., and Benson, S. W., Pressure Counterbalance Apparatus for The Measurement of The Electrical Conductivity of Aqueous Solutions above their Critical Temperatures, *Rev. Scient. Instru.*, 22:765–769 (1951)
72. Fogo, J. K., Benson, S. W., and Copeland, C. S., The Electrical Conductivity of Supercritical Solutions of Sodium Chloride and Water, *J. Chem. Phys.* 22:212–216 (1954)
73. Franck, E. U., Hochverdichteter Wasserdampf I. Elektrolytische Leitfahigkeit in KCl-H_2O Losungen bis 750°C., *Zeit. Physik. Chem.*, 8:92–106 (1956)
74. Franck, E. U., Experimental Investigations of Fluids at High Pressures and Elevated Temperatures, North American Treaty Organization (NATO) Advanced Study Institute, Series C, C41 (High Pressure Chemistry) (1978)
75. Frauck, E. U., Survey of Selected Non-Thermodynamic Properties and Chemical Phenomena of Fluids and Fluids Mixtures, in: *Chemistry and Geochemistry of Solutions at High Temperatures and Pressures*, (D. T. Rickard, and F. E. Wickman, eds.), *Proc. Noble Symp*., 13/14:65–88, Pergamon Press, New York (Sept. 1979)
76. Seward, T. M., The Stability of Chloride Complexes of Silver in Hydrothermal Solutions up to 350°C, *Geochim. Cosmochim. Acta*, 40:1329–1341 (1976)
77. Seward, T. M., The Stability of Chloride Complexes of Silver in Hydrothermal Solutions up to 350°C, *Geochim. Cosmochim. Acta*, 40:1329–1341 (1976); Seward, T. M., Metal Complex Formation in Aqueous Solutions at Elevated Temperatures and Pressures, in: *Chemistry and Geochemistry of Solutions at High Temperatures and Pressures*, (D. T. Rickard and F. E. Wickman, eds.), *Proc. Noble Symp.*, 13/14:113–132, Pergamon Press, New York (Sept. 1979)
78. Marshall, W. L., Conductances and Equilibria of Aqueous Electrolytes over Extreme Ranges of Temperature and Pressure, *Pure Appl. Chem*., 18:167–186 (1968)
79. Marshall, W. L., Complete Equilibrium Constants, Electrolyte Equiliria and Reaction Rates, *J. Phy. Chem*., 74:346–335 (1970)
80. Ryzhenko, B. N., A Conductance Cell for Use at high Temperatures and Pressures, *Geokhimiya*, 1963:41 (1963)
81. Smolyakov, B. S., Limiting Equivalent Ionic Conductances up to 200°C, *Intl. Corrosion Conf. Series., Proc. High Temperature High Pressure Electrochemistry in Aqueous Solutions Conf.*, (NACE-4), pp. 177–181 (1973)

DropBooks

82. Helgeson, H. C. and Kirkham, D. H., Theoretical Prediction of The Thermodynamic Behavior of Aqueous Electrolytes at High Pressures and Temperature: I: Summary of The Thermodynamic/Electrostatic Properties of The Solvent,*Amer. J. Sci.*, 274:1089–1198 (1974)

83. Helgeson, H. C. and Kirkham, D. H., Theoretical Prediction of The Thermodynamic Behavior of Aqueous Electrolytes at High Pressures and Temperature, III: Equation of State for Aqueous Species at Infinite dilution, *Amer. J. Sci*., 276:97–240 (1976)

84. Quist, A. S., and Marshall, W. L., Electrical Conductances of Aqueous Sodium Chloride Solutions from 0 to 800°C and to Pressures to 4000 bars. *J. Phy. Chem.*, 72:684–703 (1968)

85. Marshall, W. L. and Frantz, J. D., Electrical Conductance Measurements of Dilute, Aqueous Electrolytes at Temperatures to 800°C and Pressures to 4000 bars, Techniques and Interpretations, in: *Hydrothermal Experimental Techniques*, (G. C. Ulmer and H. L. Barnes, eds.), pp. 261–292, John Wiley and Sons, New York (1987)

86. Hawkins, D. B. and Roy, R., Electrolytic Synthesis of Kaolinite Under Hydrothermal Conditions, *J. Am. Ceram. Soc*., 45:507–508 (1962)

87. Yoshimura, M., Yoo, S-E., Hayashi, M., and Ishizawa, N., Preparation of $BaTiO_3$ Thin Film by Hydrothermal Electrochemical Method, *Jpn. J. Appl. Phys*., 28:L2007–L2009 (1989)

88. Cho, W-S., Yashima, M., Kakihana, M., Kudo, A., Sakata, T., and Yoshimura, M., Room-Temperature Preparation of Highly Crystallized Luminescent $SrWO_4$ Film by an Electrochemical Method, *J. Am. Ceram. Soc.*, 78:3110–3112 (1995)

89. Kajiyoshi, K., Hamaji, Y., Tomono, K., Kasanami, T., and Yoshimura, M., Microstructure of Strontium Titanate Thin Film Grown by the Hydrothermal–Electrochemical Method, *J. Am. Ceram. Soc*., 79:613–619 (1996)

90. Basca, R., Ravindranathan, P., and Dougherty, J. P., Electrochemical, Hydrothermal, and Electrochemical-Hydrothermal Synthesis of Barium Titanate Thin Films on Titanium Substrates, *J. Mater. Res*., 7:423–428 (1992)

91. Bendale, P., Venigalla, S., Ambrose, J. R., Verink, E. D., Jr., and Adair. J. H., Preparation of Barium Titanate Films at 55°C by "An Electrochemcial Method," *J. Am. Ceram. Soc*., 76:2619–2627 (1993)

92. Bard, A. J. and Faulkner, L. R., *Electrochemical Methods—Fundamentals and Applications*, Wiley, New York (1980)

93. Kajiyoshi, K., Tomono, K., Hamaji, Y., Kasanami, T., and Yoshimura, M., Growth of Strontium Titanate Thin Films of Controlled Thichness by the Hydrothermal-Electrochemical Method, *J. Am. Ceram. Soc*., 77:2889–2897 (1994)

94. Macdonald, D. D., Scott, A. C., and Wentrcek, P., External Reference Electrodes for Use in High Temperature Aqueous Systems, *J. Electrochem. Soc*., 126:908–911 (1979)

95. Macdonald, D. D., Scott, A. C., and Wentrcek, P., Silver-Silver Chloride Thermocells and Thermal Liquid Junction Potentials for Potassium Chloride Solutions at Elevated Temperatures, *J. Electrochem. Soc*., 126:1618–1624 (1979)

96. Weyl, W., Uber Metallammonium-Verbindungen; *Ann. Physik*, 121:606–610 (1864)

97. Seely, C. A., On Ammonium and the Solubility of Metals Without Chemical Action. *J. Franklin Inst*., 61:110 (1871)

98. Jacobs, H., and Schmidt, D., High-Pressure Ammonolysis in Solid-State Chemistry, in: *Current Topics in Materials Science* (E. Kaldis, ed.), 8:383–427 (1982)

99. Wakayama, H., Fukushima, Y., and Yamasaki, N., Wet Oxidation of Waste Oil, in: Advanced Materials '92, (R. Yamanoto, et al., eds.), *Trans. Mat. Res. Soc. Jpn.*, 18A:775–778 (1994)

100. Turlakov, V. N., Safronov, G. M., Kleshchev, G. V., and Simonov, A. V., Experimental Autoclave with Transparent Windows for Studying Hydrothermal Solutions, *Izvestia Akad. Nauk, Inorg. Mater.*, 6:1216–1217 (1970)

101. Kuznestov, V. A. and Lobachev, A. N., Hydrothermal Method for the Growth of Crystals, *Soviet Physics – Crystallography*, 17:775–804 (1973)

102. Ikornikova, N. Yu., Lobachev, A. N., Vasenin, A. R., Egorov, V. M., and Antoshin, A. V., Apparatus for Precision Research in Hydrothermal Experiments, in: *Crystallizatioin Processes Under Hydrothermal Conditions*, (A. N. Lobachev, ed.), pp. 241–255, Consultants Bureau, New York (1973)

103. Buback, M. and Franck, E. U., Measurements of the Vapor Pressures and Critical Data of Ammonium Halides, *Berichteder Bunsengesellschaft fur Physikalische Chemie*, 76:350–354 (1972)

104. Hosaka, M., and Taki, S., Raman Spectral Studies of SiO_2–NaOH–H_2O System Solution Under Hydrothermal Conditions, *J. Crystal Growth*, 100:343–346 (1990)

105. Yanagisawa, K., Sasaki, M., Nishioka, M., Ioku, K., and Yamasaki, N., Preparation of Sintered Compacts of Anatase by Hydrothermal Hot-Pressing, *J. Mat. Sci. Letts*., 13:765–766 (1994)

106. Nishioka, M., Yanagisawa, K., and Yamasaki, N., Solidification of Sludge Ash by Hydrothermal Hot Pressing Method, *Res. J. Water Pollution Control Federation*, 62:926 (1991)

107. Yamasaki, N., Yanagisawa, K., Nishioka, M., and Kanahara, S., Solidification of Radioactive Waste by Hydrothermal Hot Pressing Method, *J. Mat. Sci. Letts*., 5:355 (1986)

DropBooks

108. Nakane, Y., Hashida, T., Takahashi, H., and Yamasaki, N., Strengthening of Hydrothermal Hot Pressed Concrete Wastes by the Addition of Fresh Cement, *J. Ceram. Soc. Jpn.* (Int. Edition), 103:513–516 (1995)

109. Yamasaki, N., Xiang, L., and Feng, Q., Formation of PbO Powder by Hydrothermal Oxidation of Granular Pb Metal, *J. Mater. Sci. Letts.*, 15:2153–2157 (1996)

110. Habashi, F.,*A Textbook of Hydrometallurgy*, Libraire Universitaire du Quebec, Quebec, Canada (1993)

111. Thomas, K. G., Research, Engg. Design, and Operation of a Pressure Hydrometallurgy Facility for Gold Extraction, CANMET, Ottawa, Canada (1994)

112. Habashi, F., Industrial Autoclaves for Pressure Hydrometallurgy, in: *Proc. 2nd Intl. Conf. Solvothermal*, pp. 65–67, Reachtions, Takamatsu, Jpn., (Dec. 18–20, 1996)

113. F. Habashi, (ed.), *Handbook of Extractive Metallurgy*, 4 Vols., pp. 2500, Wiley–VCH, Germany (1997)

114. Moriyoshi, T., Uosaki, Y., Kimura, H., and Ikemoto, N., Hydrothermal Decomposition of Simple Organic Compounds, in: *Proc. 2nd Intl. Conf. Solvothermal Reactions*, pp. 50–53, Takamatsu, Jpn., (Dec. 18–20, 1996)

115. Uchida, H., Amiya, M., Iwai, Y., and Arai, Y., Separation of Dimethylnaphthalene Isomers by Supercritical Phase Absorption using Zeolite, in: *Proc. 2nd Intl. Conf. Solvothermal Reactions*, pp. 127–130, Takamatsu, Jpn., (Dec. 18–20, 1996)

116. Roy, R., Accelerating the Kinetics of Low-Temperature Inorganic Syntheses., *J. Solid State Chem.*, 111:11–17 (1994)

117. Burns, J. H., and Bredig, M. A.,*J. Chem. Phys.*, 25:1281 (1956)

118. Dachille, F., and Roy. R., High-Pressure Phase Transformations in Laboratory Mechanical Mixers and Mortars,*Nature*, 186:34, 71(1960)

119. Boldyrev, V. V.,*Rev. Solid State Science*, 7:1 (1989)

120. Boldyrev, V. V., Kabibullin, A., Khkosova, N. V., and Avaakumov, E. G., Hydrothermal Reactions Udner Mechanochemical Treatment, *J. Mater. Synth. Process*, 4:377–381 (1996)

121. Suslick, Sonochemistry,*Science*, 247:1439–1445 (1990)

122. Srikanth. V., Roy, R., and Komarneni, S., Acoustic-Wave Stimulation of the Leaching of Layer Silicates,*Mats, Lett.*, 15:127–129 (1992)

123. Fang, Y., Agarwal, D. K., Roy, D. M., and Roy, R., Fabrication of Porous Hydroxyapatite Ceramics by Microwave Ceramics, *J. Mater. Res.*, 7:490–494 (1992)

124. Abu-Sharma, A., Morris, J. S., and Koirtyohann, S. R., Wet Ashing of Some Biological Samples in Microwave Oven., *Anal. Chem.*, 47:1475–1477 (1975)

125. Kingston, H. M. and Jassie, L. B., (eds.), *Introduction to Microwave Sample Preparation*, American Chemical Society, Washington, DC. (1988)

126. Komarneni, S., Roy, R., and Li, Q. H., Microwave-Hydrothermal Synthesis of Ceramic Powders, *Mater. Res. Bull*., 27:1393–1405 (1992)

127. Komarneni, S., Pidugu, R., Li, Q. H., and Roy, R., Microwave-Hydrothermal Processing of Metal Powders, *J. Mater. Res.*, 10:1687–1692 (1995)

128. Komarneni, S., Enhanced Reaction Kinetics Under Microwave-Hydrothermal Conditions, in: *Proc. 2nd Intl. Conf. Solvothermal Reactions*, pp. 97–99, Takamatsu, Jpn., (Dec.18–26, 1996)

129. Komarneni, S., Microporous Microporous Metal Intercalated Clay Nanocomposites, in: *Ceramic Transactions, Porous Materials*, (K. Ishizaki, L. Sheppard, S. Okada, T. Hamasaki, and B. Huybrechts, eds.), 31:155–68, American Ceramic Society, Westerville, OH (1993)

130. Strubel, G., *Dt. Gemmol. Ges*., 24:138–144 (1975)

131. Vidale, R., Pore Solution Compositions in a Pelitic System at High Temperatures, Press and Salinities, *Amer. J. Sci.*, 283 A:298-313 (1983)

132. Jacobs, G. K., and Kerrick, D-M., A Simple Rapid-Quench Design for Cold-Seal Pressure Vessels, *Amer. Min*., 65:1053–1056 (1980)

DropBooks

4

Physical Chemistry of Hydrothermal Growth of Crystals

4.1 INTRODUCTION

This is perhaps the least known aspect in the hydrothermal growth of crystals. No book on crystal growth gives a complete picture of the theoretical aspects of hydrothermal growth. Similarly, no author has produced a definitive discussion of the physical chemistry of hydrothermal growth of crystals, covering aspects of physicochemical and hydrodynamic principles, solutions, solubility, phase equilibria, thermodynamics, kinetics, modeling or intelligent engineering of the hydrothermal reactions, and so on. The Nobel Symposium organized by the Royal Swedish Academy of Sciences during 1978, followed by the First International Symposium on hydrothermal reactions organized by the Tokyo Institute of Technology in 1982, helped in setting a new trend in hydrothermal technology by attracting physical chemists in large number.[1][2] The hydrothermal physical chemistry today has enriched our knowledge greatly through a proper understanding of hydrothermal solution chemistry. There are several groups all over the world working on various aspects of physical chemistry under hydrothermal conditions.

4.1.1 Physico-Chemical and Hydrodynamic Principles of the Hydrothermal Growth of Crystals

This is one of the fundamental aspects of hydrothermal growth of crystals. There are two aspects to be discussed here:

i. The physico-chemical studies on various aqueous solutions studied within a wide range of pressure temperature conditions.

ii. The physical chemistry of the hydrothermal growth of crystals.

Each one of these has been studied extensively. However, the correlation of the two works has not been done with enough accuracy.

Ezersky et al. (1993a, 1993b) have studied the hydrodynamics under hydrothermal conditions using a shadowgraph technique.[3][4] This facilitated understanding of the spatiotemporal structure of hydrothermal waves in Marangoni convection. However, a lot more experimental and theoretical developments are needed to clarify and complete the description of the hydrothermal waves. Thus, an emphasis is made on some of the basic physico-chemical aspects of the hydrothermal growth of crystals.

DropBooks

During the crystallization process from saturated solutions, the mol number of the solute compounds changes and, therefore, the free energy is represented as a function of not only temperature and pressure but also the mol numbers:

Eq. (1) $$G = f(T,P,n_1,n_2,....n_i)$$

Eq. (2) $$DG = (\delta G/\delta T)_{p,n}\, dT + (\delta G/\delta P)_{T,n} dP + (\delta G/\delta n_1)_{P,T,n}\, dn_1 + (\delta G/\delta n_1)_{P,T,n} dn_2$$

where: n_i = constant mol number of all components,
n_j = constant number of components except one.

The variation in the free energy can be expressed in terms of the chemical potential:

Eq. (3) $$(\delta G/\delta n_i)_{P,T,n} = \mu_i$$

When P and T are kept constant, Eq. (2) becomes

Eq. (4) $dG_{P,T} = \mu_i\, dn_1 + \mu_i\, dn_2 + \ldots,$ or $dG_{P,T} = (\Sigma dn_i)_{P,T}$

The integration of Eq. (4) gives

Eq. (5) $G_{P,T} = \Sigma_i\, n_i$

Differentiation of Eq. (5) gives

Eq. (6) $$dG_{P,T} = n_1 d\mu_1 + n_2 d\mu_2 + \ldots + n_i d\mu_i + \mu_i\, d\mu_1 + \mu_i\, d\mu_2 + \ldots + \mu_i\, d\mu_i = \Sigma n_i d\mu_i + \Sigma \mu_i\, dn_i$$

By equating Eqs. (4) and (6) we get

Eq. (7) $\Sigma n_i d\mu_i = 0$

Equation (7) is considered as the overall equilibrium condition in the system with variable mol numbers under constant P and T.

Let us consider a hydrothermal system containing n_A mol of solid A and partially soluble (n_{1A} mol) in n_B mol solvent. Then the free energy of the system corresponds to Eq. (5):

Eq. (8) $G = n_A\, \mu_A + n_{1A}\, \mu_{1A} + n_B\, \mu_B$

If the process of dissolution of the solid components continues, then the free energy dG becomes

Eq. (9) $G + dG = (n_A - dn)\mu_A + (n_{1A} + dn)\mu_{1A} + n_B \mu_B$

The change in the free energy corresponding to this, under constant P and T, becomes

Eq. (10) $dG = (\mu_{1A} - \mu_A)dn$

or

Eq. (11) $dG/dn = \mu_{1A} - \mu_A$

If $\mu_{1A} < \mu_A$, then dG/dn is negative and the process occurs on its own, since the free energy decreases. When $\mu_{1A} > \mu_A$, the crystallization

of the substance from solution B takes place and the chemical potential decreases, and when $\mu_{1A} = \mu_A$, the process reaches the equilibrium state. Consequently, the solute component changes over from the phase wherein its chemical potential is higher into the phase where its chemical potential is lower. The phase transition stops when the chemical potential of the component becomes equal in both phases. It is observed that the above-considered mechanism is realized only when, in the non-equilibrium process, the changes in *dG* do not depend upon the chemical potential and concentration of other components of the solution. However, consideration of the above relationship may help in understanding the physico-chemical principles of the hydrothermal process.

Most hydrothermal crystal growth experiments are carried out under the conditions of temperature gradient in standard autoclaves. The growth of a single crystal into the seed can be carried out in two ways:

a. Recrystallization of the solid substance, including its dissolution in the liquid phase, convective mass transfer of the dissolved part of the substance to the growth zone or seed.

b. Dissolution of the mixture of the nutrient components with the help of their convective mass transport into the growth zone and interaction of the dissolved components on the seed surface.

DropBooks

The methodology of the growth of single crystals on a seed is the establishment of growth conditions in which the process is represented by the sum of macro- and micro-processes occurring between the interface boundary of the solution and the crystal. The composition and concentration of the solution, temperature and pressure, hydrodynamic conditions, and surface contact of the phases are some of the basic physical and chemical parameters which determine the regime and rate of dissolution of the nutrient, mass transport, and possibility of the formation of new phases.

The isothermal chemical reaction can be expressed in terms of the van't Hoff equation

Eq. (12) $$\Delta G_{P,T} = RT \ln \pi a' - RT \ln K_{ai'}$$

where:

$\pi a'$ = $\pi'(a'_i, y_i)$

K_a = $\pi'(a'_i, y_i)$, is the thermodynamic equilibrium constant

y_i = activity coefficient

a_i = initial non-equilibrium activity of the nutrient component in the solution

a_i = equilibrium activity of the nutrient components in the solution

From Eq. (12) it is observed that ΔG depends upon the relative values of $\pi a'$ and K_a when

Eq. (13) $\pi a' < K_a$; $\Delta G < 0$

Eq. (14) $\pi a' = K_a$; $\Delta G = 0$

Eq. (15) $\pi a' > K_a$; $\Delta G > 0$

For example, in Eq. (13) the process is irreversible and the reaction takes place from left to right. In the case of Eq. (14), the reaction takes place under equilibrium condition and, for example, in Eq. (15) the process becomes reversible. As a result, the changes in ΔG in Eq. (12), for example, can be represented as follows:

$$\Delta G = RT \ln(a_i / a'_i),$$

where a_i/a'_i is the analogue of the relative supersaturation.

If the activity coefficient $y \approx 1$ or, in the given region, y does not depend upon the concentration then, for example in Eq. (12), the activity coefficient can be replaced by the mol fraction. Then the ratio a_i/a'_i is replaced by S_i/S'_i, where S'_i = undersaturated solubility.

Equilibrium concentration of the supersaturated solution. The ratio S_i/S'_i is called the relative supersaturation or degree of supersaturation.

In recent years there has been good progress on the experimental side. Much credit goes to the Russian hydrothermal crystal growers. Balitsky and Bublikova (1991) have studied the physico-chemical foundation of malachite synthesis. Similarly, Kuznetsov (1991) has reviewed the physical chemistry of hydrothermal crystal growth and the crystallization of some A_2B_6 crystals. Further, Popolitov (1991) has reviewed the physical

chemistry of the hydrothermal growth of tellurium dioxide crystals. The reader can get valuable information in the book *Hydrothermal Growth of Crystals.*[5]

4.2 BASIC PRINCIPLES OF PHASE FORMATION UNDER HYDROTHERMAL CONDITIONS

A *phase* is defined as a part of the system that is homogeneous throughout and is physically separable from other phases by distinct boundaries. The number of components in a system is the minimum number of chemical constituents that must be specified to describe the composition of all phases present. Phase relationships are conveniently represented by means of phase diagrams. Phase diagrams and the phase rules apply only to systems at equilibrium. These data are extremely important to any crystal grower for successful growth of crystals. Gibbs deducted a quantitative relationship for phase rule:

$$F = C - P + 2$$

DropBooks

where F = degrees of freedom, C = number of components, P = number of phases.

The above relation holds true if pressure, temperature, and composition are the only variables. If other variables such as magnetic, electric or gravitational fields are considered, the numerical value 2 on the right-hand side of the equation will increase by the number of new variables considered.

The hydrothermal method is considered as one of the best methods to study phase relationships in numerous systems, and the *PTX* diagrams thus obtained are published from time to time. Phase equilibria have been considered in detail by several workers. A reader can get valuable information in the works of Brebrick (1993) published in *Handbook of Crystal Growth* (D. T. J. Hurle, ed.). Hence, we restrict our discussion to some basic systems and non-conventional phase diagrams.

Among the binary systems, the H_2O-CO_2 system is important with regard to the role of H_2O and CO_2 vapor pressures in native mineral formation and in the hydrothermal synthesis of inorganic compounds. Figure 4.1 shows the phase diagram for the H_2O-CO_2 system.[6] It is found that, below the critical temperature of water, the dependence V versus P

has a gap at the pressure corresponding to the pressure of water at its critical density. The isochores of real mixtures are linear up to the immiscibility dome that gives a possibility to experimental data in the calculation of pressures of mineral formation from the gas-liquid inclusions.

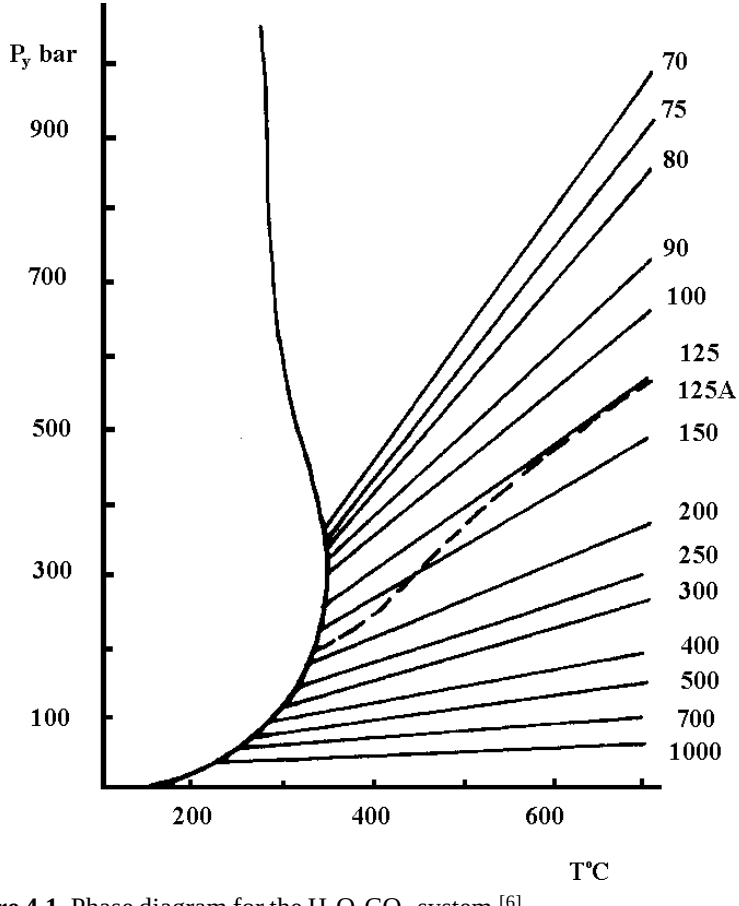

Figure 4.1. Phase diagram for the H_2O-CO_2 system.[6]

The non-conventional phase diagrams plotted for equilibrium conditions are popular, especially among Russian workers. These diagrams are popularly known as *composition diagrams* or *NC* diagrams, where N is the nutrient composition and C is the concentration of the solvent

mineralizer. Hundreds of phase diagrams of compositions are available, especially in the Russian literature. An example of such a diagram is given in Fig. 4.2 corresponding to the system Na_2O-ZrO_2-SiO_2.[7] Similarly, the distribution of the silicon-oxygen radical in the rare earth silicates is shown in the NC diagram in Fig. 4.3 corresponding to the system Na_2O-RE_2O_3-SiO_2-H_2O under hydrothermal conditions.[8] The solid lines indicate the regions of monophase crystallization and dashed lines indicate the beginning of crystallization of the excess component. These non-conventional diagrams are relatively easy to obtain and are highly useful for the growth of single crystals as they clearly depict the growth conditions. Similarly, just as in the case of conventional phase diagrams—even in the phase diagrams of crystallization, the components can be represented for example, in a ternary system as a triangle. Figure 4.4 shows the phase diagram of crystallization in the system LiO_2-Ta_2O_5-H_2O at 750°C and 1700 atm.[9]

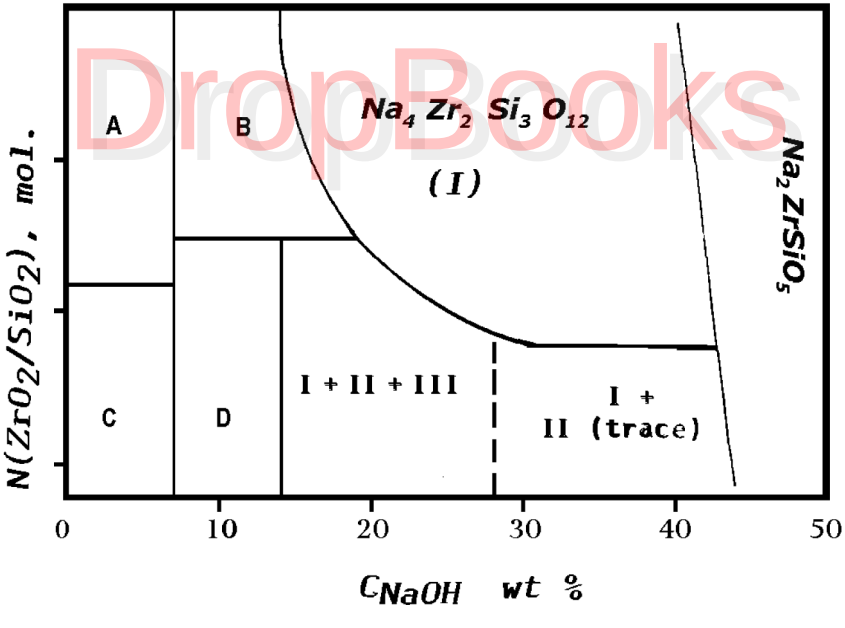

Figure 4.2. NC diagram for the system Na_2O-ZrO_2-SiO_2.[7]

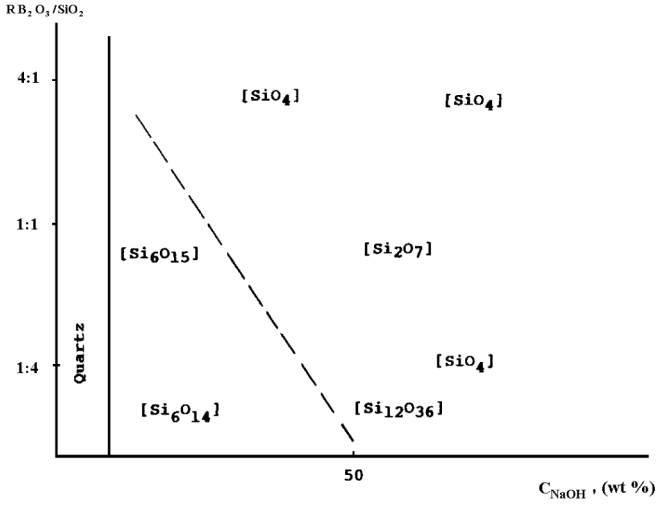

Figure 4.3. NC diagram for the system Na_2O-RE_2O_3-SiO_2-H_2O under hydrothermal conditions.

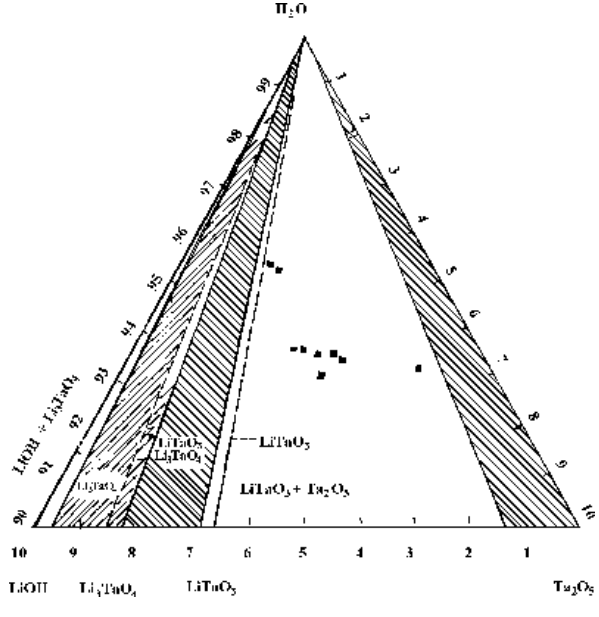

Figure 4.4. The phase diagram of crystallization in the system LiO_2-Ta_2O_5-H_2O at 750°C and 1700 atm.

4.3 SOLUTIONS, SOLUBILITY AND KINETICS OF CRYSTALLIZATION

This is one of the most important aspects of the hydrothermal growth of crystals. Initial failures in the hydrothermal growth of a specific compound are usually the result of lack of proper data on the type of solvents, the solubility, and solvent-solute interaction. Despite the large amount of literature data already available, it is still a highly attractive field in hydrothermal research, geoscience, and so on. For example, geologists are now in a position to tell us much about the conditions of formation of hydrothermal ore deposits (e.g., temperature, pressure, oxidation potential, pH, fluid salinity, etc.), but in order to fully understand the mechanisms of transport and deposition of ore minerals, information about metal complex formation, stability, and stoichiometry in high-temperature–high-pressure aqueous electrolyte solutions, thermodynamic properties of electrolytes at high pressures and temperatures, phase behavior, transport phenomena, and electrical and optical properties, is necessary.[10]-[12] Unfortunately, most of the studies have been performed only at the saturated vapor pressure of the system and very few combined high-temperature–high-pressure experiments have been designed to yield thermodynamic data.

PropBooks

Recent advances in computer technology, which have seen both speed and storage capacities dramatically increased, offer the possibility that chemical speciation modeling of multicomponent electrolyte solutions can be made much more reliable than it has been. Automation of the whole calculation process involving the assessment and selection of data, the determination of basis sets, the formation of equations and the methods by which results are evaluated is now within reach. This should be seen as the provision of technical assistance rather than as a substitute for human expertise. Nevertheless, by reducing errors and by ensuring that assumptions are recorded systematically, many of the problems that have been so apparent in the literature may be better controlled in the future.[13][14]

Sterner et al. (1997) have developed a new computer algorithm, INSIGHT, which facilitates the nonlinear thermodynamic analysis of large heterogeneous data sets for the purpose of developing accurate equations of the state of aqueous solutions and their interactions with other substances.[15] The code is capable of incorporating a diverse array of primary thermophysical data including osmotic, vapor pressure, freezing

point depression, solubility [fixed pH] [fixed pCO_2], electromotive force data, speciation information obtained from spectroscopic measurements and molecular dynamic simulations, enthalpies of mixing, dilution and solution heat capacity, volumetric, and compressibility data, together in a global, polythermal polybaric, thermodynamic analysis while simultaneously solving chemical equilibria within the aqueous phase via Gibbs energy minimization.

A hydrothermal solution is generally considered as a thermodynamically ideal one, yet in the case of strong and specific interaction between the solute and the solvent or among the components of the soluble substance in them, significant deviations from Raoult's law occur. Consequently, real hydrothermal solutions differ from ideal solutions and their understanding requires knowledge of the influence of the solvent in the process of dissolution and crystallization of various compounds. Obviously, as shown in most of the experiments, the type of solvent and its concentration determine a specific hydrothermal process and its important characteristics such as the solubility of the starting materials, quantity of the phases, their composition, output of the phases, kinetics and growth mechanism of single crystals. The value of the changes in the Gibbs free energy in reaching an equilibrium condition varies with the transition from one solvent to another and it can be shown as:

Eq. (16) $\Delta G = \Delta H - T\Delta S = RT \ln K$, or $K = \exp(-\Delta H/T) \exp(\Delta S/R)$

where K = equilibrium constant.

The above expression shows the influence of enthalpy and entropy on the equilibrium constant, so that the enthalpy and entropy of the solubility (at constant P and T) are different for different solvents. Also, the solubility of one and the same solid substance changes with the solvent.

At the moment, there is no theory which can explain and estimate the solubility in real solutions. However, many of the problems connected with solubility can be explained on the basis of overall physico-chemical principles or laws.

In some cases, it is better to use the empirical rule which agrees with the fact that solubility becomes high in solvents with higher dielectric constant (ε) and types of chemical bond which are closer to those of the solute substance. Deviation from this group has a place in the case where specific interaction between solid substance and the solvent occurs.

The synthesis and recrystallization of a specific compound and the growth of single crystals on the seed are all carried out using different solvents on the basis of physico-chemical considerations. The following conditions are adopted in selecting the most suitable mineralizers:

i. Congruence of the dissolution of the test compounds.

ii. A fairly sharp change in the solubility of the compounds with changing temperature or pressure.

iii. A specific quantitative value of the absolute solubility of the compound being crystallized.

iv. The formation of readily-soluble mobile complexes in the solution.

v. A specific redox potential of the medium ensuring the existence of ions of the required valence.

Additionally the solvent should have the desired viscosity, insignificant toxicity, and very weak corrosion activity with respect to the apparatus.

These factors fulfill the requirement of the hydrothermal mineralizer in addition to determining the values of solubility of the compound under investigation.

DropBooks

The interaction between the solute and solvent is called *solvation.* Solvent molecules become linked to the dissolved molecules or ions, and the resulting species containing solvent molecules are *solvates*. Depending upon the reactants, the linkage between the solvent and the solute may exhibit different specific (coordination, hydrogen bond formation, etc.) and non-specific (electrostatic) factors, or solvation processes of different strength and, hence, solvates include very varied formations. Therefore, it is not possible to find a single physical parameter characterizing the solvent which, in itself, could rationalize the solvation process. Simple ions may differ considerably in their electronic structures, charges and radii, and even larger differences are exhibited by solvent molecules representing different types of chemicals. Hence, solvated ions may also be very different as regards the number of solvent molecules bound to the ion (the *solvation number*), the forces giving rise to the binding, and the resulting physical and chemical properties like spatial requirements (there are various ways of determining the solvation number-viscosity measurements, pH, conductivity measurement, density measurements, etc.). The specific solvation process is the result of various types of

complex formation between the solvent-solute components. In the case of homogeneous aqueous solutions of specific solvation, an activated complex theory can be considered,[16] according to which the rate constant, ξ, of the reaction type $A + B \equiv X^{\neq} \rightarrow$ reaction products ($X^{\neq}$ is the activated complex) is determined by

Eq. (17) $$\xi = (kTK^{\neq}/h)\ (\nu_A \nu_B / \nu^{\neq})$$

The concentration of the activated complex X may be determined by the following equation:

Eq. (18) $$[X^{\neq}] = K^{\neq}\ (C_A)\ (C_B)\ \nu_A \nu_B / \nu^{\neq}$$

where h is the Planck constant, $K^{\neq}$ is the equilibrium constant of the activated complex, C_A, C_B are the concentrations of the components A and B, and ν_A, ν_B, $\nu^{\neq}$ are the activity coefficients of the nutrients and active complex, respectively.

In non-specific solvation when the medium is not homogeneous, i.e., the solvent-solute interaction is not homogeneous and continuous, such an interaction plays a significant role only for ionic compounds.[17] The classical electrostatic model links the rate of reaction constant ξ (in a given known dielectric value ε), with the rate constant (in the medium with $\varepsilon = \infty$), Eq. (18):

Eq. (19)
$$\ln \xi = \ln \xi_0 + \frac{e^2}{2\varepsilon kT}\left[\frac{Z_A^2}{r_A} + \frac{Z_B^2}{r_B} - \frac{(Z_A + Z_B)}{r_{\neq}}\right] + ¾\varepsilon kT\left(\frac{\mu_B^2}{r_B^3} - \frac{\mu_{\neq}^2}{r_{\neq}^3}\right)$$

where r is the radius of the particle, μ is the dipole moment of the particles, Z is the charge number, k is the Boltzmann constant, T the temperature, and e the electron charge.

This equation shows that the log of the rate constant depends linearly upon the reverse (negative) values of the dielectric constants.

Let us consider briefly the role of water as a solvent in the hydrothermal growth of crystals. Water is the major component of hydrothermal solutions, always with a varied chemical composition in the

laboratory and in nature. All the solutions used in hydrothermal experiments vary from one another in their properties, ability to dissolve and crystallize, and in the nature of the linking between water and electrolyte. Moreover, the properties of each solution depend upon physico-chemical aspects and the structure of the pure water. The formation of associates and complexes in the aqueous solutions of electrolytes is possible because of the presence of structural water, i.e., consisting of water molecules with directional hydrogen bonding. The experimental *P-V-T* behavior of water has been reviewed and summarized by several workers.[19]-[22] Several chemical changes arise from changes in ionic dissociation of the solution. Therefore, it is better to understand the characteristics of the pure water under hydrothermal conditions. The hydrogen ions show an influence on the solubility of various compounds under hydrothermal conditions.

4.4 THERMODYNAMIC PRINCIPLES OF SOLUBILITY

Thermodynamic principles enable one to determine how to design a reaction to yield phase-pure phases. Without knowledge of how to do this, it is impossible to distinguish a process that is being controlled by thermodynamics versus kinetics. A large number of publications have appeared on this aspect based on both the theoretical and experimental data. Several models have been proposed in order to understand the hydrothermal synthesis of a variety of compounds like ABO_4 (*A* = alkaline earth elements, *B* = Ti, Zr, Hf), HAp, sulphides of gold, silver, iron, copper, and so on.[23[-[28] Thermodynamic studies yield rich information on the behavior of solutions with varying pressure-temperature conditions. Some of the commonly studied aspects are solubility, stability, yield, dissolution-precipitation reactions, and so on, under hydrothermal conditions. The thermodynamic principles of solubility are discussed here in brief. It is well known that

PropBooks

Eq. (20) $$\Delta G^0_{sol} = \Delta H^0_{sol} - TAS^0_{sol}$$

where ΔG^0_{sol}, ΔH^0_{sol} and ΔS^0_{sol} are the changes in the corresponding free energy, enthalpy, and entropy of dissolution.

If $\Delta G^0_{sol} < 0$, then dissolution takes place. When $\Delta G^0_{sol} = 0$, the system exists in the equilibrium state; when $\Delta G^0_{sol} > 0$, crystallization is thermodynamically possible.

With a change in the enthalpy, it is observed that either:

i. In the entire temperature interval $\Delta H^0_{sol} < 0$.

ii. In the low temperature region $\Delta H^0_{sol} > 0$, whereas in the high temperature region $\Delta H^0_{sol} < 0$.

iii. In the entire temperature region $\Delta H^0_{sol} > 0$.

If entropy is considered in Eq. (20) then with an increase in the temperature, just like ΔH^0_{sol}, the ΔS^0_{sol} may also change. Here also we can expect three possibilities:

i. In the entire temperature region, $T\Delta S^0_{sol} < 0$.

ii. In the low temperature region, $T\Delta S^0_{sol} > 0$, whereas in the high temperature region, $T\Delta S^0_{sol} < 0$.

iii. In the entire temperature interval $T\Delta S^0_{sol} > 0$.

In the first case, the entropy helps in the dissolution process. In the second case, it can be both helping and reducing, and in the third case, it reduces the dissolution process.

In the majority of cases, the solubility of the solid substances in a liquid phase is limited. Solubility is an important physico-chemical and technological parameter whose estimation determines any dissolution process. It acts as a factor which strongly influences the kinetics or rate of dissolution. Solubility depends upon the nature of the substance, its aggregate state, temperature, pressure and a series of other factors. Quantitative dependence of the solubility of the solid substance on the temperature at a given constant pressure is given by

Eq. (21) $$(\delta \ln S/\delta T)_P = (Q_2/RT^2)\,(\delta \ln a_2/\ln S_{P.T.})$$

where: S = solubility of the solid substance

a_2 = activity of the solid substance

Q_2 = heat of dissolution of one mol of the substance in the saturated solution

R = gas constant

The solubility of the solid substance may be expressed as a set of two processes: *(a)* melting of the solid substance, *(b)* mixing of two liquids.

In the case of ideal solubility of the solid substance, the heat of the second process is equal to zero and $\bar{Q}_2$ is equal to the heat of melting of the

solid substance: $\bar{Q}_2$ = % melting and does not depend upon the selection of the solvent, where if $\delta \ln a_2/\delta \ln S = 1$, then Eq. (21) can be written as

Eq. (22) $$(\delta \ln S/\delta T)_P = \%_{\text{melting}}/RT^2$$

such that the right-hand side is > 0, i.e., with an increase in the growth temperature, ideal solubility of the solid substance in an ideal solution increases. The dependence of the solubility of any substance in the solution and the pressure is expressed as

Eq. (23) $$(\delta \ln S/\delta T)_T = (V^0_{\text{solid}} - V_{\text{liquid}}/RT)\,(\delta \ln a_2/\delta \ln S)_{P.T.}$$

where V_{liquid} = partial molar volume of the soluble substance in the solution, V^0_{solid} = molar volume of that substance in the solid phase. In the case of an ideal solution, $\ln a_2 = \ln S$, $\delta \ln a_2/\delta \ln S = 1$, and Eq. (23) becomes

Eq. (24) $$(\delta \ln S/\delta P)/T = (V^0_{\text{solid}} - \bar{V}_{\text{liquid}})/RT$$

Thus, in the case of ideal solutions of the solid substance in the investigated media, the solubility decreases with an increase in the pressure, if the molar volume of the soluble substance increases during its melting. Similarly, if $V^0_{\text{solid}} - \bar{V}_{\text{liquid}}$, then the solubility should increase with an increase in the pressure (in the case when the partial volume of the liquid is equal to the volume of the melting salt).

DropBooks

In recent times, many aspects of hydrothermal chemistry have been experimentally studied, particularly in the past decade. The credit goes to workers like Franck, Seward, Hegleson, and others.[10]–[12][29] However, most of these studies do not give an insight into the complete physical chemistry of the hydrothermal media as they represent mainly the lower *PT* conditions. Helgeson has reviewed exhaustively the thermodynamic properties of electrolytes at high pressures and temperatures.

An understanding of theory and the experimental results on the hydrothermal physical chemistry is very essential to the crystal grower. Here, in the experimental work, some of the basic properties of the hydrothermal medium like viscosity, dielectric constant, compressibility and coefficient of expansion, etc., are discussed briefly in the crystal growth context. Since diffusion is inversely proportional to solvent viscosity, we would expect very rapid diffusion in hydrothermal growth.

This leads to the growth of perfect single crystals with well developed morphology. We can expect higher growth rates, a narrower diffusion zone close to the growing interface and less likelihood of constitutional supercooling and dendritic growth. It is, thus, no wonder that quartz growth rates as high as 2.5 mm/day without faults or dendritic growth have been observed.[30] Figure 4.5 shows the viscosity of water as a function of density and temperature. It has been demonstrated for many cases that the mineralizer solutions (typically 1 M NaOH, Na_2CO_3, NH_4F, K_2HPO_4, etc.) are close to the properties of water. For 1 M NaOH at room temperature, $\eta_{solution}/\eta_{H_2O} = 1.25$,[31] one can expect that the viscosity of hydrothermal solutions can be as much as two orders of magnitude lower than "ordinary" solutions. The mobility of molecules and ions in the supercritical range is much higher than under normal conditions. Also, electrolytes, which are completely dissociated under normal conditions, tend to associate with rising temperature.[32]

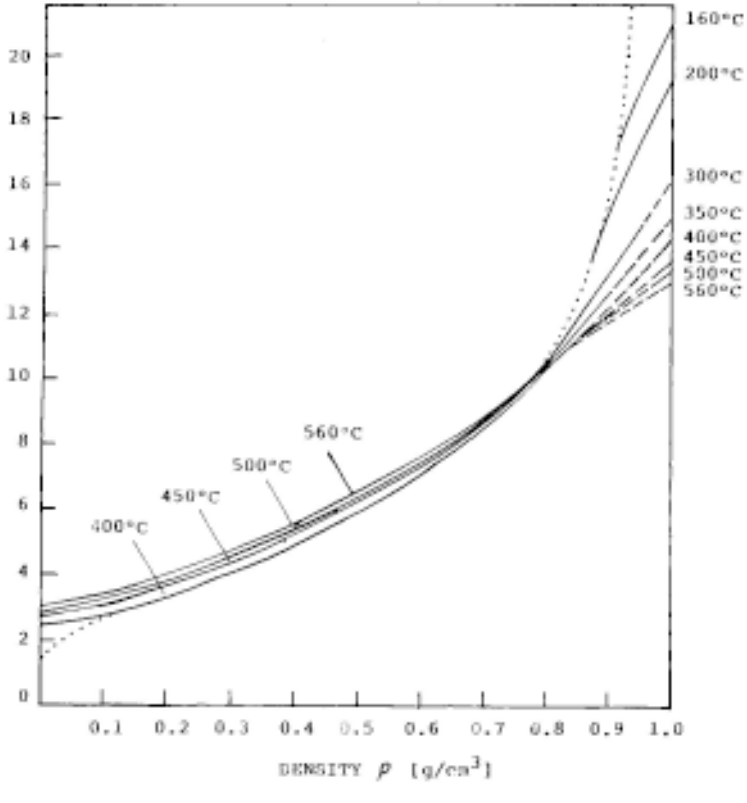

Figure 4.5. Viscosity of water as a function of density and temperature.[29]

The dielectric constant is one of the important properties of a solution. A knowledge of the temperature dependence of the relative dielectric constant is of great importance for understanding the hydration/dehydration phenomena and reactivities of a variety of solutes in supercritical water. More than forty years ago, Hasted et al. (1948) observed that the dielectric constant of electrolyte solutions (ε) can be regarded as a linear function of molarity up to 1–2 M, depending on the electrolyte.[33] Franck[29] has discussed ionization under hydrothermal conditions and made most careful and complete conductivity studies, and shown that the conductance of hydrothermal solutions remains high in spite of a decrease in ε, because that effect is more than compensated for by an increase in the ion mobility brought about by decreased viscosity under hydrothermal conditions. Figure 4.6 shows the dielectric constant of water.[34] Thermodynamic and transport properties of supercritical water are remarkably different from those of ambient water. Supercritical water is unique as a medium for chemical processes. The solubility of nonpolar species increases, whereas that of ionic and polar compounds decreases as a result of the drop of the solvent polarity, and the molecular mobility increases due to a decrease in the solvent viscosity (η). Drastic changes of ionic hydration are brought about by the decrease in the dielectric constant (ε) and density (ρ). Largely as a consequence of the dramatic decrease in the dielectric constant of water with increasing temperature at constant pressure and/or decreasing pressure at constant temperature, "completely" dissociated electrolytes at low temperatures and pressures may become highly associated in the supercritical region. Computer-simulation studies have been carried out on this topic, which are helpful for the interpretation from the molecular point of view. Virial expansion of Debye-Hückel theory affords a basis for extrapolating thermodynamic observations of "completely" dissociated electrolytes to high pressures and temperatures, where they may be highly associated. However, the Debye-Hückel equation fails to represent adequately the observed activity coefficients for dilute solutions of 2:2 electrolytes. Landolt-Börnstein (1980) have estimated the compressibility of water from the *PVT* curves.[35] The hotter and less dense the fluid is, the larger is its compressibility. It is an important factor used in the calculation of density change with pressure. The coefficient of thermal expansion is also an important parameter that helps in the growth of flawless and strain free crystals. It can be calculated from *PVT* data. Water has a much increased coefficient of expansion under hydrothermal conditions. *PVT* measurements for water and other solvents

ProfoBooks

are rather rare. Water above critical temperature (t_c = 374.2°C) and critical pressure (p_c = 22.1 MPa) is called *supercritical water*. At the critical point, the phases of liquid and gas are not distinguishable. There are extensive studies on the structure of water under ambient conditions, but the structure of water at high temperatures and high pressures are not well investigated, mainly due to experimental difficulties. In recent years, there has been increased interest in the study of the structure, dynamics, and reactivity of supercritical and subcritical water from the chemical, physical, geological and engineering points of view. There are several reasons for this trend. Water at high temperatures and high pressures is believed to have played a major role in creating organisms on the earth, the compounds necessary for them, and fossil fuels produced after their death.

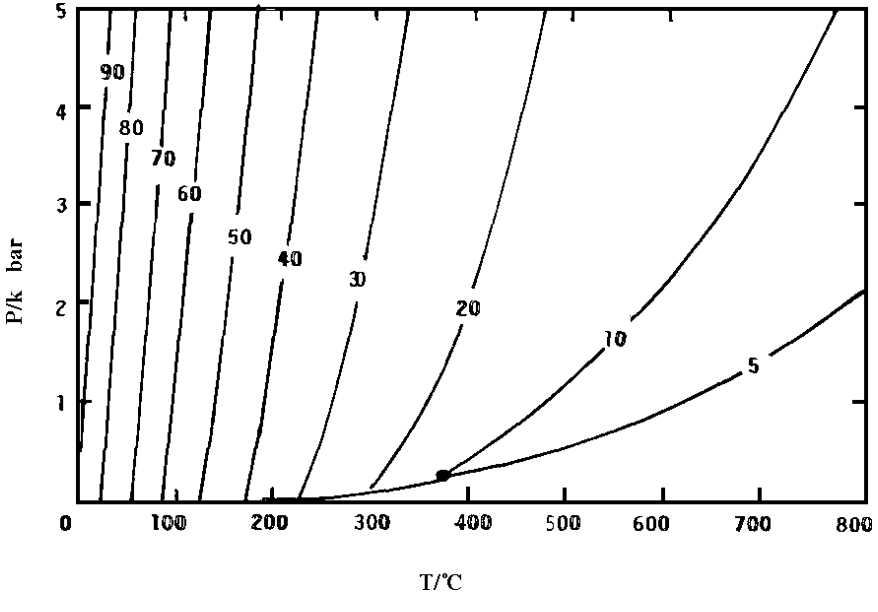

Figure 4.6. Dielectric constant of water.[34]

Seward (1997), Nakahara et al. (1996), Yamaguchi et al. (1996), Nakahara et al. (1997), and Ohtaki et al. (1997) have carried out extensive experimental work on the aqueous systems at high temperatures and pressures using conductivity, potentiometric, spectrophotometric, solubility, *PVT*, and calorimetric methods. However, insight into the configurational aspects of ion solvent interactions under hydrothermal conditions has come

mainly from neutron diffraction studies and more recently from synchrotron x-ray absorption (EXAFS) spectroscopic measurements.[36]-[40] These latter studies have confirmed that cation-oxygen (*nearest-neighor water*) distances decrease with increasing temperature and are accompanied by an associated decrease in the number of first shell solvated water molecules as has been shown for Ag^+, Sr^+, and other cations (Seward, 1997).[36]

Water is an environmentally safe material and cheaper than other solvents, and it can act as a catalyst for transformation of desired materials by tuning temperature and pressure. The larger the reaction barrier height, the larger the temperature effect on the reaction. For example, reactions whose Arrhenius activation energies are 42, 83, and 125 kJ mol^{-1} in water at 25°C, are accelerated by factors of 8.2×10^3, 6.6×10^7, and 5.4×10^{11}, respectively, at 400°C.[41] Thus, a new reaction pathway, which is not available in ambient water due to a high barrier, low solubility, or low molecular diffusion rate, can be made accessible thermally in supercritical water. Studies of the structure dynamics and reactivity of supercritical water lead to a better understanding of how complicated compounds are adaptively evolved from simple ones in hydrothermal reactions. It is important to elucidate how the structure and dynamics of supercritical water are controlled by intermolecular interactions (density) as well as kinetic energies (T). This is a new frontier of solution chemistry. The PVT data for water up to 1000°C and 10 kbar is known accurately enough (within 1% error).[42]-[44] At very high PT conditions (1000°C and 100 kbar), water is completely dissociated into H_3O^+ and OH^-, behaving like a molten salt, and has a higher density of the order of 1.7–1.9 g/cm^3. Figure 4.7 shows the temperature-density diagram of water, with pressure as a parameter.[44]

When aqueous solutions are heated up to the solvent critical point, the partial molal volume of "hydrophilic" species become largely negative and that of "hydrophobic" ones largely positive due to a divergent behavior of the solvent compressibility. It is well known that, as distances of the intermolecular charge separation decreased along the reaction coordinate, these "hydrophilic" species were dehydrated in supercritical water due to the low dielectric constant of the solvent. The desolvation effect was pronounced in the solvent with a low dielectric constant over a long range. One can regard this dehydration effect on the ionic and dipolar species as the catalytic effect of supercritical water because of its ability of lowering the height of the reaction barrier. Similarly, the conductance data for dilute alkali metal halide solutions at elevated temperatures and pressures have been usually interpreted in terms of the formation of simple, neutral ion

DropBooks

pairs. It has nevertheless been recognized that higher order polynuclear species (e.g., triplets, quadruplets, etc.) may form in electrolyte solutions having a low dielectric constant at ambient temperatures. By analogy, one might therefore expect the formation of such polynuclear ions or clusters in near critical region and at supercritical temperatures and pressures in aqueous electrolyte solutions. Recently, Driesner and Seward (1997) have carried out the molecular dynamics simulations of ion pairing and cluster formation in a 1 M NaCl solution at 380°C and near critical pressures indicating the presence of simple monatomic ions and ion pairs together with triple ions such as Na_2Cl^+ and $NaCl_2^-$ as well as the Na_2Cl_2 and more complicated polynuclear species.[45] Combined molecular dynamics simulations and *EXAFS* measurements on 1 M $SrCl_2$ solutions up to 300°C also indicate the presence of Sr^{2+}, Cl^-, $SrCl^+$, $SrCl_2$ as well as cluster species such as $Sr_2Cl_2^{2+}$ and $Sr_2Cl^+_2$.[45] Insight into ion pair and cluster formation is of importance to the understanding of many phenomena operating in hydrothermal systems in the earth's crust, including mineral equilibria, stable isotope fractionation and element transport.

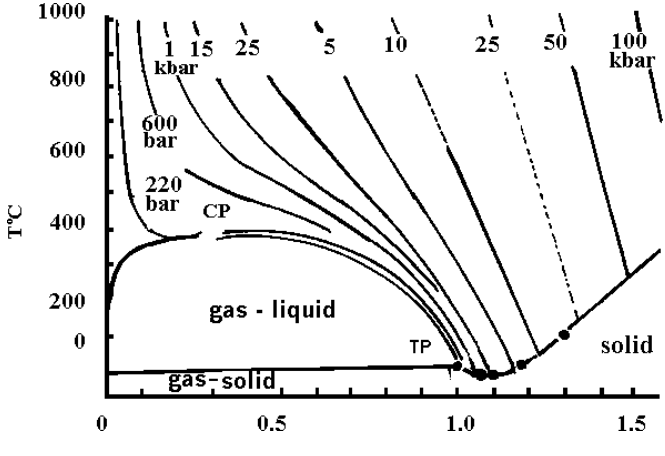

Figure 4.7. Temperature-density diagram of water, with pressure as a parameter.[44]

Benning and Seward (1996) have studied the stepwise metal complex formation of the $AuHS^0$ and $Au(HS)_2^-$ complexes and their thermodynamic data in sulphide aqueous solutions up to 400°C and 1500 bar.[46] However, a major source of uncertainty in the study of metal

hydrosulphide complexes at high temperatures and pressures has been the lack of reliable data for K_1, the first ionization constant for H_2S. There is a major lack of experimental data pertaining to metal complex equilibria in supercritical aqueous systems as well as in binary solvent systems such as H_2O-CO_2. Walther and Schott (1988) applied the dielectric constant approach to study the speciation and ion pairing at high temperature and pressure.[47] These authors have proposed many theoretical and empirical relations to account for various aspects of solubility behavior and speciation. The calculation of the dielectric-constant dependence of ion pairing at high temperatures and pressures allows the prediction of speciation in complex fluids at high temperature and pressure for reduced activities of H_2O. Using this approach, the behavior of aqueous silica in complex solutions at high temperatures and pressures has been studied. Such data are of enormous importance to understanding the geochemistry of element transport by hydrothermal fluids migrating in the earth's crust.[36]

In the hydrothermal growth of crystals, the *PVT* diagram of water proposed by Kennedy (1950) is very important (Fig. 2.6).[48] Usually, in most routine hydrothermal experiments, the pressure prevailing under the working conditions is determined by the degree of filling and the temperature. When concentrated solutions are used, the critical temperature can be several hundred degrees above that of pure water.[49] The critical temperatures are not known for the usually complex solutions at hand; hence one cannot distinguish between sub- and supercritical systems for reactions below 800°C. Although the temperature in the growth zone and the actual vapor pressure are not known to 100% accuracy, the *PVT* diagram of Kennedy is used by most hydrothermal crystal growers routinely. The *PVT* relations in $AlPO_4$ and SiO_2 systems have been reviewed.[50]-[52] Also, the *P-T* behavior of the quartz-water system has been well discussed by Brebrick.[53]

DropBooks

4.5 KINETICS OF CRYSTALLIZATION UNDER HYDROTHERMAL CONDITIONS

Hydrothermal crystallization is only one of the areas where our fundamental understanding of hydrothermal kinetics is lacking. Because, in majority of the cases, we have little knowledge about the intermediate phases forming in solution. Thus, our fundamental understanding of hydrothermal crystallization kinetics is at an early stage. In the absence of

predictive models, we must empirically define the fundamental role of temperature, pressure, precursor, and time on crystallization kinetics of various compounds. Insight into this would enable us to understand how to control the formation of solution species, solid phases and the rate of their formation.

The importance of kinetics of crystallization studies was realized with the commercialization of the synthesis of zeolites during 1950s and 1960s. Following this, a large number of publications appeared from the Soviet laboratories on kinetics studies related to the growth of single crystals under hydrothermal conditions. During this period, the anisotropy of the rate of growth of the faces of the crystals during growth on a seed acquires particular importance, since it makes it possible to orient the seed crystal platelets in such a way that the growth surface coincides with the rapidly growing face.[54]-[58] At the same time, Laudise and co-workers have studied the crystallization kinetics of quartz and zincite.[59]-[61]

These studies were based on the experience in the growth of crystals in aqueous solutions which shows clearly the relationship between the anisotropy of the rates of process: temperature, supersaturation and the presence of "foreign" components, including the solvent under hydrothermal conditions. These parameters can be varied over very wide limits.

The influence of the solvent is specific for each crystal. In the case of ZnO, for example, the presence of NH^+_4 ions in the solution produces a marked increase in the rate of growth of the prismatic faces, which under ordinary conditions does not exceed hundredths of mm/day.[61] For calcite under conditions of increased oxygen activity the faces of the scalenohedra, $(21\bar{3}1)$ and $(10\bar{1}0)$ become predominant.[62]

Various general laws characterizing the relationship between the anisotropy of the rates of growth of the faces and the chemical nature of the solvent have been studied by several workers. Some major conclusions have been drawn based on the studies on the growth of various crystals.

Supersaturation in hydrothermal experiments is given by the magnitude of the temperature gradient (ΔT) between the dissolution and growth zones, so that the relationship between the rate of growth and the magnitude of ΔT is usually investigated. If the solubility changes with temperature according to a law which is close to linear with ΔT, the growth rate is also practically linear. For all crystals, which have been studied under hydrothermal conditions, the rates of growth of the faces increase

linearly with supersaturation. The high activation energies of the growth of the faces, combined with other factors—the anisotropy of the rates of growth of the faces, the marked dependence of the rate of crystallization on the composition of the solution, etc.—provide strong evidence in support of the suggestion that in hydrothermal crystallization under conditions of excess mass transfer, a primary role is played by surface processes taking place directly at the crystal-solution interface. It should be remembered that the activation energy of diffusion in solutions usually does not exceed 4–5 kcal/mole,[63] and the activation energies of dissolution rarely exceed 10 kcal/mole. These values are much lower than the activation energies of growth, indicating that diffusion in the solution and dissolution of the charge do not limit the rate of crystallization with increase in the concentration of the solution. The rate of the crystallization can increase in two ways. For crystals that do not contain components of the solvent, the rate increases sharply at low concentrations and remains practically unchanged at high concentrations. Similarly, in some cases, an increase in the rate of growth of the faces with increase in pressure has been observed. Pressure apparently does not have any significant direct effect on the rate of growth of crystals, but it may have an influence through other parameters: mass transfer and solubility.

DropBooks

Kuznetsov (1966) reported the effects of temperature, seed orientation, filling, and temperature gradient, ΔT, on the growth kinetics of corundum crystals.[55] The activation energies for growth on the $(11\bar{2}0)$ and $(10\bar{1}1)$ faces, together with some preliminary evidence on the rate-limiting step in the hydrothermal crystallization of Al_2O_3. Figures 4.8 and 4.9 show the growth rates as functions of fillings: x: $(10\bar{1}1)$; o: $(11\bar{2}0)$, and relation of $\log R$ to $1/T$ for the filling factors given on the curves: x: $(10\bar{1}1)$, o: $(11\bar{2}0)$. The activation energies calculated from Fig. 4.9, are 32 kcal/mole for $(10\bar{1}1)$ face and 17.5 kcal/mole for $(11\bar{2}0)$ face.[55]

Riman and co-workers have investigated the crystallization kinetics of ABO_3 (A = alkaline-earth elements, B = Ti, Zr, Hf) and their solid solutions[23][24][64][65] The fundamental role of temperature, pressure, precursor, and time on crystallization kinetics of perovskite oxides has been studied in detail. Early work by Battelle Laboratories set the stage for the development of hydrothermal processes that provide excellent morphological control for a variety of ceramic chemistries.[66] The morphology control and size of lead zirconate titanate and lead titanate precipitated from organic mineralizer solutions have been worked out in detail. Kaneko and Imoto (1975) have investigated the effects of pressure, temperature,

time, and Ba:Ti ratio on the kinetics of a hydrothermal reaction between barium hydroxide and titania gels to produce barium titanate powders.[67] Ovramenko et al. (1979) conducted kinetic studies to compute an activation energy (*Ea*) of 21 kJ/mole.[68] In contrast, Hertl (1988) calculated activation energy of 105.5 kJ/mole.[69] However, this discrepancy may be due to the difference in source of titania precursor as well as other reaction conditions (e.g., temperature). Computations performed in the composition temperature-pressure space facilitate the construction of stability diagrams, speciation diagrams and yield diagrams (Fig. 4.10).[70] In addition, the authors have carried out kinetic analysis based on reaction progress, yielded into the reaction-rate regime for various perovskite type oxides.

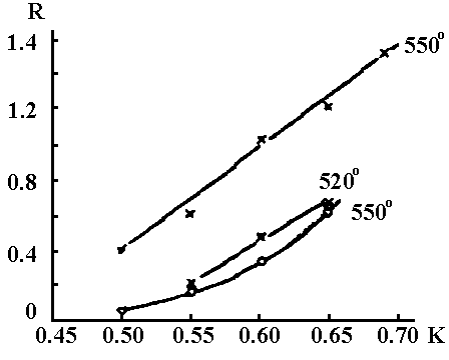

Figure 4.8. Growth rates as a function of filling: x) (1011); o) (1120).[55]

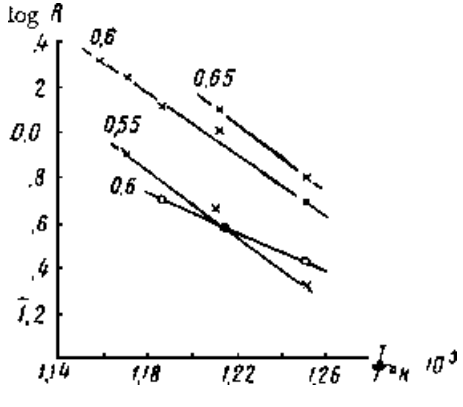

Figure 4.9. Relation of log$R$ to $^1/_T$ for the filling factors: x) (1011); o) (1120).[55]

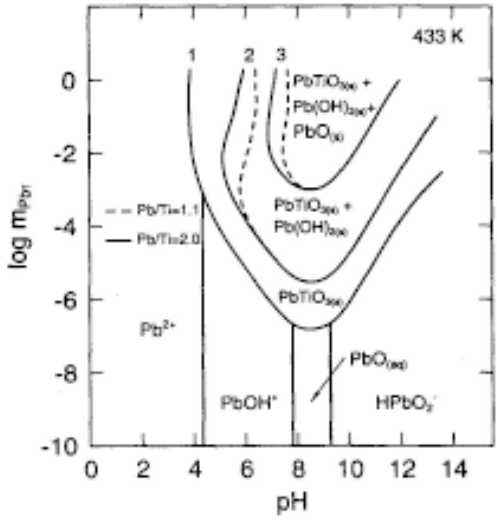

Figure 4.10. Stability diagrams, speciation diagrams and yield diagrams.[70]

Other materials of commercial interest in the present day context whose kinetics of crystallization have been studied in detail are zeolites and hydroxyapatite.[71]-[73] Various approaches or models have been proposed to understand the reaction mechanism of these compounds. The models based on the dissolution process, growth process, surface diffusion, structure directing chelates, or amines in the synthesis of zeolites, etc., have been used as the parameters in the study of crystallization kinetics. These studies have helped in the preparation of phase-pure zeolites and hydroxyapatite particles with a perfect control over the morphology, grain size, rate of crystallization and so on.

In the recent years, microwave hydrothermal is being popularly used to greatly enhance the reaction kinetics. Also, efforts have been made to have better control over the particle size, shape, yield, and purity.[74]-[76] However, the reaction kinetics of most of the compounds under microwave hydrothermal have not been understood precisely.

4.5.1 Experimental Investigations of Solubility

The selection of a suitable solvent and the theoretical aspects of solubility have been discussed in the previous section. Here, let us consider the experimental aspect, its determination, and role in growing single crystals. There are two principal methods for determining the solubility

DropBooks

under hydrothermal conditions. The first one is a sampling technique and has been described in detail by Morey and Hesselgesser.[77] It is especially useful where two fluid phases are present. In this technique, a suitably designed valve is arranged so that a fluid sample small enough so as not to perturb equilibrium can be withdrawn and chilled from an isothermal hydrothermal autoclave at operating conditions. If only one fluid phase is present, a weight loss method has been proved to be somewhat less cumbersome.[78] It is quite difficult to study the solubility of crystals under hydrothermal conditions if the compound does not form any metastable solutions over a wide temperature range. If there is a considerable metastable range of this kind, however, we may use the least troublesome method of studying solubility at high temperatures and pressures—the method of weight loss. If a weighed single crystal (or crystals) is placed in the capsule under conditions where the phase is stable and where the fluid phase is liquid alone or gas alone, the weight loss will be a measure of solubility. However, special care must be exercised to avoid overshooting, to ensure that the desired temperature is reached during warm up, to avoid losing material before weighing, or weighing material that has precipitated during the quenching. In many cases, the solubility obeys the van't Hoff equation and is linearly dependent on solution density.[79] The ratio of solubility to mineralizer concentration often gives clues to the species present.[80] Several additional difficulties were encountered with the silicates, alumino-silicates, phosphates, etc. They were first noticed while studying the solubility of quartz. These difficulties principally arise from phase separation of the solution under certain conditions, and the formation of a "heavy" phase enriched with silicon.[81] For example, it was shown by the authors of Ref. 82, in connection with the solubility of albite in H_2O at 200–350°C, that under these conditions there was a partial decomposition of the albite forming analcime. Hence, in this case, the true solubility of albite in water was not really being determined. Therefore, to obtain the true solubility of any compound which forms the heavy phases or other metastable phases, it has to be determined under conditions similar to its conditions of synthesis, so as to determine its optimum growth conditions. Russian workers at the Institute of Crystallography have designed an apparatus to suit the solubility study of various compounds (Fig. 3.22).

Let us consider the solubility studies of some selected compounds like zincite and malachite. Solubility of a compound may be positive or negative. If the solubility of a compound increases with increasing temperature, it is positive. If the solubility of the compound decreases with

increasing temperature, it is negative. Some compounds show positive solubility up to a certain temperature and then show negative solubility and vice versa. Quartz and berlinite form the best examples. The majority of the earliest hydrothermal experiments, carried out in the 19th century, had pure water as the mineralizer. Today we use a great variety of mineralizers, especially aqueous solutions of salts, acids, bases, etc., at very low concentrations. Likewise, there are a great numbers of non-aqueous solvents. Hannay and Hogarth used an alcoholic solution as a mineralizer a century ago.[83] Usually non-aqueous solvents are preferred when the required solubility cannot be reached in an aqueous medium. However, the composition of the effective solvents used in growing crystals is fairly standard. Pure water can be a good solvent at very high temperature and pressure conditions. The use of various acids, salts and bases considerably reduce the *PT* conditions. The commonly used non-aqueous solvents are NH_3, HF, HCl, HBr, Br_2, S_2Cl_2, S_2Br_2, $SeBr_2$, $H_2S + (C_2H_5)_3$, NH_4Cl, C_2H_5OH, CS_2, CCl_4, C_6H_6, CH_3NH_2, etc. In the past decade, the growth conditions have been further reduced with the use of some acid solvents. For example, high molar acids like HCl, H_2SO_4, H_3PO_4, HNO_3, HCOOH are freely used in the growth of various compound and this has brought down the growth temperature to below 300°C. In recent years, mixed solvents have been used in the growth of some compounds like $AlPO_4$. The mixed solvents are found to be highly effective. The reduction in the growth temperature considerably reduces the working pressure, which in turn helps in the use of simple apparatus. Even silica autoclaves can be used, which facilitate direct visibility of the growth medium just as in any other low temperature solution growth. This has greatly attracted the attention of crystal growers in the last two years and a great variety of compounds which hitherto were produced only at high temperature and pressure have been today obtained at lower *PT* conditions. Hence the mineralizer plays an important role in the hydrothermal growth of crystals and it has changed the tendency and perspective of the method. All these aspects can be very well described with reference to quartz, berlinite, sodalite, and α-TeO_2. The reader is advised to refer the works of Pearson[84][85] regarding the empirical selection of solvents based on the hard and soft acids and bases.

DropBooks

Solubility of Zincite. The solubility of zincite has been studied in great detail during the 1970s by several workers.[60][61][77] Measurements of the solubility of zincite has been performed first in noncomplexing solutions (HTr, NaTr) at various ionic strengths (0.03–1.0 molal NaTr) and

temperatures (50–290°C) to determine the equilibrium quotient of the reaction:

Eq. (25) $$ZnO_{cr} + 2H^+ \rightarrow Zn^{2+} + H_2O$$

Figure 4.11 represents an example of the solubility obtained at 200°C and 0.1 molal by approaching equilibrium from undersaturation (triangles), whereby the pH was changed by titration of acid into the cell during the experiments. The solid line represents the best fit of the data with a slope of -2 dictated by reaction (25). The solubility is shown in this figure to be reversed by a back titration (inverse triangles) with a basic titrant causing ZnO to precipitate.

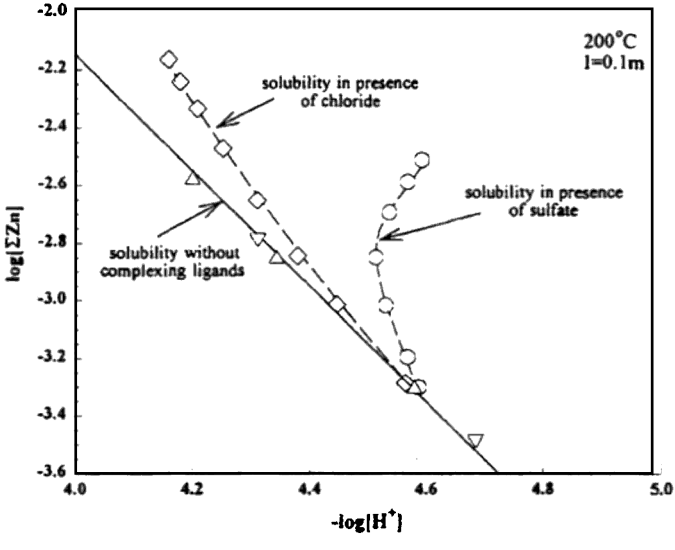

Figure 4.11. Solubility of zincite obtained at 200°.[86]

The dissociation quotients of reaction (25) were regressed against a variety of temperature–ionic-strength functions using the ORGLS general least squares program of Busing and Levy.[87] At infinite dilution, good agreement is obtained with previous experimental and model values (i.e., Khodakovsky and Yelkin, 1975;[88] Ziemniak, 1992[89]) except for the values obtained which deviate from our fit at 250 and 250°C.

In this figure, comparison is also made between these solubilities and those obtained in experiments performed by titration of solution containing chloride (diamond) and sulfate (circle) into the cell. It is clearly shown that the effect of addition of either chloride or sulfate is to increase the concentration of zinc. At this temperature, ionic strength, and stability constants of the reactions:

Eq. (26) $Zn^{2+} + SO_4^{2-} \rightarrow ZnSO_4^0$

Eq. (27) $Z^{2+} + Cl^- \rightarrow ZnCl^+$

Eq. (28) $Zn^{2+} + 2Cl^- \rightarrow ZnCl_2^0$

were obtained. The dashed curves in Fig. 4.11 are generated from these stability constants and are shown to reproduce the experimental points.[86] For reaction (26) there are no published experimental data with which to compare these results. In order to compare with literature data, the constants for reactions (27) and (28) are extrapolated to infinite dilution at 200°C. Good agreement with Bourcier et al. (1993) and Ruaya and Seward (1986) is obtained for the dichloro-zinc complex stability constant.[90][91] However, the result for the monochloro-zinc complex disagrees markedly.

DropBooks

Solubility of Malachite. The growth of malachite single crystals has posed a challenge in the past decade. Several original methods, which allow nearly all textural varieties found in natural malachite, have been devised. Malachite solubility in pure water and electrolytic aqueous solutions has not been understood precisely. Symes and Kester (1984) studied the peculiarities of malachite dissolution in pure and sea water in order to reveal the conditions necessary for its precipitation.[92] Sulyapnikov and Shtern (1972) determined the maximum copper concentration during malachite dissolution in solutions of $NaHCO_3$ and $KHCO_3$ of different concentrations at temperatures up to 200°C and different amounts of CO_2.[93] Their data has shown that, under normal conditions, the copper content in these solutions changes, strongly depending on the time of the solution mixing with the powder of the basic copper carbonate. Balitsky and Bublikova (1991) have investigated malachite solubility in 1,2,3 M solutions of ammonium hydroxide at temperatures 20, 25, 50 and 75°C (P = 1 bar). Figure 4.12 shows kinetic curves of malachite dissolution in ammonia aqueous solutions at 20°C (1–10 M NH_4OH; 2 M NH_4OH; 3–3.0 M

NH_4OH). As can be seen from Fig. 4.12, equilibrium copper contents in the ammonia solutions increase as ammonia concentration increases and they decrease as temperature rises.[94]

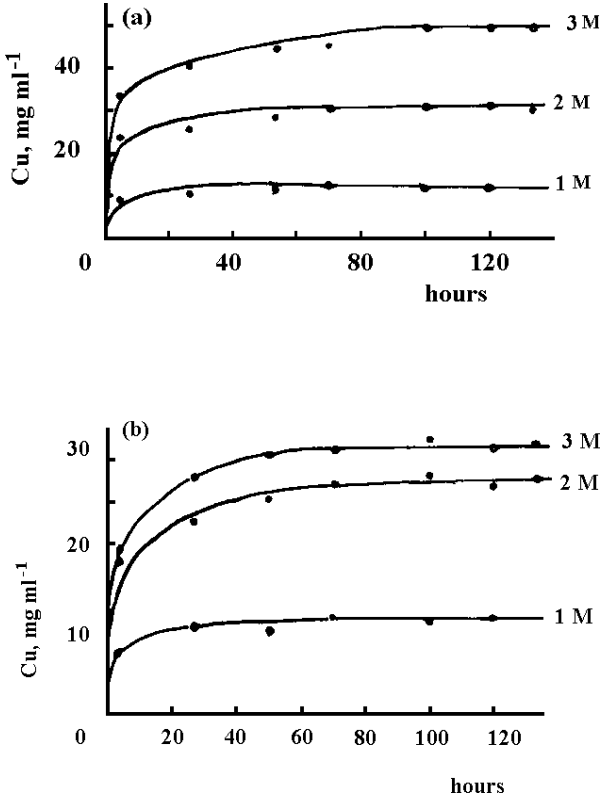

Figure 4.12. Kinetic curves of malachite dissolution in ammonia aqueous solutions at 20°C.[94]

These examples give a more or less complete picture with regard to the type of solvent, the *PT* conditions, and the progress made in the search for new solvents for various inorganic compounds under hydrothermal conditions. All these studies yield crystal growth kinetics, the phase pure product.

Thus, the hydrothermal physical chemistry is a fast growing field that is going to play a key role in the 21st century in the preparation of future materials. The physico-chemical data will provide an insight into the actual hydrothermal reaction mechanism and in turn will bring down the *PT* conditions of preparation of materials.

REFERENCES

1. *Chemistry and Geochemistry of Solutions at High Temperatures and Pressures,* (F. E. Wickman and D. Rickard, eds.), in: *Proc. Nobel Symp. Phys. Chem. Earth*, 13/14:562 (1981)
2. Somiya, S., *Proc. First Int. Symp. Hydrothermal Reactions*, Gakujutsu Bunken Fukyu-Kai, Tokyo, pp. 975 (1983)
3. Ezersky, A. B., Garcimartin, A., Burguete, J., Mancini, H. L., and Perez-Garcia, C., Hydrothermal Waves in Marangoni Convection in a Cylindrical Container, *Phys. Rev. E.*, 47:1126–1131 (1993)
4. Ezersky, A. B., Garcimartin, A., Mancini, H. L., and Perez-Garcia, C., Spatiotemporal Structure of Hydrothermal Waves in Marangoni Convection, *Phys. Rev. E.*, 48:4414–4422
5. Hydrothermal Growth of Crystals, (K. Byrappa, ed.) *Prog. Crystal Growth Charact. Mater.*, 21:1–365 (1991)
6. Zakirov, I. V., *Experimental Investigations of PVT Relations in the H_2O-CO_2 System*, Ph. D. Thesis (Moscow State University, Moscow) (1987)
7. Ilijushin, G. D., Demianets, L. N., Iljukhin, V. V., and Belov, N. V., *Dokl. Akad. Nauk USSR* (in Russian), 217:1133 (1983)
8. Dimitrova, O. V., *Investigations of the Phase Formations in the System Na_2O-RE_2O_3-SiO_2-H_2O Under Hydrothermal Conditions*, Ph.D. Thesis (Moscow State University, Moscow) (1985)
9. Kolb, E. D. and Laudise, R. A., *J.Cryst. Growth*, 33:145 (1976)
10. Hamann, S. D., Properties of Electrolyte Solutions at High Pressures And Temperatures. in: *Proc. Nobel Symp. Organized by the Royal Swedish Academy of Sciences,* (D. T. Rickard, and Fr. E.Wickman, eds.), Pergamon Press, New York, pp. 90–111 (Sept. 17–21, 1979)
11. Seward, T. M., Metal Complex Formation in Aqueous Solutions at Elevated Temperatures and Pressures, in: *Proc. Nobel Symp. Phys. Chem. Earth*, 13/14:113–132 (1981)
12. Helgeson, H. C., Prediction of the Thermodynamic Properties of Electrolytes at High Pressures and Temperatures, in: *Proc. Nobel Symp. Phys. Chem. Earth*, 13/14:113–177 (1981)
13. Read, D. and Broyd, T. W., CHEMVAL / MIRAGE report, "Verification of Specification Models," Atkins, W. S, CEC Contract FI. IW0077 (1988)
14. May, P. M., Towards More Reliable Chemical Specification Models of Multicomponent Electrolyte Solutions, in: *Proc. 5th Int. Symp. Hydrothermal Reactions*, (D. A. Palmer and D. J. Wesolowski, eds.), pp. 32–34 Gatlinburg, Tennessee, USA (July 20–24, 1997)

DropBooks

15. Sterner, S. M., Felmy, A. R., Rustad, J. R., and Pitzer, K. S., Thermodynamic Analysis of Aqueous Solutions Using INSIGHT, in: *Proc. 5th Int. Symp. Hydrothermal Reactions,* (D. A. Palmer and D. J. Wesolowski, eds.) pp. 35–38, Gatlinburg, Tennessee, USA (July 20–24, 1997)

16. Atkins, P. W., *Physical Chemistry*, p. 745 (ELBS, Oxford Univ. Press, Oxford) (1986)

17. Krestov, G. A., *Thermodynamics of Ionic Processes in Solutions Chemistry*, p. 116 (1973)

18. Deidler, K., *Kinetics of Organic Reactions M*, p. 237, Mir, Moscow (1966)

19. Kennedy, G. C., and Holser, W. T., Pressure-Volume-Temperature and Phase Relations of Water and Carbon Dioxide, in: *Handbook of Physical Constants*, (S. P. Clark, Jr. ed.) pp. 371–383, Geological Society of America, Washington, D.C. (1966)

20. Köster, H. and Franck, E.U., Das Spezifische Volumen des Wassers be: Hohen Drücken bis 600°C und 100 kbar, *Ber. Bunsenges*, 73:716–722 (1969)

21. Tödheide, K., Water at High Temperatures and Pressures, in: *Water A Comprehensive Treatise*, Vol. 1 (F. Franks, ed.), pp. 463–514, Plenum Press, New York (1972)

22. Cummings, P. T., Molecular Simulation of Supercritical Water and of Ionic Association in Supercritical Aqueous Solutions, in: *Proc. 5th Int. Symp. Hydrothermal Reactions*, (D. A. Palmer, and D. J. Wesolowski, eds.) pp. 153–156, Gatlinburg, Tennessee, USA (July 20–24, 1997)

23. Riman, R. E., Lencka, M. M., Mc Candlish, L. E., Gersten, B. L., Andrenko, A., and Cho, S. B., Intelligent Engineering of Hydrothermal Reactions., in: *Proc. 5th Int. Symp. Hydrothermal Reactions,* (D. A. Palmer, and D. J. Wesolowski, eds.) pp. 74–78, Gatlinburg, Tennessee, USA (July 20–24, 1997)

24. Lencka, M. M. and Riman, R. E., Thermodynamics of the Hydrothermal Synthesis of Calcium Titanate With Reference to Other Alkaline-Earth Titanates, *Chem. Mater*., 7:18–25 (1995)

25. Lencka, M. M. and Riman, R. E., Thermodynamic Modeling of Hydrothermal Synthesis of Ceramic Powders, *Chem. Mater*., 5:61–70 (1993)

26. Brown, W. E. and Chow, L. C., Thermodynamics of Apatite Crystal Growth and Dissolution., *J. Crystal Growth*, 53:31–41 (1981)

27. Benning, L. G. and Seward, T. M., Hydrosulphide Complexing of Au^{1+} in Hydrothermal Solutions from 150–400°C and 500–1500 Bar, *Geochim Cosmochim Acta*, 60:1849–1871 (1996)

28. Woitsekhowskaya, M., Roberts, R., Cline, J., Hemley, J. J., and Weaver, K., Gold and Arsenic in Iron Sulfides From the Getchell Deposit, Nevada: Thermodynamic Evaluation, in: *Proc. 5th Int. Symp. Hydrothermal Reactions*, (D. A. Palmer and D. J. Wesolowski, eds.) p. 301, Gatlinburg, Tennessee, USA (July 20–24, 1997)

29. Franck, E. U., Water and Aqueous Solutions at High Pressures and Temperatures, *Pure Appl. Chem.*, 24:13–30 (1970)
30. Laudise, R. A., Ballman, A. A., and King, J. C., *J. Phys. Chem. Solids*, 26:1305 (1965)
31. Handbook of Physics and Chemistry, 64th Ed., (R. C. Weast, ed.) CRC Press, Boca Raton, D261 (1983)
32. Helgeson, H. C., *Phys. Chem. Earth* 13/14:133 (1981)
33. Hasted, J. B., Ritson, D. M., and Collie, C. H., *J. Chem. Phys.*, 16:1 (1948)
34. Uematsu, M., Harder, W., and Franck, E. U., The Dielectric Constant of Water, Technical Paper 38p (WLKg. Gp. 3), Int. Assoc. for Prop., of Stern. Inter. Mtg. Kyoto Mtg. Jpn. (1976)
35. Landolt-Börnstein, Numerical Data and Functional Relationships, Gr. IV, Vol. 4, *High-pressure Properties of Matter* (G. Beggerow and K. L. Schafer, eds.), p. 91, Springer, Berlin (1980)
36. Seward, T. M., Hydrothermal Solution Speciation (Solvation to Ion Pairing and Complexing), in: *Proc. 5th Int. Symp. Hydrothermal Reactions*, (D.A Palmer and D.J Wesolowski, eds.) pp. 7–9, Gatlinburg, Tennessee, USA (July 20–24, 1997)
37. Nakahara, M., Nobuyuki, M., and Wakai, C., NMR Study of Hydrogen Bonds and Water Structure in Super- and Subcritical Conditions, in: *Proc. 2nd Int. Conf. Solvothermal Reactions*, pp. 9–12, Takamatsu, Jpn. (Dec. 18–20, 1996)
38. Yamaguchi, T., Fujita, H., Hidaka, K., and Wakita, H., Structure of Water and Methanol at Subcritical and Supercritical States by X-ray Diffraction, in: *Proc. 2nd Int. Conf. Solvothermal Reactions*, pp. 13–15, Takamatsu, Jpn. (Dec. 18–20, 1996)
39. Nakahara, M., Yamaguchi, T., and Ohtaki, H., The Structure of Water and Aqueous Electrolyte Solutions Under Extreme Conditions, *Recent Res. Dev. Phys. Chem.*, 1:17–49 (1997)
40. Ohtaki, H., Radnai, T., and Yamaguchi, T., Structure of Water Under Subcritical and Supercritical Conditions Studied by Solution X-ray Diffraction, *Chemical Society Reviews*, pp. 41–51 (1997)
41. Nakahara, M., Very High Temperature and High Pressure Reactions, in: *Encyclopedia of Experimental Chemistry*, 11:149–168, Jikken Kagaku Koza, Muruzen, Tokyo (1993)
42. Haman, S. D., *Phys. Chem. Earth*, 13/14:89 (1981)
43. Todheide, K., Ber. Bunsenges. *Physik. Chem.*, 86:1005 (1982)
44. Frank, E. U., *Int. Corros. Conf.* Ser., 109 (1973)
45. Driesner, T. and Seward, T. M., *Geochim. Cosmochim. Acta*, 61:65 (1997)

PrintBooks

46. Benning, L. G. and Seward, T. M., Hydrosulphide Complexing of Au^{1+} in Hydrothermal Solutions from 150°–400°C and 500–1500 bar, *Geochim Cosmochim Acta*, 60:1849–1871 (1996)

47. Walther, J. V. and Schott, J., The Dietectric Cnstant Approach to Speciation and Ion Pairing at High Temperature and Pressure, *Nature*, 332:635–638 (1988)

48. Kennedy, G. C.,*Am. J.Sci.*,248:540–543 (1950)

49. Popolitov, V. I., D. Sc. Thesis, Inst. of Crystallography, Russian Acad. of Sciences, Moscow (1990)

50. Kolb, E. D., Key, P. L., Laudise, R. A., and Simpson, E. E., *Bell. Sys. Tech. J.*, 61:639 (1983)

51. Marshall, W. L., Jones, E. V., and Jones, J., *Inorg. Nucl. Chem.*, 36:2313 (1974)

52. Laudise, R. A., Sunder, W. A., Belt, R. F., and Gashurov, G., *J. Cryst. Growth*, 102:427 (1990)

53. Brebrick, R. F., Phase Equilibria, in: *Handbook of Crystal Growth*, (D. T. J. Hurle, ed.) Vol. 1a, pp. 43–102, Elsevier Science, B.V., The Netherlands (1993)

54. Kuznetsov, V. A. and Lobachev, A. N., Hydrothermal Method for the Growth of Crystals, *Soviet Physics-Crystallgraphy*, 17:775–804 (1973)

55. Kuznetsov, V. A., *Hydrothermal Crystallization Kinetics of Corundum*, Sov. Phys.-Crystallogr., 10:561–564 (1966)

56. Kuznetsov, V. A., *Kinetics of Hydrothermal Crystallization of Corundum, II*, Effect of Solventson Crystallization, *Sov. Phys-Crystallogr.*, 12:608–611 (1968)

57. Lobachev, A. N., Demianets, L. N., Kuzmina, I. P. and Emelianova, E. N., Investigation of the Solubility and Crystallization Kinetics of Sodium-Zinc Germanate (Na_2ZnGeO_4) Under Hydrothermal Conditions, *J. Crystal Growth*, 13/14:540–544 (1972)

58. Popolitov, V. I. and Lobachev, A. N., Kinetics and Structure Aspect of the Growth of Single Crystals of Bismuthinite Under Hydrothermal Conditions, *Sov. Phys. Crystallogr.*, 81:131–132 (1973)

59. Laudise, R. A. and Ballman, A. A., *J. Phys. Chem.*, 64:688 (1960)

60. Laudise, A. A., Kolb, E. D., and Caporaso, A. J., *J. Amer. Ceram. Soc.*, 47:9–12 (1964)

61. Kolb, E. D. and Laudise, R. A., *J. Amer. Ceram. Soc.*, 49:302–305 (1966)

62. Ikornikova, N. Yu., D. Sc. Thesis, Institute of Crystallography, Academy of Sciences USSR, Moscow (1970)

63. Samoilov, O. Ya., The Structure of Aqueous Solutions and the Hydration of Ions, Akad. Nauk USSR Publication, Moscow (1957)

64. Riman, R. E., Lencka, M. M., Mc Candlish, L. E., Gersten, B. L., Andrenko, A., and Cho, S. B., *Intelligent Engineering of Hydrothermal Reactions*, in: *Proc. 2nd Int. Conf. Solvothermal Reacts.*, pp. 148–151, Takamatsu, Jpn. (Dec. 18–20, 1996)

65. Lencka, M. M., Andrenko, A., and Riman, R. E., Hydrothermal Precipitation of Lead Zirconate Titanate Solid Solutions:Thermodynamic Modeling and Experimental Synthesis, *J. Am. Ceram. Soc.*, 78:2609–2618 (1995)

66. Staumbagh, E. P. and Miller, J. F., in: *Proc. of the 1st Int. Symp. on Hydrothermal Reactions*, (S. Somiya, ed.) pp. 858–871, Gakujutsu Bunken Fukyu-Kai, Tokyo, Jpn. (1983)

67. Kaneko, S. and Imoto, F., Synthesis of Fine-Grained Barium Titanate by a Hydrothermal Reaction, *Nippon Kagaku Kaishi*, 6:985–990 (1975)

68. Ovramenko, N. A., Shvets, L. I., Ovcharenko, F. D., and Kornilovich, B. Y., Kinetics of Hydrothermal Synthesis of Barium Metatitanate, *Izv. Akad. Nauk USSR, Inorg. Mater.*, 15:1982–1985 (1979)

69. Hertl, W., Kinetics of Barium Titanate Synthesis, *J. Amer. Ceram. Soc.*, 71:879–883 (1988)

70. Eckert, J. O., Jr., Hung-Houston, C. C., Gersten, B. L., Lencka, M. M., and Riman, R. E., Kinetics and Mechanisms of Hydrothermal Synthesis of Barium Titanate, *J. Amer. Ceram. Soc.*, 79:2929–2939 (1996)

71. Lindner, T. and Lechert, H., *Chelate Ligands as Mineralizing Agents in Hydrothermal Synthesis of Faujasite-Type Zeolites: A Kinetic Study*, *Zeolites*, 16:196–206 (1996)

72. Sheikh, A. Y., Jones, A. G. and Graham, P., *Population Balance Modeling of Particle Formation During the Chemical Synthesis of Zeolite Crystals, Assessment of Hydrothermal Precipitation Kinetics, Zeolites*, 16:164–172 (1996)

73. Onuma, K., Ito, A., Tateishi, T. and Kameyama, T., Growth Kinetics of Hydroxyapatite Crystal Revealed by Atomic Force Microscopy, *J. Crystal Growth*, 154:118–125 (1995)

74. Komarneni, S., Roy, R., and Li, Q. H., Microwave-Hydrothermal Synthesis of Ceramic Powders, *Mater. Res. Bull.*, 27:1393–1405 (1992)

75. Fang, Yi, Agarwal, D. K., Roy, D. M., and Roy, R., Fabrication of Porous Hydroxyapatite Ceramics by Microwave Processing, *J. Mater. Res.*, 7:490–494 (1992)

76. Komarneni, S., Enhanced Reaction Kinetics Under Microwave-Hydrothermal Conditions, in: *Proc. 2nd Int. Conf. Solvothermal Reactions*, pp. 97–100, Takamatus, Jpn. (Dec. 18–20, 1996)

77. Morey, G. W. and Hesselgesser, J. M., *Am. J. Sci.*, 367 (1952)

78. Laudies, R. A., *J. Am. Chem. Soc.*, 81:562 (1959)

DropBooks

79. Laudies, R. A., in: *Progress in Inorganic Chemistry*, 3:1 (F. A. Cotton, ed.) Wiley-Interscience, New York (1962)
80. Marshall, D. J. and Laudise, R. A., in: *Crystal Growth* (H. S. Peiser, ed.), p. 557, Pergamon, New York (1966)
81. Bryatov, L. V., *Some Problems Relating to the Solubility and Growth of Quartz Crystals*, Ph.D. Thesis, Inst. of Crystallography, Acad. of Sciences, Moscow (1955)
82. Frederickson, A. P. and Cox, I. E., *Am. Mineral*, 39:738 (1954)
83. Hannay, J. B. and Hogarth, *J. Proc. R. Soc. London*, 30:178 (1880)
84. Pearson, R. G., *J. Chem. Education*, 45:581 (1968)
85. Pearson, R. G., *J. Chem. Education*, 45:645 (1968)
86. Benezeth, P., Palmer, D. A., and Wesolowskii, D. J., Potentiometric Stuides of Aluminum Hydroxide and Zinc Oxide Solubility to High Temperature, in: *Proc. 5th Int. Symp. Hydrothermal Reactions*, (D. A. Palmer and D. J. Wesolowski, eds.) pp. 149–152. Gatlinburg, Tennessee, USA (July 20–24, 1997)
87. Busing W. R. and Levy H. A., *ORNL-TM*-271 Report (1962)
88. Khodakovskiy I. L. and Yelkin A. Y., *Geokhimi.*, 10:1490–1498 (1957)
89. Ziemniak, S. E., *J. Solution Chem*., 21:745–760 (1992)
90. Bourcier, W. L., Knauss, K. G., and Jackson, K. J., *Geochim. Cosmochim. Acta*, 57:747–762 (1993)
91. Ruaya J. R. and Seward T. M., *Geochim. Cosmochim. Acta*, 50:651–661 (1986)
92. Symes, J. L. and Kester, D. R., *Geochim. Cosmochim. Acta*, 48:2219 (1984)
93. Shlyapnikov, D. S. and Shtern, E. K., *Dokl. Acad. Nauk USSR*, 207:966 (1972)
94. Balitsy, V. S. and Bublikova, T., in: *Hydrothermal Growth of Crystals*, (K. Byrappa, ed.) *Prog. Cryst. Growth Charact. Mater.*, 21:139 (1991)

5

Hydrothermal Growth of Some Selected Crystals

The hydrothermal technique has produced a wide variety of minerals and crystals, both in nature and in laboratory. In fact, it is the only technique to synthesize some of the inorganic compounds like quartz, berlinite, and so on. However, the method has some limitations as far as the size is concerned. Except quartz, the method has not yielded large single crystals. Although berlinite, gallium berlinite, and lithium tetraborate show many superior piezoelectric properties compared to α-quartz, it is not possible to obtain them as large as α-quartz crystals. Further, it is difficult to discuss here the growth of all the compounds of hydrothermal origin. Hence, the scope of this chapter has been restricted only to the growth of most important crystals.

DropBooks

5.1 QUARTZ

Quartz is one of the most abundant minerals and occurs both as an essential and accessory constituent of the rocks. References to quartz are known from 1505 onwards. It may have been derived from the Saxon word *querkluftertz,* or cross-vein-ore, which could easily have become condensed to *querertz* and then to *quartz*.[1]

Quartz, SiO_2, exists both in crystalline and amorphous forms in nature. The crystalline form of quartz has over 22 polymorphic modifications. The three principal crystalline forms of SiO_2 (quartz, tridymite, and cristobalite) possess a well-defined field of stability under equilibrium conditions for each one of them. The transformations from one to another are, however, somewhat sluggish, so that the higher temperature forms, cristobalite and tridymite, can exist metastably below their inversion temperatures. Each crystalline form of quartz, metastable tridymite and metastable cristobalite, has furthermore low- and high-temperature modifications designated as α- and β-, respectively.[2]-[4] Amongst them, α-quartz, which is stable below 573°C at atmospheric pressure, is the most popular and technologically very important. The structure of α-quartz is shown in Fig. 5.1.[5][6] The α-quartz has trigonal symmetry, belongs to the enantiomorphous crystal class 32, and its space group is $P3_121$ or $P3_221$ according to its right–or left–handedness. Its structure was among the first to be investigated by x-ray techniques as early as 1914 by Bragg.[6] The structure of quartz is made up of SiO_4 tetrahedra, which are linked by sharing each of their corners with another tetrahedron. In the 3-dimensional framework thus formed, every Si^{4+} has four oxygens and every oxygen has two silicons as nearest neighbors. There are several works on the hydrothermal synthesis of other varieties of silica—like coesite, β-quartz, stisshovite, cristobalite and tridymite.[7]–[10] However, the scope of this chapter has been restricted to the growth of large size single crystals of quartz by the hydrothermal technique. In this respect, it is only the α-quartz, which could be grown as large bulk single crystals, whereas the other varieties of silica have been obtained so far only as fine crystalline products, or tiny cristallites.

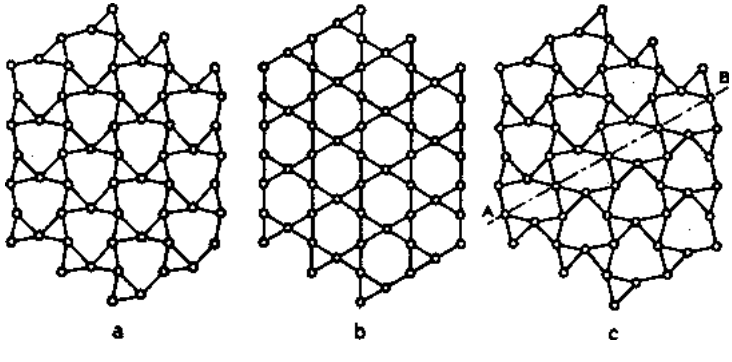

Figure 5.1. Structure of α-quartz.[5]

The α-quartz is one of the most extensively studied materials. It is the most popular, and technologically very important among all the hydrothermally grown crystals or materials. Quartz as a piezoelectric crystal has the ability to convert electric waves into mechanical waves and to reverse the process. Because of this property, quartz is widely used in filters, timing and frequency control applications, optical fibers, dielectric applications, and so on. In the recent years, quartz "tuning forks" have become essential for timing functions in electronic watches and in timing circuits for computers and telecommunications. Quartz crystal is one of the most transparent materials over a wide range of optical frequencies from UV (ultraviolet) to IR (infrared) regions, and it has double refraction (birefringence) and optical rotation power. Because of these properties, the quartz crystal is utilized as optical device on a large scale. Typical applications are in optical low pass filters (OLPF) for video cameras and waveplates for optical pick up. Table 5.1 gives a wide range of applications for α-quartz.

Table 5.1. Applications for α-quartz

Industrial equipment	Precision oscillators, optical fibers, dielectric materials, radiocommunications, cable communications, electronic applications, measurement equipment, pagers, security systems (alarms)…
Consumer equipment	Electronic hand calculators, watches, clocks, timers, cable TVs, color TVs, video recorders, RF converters, transceivers, radio equipment, microphones, electronic appliances, microphones, microcomputer and computer terminals, TV-game machines, telephones, copy machines…

DropBooks

The principal source of electronic grade natural quartz is Brazil. Today, the electronic industries are largely inclined to use synthetic quartz, because natural quartz crystals are generally irregular in shape, automatic cutting is cumbersome and the yield is low. Over 3000 tons of quartz are produced annually for a variety of applications. These applications range from optical components (due to its high transparency) to precise time and frequency oscillators based on its piezoelectric properties. The important

countries contributing to the world production are USA, Japan, China, Korea, Taiwan, Poland, Belgium, France, Germany, Russia, and so on. Japan alone produces more than 50% of the worldwide production, followed by USA.[11] Figure 2.11 shows a photograph of synthetic quartz crystals pulled out from the world's largest autoclave located at the Toyo Electric Co., Japan.[12] The inner diameter of the autoclave is 65 cm. To quote an example, the combined production quantity of quartz crystal units, filters, and oscillators in 1980 was 390 million pieces in Japan and it was remarkably increased to 2.13 billion pieces in 1990. The hydrothermal growth of quartz has been described and reviewed in several earlier works.[12]–[17] Hence, we will only consider the conventional method of the growth of α-quartz and its kinetics data in brief. Instead, we discuss the more recent developments in the growth of high purity and low dislocation quartz.

The α - β transition in quartz takes place at about 573°C, and the crystal growth of quartz insists upon a growth technique suitable to the low-temperature crystal growth process. This led to the development of hydrothermal process. In fact, much of our knowledge of the hydrothermal technique has resulted from the success in the growth of quartz crystals. The first publication in hydrothermal research is again pertaining to the synthesis of quartz by Schafhaul during 1845.[18] The best known source of natural quartz, even today, is Brazil, which has large occurrences of high quality electronic grade quartz. As a matter of fact, Brazil was the only supplier of large crystals of high quality natural quartz for electronic applications until World War II. Shortages in U.S.A and Europe caused by German submarine activity prompted efforts to synthesize large crystals of quartz, in the laboratory, using seeds. Spezia (1900–1909) was the first to attempt the seeded growth of quartz crystals and to carry out a systematic study of the solubility. However, the growth rate was poor. It was only during World War II that Nacken could achieve higher growth rates for quartz by the hydrothermal technique. The pilot scale production of quartz began during mid 1950s in U.S.A. and erstwhile USSR. Several countries attempted the artificial growth of large size single crystals of quartz. Especially, after the publication of the works of Nacken in 1950[19] and the captured German reports,[20][21] several laboratories began studying quartz crystal growth almost simultaneously and the hydrothermal technique became a very popular tool for developing many complex inorganic compounds. Industrial scale production occurred essentially during 1960s and 1970s, with a peak development between 1968 and 1976, especially in USA, Japan, and Europe.

In the growth of α-quartz by the conventional method, the autoclaves used by most of the workers were modified Bridgman type autoclaves. The design and construction of the modified Bridgman autoclave is described in Ch. 3. The typical laboratory size autoclave is 1" diameter × 1' length. The pressure autoclave used in Europe and USA is 13 inches diameter and > 10' length with 350 liters internal volume, which gives some 150 kg of quartz per cycle. But an evolution concerning vessel's dimensions has to be noted, especially in Japan, where autoclaves with 1000 liters to 5000 liters of internal volume are in operation producing 500 to 2000 kg quartz per cycle. The evolution of the autoclaves, the sealing involved, and the volume are discussed in Ch. 3. These larger internal volume autoclaves are provided with Grey-Loc type of sealing. Parallel to the increase in output, electronic components manufacturers have been looking, for the past 2½ decades, for a material with steadily increasing performances for professional applications in the telecommunications field, civilian as well as military.

In the growth of α-quartz, available nutrient material such as small particle size α-quartz, silica glass, high quality silica sand, or silica gel is placed in a liner made up of iron or silver with a suitable baffle and a frame to hold the seed plates. A mineralizer solution with a definite molarity is poured into the liner to make the required percent fill. The increased solubility in the presence of mineralizer increases the supersaturation without spontaneous nucleation and consequently allows more rapid growth rates on the seeds. Figure 3.3 shows the cross section of the modified Bridgman autoclave used in the growth of quartz crystals. The commercial autoclaves used have 10 inch inner diameter, and are10 feet long unlined. These autoclaves can work at conditions up to 30,000 psi and 400°C. Most of these experiments are carried out for 25 to 90 days to obtain full size crystals, 4 cm in the *Z*-direction and 12.5 to 15 cm in *Y*-direction. Temperature gradient is varied according to the nutrient used. About 1N NaOH or Na_2CO_3 is the most commonly used mineralizer. The solubility change with temperature is smaller in NaOH and slightly larger in Na_2CO_3. The temperature of the autoclave at the nutrient zone is usually kept at 355-369°C and, in the growth zone, it is kept at 350°C. The addition of lithium improves the growth rate and small amounts of Li salts are routinely added to the solution.[22] The solubility is also, to some extent, a function of increasing pressure. The pressure is controlled by the percent fill in the autoclave, and it is usually about 80% for hydroxyl mineralizer (20,000 psi internal pressure). In most of the experiments, the

BrownBooks

percent opening of the baffle is 20%; even lower percents are used by several workers. However, the actual percent opening of baffle area and its geometry are not disclosed, especially by commercial growers.

The optimum growth conditions for synthesis of quartz based on the work in Bell Laboratories are:[23][24]

Dissolution temperature	-	425°C
Growth temperature	-	375°C
Pressure	-	15,000–25,000 psi.
Mineralizer concentration	-	0.5–1.0 M NaOH
Temperature gradient (ΔT)	-	50°C
% fill	-	78-85%
Growth rate in (0001)	-	1.0–1.25 mm/day

The quality of the grown crystals is also a function of the seed orientation and its quality. Strained seeds generally produce a strained growth region.[25] The seeds are polished to a very fine finish before use. Most high quality crystals are grown using seeds with surfaces perpendicular to *Z*-direction since the *Z*-growth region is the lowest in aluminum concentration. Though the main part of quartz production consists in of *Y-bar* crystals, that is, small crystals (*Z* = 20 to 25 mm, 64 mm seed) capable of several Y-bars per crystal, the pure *Z-bars* are also produced, representing 10 to 20% of this production. In medium and high quality grades, we notice a rise in demand for crystals of very large dimensions and upper medium quality, especially in USA, for manufacturing wafers used in surface wave applications.[11] Earlier, most of the seeds used were natural quartz cut into a definite orientation, but in recent years this practice is only used when a high quality crystal is desired.

The growth of quartz crystals has been understood precisely with reference to the growth temperature, temperature gradient, percent of fill, solubility, percent of baffle open, orientation and nature of seed, and type of nutrient. Also, many kinetic studies have been carried out.[13][14] Figures 5.2 and 5.3 show the solubility of quartz with temperature, growth rate as a function of seed orientation, and growth rate as a function of percent of fill. Figure 5.4 shows hydrothermally grown quartz crystals.

The type of crystal to be grown depends on the application, as different properties are required in each case. For optical use, high uniformity, low strain and low inclusion counts are needed since all of these can affect the transparency. For surface acoustic wave devices, large pieces

are needed which can take a very high quality surface finish. The quality of the material required for resonators used in time and frequency devices varies with the application. The more precise the need, the more stringent are the requirements. For most applications, a truly high quality material is not needed. For high precision uses, such as in navigational devices and satellites, a very high quality material must be used. Most of the recent research on quartz growth is for improved resonator performance, which requires the growth of high quality, and low dislocation quartz, which is discussed in Sec. 5.2.6. Figure 5.5 shows the fabrication of resonators from a single crystal.

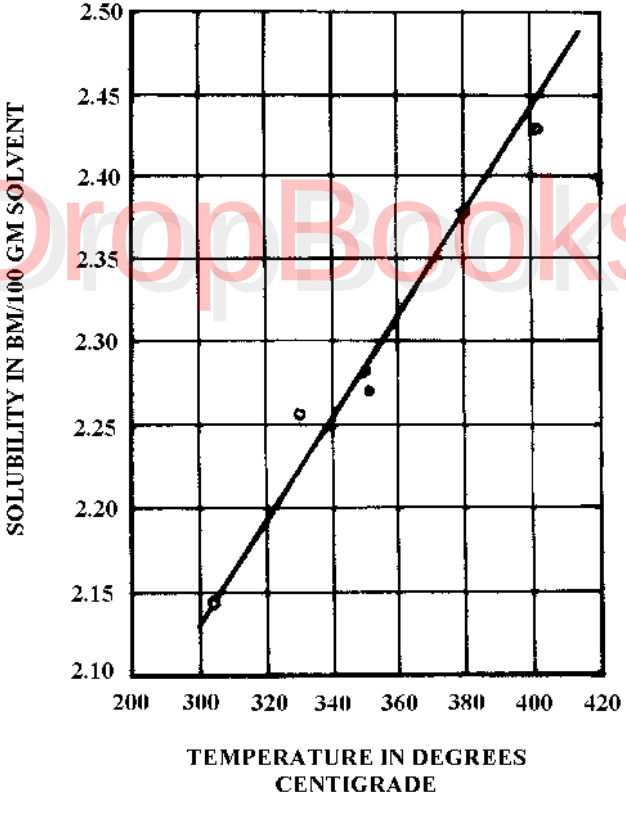

DropBooks

Figure 5.2. Solubility of quartz with temperature.[14]

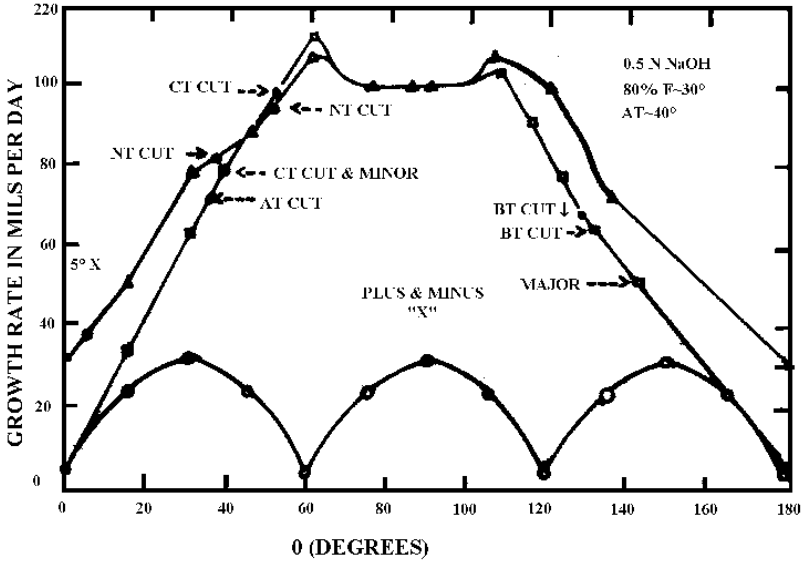

(a)

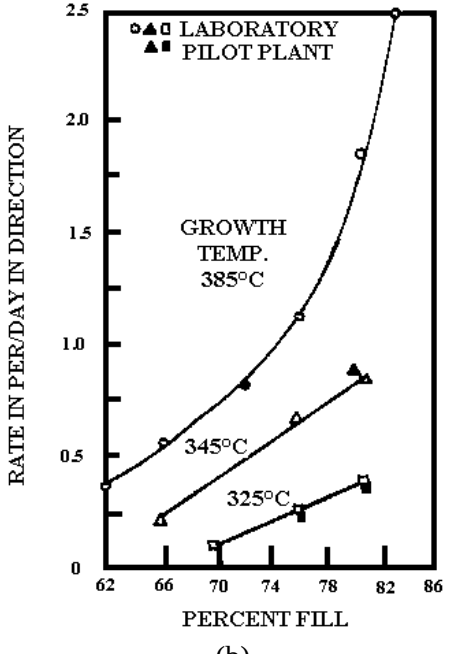

(b)

Figure 5.3. Growth rate of quartz as *(a)* a function of seed orientation, and, *(b)* a function of percent of fill.[14]

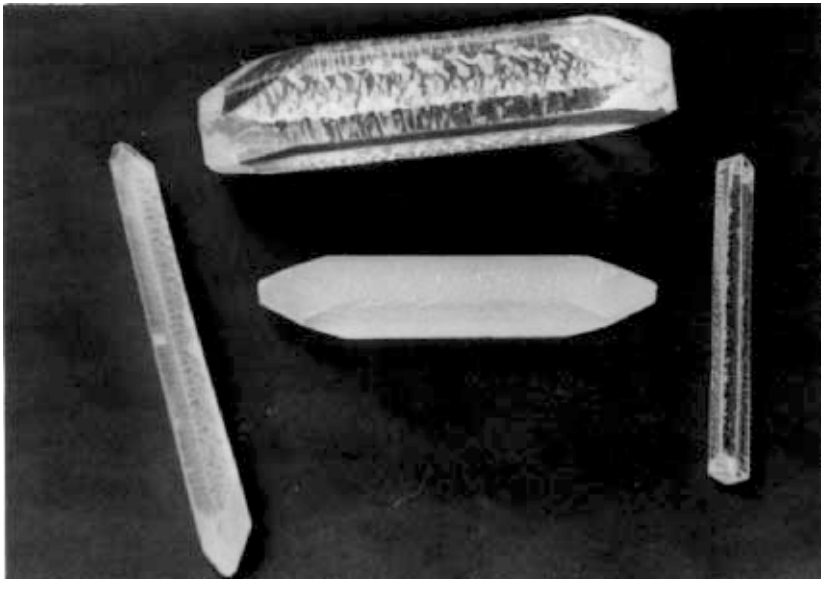

Figure 5.4. Hydrothermally grown quartz crystals.[17]

DropBooks

Figure 5.5. Fabrication of resonators from a single crystal.[16]

5.2 GROWTH OF HIGH-QUALITY (AND DISLOCATION FREE) QUARTZ CRYSTALS

It is well known that the hydrothermal growth of quartz in the industrial sector is at least 45 years old. Though many improvements have been brought about, it is still more an art than a truly reproducible industrial and scientific process. We discussed in Ch. 1 the shortcomings in the hydrothermal growth of crystals, especially with reference to the theoretical knowledge. This applies even to quartz growth under hydrothermal conditions. The growth of high quality quartz crystals insists on so many parameters like phase relationships, nutrient's solubility, thermodynamics (state equations, kinetics of reaction, impurities repartition), crystal defects characterization, and so on. The other aspect is that the needs for cheaper material in a wide range of applications like clocks, microprocessors, etc., result in content with a medium quality product, and the low profitability precludes financing long and expensive studies. Though much of the recent publications on quartz is on the possibility of obtaining/growing high quality quartz crystals for stringent electronic applications, this group is still in minority. Except for quartz, no other material coming from hydrothermal synthesis has sizable industrial use; even though $AlPO_4$, $GaPO_4$, $Li_2B_4O_7$, and microcrystallites show interesting promise, industry does not seem ready to make an important R & D effort concerning these products. Thus, it is difficult to get financial support to acquire a better knowledge of hydrothermal growth, which is highly intricate and necessitates an important effort for a long duration of time. Private industry cannot deal alone with the costs of such a program; even in the USA, research programs are government sponsored, especially in defense field.[11]

Several criteria are used to evaluate the quality of quartz crystals. The most commonly used criterion is the Q value or quality factor, which is a measure of the acoustic loss of the material. It is important for a resonator to have high electrical Q value and superior frequency-temperature characteristics. In a piezoelectric resonator, electrical energy and mechanical energy are interconvertible. In such a case, Q is expressed as:

$$Q = \frac{[X]}{R}$$

where X is the inductive or capacitive reactance at resonance and R is the resistance.

The quality factor, Q, can be considered as the inverse of the fraction of the energy lost per cycle. The highest values of Q are required in order to prevent loss of energy into coherent phonons. The acoustic Q for natural α-quartz crystal varies in the range of 1 to 3×10^6 while for synthetic quartz crystals, the value drops down to 2.105 to 1.106. Thus, in the last two decades, the main objective among quartz crystal growers has been to improve Q, which in turn leads to the production of a low concentration of physico-chemical and structural defects. We shall discuss the growth of such quartz crystals of high quality through the study of growth rate, mineralizers, solubility liner material autoclave, seed effect, nutrient effect, and finally the recent advances in the processing of defect-free quartz for stringent electronic applications.

5.2.1 Growth Rate

Growth rate is determined by the ratio of increase in thickness of seed and duration of the run. The growth rate along the main crystallographic axes, R_c, is determined by dividing the thickness of the layer grown on the seed, $(h_1 - h_0)/2$, by the run duration t, and is expressed in mm per day. A much more precise procedure is to determine R_c as a function of weight increment provided the surface area does not change during the run, $R_c = (P_t - P_o)/2S_t\,\delta$, where $\delta = 2.65 \text{g/cm}^3$ is the density of quartz. The growth rate increases with the run duration, the increment being relatively faster during the early hours and days.[26] The growth rate depends upon various factors like growth temperature, experimental pressure (% fill), impurities concentration, presence of defects, seed orientation, solvent/mineralizer, % of baffle opening, and so on. It has also been known for sometime that, qualitatively, acoustic Q is inversely proportional to the growth rate and directly related with to chemical impurities which will be discussed separately. The internal friction (inverse of mechanical Q) is dependent on growth rate of synthetic quartz crystals. This was first demonstrated by Brown.[27] Chakraborty (1977) has studied the dependence of mechanical Q on the growth rate of quartz crystals using different mineralizers, and concludes that the inverse relationship (exponential) between mechanical Q and growth rate is independent of the nature of the solvent in which the crystals have been grown.[28] Thus, the mechanical Q is not dependent on growth rate only, but also upon various other operational variables. For example, for growth on surface normal to (0001) (basal plane growth) or on samples 5° from (0001) (+5° X cut surface), high Q quartz ($Q > 10^6$) can be grown at rates below 20 mil/day

DropBooks

(0.5 mm/day) while even in the presence of Li^+, *Q*'s above 10^6 have ordinarily not been obtained at growth rates much above 60 mil/day (1.5 mm/day). Techniques for obtaining high *Q* at high rates have obvious economic importance. In particular, rates above 100 mil/day (2.5 mm/day) with *Q*'s > 10^6 would provide significant savings in both capital and operating expenses in commercial quartz growth.[29]

5.2.2 Seed Effect

The seed plays a predominant role in the quality of the resulting crystal. For higher frequency applications, a smaller *X*-axis dimension is needed. Material with growth along the *Z*-axis (*Z*-growth material) is desired for resonators as it has been shown that this material is about an order of magnitude lower in aluminum concentration.[30] The thickness of the seed is usually between 1 to 2 mm. Until recently, it was necessary to use natural seeds for the preparation of low dislocation crystals. This is an extremely tedious process since only a small portion of natural crystal is of sufficient quality for seed use, resulting in a complicated selection process. The seeds must also be of sufficient size for useful crystal growth. Christie et al. (1983) have reported that small seeds can be fastened together to make longer seeds, but this has not always been successful.[31] Most seeds used today are fabricated from synthetic quartz crystals. This is a much simpler process since the seeds can be cut parallel from the original seed. Most crystals grown from synthetic seeds, however, contain a large number of dislocations of the order of several hundred per square centimeters. This results in the formation of etch channels in the resonator, which weaken it mechanically and cause problem when electronic devices are deposited on the surface.[32] The studies of Armington and Larkin (1985) have shown that, when a seed perpendicular to the *Z*-axis (but from the *X*-growth region) is used, the dislocation density can be reduced to below ten, and sometimes to zero dislocations per square centimeter (Table 5.2, Figs. 5.6, and 5.7).[33] Although the reasons for this are not entirely understood, it may be related to the fact that, unlike dislocations in the *Z*-region where they form at the seed and grow close to the *Z*-axis, most dislocations in the *X*-region grow at an angle of at least 45°, and are usually close to 90° from the *Z*-axis. Studies have shown that aluminum in the seed does not migrate into the growth regions. Thus, the purity of the crystals produced using seeds cut from the *X*-region is as good as crystals produced from the usual *Z*-seed.

Table 5.2. Dislocation Density in Different Seeds

Seed	Mineralizer	Etch Channel Density
Z	Hydroxide	253
Z	Carbonate	247
X+	Hydroxide	1
X+(reused)	Hydroxide	14

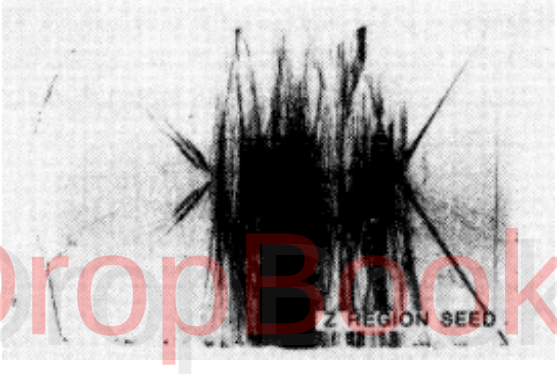

DropBooks

Figure 5.6. Dislocation density in quartz.[33] *(Courtesy of A. F. Armington.)*

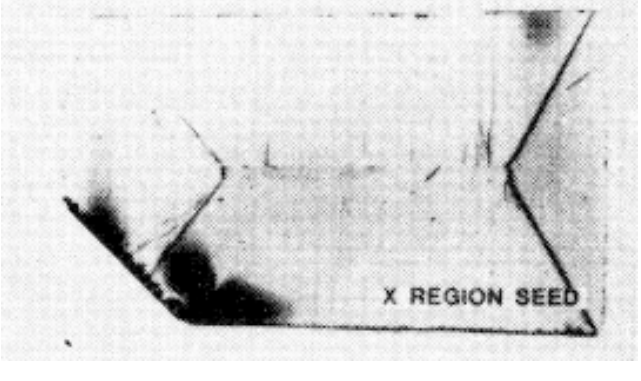

Figure 5.7. Dislocation density in quartz.[33] *(Courtesy of A. F. Armington.)*

5.2.3 Nutrient Effect

The quality of the nutrient has a profound effect on the purity of the grown crystal. It appears that most of the impurities incorporated into the crystal come from the nutrient and not from the autoclave walls. The search for new sources of nutrient is not a new field of research. In the 19th century, earlier workers tried several varieties of nutrient materials to obtain α-quartz under hydrothermal conditions. However, the results were not satisfactory owing to the lack of knowledge on the solubility data for quartz, which resulted in a very low growth rate. In this respect, some serious efforts were initiated by Kolb et al. during 1976. They examined new sources of nutrient to replace Brazilian α-quartz for hydrothermal crystallization.[34] It was found that the acoustic *Q* strain depends upon the source of the nutrient and also its geographic region/location. Both vein and appropriately chosen pegmatite quartz can be used as nutrient. High purity sand can be used as nutrient provided process conditions are altered so as to compensate for its effective lower surface area. Non α-quartz nutrients such as silica glass and silica gel produce initially higher supersaturation and fast growth rates leading to poor quality of crystal growth. However, alterations in process conditions can be made to reduce initial growth rates and prepare reasonable quality crystals. Therefore, in the growth of high quality quartz crystals, *Z*-growth material and recrystallized glass is used as the nutrient material. If future requirements become more stringent, particularly for radiation damage, it will be necessary to reduce the aluminum content even further. In this case, recrystallized glass will be the leading candidate, as higher purity glass is available. This generally requires two runs, since the glass must first be converted to α-quartz.

There are several laboratories throughout the world working to find a suitable nutrient for high quality quartz growth. Hosaka and Miyata (1991) have obtained high quality α-quartz crystals using cristobalite as the nutrient.[35] The authors have used high-purity α-cristobalite powder compacted into grains of 0.5–1.00 mm or into lumps of approximately 1 cm in diameter for the hydrothermal synthesis of α-quartz.

Alpha-cristobalite is a polymorphic form of silica as are quartz and tridymite and has a higher solubility than quartz.[36] Alpha-cristobalite powder[37] has the following advantages: it can be obtained in a high-purity state with low contents of Al and alkaline metallic ions, and can be prepared with relative ease as particles of uniform size. As compared with

the conventional growth of synthetic quartz crystals using Brazilian lascas, the use of α-cristobalite powder may be expected to allow:

(i) Synthesis of high-purity large quartz crystals.

(ii) Synthesis of micro quartz crystals having uniform grain size.

Hosaka (1991) had attempted to crystallize micro quartz crystals by hydrothermal hot pressing method using α-cristobalite powder as a source material.[38] Figure 5.8 shows α-quartz crystals grown at high (left) and low (right) fillings using α-cristobalite as the nutrient. The % fills or pressure greatly influences the growth rate. However, a considerable amount of work has to be carried out for the industrial production of α-quartz using cristobalite as the nutrient.

Figure 5.8. *Alpha*-quartz crystals.[38]

5.2.4 Solubility

Solubility is one of the most important aspects in hydrothermal crystal growth. The early literature survey clearly shows that the very slow growth rate achieved until the works of Nacken (Germany 1950) and Wooster and Wooster (1946) were published was mainly attributed to the lack of knowledge of the solubility of quartz.[19][39] The same applies to other compounds also. The first systematic study of the solubility of quartz was carried out by Spezia (1905).[40] Since then, a lot of progress has been achieved in the understanding of the solubility in general for various inorganic compounds. During 1960s, new methods of investigating the solubility and the new experimental set up for the determination of solubility under hydrothermal conditions were proposed.[41][42]

The solubility of quartz in pure water was found to be too low for crystal growth (0.1–0.3 wt %), but the solubility could be markedly increased by the addition of OH^-, Cl^-, F^-, Br^-, I^-, and acid media which act as mineralizers. For example, the reactions

$$SiO_2 + 2OH^- \rightarrow SiO_3^{2-} + H_2O$$

$$2OH^- + 3SiO_2 \rightarrow Si_3O_7^{2-} + H_2O$$

show the formation of various complexes or species during the hydrothermal crystallization of quartz. Hosaka and Taki have used Raman spectra to identify and quantify such species.[43]

In pure aqueous solutions (even at 400°C and 25000 psi), the solubility of quartz is too low to allow growth to take place in any reasonable time. Alkaline additions, such as NaOH, Na_2CO_3, KOH and K_2CO_3 are all effective as mineralizers in this pressure and temperature range. A small increase in molarity results in only a slight increase in the growth rate, whereas large increase begins to produce an additional phase along with quartz. The minimum molarity for good growth rate is about 0.25 M for NaOH. Concentrations of about 4.0 M for NaOH and 2.0 M for KOH form sodium or potassium silicates along with α-quartz. Laudise and Ballman (1961) have measured the solubility of quartz in 0.5 M NaOH as a function of % fill and temperature. The quartz solubility dependence on % fill is shown in Fig. 5.9.[44]

An important result of solubility determinations is the delineation of the pressure, temperature, and composition regions where the temperature coefficient of solubility is negative. These regions are to be avoided in the growth of quartz, since they require a different setup; otherwise, they result in the loss of seed crystals.

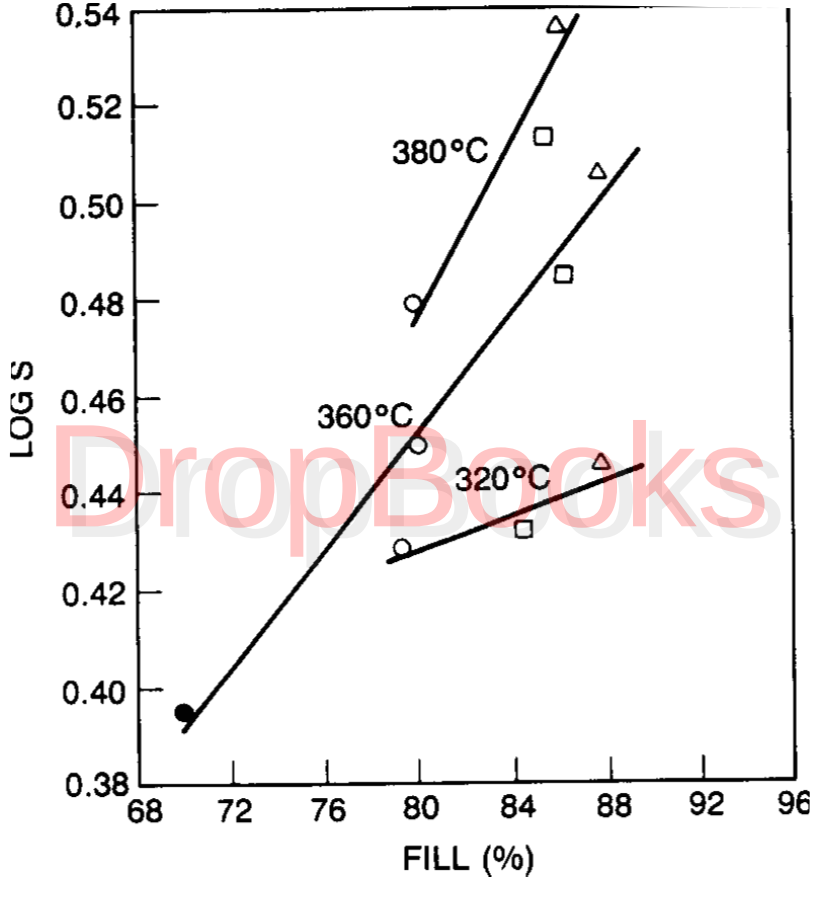

DropBooks

Figure 5.9. Quartz solubility dependence on % fill.[44]

In recent years, mixed solvents are being used even in the growth of quartz. High-quality large quartz crystals have been obtained in NaCl and KCl solutions, NaOH and Na_2CO_3 solutions, (10%).[45][46] Most of the literature data available on the solubility of α-quartz deals with the data in various solutions at elevated temperatures and pressures. It was recently observed that, in the growth of quartz crystals under hydrothermal conditions, the evaluation of pressure generation and its effect on the dissolution in different aqueous solutions are the important steps. Hence the authors have studied the solubility of α-quartz in NaOH (1M) + Na_2CO_3 (1M) using high-pressure conditions from 200 MPa to 350 MPa at temperatures of 400°C.[46] The impetus for this work was provided by the fact that high frequency applications of α-quartz require sheets with small thickness of the same order of size as the defects (such as inclusions, etch pits and dislocations). Thus, the pressure can make new solvents viable for hydrothermal growth, especially by reducing their concentrations. Figures 5.10 and 5.11 show the solubility limit comparison between NaOH (1M) and Na_2CO_3 (1M) vs. pressure at 400°C; and log solubility (S_1) in NaOH (1M) and in Na_2CO_3 (1M) vs. 1/*P*. These experimental results show that Na_2CO_3 appears to be a better solvent than sodium hydroxide in high-pressure domain for a temperature close to 400°C. From Fig. 5.11, the enthalpy values have been calculated and the values are as follows:

$\Delta H_T = 2395 \pm 5$ cal/mole for NaOH (1M); $200 \leq P \leq 350$ MPa

$\Delta H_T = 4001 \pm 2$ cal/mole for Na_2CO_3 (1M); $150 \leq P \leq 350$ MPa

5.2.5 Defects Observed in Synthetic α-quartz Single Crystals

The defects present in the synthetic α-quartz crystals play an important role in determining its quality and in turn applications. Much of the recent works on quartz is essentially focussed on the defect studies. All the defects present in quartz can be classified into two types:

- The physico-chemical defects
- The structural defects

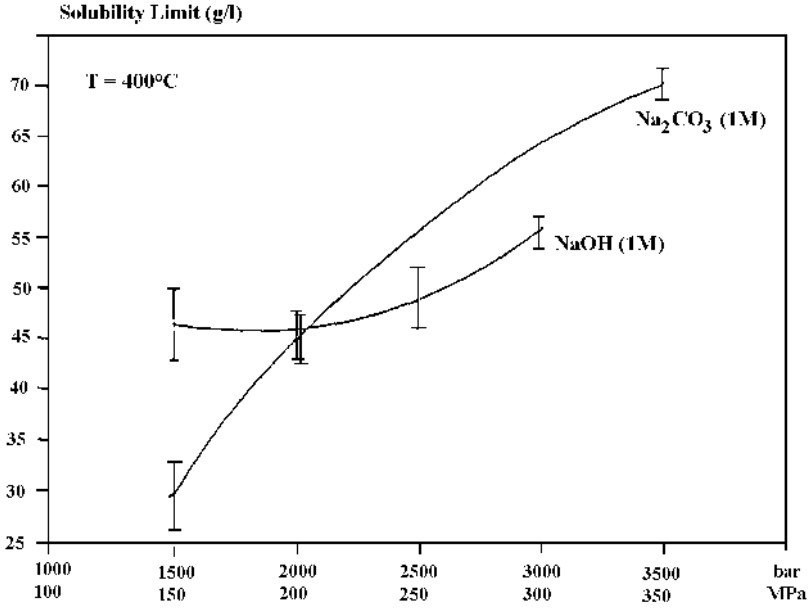

Figure 5.10. Solubility limit comparison between NaOH (1M) and Na_2CO_3 (1M) vs. pressure at 400°C.[46]

DropBooks

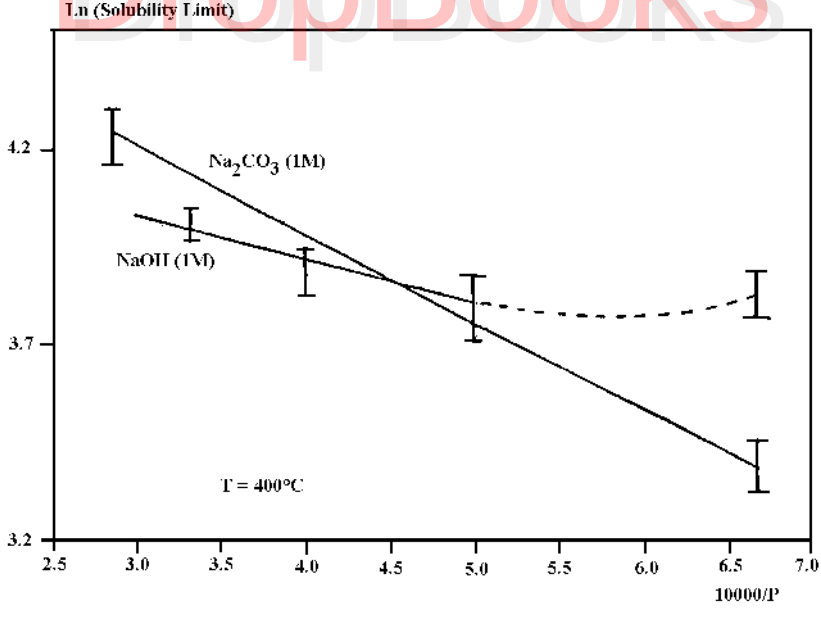

Figure 5.11. Log solubility (S_1) in NaOH (1M) and in Na_2CO_3 (1M) vs. $1/P$.[46]

Physico-chemical defects are mainly induced by the nature of the nutrient or the solvent and also by chemical contamination of the solution by the metal constituting the reaction vessel. Quite often, solid or liquid inclusions like $NaFe^{3+}Si_2O_6$ (acmite) are inserted in the α-quartz. The most important impurity in quartz is H^+, which easily fits interstitially in the large (1 Å) channels that lie parallel to the *c*-axis to charge compensate for Al^{3+} which goes to a Si^{4+}. It enters the lattice from the growth solutions as OH^-, the O^{2-} being incorporated in the SiO_2 lattice. In thermodynamical conditions, different cations (in particular Li^+) can be in the interstitial positions, in particular for compensating the $Si^{4+} \rightarrow M^{3+}$ cationic substitution into the α-SiO_2 lattice. Figure 5.12 shows the effect of growth rate on Al^{3+} concentration in the *Z*-region of grown crystals using hydroxide mineralizer.[47] Aluminum concentration was determined by EPR.[16] Similarly, Laudise has studied the dependence of the effective partition coefficient for OH^- impurity in quartz on growth rate (Fig. 5.13).[48] Lithium salt is added to the solvent to check the aluminum concentration in the grown crystal. The entry of Al occurs in the use of (OH) and (CO_3) based mineralizers. Table 5.3 gives the distribution of impurities in different sectors of synthetic quartz, which has been studied by Yoshimura et al. (1979), and Iwasaki and Kurashige (1978).[49][50]

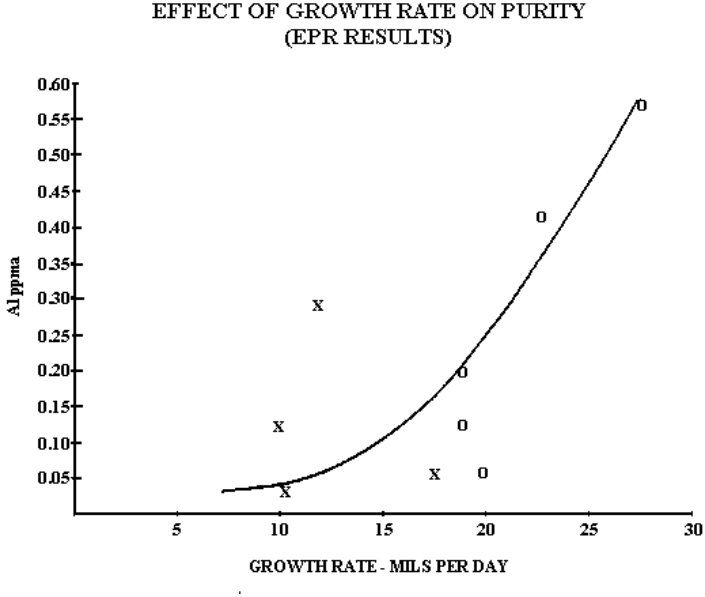

Figure 5.12. Effect of growth rate on $A1^{3+}$ concentration in the *Z*-region of growth crystals.[16]

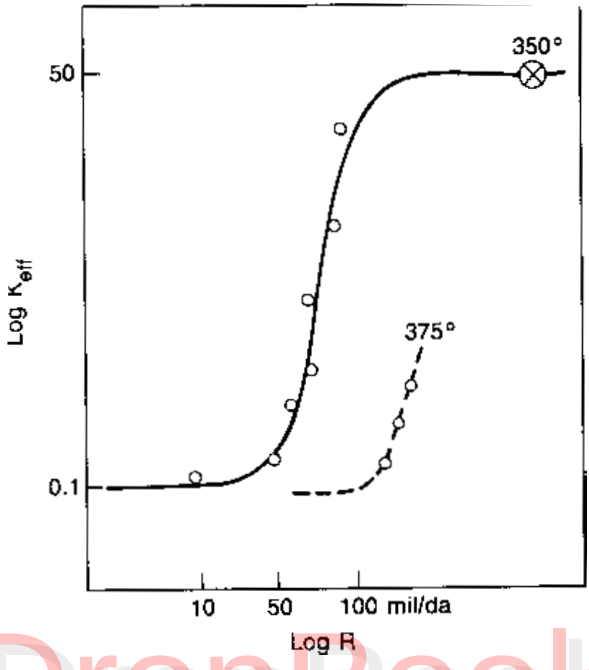

DropBooks

Figure 5.13. Effective partition coefficient for OH^- impurity in quartz on the growth rate.[48]

Table 5.3. Impurities in Synthetic Quartz Crystals (ppm)

Sector	Al	Na	Li
Z	5	1	0.5
+X	31	9	5
-X	122	40	5
S	85	26	16

The structural defects in quartz are basically the dislocations. Their origin can be due, generally, to foreign particles, thermodynamical parameters governing the crystal growth, or hydrodynamic conditions inside the reaction vessel.

5.2.6 Processing of α-quartz for High Frequency Devices

The study of the type of defects present on silica surfaces would be of great importance for a better understanding of electrical or piezoelectric properties. The development of high frequency devices (24 MHz $\rightarrow$ 100 MHz or more) induce some strong constraints concerning the shaping of the α-SiO_2 material. The low defect, high purity synthetic quartz should have the following characteristics:[51]

Parameter	Desirable	So far achieved
Etch channel density	< 10 / cm ^{2}	< 86
Inclusion density	< 10 / bar	
Impurity concentrations (ppb)		
Al	< 200	700
Li	< 300	300
Na	< 500	1640
K	< 40	300
Fe	< 100	1800
Q (3500/3800 cm^{-1})	< 2.5 x 10^6	> 2.5 x 10^6
Strain	none	variable
Fringe distortion	< 0.05 RMS	variable

The existence of defects, either physico-chemical or structural, in synthetic quartz crystals leads to the critical modifications of devices. There are three different parameters on which the quality of quartz depends:[52]

i. Chemical impurities, e.g., $(OH)^-$ distribution, induce a large decrease of the acoustic *Q*. The substitution $O^{2-} \rightarrow (OH)^-$ being coupled with the cationic one ($Si^{4+} \rightarrow M^{3+}$), the M^{3+} impurities can play an important role concerning the chemical aging of resonators and its behavior vs. ionizing radiations.

ii. Crystal defects like dislocations, etching channels, fractures, etc., which influence the acoustic distribution.

iii. Inclusions (iron, sodium, acmite, aluminum, etc.).

As the application of quartz goes to higher and higher frequency devices, the thickness of the quartz plate drops. For example:

24 MHz range applications: ~ 70 μm thickness

100 MHz range applications: ~ 6–7 μm thickness

The thinning down of the quartz plate depending upon the frequency measurements and can be expressed as

DropBooks

$$F(\text{MHz}) = \frac{K(\text{MHz}\,\mu\text{H}^{-1})}{e(\mu\text{m})}$$

where *e* is the plate thickness, *K* is a constant characteristic of the material and of its orientation, and *F* is the resonance frequency.

Sweeping is one of the most popularly used techniques in recent years to enhance the performance of quartz resonators. Sweeping or solid state electrolysis or electro-diffusion is generally performed under vacuum or air or hydrogen or desired atmosphere.[53]-[55] During sweeping, the crystal is placed in an electric field and heated. Figure 5.14 shows the schematic diagram of the sweeping apparatus. Then, there is a migration of the impurities, and some modifications are induced within the crystal. According to the parameters used by the manufacturer during the sweeping process, and the quality of the as-grown crystals, the results could be very different. Sweeping reduces the formation of etch tunnels. The effect of sweeping is to remove lithium and sodium deposited interstitially during the growth. These ions are usually trapped along an angstrom-wide

tunnel, which is parallel to the *Z*-axis in the quartz crystal lattice. These ions, in an interstitial position, interact with aluminum impurities substitutional in the lattice to form Al-Li centers, which have shown to be weakly bonded and are the cause of low radiation tolerance in a resonator. In the sweeping process, these are replaced by Al-OH or Al-hole centers, which have a much higher radiation tolerance.

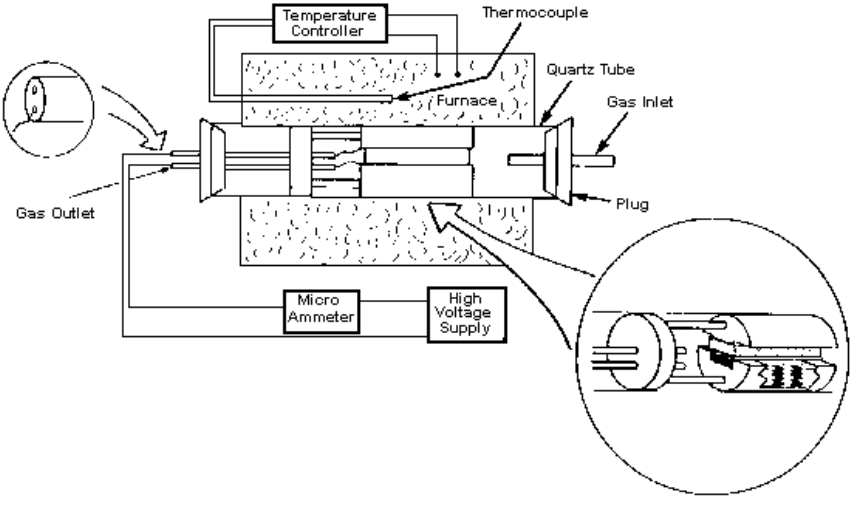

Figure 5.14. Schematic diagram of the sweeping apparatus.[55]

Sweeping is influenced by the electric field, strength, electrode type, and atmosphere. It takes less time in air due to the availability of water in the atmosphere.[56] Electrodes, usually platinum, or gold or aquadog are deposited on each of the *Z* surfaces of a lumbered bar. The crystal is then subjected to a field of 1000–2000 volts/cm (thickness) at temperature 500–550°C. The current is continuously measured and the sweeping is considered completed when the current has dropped to a constant value. It takes usually 5 to 7 days to remove alkalies. In some quartz, the sweeping may take 7 days or even more. Sweeping has also been used to dope quartz crystals in order to determine the effect of the dopant on the properties of the crystallization of quartz. A vast amount of literature data shows that sweeping can not become a routine process even

if all the same experimental conditions are ever applied. The quality of the swept crystal can change in such a way that the modifications are sometimes unexpected. So, each industrially swept crystal must be controlled before using. Some of the controlling techniques are the x-ray topography and the infrared spectroscopy. These techniques help to characterize the physico-chemical defects and the α_{3500} value (Q factor). The reader can refer to the works of Refs. 12, 57, and 58.

There are several other techniques employed for the fabrication of piezoelectric high- to ultrahigh-frequency devices based on quartz resonators. The important ones are chemical polishing and ion beam etching (IBE). The reverse thermodynamic relations are employed for the refinement of chemical polishing. Several solvents like HF and NH_4HF_2, NaOH, KOH. xH_2O, NaOH. xH_2O, etc.[59]

Similarly, the industrial chemical etching process is specially dedicated for large thickness removals without damaging the blank surface texture. This is most useful for frequency applications of quartz, because the mechanical grinding and lapping introduce surface stresses. Fluoride media is the most popularly one for this type of chemical polishing.[60] Recently, Cambon et al. (1994) have tried industrial chemical etching successfully in the temperature range of 150 to 180°C using concentrated NaOH solvents.[61] During the chemical etching process, several factors influence the process: kinetics, etching temperature, etching time, plate orientation, SiO_2 concentration, solvent concentration, wafer carrier geometry, and so on. Using this process, about 3200 quartz plates can be processed. The resonators manufactured by this process have demonstrated a high level of performance, even higher than those obtained by mechanical means.

PropBooks

Future avenues in this direction are: improvements on theoretical knowledge, improvements in the quality of solvents, nutrients, and seeds, autoclaves' technology, material used for autoclaves, dimensional ratio (diameter/length), crystallization zone/dissolution zone, basic questioning of the validity of presently used growth parameters (P,T), and better understanding of complementary treatments like sweeping, chemical etching, etc. Thus, any work on quartz is still a promising field, and it will have some important consequential effects on hydrothermal growth, in general, and facilitate the development of other materials production.

5.3 BERLINITE

Berlinite, $AlPO_4$ is named after N. J. Berlin (1812), a pharmacologist of the University of Lund. Its physical properties are shown in Table 5.4.[62] Berlinite replaces quartz in electronic devices because its large mechanical coupling factors are greater than α-quartz, and its resonant frequency is nearly independent of temperature for certain orientations.[63]–[65] Berlinite is also interesting because its presence in Ca aluminum phosphate bioglass ceramics is believed to lead to higher bioactivity of bone implants.[66][67] Table 5.5 gives a tentative comparison with quartz.

Table 5.4. Physical Properties of Berlinite and Quartz (Schwarzenbach, 1966)[62]

Properties	$AlPO_4$	Quartz
Density	2.64 (natural) 2.56 (artificial)	2.655
Hardness	6 – 7	7
n_e	1.529 ± 0.003	1.544
n_o	1.519 ± 0.003	1.535
Birefringence	+ 0.01	+ 0.009
a	4.94291	4.9138
c	10.94761	5.4052
c/*z*	5.4738 Å	
c/*a*	2.21481	1.10
c/2*a*	1.1074	
space group	$P3_121$ or $P3_221$	$P3_121$ or $P3_221$
z	3	3

Table 5.5. Tentative Comparison with Quartz (Thickness *Y* Rotated Resonators at Same Frequency)

Useful coupling coefficient (AT filter trapped resonators)	Enhanced by 1.4 – 1.5
Shift of oscillators or band width of filters (AT cut)	Twice
Angular sensitivity (1st order FTC)	Reduced
Thermal stability (higher order FTC)	Better
Q factor propagation losses	Already sufficient (may be comparable)
Thickness of plates (AT)	Reduced by 1.15
Electrode dimensions (AT)	Reduced by 1.32 (TT)
(Same plating 2D TT of TS)	Reduced by 1.23 (TS)
Nonlinear properties	To be determined
"Dry" berlinite has similar C, E, EPS constants, first order TC and much reduced higher order TC.	

DropBooks

Berlinite occurs in nature associated with augelite, attacolite, and other phosphates as small crystals at the Westana Iron mines near Nasum, Kristiaanstad, Sweden. However, the synthetic berlinite is more popular and abundant and it can be obtained as fairly big crystals. The first successful growth of berlinite crystals was by Jahn and Kordes (1953), followed by Stanely (1954).[68][69] Stanely carried out the experiments in a sealed borosilicate glass vessel placed in a low pressure environment. Mason (1950)[70] carried out the piezoelectric measurements for a small crystal of berlinite. However, the importance of berlinite only came into light in 1976 when Chang and Barsch[63] studied the piezoelectric properties of berlinite, and reported large mechanical coupling constants and that its resonant frequency was nearly independent of temperature for certain orientations.

The main problem connected with the growth of berlinite is the negative temperature coefficient of solubility, which insists on some special growth conditions, because of the lower solubility at higher temperatures, and higher solubility at lower temperatures. One of the principal problems in a systematic growth of $AlPO_4$ crystals is the growth rate relationship in H_3PO_4, and the lack of good solubility data (because of the negative temperature coefficient of solubility) at the constant fill conditions, which are essential for successful growth.[71]

Although so much of progress has been achieved in the growth of berlinite crystals, our knowledge on $AlPO_4$ is still comparable to that of quartz some thirty years ago, particularly with reference to solubility, reproducibility, crystal perfection, phase equilibria data, crystal size, etc.

Today it is possible to grow more than 500 kgs of dislocation-free high-purity quartz in a single experimental run. However, in the case of berlinite, it can not be more than a few hundred grams. The major problem is the highly corrosive phosphoric acid media in which the growth takes place.

5.3.1 Crystal Chemical Significance of the Growth of $AlPO_4$ Crystals

Berlinite is isostructural with quartz, $Si(SiO)_4$, and the artificial compound $AlAsO_4$. It shows the same thermal inversion as SiO_2,[72] although, at slightly lower temperatures, it crystallizes in hexagonal system—trigonal trapezohedral class-32. Artificial crystals are very similar to quartz with $(10\bar{1}1)$ $(01\bar{1}1)$ and (1011) faces. The natural crystals are massive and granular. As mentioned above, berlinite is isostructural with quartz but has a doubled *c*-parameter. It consists of alternating AlO_4 and PO_4 tetrahedra linked with vertices. Sosman[73] has reviewed all the forms of silica reported up to 1960. According to him, there are twenty-three polymorphic modifications of quartz, and eleven of them are the basic ones. Berlinite, although isostructural and isoelectronic with quartz, shows only six polymorphic modifications analogous to six major varieties of silica. Figure 5.15 shows six polymorphic modifications of berlinite analogous to six polymorphic modifications of quartz. The structure of all the six forms of berlinite can be described under three subgroups, i.e., quartz, tridymite, and cristobalite with higher and lower temperature forms.

The growth of any compound does not depend only upon the growth techniques and growth parameters like the starting materials, flux agents, mineralizer, temperature, pressure, rate of heating or rate of cooling, but also upon its crystal chemical parameters. A systematic study of the synthesis of ABO_4 compounds (A = Al, Fe, Cr, Co, Ga, B, Mn; B = P, As and V) and quartz with reference to their crystal chemical significance yields very interesting data which help to understand the growth technique of ABO_4 compounds.[74][75]

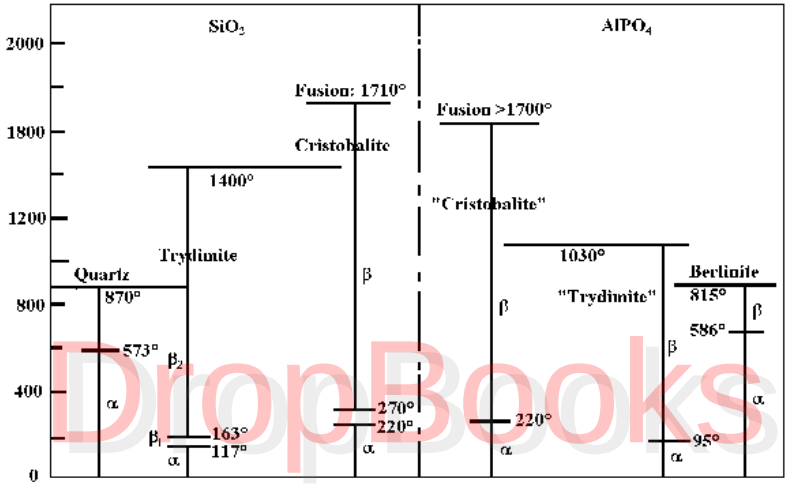

Figure 5.15. Six polymorphic modifications of berlinite analogs to six polymorphic modifications of quartz.

5.3.2 Solubility of Berlinite

Solubility is an important parameter in the successful growth of any compound in the form of large single crystals. The lack of solubility data is responsible for the earlier failures in the growth of $AlPO_4$ crystals. It was only in the late 1970s and early 1980s that reports on the solubility of $AlPO_4$ appeared in the literature. The problem associated with the growth of large single crystals of $AlPO_4$ is directly related to the lack of a

systematic study of the solubility and partly to the P_2O_5 pressure. Although, several reports have appeared on the solubility measurements with reference to various parameters, still there is no unanimity in the results. The solubility of berlinite was first determined by Jahn and Kordes (1950) in orthophosphoric acid above 300°C and it was found positive (Fig. 5.16).[68] Subsequently, Stanley (1954) reported a negative solubility for berlinite in 6.1 M H_3PO_4 (Fig. 5.17).[69] The solubility of $ALPO_4$ varies widely with the type of solvent used. Some authors claim that solubility of $AlPO_4$ in HCl is similar to that in H_3PO_4. The most important difference is the higher solubility at comparable mineralizer concentration.

The authors[76] have made an attempt to study the solubility of $AlPO_4$ in some new solvents like HCOOH, NH_4Cl, Na_2CO_3, $NH_4H_2PO_4$, NaF, KF, LiF, etc. The solubility of $AlPO_4$ (in wt %) as a function of temperature and at a pressure of 2 kpsi in 2M HCOOH solution is shown in Fig. 5.18.

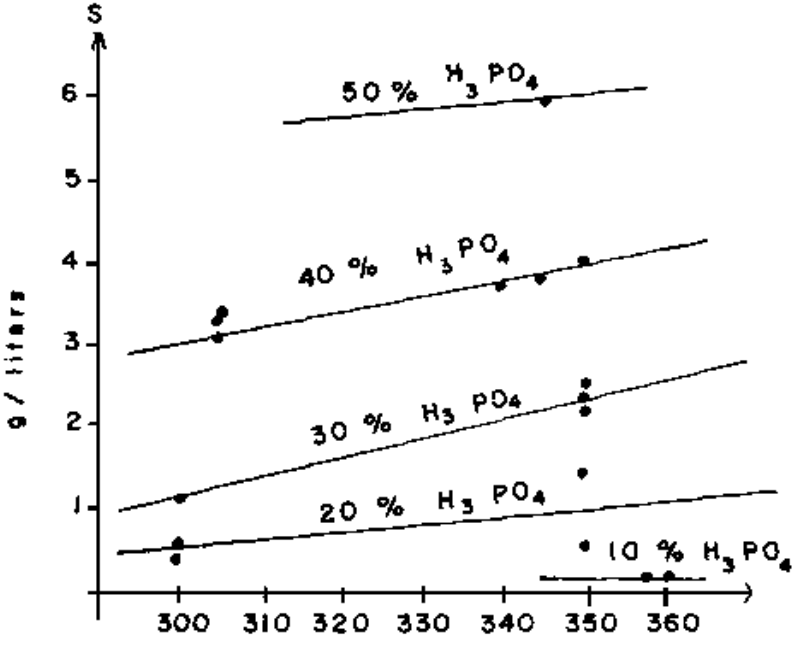

Figure 5.16. Solubility of berlinite in orthophosphoric acid above 300°C.[68]

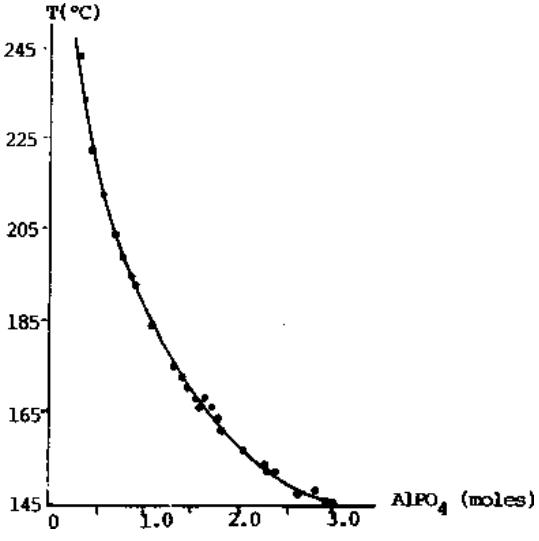

Figure 5.17. Negative solubility for berlinite in 6.1 M H_3PO_4.[69]

DropBooks

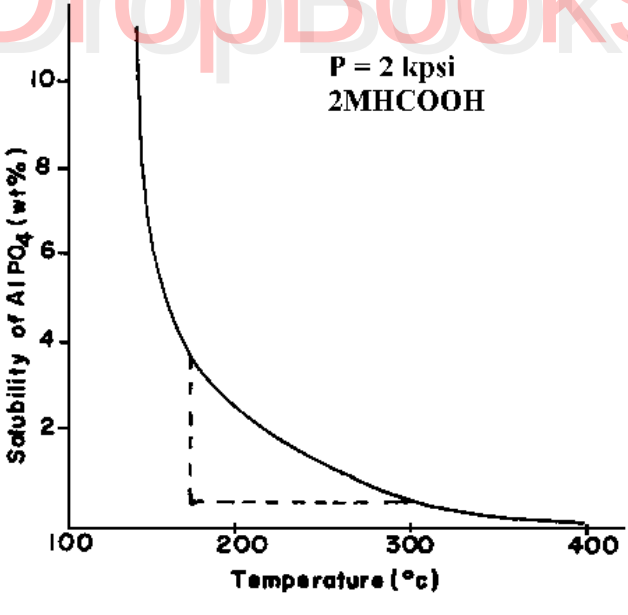

Figure 5.18. Solubility of $A1PO_4$ (in wt %) as a function of temperature.[76]

Recently, it has been shown that the solubility of $AlPO_4$ in H_2SO_4 is retrograde with respect to temperature and higher than in H_3PO_4 and HCl at comparable temperature, pressure, and acid molarity. However, the viscosity of sulphuric and phosphoric acid solutions is greater than that of HCl. Hence, the addition of HCl to H_2SO_4 would form a more efficient solvent for the growth of $AlPO_4$.[77] Figure 5.19 shows solubility as a function of temperature in H_2SO_4 + HCl mixtures. The authors have also carried out thermodynamic interpretation of the solubility data. The dissolution of berlinite in the mixtures of acids H_2SO_4 and HCl is a process of complex formation between Al^{3+} and the ligands present in the solution: OH^-, H_2O, Cl^-, HSO_4^-, SO^-_4, $H_2PO^-_4$. At low temperature, the complexes are similar to those of $AlPO_4$ in HCl; that is with Al-Cl complexes predominating. Even polynuclear complexes might form a broader metastable zone.

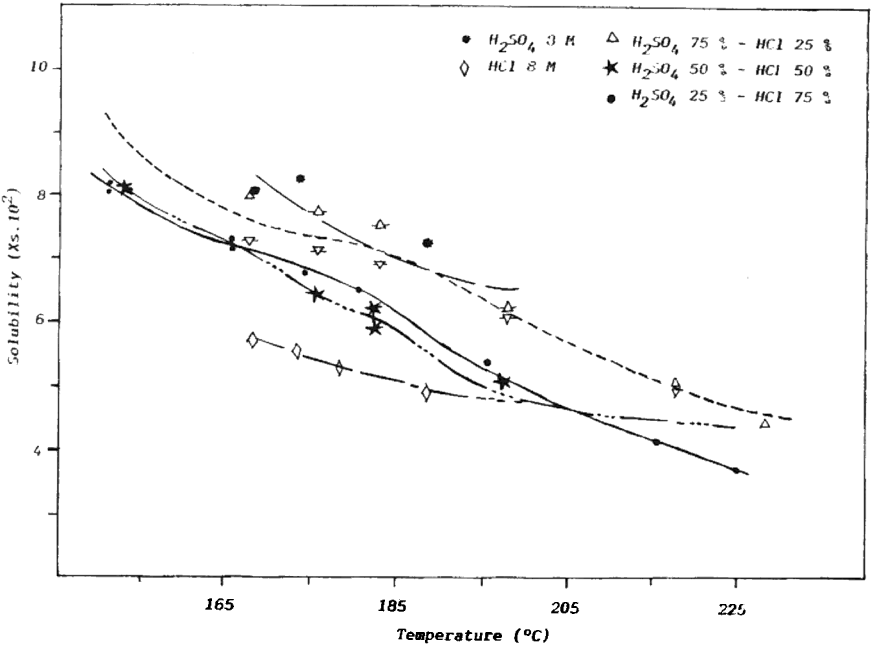

Figure 5.19. Solubility as a function of temperature in H_2SO_4 + HCI mixtures.[17]

With the rise in temperature, the association of Cl^- with H^+ increases the yield of HCl and destabilizes the $[Al^{3+}]$ complex. Under these circumstances, sulphate and monohydrogen phosphates replace chloride ligands and force a change in the coordination number of Al from six to four due to the steric effect. Similarly, H^+ also tends to destabilize the complex with sulphate and becomes $H_2PO^-_4$ hegemonic ligand as its association constant with H^+ does not vary significantly with a rise in temperature. Finally, the nucleation takes place by polymerization of tetrahedral $[Al^{3+}]$ complexes.

Table 5.6 gives comparative data of solubility of $AlPO_4$ obtained for various mineralizers under varying experimental condition.[76]

Table 5.6. Comparative Data of Solubility

Solvent	T (°C)	P (Kpsi)	Time (days)	Remarks
3M HCOOH	300	1	5	—
3.05M NaOH	170	10	3	Residue not $AlPO_4$
2M NH_4Cl	300	1	5	High solubility
4.62M Na_3PO_4	300	10	3	Residue not $AlPO_4$
2M HCOOH	300	11	5	Good solubility
3M Na_2HPO_4	300	10	5	1 % solubility
2.5M NH_4Cl	300	1	5	Fairly good solubility
3.05M CH_2COOH	170	10	3	Negligible solubility
2M $NaHCO_3$	300	1	5	Fairly good solubility
2M NaCl	300	1	5	Negligible solubility
3.05M NaCl	170	10	3	4 % solubility
2M NaF	300	1	5	Good solubility
2M KF	300	1	5	Good solubility
2M LiF	300	1	5	Good solubility
3.05M NH_4HF_2	300	10	5	Residue not $AlPO_4$
2M $NH_4H_2PO_4$	300	1	5	Negligible solubility
2M HCl	300	1	5	Good solubility
3.05M NH_4HF_2	170	10	5	Residue not $AlPO_4$
3.05M HNO_3	170	10	5	Negligible solubility
3.05M NaCl	300	10	4	Negligible solubility
1.0M Na_2CO_3	300	1	5	Negligible solubility

DropBooks

5.3.3 Crystal Growth

Berlinite could be best grown only by hydrothermal technique. The α-berlinite is stable up to 584°C, and below 150°C the hydrates and $AlPO_4.H_2O$ are stable. Therefore, the growth temperature should be greater than 150°C but less than 584°C. However, the solubility and *PVT* studies have clearly shown that crystal growth must be carried out at less than 300°C because of the reverse solubility. Several versions of the hydrothermal growth of berlinite single crystals have been tried to suit the solubility.

Nutrient Preparation. Berlinite in small crystal form can be obtained by hydrothermal reactions of H_3PO_4 with different chemicals containing aluminate.[69][78]–[80] Normally, high purity alumina is used as the nutrient, because of the purity of the grown crystals. The crystallization reaction is:

$$Al_2O_3 + 2H_3PO_4 \rightarrow 2AlPO_4 + 3H_2O$$

These fine crystals of aluminum orthophosphate are in turn used as the nutrient to grow bigger single crystals of berlinite.

The temperature coefficient of solubility of $AlPO_4$ is negative in the temperature-pressure range below 300°C. Thus, in the usual hydrothermal temperature gradient where the bottom of the autoclave is hotter than the top, $AlPO_4$ would be expected to nucleate preferably in the bottom region, so one would like to place the seed in the lower hotter region and nutrient in the upper cooler region.

The most important modifications suggested from time to time in the growth of berlinite crystals are as follows:

i. Crystal growth by slow heating method.

ii. Crystal growth by composite gradient method.

iii. Crystal growth by temperature gradient.

iv. Growth on seeds.

Chai[79] suggested the following nutrient preparation conditions for large (kgs) quantities, where the temperature is cycled:

Solvent H_3PO_4 (molar)	6.1
% Fill	81
$AlPO_4$ charge (gm)	45 presaturation at 25°C
Initial temperature (°C)	150
Final temperature (°C)	275
Differential temperature, *dT* (°C)	1 – 2
Heating rate (°C)/day	10
Method of heat rate increase	10
Yield (gm)	
> 60 mesh*	19.5 gm (70 % yield)
< 0 mesh	8.1 gm
Total yield	27.6 gm
Run duration (day)	15

* 60 mesh = 0.25 mm

Crystal Growth By Slow Heating Method. The method was previously described in Refs. 76 and 81–85, and it was mainly used for improving the quality of seeds and to enhance the size of the crystal with conditions similar to those used to obtain nucleations. A major drawback of this method is the impossibility of obtaining crystals of sufficient size in one operation due to the limited quantity of aluminum phosphate available in the solution.

DropBooks

Synthesis of berlinite crystals under lower temperature and pressure conditions using slow heating method was carried out using acid digestion bombs (T = 100–250°C; P = 100–300 atm) and smaller Morey autoclaves (T = 200–250°C; P = 300–1000 atm). The nutrient was taken in teflon liners.

The experiments at higher temperature (T > 500°C and P > 100 bars) yielded the β-berlinite. With an increase in the pressure, other high-pressure modifications of aluminum orthophosphate belonging to the cristobalite form were obtained.

Crystal Growth By Composite Gradient Method. In order to gain more flexibility in adjusting the growth rates for *Z* seeds and to avoid the preliminary work of crystal growth, nutrients of sufficient size (that did not cause crystallites to drop on crystals) needed to be obtained. A modification of the horizontal gradient method was originally proposed in Ref 87. Recently, berlinite crystals have been obtained by this method

successfully.[87] The autoclave used in the initial experiment is shown in Fig. 5.20. The following growth conditions were chosen by the authors[86][87] after experimental trials:

- Silica glass autoclave: 100 cm, diameter 30 mm
- Ratio hot/cold zone: *x* /1
- Solution: H_3PO_4, $H_2O/AlPO_4$ (6.5/1.1)
- Growth temperature: 170°C
- Horizontal temperature difference: $5 < T < 30$°C
- Construction diameter: 10 mm
- Powdered nutrient
- Filling: 80 %

Growth With Reverse Temperature Gradient. This is a more popular and widely used method in the growth of berlinite crystals. Here, the nutrient is kept in a casket at the upper portion of the autoclave, which is cooler. The nutrient is nothing but the crystalline powder or fine grains of $AlPO_4$ obtained by a slow heating method. The temperature of the bottom of the liner is kept at slightly higher temperature and this is the zone of crystallization, where berlinite can be crystallized either spontaneously or on seeds.[88]

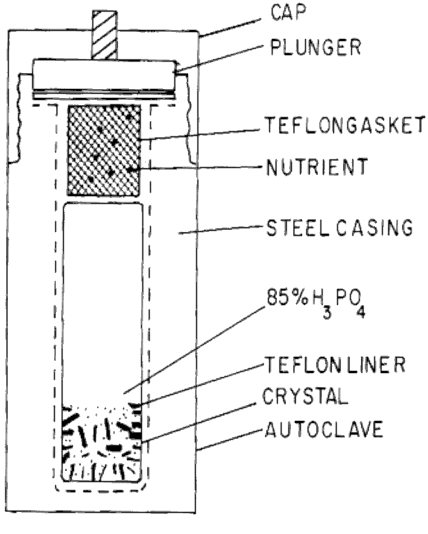

Figure 5.20. Autoclave used in the berlinite synthesis.[76]

Crystal Growth On Seeds. Spontaneously nucleated seeds and oriented seeds cut from grown crystals are mounted on a platinum frame which is placed in the bottom (hotter) region of an autoclave, and the nutrient (~ 60 mesh particle size prepared as described earlier) is placed above in a platinum gasket in the upper region (or in a teflon gasket). Thus, the seeds are in the warmer supersaturated region at the bottom of the autoclave and the temperature gradient achieved by cooling the top allowed proper convection. The schematic diagram showing the position of seeds, nutrient, and the baffle is represented in Fig. 5.21.

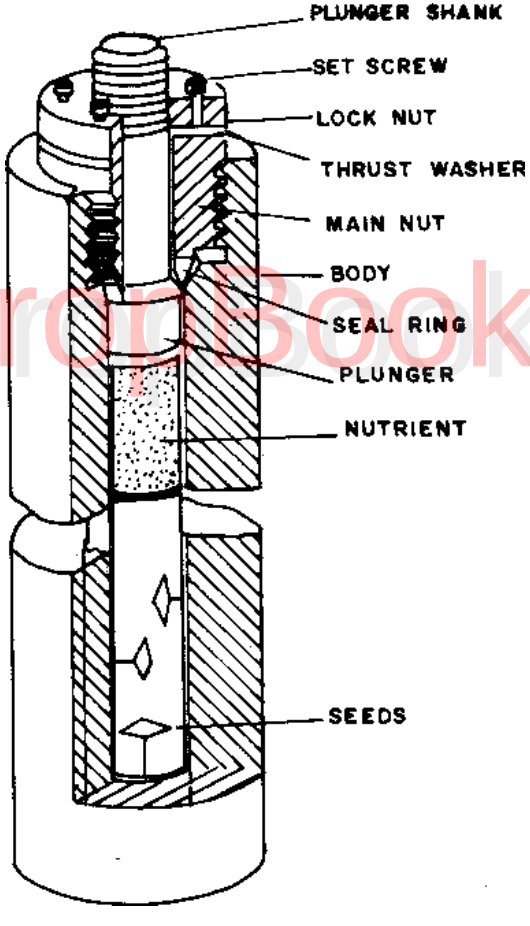

DropBooks

Figure 5.21. Schematic diagram showing the position of seeds, nutrient, and the baffle in the growth of berlinite crystals.[78]

In the growth of berlinite on seeds, the orientation of the seed is very important because the growth rate and perfection depend upon the seed orientation. According to Laudise (1985),[78] the growth rates are shown for seeds whose faces are indicated below:

(0001) (basal plane)	: :	0.25–0.50 mm/day
$(10\bar{2}\bar{1})$ (*X* cut)	: :	0.23–0.30 mm/day
$(10\bar{1}\bar{0})$ (*Y* cut)	: :	0.12–0.15 mm/day
$(01\bar{1}\bar{1})$ (minor rhombohedral face)	: :	0.12 mm/day
$(10\bar{1}\bar{1})$ (major rhombohedral face)	: :	0.15 mm/day

The relative growth rates are in general agreement with the morphology of the equilibrium form, as judged from observing spontaneously nucleated crystals, which are bounded by small prism $(10\bar{1}\bar{0})$ faces and terminated by minor and major rhombohedral faces. Thus, it would be expected that the rates on prism, major, and minor faces, are smaller than for $(11\bar{2}0)$ and (0001) faces, since the latter two do not exist as bounding equilibrium surfaces. In general, the morphology of the spontaneously nucleated crystals depends upon various parameters like pressure, temperature, volume, and composition of the nutrient and mineralizer.[89]–[91] For example, impurities in the powder come into the corresponding nutrient and caused twinning. The starting material like sodium aluminate or aluminum hydroxide gives needle-like crystals, whereas, pure $AlPO_4$ gives rhombohedral and pyramidal crystals.[76]

Yaroslavskii and Popolitov (1990) have studied the growth of berlinite on seeds in detail using fine crystalline charge and also aluminophosphate glass charge as nutrients.[92] They found that dissolution rate of aluminophosphate glass charge is three times greater than that of the crystalline charge. The solubility growth rate and crystal quality have been studied in great detail using different solvents like H_3PO_4, HCl, HNO_3, H_2SO_4. If the acid concentrations are increased above 2.5M, the spontaneous crystals form, and mother liquor is captured by the edges of the growing crystal. The growth rates differ greatly between the fine crystallization charge and aluminophosphate charge. The temperature gradient has been varied from 5–50°C. When the ΔT is high (40–50°C), it introduces macro inclusions and gas-liquid inclusions, and are clearly visible upon passing bright light through the crystal. The growth rates observed by the authors are rather high at 0.35–0.50 mm/day in H_3PO_4, 0.35–0.45mm/ day in HCl, 0.25–0.35 mm/day in HNO_3, and 0.2–0.3 mm/day

in H_2SO_4 solvent media. The growth rate of α-berlinite on [10$\bar{1}$0] and [0001] seed plates against the solvent concentration, growth temperature and temperature gradient are shown in Figs. 5.22 *a, b,* and *c*. The growth rate from aluminophosphate glass is 1.5–2 times greater than that from fine crystalline charge under the same conditions for mild process parameters.

5.3.4 Morphology

Although $AlPO_4$ crystals obtained spontaneously are small in size, they exhibit distinct morphological features. The crystal size varies from 0.5 to 4 mm and the common forms are hexagonal, rhombohedral, rod shaped, needle-like, and occasionally rounded. The morphological forms of $AlPO_4$ mainly depend upon the nutrient composition and the solvent in action. Data on the dependency of the morphological features, and the nutrient composition, as well as the solvent used are given in Table 5.7.

A typical morphology of $AlPO_4$ is shown in the schematic diagram (Fig. 5.23) consisting of major and minor rhombohedral faces. Figures 5.24 *a* and *b* show the characteristic photographs of the berlinite crystals.

DropBooks

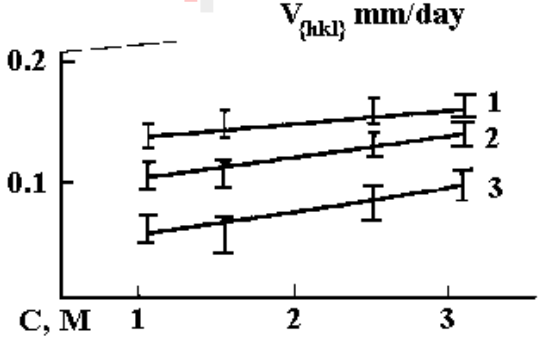

(a)

Figure 5.22. Solution concentration, growth temperature, and temperature gradient vs. growth rate *(a)–(c)*.[92]

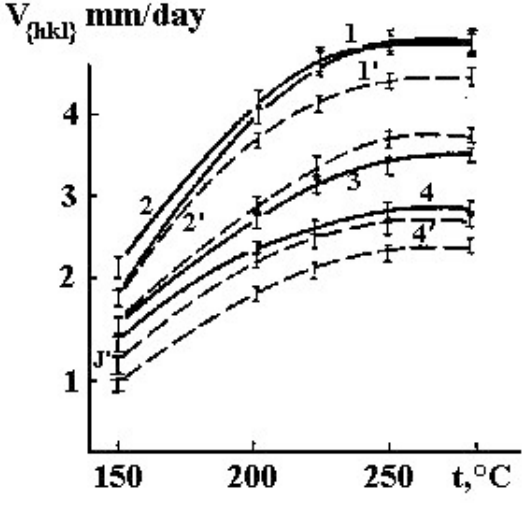

(b)

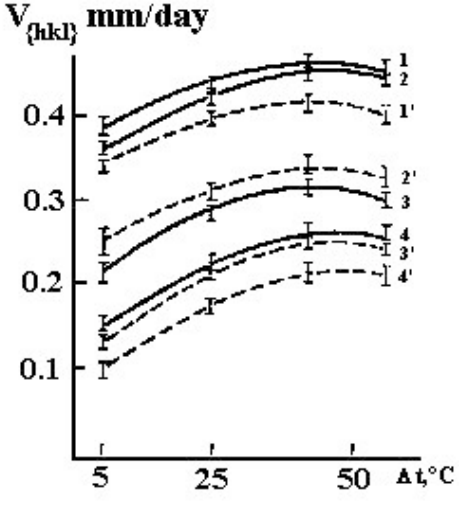

Figure 5.22. *(Cont'd.)*

Table 5.7. Morphology of Aluminum Orthophosphate Crystals

Nutrient composition	*T* °C	Morphology
$Al_2O_3 + H_3PO_4$ mineralizer HCl (1.5M)	280	Hexagonal and rhombohedral
$Al_2O_3 + H_3PO_4$ mineralizer NaCl (2M)	300	Rhombohedral
$Al_2(OH)_3 + H_3PO_4$ mineralizer NaF (2.5M)	300	Rods, needles or acicular
$Al_2O_3 + H_3PO_4$ mineralizer NH_4Cl (4M)	300	Small hexagonal, rhombohedral and equil-dimensional
$Al_2O_3 + H_3PO_4$ mineralizer HCOOH (2M)	280	Hexagonal and rhombohedral
$Al_2O_3 + H_3PO_4$ mineralizer $NaHCO_3$ (3M)	300	Hexagonal, rhombohedral and slightly irregular
$AlCl_3 + H_3PO_4$ mineralizer HCl (2M)	270	Hexagonal

DropBooks

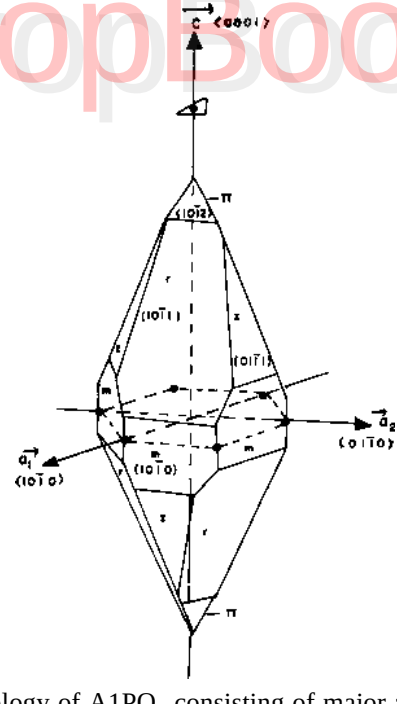

Figure 5.23. Morphology of $A1PO_4$ consisting of major and minor rhombohedral faces.[83]

It is observed that these admixtures play an important role in the process of crystallization of $AlPO_4$. In the actual experiments without any admixtures, well-developed rhombohedral and hexagonal crystals have been obtained, but with the addition of various admixtures the crystal changes to fibrous, rod shaped, acicular, massive, equi-dimensional and irregular shapes (Figs. 5.24 *c, d*). In the case of Zr and Ti as the admixtures, fibrous or acicular crystals of berlinite have been obtained; such results were earlier obtained only in experiments containing $Al(OH)_3$ as the starting component.[76][91]

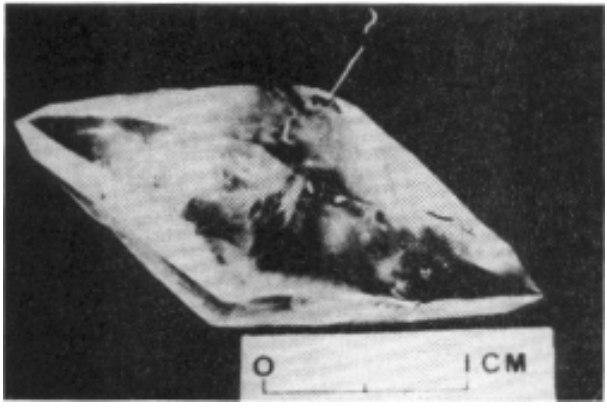

(a)

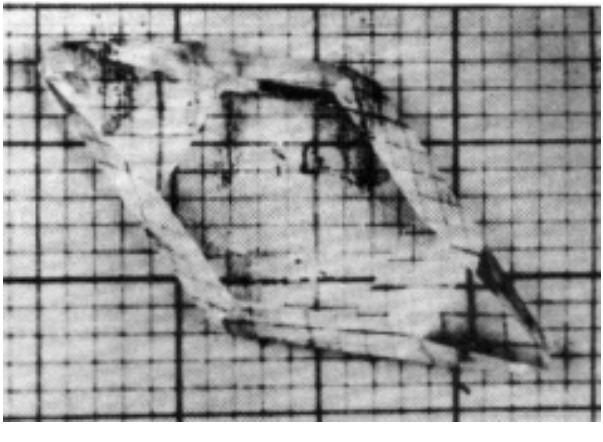

(b)

Figure 5.24. Characteristic photographs of the berlinite crystals *(a-d)*.[76][83]

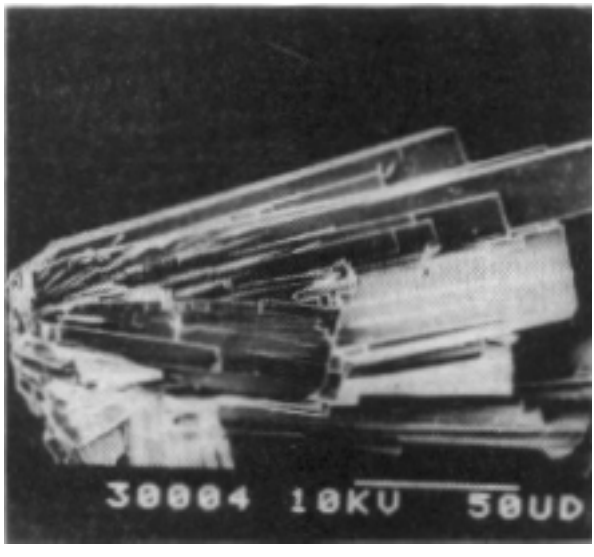

(c)

DropBooks

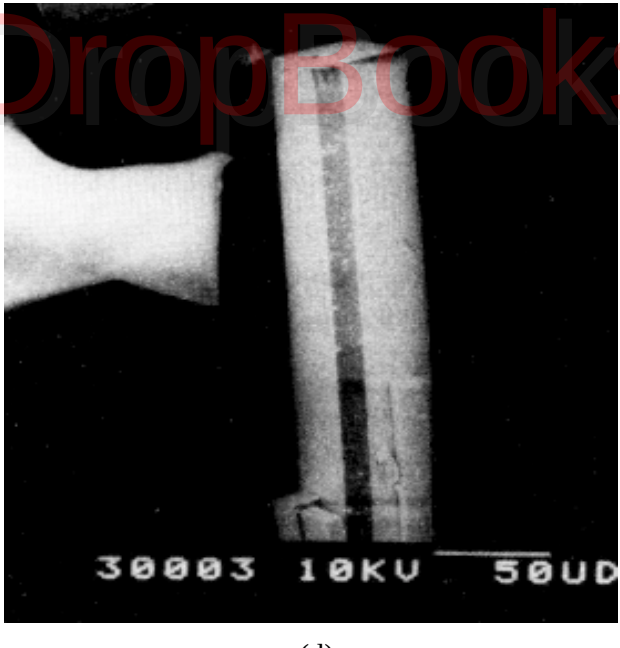

(d)

Figure. 5.24. *(Cont'd.)*

Growth defects in synthetic berlinite samples have been studied by several workers through x-ray topography.[89][93] The berlinite crystals, in general, show internal structural defects along with a high density of defects on x-ray Lang topography. It can be seen that crystals which appear transparent from outside contain many internal defects. Figure 5.25 shows a typical Lang x-ray topograph taken in (2110) face.[83] Line defects were attributed to the disorder in crystal structure and more likely to the impurities existing in the boundary of repetitive overgrowth. However, it is possible to distinguish various types of contrasts that differ by their temperature behavior. Dislocation-related contrasts vary slightly with temperature, but they appear more strongly, especially after the second thermal cycle. The variation of contrast present in the topography for the growth bands can be interpreted in terms of localized variations of the deformation in the sample with temperature. These variations appear in the same temperature range as the anomalies observed in propagation loss, frequency, and temperature characteristics. These anomalies have been attributed to water impurities in these hydrothermally grown crystals.[94][95] This explanation is qualitatively valid and in good agreement with the changes of the deformation contrast observed during the thermal cycles. The contrast due to the water impurity content is observed in selected areas and is predominantly located at growth bands that correspond to the adsorption of water on some growing faces during the cycle.

Figure 5.25. Lang x-ray topograph taken in (2110) face.[83]

A combination of selected growth conditions reducing the water content and using heat treatment to control the water distribution could be of great interest for improving the piezoelectric device application of berlinite. The choice of the seed is fundamental for the production of good crystal and a selection of excellent slices for this use is absolutely necessary when this condition is fulfilled. The x-ray topographs obtained on different crystals have shown that the quality was improved but the remaining defects could be classified into two classes. This is due to the defects present in the seed which have been developed in the grown crystals (dislocations and sometimes twins) and those which were carried during the start of the growth (bundles of dislocations) or during the growth (growth bands).

No fundamental differences were found by x-ray topography between the horizontal gradient, vertical gradient, and slow heating methods, when good seeds and optimized conditions were used.[92] The two principal imperfections readily observable are *crevice flawing* and *cracks*. When growth is on a non-equilibrium face, there is a tendency for higher growth rates and the formation of *hillocks* which tend to protrude across the solute-depleted diffusion layer near the growing face. The tips of such hillocks experience a high supersaturation and tend to grow faster than the regions between hillocks. This phenomenon is the hydrothermal analogue of constitutional surpercooling and may be viewed as a kind of dendritic growth.[96][97] Entrapment of solution between hillocks leads to bubbles of solutions in the grown material, which are observed as *viels*. Thus, growth at slower rates and on equilibrium faces produces a greatly reduced tendency for crevice flawing.

PropBooks

Cracks are often observed in hydrothermally grown material. In the case of quartz[25][98] we found that they were associated with strain caused either by strain in the seed propagating into the grown crystal or by strain associated with dislocations arising at inclusions in the new growth. It was further observed in quartz that disorder regions in seeds propagated into crystals and strain free seeds were much less likely to produce cracked growth.

At an annealing temperature which is high enough, berlinite becomes milky, and in TEM pictures one observes a large density of bubbles with a mean size of about 1000 Å; while in untreated, as-grown berlinite no such bubbles are visible. Further more, the growth of these bubbles is accompanied by a severe increase in the dislocation density of the order of 10^5 cm^{-2} or less, but in the heat treated crystals this density

reaches 10^9 cm^{-2}. An increase of at least six orders of magnitude is produced, like for wet quartz, which exhibits the same dramatic dislocation multiplication. This situation can be observed in berlinite, where bubbles with a mean diameter of 250 Å can be observed together with a very high density of dislocation.[94][98] Recently, Morris and Chai (1998) have studied the imperfect low-angle boundaries and fracture in hydrothermally grown berlinite crystals obtained on multiple-seed plate arrays.[99]

5.3.5 Thermal Behavior

The stability range of any material with a device potential is an important parameter. Byrappa et al. (1986) have reported the differential thermal analysis for containing various admixtures (Fig. 5.26).[100] For pure berlinite, the inversion temperature was reported to be at 586°C and this is similar to that reported by Beck (1949).[72] However, there are reports fixing this transition temperature at 581°C[101] and at 579°C.[102] Such a variation in the α-β inversion temperature can be explained by the effect of the starting materials, the presence of admixtures in the final products, and even the metals from the mineralizers which also act as admixtures.

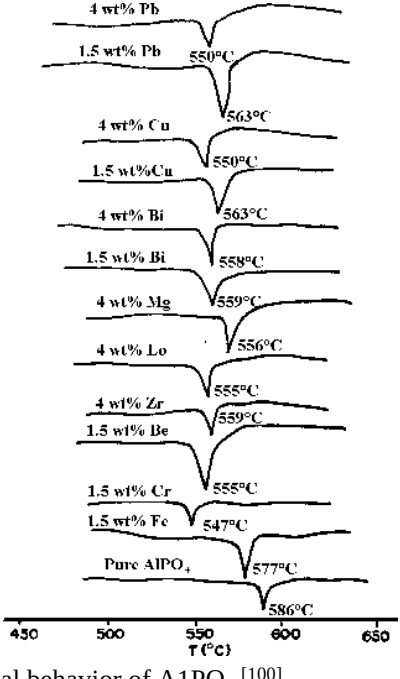

Figure 5.26. Thermal behavior of $A1PO_4$.[100]

Studies on the thermal expansion of berlinite have not been reported much in the literature. Byrappa and Prahallad (1989) have reported the thermal expansion of berlinite in detail.[103] The thermal expansion values vary depending upon the percentage of concentration of impurities in the crystal.

The values of thermal expansion for α-berlinite containing various admixtures are given in Table 5.8, and the values are, in general, very low for these materials because of the covalent bonding. Alpha-berlinite is relatively stable compared to β-berlinite with reference to the action of the dopants. The difference in α_a (max) - α_a (min) = 0.39 $\times 10^{-5}$ and α_c (max) - α_c (min) = 1.572 x 10^{-5} C^{-1}, which shows that the *c*-axis is more susceptible to thermal expansion than the *a*-axis. The coefficient of thermal expansion is quite high when rare earths are used as admixtures.

Table 5.8. Thermal Expansion of α-Berlinite Containing Admixtures[103]

Admixture	Ionic radii	Atomic weight	a	c	v
—	—	—	1.63×10^{-5}	1.068×10^{-5}	4.38×10^{-5}
Sr	0.63	51.996	1.90×10^{-5}	1.89×10^{-5}	5.77×10^{-5}
Fe	0.64	55.847	1.98×10^{-5}	1.13×10^{-5}	5.16×10^{-5}
Cu	0.72	63.546	1.76×10^{-5}	1.81×10^{-5}	5.39×10^{-5}
Nd	0.99	144. 24	2.02×10^{-5}	2.64×10^{-5}	6.78×10^{-5}
La	1.016	138. 905	1.75×10^{-5}	2.64×10^{-5}	6.22×10^{-5}

- concentration of the admixture in the nutrient was 1.5 wt %

DropBooks

5.3.6 Piezoelectric Properties of Berlinite

The piezoelectric properties of berlinite have been studied in detail by several authors. Chang and Barsch (1976),[63] and Ballato and Iafrate (1976)[104] pointed out attractive properties of *Y* rotated and doubly rotated cuts of berlinite in terms of its large coupling coefficient (twice that of quartz), with a constraint of zero first order frequency temperature coefficient (FTC). Several groups appeared throughout the world immediately to study the growth and characterization (with reference to its first, second

and third order frequency temperature coefficient) of berlinite. Figure 5.27 shows the comparison of *Y* quartz and *Y* berlinite resonators. It can be noticed that the *Q* factor is greater by an order of magnitude than for resonators. In Fig. 5.27, also given the frequency response of the *Y* quartz plate of similar design whose *Q* factor is not so different and whose coupling coefficient is smaller. The higher order temperature coefficients measured with different crystals, even with different plates of the same crystal, show values much larger than for quartz resonators of the corresponding orientation. Table 5.9 gives the comparison between quartz and berlinite. However, it has been demonstrated that the water dissolved in berlinite crystal induces low values of two factors and impairs significantly the intrinsically very favorable thermal behavior of this material.

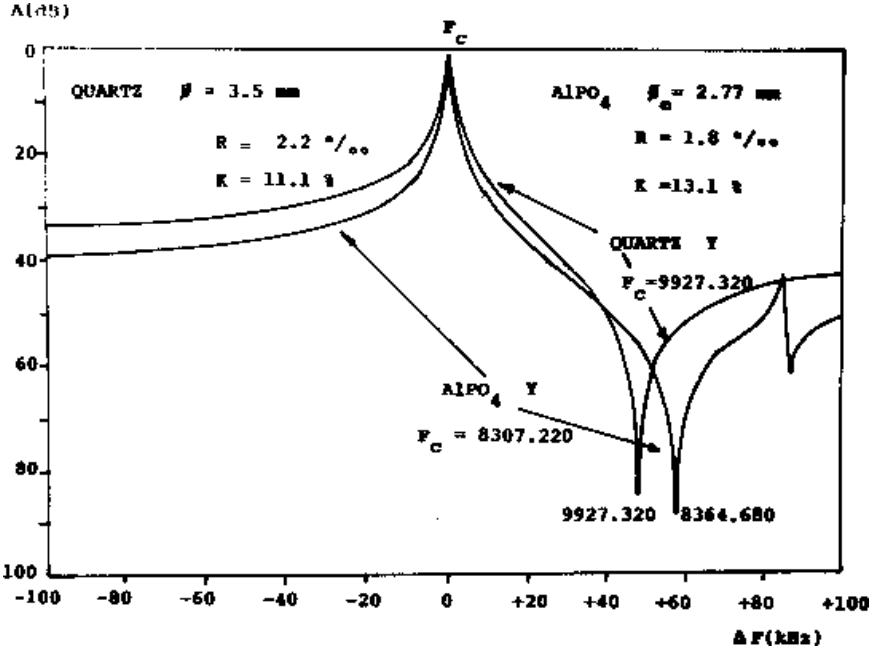

Figure 5.27. Frequency response of the *Y* quartz plate.[63]

Table 5.9. Tentative Comparison with Quartz (Thickness *Y* Rotated Resonators at same Frequency)

Useful coupling coefficient (AT filter trapped resonators)	Enhanced by 1.4 – 1.5
Shift of oscillators or band width of filters (AT cut)	Twice
Angular sensitivity (1^{st} order FTC)	Reduced
Thermal stability (higher order FTC)	Better
Q factor propogation losses	Already sufficient (may be comparable)
Thickness of plates (AT)	Reduced by 1.15
Electrode dimensions (AT)	Reduced by 1.32 (TT)
(Same plating 2D TT of TS)	Reduced by 1.24 (TS)
Nonlinear properties	To be determined

DropBooks

"Dry" berlinite has similar C, E, EPS constants, first order TC and much reduced higher order TC.

Jumas et al. (1987) gave an excellent comparison of piezoelectric properties of $AlPO_4$ to quartz.[92] According to them, the coupling coefficients measured with AT resonators with filter type response were about 11%. For quartz, the maximum values were 7.4%, and this permits one to obtain filters with twice the bandwidth. The electric constant of berlinite is lower by a factor of 1.2 to 1.35 than the corresponding constant of quartz, but the density is very similar. The frequency constants Nfa and Nfr (Nfa = 4 hx; Nfr = 4hxfr, where 2h is the thickness of the plate) are lower than those for the corresponding orientation of quartz by a factor 1.1 to 1.7; for the AT cuts the factor is 1.15.

The first, second, third, etc., order frequency temperature coefficients of berlinite are mostly dependent on the temperature coefficient (TC) of the pertinent elastic constants and the dilation coefficient.[105] As the latter are similar to those of quartz,[63] most of the better thermal behavior observed with "dry" berlinite, as compared to quartz, results from smaller values of the TC of elastic constants. For some other constants, similar things may also be expected. In Fig. 5.27, the results of Poignant are given, indicating a similar behavior of the TC of C33 for quartz and berlinite.[83] It is also expected that for other analogues of quartz with similar α-β phase transition and reduced elastic constants, similar or better thermal behavior of resonators could be obtained.

This point is of great importance for frequency generation and filtering applications of resonators, for which it is fundamental to obtain a frequency response free of unwanted (unharmonic) modes. For identical cut, resonant frequency, and plating, it can be shown that smaller dimensions of electrodes are required for berlinite than for quartz to obtain a frequency response without spurious unharmonic modes (trapping of only one mode).

Shannon and his group (1993) have studied in detail the dielectric properties of berlinite with reference to the presence of $(OH)^-$.[106][107] It has been well established that water in berlinite is found in both macroscopic and microscopic inclusions. Because crystals are grown from H_3PO_4 or H_3PO_4/HCl solutions, it is likely that the inclusions also contain this acidic solution and consequently, high concentrations of H_2PO_4, HPO^-_4 and /or Cl^- ions. Quantitative NMR determination of proton content unequivocally determines the H_2O and hydroxyl content, whereas complementary IR absorbency studies of the 3300 cm^{-1} band confirm the molar absorption coefficient of 81 $l mol^{-1}$ cm^{-1} originally determined for liquid H_2O by Thompson (1965).[108] The dielectric constant variability of berlinite prepared by different investigators is believed to result from *(i)* a variation in H_2O content in microscopic and macroscopic inclusions and *(ii)* unidentified crystalline defects.

5.4 GALLIUM PHOSPHATE, $GaPO_4$

Gallium phosphate, like aluminum phosphate, belongs to the family of quartz and quartz-like MXO_4, where M = B, Al, Ga, Fe, Mn, and X = P, As.[109] Amongst them, $AlPO_4$ and $GaPO_4$ have been studied

extensively with reference to their crystal growth, crystal chemistry, and physical properties, especially piezoelectric properties.[75][110]–[114] Both $AlPO_4$ and $GaPO_4$ exhibit piezoelectric characteristics which are superior to those of conventional α-quartz. As evident from Table 5.10, for the same AT cut, $GaPO_4$ exhibits larger coupling coefficient which makes $GaPO_4$ a most promising material in the field of wide band filters. In addition to this, the $\alpha - \beta$ phase transition for $GaPO_4$ occurs at 976°C, and hence, it can be used in a very wide range of temperatures for filters and sensor devices.[115]–[118]

Table 5.10. Comparison of Some Piezoelectric Characteristics[109]

Parameter	Quartz	Aluminum Phosphate (Berlinite)	Gallium Phosphate
Coupling coefficient* K%	8.5	11.0	> 16.0
Surtension coefficient* Q	3.10^6	10^6	$> 5.10^4$
α - β Phase transition °C	573	584	No

DropBooks

* AT cut

5.4.1 Crystal Growth of Gallium Phosphate

The synthesis of gallium orthophosphate does not differ much from the synthesis of berlinite. It is usually carried out by the hydrothermal technique at temperatures less than 250°C. On the whole, the growth of aluminum and gallium phosphates is carried out using reverse temperature gradient, or slow temperature, increasing essentially in the acid media like H_3PO_4,[119] H_2SO_4, HCl + H_2SO_4, H_3PO_4 + H_2SO_4,[113][117][118] HCl,[117][120] KF, NaOH.[120] The starting material/nutrient for $GaPO_4$ growth is prepared usually by solid state reactions with Ga_2O_3 and $NH_4H_2PO_4$, twice at 1000°C for 24 hours and subsequently hydrothermally treated at 150°C for 30 hours in 4M H_3PO_4 solution. The resultant product is generally a single phase of $GaPO_4$. Like berlinite, the gallium phosphate also shows a retrograde solubility in all the solvents

below 400°C, and above this temperature, the solubility becomes positive.[110][114][120] Hence, the nutrient is kept at the low-temperature zone (i.e., dissolution region), and the seed crystal is kept at higher temperature zone (i.e., crystallization region). The temperature gradient (5 to 40°C) is selected according to the quality and the growth rate required. Figure 5.28 shows the schematic representation of the growth of berlinite crystals and the same experimental setup can be used for the growth of gallium orthophosphate crystals. The growth of gallium orthophosphate can be carried out at 180°C for seven to ten days. By this arrangement, it was expected that the dissolved nutrient would be efficiently used to grow single crystals on the seed without the occurrence of spontaneous nucleation. As the lattice parameters of both berlinite and gallium phosphate are very close, some authors have used even berlinite crystals with a definite orientation/cut as seeds, and obtained $GaPO_4$ epitaxy on $AlPO_4$ seeds using 6M H_2SO_4 solvent, at a temperature greater than 200°C.[117] The experimental temperature is critical in the case of gallium phosphate because the crystals obtained at a temperature less than 200°C show the presence of water, which deteriorates the piezoelectric characteristics. Hence, it is advisable to use acid mineralizers with a boiling temperature of 225–240°C. Practically, there is no water in such a solvent, and it consists of orthophosphoric acid (90%) and pyro-phosphoric acid (10%). The solubility is presaturated with $GaPO_4$ to avoid the dissolution of the seeds. To keep the solution from boiling during the crystal growth, inert gas is pumped into an autoclave up to 50 bars.[121]

Cochez et al. (1994) have proposed the following scheme for the growth of α-$GaPO_4$ as the best method:[117]

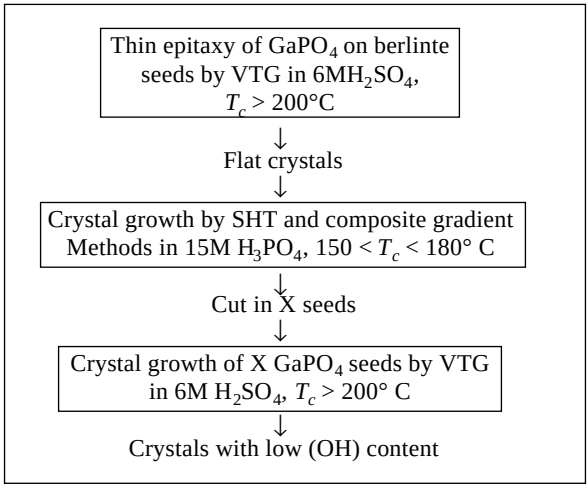

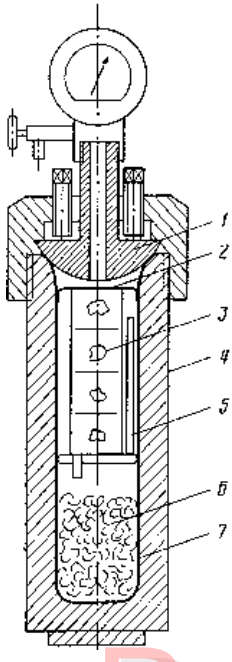

Figure 5.28. Schematic representation of the growth of berlinite crystals.[119]

DropBooks

The first stage of $GaPO_4$ crystal growth process is the epitaxy of $GaPO_4$ on berlinite seeds. The second stage consists of growing 2–d crystals through the slow heating method, or the horizontal gradient method, or the composite method (i.e., the combination of the first two). In the third stage, the X seeds are grown which helps in reducing the $(OH)^-$ content in the crystals.

Popolitov and Yaroslavskii (1990) have studied the crystallization processes of α-$GaPO_4$ under hydrothermal conditions.[120] They have studied the rate of crystallization, (i.e., the amount of $GaPO_4$ crystals formed per unit time), action of solvent, its concentration and the temperature regime. Gallium phosphate glass (prepared by sol-gel method) has been used as the nutrient with Ga:P ratio = 1: 1.5. The experiments were carried out in the temperature range 200–300°C, P = 20 – 35 MPa using teflon liners, with a temperature gradient of 4–5°C. The yield of $GaPO_4$ single crystals as a function of growth temperature and concentration of different solvents used is shown in Figs. 5.29 and 5.30. All the curves shown in Figs. 5.29 and 5.30 are described by a simple exponential

equation: $M = KC^n$, where K is the rate of bulk crystallization, C is the solvent concentration, and n is the formal order of bulk crystallization. Table 5.11 gives the values of K, C, and n for aqueous HCl, HNO_3, KF, and NaOH at 200, 250, and 300°C.

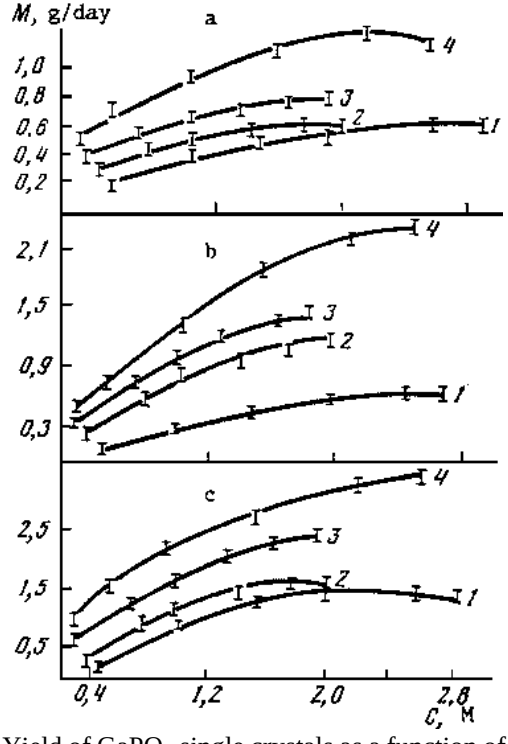

Figure 5.29. Yield of $GaPO_4$ single crystals as a function of growth temperature and concentration of different solvents.[120]

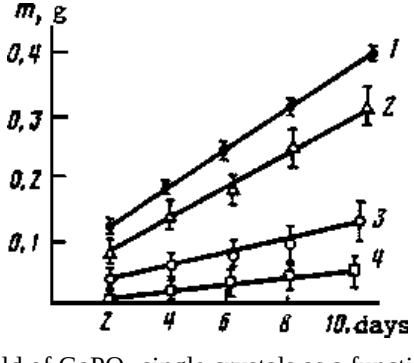

Figure 5.30. Yield of $GaPO_4$ single crystals as a function of time.[120]

Table 5.11. Crystallization Kinetics for $GaPO_4$

Solvent	HCl			HNO_3			KF			NaOH		
T, °C	200	250	300	200	250	300	200	250	300	200	250	300
K	0.22	0.48	0.76	0.11	0.28	0.41	0.09	0.14	0.26	0.04	0.05	0.15
n	0.61	0.58	0.57	0.58	0.50	0.47	0.20	0.22	0.18	0.30	0.28	0.27

Also, the authors[120] have calculated the activation energy for the formation of $GaPO_4$ single crystals from the Arrhenius equation. Similarly, the solubility of α-$GaPO_4$ has been studied by several workers within a wide range of *PT* conditions (T = 200–500°C, P = 50–1000 atm).[112][114][117][122] Figure 5.31 shows the solubility of $GaPO_4$ in the phospho-sulphuric acid solution 15M H_3PO_4 + 9M H_2SO_4 in terms of % in H_2SO_4. There is an increase in the solubility with a progressive enrichment in H_2SO_4 in the solvent. However, it always remains lower than in pure H_2SO_4. The solubility remains retrograde in all the studies up to 400°C.

DropBooks

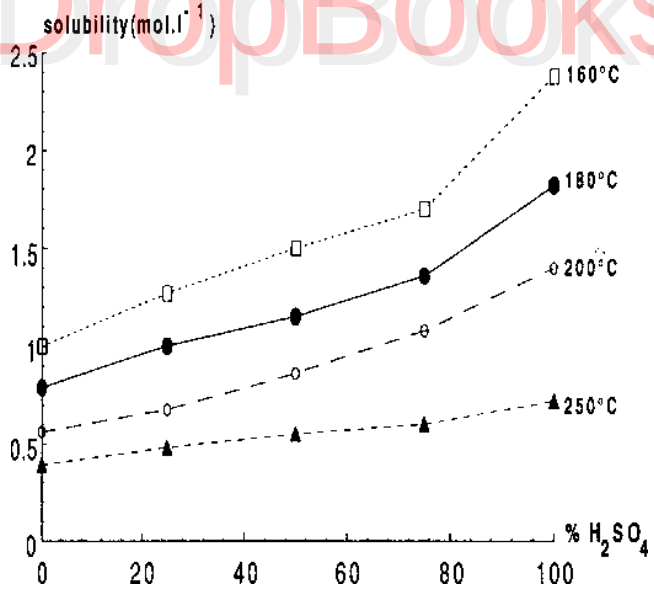

Figure 5.31. Solubility of $GaPO_4$ in the phospho-sulphuric acid solution 15M H_3PO_4 + 9M H_2SO_4.[114] *(Courtesy of the Gauthier-Villars/ESME, Paris.)*

5.4.2 Morphology

The morphology of the $GaPO_4$ single crystals is shown in Fig. 5.32.[120] The commonly appearing faces are $[10\bar{1}1]$, $[01\bar{1}1]$, $[10\bar{1}0]$, $[10\bar{1}2]$. Figure 5.33 shows the characteristic photographs of $GaPO_4$ crystals obtained by hydrothermal method. The growth rates along various crystallographic directions decrease in the following sequence:

$$\gamma(0001) >> \gamma(01\bar{1}2) > \gamma(10\bar{1}0) > \gamma(01\bar{1}1) > \gamma(10\bar{1}2) > \gamma(10\bar{1}1)$$

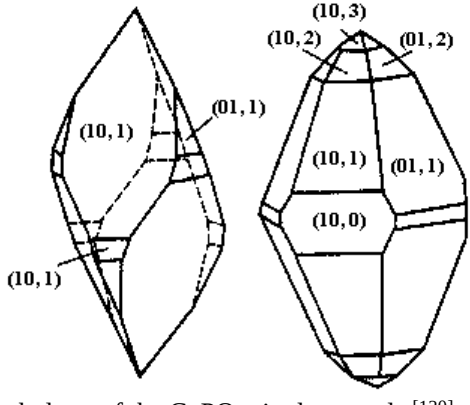

Figure 5.32. Morphology of the $GaPO_4$ single crystals.[120]

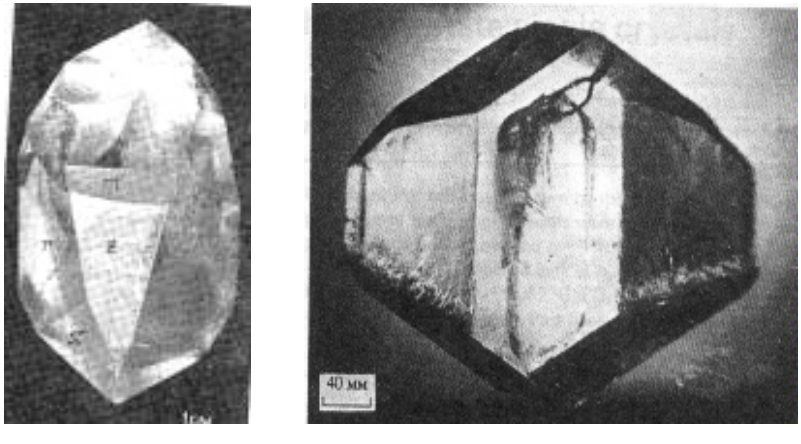

Figure 5.33. Characteristic photographs of $GaPO_4$ crystals obtained by the hydrothermal method.[121]

The common twins observed in $GaPO_4$ are according to the Dauphine, Brazil and Laydolt's twinning laws. This has been discussed in great detail in Ref. 121. The x-ray topographic studies on $GaPO_4$ have been carried out by Capelle et al.[118]

5.4.3 Dielectric Properties of Gallium Phosphate

The influence of the growth rate on the quality of the $GaPO_4$ crystals has been studied through infrared spectrometry by Cochez et al. (1993).[114] As conventionally done for quartz and berlinite, the $(OH)^-$ impurity content was monitored by infrared measurements in the wave number range of 4000 to 2500 cm^{-1}, using the relation:

$$\alpha = {}^1/_d \text{ cm log } (T_{3800}/T_{3167})$$

where T_{3800} and T_{3167} are respectively the transmittances at 3800 and 3167 cm^{-1} respectively. The strongest absorption band of Al-OH for berlinite appears at 3291 cm^{-1} and it is shifted to 3167 cm^{-1} for Ga-OH in case of $GaPO_4$ (Fig. 5.34). The α values obtained by the authors are 1.6 and 2.2 for two of their characteristic $GaPO_4$ samples. It can be observed that the $(OH)^-$ content increases with the temperature gradient.

DropBooks

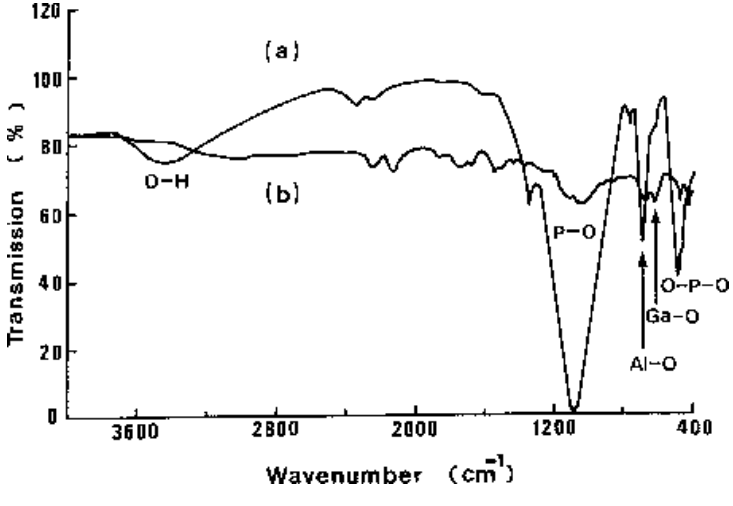

Figure 5.34. FT-IR spectra of *(a)* $A1PO_4$ (wet) and *(b)* as-grown single crystals of $GaPO_4$.[114] *(Courtesy of the Gauthier-Villars/ESME, Paris.)*

The dielectric properties have been studied in detail by Hirano et al. (1990) for $GaPO_4$ crystals.[75] According to the authors, the frequency independence of $\in'$ at room temperature in this crystal indicates that mainly electronic ionic polarizations contribute to the dielectric constant of $GaPO_4$. These two polarizations always exist below 10^{13} Hz.

Figure 5.35 shows the extrapolation of possible piezoelectric properties to other quartz-like materials.[109] Table 5.12 gives the extrapolation of AT cut characterizations from well-known quartz and quartz-like materials.

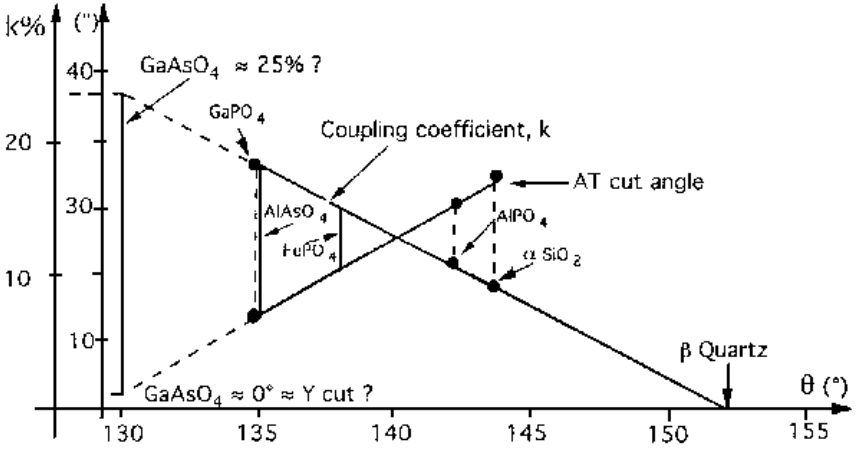

Figure 5.35. Extrapolation of possible piezoelectric properties to other quartz-like materials.[109] *(Courtesy of the Academic Press, Orlando, Florida.)*

Table 5.12. Extrapolation of AT Cut Characteristic from Well-known Quartz and Quartz-like Materials

Material	SiO_2	$AlPO_4$	$FePO_4$	$AlAsO_4$	$GaPO_4$	GeO_2	$GaAsO_4$
AT cut angle (°)	-35.25	-33.02	≈ -20	≈ -15	≈ -15	≈ 0	≈ 0
coupling coefficient *k* (%)	8.5	11.0	≈ 15	≈ 18	≈ 18	≈ 25	≈ 25
c/a	2.20	2.22	2.23	2.23	2.26	2.27	2.28

Cochez et al. (1994) have well-studied and extrapolated the relations that exist between the crystal structure distortions, expressed in terms of the M-O-X angle (where M = B, Al, Ga, Fe, Mn, and X = P, As) value and different physical properties.[117] For instance, piezoelectric characteristics of the AT cut and dielectric constant anisotropy of three known materials (SiO_2, $AlPO_4$, and $GaPO_4$) have been linearly related to their M-O-X angle value successfully. Conversely, knowledge of the M-O-X value allows prediction of physical properties for quartz-like crystals that have not been synthesized. Consequently, using only M-O-X angles, one can describe the structural strains, the α-β transition existence, and some physical properties, such as density, piezoelectric characteristics, and elastic constants.

Based on this reasoning, $GaAsO_4$ and GeO_2 appear to be the most promising materials for piezoelectric applications, unfortunately, the concomitant increase in structural distortions from quartz to $GaAsO_4$ and GeO_2 make their crystal growth very difficult. Thus, from the crystal growth point of view, $GaPO_4$ seems to be the best compromise for industrial development because of its high AT cut coupling coefficient and large temperature range stability with a few drastic packing distortions. If the size of the $GaPO_4$ crystals grown by the hydrothermal technique is increased at least by one fourth the value of the quartz, then $GaPO_4$ would be the best piezoelectric material of the 20th century and probably of the early 21st century as well.

DropBooks

5.5 POTASSIUM TITANYL PHOSPHATE (KTP)

Potassium titanyl phosphate, $KTiOPO_4$ (*KTP*) is one of the best nonlinear optical materials increasingly being used commercially for the second harmonic generation (*SHG*) and parametric oscillation since its discovery and introduction in 1976.[123] It all began when there was a search for a suitable crystal to convert efficiently the near-infrared light at 1.06 μm, which is useful in laser surgery. However, from the surgeon's point of view there is a difficulty as the near-infrared is not visible clearly. Thus, the solution for this problem was to use a second crystal which efficiently converts the near-infrared to the visible—a harmonic generator crystal.[124][125] The requirement was for a material with high conversion efficiency and appropriate index of refraction characteristics to allow phase matching. The AT & T Bell Labs group[124] tried with $LiNbO_3$.

Subsequently, the DuPont group discovered KTP to be phase matchable most efficiently at 1.064 μm to easily visible green light at 0.53 μm. It has very high laser damage resistance, coupled with low optical losses and it is transparent over a wide range of wavelengths with favorable angular, spectral and temperature bandwidthsn and has high conversion efficiencies.[123][126][127] Also, it was found that KTP's conversion efficiency was twice that of $LiNbO_3$ and hence is the most commonly used 0.53 μm harmonic generator. The additional advantage is that the preparation of $LiNbO_3$, which could be grown from the melt, was very expensive. Also, the starting materials for the growth of $LiNbO_3$ were equally expensive. In contrast to this, the starting materials for the growth of KTP are rather cheaper and the growth techniques are relatively inexpensive. The lower cost preparative methods could have an impact on its use, and indeed, more generally on the commercialization of nonlinear optical materials and electrooptic devices and systems on the whole. KTP crystals are mechanically, chemically and thermally stable and non-hygroscopic. It is remarkable for both high nonlinear optical coefficients and high conversion efficiency. The material has excellent physical properties, and can be used in a type II phase-matching configuration. In the recent years, KTP has been developed for quasi-phase-matched guided-wave devices to access the visible spectrum.

KTP belongs to the family of compounds that have the formula unit $MTiOXO_4$, where M = K, Rb, Tl, NH_4 or Cs (partial) and X = P or As. All members belong to the orthorhombic space group, $P_{na21,}$ point group, mm2, with the following lattice cell parameters: a = 12.814, b = 6.404, c = 10.616 Å, V = 371.115 $Å^3$. An important crystallographic property with reference to the optical, chemical and solid-state behavior of KTP is that there are two formula units in the asymmetric unit so that the proper solid-state formula is $K_2(TiOPO_4)_2$. The structure of KTP is composed of helices of TiO_6 octahedra linked via phosphate bridges. This leads to an open framework structure in which the charge-balancing cations are incorporated within the channels (Fig. 5.36).[128] The nature of the $KTiOPO_4$ host framework suggested the possibility that modification of the internal structural characteristics, and hence the electro-optic properties, might be achieved by gas-phase absorption and description. The K-ion exists in a high-coordination number site and is weakly bonded to both the Ti octahedral and P-tetrahedral channels existing along the *Z*-axis [001] direction, where K can diffuse with a diffusion coefficient several orders of magnitude greater than in the *X*-*Y* plane.

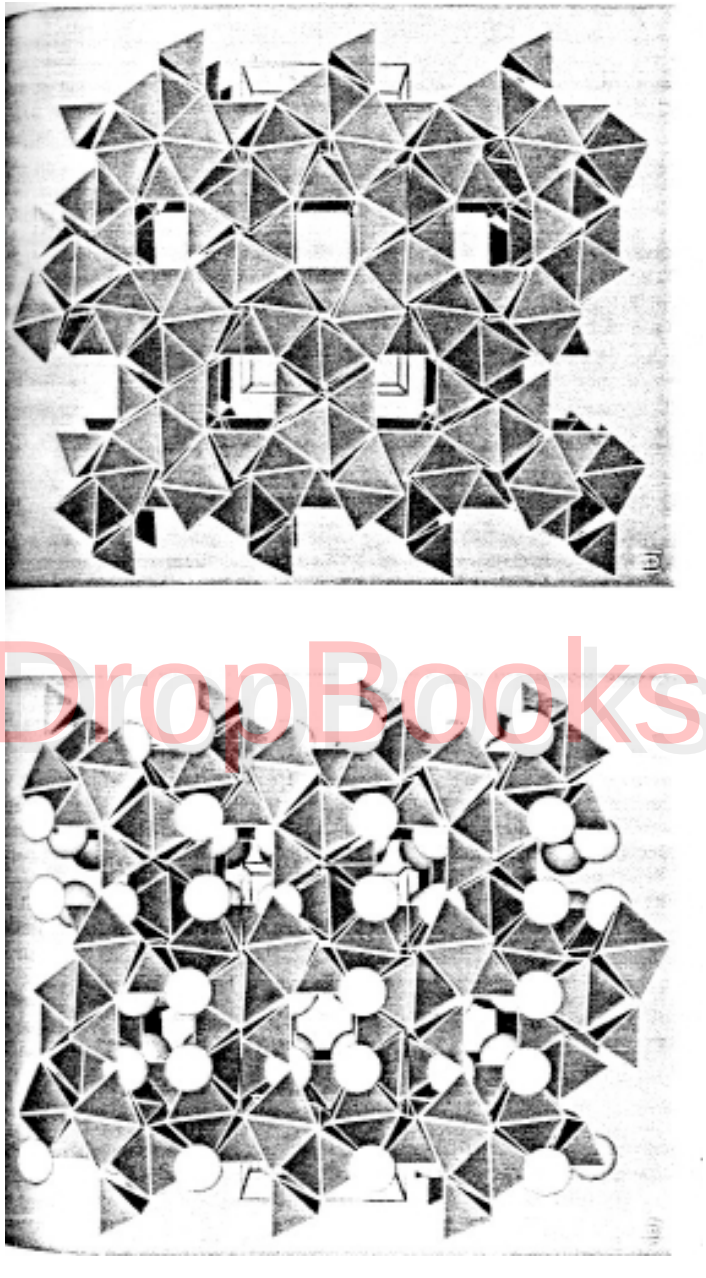

DropBooks

Figure 5.36. Structure of $KTiOPO_4$.[128]

In spite of the above-mentioned unique properties of KTP, its application has been limited by a shortage of crystals of sufficient size and quality. In particular, the crystal growth processes have tended to be plagued by spurious nucleation problems and the inclusions of the solvents. The first attempt to prepare KTP crystals was by Ouvard during 1890, who melted TiO_2, $K_4P_2O_7$ and K_3PO_4.[129] Masse and Grenier (1971) prepared KTP in the polycrystalline form.[130] However, the single crystals of KTP were first obtained by Zumsteg et al. (1976) at the DuPont Experimental Station.[123]

5.5.1 Crystal Growth of KTP

KTP decomposes before melting at 1148°C. Thus, incongruent melting and glass formation make it impossible to grow KTP crystals directly from the melt. Similarly, growth from aqueous solution at low temperature (less than 300°C) is impossible because of the low solubility of KTP. Therefore, large single crystals of KTP can be grown by both high temperature and pressure hydrothermal and flux techniques. There are several problems with reference to the quality of the crystals grown by the flux method. When pure phosphate self-fluxes are used, the main problem is the high melt viscosity. Its tendency to spuriously nucleate and also to leave behind major structural defects in the crystals has motivated the researchers to look for better fluxes. We have summarized the advantages and disadvantages of both flux and hydrothermal methods and quality of KTP crystals in Table 5.13. Similarly, the main problem with the use of the hydrothermal technique for the growth of KTP crystals is the higher pressure-temperature conditions of growth. In fact, when Zumsteg et al. (1976)[123] and Berlien and Gier (1976)[131] synthesized KTP by the hydrothermal method, the pressure-temperature conditions were quite high (P = 1.5 to 3 kbar, T = 650° to 700°C). The crystal size was not more than a few millimeters since the experiments were carried out in small platinum or gold capsules. Liu et al. (1982, 1984) have reported the growth and properties of hydrothermally grown KTP.[132][133] They prepared nutrient by the reaction of KH_2PO_4 and TiO_2 at 1250°C. The hydrothermal "flux" was 1.5 KH_2PO_4, 1.0 TiO_2 in Ag^- or Au^- lined autoclaves at a pressure of 24–28 kpsi (1.66-1.93 kbar) and 520–560°C in a gradient of 30–70°C. Growth rate on (011) was 0.2–1.8 mm/week. The higher pressure-temperature conditions do not yield large size crystals and the cost of the experiments involved is rather high. This led to the serious

Table 5.13. Difference Between Flux and Hydrothermally Grown KTP Crystals

Flux Grown KTP	Hydrothermally Grown KTP
- Temperature is constantly lowered and crystals grow through continuous change in solubility	Temperature is constant, and crystal growth occurs through continuous transport of nutrient by convection currents.
- Growth temperature is high (> 950°C)	Growth temperature is moderate (< 500°C)
- Pressure atmospheric	Pressure < 1.4 bar
- Growth rate is ≥ 1 mm/day	Growth rate < 0.6 mm/day
- Experimental duration: 7 to 10 days	Experimental duration several weeks (~ 30 days)
- Incorporation of fluxes into the lattice, & concentration of nonstoi-chiometric defects occurs	Incorporation of $(OH)^-$ into the lattice, as crystals are grown at lower temperature
- Reduced stoichiometry, thermooptic effect, poorer quality, susceptible to optical damage (less damage resistant)	Increased chemical stoichiometry, uniform refractive index, high quality, higher resistance to optical damage (most damage resistant)
- Cost of production-less expensive	Cost of production-very expensive
- Limited or slow incorporation in laser devices	More useful for laser applications
- Poor in perfection, purity and homogeneity	Better, perfect, purity and homo-geneity
- Suffers from blackening at the end part of the negative pole when placed in DC field	Does not
- Higher ionic conductivity	Lower ionic conductivity
Growth morphology is more or less the same	

DropBooks

efforts from several groups, particularly with reference to the *PVT* relations in several related systems like K_2O-TiO_2-P_2O_5, which ultimately brought down the pressure-temperature conditions to the tune of $P = 700$ bars, $T = 375$–$425°C$. The credit goes to Laudise and Belt for contributing extensively on the *PVT* relations of the KTP systems and also for growing large size single crystals of KTP by the hydrothermal technique.[134]–[137] The earlier hydrothermal experiments on KTP were carried out using platinum or gold lined autoclaves with Tuttle seals (cold-cone seal closures). The crystalline KTP nutrient in appropriate dimensions and quantity was introduced into the bottom part (dissolution zone), and the seeds (cut in proper directions) were suspended on a frame in the upper part (growth zone) of the liner cavity. A baffle separated them so as to control the solution convection for establishing a suitable temperature gradient. The mineralizers used in the earlier experiments were usually KF and K_2HPO_4 taken with a definite molarity. The percent fill (70–80%) and percent open area of the baffle (5 to 10%), temperature gradient (Δt = 10–80°C) were selected appropriately. Under such experimental conditions, the crystals are usually $16 \times 15 \times 7$ mm^3.

At present, several variants of hydrothermal growth of KTP single crystals are known.[134][135][138] Laudise et al. (1990) have carried out *PVT* measurements on 2M K_2HPO_4 and 2M K_2HPO_4 saturated with KTP (Figs. 5.37*a* and *b*).[138] It was important that growth be conducted in the absence of a gas-liquid interface, otherwise seeds in the gas phase do not grow, and bubbling, boiling, and bumping contribute to poor quality deposition. They made nutrient by the reaction of KH_2PO_4 and TiO_2 in platinum at 1250°C. The hydrothermal flux was 1.5 KH_2PO_4-1.0TiO_2 in gold or silver lined autoclaves at $P = 1.66$–1.93 kbar, $T = 520$–$560°C$ and $\Delta T = 30$–$70°C$. Growth rates on (011) were 0.2–1.8 mm/week. Laudise and co-workers have discovered much lower *PT* conditions for KTP growth, permitting the use of ordinary, unlined steel autoclaves in a K_2HPO_4 solvent. By using the reaction $KH_2PO_4 + TiO_2 \rightarrow KTiOPO_4 + H_2O$ to form KTP, they carried out a phase stability study, the results of which are shown in Fig. 5.38. Figure 5.38 shows only the water-rich corner of the complete ternary. Everywhere along the line A-H_2O, mole ratio KPO_3/TiO_2 = 1.00, the same as in KTP. Arrow 1 in Fig. 5.38 at $\cong$ 65 mol % $KPO_3/KPO_3 + TiO_2$ ($KPO_3/TiO_2 \cong 1.8$) is at or close to the boundary of the phase fields α + KTP and KTP at 600°. Alpha *(α)* is not a completely characterized phase, probably less K than in KTP. The boundary is probably nearly the same position at 500°C. Arrow 2 in Fig. 5.38, approxi-

mately 50 mol % $KPO_3/KPO_3 + TiO_2$ ($KPO_3/TiO_2 \cong 1.0$), is the boundary between the phase fields KTP and KTP + TiO_2 (anatase) at 600°C. It coincides with the line A-H_2O. Arrow 3, at approximately 58 mol % $KPO_3/KPO_3 + TiO_2$($KPO_3/TiO_2 \cong 1.4$), indicates that the boundary between the phase fields KTP and KTP + TiO_2 (anatase) at 500°C and lies at stoichiometry: richer in KPO_3 than A-H_2O. It moves to the left at lower temperatures. Assuming the validity of the boundaries defined by the arrows 1, 2 and 3, the appropriate phase boundaries have been drawn in Fig. 5.38 so as to terminate in the complete phase diagram on the KPO_3-TiO_2 axis at K(TiO)PO. Thus, the lines EC(1)G, F(3)H and D(2)A terminate at KTP. The line EF schematically represents the solubility of KTP at 500°C. It does not intersect A-D-H_2O, so KTP is incongruently saturating at 500°C, i.e., the mole ratio of KPO_3/TiO_2 in the liquid, where KTP is the only stable solid phase, ≠ to the ratio in KTP. Somewhere in the TiO_2-rich part of the diagram, anatase would probably be the sole stable phase and, in the KPO_3-rich region, E would probably be the sole stable phase. The authors did not try to find these boundaries because they are not directly relevant to KTP growth.

DropBooks

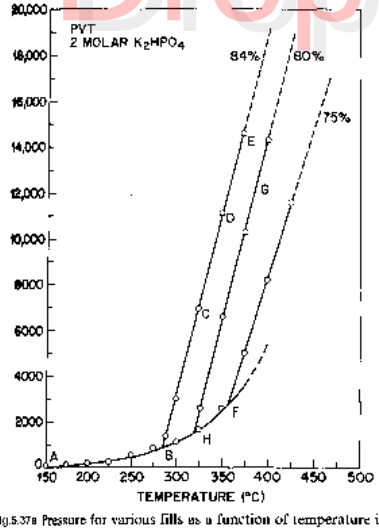

Fig.5.37a Pressure for various fills as a function of temperature in 2M K_2HPO_4.

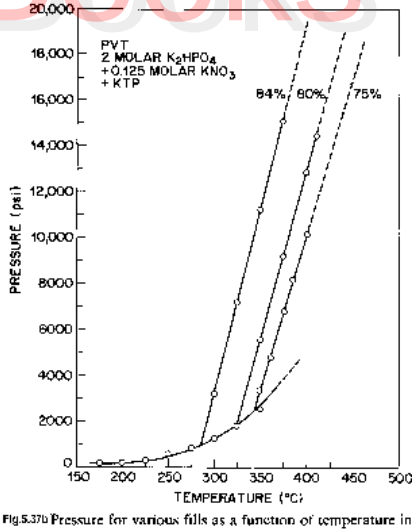

Fig.5.37b Pressure for various fills as a function of temperature in 2M K_2HPO_4 + 0.125M KNO_3 saturated with KTP.

Figure 5.37. PVT relations in KTP system.[138]

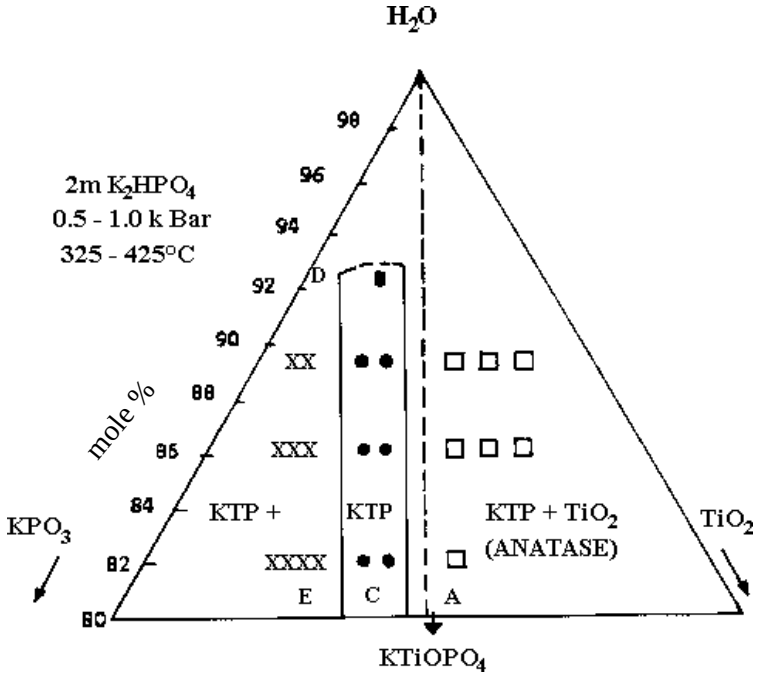

Figure 5.38. Phase diagram for KTP system.[138]

Typical conditions used in growth runs are as follows:

Autoclave:	- Pt lined, 1" ID x 6" IL (2.5 cm × 15 cm)
Mineralizer:	- 2 m K_2HPO_4 + 0.5 m KPO_3
% Fill:	- 75 %
Crystallization temperature:	- 375°C
Nutrient (dissolving) temperature:	- 425°C
Temperature differential (ΔT):	- 50°C
Seed orientation (201), (011):	- rates from 2.6 to 5.7 mil/day (~ 0.07–0.14 mm/day), (010) rate generally higher, quality good
(Seed orientation based on a = 12.80 Å, b = 6,400 Å, c = 10.580 Å)[138]	
Spontaneous wall nucleation:	- moderate; crystals clear but not too well formed

The growth rates are for the total increase in crystal thickness or time of the run. Increasing ΔT to 75°C and increasing KPO_3 decreased the growth rate, but growing without KPO_3, i.e., with the mineralizer (2 m K_2HPO_4) alone, did not markedly effect the growth rate or quality. Growth in KH_2PO_4 or KPO_3 alone was very slow.

In the growth of KTP, like quartz, the seed orientation is very important. The growth rates are different in different seed orientations and the highest rate for KTP has been obtained on (011) seed crystal.[139]

The crystals grown at lower growth rates are superior in quality. Therefore, proper care has to be taken to achieve the optimum growth rate under hydrothermal conditions by selecting appropriate growth parameters, because a combination of several growth parameters act upon the growth rate and crystal quality of KTP.

5.5.2 Solubility of KTP

The solubility of KTP is an important aspect. The higher experimental temperature pressure adopted in the earlier works were due to lack of accurate data on the solubility of KTP and added to that the solubility of KTP is rather low in most of the conventional solvents.

PropBooks

The solubility of KTP in 1M K_2HPO_4 + 0.5 KPO_3 solutions has been studied in detail.[138] Figure 5.39 shows the solubility of KTP (in wt%) in 1M K_2HPO_4 + 0.5 KPO_3 at 10 kpsi. The solubility data indicate good solubility for growth at 600°C and a positive temperature coefficient.

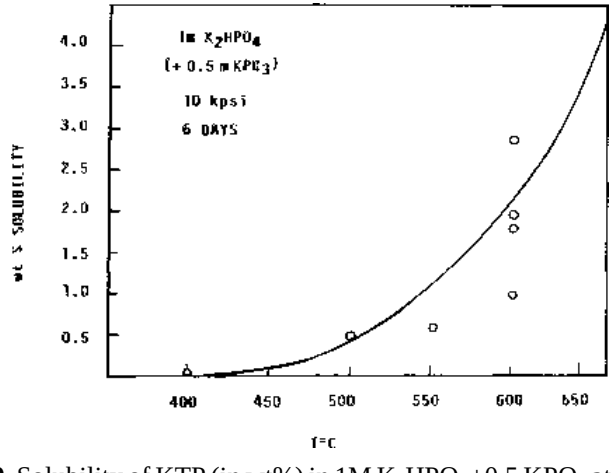

Figure 5.39. Solubility of KTP (in wt%) in 1M K_2HPO_4+0.5 KPO_3 at 10 kpsi.[138]

KTP crystals, using a complex mixture of water soluble phosphate glasses, KTP, solvents and water, have been obtained by several researchers. The glass composition is K_2O (42–70), TiO_2 (1–18), P_2O_5 (26–55) (mol%). The optimum ratio K/P is equal to 0.8–2.5, optimum glass composition is K_2O (55–60), P_2O_5 (38–42), (TiO_2 (1–5) (mol%).

Byrappa (1996) has carried out an extensive study on the solubility of KTP.[140] The main objective of this study was to find a suitable mineralizer solution in order to increase the growth rate, solubility, and crystal quality, but at reduced *PT* conditions. As well-known from the literature survey, the hydrothermal technique is most suitable for the growth of KTP crystals as it produces high-quality defect-free crystals. However, the main problem with the use of the hydrothermal technique for the growth of KTP crystals is the higher *PT* conditions of growth. In fact, when the early hydrothermal experiments were carried out, the *PT* conditions were rather high (P = 1.5 to 2 kbar; T = 650° to 700°C). The higher *PT* conditions do not yield large size crystals and the cost of the experiments involved is rather high. Subsequently, the inflow of the research data particularly on the *PVT* relations in several related systems of K_2O-TiO_2-P_2O_5, has brought down the *PT* conditions to the tune of P = 10 kpsi and T = 375–425°C.

Investigators have carried out hydrothermal experiments within a wide range of *PT* conditions using Morey and Tuttle type autoclaves. The nutrient materials were taken in teflon liners for experiments at lower *PT* conditions (using Morey type of autoclaves) and in platinum liners for experiments at higher *PT* conditions (using Tuttle type of autoclaves). A series of mixed mineralizers like H_2SO_4 + KOH, KF + HCl, HF + KF, H_2SO_4 + HCl + KF in different ratios were tried in order to bring down the *PT* conditions of crystallization of KTP crystals. The pressure in the system was calculated from *PVT* relations. In the case of lower *PT* experiments, the temperature was 275°C and the pressure was approximately 100 bars. The experiments were carried out for 8–10 days and spontaneously nucleated small crystals of KTP were obtained. The resultant product was washed thoroughly in distilled water to remove the excess solvents and the crystals were collected and dried. The size of the crystals were around 1 mm, colorless, transparent, and exhibited vitreous luster. The faces were developed in most of experiments. The solubility measurements were carried out on KTP crystals using the above said mixed mineralizers under hydrothermal conditions. Figure 5.40 shows the solubility curves for KTP. Figure 5.41 shows a representative photograph of a KTP crystal obtained by the hydrothermal method. Similar experiments

were carried out under elevated *PT* conditions (P = 500 bars and T = 325°C). The crystals were better in quality compared to the crystals obtained under lower *PT* conditions.

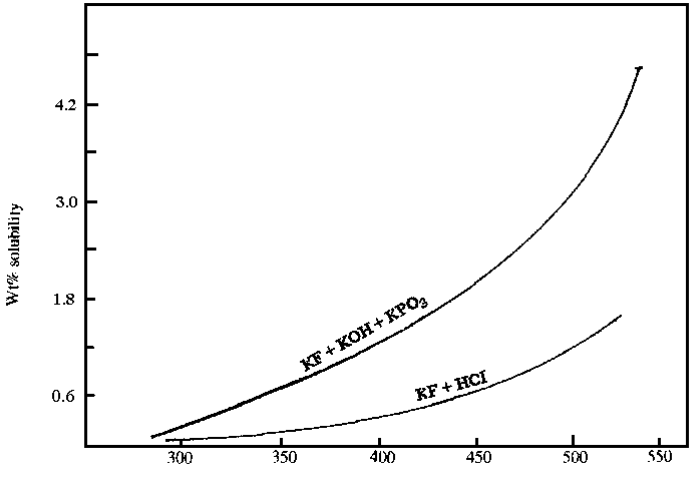

Figure 5.40. Solubility curves for KTP.[140]

DropBooks

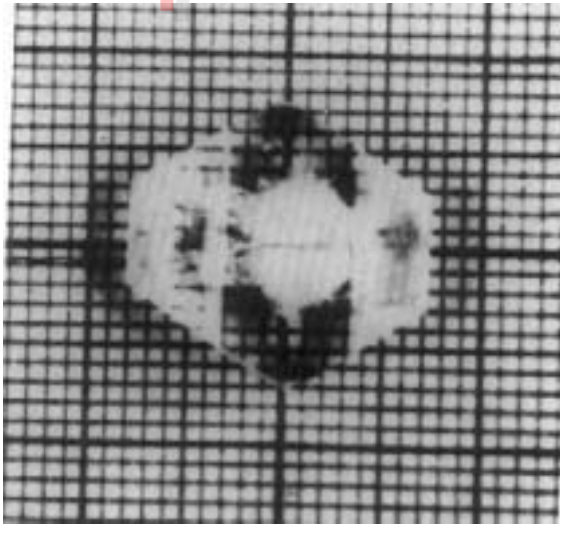

Figure 5.41. Representative photograph of a KTP crystal obtained by the hydrothermal method.[138]

Belt et al. (1989) have reported the growth of KTP single crystals in 4-liter capacity autoclaves at temperatures of 475°C and 1.5 kbar.[139] Gold liners were used here exclusively as corrosion resistance to the phosphates. Baffle openings were adjusted in the range of 20% with T = 30–40°C and the total run durations were 40–50 days. The growth rates sustained were 0.5–1.0 mm/side/week on (011) seed crystals.[126]

Belt and his group from Airtron Division of Litton Systems have increased the autoclave volume further and developed the low-temperature hydrothermal process in 5-liter systems. These large autoclaves have produced the largest KTP single crystals available in the world, see Fig. 5.42. These crystals are typically 4 × 5 × 8 cm and easily provide finished parallelpipeds of 1–1.5 cm^2 apertures and up to 2 cm long when material is extracted from either side of a seed. The schematic diagram of the large KTP crystals grown in 5-liter autoclaves is shown in Fig. 5.43. The rectangle in the center is seed plate, and the numbers identify prominent planes.[137] A successful large-scale hydrothermal growth process affects the size, cost, yield, and quality of KTP crystals. The cost of an autoclave is governed by its size, the type of alloys used, and availability of heat-treated billets from which the autoclaves are fabricated. Thus, lower-temperature experiments can use autoclaves made from more-common steel alloys, in turn lowering the cost.

The darkening of KTP crystals caused by the lack of oxygen in the growth process can be overcome by introducing an oxidizing agent, for example, 1–5 wt% of H_2O_2, into the mineralizer solution.

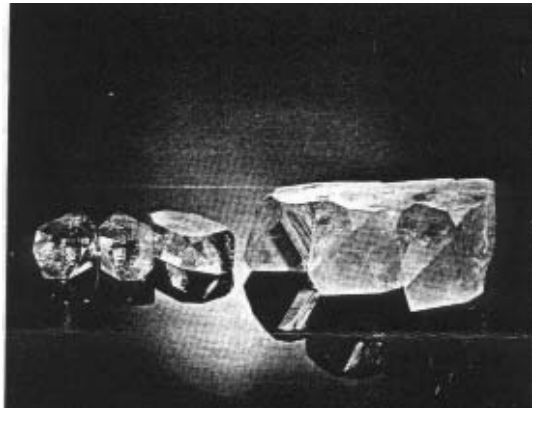

Figure 5.42. KTP single crystals grown using large autoclaves (5 liter). *(Photo courtesy of R. F. Belt.)*

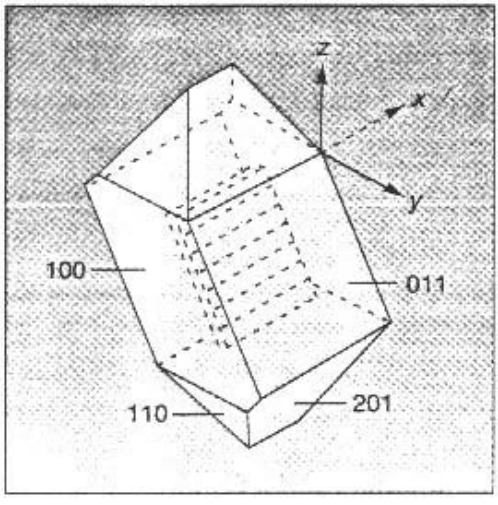

Figure 5.43. Schematic diagram of the large KTP crystals grown in 5-liter autoclaves.[137] *(Courtesy of the PennWell Publishing Co., USA.)*

5.5.3 Morphology

DropBooks

The morphology of KTP crystals is quite interesting and it does not vary much from flux-grown to hydrothermally grown. KTP usually grows as multifaceted crystal with fourteen faces typical for the KTP structure. The commonly seen crystal faces are {100}, {011}, {201} and {110} faces. These faces possess different growth rates and their relative sequence remains constant, even though the absolute growth rate of each face may vary with growth temperature gradient, solvent concentration, and so on. The average growth rates for various faces of hydrothermal KTP are given in Table 5.14.

Table 5.14. Average Growth Rate for Various Faces of Hydrothermal KTP

Growth Rate (10^{-3} mm/day)			
{100}	{201}	{011}	{110}
90	97	123	156
65	72	88	110
40	45	53	71

The {100} face has the largest area and, thus, the smallest growth rate among the faces. The width and height of the steps in KTP are inversely proportional to the growth rate or to the ΔT in different runs. Since KTP grows as multifaceted crystal, cutting and polishing of the crystal are quite cumbersome. Therefore, the growth of KTP with increased volume at lower cost is (very important) most desirable.

As shown in Table 5.13, the properties of KTP crystals vary with the growth method. Hydrothermally grown KTP crystals generally show an absorption band between 3550–3600 cm^{-1} due to the presence of $(OH)^-$. Generally, if a crystal used for a nonlinear interaction has even a small amount of absorption, the efficiency of the nonlinear interaction will be decreased. Absorption of the laser radiation occurs through the volume of the crystals illuminated by the laser beam. Thus, heating of the crystal occurs through this volume also. Cooling, on the other hand, occurs by conduction. Consequently, heating the surface of the crystal establishes thermal gradients within the crystal. As the refractive index depends on the temperature through the thermo-optic effect, gradient variations in the refractive index will also be generated. Variations in the refractive index will result in non-ideal phase matching throughout the volume of the nonlinear interaction. As the nonlinear interaction is quite sensitive to the variations in phase matching, the heating of the crystal can cause a significant degradation in the efficiency of the nonlinear interaction.[141]

Several authors have measured the ionic conductivity in pure and doped KTP crystals.[142][143] The ionic conduction property of these crystals allows ion-exchanged wave-guides to be formed readily in them.

5.6 POTASSIUM TITANYL ARSENATE

Recently, it has been shown that the nonlinear optic and electro-optic coefficients of potassium titanyl arsenate (KTA) crystals are significantly superior to those of KTP crystals.[144] Similarly, the arsenate isomorphs, like KTA, RTA, and CTA, unlike the phosphate isomorphs, are prone to ferroelectric multi-domain formation which renders these crystals useless in practical applications. KTA belongs to the class of forty compounds which are all structurally characterized by corner-linked octahedrally coordinated titanium chains connected with tetrahedrally coordinated phosphorus or arsenic bridges.

KTA can be prepared by methods analogous to those used for KTP. Brahmani and Durand (1986) have reported the structure of KTA

crystals[145]. The reputed effective nonlinear coefficient (d_{eff}) of KTA is 1.6 times that of KTP. This favorable property has encouraged several groups to carry out the hydrothermal growth of KTA at temperatures less than 600°C. Belt and Ings (1993) have hydrothermally grown KTA crystals using KH_2AsO_4 and KOH mineralizers. Flux grown KTA crystals were used as the seed crystals by these workers.[146] These authors have also studied the *PVT* relationship, solubility, and the growth rates and growth morphology in detail; with the pressure balancing method, growth rates of 0.2–0.4 mm/side/day can be achieved on {011} seeds. The experiments have been carried out in large size autoclaves of 4- to 5-liter capacities. Figure 5.44 shows the characteristic photographs of KTA single crystals obtained by Belt and Ings under hydrothermal conditions. The ideal morphology of KTA crystals is shown schematically in Fig. 5.45. The experimental conditions are given in Table 5.15.

DropBooks

Figure 5.44. Characteristic photographs of KTA single crystals obtained by Belt and Ings under hydrothermal conditions.[146]

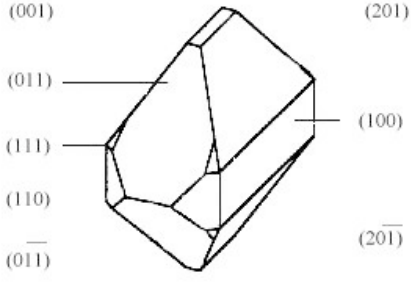

Figure 5.45. Ideal morphology of KTA crystals is shown schematically.[146]

Table 5.15. Summary of the Experimental Parameters of the Hydrothermal Growth Experiments in Production-Sized Autoclaves

Run No.	Mineralizer	% Fill		Nutrient	Nutrient temp. (°C)	Pressure (atm)	Seeds	Gradient (°C)	Run time (weeks)	Results
		Inner	Outer							
1	4M KH_2ASO_4	80	57	Flux grown KTA	560	1700	Unoriented flux growth KTA	28	2	Slight growth on KTA seeds
2	4M KH_2ASO_4	78	58	Flux grown KTA	590	1820	(201), (011) and (100) flux grown KTA	50	1.5	0.1 mm/side/week on (201) and (011) seeds, 0.2 mm/side/ week on (100) seeds
3	4M KH_2ASO_4	77	57	Flux grown KTA	590	1700	(201) and (011) flux grown KTA	30	2	0.2 mm/side/week on (201) and (011) seeds
4	4M KH_2ASO_4	77	57	Flux grown KTA	590	1700	(201) flux grown KTA	40	4	0.4 mm/side/week on (201) and (011) seeds, 0.2 mm/side/week on (100) seeds

Some authors have studied the ionic conductivity in KTA crystals and usually the ionic conductivity is one order of magnitude lower than KTP crystals. The ionic conductivity is found to be one-dimensional, i.e., along *Z*-direction only.

The structure of KTP family has the typical formula $\{K^+\}$ $[Ti^{4+}]O$ $(P^{5+})O_4$, where the flower brackets indicate nine- or eight-fold coordination, the square brackets six-fold octahedral coordination and the parentheses four-fold tetrahedral coordination. Different isovalent and aliovalent substitutions in a given structure are quite interesting, and could, perhaps, result in different structural and optical properties. Cheng et al.[147] have found that stability of KTA crystals is higher compared to other KTP-like compounds, Nb-doped KTP crystals are observed to be stable, and K_{1-x} Ti_{1-x} Nb_xO PO_4 single crystals with $x \approx 0.25$ have been obtained without any charge compensator. Partial charge compensation of Nb^{5+} in K_{1-x} Ti_{1-x} Nb_xO PO_4 crystals by Ga^{3+}, Fe^{3+} and Mg^{2+} has been reported. However, complete substitution of Ti^{4+} in single crystals of KTP with any aliovalent cation pair has not been achieved by any method.

On the contrary, complete substitution of Ti^{4+} with Nb^{5+}-Mg^{2+} and Nb^{5+}-Zn^{2+} cation pairs was reported to be possible in the case of KTA crystals. This result, suggested Chani et al. (1997), that it might be possible to prepare new aliovalent analogous of KTA containing Nb^{5+}-M^{3+} (M = Al, Cr, Ga, Fe, In) cation pairs in octahedral positions of KTP structure.[148] KTA crystal was the chosen basic material for this purpose as it was noted to be most stable compared to KTP.[147]

BlopBooks

Lattice parameter values, in general, were found to increase with increasing M^{3+} cation radius, as expected. The results of compaction measurements indicate that Ti-free crystals with the structure of KTP have tendency to create potassium vacancies. This result is in good agreement with that reported for nonsubstituted KTP crystals. Structural analogues of KTP corresponding to K [Ta, M]O AsO_4 were prepared by solid-state reaction. However, no KTP phase formation was observed in K [Nb, M]O PO_4 and K [Ta, M]O PO_4 systems.

The growth of KTP family of materials on the whole is fascinating and challenging for both technologists and academicians.

5.7 CALCITE

Calcite, $CaCO_3$ is an important carbonate mineral and it occurs commonly in nature both as well-developed crystals and amorphous material. The pure and optically clear calcite is called Iceland spar. Calcite is polymorphous and exists in at least five modifications. The two polymorphs commonly found in nature are calcite and aragonite. In addition, there are two synthetic forms known only at high pressures: calcite II and calcite III. Vaterite (γ-$CaCO_3$) is a metastable hexagonal form which crystallizes at ordinary temperatures and pressures.[149]

Calcite single crystals form an important optical material owing to its large birefringence and transparency over a wide range of wavelengths. This property makes it one of the significant materials for polarized devices such as optical isolaters and *Q* switches. It also exhibits antiferromagnetic properties. Although there are many deposits of calcite in the world, the optically clear quality calcite (for example, Iceland spar) has been depleted in recent years, leading to its shortage in nature. However, the demand for optically clear calcite single crystals is increasing greatly with the development of laser devices such as optical isolators,[150][151] and similarly, the chemical impurities and growth defects depend upon the geological settings and often lead to variations of refractive index and internal light scattering centers, and low optical damage resistance. Hence, the artificial means of obtaining optically pure calcite is becoming very popular. Many laboratories throughout the world have attempted to obtain calcite, but most of them have suffered from size or quality problems. In fact, the first publication on the synthesis of calcite appeared in 1883. Lemberg[152] heated basalt for six months with distilled water. It took up 2.43 % H_2O, which was not removed over H_2SO_4 in two weeks; the solution remaining in the tube had a slightly alkaline reaction. The same basalt heated with K_2CO_3 solution for nine months gave a glass rich in H_2O, and $CaCO_3$ crystals. A glass made from palagonit from Vidoe heated for three months with distilled H_2O was little attacked, but the product contained 8.61 % H_2O. Similarly, melted labradorite, heated for thirteen months with K_2CO_3 solution gave a glass rich in K, and the Ca replaced had formed $CaCO_3$. Further Lemberg obtained $CaCO_3$, while the MgO remained combined with the SiO_2 after heating augite with K_2CO_3 solution for one year at 100°C. When anorthite, with a little augite, was heated for 189 hours at 180–190° with Na_2CO_3 solution, the product consisted of calcite crystals, amorphous substances, and a

columnar mineral similar to cancrinite. Later, Friedel and Sarasin (1885) obtained small calcite crystals by heating $CaCl_2$, precipitated $CaCO_3$, and 60–70 cc H_2O for ten hours at 500°C; with 20 gms $CaCl_2$ and a few grams $CaCO_3$ the crystals were large enough for goniometric measurements. Crystals obtained were simple rhombohedra.[153] There was no aragonite in the product. However, all these earlier works on the synthesis of calcite were purely of geological/mineralogical interest, and the size of the crystals obtained was in no way nearer to the fabrication of devices. The most significant problem for the growth of calcite crystals is that the growth techniques are restricted due to the dissociation of $CaCO_3$ at high temperatures. Several techniques have been employed to grow calcite single crystals like low temperature solutions,[154][155] gels,[156][157] fluxes or eutectics,[158][159] top seeded solution growth,[160] travelling solvent zone melting,[161] hydrothermal hot pressing,[162]–[164] and hydrothermal.[150][151][165]–[170] Calcite crystals grown by most of these methods encounter several problems including the presence of large thermal stress, CO_2 dissociation, and alkaline carbonate flux inclusions which cause serious defects and contamination by metal ions. On the other hand, the hydrothermal method is one of the most promising techniques for growing unstable crystals such as a carbonate compound, with the advantage of suppressing the dissociation of CO_2 and yielding high quality crystals in a homogeneous ambient at relatively low temperatures.[171] Also, this technique is closer to the conditions in which calcite grows in nature.

DropBooks

Many researchers have tried to grow calcite single crystals at relatively low temperatures since calcite crystals dissociate to form CaO and CO_2 above 900°C under atmospheric pressure. Varieties of solvents have been used for hydrothermal growth of calcite, but none of them have succeeded in growing large single crystals. The solubility of calcite is very interesting. It has been studied in water under various CO_2 pressures.[172][173] The CO_2 pressure would be concerned with dissolution and precipitation of calcite in nature. Thus, hydrothermal growth under variable CO_2 pressures is also very interesting from the point of view of geochemistry. The solubility is positive for increasing CO_2 pressure and negative for increasing temperature. This behavior of calcite has posed a real problem in the search for a suitable solvent to obtain higher/optimum growth rates. Despite this, a large number of reports concerning calcite growth, hydrothermal reaction of calcite in chloride, and other chloride solutions have appeared. Because natural calcite crystals are formed in both chloride and carbonate hydrothermal solutions and these chloride solutions are almost

analogous to natural carbonate thermal springs. Ikornikova has done an extensive work on the aspects of solubility, designing an apparatus to grow calcite crystals with changing CO_2 concentration as the pressure is reduced at constant temperature, crystal growth kinetics, and mechanism.[166]

For hydrothermal crystal growth of calcite, several inorganic solvents like NaCl, LiCl, $CaCl_2$, $NaNO_3$, $Ca(NO_3)_2$, NH_4NO_3, K_2CO_3, and carbonic acid have been employed as mineralizers. The growth conditions vary from 150°C and 15 MPa, to 600°C and 200 MPa. No one has used organic salt solutions to grow calcite crystals under hydrothermal conditions. Yamasaki and his group have tested the solubility of calcite in ammonium acetate solution.[170] However, there is no unanimity with respect to solubility owing to the change in the sign of the temperature coefficient of CO_2 solubility in H_2O, as shown in the isobaric diagram Fig. 5.46. The diagram clearly shows two regions: I and II, lying on the two sides of the 200 bar isobar, which is close to the isobar of the critical pressure of water. The pH of the system falls with increasing P_{CO_2} under standard conditions. This is connected to the fact that with increasing CO_2 solubility, the concentration of both the hydrocarbonate and the hydrogen ions increases. The solubility of calcite in aqueous solutions of carbon dioxide was studied between 10–300°C and 1–100 bar.[172][173] At the same time, for T = constant, the solubility rises exponentially with increasing P_{CO_2}. Later experiments at 200–600°C and 200–1400 bar in solutions of 10–100 mg/ml CO_2 showed that absolute solubilities of calcite at high temperatures and pressures were almost an order of magnitude lower than those measured at pressures up to 100 bar.[174] The following groups have carried out extensive studies on the solubility of calcite: *i)* Ikornikova of Russia, during 1960s and 1970s—using chloride solutions; *ii)* Belt, USA, during 1970s—using carbonate solutions; *iii)* Hirano, Japan, during 1980s and early 1990s—using nitrate solutions; *iv)* Kodaira, Japan, during 1990s—using H_2O-CO_2; *v)* Yamasaki, Japan, during 1990s to date—using ammonium acetate and other organic solvents. Each one of the last three groups claims superiority of their solvents over the others. Figures 5.47 and 5.48 show the solubility curves for calcite in different solvents. Yanagisawa et al. (1996) have studied the effect of pH of CH_3COONH_4 on the growth of calcite.[170] It was found that calcite crystals could not grow in the CH_3COONH_4 solutions with a low pH. This has been explained by the change in the existing ion species in the solution. A high growth rate was obtained in the solutions with a pH of 7.0–7.5. Beyond a pH of 7.5, the

growth rate falls again. The pH of solution decreased with the increase in temperature, and it reached 6.0 at 200°C. This result suggested that H_2CO_3 was the main dissolved species in the solution at 250°C. When calcite dissolves in water, the carbonate ion must change its ionic form to HCO_3^-, which is very essential for the crystal growth of calcite, whereas H_2CO_3 does not contribute to the growth of calcite crystals. The formation of the ionic species HCO_3^- has been noticed by several workers like Kikuta and Hirano in the NH_4NO_3 solutions from FT-IR studies.[174] This suggests that calcite dissolves in the solvent below 200°C as follows:

$$NH_4NO_3 + CaCO_3 + H_2O \rightarrow Ca^{2+} + HCO_3^- + NO_3^- + NH_4^+ + OH$$

$$2NH_4F + CaCO_3 + H_2O \rightarrow CaF_2 + HCO_3^- + 2NH_4^+ + OH^-$$

$$(NH_4)_2\,SO_4 + CaCO_3 + H_2O \rightarrow CaSO_4 + HCO_3^- + 2NH_4^+ + OH^-$$

This work strongly confirms that a small amount of additives such as phosphate, sulphate, borate, and ethylene glycol effectively arrested the growth of calcite.

DropBooks

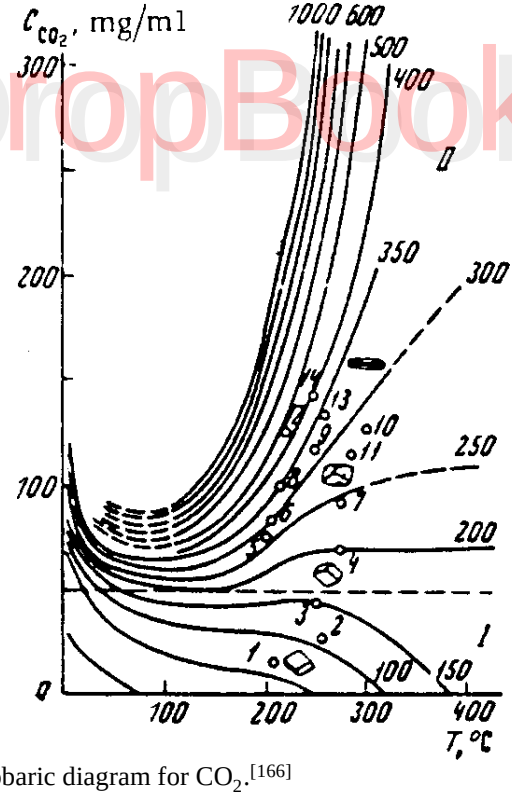

Figure 5.46. Isobaric diagram for CO_2.[166]

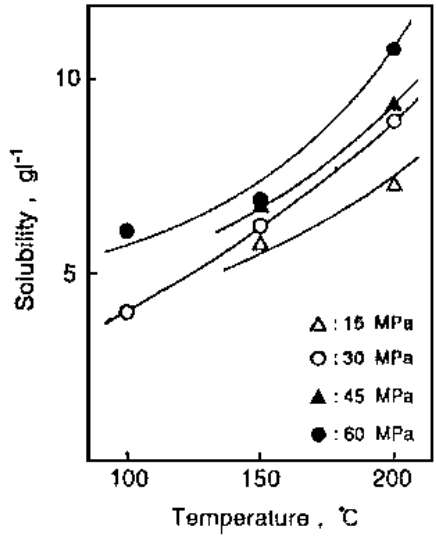

(a)

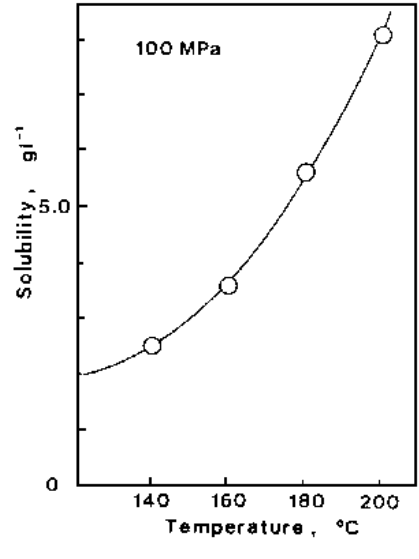

(b)

Figure 5.47. Solubility curves for calcite in different solvents, *(a)* in 1mNH_4NO_3 and *(b)* in 3mNH_4NO_3.[171]

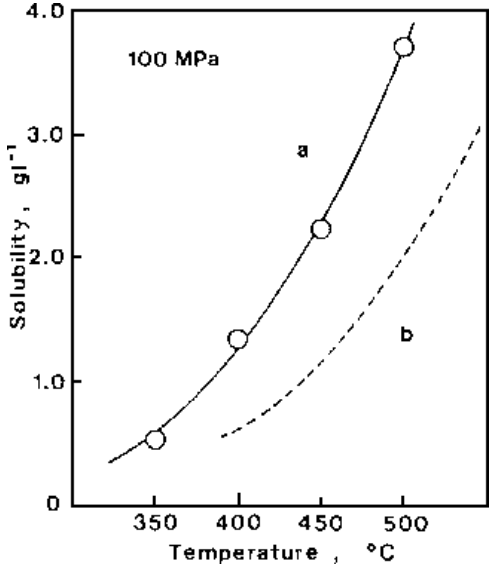

(a) 1.5mCa$(NO_3)_2$
(b) 3mNaCl

DropBooks

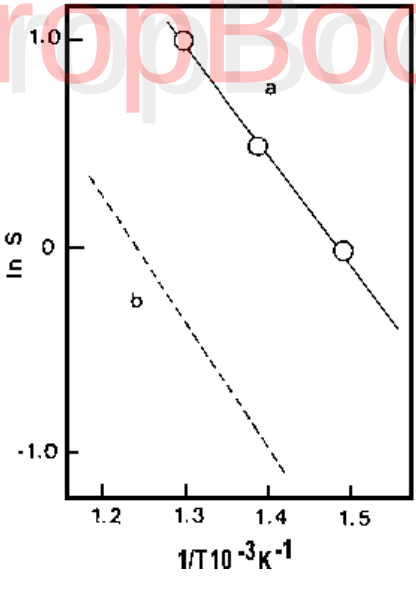

(a) 1.5mCa$(NO_3)_2$
(b) 3mNaCl

Figure 5.48. Solubility curves for calcite in different solvents.[168]

5.7.1 Crystal Growth

Solubility of calcite can be both positive and negative for increasing CO_2 pressure and increasing temperatures, respectively. Therefore, the growth of calcite crystals insists on a special experimental setup. Figure 5.49 shows the arrangement of the apparatus designed by Ikornikova for growing calcite crystals in aqueous solutions of CO_2 with a negative temperature coefficient of solubility, together with curves illustrating the height distribution of temperature and CO_2 concentration.[166] The crystals obtained by this means, with seed crystals at the bottom and nutrient at the top followed by a temperature gradient between the two zones separated through a baffle, have rhombohedral faces covered with stepped pyramids. Similarly, Ikornikova has designed another apparatus for synthesizing calcite crystals in aqueous solutions of carbonic acid under isothermal conditions. The autoclave used is a rocking autoclave. Figure 5.50 shows the schematic diagram of the apparatus used in the synthesis of calcite. The autoclaves in both the cases are either glass or teflon lined.[166][169] In this case, usually at pressure under 150 kg/cm^2, rhombohedral calcite crystals without any pinacoid are formed. The pinacoid appears on crystals formed at pressures greater than 200 kg/cm^2.

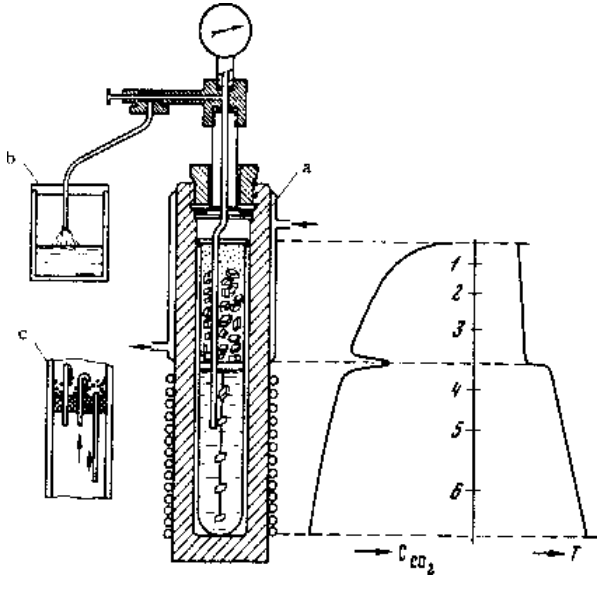

Figure 5.49. Arrangement of the apparatus for the growth of calcite.[166]

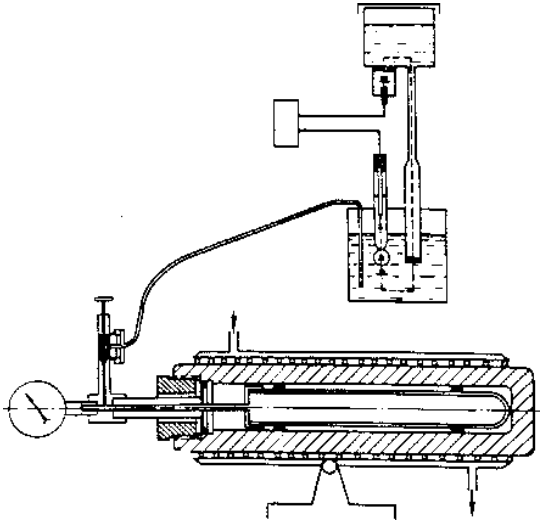

Figure 5.50. Schematic diagram of the apparatus used in the synthesis of calcite.[166]

Kinloch et al. (1974) have obtained calcite single crystals in large autoclaves (23 cm internal diameter × 280 cm length)—commercial production using 6 M K_2CO_3 mineralizer. As K_2CO_3 attacks autoclaves made of ferrous alloys, the autoclaves were provided with cylindrical silver and platinum cans.[150] The following are the experimental conditions used by these workers:

DropBooks

Nutrient:	-	45 Kg. of optical grade crystals of Mexican origin
Seeds:	-	Natural calcite crystals cutting rhombohedra with 10–20 cm^2 surfaces and 1–2 cm thick
Solvent :	-	6 m K_2CO_3
Nutrient temperature:	-	435–445°C
Seed temperature range:	-	410–425°C
% Fill:	-	86 % (1.72 Kbar)
Baffle opening:	-	8 %
Temperature gradient:	-	5 to 10°C
Experimental duration:	-	30 to 50 days
Growth rate obtained:	-	50 μm/day/face for {1011} face

Much of the recent works on the growth of calcite single crystals are being carried out under moderate to lower temperatures (200–150°C) using several new solvents like ammonium nitrate, ammonium acetate, and so on. The results are far better than crystals obtained under higher temperatures because of the reduced thermal strain. Recent workers use teflon liners. A considerable amount of progress has been achieved in the single crystal growth of calcite with reference to the solubility, growth rate, reaction kinetics, seed orientation, morphology, surface morphology, optical and laser quality, and so on. Figure 5.51 shows the schematic diagram of the autoclave for hydrothermal crystal growth of calcite commonly used in recent years. It is well confirmed that the ammonium nitrate and acetate solvents are more effective than chloride solvents from the viewpoint of calcite crystal growth. The calcite crystals dissolve in ammonium nitrate or acetate solutions, accompanied by the evolution of ammonia. This reaction increases the dissolution of calcite in the hydrothermal solution which gives an advantage of lowering the pressure, temperature conditions of the growth, and in turn facilitates the use of teflon liners. Great improvements are achieved by using a baffle plate and band heater to control the temperature gradient and the transport behavior. Higher temperature gradients give higher growth rates, especially at higher growth temperatures. Usually the growth rate varies from 25 μm/day to 213 μm/day. The rhombohedral face (1011) is the fastest growing face. Hence, natural calcite crystals cleaved at (1011) plane are used generally as seed crystals. Yanagisawa et al. (1996) have obtained the highest growth rate reported so far, for calcite, 213 μm/day using ammonium acetate solvent at 230°C and a temperature gradient of 20°C. However, the optical quality of the calcite crystal was relatively poor. Only under experimental conditions, such as temperature gradient of 15°C and growth temperature of 235°C, was the growth of transparent calcite crystals achieved at 57 μm/day. Figure 5.52 shows the hydrothermally grown calcite crystals by different authors. When as-cleaved crystals are used, the calcite crystals obtained are usually opaque or not transparent, and the surfaces show a greater degree of defects like growth hillocks, a lot of small secondary grown crystals, and strains. The crystals grown on the etched seed crystals are usually transparent and the surfaces are very smooth. Figure 5.53 represents the characteristic photographs of calcite single crystal grown in NH_4NO_3 solution using as-cleaved and etched seeds. Similarly, Figure 5.54 represents the surface morphology of the calcite crystals using as-cleaved and etched seeds. Recently, Lee (1998)

has re-attempted the solvent NH_4Cl, first reported by Ikornikova,[165] to obtain calcite single crystals[175] to suppress the spontaneous mineralizer. It was observed that the addition of such an organic additive played an important role in suppressing the formation of spontaneous nuclei; usually higher % fill (81–83%) was selected in all the experiments and the pressure-temperature conditions were kept low. Hence, teflon was used as the liner.

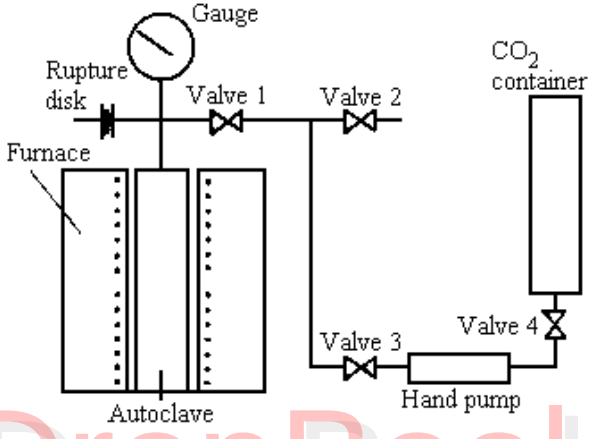

Figure 5.51. Schematic diagram of the autoclave.[169]

DropBooks

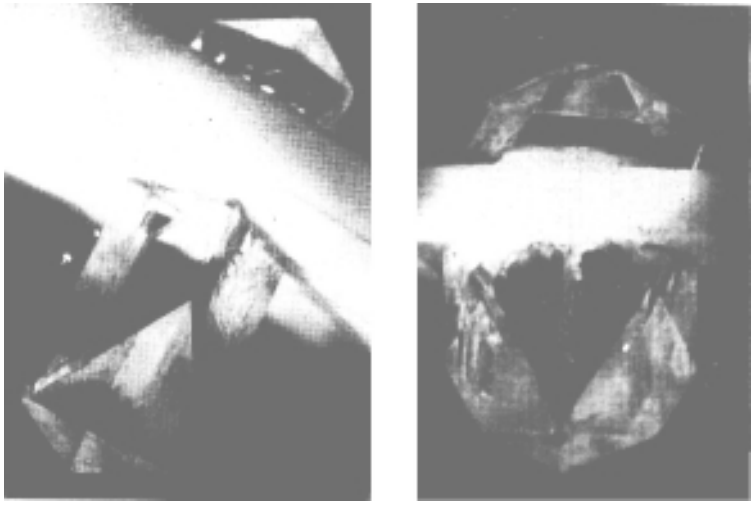

Figure 5.52. Hydrothermally grown calcite crystals.[166]

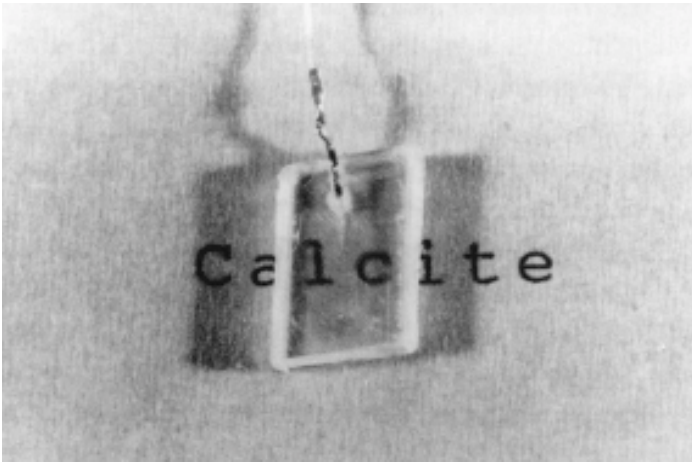

Figure 5.53. Characteristic photograph of calcite single crystal grown in NH_4NO_3 solution.[168]

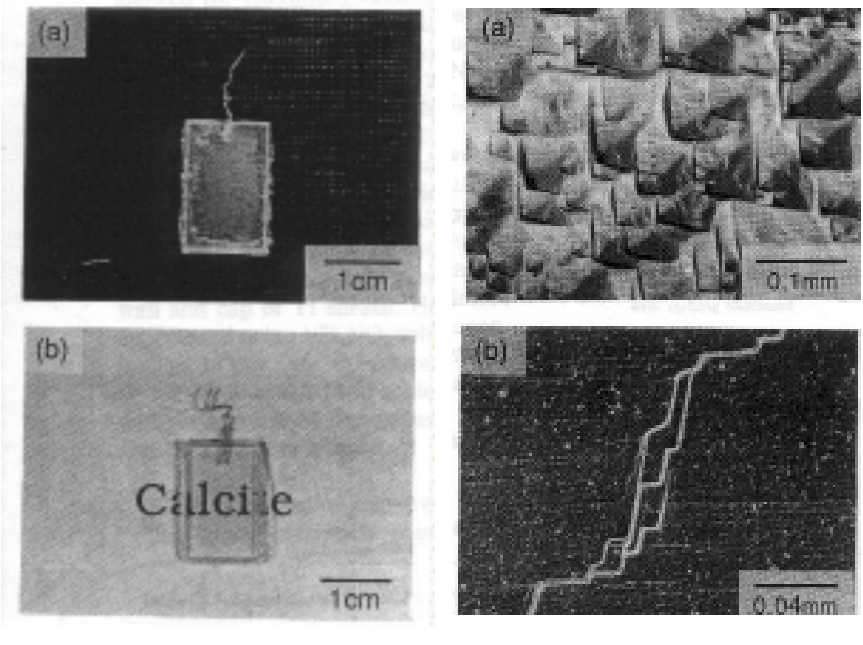

Figure 5.54. Surface morphology of the calcite crystals using as-cleaved and etched seeds.[168]

5.7.2 Hydrothermal Hot Pressing of Calcite

The hydrothermal hot pressing is being applied in recent years for the solidification of $CaCO_3$. The hydrothermal hot pressing (HHP) technique is a method by which hard solid bodies of powders can be produced in a short time and at a relatively low temperature under saturated vapor pressure. This process is very similar to diagenesis[176] in geology, therefore, a diagenesis process, such as for limestone, may be resurrected by using this technique. The results, using the hydrothermal hot pressing technique, may bring in some new information to the sedimentary process and a new technology of forming fabrication processes. Yamasaki and Weiping (1993) have obtained $CaCO_3$ by hydrothermal hot pressing with sea water, and they have designed a "quasi-diagenesis" experiment. Initially, the $CaCO_3$ powder was synthesized in seawater, and this powder was then solidified by the hydrothermal hot pressing technique. Various ions of sea water, Cl^-, Na^+, K^+, SO^{2-}_4, etc., were absorbed on the surface of the synthesized $CaCO_3$ sample powder during the precipitation process, and these ions formed soluble salts such as NaCl and $CaSO_4$ under hydrothermal hot pressing conditions, that is, the solubility of the synthetic $CaCO_3$ powder surface may have increased rapidly in the presence of $CaSO_4$, and NaCl solution under hot pressing conditions. Consequently, it was revealed that the small grains were dissolved, and then recrystallization occurred, or the grains adhered to the surface of larger grains and formed large grain growth during hydrothermal hot pressing. The solidification process was carried out by a dissolution-recrystallization mechanism during the hot pressing process.

DropBooks

Yamasaki et al. (1993) have solidified the powders of calcium carbonate with sodium carbonate by mechanical compression under hydrothermal conditions. The effects of hydrothermal conditions such as temperature, pressure, and ratio of Ca/Sr on the reaction process and microstructure of the solidified bodies have been studied.[163]

The growth of calcite single crystals is becoming very popular in recent years with the fast decrease in the availability of natural calcite. Although the growth of calcite has been better understood in the last five to six years, still there is no unanimity with reference to the solvent and experimental conditions. There is no doubt that calcite crystal growth is one of the flourishing and challenging topics.

5.7.3 Growth of Related Carbonates

There are several works in the literature dealing with the growth of other carbonates like $MnCO_3$ (rhodochrosite), $FeCO_3$ (siderite), $CaCO_3$ (spherocobaltite), $CdCO_3$ (otavite), $NiCO_3$, and so on. Most of these are the important carbonate minerals, and their growth carries a great significance to the geological literature.

$MnCO_3$ (Rhodochrosite). The crystallization of rhodochrosite crystals takes place in LiCl solutions (1–25 wt%) at temperatures 400–450°C, and pressure 680–2500 atm., the ΔT = 10–50°C.[177] In the experiments with 20–25% LiCl solutions at ΔT = 10°C, T = 430°C, and P = 960 atm, Ikornikova has obtained transparent crystals of rhodochrosite with a size of 5–7 mm.

$FeCO_3$ (Siderite). The synthesis of siderite is slightly more difficult than $MnCO_3$ having to do with the stability during the variation in the oxygen potential. Ikornikova (1970) has obtained transparent crystals of $FeCO_3$ in NH_4Cl solutions at T = 300–350°C, P = 600–800 atm and P_{CO_2}–300 atm.[178]

$CaCO_3$ (Spherocobaltite). The growth of spherocobaltite crystals has been carried out on the seeds in the LiCl solution. Autoclaves of 300 cm^3 using titanium liners have been used. Separate experiments have been carried out in 1.2–1.7 liter autoclaves with platinum liners. Spontaneously grown crystal was used as a seed crystal. However, detailed studies on the growth of spherocobaltite are not known.[177][178]

$CdCO_3$ (Otavit). Monocrystals of otavit were first obtained by Ikornikova.[177] Crystals were grown in LiCl (5–20%) and NH_4Cl (1–5%) solutions in the temperature interval 300–550°C, ΔT = 15–20°, P = 700–900 atm. The size and quality of the crystals in the growth zone were regulated through the concentration of solution and temperature gradient.

$NiCO_3$. Monocrystals of carbonate of nickel could be obtained at T > 150–500°C and P > 1500 atm using $NiCO_3$, $Ni(OH)_2$. During the evolution of CO_2 in the autoclave, the crystallization of $NiCO_3$ takes place at much lower pressure and NH_4Cl (2–10%) solution.[179]

Figures 5.55, 5.56, and 5.57 show photographs of some selected hydrothermally synthesized carbonates in the hydrothermal laboratory of K. Byrappa.

The growth of carbonates, in general, is quite interesting academically, technologically, and geologically.

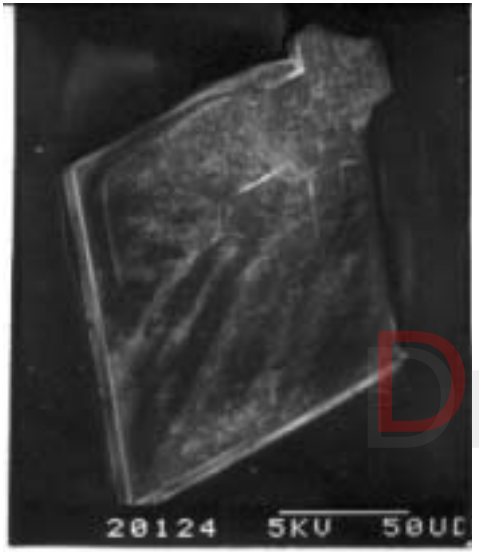

Figure 5.55. $ZnCO_3$ crystal.

Figure 5.56. $SrCO_3$ crystal.

Figure 5.57. $BaCO_3$ crystal.

DropBooks

(Photographs courtesy of J. A. K. Tareen and B. Basavalingu.)

5.8 HYDROXYAPATITE (HAp)

Apatite is a common mineral in igneous, sedimentary and metamorphic rocks,[180] which has the general chemical formula of $A_{10}(BO_4)_6X_2$, where A = Ca, Sr, Ba, Fe, Pb, Cd, and many rare earth elements; BO_4 = PO_4^{3-}, VO_4^{3-}, SiO_4^{4-}, AsO_4^{3-}, CO_3^{2-}; X = OH^-, Cl^-, F^-, CO_3^{2-}. Water exists in different forms.[181][182] The presence of the elemental phosphorus, which is a major component of apatite, was first reported in the 17th century and the phosphorus in mineral pyromorphite (lead apatite) was discovered in 1779.[183][184] Since the first synthesis of apatite done in the middle of 19th century,[185] a lot of studies in the geochemical, crystallochemical, biological, and other fields have been carried out. In fact, most of the geochemical and crystallochemical studies were carried out on natural apatites, whereas biological or other recent studies were mainly done using synthetic apatites. However, many efforts have been made to prepare large single crystals of HAp with only limited success. The interest in the synthesis of hydroxyapatite is linked with its importance as a major constituent of the inorganic component in bones and teeth where it occurs as tiny crystals. Since it has been recognized to be one of the best biocompatible materials, there have been many reports on the biological aspects.[186]–[188] HAp crystals have selective adsorption ability of proteins depending on crystal planes and are used as an adsorbent in liquid chromatography.[189] Recent interest in the material has spread to the fields of electronics and surface science (or adsorption chemistry), where sintered or powder HAp is expected to function as, for example, gas sensors, catalysts, and chromatographic absorbers. The fabrication processing of HAp has also progressed with the growing importance of the biological applications of HAp as artificial bone and teeth.[190] Table 5.16 gives the physico-chemical properties of apatites.[191] However, a detailed knowledge of chemical and physical properties of HAp, including those relevant to the behavior in a biological environment, depends on the availability of sufficiently large single crystals of known chemical composition. Even today most of the studies on chemical properties, mechanical properties, biological responses and the prosthetic application of HAp are based on polycrystalline bodies with random crystal arrangement including sintered bodies, powders, granules and coatings.

Table.5.16. Physico-chemical Properties of Synthetic Hydrothermal or Natural Fluorapatite[191]

Properties	Values	Comments
Theoretical Formula	$Ca_{10}(PO_4)_6(OH)_2$	composition varies with sample preparation
Space Group	$P6_{3/m}$ (hexagonal) $P2_{1/b}$ (monoclinic)	mono. ↔ hexa. transition may occur at ca. 200°C
Lattice Parameters (LP)	a = 9.41-9.44 Å c = 6.84-6.94 Å	large discrepanices in L.P. of *'Wet Chemically'* HAp
Theoretical Density	3.16 g/cm^3	varies with composition
Moh's Hardness	3(CO_3-Ap) 5(HAp)	water and CO_3 in apatite lattice lower hardness
Heat Capacity	184.07 cal/K.mol at 298.16 K 950°C 180.16 cal/K.mol at 298.15 K	"wet" HAp following calcined at "wet" HAp following calcined at 1100°C
Thermal Expansion Coefficient	11-14 x 10^{-6} K^{-1}	*'wet'* HAp expands non-linearly
Melting Point	1614°C	'synthetic' HAp, hot-stage microscope method
Surface Energy	S(001)=95±25MPa	Natural FAp, slow cleavage method
Stiffness Coefficient at room temp (Mbars)	C11=1.434, C33=1.805 C44=0.415, C12=0.445 C13=0.575, C66=0.495	Natural FAp, ultrasonic pulse superposition
Dielectric Constant	7.40-10.47	varies with composition
Refractive Indices	n_w=1.649-1.651, n_c=1.642-1.644	relationship between indices & composition is shown in Ref. 1
Optical Frequency	2.71 (‖c) 2.69 (⊥c)	varies with composition

DropBooks

Daubrée (1851) was the first to synthesize apatite by passing phosphorus trichloride vapor over red-hot rime.[185] Since then a number of reports on the preparation of HAp by various methods have appeared in the literature, and the results prior to 1951 have been reviewed by Jaffe (1951).[186] Yoshimura and Suda (1994) have reviewed the preparation methods for HAp and grouped all the methods into three categories, as given in Table 5.17.[191] First is the conventional *solid state reaction method* at high temperature, the second is the *wet chemical method* at relatively low temperature and the third, which is a very important method today, is the *hydrothermal method* using high-temperature–high-pressure aqueous solutions.

Table.5.17. Preparation Techniques for Hydroxyapatite[191]

Techniques	Starting Materials	Synthetic Conditions	Comments
Solid State Reaction	$Ca_3(PO_4)_2$+ $CaCO_3$ $Ca_2P_2O_7$+ $CaCO_3$	900-1300°C, usually with water vapor	Ca/P-1.67, large grain size, irregular forms, inhomogeneous flowing
Wet Chemical Method	$Ca(NO_3)_2$+$(NH_4)_2$ HPO_4 $Ca(OH)_2$+ H_3PO_4	R.T.-100°C pH: 7-12	Ca/P < 1.67 fine irregular crystals with low crysatllinity inhomogeneous
Hydro-Thermal Method	wet chemically prepared HAp, other calcium phosphates, seeding	100-200°C (1-2 MPa), 300-600°C (1-2 Kbar)	Ca/P=1.67 homo-geneous, fine single crystals or large crystals
Gel Growth Method	Gel + Ca^{2+} + PO_4^{3-}	R.T.-60°C, pH: 7-10	large Monetite, Brushite, OCP, but small HAp
Flux Growth Method	CaF_2, $CaCl_2$ as flux $Ca(OH)_2$ as flux	1325°C (FAp,ClAp) HAp	large crystals with little lattice strain

The solid state reaction method has generally been used for processing ceramic powders and for studying phase stabilities. The powders prepared by this method, however, usually have irregular forms with a large grain size, and often have heterogeneity in composition due to incompleted reaction resulting from small diffusion coefficients of ions within solids.

The wet chemical method is a relatively easier method for obtaining HAp. Besides, the reaction in any living organisms may occur in aqueous solutions at low temperatures. Many experiments on the preparation of HAp by this method have been reported which investigate the formation mechanism of any calcium phosphates *in vitro*, in addition to *in vivo*. The powders prepared by this method, however, do not seem to be appropriate as the starting materials for ceramics because they are usually less crystallized, heterogeneous in composition, and irregularly formed. Sol-gel, alkoxide, and other chemical methods have also been used. CVD, plasma spray method and other (electro) chemical methods have been mainly used to form HAp layers on substrates.

The hydrothermal method enables us to prepare well crystallized, compositionally homogenous, uniform and easily sinterable powders due to great effects of the high-temperature–high-pressure aqueous solutions.

DropBooks

The growth of HAp crystals has been carried out by several other methods like the gel growth method.[192] There are several reports on the melt growth and flux growth of apatites of different compositions. Johnson (1961) has used the melt growth for the preparation of single crystals of apatite from the stoichiometric melt. These crystals grown from the melt at high temperatures, however, are usually severely strained due to the large temperature gradients existing during the growth.[193] Prener (1967) used the flux growth method, which is an excellent method since the fluxes like CaF_2, $CaCl_2$, and $Ca(OH)_2$ mixed with the starting apatite powders make lower liquidus temperature, far below needed for the melt growth method, resulting in the production of less strained apatite crystals.[194] Recently, Oishi and his group have obtained chlorapatite and fluorapatite crystals by the flux method using NaCl, KF and Ca_2ClPO_4 fluxes.[195]–[197] Masuda et al. (1990) have used the sol-gel method to obtain HAp from metal alkoxides.[198] Brendel et al. (1992) have used the polymerized method to achieve HAp coatings.[199] Likewise, many other methods are utilized in the processing of apatites. Thus, for the growth of HAp, the volatility of water at the necessary high temperatures makes hydrothermal conditions unavoidable.

5.8.1 Crystal Structure of Apatite

Most of the studies concerning the crystallochemical, geochemical and phase stability related aspects of apatite have been carried out on natural or hydrothermally synthesized large single crystals. The crystal structure of fluorapatite (FAp) was first determined by Naray-Szabo (1930) and by Mehmel (1930) independently.[200][201] Followed by these, several publications appeared on the structure of various forms of apatite.[202]–[204] The general agreement on the crystallographic aspects is as follows:

a) Apatite shows ionic bonding character, and it is made up of a close packing of large oxygen ions, resulting in the hexagonal crystal system.[205]

b) The space group of fluorapatite (FAp) is $P6_{3/m}$.[200]–[204]

c) Although the space group of HAp is believed to be $P6_{3/m}$, HAp prepared at high temperature is P 21/b (monoclinic) at room temperature,[200] nearly identical with chlorapatite (ClAp).

d) A phase transition in HAp is suggested to occur at ~ 200°C, probably due to the order-disorder orientation at $(OH)^-$ ions along the *c* axis.[206][207]

5.8.2 Phase Equilibria

The phase equilibria in the system $CaO\text{-}P_2O_5\text{-}H_2O$ have been extensively studied by the solid state reactions method under atmospheric pressure of water vapor by Van Wazer (1958),[208] and in aqueous systems at temperatures lower than 100°C by Brown et al. (1991, 1992).[209][210] Biggar (1966) has studied the phase equilibria in the system $CaO\text{-}P_2O_5\text{-}H_2O$ in the temperature range 700 to 950°C, and *P* of 1 kbar.[211] Feng and Rockett (1979) have studied the system $CaO\text{-}P_2O_5\text{-}H_2O$ at 200°C.[212] Figure 5.58 shows the $Ca(OH)_2\text{-}Ca_3(PO_4)_2\text{-}H_2O$ at 1000 bar with 50 wt% H_2O. Skinner (1974) found that the field of stability of hydroxyapatite alone with water in the triangle $CaO\text{-}P_2O_5\text{-}H_2O$ was confined to a narrow band joining the representative point of stoichiometric hydroxyapatite to the water representative point of the phase diagram.[213] There are several other phase equilibria studies on the apatite system and the reader can refer to the works.[191][214] Andrade et al. (1997) carried out a detailed

thermodynamic analysis of the system Ca-P-H_2O based on the development of the Eh-pH and Pa_C-pH (where $Pa_{Ca} = -\log_{10} a_{Ca}$) diagrams at different temperatures and different activities of phosphorous and calcium in aqueous solution. The hydroxyapatite precipitated at ambient temperature (30°C) was hydrothermally treated at 150°C.[215] Figures 5.59–5.63 show the Eh-pH diagrams of the Ca-P-H_2O system at 25°C and 300°C, for 1.67 molal activity of the Ca and 1 molal activity of pressure in the aqueous solution. Figures 5.61 and 5.62 present the Pa_{Ca}- pH diagrams (where $Pa_{Ca} = -\log_{10} a_{Ca}$), for the same system with $a_{Ca} = 1.67$ aP and show that the pH value for the point of minimum solubility of the hydroxyapatite clearly decreases with an increase in the temperature of the system. At each temperature level, HAp predominates in the higher pH range, while $Ca_3(PO_4)_2$, $Ca_2P_2O_7$ and $CaH_6P_2O_9$ have their predominate pH range successively in the more acid direction. The stability of the calcium phosphates at higher temperatures can be seen in Fig. 5.63. The equation numbers indicated in Fig. 5.63 refer to the following reactions:

(1) $3CaHPO_4\,(c) = Ca_3(PO_4)_2\,(c) + H_3PO_4\,(c,l)$

(2) $3CaH_2PO_4\,(c) = Ca_3(PO_4)_2\,(c) + 4H_3PO_4\,(c,l)$

(3) $Ca_{10}H_2P_6O_{26}\,(c) = 3\,Ca_3(PO_4)_2\,(c) + CaO\,(c) + H_2O\,(g)$

(4) $CaH_5PO_6\,(c) = CaHPO_4\,(c) + 2H_2O\,(g)$

(5) $CaH_6P_2O_9\,(c) = Ca(H_2PO_4)_2\,(c) + H_2O\,(g)$

DropBooks

The Eh-pH and Pa_{Ca}-pH diagrams have shown that HAp may be obtained at both atmospheric and hydrothermal conditions.

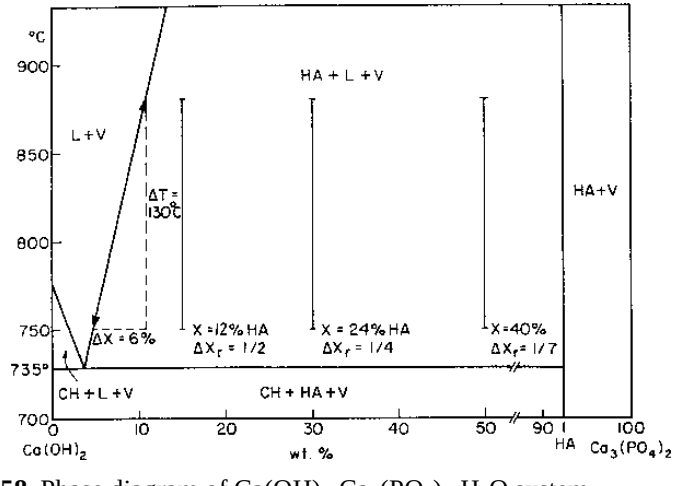

Figure 5.58. Phase diagram of $Ca(OH)_2$-$Ca_3(PO_4)_2$-H_2O system.

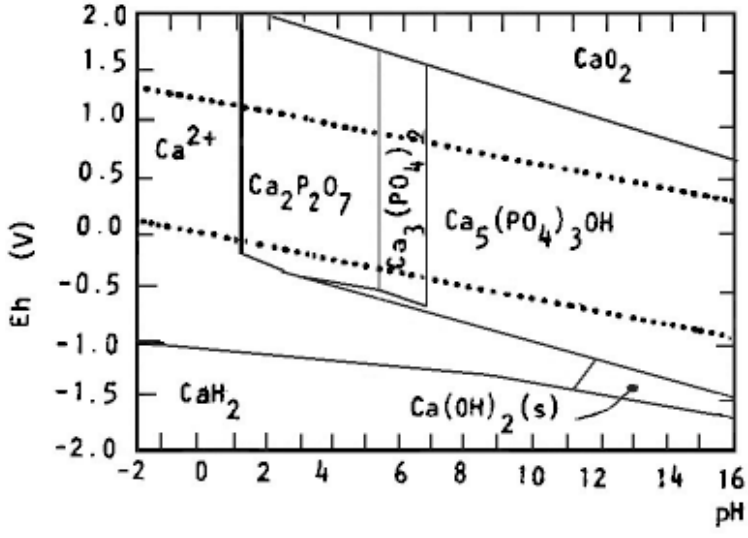

Figure 5.59. Eh-pH diagram of the Ca-P-H_2O system at 25°C for 1.67 molal activity of Ca and a_{Ca}=1.67 a_P.[215]

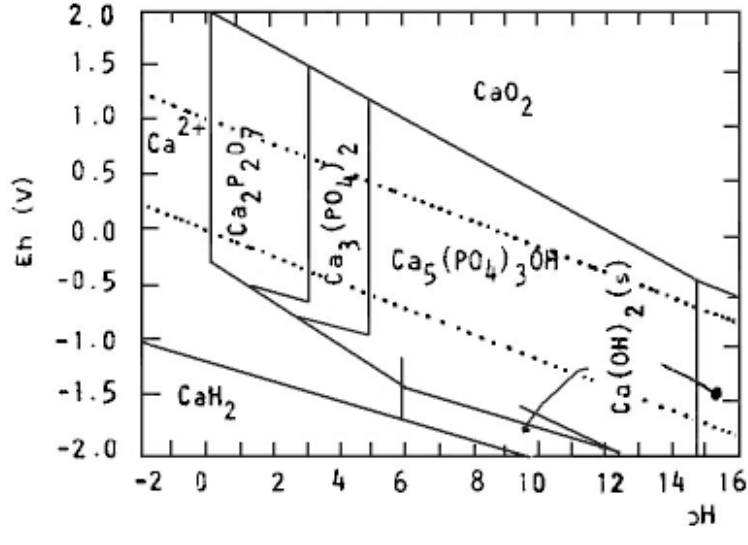

Figure 5.60. Eh-pH diagram of the Ca-P-H_2O system at 300°C for 1.67 molal activity of Ca and a_{Ca}=1.67 a_P.[215]

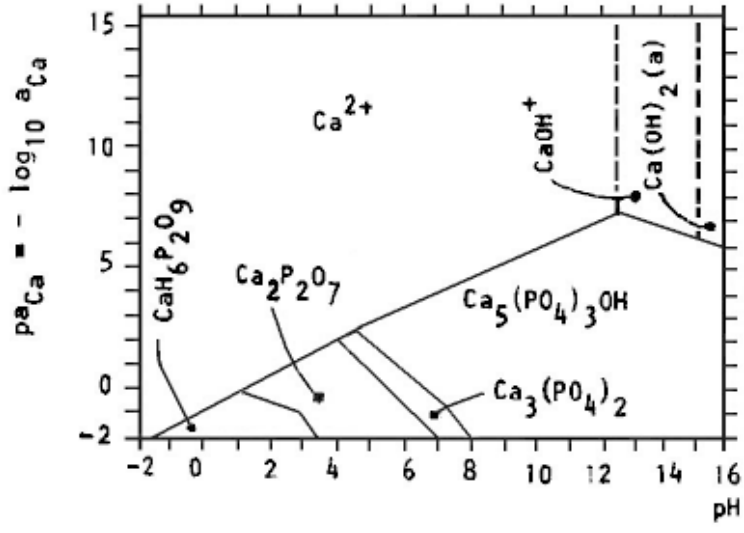

Figure 5.61. Pa_{Ca}-pH diagrams of the Ca-P-H_2O system at 25°C for a_{Ca}=1.67 a_P.[215]

DropBooks

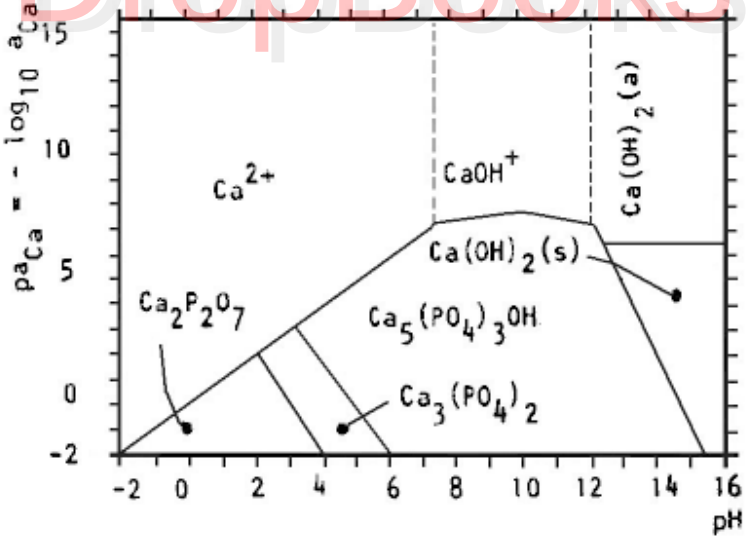

Figure 5.62. Pa_{Ca}-pH diagrams of the Ca-P-H_2O system at 300°C for a_{Ca}=1.67 a_P.[215]

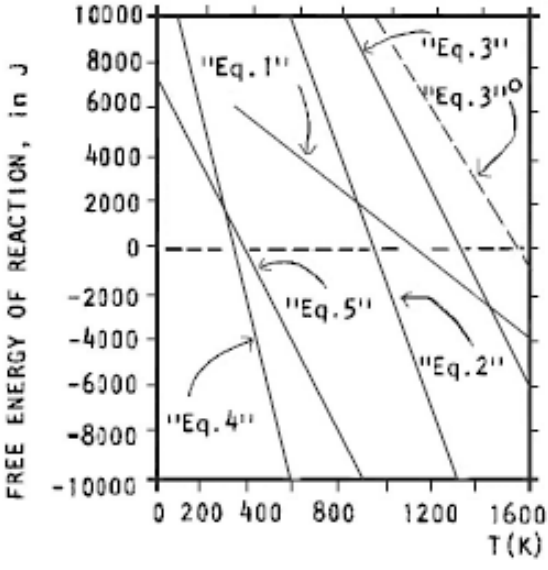

Figure 5.63. Free energy of reaction against temperature for some calcium phosphates according to Eq. (1) to Eq. (5) for water vapor fugacity equal to 0.03 atm, except for the dashed line, Eq. (3), which corresponds to water vapor fugacity equal to 1.0 atm.[215]

5.8.3 Crystal Growth

There are a large number of publications on the preparation of large HAp single crystals. Table 5.18 gives the representative works on the hydrothermal synthesis of HAp large single crystals.[218]–[225] Morey and Ingerson (1937) first attempted the hydrothermal synthesis of HAp crystals.[216] Since then, several reports have appeared in the literature. Roy (1971) grew prismatic single crystals of HAp, up to 4 mm length hydrothermally, from melts in the system $3CaO\text{-}P_2O_5\text{-}Ca(OH)_2$ and $3CaO\text{-}P_2O_5\text{-}Ca(OH)_2\text{-}H_2O$.[221] Mengeot et al. (1973) first succeeded preparing HAp single crystals of up to 7 × 3 × 3 mm in size by controlling the temperature gradient.[222] This work also revealed for the first time that HAp exhibited retrograde solubility in hydrothermal fluids between 300°C and 670°C under pressure of 3 kbar to 4 kbar. With the appearance of this report, most of the researchers placed nutrients at the cooler zone. Here, dissolution occurs and HAp crystals grow at the hotter region where the seed crystals are placed. This arrangement facilitated the growth of larger

HAp single crystals. However, the preparation of large single crystals of HAp has encountered several difficulties such as the tendency to incorporate impurities, the stability of nonstoichiometric composition, and the restricted field of crystallization in the phase diagram $CaO-P_2O_5-H_2O$, where HAp and H_2O only exist.

Table 5.18. Hydrothermal Synthesis of Hydroxyapatite Large Single Crystals[191]

Starting Materials	Synthetic Conditions	Comments
$CaHPO_4$ wet chemically prepared HAp	300°C 1250 lb/in^2, for 10 days 500°C, 354 bars, for 10 days	0.3 mm in length 2.35 mm in length, 0.2 mm in diameter
$CaHPO_4$	350°C, 100 MPa	2 mm
$Ca_3(PO_4)_2{\cdot}Ca(OH)_2$ or $Ca_3(PO_4)_2{\cdot}Ca(OH)_2$ $-H_2O$ system	15000 psi, held at 850-900°C, then cooled 20°C/h. to ~750°C, quenched	4 mm in length
synthesized HAp as nutrient & HAp seed	300-670°C, 45000-60000 psi	7 × 7 × 3mm, identify the retrograde solubility of HAp
$Ca_3(PO_4)_2{\cdot}Ca(OH)_2$ $-CaCO_3-H_2O$ system, $Ca(OH)_2$ as flux	oscillating temperature technique, 750-800°C, 14500-17500 psi	8 × 0.5 mm
$CaHPO_4{\cdot}2H_2O$	100-300°C, 2 kbar	0.1 mm
wet chemically, followed by Soxhlet extracted HAp	430-500°C, 2 kbar	3.5 mm, check the retrograde solubility of HAp

DropBooks

In the recent years, Ito and his group have done excellent work on the single crystal growth of HAp.[226][227] Single crystals of carbonate-containing HAp have been grown hydrothermally by gradually heating with a temperature gradient applied to the vessel, using $CaHPO_4$, H_2O and carbon dioxide as dry ice. The hydrothermal reaction for the formation of HAp can be written as follows:

$$10CaHPO_4 + 2H_2O \rightarrow Ca_{10}(PO_4)_6(OH)_2 + 4H_3PO_4$$

Crystal growth experiments were performed, slowly hydrolyzing $CaHPO_4$ by gradually heating a pressure vessel with a temperature gradient applied.

Kikuchi et al. (1994) have obtained Sr-substituted HAp crystals of size $0.2 \times 0.2 \times 5$ mm^3 under hydrothermal conditions.[228] The starting materials such as calcium and strontium hydrogen phosphate ($SrHPO_4$) were gradually heated with a temperature gradient. The crystal growth occurred at low pH.

In most of the works, the effects of CO_3^{2-} on the morphology of the crystals have been reported: needle-like crystals are predominant if the carbonate content is higher than 0.1%, whereas equiaxial crystals occur if the carbonate content is below 0.1%. Hata et al. (1983) synthesized Cd hydroxyapatite single crystals, partly substituted with the first series transition elements for Cd ion, to investigate the substitution effects on the crystal growth and structural changes.[229] These crystals form a superstructure of pure Cd HAp. Nagata et al. (1995) have studied the synthesis of HAp crystals in the presence of methanol and studied the morphological variations in HAp crystals.[230] It was found that the products obtained from the slurries without methanol were rod-like or granular crystals. Addition of methanol to the slurries caused an increase in the ratio of plate-like crystals to rod-like crystals or granular crystals. When the weight of methanol added was equal to the weight of the slurries, only plate-like crystals were obtained.

Although several workers have reported a negative temperature coefficient of soluble for HAp, but there is no systematic study either on the experimental or theoretical side. In this respect, Vereecke et al. (1990) reported the calculation of the solubility diagrams and the effects of some parameters such as T (< 100°C), pH; partial CO_2 pressure, and ionic strength.[231] According to this report, the solubility of HAp is lowered with temperature indicating the retrograde solubility of HAp below 100°C.

Onuma et al. (1998) and Kanzaki et al. (1998) have carried out the direct growth rate measurement of HAp single crystals by Moire phase shift interferometry and AMF.[232][233] They carried out direct investigations of the growth kinetics for each crystal face of HAp. It was found that the *a*-face grew by step-flow combined with two-dimensional nucleation, and the rate-determining process of the growth was found to be the incorporation of a growth unit at the step front, from the measurement of step velocities. The growth rate of the *a*-face was estimated to be of the order of 10^{-4} nm/s from the step advancing rate. This value is about 3–4 orders of magnitude smaller than those for soluble inorganic crystals.[232] In contrast, the growth kinetics of HAp (0001), *c*-face, remain unclear. These authors have concluded that the volume diffusion process for growth is strong during the initial stages. It is believed that a strong bond site exists in the [0001] direction and there is no strong bond site in the [$10\bar{1}0$] direction, which makes the rate-determing process between *c*- and *a*-faces different. Figure 5.64 shows the carbonate-containing hydroxyapatite single crystals grown on the polycrystalline hydroxyapatite disk and Fig. 5.65 shows carbonate-containing hydroxyapatite single crystals.

DropBooks

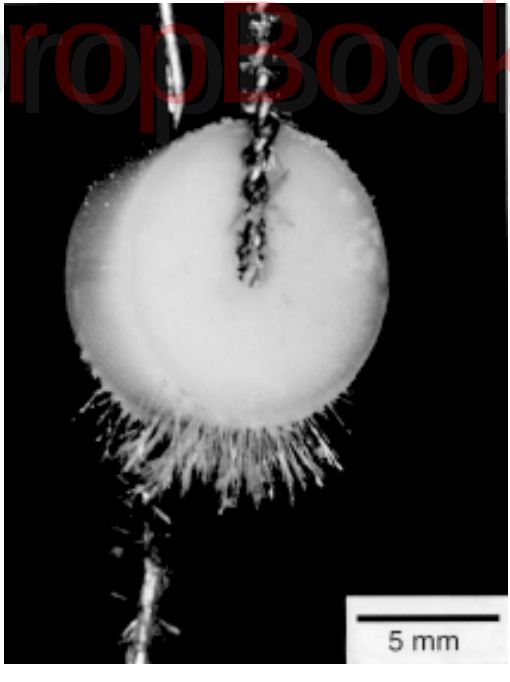

Figure 5.64. Carbonate-containing hydroxyapatite single crystals grown on the polycrystalline hydroxyapatite disk. *(Photo courtesy of A. Ito.)*

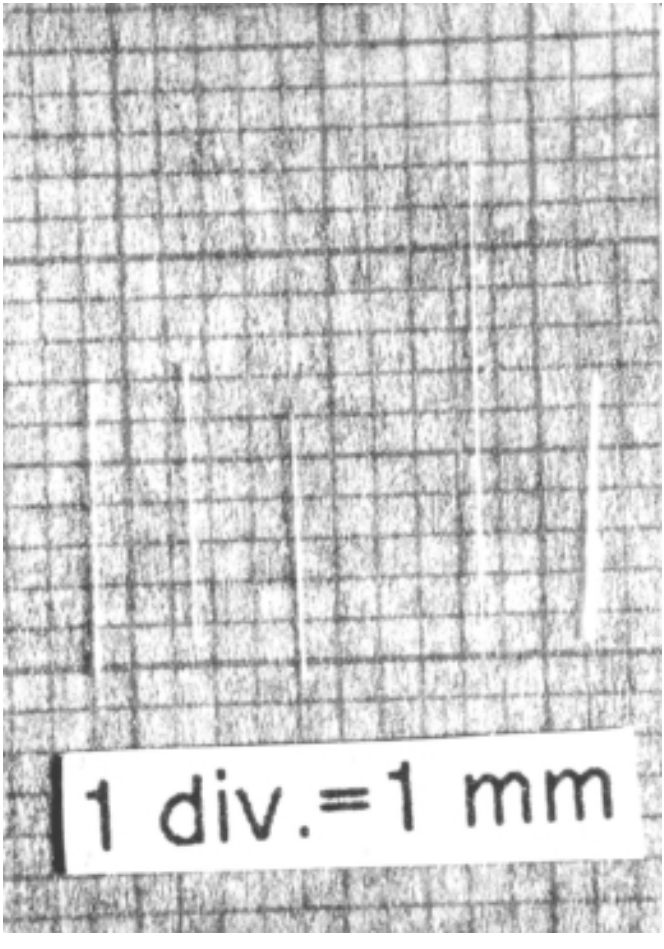

Figure 5.65. Carbonate-containing hydroxyapatite single crystals. *(Photo courtesy of A. Ito.)*

Like zeolites, hydroxyapatite is also an important technological material owing to its widespread applications attracting the attention of sicentists from interdisciplinary branches of science—including physicists, chemists, ceramists, medical doctors, engineers, and so on. Also, three International Symposiums on Apatite have been held. The importance of this material as a biomaterial, composite material, whiskers, fine particles, and so on, are discussed in Ch. 10.

REFERENCES

1. Tomkeieff, S. I., On the origin of the name "Quartz," *Min. Mag*., 26:172 (1942)
2. Sosman, R. B., *The Properties of Silica*, New York (1927)
3. Chao, E. C. T., Fahey, J. J., Littler, J., and Milton, D. J., Stisshovite, SiO_2, A Very High Pressure New Mineral from Meteor Crater, Arizona, *J. Geophys. Res.*, 67:419–423 (1962)
4. Ramsdell, C. S., The Crystallography of "Coesite," *Amer. Min*., 40:975 (1955)
5. Wei, P., The Structure of α - Quartz, *Zeit. Krist*., 92:355 (1935)
6. Bragg, W. H., The X-ray Spectra Given by Crystals of Sulphur and Quartz. *Proc. Roy. Soc.*, 89:575 (1914)
7. Hosaka, M., Miyata, T., and Sunagawa, I., Growth and Morphology of Quartz Crystals Synthesized Above the Transition Temperature, *J. Crystal Growth*, 152:300–306 (1995)
8. Arndt, J. and Rombach, N., Synthesis of Coesite from Aqueous Solutions, *J. Crystal Growth*, 35:28–32 (1976)
9. Dyuzheva, T. I., Lityagina, L. M., Bendeliani, N. A., Nikolaev, N. A. and Dorokhova, G. I., Hydrothermal Synthesis of Coesite (SiO_2), Crystallography Reports, 43:511–513 (1998)
10. Barth, T. F. W. The Cristobalite Structure: I High-Cristobalite; II Low-Cristobalite., *Amer. J. Sci*., 23:350; 24:97 (1932)
11. Buisson, X and Arnaud, R., Hydrothermal Growth of Quartz Crystals in Industry, Present Status and Evolution, *J. de Phesique* IV, 4[C_2]:25–32 (1994)
12. Taki, S., Improvement of Growth Process and Characterization of Quartz Crystals, in: The Role of Crystal Growth for Device Development (N. Nizeki, ed.) *Prog. Crystal Growth Charact. Mat.*, 23:313–339 (1991)
13. Laudise, R. A. and Nielsen, J. W., in: *Solid State Phys*., (F. Seitz and D. Turnball, eds), 12:149, Academic Press, New York (1961)
14. Ballman, A. A. and Laudise, R. A., in: *Art and Science of Growing Crystals* (J. J. Gilman, ed.), p. 231, Wiley, New York (1963)
15. Kuznetsov, V. A. and Lobachev, A. N., Hydrothermal Method for the Growth of Crystals, *Soviet Physics-Crystallography*, 17:775–804 (1973) (Translated English edition)
16. Armington, A. F., Recent Advances in the Growth of High Quality Quartz, in: *Hydrothermal Growth of Crystals* (K. Byrappa, ed.), *Prog. Crystal Growth Charact. Mat*., 21:97–111 (1990)

DropBooks

17. Byrappa, K., Hydrothermal Growth of Crystals, in: *Handbook of Crystal Growth* (D. T. J. Hurle, ed.), Vol. 2, Elsevier Science Publishers, The Netherlands, 464:562 (1994)
18. Schafhaul, K. F. E., *Gelehrte Anzeigen Bayer, Akad*., 20:557 (1845)
19. Nacken, R., Hydrothermal Syntheses als Grundlage fur Zuchtung von Quarzkristallen, *Chem. Z.*, 74:745–749, (1950)
20. Nacken, R., Artificial Quartz Crystals, etc., U.S. Office of Technical Services Report, PB-6948 (1946)
21. Nacken, R., Artificial Quartz Crystals, etc., U.S. Office of Technical Services Report, PB-18-748 and 28-897 (1946)
22. Laudise, R. A., Ballman, A. A., and King, J. C., Impurity Content of Synthetic Quartz and Its Effect Upon Mechanical Q, *J.Phys. Chem. Solids*, 26:1305–1308 (1965)
23. Laudise, R. A., Hydrothermal Crystal Growth—Some Recent Results, in: *Advanced Crystal Growth* (P. M. Dryburgh, B. Cockayne, and K. G. Barraclough, eds.), Prentice Hall, NewYork, 267–288 (1987)
24. Laudise, R. A. and Sullivan, R. A., Pilot Plant Production of Synthetic Quartz, *Chem. Engg. Prog.*, 55:55–59 (1959)
25. Barns, R. L., Kolb, E. D., Laudise, R. A., Simpson, E. E., and Kroupa, K. M., Production and Perfection of *'Z-face'* Quartz, *J. Crystal Growth*, 34:189–197 (1976)
26. Kirov, G. K., Initial Growth Stages of Man-made Quartz Crystals and Growth Mechanism of their (0001) Face, *Cryst. Res. Technol*., 27:335–342 (1992)
27. Brown, C. S., Internal Friction in Synthetic Quartz, *Proc. Phys. Soc*. (London), 75:459 (1960)
28. Chakraborty, D., Dependence of Mechanical Q on Growth Rate of Quartz Single Crystals, *J. Crystal Growth*, 41:177–180 (1977)
29. Lias, N. C., Grudenski, E. E., Kolb, E. D., and Laundise, R. A., The Growth of High Acoustic Q Quartz at High Growth Rates, *J. Crystal Growth*, 18:1–6 (1973)
30. Lipson, H. G. and Armington, A. F., Aluminum a-d Hydroxide Distribution in Cultured Quartz Grown from $^{+}$x Seeds, *J. Crystal Growth*, 80:51–59 (1987)
31. Christie, I. R. A., Croxall, D. F. and Isherwood, B. J., UK Patent 2079175B, (Dec. 7, 1983)
32. Armington, A. F., Larkin, J. J., O'Conner, J. J., Cormier, J. E., and Horrigan, J. A., *Proc. 35th Annual Frequency Symposium*, E1A, p. 297, Washington, D.C. (1981)
33. Armington, A. F. and Larkin, J. J., The Growth of High Purity, Low Dislocation Quartz. *J. Crystal Growth*, 71 :799–806 (1985).

34. Kolb, E. D., Nassau, K., Laudise, R. A., Simpson, E. E., and Kronpa, K. M., New Sources of Quartz Nutrient for the Hydrothermal Growth of Quartz, *J. Crystal Growth*, 36:93–100 (1976)
35. Hosaka, M. and Miyata, T., Hydrothermal Growth of α-Quartz Using High-Purity α-Cristobalite as Feed Material, *Mat. Res. Bull.*, 28:1201–1208 (1993)
36. Avakov, V. A. and Vinogradov, B. N., Solubility of SiO_2 Polymorphs, *Izv. Vyssh. Ucheb. Zaved., Khim. Teknol.*, 17:879–882 (1972)
37. U.S. Patent No. 4853198 (Aug. 1, 1989)
38. Hosaka, M., Synthesis of Micro α-Quartz Crystals by Hydrothermal Hot-Press Method, *J. Crystal Growth*, 112: 291 (1991)
39. Wooster, N. and Wooster, W. A. Preparation of Synthetic Quartz, *Nature*, 157:297 (1946)
40. Spezia, J. G., La Pressione e Chimicament Inattiva Nella Solubilita e Ricostituzione del Quarzo, Atti Accad. Sci. Torino Contribuzioni di Geologia Chimica, 40:254–262 (1905)
41. Shternberg, A. A., Controlling the Growth of Crystals in Autoclaves, in: Crystallization Processes under Hydrothermal Conditions (A. N. Lobachev, ed.), p. 225–240, Consultants Bureau, New York (1973)
42. Demianets, L. N., Emelyanova, E. N., and MelniKoV, O. K., Solubility of Sodalite in Aqueous Solutions of NaOH under Hydrothermal Conditions, in: Crystallization Processes under Hydrothermal Conditions (A. N. Lobachev, ed.), p. 125–150, Consultants Bureau, New York (1973)
43. Hosaka, M. and Taki, S., Hydrothermal Growth of Quartz Crystals in NaCl Solution, *J. Crystal Growth*, 100:343–346 (1990)
44. Laudise, R. A. and Ballman, A. A., The Solubility of Quartz under Hydrothermal Conditions, *J. Phys. Chem.*, 65:1396–1400 (1961)
45. Hosaka, M. and Taki, S., Hydrothermal Growth of Quartz Crystals in NaCl Solution, *J Crystal Growth*, 52:837–842 (1981)
46. Lafon, F. and Demazean, G., Pressure Effects on the Solubility and Crystal Growth of α - Quartz, *J. de Physique* IV, 4[C_2]:177–182 (1994)
47. Martin, J. J. and Armington, A. F., Effect of Growth Rate on Quartz Defects, *J. Crystal Growth*, 62:203–206 (1983)
48. Laudise, R. A., What is Materials Chemistry? in: *Materials for Nonlinear Optics (Chemical Perspectives)* (S. R. Marder, J. E. Sohn, and G. D. Stucky, eds.), *American Chemical Soc.*, p. 410–433, Washington D.C. (1991)
49. Yoshimura, J., Miyazaki, T., Wada, T., Kohra, K, Ogawa, T., and Taki, S., *J. Crystal Growth*, 46:691–700 (1979)
50. Iwasaki, F. and Kurashige, M., *J. Appl. Phys.*, 17:817–820 (1978)

BrightBooks

51. Johnson, G. R., Irvine, R. A., and Foise, J. W., A Parametric Study of the Variables Involved in Quartz Growth, *IEEE Proc. 44th Annual Symposium on Frequency Control,* p. 216–221 (1990)
52. Demazeau, G. and Lafon, F., Hydrothermal Crystal Growth of α - Quartz: New Specificities Correlated to Applications, *J. de Physique* IV, 4 [C_2]:13–18 (1994)
53. Lipson, H. G., Kahan, A., and O' Connor, J., Aluminum and Hydrogen Defect Centers in Vacuum Swept Quartz, *IEEE Proc. 37th Annual Symposium on Frequency Control*, p. 169–173 (1983)
54. Gualtieri, J. G., The Influence of Temperature and Electric Field on the Etch-Channel Density in Swept Cultured Quartz, *IEEE Proc. 39th Annual Symposium on Frequency Control*, p. 247–254 (1985)
55. Martin, J., Electro-Diffusion or Sweeping of Ions in Quartz, *IEEE Proc. 41st Annual Symposium on Frequency Control*, p. 167–174 (1987)
56. Fraser, B., in: *Physical Acoustics* (W. P. Mason, ed.), 5:54 (1968)
57. Bahadur, H., Sweeping and Irradiation Effects on Hydroxyl Defects in Crystalline Natural Quartz, *IEEE Trans. Ultrasonics, Ferroelectrics, and Frequency Control*, 41:820–833 (1994)
58. Zecchini, P., Yamni, K., and Viard, B., Modifications Induced by Sweeping and Observed in Quartz Crystals According to Their α_{3500}-Value, *J. de Physique* IV, 4 [C_2]:189–194 (1994)
59. Deleuze, M., Cambon, O., Goiffon, A., Ibanez, A., and Philippot, E., Controlled Dissolution of Quartz Material, Part I, Controlled Dissolution of Quartz Plates in Potassium and Sodium Hydroxides: Chemical Thinning Down of SC Cuts, *J. de Physique* IV, 4 [C_2]:79–84 (1994)
60. Brauer, K. and Muller, E., Correlation Between Parameters of Plastic Deformation in Doped NaCl Crystals, *Cryst. Res. Technol*., 19:K101–109 (1984)
61. Cambon, O., Deleuze, M., Michel, J. P., Aubry, J. P., Goiffon, A., and Philippot, E., Controlled Dissolution of Quartz Material, Part II, Quartz Chemical Etching Applied to Blanks Industrial Manufacturing, *J. de Physique* IV, 4 [C_2]:85–91 (1994)
62. Schwarzenbach, D., Verfeinezung der Struktur der Tiefquarz-Modification von $AlPO_4$, *Z. Krist.*, 123:161–185 (1966)
63. Chang, Z. P. and Barsch, G. R., Elastic Constants and Thermal Expansion of Berlinite, *IEEE, Trans. on Sonics and Ultrasonics*, 23:127–130 (1976)
64. O'Connell, R. M. and Corr, P. H. Temperature Compensated Cuts of Berlinite and β-Eucryptite: For Saw Devices, *Proc. 31st Annal. Freq. Control Symp*., p. 182–186 (1977)
65. Kolb, E. D., Glass, A. M., Rosenberg, R. L., Grenier, J. C., and Laudise, R. A., *Proc. 35th Ultrasonic Symp*., New York (1981)

66. US Patent 4,698, 318, Vogel, J., Holand, W., and Vogel, W. (1987)
67. Vogel, W, Vogel, J., Holand, W., and Wange, P., Development of Bioactive Silica-Free Phosphate Glass Ceramics for use in Medicine, wiss. Z. Friedrich Schiller Univ., *Jena, Math. Natur wiss. Reihe*, 36:841–854 (1987)
68. John, V. M. and Kordes, *Chem. of Earth*, 70:75–89 (1953)
69. Stanley, J. M., Hydrothermal Synthesis of Large Aluminum Phosphate Crystals, *Ind. and Eng. Chem.*, 468:1684–1689 (1954)
70. Mason, W. P. *Piezoelectric Crystals and their Application Ultrasonic*, Van Nostrand, New York, pp. 206 (1950)
71. Kolb, E. D. and Laudise, R. A., Hydrothermal Synthesis of Aluminum Orthophosphate, *J. Cryst. Growth*, 43:313–319 (1978)
72. Beck, W. R., Crystalographic Inversions of the Aluminum Orthophesphate Polymorphs and Their Relation to Those of Silica, *J. Amer. Ceram.* Soc., 32:147–153 (1949)
73. Sosman, R. S., *Phases in Silica*, Rutger University Press (1964)
74. Srikantaswamy, S., *Synthesis and Characterization of ABO_4 Crystals*, Ph.D. Thesis, Univ. of Mysore, Mysore, India (1988)
75. Byrappa, K. and Srikantaswamy, S., Recent Progress in the Growth and Characterization of Aluminum Orthophosphate Crystals, *Prog. Crystal Growth and Charact.*, 21:199–254 (1990)
76. Byrappa, K., Venkatachalapathy, V., and Puttaraj, B., Crystallization of Orthophosphate, *J. Mater. Sci.*, 19:2855–2862 (1984)
77. Byrappa, K., Srikantaswamy, S., Gopalakrishna, G. S., and Venkatachalapthy, V., Infrared Spectra of Aluminum Orthophosphate Crystals, *J. Mater. Sci. Letts.*, 5:203–205 (1986)
78. Laudise, R. A., *Crystal Growth of Electronic Materials*, (Kaldis, ed.) Elsevier Science Publ., pp. 159 (1985)
79. Chai, B. H. T., Shand, M. L., Bucher, I., and Gillee, M. A., *Proc. IEEE Ultrasonic Symp.*, pp. 557 (1979)
80. U.S.Patent, 4:234–733, Chai, B. H. T. (1982)
81. Croxall, D. F., Christie, L. R. A., Isherwood, B. J., Todd, A. G., and Brich, J., The Growth and Assessment of Berlinite Single Crystals, *Proc.2nd European Conf. on Crystal Growth*, Lancaster England, C 118 (Sept. 10–15, 1979)
82. Schulz, H. and Kluckou, R., in: *Crystal Growth* (H. S. Peiser, ed.), Pergamon Press, New York (1967)
83. Poignant, H., *Hydrothermal Synthesis of Berlinite*, Ph.D. Thesis Univ. of Rennes (1979)
84. Kolb, E. D., Grenier, J. C., and Laudise, R. A., Solubility and Growth of $AlPO_4$ in a Hydrothermal Solvent: HCl, *J. Crystal Growth*, 51:178–185 (1981)

DropBooks

85. Bryappa, K., Srikantaswamy, S., Gopalakrishna G. S., and Venkatachalapath, V., Influence of Admixtures on the Crystallization and Morphology of $AlPO_4$ Crystals, *J. Mater. Sci.*, 21:2202–2206 (1986)

86. Krauss, V. and Lehann, G., *Z. Naturforsch,* 309:28 (1975)

87. Detaint, J., Phillipport, E., Jumas, J. C., Schwartzel, J., Zarka, A., Capelle, B., and Doukhan, J. C., *39th Annual Frequency Control Symposium,* Phildelphia (1985)

88. Byrappa, K., Shashidhara J., Prasad, and Srikantaswamy, S., Growth and Properties of New Polymorphic Modification of $AlPO_4$, *J. Crystal Growth,* 79:232 (1986)

89. Jumas, J. C., Goiffon, A., Capelle, B., Zaraka, A., Doukhan, J. C., Schwartzel, J., Detaint, J., and Phillipot, F., Crystal Growth of Berlinite, $AlPO_4$: Physical Characterization and Comparison with Quartz, *J. Crystal Growth,* 80:133–148 (1987)

90. Poignant, H., Marechal, L. Le., and Toudic, Y., Etude De La Solubilite du Phosphate d'aluminium ($AlPO_4$) dans des Solutions Hydrothermales d'acide orthophosphoriaue H_3PO_4, *Mater. Res. Bull.*, 14:603–612 (1979)

91. Hasegawa, K., Minegishi, K., and Somiya, S., Effects of Starting Materials and Temperature on the Hydrothermal Synthesis of Aluminum Orthophosphate, *Proc. Ist International Symposium of Hydrothermal Growth,* Tokyo, pp. 509–518 (1982)

92. Yaroslavskii, I. M. and Popolitov, V. I., Growth of Single Crystals of Aluminum Monophosphate (Berlinite), *Izv. Akad. Nauk SSSR,* Neorg. Materialy, 26:1055–1059 (1990)

93. Capulle, B., *Appl. Cryst.*, 18:533–534 (1985)

94. Detaint, H., Poignant, and Toudic, Y., Experimental Thermal Behavior of Berlinite Resonators, *24th Symposium on Frequency Control,* 28–30 (May, 1980)

95. Steinberg, R. F., Roy, M. K., Ester, A. K., Chai, B. H. T., and Morris, R. C., *Ultrasonic Symposium,* Dallas, USA, 14–16 (Nov. 1984)

96. Laudise, R. A., *The Growth of Single Crystals*, p. 109, Prentice Hall, Engelwood Cliffs, N. J. (1970)

97. Laudise, R. A, *Treatise on Solid State Chemistry*, 5:109 (N. B. Hanvy, ed.), Plenam, New York (1970)

98. Detaint, J., Philippot, E., Jumas, J. C., Schwartzel, J., Zarka, A., Capelle, B. and Doukhan, J. C., Crystal growth, Physical Characterization and BAW Devices Applications of Berlinite, 3th Annual Frequency Control Symposium, Philadelphia, USA (May 29–31, 1985)

99. Morris, R. C., Chai, B. H. T., Imperfect Low-Angle Boundaries and Fracture in Hydrothermally Grown Berlinite Crystals, *J. Crystal Growth,* 191:108–112 (1998)

100. Byrappa, K., Srikantaswamy, S., Gopalakrishna, G. S., and Venkatachalapathy, V., Influence of Admixtures on the Alpha-Beta Berlinite Inversion, *J. Mater. Sci. Letts*., 5:347–348 (1986)

101. Troccaz, M., Berger, C., Richard, M., and Byraud, L., Etude de la transformation de phase α–β de la variété «Phosphoquartz» de l'orthophosphate d'aluminium $AlPO_4$, *Bull. Soc. Chim. de France*, 11:4256 (1967)

102. Lang, R., Datars, W. R., and Calvo, C., *Phys. Letts*., 30A:340 (1969)

103. Byrappa, K. and Prahallad, U. D., Thermal Expansion of Berlinite, *J. Mat. Sci. Letts*., 8:1667–1669 (1989)

104. Ballato, A. D. and Iafrate, G. J., The Angular Dependence of Piezoelectric Plate Frequencies and Their Temperature Coefficients, *Proc. 30th Frequency Control Symposium*, pp. 141–156 (1976)

105. Bechman, R., Ballato, A. D., and Lukaszek, T. T., High Order Temperature Coefficients of the Elastic Stiffness and Compliance of α-Quratz, *Proc. IREE*, 30:1812 (1982)

106. Shannon, R. D., Vega, A. J., Chai, B. H. T., and Rossman, G. R., Effect of H_2O on Dielectric Properties of Berlinite: I. Dielectric Constant, *J. Phys. D; Appl. Phys*., 26:93–100 (1993)

107. Fontanella, J. J., Wintersgill, M. C., Shannon, R. D., and Chai, B. H. T., Effect of H_2O on Dielectric Properties of Berlinite: II. Dielectric Loss, *J. Phys. D; Appl. Phys*., 26:101–105 (1993)

108. Thompson, W. K., Infrared spectroscopic studies of aqueous systems, I. *Trans. Faraday Soc*., 61:1635–1640 (1964)

109. Philippot, E., Palmier, D., Pintard, M., and Goiffon, A., A General Survey of Quartz and Quartz-Like Materials: Packing Distortions, Temperature and Pressure Effects, *J. Solid State Chem*., 123:1–13 (1996)

110. Hirano, S., Miwa, K. and Naka, S., Growth of Gallium Orthophosphate Crystals, *J. Crystal Growth* 79:215–218 (1986)

111. Nakae, H., Kihara, K, Okuno, M. and Hirano, S., The Crystal Structure of The Quartz-Type Form of $GaPO_4$ and Its Temperature Dependence, *Zeit. Krist.*, 210:746–753 (1995)

112. Hirano, S. and Kim, P., Physical Properties of Hydrothermally Grown Gallium Orthophosphate Single Crystals, *J. Mat. Sci.*, 25:4772–4775 (1990)

113. Hirano, S., Kim, P., and Orihara, H., Dielectric Properties of Hydrothermally Grown Gallium Orthophosphate Single Orgstals, *J. Mat. Sci.*, 25:2800–2804 (1990)

114. Cochez, M., Ibanez, A., Goiffon, A., and Philippot, E., Crystal Growth and Infrared Characterization of $GaPO_4$ in Phospho-Sulphuric Media, *Eur. J. Solid State Inorg. Chem.*, 30:509–519 (1993)

PrepBooks

115. Foulon, J. D., Giuntin, J. C., and Philippot, E., Dielectric Properties of an α-Quartz Type Material: $GaPO_4$, *Eur. J. Solid State Inorg. Chem.*, 31:245–256 (1994)

116. Hirano, S., Kim, P., and Orinara, H., Dielectric Properties of Hydrothermally Grown Gallium Orthophosphate Single Crystals, *J. Mat. Sci.*, 25:2800–2804 (1990)

117. Cochez, M., Foulon, J. D., Ibanez, A., Goiffon, A., Philippot, E., Cappelle, B., Zarka, A., Schwartzed, J., and Detaint, J., Crystal Growth and Characterization of A Quartz-Like Material: $GaPO_4$, *J. de Physique* IV, 4[C_2]:183–188 (1994)

118. Capelle, B., Zarka, A., Schwartzel, J., Detaint, J., Philippot, E., and Denis, J. P., Characterization of Piezoelectric Materials: Old and New Crystals, *J. de Physcique* IV, 4[C_2]:123–134 (1994)

119. Zvereva, O. V. and Mininzon, Yu-M., Growth Elucidation of Gallium Orthophosphate Under Hydrothermal Conditions, *Kristallografia*, 37:1051–1054 (1992)

120. Popolitov, V. I. and Yaroslavskii, I. M., Crystallization of Gallium Monophosphate, *Izv. Akad. Nauk SSSR*, Neorg. Materialy, 26:892–894 (1990)

121. Zvereva, O. V., Mininzon, Yu, M., and Demianets, L. N., Hydrothermal Growth of OH^- free $AlPO_4$ and $GaPO_4$ Crystals the Way of Twin Reducing, *J. de physique* IV, 4[C_2]:19– 24 (1994)

122. Shigarov, A. S., Zvereva, O. V., and Mininzon, Yu. M., Investigation of the Solubility of Gallium Orthophosphate, $GaPO_4$ Under Hydrothermal Conditions, *Kristallografia*, 39:717–719 (1994)

123. Zumsteg, F. C., Bierlein, J. D., and Gier, T. E., K_xRb_{1-x} $TiOPO_4$ A New Nonlinear Optical Material, *J. Appl. Phys.*, 47:4980–4985 (1976)

124. Ashkin, A., Boyd, G. D., Dziedzic, J. M., Smith, R. E., Ballman, A. A., Levinstein, J. J., and Nassau, K., Optically-Induced Refractive Index in Homogeneities in $LiTaO_3$ and $LiNbO_3$, *Appl. Phys. Letts.*, 9:72–77 (1966)

125. Okada, M. and Ieiri, S., Influence of Self-induced Thermal Effects on Phase Matching in Nonlinear Optical Crystals, *IEEE J. Quantum Electron*, QE-7:560–563 (1971)

126. US Patent, 3,949, 323, Bierlein, J. D., Assigned to E. I. Du Pont de Nemours and Company (Apr. 6, 1976)

127. US Patent, 4,231,838, Gier, T. E., Assigned to E. I. Du Pont de Nemours and Company (Nov. 4, 1980)

128. Tordjman, I, Masse, R., and Guitel, J. C., Structure Cristalline du Monophosphate $KTiPO_5$, *Z. Kristallogr.*, 139:103–115 (1974)

129. Ouvard, L., Compt. Rend. (Paris) 121:117 (1890), as reported in The Gmelin Handbook, Vol. 41, T, 8th ed. (1951)

130. Masse, R., and Grenier, J. C., Phase Transformation of $AlPO_4$:Fe^{3+} by Electron Paramagentic Resonance, *Bull. Soc. France. Mineral. Crist*., 94:437 (1971)

131. US Patent 3,949,323, Bierlien, J. D. and Gier, T. E. (Apr. 6, 1976)

132. Liu, Y. S., Drafall, L., Dentz, D., and Belt, R., Nonlinear Optical Phase-Matching Properties of $KTiOPO_4$ (KTP), G.E. Tech. Inf. Series Rep. No. 82 CR DO16, General Electric Company, Schenectady, New York (1982)

133. Liu, Y. S., Dentz, D., and Belt, R., High-Average-Power Intracavity Second-Harmonic Generation Using $KTiOPO_4$ in an Acousto-Optically Q-Switched Nd: YAG Laser Oscillator at 5 KHz, *Opt, Lett*., 9:76 (1984)

134. Laudise, R. A., Cava, R. J., and Caporaso, A. J., Phase Relations, Solubility and Growth of Potassium Titanyl Phosphate, KTP, *J. Cryst. Growth*, 74:275–281 (1986)

135. Laudise, R. A., Hydrothermal Crystal Growth—Some Recent Results, in: *Advanced Crystal Growth* (P. M. Dryburgh, B. Cockayne, and K. G. Barraclough, eds.) p. 267–286, Prentice Hall, New York (1987)

136. US Patent 4654111, Laudise, R. A. (March 31, 1987)

137. Belt, R. F., and Iradi, T., Hydrothermal Growth Produces Large KTP Nonlinear Crystals, *Laser Focus World*, p. 155–162 (Nov. 1993)

138. Laudise, R. A., Sunder, W. A., Belt, R. F., and Gashurov, G., Solubility and *P-V-T* relations and the Growth of KTP, *J. Crystal Growth*, 102:427–433 (1990)

139. Belt, R. F., Low Temperature Hydrothermal Growth of Potassium Titanyl Phosphate (KTP) in 4 liter Autoclaves, Extended Abstract ICCG-9, p. 428, Sendai, Jpn. (Aug. 20–25, 1989)

140. Byrappa, K., Board of Res. in Nuclear Sciences, *Dept. of Atomic Energy, Tech. Report*, p. 4, Bombay (1996)

141. Gettemy, D. J., Harker, W. C., Lindholm, G., and Barnes, N. P., Some Optical Properties of KTP, $LiIO_3$, and $LiNbO_3$, *IEEE. J. Quantum Electronics*, 24:2231–2237 (1988)

142. Bierlein, J. D., Ferretti, A., Brixner, L. H., and Hsu, W. Y., Fabrication and Characterization of Optical Wave Guides in $KTiOPO_4$, *Appl. Phys. Letts*., 50:1216–1219 (1987)

143. Van der Poel, C. J., Bierlein, J. D., Brown, J. B., and Colak, S., *Appl. Phys. Letts*, 57:2974–2977 (1990)

144. Bierlein, J. D., Vanherzeele, H., and Ballman, A., Linear and Nonlinear Optical Properties of Flux Growth KTP, *Appl. Phys. Letts*., 54:783–787 (1989)

145. Brahimi, M. and Durand, J, Structure et propriétés d'optique nonlinéaire de $KTiOAsO_4$, *J. Rev. Chim. Mineral*, 23:146–148 (1986)

ProBooks

146. Belt, R. F. and Ings, J. B., Hydrothermal Growth of Potassium Titanyl Arsenate (KTA) in Large Autoclaves, *J. Cyrstal Growth*, 128:956–962 (1993)

147. Cheng, L. K., Cheng, L. T., Galperin, J., Morris Hotsenpiller, P. A., and Bierlein, J. D., Crystal Growth and Characterization of $KTiOPO_4$ Isomorphs from the Self-fluxes, *J. Crystal Growth*, 137:107–115 (1994)

148. Chani, V. I., Shimamura, K., Endo, S., and Fukuda, T., Substitution of Ti^{4+} with Nb^{5+}- M^{3+} (M = Al, Cr, Ga, Fe, In) in Crystals of $KTiOAsO_4$, *J. Crystal Growth*, 17:117–122 (1997)

149. Deer, W. A., Howie, R. A., and Zussman, J., *An Introduction to the Rock-Forming Minerals*, p. 473, Longman Group Limited, England (1966)

150. Kinloch, D. R., Belt, R. F., and Puttbach, R. C., Hydrothermal Growth of Calcite in Large Autoclaves, *J. Crystal Growth*, 24/25:610–613 (1974)

151. Hirano, S. and Kikuta, K., Solubility and Hydrothermal Growth of Calcite Single Crystals in Hitrate Solutions, *J. Crystal Growth*, 79:223–226 (1986)

152. Lemberg, J., Ueber silicatumwandlungen, Z. *Deut. Geol. Ges*., 35:557–618 (1883)

153. Friedel, C. and Sarasin, E., *Bull. Soc. Min*., 8:304–305 (1885)

154. Gruzensky, P. M.., in: *Crystal Growth* (H. S. Peiser, ed.) p. 365, Pergamon, Oxford (1967)

155. Kaspar, J., in: *Growth of Crystals*, Vol. 2, Consultants Bureau, New York (1959)

156. Morse, H. and Donnay, D. H., *Bull. Soc. Franc. Mineral*, 54:19–25 (1931)

157. Nickl, H. J. and Henisch, H. K., Growth of Calcite Crystals in Gels, *J. Electrochem. Soc*., 116:1258–1264 (1969)

158. Nester, J. F. and Schroeder, J. B., Growth of Synthetic Calcite Single Crystals, *Am. Mineralogist*, 52:276–280 (1967)

159. Belin, C., Brissot, J. J., and Jesse, R. F., The Growth of Calcite Single Crystals by Travelling Solvent Zone Melting, *J. Crystal Growth*, 13/14:597–600 (1972)

160. Balascio, J. F. and White, W. B., Growth of Single Crystal Calcite by Top-Seeded Solution Growth Technique, *J. Crystal Growth*, 23:101–105 (1974)

161. Belin, C., On the Growth of Large Single Crystals of Calcite by Travelling Solvent Zone Melting, *J. Crystal Growth*, 34:341–345 (1976)

162. Yamasaki, N. and Weiping, T., Hydrothermal Hot Pressing of Calcium Carbonate with Sea Water, *J. Mat. Sci. Letts*., 12:516 –519 (1993)

163. Yamasaki, N., Weiping, T., and Yanagisawa, K., Solidification of $CaCO_3$ Containing $SrCO_3$ by Hydrothermal Hot Pressing, *J. Mat. Res*., 8:1972–1976 (1993)

164. Yamasaki, N., Weiping, T., Lei, H., and Hosoi, K., Solidification of Aragonite-type $CaCO_3$ Powder Containing Chitosan with Acetic Acid by Hydrothermal Hot Pressing, *J. Mat. Sci. Letts.*, 14:1751–1753 (1995)

165. Ikornikova, N. Yu., Growth Characteristics of Calcite Crystals in Aqueous Solutions of Carbonic Acid, in: *Crystallization Processes under Hydrothermal Conditions* (A. N. Lobachev, ed.), pp. 93–112, Consultants Bureau, New York (1973)

166. Ikornikova, N. Yu., *Hydrothermal Synthesis of Crystals in Chloride Systems* (in Russian), pp. 1–222, Nauka, Moscow (1975)

167. Higuchi, M., Takeuchi, A., and Kodaira, K., Hydrothermal Growth of Calcite Single Crystals from H_2O-CO_2-$CaCO_3$ System, *J. Crystal Growth*, 92:341–343 (1988)

168. Hirano, S. and Kikuta, K., Hydrothermal Growth of Calcite Single Crystal in $Ca(NO_3)_2$ and NH_4O_3 Solutions, *J. Crystal Growth*, 94:351–356 (1989)

169. Higuchi, M., Miyauchi, D., Takeuchi, A., and Kodaira, K., Hydrothermal Growth of Calcite Single Crystals from H_2O-CO_2-$CaCO_3$ System under Controlled CO_2 Pressure, *J. Crystal Growth*, 110:39–43 (1992)

170. Yanagisawa, K., Feng, Q., Ioku, K., and Yamasaki, N., Hydrothermal Single Crystal Growth of Calcite in Ammonium Acetate Solution, *J. Crystal Growth*, 163:285–294 (1996)

171. Hirano, S., Yogo, T., Kikuta, K. and Yoneta, Y., Hydrothermal Growth of Calcite Crystals in Nitrate Solutions, *J. Ceram. Soc. Jpn.*, 101:113–117 (1993)

172. Malinin, S. D., in: *Geochemical Investigations at High Temperatures and Pressures*, p. 48, Nauka, Moscow (1965)

173. Ellis, A. I., The Solubility of Calcite in NaCl Solutions at High Temperatures, *Amer. J. Sci.*, 261:259–267 (1963)

174. Kikuta, K. and Hirano, S., Hydrothermal Growth and Dissolution Behaviour of Calcite Single Crystal in Nitrate Solutions., *J. Crystal Growth*, 99:895–899 (1990)

175. Lee, Y-K., Chung, S. J., Hydrothermal Growth of Calcite Single Crystals in NH_4Cl Solution, *J. Crystal Growth*, 192:350–353 (1998)

176. Gorai, M. and Syuutou, K., in: *Tikaku Ganseki Koukutsu*, p. 123, Kyuyitsu Publishing House, Jpn. (1981)

177. Ikornikova, N. Yu., Formation and Crystal Growth of Trigonal Carbonates, in: *Hydrothermal Synthesis of Crystals*, pp. 114–140, Nauka, Moscow, (1968)

178. Ikornikova, N. Yu., Crystal Growth Elucidation of the Calcite Crystals in Aqueous Solutions of HCl, in: *Investigations of the Crystallization Processes under Hydrothermal Conditions*, pp. 85–102, Nauka, Moscow (1970)

DropBooks

179. Ikornikova, N. Yu., *Hydrothermal Synthesis of Crystals in Chloride Systems*, p. 220, Nauka, Moscow (1975)

180. Deer, W. A., Howie, R. A., and Zussman, J. (eds.), *Rock-Forming Minerals*, Vol. 5: *(Non-Silicates)* Longmans, Green and Co. Ltd., pp. 323–338 (1962)

181. Simpson, D. R., Problems of the Composition and Structure of the Bone Minerals, *Clin. Ortho. Relat. Res.*, 86:260–286 (1972)

182. Holcomb, D. W. and Young, R. A., Thermal Decomposition of Human Tooth Enamel, *Calcif. Tissue Int.*, 31:189–201 (1980)

183. Waggaman, W. H., *Phosphoric Acid, Phosphates and Phosphatic Fertilizers, 2nd ed.*, p. 3, Reinhold Publishing Corp., New York (1952)

184. Toy, A. D. F., The Chemistry of Phosphorus, in: *Inorganic Chemistry*, Vol. 3., Pergamon Press (1973)

185. Daubree, A. Experiences sur la production artificielle de l'apatite, de latopaze, et de quelques autres métaux fruoriféres, *Compt. Rend. Acad. Sci. Paris*, 32:625 (1851)

186. Ducheyne, P., Kokubo, T., and Van Blitterswijk, C. A., (eds.), *Bone-Bonding Biomaterials*, Rees Healthcare Communications (1992)

187. Aoki, H., *Science and Medical Applications of Hydroxyapatite*, Japanese Association of Apatite Science, JAAS (1991)

188. Hench, L. L., Bioceramics: From concept to clinic, *J. Am. Ceram. Soc.*, 74:1487–1510 (1991)

189. Yanagisawa, K., Toya, H., Feng, Qi, and Yamasaki, N., *In-situ* formation of HApcrystals under hydrothermal conditions, *Phosphorus Res. Bull.*, 5:43–46 (1995)

190. Kanazawa, T. (ed.), *Inorganic Phosphate Materials*, Elsevier Science Publishers, p. 15, Amsterdam (1989)

191. Yoshimura, M. and Suda, H., Hydrothermal Processing of Hydroxyapatite: Part, Present and Future, in: *Hydroxyapatite and Related Materials* (P. W. Brown and B. Constanz, eds.), CRC Press, Inc., pp. 45–72 (1994)

192. Mc Cauley, J. W. and Roy, R., Controlled Nucleation and Crystal Growth of Various Calcium Carbonate Phases by the Silica Gel Technique, *Am. Miner.*, 59:947–963 (1974)

193. Johnson, P. D., Some Optical Properties of Powder and Crystal Holophosphatephosphorous, *J. Electrochem. Soc.*, 108:159–162 (1961)

194. Prener, J. S., The Growth and Crystallographic Properties of Calcium Fluor- and Chlorapatite Crystals, *J. Electrochem. Soc.*, 114:77–83 (1967)

195. Oishi, S., and Kamiya, T., High-Temperature Solution Growth of Chlorspodiosite and Chlorapatite Crystals, *J. Chem. Soc. Jpn.*, 10:1129–1132 (1993)

196. Oishi, S. and Kamiya, T., Flux Growth of Fluorapatite Crystals, *J. Chem. Soc. Jpn.*, 9:800–804 (1994)

197. Oishi, S. and Sugiura, I., Growth of Chlorapatite Crystals from a Sodium Chloride Flux, *Bull. Chem. Soc. Jpn.*, 70:2483–2487 (1997)

198. Masuda, Y., Matsubara, K., and Sakka, S., Synthesis of HAp from Metal Alkoxides Through Sol-Gel Technique, *J. Ceram. Soc. Jpn.*, 98:1255–1266 (1990)

199. Brendel, T., Engel, A., and Russel, C., Hydroxyapatite Coating by a Polymeric Route, *J. Mater. Sci., Mater. Med.*, 3:175–179 (1992)

200. Náray-Szabo, S., The Structure of Apatite $(CaF)Ca_4(PO_4)_3$, *Zeit. Krist.*, 75:387–398 (1930)

201. Mehmel, M., Uber die Struktur des Apatits, *Zeit. Krist.*, 75:323–331 (1930)

202. Hendricks, S. B., Jefferson, M. E., and Mosley, V. M., The Crystal Structures of Some Natural and Synthetic Apatite-like Substances, *Zeit. Krist.*, 81:352 (1932)

203. Posner, A. S., Perloff, A., and Diorio, A. F., Refinement of the Hydroxyapatite Structure, *Acta Cryst.*, 11:308–309 (1958)

204. Kay, M. I., Young, R. A., and Posner, A. S., Crystal Structure of Hydroxyapatite, *Nature*, 204:1050–1052 (1964)

205. Elliott, J. C., The Problems of the Composition and Structure of the Mineral Components of the Hard Tissues, *Clin. Ortho. Relat. Res.*, 93:313–345 (1973)

206. Elliott, J. C., Mackie, P. E., and Young, R. A., Monoclinic Hydroxyapatite, *Science*, 180:1055–1057 (1973)

207. Van Rees, H. B., Mengeot, M., and Kostiner, E., Monoclinic-Hexagonal Transition in Hydroxyapatite and Deuterohydroxyapatite Single Crystals, *Mat. Res. Bull.*, 8:1307–1310 (1973)

208. Van Wazer, J. R., *Phosphorus and its Compounds*, Vol. 1, *Chemistry*, Wiley-Interscience, New York (1958)

209. Brown, P. W., Phase Relationships in the Ternary System $CaO\text{-}P_2O_5\text{-}H_2O$ at 25°C, *J. Am. Ceram. Soc.*, 75(1):17–22 (1992)

210. Brown, P. W., Hocker, N., and Hoyle, S., Variations in Solution Chemistry During the Low-Temperature Formation of Hydroxyapatite, *J. Am. Ceram. Soc.*, 74(8):1848–1854 (1991)

211. Biggar, A. M., *Min. Mag.*, 35:1110–1115 (1966)

212. Feng, S. S. and Rockett, T. J., The System $CaO\text{-}P_2O_5\text{-}H_2O$ at 200°C, *J. Amer. Ceram. Soc.*, 62:619–620 (1979)

213. Skinner, H. C. W., Studies in the Basic Mineralizing System, $CaO\text{-}P_2O_5\text{-}H_2O$, *Calcif. Tiss. Res.*, 14:3–4 (1974)

DropBooks

214. Eysel, W. and Roy, D. M., Hydrothermal Flux Growth of Hydroxyapatites by Temperature Oscillation, *J. Crystal Growth*, 20:245-250 (1973)

215. Andrade, M. C., Ogasawara, T., and Silva, F. T., Hydrothermal Crystallization of HAp, in: *Proc 2nd Int. Symp. Apatite*, 2:41–47 (1997)

216. Morey, G. W. and Ingerson, E., The Pneumatolitic and Hydrothermal Alteration and Synthesis of Silicates, *Econ. Geol*., 32:607–760 (1937)

217. Hayek, E., Lechtleitner, J., and Bohler, W., Hydrothermal Synthesis of Hydroxylapatite, *Angew. Chem*., 67:326 (1955)

218. Perloff, A. and Posner, A. S., Preparation of Pure Hydroxyapatite Crystals, *Science*, 124:583–584 (1956)

219. Jullmann, H. and Mosebach, R., Zur Synthese, Licht-und Doppelbrechung des Hydroxylapatits, *Naturforsch*, 21B:493–494 (1966)

220. Kirn, J. F. and Leidheiser, H., Jr., Progress in Efforts to Grow Large Single Crystals of Hydroxyapatite, *J. Cryst. Growth*, 2:111–112 (1968)

221. Roy, D. M., Crystal Growth of Hydroxyapatite, *Mat. Res. Bull.*, 6:1337–1340 (1971)

222. Mengeot, M., Harvill, M. L., and Gilliam,O. R., Hydrothermal Growth of Calcium Hydroxyapatite Single Crystals, *J. Cryst. Growth*, 19:199–203(1973)

223. Eysel, W. and Roy, D. M., Hydrothermal Flux Growth of Hydroxyapatites by Temperature Oscillation, *J. Cryst. Growth*, 20:245–250 (1973)

224. Aoki, H., Kato, K., and Shiba, M., Synthesis of Hydroxyapatite Under Hydrothermal Conditions, in: Kinetic Analysis of the Reaction Process from Monetite into Hydroxyapatite, *J. Dent. Apparatus and Materials*, 13(27):170–176 (1972)

225. Arends, J., Schuthof, J., van der Linden, W. H., Bennema, P., and van en Berg, P. J., Preparation of Pure Hydroxyapatite Single Crystals by Hydrothermal Recrystallyzation. *J. Crystal Growth*, 46:213–220 (1979)

226. Ito, A., Nakamura, S., Aoki, H., Akao, M., Teraoka, K., Tsutsumi, S., Onuma, K., and Tateishi, T., Hydrothermal Growth of Carbonate-Containing Hydroxyapatite Single Crystals, *J. Crystal Growth*, 163:311–317 (1996)

227. Ito, A., Teraoka, K., Tsutsumi, S., and Tateishi, T., Single Crystal Hydroxyapatite: Preparation, Composition and Mechanical Properties, *Bioceramics*, 9:189–192 (1996)

228. Kikuchi, M., Yamazaki, A., and Otsuka, R., Crystal Structure of Sr-Substituted HAp, Synthesized by Hydrothermal Method, *J. Solid State Chem*., 113:373–378 (1994)

229. Hata, M. and Marumo, F., Synthesis and Superstructure of $(Ca,M)_5(PO_4)_3OH$ (M = Mn, Fe,Co,Ni,Cu,Hg), *Miner. J*., 11:317–330 (1983)

230. Nagata, F., Yokogawa, Y., Toriyama, M., Kawamoto,Y., Suzuki, T., and Nishizawa, K., Hydrothermal Synthesis of HAp Crystals in the Presence of Methanol, *J. Ceram. Soc., Jpn.*, 103:70–73 (1995)

231. Vereecke, G. and Lemaitre, J., Calculation of the Solubility Diagram in the System $Ca(OH)_2$-H_3PO_4-KOH-HNO_3-CO_2-H_2O, *J. Crystal Growth*, 104:820–832 (1990)

232. Onuma, K., Kanzaki, N., Ito, A., and Tateishi, T., Growth Kinetics of the HAp (0001) Face Revealed by Phase Shift In Terferometry and Atomic Force Microscopy, *J. Phys. Chem. B.*, 102:7833–7838 (1998)

233. Kanzaki, N., Onuma, K., Ito, A., Teraoka, K., Tateishi, T., and Tsutumi, S., Direct Growth Rate Measurement of HAp Single Crystal by Moire Phase Shift Interferometry, *J. Phys. Chem. B.*, 102:6471–6476 (1998)

DropBooks

6

Hydrothermal Synthesis and Growth of Zeolites

6.1 INTRODUCTION

Zeolites form an important group of hydrated aluminosilicate minerals of the alkalies and alkaline earths, with an infinitely three-dimensional anion network and with the atomic ratio O:(Al + Si) = 2. The history of zeolites began with the discovery of stilbite in 1756 by a Swedish mineralogist, A. F. Crönstedt, who heated this silicate mineral, which fused readily with marked intumescence. The name zeolite signifies *boiling stone,* the meaning derived from the two Greek terms, z*ein*, to boil, and *lithos*, stone, an allusion to the intumescence of most zeolites with a borax lead, and refers to the frothy mass which will result when a zeolite is fused in the blowpipe. Volatile zeolitic water forms bubbles within the sinter or melt.[1][2]

Zeolite minerals were first recognized as minor, but were later regarded as widespread components in amygdales and fissures, chiefly in basic volcanic rocks. They are also found in veins and other later-stage hydrothermal environments. Big crystals of zeolites can develop in these amygdales and fissures through the mineralizing action of trapped or circulating solutions on the alkaline matrix. It is these crystals which, because of their

beauty and diversity of form, usually comprise zeolite collections.[3] Zeolites are also found in some igneous rocks and occur as alteration products of aluminosilicates, such as the felspars or felspathoids. Their occurrence is not just restricted to basalt matrices, although the scale and variety of natural depositions has been appreciated only over the last three decades. They occur as authigenic minerals in sandstones and other sedimentary rocks. Loew (1875) reported chabazite in a sedimentary tuff bed near Bowie, Arizona.[4] Similarly, Murray and Renard (1891) reported the presence of zeolites in marine sediments. Several kinds of zeolites were identified by Coombs (1954).[5]

6.2 MINERALOGY OF ZEOLITES

Zeolites belong to the tectosilicates group covering the felspars and felspathoid family of minerals. However, the structure of felspars is a more compact framework, with or without relatively small cavities. Thus, the cations and framework are strongly interdependent so that the cations cannot easily move unless framework bonds are broken, and replacement of Na or K by Ca necessarily involves a change in the Si:Al ratio, whereas the structure of felspathoids have more open framework so that the ions can be moved, removed, or interchanged through the channels/cavities without disturbing the framework. The cavities are usually filled with water molecules.

PropBooks

Finally, the zeolites' structures contain larger cavities/channels and, therefore, many exhibit, to a greater extent, the properties of ion exchange and molecular adsorption. Further, these cavities or channels in zeolites are usually filled with water molecules. These are relatively loosely bound to the framework and cations and, like the cations, these can also be removed and replaced without disrupting framework bonds. Accordingly, the felspars are anhydrous aluminosilicate minerals with a density of 2.6–2.7, followed by felspathoids (density 2.3–2.5) and zeolites (density 2–2.3). The hardness decreases from felspar to the zeolite end of the minerals owing to the above stated structural features. Thus, the characteristic feature of zeolite mineralogy is the presence of OH^- molecules in the structural channels, which are loosely bonded to the cation framework. The cations can be removed and replaced by other metals without disrupting framework bonds.

There are over 46 naturally occurring zeolite minerals, belonging to some major structure types. The channel systems in various zeolites are formed by different combinations of linked rings of tetrahedra. The wider the

channels at their narrowest parts, the larger the cation that can be introduced into the structure. A grading of the zeolites according to the openness of structure is given in Table 6.1.

Table 6.1. Numbers of Tetrahedra in Rings and Approximate Diameters of Channels in Various Felspathoids and Zeolites

Minerals	No. of Tetrahedra in Rings	Minimum Diameter of Widest Channel
Sodalite, Nosean	4 and 6	2.2 Å
Analcite4 and 6	2.2 Å	
Harmotome, Phillipsite	4 and 8	3.2 Å
Levyne	4, 6, and 8	3.2 Å
Erionite	4, 6, and 8	3.6 Å
Chabazite	4, 6, and 8	3.9 Å
Heulandite	5, 6, and 8	—
Gmelinite	4, 6, 8, and 12	6.4 Å
Faujasite	4, 6, and 12	9 Å

When zeolites are heated, water is given off continuously rather than in separate stages at definite temperatures and the dehydrated or partially dehydrated mineral can reabsorb water to its original amount when it is again exposed to water vapor. Dehydrated zeolites can also absorb other liquids or vapors in place of water, e.g., ammonia, alcohol, NO_2, H_2S, etc. The base-exchange properties of zeolites were first reported by Eichorn (1858) and have been reviewed by Hey (1930) who also investigated in detail the base-exchange of various members of the group.[6][7] The colloidal properties of the zeolites have been reviewed by Marshall (1949).[8] McBain (1954) introduced a new term, *molecular sieve*, to zeolites to describe porous materials which can act as sieves on a molecular scale, not just limited to aluminosilicate zeolites but to a large number of other zeolites like alumniophosphate zeolites, vanadophosphophosphate zeolites, titanophosphate zeolites, etc.[9] The zeolites and related materials, like phosphate-based molecule sieves, are microporous solids with a broad range of physicochemical properties, which are listed in Table 6.2.[10]

Table 6.2. Physicochemical Properties of Zeolites and Molecular Sieves[10]

Property	Range
Pore size	~ 4–13 Å
Pore shape	Circular, elliptical
Dimensionality of pore system	1-D, 2-D, 3-D
Pore configuration	Channels, cages
Surface properties	Hydrophilic, hydrophobic (high silica)
Void volume	Less than ~50%
Framework oxide compostion	Si, Al, P, Ga, Ge, B, Be, Zn:minor Ti, Fe, Co, Cr, V, Mg, Mn:minor

The commercial success of molecular sieves is largely due to the continual discovery of new materials whose diverse properties have allowed process improvements and the development of new technologies. Thus, the ability to control the materials' properties through synthetic efforts has been and will continue to be of paramount importance. Davis and Lobo (1992) and Feijen, et al. (1994) have reviewed the recent applications of zeolites.[10][11] Accordingly, the zeolites are no longer of interest to only those who are working in ion exchange. Distinction between the microscopic structure and the macroscopic properties of these materials allows one to use molecular sieves to recognize, discriminate, and organize molecules with a precision that can be < 1 Å. Also, it has expanded to other exciting areas such as supramolecular catalysis, photochemistry, nanochemistry, and electrochemistry. In this chapter, the major developments in the field of zeolites, covering aspects of their crystallization mechanism and applications, are discussed.

DropBooks

6.3 CRYSTAL CHEMISTRY OF ZEOLITES

There are 46 known zeolite minerals in nature and over 150 synthetic zeolites known in the literature. The number of synthetic zeolites is increasing day by day, particularly after the discovery of aluminophosphate zeolites by Wilson et al. (1982).[12] Despite the remarkable structural diversity in aluminophosphate zeolites, the product compositions are very similar:

$$xR + Al_2O_3 + (1.0–0.2)\ P_2O_5 + yH_2O$$

where *R* is an amine or quaternary ammonium ion. This organic species seems to exert a unique structure directing influence during crystallization of zeolites. Actually, when the first atlas of zeolite structure types was published in 1970, some twenty-seven zeolite structure types were reported.[13] During 1978, the structure commission of IZA published about thirty-eight entries in the *Atlas of Zeolite Structure Types* by Meier and Olson.[14] Later, in 1987, the 2nd edition of *Atlas*, comprising sixty-four structure types, was published.[15] The 3rd edition of the *Atlas* in 1992, compiled by Meier and Olson, covers up to 1991 and carries about 85 entries of zeolite structure types.[16] The *Atlas* has become a frequently quoted work of reference and such a publication has to be frequently updated. The current 4th edition of the *Atlas* has ninety-eight entries of zeolite structure types covering data through the end of 1995.[17] When new structure types are reported, the commission publishes them on the world wide web in Europe: (http://www.IZA-SC.ETHZ.CH/IZA-SC/) and on a mirror site in North America: (http://www-IZA-SC.CSB.YALE.EDU/IZA-SC/).

There are several zeolites' structure types reported from phosphates, and they apparently constitute two distinctive categories of microporous materials. The microporous zeolite type materials are listed in Table 6.3.[17]

The primary building block of the zeolite structure is a tetrahedron of four oxygen atoms surrounding a central Si atom (SiO_4). These are connected through their corners of shared oxygen atoms to form a wide range of small secondary building units. They are interconnected to form a wide range of polyhedra, which in turn connect to form the infinitely extended frameworks of the various specific zeolite crystal structures. Different combinations of the same secondary building unit may give numerous distinctive structural polyhedra formed from smaller ring units. The net negative charge on the framework is balanced by the presence of cations, in most cases Ca, Na, or K, which are situated in cavities within it. The zeolite framework is structurally almost independent of the (Na, Ca, K) cations, and, as the latter do not fill all the cavities, replacements of the type $Ca \leftrightarrow 2(Na,K)$ can also occur. Figures 6.1 and 6.2 show the basic structure of zeolite frameworks.[18][19] The structural complexity of zeolites is because of the various ways in which the tetrahedral groups are linked by the common sharing of oxygen ions to form polynuclear complexes. Considerable variation in the chemical composition results from the substitution of cations, such as those listed in Table 6.4.[19] They give rise to zeolite and zeolite like materials of a very wide diversity. Thus, some simple criteria are used to establish the zeolite frameworks. The most important one is the framework density (FD), which means the number of T-atoms (temperature

atoms) per 1000 Å^3. Figure 6.3 *(a)* and *(b)* show the distribution of these values for porous and dense frameworks whose structures are well established.[20] In Fig. 6.3*(a)*, a distinct gap between zeolite type and dense tetrahedral framework structures is seen. The boundary ranges from just under 20 to over 21 T-atoms per 1000 Å^3, depending on the type of smallest rings present. Figure 6.3*(b)* shows the correlation between pore size of molecular sieves and the diameter (σ) of various molecules. While, for zeolites, the observed values range from about 11.1, for structures with the largest pore volume, to around 20.5. To date, framework densities of less than twelve have only been encountered for interrupted framework, like in cloverite, and hypothetical networks.[21][22] The framework density is obviously related to the pore volume, but does not reflect the size of the pore openings, and to some extent it depends on the composition for structural and chemical reasons. The list of zeolite structure types also comprises interrupted frameworks of zeolite-like materials, provided the framework atoms, other than oxygen, are tetrahedrally coordinated, at least in the calcined form.

Table 6.3. Microporous Zeolite-Type Materials[17]

Silicates			Both Silicates and Phosphates	Phosphates
AFG	LOV	RSN	ABW	AEI
*BEA	LTL	RTE	AFI	AEL
BIK	LTN	RTH	ANA	AET
BOG	MAZ	RUT	AST	AFO
BRE	MEI	SGT	BPH	AFR
CAS	MEL	STI	CAN	AFS
-CHI	MEP	THO	CHA	AFT
CON	MER	TON	ERI	AFX
DAC	MFI	VET	FAU	AFY
DDR	MFS	VNI	GIS	AHT
DOH	MON	VSV	LAU	APC
EAB	MOR	WEI	LEV	APD
EDI	MTN	-WEN	LOS	ATN
EMT	MTT		LTA	ATO
EPI	MTW		RHO	ATS
EUO	NAT		SOD	ATT
FER	NES			ATV
GME	NON			AWW
GOO	OFF			-CLO
HEU	-PAR			DFO
JBW	PAU			VFI
KFI	PHI			WEI
LIO	-RON			ZON

DropBooks

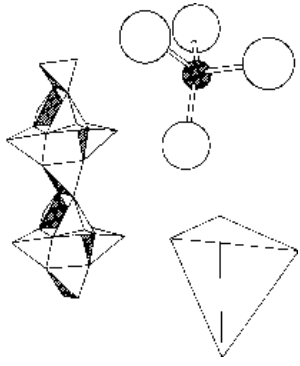

Figure 6.1. Basic structure of zeolite frameworks.[18]

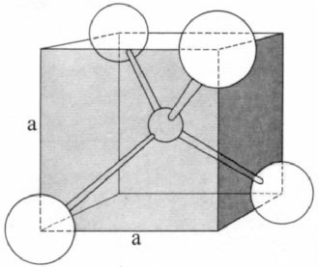

Figure 6.2. Basic structure of zeolite frameworks.[19]

Table 6.4. Coordination of Cation with Oxygen in Silicate Structures[19]

Ion	Radius (Å)	Radius Ratio	Coordination No.	Bond Strength
B^{+3}	0.20	0.20	3, 4	1 or $^3/_4$
Be^{+2}	0.31	0.25	4	$^1/_2$
Li^{+}	0.60	0.34	4	$^1/_4$
Si^{+4}	0.41	0.37	4, 6	1
P^{+5}	0.34	0.34	4, 6	$^5/_4$ or $^5/_6$
Al^{+3}	0.50	0.41	4, 5, 6	$^3/_4$ or $^1/_2$
Ge^{+4}	0.44	0.43	4, 6	1 or $^2/_3$
Ga^{+3}	0.62	0.46	4, 6	$^3/_4$ or $^1/_2$
Mg^{+2}	0.65	0.47	6	$^1/_3$
Na^{+}	0.95	0.54	6, 8	$^1/_6$ or $^1/_8$
Ca^{+2}	0.99	0.67	7, 8, 9	$^1/_4$
K^{+}	1.33	0.75	6, 7, 8, 9, 10, 12	$^1/_9$
NH_4^{+}	1.50	0.85	9, 12	$^1/_9$ or $^1/_{12}$

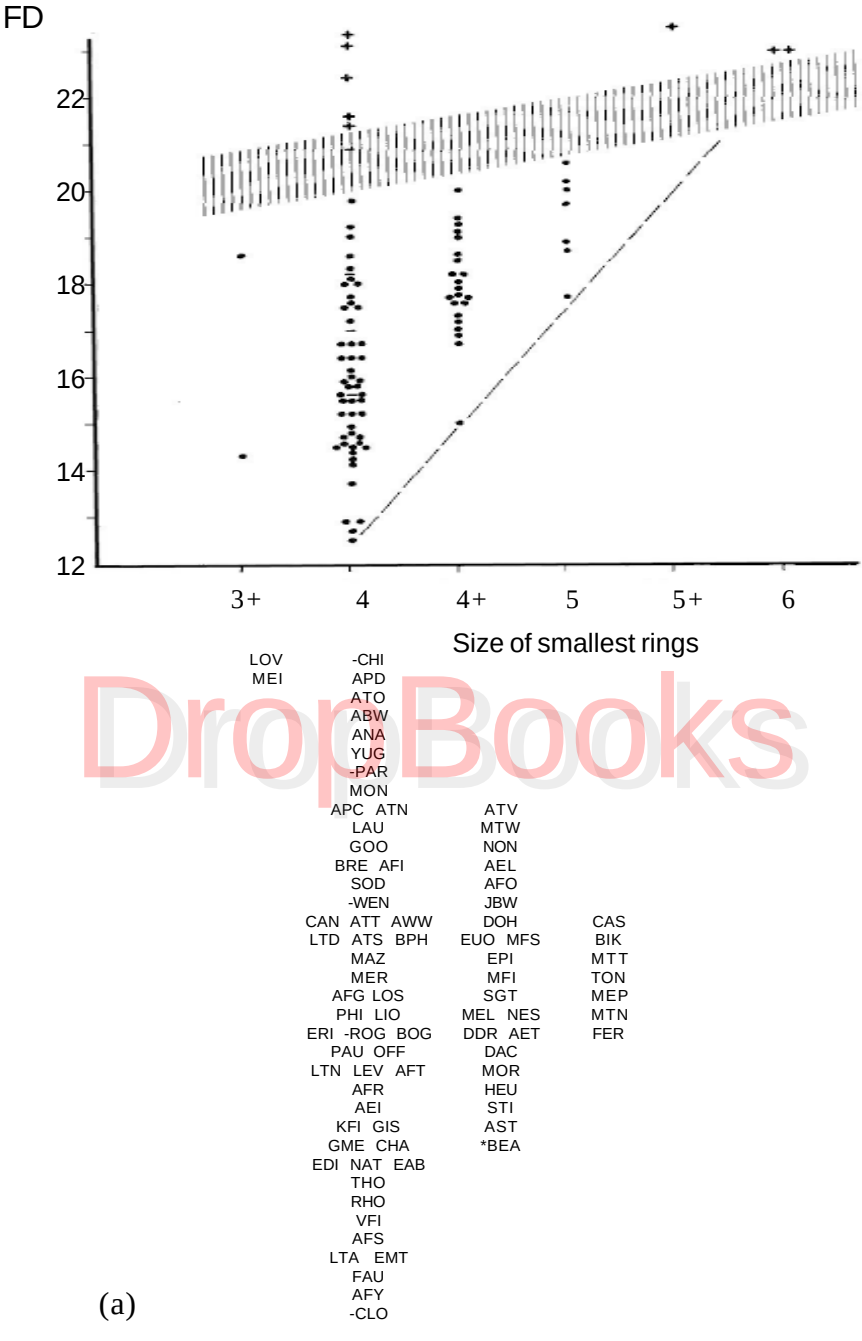

DropBooks

Figure 6.3. *(a)* Distinct gap between zeolite type and dense tetrahadral framework structure.[20] *(b)* Correlation between pore size of molecular sieves and the diameter (σ) of various molecules.[10]

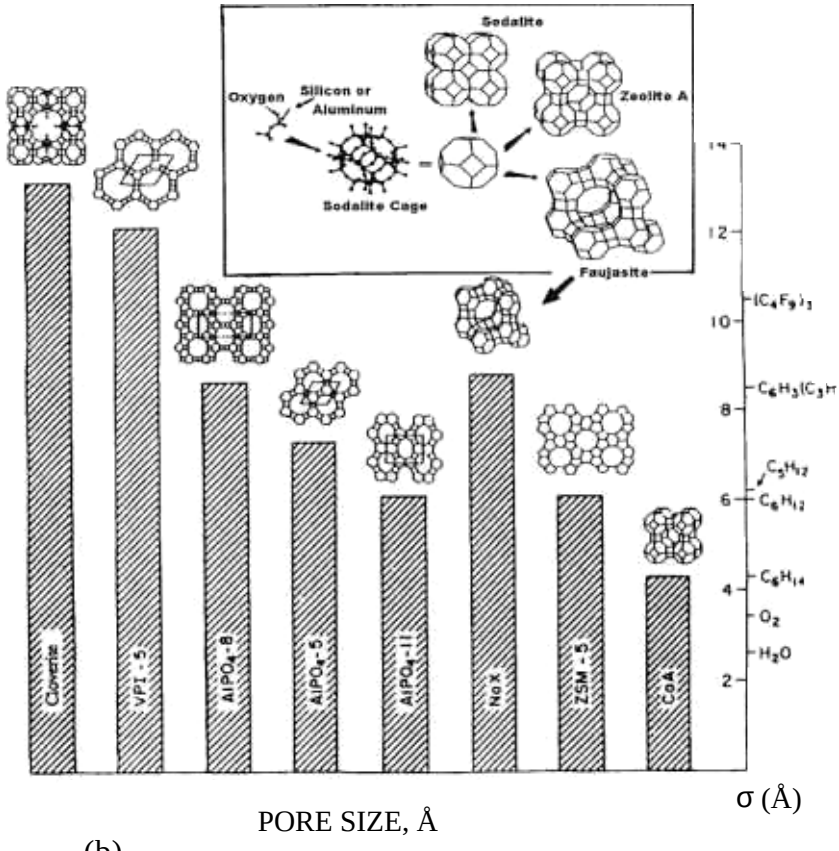

(b)

Figure 6.3. *(Cont'd.)*

The chemistry of zeolites is based on the tetrahedron (TO_4), where, T = Si, Al or P. However, zeolites are so diverse that secondary structural units based on small grouping of linked tetrahedra, are needed in describing and systematizing their topologies. A detailed structural classification of natural and synthetic zeolites has been proposed by several workers, like Breck (1974), Smith (1974), and Barrer (1981).[18][21][22] However, Meier (1968) was the first to propose a classification based on second building units contained in the structure.[23] The classification based upon secondary building units (SBU) is given below. Table 6.5 gives the building units in zeolite structures.[24] Some of the synthetic zeolites are structurally related to minerals and are included in the above classification; however, for many of the synthetic zeolites structures are not known, therefore, in many cases the

framework may be considered as made up of larger polyhedral units, such as the truncated cubo-octahedron (a-cage), truncated octahedron (b-cage), double 8 with 4 ring bridges (g-cage), double 8 ring (d-cage) and can crinite.[16]

Group	Secondary Building Units
1	Single 4 ring (S4R)
2	Single 6 ring (S6R)
3	Single 8 ring (S8R)
4	Double 4 ring (D4R)
5	Double 6 ring (D6R)
6	Double 8 ring (D8R)
7	Complex 4-1, T_5O_{10} unit
8	Complex 5-1, T_8O_{16} unit
9	Complex 4-4-1, $T_{10}O_{20}$ unit

Table 6.5. Building Units in Zeolite Structures[23]

Primary building units (PBU)	Tetrahedra (TO_4)
	Tetrahedra of four oxygen ions with a central ion of Si^+, Al^+, P^+, etc.
Secondary building units (SBU)	Single rings: S-4, S-5, S-6, S-8, S-10, S-12
	Double rings: D-4, D-6, D-8
Larger symmetrical polyhedra	Truncated octahedron (T.O.) or sodalite unit.
	11-hedron or cancrinite unit.
	14-hedron or gmelinite unit.

DropBooks

Qinhua and Aizhen (1990) have summarized the structure of zeolites as follows: the primary building block $(SiO_4)^{4-}$ tetrahedron (Fig. 6.4 *a*) and the tetrahedra are connected through their corners of shared oxygen atoms to form a wide range of small secondary building units (Fig. 6.4*b*).[25] They are interconnected to form a wide range of polyhedra (Fig. 6.4 *c*), which in turn connect to form the infinitely extended frameworks of the various specific zeolite crystal structures. In Figs. 6.4 *a-d*, showing the

structure of zeolites, the corners of the polyhedra represent Si or Al atoms and the connecting lines represent the shared oxygen atoms. Individual structures may comprise only one basic unit or many of them. A record is held by the mineral paulingite, which contains five such polyhedra.

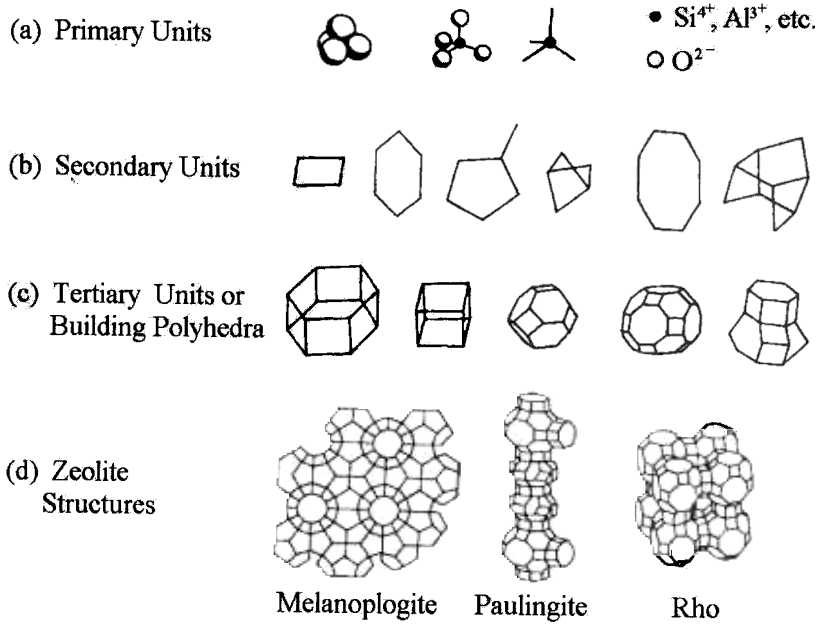

Figure 6.4. Development of zeolite structures.[25]

Different combinations of the same secondary building unit may give numerous distinctive zeolite structures. Figure 6.5 shows an example of three different zeolites that have the same structural polyhedron (cubo-octahedron), but probably form from smaller ring units.

The IUPAC commission on zeolite nomenclature has framed rules and designations consisting of three letters that have been used through the assignment of structure type codes.[26] This is subjected to review and clearance by the IZA Structure Commission according to a decision of the IZA Council (taken at the time of the 7th IZC in Tokyo, 1986). These mnemonic codes should not be confused or equated with actual materials. Structure types do not depend on composition distribution of the various

possible temperature atoms (Si, Al, P, Ga, Ge, B, Be, etc.), cell dimensions, or symmetry. The codes are generally derived from the names of the type materials and they do not include numbers and characters other than capital Roman letters. Structural criteria alone does not provide an unambiguous numbering scheme, therefore, to facilitate later additions and simple indexing, the structure types have been arranged in alphabetical order according to the structure type codes. For interrupted frameworks, the three-letter code is preceded by a hyphen for each structural type, the information given in bold type also includes the full type name, the maximum topological symmetry (i.e., the highest symmetry special group), a listing of the topologically distinct temperature atoms, their number unit cell, andthe maximum point symmetry of the respective temperature sites (in parentheses). The reader can get more detailed information in Refs. 13–17.

DropBooks

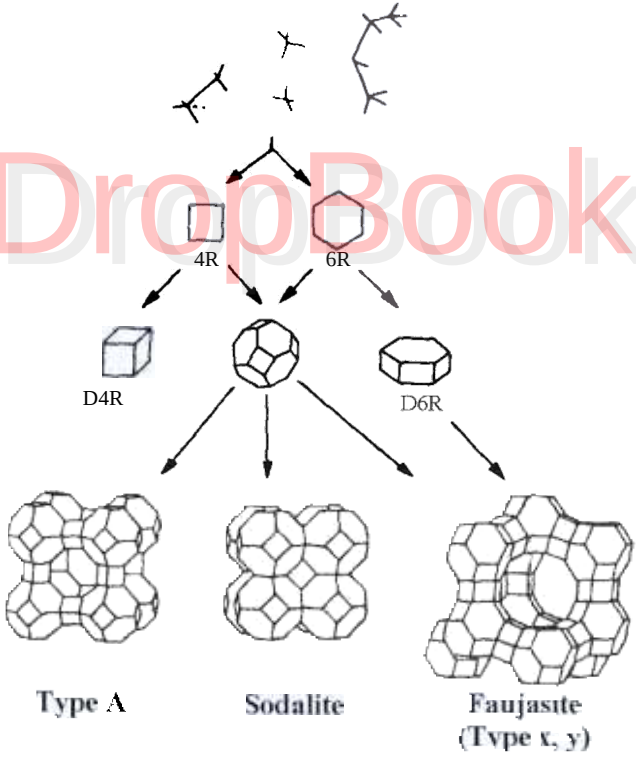

Figure 6.5. Three different zeolites.

6.4 COMPARISON BETWEEN NATURAL AND SYNTHETIC ZEOLITES

Ever since the discovery of stilbite by a Swedish chemist, Crönstedt (1756), a large number of publications have appeared both on natural and synthetic zeolites. In the last century, Wöhler (1848) attempted to recrystallize apophyllite by heating it in water solutions at 180–190°C under 10–12 atm. pressure. There are thousands of reports on various aspects of both natural and synthetic zeolites.

All the natural zeolites can be included in the following genetic types:[27]

1. Crystals resulting from hydrothermal or hot-spring activity involving reaction between solutions and basaltic lava flows.
2. Deposits formed from volcanic sediments in closed alkaline and saline lake systems.
3. Similar formations from open freshwater lake or groundwater systems acting on volcanic sediments.
4. Deposits formed from volcanic materials in alkaline solids.
5. Deposits resulting from hydrothermal or low-temperature alteration of marine sediments.
6. Formations which are the result of low-grade burial metamorphism.

The above reactions occur in open systems and may be as vast in scale as in the range of variables such as pressure, temperature, and time. Zeolites' formation, either in nature or in the laboratory, takes place under conditions in which water is present in considerable amounts, often at elevated temperatures and hence, under hydrothermal conditions. Thus, zeolites have been made in the laboratory only by the hydrothermal method because the open aluminosilicate host framework must be stabilized during growth by being filled with guest molecules. In particular, zeolites never form under acid hydrothermal conditions. The sodalites and cancrinites, like zeolites, have open frameworks, but their synthesis can be achieved pyrolytically as well as hydrothermally because nonvolatile salts can act like zeolitic water and as stabilizers by occupying the pore spaces within the aluminosilicate framework. In hydrothermal synthesis using alkaline salt solutions, water and salts may compete as stabilizers so that each may be present within

the intracrystalline pores.[28] However, the laboratory synthesis of zeolites differs much from that of the natural process, as the laboratory synthesis involves a closed system. Early attempts to synthesize zeolite centered around imitating geological conditions and it was mainly the recrystallization of zeolites taking place until the first synthesized analcime. In 1948, the first synthesis of a zeolite that did not have a natural counterpart was carried out by Barrer.

Laboratory synthesis has evolved by duplicating the conditions under which natural zeolites were produced. However, the one condition that we can never duplicate is crystallization of time, which covers 1000 years or more. The laboratory systems operate at high pH (>12, usually >14 for aluminosilicates, and >7 for aluminophosphates zeolites) and high temperature and, thereby, produce smaller, less-perfect, crystals. So, the majority of the synthetic zeolites are formed under non-equilibrium conditions and are metastable phases produced at supersaturated conditions.

Experimental results indicate that, the less stable the phase, the greater the chance that, initially, it will nucleate and grow fast, but its chance of subsequent survival is less.

Synthetic zeolites represent metastable structures that may, under given conditions, be transformed into other thermodynamically more stable types of zeolites. Also, the synthetic zeolites contain both inorganic and organic cations. Although more than 150 synthetic zeolites have been reported, many important types have a number natural mineral counterpart. Conversely, synthetic counterparts of many zeolite minerals are not yet known. In recent years some minerals having zeolite structure have been reported; one such example is cavansite, $Ca(VO)(Si_4O_{10})\,4H_2O$, which was reported by Staples, et al., (1973), from cavities and veinlets in basalts and tuffs in Oregon, U.S.A.[29] Its crystal structure was reported by Evans (1973).[30][31] Subsequently, this mineral was reported from several other localities. Powar and Byrappa (1998) have reported cavansite from India and they have carried out detailed x-ray, thermal, and infrared studies.[32] The paragenesis of the mineral cavansite is closer to zeolites. It has a three-dimensional/vanadosilicate network analogous to gismondine. However, based on a detailed infrared spectroscopic study, it was found that in cavansite water molecules occur both as loosely held and tightly bound crystal water.[32] Thus, the possibility of the existence of such new minerals having the structures of zeolites cannot be ruled out.

In recent years, the compositional-structural range of molecular sieves have been significantly increased by the discovery of crystalline microporous aluminophosphate based frameworks, beginning with the

DropBooks

aluminophosphates or $AlPO_4$-n molecular sieves, followed by silicoaluminophosphates, titanium aluminophosphates, metal aluminophosphates, and metal silicophosphates, designated as SAPO-n, TAPO-n, MeAPO-n, and MeAPSO-n, respectively.

In 1961, d'Yvoire reported the synthesis of several aluminophosphate hydrates, H_1, H_2, H_3, and H_4, etc. These materials were prepared from dilute aqueous solutions of alumina and phosphoric acid with a P_2O_5:Al_2O_3 ratio of 2.7.[33]

Much of the success in the laboratory synthesis has been achieved by duplicating the conditions under which natural zeolites were produced. In nature, water plays a key role in the crystallization of zeolites, whereas in the laboratory the zeolites structure formation insists on the presence of the organic molecules. Tables 6.6 to 6.8 give the natural zeolites whose structures were successfully duplicated from silica/alumina gels and alkali metal, alkaline earth metal, or alkyl ammonium cations, respectively.[34] One can expect more examples in the future with respect to the discovery of natural counterparts of existing synthetic zeolites. Table 6.9 gives a list of several synthetic zeolites with structures reasonably well defined, but with no counterparts in natural zeolites. New synthetic zeolites' phases will continue to grow in numbers faster than the natural zeolites.

Table 6.6 Synthetic Counterparts of Natural Zeolites—Alkaline Metal[34]

Zeolite	Alkali	Investigator	Date
Mordentie	Na	Barrer, R. M.	1948
Analcime	Na	Barrer, R. M.	1949
Phillipsite	Na	Barrer, R. M.	1951
Cancrinite	Na	Barrer, R. M.	1952
Natrolite	Na	Barrer, R. M.	1952
Faujasite	Na	Milton, R. M.	1956
Gmelinite	Na	Barrer, R. M.	1959
Chabazite	Na	Milton, R. M.	1960
Erionite	K.Na	Breck, D. W.	1960
Clinoptilolite	Li	Ames, L. L., Jr.	1963
Ferrierite	Na	Senderov, E. E.	1963
Gismondine	Na	Taylor, A. M. and Roy, R.	1964
Bikitalite	Li	Drysdale, D. J.	1971
Edingtonite	K	Barrer, R. M.	1974

Table 6.7. Synthetic Counterparts of Natural Zeolites—Alkaline Earths[34]

Zeolite	Alkali	Investigator	Date
Heulandite	Ca	Roy, R.	1960
Scolecite	Ca	Roy, R.	1960
Wairakite	Ca	Roy, R.	1960
Epistilbite	Ca	Roy, R.	1960
Garronite	Ca	Barrer, R. M.	1961
Thomsonite	Ca	Barrer, R. M.	1961
Yugawaralite	Sr	Barrer, R. M.	1964
Clinoptilolite	Sr	Barrer, R. M.	1964
Harmotone	Ba	Barrer, R. M.	1964

Table 6.8. Synthetic Counterparts of Natural Zeolites—Alkylammonium[34]

Zeolite	Alkali	Investigator	Date
Offretite	TMA, [a]Na, K	Robson, H. E.	1966
Levynite	$[CH_3N\ N]^+$, K	Kerr, G. T.	1969
Maxxite	TMA, [a]Na	Barrer, R. M.	1970

DropBooks

Table 6.9. Natural Zeolites with No Synthetic Counterpart

Zeolite	Year Discovered
Stilbite	1756
Laumontite	1785
Mesolite	1813
Brewsterite	1822
Herschelite	1825
Kehoeite	1893
Gonnardite	1896
Dachiardite	1905
Stellerite	1909
Viseite	1942
Paulingite	1960
Merlinoite	1977

6.5 SYNTHESIS OF ZEOLITES

Efforts to synthesize zeolites can be traced as far back as 1848 when Wöhler first recrystallized apophyllite by heating it in water solutions at 180–190°C under 10–12 atm.[35] Followed by this, several more attempts were made during the 1860s when Claireville synthesized zeolites by the hydrothermal method in 1862.[36] The hydrothermal reaction merges into a low-temperature reaction and indeed, in zeolite synthesis the trend has been interalia for greater experimental convenience, to grow zeolites at or below 100°C provided reaction rates are adequate. It was only during the 1940s that great attention was devoted to zeolite synthesis as a result of the pioneering work by Barrer, Milton, and co-workers.[37][38] Even now, the area of zeolite synthesis is still expanding and hence, is resulting in the discovery of synthetic zeolites with new topologies and new catalytic sorption and separation properties. Generally, three processes are used to produce zeolites:

1. Preparation of molecular sieve zeolites as high purity crystalline powders.
2. The conversion of clay minerals into zeolites.
3. Processes based on the use of other naturally occurring raw materials.

It is not surprising that much effort is made to unravel the mechanisms responsible for the formation of zeolites from its precursors. Using this knowledge, concepts may be derived for *tailor-made zeolite synthesis*, making the *art* of creating zeolite synthetics a real scientific issue. Hydrothermal synthesis of aluminosilicate zeolites involves a few elementary steps by which a mixture of Si and Al species, metal cations, organic molecules, and water, are converted via an alkaline supersaturated solution into a microporous crystalline aluminosilicate. The complex chemical processes involved in this transformation can be denoted as *zeolitization*. Since the1940s, systematic studies on synthesis have been disclosed. During 1948, Barrer synthesized the first zeolite that did not have a natural counterpart.[37] However, zeolite technology was initiated during the late 1940s on a large scale, essentially by the groups of Barrer and Milton. They developed hydrothermal synthesis using reactive alkali-metal aluminosilicate gels at low temperatures (~100°C) and pressure (autogenous). By 1958, under the leadership of Milton, the Linde Division of Union Carbide had successfully synthesized nearly all the commercially important zeolites.[38]–[42]

The next advance in zeolite synthesis was again due to Barrer. In 1961, Barrer and Denny reported zeolites' synthesis using alkylammonium cations.[37][43] They noted that the addition of alkylammonium ions to sodium aluminosilicate gels increased the framework Si/Al ratio.[43] At about the same time, G. Kerr, at Mobil Oil Company, began using organic molecules in zeolite synthesis.[44] The use of organic materials in zeolite synthesis was quickly expanded after the initial work of Barrer and Denny.[43]

In 1961, d'Yvoire reported the synthesis of several aluminophosphate hydrates, followed by the scientists of Union Carbide Laboratories who synthesized a new generation of aluminophosphate zeolites in the late 1970s.[33] Initial success resulting in the discovery of the aluminophosphate zeolites, was reported by Wilson, et al., (1982).[12] Specific reference to these developments (listed in Table 6.10) may be found in several historical reviews.[45][46] The addition of Si and P framework elements resulted in silicoaluminophosphate (SAPO) zeolites which was also reported by Wilson, et al., (1983).[47] The metal aluminophosphate (MeAPO) zeolites with the framework containing aluminum, phosphorus, and metal cation (Me), where Me = Mg^{2+}, Mn^{2+}, Fe^{2+}, Fe^{3+}, Co^{2+}, and Zn^{2+}, were reported by Flanigen, et al., (1986).[48]

ProPBooks

Until recently, zeolite synthesis has been mainly an empirical science in which a large number of experiments were used to change synthetic parameters systematically with a hope of obtaining new phases and crystal composition. The zeolite synthesis is now being gradually replaced by methods based on the use of new characterization techniques, which will provide a better understanding of the gel chemistry, nucleation, crystal growth, crystallization kinetics, and structure directing phenomenon.

The general route whereby zeolites can be synthesized in a laboratory or a plant scale is shown in Table 6.11.[49] The structure-directing agents listed are only examples of a wide range of materials that have been used. Zeolites have been synthesized only by the hydrothermal method. It involves silica, alumina, and/or phosphorus species, metal cations, organic molecules, and water, which are converted via an alkaline supersaturated solution into microporous crystalline zeolites. The complex chemical processes involved in this transformation can be denoted as *zeolitization*. The process of zeolitization is thermally activated and usually takes place at elevated temperatures in order to achieve a high yield of crystals in an acceptable period of time.

Table 6.10. Development in Zeolite Science and Technology[37]

Early History		
1756	Cronstedt, A. F.	Described natural zeolites
1840	Damour, A.	Observed reversible dehydration
1858	Eichhorn, H.	Reported ion-exchange properties of zeolites
1862	Claireville, H, de St.	Early hydrothermal synthesis (levyne)
1876	Lew	Reported sedimentary zeolites in tuff deposits
1896	Friedel, G.	Observed organic liquid sorption; proposed open spongy framework structure
1909	Grandjean, F.	Reported gas sorption (NH_3, air, H_2)
1925	Weigel, O. and Stermhoff, F.	Observed molecular sieve effect
1930	Tayior, W. H. and Pauling, L.	Structure determination of anaicime and natrolite
1932–1940s	Barrer, R. M	Systematic studies of synthesis, ion-exchange sorption and dehydration
Industrial Era		
1949–1954	Union Carbide	Synthesis of zeolite A and zeolite X (synthetic faujasite)
1954	Union Carbide	Commercialized zeolite-based gas purification and separation processes; early catalytic applications
1955–1962	Mobil	Commercialized rare earth zeolite X cracking catalyst
1958–1964		Discovery and commercialization of significant sedimentary zeolite deposits in western U.S. and Japan
1958	Mobil	Zeolite synthesis with organic cations
1962–1980s	Mobil/Union Carbide	Synthesis of high silica zeolites
1982	Union Carbide	Synthesis of microporous $AlPO_4$ molecular sieves
Recent Developments		
1985–1994	Academic and Industrial Researchers	Synthesis of “large pore” (i.e., VPI-5, cloverite) and mesopore (MCM-41) materials, new silica zeolites and clathrates, advanced materials applications

Table 6.11. Molecular Sieve Zeolite Preparation Process[49]

Molecular sieve process	Zeolite preparation process	
	Reactants	Products
Hydrogel	Reactive oxides Soluble silicates Soluble aluminates Caustic	High purity powders Gel preform Zeolite in gel matrix
Clay Conversion	Raw kaolin Metakaolin Calcined kaolin Soluble silicate Caustic sodium Chloride	Low to high purity powder Binderless, high purity Preform zeolite in clay Derived matrix.
Others	Natural SiO_2 Acid treated clay Amorphous mineral Volcanic glass Caustic $Al_2O_3, 3H_2O$	Low to high purity powder Zeolite on ceramic support Binderless preforms

DropBooks

In spite of the success of the last 45 years in the synthesis of zeolites, the factors controlling the synthesis of perous crystalline aluminosilicates or aluminophosphates are not well defined. In this connection, the IZA Synthesis Commission has given an outline of a thorough report of a molecular sieve synthesis and the following product characterization.[49] The *priority* designation is a consensus opinion of the committee as to the importance that we attach to the item. The simplest experiments will lack details in some of these categories, but not in all cases. The author should consider whether the particular procedure is unique in any way and might be significant in the overall result. Negative answers to the implied question can be helpful.

Similarly, the IZA Synthesis Commission gives two more outlines dealing with the background material and synthesis report of a hydrothermal zeolite. The background material covers aspects like source materials, gel preparation, crystallization, product recovery, and characterization. These aspects have been discussed in great detail by several authors from time to time.

Synthetic zeolites are generally made by mixing solutions of aluminates and silicates, often with the formation of a gel, and by maintaining the mixture at temperatures of 100°C or more for selected periods.[37][49]

The synthesis of zeolites involves several steps, as shown below:

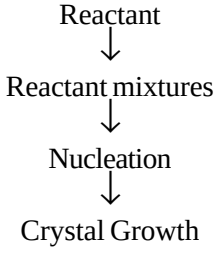

The mechanisms of zeolite formation are very complex due to the plethora of chemical reactions, equilibria, and solubility variations that occur through the heterogeneous synthesis mixture during the crystallization process.

The process of zeolitization is thermally activated and usually takes place at elevated temperatures in order to achieve a high yield of crystals in an acceptable period of time. The variables in the synthesis of zeolites are temperature, alkalinity (pH), and chemical composition, of the reactant mixtures. These variables do not necessarily determine the products obtained in hydrothermal reactions, because nucleation appears to be kinetically rather than thermodynamically determined and controlled. The kinetic variables include the treatment of reactants prior to crystallization, their chemical, and physical nature.[10][50]

With reference to the source materials, one would hope that a mole of SiO_2 would be equivalent to another SiO_2, from whatever source, when compounded into a gel. Experience teaches us that this is not the case; SiO_2 and Al_2O_3 are to some degree polymeric before gelation. Any reagent contains some unsuspected impurities, which can be active on the synthesis. To duplicate the work, one has to repeat with the same source material. The starting material can not be just *silica,* but *precipitated silica, fumed silica,* or *silica sol,* from a designated supplier. For very high silica phases, the alumina content of the silica source may be very important. Besides, one has to carefully prepare the gel and the step-by-step procedure has to be followed as noted. These steps include the order of mixing, the device used to mix, the aging time and temperature, nucleation, and batch composition. For example, the ingredients are not added sequentially, but combined into two (or three) subgroups that are blended to make the final gel. After a careful preparation

of the precursor, a suitable reaction vessel has to be selected to provide the desired temperature, pressure, agitation, and the facility to withdraw an occasional sample. Several companies from the USA, Japan, and Germany, manufacture autoclaves with all such facilities for the synthesis of zeolites. Figure 3.27 shows the Parr autoclave commonly used in zeolite synthesis. For the commercial production of zeolites, large size autoclaves or batch reactors are usually employed. The rate of heating is very important. If possible, a periodic/continuous monitoring facility is necessary to obtain the values of pH, percent of crystallinity, and the rate of crystallization. After carrying out the experimental runs, the filtration, washing, drying, and yield estimation are to be done carefully. For a better reproducibility of the results, the above aspects are to be kept in mind.

Several techniques are used to characterize the zeolite phases obtained. The most commonly used techniques are x-ray powder diffraction, Rietvield technique of structure refinement, neutron scattering, NMR, IR, Thermal, SEM, Laser Raman, measurement of sorptive capacity, particle size and pore size distribution, and so on.

Davis and Lobo (1992) have proposed two extremes of the mechanisms of zeolite synthesis, *(i)* the solution-mediated transport mechanism, and *(ii)* the solid-phase transformation mechanism.[10] Figure 6.6 shows the schematic illustrations of *(A)* the solution-mediated transport, and (*B*) solid-hydrogen transformation crystallization mechanisms. The first one involves the diffusion of aluminate, silicate, and/or aluminosilicate species from the liquid phase to the nucleation site for crystal growth. There are many examples of solution-mediated transport in the crystallization of aluminum-rich zeolites. Ueda, et al., (1984), have prepared zeolites Y, S (GME), and P (GIS), which were synthesized from clear solutions, i.e., without the presence of hydrogel (solid phase).[51] The solid-phase transformation mechanism suggests that the solid hydrogel reorganizes in forming the zeolite structure. Xu, et al., (1989) have well illustrated this process by the synthesis of ZSM-35 (FER) and ZSM-5 from nonaqueous reaction mixtures.[52] There are several such reports on the synthesis of various zeolites using both of the proposed mechanisms of zeolite crystallization. In some cases, zeolites like Z.Y were found to crystallize by a combination of the two mechanisms. As a particular structure can be formed via different crystallization processes, extreme caution is necessary when attempting to generalize conclusions from one zeolite to a class of zeolites or molecular sieves. Here, the authors discuss

BioBooks

some of the important aspects/factors influencing zeolite synthesis. For the sake of convenience, the authors deal with aluminosilicate zeolites followed by aluminophosphate zeolites and the family of microporous compounds.

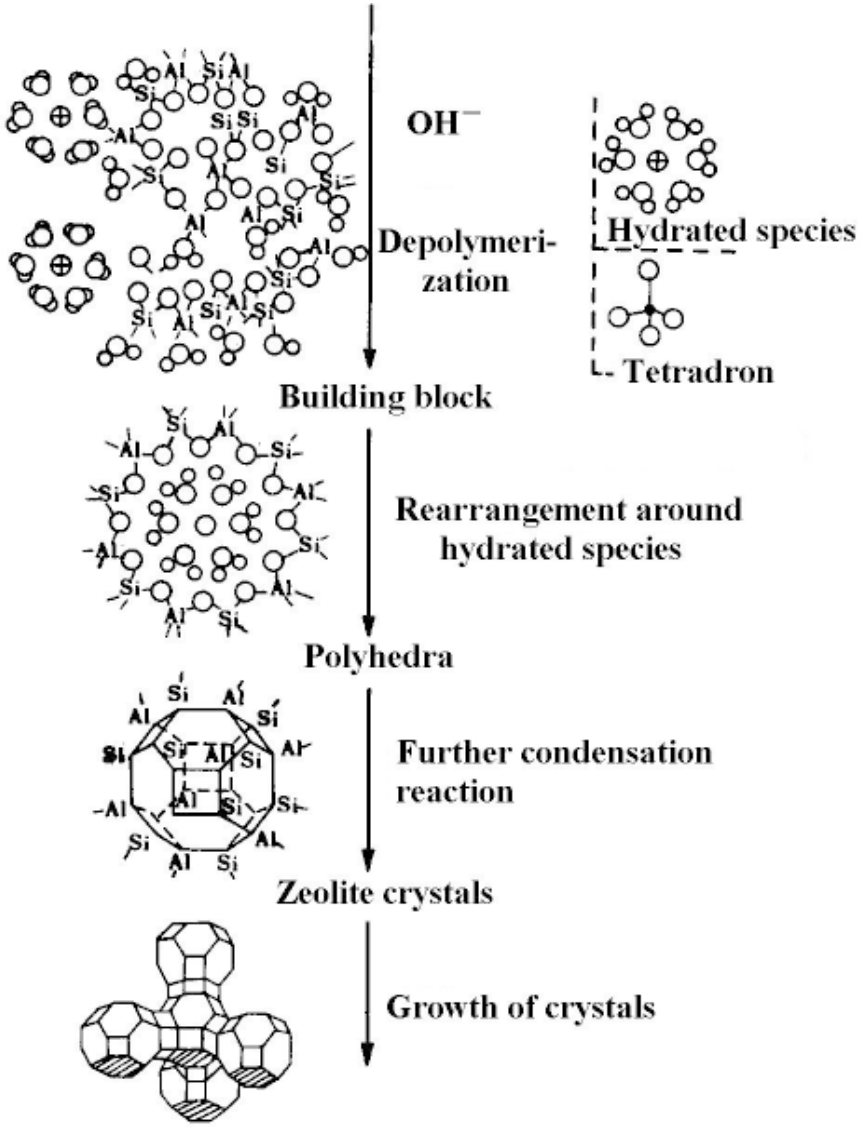

Figure 6.6. *(a)* Schematic illustrations of the solution-mediated transport. *(b)* Solid-hydrogen transformation crystallization mechanism.[10]

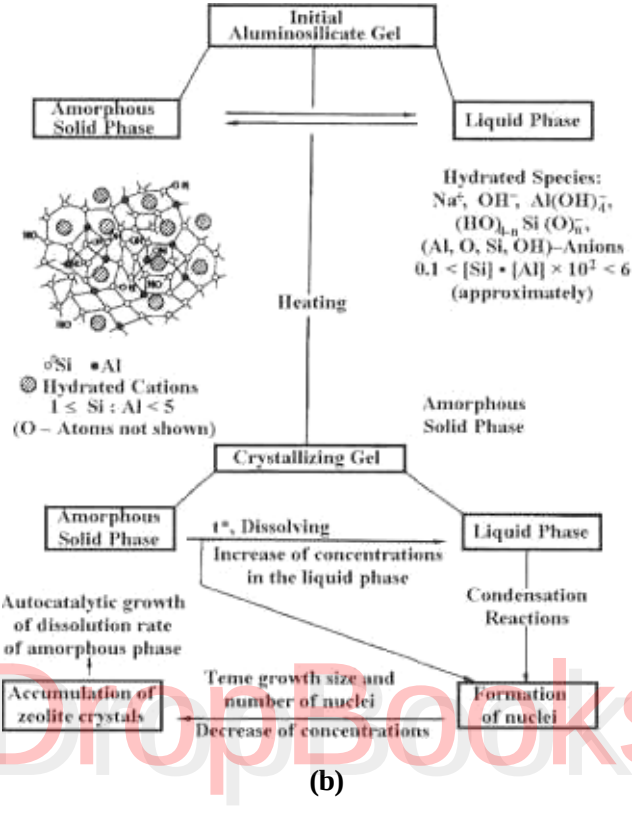

(b)

Figure 6.6. *(Cont'd.)*

6.5.1 Molar Composition

The chemical composition of a synthesized hydrogel is expressed generally in terms of an oxide formula, SiO_2 (P_2O_5), Al_2O_3, bMxO, cNyO, dR, and eH_2O, in which *M* and *N* stand for (alkali) metal ions and *R* for organic templates. The relative amount of Si, P, Al, M, N, and R, is one of the key factors determining the outcome of the crystallization. Next to the nature of the template used (inorganic and organic cations), the ratios SiO_2/Al_2O_3, P_2O_5/Al_2O_3, MxO(NyO)/SiO_2, MxO(NyO)/P_2O_5, R/SiO_2, R/P_2O_5, and H_2O/SiO_2 or H_2O/P_2O_5, can intervene during zeolitization. Such a variation greatly influences the crystallization processes right at the level of nucleation and crystallization kinetics, the nature of the crystallization

material, the lattice Al content and distribution, the crystal size and morphology.[53][54] For example, the synthesis of high-silica zeolites requires the addition of organic molecules into the reaction mixture, an exception is ZSM-5 which can be synthesized without the use of organic reagents in a very narrow range of Na^+ and Al^{3+} concentrations and the reaction temperatures are normally higher (~100–200°C) than those used to crystallize aluminum-rich zeolites.[55] Similarly, aluminum-rich zeolites, e.g., Z.A, X, P, sodalite, chabazite (CHA), and edingtonite (EDI), have pore volumes in the range ~ 0.4–0.5 cm^3 void/cm^3 of crystal and are formed near 100°C; whereas the alkali-metal cations in the synthesis of zeolites act as the source of hydroxyl ions (alkali-metal hydroxides commonly used in zeolites synthesis) and have a limited structure directing role as well.[56] Recently, it has been observed that cation-water complexes stabilize small aluminosilicate anions that are responsible for forming unique zeolite structures primarily through electrostatic and steric factors.[57]

Figure 6.7 shows a crystallization diagram for the system Na_2O-Al_2O_3-SiO_2-H_2O for a temperature of 363 K and $(Al_2O_3 + SiO_2)/H_2O$ = 0.0005. An interesting factor that can be seen from this diagram is that the content of alkali has a much stronger influence on the kind of crystallizing zeolite than the SiO_2/Al_2O_3 ratio. The primary influences of compositions of reaction mixture are given in Table 6.12.[58]

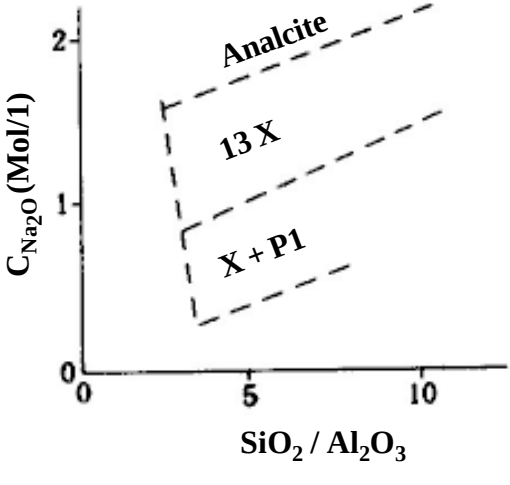

Figure 6.7. Crystallization diagram for the system Na_2O-Al_2O_3-SiO_2-H_2O for a temperature of 363 K and $(Al_2O_3 + SiO_2)/H_2O$ = 0.0005.[25]

Table 6.12. Primary Influence of the Compositions of Reaction Mixture[58]

Mole Ration	Primary Influence
SiO_2/Al_2O_3	Framework composition
H_2O/SiO_2	Rate, crystallization mechanism
OH^-/SiO_2	Silicate molecular weight, OH^- concentration
Na^+/SiO_2	Structure, cation distribution
R_4N^+/SiO_2	Framework aluminum content

The earliest synthetic zeolites were essentially Al-rich or had a low Si to Al ratio and their Al concentrations were equivalent to Si, however, Al-O-Al linkages have not been observed in zeolites.[59] Loewenstein first rationalized the absence of Al-O-Al linkages in tectoaluminosilicates on the basis of clusters of negative charges.[60] Thus, if Al-atoms do not have Al-atoms in their second coordination sphere, then $Si/Al \geq 1$. Low-silica zeolites are defined as having $1 \leq Si/Al < 2$, while intermediate Si/Al zeolites contain $2 < Si/Al \leq 5$. Table 6.13 gives a number of molecular sieve structures and representative materials according to their Si/Al ratio. In the late 1960s and early 1970s high-silica zeolites with $Si/Al > 5$ were synthesized. As the Si/Al ratio increases, the properties of zeolites are significantly altered. At higher Si/Al ratios, the crystals are hydrophobic. In the early 1980s, silica-free molecular sieves were based on the aluminophosphate compositions.[47][61]–[63] The role of organics and their concentrations are discussed in detail separately in the forthcoming sections.

DropBooks

6.5.2 The Aging of Hydrogel

After the preparation of the precursor or the hydrogel, using desired ratio of the starting materials as explained in the previous section, the hydrogel, is usually kept for a certain period of time below the crystallization temperature. This aging (ripening) period is very crucial in the synthesis of a desired zeolite, and it differs from aluminosilicate zeolites to aluminophosphate zeolites.[64] One of the important steps occurring during the aging period is the (partial) dissolution or depolymerization of the silica sol, which is promoted by the alkaline conditions for

zeolite synthesis.[37] Cook and Thompson (1988) have simulated the hydrothermal zeolite synthesis with the aging of the amorphous gel at low temperature followed by elevated temperature crystallization by population balance methods.[65]

Table 6.13. Compositions of Zeolites and Molecular Sieves

Si/Al ≤ 2 Low-Silica	2 < Si/Al ≤ 5 Intermediate Silica	5 < Si/Al High-Silica	Phosphate
ABW, Li-A(BW)	BHP, linde Q	BEA, zeolite beta	AEI, $AlPO_4$-18
AFG, afghanite[a]	BOG, boggsite[a]	DDR, decadodecasil 3R	AEL, $AlPO_4$–11
ANA, analcime[a]	BRE, brewsterite[a]	DOH, dodecasil 1H	AET, $AlPO_4$ – 8
BIK, bikitaite[a]	CAS, Cs-aluminosilicat	EUO, EU-1	AFI, $AlPO_4$ –5
CAN, cancrinite[a]	CHA, chabazite[a]	FER, ferrierite	AFO, $AlPO_4$-41
EDI, edingtonite[a]	CHI, chiavennite[b]	LEV, NU-3	AFS, MAPSO-46
FAU, NaX	DAC, dachiardite[a]	MEL, ZSM-11	AFT, $AlPO_4$-52
GIS, gismondine[a]	EAB, EAB	MEP, melanophlogite	AFY, CoAPO-50
GME, gmelinite[a]	EMT, hexagonal faujasite	MFI, ZSM-5	APC, $AlPO_4$-C
JBW, NaJ	EPI, epistibite[a]	MFS, ZSM-57	APD, $AlPO_4$-D
LAU, laumontite[a]	ERI, erionitea	MTN, dodecasil 3C	AST, $AlPO_4$-16
LEV, levyne[a]	FAU, faujasite,[a] NaY	MTT, ZSM-23	ATF, $AlPO_4$-25
LIO, liottite[a]	FER, ferrierite[a]	MTW, ZSM-12	ATN, MAPO-39
LOS, losod	GOO, Goosecreekite[a]	NON, nonasil	ATS, MAPO-36
LTN, NaZ-21	HEU, heulandite[a]	SGT, sigma-2	ATT, $AlPO_4$-12 TAMU
NAT, natrolite[a]	KFI, ZK-5	SOD, sodalite	ATV, $AlPO_4$-25
PAR, partheite[a]	LOV, lovdarite[b]	TON, theta-1	AWW, $AlPO_4$-22
PHI, phillipsite[a]	LTA, ZK-4	ZSM-48	BPH, beryllo-phosphate-H
ROG, roggianite[a]	LTL, linde L.		CAN, tiptopite[a]
SOD, sodalite	MAZ, mazzite[a]		CHA, SAPO-47
THO, thomsonite[a]	MEI, ZSM-18		CLO, cloverite
WEN, wenkite[a]	MER, merlinoitea		ERI, $AlPO_4$-17
	MON montasommaite[a]		FAU, SAPO-37
	MOR, mordenite[a]		GIS, MgAPO-43
	OFF, offretite[a]		RHO, pahasapaite[a]
	PAU, paulingite[a]		SOD, $AlPO_4$-20
	RHO, rho		VFI, VPI-5
	STI, stilbite[a]		
	YUG, yugawaralite[a]		

[a] Natural materials. [b] Beryllosilicates (natural).

The amorphous gel is formed at room temperature, homogenized, and left to age for a period of time at room temperature. The subsequent crystallization at elevated temperature after aging proceeds more quickly than in the non-aged case. Several authors have noted that germ nuclei

formed within the gel (or the solution) during gel aging grow to observable sizes upon subsequent high-temperature synthesis.[66][37] Zhdanov and Samulevich (1980) reported that aging zeolite Na A gels for up to three days resulted in a more rapid conversion upon heating and in smaller final crystal sizes.[66] They concluded that nuclei form during aging and then grow to observable size during heating. Subotic and Bronic (1986) reported experimental values of percent crystallinity vs. time for zeolite Na A syntheses at 80°C, for which some of the amorphous gel/water solutions had been aged at 25°C for as many as 17 days prior to crystallization.[67] Upon heating the aged solutions, those aged for longer times were shown to crystallize faster after a shorter induction time. These data have been plotted in Fig. 6.8. The evolution of the average zeolite crystal size with time, based on the computer simulations is shown in Fig. 6.9. As the aging time increases, the number of nuclei increases, thereby decreasing the final average crystal size. This result is perfectly logical, as with more nuclei present the reagent mass is distributed among more crystals, resulting in smaller crystals on average. Figure 6.10 shows the number of nuclei formed per day by dividing values of Ns (No. of nuclei formed during aging).

DropBooks

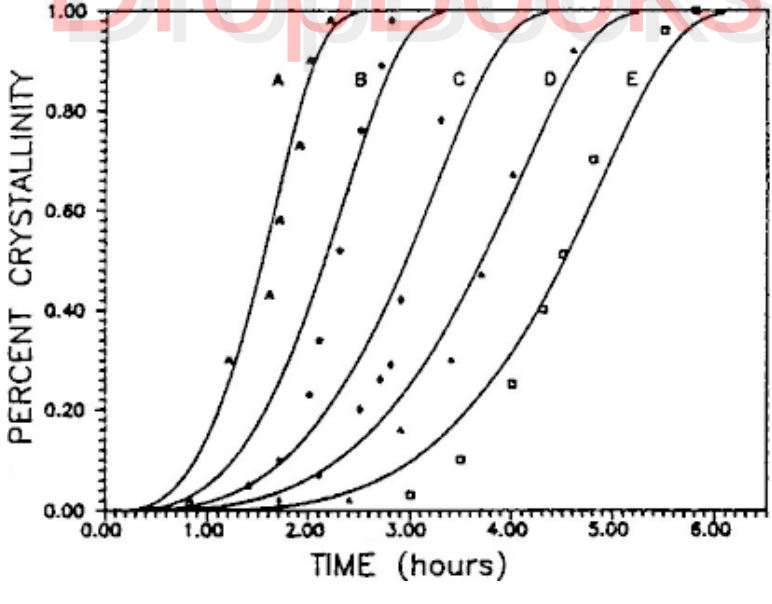

Figure 6.8. Crystallization curve simulated assuming nuclei form during reaction time.[67]

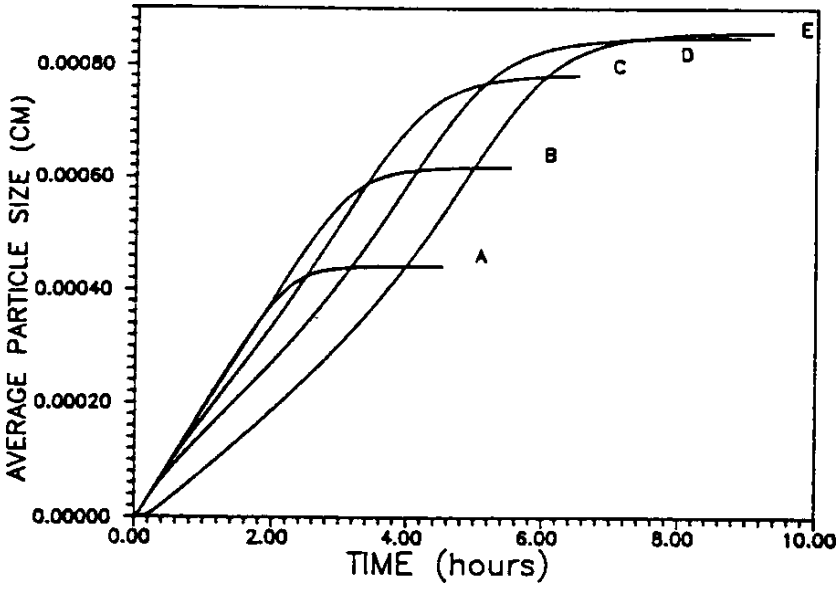

Figure 6.9. Evolution of the average zeolite crystal size with time.[67]

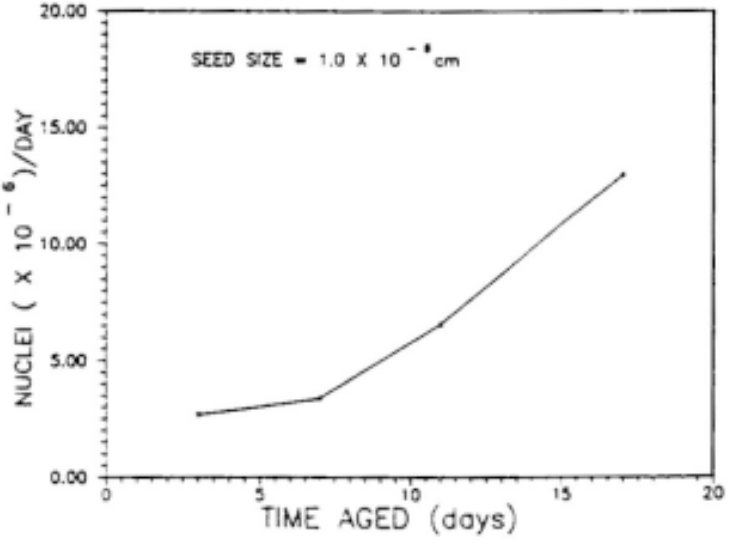

Figure 6.10. Number of nuclei formed per day by dividing values of Ns.[67]

Wu and Chao (1995) have studied systematically the gel aging through Raman spectroscopy and DTG.[68] Figures 6.11 and 6.12 show the room temperature for Raman spectra of the gel phase obtained during aging at ambient temperature, and reaction at 115°C during the synthesis of faujasite zeolites.[68] In the early stages of aging, insoluble silica and unreacted Al $(OH)^-_4$ retained in the gel, A, give bands at Ca. 441 cm^{-1} and Ca. 617 cm^{-1}, respectively. At the end of aging, the Al $(OH)^-_4$ species in the solid part and Al species in the solution part of gel A are found almost to disappear, and this disappearance might be a result of the formation of the aluminosilicate hydrogel, which is considered to be the precursor of zeolite. Upon heating, the insoluble silica dissolves progressively so that the concentration of silicates in solution measured by ICP-AES increases significantly. After the sample has been heated for 1–5 days, the cyclic tetrameric aluminosilicate and silicate anions are observed at 479–489 cm^{-1}.

DropBooks

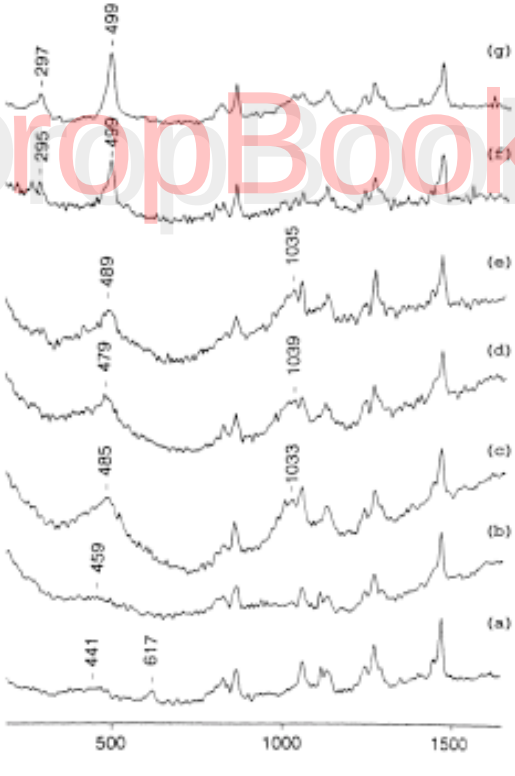

Figure 6.11. Raman spectra of the gel phase obtained during aging at ambient temperature, and reaction at 115°C during synthesis of faujasite zeolites.[68]

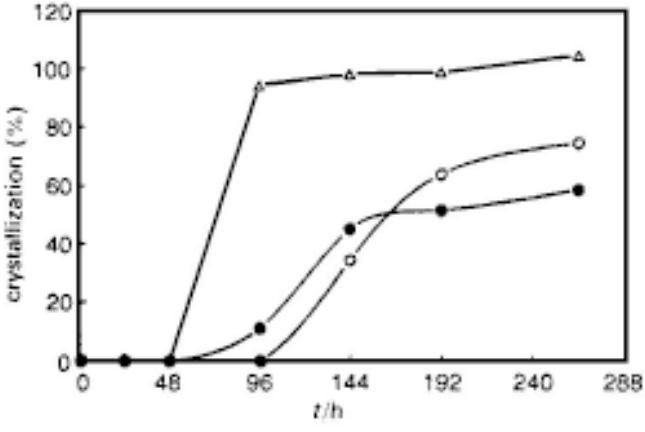

Figure 6.12. Crystallizaton curve of EMT (○: E-4 or gel A, Δ: A-1) and FAU (●: E-8 or gel) for the 18-crown-6 ether preparations.[68]

The DTG curves have been recorded for gel after different hours of aging at room temperature by Wu & Chao (1995) and the results are shown in Figs. 6.13 and 6.14. The TG/DSC thermal analysis with on-line mass spectrometry showed three distinct stages of weight loss on the faujasites, 25–200°C, 200–300°C, and 300–500°C. The first endotherm is mainly due to the desorption of water, while the second and the third result from the exothermic decomposition of organics in faujasite zeolites.

Similarly, Bell (1989) and Gilson (1992) have attempted to identify the nature and relative amounts of the silicate and aluminosilicate species present in the mother liquor using ^{29}Si and ^{27}Al NMR spectroscopy.[69][70] However, ^{29}Si NMR technique has an important limitation, i.e, silicate species containing more than 12 Si atoms have never been unequivocally identified.[63] This information has been used to understand the effect of aging of hydrogel in zeolite synthesis.

These studies indicate that the zeolite nuclei, the hydrogel or precursor, and the liquid solution, are in equilibrium during crystallization, and because of the existence of this equilibrium, the specific precursor or hydrogel can play a very important role in influencing the form of nuclei and final productions. Also, the encapsulation of organic templates or inorganic cations in the hydrogel seems to determine the type of zeolite production.

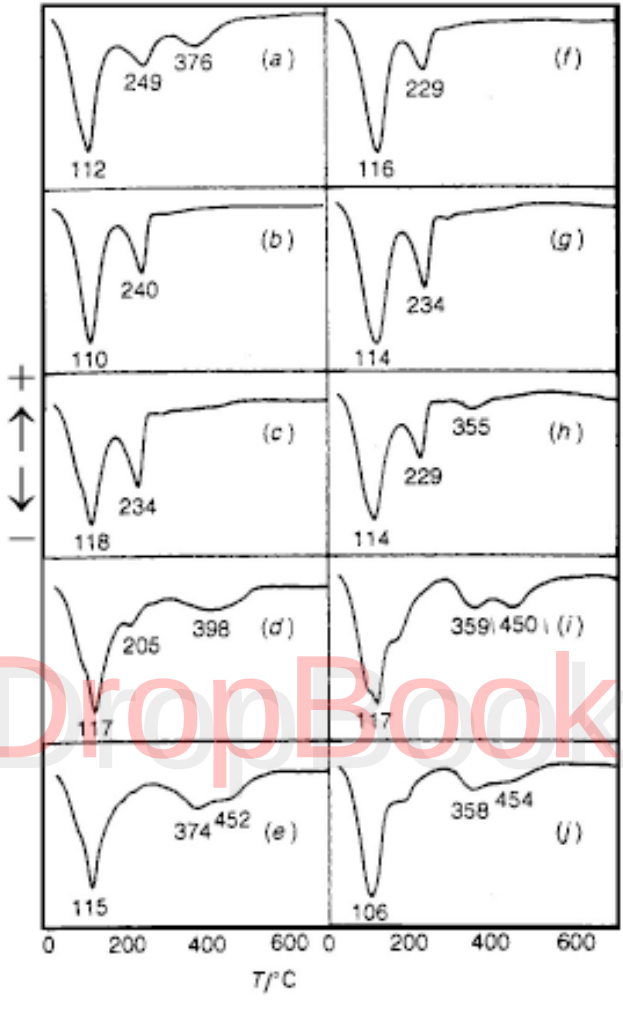

DropBooks

Figure 6.13. DTG curves of different gels.[68]

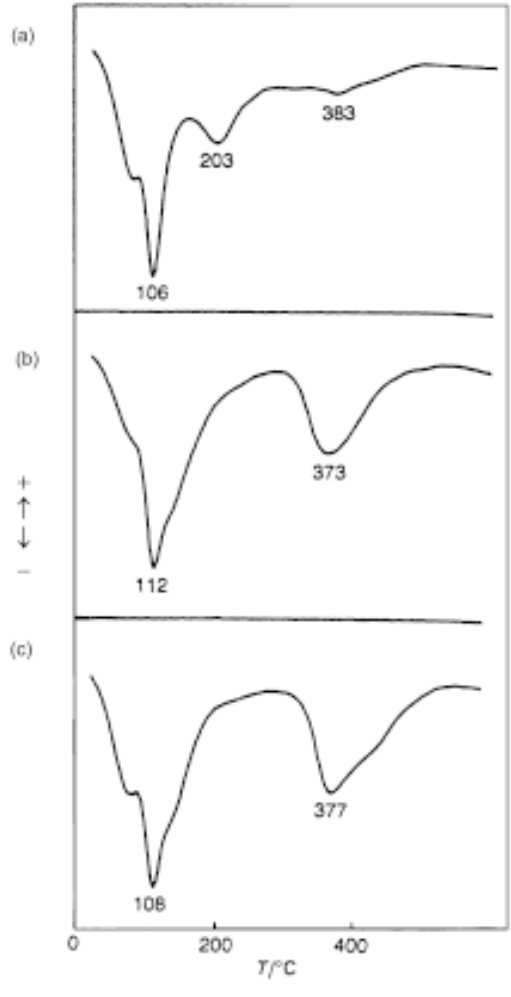

Figure 6.14. DTG curves of different gels.[68]

6.5.3 Water in Zeolite Synthesis

As mentioned earlier, zeolites could be synthesized only by the hydrothermal method. The versatility of hydrothermal chemistry owes much to the mineralizing role of water.[37][71] The factors that promote reactivity in aqueous magmas include:[72]

1. Stabilization of porous lattices as zeolites by acting as space fillers, referred to above.
2. Through its presence, especially at high pressures, water may be incorporated into hydrous glasses, melts, and solids. Through chemisorption into siliceous materials, Si-O-Si, and Al-O-Si, bonds hydrolyze and re-form. Chemical reactivity is enhanced and magma viscosity is lowered.
3. High pressures of water can modify phase equilibrium temperatures.
4. Water is a good solvent, a property that assists disintegration of solid components of a mixture and facilitates their transport and mixing.

DropBooks

Water is important as a guest molecule in zeolite structures with relatively high Al contents and consequently, aqueous media favor their formation while salts have a parallel role in the stabilization of sodalite and cancrinite. Highly siliceous zeolites, such as silicalite and ZSM-5, which have zeolitic structures, but contain very little Al^{III} and M^{m-}, are less hydrophilic than aluminous zeolites and their structures can be stabilized by certain organic guest molecules, notably amines, alcohols, and amino-alcohols. In general, the zeolitic water can be removed leaving the unchanged hydrous zeolite. In hydrothermal systems, the good solvent powers of water promote mixing, transport of materials, and facilitates nucleation and crystal growth. Water stabilizes zeolite structures by filling the cavities and forming a type of solid solution. The stabilizing effect is such that the porous aluminosilicates will not form in the absence of a *guest* molecule, which may be a salt molecule as well as water. However, the water concentration or the degree of dilution is of minor importance for the synthesis of ZSM-5, which can crystallize out of gels with an extremely wide range of H_2O/SiO_2 ratios (from 7 to 22). Some years ago Flanigen and Patton introduced a new route for zeolite synthesis that involved the use of F^- as the mineralizing agent.[73] This

method was further developed by Guth and Kessler (1989).[74] Replacement of OH^- by F^- allows the crystallization of zeolites, pure-silica ZSM-5, MFI, FER, MTT, MTN, and TON, at neutral or acidic conditions.

6.5.4 Temperature and Time

Temperature and time have a positive influence on the zeolite formation process, which occurs over a considerable range of temperatures. Based on geological evidence, an upper limit of 623 K has been suggested. Analcime has been obtained at 639 K, mordenite up to 703 K, clinoptilolite to 643 K and ferrierite at 648 K.[37] A rise in temperature will increase both the nucleation rate and the linear growth rate (expressed as $K = 0.5\,\delta l/\delta t$ with l = crystal size), hence, the crystallinity of the samples normally increases in time. As far as time is concerned, zeolite synthesis is governed by the occurrence of successive phase transformations. (Ostwald rule of successive phase transformation.) The thermodynamically least favorable phase will crystallize first and will be successively replaced in time by more stable phases.[37] The best example is the crystallization sequence of amorphous → faujasite → Na-P (Gismondine type).

The temperature, however, can also influence the type of product that has to be to crystallized. A rise in temperature leads to the crystallization of more dense products as the fraction of water in the liquid phase, which has to stabilize the porous products by filling the pores, will drop. Therefore, the existence of an upper limit for the formation of zeolites is to be expected. The use of nonvolatile pore space occupying (filling) species would, in principle, allow a high-temperature synthesis of open, porous structures.[11]

Temperature can obviously affect the rate of nucleation and crystal growth. The rate of nucleation and the linear rate of crystal growth are shown as follows:[25]

$$\mathrm{D}N/\mathrm{d}t = A\,[\exp\,(Et)^{-1}]$$

$$r = kt$$

The coefficients, *K*, *A*, and *E*, in Table 6.14, and *K* in Table 6.15, all increase with temperature, indicating that linear rates of crystal growth (coefficients *K*) and rates of nucleation (coefficients *A* and *E*) both increase with rising temperatures.

Table 6.14. K, A, and E, for Zeolite NaA as Function of Alkalinity and Temperature[77]

T (k)	H_2O/Na_2O	K (μmh^{-1})	$A \times 10^6$	E
343	20	0.050	20.0	0.102
343	30	0.027	13.2	0.033
343	40	0.017	9.0	0.115
333	20	0.03	1.0	0.062
343	20	0.05	20.0	0.102
353	20	0.06	200.0	0.132

Table 6.15. Linear Rates $K = 0.5\,\Delta 1/\Delta t$ for Growth of NaX[66]

T (k)	343	353	363	373
K(μmh^{-1})	0.0175	0.0375	0.0625	0.1071

DropBooks

When the temperature is elevated, the induction time of s-shaped crystallization curves is shortened. It is also observed that the temperature strongly affects the induction time. Zhdanov and Samulevich[66] have developed a method to analyze nucleation and crystal growth

$$\frac{d\ln(1/\theta)}{d(1/T)} = \frac{En}{R}$$

where θ is the induction time, that is, a point on the crystallization curve where the conversion into the crystallization phase just begins. The apparent activation energy for nucleation of phillipsite was given as 13.5 and 14.3 kcal/mole with and without stirring respectively, while, for the Al-free end member of the ZSM-5 series (silicalite 1), this energy was given as 9.1 kcal/mole.[75][76] The En value for NaY was obtained as 17 kcal/mole.[76]

6.5.5 Alkalinity (pH)

Alkalinity of the media plays a vital role in crystal growth, materials synthesis/preparation, and processing, on the whole. It

influences the supersaturation, kinetics, morphology, shape, size, and crystallinity, of the particles or materials as the OH^- anions fulfill the crucial role of mineralizing agent. The pH is influenced by the reactants and their concentrations/ratios, followed by temperature and time. Further, with the introduction of organics, the pH changes rapidly in the system, hence, pH is the key parameter in determining the crystallization rate. An increase in OH^- concentration will generally bring about an accelerated crystal growth and a shortened induction period before viable nuclei are formed.

In zeolite synthesis, pH of the alkaline solution is usually between 8 and 12. The major role of pH is to bring the Si and Al oxides or hydroxides into solution at an adequate rate. It is well known that OH^- is a powerful mineralizer. Water as a mineralizer has been discussed in detail in Ch. 4. Water has much increased the coefficient of expansion under hydrothermal conditions. The *PVT* measurements for water and other solvents are rather rare. The *PVT* data for water up to 1000°C and 10 Kbar are known accurately enough up to within 1% error.[71] Figure 4.7 shows the temperature-density diagram of water, with pressure as a parameter.[71] At a very high *PT* condition (1000°C and 100 kbar), water is completely dissociated into H_3O^+ and OH^-, behaving like a molten salt, and has a higher density, of the order of 1.7–1.9 g/cm^3.

The OH^- ion is a good complexing agent, which can bring amphoteric oxides and hydroxides into solution. An increase in pH will accelerate crystal growth and shorten the induction period (period before formation of viable nuclei) by an enhanced reactant concentration.[22][78] For example, the values shown for Linde zeolite, Na-A, Table 6.15, indicates that the nucleation rate dN/dt, for both coefficients A and E increase strongly with increasing pH. The solubility of silica increases nearly exponentially with the concentration of alkali and, in the resultant mixture, a range of silicate anions may appear with various degrees of oligomerization. In the case of alumina at high pH minimal oligomerization, there is the dominant anion, always being $Al(OH)^-_4$. The high pH causes supersaturation of silicate and aluminate and the formation of a large number of nuclei. The growth of these nuclei proceeds until the aluminum in the gel is exhausted so that the alkaline media enable ready mixing of reactants and also facilitate nucleation and crystal growth. Lechert (1998) has given the importance of pH values in the crystallization of zeolites.[79]

6.5.6 Structure Directing and Composition Determining Species (Templating)

Templating has become an important tool for material preparation and processing. Both organic and inorganic agents can be used as templating agents. Generally speaking, this processing route uses channels, layers, and cavity spaces of nanoporous host structures to grow nanoscale objects.[80] In some aspects, templating is related to biomimetics as the controlled nucleation and growth of inorganic phases in the organic host is an important step of biomineralization.[81] There exists a variety of organic and inorganic host materials with one, two, and three-dimensional structures as reviewed in Ref. 80. The concept of template in molecular sieve synthesis is not new.

In zeolite synthesis the term *templating* is used in a loose sense to refer to the filling of the void spaces of a zeolite structure by the bulky organic/inorganic cations frequently used as structure directing or structure-stabilizing agents. They contribute to the formation of the zeolite lattice during the zeolitization. Process *(i)* by influencing the gelation and/or nucleation processes; *(ii)* by lowering the chemical potential of the lattice formed by the inclusion of the templates during zeolite synthesis. Templating contributes to the stability through new interacts (hydrogen-bonds, electrostatic and London dispersion interactions), and further controls the formation of a particular topology through its geometry (form and size).[82] Thus, the action of a template appears to have both electronic and steric components. It is evident that changes in the cation density provoked by geometrical or physical properties of the template will be reflected in the chemical composition (Si/Al ratio) of a given topology. In the early 1960s, the TMA cation was introduced as the first organic cation to be used in zeolite synthesis.[43][83]

DropBooks

Thus far, it has not been possible to predict the actual role of templates and which template is reported to obtain a particular structure and composition. Therefore, in selecting possible templates, one has to bear in mind some general criteria regarding templating potential in zeolitization, such as solubility in the solution, stability under synthesis conditions, steric compatibility, and possible framework stabilization, and the most important practical issue is to remove the template without destroying the framework. The synthesis of Omega zeolite is strongly favored by the presence of TMA^+ ions, thus, templates can be structure-making or structure-breaking agents.[84][70] Also, it is well-known that neutral molecules, as well as cations or ion pairs, are able to fulfill structure and composition directing functions. Each one of these can be organic or inorganic in nature. Recently,

Feng, et al., (1998), have carried out the amine directed synthesis for some of the zeolites.[85]

The cations influence greatly the type of zeolite that crystallizes from aqueous alkaline magmas. Also, in the laboratory, synthesis of zeolite cations occupy an important place, not only as structure and composition directing agents, but also as agents influencing the rate of zeolite synthesis.[25][37] The species like Na^+, Li^+, Cs^+, K^+, Rb^+, Ca^{2+}, Sr^{2+}, tetra-alkyl-ammonium cations (TMA^+, TEA^+, TPA^+, dihydrozyethyl-dimethylammonium, etc.), dialkyl and trialkyl amines, phosphonium compounds, etc., are frequently used. Sometimes, neutral molecules, like crown-ethers, are used to form charged species upon complexation of an alkali metal cation.

Structure making cations are small cations, like Na^+ and Li^+, which interact strongly with water molecules because of their high charge density. As a result of this, the original hydrogen bonds are broken and the water molecules will be (reorganized) organized around the cations. This water-cation interaction is shown schematically in Fig. 6.15.

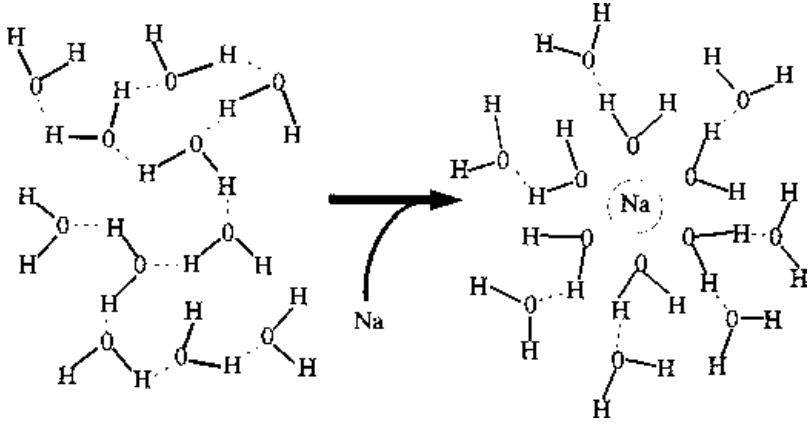

Figure 6.15. Schematic diagram of water-cation interaction.[37]

The structure-breaking cations are large cations, like NH^+_4, K^+, and Rb^+, which also interact with the water molecules, break the original hydrogen bonds, and, therefore, are known to break the water structure.[70] However, there are some large cations, like tetra alkylammonium, which seem to organize the water structure, the other templating neutral molecules used are amines, ethers, alcohols, di, and triols, etc.[82][86]

The presence of salts, e.g., NaCl, KCl, KBr, CaF_2, $BaCl_2$, $BaBr_2$, during zeolite synthesis can be an important factor as these ion pairs may be occluded (possibly next to water molecules) into the pore system, thereby stabilizing the pore structure. These nonvolatile species increase the silica, which is soluble with an increase in temperature and open several new pathways for zeolites synthesis and also for new products besides improving crystallinity and yield.

The reader can go through the excellent reviews given in Refs. 87 and 88 on the role of organic substances in the synthesis of zeolites. Table 6.16 indicates that organic bases facilitate the formation of several novel structures, especially those with extremely silica-rich zeolites, such as the pentasils, ZSM-5 and ZSM-11, and also zeolite Nu-1 and Fu-1.[37] Table 6.17 shows the organic zeolite structure relationships.[77] In recent years, several zeolites, like ZSM-5, mordenite, and other related zeolite structures, could be synthesized in the absence of any organic compound, here the hydrated Na^+ ions are able to function as templates for the formation of secondary building units.

In recent years, templating has found several new applications.[89] Among the inorganic materials zeolites have been widely used as hosts for a variety of materials, including conjugated polymers, selenium, chains, etc. Zeolites as well as glass or alumina nanoporous membranes have been used to fabricate organic and inorganic tubules or fibrils.[90] Carbon nanotubes can serve as removable templates for other inorganic nanorods/nanowires, e.g., GaN, Cu, or V_2O_5.[91] The mesoporous materials can be fabricated with a variety of shapes and sizes, from nanostructures, to almost millimeter-size objects.[92] Figures 6.16*(a)* and *(b)* show the number of papers published (including patents and some important conference proceedings) in the years between 1989 and 1997 and the countries actively engaged in templating research. Figure 6.16*(a)* shows a remarkable increase in the number of papers and, moreover, the increasing tendency will likely continue into the future.

DropBooks

6.5.7 Nucleation

This forms an important part of zeolite synthesis and it is one of the most complicated aspects because the chemical precursors here are more complex and varied compared to the chemical precursors in the formation of many ionic solids, like M^+Cl (M^+ = Li, Na, K, Rb, Cs). Nevertheless, the stages of nucleation are more or less the same in all cases, i.e., small

aggregations of precursors give unstable germ nuclei, some of these embryos become large enough to be stable nuclei and spontaneous deposits of more material on such nuclei results in larger crystallites.

The analysis of metastable solution structure is intimately related to nucleation theory. There are several approaches to understanding the nucleation, *(i)* the classical theory, and *(ii)* the modern nucleation theory.[93][94]

Table 6.16. Some Zeolite Syntheses in Presence of Organic Bases[25]

Cations	Zeolite Type	Cations	Zeolite Type
TMA^+	Sodalite	$Li^+ + Cs^+ + TMA^+$	Camcrinite
	Gismondine		Li-ABW
$Na^+ + TMA^+$	Sodalite		Zeolite A
	Cancrinte		Edingtonite (K-F)
	Gismondine		Anulcime
	Zeolite A (isotypes N-A, α, ZK-4)		Offretite (O)
			Zeolite (ZK-5 (KFL)
	Funijusite		Zeolite ZSM-2
	Zeolite TMA-E (EAB)		Gismondine
	Muzzite (zeolites W, ZSM-4)		Sodalite
	Zeolite (Na, TMA)-V	$Na^+ + K^+ +$	Erionite
	benzyltrimethylammonium (isotypes N and Z-21)		Losod
	Zeolite Nu-1	$Na^+ +$ N	Losod
	Zeolite Fu-1	$Na^+ +$ O N O	
$Ca^{2+} + TMA^+$	Sodalite	$Na^+ +_{neopentyltrimethylammonium}$	Losod
	Gismondine		
$Ba^{2+} + TMA^+$	Erionite		
	Zeolite L	$Na^+ + CH_3N^-$ N^+CH_3	Zeolite ZK-5 (KFL)
	Erionite		Levynite
	Oilretite	$Na^+ +_{primary\ n\text{-}alkylamines} (C_2 to C_{12})$	Zeolite ZSM-5 (MFL)
		$Na^+ +_{isopropylamine,\ dipropylamine}$ or dibutylamine	Zeolite ZSM-5
	Chabazite		
$Na^+ + NH_2(CH_2)_6NH_2$	Zeolite ZSM-5(MFL)		
$NH_{4+tetrapropylammonium}$	Zeolite ZSM-5		
$Na_{+tetrapropylammonium}$	Zeolite ZSM-5		
$Na^+_{+tetrapropylammonium}$	Zeolite ZSM-8		
$Na^+_{+tetrapropylammonium}$	Zeolite ZSM-11(MFL)		
$Na^+_{+benzyltriphenylammonium}$	Zeolite ZSM-11		
$Na^+_{+tetrapropylammonium}$	Zeolite ZSM-11		
$NH_4^+{}_{+tetrapropylammonium}$	Zeolite ZSM-11		
	Zeolite ZSM-10		
$K^+ + CH_3N$	NCH_3		
$Na^+_{+K^+ + tetrapropylammonium}$ with $Cr(OH)_3$, $Fe(OH)_3$, $Al(OH_3)$	Zeolite ZSM-8		

Table 6.17. Organic Zeolite Structure Relationships[77]

Organic	Structure	Structure Type
TEA	β	?
	ZSM-8	ZSM-5
	ZSM-12	?
	ZSM-20	Faujasite
	Mordenite	Mordenite
	ZSM-25	?
Methyltrienthyl-ammoulum	ZSM-12	?
TPA	ZSM-5	ZSM-5
n-Propylamine	ZSM-5	ZSM-5
TBA	ZSM-11	ZSM-11
Choline	ZSM-38	Ferrierite
	ZSM-34	Erionite-Oflretite
	ZSM-43	?
	CZH-b	?
TMA + TBA	ZSM-39	ZSM-39
TMA + n-propylamine	ZSM-39	ZSM-39
	ZSM-48	ZSM-12?
Pyrrolidine	ZSM-35	Ferrierite
	ZSM-21	Ferrierite
	ZSM-23	?
1, 2-Diaminoethane	ZSM-5	ZSM-5
	ZSM-21	Ferrierite
	ZSM-35	Ferrierite
1, 3-Diaminoethane	ZSM-35	Ferrierite ZSM-5
	ZSM-5	
1, 4-Diaminoethane	ZSM-35	Ferrierite, ZSM-5
	ZSM-5	
1, 5-Diaminoethane	ZSM-35	ZSM-5
1, 6-Diaminoethane	ZSM-5	ZSM-5
1, 7-Diaminoethane	ZSM-11	ZSM-11
1, 8-Diaminoethane		ZSM-11
ZSM-11		
	ZSM-48	
1, 9-Diaminoethane	ZSM-11	ZSM-11
1, 10-Diaminoethane	ZSM-11	ZSM-11
DDO	ZSM-10	?
	ZK-5	?
MDO	ZK-20	Levynite
MQ	LZ-132	Levynite
	Nu-	Levynite
TQA	ZSM-18	?
BP	LOSOD	LOSOD
Dihexamethylene-triamine	ZSM-30	?
Neopentylamine	Mordenite	Mordenite

DropBooks

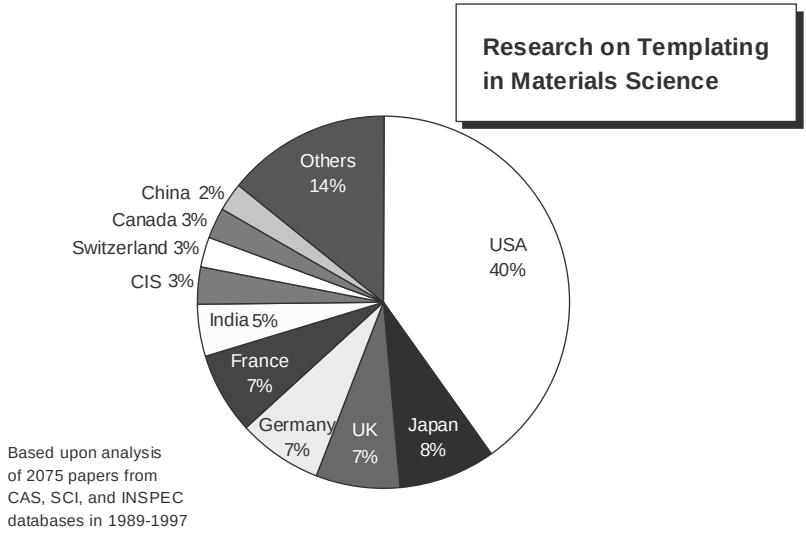

(a)

Figure 6.16. *(a)* Pie chart of the countries activey engaged in templating research based on the number of papers published (including patents and some important conference proceedings) in the years between 1989 and 1997. *(b)* Histogram of number of papers published (including patents and some important conference proceedings) in the years between 1989 and 1997. *(c)* Number of papers published in the journals on templating between 1989 and 1997.[89]

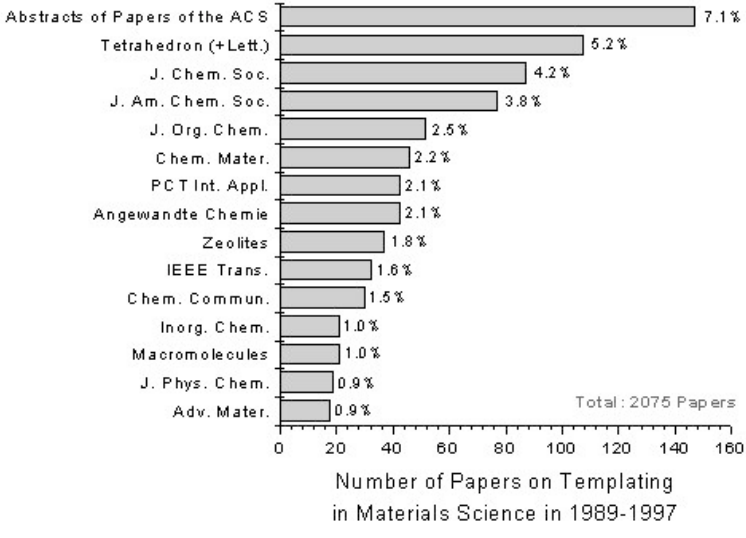

(b)

DropBooks

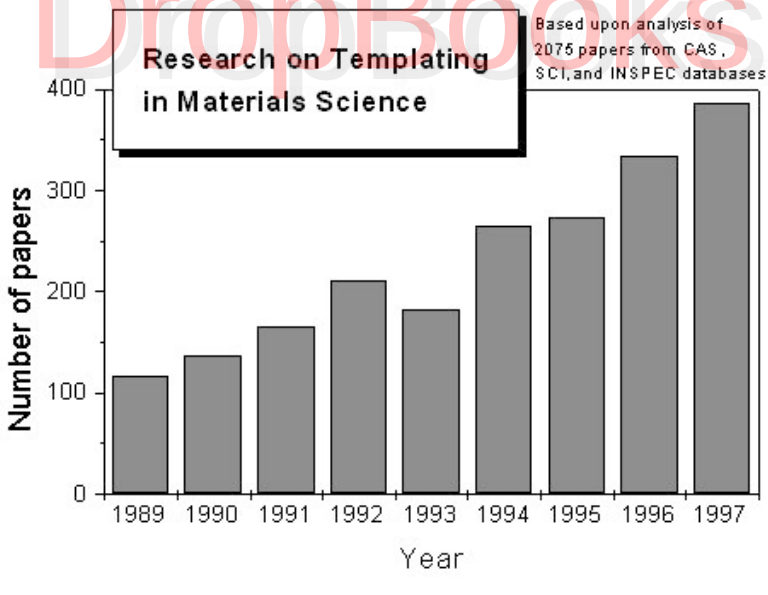

(c)

Figure 6.16. *(Cont'd.)*

In the first case, if a solution is in a metastable state (supersaturated solution) it will, sooner or later, enter another state, which is stable. Gibbs was the first one to propose that the work of the critical nucleus formation can be considered as a measure of the metastable state stability. Gibbs' idea was further developed by Volmer-Doring, Frenkel, Zeldovich, and Lifshitz-Spyozov, using thermodynamic concepts. The modern theoretical models of nucleation are based on the field-theoretic approach to nonequilibrium dynamics of the metastable state. These models provide an alternative to the classical theories.

Nucleation, on the whole, occurs from supersaturation, and it can be of two types, homogeneous and heterogeneous nucleation, the former occurs spontaneously, and the latter is induced largely by the presence of impurities or foreign particles present in the solution.

Barrer (1982) has summarized the general properties of nucleation that can be applied to zeolite synthesis also.

1. Rates of nucleation increase with the extent of undercooling, i.e., with increasing metastability; however, viscosity also tends to increase, often rapidly, as temperature falls, so that effects of the degree of undercooling and of viscosity oppose one another in influencing nucleation rates that can then pass through a maximum as temperature falls.
2. An incubation period is observed, particularly in condensed phases, during which nucleation cannot be detected. Even in seeded solutions, metastable regions of supersaturation can occur within which nucleation is not detectable. In many phase studies involving solutions, well-defined composition boundaries are found beyond which nucleation occurs freely so that under appropriate conditions the rate of nucleation increases extremely rapidly with the degree of supersaturation.
3. The extent of the incubation time can be changed significantly by very small changes in composition.
4. The onset of nucleation often depends on the previous history of the system.

The formation of nuclei takes place during the entire process of crystallization, but the rate of nucleation increases only during its initial stage. During the formation of viable nuclei, different kinds of germ nuclei (embryos) will form by chemical aggregations of the precursor species mentioned above

and disappear again upon depolymerization.[37] As a result of such fluctuations, in time the germ-nuclei will grow and eventually form different kinds of nuclei with dimensions having the critical size to become viable, i.e., nuclei on which crystal growth occurs spontaneously.

The nucleation theory with reference to the zeolite synthesis can be approached from different angles. Subotic and Bronic (1986) have developed a theory guided by their experimental observation.[67] In this connection, the theory proposed by Zhdanov (1971) and Samulevich (1980) infers that zeolite nuclei must be hidden in the amorphous gel and released during gel dissolution.[50] The basis for their theory is the empirical equation:

$$f(t) = \frac{mz(t)}{mz(tq)} = Kf$$

where: f = % zeolite relative to the final equilibrium value, t = crystallization time, q = constant power, K = constant coefficient.

Warzywoda and Thompson (1989) proposed the autocatalytic nucleation that can be incorporated in the population balance formalism, which allows inclusion of gel and solution material balances.[95] Using the population balance formalism, one can simulate crystal size distribution behavior and extend these simple analyses to other crystallizer types. However, it has been shown that the predicted nucleation rate profile for such a process is unlikely, as observed experimentally. Nuclei released from the gel are nucleated much later in the crystallization process than observed experimentally.[95]

DropBooks

The net free energy of formation of spherical nucleus can be expressed in terms of degree of supersaturation (S), the density (ρ) and surface energy (σ) of the nucleus as:[95]

$$\Delta g = \frac{16\pi\sigma^3 (MW)^2}{3(RT\rho \ln S)^2}$$

It is obvious from the above equation that from a saturated solution ($S = 1$, $\ln S = 0$) no spontaneous nucleation can occur as the value for Δg equals infinity. For a supersaturated solution ($S > 1$), Δg has a finite negative value and hence, spontaneous nucleation is possible.[95]

The nucleation rate, J (number of viable nuclei formed per unit of time) is commonly described as an Arrhenius rate equation.[96]

$$J = A \exp\left(\frac{-\Delta g}{RT}\right)$$

The above relation predicts an exponential increase in the nucleation rate for an increasing supersaturation degree once a critical degree of supersaturation has been reached.

Experimentally, the rate of nucleation can be derived from crystal size distribution measurements in the final crystallization product and size increase measurements of the largest crystals during the course of crystallization.[11][17] As the nucleation and crystal growth are assumed to consume the same precursor species, the nucleation rate is expected to go through a maximum and decline again after a certain period of time when the consumption of precursor species by crystal growth will limit their availability for forming new nuclei.[96]

Several kinetic models have been proposed for the crystallization of zeolite based on the above considerations. A reader can get more information in Refs. 25, 37, 95, and 97. Figure 6.17*(a)* shows *(1)* the growth in the number of nuclei and *(2)* change in the rate of their formation during crystallization A, and *(b)* crystallization of zeolites as a function of time. Figures 6.18*(a)* shows *(1)* the crystal size growth of Na-X zeolite during crystallization of the gel and *(2)* the histogram of crystal size distribution in the final product; *(b)* shows *(1)* the derivative of curves (1) and (2) of Fig. 6.18 *(a)*, *(2)* nucleation kinetic curve, and *(3)* the crystal mass growth curve for Na-X zeolite, calculated from the data in Fig. 6.18 *(a)* and *(b)*.

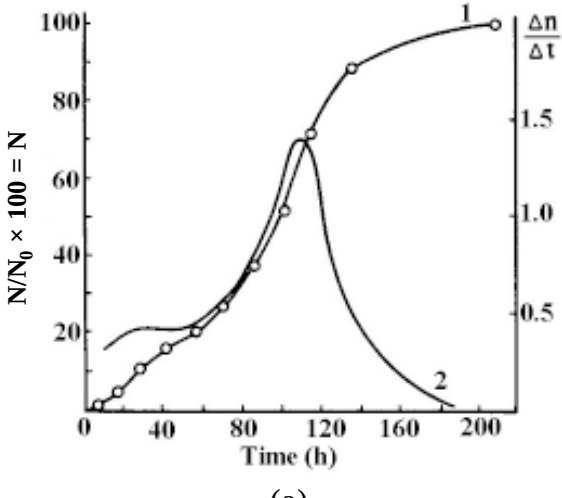

(a)

Figure 6.17. *(a)* Growth of number of nuclei (1) and change in rate of their formation (2) during crystallization of zeolite (A). *(b)* Crystallization of zeolites as a function of time; *1)* zeolite A, 373 K, *2)* zeolite X, 373 K, and *3)* mordenite, 573 K.

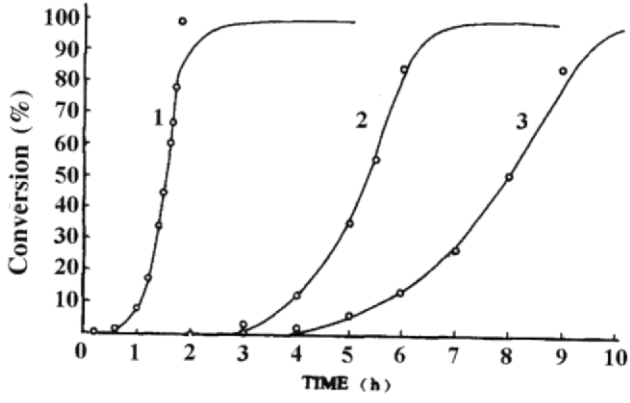

(b)

Figure 6.17. *(Cont'd.)*

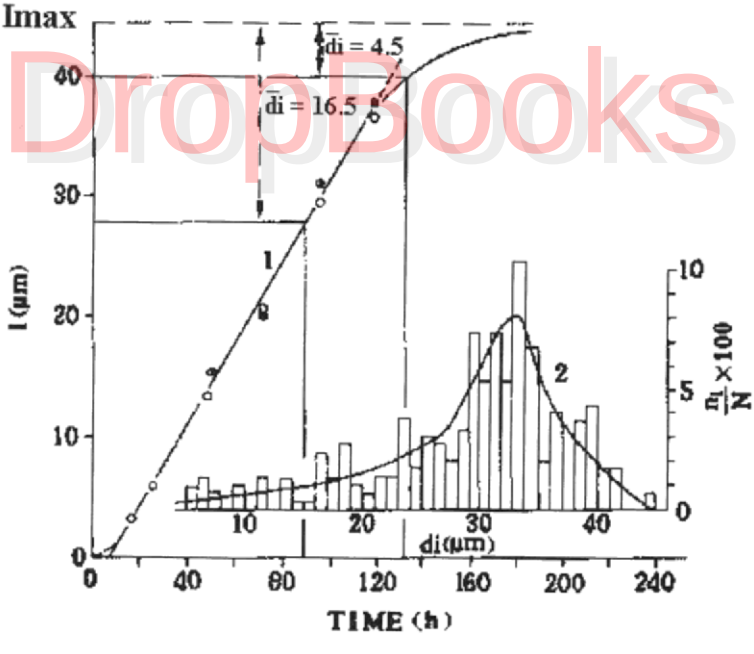

(a)

Figure 6.18. *(a)* Crystal size growth of Na-X zeolite during crystallization of the gel (1) and the histogram of crystal size distribution in the final product (2). *(b)* (1) Derivative of curves 1 and 2 of *(a)*, (2) nucleation kinetic curve (3) and the crystal mass growth curve for Na-X zeolite.[25]

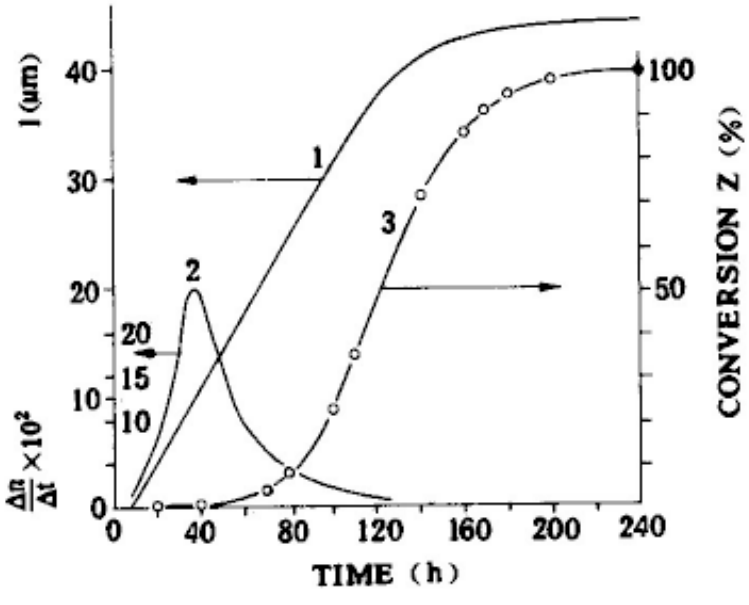

(b)

Figure 6.18. *(Cont'd.)*

In recent years there has been considerable progress made in the field of accelerating the kinetics of low-temperature inorganic synthesis.[98] Several techniques, like sonochemical (acoustic wave stimulation), ionizing and nonionizing radiation, microwave hydrothermal, hydrothermal process with superimposed electric fields, hydrothermal process with mechanical forces, and mechanochemical, including very high uniaxial pressure and shear. In order to have a coherent approach to correlate the kinetics of crystallization with crystal size distribution, Figure 6.19, shows the conceptual diagram of nucleation and crystallization of zeolite A. Carmona, et al., (1997) have explored the crystallization of VPI-5, a microporous $AlPO_4$ phase, using conventional boiling and refluxing systems, conventional hydrothermal reactors,[99] microwave activated refluxing systems, and microwave hydrothermal reactors. They explained the microwave activation techniques in terms of the influence of microwaves in the change of coordination of Al in the gel from octahedral Al (o) to tetrahedral Al (T), to yield the specific Al (o)/Al (T) ratio in the gel precursor necessary to direct the crystallization of VPI-5, and in terms of the rapid heating obtained by using microwaves necessary to reduce the probability of the formation of intermediate metastable phases.[99]

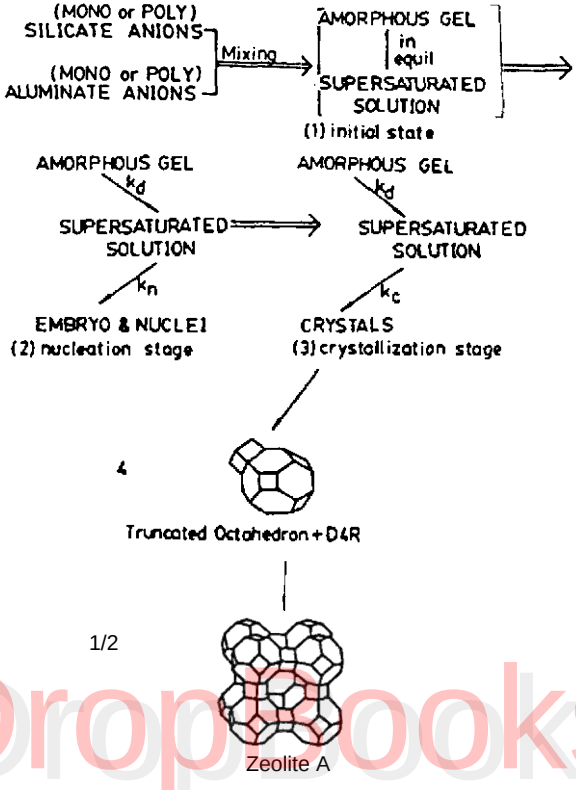

DropBooks

Figure 6.19. Conceptual diagram of nucleation and crystallization of zeolite A.[25]

6.6 CRYSTAL GROWTH

The synthesis of zeolites at temperatures around 100°C usually produces crystals in the size range 0.1–10 μm. In applications as catalysts, sorbents, and ion exchangers, this size range is fully suitable. The small size indicates that once nucleation begins there is rapid formation of numerous tiny particles all competing for the available chemical nutrients. In order to carry out the single crystal x-ray diffraction studies, zeolites should be 100 μm, or even more, in diameter. Similarly, for other examinations, like molecule and ion-selective membranes or other electrochemical studies, bigger crystals are required. Therefore, crystal growth of zeolites can be both challenging and interesting as well. Natural zeolites occur as large single crystals, however, these are often impure, rare, and require conditions that cannot be reproduced in the laboratory.[46] Large zeolite crystals are difficult

to produce in the laboratory by conventional hydrothermal synthesis where crystal formation is controlled to a large extent by the solubility of the reagent gel particles, the rate of generation of nucleation centers, and the solubility of the resulting products.[50] The low solubility of the crystallization products leads to a high degree of supersaturation, causing high nucleation leading to the formation of small crystals. A careful monitoring of the reactants, dilution temperature, agitation, and crystallization time, has yielded some large crystals of some zeolite types. Similarly, the use of slow-release complexing agents seeding sub and supragravity conditions to increase crystal size are met with limited success. There are several works on the crystal growth of zeolites.

Crystal growth succeeds nucleation, i.e., the nuclei will grow by addition or condensation of precursor species towards full-grown crystals. The autocatalytic nature of the first stage of the crystallization reflects the self-accelerating behavior of a crystallization process.

Crystal size can be influenced by experimental factors which alter the numbers of viable nuclei that develop so that if these numbers are reduced a greater share of the chemical nutrients is available for each growing crystal. The use of seed crystals can be similarly employed in the case of zeolites, Na-Y, Na-X. The smaller the number of seeds involved the larger the average size of the final crystals because a larger amount of chemical nutrient is available for each crystal before these nutrients are exhausted. Ghobarkar (1992), Ghobarkar and Schaf (1996*(a)*; 1996*(b)*; 1997), Kuperman, et al. (1993), Mel'nikov, et al. (1973), Demianets, et al. (1973), have carried out extensive work on hydrothermal crystal growth of several zeolites and studied their morphology in detail.[100]-[106] Figures 6.20–6.23*(a)–(j)* show the characteristic photographs of various zeolite crystals obtained under hydrothermal conditions. Kuperman, et al. (1993) have used a nonaqueous solvent, a mineralizing agent, reagent quantities of water, an optional organic template, silica or silica and alumina, or alumina and phosphorous, oxide sources to obtain giant crystals of zeolites and molecular sieves.[104] A close examination of the reactant products, under a polarizing microscope, didn't show any twining. Ghobarkar and Schaf (1996, 1997) have carried out hydrothermal experiments and found that at 1 kbar pressure and an experimental duration of 6 weeks maximum, the zeolite phases, thomsonite and edingtonite, were formed in the whole temperature range between 80°C and 230°C, and at 1 kbar pressure and at an experiment duration of 8 weeks maximum, the zeolite phase-natrolite was formed in a temperature interval between 80°C and 150°C.[102][103]

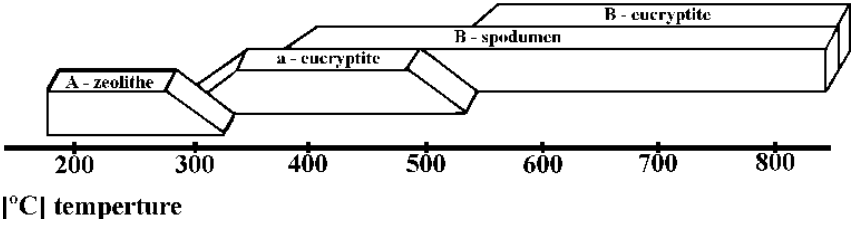

(a)

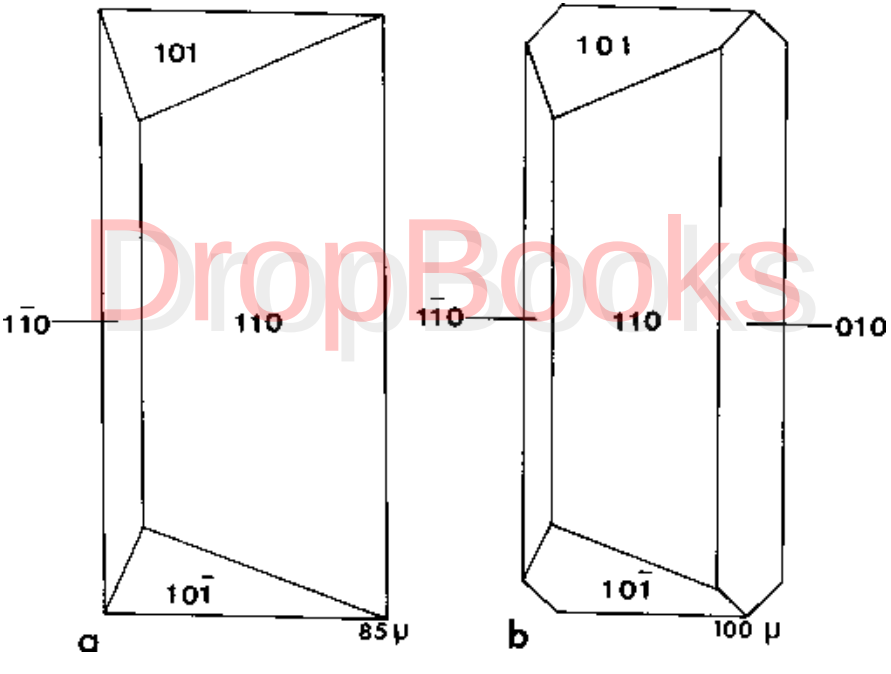

DropBooks

(b)

Figure 6.20. *(a)* Schemetic diagrams of zeolite crystals obtained under hydrothermal conditions. Development of mineral phase depending on the temperature. *(b)* Crystal of A-zeolite at (a) 150°C and (b) 250°C.[100]

(a)

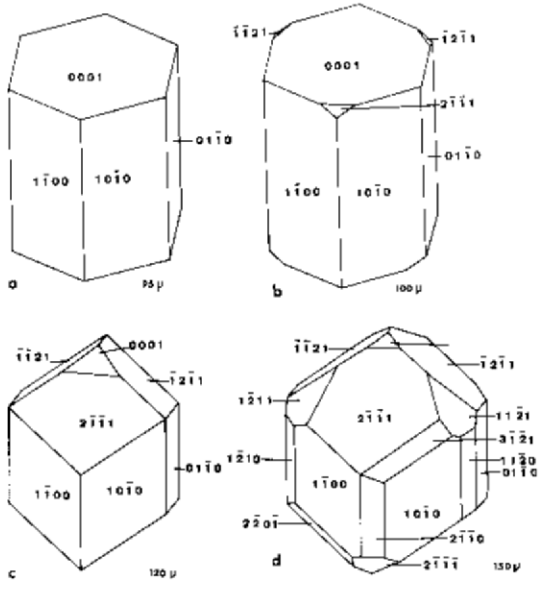

(b)

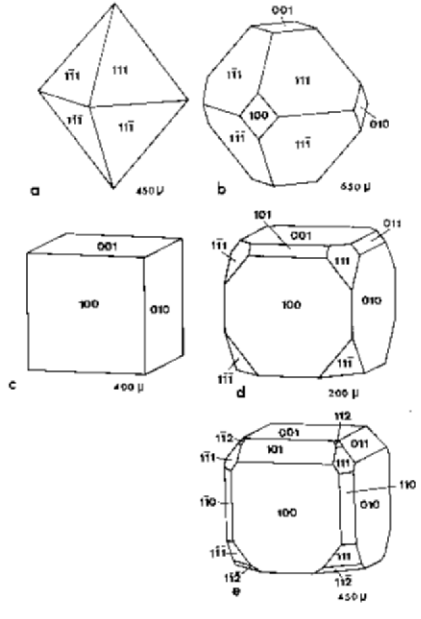

Figure 6.21. ***(a)*** Crystal of α-eucryptite at (a) 300°C, (b) 350°C, (c) 400°C, and 450°C (d). ***(b)*** Crystals of β-spodumene at (a) 350°C, (b) 400°C, (c) 500°C, (d) 550° and (e) 650°C.[100]

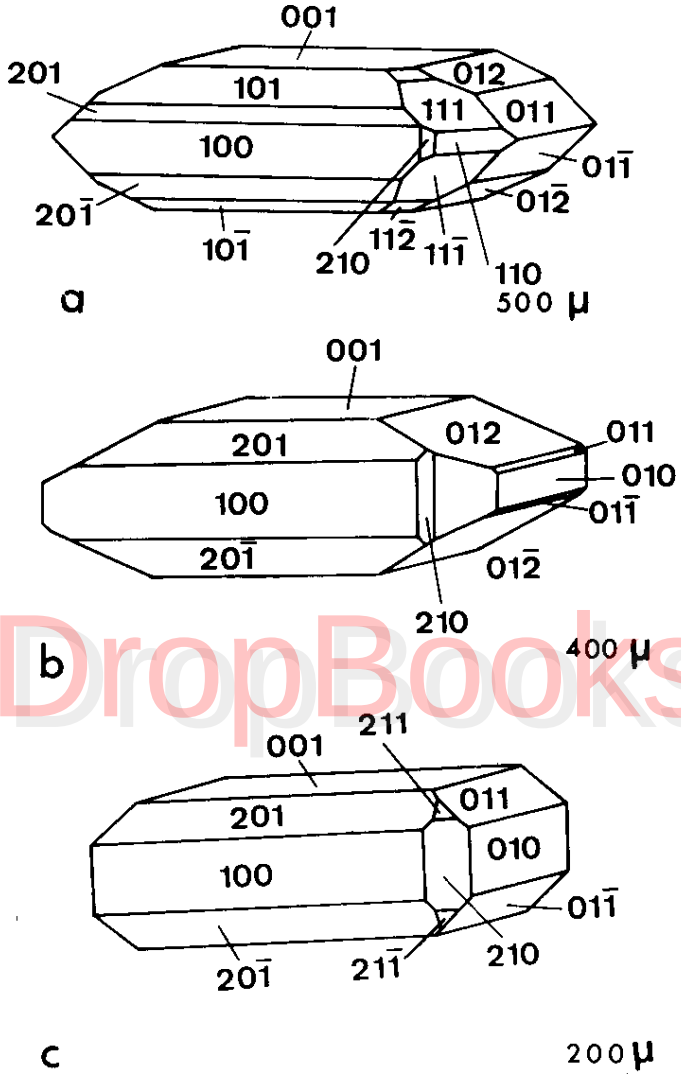

(a)

Figure 6.22. ***(a)*** Crystal of β-eucryptite at (a) 500°C, (b) 750°C, and (c) 850°C. ***(b)*** Sem and schematic diagram of Natrolite. ***(c)*** Crystal morphology of Thomsonite and Edingtonite.[102]

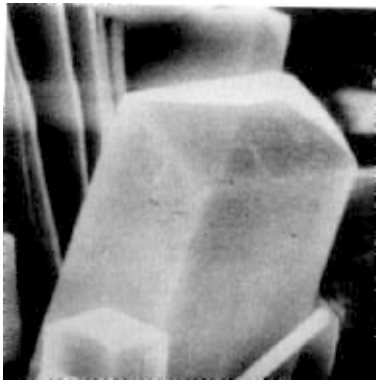

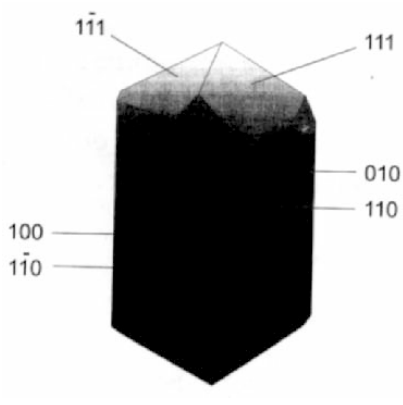

(b)

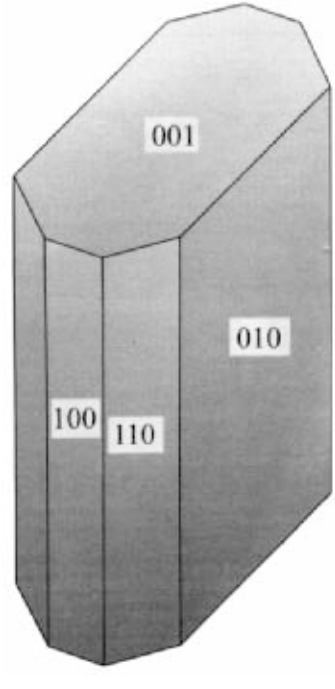

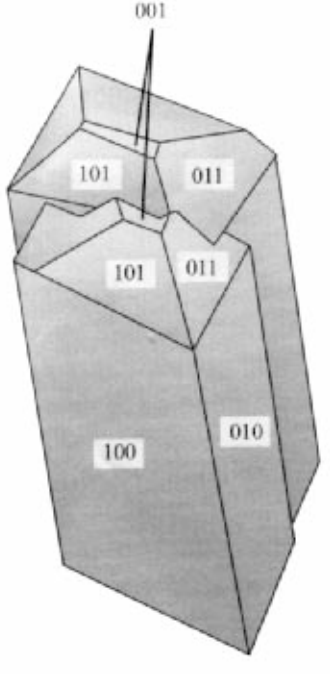

(c)

Figure 6.22. *(Cont'd.)*

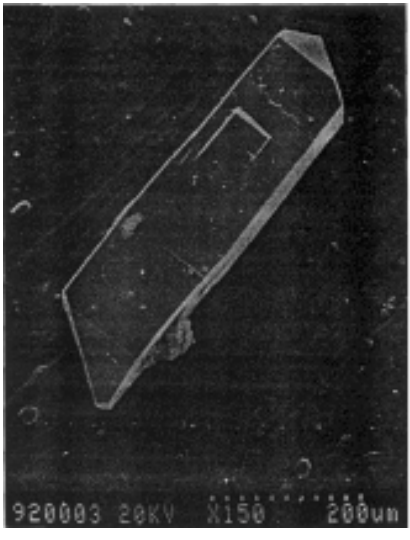

(a)

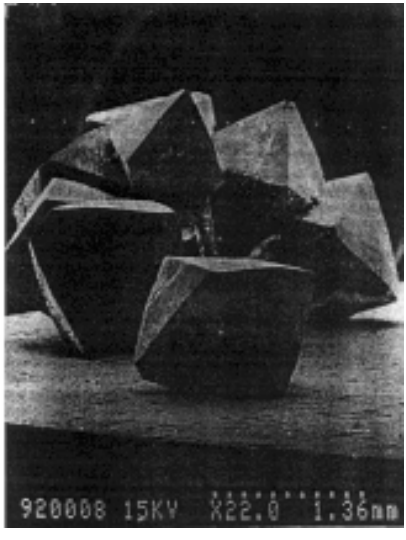

(b)

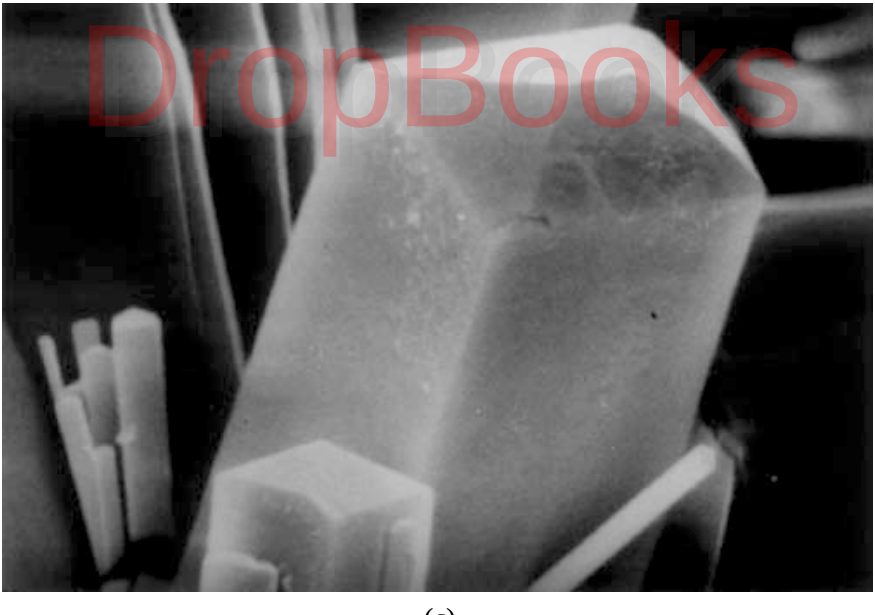

DropBooks

(c)

Figure 6.23. SEM of crystals of *(a)* silicaline-1, *(b)* dodecasil-3C, *(c)* Natrolite, *(d)* Chabasite, *(e)* A-Zeolite, *(f)* Merilonite, *(g)* Dachiardite, *(h)* Thomsonite, *(i)* Epistilbite, and *(j)* Gmelinite. *(Photos courtesy of Prof. Ghobarkar, H.)*

(d)

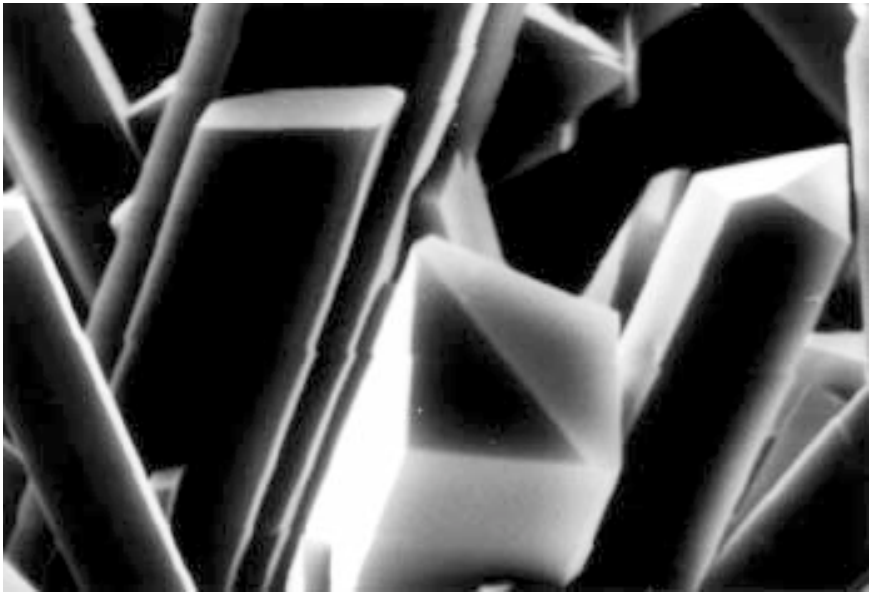

(e)

Figure 6.23. *(Cont'd.)*

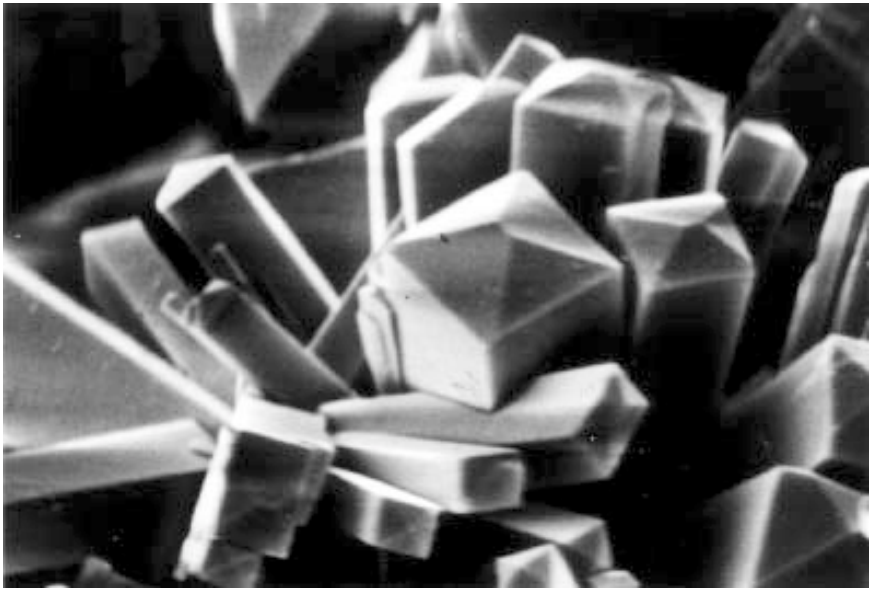

(f)

DropBooks

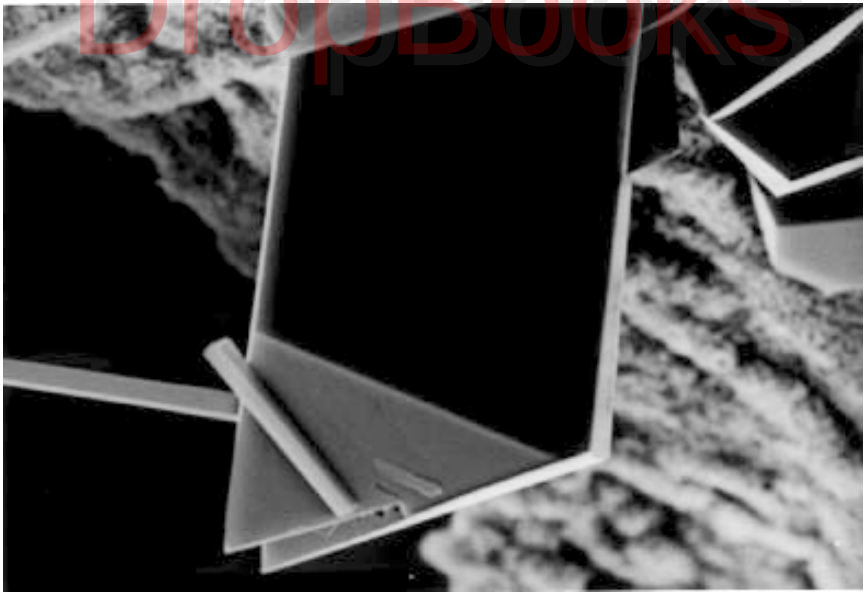

(g)

Figure 6.23. *(Cont'd.)*

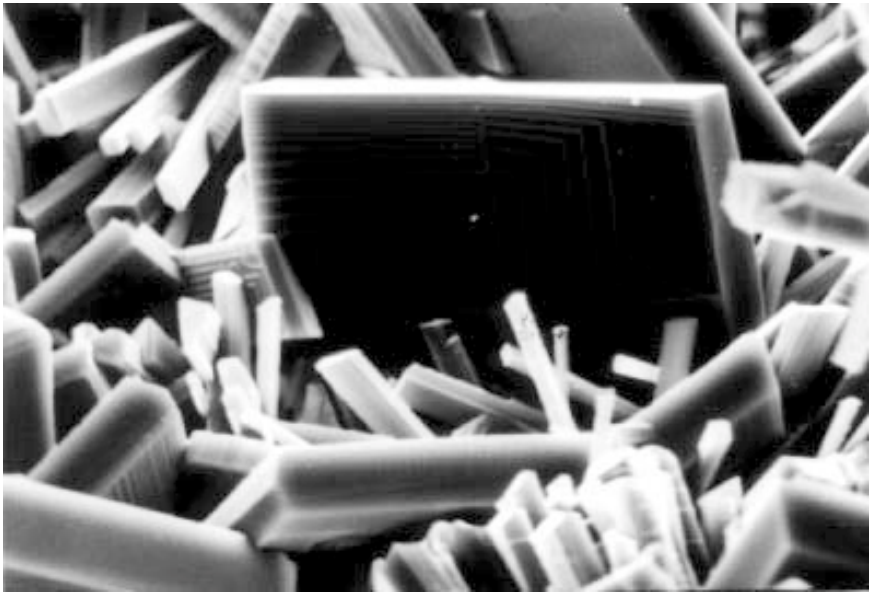

(h)

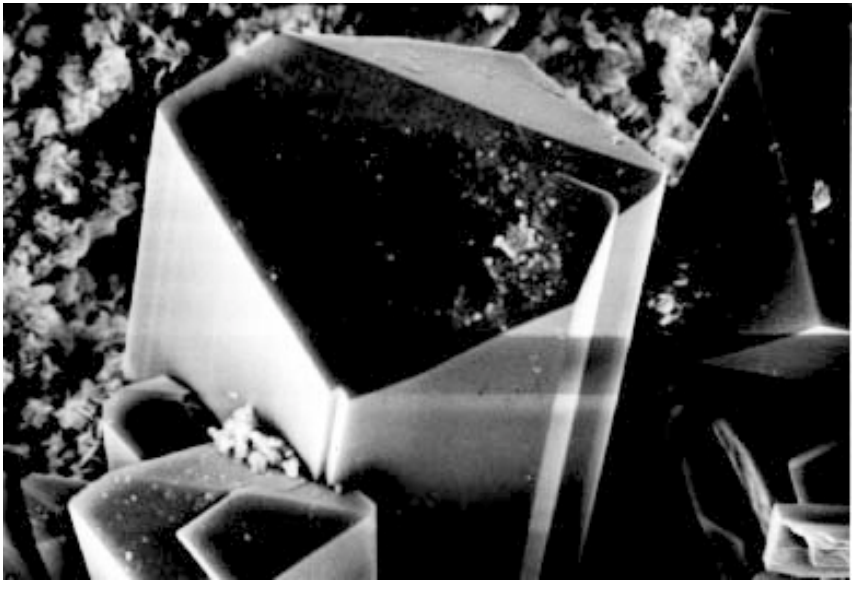

(i)

Figure 6.23. *(Cont'd.)*

(j)

Figure 6.23. *(Cont'd.)*

DropBooks

Among all the zeolite groups of materials, only sodalite has been obtained as bulk single crystals, owing to its attractive optical properties as nanocomposites in quantum electronics and nonlinear optics. Sodalites may be represented by the general formula $M_8\,[AlSO_4]_6.\,X_2$, where M = Na, Li, Ag, …, and X = Cl, Br, ClO_4, …. The sodalite framework consists of alternating SiO_4 and AlO_4 corner sharing tetrahedra forming four and six rings, which make up the basic β-case unit common to several zeolites. A semi-condensed structure is formed through linkage of the β-cases via six rings, with M_4 X clusters located at the center of each cage as shown in Fig. 6.24.[107] The replacement of the framework Al and Si by the larger Ga and Ge affects the structure, the introduction of larger framework atoms may also allow the enclathration of larger anions which can't be normally incorporated into aluminosilicate sodalites. The most promising method for the production of sodalite single crystals is the hydrothermal method, as any attempt to grow sodalite from the melt simply produces glass of an analogous composition while growing from solution in the melt yields small crystals of < 2 mm.[106] Thus, sodalite is normally synthesized from strong basic media under mild

hydrothermal conditions, however, by using ethylene glycol as a solvent, Bibby and Dale (1985) prepared a purely siliceous sodalite.[37][108] In fact, the exploration in hydrothermal systems of reactions yielding salt-bearing sodalites began nearly 120 years ago.[109][110] Carlgren and Cleve (1892) made the sodalites from Kaolinite and aqueous caustic soda containing the relevant dissolved salts at temperatures ranging from about 185°C to 220°C. Sodalite can also be made very easily in the absence of any salts, then they contain only zeolitic water and a limited amount of soda.[110] However, the production of large single crystals under hydrothermal conditions is very long and cumbersome. In fact, some experiments have been carried out for six months. Demianets, et al. (1992) have studied the solubility of sodalite in aqueous solutions of NaOH (10–40 wt%) between 200 and 300°C. Figure 6.25 shows the dependence of solubility of sodalite and the NaOH concentration at constant temperatures. The soluble curve of natural sodalite (hackmanite) lies rather below the curve plotted for the soluble of artificial sodalite. The synthetic mineral dissolves considerably at a rapid rate.[106]

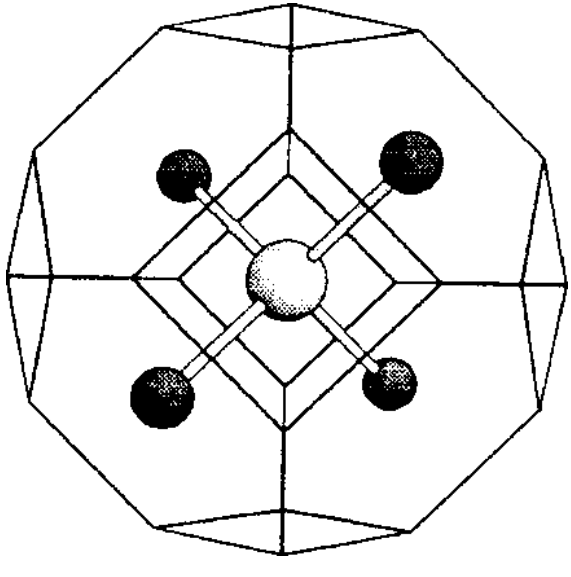

Figure 6.24. Sodalite cage containing M_4X cluster.[107]

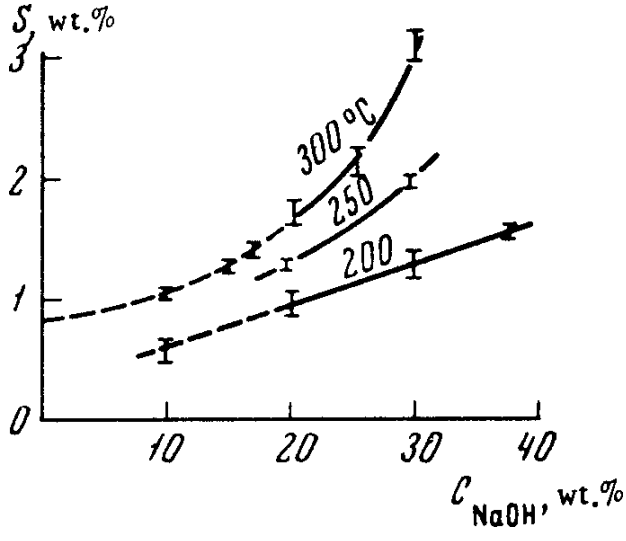

Figure 6.25. Dependence of solubility of sodalite and the NaOH concentration at constant temperature.[106]

DropBooks

Mel'nikov, et al. (1973) have carried out the hydrothermal growth of bulk sodalite crystals using seed crystals and have studied the kinetics of crystallization in detail. The experimental temperature was varied from 150 to 400°C in steps of 50°C. Figure 6.26 shows the relation between the growth rates of sodalite crystals in the directions and the temperature gradient *(a)* 200°C, *(b)* 250°C, *(c)* 300°C, and *(d)* 350°C.[105] The mass transfer associated with the crystallization of sodalite depends linearly on the temperature gradient for a constant growth temperature. They have found a direct relationship between the growth rates of the sodalite faces and the temperature drop at constant temperature and an exponential temperature dependence at constant supersaturation.[105] Recently, Hayashi, et al. (1998) have grown millimeter sized aluminosilicate sodalite single crystals under hydrothermal conditions.[112]

In spite of the interesting results obtained by the above authors, the quantum of data available on crystal growth is just meager compared to the synthesis of zeolites. It has to be understood in greater detail.

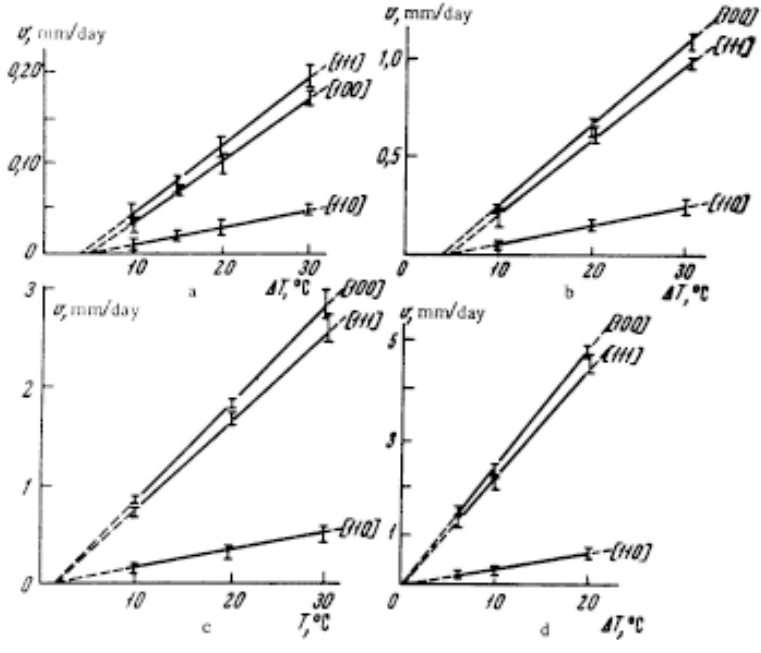

Figure 6.26. Relation between the growth rates of sodalite crystals.[105]

6.7 ALUMINOPHOSPHATE ZEOLITES

Aluminophosphate zeolites represent a new class of microporous inorganic solids with the potential to be as useful and as scientifically challenging as the aluminosilicate zeolites and form a part of the history of framework of oxide molecular sieves. The basis for the synthesis of such zeolites is the crystal chemical similarities between Si and P, and $AlPO_4$ and SiO_2 in particular. The unique feature of these zeolites is the compositional similarity and a great structural diversity. The basic structural units consist of alternating Al and P with Al exhibiting octahedral coordination and pressure, and tetrahedral coordination. The two waters of hydration occupy positions in the coordination sphere of Al.

The synthesis of aluminophosphate zeolites does not differ much from that of the synthesis of aluminosilicate zeolites, the procedure is as follows: equimolar amounts of a reactive hydrated alumina like boehmite, and phosphoric acid are dissolved in water. An aluminophosphate gel is formed, to which a templating agent (R), an organic amine or a quaternary

ammonium salt, is added. This mixture is digested quiescently in the preferred temperature range of 125–200°C. A crystallization product is formed, which is worked up using procedures typical of zeolite synthesis. About 23 structure analogs of three zeolites, *(i)* erionite ($AlPO_4$-17), *(ii)* sodalite ($AlPO_4$-20), and *(iii)* analcime ($AlPO_4$-24), have been obtained.[111] Some of the novel structures are $AlPO_4$-5, -11, -14, -18, -31, and -33. Among these, $AlPO_4$-5 was the first $AlPO_4$ molecular sieve synthesized and it was found to be a novel structure belonging to the hexagonal system. Similarly, in the preparation of aluminophosphate zeolites, the precursor gel contains four components, an alumina source, a phosphate source, water, and an organic amine or quaternary ammonium salt. The relative concentrations of the reactants are very important and, similarly, without the presence of organics no aluminophosphate zeolites molecular sieves can be formed. In most of the cases, the ratio of Al:P is 1.0. The commonly used organics are amines and quaternary ammonium cations i–Pr_2NH, n–Pr_2NH, n–BuEtNH, Et_2NH, n–Bu_2NH, n–Pe_2NH, Me_2NH, n–$BuNH_2$, n–$HexNH_2$. A wide variety of templating agents has yielded almost as wide a variety of structure types. The various structure types include a broad range of pore size and volumes as broad as that found among synthetic zeolites. The $AlPO_4$ frameworks have excellent thermal and hydrothermal stability. The surface character of the $AlPO_4$ molecular sieves differs from that of the silica molecular sieves even though both framework types are neutral with no extra-framework cations. The molecular sieve silicalite is hydrophobic and the $AlPO_4$ molecular sieves are moderately hydrophilic. Zeolites are hydrophilic due to the interaction of the dipole of the H_2O molecule with the electrostatic fields of the anionic aluminosilicate framework and the balancing non-framework cations. The hydrophilicity of the $AlPO_4$ materials is apparently due to the difference in electronegativity between Al (1.5) and P (2.1). Neither mechanism is possible with silica molecular sieves. The $AlPO_4$ molecular sieves do exhibit less affinity for H_2O than the hydrophilic zeolites, such as type A or type X.

DropBooks

The problems associated with the aluminophosphate zeolites crystallization are traced to the similarity in the composition and diversity in the structure. Therefore, one has to monitor carefully each step in order to prepare a desired zeolite phase and its reproducibility. In the case of aluminophosphate zeolites crystallization, the gel preparation, gel pretreatment, gel aging, pH of the media, experimental duration, experimental temperature of synthesis, molar proportions of the starting material, type of organics, and the time of addition of organics, and alumina source play an important role. The aluminosilicate zeolites are crystallized in a strong basic

medium with a pH of the reaction mixture > 13, whereas, for the successful crystallization of aluminophosphate zeolites, the pH range of the hydrous gel is found to be in the range of 3.5–6.0.[113] Any slight change in the above listed parameters largely influences the resultant product. Figures 6.27 and 6.28 show the possible experimental procedures for treating the $AlPO_4$ gel.

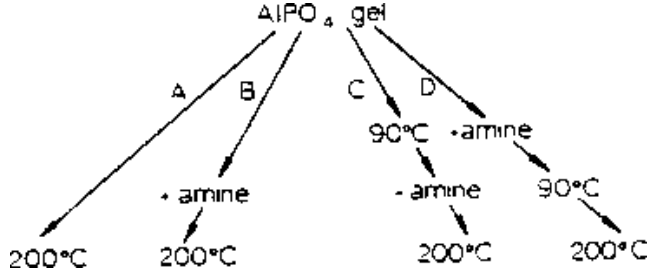

Figure 6.27. Possible experimental procedures for treating the $AlPO_4$ gel.[114]

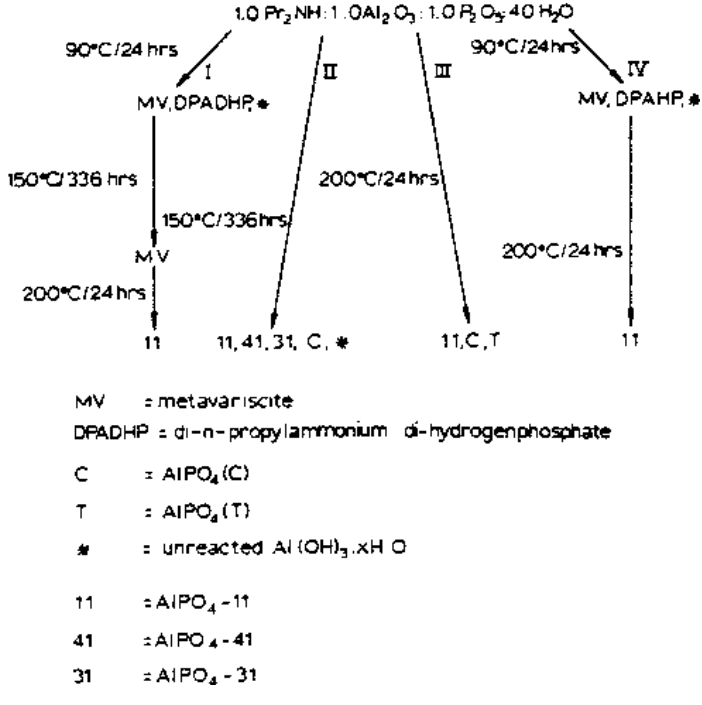

Figure 6.28. Effect of various hydrothermal treatments on the amine containing $AlPO_4$ gel.[114]

It was well known that the largest ring in silica zeolites consisted of twelve tetrahedral (12 T atoms) and this concept remained for over 180 years, since the first discovery of natural zeolite with 12-T atom rings, viz., gmelinite, took place during 1807.[18][19] Davis, et al., (1989) have synthesized for the first molecular sieve with rings that possess greater than 12-T atoms.[114] Virginia Polytechnic Institute No. 5 (VPI-5) is a family of aluminophosphate based molecular sieves with the same 3-d topology. The extra-large pores of VPI-5 contain unidimensional channels circumscribed by rings that have 18-membered rings and possess free diameters of approximately 12 to 13 Å.[114] It was only during 1996 that Freyhardt, et al., synthesized the first aluminosilicate zeolite with its ellipitcal 14-tetrahedral-atom pore opening.[115] For the synthesis of VPI-5, pseudoboehmite, 85 wt% H_3PO_4, tetrabutylammonium hydroxide (TBA) and n-dipropylamine (DPA) were used. Schmidt, et al. (1992) have studied the VPI-5 synthesis in detail.[116] Here, we describe only the synthesis of VPI-5 to show the peculiarities involved in the synthesis of aluminophosphate zeolites in general. In this regard, the experimental results of Schmidt, et al. (1992) are very interesting for a reader.[116] The reaction temperature was varied from 100–200°C using two different gel compositions in order to find the optimum conditions for VPI-5 crystallization. Figure 6.29 shows the dependence of the various $AlPO_4$ phases upon the reaction temperature for different molar ratios.

DropBooks

The change in temperature results in the appearance of various other phases like AlPO-11, AlPO-H3, in addition to VPI-5. Figure 6.29 clearly indicates a very narrow temperature range for the crystallization of VPI-5, which depends essentially upon the molar ratio of DPA = Al_2O_3:P_2O_5:H_2O. It has been shown that the use of bigger autoclaves can reduce the formation of other phases which might be connected with slower heating rate and temperature gradients/thermal currents within the liners.

Similarly, Schmidt, et al. have studied the effect of reaction time on the crystallization of $AlPO_4$ phases. Figure 6.30 shows the dependence of the various $AlPO_4$ phases upon reaction time at 124°C for the molar ratio 1 DPA:1 Al_2O_3:1 P_2O_5 = 40 H_2O. Thus, the hydrothermal crystallization of aluminophosphate zeolites from the reaction gel mixture is usually controlled kinetically and the first nucleus that reaches the critical size will determine the final production.

Figure 6.31 shows a schematic representation of the triple helix of water molecules within the 18-ring channel.

A majority of the aluminophosphate zeolites undergo phase transitions when calcined. For example, when VPI-5 is heated to 130°C under ambient pressure, it leads to a total phase transition of VPI-5 to AlPO-8. Figure 6.32 shows the schematic representation of the transformation of VPI-5 into $AlPO_4$-8.[117] This transformation takes place after the removal of water under specific washing and drying steps of the as-synthesized materials, the transformation may be complete when occluded water is removed above 100°C.

Thus, the synthesis of aluminophosphate zeolites involves a careful understanding of the influence of several experimental parameters.

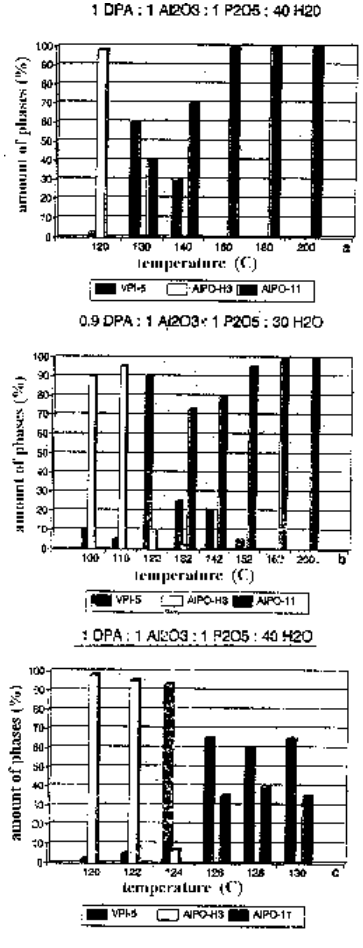

Figure 6.29. Dependence of various $AlPO_4$ phases upon reaction temperature for different molar ratios.[116]

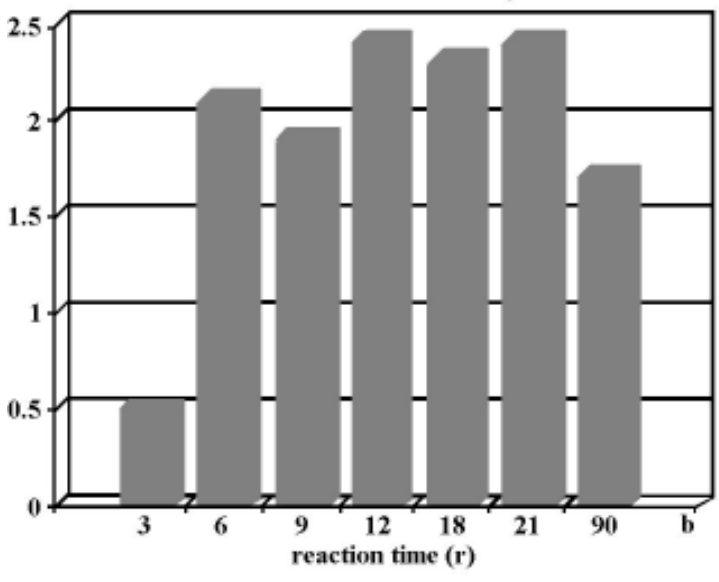

Figure 6.30. Dependence of the various $AlPO_4$ phases upon reaction time at 124°C for the molar ratio: 1:DPA:1 Al_2O_3:1 P_2O_5 = 40 H_2O.[116]

DropBooks

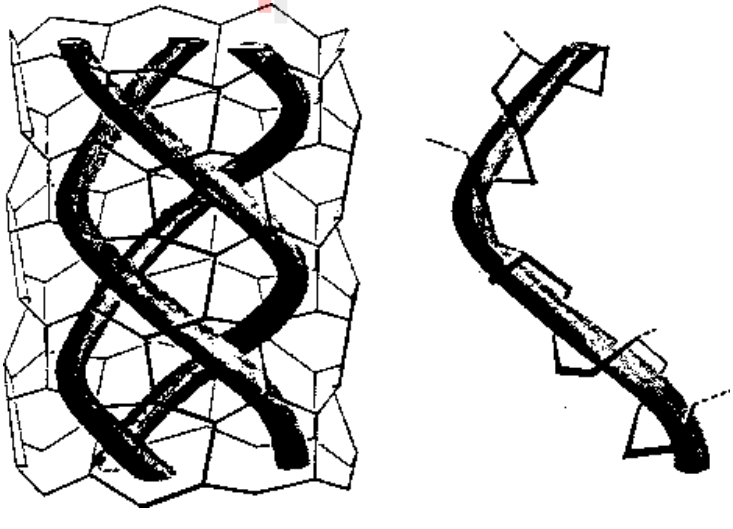

Figure 6.31. Schematic representation of the triple helix of water molecules within the 18-ring channel.[116]

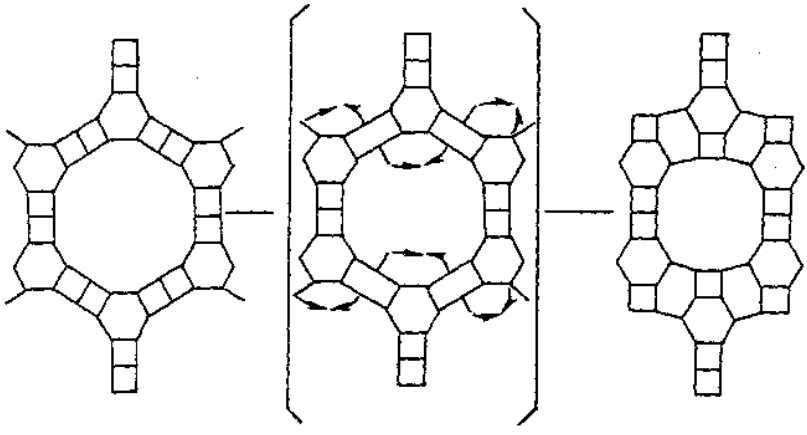

Figure 6.32. Schematic representation of the transformation of VP-5 into $AlPO_4$-8.[117]

6.8 GROWTH OF ZEOLITE THIN FILMS AND CRYSTALS AT INORGANIC/ORGANIC INTERFACES (PREPARATION OF ZEOLITE-BASED COMPOSITES)

There is a growing interest in the development of inorganic films and membranes with controllable porosity owing to their promising applications in asymmetric membranes, catalytic monoliths, and chemical sensors.[118]-[121] The interest in microporous thin films is primarily motivated by their potential molecular sieving action, large surface areas, and controlled host-sorbate interactions, especially at low vapor pressures. Some authors have explored several possibilities/strategies for thin film formation, including dip-coating of zeolite/silica sol suspensions, and chemical attachment of zeolite crystals via molecular coupling layers.[120][121] Similarly, zeolites also have been embedded into polymers, covered with glazes and extruded into composite monoliths.[122][123] It was observed that in order to enhance control of molecular selectivity in sensors, it would be desirable to tune or switch the pore size of zeolite crystals in the film. Thus, the authors have adopted such a concept by forming zeolite CaA/silica composite thin films and controlling the zeolitic pores through *in-situ* cation exchange and developed several composites. One such composite typically consists of 100 $\mu g/cm^2$ of zeolite crystals and 10 $\mu g/cm^2$ of amorphous silica over-layer. The

thickness of the silica layer is estimated to be about 20 nm when assuming a density of 2.2 g/cm^3 and a smooth surface. Systematic studies of the cation exchange in zeolite/silica composite films and sorption in the composite films have been carried out by Yan and Bein (1995).[121] Figures 6.33*(a)* and *(b)* show the assembly of zeolite CaA crystals on a silozane layer on a gold surface, and stabilization with 20 nm silica layer. Figure 6.34 shows the mass changes of zeolite silica composite films exchanged with different cations on a piezoelectric substrate. Figure 6.35 shows a schematic diagram of the SAW device covered with molecular sieve layer. Figure 6.36 shows the proposed reaction scheme for the design of zeolite layers and films on organophosphate films: *(a)* aluminophosphate nuclei attach on organophosphonate film, *(b)* growth of hexagonal crystals, the SEM pictures have shown that the $AlPO_4$-5 crystals grow with their *c*-axes oriented similar to the gold surface, Fig. 6.37. It was also found that changing the water concentrations in the hydrothermal synthesis and temperature of synthesis has a profound effect on the orientation morphology and aspect ratios of the surface-attached crystals. Table 6.18 gives the effect of water concentration on the morphology of surface attached $AlPO_4$-5 crystals.

Thus, the molecular selectivity of zeolite thin films can be precisely tuned by gating the entry of molecules into the zeolite pores.

Bein (1996) has reviewed the zeolite molecular sieve films and membranes.[124] These zeolite-based, nano-structured materials offer the potential to organize matter and to manipulate molecules with high spatial precision at the nanometer level. Pure zeolite membranes (20–250μm thick) consisting of ZSM-5 crystals have been prepared between 180°C (for 0.3–9 days) on substrates including teflon, silver, stainless steel and Vycor glass.[125] Sano, et al. (1992) have proposed a new preparation method for highly siliceous zeolite films. Similarly, these authors have obtained a pure ZSM-5 zeolite film ca. 30–100 μm in thickness; it is made up of zeolite crystals, which can be obtained on a teflon slab.[126] At first, silicalite was hydrothermally synthesized in the presence of cellulose moldings, such as a filter paper. Figure 6.38 shows the SEM photograph of a silicalite-cellulose composite prepared in 48 hours. Carbon membranes (in the form of hollow fibers) constitute a novel type of support for zeolite layers. Figure 6.39 shows such hollow-fiber carbon zeolite membranes.[127] Layers with molecular

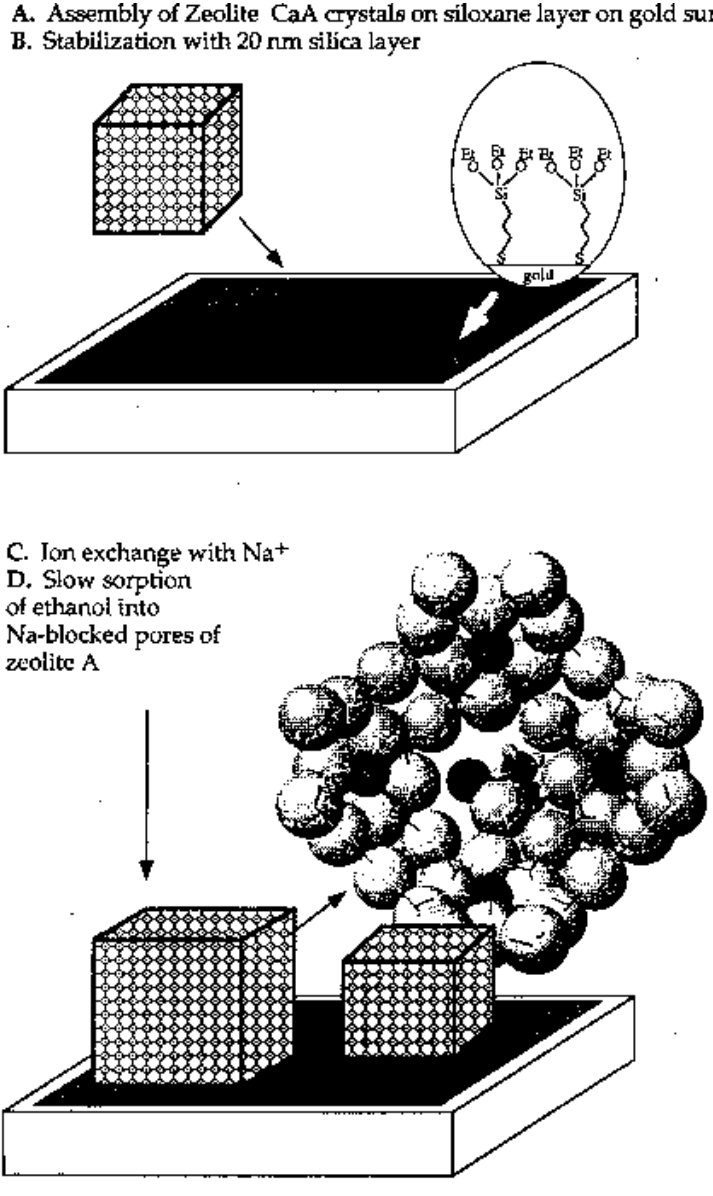
A. Assembly of Zeolite CaA crystals on siloxane layer on gold surface
B. Stabilization with 20 nm silica layer
gold
C. Ion exchange with Na+
D. Slow sorption of ethanol into Na-blocked pores of zeolite A

[a] The slow sorption of EtOH into the partially blocked eight-ring windows is depicted. Sodium ions appear in gray, framework Al, Si in black, and oxygen in light gray.

Figure 6.33. Assembly of zeolite CaA crystals on silozane layer on gold surface, and stabilization with 20 nm silica layer.[121]

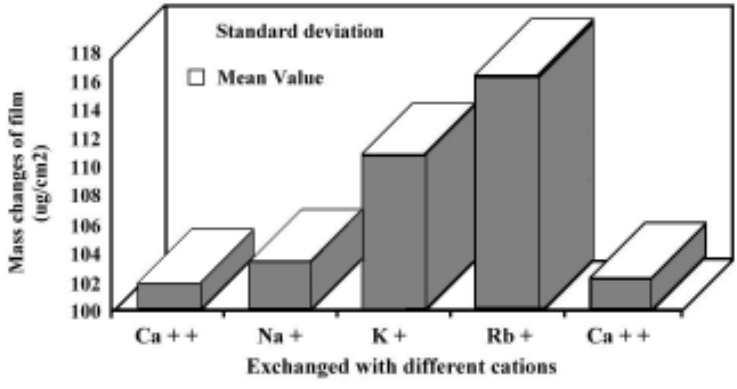

Figure 6.34. Mass changes of zeolite silica composite films exchanged with different cations on a piezoelectric substrate.[124]

DropBooks

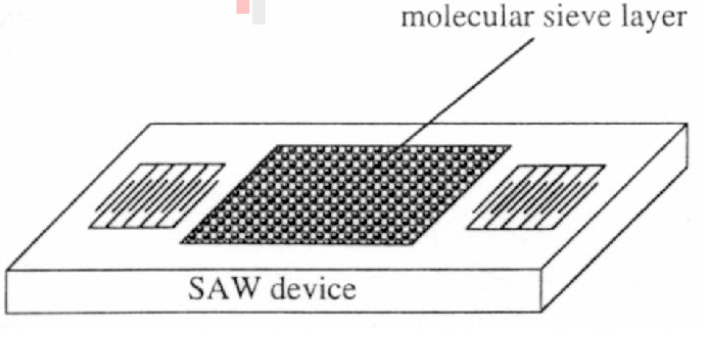

Figure 6.35. Schematic diagram of SAW device covered with molecular sieve layer.[124]

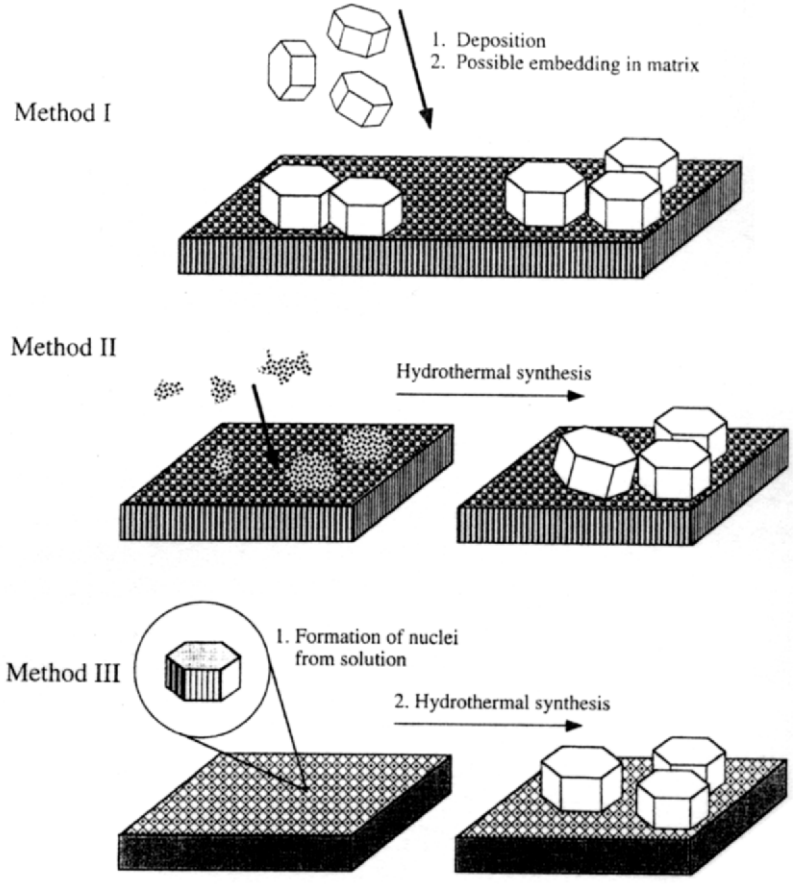

Figure 6.36. *Method I,* Proposed reaction scheme for design of zeolite layers and films on organophosphate films. *Method II,* Aluminophosphate nuclei attach on organophospnonate film and *Method III,* growth of hexagonal crystals.[124]

DropBooks

Figure 6.37. SEM pictures show that the $AlPO_4$-5 crystals grow with their c-axes oriented similar to the gold surface.[124]

Table 6.18. Effect of Water Concentration On the Morphology of Surface Attached $AlPO_4$-5 Crystals[124]

Water content (d)	Crystal		
	Length (μm)	Width (μm)	Orientation
300	30–50	40–50	Vertical
400	20–30	3–6	Tilted
600	30–50	2–10	Tilted

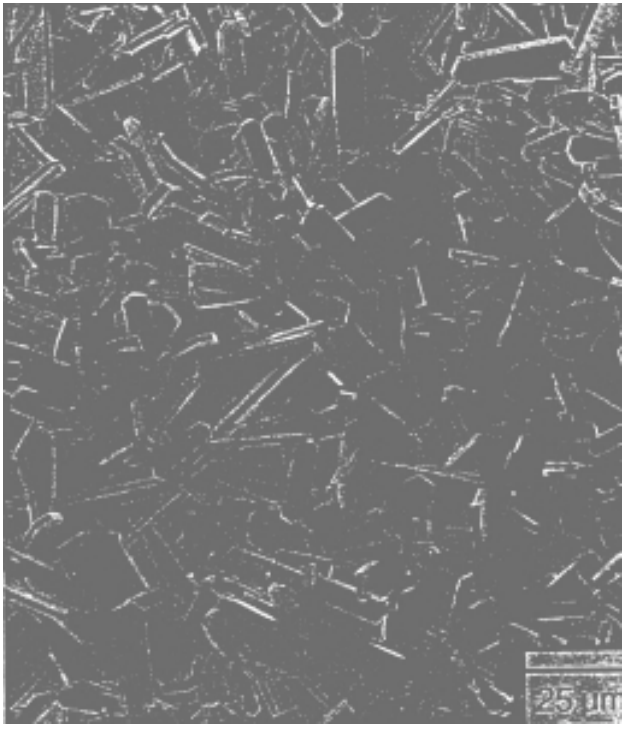

Figure 6.38. Shows SEM photograph of silicalite-cellulose composite prepared in 48 hours.[126]

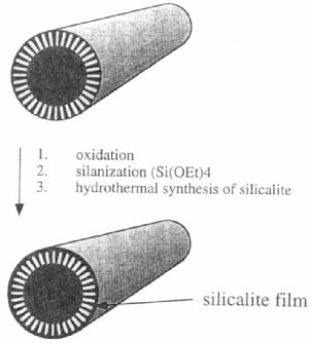

Figure 6.39. Hollow-fiber carbon zeolite membranes.[127]

sieving properties were formed by embedding microcrystals of Z, Y, and Chabazite, in a glassy silica matrix.[128]

Molecular sieve films are the promising candidates for applications in chemical sensors, especially in industrial process control, environmental and indoor air-quality monitoring, effluent and auto-exhaust control, and medical monitoring. Noack, et al. (1994) have obtained columnar $AlPO_4$-5 crystals aligned and embedded in nickel (by galvanic deposition) and studied in the permeation of heptane and different aromatic hydrocarbons (Figures 6.40 *a–b*).[129] There have been a few works that mimic some features of biomineralization to grow oriented zeolite molecular sieve films. Such self-assembled layers include self-assembled

DropBooks

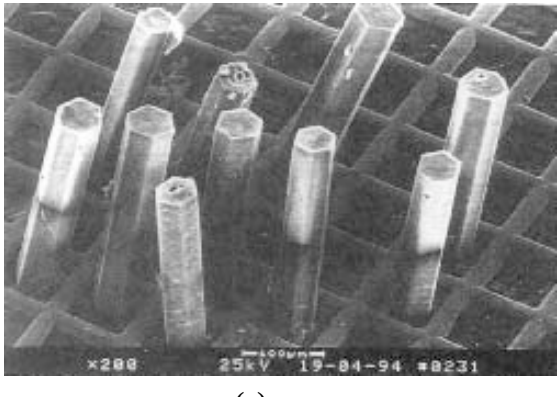

(a)

Figure 6.40. *(a* and *b)* Columnar $AlPO_4$-5 crystals aligned and embedded in nickel.[129]

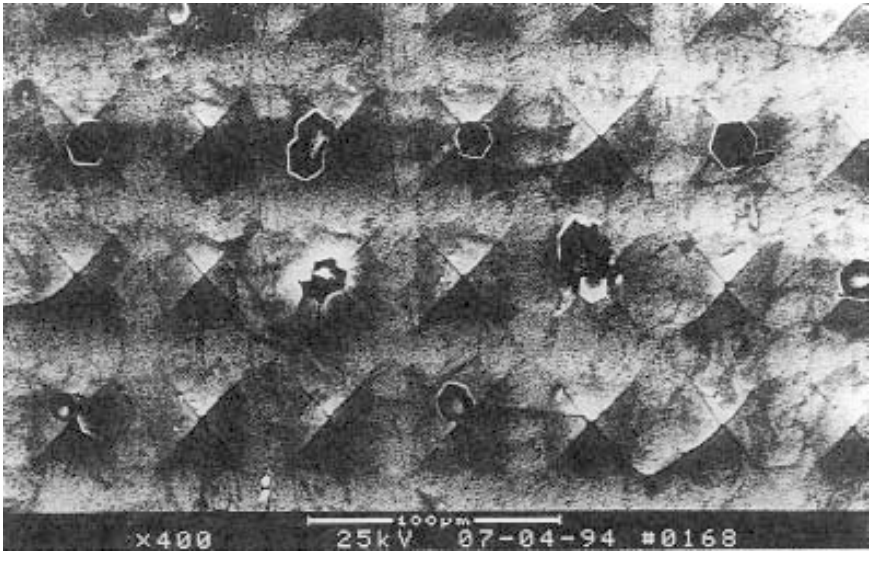

(b)

Figure 6.40. *(Cont'd.)*

functional layers and they have potential applications in microelectronics and nonlinear optical devices.[130]

Thus, there is a great variety of synthesis approaches regarding the design of molecular sieve layers and membranes. These aspects will play a major role in the future zeolite research.

6.9 APPLICATIONS OF ZEOLITES

The conventional applications of zeolites are adsorptive, gas separation, shape-selective catalysis, and ion exchange.[25][37] In recent years, there is an increased research activity in molecular sieve science and technology towards the development of advanced materials. There are several reports available in the literature dealing with the controlled incorporation of guest compounds into a zeolitic framework to get new optical, electronic, and magnetic materials, such as intrazeolite sulfides, selenides, silver compounds, carbonyls, the intra-crystallization polymerization of acetylene, and pyrrole, the formation of metal clusters, and trapped supramolecular compounds (ship-in-one-bottle).[131][134]

The application of zeolites as catalysts is basically dependent upon the accessibility to reactants of intra-crystallization, catalytically active centers, and upon the shape and size of the penetrant molecules. Specific catalytic actions can depend upon zeolite basicity, the generation of acid sites within the crystals, or upon the introduction of particular cations (by ion-exchange), or of elements such as S, Te, and Se, or metals like Pt, into the crystals.

The catalytic oxidation of H_2S by O_2 exemplifies a process in which the best catalysts are the basic Na and K-forms of zeolites X and Y.[135] The catalytic activity is directly proportional to the number of AlO_4 tetrahedra and inversely related to the electrostatic potential of the exchange ions introduced (K^+, Na^+, Li^+, and Ca^{2+}). However, it is the hydrocarbon chemistry which has placed zeolites in a unique place in science and technology, especially with H-zeolites providing Brönsted acid sites and reactions proceeding via carbonium ions. The acid centers form the reversible reaction.

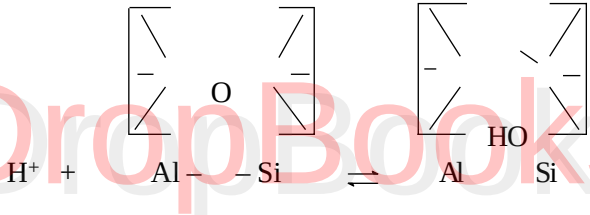

DropBooks

Various shape-selective catalyses have been described in several zeolites. In Ca-A zeolite, chemical dehydration of n-butanol (which penetrates the crystals), but not of isobutanol (which does not penetrate), was observed. Whereas, Ca-X zeolite doesn't show this kind of selectivity, but it sorbs both alcohols readily. Similarly, n-paraffins and n-olefines (which entered the Ca-A) were readily combusted with O_2 while iso-paraffins and iso-olefines, which didn't enter Ca-A, did not react appreciably.[136] Shape-selective catalysis has also been observed in several other zeolites and prominent among them is ZSM-5, MFI. This sorbs and cracks mono-methyl in addition to n-paraffins and is used to dewax heavy oils.

Mirajkar, et al. (1993) have studied the sorption properties of Al-omega and Ga-omega zeolites.[137] Figure 6.41 shows the sorption uptakes (*P/Po* = 0.8, 298 K) of samples of different crystallinity for Al-omega and Ga-omega zeolites synthesized at 398 K. These curves typically show that sorption uptake increases as the degree of crystallinity increases, water being a polar molecule and comparatively small in size, is able to become occluded

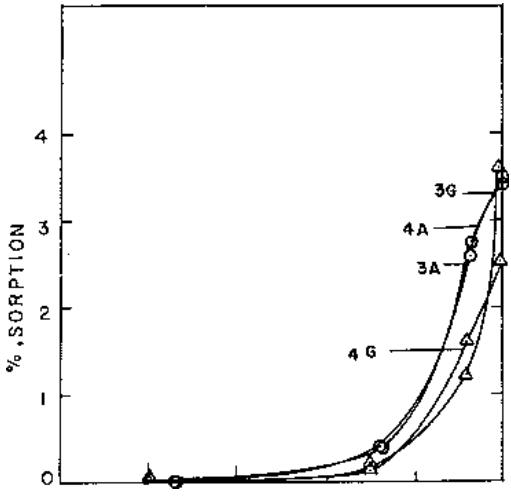

(a)

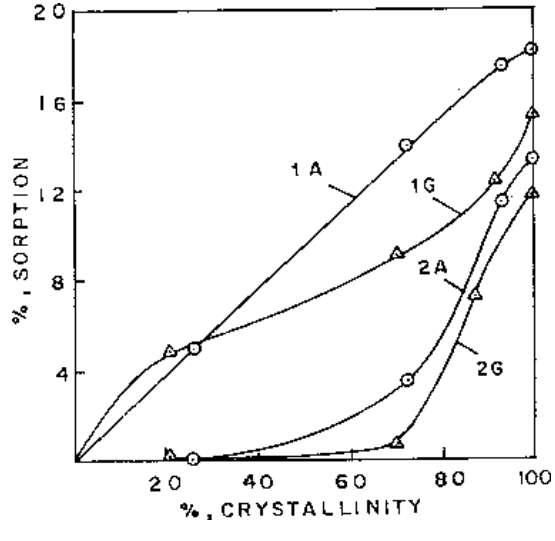

(b)

Figure 6.41. *(a, b)* Sorption uptakes (P/Po = 0.8, 298K) of samples of different crystallinity for Al-omega and Ga-Omega zeolites synthesized at 398 K.[137]

Table. 6.19. Adsorption (wt%) on Al- and Ga-omega Zeolites, *P/Po* = 0.8 and *T* = 298 K[137]

Synthesis	Al-omega			Ga-omega		
Temp. (K)	383	398	413	383	398	413
Adsorbate						
water	20.45	18.10	17.30	17.50	14.89	15.3
n-butylamine	17.19	13.22	10.10	15.50	11.69	9.6
n-hexane	6.70	3.51	2.09	4.70	3.57	1.8
cyclohexane	6.50	3.33	2.25	4.61	2.27	1.8

in cavities of samples of low crystallinity. Table 6.19 gives the adsorption (wt%) on Al- and Ga-omega zeolites *P/Po* = 0.8 and T = 298 K.

The sorption uptakes are found to decrease with the increase in experimental temperature and this decrease is consistent with the observed increase in the crystallite size.

As the molecular size of the probe molecules increases, a decrease in sorption uptake with an increase in crystallite size becomes appreciable on account of their different packing in the zeolite voids; Al-omega shows higher sorption uptake than for Ga-omega zeolite. These omega zeolites are stable up to a temperature of 1000°C.

DropBooks

The $AlPO_4$ molecular sieves show excellent physical properties. Many are thermally stable and resist loss of structure at 1000°C. Those studied for hydrothermal stability, including $AlPO_4$-5, 11, and 17, show no structure loss when treated with 16% steam at 600°C. The adsorption properties of selected $AlPO_4$ molecular sieves are listed in Table 6.20. The different structure types are arranged in order of decreasing pore size, which is controlled by the ring size. The ring size refers to the number of tetrahedral atoms (Al or P). For the 12-T ring structures, $AlPO_4$-5 and $AlPO_4$-31, adsorption of neopentane has been observed. The 10, or puckered 12-ring of $AlPO_4$-11 adsorbs cyclohexane, but not neopentane. The pore size is similar to that of ZSM-5. Two of the 8-ring structures, $AlPO_4$-17 and $AlPO_4$-18, sorb butane, but not isobutane. $AlPO_4$-14 and $AlPO_4$-33 sorb xenon, but not butane, indicating somewhat puckered 8-ring structures. Similarly, 16-ring structures of $AlPO_4$-16 and $AlPO_4$-20 absorb only water. The pore volumes are near saturation values, O_2 at 183°C and H_2O at ambient temperature.

In general, the H_2O pore volumes are usually greater than the O_2 pore volumes, reflecting the presence of additional pore volume accessible to H_2O, but not to O_2. The model of $AlPO_4$-5 structure shown in Fig. 6.42 indicates large pore voids capable of absorbing O_2 or H_2O, the small voids, shown in Fig. 6.43*(a)–(b)* are outlined by columns of twisted chains of 4 and 6-rings parallel to the c-axis, adsorb H_2O only. In $AlPO_4$-5 these small voids apparently sorb about 0.12 cm^3/g. Figure 6.44 shows the O_2

Table 6.20. Typical Adsorption Pore Volumes for Selected $AlPO_4$-based Structure Types

		Adsorption Capacity (cc/100g)[a]						
Adsorbate =		H_2O	O_2	n-butane	n-hexane	isobutane	cyclohexane	neopentane
Kinetic Dia.(nm) =		0.265	0.346	0.43	0.43	0.50	0.60	0.62
P/Po =		0.9	0.9	0.4	0.3	0.3	0.5	0.6
Temp. (C) =		22	-183	22	22	22	22	22
Structure	Ring Size[b]							
5	12	26	16	13				12
36	12	31	21	14				13
46	12	35	30		28			26
11	10	18	13		11		11	2
31	10 or 12	21	13		11		9	11
41	10 or 12	21	12		10		8	11
34	8	33	27	23		2		
35	8	31	17	1				
39	8	23	9	1				
44	8	35	25		10			
47	8	35	27	25				
16	6	28	4	1				
20	6	32	2	1				

[a] Determined by standard McBain-Baker gravimetric techniques after calcination at 500-600°C in air. Samples activated at 350°C, 0.01torr, prior to measurement.

[b] Number of tetrahedral atoms (Al, P, Me) in ring controlling pore size. When structure is not known, it is estimated from adsorption measurements.

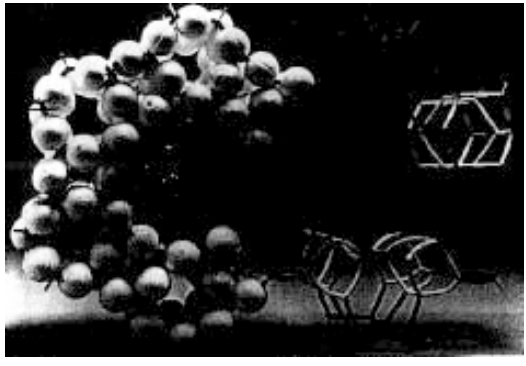

Figure 6.42. The model of $AlPO_4$-5 structure.[111]

(a)

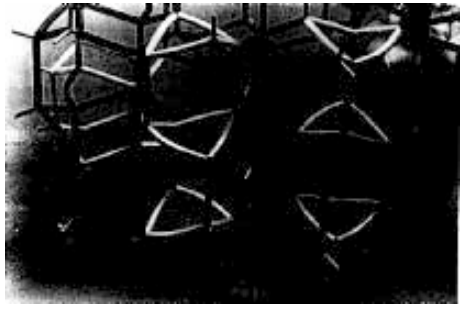

(b)

Figure 6.43. *(a, b)* Columns of twisted chains of 4 and 6-rings parallel to the c-axis, adsorb H_2O.[111]

DropBooks

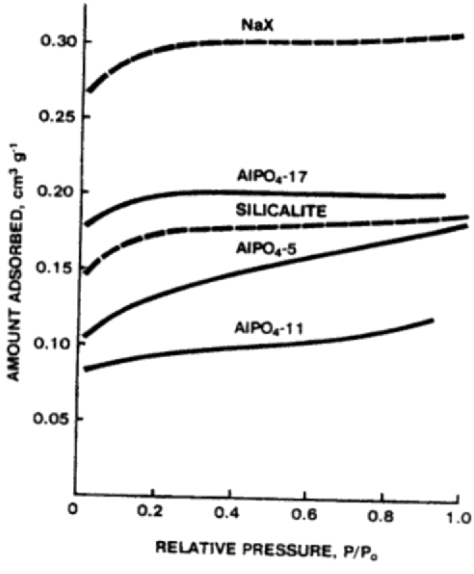

Figure 6.44. Graph of O_2 isotherms of $AlPO_4$-5, 11, and 17.[111]

isotherms of $AlPO_4$-5, 11, and 17, compared with those of a typical zeolite, NaX, and a silica molecular sieve, silicalite. The $AlPO_4$-5 and 17 have saturation pore volumes of approximately 0.2 cm^3/g, similar to that of silicalite, while $AlPO_4$-11 has a relatively small O_2 pore volume (~ 0.1 cm^3/g).

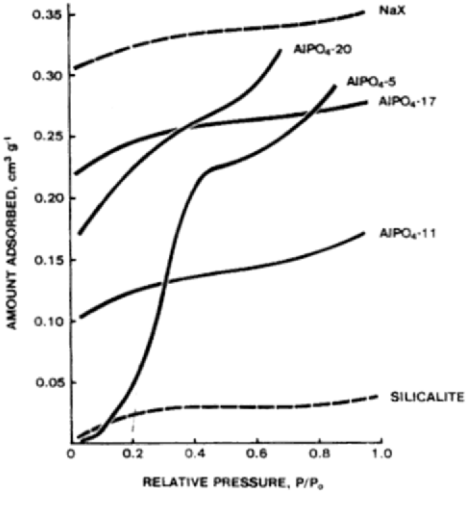

Figure 6.45. The H_2O adsorption isotherms for $AlPO_4$-5, 11, 17 and 20.[111]

Figure 6.45 shows the H_2O adsorption isotherms for $AlPO_4$-5, 11, 17, and 20. For comparison, the hydrophilic NaX and the hydrophobic silicate are considered. A very unusual shape has been obtained for the $AlPO_4$ adsorption curve for O_2 and paraffins.

In recent years, with the discovery of VPI-5 and other large pore zeolites, several advantages have been found. $AlPO_4$-5 adsorbs O_2 and some hydrocarbons except for triisopropylbenzene. The triisopropylbenzene is too large to penetrate the 12 T-atom ring of $AlPO_4$-5. VPI-5 reveals two phenomena not observed for $AlPO_4$-5; firstly, triisopropylbenzene is adsorbed; secondly, the adsorption capacity monotonically decreases with increasing adsorbate size. Since VPI–5 contains larger pores of 12–13 Å, all adsorbates other than triisopropylbenzene have the possibility of fitting more than one molecule across the diameter. In other words, packing of adsorbate molecules may be important in these extra-large pores. Table 6.21 gives the adsorption capacity of $AlPO_4$-5 and VPI-5 for various adsorbates.[114] Davis, et al. (1989) have measured the complete argon adsorption isotherms at liquid argon temperatures.[114] The data obtained from NaX and VPI-5 are shown in Fig. 6.46. Thus, the zeolites with large pore diameters are becoming

Table 6.21. Adsorption Capacity of Molecular Sieves at P/Po = 0.4[114]

Kinetic Diameter, Å	Adsorbate[a]	Capacity, cm^3/g $AlPO_4$-5	VPI-5
3.46	O_2	0.146	0.228
4.30	n-Hexane	0.139	0.198
6.00	Cyclohexane	0.145	0.156
6.20	Neopentane	0.137	0.148
8.50	Triisopropylbenzene		

[a] Adsorption at room temperature except for O_2 which was performed at either liquid N_2 or O_2 temperatures.

essential materials for the adsorption of large molecules, which either absorb or adsorb very slowly into known molecular sieves.

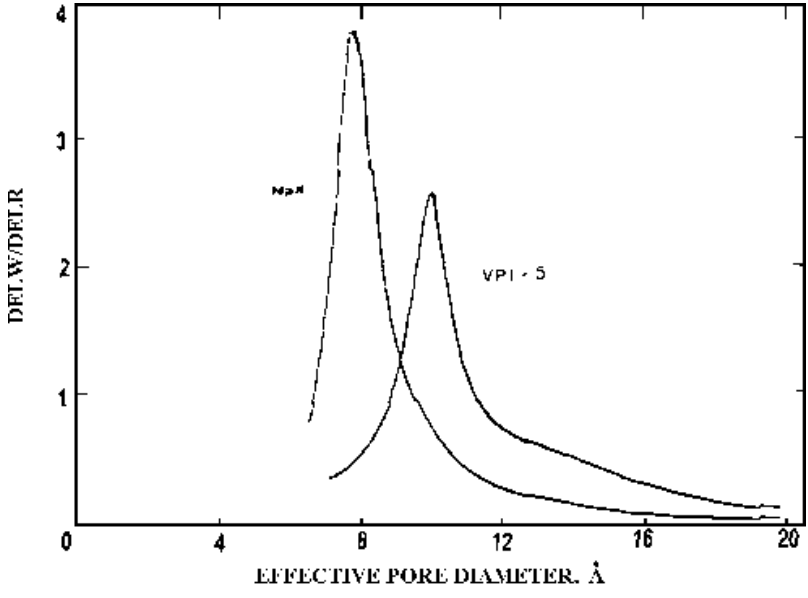

Figure 6.46. Effective pore size distribution.[114]

6.10 OXIDATIVE CATALYSIS ON ZEOLITES

Oxidation processes constitute one of the most common classes of chemical reactions. The endeavor by investigators to create economically more effective and ecologically clean technologies has stimulated the search for new catalysts exhibiting a high selectivity.

Though zeolites were not regarded as promising catalysts for oxidation reactions, considerable changes have taken place in the last decade. It was during the early 1980s, that titanosilicate zeolites, having a structure of the ZSM-type, and the discovery of their unique properties in oxidation reactions involving H_2O_2 took place. Thus, titanosilicates become the effective catalysts of a wide range of reactions occurring in the liquid phase, such as the oxidation of alcohols, epoxidation of alkenes, hydroxylation of aromatic compounds, and the conversion of cyclohexanone into an oxime.[136]-[142] These advances in liquid phase oxidation of primary and secondary alcohols to the corresponding carbonyl compounds have been assessed as one of the most important achievements in the field of organic synthesis. The partial oxidation of hydrocarbons is achieved, as a rule, in the presence of transitional metal oxides. Their activity is due to more or less facile electron transfer and their capacity for the reversibility of their oxidation state in interaction with oxygen in the substance. Oxidized zeolites themselves cannot serve as oxidation cata-

lysts, but the possibility of their use as carriers, nevertheless, is of great interest. However, because of the serious environment problems associated with Cr-containing effluent, attention has been focused on the use of catalytic amounts of soluble chromium compounds in conjunction with, e.g., tetra-butyl hydroperoxide (TBHP) as the stoichiometric oxidant. The use of heterogeneous catalysts in the liquid phase, on the other hand, offers several advantages compared with their homogenous counterparts, e.g., ease of recovery and recycling and enhanced stability. Kharitonov, et al. (1992) have studied the reactions involving gasoline oxidation with nitrous oxide, and the best results were obtained in the oxidation of benzene to phenol in the presence of iron-containing ZSM-5 zeolites.[142]

An approach to create solid catalysts with novel activities is to incorporate redox metals by isomorphous substitution into the lattice framework of zeolites and related molecular sieves. Since the discovery of aluminophosphate molecular sieves in 1982, much attention has been focused on the incorporation of various elements into the framework of these molecular sieves.[143] Modified compositions of these silica or aluminophosphate-based materials are expected to expand the scope of their catalytic applications as mesoporous materials and optimized advanced catalysts. These materials have been the most promising class of three-dimensional host frameworks with controlled microporosity. Atomic-scale engineering of catalytic functions of isolated redox sites in the confined environments of zeolitic channels is also of great interest.

DropBooks

Rabo, et al. (1973) showed that Na, Ca, Be, and La, forms of Z,Y containing residual protons reacted with NaCl, at 575–675 K, with the evolution of HCl.[144][145] Clearfield, et al., (1973) and Clearfield (1990) demonstrated the introduction of cations, such as Zn^{2+}, Cu^{2+}, Co^{2+}, Ni^{2+}, Mn^{2+}, and Cr^{3+}, Cr^{5+}, Mo^{5+}, Ga^{3+}, V^{4+}, into zeolites A, X, and Y, by the reaction of their chlorides with the H forms of the zeolites phosphates and molybdates.[146][147] Figure 6.47 shows the activity of Cr/H-ZSM-5 in CH_4 burnt at 500°C.[148][149] The catalytic activity of the Cr/H-ZSM-5 system increased linearly with the rise of chromium content up to 1.5 wt%, showing considerable site homogeneity. The activity of the catalyst reached a maximum point when the number of isolated Cr^{5+} cations capable of changing valence state upon redox treatment, reached maximum. Stabilization of isolated Cr^{5+} ions in a coordinatively unsaturated environment inside H-ZSM-5 may be a reason for such unusually high intrinsic catalytic activity.[150] Similarly, a complete oxidation of CH_4 over Mn/H-ZSM-5, Cu/H-ZSM-5, and V/H-ZSM-5, has also been studied in detail by Kucherov, et

al.[148] Ethane oxidation with N_2O over H-ZSM-5 and Cu/H- ZSM-5 has been studied by Kucherov, et al. (1991, 1992).[150][151] The C_2H_6 oxidation by N_2O, as distinct from O_2, proceeds on both H-ZSM-5 and Cu/H-ZSM-5. At $T > 430°C$, a stable 100% conversion took place on H-ZSM-5, but the decrease in temperature to 410–400°C led to a drastic drop in C_2H_6 and N_2O conversion with fast cooking of zeolite. The oxidation of ethane with N_2O was treated as a complex heterogeneous-homogeneous process (catalytic decomposition of N_2O and subsequent gas-phase C_2H_6 oxidation

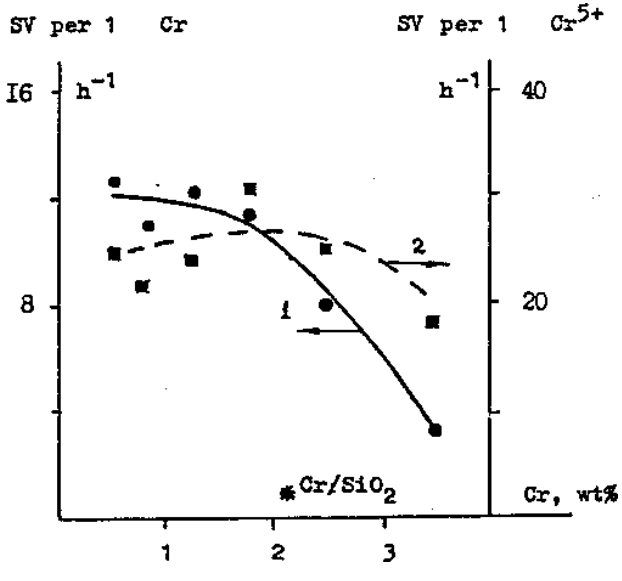

Figure 6.47. Activity of Cr/H-ZSM-5 in CH_4 burnt at 500°C.[148]

with the participation of excited molecules and coupling products).[151][152] Thus, the modification of pentasils by transition metal cations permits the preparation of promising catalysts for both complete oxidation of alkanes and NOx decomposition.

Guth, et al. (1986, 1989) have developed a new route of the synthesis of microporous compounds in the presence of fluorine.[74] The addition of fluoride ions in the reaction medium seems to induce mineralization and allows the crystallization of zeolites at neutral or acidic pH and the partial substitution of silicon by other tri or tetravalent metals, like B^{3+}, Al^{3+}, Ga^{3+}, Fe^{3+}, Ge^{4+}, and Ti^{4+}. Just like in other phases, fluorine is also incorporated in the open frameworks, and the best example is cloverite, with three-dimensional 20-membered ring channels, in which fluorine is located at

the center of a double 4-ring (D4R) cage.[153][155] A similar structural diversity is associated, in part, with the ability of vanadium-oxygen compounds to form tetrahedral, square-pyramidal, and octahedral coordination polyhedra, and to build larger aggregates by condensation of polyhedra through shared oxygen atoms.[156][157] Such works produce novel structures/frameworks that encapsulate organic guests to produce large cavities or tunnels. After the organic template is removed by ion exchange or thermal methods, the solid may sorb substrate molecules in a size and shape-selective fashion.[158] Similarly, there are several mixed tetrahedral-octahedral framework structures which are both novel and different from the traditional aluminosilicate zeolites, where only TO_4 tetrahedra (T = Si, Al, or Ge) are the basic building units. Mixed TO_6 and TO_4 units are also found in the structures of recently synthesized microporous stannosilicates, germanates and gallophosphates.[159][160]–[162] These compounds show good ionic conductivity and humidity sensing property as seen in microporous Na-germanates. Leonowicz, et al. (1994) have obtained a new boron, MCM-22, zeolite that contains structural features previously unknown among zeolites. The high-resolution electron micrographs and synchrotron x-ray diffraction powder data reveal two independent pore systems, both of which are accessed through rings composed of 10 tetrahedral (T) atoms (such as Si, Al, and B). One of these pore systems is defined by 2-*d*, sinusoidal channels. The other consists of large supercages whose inner free diameter, 7.1 Å, is defined by 12 T-O species (12-rings) and whose inner height is 18.2 Å. These coexisting pore systems may provide opportunities for a wide variety of catalytic applications in the petrochemical and refining industries.[163]

DropBooks

Caro, et al. (1992) have obtained aligned molecular sieve crystals as nonlinear optical materials.[134] As is well-known, the formation of Längmuir-Blodgett films and the crystallization of non-centrosymmetric organic crystals are widely studied as promising techniques to get ordered molecular arrangements for nonlinear optics and optoelectronics.[164] The required bulk alignment of molecular dipoles can also be achieved by their adsorption in the pores of appropriate molecular sieve matrices. Caro, et al. (1992) have studied the optical second harmonic generation (SHG) by para-nitro-aniline (PNA) adsorbed in $AlPO_4$-5 crystals. No SHG effects could be observed for the unloaded $AlPO_4$-5 matrix. Figure 6.48 shows the experimental arrangement of the ps-Nd:YAG laser device and the position of the $AlPO_4$-5 crystal in the laser light beam.[134] The relative intensity of the SHG signal as a

function of the angle between the polarization plane of the incident laser light and the *c*-axis (length direction [001]) of $AlPO_4$-5 crystal is plotted in Fig. 6.49. The vanishing of the SHG intensity for $\phi = 90°$ indicates that the molecules are well aligned by the molecular sieve channels, i.e., their

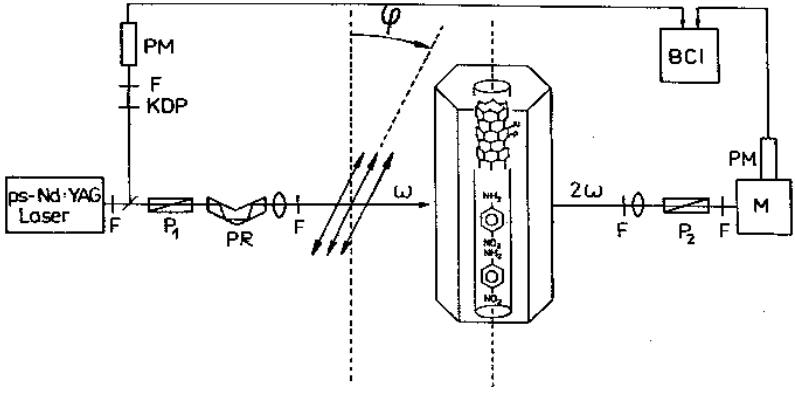

Figure 6.48. Experimental arrangement of the ps-ND:YAG laser device and the position of the $AlPO_4$-5 crystal in the laser light beam.[134]

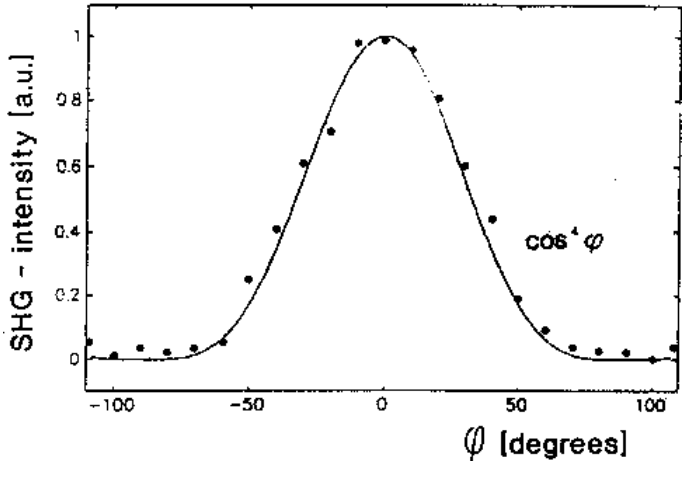

Figure 6.49. Relative intensity of the SHG signal as a function of the angle between the polarization plane of the incident laser light and the *c*-axis (length direction [001]) of $AlPO_4$-5 crystal is plotted.[134]

orientational distribution is sharp.[164] Alvaro, et al. (1998) have prepared a series of four europium complexes incorporated into three different zeolites. Also, the chemiluminescence of Eu^{+3} exchange Y-zeolite upon thermal decomposition of tetramethyl 1, 2-dioxetane has been reported.[165]

Smolin, et al. (1998) have introduced CdS clusters in pores of zeolite-Z. It is shown that these clusters are built up around the S atoms that are situated at the centers of the large cavities of zeolites and coordinated tetrahedrally by Cd atoms. These atoms are bound through sulfur atoms with Cd cations situated near the walls of the cavity in the environment of the aluminosilicate framework oxygens.[166]

Thus, the study of zeolites is a very popular field. A great diversity, both in terms of compositions and applications, is being reported for zeolites. New structures have been discovered. All these suggest a great future for the zeolites, covering fields of selective and shape catalysis, oxidative catalysis, micro-electronics, optoelectronics, environmental issues, and so on.

REFERENCES

DropBooks

1. Crönstedt, A. F., *Akad. Handl. Stockholm*, 17:120 (1756)
2. Deer, W. A., Howie, R. A., and Zussman, J., *Rock-Forming Minerals*, Longmans, 4:351 (1967)
3. Dana, E. S., *A Text Book of Mineralogy*, p. 640, John Wiley and Sons, Inc., New York (1955)
4. Loew, D., *U.S. Geog. and Geol. Explor. and Surv. West of 100th Meridian*, Pt. 6, 3:569 (1875)
5. Coombs, D. S., The Nature and Alteration of Some Triassic Sediments, *Trans. Roy. Soc. New Zealand*, 82:65 (1954)
6. Eichorn, H., *Ann. Phys. Chem.*, 105:130 (1858)
7. Hey, M. H., Studies on the Zeolites Part I, General Review, *Min. Mag.*, 22:422 (1930)
8. Marshall, C. E., *The Colloid Chemistry of the Silicate Minerals*, Academic Press, New York (1949)
9. McBain, J. W., *The Sorption of Gases and Vapors by Solids*, Rutledge and Sons, London (1932)
10. Davis, M. E. and Lobo, R. F., Zeolite and Molecular Sieve Synthesis, *Chem. Mater.*, 4:756–768 (1992)

11. Feijen, E. J. P., Martens, J. A., and Jacobs, P. A., Zeolites and Their Mechanism of Synthesis, in: *Zeolites and Related Microporous Materials: State of the Art 1994*, (J. Weitkamp, H. G. Karge, H. Pfeifer, and W. Holderich, eds.*), Studies in Surface Science and Catalysis*, 84:3–21 (1994)
12. Wilson, S. T., Lok, B. M., Messina, C. A., Cannon, T. R., and Flanigen, E. M., Aluminophosphate Molecules Sieves; A New Class of Microporous Crystalline Inorganic Solids, *J. Am. Chem. Soc*., 104:1146–1147 (1982)
13. Meier, W. M. and Olson, D. H., Atlas of Zeolite Structure Types, *Adv. Chem. Ser*., 101:155 (1970)
14. Meier, W. M. and Olson, D. H., *Atlas of Zeolite Structure Types*, Structure Commission of the IZA (1978)
15. Meier, W. M. and Olson, D. H., *Atlas of Zeolite Structure Types*, Structure Commission of the IZA, Butterworth-Heinemann (1987)
16. Meier, W. M. and Olson, D. H., *Atlas of Zeolite Structure Types*, Structure Commission of the IZA, Butterworth-Heinemann (1992)
17. Meier, W. M., Olson, D. H., and Baerlocher, C., *Atlas of Zeolite Structure Types*, in: *Zeolites*, 17:1–230 (1996)
18. Breck, D. W., *Zeolite Molecular Sieves: Structure, Chemistry and Use*, Wiley and Sons, London (1974)
19. Breck, D. W., Structure of Zeolite, in: *Zeolite Molecular Sieves*, pp. 29–185, Wiley Interscience Publication, New York (1974)
20. Brunner, G. O. and Meier, W. M., Framework Density Distribution of Zeolite Type Tetrahedral Nets, *Nature*, 337:146 (1989)
21. Smith, J. V., *Felspar Minerals*, Vol. 2, Springer, Berlin (1974)
22. Barrer, R .M., Zeolites and their Synthesis, *Zeolites*, 1:130–140 (1981)
23. Meier, W. M., in: *Molecular Sieves*, p. 10, Soc. Chem. Ind., London (1968)
24. Flanigen, E. M., Crystal Structure and Chemistry of Natural Zeolites, in: *Reviews in Mineralogy, Vol. 4, Mineralogy and Geology of Natural Zeolites*, (A. M. Frederick, ed.), pp. 19–52, Mineralogical Society of America, New York (1986)
25. Qinhua, Xn and Aizhen, Yan., Hydrothermal Synthesis and Crystallization of Zeolites. in: Hydrothermal Growth of Crystals, (K. Byrappa, ed.), *Prog. Crystal Growth and Characterization,* 21:29–70 (1990)
26. Barrer, R. M., Chemical Nomenclature and Formulation of Compositions of Synthetic and Natural Zeolites, *Pure and Appl. Chem*., 51:1091 (1979)
27. Munson, R. A. and Sheppard, R. A., *Minerals Sci. Eng.,* 6:19 (1974)
28. Barrer, R. M. and Cole, J. F., *J. Chem. Soc. A,* p. 1516 (1970)

29. Staples, L. W., Evans, H. T. Jr., and Lindsey, J. R., Cavansite and Pentagonite, New Dimorphous Calcium Vanadium Silicate Minerals from Oregon, *Amer. Mineral.*, 58:405–411 (1973)
30. Evans, H. T., Jr., The Crystal Structures of Cavansite and Pentagonite, *Amer. Mineral*, 58:412–424 (1973)
31. Rinaldi, R., Pluth, J. J., and Smith, J. V., Crystal Structure of Cavansite Dehydrated at 220°C, *Acta Crystallogr*., B31:1598–1602 (1975)
32. Powar, K. B. and Byrappa, K., X-Ray, Thermal, and Infrared Studies of Cavansite from Wagholi Western Maharashtra, India., *J. Geol. Soc*., Japan, (Submitted).
33. d'Yvoire, F., *Bull. Soc. Chem.*, (France) (1762, 1961)
34. Robson, H, Synthesizing Zeolites, *Chemtech*, 176–180 (March, 1978)
35. Wöhler, (cited by Bunsen, R.), *Ann.*, 65:80 (1848)
36. Claireville, H. de St., (1862) (cited by Morey, G. W. and Niggli, P.), The Hydrothermal Formation of Silicates, a Review, *J. Am. Chem. Soc*., 35:1086–1130 (1913)
37. Barrer, R. M., *Hydrothermal Chemistry of Zeolites*, Academic Press, London (1982)
38. Milton, R. M., *Zeolite Synthesis*, (M. L. Occelli and H. E. Robson, eds.) ACS Symp. Ser. No. 398, p. 1 (1989)
39. Milton, R. M., to Union Carbide, U.S.P. 2,882,244 (1959)
40. Milton, R. M., U.S.P. 2,996,358 (1961)
41. Milton, R. M., U.S.P. 3,010,789 (1961)
42. Milton, R. M., to Union Carbide, U.S.P. 3,030,181 (1962)
43. Barrer, R. M. and Denney, P., Hydrothermal Chemistry of the Silicates, Part IX Nitrogenous Aluminosilicates, *J. Chem. Soc.*, pp. 971–1000 (1961)
44. Kerr, G. T., *Inorg. Chem*., 5:1539 (1966)
45. Higgens, J. B., Silica Zeolites and Clathrasils, in*: Mineralogy of Silica*, pp. 507–543, *Reviews in Mineralogy*, Mineralogical Society of America, New York
46. Hay, R. L., in: *Natural Zeolites* (L. B. Sand and F. A. Mumpton, eds.), pp. 135–143, Pergamon, Oxford (1978)
47. Wilson, S. T., Lok, B. M., Messina, C. A., Cannan, T. R., and Flanigen, E. M., *Aluminophosphate Molecular Sieves, A New Class of Microporous Crystalline Inorganic Solids*, Am. Chem. Soc., p. 79–110 (1983)
48. Flanigen, E. M., Lok, B. M., Patton, R. L., and Wilson, S. T., in: *New Developments in Zeolite Science and Technology*, (P. A. Jacobs, ed.), p. 103, Elsevier, Amsterdam (1986)

DropBooks

49. *Zeolite Synthesis,* (M. L. Occelli and H. E. Robson, eds.), ACS Symposium Series 398, Am. Chem. Soc. Washington, D.C. (1989)
50. Zhdanov, S. P., *Some Problems of Zeolite Crystallization, Molecular Sieve Zeolite - I,* (E. M. Flanigen and L. B. Sand, eds.), *Adv. Chem. Ser.,* 101:20, Am. Chem. Soc., Washington, D.C. (1971)
51. Ueda, S., Kageyama, W., and Koizumi, M., in: *Proc. 6th International Zeolite Conference,* (D. Olson and A. Bisio, eds.), p. 905, Butterworth, Surrey (1984)
52. Xu, W., Li, J., Li, W., Zhang, H., and Liang. B., Nonaqueous Synthesis of ZSM-35 and ZSM-5, *Zeolites,* 9:468–473 (1989)
53. Dai, F-Y., Suzuki, M., Takahashi, H., and Saito, Y., in: New Developments in Zeolite Science and Technology, *Proc. 7th International Zeolite Conference,* (Y. Murakami, A. Lijima, and J. W. Ward, eds.), p. 223, Kodansha, Elsevier, Tokyo, Amsterdam (1986)
54. Dwyer, J., Karim, K., Smith, W. J., Thompson, N. E., Harris, R. K., and Apperley, D. C., A Comparison of Siliceous Faujasite Zeolites Produced by Direct Synthesis or by Secondary Synthesis, *J. Phys. Chem.*, 95:8826–8831 (1991)
55. Dai, F. Y., Suzuki, M., Takahashi, H., and Saitoy, Y., *Stud. Surf. Sci. Catal.*, 28:223 (1986)
56. Flanigen, E. M., *Adv. Chem. Ser*., 121:114 (1973)
57. Dutta, P. K., Pur, M., and Shieh, D. C., *MRS Soc. Symp. Proc.*, 111:101 (1988)
58. Rollman, L. D., Templates in Zeolite Crystallization, *Adv. Chem. Ser.*, 173–387 (1979)
59. Flanigen, E. M., in: *Proc. 5th International Conference Zeolites,* (L. V. C. Rees, ed.), p. 760, Heyden, London (1980)
60. Loewenstein, W., The Distribution of Aluminum in the Tetrahedra of Silicates and Aluminates *Am. Mineral*., 39:92–96 (1954)
61. Flanigen, E. M., Patton, R. L., and Wilson, S. T., *Stud. Surf. Sci. Catal*., 37:13–27 (1988)
62. Gier, T. E. and Stuckey, G. D., *Nature,* 346:508 (1991)
63. Xu, R., Chen, J., and Feng, C., New Families of M(III)X(V)O4 - Type Microporous Crystals and Inclusion Compounds, *Stud. Sur. Catal.*, 60:63–72 (1991)
64. Katovic, A., Subotic, B., Smit, I., Despotovic, Lj. A., and Curic, M., in: *Zeolite Synthesis*, (M. L. Ocelli and H. E. Robson, eds.), ACS Symp. Ser., Nr. 398, p. 124 (1989)
65. Cook, J. D. and Thompson, R. W., Modeling the Effect of Gel Aging, *Zeolites*, 8:322–326 (1988)

66. Zhdanov, S. P. and Samulevich, N. N., in: *Procs. 5th International Conference on Zeolites*, (L. V. C. Rees, ed.), p. 75, Heyden, London (1980)

67. Subotic, B. and Bronic, J., in: *Proc. 7th International Zeolite Conference*, p. 45, Tokyo (1986)

68. Wu, C. N. and Chao, K. J., Synthesis of Faujasite Zeolites with Crown-Ether Templates, *J. Chem. Soc. Faraday Trans.*, 91:167–173 (1995)

69. Bell, A. T., in: *Zeolite Synthesis*, (M. L. Occelli and H. E. Robson, eds.), ACS Symp. Ser., Nr. 398, p. 66 (1989)

70. Gilson, J. P., in: *Zeolite Microporous Solids: Synthesis, Structure and Reactivity*, (E. G. Derouane, F. Lemos, C. Naccache, and F. R. Ribeiro, eds.), *NATO ASI Ser.*, 352:19, Kluwer Academic Publishers, Dordrecht (1992)

71. Byrappa, K., Hydrothermal Growth of Crystals, in: *Handbook of Crystal Growth* (D. T. J. Hurle, ed.), p. 465, Elsevier North-Holland, Amsterdam (1994)

72. Barre, R. M., *Trans. 7th International Ceramic Congress*, p. 379, London (1960)

73. Flanigen, E. M. and Patton, R. L., U. S. Patent 4,073,864 (1978)

74. Guth. J. L., Kessler, H., Higel, J. M., Lamblin, J. M., Patarin, J., Seive, A., Chezcau, J. M., and Wey, R., *ACS Symp. Ser.*, 398:176 (1989)

75. Hayhurt, D. T. and Sand, L. B., Molecular Sieves II, *ACS Symp. Ser.*, 40:219 (1977)

76. Chao, K. J., Tasi, T. G., Chen, M. S., and Wang, I., Kinetic Studies On The Formation of Zeolites, ZAM-5, *J. Chem. Soc. Faraday I*, 77:465–555 (1981)

77. Qinhua, Xu, Shullin, B., and Jialu, D., *Scientia Sinica (Ser. B)*, 25:349 (1982)

78. Witte, B. D., Patarin, J., Nouen, D. Le., Delmotte, L., Guth, J. L., and Cholley, T., Cyclic Polyols: A New Class of Structure-Directing Agents? Study of Inositol in the Synthesis of FAU and LTA-Type Zeolites, *Microporous Mesoporous Mater.*, 23:11–22 (1998)

79. Lechert. H., The pH Value and its Importance for the Crystallization of Zeolites, (H. Robson, ed.), *Microporous Macroporous Material*, 22:519–523, Karl Petter, Lillerud (1998)

80. Ozin, G. A., Nano Chemistry Synthesis In Diminishing Dimensions, *Adv. Mat.*, 4:612–649 (1992)

81. Mann, S., *Nature*, 365:499–505 (1993)

82. Guth, J. L, Caullet, P., Sieve, A., Patarin, J., and Delprato, F., in: *Guidelines For Mastering The Properties of Molecular Sieves*, (Barthomeuf, ed.), p. 69, Plenum Press, New York (1990)

DropBooks

83. Kerr, C. T., *Inorg. Chem.*, 5:1537 (1960)
84. Qiuhua, Xu, Huizhu, Z-qng, Jialu, D., and Rui, W., *Kexue Tongbao*, 25:833 (1980)
85. Feng, P., Bu, X., Gier, T. E., and Stucky, G. D., Amine-Directed Syntheses and Crystal Structure of Phosphate Based Zeolite Analogs., *Microporous Mesoporous Mat*., 23:221–229 (1998)
86. Jansen, J. C., in: *Introduction to Zeolite Science and Practice*, (H. Van Bekkum, E. M. Flanigen, and J. C. Jansen, eds.) p. 77, Elsevier, Amsterdam (1991)
87. Lok, B. M., Cannan, T. R., and Messina, C. A., The Role of Organic Molecules in Molecular Sieve Synthesis, *Zeolites*, 3:282–291 (1983)
88. Moini, A., Schmitt, K. D., Valyocsik, E. W., and Polomski, R .F., The Role of Diquatemary Cations as Directing Agents in Zeolite Synthesis, in: *Zeolites and Related Microporous Materials: State of the Art*, (J. Weitkamp, H. G. Karge, H. Pfeifer, and W. Holderich, eds.), *Studies in Surface Science and Catalysis*, 84:23–28 (1994)
89. Yoshimura, M., Suchanek, W., and Byrappa, K., Soft, Solution Processing—A Strategy for Advanced Materials Processing in the 21st Century, *MRS Bull.*, September Issue (2000).
90. Martin, C. R., Membrane-Based Synthesis of Nanomaterials, *Chem. Mater.*, 8:1739–1746 (1996)
91. Ajayan, P. M., Stephan, O., Redlich, P., and Colliex, C., *Nature*, 375:564–567 (1995)
92. Schact, S., Huo, Q., Voigt-Martin, I. G., Stucky, G. D., and Schuth, F., *Science*, 273:768–771 (1996)
93. Mutaftschiev, B., Nucleation Theory, in: *Handbook of Crystal Growth*., (D. T. J. Hurle, ed.), 1:187–247, Elsevier Science Publishers, B. V., U.K. (1993)
94. Myerson, A. S. and Izmailov, A. F., The Structure of Supersaturated Solutions, in: *Handbook of Crystal Growth*, (D. T. J. Hurle, ed.), 1:250–305, Elsevier Science Publishers, B. V., U.K. (1993)
95. Warzywoda, J. and Thompson, R. W., Zeolite Crystallization with Autocatalytic Nucleation, *Zeolites*, 9:341–345 (1989)
96. Jacobs, P. A., in: *Zeolite Microporous Solids: Synthesis Structure and Reactivity*, (E. G. Derouane, F. Lemos, C. Naccache, and F. R. Ribeiro, eds.), p. 3, NATO ASI Ser. Vol. 352, Kluwer Academic Publishers, Dordrecht (1992)
97. Chen, W. H., Hu, H. C., and Lee, T. Y., Transient Crystallization and Crystal Size Distribution of Zeolite A., *Chem. Eng. Sci*., 48:3683–3691 (1993)
98. Roy, R., Accelerating the Kinetics of Low-Temperature Inorganic Syntheses, *J. Solid State Chem.*, 111:11–17 (1994)

99. Carmona, J. G., Clemente, R. R., and Morales, J. G., Comparative Preparation of Microporous VPI-5 Using Conventional and Microwave Heating Techniques, *Zeolites*, 18:340–346 (1997)

100. Ghobarkar, H., The Morphology of Some Hydrothermally Synthesized Li-Minerals: A–Z, α-Eucryptite, β-Spodumene and β-Eucryptite, *Cryst. Res. Technol*., 27:181–185 (1992)

101. Ghobarkar, H. and Schaf, O., The Morphology of Hydrothermally Synthesized Natrolite, *Cryst. Res. Technol*., 31:K54–K57 (1996)

102. Ghobarkar, H. and Schaf, O., Hydrothermal Synthesis and Morphology of Thomsonite and Edingtonite, *Cryst. Res. Technol*., 32:653–657 (1997)

103. Ghobarkar, H. and Schaf, O., The Morphology of Hydrothermally Synthesized Mesolite, *Cryst. Res. Technol*., 31: K67–K69 (1996)

104. Kuperman, A., Nadimi, S., Oliver, S., Ozin, G. A., Garces, J. M., and Olken, M., Non-Aqueous Synthesis of Giant Crystals of Zeolites and Molecular Sieves, *Nature*, 365:239–242 (1993)

105. Mel'nikov, O. K., Litvin, B. N., and Triodina, N. S., Crystallization of Sodalite on a Seed, in: *Crystallization Processes Under Hydrothermal Conditions*, (A. N. Lobachev, ed.), p. 151–172, Consultants Bureau, New York (1973)

106. Demianets, L. N., Emelyanova, E. N., and Mel'nikov, O. K., Solubility of Sodalite in Various Solutions of NaOH Under Hydrothermal Conditions, in: *Crystallization Processes Under Hydrothermal Conditions*, (A. N. Lobachev, ed.), pp. 125–149, Consultant Bureau, New York (1973)

107. Johnson, G. M. and Weller, M. T., Synthesis and Characterization of Gallium and Germanium Containing Sodalites, in: Progress in Zeolite and Microporous Materials, (H. Chon, S. K. Ihm, and Y. S. Uh, eds.), *Stud. in Surf. Sci. Cat*., 105:269–275 (1997)

108. Bibby, D. M. and Dale, P., Synthesis of Silica-Sodalite from Nonaqueous Systems, *Nature*, 317:157–158 (1985)

109. Lemberg, J., Ueber Silicatumwandlungen, *Z. Deut. Geol. Gesell*, 33:579–611 (1883)

110. Carlgren, O. and Cleve, P. T., Uber Einige Ammoniakalische Platinverbindungen, Z. *Anorg. Chem.*, 2:65–75 (1892)

111. Wilson, S. T. and Flanigen, E. M., Synthesis and Characterization of Metal Aluminophosphate Molecular Sieves, in: *Zeolite Synthesis*, pp. 329–345, American Chemical Society, Washington, D.C. (1989)

112. Hayashi, T., Shiga, H., Sadakata, M., and Okubo, T., Hydrothermal Growth of Millimeter-Sized Aluminosilicate Sodalite Single Crystals in Noble Metal Capsules, *J. Mater. Res*., 13:891–895 (1998)

DropBooks

113. Ren, X., Komarneni, S., and Roy, D. M., The Role of Gel Chemistry in Synthesis of Aluminophosphate Molecular Sieves, *Zeolites*, 11:142–148 (1996)

114. Davis, M. E., Montes, C., and Garces, J. M., Synthesis of VPI-5, in: *Zeolite Synthesis*, pp. 291–304, Am. Chem. Soc., Washington, D.C. (1989)

115. Freyhardt, C. C., Tsapatsis, M., Lobo, R. F., Balkus, K. J. Jr., and Davis, M. E., A High-Silica Zeolite with a 14-Tetrahedra-Atom Pore Opening, *Nature*, 384:295–296 (1996)

116. Schmidt, W., Schuth, F., Reichert, H., Unger, K., and Zibrowius, B., VPI-5 and Related Aluminophosphates: Preparation and Thermal Stability, *Zeolites*, 12:1–8 (1992)

117. Maistriau, L., Gabelica, Z., Derouane, E. G., Vogt, E. T. C., and Van Oene, J., Solid-State N.M.R. Study of the Transformation of VPI-5/MCM-9 into AlPO4-8/SAPO-8., *Zeolites*, 11:583–592 (1991)

118. Gopel, W., Jones, T. A., Kleitz, M., Lundstrom, J., and Seiyama, T., *Chemical and Biochemical Sensors*, VCH, New York (1991)

119. U.S. Patent No. 5,151,110 , Bein, T., Brown, K., Frye, C. G., and Brinker, C. J., (1992)

120. Feng, S. and Bein, T., Vertical Aluminophosphate Molecular Sieve Crystals Grown at Inorganic-Organic Interfaces, *Science*, 265:1839–1841 (1994)

121. Yan, Y. and Bein, T., Zeolite Thin Films with Tuneable Molecular Sieve Function, *J. Am. Chem. Soc*., 117:9990–9994 (1995)

122. Hennepete, H. J. C., Bargemen, D., Mulder, M. H. V., and Smith, C. A., Zeolite-Filled Silicone Rubber Membranes, Part I, Membrane Preparation and Pervaporation Results, *J. Member Sci*., 35:39–55 (1985)

123. Geus, E. R., Schoomian, J., and Van Bekkum, H., in: *Synthesis Characterization and Novel Applications of Molecular Sieve Materials* (L. Bedrad, T. Bein, M. E. Davis, J. Garces, V. A. Maroni, and G. D. Stucky, eds.), p. 231, Mater. Res. Soc., Pittsburgh, PA. (1993)

124. Bein. T., Synthesis and Applications of Molecular Sieve Layers and Membranes, *Chem. Mater.*, 8:1636–1653 (1996)

125. Tsikoyiannis, J. G. and Haag, W. O., Synthesis and Characterization of a Pure Zeolite Membrane, *Zeolites*, 12:126–130 (1992)

126. Sano, T., Kiyozumi, Y., Maeda, K., Toba, M., Niwa, S., and Mizukami, F., New Preparation Method for Highly Siliceous Zeolite Films, *J. Mater. Chem*., 2:141–142 (1992)

127. Smith, S. P. J., Linkov, V. M., Sanderson, R. D., Petrik, L, O'Conner, C. T., and Keiser, K., *Microporous Mater*., 4:385–390 (1995)

128. Bein, T., Brown, K., Brinker, C., in: Zeolites: Facts, Figs, Future, (P. A. Jacobs and R. A. Van Santen, eds.), *Stud. Surf. Sci. Catal*., 49:887–896 (1989)

129. Noack, M., Koelsch, P., Venzke, D., Toussaint, P., and Caro, J., New One-Dimensional Membranes-Aligned $AlPO_4$-5 Moleculer Sieve Crystals in a Nickel Foil, *J. Microporous Mater.*, 3:201–206 (1994)
130. Fuchs, H., Ohst, H., and Prass, W., *Adv. Mater*., 3:10 (1991)
131. Eddy, M. E., Stucky, G. D., Herron, G., and Bein, T., *J. Am. Chem. Soc.*, 111:2564 (1989)
132. Wark, M., Lutz, W., Bulow, M., and Schulz-Ekloff, G., in: *Proc. Third German Workshop on Zeolite Chemistry*, Berlin (Mar. 18–19, 1991)
133. Weitkamp, J., Proc. ZEOCAT 9O, Catalysis and Adsorption by Zeolites., in: *Stud. Surf. Sci. Catal.*, (O'hlmann, et al., eds.), 65:21 (1990)
134. Caro, J., Finger, G., Kornatowski, J., Richter-Mendan, J., Lutz, W., and Zibrowius, B., Aligned Molecular Sieve Crystals, *Adv. Mater.*, 4:273–276 (1992)
135. Ziolek, M. and Dudzik, Z., Catalytic Active Centers in $H_2O + O_2$ Reaction on faujasiter, *Zeolites*, 1:117–121 (1981)
136. Weisz, P. B. and Erdol, U., *Kohle*, 18:527 (1965)
137. Mirajkar, S. P., Eapen, M. J., Tamhankar, S. S., Rao, B. S., and Shiralkar, V. P., Hydrothermal Synthesis of Al and Ga-Substituted Omega Zeolite, *J. Inclus. Phenom. Molecular Recognition in Chemistry*, 16:139–153 (1993)
138. Perego, G., Bellussi, G., Corno, C., et al., New Developments in Zeolite Science and Technology, *Proc. 7th Intl. Conf. in Zeolites*, Tokyo, p. 129, Elsevier, Amsterdam (1986)
139. Notary, B., Innovation in Zeolites Materials Science, *Proc. International Symposium*, Nieuwpoort, p. 413, Elsevier, Amsterdam (1988)
140. Romano, U., Esposito, A., Maspero, F., et al., New Developments in Selective Oxidation, *Proc. International Symposium, Rimini*, Paper B1, Prepr. Univ. Bologna (1989)
141. Roffia, P., Leofanti, G., Casana, A., et al., New Developments in Selective Oxidation, *Proc. International Symposium, Rimini*, Paper 42, Prepr. Univ. Bologna (1989)
142. Kharitonov, A. S., Sobolev, V. I., and Panov, G. I., Hydrothermal of Aromatic Compounds With Nitrous Oxide, New Possibilities of Oxidative Catalysis on Zeolites, *Uspekhi Khimi*, 61:2062–2077 (1992)
143. Wilson, S. T. and Flanigen, E. M., Eur. Pat. Appl. 132,708 (1985)
144. Rabo, J. A., Poutsma, M. L., and Skeels, G. W., in: *Proc. 5th Intl. Congr. Catal.*, (J. Hightower, ed.), p. 1353–1361, North-Holland, New York (1973)
145. Rabo, J. A., Salt Occlusion in Zeolite Crystals, in: Zeolite Chemistry and Catalysis, *ACS Monograph 171*, (J. A. Rabo, ed.), pp. 332–349, Am. Chem. Soc., Washington, D.C. (1976)

DropBooks

146. Clearfield, A., Saldarriaga, C. H., and Buckley, R. C., *Proc. Third Int. Conf. Molr. Sieves*, (J. B. Uytterhoeven, ed.), Paper 130, pp. 241–245, Univ. Leuven Press, Zurich (1973)

147. Clearfield, A., Hydrothermal Synthesis of Selected Phosphates and Molybdates, in: Hydrothermal Growth of Crystals, (K. Byrappa, ed.), *Prog. Crystal Growth Charact.*, 21:1–28 (1990)

148. Slinkin, A. A., Kucherov, A. V., Goryashenko, S. S., and Slovetskaya, K. I., in: *Proc. All-Union Conf. Use of Zeolites in Catalysis*, p. 191, Moscow (in Russian) (1989)

149. Slinkin, A. A., Kucherov, A. V., Goryaskenko, S. S., Aleshin, E. G., and Slovetskaya, K. I., in: *Proc. 8th Soviet-French Seminar Catal*., p. 153, Novosibirsk (1990)

150. Kucherov, A. V. and Slinkin, A. A., Solid-State Reaction as a Way to Transit Metal Cation Introduction Into High-Silica Zeolites*., J. Molecular Catalysis*, 90:323–354 (1994)

151. Kucherov, A. V., Kucherova, T. N., and Slinkin, A. A., in: *Recent Res. Rep. Int. Symp. Zeolites Chemistry Catalysis*, p. 69, Prague (Sept. 8–13, 1991)

152. Kucherov, A. V., Kucherova, T. N., and Slinkin, A. A., *Kinet. Katal.*, 33:877 (1992)

153. Loiseau, T. and Ferey, G., Oxyfluorinated Microporous Compounds, *J. Solid State Chem*., 111: 403–415 (1994)

154. Riou, D. and Ferey, G., Oxyfluorinated Microporous Compounds, *J. Solid State Chem*., 111:422–426 (1994)

155. Loiseau, T., Retoux, R., Lacorre, P., and Ferey, G., Oxyfluorinated Microporous Compounds, *J. Solid State Chem*., 111:427–436 (1994)

156. Muller, A. and Pope, M. T., *Angew. Chem. Intl. Ed. Engl.*, 30:34 (1991)

157. Soghomonian, V., Chen, Q., Haushalter, R. C., and Zubieta, J., Vanadium Phosphate Framework Solid Constructed of Octahedra, Square Pyramids, and Tetrahedra With a Cavity Diameter of 18.4 Å, *Angew Chem. Int. Ed. Engl*., 32:610–612 (1993)

158. Haushalter, R. C. and Mundi, L. A., Reduced Molybdenum Phosphates: Octahedral Tetrahedral Framework Solids With Tunnels, Cages and Micropores, *Chem. Mater.* 4:31–48 (1992)

159. Corcoran, E. W., Nawsam, J. M. Jr., King, H. E. Jr., and Vaughan, D. E. W., in: *Zeolites Synthesis*, (M. Occelli and H. E. Robson, eds.), p. 603, Am. Chem. Soc., Washington, D.C. (1989)

160. Feng, S., Xu, R., Yang, G., and Shun, H., *Chem. J. Chinese Univ. (Engl. Ed.)*, 4:9 (1988)

161. Wang, T., Yang, G., Feng, S., Shang, C., and Xu, R., *J. Chem. Soc. Chem. Commun*., p. 2436 (1989)

162. Feng, S., Tsai, M., and Greenblatt, M., Preparation, Ionic Conductivity, and Humidity-Sensing Property of Novel, Crystalline Microporous Germanates, Na_3Hge7O_{16}. × H_2O, x = 0–6.1, *Chem. Mater*., 4:388–393 (1992)

163. Leonowicz, M. E., Lawton, J. A., Lawton, S. L., and Rubin, M. K., MCM-22: A Molecular Sieve With Two Independent Multidimensional Channel Systems, *Science*, 24:1910–1913 (1994)

164. Fuchs, H., Ohst, H., and Prass, W., *Adv. Mater*., 3:10 (1991)

165. Alvaro, H., Fornes, V., Garcia, S., Garcia, H., and Scaiano, J. C., Intrazeolite Photochemistry 20, Characterization of Highly Luminescent Europium Compleaes Mride eolites, *J. Phys. Chem*. B., 102:8744–8750 (1998)

166. Smolin, Yu. I., Shepelev, Yu. F., Lapshin, A. E., and Vasileva, E. A., CdS Clusters in Pores of Zeolites X, *Crystallography Reports*, 43:387–394 (1998)

DropBooks

7

Hydrothermal Synthesis and Growth of Coordinated Complex Crystals (Part I)

7.1 INTRODUCTION

Hydrothermal synthesis and growth of complex coordinated crystals are not new especially for silicates. In fact, the hydrothermal technology was clubbed under silicate technology in the earlier days. Silicates have drawn the attention of crystal chemists right from the earliest days owing to their abundance, structural diversity, and wide spread applications in various technologies. Thus, the synthesis of complex coordinated complexes began in the 19th century. However, during the1960s and 1970s the importance of the hydrothermal technique for the synthesis of inorganic materials without natural analogs was realized. Since then a large variety of complex coordinated complexes are being obtained with very complex crystal structures. This group covers silicates, phosphates, vanadates, arsenates, molybdates, tungstates, fluorides, sulphates, selernides, borates, and so on, with a great variety of cations starting from alkali, alkaline-earth, transitional to rare earth metals. The number of all such compounds exceeds several hundreds owing to their academic and technological interest and here it is impossible to discuss each and every compound. Therefore, we have discussed these compounds in two parts for the

sake of the reader's convenience. Part I covers silicates, germanates, phosphates, vanadates, and borates (Ch. 7). The remaining group of complex coordinated compounds are discussed in Part II (Ch. 8). The literature survey shows that among all these compounds, the silicates and germanates have taken a unique place in the hydrothermal research because of their diversified compositions and structures. Here, these compounds will be discussed in two categories: *i)* rare earth silicates and phosphates; and *ii)* transitional metal silicates and phosphates.

7.2 CRYSTAL CHEMICAL BACKGROUND

It is interesting to note that there is a close relationship between crystal chemistry and crystal growth of these compounds. The primary requirement for any material/crystal/mineral with a device potential is the understanding of its scientific foundation, particularly the consequences of the sub-microscopic crystal structure, i.e., the spatial arrangement of atoms, ions, molecules, and the types of chemical bonds between them. It is the chemical bond more than anything else that determines the structure and the properties of a crystal. A crystal chemical knowledge helps in tailoring a given phase or a given structure that is to optimize chemical classification, crystal structure, and defect structure with respect to the desired properties. Therefore, the present authors briefly discuss the structural diversity of silicates and the Si-O chemical bond.

DropBooks

Silicates are the compounds containing Si and O. Their main specific structural feature is the presence of Si-atoms in a 4-fold coordination with oxygen, which is favored by the ratio rSi:rO = 0.28. Table 7.1 gives the different types of coordinations of cations as a function of ionic radii ratio. Bond lengths and bond angles in Si-tetrahedra tend to be close to their mean values: d(Si-O) = 1.62 Å; angle O-Si-O = 109°.47'; Si-O-Si = 140°. Si atoms are found in 6-fold coordination in relatively small groups, basically in high-pressure silicates, and in 5-fold coordination in some of the organosilicate compounds.[1]

The structures of silicates and related compounds contain tetrahedral anions of different configuration (single tetrahedron, pyrogroups, rings, chains, layers, frameworks, etc.). Their comparative analysis considerably extends scientific ideas on structures of crystalline materials. The attention to silicates is connected to their wide-spread abundance in the continental crust (Table 7.2), the exceptional variability of tetrahedral

anions in their structures, and a wide-spread application of silicates in modern technology. Silicates are widely being used in ceramic, optical, electronic, piezoelectric, optoelectronic, etc., industries.[2]

Table 7.1 The Different Types of Coordinations of Cations As a Function of Ionic Radii Ratio[1]

C N	Coordination	Ionic Radii Ratio
2	Dumb-bells	< 0.15
3	Triangle	0.15-0.22
4	Tetrahedron	0.22-0.41
6	Octahedron	0.41-0.73
8	Cube	0.73-1.37

Table 7.2. Bulk Content of Silicates In Continental Crust[2]

Mineral	Percentage	Total
Feldspars	64.0 %	
Pyroxenes + Amphiboles	9.0 %	
Quartz	18.0 %	96.5 %
Biotite	4.0 %	
Olivine	1.5 %	

The compounds that are nearer to silicates in the crystal chemical sense are phosphates with over 350 minerals. According to Corbridge, the term *phosphate* may be used to include all phosphorus compounds which contain P-O linkages.[3] Similarly, the author[4] calls all the simple and complex oxides obtained from phosphoric acid solutions phosphates. For a free atom of phosphorus, the distribution of electrons in the valence cell is written as follows:

Eq. (1)

$3s$	$3p$
↓↑	↑↑↓

It means that the phosphorus atom can form the bonds due to 3*p* electrons and another two owing to 3*s* electrons. Hence, the phosphorus atom participates in the reaction with oxygen to exist in a trivalent state, forming phosphides and in a pentavalent state forming phosphates. As a result of sp^3 hybridization (l*s* and 3*p* orbitals of P), four similar energy orbits develop and during the interaction of phosphorus with oxygen, it leads to the formation of a stable tetrahedral group [PO_4]. However, the P-O bonds in such a tetrahedron will not be purely ordinary (σ bonds), but it includes a distinct fraction of short bonds (π bonds) as well. It is well known that the P-O tetrahedra are susceptible to the condensation reactions due to the formation of bridging bonds -P- O-P- or P-O (M). The possibility of the development of such bonds make the *p* orbit of the bridging oxygen (which is arranged perpendicular to the plane POP) to interact with *d* orbits of the P atoms to form π bonds. The bond lengths and bond angles in P tetrahedra are given as follows: d(P-O) = 1.54 + 0.02 Å, P-O (terminal) = 1.51 Å, angle O-P-O = 109.4 ± 5° and angle P-O-P = 156 to 167°. P-O (bridging) = 1.64 Å. Although the bond length tends to be close to its mean value, the bond angle, especially angle P-O-P, is obtuse and the rotation flexibility along the P-O-P linkage allows a variety of related orientation of adjacent tetrahedra.[5] From the crystal chemistry of phosphates, it is evident that the variation in the bond lengths and bond angles is quite large and it is difficult to find an analog to [PO_4]-tetrahedra among the inorganic compounds.[6] Hence, a thorough study of the crystal chemistry of silicates and phosphates, in turn, helps to understand crystal chemistry of analogous compounds like germanates, vanadates, arsenates, sulphates, borates, etc.

Germanates and phosphates form the nearest analogs of silicates owing to the nearer ionic radii and charge values. All three types of tetrahedra [SiO_4, GeO_4, and PO_4] form condensed radicals, but the ability to undergo polycondensation is high for silica tetrahedra when compared with Ge, P, and other tetrahedra (VO_4, AsO_4, SO_4, BO_4, BeF_4 etc.) having nearer ionic radii. This is probably connected with a significantly lower number of different P:O and Ge:O ratios (10 and 9 respectively) when compared with a similar Si:O, which is 28 as observed in phosphates, germanates, and silicates.[7] This characteristic property of Si tetrahedra can be explained based on two factors: *i)* suitable value of valence charge

DropBooks

of silicon equivalent to one (this separates silicon from phosphorus), *ii)* characteristic radius ratio $rSi^{4+}:rO^{2-}$ for the formation of tetrahedral coordination. In this respect, Si tetrahedra differ from Ge tetrahedra for which the radius ratio $rGe^{4+}:rO^{2-}$ (0.38) is nearer to the upper stability limit of the tetrahedral coordination (0.41). The possible valence states and the coordination number of basic cations capable of forming oxide complexes are given in Table 7.3. All these elements represented in Table 7.3 form the tetrahedral coordination. Besides, the linking of $[TO_4]$-tetrahedra (T is the tetrahedral cation) is different for different cations. For example, out of more than six hundred structures refined for natural and synthetic sulphates, only in four structures, viz, $K_2S_2O_7$,[8] $nK_2S_2O_7 \cdot V_2O_5$,[9] CdS_2O_7,[10] and $Te(S_2O_7)_2$,[11] have the pyrogroups $[S_2O_7]$ been established recently. Structurally, a very important phosphate mineral, canaphite, having pyrophosphate groups $[P_2O_7]$ formed by the linking of two tetrahedra at the vertices, was reported recently.[12] Before the discovery of this mineral in 1988, there was a unanimous opinion with regard to the absence of condensed phosphate minerals, although more than 320 phosphate minerals are known in nature. However, vanadates, which usually form 4-, 5- and 6-fold coordinations with oxygen, contain the condensed V-tetrahedra. For example, chervetite, $Pb_2V_2O_7$ having pyrogroup-$[V_2O_7]$ formed by the linking of two $[VO_4]$-teterahedra with one of the corners sharing, has been reported so far.[13] In contrast, such condensed radical groups or pyrogroups, i.e., $[As_2O_7]$ complexes, have not been reported among arsenates.

Table 7.3. Valency States and Coordination Numbers of Basic Oxide Complexes[1]

Group	Element	Valency States					Coordination			
		2	3	4	5	6	3	4	5	6
III	B	-	+	-	-	-	+	+	-	-
IV	Si	-	-	+	-	-	-	+	+	+
	Ge	-	-	+	-	-	-	+	-	+
V	P	-	+	+	+	-	-	+	-	-
	V	+	+	+	+	-	-	+	+	+
	As	-	+	-	+	-	-	+	-	-
VI	S	+	-	+	-	+	-	+	-	-

Main Concept of Silicate Structures. In silicate structures (Si,O)-tetrahedral anions should be adjusted to the cationic polyhedral fragments.[14] In particular, this principle was confirmed by the structures with big cations (K, Na, Ca, RE …), which always contain (Si, O)-complexes on the basis of pyrogroups $[Si_2O_7]$ commensurable with the edges of cationic polyhedra.

Several quantitative correlations actually complete this qualitative approach. For example, there are more than 60 compounds with a general formula $M_a[T_2O_7]_b$, where T = As, Be, Cr, Ge, P, S, Si. They can be subdivided into two groups: *a)* tortveitite-like with angle T-O-T > 140°; *b)* bichromate-like with angle T-O-T < 140. Figure 7.1 illustrates that the frontier between both groups corresponds to the equation r/T/ = 1.5r/M-1.1, where r-radii of tetrahedral (T) and nontetrahedral (M) cations.[15] Thus, the increasing number of refined structures allows the establishment of a quantitative relationship between the configuration of tetrahedral complexes and properties of the non-tetrahedral cations.

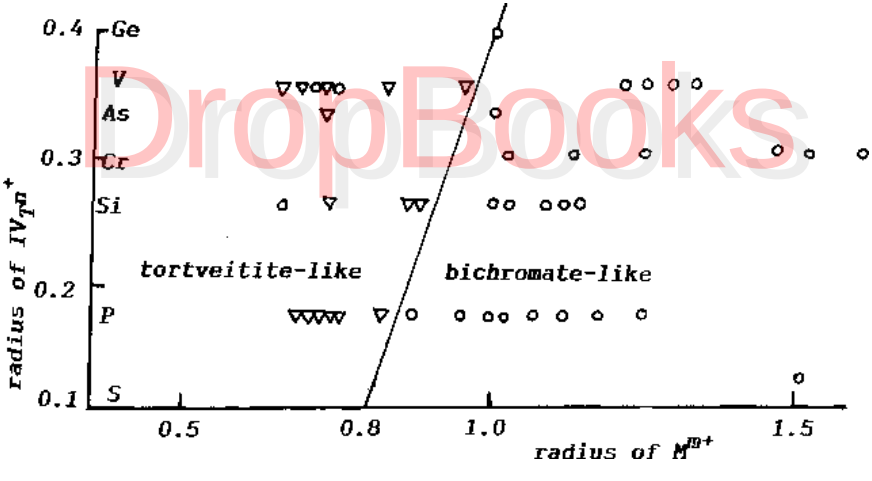

DropBooks

Figure 7.1. Correlation between the stability of tortveitite-like and bichromate-like structures $Ma[T_2O_7]$ and radii of M- and T- cations.[1]

Among these complex coordinated compounds, silicates have been studied extensively, followed by germanates, phosphates, and others. Although silicates and germanates have a systematic structural classification their analogous compounds—like phosphates, vanadates, arsenates, etc.—do not have a systematic classification. It is extremely difficult to classify phosphates, unlike silicates, because of high complexity in the phosphates' internal structures.[16] Similarly, the other analogous compounds such as borates, vanadates, arsenates, and sulphates, have not been studied in detail and they do not have any systematic structural classification. This is probably connected with their lesser abundance in nature and also lesser degree of structural diversities.

One of the main crystal chemical problems is connected with predictions of structural transformations of elevated temperatures and pressures. The hydrothermal technique especially is very handy in this context.

The diversity of (Si,O)-complexes, described in an earlier section has been attributed to silicate stability at relatively lower depths. The lower coordination number of oxygen[2][3] in these structures makes them unstable in the mantle. High-pressure structural studies[17] show that the decrease of Si-O distance until the "critical" value–1.59 Å–leads to a change of Si-tetrahedra by Si-octahedra. There is a certain advantage in such transformations, because Si-octahedra with longer distances Si-O can be linked not only by corners, but also by edges and even by faces. Thus, the coordination number of oxygen becomes greater, and at the same time the distribution of Si-atoms becomes more compact.[18] The "critical" value 1.59 Å is not accidental and is confirmed by the correlation between interatomic distances and angles in Si-tetrahedra.[19] Lg2/d (Si-O) avg/ = Lgd (Si-Si) – Lg $\angle$ (Si-O-Si) /2 with fixed Si-Si distances = 3.06 Å and $\angle$ $(Si\text{-}O\text{-}Si)_{max}$ = 180°, one gets d $(Si\text{-}O)_{min}$ = 1.59 Å. This value was obtained in the structure of forsterite Mg_2SiO_4 at P = 14. 9 GPa.[20]

The stability of Si-tetrahedra depends on the properties of nontetrahedral M-cations. The presence of M-cations with a high value of electronegativity leads to a decrease in the coordination of oxygen atoms. Consequently, under high pressures these structures transform into structures with Si-octahedra more easily.[21]

McDonald and Cruickshank (1967)[22] have shown that in structures with electronegative M-cations the distances Si-O bridging and Si-O terminal become more equal. According to Brown (1978),[23] this effect is followed by a decrease of $(Si\text{-}O)_{avg}$ distances in Si-tetrahedra. In other words, chemical deformations connected with the presence of M cations with high electronegativity is similar to the high-pressure structural deformations.

The concept of emphasizing the dominating role of cations in the structure reformation is used for the interpretation of structural transformations under high pressure. The compressibility of cationic polyhedra (β) is inversely proportional to the polyhedral charge density z/d,[24] where d-distance between central cation and O-atoms. The behavior of Si-tetrahedra mainly depends on the compressibility of the M-polyhedra, which can be considered as initial.[25] For example, Mg_2SiO_4, under high pressure successively transforms from α- and β- modifications with decreasing ratios (Mg-O)/(Si-O):1.291 (α), 1.860 (β) and 1.251 (γ). The significant compressibility of the Mg-octahedra during the transformation from the α- to the γ- form initiates the unexpected expansion of the Si-tetrahedra; d(Si-O) in α-Mg_2SiO_4 = 1.636 Å while in γ-Mg_2SiO_4 = 1.655 Å.[26] It is noteworthy that the structural alterations in these compounds as in some other silicates result in oxygen atom packing ordering.[27]

DropBooks

According to Ringwood,[28] high-pressure transformations of silicates can be studied on the basis of their germanate analogs. This idea can be understood if one takes into account that the ratio r_{cation}/r_{oxygen} should be increased under high pressure. At atmospheric pressure, rGe^{4+} is greater than rSi^{4+} for 20%. Therefore, the structures of germanates at normal pressure reflect many specific features of high-pressure deformations in silicates. As an example, the authors compare the high-pressure structural changes in quartz[29] with chemical deformations in its structure, where Si-atoms were partially substituted by Ge.

These crystals bear composition $(Si_{0.86}Ge_{0.14})O_2$ which is considered to be unique because, hitherto, the GeO_2 concentration in the synthetic quartz crystals never exceeded 0.13 molar %. The common tendencies in quartz under high pressure and with the substitution of Si for Ge are connected with: *i)* a decrease in angle T-O-T (Fig. 7.2); *ii)* a decrease in intertetrahedral distances O-O; *iii)* a similar change in tilt angles between tetrahedra (Fig. 7.3*a*); and *iv)* an increase in tetrahedral distortion (Table. 7.4).[30]

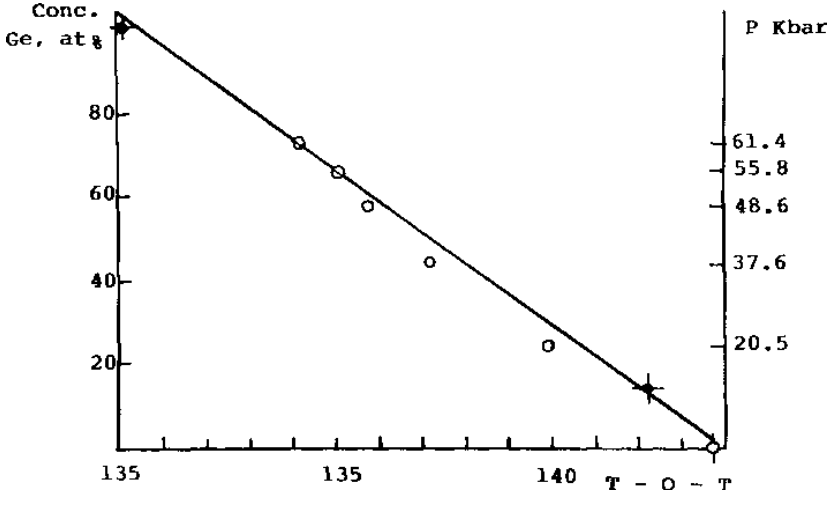

Figure 7.2. Decrease in T-O-T with the substitution of Si for Ge.[7]

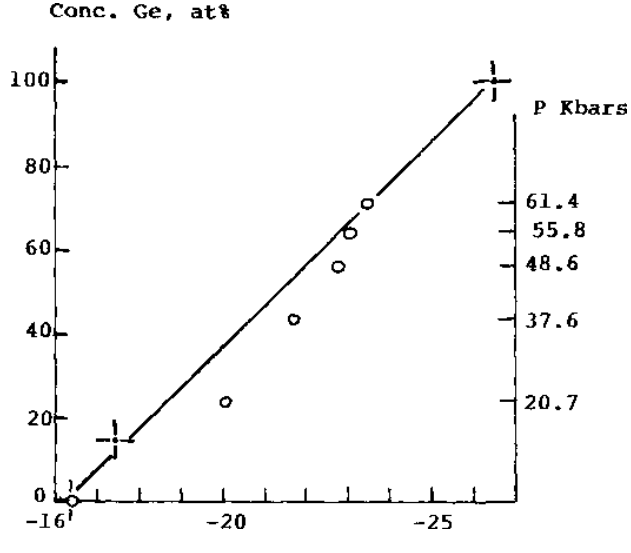

Figure 7.3. Decrease in the tilt angles between tetrahedra.[7]

Table 7.4. Comparison of Structural Parameters in Quartz Under High Pressure With The Substitution of Si for Ge[7]

Structural parameter	Pressure		Substitution of Si for Ge	
	1 bar	61.4 kbar	$(Si_{0.86}Ge_{0.14})$	GeO_2
∠T-O-T	143.73	134.2	142.2	130.1
inter-tetrahedral	3.331	2.925	3.304	3.024
distances O-O Å	3.411	3.064	3.406	3.193
tilt angle	-16.37	-23.47	-17.41	-26.55
(O-T-O)-angle's dispersion	0.67	5.51	1.04	10.09

The structural comparison in silicates and germanates allows explanation of the different crystal chemical phenomena. One of them is connected with the question of why GeO_2 does not crystallize with coesite structure while stishovite—a form of GeO_2—mineral argutite is known even in nature.

The structural changes of coesite under high pressure are connected with significant dispersion in Si-O-Si angles. It is noteworthy that the smallest angle sharply decreases. Moreover, under high pressure, the temperature factor of O_1, which participates in bond Si-O_1-Si with an angle equal to 180°, increases up to about 30%, while the temperature factors of other atoms decrease. Substitution of Ge for Si would reinforce the tendencies and would lead to structural distortions, in other words, to the displacement of O_1 and the distortion in angle Si-O_1-Si = 180°.

DropBooks

The tetrahedral complexes are being extensively studied and characterized, owing to their applications in technologies such as laser, superionic, ferroelectric, ion-exchange, piezoelectric, opto-electronics, and a host of others. We initially discuss the silicate structure, followed by phosphates, borates, vanadates, sulphates, etc., with reference to their properties. Only some representative compounds have been discussed covering all the tetrahedrally coordinated compounds.

In principle, there are several ways to search new crystalline phases under hydrothermal conditions:

- The investigation of phase diagrams of crystallization for complicated systems and of hydrothermal chemistry of individual elements.
- The direct search for new compounds with the preset physical properties.

- The study of hydrothermal reactions under new pressure temperature conditions.
- The modification of known compounds with the help of isomorphic displacements or of special doping.

The above aspects have been discussed, in this book, for silicates, germanates, phosphates, borates, arsenates, vanadates, molybdates, tungstates, fluorides, etc.

The study of the phase diagrams of crystallization is the first step in the search of new compounds, the conditions of their synthesis, and the prediction of their physical properties. The next step in the hydrothermal synthesis is the selection of compounds with promising properties and the development of methods providing the synthesis of crystals with sizes appropriate for their practical use in science and technology. The study of phase interactions in multi-component systems yields a wealth of information for hydrothermal physical and crystal chemistry and simulation of natural processes. In fact, the number of single crystals grown on seeds under hydrothermal conditions is much smaller than that of spontaneously grown single crystals. Today we have the techniques for crystal growth on seeds for the following materials:

Oxides:	quartz SiO_2, GeO_2, zincite ZnO, cuprite Cu_2O, sapphire Al_2O_3, ruby Al_2O_3: Cr^{3+}, TeO_2, ABO_4 (A-Sb, B-Sb, Nb).
Sulphides:	ZnS, HgS.
Complex oxides:	sillenite $Bi_{12}TO_{20}$ (T=Si, Ge etc.), garnets $Ln_3Fe_5O_{12}$, ferrites $LnFeO_3$.
Silicates:	nepheline (Na, K) $AlSiO_4$, cancrinite $Na_8Al_6Si_6O_{24}(OH,Cl)_2 . NH_2O$, sodalite $Na_8Al_6Si_6O_{24}(OH)_2 . NH_2O$; beryl (emerald) $Al_2Be_3Si_6O_{18}$: Cr^3, eulytine $Bi_4(SiO_4)_3$.
Phosphates:	$AlPO_4$, $GaPO_4$, $KTiOPO_4$, $KTiOAsO_4$.
Carbonates:	$CaCO_3$, $CoCO_3$, $MnCO_3$.
Germanates:	$KAlGeO_4$, $Na_8Al_6Ge_6O_{24}(OH)_2$ nH_2O (two modifications), $Bi_4Ge_3O_{12}$.

The number of spontaneously nucleated crystals/compounds is very high and it is practically impossible to list the individual phases and their preparation conditions. Therefore, we have made an effort to group them into broader divisions and discuss only some selected phases.

7.3 RARE EARTH SILICATES

Among silicates obtained under hydrothermal conditions, the rare earth silicates are the most extensively studied ones owing to their academic as well as technological importance. The rare earth elements have a significant influence on the crystallization of various rocks and minerals and in the magmatic processes on the whole. Their distribution in various rocks and minerals clearly demonstrates the physico-chemical influence they exert upon the crystallization of the magma. Their distribution and association further depend upon the alkalinity of the melt. Therefore, an extensive work has been carried out on various alkali-rare earth metal silicate systems in order to understand the crystallization of a large number of rare earth silicates with and without alkali metals. A majority of these rare earth silicates were found to be new phases, and most of them carry technological significance owing to their unique physical properties. Although a great amount of work has been done on the synthesis of several hundreds of phases of rare earth silicates with and without alkali metals, there are only a few publications dealing with their crystal growth and seeded growth. Nevertheless, a vast literature data accumulated on these compounds yield a great variety of interesting results with reference to the phase formation, pressure-temperature conditions, starting materials, type of rare earth element, alkali metal, the role of solvent, and so on. A large number of structure types have been obtained, which clearly indicates the importance of these rare earth silicates from the academic point of view. Besides, these rare earth silicates exhibit very interesting physical properties, which have been studied by various authors and they have correlated these properties with their molecular structures. Though it is extremely difficult to discuss each and every aspect dealt in the literature, we have made a sincere attempt to provide an overall picture of these rare earth silicates of hydrothermal origin with a special reference to their phase formation and structure types.

ProofBooks

7.4 PHASE FORMATION OF RARE EARTH SILICATES (IN AQUEOUS SOLVENTS)

It is well known that the hydrothermal solutions contain significant amounts of chlorides, carbonates, and other well soluble components. The distribution and mobility of the rare earth elements greatly depend upon

their interaction with Cl, F, SO_4, and CO_3 species. The formation of silicates in nature takes place essentially from fluoride solutions having alkaline character. Among them, the main role is played by the hydroxides of Na and K. In laboratory synthesis of rare earth silicates, essentially aqueous solvents of hydroxides and carbonates of Na and K, and, similarly, chloride, fluorides, and their mixtures, are commonly used as solvents. The solubility increases above 60°C in NaOH solutions, especially above the melting point of NaOH (476°C), there exists a complete mixing. Similarly, the increase in the concentration of NaOH with temperature further improves the solubility.[31][32] Such studies have been carried out on carbonate solutions in detail.[33][34] Table 7.5 shows the solubility of Na_2CO_3 in water.

Table 7.5. Solubility of Na_2CO_3 in Water[33]

P (atm)	Na_2CO_3 in wt %	P (atm)	Na_2CO_3 in wt %	P (atm)	Na_2CO_3 in wt %
475°C		500°C		540°C	
900	1.5–2	1735	55	1200	< 1.0
1300	3.5–4	1905	88	1300	1.0
1550	16	520°C		1400	1.0
1625	28	1200	1.5		
1637	37	1400	3.5		
1833	44	1500	3.5		
1955	49-50				

The bonding of the rare earth elements in the form of soluble species could be represented as follows:[35]

Eq. (2) $$R^{I}_{y}\, X_z \leftrightarrow R^{+3} \leftrightarrow [R_{en}\, (AX)m]$$

where R = rare earth ion
X and (AX) = any acidic ions
I and II = electroneutral compounds or complex anions.

For example, rare earth elements with carbonate ions would form complex anions of $[R\,(CO_3)_3]$ type, which can migrate and in the presence of alkali elements would form $Na_3[R(CO_3)_3]_3$. From Lu to La, the stability of such complexes would increase with an increase in the alkali concentration in the medium. Thus, in natural processes, rare earth elements must

have migrated as the soluble complexes of carbonates, fluorides, chlorides, and may be sulphates. Such complexes, in turn, participate in chemical reactions to form more stable complexes with additional anions of CO_3, F, Cl, O_4, and OH, thus, the study of rare earth silicates in aqueous solutions of Na_2CO_3, Na_2SO_4, NaCl, and NaF. In fact, the solubility of Na_2CO_3, Na_2SO_4, NaF in water decreases with an increase in temperature, and increases with an increase in pressure. The solubility of NaCl in water increases with an increase in temperature and pressure. These studies on the behavior of solvents with temperature and pressure have helped in the understanding of the phase formations in various rare earth silicates and analogous systems.

Although the study of various rare earth silicate systems began during the 1970s extensively, the objective was to understand the distribution and mobility of rare earth elements in natural systems. The importance of the addition of alkali elements into the systems was realized in the 1980s, because the alkali and rare earth metals together play an important role in the formation of various phases. Several new phases were discovered and with the availability of a vast amount of structural data on these alkali rare earth silicates, their physical properties became known to the scientific community. Some of these alkali rare earth silicates exhibit very interesting mixed framework structures. Among the cations in the alkali rare earth silicates with mixed framework structures, the alkali ion can serve as a mobile charge carrier. It provides interesting opportunities for the development of potentially new fast ion conductors because of the extensive possibilities for crystal chemical tailoring. The chemical stability for silicates and a large number of related phases are available for investigation.[36][37] High Ionic conductivity has been reported in $Na_5RSi_4O_{12}$ (where R = La-Lu, Sc, Y) ring silicates, almost simultaneously from three different laboratories.[38]–[43] Hydrothermal synthesis of $Na_5YSi_4O_{12}$, $Na_5Sc\ Si_4O_{12}$, $Na_5Er\ Si_4O_{12}$, etc., has been reported in the literature. The crystal structure of $Na_5RSi_4O_{12}$ was reported by Maksimov et al.[43] and it is shown in Fig. 7.4. Thus, the importance of the rare earth silicates was established during the 1980s. Here, we discuss the behavior of various rare earth silicates and alkali rare earth silicate systems under hydrothermal conditions within a wide range of pressure temperature conditions. Also, the role of different mineralizers and the starting molar ratios on their crystallization has been studied to obtain a general picture, instead of describing each and every rare earth silicate compound and its synthesis.

ProBooks

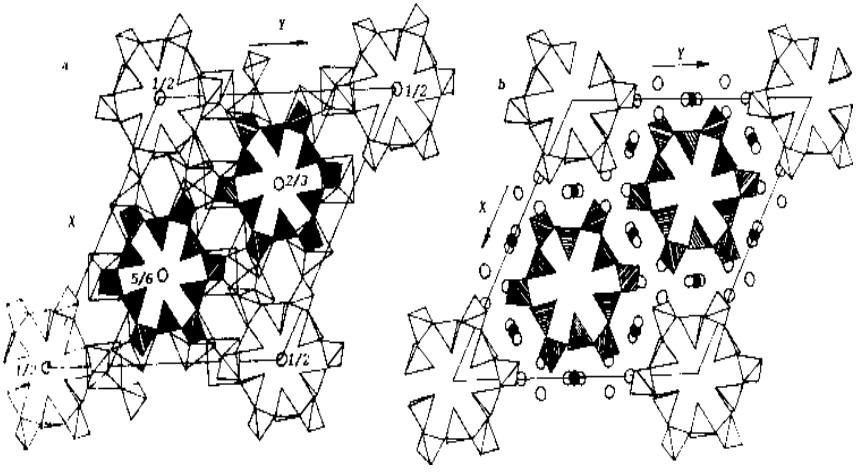

Figure 7.4. Crystal structure of $Na_5RSi_4O_{12}$.[43]

In the carbonate solutions and in mixed solutions of NaOH + Na_2CO_3, two new phases crystallize and when RE_2O_3: SiO_2 = 1:4, NaR Si_6O_{14} crystallizes, where R = La-Eu. These crystals are quite stable in pure Na_2CO_3 solution and NaOH up to 10%. With an increase in the concentration of the solutions, apatite like phase forms, and with a decrease in the concentration of the solutions, the stability of $NaRSi_6O_{14}$ falls along with the stability field of quartz. In a pure carbonate solution, together with $NaRSi_6O_{14}$, quartz always crystallizes. With an addition of NaOH, the quantity of quartz reduces but doesn't disappear totally.

When R_2O_3:SiO_2 approaches 1:1, the system gives another phase $Na_3RSi_6O_{15}.2H_2O$, which is the characteristic phase for the entire rare earth series, and it persists up to the concentration of NaOH = 30%, and beyond 30 % of NaOH, it separates into two types: $Na_3R[Si_2O_7]$ for the second half of the series (yttrium series) and $Na_2R[SiO_4]$ (OH) for the first half of the rare earth series (lanthanum series). An overall scheme of crystallization shows that when mixed mineralizers (NaOH + N_2CO_3) are used, the crystallization pattern changes, and is shown for the Nd representative in Fig. 7.5[44] It is interesting to see that with a decrease in the amount of H_2O in the alkali-carbonate system the field of $Na_3RSi_6O_{15}\cdot 2H_2O$ also decreases and only one phase NaR_6O_{14} crystallizes. In the NaOH + Na_2CO_3 solution and at T = 550–600°C and P = 1–2 kbar and only in experiments with NaF and NaCl, it is shown that

the surplus silica for the lighter rare earth series in the system, only $NaRSi_6O_{14}$ crystallizes in all cases, of course, the crystal morphology varies from those obtained using carbonate solutions. Figure 7.6 shows the crystallization fields for the system Na_2O-R_2O_3-SiO_2-H_2O, T = 450–650°C, P = 400–2500 atm (*i.* Surplus R_2O_3; *ii.* Surplus SiO_2).[35] In NaF solution this compound crystallizes as fine crystalline mass. It can be concluded that under hydrothermal experimental conditions, the presence of F, Cl, CO_3, and SO_4 anions in the solvents greatly influences the $[SiO_4]$ anions to form highly complex anions like $[Si_6O_{15}]$ and $[Si_6O_{14}]$. It is interesting to note that rare earth elements, including the lighter rare earths (La-Nd), form chain silicates with discrete polyhedra. Such discrete rare earth polyhedra were first observed among silicates, and, subsequently, in germanates, phosphates, and so on.[44]–[46]

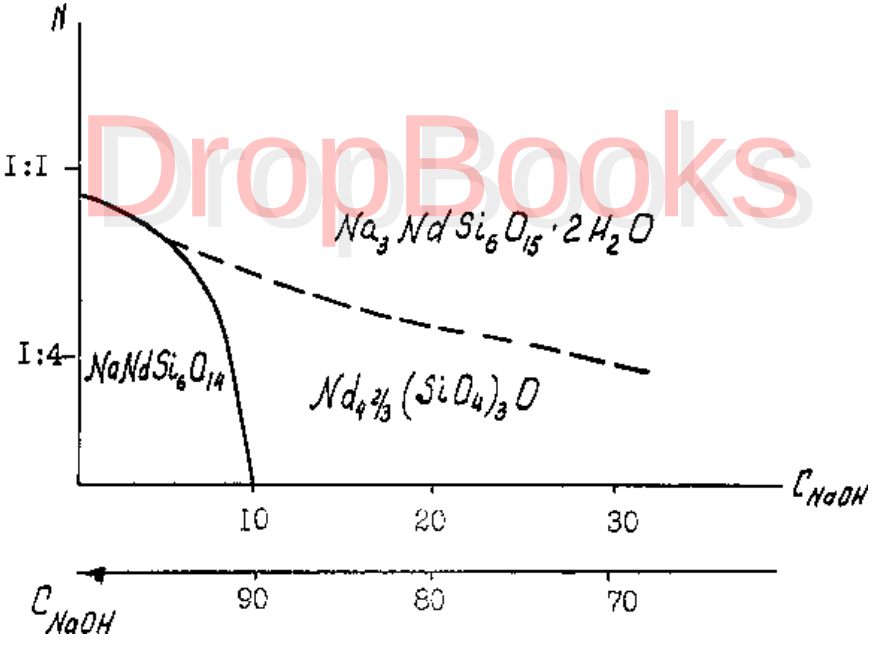

Figure 7.5. Crystallization pattern Nd silicate.[44]

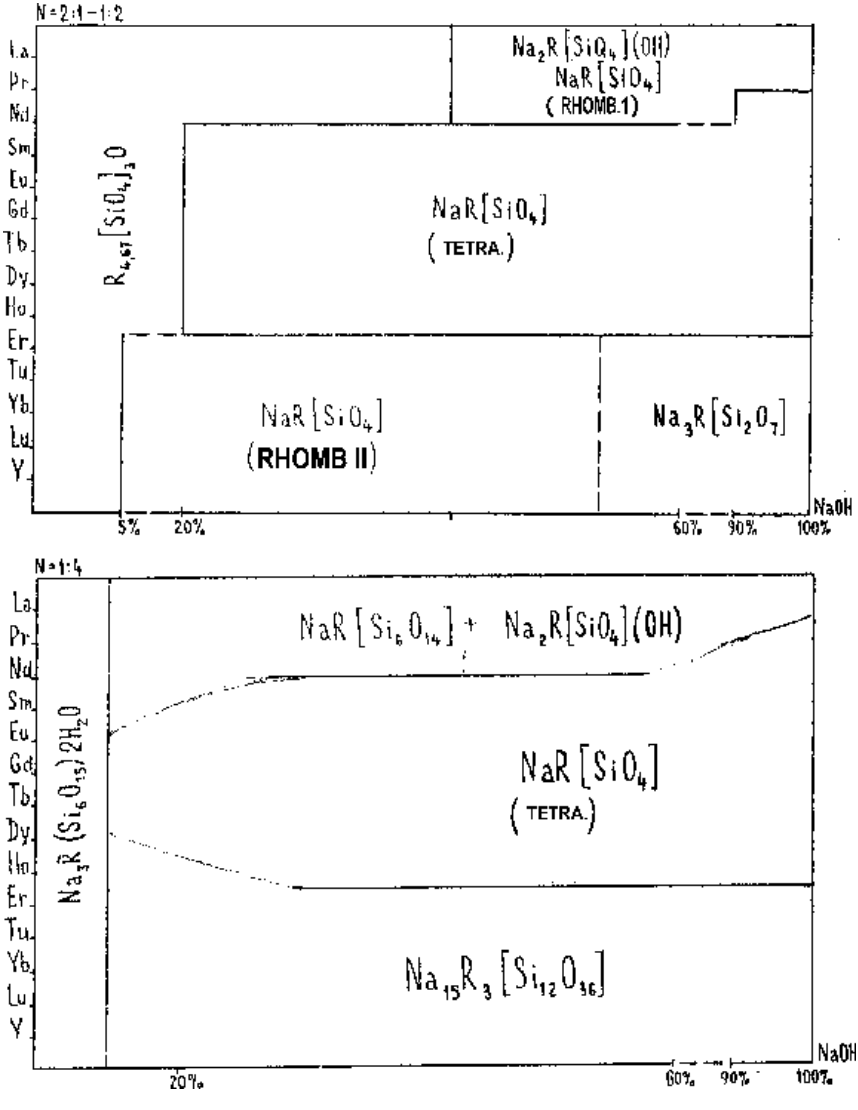

Figure 7.6. Crystallization fields for the system Na_2O-R_2O_3-SiO_2-H_2O, T = 450–650°C, P = 400–2500 atm (*i.* surplus R_2O_3; *ii.* surplus SiO_2).[35]

Haile et al. (1993)[47]–[49] studied the hydrothermal synthesis of new alkali silicates, potassium neodymium phases, and sodium phases, in great detail. The alkali silicates are interesting, both scientifically and technologically, as fast ionic conductors because of their typical open framework structures and the unique possibilities for crystal chemical tailoring. Their studies on the systems K_2O-Nd_2O_3-SiO_2 and Na_2O-Nd_2O_3-SiO_2 yielded: $K_3NdSi_3O_8(OH)_2$, $K_3NdSi_7O_{17}$, $K_5NdSi_9O_{22}$, $K_8NdSi_{12}O_{32}{\cdot}OH$, $K_3NdSi_6O_{15}$, $K_3NdSi_6O_{15}$ (P_{bam}), $K_2Nd{\cdot}Si_4O_{10}{\cdot}OH$, and $KNd_9(SiO_4)_6O_2$, out of which the first four have no known isomorphs. Similarly, of $NaNdSi_6O_{14}$, $Na_3NdSi_6O_{15}$ $2.5H_2O$, $NaNd_9(SiO_4)_6O_2$, $Na_3YSi_6O_{15}$, $Na_3YSi_7O_{17}$, $Na_7YSi_{12}O_{29}$, $Na_3YSi_3O_9$, $Na_5YSi_4O_{12}$, $Na_6YSi_{13}O_{29}$ $(OH)_3$ and $NaYSi_6O_{14}$, six are new. The synthesis has been carried out in aqueous solutions of MOH, M_2CO_3, MF, MHF_2 (where M = Na, K), $K_2B_4O_7$ as solvent, and either a glass of high silica content, $4K_2O$ (Na_2O)-Nd_2O_3-$17SiO_2$, or a mixture of Nd_2O_3, vitreous silica and K_2CO_3(Na_2CO_3) as the precursor material. Pressures, temperatures, and solution molarities utilized ranged from 0.3 to 1.4 kbar, from 350 to 600°C, and up to 10 M respectively. The authors found that high-solution molarities, high temperatures, and to some extent, high-pressures and long reaction-time favored the crystallization of phases with low "connectivities" between [SiO_4] tetrahedra in the structure. A decrease in the ratio of interstitial oxygen atoms and hydroxyl groups broadly corresponds to a progressive change from a 3-*d* structure, to one that is layered, to one based on chains or rings and eventually, to one that contains discrete radicals, typically $[SiO_4]^{-4}$ groups. The changes in the structure of the crystallization phase occur via changes in the structure of the silicate species in the solution. The latter, in turn, responds to changes in the experimental conditions in accordance with a generalized reaction:

ProfBooks

Eq. (3) $$Si_xO_y^{2(2x-y)} + 2zOH^- \leftrightarrow Si_xO_y^{2(2x-y-z)} + H_2O$$

The synthesis in the Na_2O-Nd_2O_3-SiO_2-H_2O system is much more sensitive to the basic alkali content than in the K_2O-Nd_2O_3-SiO_2-H_2O system, with the apatite-type phase forming at much lower hydroxide and carbonate concentrations. High SiO_2 solubility in the presence of Na_2O is also responsible for the much greater quantity of gelatinous material that resulted from these experiments.

It is interesting to note that the crystallization of various phases and the stoichiometries of the phases depend mainly on the type and

concentration of the alkali metals. The apatite-type phases have been obtained at the highest KOH molarity. The two quantities, Si:O and mol % SiO_2, are necessarily related in a system where the non-silicon cations are mono- and trivalent. The former has in addition, a very direct relationship to the linkage of tetrahedra in the silicate framework. A low Si:O ratio implies that if any or some oxygen atoms are bonded to more than one silicon, the connectivity of the framework is low. The change observed in the nature of the crystallized phase upon an increase in the potassium content, corresponding to a lowering of the connectivity of the structure. The phase encountered at the lowest KOH concentration is an ideal Si_2O_5 layered silicate, ($K_3NdSi_6O_{15}$, P_{bam} form) with all SiO_4 tetrahedra sharing apices with three others. The phase encountered at the highest KOH molarity is an orthosilicate, ($KNd_9(SiO_4)_6O_2$) structurally composed of isolated SiO_4 tetrahedra. Similarly, $K_3NdSi_7O_{17}$, produced at lower KHF_2 concentrations has an interconnected, 3-*d* silica framework, whereas $K_2NdSi_4O_{10}OH$, obtained at higher concentrations, is based on infinite (Si_2O_5) tubular units.

The concept of classifying compounds as "chain breakers" (for example, K_2O) and "chain formers" (for example, P_2O_5) has been well developed in silicate glass technology, yet rarely used in the context of silicate crystal growth. As the hydrothermal growth involves a solution in addition to the growing silicate phase, it is by no means obvious that such an approach should be applicable in this context. Ikornikova (1971)[50] has studied aqueous solutions of SiO_2 and Na_2O, and has observed that at low alkali to silica ratios in the solute, but high overall solute concentrations, silica is dissolved as long chain polymers or colloidal particles (5–20 Å in radius) that have an overall composition ranging between $Si_2O^{2-}_5$ and SiO_3^{2-}. As the alkali to silica ratio in the liquid is increased, such agglomerates break apart, coordination decreases, and the predominant species become more negatively charged pyrosilicate ($Si_2O^{6-}_7$) and orthosilicate (SiO_4^{4-}) groups. In this particular system, we expect reactions such as

Eq. (4) $$2Si_6O_{15}^{-6}(aq) + 4OH^- \leftrightarrow Si_{12}O_{32}^{-16}(aq) + 2H_2O$$

Eq. (5) $$Si_3O_8^{-4}(aq) + 8OH^- \leftrightarrow 3SiO_4^{-4}(aq) + 4H_2O$$

to take place. The dissolved species on the left-hand side of Eq. (4) has Si:O ratio 0.4 and comprises the basic unit of $K_3NdSi_6O_{15}$, while that on the right-hand side has a ratio of 0.375 and it corresponds to the silicate

layer in $K_8Nd_3Si_{12}O_{32}OH$. Similarly, Eq. (5) represents the equilibrium between the aqueous counterparts of $K_8Nd_3Si_{12}O_{23}OH$ and $KNd_9(SiO_4)_6O_2$ (Si:O = 0.25 on the right).

As the OH^- concentration is raised, the right hand sides of Eqs. (4) and (5) are increasingly favored, Si-O-Si bonding decreases, the fraction of oxygen atoms bonded to only one silicon increases, and the average size of the dissolved silica complexes decreases. During hydrothermal growth, it is expected that these complexes act as precursors to the crystalline precipitate such that, as the aqueous concentration of a particular species is increased, the likelihood of a structure into which it is easily incorporated will precipitate, correspondingly increases. It is in this manner "an increase in the alkali content in the liquid phase causes a decrease in the connectivity of the silica framework in the resultant crystalline phase."

The anionic species present in the solvent plays a decisive role in determining the solution molarity required for the synthesis of the various compounds. Much lower concentrations are required to obtain $K_8Nd_3Si_{12}O_{32}OH$ from $K_2B_4O_7$. For example, concentration < 1M $K_2B_4O_7$ provides twice as many potassium ions as 1M KOH. The absence of $KNd_9(SiO_4)_6O_2$ from K_2CO_3 experiments, even at very high concentrations, suggests that, in accordance with reactions shown above, pH is also an important factor. The higher pH values cause not only greater SiO_2 dissolution, but also the break up of dissolved silica complexes into smaller species. The reasons that the fluorine compounds gave rise to entirely different phases remain unclear. The low concentrations at which these fairly pH neutral compounds caused the formation of $K_3NdSi_7O_{17}$ rather than $K_3NdSi_6O_{15}$ (derived when pure water served as the solvent) indicates that some variable other than pH, possibly the high reactivity of F^- with Si^{4+}, is playing a significant role.

Higher temperatures slightly favored the formation of low Si:O phases. This was true in spite of the fact that at high temperatures (at constant molarity) the percent fill of liquid was lowered to compensate for the decrease in the density of water, leading to a systematic reduction in the total alkali content. If such a change in experimental conditions was to occur alone, that should result in the synthesis of the high Si:O phases. If we accept that changes in the structure of silica in solution are responsible for changes in the structure of the precipitate, the result implies that high temperatures are particularly effective in shifting the above two reactions to the right, thereby causing dissolved silica complexes to break apart into smaller species.

DropBooks

Higher pressures also favor the low Si:O phases. In this case, however, experiments performed at 1400 bar pressure were given higher percent than those performed at 825 bar (constant molarity), to reflect the increase in solvent density at the higher pressure. It is, therefore, not clear whether the change in crystallized phase resulted from an increase in the pressure or increase in the total alkali content.

Lastly, although only a limited number of experiments have been performed with variation in the crystallization time, a tendency towards the formation of the low Si:O ratio apatite-type phase with increasing time has been observed in the 5M KOH experiments. The reason may be that the glass, with a relatively high solubility, quickly supersaturates in the solution with respect to the crystalline phases. As the initial silica content in the solution is high, dissolved species are large, and the higher silica content phase—$K_8Nd_3Si_{12}O_{32}OH$—precipitates preferentially over $KNd_9(SiO_4)_6O_2$ in the solution. If more time is given, $K_8Nd_3Si_{12}O_{32}OH$ slowly redissolves, but the total silica content in the solution remains low. Therefore, dissolved species are reduced in size, and the apatite-type phase eventually precipitates.

The conditions (average temperature, estimated pressure, solvent type and molarity, solid to liquid ratio, total alkali content, and time) that gave rise to $K_3NdSi_3O_8(OH)_2$ growth using the temperature gradient technique broadly correspond to those that caused $K_8Nd_3Si_{12}O_{32}OH$ and $KNd_9(SiO_4)_6O_2$ co-crystallization isothermally. As $K_3NdSi_3O_8(OH)_2$ has a silicon to (bonding) oxygen ratio of 0.3, a structure based on trisilicate chains[51] and a composition that closely resembles the combined stoichiometry of the nutrient and the mineralizer is formed.

The reasons for the appearance of the different phases under different conditions have been explained in terms of their differing structures, rather than differing stoichiometries, and in terms of silicate solution chemistry. It is generally accepted that during hydrothermal growth, the nature of the dissolved species determines the nature of the crystalline product. We have observed a decrease in the connectivity of the silicate framework in the product phase, as measured by the Si:O ratio (or, alternatively, SiO_2 mol%), with increasing solution molarity (alkali content), temperature and, to some extent, pressure. Therefore, it is concluded that higher solubilities under these conditions coincide with a decrease in the average size of the dissolved complexes, and are responsible for the change in the structural nature of the crystalline product. Longer times also appear to favor the crystallization of low Si:O ratio phases. These

observations provide guidelines by which new phases with some desired structural feature might be synthesized. Stoichiometric parameter other than the Si:O ratio and the SiO_2 mol% are not easily correlated to the experimental variables. The mole percent alkali in the product phase, for example, does not monotonically increase as the molarity of the solution is increased. Lastly, it is observed that when phases of low silica content form, overall mass balance is maintained via the presence of a high silica content gel. It is most probable that this gel precipitates out of solution as the autoclave is quenched.

Such studies greatly help in understanding the hydrothermal chemistry of silicates and their crystallization mechanism. Hitherto, only zeolites have such a vast amount of data on their hydrothermal chemistry. Another approach to the hydrothermal chemistry of silicates has been treated in the forthcoming sections under degree of silification.

7.5 CRYSTAL CHEMICAL SIGNIFICANCE OF PHASE FORMATION

ProBooks

The study of the crystallization of various rare earth silicates and their correlation with the crystal chemistry has not been carried out effectively. In laboratory conditions, it is interesting to understand the conditions of synthesis and the structure with the change in the ionic radii of rare earths. Such studies have revealed the mechanism of formation of some of the fine crystal structures.

Silicates of rare earth elements owing to their ionic radii belong to a large group of silicates with larger cations. During the 1950s, the academican N. V. Belov framed the structural principles for these silicates. Further, the structure formation of silicon-oxygen radicals shall be treated essentially, as a result of cationic motif. Their differentiation as chains, ribbons, cages, and rings is relatively more popular, but a significant variation depending upon their geometric relationship of cationic polyhedra and Si-O radicals can also be observed.[52]

Natural rare earth silicates are considered as very complex ones containing a wide range of cations like Ca, Fe, Be, Al, Ti, Sr, Mn, Ba, and Na. Their crystal chemical elucidation is highly related to the naturally occurring rare earth elements. Thus, we can have two broad groups: alkali rare earth silicates and rare earth silicates without alkalis covering both natural and synthetic rare earth silicates. Figure 7.7 shows the tetrahedral

arrangement in silicates with $[Si_6O_{14}]$ radical. The typical compounds are $Na_4[Si_6O_{14}]$ and $NaNd[Si_6O_{14}]$.[50]

Today, over fifteen structure types of mixed rare earth silicates without alkalis, and twenty-one structure types of rare earth silicates with alkali cations have been reported. Their crystal chemical characteristics are presented in Tables 7.6 to 7.9.[35][53]

Table 7.6. Crystal Chemical Characteristics of Rare Earth Silicates[35]

Crystal chemical group	R-element	Symmetry
$Na^{X}R^{IX}[SiO_4]$	La-Nd	Orthorhombic *(i)*
$Na^{VII}R^{VIII}[SiO_4]$	Pr-Ho	Tetragonal
$Na^{V1}R^{VI}[SiO_4]$	Ho-Lu	Orthorhombic *(ii)*
$Na*_{13}R_3{}^{VI}[Si_{12}O_{36}]$	Ho-Lu,	Y Monoclinic
$Na*R^{VI}[Si_2O_7]$	Er-Lu,	Y Orthorhombic
$Na*R^{VI}[Si_6O_{14}]$	La-Eu	Orthorhombic
$Na_2*R^{VIII}[SiO_4](OH)$	La, Pr	Orthorhombic
$Na*R^{VII}[Si_6O_{13}](OH)_2$	La-Lu	Orthorhombic

* Co-ordination number of Na in the work is not given.

Table 7.7. Crystal Chemical Characteristics of Silicates[35][53]

Compound	O/Si	SiO_2/ R_2O_3	Si/ Na+R	Structural motif Si-O	R-O	*Co-No. R	*Co-No. of Na
$R_{4.67}[SiO_4]_3O$	4	0.78	0.64	$[SiO_4]$	3d- bond	9.7	—
$NaR[SiO_4]$	4	2	0.5	$[SiO_4]$	$[R_2O_8]_{\infty\infty}$	9	10
$NaR[SiO_4]$	4	2	0.5	$[SiO_4]$	4 –mem-bered ring	8	7
$NaR[SiO_4]$	4	2	0.5	$[SiO_4]$	$[R_2O_8]_{\infty\infty}$	6	6
$Na_2R[SiO_4](OH)$	4	2	0.33	$[SiO_4]$	3d- bond	8	5; 7
$Na_3R[Si_2O_7]$	3.5	4	0.5	$[Si_2O_7]$	$[RO_6]_0$	6	4; 5
$Na_{15}R_3[Si_{12}O_{36}]$	3	8	0.66	$[Si_{12}O_{36}]$	$[RO_6]_0$	6	4; 6
$Na_3R[Si_6O_{15}]2H_2O$	2.5	12	1.5	$[Si_6O_{15}]$		7	—
$NaR[Si_6O_{14}]$	2.33	12	3	$[Si_6O_{14}]$	$[R_3O_{12}]_\infty$	8	4; 8

* Co-No. = Coordination number.

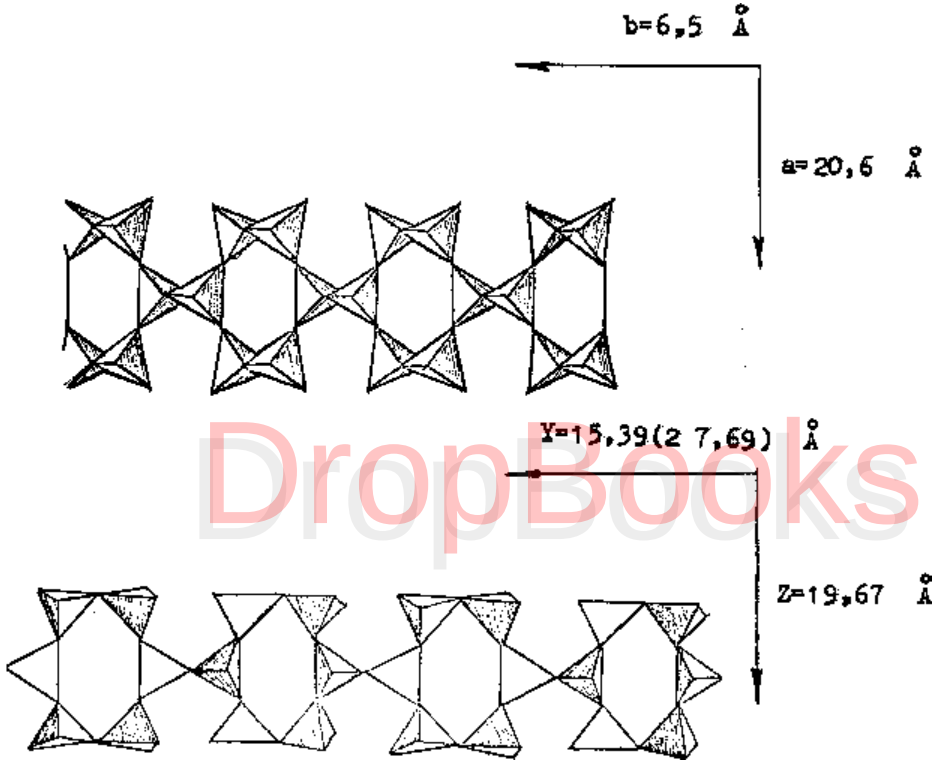

DropBooks

Figure 7.7. Tetrahedral arrangement in silicates with $[Si_6O_{14}]$ radical.[7]

Table 7.8. Structure Types of Rare Earth Silicates[35][53]

Compound	Representative	Cell parameter (Å)	Rare Earth, Co. No., Average bond distance Å	Tetrahedral radical form	Rare earth polyhedra
$R_2[SiO_4]O$ R=La-Tb	$Gd_2[SiO_4]O$	$P2_1/c$ z = 4 a = 9.12 b = 7.06 c = 6.73 β = 107.58°	Gd_1 7 2.39 Gd_2 9 2.49	orthotetra-hedra	framework
$R_2[SiO_4]O$ R=Tb-Lu,Y	$Yb_2[SiO_4]O$	B2/ b z = 8 a = 14.28 b = 10.28 c = 6.653 γ = 122.2°	Yb_1 7 2.33 Yb_2 6 2.33	orthotetra-hedra	framework
$R_{4.67}[SiO_4]_3O$ R = La-Lu	$Gd_{4.67}[SiO_4]_3O$	$P6_3/m$ z = 2 a = 9.431 b = 9.873	Gd_1 7 2.41 Gd_2 9 2.53	orthotetra-hedra	framework
	α - $Eu^{2+}{}_2[SiO_4]$	$P2_1/c$ z = 4 a = 5.661 b = 7.101 c = 11.518 β = 122.01	Eu_1 8 2.62 Eu_2 10 2.86	orthotetra-hedra	framework
	β - $Eu^{2+}{}_2[SiO_4]$	Pnma z = 4 a = 7.137 b = 5.665 c = 9.767	Eu_1 10 2.86 Eu_2 7 2.57	orthotetra-hedra	framework
$R_2Si_2O_7$ R = La-Eu	$Sm_2Si_2O_7$	$P4_1$ z = 8 a = 6.695 b =24.40	Sm_1 7 2.42 Sm_2 9 2.56	diortho-	framework
$R_2Si_2O_7$ R = Ho-Lu,Sc	$Yb_2Si_2O_7$	C2/m z = 2 a = 6.802 b = 8.875 c = 4.703 β = 102.12°	Yb 6 2.24	diortho-	ribbon
$R_2Si_2O_7$ R = Ho-Er	$Er_2Si_2O_7$	$P2_1/$ b z = 2 a = 4.683 b = 5.556 c = 10.79 γ = 96°	Er 6 2.26	diortho-	layer

(Cont'd.)

Table 7.8. *(Cont'd.)*

Compound	Representative	Cell parameter (Å)	Rare Earth, Co. No., Average bond distance Å			Tetrahedral radical form	Rare earth polyhedra
$R_2Si_2O_7$ R = Eu-Ho	$Gd_2Si_2O_7$	Pna21 z = 4 a = 13.87 b = 5.073 c = 8.33	Gd	7	2.40	diortho-	framework
$R_2Si_2O_7$ R = Sm-Eu	$Eu_2Si_2O_7$	P_1-P_I z = 4 a = 8.517 b =12.848 c = 5.385 α =91.65° β =92.24° γ =90.44°				diortho-	
$R_2Si_2O_7$ R = La-Sm	$Nd_2Si_2O_7$	$P2_12_12_1$ z = 4 a = 5.394 b =12.95 c = 8.72	Nd	8	2.53	diortho-	framework
$R_2[Si_2O_7]$ R = Tm-Lu	$Yb_2[Si_2O_7]$	$P4_12_12$ z = 4 a = 6.574 c =11.98				diortho-	framework
	$(Y,Th)_2[Si_2O_7]$	$P2_1$ /m z = 2 a = 7.50 b = 8.06 c = 5.02 β = 112°	Y	6	2.36	diortho-	layer
	$Y_3[Si_3O_{10}](OH)$	$P2_1$ /n z = 6 a =10.343 b = 7.284 c =11.093 γ =96.92°	$Y_{1.2}$ Y_3	7 8	2.32 2.43	triotho-	layer
$R_4[Si_3O_{10}]$ $[SiO_4]$ $[SiO_4]$ R = Eu-Er	$Ho_4[Si_3O_{10}]$	P_1 z = 4 a = 6.664 b = 6.674 c = 12.110 α =94.07° β =89.97° γ =91.66°	Ho	8	2.44	triortho - + ortho-tetrahedra	ribbon

DropBooks

Table 7.9. Structure Types of Alkali Rare Earth Silicates[35][53]

Compound	Representative	Cell parameter (Å)	Rare Earth, Co. No., Average bond distance Å			Tetrahedral radical form	Rare earth polyhedra
$NaR[SiO_4]$ R = Er-Lu,Y	$NaY[SiO_4]$	$Pbn2_1$ z = 4 a = 5.09 b =10.96 c = 6.35	Y	6	2.26	orthotetra-hedra	discrete polyhedra
$Na\ R[SiO_4]$ R = Nd-Ho	$NaSm[SiO_4]$	14/m z = 8 a =11.89 c = 5.45	Sm	8	2.51	orthotetra-hedra	framework
$NaR[SiO_4]$ R = Ce-Nd	$NaNd[SiO_4]$	$Pna2_1$ z = 12 a =20.00 b = 9.28 c = 5.45	Nd	8	2.45	orthotetra-hedra	column
	$KNd_9[SiO_4]_6O_2$	$P6_3$ z = 1 a = 9.576 c = 7.009	Nd (K,Nd) (K,Nd)	7 9 9	2.48 2.48 2.75	orthotetra-hedra	framework
	$LiY[SiO_4]$	$P2_1/b$ z = 4 a = 5.368 b =10.806 c = 6.195 γ =113.40°	Y	7	2.01	orthotetra-hedra	layers from 6-membered ring, Seven sided
$Na_2R[SiO_4]OH$ R = La-Pr	$Na_2La[SiO_4]OH$	Pnma z = 4 a = 9.72 b = 7.57 c = 6.81	La	8	2.59	orthotetra-hedra	framework
	$4\{NaYSiO_4\}NaF$	1_4 z = 8 a =11.579 c = 5.396				orthotetra-hedra	framework
$Na_3R[Si_2O_7]$ R = Er-Lu,Y,Sc	$Na_3Sc[Si_2O_7]$	Pbnm z = 4 a = 5.354 b = 9.347 c =13.089	Sc	6	2.10	diortho-hedra	discrete poly
	$Na_6YSc[Si_2O_7]_2$	$P6_3$ z = 4 a =10.726 b =13.491	Y	6 6	2.62 2.71	diortho-hedra	discrete poly

(Cont'd.)

Table 7.9. *(Cont'd.)*

Compound	Representative	Cell parameter (Å)	Rare Earth, Co. No., Average bond distance Å			Tetrahedral radical form	Rare earth polyhedra
	$K_3Eu[Si_2O_7]$	P6c2 z = 6 a = 9.956 c =14.455	Eu	6	2.31	diortho-	discrete polyhedra
	$K_3Y[Si_3O_8(OH)_2]$	Pmnb z = 4 a = 13.536 b = 13.17 c = 5.867	Y	6	2.23	Triothor-	discrete polyhedra
	$Na_4Sc_2[Si_4O_{13}]$	$Pna2_1$ z = 4 a =14.442 b = 5.288 c =14.219	Sc	6	2.11	tetra-	polyhedra
	$K_4Sc_2[Si_4O_{12}](OH)_2$	Pbam z = 8 a =12.725 b =12.741 c = 8.441	Sc	6	2.09 -2.16	4-membered ring	chain
$Na_5RSi_4O_{12}$ R=Sm-Lu,Y,Sc	$Na_5LuSi_4O_{12}$	R32 z = 16 a =21.926[4] c =12.556[2]	Lu	6	2.20	12-membered ring	discrete polyhedra
	$LiScSi_2O_6$	C2/c z = 4 a = 9.8033 b = 8.9581 c = 5.3512 β =110.281°	Sc	6	2.107	Chains with Period of 2 tetrahedra	layer
	$Na_{12}Y_4Si_{12}O_{36}$	$P2_12_12_1$ z = 16 a =15.033 b =15.142 c =15.213	Y	6	2.20 -2.36	Chains with Period of 24 tetrahedra	discrete polyhedra
$NaRSi_6O_{14}$ R=La-Lu	$NaPrSi_6O_{14}$	Ibam z = 8 a = 7.682 b =15.445 c =19.724	Pr	6	2.41	Tripple layered column	Column
	$NaNdSi_6O_{13}(OH)_2 nH_2O$	Cmm2 z = 4 a =30.87 b = 7.387 c = 7.120	Nd	7	2.44	layers with 8-, 6-, 5-, & 4- membered rings	discrete polyhedra

(Cont'd.)

DropBooks

Table 7.9. *(Cont'd.)*

Compound	Representative	Cell parameter (Å)	Rare Earth, Co. No., Average bond distance Å			Tetrahedral radical form	Rare earth polyhedra
$K_3RSi_6O_{15}$ R =La-Lu	$K_3NdSi_6O_{15}$	Pbam z = 4 a =16.011 b =14.984 c = 7.276	Nd	6	2.38	layers with 8-, 6-, 5-, & 4- membered rings	discrete polyhedra
$K_8R_3[Si_6O_{16}]_2$ (OH) R =La-Lu	$K_8Yb_3[Si_6O_{16}]_2$ (OH)	P1 z = 1 a = 6.808 b = 11.434 c = 11.449 α = 88.52 β = 90.91 γ =100.10	Yb	6	2.26	layers with 12-, 8-, & 6-membered rings	discrete & bicapped polyhedra
	$K_2Ce[Si_6O_{15}]$	12/ b z =4 a =13.058 b =11.854 c = 8.698 γ =90.15	Ce	8	2.23	framework	discrete

* Co-No. = coordination number

In these compounds, the following anionic groups have been identified: ortho-, diortho-, mixed ortho- and triortho-groups, tetraortho-groups, discrete 4-membered rings, discrete twelve-membered rings, spiral chains, layers from 6-, 8-, and 12-membered rings, triple column and Si-O framework. Various types of anionic radicals, found in rare earth silicates are given in Table 7.10.[53]

Table 7.10. Anionic Structural Motif in Rare Earth and Alkali Rare Earth Silicates[53]

Radical form	Representative Structure type	Rare eath Polyhedra	Co. No. of Rare Earth Cations
Orthotetrahedra $[SiO_4]$	$Gd_2[SiO_4]O$	framework	7, 9
	$Yb_2[SiO_4]O$	framework	6, 7
	$Ge_{4.66}[SiO_4]_3O$	framework	7, 9
	$Eu_2[SiO_4]$	framework	8, 10
	$NaNd[SiO_4]$	column	9
	$NaSm[SiO_4]$	4-membered ring	6
	$NaY[SiO_4]$	discrete polyhedra	6
	$4\{NaYSiO_4\}NaF$	4-membered ring	6
	$Na_2La[SiO_4](OH)$	framework	8
	$KNd_9[SiO_4]_6O_2$	framework	7, 9
diortho- $[Si_2O_7]$	$La_2[Si_2O_7]$	framework	7, 8, 9
	$Yb_2[Si_2O_7]$	6-membered ring	6
	$Er_2[Si_2O_7]$	layer	6
	$Gd_2[Si_2O_7]$	framework	7
	$Eu_2[Si_2O_7]$	framework	8
	$Nd_2[Si_2O_7]$	framework	8
	$Yb_2[Si_2O_7]$	framework	7
	$(Y,Th)_2[Si_2O_7]$	layer	6
	$Na_3Sc[Si_2O_7]$	discrete polyhedra	6
	$Na_6YSc[Si_2O_7]_2$	discrete polyhedra	6
	$Na_3Y[Si_2O_7]$	discrete polyhedra	6
	$K_3Eu[Si_2O_7]$	discrete polyhedra	6
triortho $[Si_3O_{10}]$	$Y_3[Si_3O_{10}](OH)$	layer	7, 8
	$K_3Y[Si_3O_8](OH)_2$	discrete polyhedra	6
tetraortho- $[Si_4O_{13}]$	$Na_4Sc_2[Si_4O_{13}]$	bicapped polyhedra	6
Mixed ortho- and triortho- $[SiO_4]$ & $[Si_3O_{10}]$	$Ho_4[Si_3O_{10}][SiO_4]$	ribbon	8
Ring: $[Si_4O_{12}]$ Four	$K_4Sc_2[Si_4O_{12}](OH)_2$	column	6
Twelve $[Si_{12}O_{36}]$	$Na_5Lu[Si_4O_{12}]$	discrete polyhedra	

(Cont'd.)

DropoBooks

Table 7.10. *(Cont'd.)*

Radical form	Representative Structure type	Rare eath Polyhedra	Co. No. of Rare Earth Cations
Spiral Chain $[Si_{24}O_{72}]$	$Na_3Y\ [Si_3O_9]$	discrete polyhedra	6
Layers: from 6,8, 12- rings $[Si_3O_8]$	$K_8Yb_3[Si_6O_{16}]_2$ (OH)	discrete and twinned polyhedra	6
- from 4,5,6,8-rings	$NaNd[Si_6O_{13}]$ $(OH)_2$; nH_2O	discrete polyhedra	7
- from 4,6,8-rings $[Si_2O_5]$	$Na_2Ce[Si_6O_{14}]$ (OH).n H_2O	discrete polyhedra	7
	$K_3Nd[Si_6O_{15}]$	discrete polyhedra	6
Three Storeyed Column $[Si_3O_7]$	$NaNd[Si_6O_{14}]$	column	6
framework $[Si_2O_5]$	$K_2Ce[Si_6O_{15}]$	discrete polyhedra	6

* Co-No. = coordination number

Orthotetrahedra (Orthosilicates)–have a free oxygen not shared with neighboring [Si-O] tetrahedra, but are bonded only with the rare earth cations. $R_2[SiO_4]O$ has two structure types: $Eu^{+2}{}_2[SiO_4]$ and $Gd_2[SiO_4]O$: $NaR[SiO_4]$ has three structure types, and similarly in the apatite type $R_{4.66}[SiO_4]_3O$ and $KNd_9[SiO_4]_6O$.

Diortho-group (Diorthosilicates)–contains compounds of $R_2[Si_2O_7]$ (seven structure types)—$Y_2[Si_2O_7]$, $Sc_2[Si_2O_7]$, $Na_3R[Si_2O_7]$, $K_3R[Si_2O_7]$ and $Na_6YSc[Si_2O_7]$.

Triorthosilicates are always characteristic of $Y_3[Si_3O_{10}]$ and $K_3Y[Si_3O_8](OH)_2$ (Fig. 7.8).[54][55] Likely triortho groups in the form is sufficiently rare Si-O radical and twice observed in Gd-silicates: $Na_4Gd_2[Si_3O_{10}]$[56] and $Na_2Gd_3[Si_3O_{10}]$.[57]

Tetraortho-groups $[Si_4O_{13}]$ as seen in $Na_4Sc_2[Si_4O_{13}]$ is a linear radical which extends to a series of island radicals SiO_4-Si_2O_7-Si_3O_{10}-Si_4O_{13}.

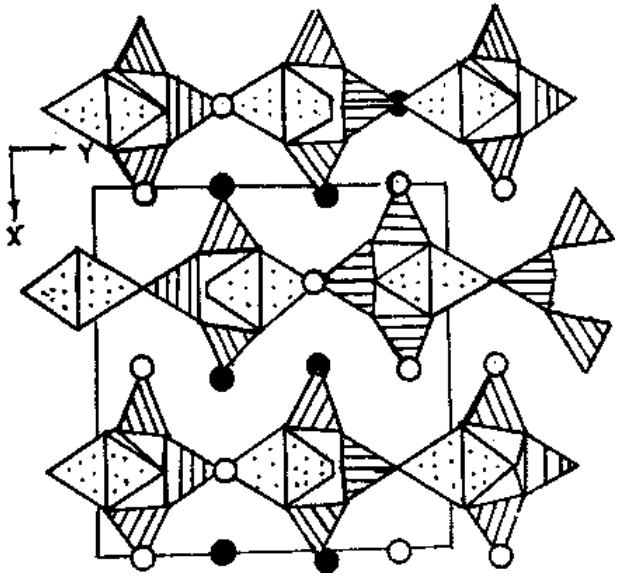

Figure 7.8. Triorthosilicates, $Y_3[Si_3O_{10}]$ and $K_3Y[Si_3O_8](OH)_2$.[54]

DropBooks

Mixed ortho- and triorthogroups $[SiO_4]$ and $[Si_3O_{10}]$ exist simultaneously in $HO_4[Si_3O_{10}]$ $[SiO_4]$. The triorthogroups have similar consideration of diverse tetrahedral anions as in earlier observed $Ca_6[SiO_4]$ $[Si_3O_{10}]$.[58]

Discrete 4-membered ring $[Si_4O_{12}]$ with 2/m symmetry exists in $K_4Sc(OH)_2$ $[Si_4O_{12}]$ structure. Likely four-membered rings with different symmetry were found in several compounds like: $Ba_2FeR_2Ti_2O_2$ $[Si_4O_{12}]_2OH{\cdot}H_2O$,[55] $Na_3CaPSiO_7$,[59] $Ca_2R_2[Si_4O_{12}]$,[60] $(Ba,K,Na)_8$ $(Ti,Nb)_9$ $(O,OH)_{10}$ $[Si_4O_{12}]_4{\cdot}nH_2O$,[61] $Ba_2(Fe,Ti,Mg)_2$ $(H_2O)[Si_4O_{12}]$,[62] $KHSiO_3$,[63] $Ba_{12}Mn_6$ $(OH,O)_2$ $[Si_4O_{12}]Cl_9$ $(OH,H_2O)_7$,[64] $(Na,K)_{2-x}$ (Nb,Ti) (O,OH) $[Si_2O_6]{\cdot}2H_2O$,[65] Ba_4Ti_4 $(Ti,Nb,Fe)_4ClO_6$ $[Si_4O_{12}]$.[66]

Discrete 12-membered ring $[Si_{12}O_{36}]$ This was observed in the structure of $Na_5Ce[Si_4O_{12}]$ (Fig. 7.9).[67] The other ring type $[Si_{12}O_{36}]$ is found in $Ba_5FeTi(OH)_4$ $[Si_6O_{18}]$.[68] The rings in either structure differ greatly from one another, for example, the latter case has higher symmetry, and the earlier case has lower symmetry.

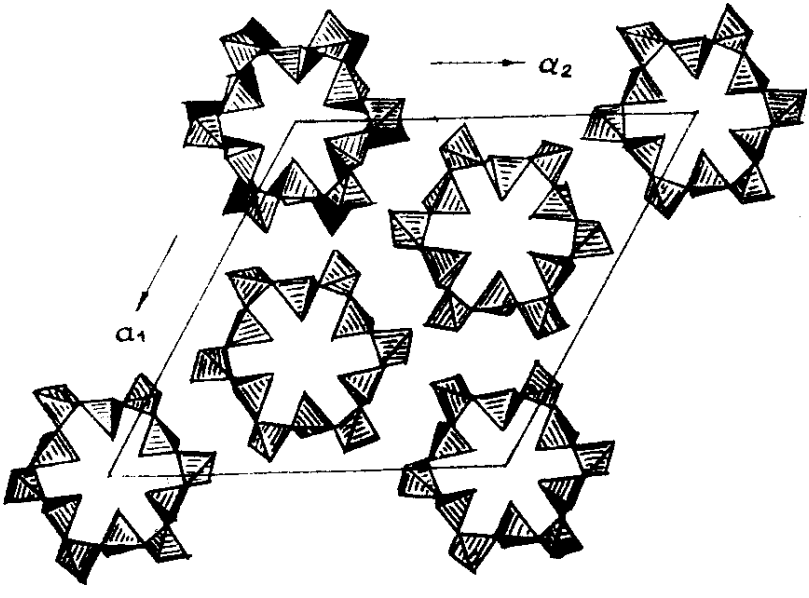

Figure 7.9. Structure of $Na_5Ce[Si_4O_{12}]$.[67]

Spiral chains $[Si_{24}O_{72}]$ are found in the structure of $Na_3Y[Si_3O_9]$. This new type of infinite spiral formation metachain silicate $[Si_{12}O_{36}]$ agrees with the formula $12[SiO_4]$-tetrahedra. Such a matachain silicate is shown in (Fig. 7.10).[69]

Layers from 6-, 8- and 12-rings $[Si_3O_8]$ have been reported in the structure of $K_8Yb_3[Si_6O_{15}]_2(OH)$ (Fig. 7.11).[70]

Layers from 4-, 5-, 6-, and 8-membered rings, $[Si_2O_5]$ was found in the structure of $NaNd[Si_6O_{13}](OH)_2 \cdot nH_2O$ (Fig. 7.12).[71] This type of layer form as a result of the condensation of the ribbon from the reflection of the 8-membered rings. Layered radical from $[SiO_4]$-tetrahedra with such an arrangement of the rings is unique among silicate structures.

Layers from 4-, 6-, and 8-membered rings, $[Si_2O_5]$ was observed in the structure of $K_3Nd[Si_6O_{15}]$ (Fig. 7.13).[72] Such an arrangement has been noticed in several other rare earth and non-rare earth silicates. Usually the layers are extended and structures are highly distorted.

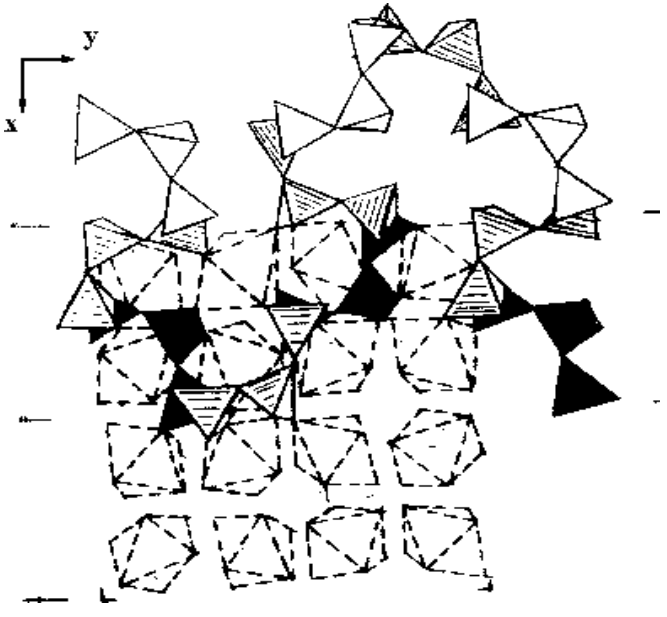

Figure 7.10. Metachain silicate.[69]

DropBooks

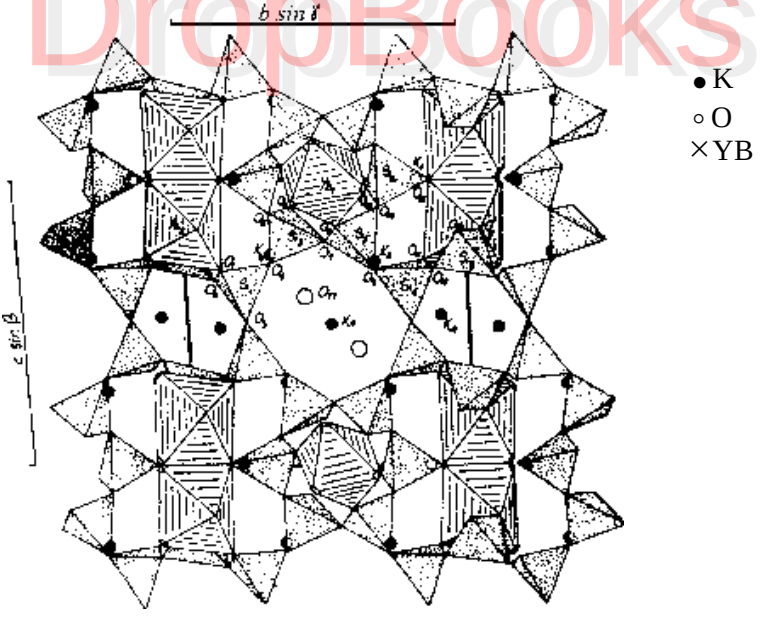

Figure 7.11. Layers from 6-, 8-, and 12- rings of $[Si_3O_8]$ in the structure of $K_8Yb_3[Si_6O_{15}]_2(OH)$.[70]

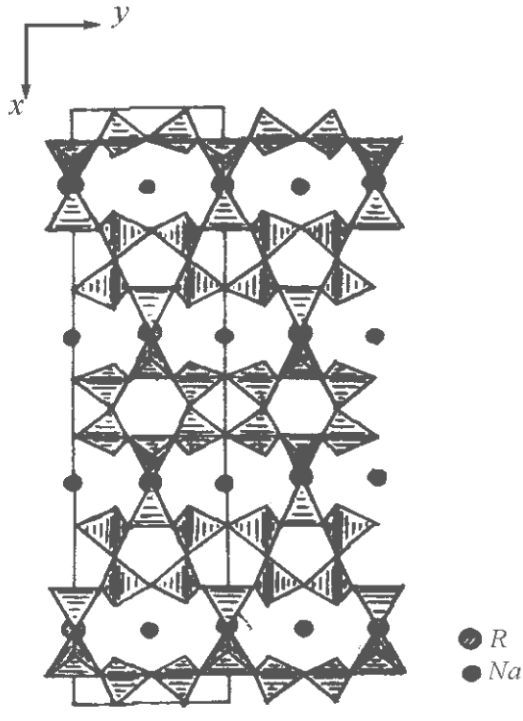

Figure 7.12. Layers from 4-, 5-, 6-, and 8-membered rings, $[Si_2O_5]$ in the structure of $NaNd[Si_6O_{13}](OH)_2.nH_2O$.[71]

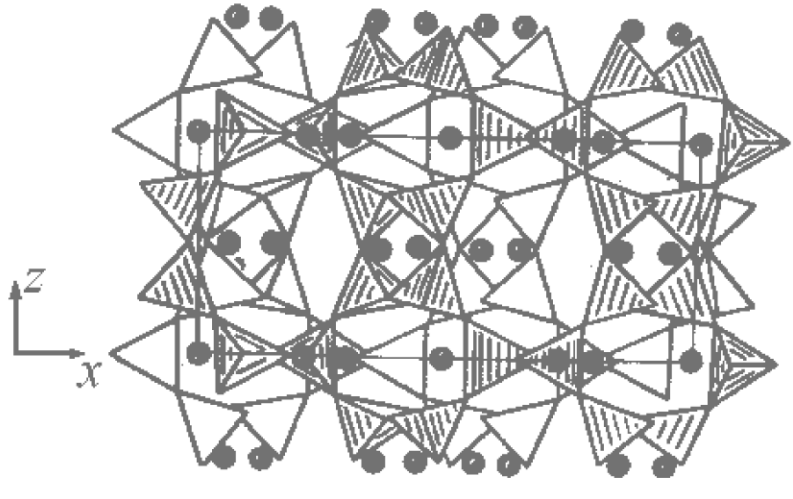

Figure 7.13. Layers from 4-, 6-, and 8-membered rings, $[Si_2O_5]$ in the structure of $K_3Nd[Si_6O_{15}]$.[72]

Triple columnar [Si_3O_7] was demonstrated in the structure of NaR[Si_6O_{14}] (Fig. 7.14).[73] The structure is made up of 3-*d* network from 12-membered complexes.

Framework [Si_2O_5] was found in the structure of K_2Ce [Si_6O_{15}] (Fig. 7.15).[74]

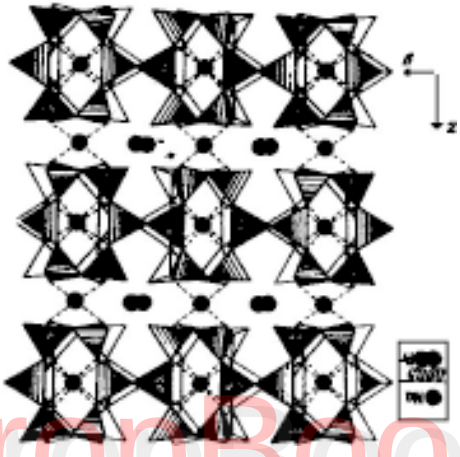

DropBooks

Figure 7.14. Triple columnar [Si_3O_7] in the structure of NaR[Si_6O_{14}].[73]

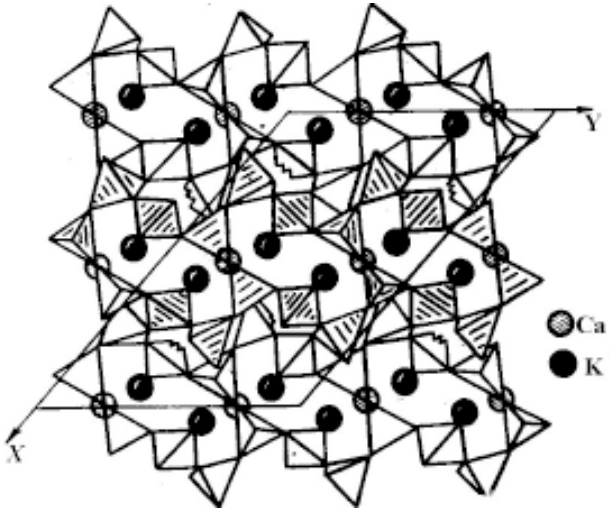

Figure 7.15. Framework [Si_2O_5] in the structure of K_2Ce [Si_6O_{15}].[74]

Thus, a wide variety of Si-O anionic motif forming unique layers, ribbons, chains, rings, and framework is characteristic of only rare earth silicates. Such complex and highly fine structures have been observed in synthetic rare earth silicates.

7.5.1 Phase Formation in Surplus R_2O_3

During the synthesis of rare earth silicates with surplus rare earth elements, the structures of the phases forming and their stability mainly depends upon the characteristics of the rare earth motif, which is closely related to the ionic radii of the rare earth elements. The ionic radii of rare earth elements vary from 1.061 Å (La) to 0.848 Å (Lu). The coordination number also varies from 6 to 8. Similarly, the variation in the ionic radii of the rare earth elements in the structure is compensated by the distortion of the 3-*d* rare earth motif, so that the structure type is retained for the entire rare earth series.

7.5.2 Silicates

In Fig. 7.6, the fields of crystallization of various phases in the system Na_2O-R_2O_3-SiO_2-H_2O are shown. In solutions with lower concentrations of NaOH, the representative phase is R_4 2/3 $[SiO_4]_3O$. Moreover, their stability (Fig. 7.16) extends towards the lower rare earth elements. The possible reasons for this is the search of their structural elucidation.

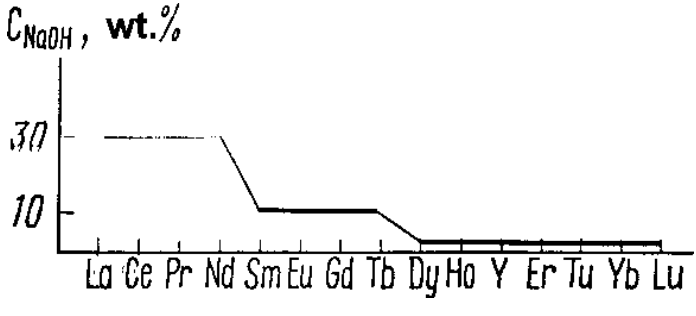

Figure 7.16. Rare earth elements.[35]

In Ref. 75 it has been shown that with a decrease in the values of rare earth cations, the stability of the $R_{18}Si_7O_{41}$ decreases especially for smaller elements (Er-Lu). If other elements like Na, Mn, Pb, Ca and so on go into the structure, the stability of the structures under hydrothermal conditions again rises. However, the stability of rare earth britolite determined mainly from the position of these other elements is in the structures.

Transition from britolite to mixed Na R-silicates takes place during the complete destruction of cationic motif and with a change in the coordination number of rare earth elements.

In highly concentrated aqueous solutions NaOH (< 80%) (Table 7.11) mixed silicates like $Na_2O{\cdot}R_2O_3{\cdot}2SiO_2$ = Na. $R[SiO_4]$ are formed covering a significant part of the rare earth series from Pr to Ho, including Y. The latter one is usually related to the heavier (Eu-Lu) rare earths with the coordination number 7, since the ionic radius of Y is slightly higher (0.99) and it lies between Nd and Sm. This emphasizes sufficiently simple means of synthesis of tetragonal modification of $NaY[SiO_4]$. The field of stability of tetragonal rare earth silicates of type Na $R[SiO_4]$ lies between Ho and Er. This is the traditional boundary for the morphotrophic series of rare earth elements. Its existence is usually based on the geometric representation of the stability of the rare earth octahedra, since the significant part of the R-O bonding is ionic (~ 75%). However, under the conditions of high potential elements with lower values of electro-negativity, as Na^+, a better model could be obtained giving the influence and an overall covalent bonding in the nature of R-O bond. It can be assumed that in the aqueous solvents, with higher concentration of Na^+, the capability of internal *f*-orbit for hybridization which is for Er-Lu, indistinctly becomes closer to zero. Therefore, the Eu-Lu group in NaOH aqueous solvent forms only silicates with octahedral coordination of the rare earth: Na $R[SiO_4]$ and $Na_3R[Si_2O_7]$.

Reduction in the influence of *f*-orbit at higher potential Na^+ can be seen as the possibility for the distortion of rare earth motif, particularly leading to the decrease in the coordination number of rare earth elements up to 6 (trigonal prism). In this case, the rare earth polyhedra form discrete groupings of rare earth prism. It is emphasized that from the point of view the size of the coordination number of rare earth equals 8, this group is more logical than the coordination number 6.

PropBooks

Table 7.11. Phase Formation in the System Na_2O-R_2O_3-SiO_2-H_2O in the Region of Surplus R_2O_3 Depending upon the NaOH Concentration [35]

	Rare Earth Elements															
CNaOH	La	Ce	Pr	Nd	Sm	Eu	Gd	TB	Dy	Ho	Er	Tu	Yb	Lu	Y	Sc
80%	A	G	C	C	C	C	C	C	C	C	F	F	F	F	C	G
80–55%	A	G	A	C	C	C	C	C	C	C	E	E	E	E	H	H
55–25%	A	A	A	A+C	C	C	C	C	C	C	D	D	D	D	D	G
25–5%	B	B	B	B	C	C	C	C	C	C	D	D	D	D	D	G
5%	B	B	B	B	B	B	B	B	B	B	B	B	B	B	B	H

A – $NaRSiO_4$ (Orthorhombic – I); C – $NaRSiO_4$ (Tetragonal);
D – $NaRSiO_4$ (Orthorombic II);

E – $Na_3Rsi_2O_7$; B – britolites $R_{4.67}(SiO_4)_3O$; F – unknown phase;
G – experiments not carried out;

H – $NaScSi_2O_6$.

The stability field of tetragonal modification of Na $R[SiO_4]$ for the lighter lanthanides ends at Pr (Table 7.11), but the La- representative crystallizes in a different structure type 'A' (orthorhombic I) and its boundary depends upon the concentration of NaOH. For lighter rare earths the characteristic feature is the significant contribution of *f*-orbit that changes the boundary corresponding to the participation of *f*-orbits in the R-O bonding. With an increase in the NaOH concentration, the coordination number for Pr and Nd decreases from 9 to 8, i.e., the reduction in the participation of *f*-orbits in the bonding. During the transition of structure type A (orthorhombic I), to type B (tetragonal), the basic nature of the rare earth motif, i.e., columns from rare earth polyhedra, is retained.

In the heavier lanthanide groups (Er-Lu), the change in the NaOH concentration does not speak on the coordination number, but the degree of association of rare earth motif changes from discrete nature in the group $Na_3R[Si_2O_7]$ up to a highly associated nature in $NaR[SiO_4]$ (orthorhombic II). For both of the groups, the characteristic feature is the octahedral surrounding for rare earth elements. Here, the end members of rare earth series are well inscribed as $[YO_6]$ and, therefore, it is easy to obtain $Na_3Y[Si_2O_4]$ (analogous to Sc-diorthosilicate).

7.5.3 Phase Formation in the Rare Earth Silicate Systems in the High Silica Region

It is well known that, in the region of surplus [Si-O], the formation of highly condensed silicates can be expected. Until now, the synthesis under such conditions was carried out in pure water and obviously, the higher the amount of [Si-O] taken, the higher its concentration and more complex silicates were obtained. However, the synthesis did not lead to the differentiation of crystalline individuals and, as a rule, resulted in the formation of coarse crystalline and fine crystalline masses. The action of silicon in the aqueous solvents of salts and alkalies remains unknown. From the works of Dimitrova, it was found that in alkaline solutions and surplus silica in the system, the heavier phases form.[35]

In order to explain the possibility of obtaining silicates in the form of monocrystals in high silica region, a series of experiments have been carried out by Dimitrova (1977)[35] and the results are shown in Fig. 7.6.

The region in which the crystallization was carried out lies in the stability field of quartz. Therefore, quartz exists in all the experiments. But this occurs only in case, when the NaOH concentration is < 15%. As the concentration of NaOH increases, quartz disappears and there appears Na silicates and similarly the heavier phases—amorphous glassy substance. Under these conditions, the formation of silicates takes place with the complexity of the anionic motif. For the lighter rare earths Na $R[Si_6O_{14}]$ forms and their structural units consist of $[Si_3O_7]_{\infty\infty}$ (O/Si = 2.33). With a decrease in the concentration of Si, another structure type having $[Si_6O_{15}]$ radical, e.g., Na R $Si_6O_{15}{\cdot}2H_2O$ (O/Si = 2.5) crystallizes. With an increase in NaOH concentration silicates of type $Na_{15}R_3[Si_{12}O_{36}]$ are obtained with Si-O radicals made up of 12-membered rings, $[Si_{12}O_{36}]$ (O/Si = 3).

In the region with high silica concentration, R_2O_3 is insufficient for the formation of complex 3-*d* cationic motif. When R_2O_3:SiO_2 = 1:4 and concentration of NaOH is 5%, Na $R[Si_6O_{14}]$ type was obtained. In this the cationic motif is represented by rare earth chains. During the increase in NaOH concentration, rare earth chain silicates cease to form with the appearance of compounds with discrete rare earth cations. In

DropBooks

$Na_{15}R_5[Si_{12}O_{36}]$ rare earth ion lies as isolated octahedra, whereas in $Na_3R[Si_6O_{15}]\cdot 2H_2O$, the rare earth ion lies as isolated seven sided polyhedra.

More recently, Haile et al. (1995)[76] carried out hydrothermal investigations in the high silica region of the Na_2O-Y_2O_3-SiO_2 system and obtained a new phase—trisodium yttrium, Ibmm, with a = 10.468, b = 15.246, c = 8.385 Å; Z = 4, and *n* atoms in the asymmetric unit. The structure is unique in the sense that silica tetrahedra form isolated $[Si_6O_{15}]$ rings, rather than layers as might be expected from the Si:O = 4. No isomorphs to $Na_3YSi_6O_{15}$ have been reported. Figure 7.17*a* shows the structure of $Na_3YSi_6O_{15}$ as viewed along *c*-axis. The SiO_4 and YO_6 units are represented as polyhedra.

Similarly, Haile et al. (1997)[77] reported another phase rich in sodium, $Na_3NdSi_6O_{15}\cdot 2H_2O$, a layered silicate in the system Na_2O-Nd_2O_3-SiO_2 under hydrothermal conditions. Although this compound has very similar lattice constants and diffraction symbol to data reported for $NaNdSi_6O_{13}(OH)\ 2\cdot nH_2O$ (special group Cmm2) by Karpov et al (1977),[71] the microprobe analysis given by Haile et al. (Table 7.12) shows the composition substantially richer in Na^+. The asymmetric unit of the structure contains 22 atomic sites: 1 Nd, 4 Na (three of which are only partially occupied). Figure 7.17*b* shows the structure of $Na_3NdSi_6O_{15}\cdot 2H_2O$ viewed along *a*. The SiO_4 and NdO_7 units are represented as polyhedra. Figure 7.17*c* shows an isolated NdO_7 polyhedron viewed along *a*, and the figure also gives oxygen-oxygen distances (Å).

Tuttle autoclaves have been used in the above works. The solvents used are either pure water or a dilute solution of a sodium base (0.1M NaOH, Na_2CO_3, or $NaHF_2$), experimental temperature was 500 to 600ºC, and pressure was 8.25×10^5 Pa.

In systems containing Fe^{3+} and weak NaOH solutions, aegirine, Na Fe Si_2O_6 type silicates were obtained, whereas, in the strongly concentrated NaOH solutions, $Na_{15}Fe_5Si_{12}O_{36}$ forms. The heavier rare earth elements (Ho to Lu) follow Fe^{+3}. Whereas, the lighter lanthanides form original structures, whose cationic nature has not been observed in natural analogs.

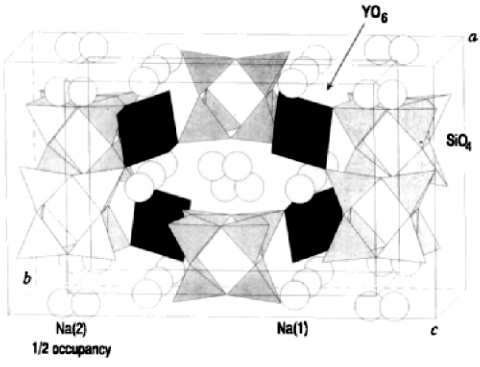

(a)

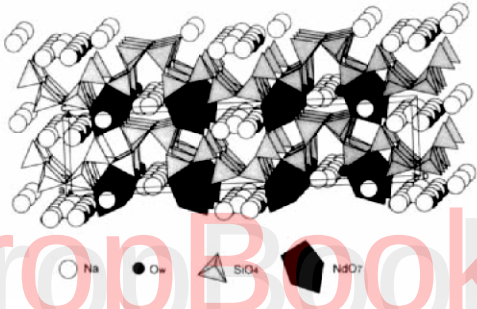

(b)

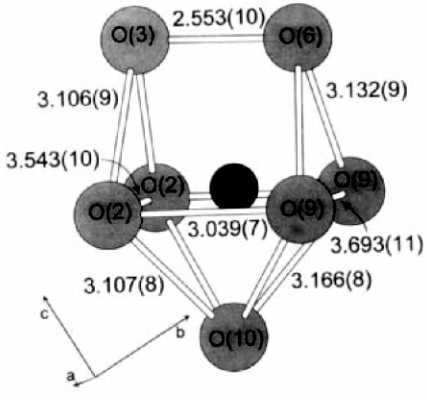

(c)

Figure 7.17. Structures of *(a)* $Na_3YSi_6O_{15}$ as viewed along *c*-axis,[76] *(b)* $Na_3NdSi_6O_{15}{\cdot}2H_2O$ viewed along *a*, and *(c)* isolated NdO_7 polyhedron viewed along '*a*', the figure also gives oxygen-oxygen distances (Å).[71]

DropBooks

Table 7.12. Results of Electron Microprobe Analyses at Three Different Locations Within a Single Crystal of the Present Sodium Neodymium Silicate[77]

The expected values are those calculated for the composition $Na_3NdSi_6O_{15}{\cdot}2H_2O$, deduced from the chemical analysis and the structure determination.

Position	Na mol%	Nd mol%	Si mol%	Total wt% oxides
1	10.81	3.49	22.40	94.55
2	10.79	3.50	22.50	94.77
3	10.74	3.46	22.24	94.19
Average	10.78 (4)	3.48 (2)	22.4 (1)	94.5 (3)
Expected	10.5	3.5	21.0	94.7

7.6 DEGREE OF SILIFICATION

One of the characteristic features of silicates is the molar ratio of rare earth oxides and silicon. Variation in the value of molar ratio varies within a wide range: from 0.78 for Na-free silicate (apatite-britolite structures) up to 12 for compounds with highly condensed [Si-O] radicals. The degree of silification (*S*) can be represented as the ratio of Si atoms to the sum of the cations:

Eq. (6)
$$S = \frac{KSi}{\left(n\,M^{++} + m\,Me^{++} + ...\right)}$$

The degree of silification decreases with an increase in NaOH concentration. This reflects the inter-relation of cationic and anionic motif (crystal chemical factor). It also reflects the phase formation, chemical environment, and conditions of synthesis (genetical factors). In case of the lower concentration of NaOH, the monocrystals can be obtained in the presence of additional anions like CO_3, Cl, F, SO_4, etc. Dimitrova (1977)[35] has studied the degree of silification for several rare earth silicate systems, and found $S \approx 3$ only for one silicate and for a majority of the silicates $S < 1$ with a higher association of cationic motif. Corresponding

to the increase in the concentration of Si from 0.27% to 16.7% the following phase changes have been observed:

Eq. (7) $R_{4\ 2/3}[SiO_4]_3O \rightarrow Na_3R[Si_6O_{15}]\cdot 2H_2O \rightarrow Na\ R[Si_6O_{14}]$
S = 0.64 1.5 3.0

The other example for silification of rare earth silicates in highly concentrated solution of NaOH (30–45%), is the (Ho-Lu) series,

Eq. (8) $Na\ R[SiO_4] \rightarrow Na\ R[SiO_7] \rightarrow Na_{15}R[Si_{12}O_{36}]$
S = 0.5 0.5 0.66

In highly concentrated solutions, the change in the concentration of Si from 48% to 60% does not influence on the degree of silification. For example, at constant concentration of Si (48%) and increase in NaOH concentration, the following chain sequence is observed:

i) For lighter lanthanides:

Eq. (9) $R_{4\ 2/3}[SiO_4]_3O \rightarrow Na\ R[SiO_4] \rightarrow Na_2R[SiO_4].(OH)$
S = 0.64 0.5 0.5

DropBooks

ii) For heavier lanthanides:

Eq. (10) $R_{4\ 2/3}[SiO_4]_3O \rightarrow Na\ R[SiO_4] \rightarrow Na_3R[Si_2O_7]$
S = 0.64 0.5 0.5

For more concentrated solutions, Si (>60%) and corresponding NaOH concentration, the lighter rare earths show the following sequence:

Eq. (11) $Na_3R[Si_6O_{15}]\cdot 2H_2O \rightarrow Na\ R[SiO_4] \rightarrow Na\ R[SiO_4]\ (OH)$
S = 3 0.5 0.33

All these phase transformations show that without depending upon the concentration of Si, the degree of silification of phases decreases with an increase in the NaOH concentration in the system.

It can be assumed that rare earth elements, having high basicity (La-Nd) in the process of phase formation, form more associated rare earth motif with a characteristic *3d* bond.[35] Only at higher concentrations

of Si, and in the presence of carbonate ions, less associated chains $[R_3O_{12}]_\infty$ as in $NaRSi_6O_{14}$, or discrete polyhedra as in $Na_3RSi_6O_{15}{\cdot}2H_2O$, are formed.

7.7 PROPERTIES OF RARE EARTH SILICATES

Rare earth silicates exhibit very interesting electrical and optical properties, which make these compounds unique in several respects. For example, the discovery of high ionic conduction in rare earth ring silicates has triggered an intensive search for technically promising superionic conductors.[78]–[81] Because the popular β-alumina had several disadvantages—like its intrinsically high anisotropy, current and stress inhomogeneities—which degrade the mechanical properties. In this respect, the rare earth silicates containing alkali metals offer lower sintering temperatures (1100°C compared to 1600°C for β-alumina), a wide chemical flexibility, and ionic conductivities possibly surpassing, at 300°C, that of β-alumina. Beyeler et al. (1980) have grown single crystals of $Na_5YSi_4O_{12}$ using the hydrothermal method and studied its directional ionic conductivity in the frequency range between 1 kHz and 50 MHz. Figure 7.18 shows the Arrhenius plot of $Na_5YSi_4O_{12}$ single-crystals.[81] Subsequently, several others have reported the high ionic conductivity in a large variety of rare earth silicates and also proposed the conduction mechanism as there is a close relationship existing between the crystal structure and the properties.[49][82]–[86] Several authors have reported ionic conductivity in various alkali rare earth silicates.[49][84][87]

The ionic conductivity is closely related to the mixed framework structure. The most important compound among rare earth silicates is $Na_5RSi_4O_{12}$, wherein, $[SiO_4]$ tetrahedra are linked to form $[Si_{12}O_{36}]$ rings parallel to the basal plane of the hexagonal cell. Maksimov et al. (1973) could locate only 48/90 of the Na^+ atoms mobile making this compound a good Na^+ ion conductor.[43] The discrete polyhedra of metalayers are mainly responsible for ionic conductivity, as in $K_3R_3(Si_6O_{16})_2OH$, where R = Gd, Ho.[70] Excess rare earth elements lead to the condensation of their polyhedra which gives low conductivity (10^{-4} to 10^{-3} ohm$^-$ cm^{-1} at 300°C).

The discrete nature polyhedra in these compounds is responsible for these special properties like photoluminescence. Figure 7.19 shows the photoluminescence spectra in $NaY[SiO_4]$ crystals.[88]

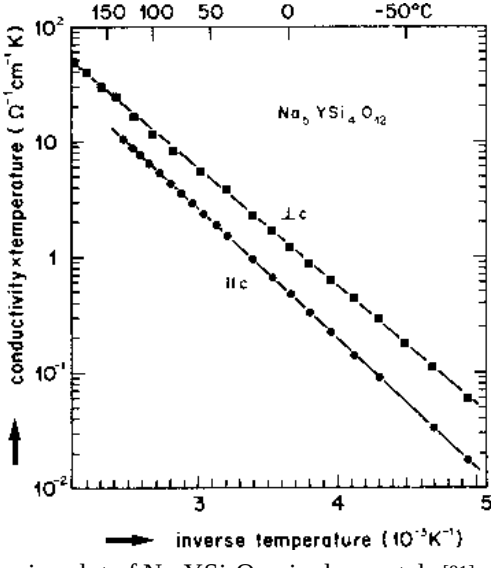

Figure 7.18. Arrhenius plot of $Na_5YSi_4O_{12}$ single-crystals.[81]

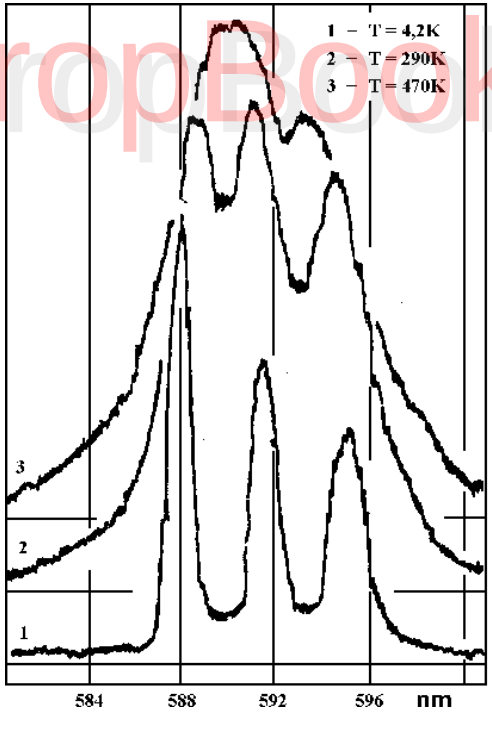

Figure 7.19. Photoluminescence spectra in $NaY[SiO_4]$ crystals.[88]

7.8 SODIUM ZIRCONIUM SILICATES

Most of the sodium zirconium silicates belong to the NASICON family.[89]–[91] There are over twenty known sodium zirconium silicates, out of which only six are minerals. The sodium zirconium silicates find extensive applications in modern technology, especially after the discovery of unique properties in these compounds as inorganic adsorbents used in industry and agriculture and for environmental safety. Among the inorganic adsorbents, zeolites were most popular initially. Unfortunately, aluminosilicate-based zeolites have one essential drawback, a low chemical stability in acid and alkaline media, which imposes certain restrictions on their application. Titanium silicates, such as $Na_2Ti_2SiO_7 \cdot 2H_2O$,[92][93] and $Na_2TiSi_2O_7 \cdot 2H_2O$,[94] are among a large family of known titanium containing minerals and synthetic compounds, and they exhibit most promising selective ion exchange properties suitable for highly alkaline nuclear waste remediation. Clearfield and his group have found that the reason for the unique behavior of crystalline titanium silicates is connected with the correspondence of the geometrical parameters of their adsorption sites (channels, cavities) to the size of the selectively adsorbed Cs^+ or Sr^+ ions.[93][95][96] By analogy, the other polyvalent metal silicates—for example, zirconium silicates—might be as fruitful in yielding the desired exchangers as was the case for titanium silicates. Moreover, zirconium silicates occur widely in nature, and their formation under hydrothermal conditions (in a wide range of temperatures from 300 to 550°C) has been given considerable attention to solve some of the general geophysical and mineralogical problems. It is reasonable to expect that some of these compounds, due to the presence of ion-exchange functional groups, as well as the existence in their structure of well-defined channels and cavities, could exhibit interesting ion-exchange properties, viz. high selectivity to certain ions and molecules. Unfortunately, the ion-exchange behavior of such zirconium silicates has not been studied in detail yet.

Na_2O-ZrO_2-SiO_2-H_2O system has been studied over a wide range of the initial component ratios, ZrO_2/GeO_2 = 3:1–1:9 (mole); NaOH concentration 0–50wt%, temperature 300–600°C, pressure 40–300 MPa by several workers.[97]–[100] The phase composition of zirconium silicates formed in Na-containing media is shown in Fig. 7.20 and the crystallization field is shown in Fig. 7.21. The analysis of the products of hydrothermal synthesis and x-ray data allows one to refine the composition of some phases. Thus, the phase earlier described as $Na_{14}Zr_2Si_{10}O_{31}$ based on the

data of chemical analysis[99][100] has, in fact, the composition $Na_8ZrSi_6O_{18}$. Its structure is analogous to $Na_8SnSi_6O_{18}$.[101] $Na_6Zr_2Si_3O_{15}$ (composition based on the data of the chemical analysis)[102] has the same structure as the synthetic germanate $Na_3HZrGe_2O_8$ (see Table 7.13).

The general scheme of zirconium silicate crystallization in hydrothermal solution with an increase in alkali concentration and temperature is shown in Fig. 7.22.

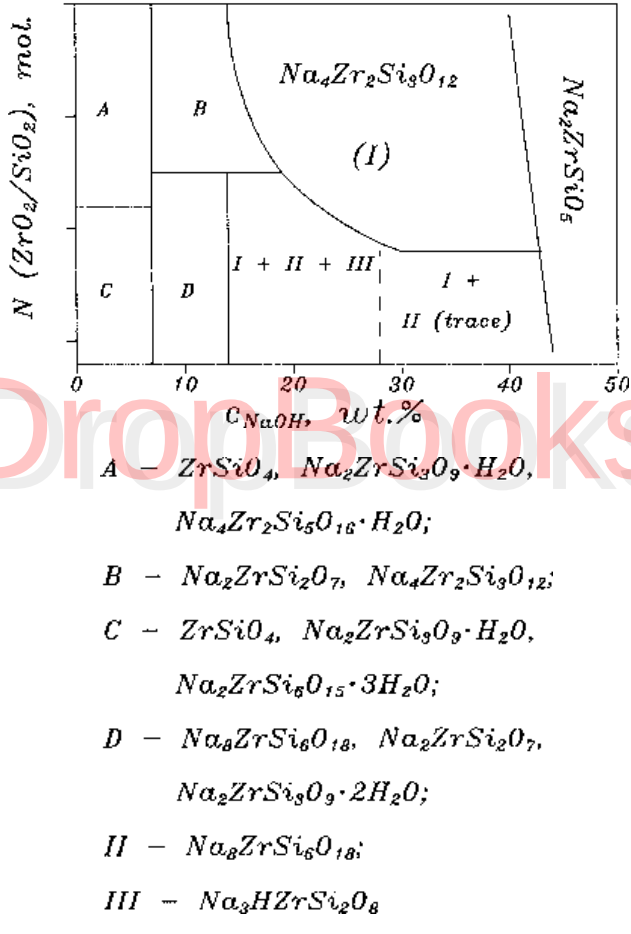

DropBooks

Figure 7.20. Phase composition of zirconium silicates formed in Na-containing media.[97]

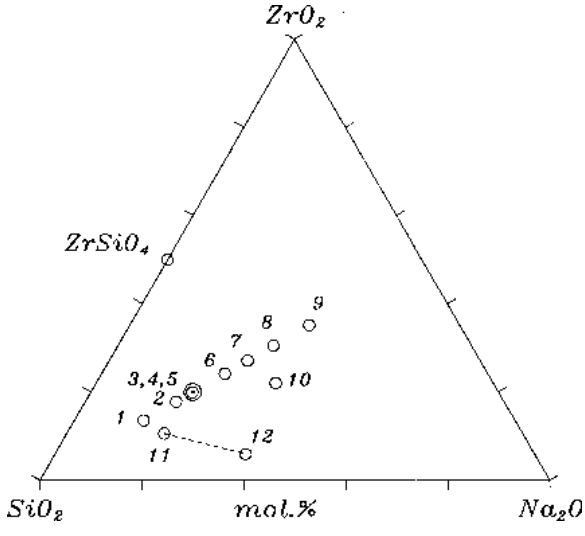

1 – $Na_2ZrSi_6O_{15} \cdot 3H_2O$;

2 – $Na_2ZrSi_4O_{11}$;

3 – $Na_2ZrSi_3O_9 \cdot 2H_2O$;

4 – $Na_2ZrSi_3O_9 \cdot 3H_2O$;

5 – $Na_4Zr_2Si_6O_{18} \cdot 4H_2O$;

6 – $Na_4Zr_2Si_5O_{16}$;

7 – $Na_2ZrSi_2O_7$;

8 – $Na_4Zr_2Si_3O_{12}$;

9 – Na_2ZrSiO_5;

10 – $Na_3HZrSi_2O_8$

11–12 – $Na_{8-x}H_xZrSi_6O_{18}$

Figure 7.21. Crystallization field in Na_2O-ZrO_2-SiO_2 system.[97]

Table 7.13. New Silicates of Zirconium[97]

Compound	Unit cell parameters			Space group
	a, Å	b, Å	c, Å	
$Na_8ZrSi_6O_{18}$	7.371 α=88.34°	—	—	R3m
$Na_8SnSi_6O_{18}$	7.344 α=87.82°	—	—	R3m
$Na_3HZrSi_2O_8$	9.036 α=87.74°	6.953 β=89.75	5.558 γ=89.16	12/m

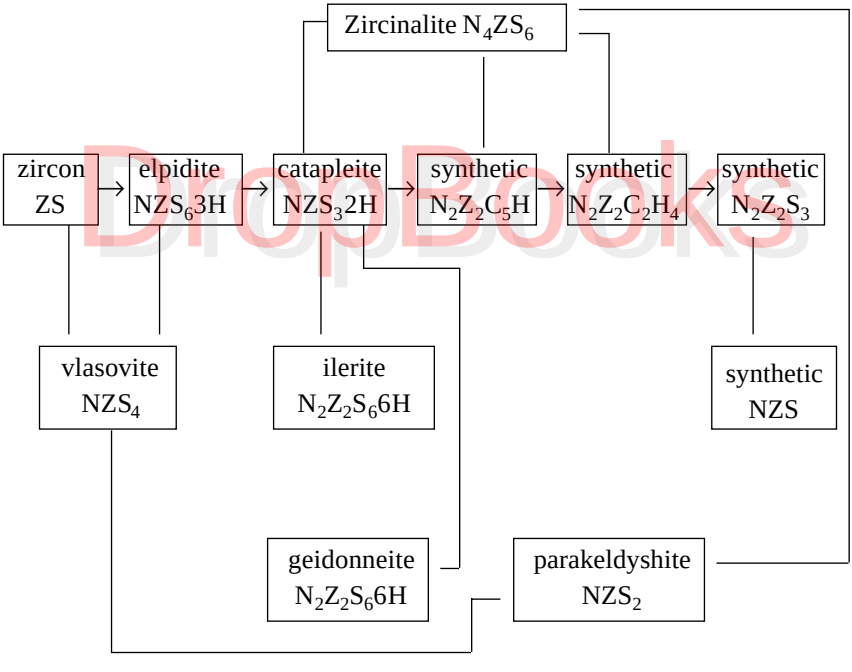

DropBooks

→ denotes the transitions with the temperature rise,
↔ denotes paragenesis, dashed lines denotes natural paragenesis,
N = Na_2O, Z = ZrO_2, S = SiO_2 and H = H_2O.

Figure 7.22. Scheme of zirconium silicate crystallization.[97]

Analogs of zirconium mineral (zircon, elpidite, vlasovite, catapleite, parakeldyshite) and $Na_4Zr_2Si_5O_{16}\cdot H_2O$ silicate (still not observed in nature) are formed in the region of solutions with the lowest concentrations. In highly concentrated solutions, the silicates with the lowest silicon content are crystallized: $Na_4Zr_2Si_3O_{12}$ and Na_2ZrSiO_5. This system illustrates the role of the solvent in the formation of crystal phases. With an increase in the NaOH concentration the process of the formation of alkali-zirconium silicates proceeds with the depolymerization of the Si-O radicals: infinite $[Si_6O_{15}]$ chains in elpidite $\Rightarrow$ infinite $[Si_4O_{11}]$ chains in vlasovite $\Rightarrow$ island $[Si_3O_9]$ rings in catapleite $\Rightarrow$ $[Si_2O_7]$ diorthogroups in parakeldyshite $\Rightarrow$ $[SiO_4]$ orthogroups in the synthetic $Na_4Zr_2Si_5O_{16}$ and $Na_3HZrSi_2O_8$ phases. Barth et al. (1988) studied the structure and ionic conduction in $Na_4ZrSi_3O_{10}$,[103] belonging to the NASICON family. Figure 7.23 shows part of the system Na_2O-ZrO_2-SiO_2-P_2O_5. $Na_4ZrSi_3O_{10}$ has been characterized as a monoclinic compound with lattice parameters which are quite similar to the monoclinic low temperature modification of NASICON.

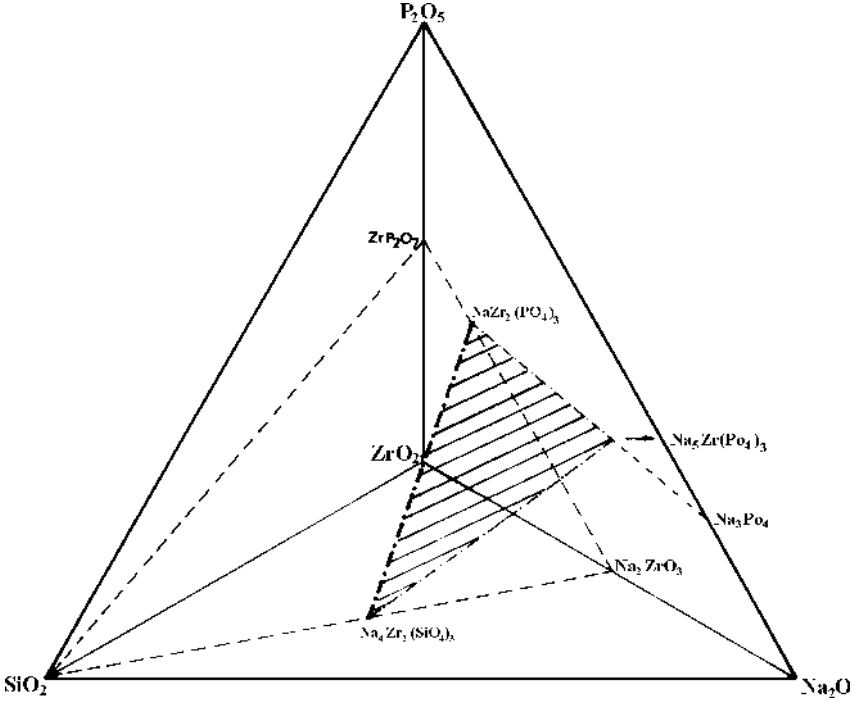

Figure 7.23. Part of the system Na_2O-ZrO_2-SiO_2-P_2O_5.[97]

In recent years there has been a general trend to synthesize these zirconium silicates under lower pressure temperature conditions Yong and Wenqin (1990, 1991) studied this system and obtained $Na_4Zr_2(SiO_4)_3$ at 290–300°C and further reduced temperature conditions (250°C) using $ZrOCl_2$, Na_2SiO_3 and NaOH solution,[104][105] and the hydrothermal chemical reaction is given below:

Eq. (12) $$2ZrOCl_2 + 3Na_2SiO_3 + 2NaOH \rightarrow Na_4Zr_2(SiO_4)_3 + 4NaCl + H_2O$$

Clearfield and co-workers have obtained a series of zirconium silicates under mild hydrothermal conditions (180–190°C) and studied the influence of the type of silicon-containing reagent, the molar ratio, and concentrations of reagents in the reaction mixture on the yield of resultant products.[95][96][106] These authors have studied the formation of several different sodium zirconium silicate phases in the systems: *i)* $Zr(OC_3H_7)_4$-silicic acid-NaOH-H_2O; *ii)* $Zr(OC_3H_7)_4$-silicon–containing reagent-NaOH($_4$M)-H_2O under mild hydrothermal conditions (T = 180–190°C, pressure generated from 50% fill). These studies have yielded several novel sodium zirconium silicates. According to these authors, the predominant phase is hydrated sodium zirconium silicates in this system in contrast to mainly anhydrous SZS (Na_2-$ZrSiO_5$, $Na_2ZrSi_2O_7$, $Na_4Zr_2Si_3O_{12}$, etc.) while carrying out the reactions at much higher temperatures (300–550°C).[97] This suggests that a relatively low temperature of hydrothermal synthesis could be one of the factors favorable for the preparation of hydrated zirconium silicates, possessing the ability for ion exchange. Then, the second controlling factor, giving a certain diversity of compounds, is the type of the initial silicon-containing reagent. The comparison shows that in a wide range of Si:Zr ratios (2–5:1) used in the systems $Zr(OC_3H_7)_4$-$Na_2Si_3O_7$- NaOH-H_2O and $Zr(OC_3H_7)_4$ - Na_2SiO_3 - NaOH-H_2O, the main product is $Na_4Zr_2Si_5O_{16}\cdot H_2O$. No formation of $Na_2ZrSi_3O_9\cdot 2H_2O$ or the novel 12.8 Å phase was found. The second feature is the formation of $Na_4ZrSi_3O_{10}$ (as admixture or main phase) even at a Si:Zr ratio of 1:1, which was not observed when silicic acid as the silicon containing reagent was used.

The hydrothermally grown crystals of the sodium zirconium silicates have a broad size range (from 0.2 to 25 mm) and an irregular form. The lack of a clearly defined morphology correlates with a low crystallinity of the compound.

DropBooks

A majority of the works on the synthesis of alkali zirconium silicates suggest that all of them are layered compounds. Thermal and chemical stability, different Zr/Si molar ratio, and intercalation ability suggest that these compounds could be promising for pillaring with inorganic and organic species for synthesis of new functionally designed and tailored catalysts, and support for catalyst and adsorbents. High affinity for some transition and toxic heavy metals makes sodium zirconium silicates attractive for high-level purification of certain technological solutions and wastes containing these elements.

7.9 GROWTH OF SELECTED SILICATES

It would be extremely difficult to describe the growth of all the silicates under hydrothermal conditions as there have been a great number of publications in this field since the 1850s. Therefore, we only discuss the synthesis of some selected silicates with an emphasis on the current trends in the growth of silicate crystals.

The first work on silicates on the whole by hydrothermal method was carried out by Wöhler (1848).[107] Followed by this, several other silicate minerals were synthesized during the 19th century. Allen et al. (1906) carried out a systematic investigation of the hydrothermal synthesis of several pyroxene and amphibole group of minerals.[108] For example, these authors quote an experiment of the synthesis of amphibole at low temperatures by Chroustschoff, who obtained hornblende in which a mixture of silicic acid, alumina, lime, magnesia, ferrous and ferric oxides, and the alkalies, partly in solution partly precipitated were heated in sealed glass vessels at a temperature of 550°C for three months. The results of these experiments were used to explain the geological relations. Later, Morey and Niggli (1913) published an exhaustive review on the hydrothermal formation of silicates, giving a complete list of silicates obtained till that time, and all the important publications were included.[109] Figure 7.24 shows the equilibrium diagram of the system diopside-anorthite at pressure 1 bar, and it was studied by Bowen (1915). Soon after this, Morey, supported by Fenner (1917), published a systematic investigation of the ternary system H_2O-K_2SiO_3-SiO_2.[110] Here, for the first time, studies were carried out in a systematic fashion with the temperature carefully controlled and measured and the pressure held constant throughout the experiment. Figure 2.6 shows the isothermal polybaric saturation curves

and the isobaric polythermal saturation curve at 1 atm pressure of H_2O vapor. This marked the beginning of the phase equilibria studies in the silicate system and, followed by this, several other important publications came out especially from the Geophysical Laboratory in Washington, pertaining to the silicate systems. In fact, Bowen developed his famous petrologic ideas based on these phase equilibrium data.[111] One of the most important phase equilibrium data among the silicate systems is for the system MgO-SiO_2-H_2O given by Bowen and Tuttle (1949).[112] This work, in many respects, laid the foundation for much of the subsequent work on silicate systems. In this work, the authors describe the change of assemblages with temperature and also show the effect of pressure on the temperatures involved. Figure 7.25 shows the pressure-temperature curves of univariant equilibrium in the system MgO-SiO_2-H_2O.[121]–[124] There are quite a large number of such silicate systems reported in the literature, contributing to the understanding of complex geological processes. Some of the systems like Al_2O_3-SiO_2-H_2O,[113]–[115] CaO-SiO_2-H_2O,[116]–[119] SrO-SiO_2-H_2O,[120] MgO-Al_2O_5-SiO_2-H_2O,[121]–[124] and alkali-Al_2O_3-SiO_2-H_2O[125]–[128] are noteworthy to mention here, as they provide a vast amount of information on the understanding of the natural geological processes leading to the formation of various rocks and minerals.

DropBooks

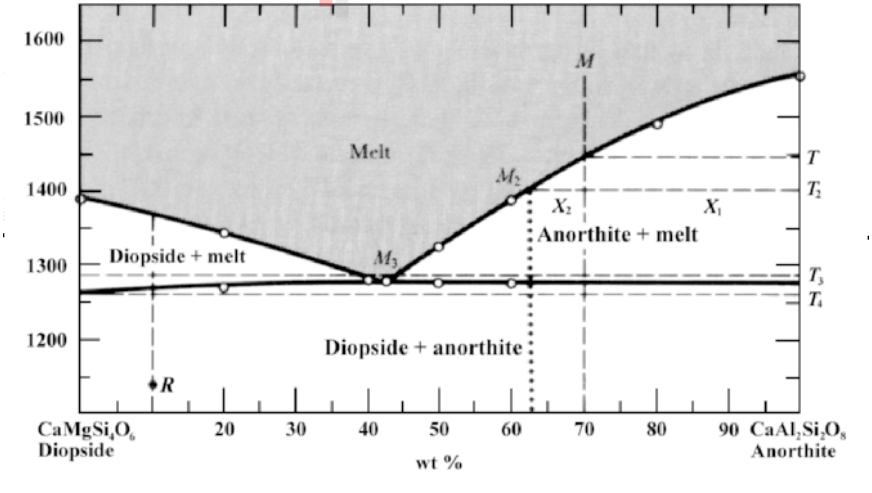

Figure 7.24. Equilibrium diagram of the system diopside-anorthite at pressure 1 bar. *Bowen, N. L., The Crystallization of Haplobasaltic, Haplodioritic, and Related Magmas,* Am. J. Sci., *40:161–185 (1915).*

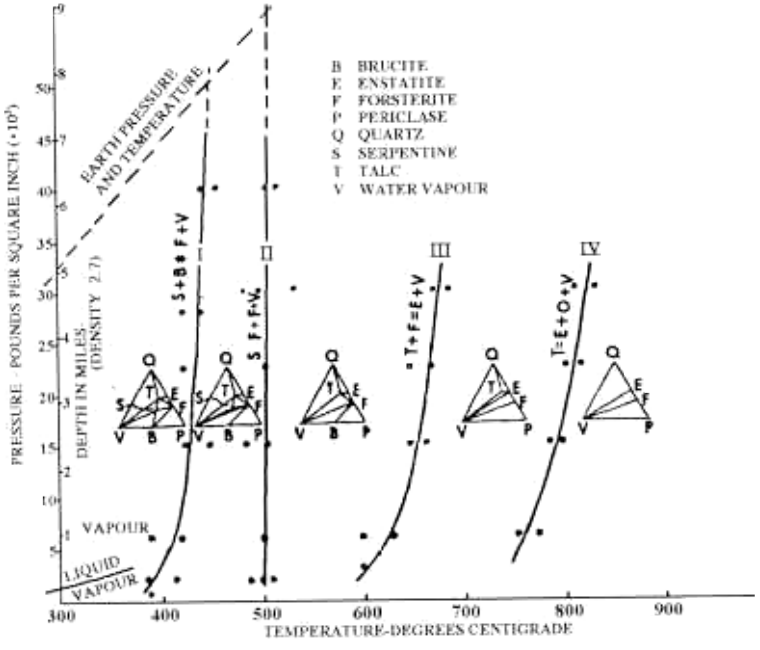

Figure 7.25. Pressure-temperature curves of univariant equilibrium in the system $MgO\text{-}SiO_2\text{-}H_2O$.[123]

We give here some of the earliest works on the synthesis of various silicates in general, before going into the systematic synthesis of selected silicates with device potential, gemstones, and of general interest.

Felspars: The high-temperature varieties of felspars have been successfully prepared by the end of the 19th century. However, the complexities in their forms and intergrowth were realized only during the 1950s.

Several hydrous and anhydrous aluminosilicates have been synthesized for the past 150 years using hydrothermal technique. Among these, the dense anhydrous alumino-silicates carried a great significance because of their role in natural metamorphic processes. Though several minerals—like garnets, sillimanite, analusite, kyamte, and epidotes—have been synthesized using hydrothermal method, no reproducible synthesis of these minerals was achieved before the work of Coes (1953),[129] whose works are briefly described here for the benefit of the readers in Table 7.14.[117]

Table 7.14. Early Hydrothermal Synthesis of Various Dense Anhydrous Aluminosilicates (Coes, 1953)[129]

Silicate	Starting Material	Pressure	Temp. °C
Jadeite	Sodium sulphate, Kaolin + silica	+ 20,000 kg/cm^4	900
$NaCr(SiO_3)_2$	Sodium dichroumate + Silica	20,000 kg/cm^2	900
Andalusite	Kaolin + Sodium salts	20,000 to 30,000 kg/cm2	600–900
Kyanite	alumina + silica	20,000 to 40,000 kg/cm^2	600–900
Sillimanite	Kaolin + fluorides	20,000 to 30,000 kg/cm^2	600–900
Topaz	Kaolin + fluorides, but higher fluoride contents or Kaoline + NH_4HF_2		
Epidote & zoisite	hydrated calcium & iron nitrates, hydrated alumina & silica	20,000 kg/cm^2	800
Garnet:			
grossularite		15,000 kg/cm^2	600–800
andradite		20,000 kg/cm^2	600–800
almandine		20,000 kg/cm^2	600–900
pyrope		30,000 kg/cm^2	900
$Mg_3Fe_2(SiO_4)_3$		30,000 kg/cm^2	900
$Mn_3Fe_2(SiO_4)_3$		20,000 kg/cm^2	800
$Fe_3Fe_2(SiO_4)_3$		20,000 kg/cm^2	800
$Mg_3Cr_2(SiO_4)_3$		20,000 kg/cm^2	800

DropBooks

The other important minerals synthesized during the 19th century by hydrothermal method are staurolite, chloritoid, beryl, vesuvianite, lanosonite, bertrandite, lowsonite, bertrandite, low temperature forms of the lithium aluminosilicates, spodumene, eucryptite, petalite, micas, clays, tourmaline, uranium minerals, and so on. Therefore, we describe the synthesis of only some technologically important silicates under hydrothermal conditions.

7.9.1 Bismuth Silicate, $Bi_{12}SiO_{20}$

Bismuth silicate, $Bi_{12}SiO_{20}$ (BSO) is of considerable interest for optical signal processing. It is popular as a photorefracting crystal. The *photorefractive effect* can be described as a combination of the photoconductive and the electro-optic effects used in a variety of applications like nonlinear mixing including active spatial filtering phase conjugation by way of degenerating four-wave mixing optical processing devices such as optical oscillators, and as a technique useful for nondestructive materials analysis. Litvin (1964) has studied the system Na_2O-Bi_2O_3-SiO_2-H_2O under hydrothermal conditions: T = 350–450°C, P = 400–500 atm in NaOH solution up to 40wt%.[130]

Figure 7.26 shows the fields of crystallization of bismuth silicates in the system Na_2O-Bi_2O_3-SiO_2-H_2O. The following phases have been obtained: α-Bi_2O_3 (bismite), Bi_2SiO_{20} (sillenite) and $Bi_4Si_3O_{12}$ (eulytite). Bi_2SiO_{20} crystallizes under hydrothermal conditions in NaOH (1–60 wt%) and KOH (1–40 wt%) solutions and 350 atm pressure.[131] Whereas, eulytite crystallizes with NaOH (21wt%), and it does not depend on the ratio of the starting components (Bi_2O_3 + SiO_2). It recrystallizes well at 380°C. However, the variation in the ratio of the starting components (Bi_2O_3 + SiO_2) restricts the field of crystallization of $Bi_{12}SiO_{20}$ on one hand and the appearance of α-Bi_2O_3 on the other hand. The process of formation of $Bi_{12}SiO_{20}$ is very sensitive to the existence of hydrogen. Surplus hydrogen leads to the establishment of $Bi_{12}SiO_{20} \rightarrow$ Bi metal transformation. The hydrothermal synthesis of bismuth silicates can be carried out in silver, platinum, copper, or titanium liners. In fact, Bi_2O_3 and SiO_2 reactions occur more rapidly than for other silicate systems, so that the entire reaction completes within two days.

BSO crystals are usually grown using Czechrolskii and hydrothermal methods. Although commercially available crystals of BSO grown by melt techniques are sufficiently of good quality for most applications; they have limitations in optical uniformity and reproducibility of photorefractive properties. Variations in the process control environment, i.e., temperature, growth rate, ambient atmosphere, rotation rates, and annealing, can affect segregation of dopants and defects in the melt growth environment. High-temperature solution growth by the hydrothermal process is capable of producing multiple crystals of large size and identical consistency while requiring only a stable temperature control system once the internal environmental conditions have been established.[132] The

Cz-grown crystals have higher trap density, whereas the hydrothermally-grown crystals have lower trap density. The hydrothermally-grown crystals are free of the typical structural defects encountered in commercial material, i.e., veils, bubbles, precipitates, and other strain producing phenomena. BSO crystals show yellow coloration. The doping studies on both Cz-grown and hydrothermally-grown material indicate that Al, Ga, Cr, Mn, and V are effective in altering absorption at different wavelengths. Harris et al. (1992) obtained low-defect colorless BSO crystals under hydrothermal conditions using a noble metal liner.[133] Figure 7.27 shows two crystals resulting from one run still mounted on the silver seed holder and the baffle. They have used 1.5 × 10 × 10 mm^3 seeds taken from a Cz-grown crystal.[100] Centimeter-size pieces of Cz-grown BSO crystals were used as the nutrient. The liner was filled with 4N NaOH solution and the external void was filled with a sodium-silicate pressure-balancing solution. The following were the experimental conditions:

Dissolution temperature – 390°C

Crystallization temperature – 385°C

ΔTemperature – 5°C

Pressure – 6000 to 12,000 psi.

Growth duration – 30 to 40 days

Growth rate – 0.1 to 0.3 mm/day

DropBooks

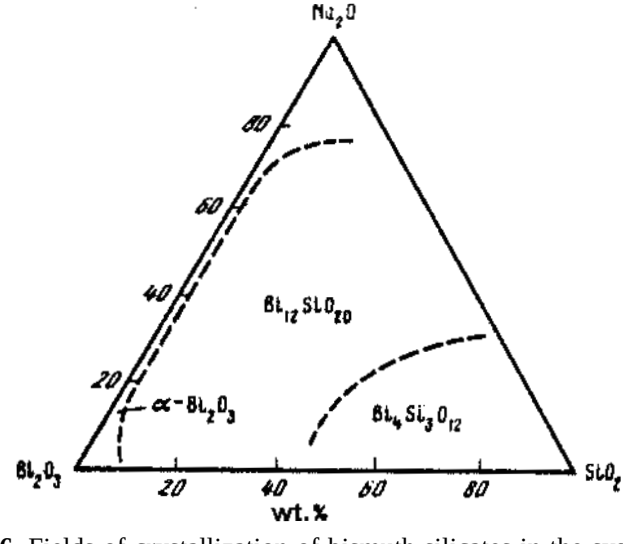

Figure 7.26. Fields of crystallization of bismuth silicates in the system Na_2O-Bi_2O_3-SiO_2-H_2O.[131]

Figure 7.27. Two crystals resulting from one run still mounted on the silver seed holder and the baffle.[133]

Little or no growth occurred at NaOH normalities less than 4N or nutrient zone temperatures less than 390°C. Excessive, unoriented growth on seeds and spontaneous nucleation on the walls of the liner occurred with normalities above 5°C. Experiments using Czechrolski-grown nutrient produced better crystals. Limited experimental data indicates that the preferred growth orientation is [100]. Most of the crystals were colorless in contrast to the straw color of Czechrolski crystals. Some were pale green, perhaps as a result of minor leaks in the platinum liner.[134] Figure 7.28 shows the absorption spectra of various BSO samples. The solid curves represent the absorption spectra taken at 10 K of a hydrothermally grown sample with those of the Cz-grown undoped and Al-doped samples. The deep-donor absorption shoulder is present in the curve for the undoped-Cz sample. The dashed curves represent the spectra taken on the three samples after they were exposed to intense monochromatic light (0.2 mw/cm^2) for 1 hr at 10 K; 3 and 3.3 eV lights were used for the undoped and Al-doped Cz samples, respectively. The additional photochromic absorption in the undoped and Al-doped Cz-BSO samples is caused by the transfer of electrons to as yet unidentified traps. The hydrothermally grown BSO crystals do not produce any photochromic absorption. Exposing them at 10 K to 3.3–3.45 eV light causes readily visible blue luminescence but no additional absorption bands are produced. Harris et al. (1994) reported the absorption coefficients of BSO crystals doped with V, Cr,

Mn, and so on.[135] They conclude that the hydrothermal material shows special promise for optical "tailoring," since the native Czechrolski defect is absent and photo-conductive sites and traps may be introduced by doping without interference from this defection. Leigh et al. (1994) reported the characterization of Czechrolski and hydrothermally grown BSO crystals.[136] They have observed significantly smaller optically- and thermally-induced conductivities in the hydrothermal material. A lower defect content also appears to inhibit the conduction processes for the hydrothermal material in terms of missing traps responsible for a hopping conduction process. Slightly higher concentrations of Fe and V were found in the hydrothermal material but these impurities do not affect the color or contribute to a 500 nm absorption in this material. However, an equivalent concentration of these impurities in the Cz-grown material from a hydrothermal charge does affect both the absorption and the TSC results. Thus, the near-intrinsic BSO can be prepared using hydrothermal growth techniques.

DropBooks

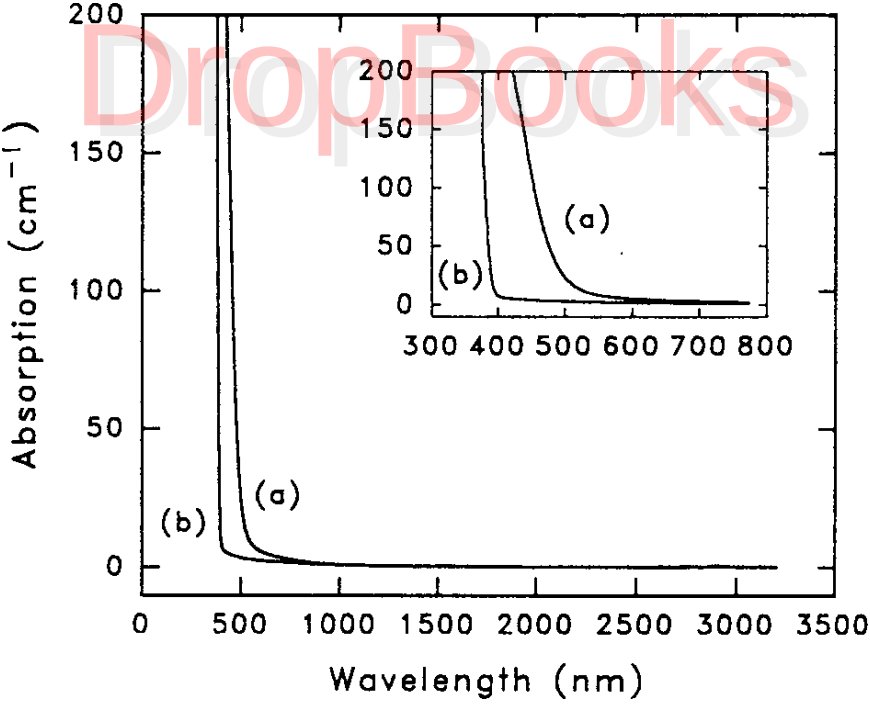

Figure 7.28. Absorption spectra of various BSO samples.[135]

There are several other reports dealing with the study of phase formations in related systems giving compounds isostructural to BSO. For example, Surnina and Litvin (1970) have studied the phase formation in the system Na_2O-Me_2O_3-Bi_2O_3-H_2O (Me = Al, Ga, In) under hydrothermal conditions.[137] Abrahams et al. (1967) obtained $Bi_{12}GeO_{20}$ crystals, germanium sillenite, which exhibit similar properties.[138] The other commonly used cations substituting for Si are Al, Ga, Fe, Ge, and Ti.

7.9.2 Beryl, $Be_3Al_2(SiO_3)_6$

Beryl is one of the most common minerals of hydrothermal origin. It occurs as well-developed crystals of large size. In fact, beryl is the largest crystal produced by nature and is commonly found in pegmatites. It is one of the most important gemstones. The presence of a little Cr^{+3} gives a green color and it is known as *emerald*. The bluish green variety is known as *aquamarine*. The greenish/yellow to iron-yellow and honey-yellow are called *golden beryl*. The rose colored variety is called *morganite* or *vorobyevite*. The alkali elements like Na^+, Li^+, and Cs^+ are sometimes present replacing the beryllium from 0.25 to 5 %.

Artificial growth of beryl crystals began in the 19th century. Hautefeuille and Perrey (1888) were the first ones to synthesize beryl crystals.[139] Espig (1935) studied the crystal structure of beryl.[140] Rogers and Sperisen (1942) prepared beryl crystals by the hydrothermal technique.[141] Wyart and Scavnicar (1957) synthesized beryl crystals by the hydrothermal technique using $NaHCO_3$ solvents.[142] Nassau (1976) has grown large crystals of beryl by the hydrothermal method.[143] Beryl, $Be_3Al_2Si_6O_{18}$, is found with a variety of impurity cations leading to its well-known beautiful colors and its favorable use as a gemstone. Probably the best work on hydrothermal growth of emerald was by Nacken.[144] He made large numbers of synthetic emeralds, using a trace of chromium to produce the color. Hexagonal prisms weighing about 0.2 gm were grown in a few days. Nassau (1976) and Hosaka (1990) reviewed the hydrothermal growth of emerald.[143] Johann Lechleitner of Innsbruck, Austria, released the first and not completely satisfactory product into the market during 1960.[145]–[147] He used faceted beryl gemstones as the seed and grew a thin layer of hydrothermal emerald on the surface, which was subsequently given a light polish (not necessarily on all faces). Such stones were marketed for a short time under the names *Emerita* and *Symerald*. Since the green skin was quite thin, the color of these emeralds was not intense, and the skin could be readily viewed by immersion of the

stone in a liquid. Lechleitner emerald can be synthesized under the following conditions:

Growth temperature - 300–400°C

Pressure - 1020 kg/cm_2

Solvent - a weak alkaline solution

Nutrient - silica (SiO_2), alumina (Al_2O_3), beryllium oxide (BeO)

The first completely synthetic hydrothermal emerald was put on the market by the Linde Division, Union Carbide Corp. in 1965. Figure 7.29 shows the emeralds grown hydrothermally by the Linde Co.; and the size of the crystal is 50 × 22 × 6 mm.

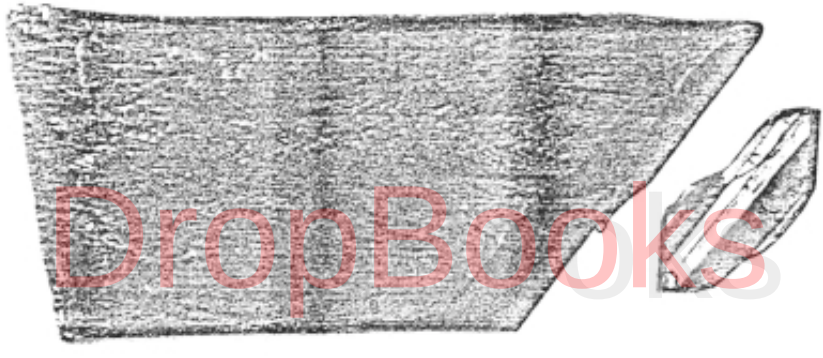
DropBooks

Figure 7.29. Emeralds grown hydrothermally by the Linde Co.; the size of the crystal is 50 × 22 × 6 mm.[144]

The first patent on beryl revealed that it could be grown in a neutral to alkali medium (pH of 7 to 12.5) using mineralizers such as alkali or ammonium halides (e.g., NH_4F + NH_4OH or KF) and that Fe, Ni, or Nd could be used as dopants.[148] The second patent dealt with the analogous growth of beryl in an acid medium (pH of 0.2 to 4.5), using similar halide mineralizers but with an acid reaction (e.g., 8N NH_4Cl) or with extra acid added.[149] Typical emerald growth conditions included pressures of 10,000 to 20,000 psi at temperatures of 500°C to 600°C resulting from a 62% fill. Small temperature gradients of 10 to 25°C were employed. The Al was supplied from gibbsite $Al(OH)_3$, Be from $Be(OH)_2$, Si from crushed crystals of quartz and Cr from $CrCl_3.6H_2O$. Growth rates as high as 1/3 mm per day could be attained. The pressure vessel was lined with gold.

Yancy (1973) could attain a growth rate of 0.8 mm/day using the above experimental conditions.[150] Figure 7.30 shows the schematic diagram for hydrothermal growth of emeralds (after Nassau, 1976).[143] In 1971, Vacuum Ventures Inc. bought the installation from Linde and supplied synthetic emerald using the trade name "Regency emerald." Regency emerald has the same inclusions as Linde emerald, and growth conditions of Regency emerald are considered to be identical to those of Linde emerald.[151] Chlorine was detected in hydrothermally grown Regency and Linde emerald.[152][153] It seems that chlorine must have been derived either from chromium chloride ($CrCl_3$) added as a coloring agent or from HCl added for increasing the acid content in the growth solution. Figure 7.31 shows the as-grown crystal of Regency emerald.[151] The crystal size is 14 × 8 × 6 mm. The seed is colorless but is green at the upper growth layer. The green emerald layer has a thickness three to four times that of the seed.

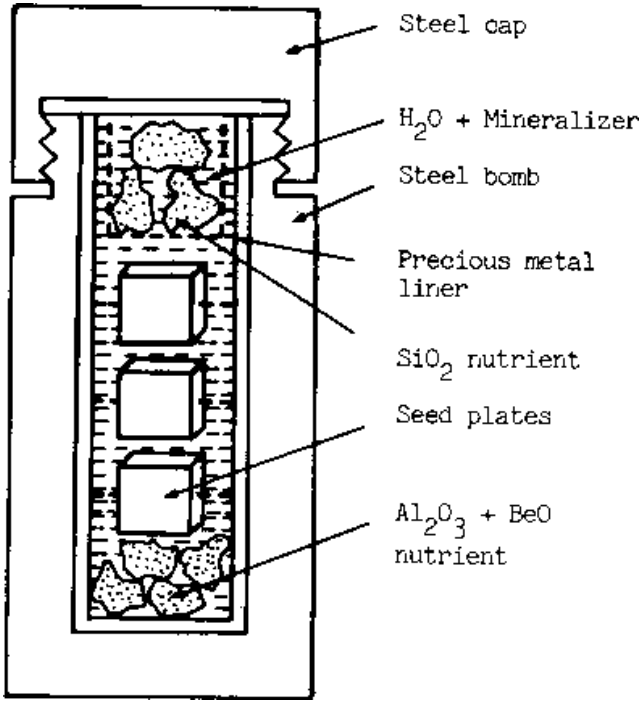

Figure 7.30. Schematic diagram for hydrothermal growth of emeralds (after Nassau, 1976).[143]

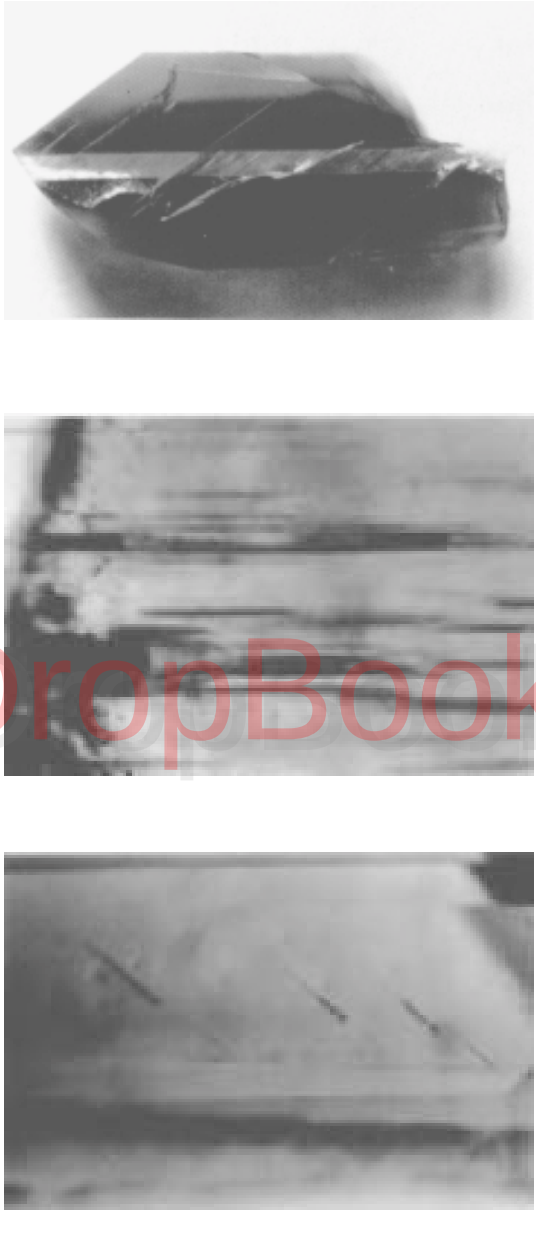

DropBooks

Figure 7.31. As-grown crystal of Regency emerald.[151]

The study of Biron synthetic emerald began in Western Australia during 1977.[154] In 1985, commercial stones were synthesized and sold through the Perth Lapidary Center under the trade name "Biron." Biron Mineral (Pvt) Ltd. is, at present, known as the Emerald Pool Mining Company (Pvt) Ltd.[155] The growth conditions remain unknown. Chlorine, chromium, and vanadium have been detected in these crystals.[154]–[156] Infrared absorption spectrometry has revealed the presence of H_2O. Microscopic examination has revealed the presence of gold crystals.[156] This may indicate that Biron emerald was hydrothermally synthesized in an autoclave lined with gold or gold alloy with chromium and vanadium used as the coloring agents. The crystals have a remarkably large growth sector and are transparent.[156] The characteristic inclusions are the particles of gold, greyish white "bread-crumb" inclusions, phenakite crystals, and rare fragments of the seed.[157]

Hydrothermal synthesis of emerald in USSR began in 1965.[158] At present, it has been improved to obtain commercially faceted emerald.[159] The Russian method of hydrothermal growth of emerald has been reported in detail by Schmetzer.[160] To cite the growth conditions of the Russian synthetic emerald from his paper:

Growth temperature - 590–620°C

Temperature gradient - 45°C, 20–100°C, 70–130°C

Pressure - 816–1530 kg/cm^2

Solvent - acidic solution or flour-bearing solutions of complex components

Nutrient - natural beryl or oxides of Be, Al and Si

Vessel - stainless steel (200–800 ml)

Seed - plate cut parallel to (5 5 10 6)

Under these growth conditions, a seed plate of 6 cm^2 in size increases its weight by 10 gm in about 20 days, and an emerald layer is 5–7 mm in this period of time. This corresponds to a growth rate of 0.2–0.3 mm/day. Cr^{3+}, Fe^{2+}, Fe^{3+}, Ni^{3+}, and Cu^{2+} have been detected through chemical analysis

as color-associated transition elements. Fe^{2+} and Cu^{2+} ions were assigned to the tetrahedral sites, and Ni^{3+}, Cr^{3+}, and Fe^{3+} ions to the octahedral sites.[160] Evolution of ions from the inner wall of the autoclave is possible. It is, therefore, unknown what ions were added during the process of growth. The length of the crystal is 6.1 cm, width: 1 cm, thickness: 0.7 cm. The Russian synthetic emerald crystals grown for commercial aims commented by Klyakhin are 10–12 cm in length, up to 2–2.5 cm in width and up to 2 cm in thickness of grown layers. Their total thickness varies within 0.8–1.4 cm.

The optical properties and physical features of commercial synthetic emeralds are presented by Sinkankas.[161] Table 7.15 lists the properties of various synthetic emeralds including the Russian hydrothermally grown emerald.

Kodaira et al. (1982) obtained hexagonal prism crystals having a maximum size of 0.3 mm in length from 0.1 N NaOH solution at 750°C. Using 0.5 N or 1 N NaOH solution as solvents, beryl crystals were precipitated with phenacite at 500 to 600°C. Temperatures higher than 650°C resulted in phenacite crystals with a small amount of beryl.[162] Figure 7.32 shows the hexagonal prism shaped crystals grown from 0.1 N NaOH solution.

DropBooks

What is most significant in the hydrothermal growth of beryl is that Al and Be hydroxides are highly reactive; the growth process is usually stopped when phenakite crystals start developing at the bottom of the vessel. The growth rate and morphology depends upon temperature, pressure, ΔT, size of the crushed quartz dopants, and so on. High growth rates produce too many inclusions.

As the sources of natural colored gemstones continue to shrink and the population growth of the world continues to increase, the size of the market for gem materials such as synthetic emerald is expected to increase (tempered, however, by occasional reverses in the world economy).

Table 7.15. Properties of Hydrothermally Grown Emeralds[144]

Refractive index	Birefringence			Specific gravity	Chelsea filter	253.7 nm UV	365 nm
Natural (Santa Terezinha)	1.580	1.588	0.008	2.70	inert to pink	none	none
Lechleitner emerald-coated natural beryl	1.586-1.597	1.580-1.587	0.006-0.010	n.d	red	pale red to bright	pale red to red
fully-synthetic beryl-emerald composite	1.567-1.573	1.562-1.567	0.005-0.006	2.67-2.69	bright red	bright red	bright red
Linde (0.3-1.2% Cr)	1.567-1.573	1.562-1.567	0.005-0.006	2.67-2.69	bright red	bright red	bright red
Regency	1.568	1.573	0.005	2.68	bright red	red	bright red
Biron	1.577	1.570	0.007	2.72	red to pink	inert	very weak dark green
	1.573	1.569	0.004-0.005	2.68-2.71	strong pink red	inert	inter
Pool	1.574	1.569	0.005	2.75	red	inert	inter
Soviet	1.583-1.586	1.577-1.579	0.006-0.007	2.70-2.71	none-to dark orange yellow	none	none to partly dark red
	1.579-1.587	1.574-1.581	0.005-0.006	2.64-2.66	no reaction	inert	dull red

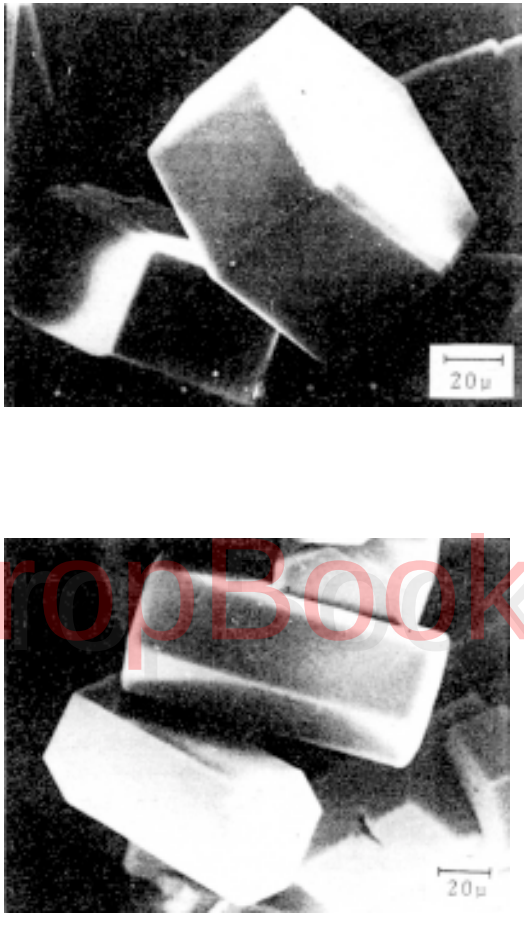

DropBooks

Figure 7.32. Hexagonal prism shaped crystals grown from 0.1 N NaOH solution.[162]

There are several other beryllium bearing silicates—like chkalovite -$Na_2BeSi_2O_6$, iron beryllosilicate-$Fe_3BeSi_3O_9(F,OH)_2$, aluminoberyllosilicate-$Na_3Al.BeSi_2O_8$, barylite-$BaBe_2Si_2O_7$ and so on—have been synthesized as single crystals using the hydrothermal method.[163]-[166] Sobolev et al. (1966) prepared chkalovite and its germainum analog by hydrothermal techniques from the system BeO-MeO_2-NaOH-H_2O (where Me = Si, Ge).[167] Beus and Dikov (1967) have studied its field of stability in hydrothermal solutions containing NaOH, Na_2CO_3, NaF, and HF, and prepared from beryllium hydroxide and nitrate with amorphous SiO_2 in hydrothermal NaOH and NaCl solutions.[168] The experimental temperature was 400–600°C, ΔT = 40–60°C, P = ~ 700 atm and the experimental duration was five days. It is possible that in natural hydrothermal process, where chkalovite is very rarely encountered, undergoes further changes owing to its chemical instability, forming other more stable beryllium compounds. Most of the beryllium bearing compounds exhibit piezoelectric properties, especially the Na^+ and Bu^{+2} bearing beryllium silicates. For example, barylite crystals cannot be synthesized by the ordinary solid-state reaction. Maeda et al. (1991) obtained this crystal under the following conditions:

P = 500 bar

T = 385°C

ΔT = 15°C

Solvent = 3 M KOH

Baffle opening = 15%

Seed = Ba Be_2 Si_2 O_7 ceramics

Likewise, there are several such reports on the hydrothermal synthesis of beryllium bearing silicates and most of them exhibit interesting electronic properties.

7.9.3 Tourmaline

Tourmaline is a complex silicate of boron and aluminum with either magnesium, iron, or the alkali metals prominent. The general formula can be written as $XY{\cdot}Al_6{\cdot}[Be_6Si_6O_{27}(OH,F)_4]$, where X = Na, Ca, K; Y = Mg, Fe, Mn, Li, Al, etc. Tourmaline crystals exhibit pyroelectric properties and the importance of the seeded growth of tourmaline was realized during the 1940s. The basic interest lies in the colorless variety of

tourmaline for pyroelectric applications. The earliest attempts to obtain tourmaline single crystals were carried out through proper selection of nutrient and the solvent.[169][170] Robbins et al. (1963) have carried out the growth of tourmaline crystals using metastable glass of tourmaline composition and the given pressure-temperature diagrams of stability.[171] Voskresenskaya (1966), and Voskresenskaya and Barsukova (1967) have carried out the synthesis of colorless tourmaline on the seeds under hydrothermal conditions.[172][173] The above authors have carried out experiments in autoclaves with a volume of 200 cm^3 at temperatures 550–600°C and pressure 2000 atm., using platinum liners. A mixture of oxides or glass of tourmaline composition was used as the nutrient. Natural tourmaline was used as seed crystals. The growth was carried out in the acidic media from aqueous solutions H_3BO_4-NaCl (NaF). The concentration of boric acid was 5–10 wt%, NaCl ~ 2.5 wt%. The seed orientation was along the (0001) face, polar in character, and crystals usually developed simple forms (1011), (0221), and (0112).

7.9.4 Nepheline

ProBooks

Nepheline is an important mineral and has the orthosilicate formula $(Na,K)AlSiO_4$, with a framework of aluminosilicate having acentric space group $P6_3$. Nepheline is of interest as piezo- and pyroelectric material. The nepheline structure is related to "tridymite intercalation stones," which allows it to vary the Na/K ratio in a wide interval. In nature, nepheline usually occurs as small glassy crystals or grains. The natural nephelite always contains silica in excess and also small amounts of potassium. Nepheline can be easily prepared artificially by fusing its constituents together in the proper proportions. The earliest experiments on the artificial synthesis began in the 19th century. Friedel (1890) treated muscovite with NaOH or KOH solution and water at 200°C to 500°C and obtained nephelite.[174][175] The end members of this row are characterized by several polymorphs, and the nepheline structural type is characteristic for Na/K ratios from 1 to 0.5.

Nepheline, $NaAlSiO_4$, is stable in NaOH solutions with concentrations 3–15 wt% at temperatures more than 450°C. Increase in temperature results in the expansion of the stability field to 20–22 wt% at 500°C. At $400 < T < 450$°C, nepheline-hydrate-I and nepheline-hydrate-II form from artificial cancrinate and sodalite. However, under the same conditions, the nepheline phase is in equilibrium with solution if synthetic

nepheline is used as the starting material. The boundary nepheline hydrate, cancrinite, seems to be metastable. Nepheline (both synthetic and natural) is replaced by cancrinate at 200–300°C and NaOH concentrations greater than 3 wt%.[176][177]

Nepheline single crystals can be grown in the field of its thermodynamic stability as in the field of its instability at $300 < T < 400$°C if the growth process is initiated by nepheline seed. In the region of instability, single crystals of nepheline grow on the seed but hydrocancrinate, $Na_8Al_6Si_6O_{24}(OH)_2 \cdot nH_2O$, crystals grow on spontaneous nuclei. At $T >$ 450°C, nepheline and cancrinate grow simultaneously if there are seeds of both nepheline and cancrinate.

Single crystals of $(Na,K)AlSiO_4$ were grown in the system Na_2O-K_2O-Al_2O_3-SiO_2-H_2O using natural nepheline as a nutrient and as a material for seeds. To minimize the mismatch between the seed and the grown layer, the potassium was introduced into the starting NaOH-solution. As a result, the composition of grown layer was close to the composition of seed plates (Table 7.16).

Table 7.16. Chemical Composition of Natural and Artificial Nepheline

Compound	oxide contents, wt%							
	SiO_2	Al_2O_3	Fe_2O_3	FeO	MgO	CaO	Na_2O	K_2O
nepheline natural (starting material)	43.63	32.37	0.41	0.17	0.76	0.36	15.94	6.0
napheline artificial (grown layer)	41.55	34.47	0.74	—	0.10	—	16.77	5.98

The unit cell parameters are equal to: a = 12.64, c = 5.16 Å (seed material), a = 12.72, c = 5.12 Å (grown layer). At temperatures of 300–350°C in the growth zone, the regeneration of seed plates takes place with the formation of the following simple forms: hexagonal prism (1010), monohedra (0001) and (0001) and sometimes hexagonal pyramids (1011), (1012). The polar symmetry is observed rarely, and the external habit usually corresponds to the point group 6/m or 6/mmm. In this case, the growth morphology and growth rates of (0001) and (0001) faces are the same, which may be caused also by twinning. Specific cellular microstructure is observed in transmission light; the cell size is 1.5–3 mm.

The mean values of growth rates for different crystallographic directions are:

$\gamma(1010)$ – 0.04 mm/day

$\gamma(0001)$ – 0.12 mm/day

$\gamma(1011)$ – 0.4 mm/day

$\gamma(1011) > \gamma(1210) > \gamma(0001) \geq \gamma(0001) > \gamma(1010)$

The faces (0001) and $(10\bar{1}0)$ grow on spiral mechanisms, the faces of pyramid grow on normal mechanisms. Nepheline crystals exhibit interesting uni-dimensional ionic conductivity. It shows anamolously high dielectric constant parallel to c-axis.[178]

7.9.5 Zincosilicates

The earliest work on the hydrothermal synthesis of zincosilicates appeared during 1974.[179] The study of zincosilicates carries a special significance with reference to their crystal chemistry and phase stability, as they occur in nature under varying geological conditions. Zincosilicates phase formation in the system Na_2O-ZnO-SiO_2-H_2O has been studied in great detail by several workers.[179]–[182] The following zincosilicates have been identified in this system: $Zn_2[SiO_4]$-willemite, $Na_2Zn[Si_2O_6]$, $NaZn[SiO_4]$, $Na_2Zn[Si_3O_8]$, $Na_2Zn_3(SiO_4)_2$, and $Na_2Zn_2[Si_2O_7]$. Figure 7.33 shows the NC-diagram of fields of crystallization of various zincosilicate phases. Figure 7.34 shows the schematic diagram of various zincosilicate phase formations. Litvin proposed the following univariant equilibrium:[176]

$$Zn_2SiO_4 + 2Na_2O + 3SiO_2 \leftrightarrow 2Na_2Zn\ Si_2O_6$$

$$3Zn_2SiO_4 + 2Na_2O + SiO_2 \leftrightarrow 2Na_2Zn_3Si_2O_8$$

$$Zn_2SiO_4 + 2Na_2O + 5SiO_2 \leftrightarrow 2Na_2ZnSi_3O_8$$

$$Zn_2SiO_4 + Na_2O + SiO_2 \leftrightarrow Na_2Zn_2Si_2O_7$$

$$2Na_3Zn_3Si_2O_8 + Na_2O + 2SiO_2 \leftrightarrow 3NaZn_2Si_2O_7$$

$$Na_2Zn_2Si_2O_7 + Na_2O + 2SiO_2 \leftrightarrow 2Na_2ZnSi_2O_6$$

$$Na_2ZnSi_2O_6 \leftrightarrow Na_2ZnSiO_4 + SiO_2$$

$$Na_2ZnSi_3O_8 \leftrightarrow Na_2ZnSi_2O_6 + SiO_2$$

$$Na_2Zn_3Si_2O_8 + 2Na_2O + SiO_2 \leftrightarrow 3Na_2ZnSiO_4$$

$$3Na_2ZnSiO_4 \leftrightarrow Na_2Zn_3Si_2O_8 + SiO_2 + 2Na_2O$$

DropBooks

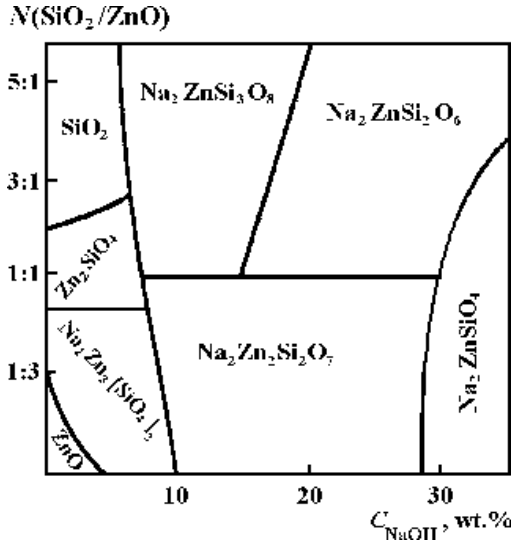

Figure 7.33. NC-diagram of fields of crystallization of various zincosilicate phases.[176]

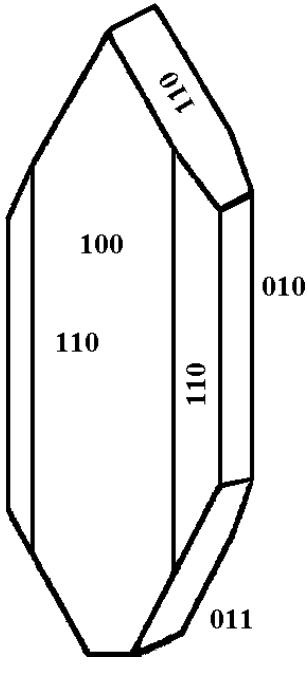

Figure 7.34. Schematic diagram of various zincosilicate phase formation.[176]

Zn_2SiO_4 (Willemite): Willemite crystallizes in pure water, in NaOH solution and in mixed solvents of NaOH + Na_2CO_3. The optimum conditions for spontaneous recrystallization of willemite are: NaOH: 4–6 wt%; T = 375–450°C; ΔT = 5–8°C, P = 400–600 atm. Single crystals of willemite grow in the form of a hexagonal prism. The fast growing face is the rhombohedral face (1120), the growth rate of which is 0.8–1.0 mm/day. When the concentration of NaOH increases beyond 10 wt%, the solubility of willemite increases and the formation of other phases begins. Also, when the NaOH concentration is 10 wt%, the boundaries of monomineralic synthesis move up to the ratio ZnO/SiO_2 = 1:2.5. Further increase in the concentration of the solvent increases the field of quartz. Willemite doped with active ions like Mn^{2+} exhibits excellent luminescence properties when exposed to UV radiation, and it is an excellent phosphor.

The field of crystallization of $Na_2ZnSi_3O_8$ falls in the silica rich region (Fig. 7.35). $Na_2ZnSi_3O_8$ crystallizes usually together with willemite, with an increase in the NaOH concentration, especially silica. $Na_2ZnSi_3O_8$ starts melting congruently and recrystallizes in the upper part of the autoclave. The presence of Na_2CO_3 helps crystals and increases the crystal size. The crystals of $Na_2ZnSi_3O_8$ could be obtained at temperatures 325–400°C, ΔT = 8 to 12°C, and P = 400–600 atm. Dipyramidal crystals with [100] and [110] faces grow under these conditions with a growth rate of 0.08 mm/day. The crystals exhibit piezoelectric effect like quartz. The crystals are colorless, transparent. The crystals doped with Mn^{2+} show good luminescence.

DropBooks

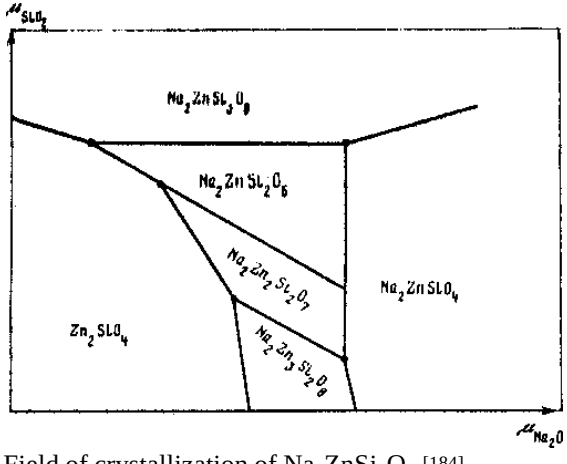

Figure 7.35. Field of crystallization of $Na_2ZnSi_3O_8$.[184]

$Na_2Zn_2Si_2O_7$: This crystallizes in 10–25% NaOH solutions at ZnO/SiO_2 > 1:1. If the concentration of ZnO increases to 7:1, this phase becomes unstable and transforms to $Na_2Zn_3[SiO_4]_2$. The crystals are thin plates—like at ZnO/SiO_2 = 2:1 to 1:1. With an increase in the ZnO in the nutrient, the crystals become thicker. The commonly seen faces are (100), (010), (210), (110), (101), and (111). Crystals are colorless, transparent, with glassy surfaces. The crystallization of $Na_2Zn_2Si_2O_7$ takes place in 15–18 wt% NaOH solution at T = 450°C, ΔT = 4–6°C, P = 400–600 atm. The growth rate is 0.3–0.5 mm/day along the direction [101].[183] The growth rate of the (001) face increases and becomes equal to the growth rate along other faces. These crystals show luminescence, and strong piezoelectric effect. Heating above 1090°C, $Na_2Zn_2Si_2O_7$ starts decomposing to ZnO and melt, and at 1325°C, it completely melts.

$Na_2Zn[SiO_4]$: Single crystals of sodium orthozincosilicate have been obtained in highly concentrated NaOH solution (30% NaOH) and it does not depend upon the ratio of the starting components. $Na_2Zn[SiO_4]$ dissolves congruently. The schematic diagram of the crystal morphology is shown in Fig. 7.37. The commonly observed forms are (100), (001), (110), and (011). Twinning is common. Crystals are colorless, Mn^{2+} rich crystals are green, Cu^{2+} rich crystals are blue. The Mn^{2+} doped $Na_2Zn[SiO_4]$ crystals show luminescence, and also significant piezoelectric effect. At T = 1060 ± 10°C, $NaZn[SiO_4]$ undergoes phase transition.

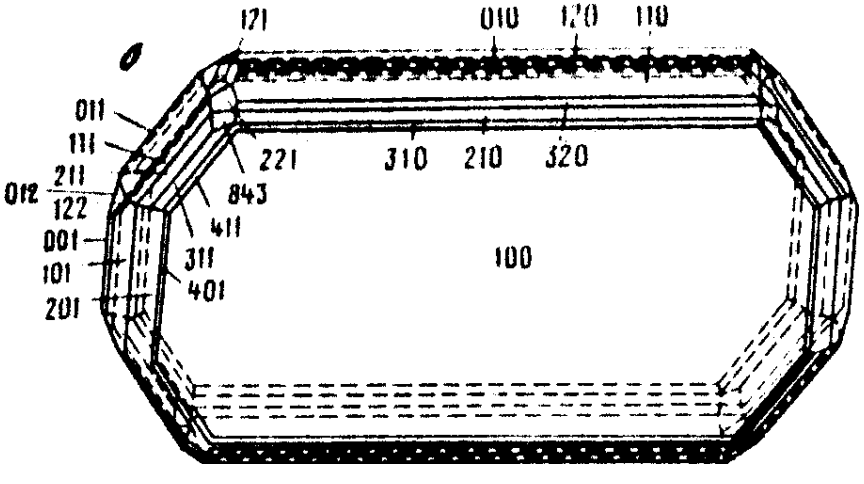

Figure 7.36. Schematic diagram of the crystal morphology.[184]

Synthetic sodium zincosilicates are a new group of crystallophosphor materials. Sodium zincosilicates doped with Mn^{2+} exhibit stronger luminescence. Also, $Na_2Zn_2[Si_2O_7]$, $Na_2Zn[Si_3O_8]$, and $Na_2Zn[SiO_4]$ show stronger piezoelectric effect than quartz. However, the basic problem is the growth of large size single crystals.

Several other compounds crystallize from the system Na_2O-MO-SiO_2-H_2O (where M = Cd, Ca, Ba, and Mn). Amongst them, the Cd and Mn bearing silicates show interesting physical properties.[176][184]–[187] Similarly, the Ca-bearing silicates carry great geological significance and such systems are being studied extensively.[188]–[191]

Several phases crystallize in the Na_2O-CaO-SiO_2-H_2O under hydrothermal conditions. Figure 7.37 shows the NC-diagram of crystallization in the system Na_2O-CaO-SiO_2-H_2O. Following are the important phases crystallizing in this system: $Ca[SiO_3]$, $Ca_6[Si_6O_{17}](OH)_2$ (xonolite), $Ca_5[SiO_4]_2$ x $(OH)_2$ (khondrodite), $Ca_6[Si_4O_{14}]$ (kilkhoanite), $Ca_8[Si_5O_{18}]$ (orthorolite), $Ca_6[SiO_4]$ $[Si_2O_7](OH)_2$ (dellaite), etc.

DropBooks

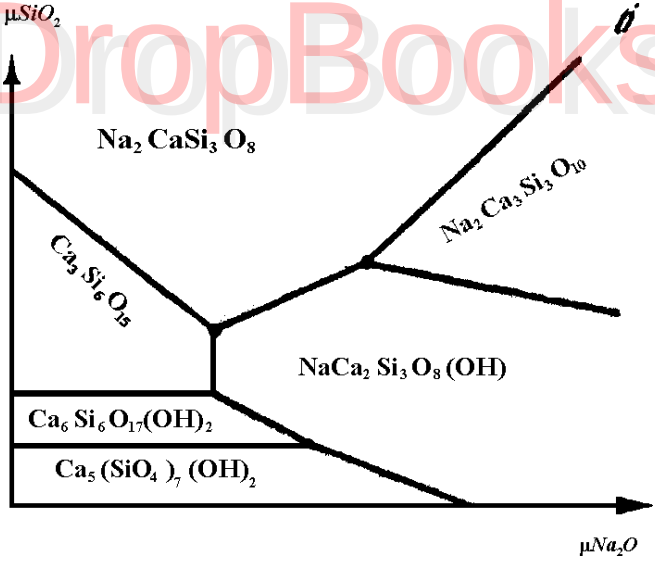

Figure 7.37. NC–diagram of crystallization in the system Na_2O-CaO-SiO_2-H_2O.[184]

The studies of the crystallization of monocationic calcium silicates reveal that they are formed in at least two ways:

i. Interaction of soluble silica with calcium compound (through neutralization reaction).

ii. Interaction of aqueous solutions of silica with amorphous or crystalline portlandite.

The ratio of SiO_2/CaO (degree of silification) regularly increases $0.5 \rightarrow 0.75 \rightarrow 1.0$. [Si-O] radical leads to the transition from discrete ortho-, diortho- group to infinite chains and then infinite ribbon $[Si_6O_{17}]_\infty$. In most of the experiments quartz also crystallizes together with xonotlite.

In the second case, the degree of silification increases insignificantly ($0.33 \rightarrow 0.4 \rightarrow 0.62 \rightarrow 0.66$) and morphotropic transitions in [Si-O] radical takes place as follows: $[SiO_4] \rightarrow [SiO_4]_2\,[Si_3O_{10}] \rightarrow [SiO_4][Si_3O_{10}]$.

Nd^{3+} doped $Ca_2Al_2SiO_7$ (gehlenite) is an efficient new laser material,[192] since its structure exhibits some disorder and can accept active rare earth ions. The unit cell is tetragonal (melilite type) with special group $P42_{1m}$. Figure 7.38 shows the Na^{3+} emission spectrum corresponding to the $^4F_{3/2} \rightarrow {}^4I_{11/2}$ transition *a)* in gehlenite, and *b)* in YAG.

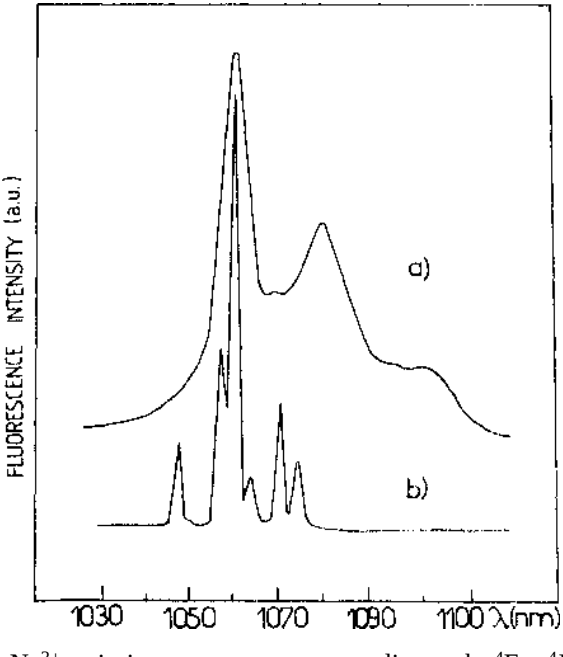

Figure 7.38. Na^{3+} emission spectrum corresponding to the $^4F_{3/2}\,{}^4I_{11/2}$ transition in *a)* gehlenite and in *b)* YAG.[192]

In the system Na_2O-BaO-SiO_2-H_2O under hydrothermal conditions below 350°C, two phases crystallize: $BaSiO_3 \cdot nH_2O$[193] and $BaSi_2O_5 \cdot 3H_2O$,[194] in the $BaCl_2$ + $Na_2H_2SiO_4$ solution, the low temperature of growth and the nature of the solution does not form silicates when BaO/SiO_2 > 1:1. At temperatures 450–550°C, pressures 400–1200 atm, and BaO/SiO_2 from 7.5:1 to 1:10, the following phases form: $BaSiO_3$, $Ba_2Si_3O_8$, $BaSi_2O_5$ (sanbornite) and $Ba_5Si_4O_{12} \cdot (OH)_2$, Na $Ba_3Si_2O_7 \cdot (OH)$.[195] Figure 7.39 shows NC-diagram of crystallization in the system Na_2O-BaO-SiO_2-H_2O, and Fig. 7.40 shows the schematic diagram of the crystal morphology of the barium silicates. From the NC-diagram, the boundaries of crystallization of $BaSi_2O_5$ and $BaSi_3O_8$ are controlled only by NaOH concentration. Further, the boundaries between monocationic barium silicate and quartz depends only on the concentration of $Ba(OH)_2$ ($M_{Ba}O$). All the transitions to $NaBa_3Si_2O_7$ (OH) are controlled mainly by the concentration of NaOH. Mn^{2+} doped $BaSi_2O_5$ shows luminescence.

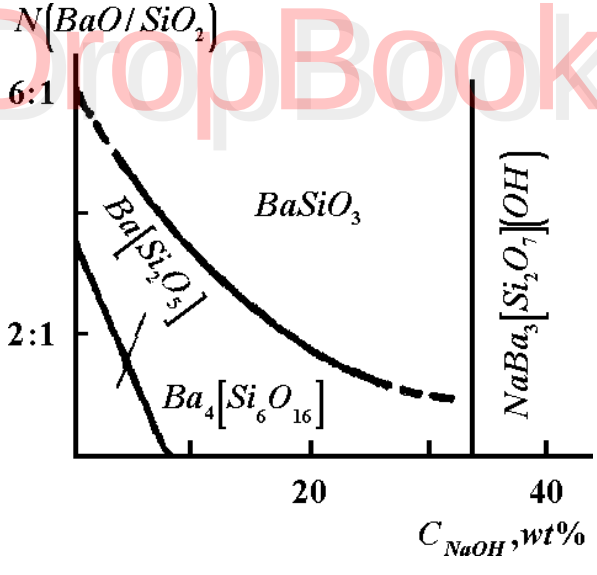

Figure 7.39. NC-diagram of crystallization in the system Na_2O-BaO-SiO_2 - H_2O.[195]

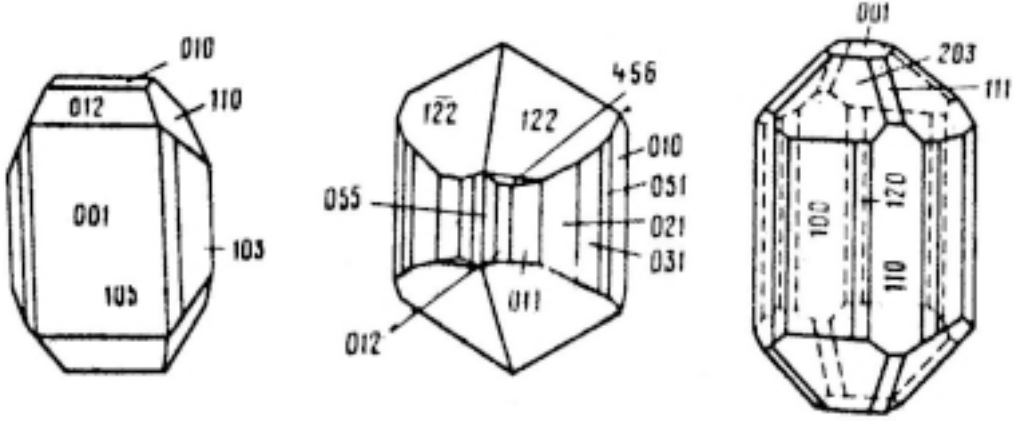

Figure 7.40. Schematic diagram of the crystal morphology of the barium silicates.[184]

The other important system Na_2O-MnO-SiO_2-H_2O gives the following phases under hydrothermal condition: Mn_7SiO_{12} (braunite), $Mn(OH)_2$ (pyrochroite), Mn_2SiO_4 (tephroite), $Na_2Mn_7Si_8O_{24}$, $Na_2Mn_6Si_7O_{21}$, $Na_2Mn_3Si_4O_{12}$, $Na_2Mn_2Si_2O_7$, Na_2MnSiO_4, $Na_6Mn_3Si_6O_{18}$, $Na_2MnSi_8O_{18}$, $Na_2Mn_7(SiO_3)_8$, $Na_2Mn_8O_{16}\cdot nH_2O$. Several of them occur in nature as minerals. Figure 7.41 shows the NC-diagram of crystallization of the system Na_2O-MnO-SiO_2-H_2O.[196] Most of these phases belong to the lower symmetry classes (monoclinic and orthorhombic) and some of them are excellent luminiscent materials. Further, these compounds crystallize at $T > 400°C$ and $MnO/SiO_2 > 1$. These compounds can be obtained using alkaline solutions, NaOH (< 20%). The major difficulties concerning this system are associated with the change in the valency of Mn^{2-} to Mn^{4+}.[197]

A majority of these sodium manganese silicates—$Mn_2[SiO_4]$, $Na_2Mn_2[Si_2O_7]$, $Na_2Mn(SiO_4)$, $Na_2Mn_7(SiO_3)_8$, $Na_6Mn_3(Si_6O_{18})$—show useful physical properties. Some of them have been obtained as single crystals using spontaneously grown crystals as seeds.[198]

DropBooks

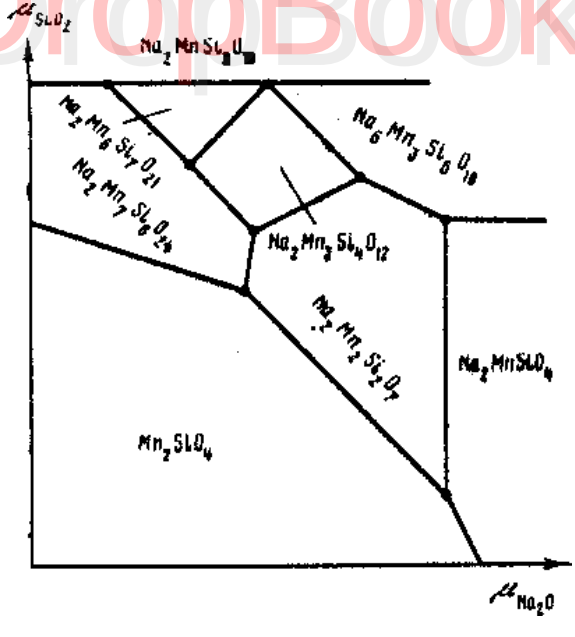

Figure 7.41. NC-diagram of crystallization of the system Na_2O-MnO-SiO_2-H_2O.[196]

7.10 HYDROTHERMAL GROWTH OF LITHIUM SILICATES

Lithium aluminum silicate systems are being studied extensively because of their ultra-low thermal expansion and their geological importance. Almost all the natural lithium aluminosilicates have been synthesized, together with a number of artificial lithium compounds with no natural analogs. However, the only exception is α-spodumene, which has never been synthesized with an adequate degree of reproducibility, in spite of high pressure-temperature conditions of synthesis (T = 600°C, P = 4000 atm).[199][200] In the Li_2O-Al_2O_3-SiO_2-H_2O system, in temperature range 400–700°C and at pressures of up to 9000 atm, α-eucryptite, β-spodumene, petalite, lithium silicate, and α-spodumene have been synthesized over a wide range of pH.[201] Instead of α-spodumene, others—like eucryptite, β-spodumene, petalite, and a number of artificial lithium compounds—have been obtained.

The results of the foregoing investigations lead to the conclusions that *(a)* spodumene is formed at pressures of over 4000 atm as indicated, in particular, by the fact that all the phases synthesized have lower densities than that of α-spodumene, and *(b)* isomorphic impurities reduce the minimum pressure required for the formation of α-spodumene.

Pure LiCl solutions at 400–700°C and pressures of 750–3000 atm, we may synthesize α-eucryptite $LiAlSiO_4$, β-spodumene β-$LiAlSi_2O_6$, and petalite $LiAlSi_4O_{10}$. The α-eucryptite is mainly formed for high Al_2O_3/SiO_2 ratios in the original charge (~ 1:1), β-spodumene for smaller ratios (1:2 to 1:3), and petalite for a high concentration of silica (ratio A/S ~ 1:8). In the neighborhood of the ratio Al_2O_3/SiO_2 ~ 1:5, we observe paragenesis of β-spodumene and quartz.

The concentration of LiCl solutions, and the temperature and pressure within the limits indicated, have little effect on phase formation in the LiCl-Al_2O_3-SiO_2-H_2O system.

The pH of the solution, together with the Al_2O_3/SiO_2 ratio, constitutes the second most important factor in the crystallization. Reducing the alkalinity of the solution (in LiCl + HCl solutions) has practically no effect on the phase formation, but on increasing the alkalinity (in LiCl + LiOH or LiOH solutions) new compounds appear and the ranges of crystallization of the phases already noted alter. First of all, lithium silicate Li_2SiO_3 appears. For a ratio of Al_2O_3/SiO_2 = 1:1 lithium silicate is synthesized for high values of the alkalinity, but with increasing concentration of SiO_2 in the original mixture the range of its stability moves in the low pH direction

(Fig. 7.42). In alkaline solutions the field of formation of petalite also widens, and the latter is synthesized for higher Al_2O_3 /SiO_2 ratios (~ 1 : 2 for pH > 10) than in LiCl solutions. The range of existence of β-spodumene, on the other hand, contracts slightly on increasing the alkalinity (Fig. 7.42), and for pH > 10 it becomes unstable, being replaced by α-eucryptite and lithium silicate.

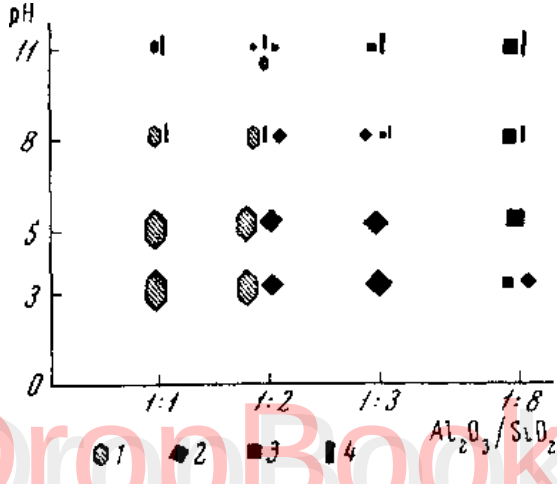

DropBooks

Figure 7.42. Fields of stability of lithium silicates in relation to the pH of the solution and the ratio of the original charge components at T = 600° to 700° and P = 2000–3000 atm. *(1)* α-$LiAlSiO_4$; *(2)* β-$LiAlSi_2O_6$; *(3)* $LiAlSi_4O_{10}$; *(4)* Li_2SiO_3.[201]

The densest of all phases synthesized is α-spodumene, which clearly indicates that the stability range lies at much higher pressures. In other words, at pressures of under 4000 atm and in the absence of impurities, no spodumene is formed. The commonly used impurities are Cr^{3+} and Fe^{3+}. The α-spodumene is synthesized in LiCl solutions at pressures over ~ 6000 atm. At lower pressures, it decomposes into α-eucryptite and β-spodumene. The partial replacement of Al^{+3} by Cr^{+3} reduces the lower limit of pressures for the formation of spodumene; spodumene containing traces of Cr^{3+} grows on the seed at 3000 atm. A complete replacement of Al_2O_3 by Fe_2O_3 or Cr_2O_3 leads to the synthesis of iron and chromium spodumene in the low-pressure range: ~ 250 and ~ 750 atm respectively. Figure 7.43 shows the characteristic photographs of α-eucryptite and β-spodumene crystals.[201]

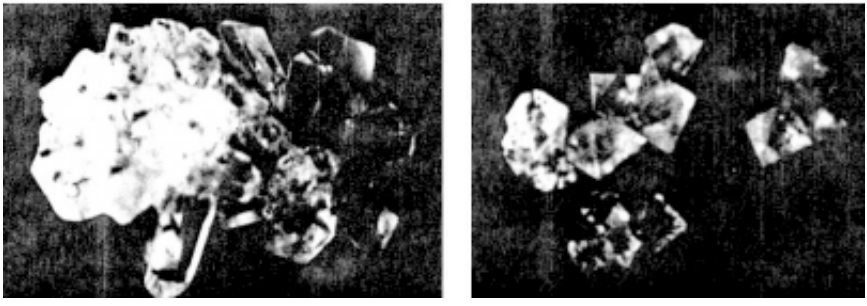

Figure 7.43. Characteristic photographs of α - eucryptite and β - spodumene crystals.[201]

Ghobarkar (1992) has studied the hydrothermal synthesis of petalite mineral phases and their morphological changes with temperature in great detail.[202] Here, petalite minerals were synthesized hydrothermally at different temperatures from a glass with the composition Li_2CO_3:Al_2O_3:SiO_2 = 1:1:8. It was found that the development of the mineral phases and the volume and habit of crystals depended on the rise of temperature from 410°C to 490°C, α-petalite crystallized in the monoclinic system with a constant change in the habit. α-petalite splits into quartz and an orthorhombic β_1-petalite from 490°C onwards. The tetragonal phase of petalite forms from 560°C to 750°C with changes in the habit.

Thus, the hydrothermal synthesis of lithium silicates is a challenging field in hydrothermal research.

7.11 HYDROTHERMAL GROWTH OF GERMANATES

Germanates form an important group of inorganic compounds having a close proximity to the silicates in many respects. The ionic radii of both Si^{4+} (0.39Å) and Ge^{4+} (0.44 Å) are closer to one another. The natural germanates are very few and, hence, their synthetic analogs permit to understand their structures, crystal chemistry, physico-chemical conditions, etc. In nature germanium usually occurs in the form of isomorphous admixtures in some relatively rare minerals (samarskite, tantalite, gadolinite, germantite, etc.) Individual germanium minerals or germanates are rather rare or very few, especially in some sulphides and sulphates.[203]–[205]

Germanates could be obtained both by flux and hydrothermal methods. However, just like silicates, even germanates insists hydrothermal conditions for the formation of a large variety of anionic groups. The flux grown germanates are very few and are represented by [GeO_4] and [Ge_2O_7] anionic groups, whereas the hydrothermally grown germanates do contain a large variety of anionic groups like [GeO_4], [Ge_2O_7], [Ge_4O_{13}], [Ge_3O_{12}], [$Ge_{10}O_{25}$], [Ge_3O_{12}], [Ge_5O_{16}], etc. These germanates with different cations can be obtained at rather lower parameters (T = 500°C, P = 1500–2000 atm). Under such conditions germanates can occupy both tetrahedral and/or octahedral position in the structure. The fixation of Si in octahedral coordination demands much higher pressure (> 10 kbar). This fact reveals an important aspect of the study of germanates crystallization, because the germanates obtained under lower *PT* conditions may be the analogs of silicates formed in the earth crust at greater depths.

The growth of germanates began as an attempt to synthesize silicates analogs during the middle of this century. Onishi (1956) and Wardani (1957) studied the geochemistry of germanium in detail.[203][204] Just like in silicates, even in germanates, we can have two types: *1)* germanates containing rare earth elements, and *2)* germanates without rare earth elements. The phase formation and crystal chemical elucidation of the germanates have been discussed in general here.

DropBooks

The natural compounds of germanium and rare earth elements are practically absent and only their synthesis allows one to study their structures, crystal chemistry, and physical and chemical characteristics in detail. Under such conditions germanium can occupy both tetrahedral and (or) octahedral positions in the structure. The fixation of Si in octahedra (coordination number 6) demands much higher pressure (more than 10 kbar). This fact reveals an important aspect of the study of rare earth germanate crystallization, because the germanates obtained under lower temperatures and pressures may be the analogs of silicate phases formed in the earth crust at large depth (high-pressures phases). The classification of germanates containing rare earth elements differ slightly from that of the silicates containing rare earth elements.

For germanium, like silicon, a tendency to form chains has been noticed. For silicon, both hydrides and halogenides have been obtained, but germanium forms only halogenides with the bond Ge-Ge.

GeO_2 is largely analogous to SiO_2, and it may form glass while cooling from the melt. One of the polymorphic modifications of GeO_2 at 1033°C has quartz structure. This GeO_2 modification becomes metastable

at < 1053°C. The stable modification of GeO_2 has the characteristic rutile, TiO_2 type structure.

Germanium may exist in solutions as a negatively charged ion and forming sulphides and tiosalts differs from silicon, but at the same time germanates and fluorogermanates are often isostructural with the corresponding silicates. Among rare earth germanates, we have alkali-free germanates and alkali rare earth germanates.

7.11.1 Rare Earth Germanates

There are some known representatives of rare earth germanates: $Ln_{4.67}[GeO_4]_3O$, $Ln_4[GeO_4]O_4$, $Ln_{13}[GeO_4]_6$ [O, (OH, F)$_2$]$_6$, $Ln_2Ge_2O_7$ (two structure types), Ln_2GeO_5 (three structure types) [206] The experiments in the system Ln_2O_3-GeO_2-R-H_2O resulted in obtaining new types of germanates (Table 7.17). Two of them correspond to the silicates structures, six germanates belong to new structure types. The crystallization of germanates was carried out at rather high AOH (AF) concentration, but alkali cations took part only in intermediate stages of the synthesis processes (solution, transport) as mineralizers. In the final composition of rare earth germanates the alkali cations were absent. The common features of all germanates obtained was the prevalence of rare earth component in comparison with germanium, $1 \leq Ln/Ge \leq 4$ (Table 7.17). For most of the new structure types, the presence of morphotropic rows are characteristic (Table 7.18). The compound $Ln_4Ge_3O_9(OH)_6$ has been found in the systems with ten rare earth elements. The structural type $Ln_3GeO_5(OH)_3$ is characteristic for eight rare earth elements. Structure formation of most rare earth germanates demands some additional anionic groups (OH, F), which usually enter into the coordination polyhedra of rare-earth cation. Crystal-chemical analysis of new rare earth germanates revealed some interesting features of their structures.

The phase formation in the system M^+_2O-R_2O_3-GeO_2-H_2O (where M = Li, Na, K, Rb, Cs; R= rare earth elements) has been studied extensively. Like in silicate systems, even in the germanate system the phase formation is determined by the type of rare earth cation and the ratio of R_2O_3/GeO_2 in the nutrient and the concentration of the solvent. In the system Na_2O-R_2O_3-GeO_2-H_2O, the following phases have been identified: La and Pr form $Na_2RGeO_4(OH)$; Nd and Sm form $NaR_3[GeO_4]_2$ $(OH)_2$, and the rest of the elements (Eu-Lu,Y) form $NaRGeO_4$ crystallizing in the rhombohedral modification (Figs. 7.44 and 7.45). For all three phases, the

Table 7.17. New Structure Types of Alkali-free Germanates of Rare Earth Elements[206]

Compound	Solvent Concentration wt%	Unit cell parameters			Space group	Coordination number of Ge; Ge-O radical
		a, Å	b, Å	c, Å		
$Y_7Ge_2O_{12}(F, OH)_5$	KF 25 %	5.551	11.283	12.131 γ = 108.81°	A2/m	4; $[GeO]_4$
$Sm_4Ge_3O_9(OH)_6$	CsOH	15.145	10.909	7.161	Cmcm	4; 6;$[Ge^{IV}Ge_2^{VI}O_9]$
$Y_4GeO_6(OH, F)_4$	KF	5.618 α=91.45°	6.276 β=109.44°	6.885 γ=111.24°	P1	4; $[GeO_4]$
$Gd_3GeO_5(OH)_3$	RbOH 30–50%	5.510	6.011	10.277 γ=104.89°	$P2_1/m$	5; $[GeO_5]$
$Sm_3GeO_5(OH)_3$	RbOH 30–50%	5.526	6.104	10.328 γ=104.76°	$P2_1/m$	5; $[GeO_5]$
$Dy_3GeO_5(OH)_3$	CsOH 40%	5.481	5.920	10.215 γ=105.02°	$P2_1/m$	5; $[GeO_5]$
$Gd_4Ge_3O_{11}(OH)_2$	CsOH 40%	6.713 α=62.19°	9.349 β=73.67°	10.128 γ=69.05°	P1	4;$[Ge_2O_7]$ + $[GeO_4]$
$Er_{13}Ge_6O_{31}(OH,F)$	CsOH	15.617	—	9.398	R3	4; $[GeO_4]$
Nd_4GeO_8	NaOH	7.475	5.727	17.927	$Pmc2_1$	4; $[GeO_4]$
$Yb_2Ge_2O_7$	KF 25%	9.827	—	—	Fd3m	4; $[GeO_4]$

DropBooks

Table 7.18. New Series of Alkali-free Rare Earth Germanates[206]

	Ce	Pr	Nd	Pm	Sm	Eu	Gd	Tb	Dy	Ho	Er	Tm	Yb	Lu	Y
$Ln_4GeO_6(OH, F)_4$															+ +
$Ln_7Ge_2O_{12}(F,OH)_5$															+ +
$LN_4Ge_3O_9(OH)_6$					+ +	+ +	+ +	+ +	+ +	+ +	+ +	+ +	+ +	+ +	
$Ln_3GeO_5(OH)_3$					+ +	+ +	+ +	+ +	+ +	+ +	+ +				
$Ln_4[Ge_2O_7][GeO_4](OH)_2$						+ +									
Ln_4GeO_8		+ +										+ +	+ +	+ +	
$Ln_{13}Ge_6O_{31}F$						+ +					+ +				
$Ln_2Ge_2O_7$ (cubic)													+ +	+ +	+ +

structure-genetic relation is olivine-like ribbon, which reflects the corresponding rare earth element motif, phase transitions: $Na_2RGeO_4(OH) \rightarrow NaR_3[GeO_4]_2(OH)_2 \rightarrow NaRGeO_4$ from Lu to La (NaOH = 20–40%) is accompanied by the rearrangement of only cationic motif and expressed in the redistribution of Na and R in olivine-like ribbon (Fig. 7.46).

Thus, the structural elucidation of the rare earth silicates and germanates in the R_2O_3 rich region of synthesis, shows that the structure determining factors are the *3-d* arrangement of rare earth polyhedra and the stability of which depends upon the NaOH solution. For lighter rare earth elements the *3-d* arrangement remains stable even at higher concentration of NaOH. However, the *3-d* arrangement loosens at the expense of the enrichment of Na-Polyhedra, e.g., structures of $NaNdSiO_4$ and $Na_2PrSiO_4(OH)$.

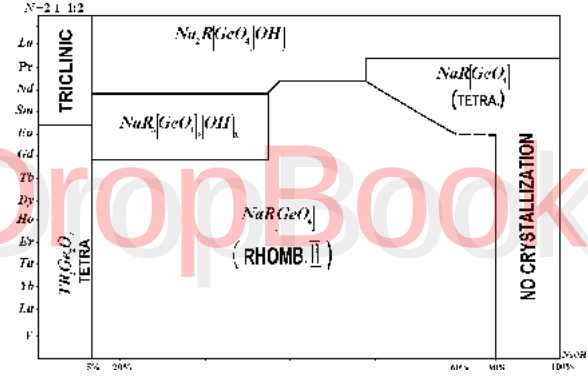

Figure 7.44. NC-diagram for sodium rare earth germinate system: $T = 450°C$.[206]

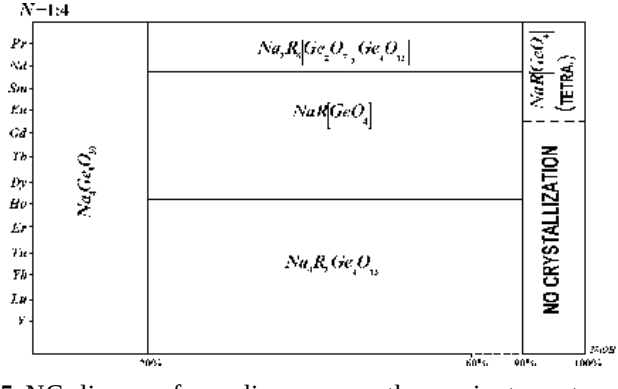

Figure 7.45. NC-diagram for sodium rare earth germinate system: $T = 650°C$, $P = 400–2500$ atm.[206]

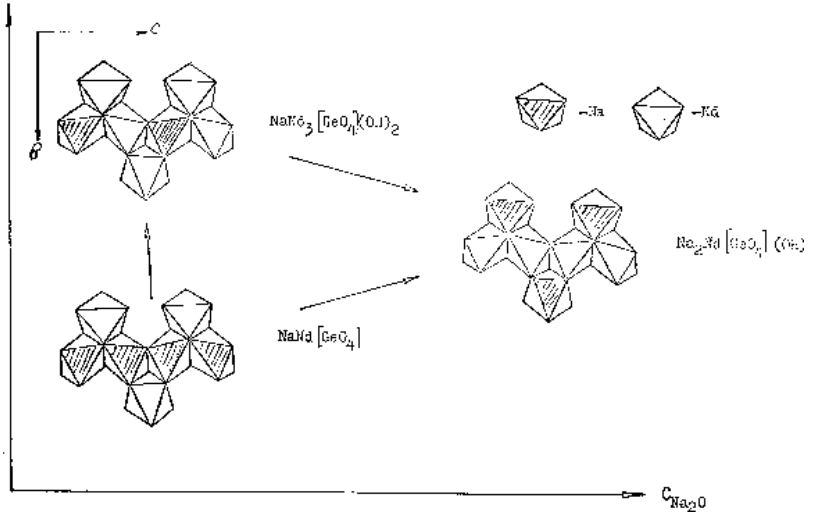

Figure 7.46. Change in rare earth motif during phase transition.[206]

For heavier rare earth elements, in which the amphoteric character is sufficiently strong, the decondensation of the cationic motif occurs from *3-d* bonding britolite up to *2-d* network $[R_2O_8]_{\infty\infty}$ and at the end discrete polyhedra-octahedra in $Na_3RSi_2O_7$. The same picture appears even for germanates. However, there is some variation from silicate systems, which are absent in germanates, wherein the rare-earth elements lie as discrete polyhedra. For example, among germanates the structure type $Na_3RSi_2O_7$ does not exist. The second important structure elucidation among germanates is connected with more of olivine type structures. Therefore, rare earth germanates are the closer analogs of silicates.

A detailed work on the system Na_2O-R_2O_3-GeO_2-H_2O indicates that with surplus R_2O_3 in the nutrient (GeO_2/R_2O_3 = 1:1 to 1:4) for groups La–Gd, three types of germanates form: $NaR_3Ge_2O_8(OH)_2$, $NaRGeO_4$, and $Na_2RGeO_4(OH)$. Their synthesis takes place with temperature gradient. $NaR_3Ge_2O_8(OH)_2$ crystallizes within a narrow interval of GeO_2/R_2O_3 ratio = 2.5:1–1.75:1 with NaOH concentration 5–42 wt% and 100% output. Crystals of 4–6 mm size, commonly as equi-dimensional crystals with pinacoidal and rhombohedral prisms belonging to the olivine type structure are formed.

$NaRGeO_4$ crystallizes over a broad field and the GeO_2 / R_2O_3 = 2:1–1:1 in the NaOH solutions of 5–80 wt% with 100% output. Crystals of 5 mm size have been obtained. This compound belongs to the structure

type olivine. At lower pressures and temperatures (P = 3–20 atm and T = 558–650°C) in the NaOH rich region (>80 wt%) for groups Nd-Eu, phases belong to the tetragonal modification and the crystals are plate-like, thick, 1–2 mm in size, and twinning is common.

$Na_2RGeO_4(OH)$ (where R = La-Nd) crystals form at GeO_2/R_2O_3 = 1:2 and concentration of NaOH > 6 wt%. Crystals have equi-dimensional habit. Output of 100% was obtained in solutions when H_2O < 10 %. $Na_2R[GeO_4](OH)$ belongs to the olivine type structures. Thus, for La-Gd group of germanates of olivine type structures in NaOH solution the following scheme, with an increase in the concentration of NaOH has been proposed:

Eq. (13) $NaR_3[GeO_4]_2(OH)_2 \rightarrow NaR[GeO_4] \rightarrow Na_2R[GeO_4](OH)$

In spite of the rearrangement of Na^+ and rare earth cations, common olivine type motif is retained over a wide interval not only on the concentration of NaOH, but also the ratio of GeO_2/R_2O_3. When GeO_2/R_2O_3 > 3:1 in 20–90 wt% NaOH solutions' complex germanates like $Na_2R_6Ge_8O_{26}$ appear for Nd and Pr representatives. However, the output is < 10 % and crystals are small (< 1 mm).

When Dy-Lu are used, a slightly different picture is seen. $NaR_2Ge_4O_{10}$ (OH), $NaRGeO_4$ and $Na_4R_2Ge_4O_{13}$ are the characteristic phases. $NaR_2Ge_4O_{10}(OH)$ phase crystallizes in < 10 wt % NaOH with GeO_2/R_2O_3 = 1:2.5–1:3.

$NaRGeO_4$ -Orthogermanates crystallize in the R_2O_3 rich region in the system Na_2O-R_2O_3-GeO_2-H_2O.

In GeO_2 rich region, for Dy-Lu groups $Na_4R_2Ge_4O_{13}$ is the characteristic phase with 100 % out put in 30–60 wt% NaOH solutions at ratio GeO_2/R_2O_3 = 2.5:1–3:1. The crystals are up to 2 mm in size.

Similarly, the rare earth germanates have been synthesized using aqueous solutions of KOH and KF.[206] Unfortunately, Output of 100% has not been obtained for several germanates. Quite often two or three phases crystallize simultaneously. All the KR-germanates have been grouped into two structure types: $K_2R_4[Ge_4O_{13}](OH,F)_4$, and $K_4R_2[Ge_4O_{13}](OH,F)_4$. Figure 7.47 shows the phase formation of rare earth germanates in the aqueous solution of KF. $K_2R_4[Ge_4O_{13}](OH,F)_4$ covers Nd-Tb rare earth cations, and the second group covers Er-Lu. When R_2O_3/GeO_2 ratio is < 1:1, the resultant product always carries $K_4Ge_9O_{20}$ in the form of hexagonal prism and plates. Surplus R_2O_3 gives K_2RF_5 (R = Tb-Lu) and

PropBooks

related phases. The boundaries of the appearance of fluorides depend upon the concentration of K and the type of rare earth ion. The expansion of the boundaries of K_2RF_5 and $K_2R[Ge_4O_{13}](OH,F)_4$ slowly moves towards La and KF solution concentration > 45 %, and the crystallization of germanates practically ceases. The crystal size decreases sharply towards the heavier rare earth elements, so that the Tb representative cannot be obtained as good single crystals of sufficiently large size. For Er-Lu groups $K_4R_2[Ge_8O_{20}](OH,F)_2$ type is obtained. The refinement of $K_4Yb_2[Ge_8O_{20}](OH,F)_2$ structure revealed $[Ge_8O_{20}]$ radical. The rare earth motif is represented by the infinite chain from rare earth octahedra shared at the vertices.

The scandium bearing system has been studied in detail. Despite the fact that it does not cover a wide range of germanates the commonly observed phases are for example, $KScGe_2O_6$, $K_2Sc_2Ge_2O_7(OH)_2$, $Sc_2Ge_2O_7$, $Na_4Sc_2Ge_4O_{13}$, $Na_2ScGeO_4(OH)$, $NaScGe_2O_6$, etc. in the K_2O-Sc_2O_3-GeO_2-H_2O and Na_2O-Sc_2O_3-GeO_2-H_2O systems respectively.[35][206] Most of these phases crystallize independently depending upon the GeO_2/Sc_2O_3 ratio and the concentration of the alkaline solution. Figure 7.48 shows the NC diagram of crystallization of various phases in the K_2O-Sc_2O_3-GeO_2-H_2O system. Figure 7.49 *(a–f)* shows the characteristic photographs of rare earth germanates.[206] Tables 7.19 and 7.20 give the structure types of alkali-free rare earth germanates, and structure types of alkali-, and alkaline earth rare earth germanates, respectively.

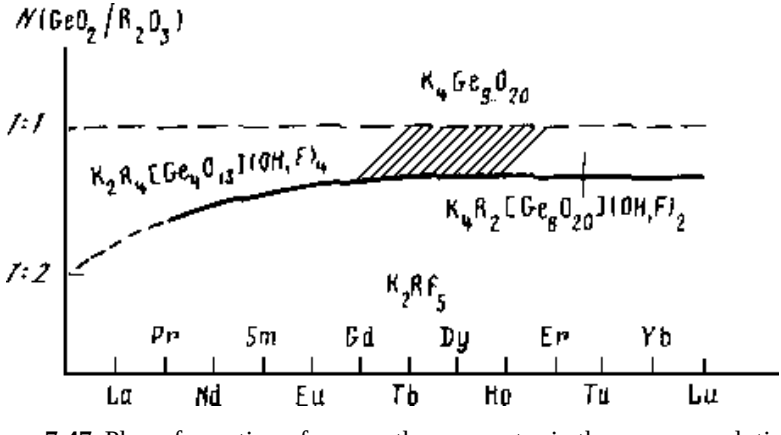

Figure 7.47. Phase formation of rare earth germanates in the aqueous solution of KF.[206]

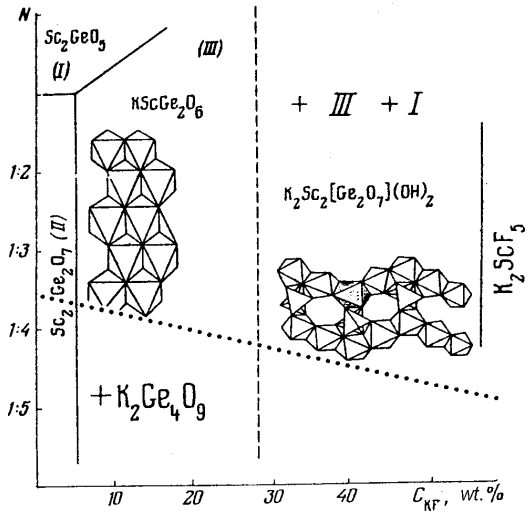

Figure 7.48. NC-diagram of crystallization of various phases in the K_2O-Sc_2O_3-GeO_2-H_2O system.[35]

DropBooks

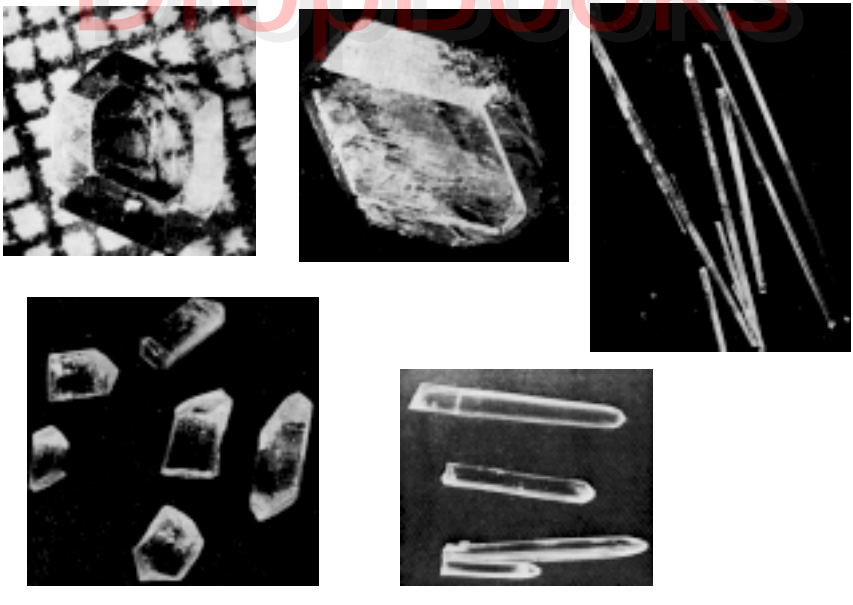

Figure 7.49. The characteristic photographs of rare earth germanates.[206] *(Courtesy of L. N. Demianets.)*

Table. 7.19. Structure Types of Alkali-free Rare Earth Germanates[206]

Compound	Representative	Cell parameter (Å)	Rare Earth, Co. No., Average bond distance Å			Tetrahedral radical form	Rare earth polyhedra
$R_2[GeO_4]O$ R =La-Tb	$Sm_2[GeO_4]O$	$P2_1/c$ z = 4 a = 9.4 b = 7.2 c = 6.9 β = 108°				orthotetra-hedra	framework
$R_2[GeO_4]O$ R =Dy-Lu,Y	$Er_2[GeO_4]O$	B2/ b z = 8 a = 14.86 b= 10.56 c = 6.83 γ =122.10°				orthotetra-hedra	framework
	$Sc_2[GeO_4]O$	B2/ b z = 8 a = 10.927 b = 10.656 c = 10.486 γ = 93.96	Sc	6	2.09	orthotetra-hedra	framework
$R_4[GeO_4]_4$ R =La-Gd	$La_4[GeO_4]O_4$	hexagonal a = 10.54 c = 7.63				orthotetra-hedra	
$R_4[GeO_4]_4$ R = Tb-Lu,Sc	$Nd_4[GeO_4]O_4$	$Pmc2_1$ z = 4 a = 7.475 b = 5.757 c = 17.927	Nd	8	2.50	orthotetra-hedra	framework
$R_{4.67}[GeO_4]_3O$ R = La-Dy	$Dy_{4.67}[GeO_4]_3O$	$P6_3/m$ z = 2 a = 9.200 c = 6.808	Dy Dy	7 9	2.33 2.40	orthotetra-hedra	framework
H type $R(OH)_3$ $6R_2$. $[GeO_4][O,(OH,F)_2]$ R = Nd-Eu	$Sm(OH)_3 \cdot 6Sm_2 \cdot$ $[GeO_4][O,(OH,F)_2]$	$P6_3/m$ z = 2 a = 15.90 c = 6.98	Sm Sm	7 9	2.51 2.48	orthotetra-hedra	framework

(Cont'd.)

Table. 7.19. *(Cont'd.)*

Compound	Representative	Cell parameter (Å)	Rare Earth, Co. No., Average bond distance Å			Tetrahedral radical form	Rare earth polyhedra
$R_2Ge_2O_7$ R =Tb-Lu	$Er_2Ge_2O_7$	P4$_1$2$_1$2 z = 4 a = 6.778 c =12.34	Er	7	2.32	diortho-groups	framework
	$Sc_2Ge_2O_7$	C2/m z = 2 a = 6.56 b = 8.690 c = 4.900 β = 102.5°				diortho-groups	layers from 6-mem bered
$R_4[Ge_3O_{10}]$ $[GeO_4]$ R = La-Pr	$La_4[Ge_3O_{10}]$ $[GeO_4]$	P1 z = 4 a =12.76 b = 7.070 c = 7.006 α = 90.95° β = 90.35° γ = 94.10°	La	8	2.56	triortho-group	framework
$R_4[Ge_3O_{10}]$ $[GeO_4]$ R = Nd-Gd	$Gd_4[Ge_3O_{10}]$ $[GeO_4]$	P1 z = 6 a =18.50 b = 6.800 c = 6.858 α = 87.88° β = 91.60° γ = 94.55°	Gd	8	2.48	triortho-group	framework
$R_2Ge_2O_7$	R = Sc, Yb	Cubic a = 9.81				octahedral framework	framework
$R_4Ge_3O_9(OH)_6$ R = Sm,Er-Lu	$Sm_4Ge_3O_9(OH)_6$	Cmcm z = 4 a = 15.195 b = 10.909 c = 7.161	Sm Sm	7 8	2.30 2.39	chains from octahedra connected with ortho-tetrahalra	framework

Co. No. = Coordination number

DropBooks

Table 7.20. Structure Types of Alkali- and Alkaline Earth, Rare Earth Germanates[206]

Compound	Representative	Cell parameter (Å)	Rare Earth, Co. No., Average bond distance Å			Tetrahedral radical form	Rare earth polyhedra
$NaR[GeO_4]$ R = Sm-Lu,Y	$NaSm[GeO_4]$	$Pbn2_1$ z = 4 a = 5.27 b = 11.70 c = 6.50	Sm	6	2.36	orth-tetra-hedra	discrete polyhedra
$NaR[GeO_4]$ R = La-Nd	$NaEu[GeO_4]$	14/m z = 8 a =11.75 c = 5.45				orth-tetra-hedra	framework
$NaR_3[GeO_4]_2$ $(OH)_2$ R = Nd-Gd	$NaSm_3[GeO_4]_2$ $(OH)_2$	Bb z = 4 a = 18.21 b =12.15 c = 5.27 γ =131.88°	Sm Sm	8 7	2.46 2.47	orth-tetra-hedra	discrete polyhedra
	$NaHo_4[GeO_4]_2$ O_2 (OH)	Pnma z = 4 a = 6.75 b =21.67 c = 6.91	Ho	7	2.33	orth-tetra-hedra	framework
$Na_2R[GeO_4]$ R = Pr-Gd	$Na_2Pr[GeO_4]$	Pnma z = 4 a = 9.52 b = 7.48 c = 6.98	Pr	8	2.51	orth-tetra-hedra	framework
	$Na_2Sc[GeO_4]$ (OH)	$P2_1ab$ z = 8 a = 12.34 b = 13.78 c = 5.53	Sc	6	1.99-2.18	orth-tetra-hedra	ribbon
	$LiNd[GeO_4]$	Pbcn z = 4 a = 5.096 b =11.923 c = 5.399	Nd	8	2.486	orth-tetra-hedra	framework
$Me_3R_2[GeO_4]_3$ Me =Sr,Ca R = Ho-Lu,Y	$Ca_3Y_2[GeO_4]_3$	Ia3d z = 8 a = 12.085				orth-tetra-hedra	
$Me_2R_3[GeO_4]_3Cl$ Me=Ca,Ba R = La,Ce	$Ca_2Ce_3[GeO_4]_3$ Cl	$P6_3/m$ z = 2 a = 9.467 c = 6.999				orth-tetra-hedra	

(Cont'd.)

Table 7.20. *(Cont'd.)*

Compound	representative	cell parameter (Å)	Rare Earth, Co. No., Average bond distance Å			tetrahedral radical form	Rare earth polyhedra
$K_2Sc_2[Ge_2O_7](OH)_2$		Pbcn z = 4 a = 7.06 b =11.35 c =10.67	Sc	6	2.11	diortho-groups	framework
$Na_4R_2[Ge_4O_{13}]$ R = Yb-Lu,Sc	$Na_4Sc_2[Ge_4O_{13}]$	$Pna2_1$ z = 4 a =14.30 b= 5.46 c=14.65	Sc	6	2.12	Tetra -groups	twinned polyhedra
$K_2R_4[Ge_4O_{13}]$ $(OH,F)_4$ R = Pr-Gd	$K_2Nd_4[Ge_4O_{13}]$ $(OH,F)_4$	$P2_1$ z = 4 a = 6.821 b = 7.438 c =17.639 γ =121.33°	Nd	7 8	2.40 2.53	Tetra-groups	framework
$Na_2R_6[Ge_2O_7]_2$ $[Ge_4O_{12}]$ R =Pr-Nd	$Na_2Pr_6[Ge_2O_7]_2$ $[Ge_4O_{12}]$	P1 z = 2 a = 7.18 b =11.61 c = 7.04 α =98.92° β =91.62° γ =102.50°	Pr	7 8	2.26-2.61 2.41-2.71	diortho-group + 4 – membered ring	framework
	$K_4Yb_2[Ge_8O_{20}]$ $(OH,F)_2$	$P2_1/m$ z = 2 a = 12.105 b = 11.896 c = 8.576 γ = 112.04°	Yb	6	2.19	tubular	columns ribbons
$MRGe_2O_6$ M = K,Na R = Sc	$NaScGe_2O_6$	Monoclinic z =2 a = 10.1 b = 9.1 c = 4.7 β = 108°				metachain with a period of 2-tetra-hedra	ribbons
$Na_5RGe_4O_{12}$ R = Gd-Lu,Y	$Na_5GdGe_4O_{12}$	R3c z = 16 a =22.781 c =12.994				12-membered rings	discrete polyhedra
$MgLa_2GeO_6$		Pm3m a = 3.90				Isolated octahedra	

Co. No. = Coordination number

DropBooks

7.11.2 Zirconium Germanates

The study of zirconium germanate crystallization continues to be popular under hydrothermal conditions. Recently the number of sodium-zirconium germanates synthesized under hydrothermal conditions has increased enormously. In the Na_2O-ZrO_2-GeO_2-H_2O system, the following germanates can be synthesized (Fig. 7.50): $ZrGeO_4$, Na_2ZrGeO_5 (Ge/Zr =1,Q_1), $Na_2ZrGe_2O_7$ (Q_2), $Na_4Zr_2Ge_3O_{12}$ ($Q_{1.5}$), $Na_3HZrGe_2O_8$ (Q_2Na), and $Na_4Zr_2Ge_5O_{16}{\cdot}H_2O$ ($Q_{2.5}$).

The subscript of letter Q indicates the value of the Ge/Zr ratio in the solid phase. The crystallization regions of these phases are shown in Figs. 7.50 and 7.51 respectively. Five sodium-zirconium germanates were synthesized in the system Na_2O-ZrO_2-GeO_2-H_2O. New compounds are marked with asterisks. All the compounds are characterized by the same Zr and Ge coordination and in all the compounds zirconium atoms occupy octahedra, while germanium atoms occupy tetrahedra.

The positions of phase boundaries (crystallization of individual compounds) are determined by the NaOH concentration and the initial ratio of zirconium and germanium oxides. The sequence of germanate formation in the hydrothermal Na_2O-ZrO_2-GeO_2-H_2O system may be represented by the scheme in Fig. 7.52.

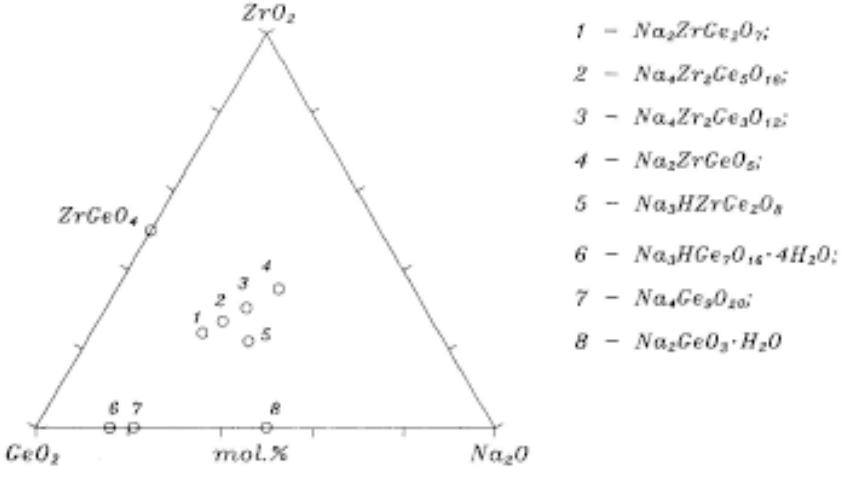

Figure 7.50. Crystallization field of sodium zirconium germanets.[97]

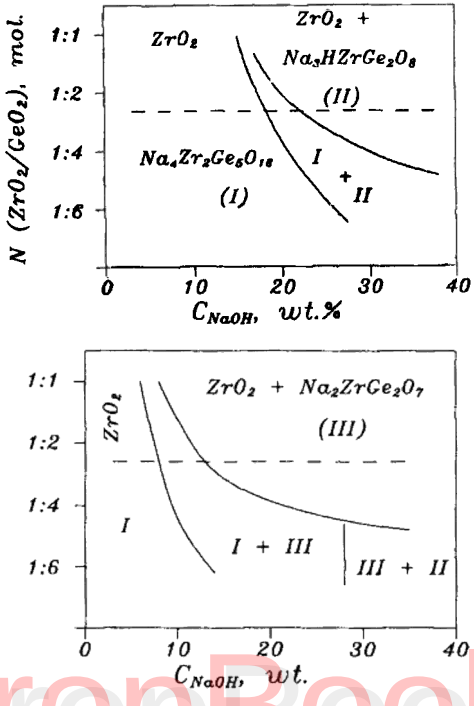

DropBooks

Figure 7.51. Crystallization field of sodium zirconium germanets.[97]

at 300°C :

$$ZrGeO_4 \longrightarrow Na_4Zr_2Ge_5O_{16}\cdot H_2O\ (Q_{2.5}) \longrightarrow Na_3HZrGe_2O_8\ (Q_2^{Na})$$

at 400°C :

$$ZrGeO_4 \longrightarrow Na_4Zr_2Ge_5O_{16}\cdot H_2O\ (Q_{2.5}) \begin{cases} \longrightarrow Na_2ZrGe_2O_7\ (Q_2) \\ \longrightarrow Na_3HZrGe_2O_8 (Q2^{Na}) \end{cases}$$

at 500°C :

$$ZrGeO_4 \longrightarrow Na_4Zr_2Ge_5O_{16}\cdot H_2O\ (Q_{2.5}) \begin{cases} \longrightarrow Na_4Zr_2Ge_3O_{12} \\ \longrightarrow Na_2ZrGe_2O_7\ (Q_2) \\ \longrightarrow Na_2ZrGeO_5\ (Q_1) \end{cases}$$

Figure 7.52. Reaction scheme of germanate formation in the hydrothermal Na_2O-ZrO_2-GeO_2-H_2O system.[97]

The formation of NaZr- germanates is accompanied by a decrease in the coordination numbers of Zr from 8 to 6 in all NaZr- germanates. If we pass from alkali-free to alkali-zirconium germanates, the GeO_2/ZrO_2 ratio first increases in a jump-wise manner and then decreases to the initial minimum value equal to unity:

Eq. (14) (q) $1 \rightarrow 2.5 \rightarrow 2 \rightarrow 1.5 \rightarrow 1$.

A decrease in the GeO_2/ZrO_2 ratio is reflected in a decrease of the condensation of germanium-oxygen tetrahedra:

n = 5, $[Ge_5O_{16}]$ island chains in $Na_4Zr_2Ge_5O_{16}\cdot H_2O$.

n = 2, $[Ge_2O_7]$ diorthogroups in $Na_2ZrGe_2O_7$.

n = 1, $[HGeO_4]$ and $[GeO_4]$ type tetrahedra in $Na_3HZrGe_2O_8$.

n = 1, $[GeO_4]$ tetrahedra in Na_2ZrGeO_5 and $Na_4Zr_2Ge_3O_{12}$.

The germanate system has no compounds analogous to silicates with the TO_2/ZrO_2 ratio = 3. The maximum GeO_2/ZrO_2 ratio is equal to 2.5. The substitution of Si by Ge results in the change of the structure type of alkali-free compound to $ZrGeO_4$ crystallizing in the scheelite type. The general scheme of the interaction between the zirconium and germanium oxides and NaOH solutions at high temperatures and pressures may be represented in the form:

Eq. (15)

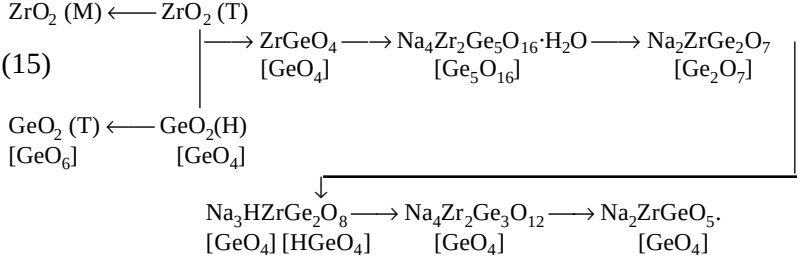
ZrO2 (M) ⟵ ZrO2 (T)
⟶ ZrGeO4 ⟶ Na4Zr2Ge5O16·H2O ⟶ Na2ZrGe2O7
[GeO4] [Ge5O16] [Ge2O7]
GeO2 (T) ⟵ GeO2(H)
[GeO6] [GeO4]
Na3HZrGe2O8 ⟶ Na4Zr2Ge3O12 ⟶ Na2ZrGeO5.
[GeO4] [HGeO4] [GeO4] [GeO4]

The sequence of the formation of NaZr and Na germanates reflects a general trend in the decondensation of Ge-O radicals with an increase of the alkali content in the system. The formation of each subsequent phase in the chain accompanied by the separation of GeO_2 either participates in the formation of the accessory phase or remains in the solution:

$$Na_4Zr_2Ge_5O_{16}\cdot H_2O \rightarrow 2Na_2ZrGe_2O_7 + GeO_2 + H_2O$$

$$3Na_4Zr_2Ge_5O_{16}\cdot H_2O \rightarrow 4Na_3HZrGe_2O_8 + 2ZrO_2 + 5GeO_2 + H_2O$$

$$3Na_2ZrGe_2O_7 \rightarrow 2Na_3HZrGe_2O_8 + ZrO_2 \ (m_{GeO2} = const)$$

$$2Na_2ZrGe_2O_7 \rightarrow Na_4Zr_2Ge_3O_{12} + GeO_2$$

$$Na_4Zr_2Ge_3O_{12} \rightarrow 2Na_2ZrGeO_5 + GeO_2$$

As the NaOH-content increases in the solution we get:

$$2ZrO_2 + 5GeO_2 + 4NaOH \rightarrow Na_4Zr_2Ge_5O_{16}\cdot H_2O + H_2O$$

$$2Na_4Zr_2Ge_5O_{16}\cdot H_2O + 2NaOH \rightarrow 5Na_2ZrGe_2O_7 + GeO_2 + ZrO_2 + 2H_2O$$

$$Na_2ZrGe_2O_7 + NaOH \rightarrow Na_3HZrGe_2O_8$$

$$\uparrow\downarrow$$

$$Na_4Zr_2Ge_3O_{12} + GeO_2 + 2NaOH$$

$$\downarrow$$

$$Na_2GeO_3\cdot H_2O.$$

DropBooks

The above reactions permit one to draw a conclusion that the stable crystallization of different phases in the above sequence which was observed with an increase in the NaOH content will also proceed with a decrease in the GeO_2 content at sufficiently high Na_2O content in the system.

The systematic study of hydrothermal crystallization in the systems Na_2O-MO_2-GeO_2-H_2O (M = Ti, Zr, and Hf) revealed the main regularities of germanate formation and growth. In these systems compounds having both network- and no-network structure can be obtained. For the compound having network the value q = Ge/M can be equal to 1,

1.5, 2, 2.5; the value p = Na/M being equal to 2. In germanates without network structure q = 1 and 1.25, p = 1, 1.5, 2, and 3.

In the network NaZr- germanates, the degree of Ge-tetrahedra condensation increases from n = 1 till n = 5. For the network NaZr-silicates which have no germanate analogs, the new crystallization branch takes place (the formation of the phases with q = 3; 3; 6, n = 3 and ∞). Such change in n-value is connected with the change of secondary structural units. The analysis of the crystal structure of the synthesized phases leads to the conclusion that the structural unit common to all sodium-zirconium germanates is a centrosymmetric closed dimer grouping of two Zr-octahedra and two Ge-tetrahedra, M_2T_2, which occupy the regular point system in the centrosymmetric groups. During structural rearrangement such groups link in another way. For silicates the cyclic dimer M_2T_4 is typical.[97][206]

7.11.3 Zincogermanates

Hydrothermal growth of zincogermanates, although not as popular as that of zincosilicates, have been studied in detail. The appreciable solubility of sodium zinc germanate in water solutions of caustic soda at elevated temperatures and pressures allows its preparation in the form of coarse well-formed crystals, the sizes of which amount to some cubic centimeters.

In the majority of the experiments, the synthesis of sodium zinc germanate was carried out in the presence of Mn^{2+} ions in the solution with the aim of preparing crystals activated by Mn^{2+}. It is well-known that Mn^{2+} is widely used as an activator for the preparation of various zinc silicate phosphors. Like in zincosilicates, zincogermanates in the presence of Mn^{2+} exhibit photo-, electro-, cathode-, x-ray, and thermo-luminescence. Among the zincogermanates, only the Na_2ZnGeO_4 phase is very popular and well studied. Similarly, Na_2CoGeO_4 has been studied in detail owing to its interesting piezoelectric and pyroelectric properties.[207]–[210]

In contrast to the Na_2O-ZnO-GeO_2-H_2O system, the Cd system, not only does a change in the alkali concentration in solution leading to an exchange of the crystallization phases, but the phase boundaries are also substantially displaced as the Cd:Ge ratio alters. For surplus GeO_2 in pure water, only the rutile form of the oxide crystallizes, together with a cadmium germanate with CdO:GeO_2 = 1:2. As the amount of CdO in the

system increases, the amount of free GeO_2 in the crystallization products diminishes. The cadmium germanate $CdGe_2O_5$ remains as a stable solid phase up to a ratio of $CdO:GeO_2$ = 1:1. Further increasing of the cadmium content leads to the formation of an olivine-like phase Cd_2GeO_4, and this remains dominant in the phase diagram of the system.[207] The Na_2O-CdO-GeO_2-H_2O has yielded eight crystalline phases under hydrothermal conditions.[207][211][212] The other germanates of interest are lead germanates, alkali gallium germanates, antimony germanates, neobium germanates, alkali aluminogermanates berium germanater bismuth germanates, titanogermanates and so on.[213]–[219]

Most of these germanates show interesting physical properties. Hence, a systematic understanding of germanate phases obtained from a wide variety of germanate systems will be of great interest in solid state science.

7.12 PROPERTIES OF GERMANATES

Amongst germanates, rare earth germanates and LISICON [$Li_{14}Zn(GeO_4)_4$] have been studied extensively owing to their unusual physical properties. Most of the germanates, especially rare earth germanates, have very high melting points, high-density and refractive indices. Table 7.21 gives the physico-chemical properties of some rare earth germanates.[206] Electrical and magnetic properties have been studied for oxyorthogermanates, R_2GeO_5 and diorthogermanates, $R_2Ge_2O_7$. These studies confirm that R_2GeO_5 and $R_2Ge_2O_7$ belong to a class of dielectrics.[220] The Sm and La-bearing germanates are diamagnetic. The magnetic transition temperatures for oxyortho- and diorthogermanates are as follows:[221]

$Tb_2Ge_2O_7$ = 2.05 ± 0.05 K

$Dy_2Ge_2O_7$ = 2.15 ± 0.05 K

$Ho_2Ge_2O_7$ = 1.45 ± 0.05 K

$Er_2Ge_2O_7$ = 1.15 ± 0.05 K

Dy_2GeO_5 = 2.50 ± 0.10 K

Er_2GeO_5 = 1.25 ± 0.10 K

Drop Books

Table 7.21. Physico-chemical Properties of Some Rare Earth Germantes[206]

Compound	d, g / cm^3	Melting temp. (T°C)	Reference Indices
La_2GeO_5	5.97	1800	1.940
Nd_2GeO_5	6.55	1820± 25	1.948
Gd_2GeO_5	7.07	1.880	1.941
Y_2GeO_5	4.83	1975± 15	1.848
Er_2GeO_5	7.28	2000± 50	1.904
La_4GeO_8	6.30	1720*	1.973
Gd_4GeO_8	7.77	1650*	1.975
Y_4GeO_8	5.10	2000	1.887
Er_4Ge_8	8.02	1600**	1.93
$La_{4.67}[GeO_4]_3$	5.89	1770	1.930
$La_2Ge_2O_7$	5.67	1680*	1.900
$Nd_2Ge_2O_7$	6.16	1820± 25*	—
$Gd_2Ge_2O_7$	6.70	1770	1.922
$Y_2Ge_2O_7$	4.69	1800± 25	1.840
α-$Er_2Ge_2O_7$	6.99	1875± 50	1.890
β-$Er_2Ge_2O_7$	—	—	1.938
$Sc_2Ge_2O_7$	4.46	1850	1.847
$La_2Ge_3O_9$	5.94	1300	1.995

* with decomposition. ** with decomposition in solid phase.

Most of the works on the investigations of physical properties of rare earth germanates deal with the luminescence properties. Their emission and absorption spectral characteristics have been studied in great detail. Figure 7.53 shows the luminescence spectra of $NaEuGeO_4$ and $NaTbGeO_4$.[222] Figure 7.54 shows the excitation spectrum of $NaGd_3[GeO_4]_2(OH)_2$: Tb^{3+} (2.5%).[223]

Several lithium germanates have been reported to show high ionic conductivity. Amongst them, $Li_{14}Zn(GeO_4)_4$ is a very well-known Li^+ ion conductor. This one phase of the solid solution phase between Li_4GeO_4-Zn_2GeO_4 is popularly known as LISICON. The electrical conductivity of LISICON is 4×10^{-3} Ω^{-1} cm^{-1} at 500 K, but it decreases to $< 10^{-6}$ Ω^{-1} cm^{-1} at room temperature.[207][208] Similarly, the alkali rare earth germanates exhibit very good ionic conductivity on par with their rare earth silicates counterparts.[82][83]

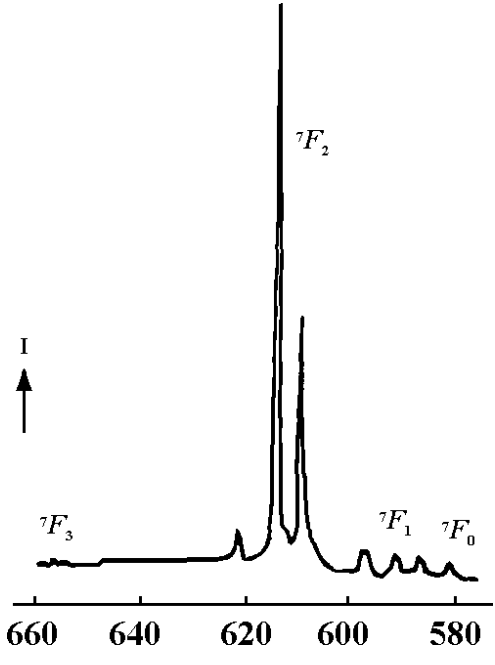

Figure 7.53. Luminescence spectra of $NaEuGeO_4$ and $NaTbGeO_4$.[222]

DropBooks

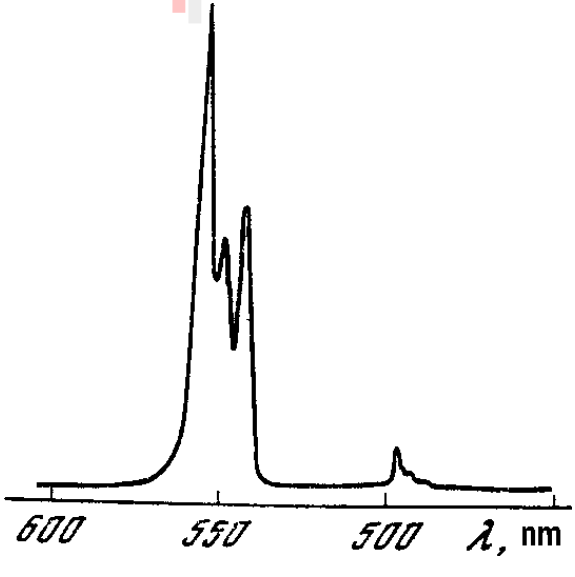

Figure 7.54. Excitation spectrum of $NaGd_3[GeO_4]_2(OH)_2$: Tb^{3+} (2.5%).[222]

7.13 HYDROTHERMAL GROWTH OF PHOSPHATES

From the time of its discovery, hydrothermal technique was known for the synthesis of silicates. In the 19th century, hydrothermal technique was included under silicate technology. Next to silicates, it was the oxides and hydroxides of various metals that dominated the hydrothermal technology during the late 19th and early 20th centuries. Subsequently, germanates, sulphides, and carbonates, etc., became popular. However, the growth of phosphates by hydrothermal technique was not attempted for a long time. It was only during the 1950s that hydrothermal technique was tested for the synthesis of phosphates,[225] and up to the 1980s there were only scanty reports on the synthesis of phosphates by hydrothermal technique. Today, the situation has changed dramatically. Hydrothermal growth of phosphates is much more popular than the hydrothermal growth of any other compound. A large variety of phosphates starting from simple ortho- to the most condensed or ultra-phosphates containing a wide range of elements have been obtained. This is probably due to the improved instrumentation techniques and the discovery of aluminophosphate zeolites. Further, the success in the growth of various phosphates has prompted the hydrothermal researchers to synthesize other inorganic compounds hitherto unattempted. Similarly, it is appropriate to state that the success in the growth of phosphates has led to the understanding of hydrothermal crystallization mechanism for various inorganic compounds. It ultimately has set a new trend in the synthesis of inorganic compounds under mild hydrothermal conditions.

There is a growing interest in the study of phosphates in the last two decades owing to their widespread application, e.g., piezoelectric, luminescent, magnetic, superionic, ceramic, solid state laser, ulter-low thermal expansion, nonlinear optic, moisture sensors, as hosts for actinide ions, and so on, in modern technology. Similarly, phosphate minerals are the important source materials of almost all the rare earth elements. Thus, the phase equilibria studies in phosphate systems help to understand the interaction between various metals and P_2O_5, and it might give possible clues to separate these rare earth elements from phosphate minerals and also to understand their genesis. It is interesting to note that there are over 300 phosphate minerals in nature that have been classified into various groups depending upon the cationic elements present in them.[226] The phosphates containing rare earth elements represent the smallest group having only 15 minerals, out of which 4 are anhydrous: monazite-(Ce, La,

Y, Th)PO_4; xenotime-YPO_4; cheralite-(R, Ce, Th)PO_4 and vitosite-$Na_3R(PO_4)$[227] (a recently reported mineral from Lovozerskii alkaline mass), where R is rare earth element. It is interesting to note that all the naturally occurring phosphates are represented by one anionic group—orthophosphate. Although a wide range of physico-chemical conditions exist in nature, we find phosphate minerals without poly-, pyro-, meta-, ultra-, etc., types, unlike the silicate minerals with a very wide variety of condensed silicates like meta-, poly-, soro-, phyllo-, etc. The reasons for the absence of condensed phosphates in nature are not clearly known. In order to understand the peculiarities among natural phosphate minerals, one has to synthesize them in the laboratory by simulating the natural conditions. However, the synthesis of phosphates was started neither to understand the peculiarities in nature nor to use them in technology. The first work on the synthesis of phosphates began in the 19th century by Berstelius in 1816.[228] He synthesized sodium pyrophosphate artificially for the first time. In 1889, K. R. Johnson obtained LaP_5O_{14}—the first artificial rare earth phosphate.[229] However, the works on the synthesis of inorganic phosphates or their growth as monocrystals attracted less attention. Even after the beginning of the synthesis of various types of rare earth phosphates from the early 40s[230][231] up to early 70s[232][233] the interest was confined only to the studies concerning the x-ray and morphological analyses. The first technological phosphate material was KDP, which was first obtained during the 1940s for telecommunication purpose. The interest on this material continues to progress. Except this, virtually phosphates did not carry any technological significance for a very long time. However, a systematic study of rare earth phosphates began in the 1970s with the developments in the field of communication and the problems associated with the miniature sources of light, particularly lasers based on dielectrics. Until recently, these materials contained a low concentration of active ions, which was a major obstacle in the attempts to use them in opto-electronics.

DropBooks

In 1973, laser beams were obtained from NaP_5O_{14} crystal containing 3.86×10^{12} ions of neodymium atoms/cm^3.[234][235] Such a high concentration of active ions led to the further decrease in size of the laser crystal to tens of micromillimeters. An analogous effect was found in the monocrystals of $MNd(PO_3)_4$ (where M = Li, Na, K),[236][237] $Na_3Nd(PO_4)_2$,[238] $K_3Nd(PO_4)_2$,[239] etc. Prior to the development of these rare

earth phosphates, laser beams were obtained in crystals mostly YAG:Nd containing only 2–3% of active ions mostly as dopants, but not as the stoichiometric components. Today it has become a flourishing field in science and technology, particularly in the field of fiber-optic communication. In 1976, the authors[240] reported a three dimensional high ionic conductivity in NASICON ($Na_{1+x}Zr_2Si_xP_{3-x}O_{12}$;$0 \leq \times \leq 3$) type of phosphate which is isostructural with $Na_3Sc_2P_3O_{12}$.[241] Later on ionic conductivity was reported in some other rare earth phosphates like $RbNdP_4O_{12}$,[242] $CsNdP_4O_2$,[228][243] etc. Since NASICON has some problems like non-stoichiometry, nonavailability of single crystals, and highly complex structures, there is a search for new materials with simple structures. The rare earth phosphates containing other elements like sodium, transitional elements and some alkaline earth elements are found to be the ideal substitutes for NASICON.[244] In all these materials the ionic conductivity, the optical properties and so on depend mainly upon the type of cation and the crystalline structure. However, the structures of many new solid electrolytes are yet to be studied because of the nonavailability of these materials in the form of single crystals. It is well known that the rare earth phosphates exhibit island, ribbon, layered, ring, and framework types of structures, which are highly distorted with a very wide variation in P-O bond lengths. The inter-isolation of the rare earth polyhedra in most of the rare earth phosphates and the distortion of the overall structures are mainly responsible for the presence of luminescence and ionic conductivity in these materials. The activation energy and ionic conductivity depend upon the radii of the rare earth cation.[245] The study of ionic conductivity in condensed phosphates needs a thorough knowledge of crystalline structure, which insists on single crystals. Similarly, rare earth phosphates, particularly orthophosphates have very high melting points (2300–2500°C) and they are known as high-temperature ceramics in addition to their common names like color luminophors and scintillators. Much recently, magnetic properties have also been reported in some orthophosphates. All these properties have not been understood precisely. Therefore, the growth of these materials in the form of single crystals is highly desirable to understand various physical characteristics. There may be over 1000 reports on the synthesis of phosphates bearing rare earth elements, alkali, alkaline earth and transitional elements. One third of them might deal with hydrothermal technique.

7.13.1 Structural Chemistry of Rare Earth Phosphates

The formation of a wide variety of phosphates, particularly rare earth phosphates is connected with the reaction susceptibility of phosphoro-oxygen anions to give various degrees of condensation. As a result of such reactions among the phosphoro-oxygen anions, there develops bridging oxygen bonds –P – O – O – P– forming pyrophosphates—$[P_2O_7]$—initially followed by more complex linear anions like $[P_nO_{3n+1}]$, rings like $[P_nO_{3n}]$ ($n < 3$), etc. It is extremely difficult to classify phosphates unlike silicates, because of high complexity in the phosphates' internal structures. For example, a recently reported structure of $(NH_4)_2Ce(PO_3)_5$[246] has two infinite crystallographically nonequivalent $(PO_3)^-$ chains, one running parallel to the *'a'* -axis, the other along *'c'* -axis, both with a period of five tetrahedra. This compound is the first example of a long chain polyphosphate with crystallographically independent chains and such a peculiarity has not been reported in silicates or germanates so far.

The phosphorus atoms participate in the form of phosphoro-oxygen anions $[H_2PO_4]^{-1}$, $[HPO_4]^{-2}$, and $[PO_4]^{-1}$ in the reactions forming respective phosphates. The $[PO_4]^{-3}$ anions are less reaction susceptible among these three, and that makes the solid state synthesis difficult. Therefore, ammonium phosphates are used in the solid phase synthesis. The acidic phosphoro-oxygen anions easily take part in the reactions during heating and in fact, high reaction susceptibility of acidic phosphoro-oxygen anions serve as a basis in working out various methods of obtaining rare earth phosphates with a particular reference to the highly condensed ultraphosphates.[247] With a slow dehydration of acid orthophosphate anion there occurs the removal of the $(OH)^{-1}$ ions and the condensation of phosphoro-oxygen anions. This was a popular method even in the 19th century, but for a long time the mechanism of the process remained unclear. Growth conditions for the required phosphate anions were selected empirical and compelled to participate in the reactions. However, higher the degree of condensation of phosphate anion the more difficult it is to ascertain the growth conditions. The process is quite complicated and very often results in the formation of a mixture of various degrees of condensed anions. McGilvery and Scott (1957) concluded that water molecules play a distinct role in the dehydration process, particularly its concentration influences not only on the rate of reaction but also on the stability of various phosphate anions.[248] For the benefit of a reader we

PropBooks

have described the hydrothermal growth of phosphates containing rare earth elements followed by transitional elements.

7.13.2 Hydrothermal Growth of Rare Earth Phosphates

The first work on the hydrothermal synthesis of rare earth phosphates was by Anthony (1957), who synthesized monocrystals of monazite, $CePO_4$ from aqueous solutions of 85% H_3PO_4 at 300°C using teflon liners.[225] Carron et al. (1958)[249] have described the formation of rare earth orthophosphates from HCl solutions at 105–300°C and at pressure of 90 atm. A more systematic work on the hydrothermal synthesis of rare earth orthophosphates was carried out by Carron et al. (1958).[250] However, there was a break in the activity of the hydrothermal synthesis of rare earth phosphates until the 1980s. This was mainly connected with the lack of growth technology, high volatility of phosphorus at higher temperatures, high reaction susceptibility of phosphorus, corrosive nature of phosphorus at higher temperatures, etc. The experiments on the hydrothermal synthesis of phosphates can not be carried out at temperatures > 500°C, because phosphorus corrodes even the metals like Pt, Ir, Mo, Au and Ni. Some of these problems could be overcome using a teflon or vitreous carbon glass liners. However, the main drawback in using these liners is sealing. If one can seal the glassy carbon liners by some means, the growth of pure phosphates can be carried out even at higher temperatures by hydrothermal method. Similarly, the use of teflon liners is again a problem, because it cannot be used beyond 300°C and 200 atm. Of course, pressure can be slightly increased by means of a counter balance technique, i.e., by creating the same pressure between the autoclave walls and inside the liner. These problems have been discussed in great detail by Byrappa and Gopalakrishna (1985),[251] Byrappa,[252] and Rabenau (1984).[253] Byrappa and Gopalakrishna (1985) have studied the rare earth phosphate system Na_2O-R_2O_3-ZrO_2-P_2O_5.[251]

The first ever report on the study of phase equilibria in the rare earth phosphate system on the whole, appeared in 1981,[254] where the phase equilibria in the system Nd_2O_3-P_2O_5-H_2O at 500°C under 100 MPa and the synthesis of NdP_5O_{14} crystals were studied. This is also the first phosphate system studied hydrothermally. All the earlier reports deal with only a part of the phase diagram. The starting materials—Nd_2O_3, P_2O_2, and 85% H_3PO_4 solution—were taken in definite amounts within a sealed golden capsule. Although this method has been included in the

hydrothermal method by the Japanese workers, the partial pressure of water under these conditions was always low and often less than 1 atm. Therefore, it can be considered as a special case of the hydrothermal method. This report was followed by another publication,[255] which deals with the hydrothermal synthesis of mixed phosphates of neodymium and alkaline metals (M_2O. $Nd_2O_3 \cdot 4P_2O_5$). Here, the authors have studied the phase formation in the alkaline rare earth phosphate system (M_2O-Nd_2O_3-P_2O_5-H_2O, where M-Li, Na, K, Rb, and Cs) under hydrothermal conditions in the temperature and pressure range 300–700°C and 0.5–600 atm respectively using vitreous carbon glass, teflon and platinum liners. The system is a four component one with temperature and pressure as constants. According to the Gibb's phase rule at the invariant equilibrium only four phases can exist ($NdPO_4$, NdP_3O_9, NdP_5O_{14}, and $MNdP_4O_{12}$). The variation in the concentration of phosphorus and alkaline metal oxides determines the fields of crystallization of different phases in the composition diagram. According to Le Chatalae's principle the increase in the potential of M_2O (P_2O_5) provides the reaction taking place with the absorption of this component. The following reactions can explain the various nonvariant point in the ternary phosphate systems:

DropBooks

$$NdPO_4 + P_2O_5 + G_1 \rightleftharpoons Nd(PO_3)_3 + G_2$$

$$2\ NdPO_4 + M_2O + P_2O_5 + G_3 2 \rightleftharpoons MNdP_4O_{12} + G_4$$

Eq. (16)

$$Nd(PO_3)_3 + P_2O_5 + G_5 \rightleftharpoons NdP_5O_{14} + G_6$$

$$2\ Nd(PO_3)_3 + M_2O + P_2O_5 + G_7 \rightleftharpoons 2\ MNdP_4O_{12} + G_8$$

$$2\ NdP_5O_{14} + M_2O + G_9 \rightleftharpoons 2\ MNdP_4O_{12} + P_2O_5 + G_{10}$$

where G is a liquid phase having transitional composition. The presence of a divariant field of stability of $MNdP_4O_{12}$ (Fig. 7.55) indicates the possibility of growing these crystals from solutions with variable concentrations of phosphorus and alkaline metals. The relevant empirical AB-diagrams of fields of crystallization, where A = M_2O/Nd_2O_3, B = $P_2O_5/M_2O + Nd_2O_3$, are given in Fig. 7.56. The dependence of *PT*-conditions and the equilibrium state of the system has been studied (Fig. 7.57 and Fig. 7.58). It is observed that with changes in temperatures, there will be different polymorphic modifications of tetraphosphates. In hydrothermal systems, the pressure measured corresponds to the pressure of aqueous solutions and its influence on crystallization process is quite important. At a constant temperature, it increases with reference to the molar fraction of

the water. In the pressure range of 1–600 atms, the boundaries of phase formation do not change. In this case, the changes in phase formation take place only during changes in the concentration of water in the ampoule. With an increase in the molar fraction of water the following phase transformation takes place:

Eq. (17)

$$MNdP_4O_{12} \rightarrow NdP_3O_9 \rightarrow NdPO_4$$
$$NdP_5O_{14} \rightarrow NdP_3O_9 \rightarrow NdPO_4$$

Using these results, Byrappa et al. (1990) reported on the hydrothermal growth of TmP_5O_{14} crystals under mild hydrothermal conditions.[256] The crystal size was much higher and crystals were well faceted than the crystals obtained by Yoshimura et al. (1981).[254] The important aspect of this work is the growth of ultraphosphates under mild hydrothermal conditions (T = 240°C, P = < 100 bars). The autoclaves used were simple Morey type provided with teflon liners. The crystallization was carried out through spontaneous nucleation.

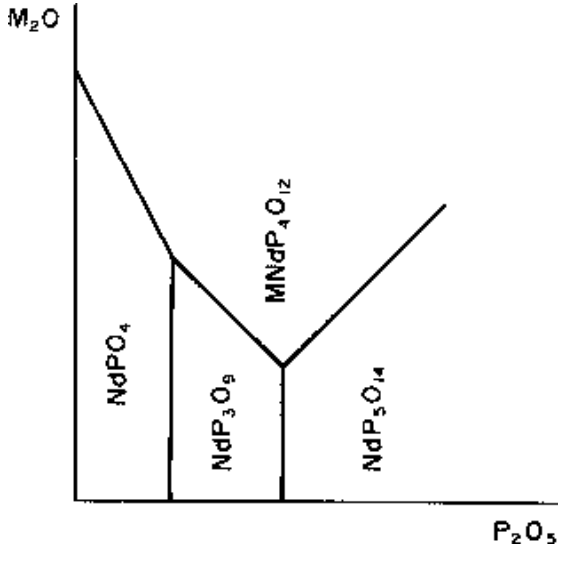

Figure 7.55. Composition diagram for the system Me_2O-Nd_2O_3-P_2O_5 -H_2O.[251]

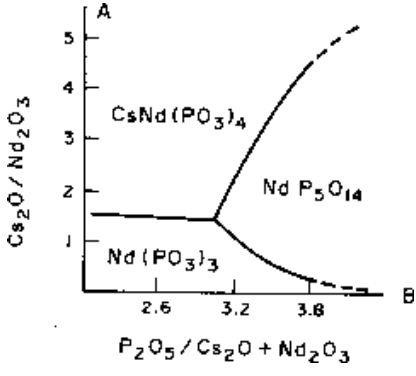

(a)

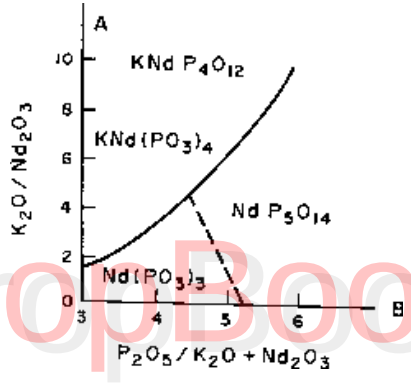

(b)

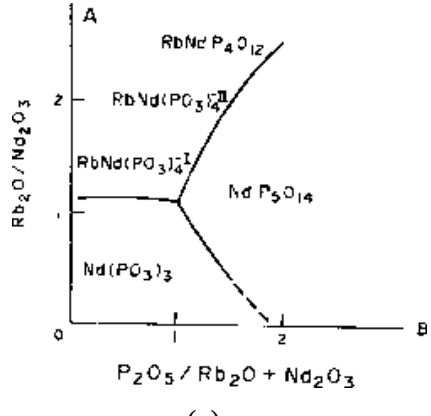

(c)

Figure 7.56. AB diagram of crystallization in *(a)* Cs_2O-Nd_2O_3-P_2O_5-H_2O: *(b)* K_2O-Nd_2O_3-P_2O_5-H_2O: *(c)* Rb_2O-Nd_2O_3-P_2O_5-H_2O systems.[256]

DropBooks

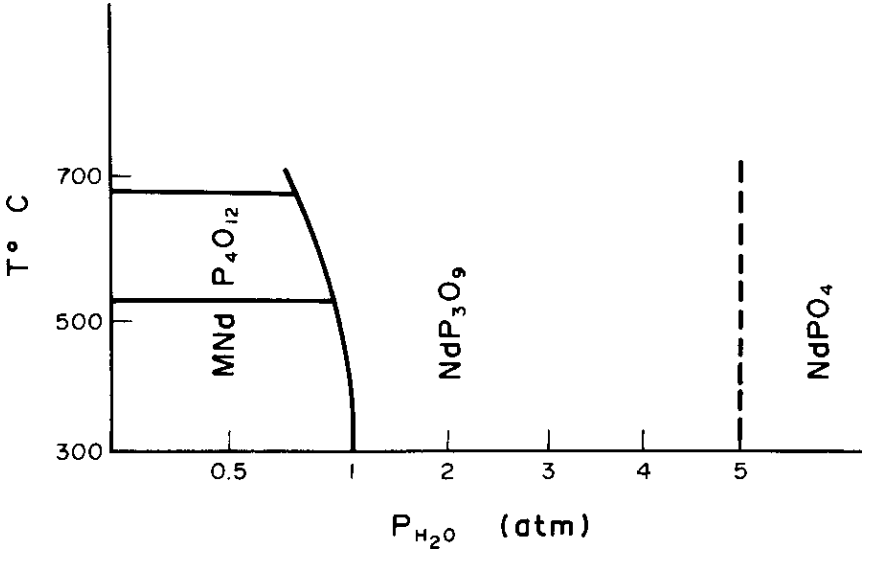

Figure 7.57. Phase transformation with reference to the changes in *PT* conditions.[257]

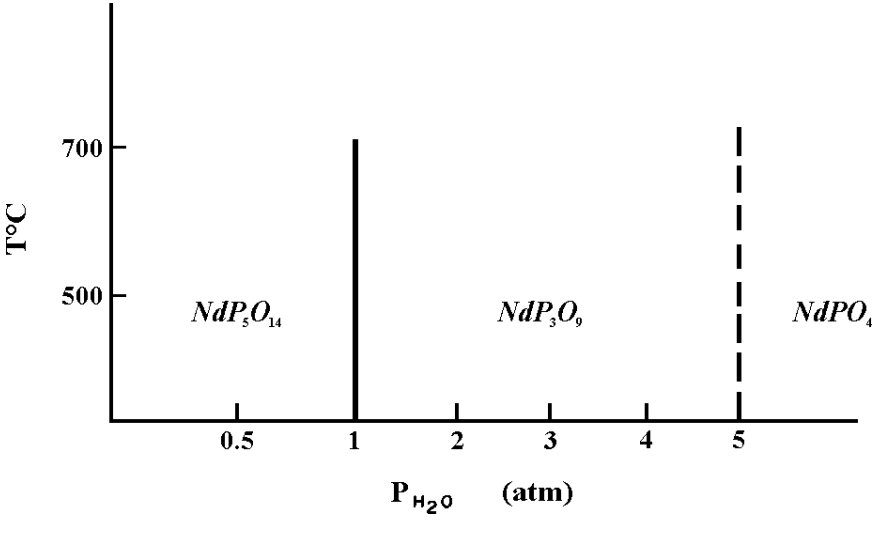

Figure 7.58. Phase transformation with reference to the changes in *PT* conditions.[257]

This is an important conclusion, particularly for geoscientists to explain the possible reasons for the absence of condensed phosphates in nature.[257] The experiments carried out under hydrothermal conditions showed that when P_{H_2O}> 6 atms, crystallization of polyphosphates or ultraphosphates ceases and is replaced by crystallization of simple orthophosphates irrespective of the temperature of the system. Similarly, even an increase in the concentration of M_2O in the system leads to decondensation, and ultraphosphates having a highly condensed state or a complex anionic structure $[P_5O_{14}]$ disappear from the products of crystallization and are replaced by polyphosphates with radicals $[P_2O_7]$, $[P_3O_9]$, $[P_4O_{12}]$, and finally $[PO_4]$. These experiments demonstrate that the structures of condensed phosphates are not stable, at least not in the presence of water. It is well-known that the magmatic or the post-magmatic processes of mineral formation are always accompanied by a certain amount of water and proceed in the presence of many types of metals. These are the conditions for the formation of orthophosphates and not condensed phosphates.[257] From the above studies, it is clear that only the hydrothermal method of studying alkaline rare earth phosphate systems revealed the formation of various phosphates depending upon the *PT*-conditions.

PropBooks

The growth of rare earth phosphates in the form of single crystals is very interesting owing to the high reaction susceptibility of phosphorus and the easy formation of phosphoro-oxygen radicals in a given system. For example, any anionic group of Nd-phosphate can be readily obtained from phosphoric acid solutions. In the liquid, from which the Nd-phosphates grow, Nd should be dissociated to form individual ions. For this purpose usually concentrated solutions or alkali melts are used. However, the process of Nd dissociation often carries a reversible character and the phase develops with Nd ions in the condensed pattern during the crystallization—for example, as in NdP_3O_9.[258] In order to achieve this, it is necessary that in the process of crystallization the Nd ions are to be held in a dissociated state, i.e., in the form of a nezoite complex (Fig. 7.59). A shell of ligands around Nd prevents the ions from inter-condensation and allows them to enter the crystal lattice as isolated ions. These ligands which often occur as tetrahedral oxy-anions $[TO_4]$ is the formation of a nezoite complex of type NdT_8O_{24}, where T = S, P, W, Mo, etc.[259] Thus, to obtain nezoite crystals, it is first necessary to bring Nd ions into a dissociated state, followed by creating the conditions for the formation of nezoite complexes, and only then does the desired crystallization take

place. The most suitable systems for this purpose appears to be Nd containing ternary systems of type M_2O-Nd_2O_3-T_xO_y, where M = H, Li, K, Rb, Cs and Tl or their admixtures. The process of crystallization is much more simple in the multicomponent systems. The quantitative ratio of the component largely determines the stoichiometric nezoitic complexes in these, i.e., the ratio of T_xO_y/Nd_2O_3 should not be less than 8. The main problem of concern is the incorporation of some components in excess than the stoichiometric ratio. As a result, the molar ratio of the nutrient components in the growth of nezoites is not regular and can be expressed approximately as $M_2O(M)/Nd_2O_3/T_xO_y = 2 > 1 < 8$. The additional amount of the components are introduced into the nutrient depending upon the individual cases. Thus, the growth of nezoites requires a definite surplus of T_xO_y components, and they may not be taken from the stoichiometric melt. Therefore, in the growth of nezoites either high-temperature aqueous solution or flux agents are used. Similarly, in the synthesis of many phosphates in the form of crystals, highly concentrated solution of phosphoric acid is used. It is considered that at over 250°C, orthophosphoric acid converts into pyrophosphoric acid and with a further increase in temperature it transfers to an even more condensed state due to the expulsion of water.[260] Figure 7.60 represents a temperature composition diagram for the system H_2O-P_2O_5, at pressure up to l atmospheres.[243] In region *(2)* of the diagram, crystallization can be carried out at normal pressure, whereas the crystal growth from solution corresponding to the composition of the region *(1)* requires the use of a hydrothermal apparatus. Here, the authors discuss the crystallization of rare earth phosphates as an example to explain the influence of the physico-chemical conditions and the primary structural units. The formation of rare earth phosphates in acidic (pH > 7.0) phosphoro-oxygen media takes place as follows:

Eq. (18)

$$R_nL + M_xP_yO_z \rightarrow R_nP_yO_z + M_xL$$
$$R_nL + M_xP_yO_z \rightarrow M_xR_nP_yO_z$$

where L = anion and it is usually Cl^-, NO_3 or SO_4, M = alkali cation and NH_4.

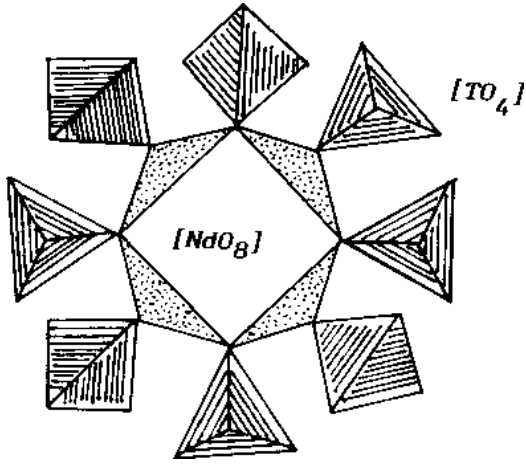

Figure 7.59. Nezoite complex.[243]

DropBooks

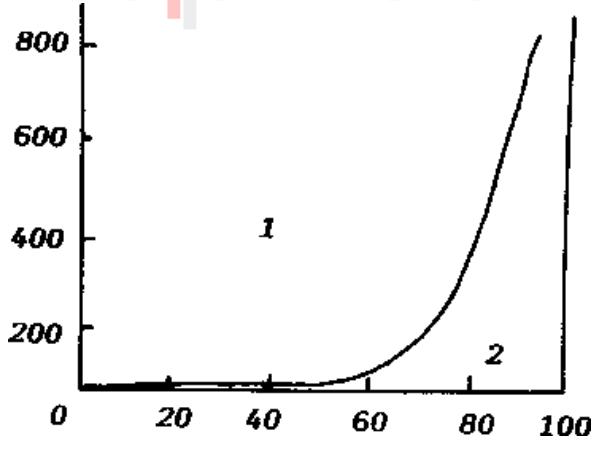

Figure 7.60. Temperature-composition diagram for the system H_2O-P_2O_5 at 1 atm pressure.[243]

As is evident, the type of rare earth phosphate determines the degree of condensation of phosphoro-oxygen anions, which depends upon the pH of the solution and concentration of P_2O_5. And during the interaction of $NdCl_3$ and YCl_3 with sodium tripolyphosphate at pH > 4.5, formation of $Nd_5(P_3O_{10})H_2O$ was established.[262] The actual process of synthesis from aqueous solution takes place in many stages. The soluble pyrophosphates $M_4P_2O_7$ (where M = NH_4, Na, K) serves as the source of phosphate anions. In the crystallization of $Na_5R(P_4O_{12})_2$, triphosphate anions $(P_3O_{10})^{-5}$ are initially stabilized in the form of solution-$(NH_4)_5P_3O_{10}$ or $Ca_5P_3O_{10}$, in which $ErCl_3$ or $NdCl_3$ dissolves followed by the crystallization of monocationic and mixed triphosphates $Er_5P_3O_{10}$, $MErP_3O_{10}{\cdot}xH_2O$ where M = Cs and NH_4.[263] By changing the partial pressure of water and the temperature of the system, the existence of phosphoro-oxygen anions (starting from orthophosphate up to ultraphosphate) can be stabilized. A required $[P_2O_7]$, $[P_4O_{12}]$ or $[P_5O_{14}]$ anion is created first in the solution and subsequently it was allowed to react with metals to obtain respective metal phosphate complexes. By such a direct method ortho-, pyro-, meta- and ultraphosphates of rare earth elements have been synthesized.

A series of mixed and simple anhydrous and hydrous rare earth phosphates have been obtained by the Russian and Chinese groups.[46][260]–[264] Under hydrothermal conditions the crystal chemistry of these rare earth phosphates have been studied in great detail and correlated with growth conditions. Xu et al. (1996,[262] 1996,[263] 1999[264]) have studied M_2O-CeO_2-P_2O_5-H_2O (M = NH_4, Na, K) system under hydrothermal conditions and obtained $M_2Ce(PO_4)_2{\cdot}H_2O$, (Ce = 4^+) an $M_3Ce(PO_4)_2$, $M_5Ce(PO_4)_3$.

Byrappa et al. (1985) synthesized $Na_2(R,Co)Zr(PO_4)_3$ (R = rare earths) crystals under hydrothermal conditions at T = 200°C and pressure 50 to 60 atm.[265][266] The experiments were carried out in Morey type autoclaves provided with teflon liners. The cross section of the autoclave used in the synthesis is shown in Fig. 7.61.

The crystallization was carried out by spontaneous nucleation that was controlled through a systematic rate of heating the alkaline component (Na_2O). It was taken in the form of a solution (NaOH) with a known molarity and this solution acts as a mineralizer. In the growth of double pyrophosphates, the addition of surplus P_2O_5 did not change the resultant product, which can be explained from the influence of H_2O vapor pressure in the system. Surplus P_2O_5 should actually result in the formation of simple or compound orthophosphates.

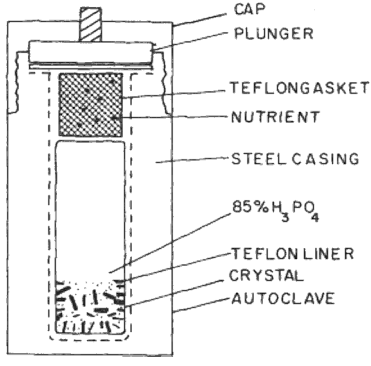

Figure 7.61. Cross section of the autoclave used in the synthesis of superionic phosphates.[265]

These rare earth orthophosphates have been obtained using the starting components in the following molar ratio:

Eq. (19) $Na_2O : M^{2+}O.\ M_2^{3+}O_3 : M^{+4}O_2 : P_2O_5 = 4.5 : 1 : 0.8 : 10$

This has been reviewed by Byrappa (1990).[267]

Bykov et al. (1990) have obtained $Li_3M_2(PO_4)_3$ (M = Fe, Sc, Cr) using different techniques including hydrothermal technique.[268] However, the resultant product was polycrystalline powder. The crystallization of $Li_3Sc_2(PO_4)_3$ was carried out from the systems: LiH_2PO_4-Sc_2O_3-H_3PO_4-H_2O; $Li_3Sc_2(PO_4)_3$-$NH_3H_2PO_4$-H_2O; and $Li_3Sc_2(PO_4)_3$-LiH_2PO_4-H_2O, besides, $Li_3Sc_2(PO_4)_3$, the other stable phases like $ScPO_4$, and scandium hydroxides have obtained.

Thus, the hydrothermal technique is becoming a popular technique to synthesize rare earth phosphates. What is most important in the case of hydrothermal synthesis of phosphates in comparison with their analogous compounds—silicates and germanates—is that it is yet to be clear as to why a wide range of structural variations have not been achieved through hydrothermal technique. The other synthesis techniques like aqueous solutions, flux, phosphoric acid solutions have resulted in very complex structures whereas the hydrothermal technique has resulted in only a few anhydrous phosphates types like ortho-, diortho-, triortho-groups, pyrophosphates, simple tetra- and ultraphosphates. Therefore, lets discuss the crystal chemistry of rare earth phosphates.

7.13.3 Structure Types of Rare Earth Phosphates

The silicates and germanates have been sufficiently well studied. However, it is only now in the recent years that the rare earth phosphates are being studied extensively. As mentioned earlier, the structures of condensed rare earth phosphates in particular do not resemble the structures of silicates and germanates but the popular representatives such as ortho-, diortho-, ring, layered, chain, ribbon structures, exist in phosphates also, rare earth silicates have forty structure types, the rare earth germanates have thirty-two structure types and rare earth phosphates have over thirty structure types.[53] From the studies on the crystallization of rare earth silicates, germanates and phosphates, it is clear that a decrease in the R_2O_3/X_xO_y (X = Si, Ge, P) ratio leads to the formation of condensed anions. Tables 7.22 and 7.23 give the structure types of alkali-free rare earth phosphates and alkali rare earth phosphates reported so far in the literature.

7.14 HYDROTHERMAL GROWTH OF MIXED VALENT METAL PHOSPHATES

The interest in the synthesis of phosphates, other than rare earth phosphates is connected with the publication of NASICON, whose ionic conductivity is equivalent to that of Na β-alumina. It has a framework structure and the general formula is $Na_{1+x}Zr_2Si_xP3_{-x}O_{12}$; $O < x < 3$.[269] It is a solid solution between $NaZr_2P_3O_{12} - Na_4Zr_2Si_3O_{12}$. NASICON poses a challenge to Materials Scientists in understanding its structure and conduction mechanism due to the lack of single crystals, non-stoichiometry in the composition, zirconium deficiency, etc. Many variations have been investigated by appropriate substitutions in the NASICON system.[265] The basic structure of most of these derivatives remains that of $Na_3Sc_2P_3O_{12}$. NASICON has two structure types viz. NASICON and anti NASICON (Hong 1976; Efremov and Kalinin 1978).[270][271]

The structure of NASICON is highly complicated because, of its solid solution nature. There are nearly a hundred atoms per unit cell, which makes it rather difficult to describe. However, simplification can be introduced by assuming that this type of structure is derived from that of glaserite $K_3Na(SO_4)_2$—a rhomobohedral super structure (Vlasse et al. 1980; Fig. 7.62).[272]

Table 7.22. Structure Types of Alkali-free Rare Earth Phosphates[7][53][243]

Compound	Representative	Cell parameter (Å)	Rare Earth, Co. No., Average bond distance Å			Tetrahedral radical form	Rare earth polyhedra
R $[PO_4]$ R =Gd-Lu, Y,Sc	Y$[PO_4]$	14/amd Z = 4 a = 6.885 c =5.982	Y	8	2.28	ortho-tetra-hedra	framework
R $[PO_4]$ R = La-Eu	Ce$[PO_4]$	$P3_121$ Z = 3 a = 7.055 c = 6.439	Ce	8	2.48	ortho-tetra-hedra	framework
R $[PO_4]$ R =La-Dy	Ce$[PO_4]$ monazite	$P2_1/n$ Z = 4 a = 6.78 b = 7.00 c = 6.44 β =103.63°	Ce	8	2.51	ortho-tetra-hedra	framework
	$YbH_2[P_3O_{10}]$	A_2 Z = 2 a = 5.617 b = 6.666 c =10.011 β =97.32°	Yb	6	2.19	triortho - groups	discrete polyhedra
R $[PO_3]_3$ R = La-Gd	Nd $[PO_3]_3$	$C222_1$ Z = 4 a =11.172 b= 8.533 c = 7.284	Nd	8	2.43	chains with a period of 6 – tetra-hedra	columns
R $[PO_3]_3$ R = Gd-Lu	Yb $[PO_3]_3$	$P2_1/c$ Z = 12 a = 11.219 b= 19.983 c = 9.999 β =97.30°	Yb	6	2.20	chains with a period of 6 tetrahedra	discrete polyhedra
R $[P_5O_{14}]$ R= La-Tb	Nd$[P_5O_{14}]$	$P2_1/c$ Z = 4 a = 8.771 b = 9.012 c =13.057 β =89.58°	Nd	8	2.43	ribbons from 8-membered rings	discrete polyhedra

(Cont'd.)

Drol Books

Table 7.22. *(Cont'd.)*

Compound	Representative	Cell parameter (Å)	Rare Earth, Co. No., Average bond distance Å	Tetrahedral radical form	Rare earth polyhedra
R $[P_5O_{14}]$ R =Dy,Ho, Er,Y	Ho$[P_5O_{14}]$	Pcmn Z = 4 a = 8.926 b=12.71 c = 8.720	Ho 8 2.32	ribbons from 8-membered	discrete polyhedra
R $[P_5O_{14}]$ R = Tb-Lu,Y	Yb $[P_5O_{14}]$	C2/c Z = 8 a =12.830 b =12.676 c =12.337 β =91.25°	Yb 8 2.30	layer from 20 & 8 mem-bered rings	discrete polyhedra

Co. No. = Coordination number

Table 7.23. Structure Types of Alkali Rare Earth Phosphates[7][53][243]

Compound	Representative	Cell parameter (Å)	Rare Earth, Co. No., Average bond distance Å	Tetrahedral radical form	Rare earth polyhedra
$Na_3Sc_2[PO_4]_3$		Bb Z = 4 a = 16.10 b = 9.109 c = 8.928 γ =127.15°	Sc 6 2.092	orthotetra-hedra	discrete polyhedra
$Na_3Sc_2[PO_4]_3$		R3c Z = 6 a = 8.927 c =22.34	Sc 6 2.080	orthotetra-hedra	discrete polyhedra
$Na_{4.5}R_{1.5}[PO_4]_3$ R=Tm,Yb,Lu	$Na_{4.5}Yb_{1.5}[PO_4]_3$	R3c Z = 6 a = 9.12 c =21.81	Yb, Na 6 2.213	orthotetra-hedra	discrete polyhedra
$Na_3R[PO_4]_2$ R =La-Er,Y	$Na_3Nd[PO_4]_2$	Pbc2_1 Z =24 a =15.874 b =13.952 c =18.470	Nd 7 2.41 Nd 6 2.43 Nd 8 2.48 Nd	orthotetra-hedra	discrete polyhedra

(Cont'd.)

Table 7.23. *(Cont'd.)*

Compound	Representative	Cell parameter (Å)	Rare Earth, Co. No., Average bond distance Å	Tetrahedral radical form	Rare earth polyhedra
$K_3Nd[PO_4]_2$		$P2_1/m$ Z = 2 a = 9.532 b = 5.631 c = 7.444 β =90.95°	Nd 7 2.44	orthotetra-hedra	discrete polyhedra
$Na_3Ce[PO_4]_2$		orthorhombic a = 14.07 b = 16.04 c = 18.61 v = 4200 Å^3	Ce — — —	—	——
$MR[PO_4]_2.H_2O$ $K_2Ce[PO_4]_2.H_2O$ M = NH_4, K, Na R = Yb,Ce		orthorhombic a = 12.793 Å b = 14.015 Å c = 15.945 Å v = 2854 Å^3	— — — —	—	—
$M_3R_2[PO_4]_3$ M=Na,K R=Ce-Gd	$K_3Ce_2[PO_4]_3$	P3m1, P31m Z = 3 a = 9.30 c =14.41	— — —	—	—
$KR[PO_3]_4$ R =Eu,Ho	$KHo[PO_3]_4$	C2/c Z = 4 a = 7.798 b =12.310 c =10.551 β =112.63°	Ho 8 2.34	4-membered rings	discrete polyhedra
β-CsR$[PO_3]_4$ R = Pr, Nd	β-CsNd$[PO_3]_4$	143d Z = 12 a =15.233	Nd 8 2.46	4-membered rings	discrete polyhedra
$LiNd[PO_3]_4$		C2/c Z = 4 a = 16.408 b = 7.035 c = 9.726 β = 126.38°	Nd 8 2.46	chains with a period of 4-tetrahedra	discrete polyhedra
α-KR$[PO_3]_4$ R =Nd,Sm, Dy,Ho,Er	α-KNd$[PO_3]_4$	P21 Z = 2 a = 8.007 b= 8.433 c= 7.280 β =91.97°	Nd 8 2.44	chains with a period of 4-tetrahedra	discrete polyhedra

(Cont'd.)

DropBooks

Table 7.23. *(Cont'd.)*

Compound	Representative	Cell parameter (Å)	Rare Earth, Co. No., Average bond distance Å	Tetrahedral radical form	Rare earth polyhedra
$NaNd[PO_3]_4$		P21/n Z = 4 a = 9.907 b =13.10 c = 7.201 β = 90.51°	Nd 8 2.45	chains with a period of 4-tetrahedra	discrete polyhedra
α-$CsR[PO_3]_4$ R = Tb,Pr,Nd	$CsNd[PO_3]_4$	$P2_1$ Z = 2 a = 7.145 b = 8.809 c =11.007 β=105.86°	Nd 8 2.45	chains with a period of 8-tetrahedra	discrete polyhedra
$MR[PO_3]_4$ M=K,Tl,Rb,Cs R=Nd,Ho,Er	$T1Nd[PO_3]_4$	$P2_1$/ Z =4 a =10.440 b = 8.050 c =11.007 β =105.86°	Nd 8 2.441	chains with a period of 8-tetrahedra	discrete polyhedra
$KYb[PO_3]_4$		$P2_1$/n Z = 4 a = 7.776 b = 8.853 c =14.831 β =96.36°	Yb 7 2.27	chains with a period of 8-tetrahedra	discrete polyhedra

Co. No. = Coordination number

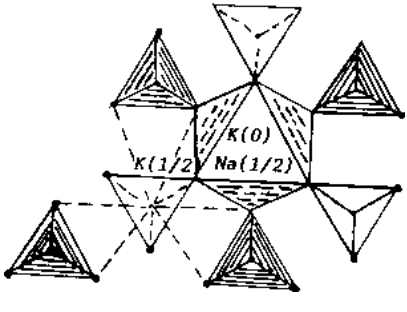

Figure 7.62. Structure of glaserite $K_3Na\ (SO_4)_2$.[272]

Hong (1976) studied the structure of NASICON, $Na_{1+x}Zr_2Si_xP_{3-x}O_{12}$, solid solution series and reported a monoclinic deformation. Space group is C_2/c in the region of x = 1.8–2.2. The first crystal structure of NASICON type material was performed in 1968 by Hagman and Kierkegaard, who studied the structure of $NaM_2(PO_4)_3$ (where M = Ge, Ti and Zr) and found them to be isomorphous.[273] $Na_4Zr_2(SiO_4)_3$ structure has been further studied by Sizova et al. (1973)[274] and Tranqui et al. (1981)[275] and reported multiple Na^+ sites leading to the nonstoichiometry in NASICON compound. Delbecq et al. (1980),[276] Susman et al. (1982),[277] Collin et al. (1983),[278] Boilot et al. (1983),[279] Clearfield et al. (1983),[280] and Baur et al (1986)[281] have reported five different lattice sites for Na^+, out of which only the Na^+ is mobile.

Stoichiometry, structure, and conductivity of NASICON are being studied by several authors consistently from time to time. Since, the structure of NASICON is highly complicated, Materials Scientists continue to strive to develop new superionic conductors with simple structures. Phosphates are found to be the most suitable ones. The structure of these phosphates consist of a three dimensional framework. A series of new NASICON analogs like $Na_3M^{2+}(PO_4)_3$, (M = Sr, Mg, Fe, Mn) [Feltz and Barth 1983.[282] $Na_2(R, M^{3+})M^{4+}(PO_4)_3$ (Byrappa et al. 1986).[267] $A_3M^{3+}(PO_4)_3$, (A = Li, Na, Ag, K; M = Cr, Fe) (Y'voire et al. 1983),[283] $ABC(PO_4)_3$ (A = K, Rb, Cs; B = Ca, Sr; C = Ln and Bi) (Keller et al. 1985) (M = Sc, Cr, Fe) (De la Rochere et al. 1983),[284] were synthesized with an intention to develop compounds having stoichiometric composition and relatively simple structures. However, all these compounds did contain only the ortho-group of radicals irrespective of a wide variety of them. Byrappa and his group have reported, for the first time, pyrophosphates showing high ionic conductivity grown by hydrothermal method (Gali et al. 1989;[285] Byrappa et al. 1989;[286] Gali and Byrappa, 1990[287]).

The hydrothermal method has not been attempted to grow phosphates widely, except for rare earth phosphates and aluminum orthophosphates during the 1950s (Jahn and Kordes 1953;[288] Stanley 1954;[289] Carron et al. 1958;[249] Kurbanov et al. 1981;[290] Yoshimura et al. 1981;[254] Yonghua et al. 1982;[291] Byrappa and Litvin 1983;[255] Y'voire et al. 1983;[292] Keller et al. 1985;[293] Gali et al. 1989;[285] Byrappa et al. 1989;[286] Gali and Byrappa 1990[287]). Only a few reports on the hydrothermal growth of superionics are seen in literature. Clearfield et al. (1986) and Genet and Barj (1983) adopted this technique to process NASICON compounds.[280][294] According to them, an insufficient amount

BrownBooks

of Si^{+4} enters the composition, but it is possible to develop stoichiometric NASICON. The problem arises when Si^{+4} is added to the system. By adopting the hydrothermal method, almost all the problems quoted earlier have been overcome by Byrappa and Gopalakrishna (1985).[251]

In the case of hydrothermal growth, the selection of the nutrient materials, including solvents, is the most important aspect. Such studies are not readily available in the literature as the hydrothermal crystal growers touch upon the solvent effect, solvent-solute interaction, complex formation, etc. only in the recent years. Keeping this in mind, the authors have made an attempt for solvent selection with reference to the superionic pyrophosphates containing different divalent metals. A full understanding of the complex system formed in solutions is inconceivable without a study of the effects of the different solvents on dissolved ionic species. The properties of a solvent are determined jointly by its general chemical nature and physical properties. These properties are involved in such a complex interaction that it is difficult to establish unambiguously how they contribute individually to the general behavior of the solvents. Complex formation reactions occurring in solutions are known to be, in effect, substitution reactions in which the legend replaces solvent molecules bound in the solvate sphere of the metal ion. Thus, it is understandable that the rates, kinetics, and mechanism of such reactions are dependent on the solvents. The magnitude of the interaction between the coordinated solvent molecules and the cation (the strength of the coordinate bond) influences the rate of exchange of the coordinated solvent with some other legend.

In the most complex-equilibrium investigations in solvent mixtures, the choice of the solvent was determined by the solubilities of the components of the system. The aim of the investigations, therefore, was not the detection of the solvent effect, but the determination of the compositions and stabilities of the complexes formed in solution. The linkage between the solvent and solute is essentially coordination type and hence, a varied acid-base complexes have been observed in the solution. Byrappa and Umesh Dutt (1994) and Byrappa and Nirmala (1999) have studied in great detail the hydrothermal crystallization mechanism of $HNaMP_2O_7$ (where M = Mn, Co, Ni, Zn, Cd, Pb) crystals.[295][296] Table 7.24 gives the experimental conditions of the growth of these novel phosphates with very interesting structures. In all the experiments 85% H_3PO_4 and NaOH solutions have been used as the solvents and only in a very few experiments, other solvents like HNO_3, HCl, H_2SO_4, HCOOH, etc. have been used.

Table 7.24. Experimental Conditions For Low Temperature Hydrothermal Synthesis (from the works of K. Byrappa)

Compound	Nutrient Components				T °C	P (bars)	Duration (days)	Size mm	Prominent Faces	Morphology
$Na_2H_3Al(P_2O_7)_2$	H_3PO_4 (ml)	NaOH (ml)	Al_2O_3 (gm)	$Zr(NO_3)_4$ (gm)						
	6	5(5M)	1	0.5	250	85	8	0.15-2	010	rhombohedral, tabular, rods, shaped, prismatic
$NaHCoP_2O_7$	H_3PO_4 (ml)	NaOH (ml)	$Co(NO_3)_4$ (gm)	$Zr(NO_3)_4$ (gm)						
	5	5(5M)	1	0.3	250	80	8	0.5-2	010	perfect rhombo-hedral, prismatic red shaped
$NaHNiP_2O_7$	H_3PO_4 (ml)	NaOH (ml)	$NiCl_2$ (gm)	$Zr(NO_3)_4$ (gm)						
	5	5(5M)	1.0	0.5	250	85	8	0.5	110	prismatic, rod shaped
	5	5(5M)	1.25	0.5	250	85	8	0.5		
	5	5(5M)	1.5	0.5	250	90	8	0.5-1.5		

(Cont'd.)

DropBooks

Table 7.24. *(Cont'd.)*

Compound	Nutrient Components				T °C	P (bars)	Duration (days)	Size mm	Prominent Faces	Morphology
$NaHMnP_2O_7$	H_3PO_4 (ml)	NaOH (ml)	$MnCl_2$ (gm)	$CaCo_3$ (gm)						
	5	5(5M)	1.5	0.75	250	85	8	1	100	rod shaped,
	5	5(5M)	1.5	1.00	250	90	8	1-3		prismatic
	5	5(5M)	1.5	1.25	250	90	8	2-3		
	5	5(5M)	1.5	1.5	250	90	8	2		
$NaHZnP_2O_7$	H_3PO_4 (ml)	NaOH (ml)	ZnO (gm)	$Zr(NO_3)_4$ (gm)						
	5	5(5M)	0.5	0.5	250	80	8	1-2	101	prismatic,
	5	5(5M)	0.75	0.5	250	80	8	1-2		needles
	5	5(5M)	1.00	0.5	250	85	8	2-5		
	5	5(5M)	1.50	0.5	250	90	8	1-3		
$NaHCdP_2O_7$	H_3PO_4 (ml)	NaOH (ml)	CdO (gm)	$Zr(NO_3)_4$ (gm)						sub-rounded,
	5	5(5M)	1	0.5	250	70	8	2-5	111	tabular, dome shaped

The hard bases H_2O, OH^-, PO_4^{-3}, NO_3, and SO_4^{2-} act upon the dissolution of the solvated complexes determining the solubility of the final resultant stable complex.[297] The following reaction series can be proposed for the formation of $HNaCoP_2O_7$:

$$3NaOH + H_3PO_4 \rightarrow Na_3PO_4 + 3H_2O$$

$$3Co(NO_3)_2 + 2H_3PO_4 \rightarrow Co_3(PO_4)_2 + 3H_2O + 6NO_2\uparrow + 3[O]\uparrow$$

$$Zr(NO_3)_4 + 4NaOH \rightarrow 4NaNO_3 + 2H_2O + ZrO_2\downarrow$$

$$2H_3PO_4 \rightarrow H_4P_2O_7 + H_2O$$

$$Na_3PO_4 + H_4P_2O_7 \rightarrow NaH_3P_2O_7 + HNO_3$$

$$Na_3PO_4 + H_4P_2O_7 \rightarrow NaH_3P_2O_7 + Na_2HPO_4$$

$$Co_3(PO_4)_2 + H_4P_2O_7 + 4H_2O \rightarrow H_2CoP_2O_7 + 2H_3PO_4 + 2Co(OH)_2$$

$$Co(NO_3)_2 + H_4P_2O_7 \rightarrow H_2CoP_2O_7 + 2HNO_3$$

$$Co(NO_3)_2 + H_4P_2O_7 \rightarrow H_2CoP_2O_7 + 2HNO_3$$

$$NaOH + H_2CoP_2O_7 \rightarrow HNaCoP_2O_7 + H_2O$$

$$Co(OH)_2 + NaH_3P_2O_7 \rightarrow HNaCoP_2O_7 + 2H_2O$$

The formation of a stable complex, i.e., $HNaCoP_2O_7$ at 250°C and 100 bars pressure, must have undergone several intermediate stages of solvation, forming stable and unstable solvated complexes like $NaNO_3$, having very low values of lattice energy constant, 755 kJ/mole, and Co, which has a desolvation energy value around 15 eV, etc. that have further interacted with each other because of their weak ionic bonding of very low charge to give a stable coordinated compound with a very high of lattice energy constant and stronger ionic bonding. But at temperatures around 250°C, the polymerization of the ortho-group of phosphates to form the pyro-group with higher lattice energy may be expected. Also, the reaction between the alkali pyrophosphate complexes with metal complexes results in the formation of stable complexes of pyrophosphate, i.e., $HNaCoP_2O_7$.

The hydrothermal crystallization of these superionic phosphates has been studied through another approach, which is quite effective from the point of hydrothermal solution chemistry.

The crystallization process involves many chemical interactions leading to the formation of a stable complex. To understand the growth of

DropBooks

title compounds, the authors have described the following possible stages of interactions:[295]

1) acid-base interactions
2) formation of metal-aqua complexes
3) interaction between acid-base and metal-aqua complexes

Acid-base Interactions. Components such as H_2O, OH^- and PO_4^{3-} are considered as the hard and form pyrophosphate complexes at around 250°C:

Eq. (20) $2H_3PO_4 \rightarrow H_4P_2O_7 + 2H_2O$

Eq. (21) $NaOH + H_4P_2O_7 \rightarrow NaH_3P_2O_7 + H_2O$

As the pH increases the stability of $NaH_3P_2O_7$ decreases (pH>3), and this leads to the formation of $Na_2H_2P_2O_7$.

Eq. (22) $NaOH + NaH_3P_2O_7 \rightarrow Na_2H_2P_2O_7 + H_2O$

The occurrence of Eq. (22) also increases the pH of the system, but the compound $Na_2H_2P_2O_7$ is stable in the pH range 3–9. The formation of $Na_3HP_2O_7$ is favored if pH > 9.

Eq. (23) $NaOH + Na_2H_2P_2O_7 \rightarrow Na_3HP_2O_7 + H_2O$

Formation of Metal-aqua Complexes. The zinc metal-aqua complexes in the hydrothermal system have been studied in detail. The tendency of zinc towards a tetrahedral coordination is evidently responsible for the existence of $[Zn(H_2O)_x(OH)_{4-x}]^{x-2}$ type aqua complexes in aqueous solutions, where the value of x depends on the pH of the medium.[298] In strong alkaline solutions, $Zn(OH)_4^{2-}$ occurs (and here x = 0). By reducing the solution pH to neutral, a dizincate $[Zn_2O(H_2O)_x(OH)_{6-x}]^{x-4}$ may be formed as a result of the association of zincate ion.

The zinc oxide forms aqua complexes when dissolved in alkaline solutions.[299] The distribution of zinc aqua ions in alkaline solution is shown in Fig. 7.63.

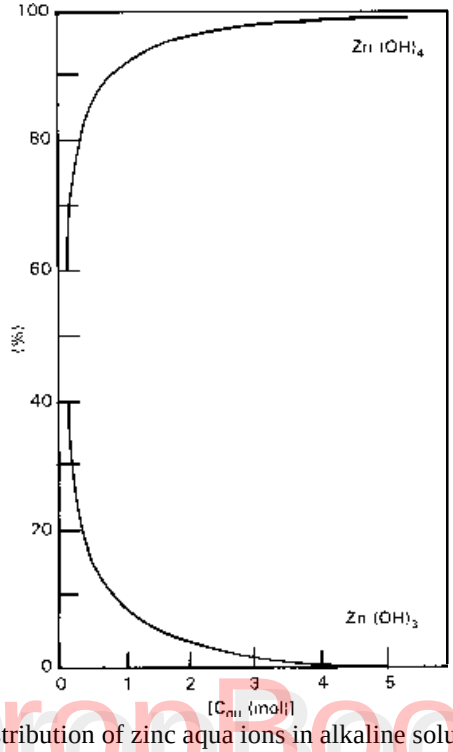

Figure 7.63. Distribution of zinc aqua ions in alkaline solution.[299]

DropBooks

Similar aqua complexes can be expected for the other divalent cations, like Mn^{2+}, Ni^{2+}, Fe^{2+}, Cu^{2+}, Pb^{2+}, Cd^{2+} and others, under hydrothermal conditions.

Although the metal cations form octahedral complexes, tetrahedral complexes are the more stable ones, and a few octahedral complexes retain their constitution for a long time depending upon their half-life of aqua-ligands.[300]

Interactions Between Acid-base and Metal-aqua Complexes. Pyrophosphoric acid forms salts due to the sequestering action of the pyrophosphate radical, the sequestering ability decreases with higher concentrations of salts, or with increasing pH. Interactions between metal-aqua complexes with the sodium salts of pyrophosphoric acid can be written as follows:

Eq. (24) $$NaH_3P_2O_7 + M(OH)_2 \rightarrow HNaMP_2O_7 + 2H_2O$$
(pH = 2–3)

Eq. (25) $Na_2H_2P_2O_7 + M(OH)_2 \rightarrow HNaMP_2O_7 + NaOH + H_2O$ (pH = 3–9)

Eq. (26) $Na_3HP_2O_7 + M(OH)_2 \rightarrow HNaMP_2O_7 + 2NaOH$ (pH > 9)

where M = Mn, Fe, Co, Ni, Cu, Zn, Pb.

The aqua complexes can form more stable complexes because of the higher desolvation energy of metal cations when compared to sodium (3.97 eV). Hence, the formation of $HNaMP_2O_7$ is expected in the system instead of stable sodium salts of pyrophsophoric acid, namely $Na_2H_2P_2O_7$ and $Na_4P_2O_7$.

The hydrothermal growth of $HNaMP_2O_7$ (where M = Mn, Co, Ni, Zn, Cd, Pb) crystals clearly show that there is a gradual change in the crystallinity and morphology from Mn end to the Pb end. Table. 7.25 shows the cations in superionic pyrophosphates. As evident from Table 7.25, higher the entropy values the lower will be the degree of crystallinity and the crystal morphology. For example, $HNaMP_2O_7$ (M = Mn, Co, Al, Ni) show good crystallinity and well-developed crystal morphology, whereas the crystals $HNaMP_2O_7$ (M = Zn, Cd, Pb) with higher entropy values have a lower degree of crystallinity. These crystals show poor morphology and are often polycrystalline.[301]

Table 7.25. Cations in Superionic Pyrophosphates[301]

Element	At.No.	At.Wt.	At.radii* (A^o)	Entropy at 298 ^oK (e.u)
Al	13	65.38	1.82	6.769
Mn	25	54.93	1.79	7.590
Co	27	58.93	1.67	6.800
Ni	28	58.70	1.62	7.137
Zn	30	65.38	1.53	9.950
Cd	48	112.41	1.71	12.300
Pb	82	207.20	1.81	15.490

* Ref. Table of periodic properties of the elements,
Sargent-Welch Scientific Company

The authors have obtained good crystals up to 6 mm size. Twinning was absent in general, except in crystals doped with additives. In the case of $(Na_{2/3}Zr_{1/3})_2P_2O_7$, Bi and Ce were added as additives even in higher concentration, but they did not enter the composition. The cations play a major role in the crystallization of pyrophosphates. Also, divalent metals enter the composition more easily than trivalent metals, particularly in condensed phosphates. A large number of experiments have been carried out using Al, Cr, Fe, Bi, Co and rare earths even in surplus amount. Only Al enters the composition easily and others need higher temperature of synthesis. The volatiles and type of cations play a major role in the crystallization of condensed phosphates. The morphology of these crystals depend upon the concentration of P_2O_5 and H_2O in the system (Byrappa 1990).[267][302] For example, in $NaHCo(P_2O_7)$ crystals, the prism faces dominate over the pyramidal faces with an increase in P_2O_5 and H_2O concentration. The morphology of these superionic pyrophosphates is very interesting and it is shown together with their schematic diagrams in Fig. 7.64 *a–e*. The crystallization was carried out by spontaneous nucleation, which was controlled by a systematic rate of heating. Hence, the crystals were well developed and of excellent quality.

The x-ray diffraction studies (both powder and single-crystal) show that these crystals belong to the lower symmetry and show very interesting morphology. A general morphology of these pyrophosphates is given in Table. 7.25.

PropBooks

In order to grow these crystals, it is very important to know their solubility, internal atomic structure, macro- and micromorphology. The solubility of these pyrophosphates was found to be positive. Similarly, the crystals obtained by the hydrothermal technique show very interesting morphology. Hence, it becomes rather easy to grow them as bulk single crystals of several centimeters in length, despite the phosphoric acid media in which the growth occurs.

The most common morphological habits observed in pyrophosphates are perfect rhombohedral, prismatic, rod shaped, etc. The crystal faces are more or less smooth and vitreous in luster, with a high degree of transparency. The prism faces dominated over all other faces in all the crystals followed by pinacoidal and dome faces. There is a clear-cut distinction in the morphology of these pyrophosphates. In most of the experiments the entry of the selective dopants was controlled in order to observe the morphological variations. The morphology of these pyrophosphates varies from one to another, depending on the cations present.

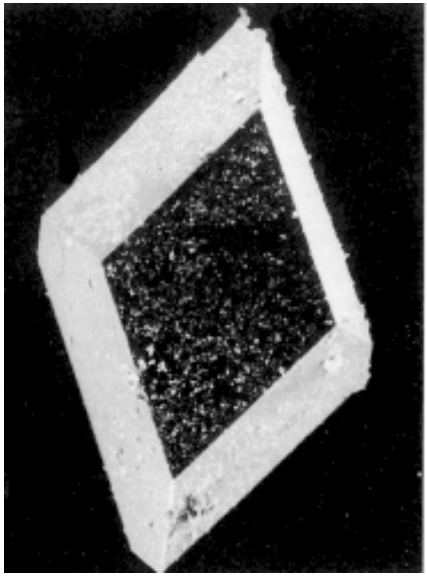

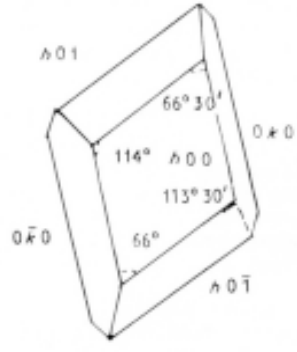

(a)

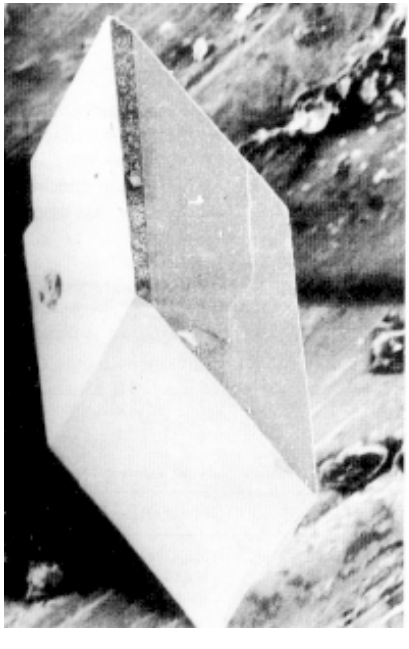

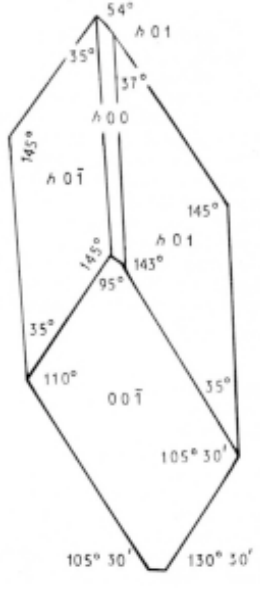

(b)

Figure 7.64. Morphology of superionic pyrophosphates.[302]

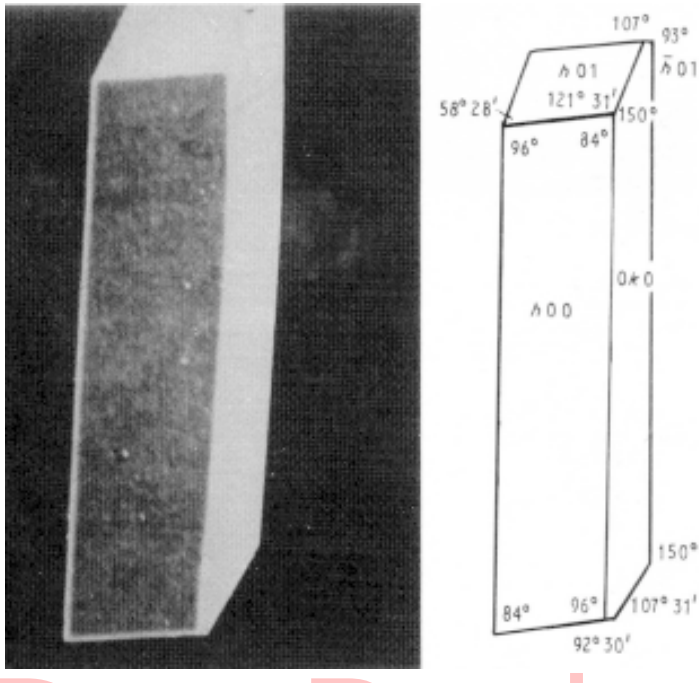

(c)

DropBooks

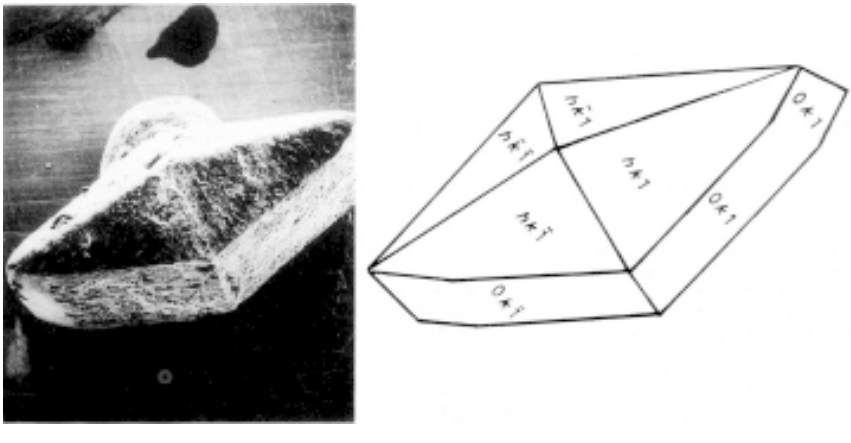

(d)

Figure 7.64. *(Cont'd.)*

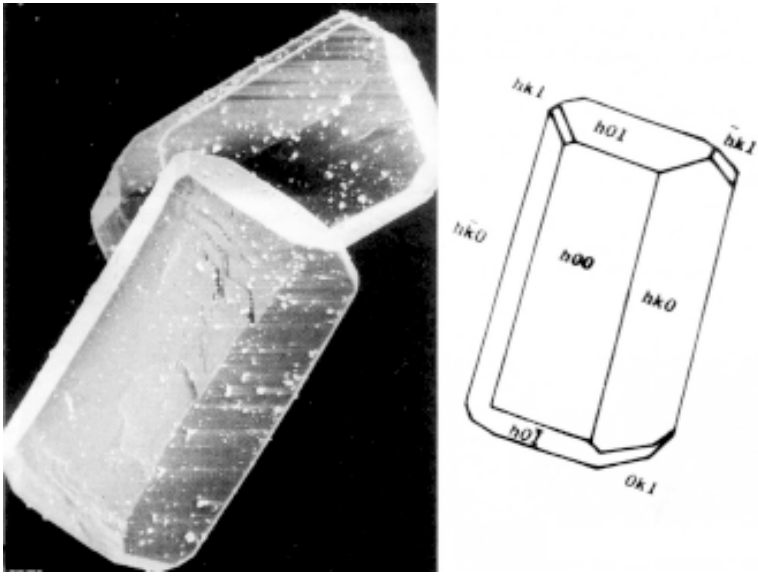

(e)

Figure 7.64. *(Cont'd.)*

To gain an understanding of the morphological variation with respect to the growth conditions, it is essential to study particularly the role of the degree of supersaturation, the concentration of water and Na_2O in the system. $NaHCo(P_2O_7)$ and $NaHZn(P_2O_7)$ crystals were selected for such a systematic study, because these compounds show a very well-developed morphology and are sensitive to such variations. In fact, both these compounds show similar morphological variations. Figure 7.64 *a–e* shows how the morphology varies with the concentration of P_2O_5. This is further represented in the schematic diagram of Fig. 7.65. The interfacial angles for the representative pyrophosphates have been measured using a Leitz phase-contrast microscope and these angles are shown in the schematic diagrams of Fig. 7.65. As the concentration of P_2O_5 and H_2O increases, the pyramidal faces are replaced by the prismatic and the pinacoidal faces.[302] Similarly, an attempt has been made to study the variation of the growth rate of $NaHCo(P_2O_7)$ crystals with concentration of P_2O_5, Na_2O and H_2O (Fig. 7.66 *a–c*). These figures show critical points, beyond which the growth rate falls sharply. This helps to fix the optimum conditions for the growth of $NaHCo(P_2O_7)$. [302]

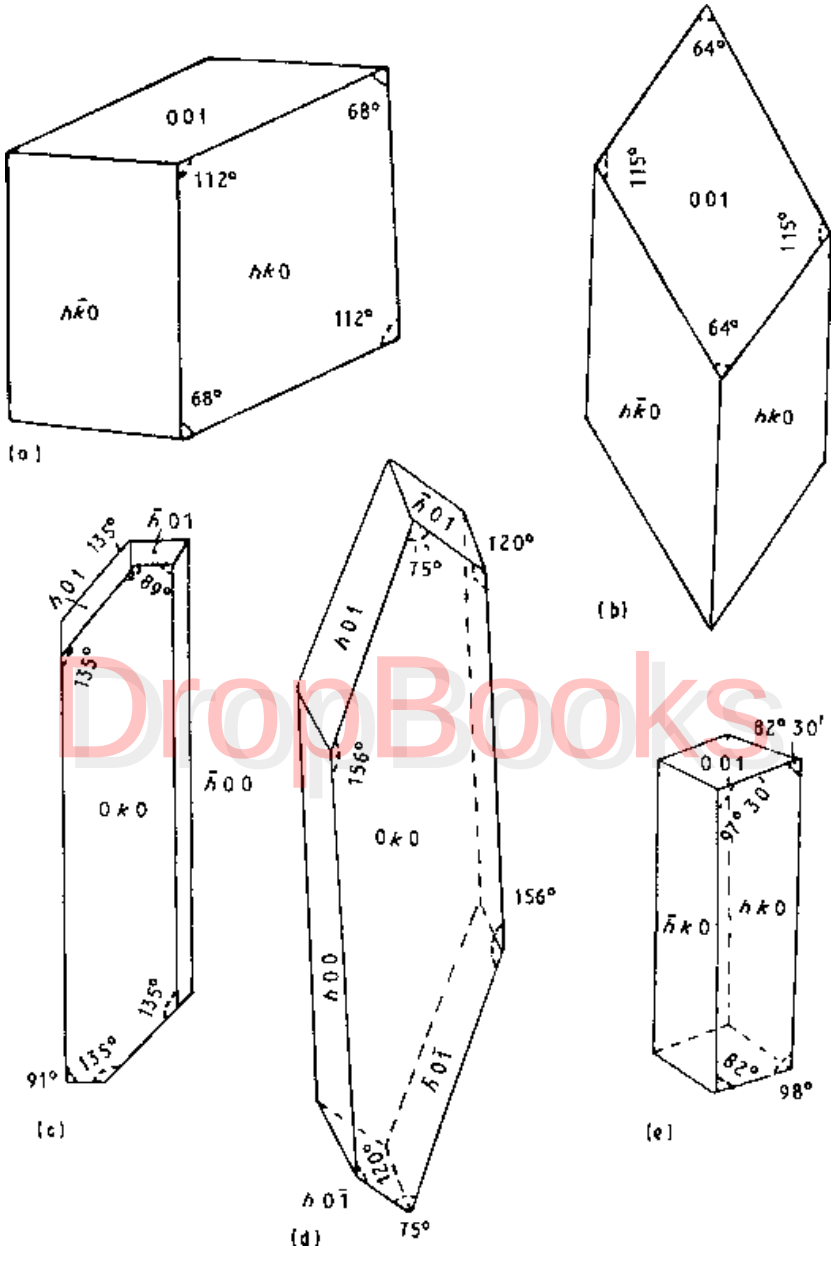

DropBooks

Figure 7.65. Schematic diagrams of the variation in morphology of superionic pyrophosphates with P_2O_5 content in the system.

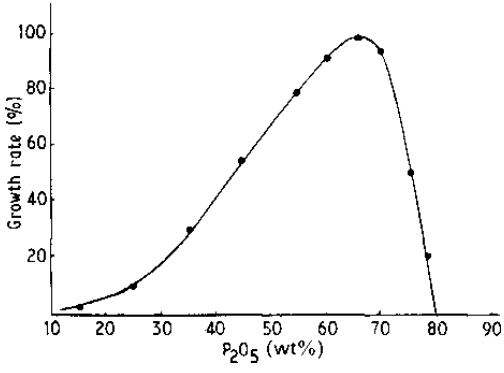

(a)

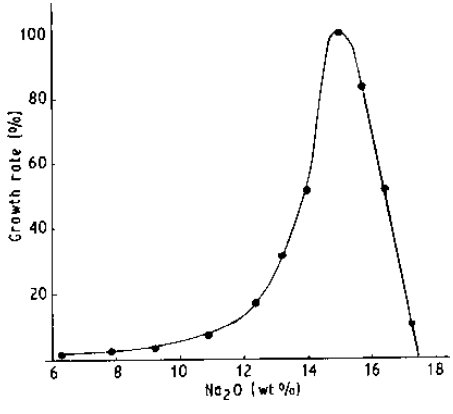

(b)

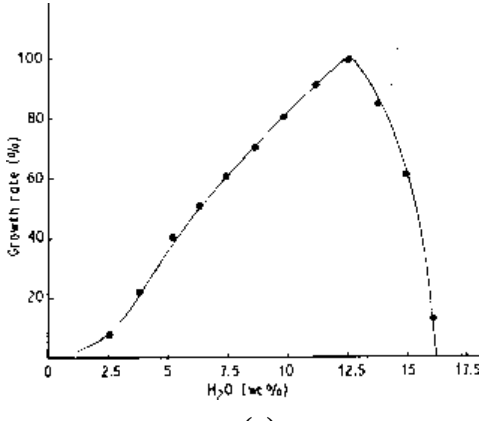

(c)

Figure 7.66. Growth rate of superionic pyrophosphate, $NaHCo(P_2O_7)$ vs. *(a)* P_2O_5 concentration, *(b)* Na_2O concentration, and *(c)* H_2O concentration.[302]

Similar features were observed in the case of $NaHZn(P_2O_7)$ crystals. Representative photographs (Fig. 7.67) of $NaHZn(P_2O_7)$ show how morphology varies with the above-mentioned growth parameters. These experiments indicate that the degree of supersaturation, concentration of cations and dopants determine the morphology of these pyrophosphates. Such studies help in the successful growth of superionic phosphates in the form of single crystals with a desired morphology. They help to understand the growth technology of these phosphates in detail.

DropBooks

Figure 7.67. Photographs of NaHZn (P_2O_7) crystals (magnification $\times$ 30).[301]

A number of factors such as the degree of supersaturation, temperature, pressure, accidental/deliberate entry of impurities and their concentration, type of the solvent, pH of the mineralizer, etc. affect the habit of crystals obtained under hydrothermal conditions. Habit modifications are also observed when significant changes in the growth temperature occur, since increase in temperature hastens the growth kinetics and in turn growth rate.

The crystal faces of most of the superionic pyrophosphates are more or less smooth and vitreous in luster with a high degree of transparency. The morphology of these pyrophosphates varies from one another depending upon the cations present.

It is interesting to observe the morphological variations in the pyrophosphates with reference to the variation in the cation. The cations used are essentially the divalent and trivalent metals such as Al, Mn, Co, Ni, Zn, Cd, and Pb. Table 7.25 shows cation properties. As evident from, Table 7.25 the Al is the smallest ion and it shows the excellent morphology (Fig. 7.64a). The crystals are very well developed and highly transparent. This is followed by Mn, which gives good crystals of excellent crystal habit. However, due to the susceptibility of Mn for the changes in the valency with sudden changes in the experimental growth parameters, there is a tendency for the formation of polymorphic modifications of Mn bearing pyrophosphates. But both the polymorphic modifications of Mn superionic pyrophosphates show excellent morphology with well developed habits, smooth and vitreous surfaces (Fig. 7.64*a*).

The cobalt bearing superionic pyrophosphate shows probably the best morphology (Fig. 7.64*b*). The crystals are very well-developed with vitreous and smooth surfaces having a high degree of transparency. The size of the cobalt bearing pyrophosphate is higher than the other pyrophosphates of this class.

It is believed that all these superionic pyrophosphates belong to the same structure type, i.e., triclinic, P1 space group. As the ionic size of the cations inserted into the structure increases, there develops a general structural distortion, which in turn affects the crystal morphology. Table 7.26 shows the variation in bond lengths of these pyrophosphates. As evident from Table 7.26, the difference in maximum and minimum bond lengths of Na-O polyhedra increases gradually towards the Zn end member. Thus, towards the Pb end member, the crystals become poorly developed. The poor morphology of Cd and Pb bearing pyrophosphates is due to the changes in the bond lengths and bond angles leading to the slightly higher degree of structural disorder as indicated by the preliminary X-ray single crystal diffraction studies. Also, it is evident from Table 7.25 that the values of entropy for Zn, Cd, and Pb gradually increase and these values are quite high compared to those of Mn, Al, Co, or Ni. Entropy is directly related to the structural disorder. Thus, the thermodynamic properties of the cations directly influence the morphology of these new novel pyrophosphates.

Table 7.26. Bond Lengths For Superionic Pyrophosphates Crystals[301]

Compound	Na-O (max)	Na-O (min)	Na-O Dif. (max -min)	M^{+2}-O (max)	M^{+2}-O (min)	M^{+2}-O Dif. (max -min)	P_1-O (max)	P_1-O (min)	P_1-O Dif. (max -min)	P_2-O (max)	P_2-O (min)	P_2-O Dif. (max -min)
$Na_2AlH_3(P_2O_7)_2$	2.929	2.397	0.532	1.940	1.855	0.085	1.599	1.495	0.104	1.587	1.500	0.087
$NaMnH\ P_2O_7$	2.79	2.32	0.47	2.20	2.00	0.2	1.64	1.52	0.12	1.58	1.49	0.09
$NaCoHP_2O_7$	3.097	2.445	0.652	2.196	2.035	0.161	1.587	1.502	0.85	1.602	1.498	0.104
$NaNiHP_2O_7$	3.385	2.315	1.07	2.157	2.016	0.141	1.593	1.505	0.085	1.607	1.497	0.11
$NaZnHP_2O_7$	3.446	2.308	1.138	2.283	2.020	0.263	1.591	1.504	0.087	1.595	1.488	0.107

DropBooks

There are several publications, but the majority of these publications essentially deal with the general synthesis of a large variety of phosphates under hydrothermal conditions and hence, in most of the cases, the resultant product contained either crystalline powder or tiny crystals. However, one can grow these as single crystals if systematic investigations are carried out as in the case of $NaHMP_2O_7$ (M = Ni, Co, Mn, Zn, Cd, Pb) crystals.

7.15 PROPERTIES OF RARE EARTH AND MIXED VALENT METAL PHOSPHATES

The rare earth phosphates are known as the laser-host materials, and mixed valent metal phosphates show very interesting physico-chemical properties, especially the superionic properties. Laser beams have been obtained from condensed rare earth phosphates containing active elements like Nd, Pr, Er, Eu. In this respect the ultraphosphates RP_5O_{14} and tetraphosphates MRP_4O_{12} (where M = Li, Na, K, Rb, Cs; R = Nd, Pr, Eu, Er) are the most popular ones. Figures 7.68 and 7.69 show the luminescence spectra of NdP_5O_{14} and α-$CsNd(PO_3)_4$ crystals of hydrothermal origin.[303][304] Similarly, ionic conductivity has been reported in some of the crystals of MRP_4O_{12}.[305] However, the ionic conductivity values are not high and not comparable to mixed valent metal phosphates. Since majority of these compounds either belong to the NASICON family or analogous to NASICON structures, they obviously exhibit high ionic conductivity. $Na_3M^{2+}(PO_4)_3$ (M = Sr, Mg, Fe, Mn); $A_3M^{3+}(PO_4)_3$ (A = Li, Na, Ag, K; M = Cr, Fe); $ABC(PO_4)_3$ (A = K, Rb, Cs; B = Ca, Sr ; C = Ln and Bi) $NaHMP_2O_7$ (M = Mn, Co, Ni, Zn, Pb, Cd); $Na_{.66}Zr_{.33})_2(P_2O_7)_2$, and so on, exhibit high ionic conductivity. The unique feature of these NASICON analogs is the thermal stability. Unlike the NASICON compound, whose ionic conductivity is hampered by the presence of multiple phase transitions from > 60°C, these compounds show only one or two phase transitions, usually > 400°C.[306] Figure 7.70 shows the DTA curves for the representative superionic pyrophosphates. Similarly $MSn_2(PO_4)_3$ (M = Na, K, NH_4) grown hydrothermally is stable up to 1200°C without phase transitions.[307]–[309] Also, some of the rare earth phosphates show ultra-low thermal expansion coefficient, which has a potential application in several fields.[310] Byrappa et al. (1994) & Sanjeev (1996) have studied the ionic conductivity in superionic pyrophosphates within a wide range

of temperature and internal frequency.[311][312] Figures 7.71 and 7.72, show the Arrhenius Plot and the complex-impedance plots for the representative superionic pyrophosphates.

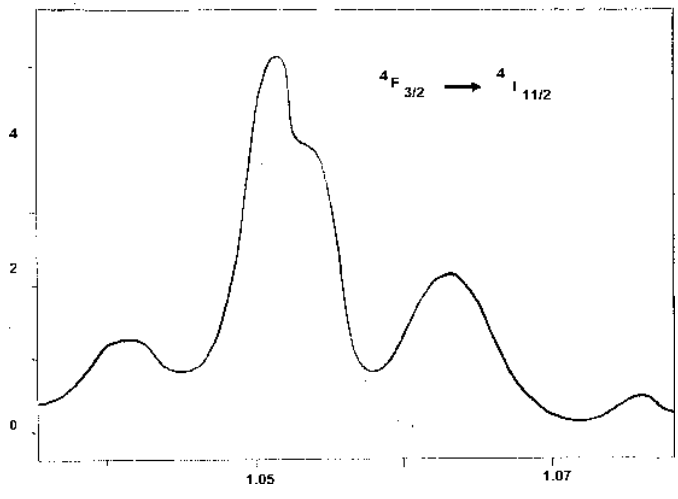

Figure 7.68. Luminescence spectra of NdP_5O_{14} crystals.[303]

DropBooks

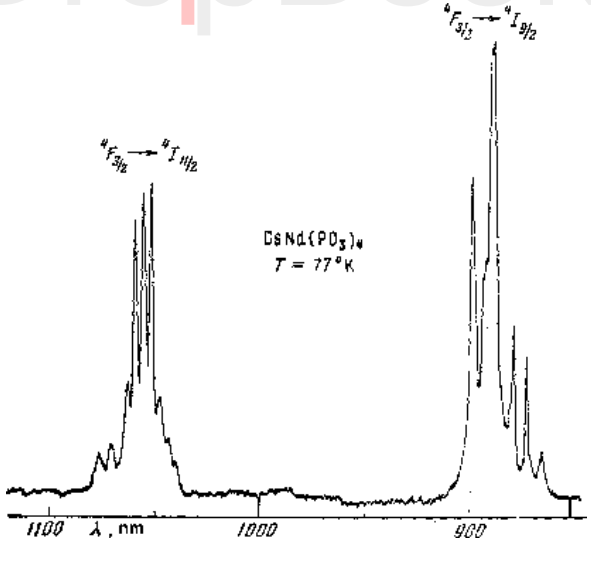

Figure 7.69. Luminescence spectra of α - CsNd $(PO_3)_4$ crystals.[304]

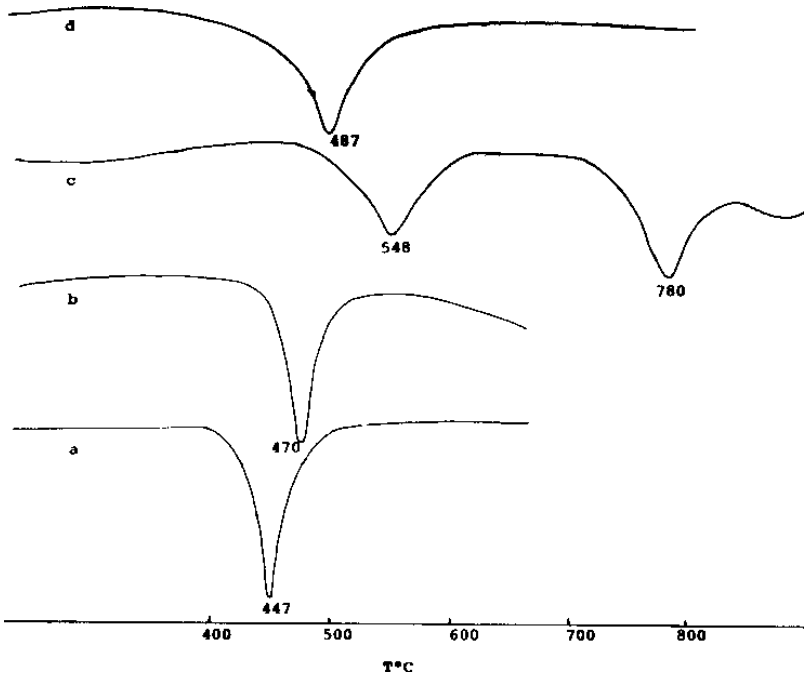

Figure 7.70. DTA curves for the representative superionic pyrophosphates.[306]

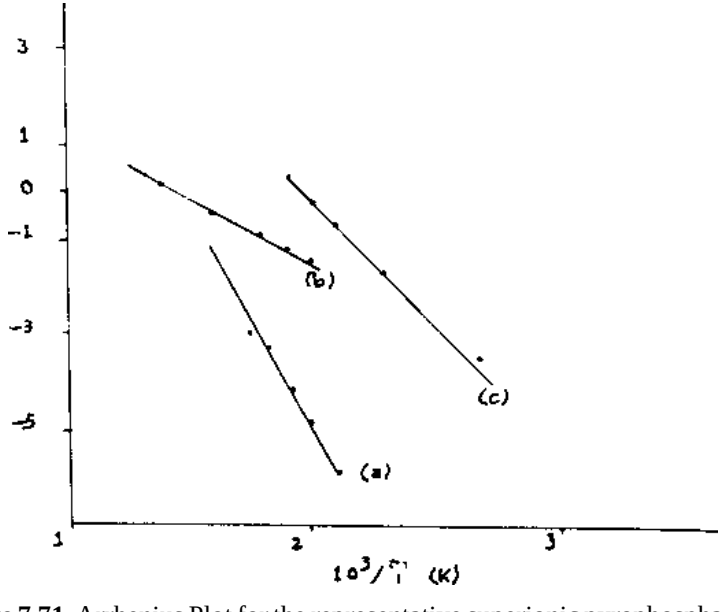

Figure 7.71. Arrhenius Plot for the representative superionic pyrophosphates.[311]

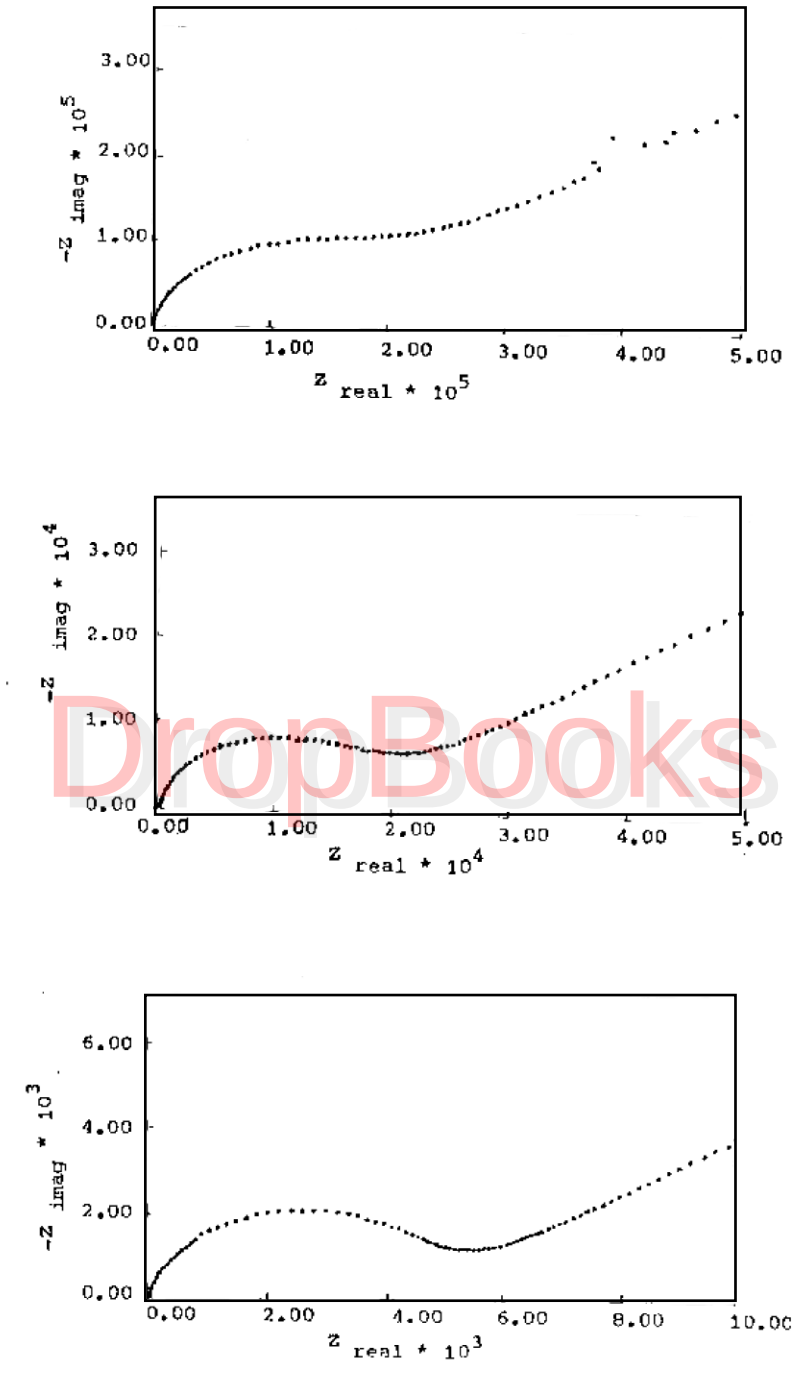

DropBooks

Figure 7.72. Complex - impedance plots for the representative superionic pyrophosphates.[311]

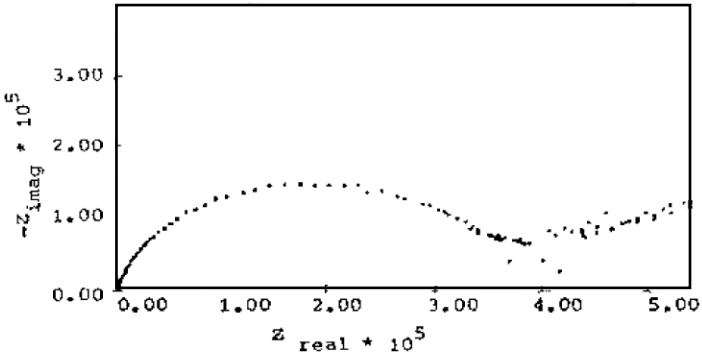

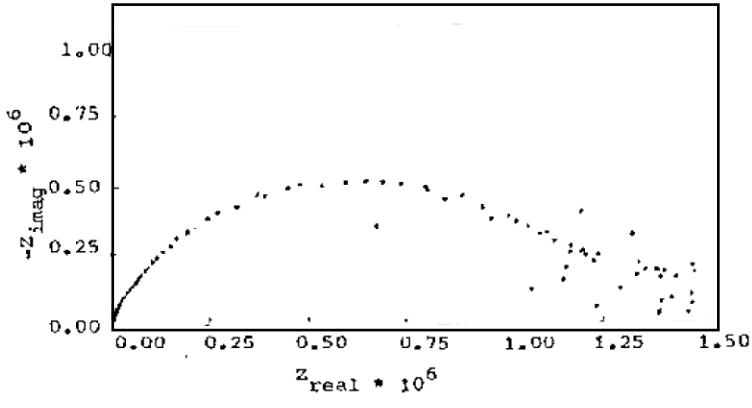

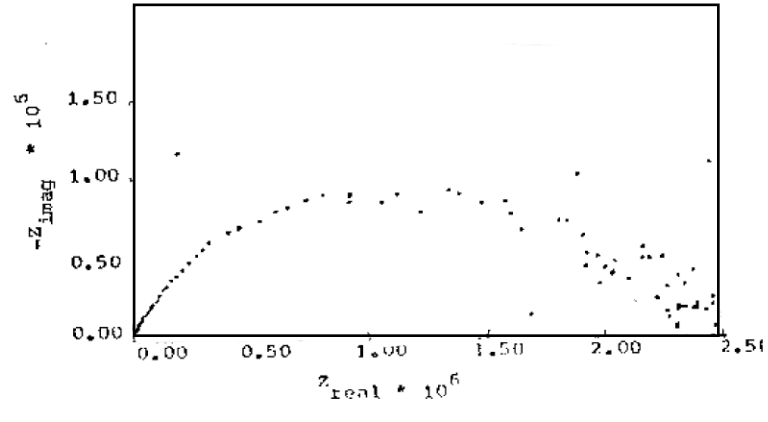

Figure 7.72. *(Cont'd.)*

$AVOPO_4$ (A = Li, Na, K) group of compounds are very interesting and isostructural with the well-known nonlinear optical material $KTiOPO_4$. These compounds have high thermal stability and magnetic susceptibility. The experimental results show that the Curie-Weiss behavior: $\lambda_M = C/CT - \theta)$, where C = 0.4168 cm^3 K/mol is the curie constant and $\theta = -67.5$ is the Weiss temperature with increasing temperature, λ_M first decreases rapidly but reaches a minimum at $T \sim 15$ K, increases up to ~ 40 K, then smoothly decreases again with temperature. (See Fig. 7.73)[313] Similarly very interesting magnetic susceptibility has been reported in several other hydrothermally prepared metal vanadyl phosphates like $K_2(VO)_3(HPO_4)_4$, $Mn_2VO(PO_4)_2,H_2O$, a-$NH_4(VO_2)(HPO_4)$, $CsMo_2O_3(PO_4)_2$ and so on.[314]–[317] Figure 7.74 shows a plot of the reciprocal magnetic susceptibility vs. temperature for $Mn_2VO(PO_4)_2.H_2O$. This compound displays Curie-Weiss behavior down to $T_N = 20$ K, at which point an antiferromagnetic transition takes place. The high temperature portion (150–300 K) was fit to the Curie-Weiss expression, yielding a Curie constant of C = 9.0 emu K^{-1} $mole^{-1}$ and a Weiss constant of $\theta = -46$ K. The effective magnetic moment μ_{eff} = 8.5 BM. The origin of the antiferromagnetic interaction most likely arises between Mn(2) and V atoms, which are 3.150 Å apart in their edge-sharing polyhedral arrangement.

DropBooks

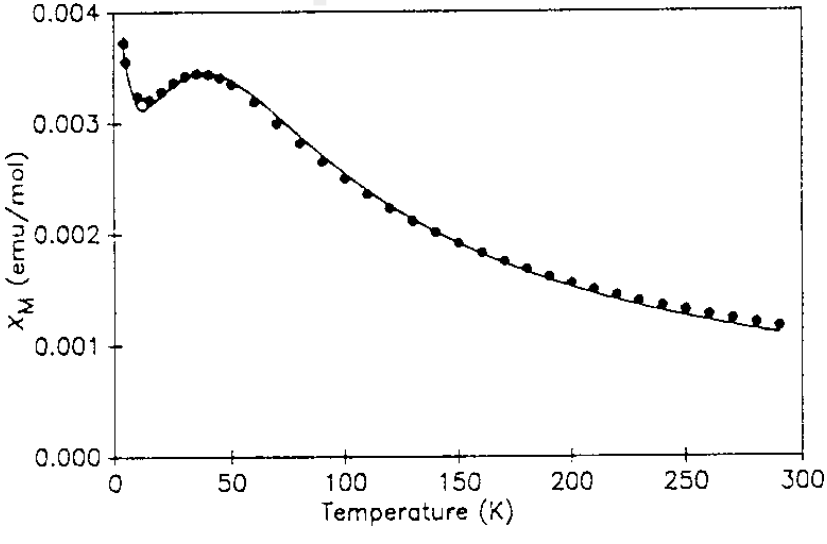

Figure 7.73. Thermal stability and magnetic susceptibility of $Mn_2VO(PO_4)_2 \cdot H_2O$.[313] *(Courtesy of the Academic Press, Orlando, Florida.)*

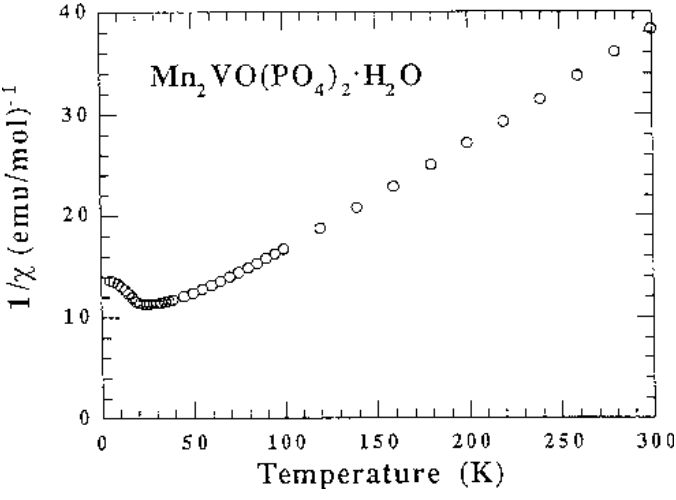

Figure 7.74. Plot of the reciprocal magnetic susceptibility vs. temperature for $Mn_2VO(PO_4)_2 \cdot H_2O$.[315] *(Courtesy of the Academic Press, Orlando, Florida.)*

7.16 HYDROTHERMAL SYNTHESIS OF VANADATES

The synthesis of vanadates is not as popular as silicates, phosphates, germanates or sulphates, because of their limited use in the modern technology unlike its analogous materials silicates or phosphates. Further, the synthesis of vanadates is relatively a recent field. The first systematic synthesis of vanadates was during the 1950s, when ABO_4 (A = Al, Ga, B, Bi, Fe, etc.; B = P, V, As) isostructural to $AlPO_4$ was obtained.[318] However, the solid state synthesis was the most popular one followed by the flux method. The main objective of the synthesis of AVO_4 (A = Al, Cr, B, Fe, Ga, Mn, etc.) was academic, and it was quite recently their technological potential was explored. For example, $FeVO_4$ shows very interesting magnetic properties. This compound shows successive phase $FeVO_4$-I $\rightarrow$ $FeVO_4$-II $\rightarrow$ $FeVO_4$-III $\rightarrow$ $FeVO_4$-IV type structures with increasing pressures.[319] During the 1970s, a series of simple and complex rare earth vanadates were synthesized with a motivation to develop new luminophors, because a majority of these vanadates, particularly mixed rare earth phosphates, contain isolated rare earth ions.[320] Whereas, simple rare earth orthovanadates show very high thermal stability owing to their very high melting points and also exhibit unique optical and magnetic properties.[321–323] All these simple rare earth orthovanadate

single crystals have been obtained by flux and melt techniques. Byrappa et al. (1987) attempted the synthesis of vanadates for the first time by hydrothermal technique, and they have obtained $NH_4Zr_2V_3O_{12}$ crystals, which show interesting proton conducting properties.[324] However, during the 1990s, it was shown that the hydrothermal technique helps in synthesizing a new class of compounds with unique structures, especially from the phosphate, vanadate and arsenate groups. This made the hydrothermal technique popular for the synthesis of novel vanadates, which exhibited interesting physico-chemical properties owing to their unique structural peculiarities. Similarly, the growth of simple rare earth orthovanadates doped with active elements was realized by hydrothermal technique quite recently.[325]

Here, we describe the growth of simple rare earth orthovanadates and mixed metal vanadates of recent importance by hydrothermal method.

7.16.1 Growth of R = MVO_4 (R = Nd, Eu; M = Y, Gd)

Single crystals of yttrium orthovanadate, YVO_4 with zircon structure, $ZrSiO_4$ having tetragonal space group I4/amd[326] find extensive applications owing to their most valuable unusual magnetic, optical and luminescent properties. Hence, they are used as highly efficient laser diode pumped microlasers,[327] an efficient phosphor[328] as very attractive polarizer material,[329] and low-threshold laser host.[330] The laser emission cross-section of Nd:YVO_4 at 1064 nm is 2.7 times greater than that of Nd:YAG.[331] As a laser host material, Nd:YVO_4 offers attractive properties such as highly polarized emission, large absorption cross-section, high thermal fracture limit, and good mechanical strength. Together, these characteristics are favorable for a broad range of diode-pumped laser applications including visible lasers. Single crystals of yttrium orthovanadates have been obtained by various techniques like Czochralski,[332][333] zone melting,[334][335] Verneuil method,[333] dissolution in melts,[336] from flux,[336][337] and top seeded solution growth.[338] However, there are no reports dealing with the hydrothermal synthesis of these crystals. This is probably connected to the high temperature and pressure conditions involved in the growth of these crystals and also to the strong belief that their growth under mild hydrothermal conditions will introduce water into the structure or to the interstices. Further, these crystals are known to have high melting points and very low solubility. Therefore, the high-temperature solutions and melt techniques were preferred over the others. In fact,

PrepBooks

several problems have been encountered in the growth of yttrium orthovanadates by the above said conventional methods. These problems might be connected to the instability of the pentavalent vanadium at high temperatures and the loss of oxygen through surface encrustation by the reaction of the melt with the crucible material. The unstable melt behavior of YVO_4 leads to the appearance of zoning in crystals due to the variation in the dopant concentration. Recently, it has been observed that YVO_4 crystals are very difficult to grow with a stoichiometric or near stiochiometric composition. Further, the most critical aspect is the appearance of metastable phases which precipitate within YVO_4 crystals.[339] The detection of correct Y-V-O stoichiometry in YVO_4 crystals is difficult.[340] Moreover, as the temperatures involved in the flux growth is about 1300°C and in melt growth above 1800°C, there is a high probability of vanadium attacking the container. In order to overcome most of these difficulties in melt and high-temperature solution techniques, Byrappa et al. (1999) have preferred hydrothermal technique as a solution to this problem.[325] Since the experiments in hydrothermal technique are carried out in a closed system, the loss of oxygen could be readily prevented. In addition, the experimental conditions adopted by the authors involve the use of teflon liners for the autoclaves and the interaction between the container and vanadium is avoided.

The experiments on the hydrothermal growth of $R:MO_4$ (R = Nd, Eu; M = Y, Gd) were carried out using Morey type of autoclaves provided with teflon liners. The use of teflon liners has helped in overcoming the entry of inclusions from the autoclave material. The schematic diagram of hydrothermal autoclave used in the present work is shown in Fig. 7.75. The starting materials such as Y_2O_3, V_2O_5, and R_2O_3 (where R = Nd, Eu,) were weighed in appropriate proportions in teflon liners. A suitable mineralizer solution of known concentration was added into the teflon liners and the entire mixture was stirred well until a homogeneous and relatively viscous solution was obtained. The temperature was kept constant at 240°C and the autogeneous pressure generated depended on the fill, usually 50–60%. The pH of the growth medium was measured before and after each experimental run. In the present work, the crystallization was carried out in all the experiments through spontaneous nucleation. Hence, an effort was made to reduce the number of nucleation centers by increasing the temperature of the crystallization reactor slowly at the rate of 10°C/h up to 100°C and beyond at the rate of 5°C/h. The nutrient materials were held at 240°C for a period of three days without any

fluctuations in the temperature. From the fourth day onwards the temperature fluctuation to the tune of ± 10°C to ± 20°C were introduced periodically to reduce the number of nucleation centers. By this means, small crystallites, which had developed earlier, dissolve leaving only bigger crystallites to grow. The authors had previously employed oscillating temperature technique to obtain bigger crystals of yttrium orthovanadates from high-temperature solutions.[336] More details can be obtained from this work. In these experiments, it was observed that as the size of the crystal increases, the crystal quality is reduced. The formation of stable complex R:YVO_4 at 240°C and around 100 bar pressure, must have undergone several intermediate stages of solvation forming stable and unstable solvated complexes from room temperature to 240°C. The representative chemical reactions are given below:

$V_2O_5 + 10\ HCl \rightarrow 2\ \underline{VCl_4} + 5\ H_2O + Cl_2 \uparrow$

$Y_2O_3 + 3\ HCl \rightarrow Y(OH)_3 + YCl_3$

$Y_2O_3 + 6\ HNO_3 \rightarrow 2\ \underline{Y(NO_3)_3} + 3\ H_2O$

$V_2O_5 + 6\ HNO_3 \rightarrow 2H_3VO_4 + 3N_2O_5 \uparrow$

$2\ VCl_4 + 4\ HNO_3 \rightarrow 2\ \underline{VOCl_3} + 2\ HCl + H_2 \uparrow + 2\ N_2O_5 \uparrow$

$2\ VOCl_3 + 8\ Y(OH)_3 \rightarrow \underline{Y_8V_2O_{17}} + 6\ HCl + 9\ H_2O$

$2\ VOCl_3 + 2\ Y(NO_3)_3 \rightarrow 2\ YVO_3 + 3\ N_2O_5 + 3\ Cl_2 \uparrow$

$YCl_3 + H_3VO_4 \rightarrow YVO_4 + 3\ HCl$

$VOCl_3 + Y(OH)_3 \rightarrow YVO_4 + 3\ HCl$

$2\ H_3VO_4 + 2\ Y(NO_3)_3 \rightarrow 2\ YVO_4 + 3\ H_2O + 3\ N_2O_5 \uparrow$

$H_3VO_4 + Y(NO_3)_3 \rightarrow YVO_4 + 3\ HNO_3$

$H_3VO_4 + Y(OH)_3 \rightarrow YVO_4 + 3\ H_2O$

___Underlined formulas represent the solid precipitation

DropBooks

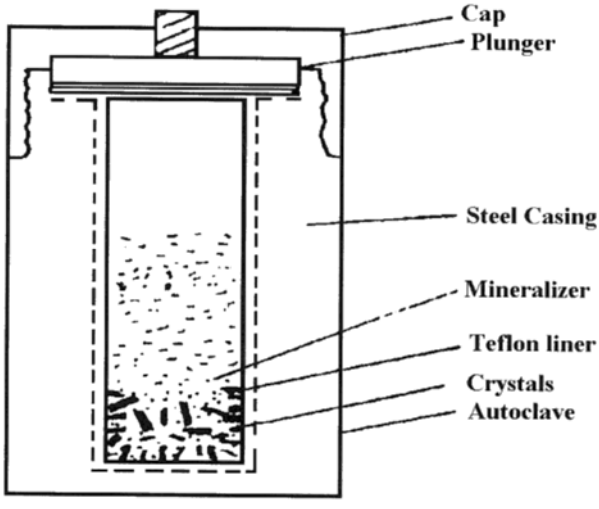

Figure 7.75. Schematic diagram of a hydrothermal autoclave.[325]

The viscosity of nitric acid and sulphuric acid greater than that of HCl to HNO_3 would form a more efficient solvent for the growth of R:YVO_4. The dissolution of rare earth vanadates in HCl and HNO_3 is a process of complex formation between R^{3+}, V^{5+}, and the ligands present in the solution OH^-, H_2O, Cl^-, NO^{3-}. With a rise in temperature, the association of Cl^- with H^+ increases the yield of HCl and destabilizes the R^{3+} complex. Under these circumstances, nitrates replace chloride ligands. Finally, the nucleation takes place by the polymerisation of tetrahedral R^{3+} complexes. The yttrium orthovanadate, YVO_4 crystals were doped with active ions like Nd or Eu, and obtained crystals of Nd:YVO_4 and Eu:YVO_4. The rare earth concentrations are in the range 5–10%. After the experimental run, the autoclaves were quenched initially using an air jet followed by water, and the products were washed thoroughly in double distilled water in an ultrasonic cleaner to remove all excess acid media. The crystals obtained were well faceted single crystals of 2 to 4 mm in size.

Solubility. Successful growth of any crystal insists on the availability of solubility data. In fact, the earlier workers did not attempt the hydrothermal growth of rare earth vanadate crystals due to the lack of the solubility data on these compounds. Mineralizers like HCl, HNO_3, HCOOH, H_2SO_4, NaOH, NaF and mixed acid mineralizers like HCl + HNO_3, HCl + H_2SO_4, HCl + HCOOH have been tried. The solubility measurements were carried out by the weight loss method. Here a crystal is kept in

equilibrium with an appropriate solution at the desired pressure and temperature conditions for a period of time greater than that is necessary to establish equilibrium. All the solubility measurements were carried out in Morey-type autoclaves. Figure 7.76 shows the solubility of R:YVO_4 (in wt%) as a function of temperature and at a pressure of 100 bar in 1.5 M HCl + 3.0 M HNO_3. R:YVO_4 shows a negative temperature coefficient of solubility under hydrothermal conditions. The enthalpy of dissolution calculated from an Arrhenius plot log S Vs 10^3/T, was found to be 4.250 kJ/mole (Fig. 7.77). The experimental temperature to study the solubility was up to 350°C. It was found that above 300°C, the solubility does not alter much, which suggests that the crystal growth beyond this temperature is not practical. Hence, from the solubility data, it is found that the temperature range between 180° to 300°C is the most ideal, and 240°C particularly is the best growth temperature. The solvents like HCl, HNO_3, H_2SO_4, and HCOOH when used alone were not good solvents since fine crystalline products having no morphology were obtained. The use of alkaline solvent did not result in the crystallization of yttrium orthovanadates but instead yttrium hydroxides, $Y(OH)_3$ or hydrous yttrium vanadates, $YVO_4.nH_2O$ were formed. Since, the use of single acid solvents did not substantially enhance the solubility, mixed acid mineralizers were tried (HNO_3 + HCl, HCl + H_2SO_4, HNO_3 + HCOOH, etc.,). It was found that 1.5 M HCl + 3.0 M HNO_3 taken in 2:1 ratio is the best solvent for the growth of R:YVO_4 crystals.

DropBooks

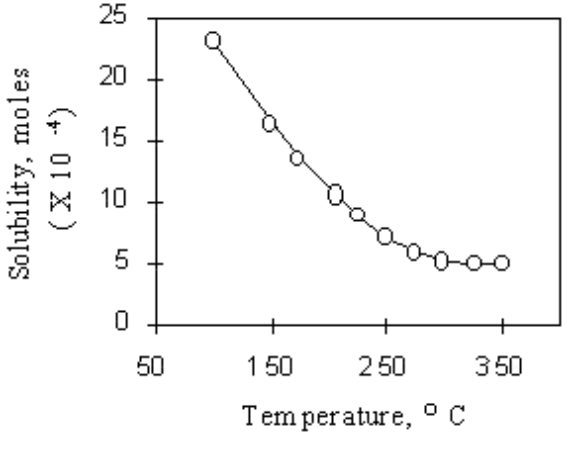

Figure 7.76. Solubility curve of Nd:YVO_4.[325]

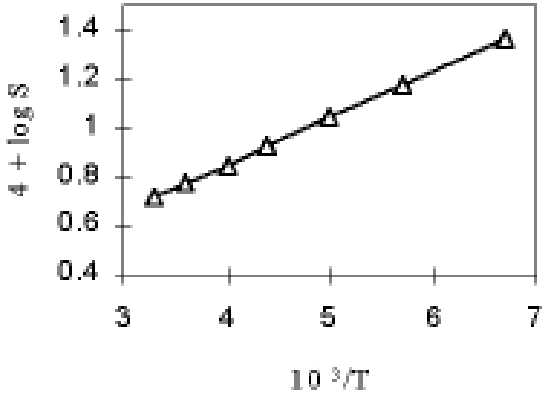

Figure 7.77. Arrhenius plot log S vs. $10^3/T$.

Rare earth orthovanadate, Nd:YVO_4 crystals were obtained under hydrothermal conditions. The earlier workers used mostly the melt technique to obtain rare earth vanadates. The study of the morphology of crystals is very important since the crystal habit is governed by the kinetics rather than the equilibrium considerations with a number of factors like degree of supersaturation, solvent type, the pH of the media, etc.[341] Thus, the authors have studied the influence of these parameters on the growth morphology of Nd:YVO_4 and Eu:YVO_4. The most commonly observed morphology is rod-shaped or prismatic habit. Since the requirement of a crystal for solid state laser host is a thin tabular platelet of 5 × 5 × 2 mm dimension, the crystals obtained either by flux or melt technique exhibiting highly facetted morphological forms have to be cut and polished to the desired shape before the device fabrication. Hence, an emphasis has been made on the influence of pH of the growth media to get the desired morphology. Figure 7.78 *a* shows photographs of doped YVO_4 crystals, and the corresponding schematic diagrams are shown in Fig. 7.78 *b*. Table 7.27 gives the morphology of the rare earth vanadates. The morphology could be changed from elongated broad hexagonal platelets to more or less cubic shape by a systematic variation in the pH of the growth media, and the thickness was controlled to ~2 mm. Thus, the largest crystals obtained through spontaneous nucleation provided by temperature oscillations were 4.2 × 4.2 × 2.0 mm in about eight days of experimental duration. Simple rare earth vanadate crystals were obtained when the pH was kept low (< 4.0), and Y $(OH)_3$ and $YVO_4.nH_2O$ crystallized when pH > 4.0. Well-developed platelets were obtained in the pH

range -0.03 to -0.15 (see morphology shown in Fig. 7.79). *In-situ* growth of the desired morphology under moderate hydrothermal conditions has shown in general, that yttrium orthovanadate crystals have a strong tendency to flattening. The authors have shown that some rare earth orthovanadates obtained by flux method, bearing Pr, Eu, and Tm are almost isometric. A study of the growth rate of the rare earth vanadate crystals was attempted and Fig. 7.80 shows the dependence of growth rate on the pH of the growth media. Higher growth rate was obtained in the pH range –0.08 to 0.08, in which the crystals grow thicker and the optical quality suffers. It has been earlier reported that the rare earth vanadates belonging to the zircon type show a tendency for banding/zoning, particularly on the (001) face.[342] The yttrium orthovanadate crystals generally show dark brown to light brown colors with a change in the dopant level. The darker colors appear when the crystals grow thicker and molar ratio is not maintained properly because the growth depends on the control of oxygen activity and surplus V_2O_5. Small quantity of hydrogen peroxide was added in order to create oxygen rich atmosphere and that in turn improved the quality of the crystals. It became honey yellow in color, uniform throughout, and the transparency also increased. The hydrothermally grown crystals do not show zoning or banding, unlike the rare earth orthovanadates obtained by other techniques.

DropBooks

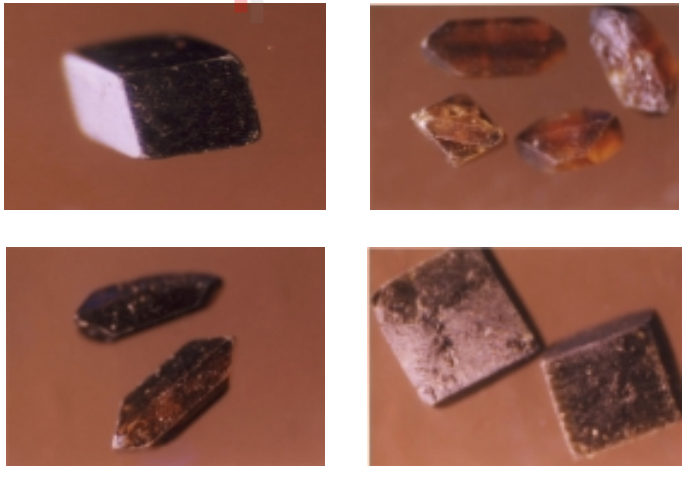

(a)

Figure 7.78. *(a)* Photographs of doped YVO_4 crystals, and *(b)* schematic diagrams.[325]

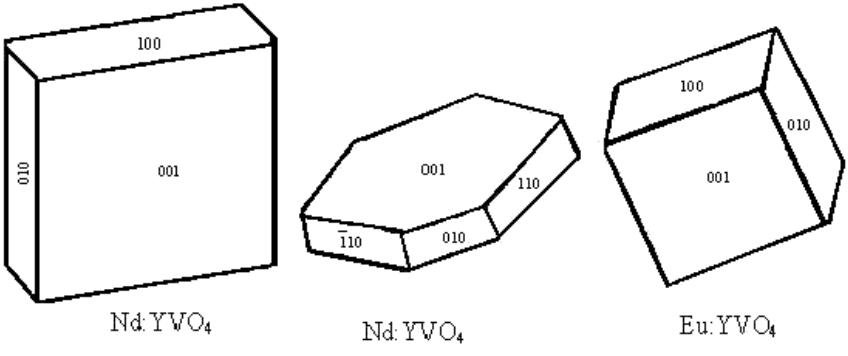

(b)

Figure 7.78. *(Cont'd.)*

Table 7.27. Morphology of Yttrium Orthovanadates

Composition	Growth temp (°C)	pH range	Common faces	Growth rate
Nd : YVO_4	240	0.05 to 0.10	(001) (010) (110)	$\gamma(110) > \gamma(010)$
Nd : YVO_4	240	-0.03 to 0.15	(001) (100) (010)	$\gamma(100) > \gamma(010)$

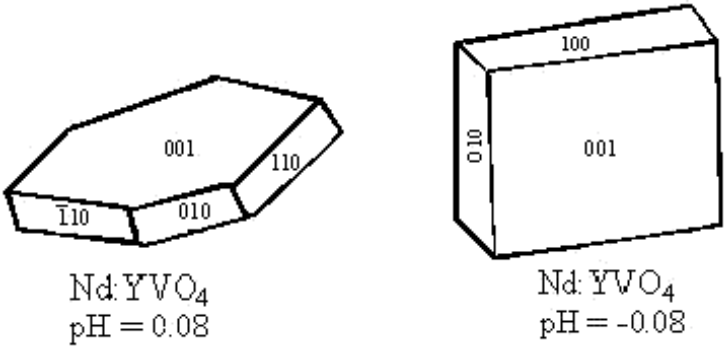

Figure 7.79. Morphology of rare earth vanadates.[325]

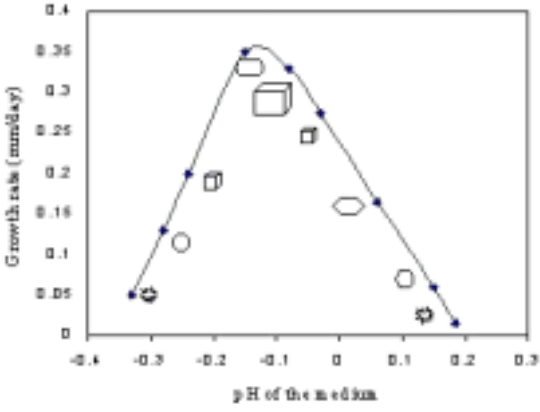

Figure 7.80. Dependence of growth rate on the pH of the growth media.[325]

7.16.2 Growth of Mixed Valent Vanadates

The first hydrothermally grown mixed valent vanadate is $NH_4Zr_2V_3O_{12}$—a proton conductor.[324] In comparison with flux and melt techniques, the hydrothermal growth of vanadates has been carried out at fairly lower temperature-pressure conditions ($T < 300°C$ and $P < 100$ bar).

DropBooks

Although, the method is not very popular for vanadates, it has helped in synthesizing several new vanadates with unique structures. Oka and his group have prepared a series of vanadates under mild hydrothermal conditions.[319]

A series of experiments were conducted by hydrothermal method to obtain $NH_4Zr_2V_3O_{12}$ crystals, the initial experiments with a varying molar ratio of the nutrient components yielded only a crystalline powder without any experimental morphology, the authors were able to finally synthesize small needle-like crystals of $NH_4Zr_2V_3O_{12}$ under the following conditions: $T = 250°C$, $P = 200$ atm; NH_4VO_3 5 gm and HCOOH (2.0M) 6ml.[324] The experiments were carried out for eight days using teflon liners in Morey-type autoclaves of capacity 50 ml. Since crystallization occurred due to spontaneous nucleation, the furnace temperature was slowly increased to control the nucleation rate (~ 5°C / hr.). The main drawback of this method is the small size of the crystals (Fig. 7.81).

Here it is appropriate to discuss the growth of some selected vanadate crystals like $FeVO_4$ and MV_3O_7 (M = Cd, Ca, Sr).

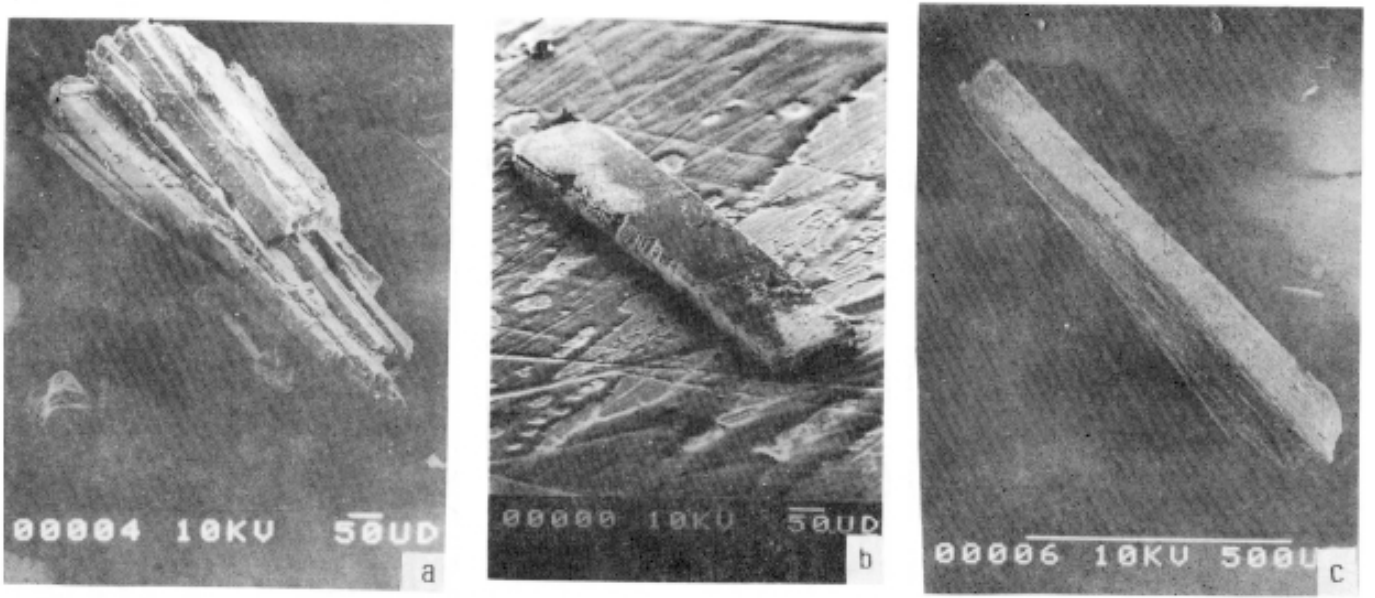

Figure 7.81. Photographs of $NH_4Zr_2V_3O_{12}$ crystals obtained under hydrothermal conditions.[324]

Iron vanadate, $FeVO_4$ exhibits four polymorphs ($FeVO_4$-I, $FeVO_4$-II, $FeVO_4$-III, $FeVO_4$-IV) belonging to triclinic, orthorhombic, orthorhombic and monoclinic respectively.[344][345] In the preparation of $FeVO_4$-II, Yao et al. (1992) used the aqueous solutions of $VOCl_2$ and $FeCl_3$ with V/Fe molar ratios of 0.5 to 1.0, where the concentration of $FeCl_3$ was fixed to 0.1 mol/liter.[346] The solutions were sealed in Pyrex ampoules and treated hydrothermally at 280°C for 40 hours. Similarly, Oka and his group prepared several layered structures of hydrated vanadium oxides, and bronzes, as these oxides in hydrated states have a tendency to adopt layered structures accommodating foreign cations in the interlayer regions. Layered phases containing alkali-metal ions, the alkali-metal intercalates $A_{0.3}V_2O_5 \cdot nH_2O$ (A = alkali ion) have been successfully synthesized under hydrothermal conditions. These vanadates are usually prepared hydrothermally at 250°C from aqueous $VOSO_4$ solutions under autogenous pressure.[346]–[348]

7.17 HYDROTHERMAL SYNTHESIS OF BORATES

ProBooks

Borates have been studied for the past 75 years. Over 85 phases have been established with 58 known compounds belonging to over 9 different structure types. The study of borates in general was purely of academic interest and did not carry any great significance until the late 1970s when mixed alkali borates were first used in miniature laser applications.[349] Subsequently, lithium boracite was reported to be exhibiting superionic properties.[350] However, these applications did not generate any special interest among materials scientists, but it is the β-barium borate, which opened a new chapter for borates.[351] The recent discovery of piezoelectric $Li_2B_4O_7$ and nonlinear optical LiB_3O_5 has attracted a great deal of attention from materials scientists, and today it is the alkali borates that are being studied extensively worldwide.[352][353] The growth of alkali borates is being carried out mostly by melt and flux techniques. There are some reports about the solid-state reactions, but the work on borates, in general by hydrothermal technique, was almost untouched except for the past decade. Only a few alkali borates have been obtained by the hydrothermal technique. The Li_2O-B_2O_3 system was first studied in 1958 by Sastry and Hummel by the flux method.[354]

In general, the alkali borates exhibit essentially framework structures made up of [BO_4] tetrahedra and [BO_3] triangles. Among alkali borates, only one compound shows a chain arrangement, some four compounds show islands, and two compounds show a layered arrangement. The ring arrangement in general is absent. On the other hand, the phosphates, silicates, and sulphates show extensive chain and ring arrangements and the crystals essentially belong to the lower symmetry. The alkali borates, because of their basic structural units made up of [BO_3] triangles and [BO_4] tetrahedra, crystallize both in higher and lower symmetry systems and show wide morphological variations. Similarly, the growth experiments clearly show that any slight change in any of the growth parameters would drastically change the resultant products. Hence, the study of morphology of alkali borates is very interesting and a wide range of morphological variations has been observed which exhibit some definite relationship with reference to the type of the structure, compound, and growth conditions.

Borates were almost ignored by hydrothermal crystal growers. It was only during the last decade that we become acquainted with an in-depth knowledge about the behavior of boron in the hydrothermal solutions and its interaction with various metal cations. Although, not much has been done on the alkali borate systems, several other borate systems like alkali transitional metal borate systems have been studied in detail. Today we have data available on several borate systems like Na_2O-CdO-B_2O_3-H_2O, Li_2O-CdO-B_2O_3-H_2O,[355] Na_2O-ZnO-B_2O_3, Li_2O-CdO-B_2O_3-H_2O·K_2O-ZnO-B_2O_3-H_2O, ZnO-B_2O_3-H_2O,[356]MgO-CdO-B_2O_3-H_2O,[357] Li_2O-ZnO-B_2O_3-H_2O,[358] under hydrothermal conditions. More than 25 different borate components have been obtained by hydrothermal technique and many of them show interesting luminescence, nonlinear, superionic, properties. For example, the Li_2O-ZnO-B_2O_3-H_2O system has been studied under hydrothermal conditions within the temperature range 250–450°C. (See Fig. 7.82 *a, b, c.*)[358] A series of lithium borates like $LiBO_2$, $Li_2B_4O_7$, $Li_3B_5O_8(OH)_2$ and mixed borates like $Li_4Zn_3B_4O_{11}$, $Li_8Zn_4B_6O_{17}$ have been obtained in this system. Further, the authors[358] have added MnO into the nutrient in a very small quantity and the experiments have been carried out using copper ampoules. It is well-known that all the zinc compounds activated with Mn_2^+ show strong luminescence in green or orange regions.[359] Hence, the authors have added a small quantity (0.5 mol %) of Mn^{2+} into the system M_2O-ZnO-B_2O_3-H_2O (M = Li, Na, K).[358]

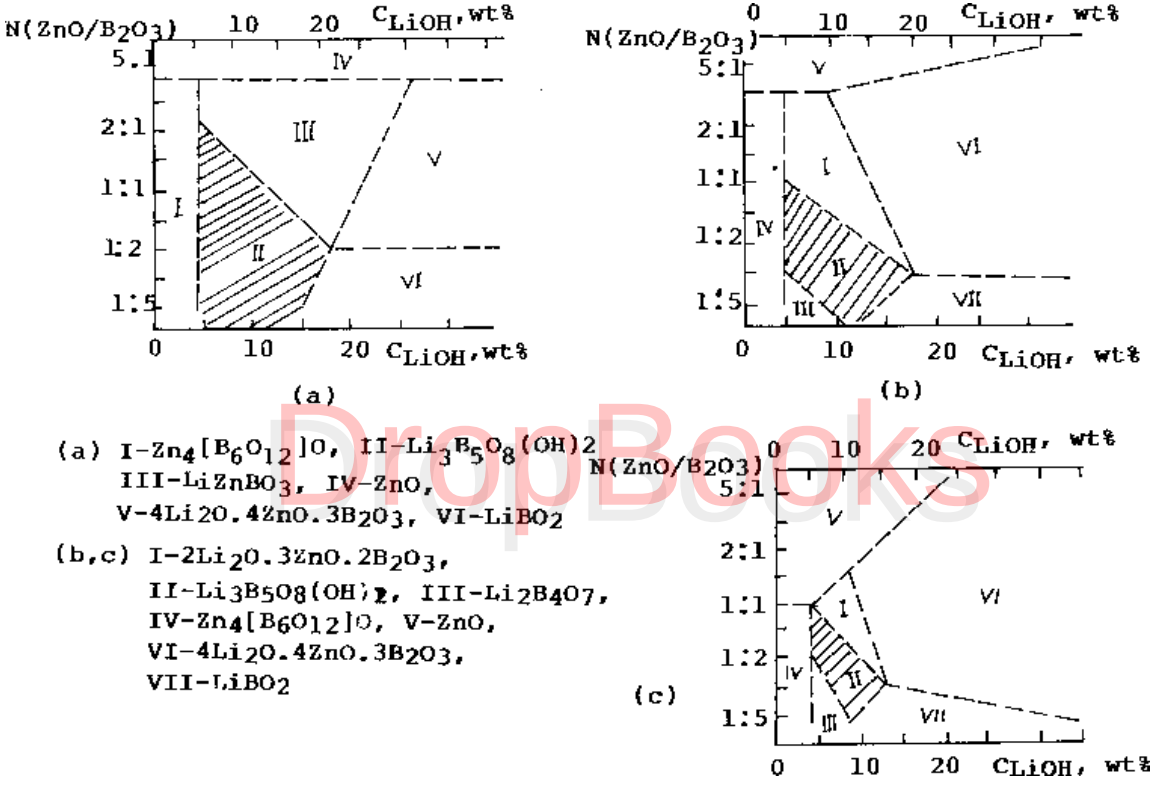

DropBooks

Figure 7.82 (a-c). Phase diagrams of Li_2O - Ln_2O_3 - B_2O_3 - H_2O.[358]

Further, it is known that Mn and Cu are the activators of $Li_2B_4O_7$ for thermally stimulated luminescence dosimeters.[360][361] Here it is appropriate to quote the earlier work of Garret et al. (1977) who, while growing $Li_2B_4O_7$ observed that only small crystals of $Li_2B_4O_7$ could be obtained because of the highly corrosive nature of Li_2O-B_2O_3 that melts the platinum crucibles. Therefore, the use of copper ampoules for the borate system is doubtful and copper might contribute to the crystallization of various other phases just like the addition of MnO in the system Li_2O-ZnO-B_2O_3-H_2O as reported earlier.[358] The authors have studied this Li_2O-B_2O_3-H_2O system under lower *PT* conditions (*T* = 200–300°C, *P* = 50-200 bar) and discovered several new phases like $Li_4H_2B_2O_6$, $LiH_2B_5O_9$, etc. The crystal structures of these compounds show that they are the potential technological materials. It is observed that in the system M_2O-CdO-B_2O_3-H_2O (M = Li, Na), the alkali concentration determines the sequence of crystallizing phases. Figure 7.83 shows the phases crystallizing in the system Li_2O-B_2O_3-H_2O under hydrothermal condition.[362] At low alkali concentrations, alkali-free borates are formed. In the cadmium systems it is CdB_2O_4, cubic borate with a framework structure and at 300°C it is aqueous borate with the composition $6CdO{\cdot}3B_2O_3{\cdot}4H_2O$ that are formed. In the right upper part of the diagram another cubic borate is formed—$Cd_4(BO_3)_2(OH)_2$. In the lithium system, the region between pure cadmium and pure lithium borates is the region where Li- and Cd-borates are crystallized. These borate structures provided a wealth of information for further development of hydrothermal and crystal chemistry of borates. This data illustrates the trend of boron atoms to occupy tetrahedral positions for higher concentration of boron and 'triangle' positions if the boron concentration is low. In the former case the B-O fragments prevail, whereas large cations play less important role (CdB_4O_7), in the latter case the B-O fragments are the links connecting Cd(Ca, K, Li) fragments. Such triangles in the $Cd_4(BO_3)_2(OH)_2$ structure impart additional rigidity to the strong Cd-O framework. Some intermediate variants are also observed—both boron coordinations are possible in a compound, e.g. in $K_2CaB_4O_5(OH)_4{\cdot}8H_2O$ and $Li_3B_5O_8(OH)_2$-II.[355]–[357] The crystals of lithium rare earth borates $Li_3Nd_2(BO_3)_3$ and $LiNd[BO_3(OH)]$ were synthesized in the systems Li_2O-Ln_2O_3-B_2O_3-H_2O at LiOH concentrations 20–30 wt%.[356]

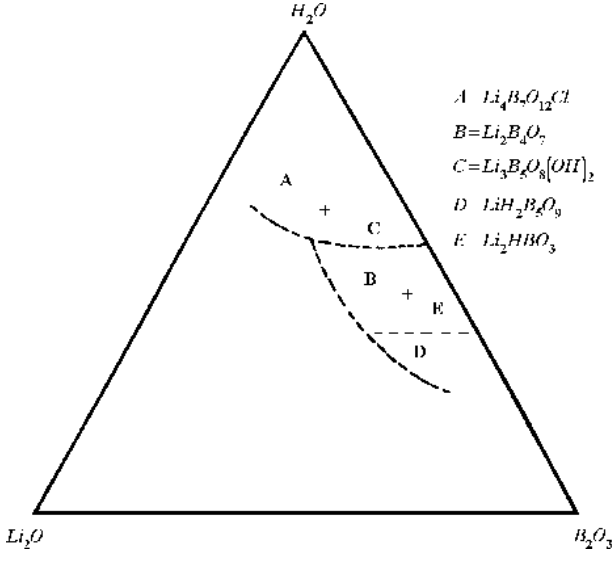

Figure 7.83. Phases crystallizing in the system Li_2O-B_2O_3-H_2O under hydrothermal conditions.[362]

DropBooks

7.17.1 Hydrothermal Growth of Selected Borates

It is practically impossible to describe the hydrothermal growth of each and every type of borate crystals. Therefore, the authors have described the hydrothermal growth of only some important borate materials and their overall growth elucidation.

$Li_2B_4O_7$. Lithium tetraborate ($Li_2B_4O_7$) is an important piezoelectric and nonferroelectric crystal which has attracted great attention in research and industry for it's application in surface acoustic wave (SAW) and bulk acoustic wave (BAW) devices. It has a lower temperature coefficient of delay than lithium niobate and tantalate and a higher electromechanical coupling constant than α-quartz. Since berlinite has several major problems in it's growth as large single crystals, lithium tetraborate is becoming an attractive prospect as a piezoelectric crystal.[363] The raw materials for the growth of $Li_2B_4O_7$ in large quantities are abundant, and the ready availability of isotopically pure ^6Li, ^{10}B, and ^{11}B as the nutrient materials make $Li_2B_4O_7$ growth both practical and economical.

Before Garret et al. (1977), only small crystals or grains of $Li_2B_4O_7$ were obtained. Although an attempt was made to synthesize $Li_2B_4O_7$ by the hydrothermal method, the size of the crystal was too small (Fig. 7.84). It always had some divalent metal oxide like MnO or CuO.[356] Perhaps this is mainly due to the corrosive nature of the Li_2O-B_2O_3 melt towards the platinum crucible. Hence, Garret et al. (1977) used the nickle crucibles. However, the method adopted by these authors is quite cumbersome because of the complexity of the technique that has a graphite susceptor and inert atmosphere. The only method advocated up to now by various authors to grow $Li_2B_4O_7$ crystals is the melt technique, particularly the Czochralski method.[364]–[366] More recently, a group of Chinese researchers have successfully obtained large crystals (2 inch dia and 4 inch length) of high quality $Li_2B_4O_7$ for the first time by Bridgman technique.[367] Almost at the same time a Japanese group has reported the preparation of $Li_2B_4O_7$ thin films by sol-gel method.[349] The $Li_2B_4O_7$ crystals obtained by the Czochralski method always show coring which is the main macrodefect thereby hindering wide industrial applications of $Li_2B_4O_7$ in the manufacture of SAW and BAW devices, i.e., a continuous or intermittent opaque region parallel to the growth direction at the central core of the crystal often occurs and is related to the growth rate, deviation of the melt composition from stoichiometry (for example, becomes Li rich) and contents of H_2O or O_2 in the melt of $Li_2B_4O_7$.[365][366] In the Bridgman growth of $Li_2B_4O_7$ the authors have observed a similar opaque core in the $Li_2B_4O_7$ crystal, and considered this defect to be a cluster of holes and a cellular structure or dendritic.[367] A few white inclusions of impurities and evidence of constitutional supercooling in the holes or on the walls of cells have been observed. Similarly, the cracking by thermal stress frequently occurs in Cz growth because, of the anisotropy of the expansion coefficient of $Li_2B_4O_7$. No cracks due to thermal stress occur in Bridgman growth of $Li_2B_4O_7$ for various orientations, since the temperature gradient in the $Li_2B_4O_7$ crystal is smaller. However, if the residual melt on the top of an as-grown crystal in <100> or <110> directions changes into polycrystalline phase by fast cooling, cracks in the $Li_2B_4O_7$ occur often in the top region. Similarly, the sol-gel technique has some disadvantages although, the method has several advantages like, it allows high purity, low processing temperature, precise composition control and the formation of bulk monoliths, fibers and coating films. The important conclusions drawn by the authors based on their work on sol-gel method is that a larger amount of water is necessary for the crystallization of

$Li_2B_4O_7$ thin films, but also to suppress the formation of undesirable crystalline phases other than $Li_2B_4O_7$.[368] Obviously, hydrothermal technique helps not only in the crystallization of $Li_2B_4O_7$ crystals at fairly lower temperatures, but also in solving many of the problems encountered in other methods as described earlier. As a contrary to the result of Garret et al.,[364] no difficulties were experienced using platinum crucibles to contain the melt by the authors.[366] Hence, in order to avoid these controversies, Byrappa and Shekar (1992) used telfon liners such that incorporation of impurities could be totally avoided.[369]

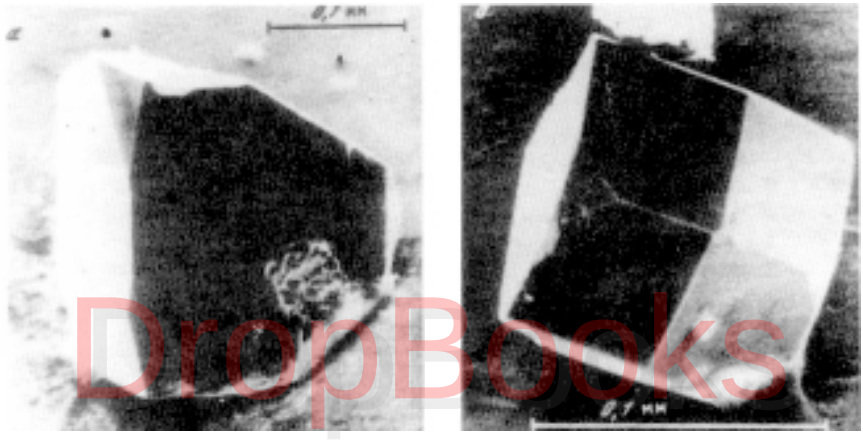

Figure 7.84. Characteristic photographs of $Li_2B_4O_7$ crystals.[356]

The experiments on the hydrothermal synthesis of $Li_2B_4O_7$ were carried out using Morey type autoclaves provided with teflon liners of capacity 25 ml. The use of teflon liners has helped in overcoming the corrosive nature of the melt (Li_2O-B_2O_3). The nutrient materials such as $LiBO_2$ or LiOH and Boric acid were taken in teflon liners. The molar ratio of the starting materials was selected through theoretical calculations. The percent fill was varied from 50–60%. Several mineralizers like HCl, HCOOH, H_2SO_4, and HNO_3 were tried in the synthesis of $Li_2B_4O_7$ crystals. The experimental conditions are given in Table 7.28. It was found that only HCOOH acts as a suitable mineralizer, whereas the other solvents like HCl and HNO_3 did not yield good crystals. Further, the molarity of HCOOH was varied from 1 M to 3.5 M and it was found that good results were obtained in 1.5M HCOOH solution.

Table.7.28. Experimental Conditions For The Growth of $Li_2B_4O_7$ Crystals[369]

No.	Nutrient Composition	Temp. (°C)	Pressure (bars)	% fill	Duration (days)	Size (mm)	Remarks
1.	$LiBO_2$ – 1.668 B_2O_3 – 2.332 HCOOH(3M) – 8 ml	250	120	70	8	4–14	bulk crystals of tetragonal and regular shapes
2.	$LiBO_2$ – 1.668 B_2O_3 – 2.332 HCOOH(2.5M) – 8 ml	250	115	65	9	1–8	polycrystalline and wedge shaped crystals
3.	$LiBO_2$ – 1.668 B_2O_3 – 2.332 HCOOH(2M) – 8 ml	250	100	60	8	3–10	wedge shaped crystals
4.	$LiBO_2$ – 1.668 B_2O_3 – 2.332 HCOOH(1.5M)–6.5ml	250	100	55	7	1–8	wedge shaped crystals
5.	$LiBO_2$ – 1.668 B_2O_3 – 2.332 HCOOH(1.5M) – 6 ml	250	90	50	8	0.5–2	well developed tetragonal crystals
6.	$LiBO_2$ – 1.668 B_2O_3 – 2.332 HCOOH(3M) – 8 ml	250	120	70	8	4–14	bulk crystals of tetragonal and regular shapes

The formation of $Li_2B_4O_7$ takes place according to the following reactions:

$$2\ LiBO_2 + 2\ HCOOH \longrightarrow 2\ LiHCOO + B_2O_3 + H_2O$$

$$LiHCOO + H_3BO_3 \longrightarrow LiB(OH)_4 + CO$$

$$2\ LiB(OH)_4 + 2\ H_3BO_3 \longrightarrow Li_2B_4O_7 + 7\ H_2O$$

The formation of the hydroxy borate ion on ionization of boric acid is spontaneous. It is possible that the intermediate solvated complexes like boric acid (it is a weak electrolyte and the complexes formed are rather stable), LiHCOO and $LiBO_2$ interact with each other because of their ionic bonding or very low charge in order to give a stable coordinated compound having a high lattice energy and relatively stronger ionic bonding, $Li_2B_4O_7$.

The crystallization was carried out in all the experiments through spontaneous nucleation. As such, the crystals obtained under the above said conditions are colorless, highly transparent and vary in size from 5 to 6 mm. The crystals are transparent and the faces are also well developed (Fig. 7.85 *a, b*). In general, the morphology of the hydrothermally grown $Li_2B_4O_7$ is very interesting and it varies widely depending upon the experimental conditions, particularly the starting materials and the percent fill. Even the size of the crystals varies depending upon the above parameters from 1 mm up to 12 mm. As the pressure in the system was decreased slowly (up to 40 atm), the size of the crystals increased. In some experiments the authors have obtained well-developed and perfect tetragonal crystals (Fig. 7.86) of small size and in some other experiments wedge shaped, massive and irregular crystals.[370] When the size of the crystals is large the crystals become less transparent. $Li_2B_4O_7$ crystals can be obtained within the following molar ratio:Li_2O:B_2O_3 = 1:7–9. The chemical analysis of the $Li_2B_4O_7$ obtained shows that the ratio Li_2O:B_2O_3 is higher than the theoretical ratio:(69.2 molar % B_2O_3-experimental ratio as against 66.6 M % of B_2O_3-theoretical) as in the case of Ref. 367. Figure 7.87 shows the schematic diagram of morphological variations in $Li_2B_4O_7$ crystals with the %fill in the autoclaves.[367]

DropBooks

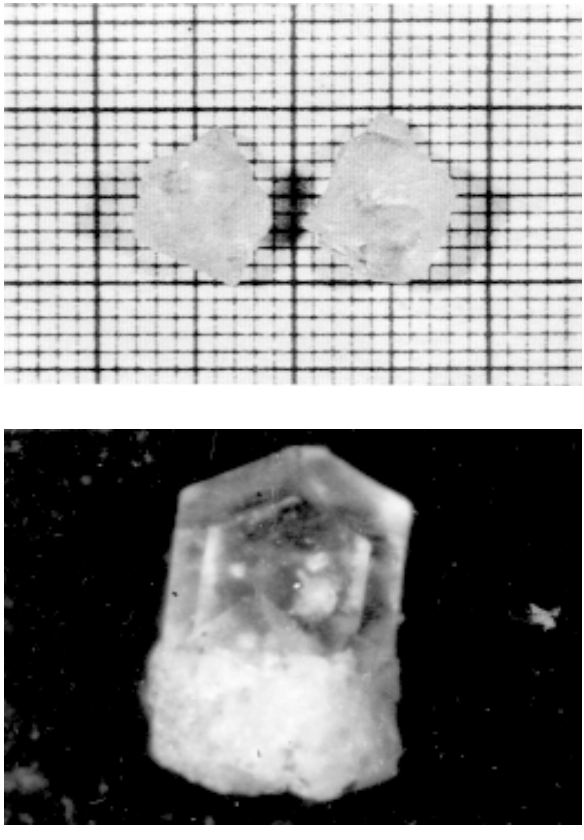

Figure 7.85. Photographs of $Li_2B_4O_7$ crystals.[370]

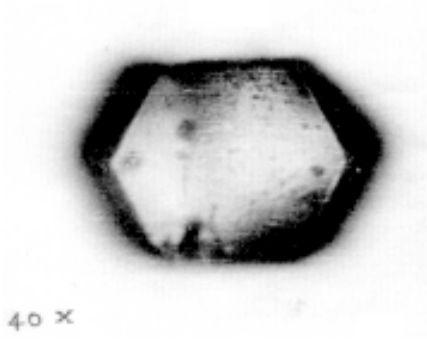

Figure 7.86. Photograph of tetragonal crystal of $Li_2B_4O_7$.[370]

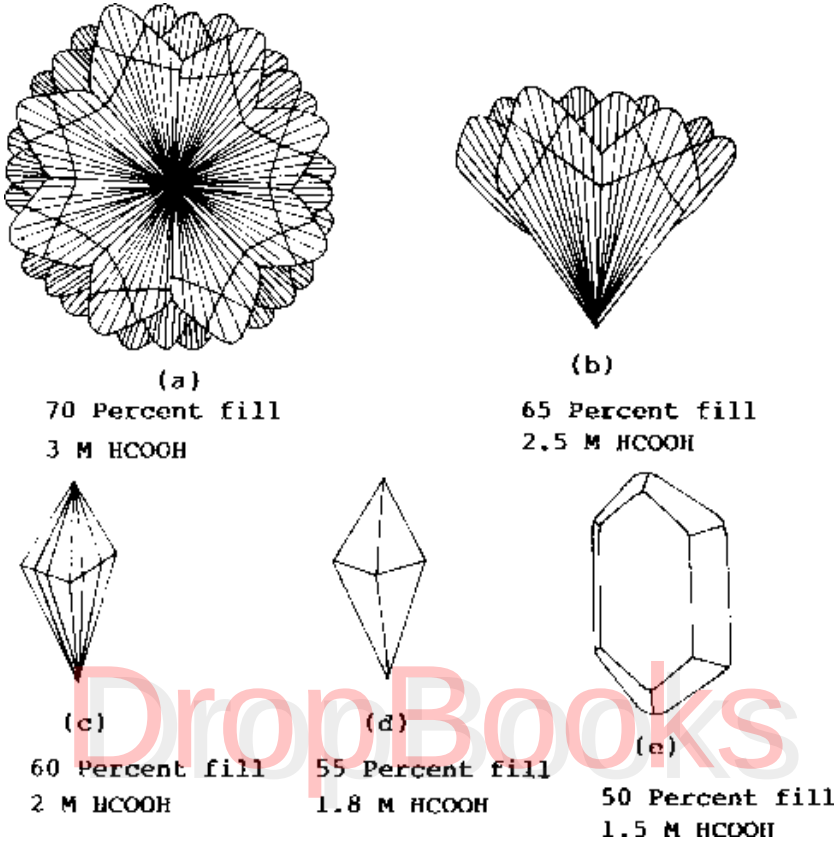

DropBooks

Figure 7.87. Schematic diagram of morphological variations.[370]

In order to reduce the number of nucleation centers, the temperature of the crystallization reactor was increased very slowly at the rate of 10°C/h up to 100°C and beyond which at the rate of 5°C/h. The nutrient materials were held at 250°C for a period of three days without any fluctuations in the temperature. From the 4th day onwards the temperature fluctuations to the tune of ± 20°C were introduced periodically in order to reduce the nucleation centers. By this means, the earlier developed small crystallites dissolve and only the bigger crystallites remain. This provides the growth of bigger crystals (12 × 12 × 10 mm). The big crystals do show cracking due to the thermal stress during the sudden quenching of the

autoclaves after the experiments. Striations and thermal cracking are commonly noticed in $Li_2B_4O_7$ crystals obtained by Czochralski and Bridgman techniques. However, the greatest advantage in the hydrothermal growth is that the thermal stress either during the growth or during the quenching can be easily overcome. Further, the hydrothermal method helps in growing the pure and large single crystals. This work has clearly demonstrated the advantages in growing $Li_2B_4O_7$crystals devoid of all the macrodefects. Even the separately crystallized $Li_2B_4O_7$ crystals with the experimental duration of 8–10 days have yielded crystals of 12 × 12 × 10mm size which shows fairly higher growth rates. Therefore, a careful study of the growth parameters and an introduction of seed will make this technique a more attractive one for $Li_2B_4O_7$. It is well-known that both $Li_2B_4O_7$ and berlinite are the most suitable piezoelectric materials having high SAW coupling coefficients for high frequency and temperature compensation. Here, it is appropriate to mention that the growth of berlinite has been proved to be extremely difficult so as to obtain large single crystals of high quality, owing to the difficulties associated with the highly corrosive nature of P_2O_5, it's high reaction susceptibility and the negative temperature coefficient of solubility. Therefore, the successful growth of high quality $Li_2B_4O_7$ by hydrothermal technique would solve the existing problems with respect to the other techniques adopted so far. Also, the use of teflon liners and the availability of isotopically pure starting materials help in getting highly pure crystals. Further, the temperature and pressure condition involved in the growth of $Li_2B_4O_7$ is relatively low and this insists upon very simple autoclave designs and higher practicability. Byrappa et al. (1993) have studied the solubility of LBO under hydrothermal conditions with reference to the molarity, percent fill, pressure, etc. in different solvents.[370] The solubility is found to be positive. The solubility measurements were carried out by weight loss method in different solvent media and these studies were performed with utmost care to obtain good results by taking the average values. The possible errors if any in our measurements are due to the fluctuations in temperature (± 1°C), weight and volume determination. Figures 7.88 *a*, *b*, and *c* show the solubility curves for LBO crystals with varying molarity of LiOH, HCOOH, pressure and temperature. As evident from Fig. 7.88, the ideal temperature for the growth of LBO crystals is within the temperature range 200 to 260°C (Fig. 7.88*a*). Similarly, the ideal molarity range of the mineralizer in the growth of LBO crystals is 1.5 to 1.8M (Fig. 7.88*b*).

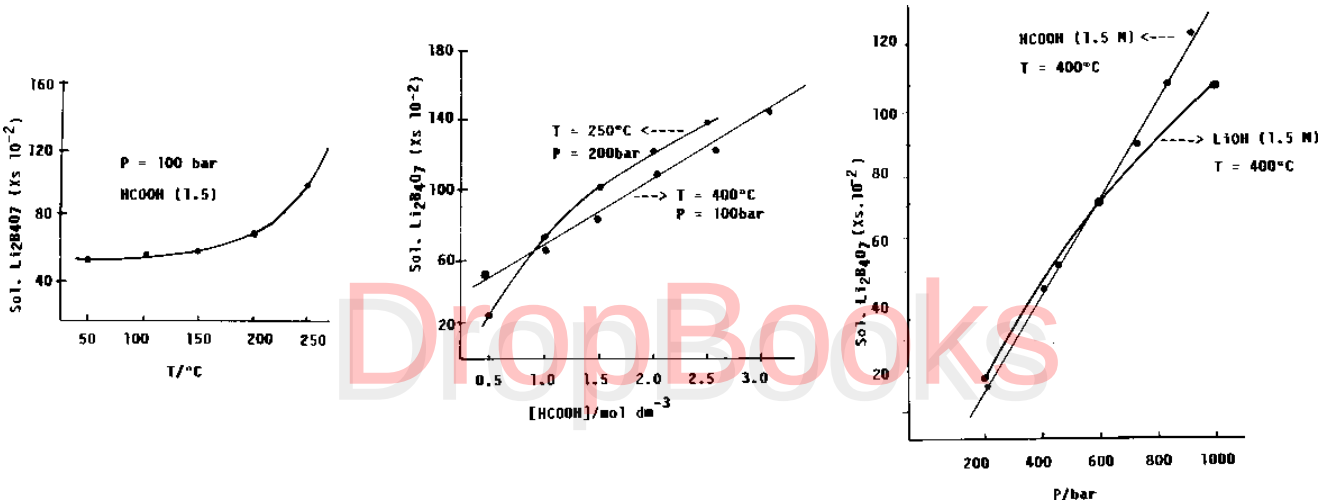

DropBooks

Figure 7.88. Solubility curves for LBO crystals.[370]

$Li_3B_5O_8(OH)_2$. The synthesis of $Li_3B_5O_8(OH)_2$ crystals has been reported earlier by the authors while investigating the system Li_2O-ZnO-B_2O_3-H_2O under hydrothermal conditions within the temperature range 250–450°C.[356] They obtained the crystals through the following chemical reactions:

Eq. (27) $$3LiOH + 5H_3BO_3 \longrightarrow Li_3B_5O_8(OH)_2 + 8H_2O$$

This has two polymorphic modifications: $Li_3B_5O_8(OH)_2$ (l) and $Li_3B_5O_8(OH)$ (ll). They have obtained a series of lithium borates: $LiBO_2$, $Li_2B_4O_7$, $Li_3B_5O_8(OH)_2$ and mixed Zn borates: $LiZnBO_3$, $2Li_2O{\cdot}3ZnO{\cdot}2B_2O_3$, $4Li_2O{\cdot}4ZnO{\cdot}3B_2O_3$. Among these, $Li_3B_5O_8(OH)_2$ crystallizes within a narrow region (as shown in Fig. 7.83) when MnO was added into the nutrient in a very small quantity. Contrary to these earlier works, Byrappa et al. (1992) obtained $Li_3B_5O_8(OH)_2$ crystals in the system Li_2O-B_2O_3-H_2O under lower *PT* conditions (T = 240°C, P = 100 atm) in the absence of any other components like MnO or CuO.[371]

The experiments were carried out using a Morey-type autoclave provided with teflon liners. The starting materials such as LiOH and H_3BO_3 were taken in teflon liners. The percent fill was varied from 50–60%. Several mineralizers were tried and the HCOOH was found to be a better mineralizer with it's molarity varying from 1.5–5 M. In most of the earlier works LiOH has been taken as a mineralizer. A change in the concentration of LiOH in the system changes the resultant lithium compound. Byrappa et al. (1992) observed that LiOH exists in the system, the presence of additional mineralizer namely HCOOH enhances the solubility of this compound and the solvation processes.[371] Figure 7.89 shows the solubility of $Li_3B_5O_8(OH)_2$ in HCOOH.[372] The formation of $Li_3B_5O_8(OH)_2$ takes place according to the following reactions:

Eq. (28) $$LiOH + H_3BO_3 \longrightarrow LiBO_2 + 2H_2O$$

Eq. (29) $$3LiBO_2 + 2H_3BO_3 \longrightarrow Li_3B_5O_8(OH)_2 + 2H_2O$$

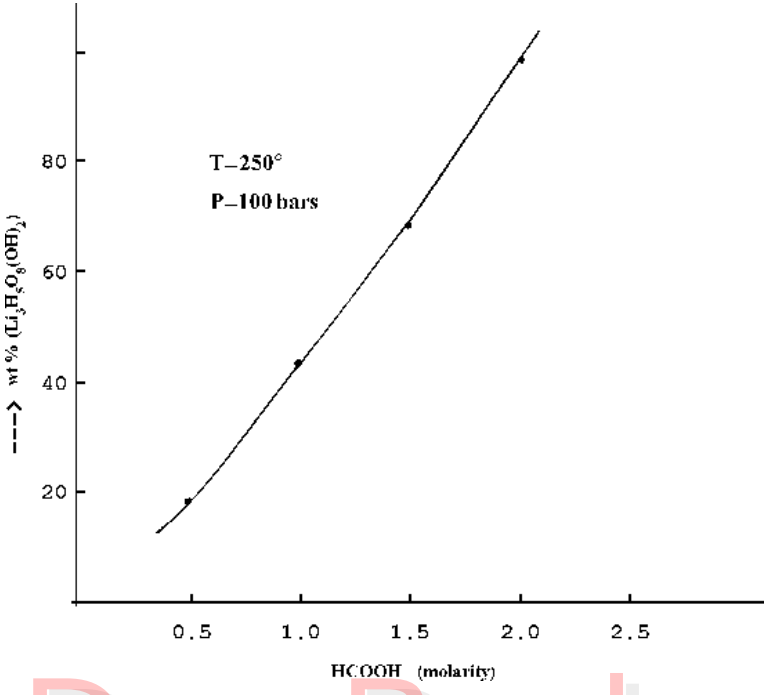

DropBooks

Figure 7.89. Solubility of $Li_3B_5O_8(OH)_2$ in HCOOH.[372]

Water is considered as the hard base and strongly acts upon the dissolution of the solvanted particles of $LiBO_2$ and determines the solubility of the final resultant acid base complex, i.e., $Li_3B_5O_8(OH)_2$. It must have been formed through several intermediate stages of solvation and formed several stable and unstable ions through an active interaction between the solute and solvent depending upon the dissolution energy of various cations and doners. Usually when HCOOH is taken as a mineralizer, LiOH forms LiHCOO which later forms $LiBO_2$ and interacts with H_2BO_3. Since the system studied is a quarternary system, it becomes extremely difficult to assess the exact stage and nature of crystallization. The reactions given are more or less hypothetical without much speculation. It is possible that the intermediate solvated complexes like LiHCOO and $LiBO_2$ interact with each other because of their weak ionic bonding or very low charge in order to give a stable co-ordinated compound with a high lattice energy and relatively strong ionic bonding, $Li_3B_5O_8(OH)_2$.

The experimental conditions in the hydrothermal synthesis of $Li_3B_5O_8(OH)_2$ are given in Table. 7.29. The size varies up to 15mm and the crystals are good in quality (Fig. 7.90). The present study also shows that $Li_3B_5O_8(OH)_2$ crystallizes within a narrow region in the system Li_2O-B_2O_3-H_2O (Fig. 7.83). The crystals were occasionally twinned and are transparent. Since, $Li_3B_5O_8(OH)_2$ crystals of size 15mm could be obtained in an experimental run of 8–10 days, a careful study of growth parameters and an introduction of the seed will enable one to grow bigger crystals.

$Li_4B_7O_{12}Cl$. In the recent years boracites have attracted attention of Materials Scientists owing to their variety of applications in modern technology, particularly after the successful application of transitional metal rare earth borates—$NdAl_3(BO_3)_4$, $Nd(Al,Cr)_3(BO_3)_4$, $Nd(Ga,Cr)_3(BO_3)_4$, etc.—as miniature laser materials.[349] Almost at the same time, high ionic conductivity was observed in lithium boracite ($Li_4B_7O_{12}Cl$).[373] This compound was successfully synthesized in 1972.[374] Later the structure of the compound was reported in 1973.[375] This compound has been reported to be obtained earlier by two techniques: *1)* through sublimation, and *2)* hydrothermally. Although the hydrothermal technique has been successfully adopted to the synthesis of this compound, the *PT* conditions were quite high and crystal size was too small and less then 1 mm. Byrappa et al. (1992) selected the suitable composition region in the phase diagram where $Li_4B_7O_{12}Cl$ could be crystallized in the presence of Cl under hydrothermal condition.[376] They took chlorine in the starting mixture as HCl with a varying molarity. Figure 7.83 shows the crystallization boundary for this compound, $Li_4B_7O_{12}Cl$. The crystallization field is rather narrow and any slight change in the composition will give rise to other varieties of lithium borates like $Li_2B_4O_7$, LiB_3O_5 and $Li_3B_5O_8(OH)_2$, etc. Therefore, one has to be extremely cautious in selecting the nutrients. The experiments were taken in a teflon liner, which was placed inside the autoclave. The capacity of the autoclave was 30 to 50ml. These autoclaves are normally provided with a safety blow-out disc. The percent filling of the liners and the experimental temperatures were used in calculating the pressure. The experiments were carried out by spontaneous crystallization. The starting materials such as lithium carbonate and boric acid were taken in the following molar ratio:

Eq. (30) $Li_2O:B_2O_3 = (0.4–0.7):(2.5–4.3)$

Table.7.29. Experimental Conditions For The Growth of $Li_3B_5O_8(OH)_2$ Crystals[371]

No.	Nutrient Composition	Temp. (°C)	Pressure (bars)	% fill	Duration (days)	Size (mm)	Remarks
1.	LiOH – 0.800 H_3BO_3 – 3.200 HCOOH(1.5M) – 8 ml	250	120	70	7	3–4	well developed tetragonal crystals
2.	LiOH – 0.800 H_3BO_3 – 3.200 HCOOH(1.8M) – 8 ml	250	120	70	10	8.0–10	wedge shaped crystals
3.	LiOH – 0.800 H_3BO_3 – 3.200 HCOOH(1.5M) – 7 ml	250	100	60	15	8.0–10	wedge shaped polycrystalline crystals
4.	LiOH – 0.800 H_3BO_3 – 3.200 HCOOH(1.5M) – 8 ml	250	120	70	8	8.0–10	wedge shaped crystals
5.	LiOH – 0.800 H_3BO_3 – 3.200 HCOOH(2M) – 7 ml	250	100	60	8	8.0–10	well developed tetragonal crystals
6.	LiOH – 0.800 H_3BO_3 – 3.200 HCOOH(1.5M) – 7 ml	250	100	60	7	8.0–10	well developed tetragonal crystals

DropBooks

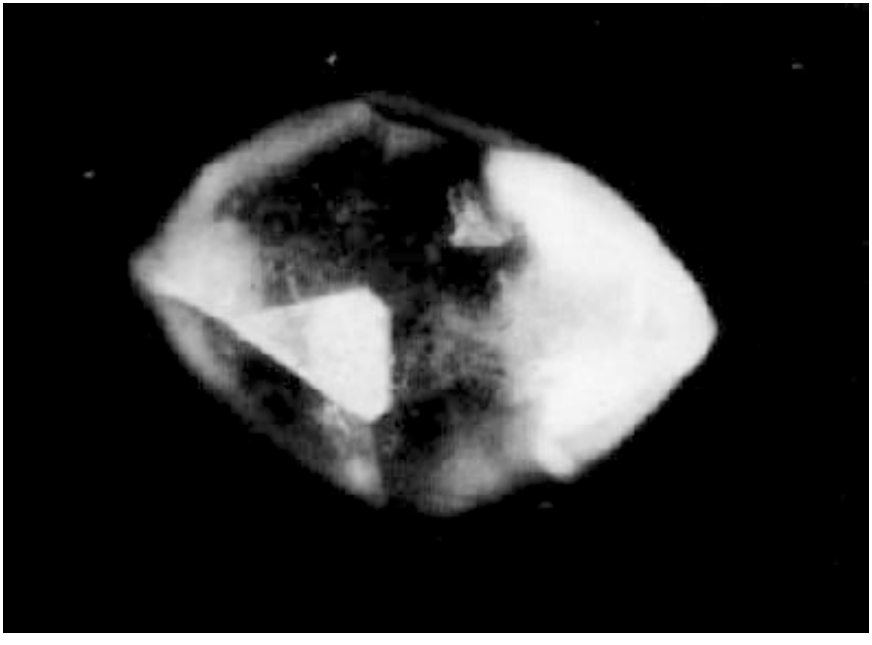

Figure 7.90. Photograph of $Li_3B_5O_8(OH)_2$ crystal.[371]

The mineralizer solution HCl was taken with a definite molarity (1.5 to 2). Since the crystallization took place through spontaneous nucleation, the temperature of the furnace was slowly increased to control the rate of nucleation. In the majority of the experiments, the percent filling varied from 50–65%. The experimental conditions under which $Li_4B_7O_{12}Cl$ crystals obtained are given in Table 7.30.[376]

These experiments yielded crystals up to 2 mm in size. In the majority of the experiments $Li_4B_7O_{12}Cl$ crystals obtained were twinned and the size varied up to 3 mm. The twinning was also controlled and the transparency of the crystals was also enhanced by means of increasing the growth temperature, quenching of the autoclaves and accurate monitoring of the experimental conditions. The rate of heating and the rate of cooling of the autoclaves and the establishment of equilibrium conditions in the system control the defect formation in these crystals.

$LiH_2B_5O_9$. The synthesis of $LiH_2B_5O_9$ crystals has been carried out for the first time by Byrappa et al. (1993). $LiH_2B_5O_9$ crystallizes within a narrow region in the Li_2O-B_2O_3-H_2O system.[377]

Table.7.30. Experimental Conditions For The Growth of $Li_4B_7O_{12}Cl$ Crystals[376]

No.	Nutrient Composition	Temp. (°C)	Pressure (bars)	% fill	Duration (days)	Size (mm)	Remarks
1.	Li_2CO_3 – 1.000 B_2O_3 – 3..000 HCl(5M) – 8 ml	250	90	60	8	1–4	transparent cunic crystals
2.	Li_2CO_3 – 0.9 B_2O_3 – 3..000 HCl(5M) – 8 ml	250	90	60	7	1–2	transparent cunic crystals
3.	Li_2CO_3 – 0.8 B_2O_3 – 3..000 HCl(5M) – 8 ml	250	90	58	7	1–2	transparent cunic crystals
4.	Li_2CO_3 – 1.000 B_2O_3 – 3..000 HCl(5M) – 8 ml	250	90	60	8	0.5–1	small transparent cunic crystals
5.	Li_2CO_3 – 1.2 B_2O_3 – 3..000 HCl(5M) – 8 ml	250	90	60	8	0.5–1	small transparent cunic crystals
6.	Li_2CO_3 – 1.000 B_2O_3 – 3..000	250	90	60	8	0.1	very small crystals

DropBooks

This new compound belonging to the monoclinic system space group (P21/a) has been obtained under hydrothermal conditions at 250°C and 100 bar pressure. The starting materials such as $LiBO_2$, B_2O_3 and solvent 1.5 M HCOOH were taken in teflon liners. The Li_2O:B_2O_3:H_2O molar ratio was 1–1.5:.5.5–6:3–3.5. The experiments were carried out using Morey type of autoclaves. The percent fill was varied from 50–60%. Several mineralizers were tried and the HCOOH was found to be a better mineralizer with its molarity varying from 1.5-2 M.

The formation of $LiH_2B_5O_9$ must have taken place according to the following reaction:

Eq. (31) $2LiBO_2 + 2HCOOH \longrightarrow 2HCOOLi + B_2O_3 + H_2O$

Eq. (32) $HCOOLi + 5H_3BO_3 \longrightarrow LiH_2B_5O_9 + CO + 7H_2O$

The reaction of $LiBO_2$ and HCOOH resulted in the formation of HCOOLi. When HCOOLi reacts with H_3BO_3 with 1:3 ratio $Li_2B_4O_7$ was formed but with an increase in the amount of H_3BO_3 (HCOOLi : H_3BO_3 = 1:5) the new compound $LiH_2B_5O_9$ has resulted.

The experimental conditions for the growth of $LiH_2B_5O_9$ are given in Table. 7.31. During the crystallization process hydrogen from HCOOH has entered the structure indicating hydrolysis process. The crystals are colorless with vitreous luster and pseudo orthorhombic symmetry.[362][372]

It is interesting to note that the growth of borates by hydrothermal method is not yet popular, and even today the flux method followed by meet method, are the most popular ones. A large group of compounds with general formula $RM_3(BO_3)_4$ (where R = Y, La-Lu, Bi, In, but M = Al, Sc, Fe, Ga, Cr) have been obtained mainly by flux method. However, the hydrothermal technique is slowly catching up because of the advantages as listed earlier in the growth of $Li_2B_4O_7$.

Applications of Borates. Borates exhibit very interesting properties like piezoelectric, pyroelectric and ferroelectrics, acousto-electric, luminescent, superionic and so on. Also, they possess good thermal and chemical stability. Owing to the possibility of wide isomorphous substitutions, one can consider these borates as polyfunctional materials with device potential. However, borates of hydrothermal origin are being used essentially as piezoelectric, ferroelectric and superionic borates.

Table.7.31. Experimental Conditions For The Growth of $LiH_2B_5O_9$ Crystals[362]

No.	Nutrient Composition	Temp. (°C)	Pressure (bars)	% fill	Duration (days)	Size (mm)	Remarks
1.	$LiBO_2$ – 2.0 B_2O_3 – 4.0 HCOOH(1.5M) – 6ml	250	100	60	7	1–4	transparent crystals
2.	$LiBO_2$ – 2.0 B_2O_3 – 4.0 HCOOH(1.5M) – 5ml	250	90	55	7	1–3	transparent crystals
3.	$LiBO_2$ – 2.0 B_2O_3 – 4.0 HCOOH(1.5M) – 7ml	250	110	65	7	5	massive crystals
4.	$LiBO_2$ – 2.0 B_2O_3 – 4.0 HCOOH(2M)–6ml	250	100	60	7	0.5–1	small transparent crystals
5.	$LiBO_2$ – 2.0 B_2O_3 – 4.0 HCOOH(3M) – 6ml	250	100	60	8	0.5	small transparent crystals
6.	$LiBO_2$ – 2.2 B_2O_3 – 4.0 HCOOH(1.5M) – 6ml	250	100	65	7	1–3	transparent crystals

DropBooks

$Li_2B_4O_7$ is known as a Li superionic conductor with its ionic conductivity of the order of $10^{-4}\,W^{-1}\,cm^{-1}$ at about 500 K, and has a large piezoelectric constant. A combination of piezoelectric and superionic properties should give rise to electro-acoustic anomalies in $Li_2B_4O_7$ crystals. Figure 7.91 shows the complex impedance plots of $Li_2B_4O_7$ at different temperatures: *a)* 299 K, *b)* 323 K, *c)* 348 K, *d)* 373 K, *e)* 398 K, *f)* 423 K, *g)* 448 K, *h)* 473 K, *i)* 498 K, *j)* 523 K, *k)* 548 K, and *l)* 573 K. The CIS studies reveal that the study of anomalies should give important information. On the physical nature of the acousto-ionic interaction and also on the characteristics of ion transport in solid electrolytes on the whole. $Li_2B_4O_7$ may be used as a dielectric resonator at about 10 MHz. The noise observed in the CIS data is not a thermal noise, but it appears to be 1/f quanturn noise.[378]

$Li_3B_5O_8(OH)_2$ shows poor ionic conductivity and behaves as a dielectric material below 498 K, with the electronic equivalent circuit representation indicating a pure capacitor type behavior. Between 299 and 523 K, the material exhibits piezoelectric behavior and at about 523 K, it shows superionic conducting behavior. The complex impedance becomes almost zero at 10 MHz.[379]

The ionic conductivity has been studied by several workers. The ionic conductivity generally varies from 10^{-2} to 10^{-3} $(ohm, cm)^{-1}$ at about 300°C. The activation energy value is around 0.4 eV (380).

Alkali borates, α-$LiBO_2$ crystals are doped with Mn^{2+} ions, and they show weak yellow luminescence (UV excitation). New alkali-free borates of divalent metals doped with Mn^{2+} ions show interesting luminescence properties. For example, Mn-activated cadmium borates show yellow-green luminescence and $Zn_4B_6O_{12}$ borate yields green luminescence.[380]-[381] Similarly, Mn^{2+} doped $LiZnBO_3$, and $2Li_2O{\cdot}ZnO{\cdot}2B_2O$, and $Na_2Zn_2MnB_{4.67}O_{11}$ show crimson luminescence, and $4Li_2O{\cdot}4ZnO{\cdot}3B_2O_3$ shows yellow luminescence.[381]

The complex coordinated complexes are best obtained under hydrothermal conditions. Such complex structures have not been able to be obtained by other crystal growth methods. Especially with the reduction in the *PT* conditions of synthesis, the method is becoming more attractive for these complexes. New structures being obtained are throwing light upon new and interesting physico-chemical properties of these compounds.

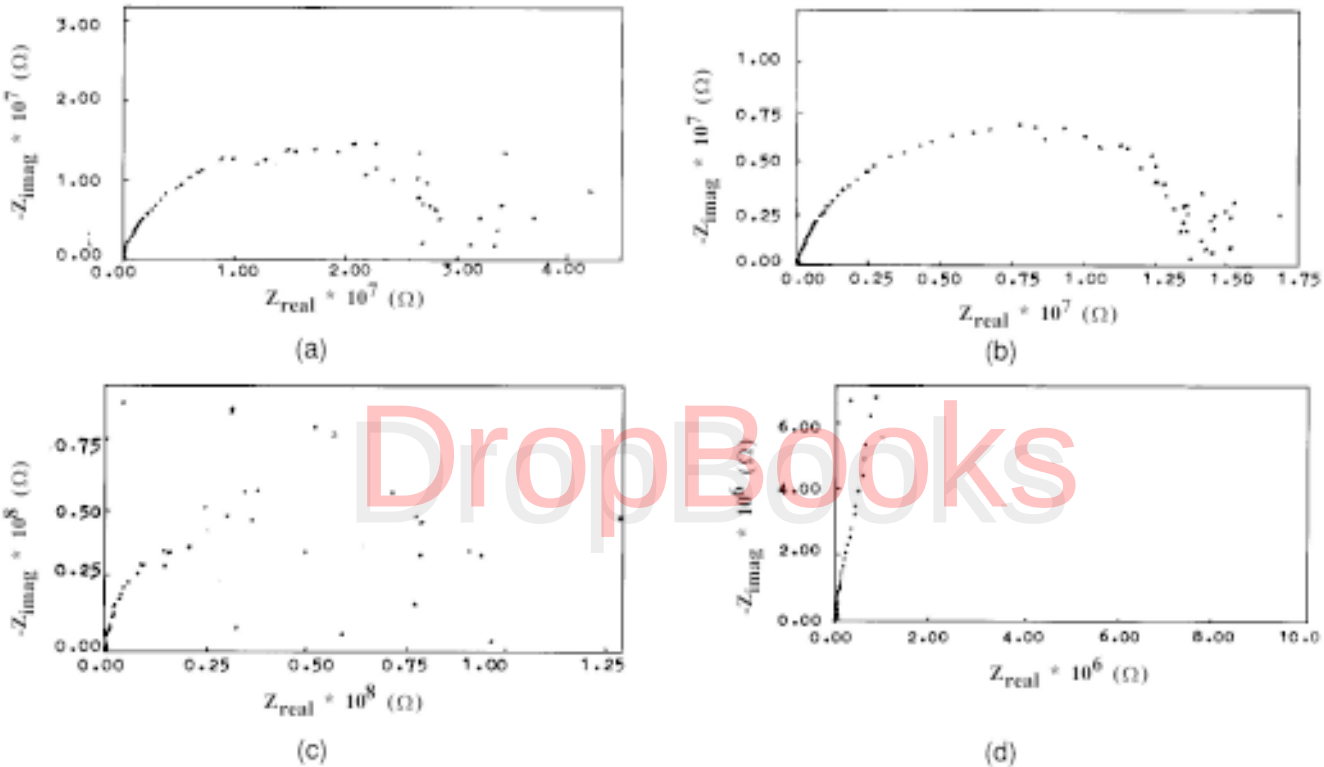

DropBooks

Figure 7.91. Complex impedance plots of $Li_2B_4O_7$ at different temperatures.[379]

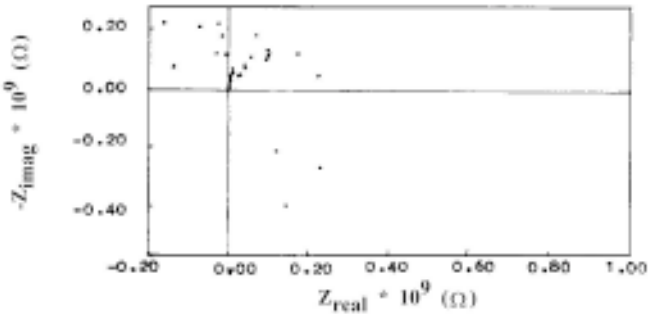

(e)

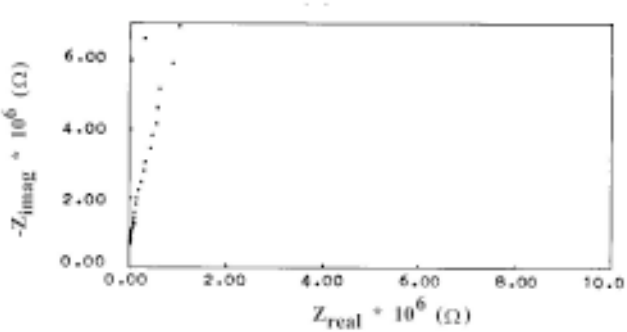

(f)

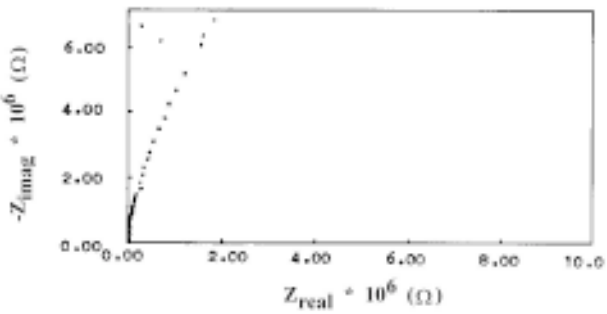

(g)

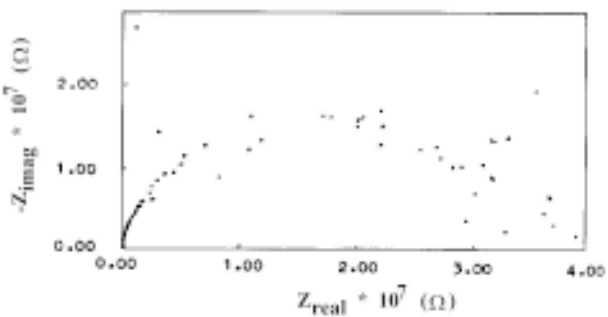

(h)

Figure 7.91. *(Cont'd.)*

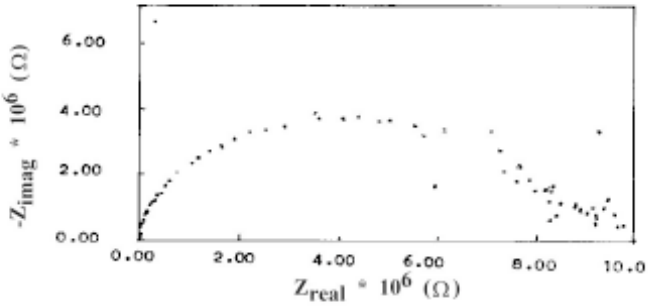

(i)

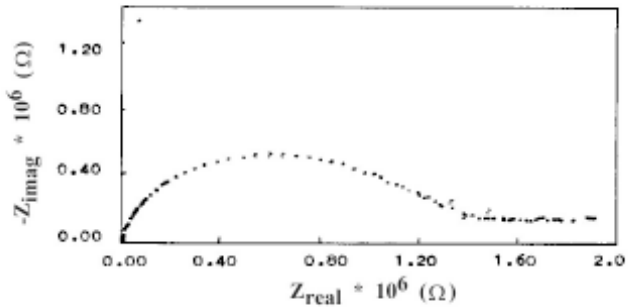

(j)

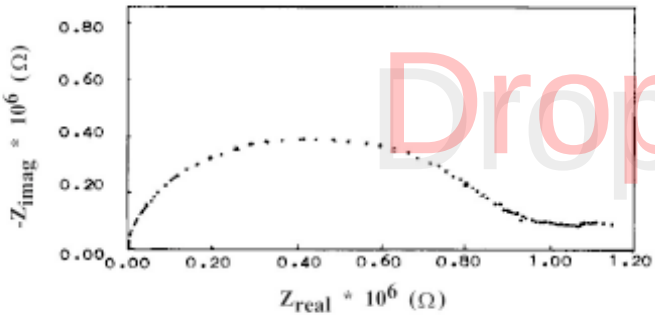

(K)

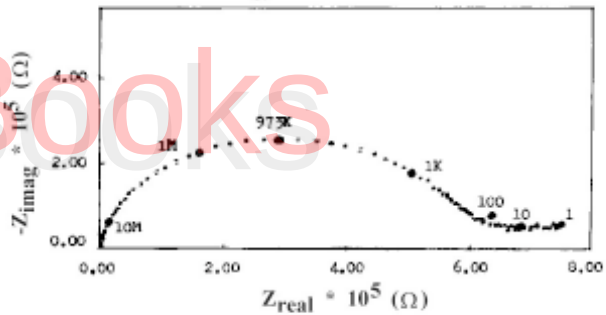

(l)

DropBooks

Figure 7.91. *(Cont'd.)*

REFERENCES

1. Byrappa, K. and Pushcharovsky, D. Yu., Crystal Chemistry and its Significance on the Growth of Technological Materials: Part 1; Silicates, Phosphates and Their Analogs. *Prog. Crystal Growth and Charact*., 24:269–359 (1992)
2. Wedeponl, K. H., *Geochemistry*, Holt, Reinhart, and Winston, New York, p. 231, (1971)
3. Corbridge, D. C. E., The Structural Chemistry of Phosphorous. 4 Preparative Methods and Growth of Rare Earth Phosphates, *Bull. Soc. Fr. Crystallogr*., 94:271 (1971)
4. Byrappa, K., Preparative Methods and Growth of Rare Earth Phosphates, *Prog. Cryst. Growth and Charact*., 3:163–198 (1986)
5. Corbridge, D. C. E., *Topics in Phosphorus Chemistry*, Plenum Press (1968)
6. Palkina, K. K., *Izvest, Akad. Nauk SSSR, Inorg. Mater*. 14:789 (1978) (in Russian)
7. Pushcharovsky, D. Yu., *Structural Mineralogy of Silicates and their Analogs*, 160 Nedra, Moscow (1986) (in Russian)
8. Lyton, H. and Truter, M. R., *J. Chem. Soc*, p. 5112 (1960)
9. Bushuev, N. N., Illarionov, V. V., and Kapilevich, S. B., *J. Inorg. Chem*. 26:2908 (in Russian) (1981)
10. Simonov, M. A., Shkovrov, S. V., and Troyanov, S. I., *Kristallographia*, 33:502 (1988)
11. Einstein, F. W. and Willis, A. C., *Acts. Cryst*., B37:218 (1981)
12. Rouse, R. C., Peacor, D. R., and Freed, R. L., *Amer. Mineral*, 73:168 (1988)
13. Kawahara, A., *Bull. Soc. to Mineral Cryst.*, 90:279 (1967)
14. Belov, N. V., *Crystal Chemistry of Large Cation Silicates, Consultants Bureau*, New York (1959)
15. Clark, G. M. and Morley, R., *Chem. Soc. Revs*., 5:269–274 (1976)
16. Byrappa, K., Plyusnina, I. I., and Dorokhova, G. I., Growth, Structure and IR-spectra of $CsRP_4O_{12}$ Crystals, *J. Mat. Sci*., U.K., 17:1847–1853 (1982)
17. Hazen, R. M. and Finger, L. W., *Comparative Crystal Chemistry Temperature and Pressure, Composition and the Variation of Crystal Structure*, J. Weily and Sons, London, p. 231 (1982)
18. Clearfield, A., Subramanian, M. A., Rudolf, P. R., and Moin, A., *Solid State Ionics* 18/19:13 (1986)
19. Hill, R. J. and Giffs, G. V., *Acta Cryst*. B53:25 (1979)
20. Kudoh, Y. and Takenchi, Y., *Z. Kristalogr*. 171:291 (1985)
21. Liebau, F., Structural Chemistry of Silicates, Springer-Verlag, Berlin, Heidelberg, p. 347 (1985)

22. McDonald, W. S. and Cruickshank, D. W. J., *Acta Cryst*., 22:37 (1967)
23. Brown, I. D., *Chem. Soc. Revs.*, 7:359 (1978)
24. Hazen, R. M. and Prewitt, Ch., *Amer. Mineral*, 62:309 (1977)
25. Urusov, V. S. and Pushcharovsky, D. Yu., *Crystal Chemical Principles of High-pressure Mineral*, p. 23 (in Russian) (1984)
26. Sasaki, S., Prewitt, Ch., Sato, Y., and Ito, E., *J.Geophys. Res.*, 87:7829 (1982)
27. Horiuchi, H. and Sawamoto, H., *Amer. Mineral*. 66:568 (1981)
28. Ringwood, A. E., Germanates as the Model of Silicates, Stable at High Pressures, in: *Problems of Petrology and Genetic Mineralogy*, p. 41, Nauka, Moscow (in Russian) (1969)
29. Levien, L., Prewitt, Ch., and D. J. Weidner, *Amer. Mineral*, 65:920 (1980)
30. Pushcharovsky, D. Yu., Vyatkin, S. V., Yamnova, N. A., and Sorokina, S. L., *Kristallographia*, 35:1172–1176 (1990)
31. Samailovich, L. A., Dependence of Pressure, Temperature, and Density of Water-Salt Solutions, p. 47, BHUUCUMC (VNIISIMS), Moscow (in Russian) (1969)
32. Zakirov, I. V., Investigations of the Thermodynamic Parameters of Hydrothermal Systems, in: *Problems for Geology and Metallogenesis of Volcanic Materials., Proc. Geology Congress*, Vladivostok, pp. 155–156 (1968)
33. Ravich, M. I. and Borovaya, F. E., Solubility of Sodium Carbonate in Water at Higher Pressure and Temperature Interval 475–540°C, *Doklady Akad. Nauk SSSR*, 180:1372–1375 (1968)
34. Ravich, M. I., Borovaya, F. E., and Smirnova, E. G., Solubility and Vapor Pressure in Potassium Carbonate-Water Systems Under High Temperature and Pressures, *J. Inorg.Chem.*, 13:1422–1427 (1968)
35. Dimitrova, O. V., Ph.D. Thesis, Moscow State Univ., Moscow (1977)
36. Haile, S. M., Wuensch, B. J., and Laudise, R. A., Hydrothermal Synthesis of New Alkali Silicates I. Potassium Neodymium Phases, *J. Crystal Growth*, 131:352–372 (1993)
37. Haile, S. M., Wuensch, B. J., and Laudise, R. A., Hydrothermal Synthesis of New Alkali Silicates II. Sodium Neodymium and Sodium Yttrium Phases. *J. Crystal Growth*, 131:373–386 (1993)
38. Shannon, R. D., Taylor, B. E., Gier, T. E., Chen, H. Y. and Berzine, T., *Am. Chem. Soc. Inorg. Chem.*, 17:958–963 (1978)
39. Shannon, R. D., Chen, H. Y., and Berzine, T., *Mater. Res. Bull.*, 12:959 (1977)
40. Hong, H. Y. P., Kafalas, J. A., and Bayard, M., *Mater. Res. Bull.*, 13:757–760 (1978)
41. Beyeler, H. U. and Hibma, T., *Solid State Commun*, 27:641–645 (1978)

DropBooks

42. Bowen, N. L., Schairer, J. F., and Willems, H. W. V., *Am. J. Sci.*, 20:405 (1930)
43. Maksimov, B. A., Kharitonov, Yu. A., and Belov, N. V., *Dok. Acad. Nauk. USSR* 213:1072 (1973)
44. Demianets, L. N., Lobachev, A. N., and Emelchenko, G. A., *Germanates of Rare Earth Elements*. Nauka, Moscow (1980)
45. Litvin, B. N., Byrappa, K., and Bebikh, L. G., Growth and Properties of Monocrystals for Miniature Lasers, *Prog. Crystal Growth Charact.* 3:257–271, U.K.(1981)
46. Pabedimskaya, E. A., Pushcharovsky, D. Yu., and Karpov, O. G., *Structure Types of Rare Earth Silicates, Germanates and Phosphates*, Moscow State, Unviersity Press, Moscow (1984)
47. Haile, S. M., Wuensch, B. J., Siegrist, T., and Laudise, R. A., Hydrothermal Synthesis of New Alkali Silicates I. Potassium Neodymium Phases, *J. Crystal Growth*, 13:352–372 (1993)
48. Haile, S. M., Wuensch, B. J., and Laudise, R. A., Hydrothermal Synthesis of New Alkali Silicates II. Sodium Neodymium and Sodium Yttrium Phases, *J. Crystal Growth*, 131:373– 386 (1993)
49. Haile, S. M., Wuensch, B. J., Siegrist, T., and Laudise, R. A., Conductivity and Crystallography of New Alkali Rare Earth Silicates Synthesized as Possible Fast-Ion Conductors, *Solid State Ionics*, 53–56:1292–1301 (1992)
50. Ikornikova, N. Yu., in: *Crystallization Processes Under Hydrothermal Conditions*, (A. N. Lobachev, ed.), pp. 93–111, Consultants Bureau, New York, (1971)
51. Haile, S. M., Ph.D. Thesis, Massachusetts Institute of Technology, USA (1992)
52. Belov, N. V., *Crystal Chemistry of Silicates with Large Cations*, Nauka, Moscow (1961)
53. Pobedimskaya, E. A., Pushcharovsky, D. Yu., and Karpov, O. G., *Structure Types of Rare Earth Silicates, Germanates and Phosphates*, Moscow State University Press, Moscow (1984)
54. Maksimov, B. A., Ilyukhin, V. V., and Belov, N. V., Crystalline Strructure of K_3Y $[Si_3O_8(OH)_2]$, *Doklady Akad. Nank USSR*, 181:400–403 (1968)
55. Dowty, E., Crystal Structure of Joaquinite, *Am. Mineral*, Am. Mineral, 60:872-878 (1975)
56. Simonov, M. A., Egorov–Tismenko, Yu. K., and Belov, N. V., New Si-O radical $[Si_3O_{10}]$ in $Na_4Gd_2[Si_3O_{10}]$, *Doklady Akad. Nauk USSR*, 179:860–863 (1968)
57. Simonov, M. A., Egorov–Tismenko, Yu. K., and Belov, N. V., Crystal Structure of Na,Gd-Triorthosilicate $Na_2Gd_3[Si_3O_{10}]$, *Doklady Akad. Nauk USSR*, 181:38–42, (1968)

58. Taylor, H. F. W., The Crystal Structure of Kilchoanite $Ca_6(SiO_4)$ (Si_3O_{10}) With Some Comments On Related Phases, *Miner. Mag*., 38:67–71 (1971)
59. Krutik, V. M., Pushcharovsky, D. Yu., Khomyakov, A. P., Pobedimskaya, E. A., Belov, N. V., Anionic Radical Mixed Type $[Si_4O_{12}]$ and P-orthotetrahedra) in Monodinic Phosphate, *Kristallografia*, 25:178–181 (1980)
60. Volodina, G. F., Rumanova, I. M., and Belov, N. V., Crystal Structure of $Ca_2R_2[Si_4O_{12}]CO_3.H_2O$, *Doklady Akad. Nauk USSR*, 149:23–26 (1963)
61. Golovastikov, N. I., Crystal Structure of Alkali Titanosilicate Labuntzovite, *Kristallografia*, 18:771–774 (1973)
62. Mazzi, F., Rossi, G., The Crystal Structure of Taramellite $Ba_2(Fe,Ti,Mg)_2$ $H_2/O_2(Si_4O_{12})$ /.–*Z. Kristallogr*., Vol. 121 (1965)
63. Hilmer, W., Die Kristallstructure des sauren Kaliummetasilikates $K_4(HSiO_3)_4$, *Acta Crystallogr*., 17:1063-1065 (1964)
64. Kampf, A. R., Khan, A. A., and Baur, W. H., Barium Cloride Silicate With An Open Framework: Verplanckite, *Acta Crystallogr*., 29:379–382 (1973)
65. Perrault, G., Boucher, C., Vicat, J., et al., Structure Cristalline du Nenadkevichite $(Na,K)_{2-x}$ (Nd,Ti) (O,OH) $Si_2O_6{\cdot}2H_2O$–*Acta Crystallogr*., 29:7 (1973)
66. Nekrasov, Yu. A., Ponomarev, V. I., Simonov, B. I., and Kheiker, D. M., Establishment Atomic Structures Biotite and Isomorphous Ratios in This Mineral. *Kristallagrafia*, Vol. 14 (1969)
67. Maksimov, B. A., Merinov, B. V., Borovkov, V. S., Ivanov–Shits, A. K., Kharitonov, Yu. A., and Belov,N. V., Specialities of Construction of Rare Earth Silicates Family, $Na_5RSi_4O_{12}$ – A New Class of Solid Electrolytes, *Kristallografia*, Vol. 24 (1979)
68. Malinovski, Yu. A., Pobedimskaya, E. A., and Belov, N. V., Crystal Structure of Traskite, *Doklady Akademi Nauk USSR*, Vol. 229 (1976)
69. Maksimov, B. A., Kalinin, V. R., Merinov, B. V., Ilyukhin, V. V., and Belov, N. V., Crystal Structure Rare Earth NaY – Metasilicate $\{Na_3YSi_3O_9\}$ x $4Na_{12}Y_4$ $[Si_{12}O_{36}]_\infty$, *Doklady Akademii Nauk USSR* (1980)
70. Pushcharovsky, D. Yu., Dago, A. M., Pobedimskaya, E. A., and Belov, N. V., Crystal Structure $K_8Yb[Si_6O_{16}](OH)$ Polymorphism Radicals $[Si_3O_8]$ – *Doklady Akademii Nauk USSR*, Vol. 258 (1979)
71. Karpov,O. G., Pushcharovsky, D. Yu., Pobedimskaya, E. A., Burshtein, I. F., and Belov, N. V., Crystal Structure of Rare Earth Silicate $NaNdSi_6O_{13}(OH)_2.nH_2O$, *Sov. Phys. Dokl.*, 22:464–466 (1977)
72. Pushcharovsky, D. Yu., Karpov, O. G., Pobedimskaya, E. A., and Belov, N. V., Crystal Structure of $K_3NdSi_6O_{15}$, *Doklady Akademi Nauk*, Vol. 234 (1977)

ProBooks

73. Karpov,O. G., Pushchrovsky, D. Yu., Pobedimskaya, E. A., and Belov, N. V., Crystal Structure of Rare Earth Silicates $NaPrSi_6O_{14}$ and $NaNdSi_6O_{14}$. New Infinite Silica Radical 3d Column $[Si_3O_7]_{\infty\,\infty}$ – *Dokl. Akad. Nauk USSR*, Vol. 226 (1976)

74. Karpov, O.G., Pobedimskaya, E.A. and Belov, N.V., Crystal Structure of K.Ce- Silicate With 3d Anion Framework $K_2CeSi_6O_{15}$, *Kristallografia*, Vol. 22 (1977)

75. Felsche J., The Crystal Chemistry of the Rare–Earth Silicates–*Struct. and Bond*., Vol. 13 (1973)

76. Haile, S. M., Maier, J., Wuensch, B. J., and Laudise, R. A., Structure of $Na_3YSi_6O_{15}$–A Unique Silicate Based on Discrete Si_6O_{15} units, and a Possible Fast Ion Conductor, *Acta Crysta.*, B51:673–680 (1995)

77. Haile, S. M., Wuensch, B. J., Laudise, R. A., and Maier, J., Structure of $Na_3NdSi_6O_{15}\cdot 2H_2O$ – A Layered Silicate With Paths For Possible Fast Ion Conduction, *Acta Crysta.*, B53:7–17 (1997)

78. Shannon, R. D., Chen, H. Y., and Berzins, T., *Mater. Res. Bull.*, 12:969 (1977)

79. Shannon, R. D., Taylor, B. E., Gier, T. E., Chen, H.-Y., and Berzins,T., *Inorg. Chem.*, 17:958–962 (1978)

80. Beyeler, H. U., Hibma, T., *Solid State Commun*., 27:641–645 (1978)

81. Beyeler, H. U., Shannon, R. D., and Chen, H. Y., Ionic Conductivity of Single–Crystal $Na_5YSi_4O_{12}$, *Appl. Phys. Lett*., 37:934–935 (1980)

82. Atomyan, L. O. and Ukshe, E. A., in: *Physical Chemistry Modern Problems*, Moscow, Chemistry, p. 90 (1983)

83. Filipenko, O. S., Atomyan, L. O., Panomerov, V. I., Litvin, B. N., Dimitrova, O. V., Leonova, L.S., Tkacheva, N. S., and Ukshe, E. A., Heterrogeneous 10-Sided Crystal Framework–A Desired Structure Factor for Ionic Conductivity in Complex Oxides, *Phyl. Chem.*, 283: 430–433 (1985)

84. Haile, S. M., Maier, J., Wuensch, B. J., and Laudise, R. A., in: *Fast Ion Transport in Solids*, (B. Scrosati, et al. eds.), Kluwer Academic Publishers, 315–326 (1993)

85. Haile, S. M., Wuensch, B. J., Laudise, R. A., and Maier, J., Structure of $Na_3NdSi_6O_{15}.2H_2O$–A Layered Silicate With Paths For Possible Fast–Ion Conduction, *Acta Crysta.* B53:7–17 (1997)

86. Haile, S. M., Maier, J., Wuensch, B. J., and Laudise, R. A., Structure of $Na_3YSi_6O_{15}$–A Unique Silicate Based On Discrete Si_6O_{15} Units, and A Possible Fast-Ion Conductor, *Acta Crist*., B51:673–680 (1995)

87. Leonova, L. S. and Ukshe, E. A., Crystal Structure and Ionic Conductivity of Solid Electrolytes $M_5RESi_4O_{12}$, where M = Na, Ag; RE = Sm $\rightarrow$ Lu, *Solid State Ionics*, 14:137–142 (1984)

88. Maksimov, B. A., Litvin, B. N., Ilyukhin, V. V., and Belov. N.V., *Kristallografia*, 14:490–493 (1968)
89. Boilot, J. P., Collin, G., and Comes, R., *J. Solid State Chem*., 50:91–94 (1983)
90. Tranqui, D., Capponi, J. J., Joubert, J. C., and Shannon, R. D., *J. Solid State Chem*., 39:219–223 (1981)
91. Huggins, R. A. and Rabenau, A., *Mat. Res, Bull*., 31:1315–3120 (1978)
92. Anthony, R. G., Philip, C. V., and Dosch, R. G., *Waste Management*, 13:503–508 (1993)
93. Clearfield, A., Bortun, A. I., and Bortun, L. N., *Solvent Extr. Ion Exch*. 14:341 (1996)
94. Bortun, A. I., Bortun, L. N., Cahill, R. A., and Clearfield, A., *Solvent Extr. Ion Exch*., 15:285–290 (1997)
95. Poojary, D. M., Cahill, R. A., and Clearfield, A., *Chem. Mater*., 6:2364–2369 (1994)
96. Poojary, D. M., Bortun, A. I., Bortun, L.N., and Clearfield, A., *Inorg. Chem*., 35:6131–6135 (1996)
97. Demianets, L. N., in: Hydrothermal Growth of Crystals, (K. Byrappa, ed.) *Prog. Cryst. Growth Charact*., 21:291–355 (1991)
98. Iljushin, G. D., Demianets, L. N., Iljukhin, V. V, and Belov, N. V., *Dokl. Akad, Nauk USSR*, 271:1133–1135 (1983)
99. Alyamovskaya, K. V. and Chukhlantsev, V. G., *Izvestiya Akademii Nauk SSSR, Neorgan. Mater*., 6:8 (in Russian) (1970)
100. Alyamovskaya, K. V. and Chukhlantsev, V. G., *Izvestiya VUZ'ov, Khimiya i Khim.Tekhnologiya* 13:7 (in Russian) (1970)
101. Safronov, A. N., Nevskii, N. N., Iljukhin, V. V., and Belov, N. V., *Dokl. Akademii Nauk SSSR*, 225:1114 –1118 (in Russian) (1980)
102. Genet, F. and Barj, M., *Solid State Ionics*, 9–10:891–895 (1983)
103. Barth, S., Felitz, A., and Jager, C., Structure and Ionic Conduction in Solids: VI. Evidence for the Non-Existence of $Na_4ZrSi_3O_{10}$ As a Definite Crystalline Phase, *Solid State Ionics*, 26:189–195 (1988)
104. Yue Yong and Pang Wenqin, *J. Chem. Soc. Chem. Commun*., pp. 1166–1169 (1990)
105. Yue Yong and Pang Wenqin, Synthesis and Crystallization of $Na_4Zr_2(SiO_4)_3$ Under Lower Temperature and Pressure Hydrothermal Conditions, *J. Mat. Sci. Letts*., 10:1009–1010 (1991)
106. Bortun, A. I., Bortun, L. N., and Clearfield, A., Hydrothermal Synthesis of Sodium Zirconium Silicates and Characterization of Their Properties, *Chem. Mater*., 9:1854–1864 (1997)
107. Wöhler, K., cited by Bunsen, Apophyllite Heated With H_2O at 180°–190°C Under a Pressure of 10–12 atm, *Ann.*, 65:80–96 (1948)

DropBooks

108. Allen, E. T., Wright, F. E., and Clement, J. K., Part I Formation and Properties of the Four Crystal Forms, *Am. J. Sci. IVth Series*, XXII:385–438 (1906)

109. Morey, G. W. and Niggli, P., The Hydrothermal Formation of Silicates, A Review, *J. Am.Chem.Soc*., 35:1086–1131 (1913)

110. Morey, G. W., The Ternary System H_2O-K_2SiO_3-SiO_2, *J. Am. Chem. Soc*., 39: 1173–1229 (1917)

111. Bowen, N. L., The Behavior of Inclusions in Igneous Magmas, *J. Geol*., 30: 513–520 (1922)

112. Bowen, N. L. and Tuttle, O. F., The System MgO-SiO_2-H_2O., *Bull. Geol. Soc. Am*. 60: 439–460 (1949)

113. Noll, W., Mineralbildung im System Al_2O_3-SiO_2-H_2O. *Neues Jahrbuch Mineralogie*, 70:65–115 (1935)

114. Noll, W., Zur Kenntnis der siallitischen Mineralumbildung. Fortschritte der Mineralogie, *Kristallographite und Petrographie* 21:85–88 (1937)

115. Noll, W., Neuere Untersuchungen von reaktionen in Wesserhaltigen Silicatsystemen. *Die Chemie* 57:90–94 (1944)

116. Taylor, H. F. W., Hydrated Calcium Silicates. Part I. Compound Formation at Ordinary Temperatures. *J. Chem. Soc*., 726:3682–3690 (1950)

117. Taylor, H. F. W., Hydrothermal Reactions in the System CaO-SiO_2-H_2O. *Proc. Intl. Symposium on Reactivity of Solids*, pp. 677–682 Gothenburg (1952)

118. Taylor, H. F. W., Hydrated Calcium Silicates. Part V. The Water Content of Calcium Silicate Hydrate –I, *J. Chem. Soc*., 33:163–171 (1953)

119. Taylor, H. F. W. and Bessey, G. E., Review of Hydrothermal Reactions in the System Lime-Silica-Water, *Magazine Concrete Res*., 4:15–26 (1950)

120. Carlson, E. T. and Wells, L. S. Hydrothermal Preparation of Some Strontium Silicates, *J. Res. Natl. Bur. Stds*., 51:2 (1953)

121. Roy, D. M. and Roy, R., Studies in the System MgO-Al_2O_3-SiO_2-H_2O, *Bull. Geol. Soc.Amer*., 63:1293–1294, (Abstr.) (1952)

122. Roy, D. M. and Roy, R., Synthesis and Stability of Minerals in the System MgO-Al_2O_3-SiO_2-H_2O, *Amer. Min*., 40:147–178 (1955)

123. Yoder, H. S., The MgO-Al_2O_3-SiO_2-H_2O System and the Related Metamorphic Facies, *Amer. Sci*., Bowen Volume, pp. 569–627 (1952)

124. Nelson, B. W. and Roy, R., Polymorphic 7Å and 14Å Phases in the MgO-Al_2O_3-SiO_2-H_2O System and Their Identification. Proceedings of the Second National Clay Conference, Columbia, Mo. (See Publn. of the National Research Council, No. 327) (1953)

125. Barrer, R. M. and White, E. A. D., The Hydrothermal Chemistry of Silicates. Part II. Synthetic Crystalline Sodium Aluminosilicates, *J. Chem. Soc*. 286:1561–1571 (1952)

126. Sand, L. B., Roy, R., and Osborn, E. F., Stability Relations of Some Minerals in the System Na_2O-Al_2O_3-SiO_2-H_2O, *Bull. Geol. Soc. Amer*., 64:1469–1470 (Abstr.)

127. Friedman, Irving, Some Aspects of the System H_2O-Na_2O-SiO_2-Al_2O_3, *J. Geol*., 59:19–31 (1951)

128. Yoder, H. S. and Eugster, H. P., Phlogopite Synthesis and Stability Range, *Geochim. et Cosmochim. Acta.*, 6:157–185 (1954)

129. Coes, L., A New Dense Crystalline Silica, *Science*, 118:131–133 (1953)

130. Litvin, B. N., Investigations of the Hydrothermal Crystallization in Some Silicate Systems, Ph.D. Thesis, Institute of Crystallography, *Acad. Nauk USSR* (1964)

131. Surnina, V. S. and Litvin, B. N., Crystallization in the Systems Na_2O-Bi_2O_3-SiO_2-H_2O and Na_2O-Bi_2O_3-GeO_2-H_2O, *Izvestia Akad. Nauk USSR, Inorganic Materials*, 6:1695–1697 (1970)

132. Armington, A. F., Recent Advances in the Growth of High Quality Quartz. In: *Hydrothermal of Crystals* (K. Byrappa, ed.), *Prog–Crystal Growth Charact.* 21:97–111 (1991)

133. Harris, M. T., Larkin, J. J., and Martin, J. J., Low-Defect Colorless $Bi_{12}SiO_{20}$ Grown by Hydrothermal Technique, *Appl. Phys. Lett*., 60:2162–2163 (1992)

134. Larkin, J., Harris, M. T., Cormier, J. E., and Armington, A. F., Hydrothermal Growth of Bismuth Silicate (BSO), *J. Crystal Growth*, 128:871–875 (1993)

135. Harris, M. T., Larkin, J. J., Cormier, J., and Armington, A. F., Optical Studies of Czochralski and Hydrothermal Bismuth Silicate, *J. Crystal Growth*, 137:128–131 (1994)

136. Leigh, W. B., Larkin, J. J., Harris, M. T., and Brown, R. N., Characterization of Czochralski- and Hydrothermal Grown $Bi_{12}SiO_{12}$, *J. Appl. Phys*., 76:660–666 (1994)

137. Surnina, V. S. and Litvin, B. N., Investigations of Phase Formations in the System Na_2O-Me_2O_3-Bi_2O_3-H_2O (where Me= Al, Ga, In) Under Hydrothermal Conditions, *Kristallografia*, 15:604–607 (1970)

138. Abrahams, S. C., Jamieson, P. B., and Bernstein, J. L., Crystal Structure of Piezoelectric Bismuth Germanium Oxide $Bi_{12}GeO_{20}$, *J. Chem. Phys*., 747:4034–4041 (1967)

139. Hautefeuille, P. and Perrey, A., *Crystal Research. Acad. Sci.*, 106:1800–1810, Paris (1888)

140. Espig, H.–Z., *Kristallogr.*, 92:387–392 (1935)

141. Rogers, A. F. and Sperisen, F., *J., Amer. Miner*., 27:762–765 (1942)

142. Wyart, J. and Scavnicar, S., Synthèse Hydrothermale du beryl, *Bull. Soc. Franc. Minèr. Crist*., 80:395–396 (1957)

143. Nacken, R., cited by Nassau, K., *J. Crystal Growth*, 35:211–217 (1976)

DropBooks

144. Hosaka, M., Hydrothermal Growth of Gem Stones and Their Characterization, in: *Hydrothermal Growth of Crystals*, (K. Byrappa, ed.) *Prog. Crystal Growth Charact.*, 21:71–96 (1990)

145. Anderson, B. W., *Gem Testing, 8th ed*., pp. 97–106, 223–229, Butterworths, London, (1971)

146. Liddicoat, R. T. Jr., *Handbook of Gem Identification, 10th ed*., pp. 106–108, 138–144, 308–313, (Gemnological Institute of America, Los Angeles,) (1975)

147. Webster, R., *Gems, 3rd ed*., pp. 83–100, 359–366, (Newns–Butterworths, London) (1975)

148. US Patent 3,567,642, Flanigen, E. M., (March 2, 1971)

149. US Patent 3,567,643, Flanigen, E. M. and Mumbach, N. R., (March 2, 1971)

150. USA Patent No.3,723,337, Yancey, P. J., (1973)

151. Brown, G. and Snow, J., *Aust. Gemmol*., 15:2, 57 (1983)

152. Hanmi, H. A., *J. Gemmol*., 18:2, 138 (1982)

153. Stockton, C., *Gems and Gemology*, 20:3, 141 (1984)

154. Darragh, P. J. and Willing, M. J., *Aust. Gemmol*., 14:12, 344 (1982)

155. Scarratt, K., *J. Gemmol*., 21:5, 294 (1989)

156. Kane, R. E. and Liddicoat, R. T. Jr., *Gems and Gemology*, 21:3, 156 (1985)

157. Brown, G. and Snow, J., *Aust. Gemmol*., 16:12, 437 (1988)

158. EmeÍyanova, E. N., Grum–Grzhimailo, S. V., Boksha, O. N., and Varina, T. M., *Sov. Phys.–Cryst.*, 10:10 (1965)

159. Takubo, H., *J. Gemmol. Soc. Jpn.*, 6:4, 3 (1979)

160. Schmetzer, K., *J.Gemmol*., 21:3, 145 (1988)

161. Sinkankas, J., *Emerald and other Beryl*, Chilton Book Company, Pennsylvania (1981)

162. Kodaira, K., Iwase, Y., Tsunashima, A., and Matsushita, T., High-pressure Hydrothermal Synthesis of Beryl Crystals. *J. Crystal Growth*, 60:172–174 (1982)

163. Bauér, Ya. and Rykl, D., Synthetic Chkalovite, *Sov. Phys. Crystallogr*., 17:615–616 (1972)

164. Bakakin, V. V. and Solov'eva, L. P., Crystal Structure of $Fe_3BeSi_3O_9(F,OH)_2$, An Example of a Wollastonite-Like Silicon-Oxygen Chain Based on Fe, *Sov. Phys–Crystallogv*., 15:999–1005 (1971)

165. Kharitonov, Yu. A., Golyshev, V. M., Rastsvetaeva, R. K., and Belov, N. V., Crystal Structure of Synthetic Sodium Aluminoberyllosilicate $Na_3AlBeSi_2O_8$, *Sov. Phys. Crystallogr*., 19:667–668 (1975)

166. Maeda, M., Uehara, T., Sato, H., and Ikeda, T., Hydrothermal Syntheses of $BaBe_2Si_2O_7$, Jap. *J. Appl. Phys*., 30:2240–2242 (1991)

167. Sobolev, B. P., Dern'yanets, L. N., Dikov, Yu. P, Ilyukhin, V. V., and Belov, N. V., Geokhimiya, 6:634–639 (1966)

168. Beus, A. A., and Dikov, Yu. P., *Geochemistry of Beryllium in Processes of Endogenic Mineral Formation,* Nedra, Moscow (1967)

169. Frondel, C., Hurlbut, C. S., and Collete, R. C., Synthesis of Tourmaline, *Amer. Miner*., 32:680–681 (1947)

170. Michel-Levy, M.C., Synthese de la tourmaline et de la jeremeiwite, *Crystal Acad. Sci*., 228:1814–1816 (1949)

171. Robbins, K. P., Yoder, Kh. S., and Shairrer, J. P., Synthesis of Tourmaline, in: *Problems in Theoretical and Experimental Petrology*; Mir Publishers, Leningrad, p. 523, (1963)

172. Voskresenskaya, I. E., Properties of Synthetic Tourmaline, in: *Mineralogy*, Lvov Univ. Press, Lvov, pp. 164–171 (1966)

173. Voskresenskaya, I. E. and Barsukova, M. L., Synthesis and Properties of Some Iron and No Iron Bearing Tourmaline, in: *Hydrothermal Synthesis of Crystals*, Nauka, Moscow, pp. 175–192 (1967)

174. Friedel, C. and Georges, *Bull.Soc.Min*., 13:129–139 (1890)

175. Friedel, C., *Bull. Soc. Min*., 19:5–14 (1896)

176. Litvin, B. N., *Hydrothermal Chemistry of Silicates of Germanats*, D.Sc., Thesis., Institute General and Inorganic Chemistry, Akad. Nauk USSR, p. 33 (1978)

177. Litvin, B. N. and Melnikov, O. K., Crystallization in the System Na_2O-Al_2O_3-SiO_2-H_2O., *Kristallografia*, 14:101–105 (1969)

178. Roth, G. and Bhm, H., Ionic Conductivity of Sodium-Nepheline Single Crystals, *Solid State Ionics*, 18/19:553–556 (1986)

179. Ingerson, E. and Tuttle, O. F., Artificial Willemite Needles, *Amer. J. Sci*., 245:313–319 (1947)

180. Roy, D. M. and Mupton, F. A., Stability of Minerals in the System ZnO-SiO_2-H_2O, *Econ. Geol*., 51:432–443 (1956)

181. Ringwood, A. E. and Major, A., High-pressure Trans-formations on the Zinc Germanates and Silicates, *Nature*, 215:1367–1368 (1967)

182. Litvin, B. N., Tarasenkova, O. S., and Belov, N. V., Synthesis and Crystal Chemical Elucidation of Compounds in the System Na_2O-ZnO-SiO_2-H_2O, at 400–500°C, in: *Physico–Chemical Petrology Series*, 4:89–101, Nauka, Moscow (1974)

183. Belyaev, L. M., Litvin, B. N., Dianova, I. M., and Melnikov, O. K., Hydrothermal Synthesis Crystallophosphors of $Na_xZn_ySi_pO_q$ type, *Kristallografia*, 11:285–287 (1966)

184. Litvin, B. N. and Popolitov, V. I., *Hydrothermal Synthesis of Inorganic Compounds*, pp. 66–81, Nauka, Moscow (1984)

DropBooks

185. Simonov, M. A., Melnikov, O. K., and Litvin, B. N., Synthesis of NaCl Silicates, in: *Hydrothermal Synthesis of Crystals*, pp. 155–159, Nauka, Moscow (1968)

186. Simomov, M. A., Egorov – Tismenko, Yu. K. and Belov, N. V., Confirmation of Crystal Structure of Na, Cd-triorthosilicate-$Na_4Cd_2Si_3O_{10}$, *Dokl. Akad. Nauk USSR*., 238:348–351 (1978)

187. Litvin, B. N., Dianova, I. M., and Kagon, L. A., Synthesis and Properties of Monocrystals of Composition $Na_2O{\cdot}2MnO{\cdot}2SiO_2$, *Kristallografia*, 9:571–574 (1964)

188. Taylor, F. W., Hydrosilicates of Calcium, in: *Proc. 5th International Congress on the Chemistry of Cement*., pp. 114–136, Stroizdat, Moscow (1973)

189. Ilyukhin, V. V., Kuznestov, V. A., Lobachev, A. N., and Bakshutov, V. S., *Hydrosilicates of Calcium*, p. 184, Nauka, Moscow, (1979)

190. Litvin, B. N. and Kudryasteva, O. V., Structural-Genetic Elucidation of Phase Formation in the System CaO-SiO_2-H_2O, in: *Proc. 6th International Congress on Chemistry of Cement*, pp. 211–213, Stroizdat, Moscow (1976)

191. Taylor, H. F. W., The Crystal Structure of Kilchoanite, $Ca_6(SiO_4)$ (Si_3O_{10}) With Some Comments on Related Phases, *Miner. Mag.*, 38:26–31 (1971)

192. Lejus, A. M., Kahn–Harari, A., Benitez, J. M., and Viana, B. Crystal Growth, Characterization and Structure Refinement of Neodymium Doped Gehlenite, a New Laser Material, $[Ca_2Al_2SiO_7]$, *Mat. Res. Bull.*, 29:725–734 (1994)

193. Funk, H., Uber barium silicathydrate und ihre hydrothermal-produkte.– *Ztschr. Anorg. Und allg. Chem.*, 296:46–62 (1958)

194. Eskola, P., Synthetic Barium Silicate, *Amer. J. Sci*., 4 :331–332 (1922)

195. Philipenko, O. S., Litvin, B. N., Pobedimskaya, E. A., and Belov, N. V., Hydrothermal Synthesis of Some Barium Silicates and Their X-ray Data, *Kristallografia*, 15:863–865 (1970)

196. Ismail-Zade, I. and Litvin, B. N., Hydrothermal Synthesis of Monocrystals of Na-Mn-Silicates and Germanates. *Azerbaizan Chemistry Journal*, 6:135–146 (1969)

197. USSR Patent, No. 1305288, 19.02.69, Litvin, B. N., Growth of Bivalent Mn-Silicates and Germanates Crystals, and Ismail-Zade, I.

198. Litvin, B. N., Fonin, V. S., Pushcharovskii, D. Yu., and Pobedimskaya, E. A., Crystallization of Silicates, in: *Crystal Growth*, pp. 96–100, Nauka, Moscow (1977)

199. Hatch, R. A., *Amer. Mineral*., 28:471–478 (1943)

200. Isaacs, T. and Roy, R., *Geochim. Cosmochim. Acta*., 15:213–219 (1958)

201. Kuznetsov, V. A., Shternberg, A. A., and Ivanova, T. K., Hydrothermal Crystallization of Lithium Silicates, Synthesis of Spodumene, in: *Crystallization Processes under Hydrothermal Conditions*, (A. N. Lobachev, ed.) pp. 173–184, Consultants Bureau, New York (1973)

202. Ghobarkar, H., The Hydrothermal Synthesis of Petalite Mineral Phases and Their Morphological Changing by Increasing of Temperature, *Cryst. Res. Technol*., 27:451–456 (1992)

203. Onishi, H., Notes on the Geochemistry of Germanium, *Bull. Chem. Soc*. Jap., 29:686–694 (1956)

204. Wardani, S. A., On the Geochemistry of Germanium–*Geochim et Cosmochim. Acta*., 13:5–19 (1957)

205. Vinogradov, A. P., *Geochemistry*, 1:6–52 (1956)

206. Demianets, L. N., Lobachev, A. N., and Emelchenko, G. A., *Germanates of Rare Earth Elements* Moscow, Nauka, (in Russian) (1980)

207. Duderov, N. G., Dem'yanets, L. N., Belokoneva, E. L., Lobachev,A. N., and Belov, N. V., New Crystalline Phases in the Na_2O-CdO-GeO_2-H_2O system. *Sov. Phys. – Crystallography*, 17:916–920 (1973)

208. Duderov, N. G., Demianets, L. N., Lobachev, A. N., Pisarevsky, Yu. V., and Silvestrova, I. M., Na_2COGeO_4 Single Crystal Growth and Study of There Piezoelectric and Elastic Properties, *J. Crystal Growth*, 44:483–491 (1978)

209. Demianets, L. N., Duderov, N. G., Lobachev, A. N., Lefaucheux, F, Robert, M. C., and Authier, A., X-ray Topographic Study of Growth Defects in Hydrothermal Na_2CoCeO_4 Single Crystals in Relation to Their Growth Conditions, *J. Crystal Growth*, 44:570–580 (1978)

210. Kuzmina, I. P., Lobachev, A. N., Vinokurov, V. M., Nizamutdinov, N. M., and Volkova, L. A., Zn–Mn isomorphism in Na_2ZnGeO_4 Crystals, *Sov. Phys. Crystallogr*., 18:110–111 (1973)

211. Belokoneva, E. L., Ivanov, Yu. A., Simonov, M. A., and Belov, N. V., Crystal Structure of Cadmium Orthogermanate Cd_2GeO_4, *Sov. Phys.–Crystallography*, 17:177–179 (1972)

212. Kornev, A. N., Dem'yanets, L. N., Maksimov, B. A., Ilyukhin, V. V. and Belov, N. V., Hydrothermal Synthesis in the KCl-CdO-GeO_2-H_2O System and the Crystal Structure of $Cd_2[Ge_2O_6]$, *Sov. Phys-Crystallogr*., 17:244–246 (1972)

213. Ivanov, S. A., Bush, A. A., Fedotov, S. V., and Zavodnik,V. E., Single Crystals of New Phase $Na_{0.67}Pb_2Ge_{2.67}O_{7.33}(OH)_{0.67}$ in PbO-GeO_2-NaOH-H_2O System: Conditions of Preparation, Atomic Structure, and Properties, *J. Structural Chemistry*, 32:13–17 (1991)

214. Uvarova, T. G., Dem'yanets, L. N., and Lobachev, A. N., Hydrothermal Synthesis of Sodium Aluminogermanate Single Crystals, *Sov. Phys. Crystallography*, 21:497–499 (1976)

215. Malinovskii, Yu. A., Pobedimskaya, E. A., and Belov, N. V., Synthesis and Crystal Structure of the Germanate–Carbonate Apatite $Ba_5[(Ge,C)(O,OH)_4]_3(OH)$. *Sov. Phys. Crystallogr*., 20:394–396 (1975)

DropBooks

216. Malinovskii, Yu. A., Pobedimskaya, E. A., Kuznetsov, V. A., and Belov, N. V., Phase Formation in the System $BaO\text{-}GeO_2\text{-}K_2O\text{-}H_2O$ Under Hydrothermal Conditions, *Sov. Phys. Crystallogr*., 20:725–728 (1976)

217. Kurazhkovskaya, V. S., Ph.D., Thesis, Moscow State University, Moscow (1971)

218. Tseitlin, M. N., Plakhov,G. F., Lobachev, A. N., Popolitov, V.I., Simonov, M.A., and Belov, N.V., Study of Crystallization in the Hydrothermal System $GeO_2\text{-}Sb_2O_3\text{-}KF\text{-}H_2O$, *Sov. Phys. Crystallogr.*, 18:525–527 (1974)

219. Verkovskii, V. Ya., Kuzmin, E. A., Ilyukhin, V. V. and Belov., Crystal Structural of Na-titanogermanate, $Na_2(TiO)$ $[GeO_4]$, *Doklady Akad. Nauk. USSR, Kristallografia*, 190:91–93 (1970)

220. Popov.V. V., Petrova, M. A., Synthesis and Electric Properties of Germanates of Rare Earth Elements, *Izv. Akad. Nauk USSR, Inorg. Mater*., 9:61–63 (1973)

221. Fournier, J., Kohlmuller, R., Surles Systemes $GeO_2\text{-}Ln_2O_3$- C, *R. Acad. Sci. (C)*, 266:136–362 (1968)

222. Emelchenko, G. A., Grechushnikov, B. N., and Ilyukhin, V. V., Spectroscopic Investigations of Rare Earth Germanates, in: *Spectroscopy of Crystals*, pp. 265–269, Nauka, Moscow (1976)

223. Hong, H. Y.-P., Crystal Structure and Ionic Conductivity of $Li_{14}Zn(GeO_4)_4$ and Other New Li^+ Superionic Conductors, *Mat. Res. Bull*., 13:117–124 (1978)

224. Ohtsuka, H. and Yamaji, A., Preparation and Characteristic of $Li_{14}Zn(GeO_4)_4$ Thin Films for Solid State Batteries, *IEEE,* CH 1855–1856:353–359 (1983)

225. Anthony, J. W., *Amer. Min.*, 42:904–910 (1957)

226. Kostov, I., *Mineralogy*, Mir Publishers, Moscow (1971)

227. Ronsbo, J. C., Khomyakov, A. P., Semenov, E. I., Voronkov, A. A., and Garanin, V. K., Neues *Jahrb. Mineral. Abhandl*. 1:42–45 (1979)

228. Berstelius, J. J., Ann. Physik, 53:393 (1816)

229. Johnson, K. R., *Ber. Deut. Chem. Ges.* 22:976 (1889)

230. Mooney, R. C. L., *J. Chem. Phys.* 16:1003 (1948)

231. Mooney, R. C. L., *Acta Crystallogr*. 3:337 (1950)

232. Jaulmes, S. C., *R. Acad. Sci*., C 268:935, Paris (1969)

233. Beucher, M., *Les Elements des Terres Rares*. Cell. No. 180/181:331 (1970)

234. Danielmeyer, H. G., Huber, G., Kruhler, W. W., and Jesser, J. F., *Appl. Phys*., 2:335–339 (1973)

235. Weber, H. P., Damen, T. C., Danielmeyer, H. G., and Tofield, B. C., *Appl. Phys. Lett*. 22:534–536 (1973)

236. Otsuka, K., Yamada, T., Nakano, J., Kimura, T., and Seruwateri, M., J. *Appl. Phys*., 46:4600 (1975)

237. Otsuka, K., Miyazawa, S., Yamada, T., and Iwasaki, H., *J. Appl. Phys*., 48:2099–2103 (1977)

238. Krühler, W. W., Plattner, R. D., Fabian, W., Mockel, P., and Grabmaier, J. G., *Opt. Commun*., 20:354–360 (1977)

239. Chin, S. R. and Hong, H. Y.-P., *Opt. Commun*., 15:345–349 (1975)

240. Goodenough, J. B., Hong, H. Y. -P., and Kafalas, J. A., *Mat. Res. Bull*., 11:203–210 (1976)

241. Hong, H. Y. P., *Mat. Res. Bull*., 11:173–180 (1976)

242. Goodenough, J. B., Proc. *International Course on Materials Science*, Erice, Italy (April 14–24, 1980)

243. Byrappa, K., Ph. D. Thesis, Moscow, State University, Moscow (1982)

244. Byrappa, K., Gopalakrishna, G. S., Viswanathiah, M. N., Venkatachalapathy, V. and Puttaraj, B., *J. Mat. Sci. Lett*., 4:565–570 (1985)

245. Atomyan, L. O., Philepenko, O. S., Ponomarev, B. I., Leonov, L. S., Tkacheva, N. S., Ukshe, E. A., Dimitrova, O. V., and Litvin, B. N., *Dokl. Acad. Nauk. USSR*, 261:874–879 (1981)

246. Rzaigui, M., Kbir Ariguib, Averbuch-Pouchot, M. T., and Durif, A., *J. Solid State Chem*., 50:240–246 (1983)

247. Chudinova, N. N., D. Sc.Thesis, Institute of General and Inorganic Chemistry, Academy of Science, USSR, Moscow (1980)

248. McGilvery, J. D. and Scott, A. E., *Can. J. Chem. Soc*., 79:3647 (1957)

249. Carron, M., Mrose, M. E., and Murata, K. J., Relation of Ionic Radius to Structures of Rare Earth Phosphates, Arsenates and Vanadates, *Amer. Min*., 43:985–989 (1958)

250. Carron, M. K., Naeser, C. R., Rose H. J. Jr., and Hildebrand, F. A., Fractional Precipitation of Rare Earths With Phosphoric Acid, U.S.Geol, Survey Bull. No.1036–N:253–273 (1958)

251. Byrappa, K. and Gopalakrishna, A., Critical Survey on the Study of Alkaline Rare Earth Phosphate and NASICON Systems With a Special Reference to the Hydrothermal Method, *Prog. Crystal Growth Character*., 11:89–107 (1985)

252. Byrappa, K., Preparative Methods and Growth of Rare Earth Phosphates, *Prog. Crystal Growth Character*., 13:163–196 (1986)

253. Rabenau, A., Lithium Nitride and Related Materials, *Proc. Int. Course on Physics of Materials*, I. I. T, Madras, India(Sept. 3–22, 1984)

254. Yoshimura, M., Fujii, K., and Somiya, S., Phase Equilibria in the System Nd_2O_3-P_2O_5-H_2O at 500°C, Under 100 MPa and Synthesis of NdP_5O_{14} Crystals, *Mat. Res. Bull*., 16:327–333 (1981)

255. Byrappa, K. and Litvin, B. N., Hydrothermal Synthesis of Mixed Phosphates of Neodymium and Alkaline Metals ($Me_2O{\cdot}Nd_2O_3{\cdot}4P_2O_5$), *Mat. Sci*., 18:703–708 (1983)

DropBooks

256. Byrappa, K., Srikantaswamy, S., and Gali, S., Hydrothermal Synthesis and Structure of TmP_5O_{14}, *J. Mat. Sci. Letts*. 9:235–236 (1990)

257. Byrappa, K., The Possible Reasons for the Absence of Condensed Phosphates in Nature, *Phys. Chem. Minerals*, 10:94–95 (1983)

258. Gorbunov, Yu. E., Ilyuhin, V. V., Kuznestov, V. G., et al, *Dok. Akad. Nauk USSR*, 222:1329 (1976) (in Russian)

259. Chiganov, A. V., and Belov, N. V., *Geochemistry*, 12:1456 (1968)

260. Palkina, K. K., Crystal Chemistry of Rare Earth Phosphates, *Inorg. Mater*., 18:1199–1221 (1982)

261. Litvin, B. N., Chemical Processes in the Growth of Single Crystals, *Inorg. Mater*., 20:898–904 (1984)

262. Xu, Y., Feng, S., and Pang, W., Hydrothermal Synthesis and Characterization of $Na_3Ce(PO_4)_2$, *Mat. Letts.*, 28:313–315 (1996)

263. Xu, Y., Feng, S., and Pang, W., Hydrothermal Synthesis and Characterization of $K_2Ce(PO_4)_2 \cdot H_2O$., *Mat. Letts*., 28:499–502 (1996)

264. Pang, W., Personal Communication. (1999)

265. Byrappa, K., Gopalakrishna, G. S., Venkatachalapathy, V., and Puttaraju, B., Crystallization and Characterization of Na_2(La, Me) Zr $(PO_4)_3$, *J. Mat. Sci*., 20:1419–1424 (1985)

266. Byrappa, K., Gopalakrishna, G. S., Kulkarni, A. B., and Venkatachalapathy, V., Synthesis and Characterization of Na_2 (R,Co)$Zr(PO_4)_3$ Crystals, *J. Less Common Metals*, 110:441–444 (1985)

267. Byrappa, K., Growth and Characterization of Some New Superionic Phosphates, *Trans. Mat. Res. Soc. Jpn.*, pp. 433–456 (1990)

268. Bykov, A. B., Chirkin, A. P., Demyanets, L. N., Doronin, S. N., Genkina, E. A., Ivanov-Shits, A. K., Kondratyuk, I. P., Maksimov, B. A., Melnikov, O. K., Muradyan, L. N., Simonov, V. I., and Timofeeva, V. A., Superionic Conductors $Li_3M_2(PO_4)_3$ (M = Fe, Sc, Cr): Synthesis, Structure and Electrophysical Properties, *Solid State Ionics*, 38:31–52 (1990)

269. Goodenongh, J. B., Hong, H. Y. P., and Kafalas, J. A., Fast Na^+ Ion Transport in Skeleton Structures, *Mater. Res. Bull*. 11:203–220 (1976)

270. Hong, H. Y.-P., Crystal Structures and Crystal Chemistry in the System $Na_{1+x}Zr_2Si_xP_{3-x}O_{12}$, *Mat. Res. Bull*., 11:173–176 (1976)

271. Efremov, V. A. and Kalinin, V. B., Determination of Crystal Structure of $Na_3Sc_2(PO_4)_3$, *Kristallografia*, 23:703–708 (1978)

272. Vlasse, M., Parent, C., Salmon, R., Flem, Le. G., and Hagenmuller, P., The Structures of the $Na_3Ln(XO_4)_2P$ Phases (Ln = rare earth X = P, V, As), *J. Solid State Chem.*, 35:318–324 (1980)

273. Hagman, L. O. and Kierkegaard, P., The Crystal Structure of $NaMe_2^{IV}(PO_4)_3$, *Acta Chem. Scandinav.*, 22:1822–1832 (1968)

274. Sizova, R. G., Voronkov, A. A., Shumyatskaya, N. V., Illyakhin, V. V, and Belov, N. N., *Dok Akad. USSR Physics Series*, 17:618 (1973)

275. Tranqui, D., Copponi, J. J., Joubert, J. C., and Shannon, R. D., Crystal Stracture and Ionic Conductivity in $Na_4Zr_2Si_3O_{12}$, *J. Solid State Chem.*, 39:219 (1981)

276. Delbecq, C. J., Marschall, S. A., and Susman, S., Evidence of a Structural Phase Change in the Fast Ionic Conductor $Na_3Sc_2P_3O_{12}$, *Solid State Ionics*, 1:145–149 (1980)

277. Susman, S. Delbecq, C. J., and Brun, T. O., Structure and Conductivity of the NASICON Analog $Na_3Sc_2(PO_4)_3$, *Proc. Electro Chemical Soc*. (Spring Meet May 9–14) Mautreal Extd. Abst., pp.1172–1173 (1982)

278. Collin, G., Boilot, J. P., dt la Rochere, M, and Comes, R. *Proc. Cont. on High temperature Solid Oxide Electrolytes*, (F. J. Salzano, ed.) (Broolthaven National Lab., New York) (Aug. 16–18, 1983)

279. Boilot, J. P., Collin G., and Colomban Ph., Nasicon and Related Compounds: A Review, *Progress in Solid Electrolytes* (T. W. Wheat, A. Ahmad., and A. Kauahox, eds) pp. 91–22, Energy, Mines and Resources, Ottawa, Canada (1983)

280. Clearfield, A., Subramanian, M. A., Rudolf, P. R., and Moini, A., Stoichiometry, Structure and Conductivity of NASICON, *Solid State Ionics* 18/19:13–20 (1986)

281. Baur, W. H., Bygar, J. R., Whitemore, D. H., and Faber, *Solid State Ionics*, 18/19:93–99 (1986)

282. Feltz, A. B. and Barth, S., Preparation and Conductivity Behavior of $Na_3M^{II}Zr(PO_4)_3$, (M^{II}: Mn, Mg, Zn) *Solid State Ionics*, 9/10:867 (1983)

283. Y'voire, F. D., Pintard-Screpel, M., and Bretey, E. Les Phasphates $Na_3M_2^{+3}(PO_4)_3$ (Cr, Fe = M) et $Na_3Cr_3(PO_4)_4$: Donnees Cristallographiques et Conductivite Ionique, *CR Acad Sci.*, Pris 290:C185–188 (1980)

284. Rochera, M. de la, Kahu, A., d' Yvoire and Bretey, E., Crystal Structure and Cution Transport Properties of the Orth-Diphosphates $Na_7(MP_2O_7)PO_4$ (M = Al, Cr, Fe) *Mat. Res. Bull.*, 20:27–34 (1985)

285. Gali, S., Byrappa, K., and Gopolakrishna, G. S., Structure of $Na_2MZr(P_2O_7)$, (M = Ni, Co) *Acta Crist.*, C45:1667–1669 (1989)

286. Byrappa, K., Gopalakrishna, G. S., and Gali, S., Synthesis and Characterization of New Superionic Pyrophasphates, *Indian Journal of Physics*, 63A:321–325 (1989)

287. Gali, S. and Byrappa, K., Structure of $(Na_{2/3}Zr_{1/3})_2P_2O_7$. *Acta Crist.*, C46:2011 (1990)

288. John, V. M. and Kordes, S., *Chem. of Earth*, 70:75 (1953)

289. Stanley, J. M., Hydrothermal Synthesis of Large Aluminum Phosphate Crystals, *Ind. and Eng. Chem.*, 468:1684 (1954)

DropBooks

290. Kurbanov, H. M., Kara-ushnov, V. Yu, and Halikov, B. C., *Orthophosphtes of Rare Earth Elements*, Donish Publishers: Dushanbe (in Russian) (1981)

291. Yonghua, L., Ninghai, H., Z-Qinglian, Endong, S., Mingyi, W., Shuzhen, L., and Shixue, W., *Kexue Tongbao* (in Chinese), 27:1126 (1982)

292. Y'voire, F. D., Pintard-Screpel, M., Brety, E., and De La Rochere, M., *Soild State Ionics*, 9 /10:851 (1983)

293. Keller, L. P., Mc Carthy, G. J., and Garvey, R. G., *Mater. Res. Bull*., 20:459 (1985)

294. Genet, F. and Barj, M., *Solid State Ionics*, 9/10:891 (1983)

295. Byrappa, K. and Umesh Dutt, *J. Mater. Sci*., 29:6468–6472 (1994)

296. Byrappa, K. and Nirmala, B., Study of Crystallization Process in Some Rare Earth Vanadate, Tungstate and Phosphate Systems Under Hydrothermal Conditions, *Indian J. of Phys*. 73(A):1–9 (1999)

297. Burger, K., *Solvation, Ionic and Complex Formation Reaction in Non-Aqueous Solvents*., p. 42, Akademiai Kiaddo, Budapest (1983)

298. Belov, N. V., *Miner, Sb*. Vol. 15 (1961)

299. Dirke, T. P., *J. Electrochem. Soc*., 101:328 (1954)

300. Jorgenson, C. K., in: *Werner Centennial Advances in Chemistry Series*, p. 161, American Ceramic Society, New York (1967)

301. Byrappa, K. and Sanjeeva Ravi Raj, B., Crystal Growth, Morphology and Properties of $NaHMP_2O_7$ (M = Ni, Co, Mn, Cd, Zn, Pb), *Ind. J. Phys*., 72(A):1–10 (1998)

302. Byrappa, K., Gopalakrishna, G. S., and Umesh Dutt, B. V., Morphology of New Superionic Pyrophosphates, *J. Mat. Sci*., 27:4439–4446 (1992)

303. Danielmeyer, H. G., Huber, H., Kruhler, W. W., and Jesser, J. F., *Appl. Phys*., 2:335 (1973)

304. Dorokhova, G. I., Ph.D. Thesis, Moscow State Univ., Moscow (1985)

305. Vashishta, J. N., Mundy, J. N., and Shenoy, G. K. (eds.), *Proc. Int. Conf. on Fast Ion Transport in Solids*, Elsevier Science Publishers, Lake Geneva, (May 21–25, 1979)

306. Byrappa, K., Fast Ionic Conductors–New Perspectives, *Indian J. Phys*., 66A:233–61 (1992)

307. Yue, Y. and Pany, W., Hydrothermal Synthesis and Characterization of $NaSn_2(PO_4)_3$, *J. MSL*, 11:148–149 (1992)

308. Xu, Y, Feng, S., and Pany, W., Hydrothermal Synthesis and Characterization of $KSn_2(PO_4)_3$, *J.Chem. Soc. Chem. Commun.*, pp. 1428–1429 (1993)

309. Xu, Y., Feng, S., and Pang, W., Hydrothermal Synthesis Characterization of $NH_4Sn_2(PO_4)_3$, *J. Solid State Chem*. 119:197–198 (1995)

310. Byrappa, K., Gopalakrishna, G. S., Mahadevappa, D. S., and Shashidharaprasad, J., in: *Physics of Materials*, (M. Yussouff, ed.) World Scientific Publishers, Singapore, p. 222 (1987)

311. Sanjeev, B. R., Ph.D. Thesis, University of Mysore, India (1996)

312. Byrappa, K., Umesh Dutt, B. V., Clearfield, A., and Damodara Poojary, M., Crystal Growth, Morphology, Structure and Properties of $HNaMP_2O_7$, Where M = Co, and Ni Ccrystals, *J. Mater. Res.*, 9:1519–1525 (1994)

313. Lii, K. H., Li, C. H., Cheng, C. Y., and Wang, S. L., Hydrothermal Synthesis Structure and Magnetic Properties of a New Polymorph of Lithium Vandyl (iv) Orthophosphate:$LiVOPO_4$, *J. Solid State Chem.*, 95:352–359 (1991)

314. Lii, K. H. and Tsai, H. J., Hydrothermal Synthesis and Characterization of Vandyl (iv) Hydrogenphosphate, $K_2(VO)_3$ (HPO_4), *J. Solid State Chem.*, 91:331–338 (1991)

315. Mar, A., Leroux, F., Guyomard, D., Verbaere, A., and Piffard, Y., Hydrothermal Synthesis and Structure of $Mn_2VO(PO_4)_2 \cdot H_2O$, *J. Solid State Chem.*, 115:76–82 (1995)

316. Amoros, P. and Bail Le, A., Synthesis and Crystal Structure of a - $NH_4(VO_2)(HPO_4)$, *J. Solid State Chem.*, 97:283–291 (1992)

317. Hoareau, T., Leclaire, A., Borel. M. M., Grandin, A., and Raveau, B., A Mixed Valent Molybdenum Monophosphate With a Layer Structure: $CsMO_2O_3(PO_4)_2$, *J. Solid State Chem.*, 116: 87–91 (1995)

318. Srikantaswamy, S., Ph.D. Thesis, University of Mysore, Mysore, India (1989)

319. Oka, Y., Yao, T., Yamamoto, N., Ueda, Y., Kawasaki, S, Azuma, M., and Takano, M., Hydrothermal Synthesis Crystal Structure and Magnetic Properties of $FeVO_4$ -II, *J. Solid State Chem.*, 123:54–59 (1996)

320. Vlasse, M., Parent, C., Salmon, R., and Flem, Le Ge., The Structures of $Na_3Ln(XO_4)_2$ Phases (Ln = rare earth, X = P,V,As), in: *Rare-Earths in Modern Sciences and Technology*, 2:195–201, Plenum Press, New York, (1980)

321. Rubin, J. J. and Utiert, L. G., Growth of Large Yttrium Vanadate Single Crystals for Optical Maser Studies, *J. Appl. Phys.*, 37:2920–2924 (1966)

322. Muto, K. and Awasu, K., Growth of Yttrium Vanadate Crystals by a Modified Floating Zone Technique, *J. Appl. Phys.*, 8:1360–1364, Jpn., (1969)

323. Tanner, B. K. and Smith, S. H., A Study of the Perfection of Flux-Grown Rare Earth Vanadates by X-ray Topography, *J. Crystal Growth*, 28:77–84 (1975)

324. Byrappa, K., Kulkarni, A. B., Desai, N. B., and Jagadeesh, H. P., $NH_4Zr_2V_3O_{12}$ proton conductor, *Bull. Mater. Sci.*, 9:323–330 (1987)

DropBooks

325. Byrappa, K., Nirmala, B., and Yoshimura, M., Crystal Growth of Nd: RVO_4 (Where R = Y,Gd) Under Mild Hydrothermal Conditions, Materials Forum, 315–317:506–513 (1999)

326. Chakoumakos, B. C., Abraham, M. M., and Boatner, L. A., *J. Solid State Chem*., 109:194 (1994)

327. Shimamura, K., Uda, S., Kochauriklin, V. V., Taniuchi, T., and Fukuda, T., *J. Appl. Phys*., 35:320, Jpn. (1996)

328. Prasad, M., Pandit, A. K., Ansari, T. H., Singh, R. A., and Wankkyn, B. M., *Phys. Lett*., A 138:61 (1989)

329. Maunders, E. A. and Deshaser, E. G., *J. Opt. Soc*., 61:68 (1971)

330. Chai, B. G., Loutts, G., Chang, X. X., Hong, P., Bass, M., Sherbakov, I. A., and Zagumenny, A. I., *Advanced Solid-State Lasers*, Technical Digest, p. 230, Optical Society of America, Washington, DC, (1994)

331. Ross, M., *IEEE J. Quantum Electron*, QE-11:938 (1975)

332. Rulin, J. J. and Utert, L. G., Growth of Large Yttrium Vanadate Single Crystals for Optical Maser Studies, *J. Appl. Phys*., 37:2920 (1966)

333. Bagdasarov, Kh. S., Karylor, V. S., and Popov, V. I., New Yttrium and Gadolinium Vanadates, in: *High Temperature Chemistry of Silicates and Oxides*, p. 123, (in Russian), Nauka, Leningrad (1972)

334. Muto, K. and Awasu, K., Growth of Yttrium Vanadate Crystals By a Modified Floating Zone Technique, *J. Appl. Phys*., 8:1360, Jpn. (1969)

335. Udalov, Yu. P. and Appen, Z. S., Izv. Akad. Nauk USSR, Neorganicheskie Materially, 18:1143 (1982)

336. Bagdasarov, Kh. S., Getman, E. I., Mikhailichenko, N. N., Mokhosoeva, I. V., Mokhosoev, M. V., and Popov, V. I., Gadolinium and Yttrium Orthovanadates, *Izv. Akad. Nauk USSR, Inorg. Mater*., 5:1581 (1969)

337. Hintzmann and Müller-Vögt, G., *J. Crystal Growth*, 5:274 (1969)

338. Terado, Y., Shimamura, K., Kochurikhin, V. V., Barashov, L. V., Ivanov, M. A., and Fukuda, T., *J. Crystal Growth*, 167:369 (1996)

339. Erdei, S., Jin, B. M., and Ainger, F. W., *J. Crystal Growth*, 174:328 (1997)

340. Erdei, S., Milmkiewicz, M., Ainger, F. W., Kaszei, B., Vandlik, J., and Surverges, A., *Mater. Letts*., 24:301 (1995)

341. Gibbs, J. W., *Collected Works* Longman, Green, London (1925)

342. Sato, M. and Utsunomiya, T., Crystal Growth of YVO_4 and Distribution of Rare Earth Ions in the Growth Crystals, *Bull. Tokyo Institute of Technology*, 98:15 (1970)

343. Müller, J. and Joubert, J. C., *J. Solid State Chem*., 14:8–13 (1975).

344. Robertson, B. and Kostiner, E., *J. Solid State Chem*., 4:29–35 (1972)

345. Young, A. P. and Schwarz, C. M., *Acta Crist*., 15:1305 (1962)

346. Yao, T., Oka, Y., and Yamamoto, N., Layered Structures of Hydrated Vanadium Oxides, Part-1, Alkali-Metal Intercalates $A_{0.3}V_2O_5 \cdot nH_2O$ (A = Na,K,Rb,Cs and NH_4), *J. Mater. Chem*., 2:331–336 (1992)

347. Yao, T., Oka, Y., and Yamamoto, N., Layered Structures of Hydrated Vanadium Oxides, Part-2, Vanadyl Intercalates $(VO)_xV_2O_5 \cdot nH_2O$, *J. Mater. Chem*., 2:337–340 (1992)

348. Oka, Y., Yao, T., Yamamoto, N., and Tamada, O., Hydrothermal Synthesis of Hydrous Vanadium Oxide Bronzes $M_xV_3O_8(VO)_y \cdot nH_2O$ (M = K,Rb,Ba), *Mater. Res. Bull*., 32:59–66 (1997)

349. Lutz, F. and Leiss, M., Recent Nd-Miniature Lasers, Extended Abstract C57, *ECCG-2*, Lancaster, UK (Sept. 10–15, 1979)

350. Reau, J. M., Levasseur, A., Maniez, G., Cales, B., Fouassier, C., and Hagenmuller, P., *Mater. Res. Bull*., 11:1087 (1976)

351. Chen, C. T., Wu, B. C., Jiang, A. D., and Yov, G. M., *Scientia Sinica*, B28: 238 (1985)

352. Garrett, J. D., Natarajan-Iyer, M., and Greedan, J. E., *J. Cryst. Growth*, 41:225 (1977)

353. Konig, V. H. and Hoppe, R., Anorg, Z., *Allg. Chem*. 439:71 (1978)

354. Sastry, B. S. R. and Hummel, F. A., *J. Am. Ceram. Soc*. 41:7 (1958)

355. Sokolova, E. V., Ph. D. Thesis, Moscow State University, Moscow (in Russian) (1980)

356. Belov, N. V., Ivaschenko, A. I., Bondareva, O. S., Lobachev, A. N., Malinovskii, Yu. A., Melnikov, O. K., and Simonov, M. A., in: *Hydrothermal Synthesis and Growth of Single Crystals*, (A. N. Lobachev, ed.), p. 158, Nauka, Moscow, (1982)

357. Yakubovich, O. V., Ph.D. Thesis, Moscow State University, Moscow (1978)

358. Bonderava, O. S., Egorov-Tismenko, Y. K., Simonov, M. A., and Belov, M. V., *Sov. Phys. Dokl.*, 23:806 (1978)

359. Terol, S., Otero de le Gaudaka, M. J., *Naturforsch, Z.*, 16A:920 (1961)

360. Dewerd, L. A., *Mater. Res. Bull*., 11:1413 (1976)

361. Takanaga, M., *Nucl. Instrum. Methods*, 175:77 (1980)

362. Byrappa, K. and Shekar, K. V. K., Phases and Crystallization in the System Li_2O-B_2O_3-H_2O Under Hydrothermal Conditions, *J. Mat. Res.* U.S.A., 8:864–870 (1993)

363. Byrappa, K. and Srikantaswamy, S., Recent Progress in the Growth of Aluminum Orthophosphate, *Prog. Crystal Growth Charact*., 21:119–254 (1990)

364. Garrett, J. D., Natarajan-Iyer, M., and Greedan, J. E., *J. Cryst. Growth*, 41: 225 (1977)

DropBooks

365. Adachi, M., *Jpn., J. Appl. Phys.* 24:72 (1985)

366. Robertson, D. S. and Young, I. M., *J. Mater. Sci*., 17:1729 (1982)

367. Fan, S., Shen, G. S., Wand, W., Li, J. L., and X. –H.Le, *J. Crystal Growth*, 99: 811–817 (1990)

368. Yamashita, H., Yoko, T., and Sakka, S., *J. Mater. Sci. Lett*., 9:796–798 (1990)

369. Byrappa, K. and Shekar, K. V. K., Hydrothermal Synthesis and Characterization of Piezoelecteric $Li_2B_4O_7$ Crystals, *J. Mat. Chem., Royal Soc. Chem*., 2:13–18 (1992)

370. Byrappa, K., Shekar, K. V. K., and Clemente, R. R., Hydrothermal Synthesis and Morphology of $Li_2B_4O_7$ Crystals, *Mater. Res. Bull*., 7:864–870 (1993)

371. Byrappa, K., Shekar, K.V.K., and Gali, S., Synthesis and Charaterization of $Li_3B_5O_8(OH)_2$ Crystals, *Cryst. Res. Technol*., 27:767–772 (1992)

372. Shekar, K. V. K., Ph.D. Thesis, Univ. of Mysore, India (1993)

373. Reau, J. M., Levasseur, A., Guy Maniez, Bernard Cales, Fouassier, C., and Hagenmuller, P., *Mat. Res. Bull.*, 11:1087 (1976)

374. Jettschko, W. and Bithetr, T.A., *Naturaf, Z*., 27B:1423–1426 (1972)

375. Levassar, M. A., Lloyd, D. J., Fouassier, C., and Hagenuller, P., *J. Solid State Chemistry*, 8:318–323 (1973)

376. Byrappa, K., Skekar, K. V. K., Kulkarni, A. B., and Gali, S., Hydrothermal Synthesis and Characterization of $Li_4Bi_7O_{12}Cl$ Crystals–Fast Ionic Conductors, *Ind. J. Phys.*, 66A:263–271 (1992)

377. Cardenas, A., Solans, J., Byrappa, K., and Shekar, K. V. K., Structure of Lithium Catena-Poly [3,4 – dihydroxopentaborate – 1:5 - m - oxo], *Acta Cryst*., C49:645–647 (1993)

378. Byrappa, K., Rajeev,V., Hanumesh, V. J., Kulkarni, A. R. and Kulkarni, A. B., Crystal Growth and Electrical Properties of $Li_2B_4O_7$, *J. Mater. Res.*, 11:2616–2621 (1996)

379. Byrappa, K., Rajeev, V., Kulkarni, A. R., and Kulkarni, A. B., $Li_3B_5O_8(OH)_2$: Crystal Growth Ionic Conductivity Studies, *J. Mater. Sci*., 32:1599–1602 (1997)

380. Sokolova, E. V., *Hydrothermal Synthesis and Crystal Structures of Cd- and Li-Cd Borates*, Ph.D. Thesis, Moscow State University, Moscow (in Russian) (1980)

381. Bondareva, O. S., *Hydrothermal Synthesis and Crystal Structures of Li, Zn and Li, Zn-Borates.* Ph.D.Thesis, Moscow State University, Moscow (in Russian) (1979)

8

Hydrothermal Synthesis and Crystal Growth of Fluorides, Sulfides, Tungstates, Molybdates, and Related Compounds

(Coordinated Complex Crystals, Part II)

DropBooks

8.1 INTRODUCTION

The hydrothermal synthesis of complex coordinated compounds covers a vast group of compounds. In Ch. 7, which is Part I of these complexes, we cover silicates, germanates, phosphates, vanadates, and borates. Here we deal with fluorides, sulphides, tungstates, titanates, molybdates, tantalates, neobates, selenides, and related compounds.

The synthesis of these compounds did not carry much geological significance in the past, hence, their synthesis began in the middle of the 20^{th} century. However, the interest was purely academic. Today, these compounds have a great technological significance.

8.2 FLUORIDES

Fluorides form a large group of inorganic compounds from the simplest to the most complicated types. In addition, we have

fluorophosphates, fluorocarbonates, fluoroarsenates, oxyfluorides, etc. These compounds contain a great variety of cations of the elements from groups 1, 2, 3, and 4, of the Periodic Table. For simple fluorides like the AF type, the optimum growth method is from flux, or melt, or gas transport, whereas for more complicated fluorine-bearing compounds, hydrothermal synthesis is the most convenient method. The hydrothermal method helps in developing new crystal structures which are difficult to obtain by other conventional methods. Among fluorides, those containing rare earth elements, particularly the active elements like Nd^{3+}, and Eu^{3+} are the most popular because of their excellent luminescent properties. The fluorides bearing Fe, Mn, and other transitional metals show good magnetic properties, however, it is the rare earth elements bearing fluorides that carry greater importance as laser host materials. Kaminskii et al. (1993) have reviewed in detail new CW-laser crystals with semiconductor laser pumping on the anisotropic fluorides with Nd^{3+} ions obtained by the hydrothermal method.[1] Similarly, Deaminates (1990) reviewed the hydrothermal growth of alkali rare earth fluorides and alkali zirconium fluorides and discussed their luminescent and ionic conductivity properties.[2] Bridenbangh et al. (1994) discussed the hydrothermal growth of alkali fluoride crystals and studied the phase equilibria of the KF-GdF_2-H_2O system in detail under hydrothermal conditions.[3]

8.2.1 Hydrothermal Synthesis of Rare Earth Fluorides

Rare earth fluorides have attracted materials scientists for more than 30 years, owing to their unusual crystal structures and physical properties, but even today the problem concerning the polymorphism of double fluorides and the nature of morphotropic transitions in these compounds has not yet been understood. The physical properties of compounds formed in the AF-LnF_3 systems (*A* is the single-charged cation) have not been studied, which may be explained by the absence of sufficiently simple methods of synthesis of double fluorides of alkali and rare earth elements single crystals. The use of hydrothermal solutions provides the study of the behavior of the whole series of rare earth elements in the presence of F-ions under the same conditions. Under hydrothermal conditions, it is easy to synthesize fluorides of compositions $ALnF_4$, A_3LnF_6, A_2LnF_5 (A = Li, Na, K, Rb, Cs), etc. These compounds form morphotropic series (K_2LnF_5) embracing most of the rare earth elements except La, Ce, Pr, and Sc.

The hydrothermal phase equilibria of the Ln_2O_3-KF-H_2O system has been studied in detail.[2][3] The stability fields of several compounds such as $KLnF_4$, K_2LnF_5, K_3LnF_6, K_2LnF_5, and KLn_2F_7, have been fixed. Figure 8.1 shows the composition diagram of the system KF-GdF_3-H_2O at 450°C and 10 kpsi. The region near *A* in Fig. 8.1 is close to the limit of $KGdF_4$ solubility, relative to KF concentration, as estimated from the solubility measurements. The single-phase field for KGd_2F_7 should not be considered to extend to the H_2O-GdF_3 join. The only information on the right side of this field was obtained at very high H_2O contents (98 mol%); this was deemed insufficient to allow projection of a phase boundary, however, the single-phase stability of KGd_2F_7 likely does not persist much farther to the right than the individual single-phase results shown. An additional two-phase field is shown along the left side of the diagram. A general point of particular interest from Fig. 8.1 is that in this hydrothermal system, the phases K_2GdF_5, $KGdF_4$, and KGd_2F_7, are formed and are stable only where KF is in excess in the stoichiometric solid, thus, they are incongruently saturating. KF must be between 17.5 and 27 total mol% for $KGdF_4$ stability where water is at 65 total mol%. A 17.5 total mol% corresponds to the stoichiometry of $KGdF_4$, indicating that the phase is probably marginally congruently soluble. However, the other boundary of the $KGdF_4$ phase field positioned at 27 mol% total KF indicates that 17 mol% KF is required to stabilize 8 mol% $KGdF_4$. Thus, it can be concluded that a large excess of KF is required to stabilize the $KGdF_4$ phase. Analogous reasoning can be applied to choose conditions for the growth of other phases in Fig. 8.1.

PropBooks

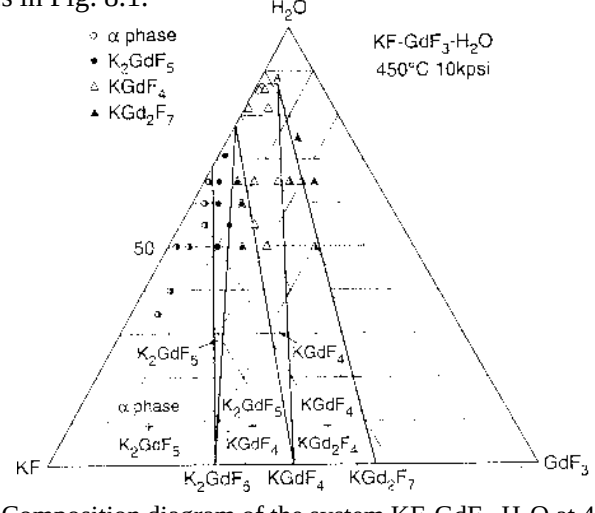

Figure 8.1. Composition diagram of the system KF-GdF_3-H_2O at 450°C and 10 kpsi.[3]

By considering the nature of the rare earth oxides' interaction with KF solutions, one can single out four rare earth subgroups. The first one (La-Pr), which showed no formation of K_2LnF_5, begins at $q = M_{KF}/MH_2O = 0.56$. In the third subgroup (Sm, Gd), the values of the q-ratio necessary for the formation of such compounds were 0.36 and 0.26, respectively; and in the fourth subgroup (Tb-Lu), the crystallization of the K_2LnF_5 phases begins for q values smoothly varying from 0.16 to 0.10. Pentafluorides are crystallized as transparent, faceted, prismatic, crystals up to 15 mm in length, of colors typical for the corresponding rare earth elements.

The conditions for the investigation of the phase relations in the fluoride systems are KF/Ln_2O_3 (molar) ratio up to 100, the $M(H_2O)/M(Ln_2O_3)$ ratio 200, temperature = 450–500°C, and pressure 100–150 MPa. Under these conditions, fluoride crystals were grown for spectroscopic studies. It has been shown that the $K_2GdF_5:Nd^{3+}$ compounds may be considered as potential media for the excitation of a stimulated emission in the range 1.06–1.35 μm, whereas the terbium-activated yttrium and gadolinium compounds may serve as luminophores with saturated green luminescence.

The solubility of $KGdF_4$ is a function of T in 12 mol% KF [defined as moles KF/(moles of KF + H_2O)] at a pressure of 10 kpsi. Figure 8.2 shows the solubility of $KGdF_4$ as a function of temperature and concentration of KF. Assuming a linear relationship between solubility and mol% KF, a slope of 0.02 moles solute dissolved/moles KF suggests the following generalized multi-staged reaction:

Eq. (1) $$KGdF_4 + n\,F^- \rightleftharpoons KGdF_{4+n}^{-n}$$

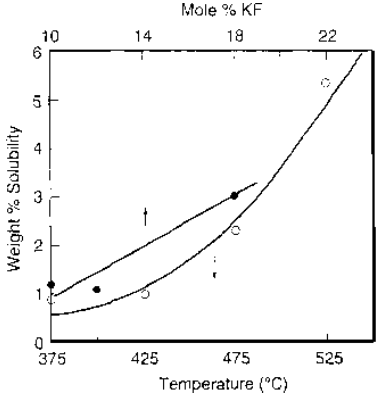

Figure 8.2. Solubility of $KGdF_4$ as a function of temperature and concentration of KF.[3]

Since reaction does not proceed easily to the right, 50 moles of KF are required to dissolve 1 mole of $KGdF_4$.[1] Past experience in growing crystals hydrothermally indicates that the magnitudes of solubility and temperature coefficients of solubility are appropriate for growth with KF mineralizer. The log of solubility versus the reciprocal of absolute temperature is approximately linear. From the slope of a log (s) versus $1/T$ plot, the heat of solution (or the heat of reaction of Eq. 1) is ~12 kcal/mol.[3] In order to obtain reasonably sized crystals, controlled transport in a temperature gradient of nutrient that is thermodynamically stable is essential. Mineralizer concentration is chosen to be within the $KGdF_4$ phase field, high enough to provide reasonable solubility. The optimum conditions are as follows: KF solvent: 16 mol%, 80% initial fill, dissolution temperature: 450°C, growth temperature: 425°C. The previously synthesized seeds of size 4 × 0.5 × 0.5 mm were placed on a point gauze basket mounted at the top of the growth zone.

The other alkali rare earth fluorides of interest are $LiKYF_5$, CsY_2F_7, KYF_4, and K_2YF_5 doped with Nd^{3+} ions up to 10 at %. These crystals were obtained at T = 450–700°C and P = 100–150 MPa, over a period of 15–20 days, and the crystal size was 5 mm.[1] Some of these single-centered laser fluorides such as $LiKYF_5$:Nd^{3+} have better physical characteristics in comparison with oxygen-containing substances. Most of these compounds crystallize in the lower symmetry. Figure 8.3 shows the fragments of the $LiKYF_5$ crystal structure.[4]

DropBooks

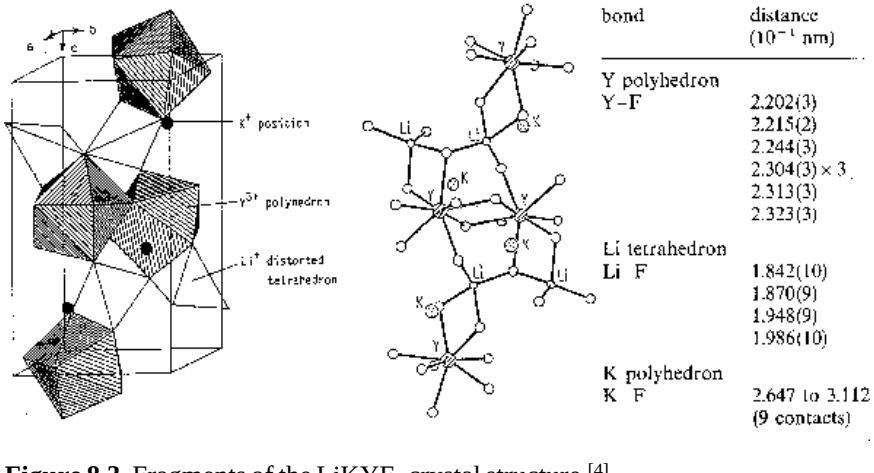

bond	distance (10^{-1} nm)
Y polyhedron	
Y–F	2.202(3)
	2.215(2)
	2.244(3)
	2.304(3) × 3
	2.313(3)
	2.323(3)
Li tetrahedron	
Li F	1.842(10)
	1.870(9)
	1.948(9)
	1.986(10)
K polyhedron	
K F	2.647 to 3.112 (9 contacts)

Figure 8.3. Fragments of the $LiKYF_5$ crystal structure.[4]

8.2.2 Spectroscopic Properties of Rare Earth Fluorides

There are over 250 Nd^{3+} doped insulating laser crystals and anisotropic single-centered fluorides with ordered structures which are unique owing to their excellent spectroscopic properties.[5][6] The most important ones are tetragonal $LiLnF_4$ crystals with a space group $I4_{1/a}$, as well as monoclinic BaY_2F_8 (space group C2/m) crystals. Similarly multi-centered disordered cubic $5NaF{\cdot}9LnF_3{:}Nd^{3+}$ crystals with space group Fm3m, may be considered as potential media for the excitation of a stimulated emission in the range 1.06–1.35 μm.[7] Being transparent in a wide spectral region, these fluorides reveal a negative d*n*/d*T* coefficient, possess a high stability with reference to short wavelength radiation of pumping Xe-flashlamps, and have satisfactory thermo-physical characteristics. This has led to the fact that these materials are rather widely used in quantum electronics. However, low distribution coefficients of Nd^{3+} ions prevent obtaining single crystals of a majority of these compounds with characteristics that are optimal for solid state lasers of the new generation, i.e., lasers using semiconductor laser-diode excitation. That is why the search for new anisotropic single-centered generating fluorides is an extremely urgent problem. These new crystals are able to generate stimulated emission at 300 K in free-running pulse operating mode on inter-stark transitions of two $^4F_{3/2} \rightarrow {}^4I_{11/2}$ and $^4F_{3/2} \rightarrow {}^4I_{13/2}$ laser channels of Nd^{3+} ions with Xe-flashlamp excitation as well as in CW mode ($^4F_{3/2} \rightarrow {}^4I_{11/2}$) under laser-diode pumping.[1][8]–[10] The radiation from these transitions promotes the formation of mainly one line, which in turn, provides the conditions favorable for the excitation of the stimulated emission at frequencies of the main intense lines. The spectroscopic data obtained have been used in the synthesis of these rare earth fluorides by the hydrothermal technique.[4] Figure 8.4 shows the luminescence spectra ($^4F_{3/2} \rightarrow {}^4I_{13/2}$) at 77 K *(a)* and 300 K *(b)* and the scheme of crystal field splitting of $^4F_{3/2}$ and $^4I_{13/2}$ transitions *(c)* of Nd^{3+} ions in K_2GdF_5. These crystals may be a prospective material for solid state lasers in the range of 3–4 μm.[2] Figure 8.5 shows the fluorescent emission spectrum and fluorescent lifetime for the Pr($^1G_4 \rightarrow {}^3H_5$) transition in $KGd_{0.98}Yb_{0.01}Pr_{0.01}F_4$ when the $^1G_4$ level is pumped directly at 1.02 μm. In $KGdF_4$ this transition is centered near 1.3 μm and is broad enough for wavelength multiplexing, the lifetime is 150 μs. Similar measurements have been made on $KGd_{.98}Yb_{.01}Pr_{.01}F_4$ and $KGd_{.94}Yb_{.05}Pr_{.01}F_4$ using three different pumping schemes; *(i)* pump Yb($^2F_{7/2} \rightarrow 2F_{5/2}$) at 0.94 μm and observed fluorescent emission at

0.97 μm from Yb($^2F_{5/2} \rightarrow {}^2F_{7/2}$); *(ii)* pump Yb($^2F_{7/2} \rightarrow {}^2F_{5/2}$) at 0.970 μm and observe emission from Pr($^1G_4 \rightarrow {}^3H_5$) at 1.3 μm; and *(iii)* pump Pr($^3H_4 \rightarrow {}^1G_4$) at 1.02 μm and observed emission from Pr($^1G_4 \rightarrow {}^3H_5$) at 1.3 μm. The results are given in Table 8.1

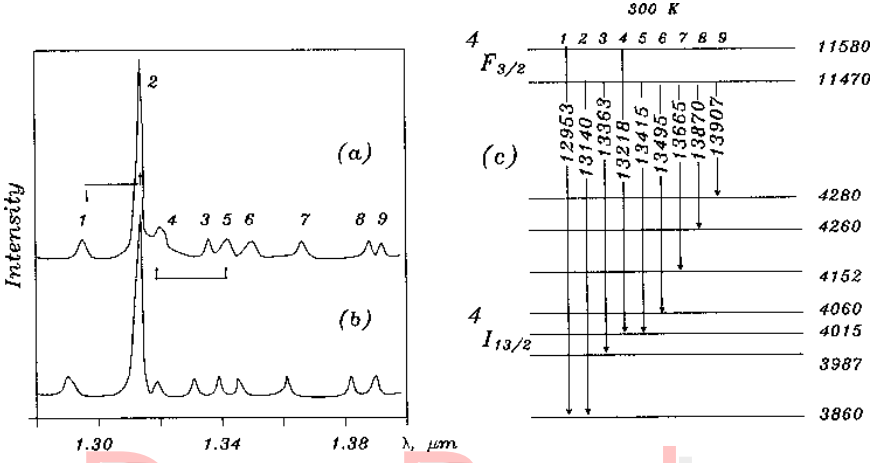

DropBooks

Figure 8.4. Luminescence spectra ($^4F_{3/2} \rightarrow {}^4I_{13/2}$) at *(a)* 77 K and *(b)* 300 K and *(c)* the scheme of crystal field splitting of $^4F_{3/2}$ and $^4I_{13/2}$ transitions of Nd^{3+} ions in K_2GdF_5.[4]

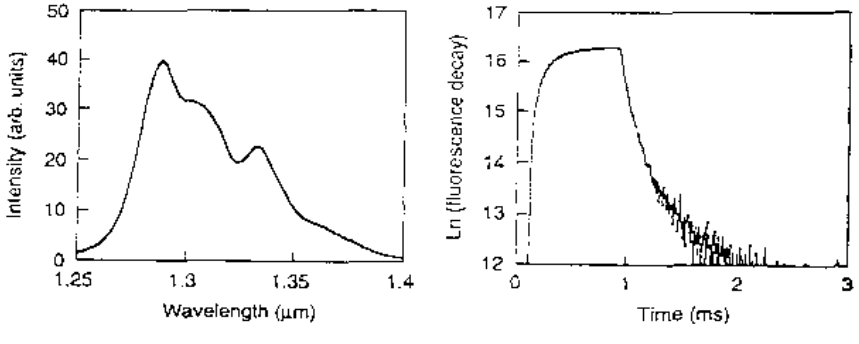

Figure 8.5. Fluorescent emission spectrum and fluorescent lifetime for the Pr($^1G_4 \rightarrow {}^3H_5$) transition in $KGd_{0.98}Yb_{0.01}Pr_{0.01}F_4$.[5]

Table. 8.1. Fluorescent Intensity and Lifetime of $KGdF_4$ Samples[4]

Sample fluorescent rare earth	Yb[a]		Pr[b]		Pr[c]	
	Intensity (a.u.)	Lifetime (μs)	Intensity (a.u.)	Lifetime (μs)	Intensity (a.u.)	Lifetime (μs)
$KGd_{0.98}Yb_{0.01}Pr_{0.01}\ F_4$	240	1120	40	150	90	600
$KGd_{0.94}Yb_{0.05}Pr_{0.01}F_4$	250	400	90	115	280	500

[a]Test conditions: pump Yb ($^2F_{5/2}$) at 0.94 μm; emission from ($^2F_{5/2} \longrightarrow {}^2F_{7/2}$) Yb at 0.97 μm.

[b]Test conditions: pump Pr ($^1G_4$) at 1.02 μm; emission from ($^1G_4 \longrightarrow {}^3H_5$) Pr at 1.3 μm.

[c]Test conditions: pump Yb ($^2F_{5/2}$) at 0.97 μm; emission from ($^1G_4 \longrightarrow {}^3H_5$) Pr at 1.3 μm.

From the data in Table 8.1, the following observations can be made. First, the lifetime of the Yb fluorescence is sufficiently long to permit energy transfer from the Yb $^2F_{5/2}$ to the Pr $^1G_4$ levels. At both doping levels, the lifetime of the Yb $^2F_{5/2}$ state is longer than the lifetime of the Pr $^1G_4$ level. Second, both the intensity and the lifetime of the Pr($^1G_4 \rightarrow {}^3H_5$) transition increase when Yb is pumped and compared to the Pr pumped.

Thus, the rare earth fluorides have found unique technological applications. Their synthesis is highly challenging.

8.3 HYDROTHERMAL SYNTHESIS OF TRANSITION METAL FLUORIDES

The hydrothermal method permits us to synthesize single crystals of some transitional metals and other ternary fluorides. The majority of these compounds show superionic, magnetic, and other important physical properties.

Among alkali-zirconium fluorides, compounds of special interest are those belonging to the A_3ZrF_7 family (A = Na, R, Rb, Cs, NH^+_4) with the characteristic OD structures. Except for Na_3ZrF_7 (its structure is a derivative of a fluorite-type structure), the above fluorides are related to the K_3UF_7 type (usually characteristic of heavy metals). Heptafluorides are usually obtained using the methods of chemical interaction at room temperature by sintering in inert fluorinating atmosphere and crystallization from KF flux.

PropBooks

Illyushin et al. (1970) have obtained several millimeters large K_3ZrF_7 single crystals under hydrothermal conditions at temperatures of 450–500°C and pressures of 100–150 MPa. The initial materials were aqueous zirconium dioxide and potassium fluoride solutions with the concentration 10–60 wt%.[11] Potassium-zirconium heptafluoride is a stable fluorine-containing crystalline phase within the range of temperatures and pressures used in hydrothermal experiments.

Conductivity (σ) of K_3ZrF_7 single and polycrystals was measured in the temperature range 300–700 K. The values of σ were calculated from the impedance (admittance) frequency plots of an electrochemical $Ag/K_3ZrF_7/Ag$ cell.The conductivity of single crystals is somewhat higher than that of polycrystals, yet no noticeable anisotropy in conductivity was observed.[11] At 300°C, conductivity is 3.9×10^{-2} and $1.17 \times$ 1–2 ohm^{-1} cm^{-1} for single and polycrystals respectively (Fig. 8.6).

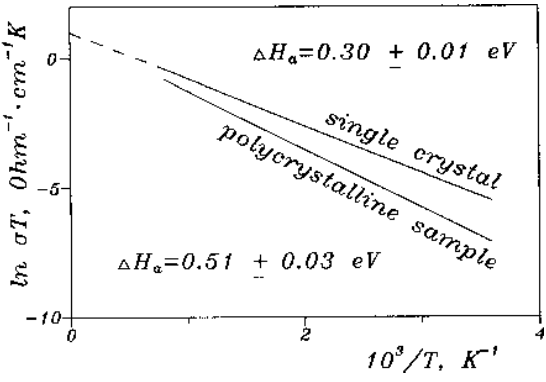

Figure 8.6. Conductivity (σ) for single and polycrystals.[11]

A synthetic Fe^{3+} variety of elpasoite, a rare natural mineral (K_2NaAlF_6), was synthesized in the course of the investigation of the phase formation in the AF-Fe_2O_3-$(NH_4)_2$ HPO_4-H_2O system with A = Na, K, Cs (T = 400°C, fill = 0.7, C_{KF} = 30–50 wt%).[12] The structural analysis yielded the composition $K_2NaH_{1.5}Fe_{0.6}F_6$ for the cubic crystals of this system (space group Fm3m). Under hydrothermal conditions, complex fluorides of the system $A^{1+}F$ - $A^{2+}F_2$ - $A^{3+}F_3$ (A^{1+} = Li, Na, K; A^{2+} = Ca, Sr, Ba, Mg, Zn; A^{3+} = B, Al, Ga) were also obtained.[13]

According to their structures, these compounds are close to well-known minerals elpasoite, K_2NaAlF_6, cryolite, Na_3AlF_6, and veberite, Na_2MgAlF_7. In these compounds, A^{2+} and A^{3+} ions are displaced by cations of iron and rare earth subgroups, respectively. Such compounds were synthesized from aqueous solutions with high HF-concentration; the stoichiometric mixtures of oxides and hydroxides served as starting materials. Such crystalline products were used as nutrients for single crystal growth though the temperature gradient technique at T = 120–280°C, (ΔT = 20–40°C).[13] Other fluorides, like $Cs_2FeF_5H_2O$, Na_3FeF_6, $Ba_3Ta_2O_2F_{12}$, were also synthesized under hydrothermal conditions.[14]–[16] The hydrothermal technique provides the possibility of growing hydrous transition metal fluorides in HF solutions under *PT* conditons.[17] This includes several fluoride systems like AF-AlF_3, AF-FeF_3, AF-$M^{2+}F_2$, AF_2-FeF_3, where A is an alkaline, ammonium or Hg_2^{2+} ion, M^{2+}, a divalent transition metal, (Mn, Fe, Co, Zn, Ni, Cu).[18][19] Some of the ternary and quaternary systems like H_2O-AF-MF_2 or MF_3 (A = Li, Na, Cs, NH_4, M = Mn, Cu, V, Cr, Fe), H_2O-BaF_2 - (ZnF_2 or VF_3), H_2O - AF- MF_2 - MF_3 (A = Li, Na, K, Rb, Cs, NH_4; M = Mn, Fe, Ni, Al, V, Cr, Fe), and H_2O-BaF_2-(MnF_2 or

NiF_2) (CrF_3 or FeF_3) have been studied.[20] The major advantages of the hydrothermal technique for fluorides are the ability to obtain low temperature varieties, rhombohedral α-FeF_3, phases with slow kinetics of formation, hexagonal $CaAlF_4$, and compounds with incongruent melting, like NH_4AlF_4.

The phases which appear in the system H_2O-FeF_3 are classified according to the growing temperature and the hydrothermal medium, H_2O or 49% HF. The iron coordination polyhedra are indicated. It is clear that high temperature and higher concentration of hydrofluoric acid favor the dehydration of the fluorides in the order Fe^{III}, Fe^{II}. The FeF_2 is grown only at extreme conditions (450°C, 49% HF).

The Mn^{II} compounds, $MnFeF_5(H_2O)_2$ and $MnFe_2F_8(H_2O)_2$, analogous to $Fe^{II}Fe^{III}F_5(H_2O)_2$ and $Fe^{II}Fe_2{}^{III}F_8(H2O)_2$, are synthesized as by-products in the presence of sodium fluoride.[21]

$NaMnFeF_6$, synthesized under hydrothermal conditions, cannot be obtained by solid state reaction at any temperature: Weberite, Na_2MnFeF_7, always forms.[22] $NaMnFeF_6$, trigonal (a = 9.042 Å, c = 4.995[5] Å) is isotopic of $NaMnCrF_6$[3][23] and undergoes endothermic decomposition at T = 546°C:[5]

DropBooks

Eq. (2) $$2\ NaMnFeF_6 \rightarrow Na_2MnFeF_7 + MnF_2 + FeF_3$$

N-$RbMnFeF_6$ crystallizes with the new structural form of NH_4MnFeF_6 described below. Above 608°C, N-$RbMnFeF_6$ adopts the modified pyrochlore structure; the irreversible phase transition N-$RbMnFeF_6$ $\rightarrow$ P-$RbMnFeF_6$ is endothermic (N and P are the two structure forms in $RbMnFeF_6$).[5][24]

The growth of ammonium phases becomes particularly accessible by the hydrothermal method. Crystals of $NH_4M^{III}F_4$ (M = Fe, V, Cr) compounds easily grow. In spite of frequent twinning, their parameters and space groups are derived. For NH_4FeF_4 (a = 7.559 Å, C = 12,754 Å), the space group is Pnma.[4][8][24]

Single crystals of $NH_4Fe^{II}Fe^{III}F_6$ are produced when the reduction of Fe^{3+} to Fe^{2+} occurs. Thus, the hydrothermal synthesis helps in a large variety of growth solutions, and the variation of the temperature leads to numerous new fluorinated phases of structural and magnetic interest. For stable compounds, the hydrothermal method represents an alternative way of crystal growth; its specificity is enhanced when low temperature (HTB-FeF_3, N-$RbMnFeF_6$) or thermally unstable phases (hydrates, ammonium compounds) are desired as single crystals.

8.4 HYDROTHERMAL SYNTHESIS OF FLUOROCARBONATES AND FLUOROPHOSPHATES

A new class of fluorides is being studied extensively in recent years, owing to their potential physical properties like nonlinear, magnetic, and electrical conductivity.[25]–[27] These materials have a high thermal and chemical stability. The hydrothermal synthesis at high temperature and pressure conditions yields these compounds. Among these, fluorides and fluorocarbonates are the most popular. These compounds contain rare earth 3*d* transition and alkaline-earth metals in their composition. The following are the most popular compounds:

Eq. (3) $M_3Ln_2(CO_3)_4F$ (M = Na, K; Ln = rare earth elements)

Eq. (4) $M^{1+}M^{2+}(CO_3)_4F$ (M^{2+} = Na,K; M^{2+} = Cu, Fe, Zn)

Eq. (5) $M^{2+}Ln(CO_3)_2F$ (M^{2+} = Ba, Mg; Ln = rare earth)

Eq. (6) $M^{2+}{}_3Ln_2(CO_3)_5F_5$ (M = Ba, Mg; Ln = rare earth)

Eq. (7) $M^{2+}M^{2+}(CO_3)F_2$ (M^{2+} = Ba, Mg; M^{3+} = Mn, Cu)

Eq. (8) $M^{2+}{}_2PO_4F$ (M^{2+} = Mn, Co)

Eq. (9) $M^{+}MPO_4F$ (M^{+} = Na, K, Cs, NH_4, M = Fe)

The crystal growth of rare earth, alkaline earth, and 3*d* transition metal fluorocarbonates is difficult, and numerous earlier attempts involving alkaline fluorides or carbonates with cobalt, iron or zinc, rare earth carbonates or fluorides failed. However, the association of alkali/alkaline earth carbonate with rare earth or 3*d* transition metal fluoride was successful.[28]–[31] Hydrothermal synthesis at high temperature and high pressure is well suited for the crystal growth of rare earth or yttrium fluorocarbonates. Several interesting compounds with unique structures have been obtained by the hydrothermal method.[30][31][34] These compounds have been synthesized by hydrothermal growth at T = 740°C and P = 200 MPa in 20 hours.

The starting materials are usually the carbonates of alkali or alkaline earth, rare earth, or 3*d* transition metal fluorides, and alkali-fluoride. Figure 8.7 shows the structural projection of $Na_3La_2(CO_3)_4F$, along Ref. 21. The

structure shows double layers along *"c"* of the lanthanum coordination polyhedra, which adopts the ten-fold (30 + 60 + 1F) coordination, similar to that of $Ba_3La_2(CO_3)_5F_2$, $BaSm(CO_3)_2F$, and $Ba_2Ce(CO_3)_2F$, for La or rare earth ions. The structure exhibits a 2*d* character with infinite $(LaO_6)_2F$; double layers parallel to the *(a, b)* plane are separated by Na^+ ions.

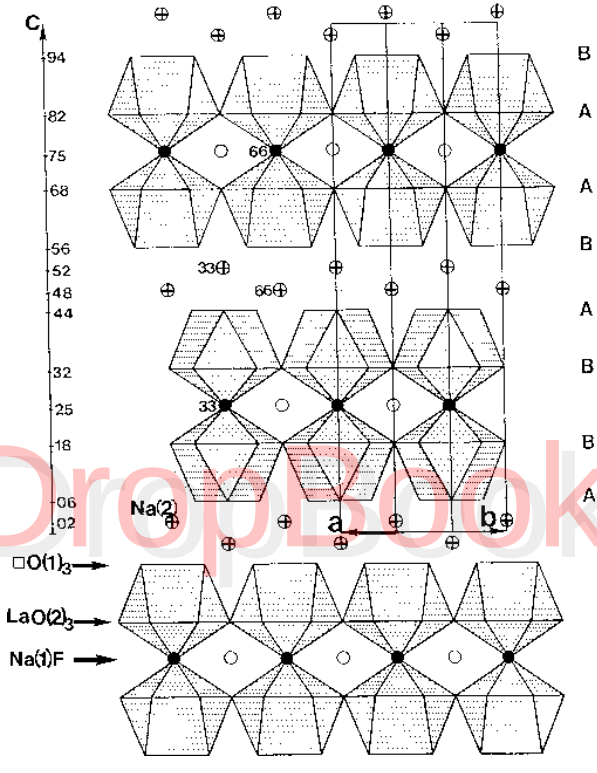

Figure 8.7. Structural projection of $Na_3La_2(CO_3)_4F$.[21] *(Courtesy of the Academic Press, Orlando, Florida.)*

The mineral type structures obtained are $PrCO_3F$ (bastnaesite type), $Ba_2Ce(CO_3)_3F$ (zhonghuacerite), $BaSm(CO_3)_2F$ (huanghoite type), $Ba_2La_2(CO_3)_5F_2$ (cebaite type), and several new structures like $Na_3La_2(CO_3)_4F$, exhibiting interesting physical properties.

The 3*d* transitional metal fluorocarbonates could be synthesized at slightly lower temperature than the rare earth fluorocarbonates. The typical experimental conditions are $T = 700°C$ and $P = 200$ MPa. Several new compounds like $BaMn(CO_3)F_2$, $BaCu(CO_3)F_2$, and $KCu(CO_3)F$, have been obtained. Under hydrothermal conditions, the association of alkaline

carbonates with 3*d* transition metal fluorides leads, in most cases, to anionic exchange and to the formation of 3*d* transition metal carbonates and alkaline fluorides. However, when the starting materials are K_2CO_3 and CuF_2 in 1:1 ratio, green crystals of $KCu(CO_3)F$ which can reach 4 mm^3 are obtained. Thus, the fluorocarbonates are being studied extensively, especially by the French group (Leblanc and coworkers).

The hydrothermal synthesis of fluorophosphates is slowly attracting the attention of materials scientists because the magnetic effects have been investigated in fluorides which present triangular cationic planes or K atom, lattices and where the coordination MF6 polyhedra are mainly connected by vertices, and super exchange interactions occur through 180° type M-F-M bridges, which frequently lead to antiferromagnetism. Several phosphate minerals adopt the general formula M_2PO_4X, where M^{2+} = 3*d* cation, Mg^{2+}, Ca^{2+} and X^- = F^-, OH^-; arsenate or vanadate series also exist. The occurrence of the triploidite substructure is said to be related to the ordered F-OH substitution on the anionic sublattice. The coordination of the M^{2+} cations is octahedral; in triploidite, the evolution of the M-F distances implies that half of the cations M^{2+} adopt a five-fold coordination, consequently, the magnetic super exchange pathway in triploidite results from that of triplite by breaking one of the three M^{2+}-F^--M^{2+} magnetic bridges and strengthening the others.[32]

The majority of these fluorophosphates, particularly the oxyfluorinated prepared under hydrothermal conditions, have been quite popular in recent years as microporous compounds belonging to the systems AF-M_2O_3-P_2O_5-amine (A = H^+, M = Al, Ga, 3*d* transition metal). The experiments are usually carried out at 217°C under autogenous pressure, for 36 to 40 hours. These compounds obtained under hydrothermal conditions show interesting crystal structures which are again difficult to obtain by other conventional methods.

8.5 OXYFLUORINATED COMPOUNDS

Oxyfluorinated compounds are being studied extensively in recent years owing to their interesting physical properties. Several phases in the systems BaF_2-TiO_2-FH_{aq} and BaF_2-M_2O_5-HF_{aq} (M = Ta or Nb) under hydrothermal conditions have been identified.[35][38] Among them, $Ba_3Nb_2O_2F_{12}.2H_2O$, $Ba_4Nb_2O_3F_{12}$, and $Ba_3Ta_2O_2F_{12}$ have interesting structures. $Ba_3Ta_2O_2F_{12}$ is a new oxyfluoride with seven-fold coordinated

Ta^{5+}. In the monocapped trigonal prism $TaOF_6$, the distances Ta-X (X = O_2 or F^-) are close to those found in an octahedral environment, which led to X-X distances smaller than the calculated values. The isolated $TaOF_6$ groups are connected together by two types of Ba^{2+} polyhedra. The $Ba_3Nb_2O_2F_{12}.2H_2O$ is a new acentric hydrated niobium oxyfluoride. Its structure is built from isolated $NbOF_6$ pentagonal bipyramids. The $Ba_4Nb_2O_3F_{12}$ is a *3d* oxyfluoride, which exhibits two kinds of coordination polyhedra for Nb atoms: the octahedral form with (NbO_2F_4), (NbO_3F_3) formulations, and the pentagonal bipyramid ($NbOF_6$). Four (NbX_6) octahedra are cris-oxygen connected to form separated $[Nb_4O_7F_{14}]^{8-}$ condensed blocks while ($NbOF_6$) pentagonal bipyramids are isolated, but linked together by Ba^{2+} cations.

In all these cases, single crystals have been prepared by the hydrothermal technique and not by other conventional methods.

The other material of technological importance among fluorides is α-PbF_2 single crystals. Lead fluoride stands out as an important optical material because of its chemical and mechanical stability, wide transparency range (from UV to medium IR), and rich substitutional chemistry (permitting the variation of its composition and, consequently, its main operational parameters), and also because its single crystals can be readily obtained from both melt and solution. Lead fluoride is poorly soluble and can be easily prepared by the reaction of HF acid with lead hydroxide or carbonate or by precipitation from aqueous solutions of these reagents with NH_4F. The α-β transformation, orthorhombic-to-cubic in PbF_2, takes place at 460°C. Beta-PbF_2 is chemically more stable, and can be readily obtained as large single crystals from the melt.[39] However, the α-PbF_2 cannot be prepared by melt or solid state reacts or flux methods. Nikolskaya and Demianets (1994) have carried out the growth of α-PbF_2 at T = 280°C using teflon liners and at T = 450°C using copper ampoules.[40] Extra-pure-grade PbF_2, 6–10% NH_4F and 10–20% KF solutions have been used as the starting materials. The temperature gradient has been maintained at 35–42°C. At a lower growth temperature of 280°C, the quantity of α-PbF_2 is higher than the crystals obtained at 450°C. The crystals are highly transparent, well faceted, elongated, and up to 8 mm in length. In some cases, the crystal length was up to 10 mm, but in this case the crystals were fragile. Figure 8.8 shows the micrographs of α-PbF_2 crystals obtained under hydrothermal conditions by Nikolskaya and Demianets (1994).[40]

ProfBooks

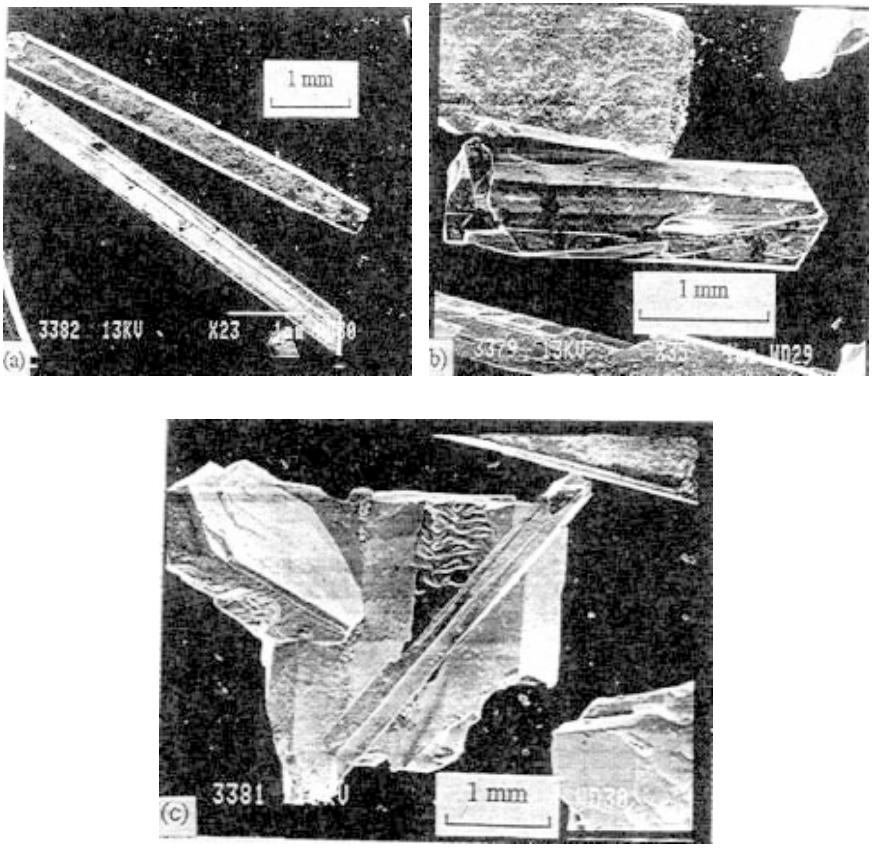

Figure 8.8. Micrographs of α-PbF_2 crystals obtained under hydrothermal conditions.[40]

8.6 PHYSICAL PROPERTIES OF TRANSITION METAL FLUORIDES AND FLUOROCARBONATES/ FLUOROPHOSPHATES/OXYFLUORIDES

These compounds exhibit essentially magnetic properties, ionic conducting, and nonlinear optical properties. The oxyfluorides exhibit microporous structures, which are highly useful as selective gas absorbers, catalysts, and so on. Here we discuss only a few representative compounds and their physical properties.

Among the fluorocarbonates, $KCu(CO_3)F$ and $BaCu(CO_3)F_2$ exhibit excellent magnetic properties.

The variation of the reciprocal susceptibility of $KCu(CO_3)F$, in the temperature range 4.2–300 K, is given in Fig. 8.9. The magnetic susceptibility is weak and nearly independent of the temperature between 300 K and 100 K, it then increases continuously from 100 K to 4.2 K.

Strong antiferromagnetic interactions must be present between nearest Cu^{2+} neighbors in order to explain the magnetic behavior at high temperature; however, this hypothesis does not appear really acceptable for two reasons:

- Super exchange interactions Cu-F-Cu possible in the infinite files along *a* are not generally very strong ($J/k \approx 100$ K)
- Super-super exchange interactions Cu-O-O-Cu (through the carbonate ions) are probably even weaker.

DropBooks

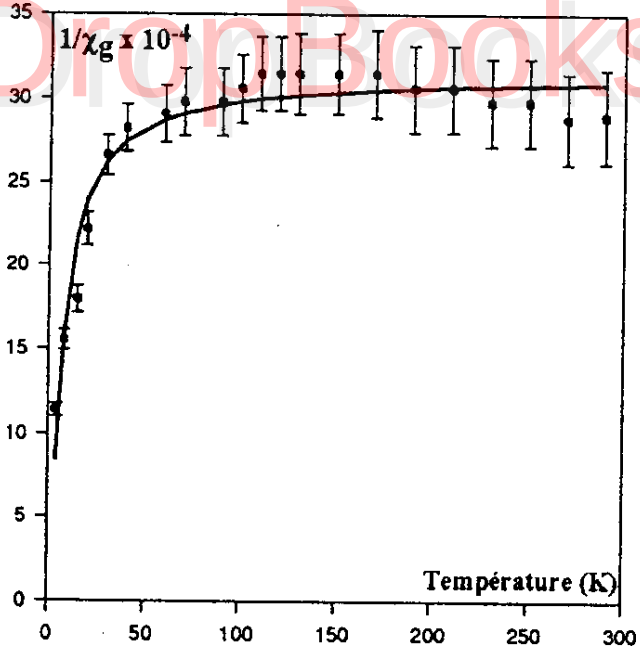

Figure 8.9. Reciprocal susceptibility of $KCu(CO_3)F$.[31] *(Courtesy of the Gauthier-Villars/ESME, Paris.)*

Ferromagnetic interactions must also take place at low temperature (T < 60 K). The variation of the inverse magnetic susceptibility with the temperature is given in Fig. 8.10 for $BaMn(CO_3)F_2$. Above $T \approx 90$ K, the linear Curie-Weiss law is well obeyed, leading to a molar Curie constant C_M = 4.39 (as compared to the theoretical value C_M = 4.375 for Mn^{2+}) and a Curie paramagnetic temperature θp = -52K. This value of θp, together with the deviation of $1/x$ from the Curie-Weiss law at T < 90 K indicates that antiferromagnetic interactions dominate, however, no clear evidence of magnetic order can be found at low temperature.[31]

Magnetic susceptibility of Mn_2PO_4F and CO_2PO_4F has been studied by Leblanc et al. (1997).[32] The variation of the inverse magnetic susceptibility Xg^{-1} with temperature (Fig. 8.11) and the absence of field dependence of the susceptibility are indicative of antiferromagnetic behavior with T_N = 15 and T_N = 14 K for Mn_2PO_4F and CO_2PO_4F, respectively. Above ~100 K, the Curie-Weiss law is well obeyed and yields θp = -50 K, C_M = 8.2 and θp = -53K, C_M = 6.4. These molar Curie constants, which give μ_{eff} = 5.70 and 5.1 μ_B, are in good agreement with the calculated value $C_M(th)$ = 8.75 (spin only value) for Mn^{2+} and with the value usually found for Co^{2+}.

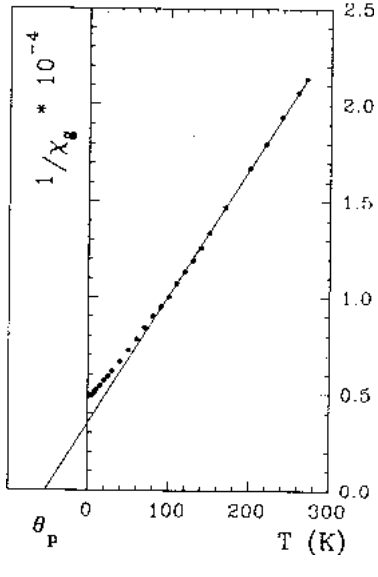

Figure 8.10. Variation of the inverse magnetic susceptibility with temperature.[31] *(Courtesy of the Gauthier-Villars/ESME, Paris.)*

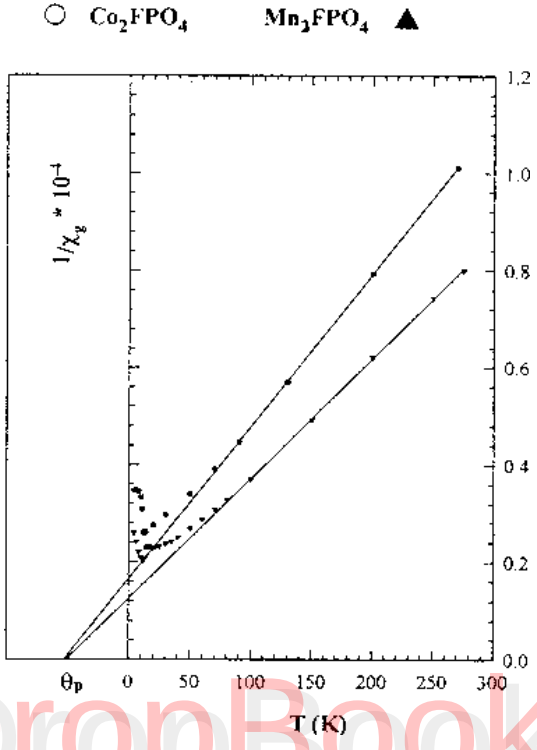

DropBooks

Figure 8.11. Variation of the inverse magnetic susceptibility Xg^{-1} with temperature.[32]

8.7 HYDROTHERMAL SYNTHESIS OF TUNGSTATES

Tungstates form an important class of materials with a wide range of divalent and trivalent metals in their composition. Among the trivalent metals, the rare earth and transitional metals are the common ones. Tungstates are either simple or mixed types, but exhibit high thermal and chemical stability in general. The important physical properties are excellent luminescent and electrical conductivity.

Tungstates can be obtained by different methods, like solid-state reactions, flux, and hydrothermal, however, it is the flux method that is very popular in the growth of a large variety of tungstates. With the recent advances in the hydrothermal chemistry of various inorganic systems and the influence of organic precursors or solvents in the growth of various inorganic compounds, the hydrothermal synthesis of tungstates is becoming popular. Several simple and complex tungstates, like

$Me^{2+}WO_4$ (Me = Ca, Cd, Mn, Fe, Ca, Sr, Ba, Cd, Mn, Zn), $M_2{}^{2+}M(WO_4)_2$, $MLn(WO_4)_2$, (M = Li, Na, K, Rb; Ln = rare earths), have been reported. In general, the synthesis of Sr and Ba tungstates are carried out using either (NaOH) solution or chloride solution, whereas for the growth of Ca, Cd, Mn, Fe, it is possible to obtain only in the chloride solutions with 100% output.[41]–[43] Wolframites of divalent metals belong to two structural groups, one crystallizing in the scheelite type covering $CaWO_4$, $SrWO_4$, and $BaWO_4$; the second one crystallizing in the wolframite structure type covering $CdWO_4$, $MnWO_4$ and $FeWO_4$. The first group usually forms bipyramidal crystals of 3–5 mm size. The second group of crystals are usually prismatic in form and their synthesis is carried out from a mixture of $M^{2+}O$ and WO_3 (M^{2+} = Cd, Mn, Fe) in 1:1 ratio at temperature 375–550°C and pressure up to 2000 atm. As mineralizers, aqueous solutions of chlorides and more complex solutions like the mixture of chlorides and fluorides, sodium wolframite and sodium chloride and sodium nitrate are used.[42][43] Among the mixed wolframites $MM^{2+}(WO_4)_2$ (M = Li, Na, K; M^{2+} = Cd, Mn, Fe) are the common ones prepared by the hydrothermal method. The wolframites of trivalent metals form two large groups, *(i)* simple trivalent metal wolframites and *(ii)* mixed trivalent metal wolframites. Besides, there are several hydrous wolframites, $Me^{3+}WO_4(OH)$,[44] oxychloride wolframite $Me^{3+}WO_4Cl$ and oxywolframites nMe_2O_3-mWO_3. The ratio of *n:m* varies in this case between 1:1 and 1:3.[45]

Most of these simple or mixed tungstates containing divalent and trivalent metals exhibit magnetic properties. However, it is the mixed rare earth tungstates which occupy a unique place in the tungstate family owing to their excellent optical, electrical, and magnetic properties. Among these high temperature polymorphs of mixed rare earth tungstates, $MR(WO_4)_2$ (M = Li, Na, K, Rb, Cs; R = rare earth elements) crystals have a common crystal structure which is similar to that of tetragonal scheelite, ($CaWO_4$) under atmospheric pressure; however, the low temperature polymorphs of these mixed rare earth tungstates belong to the monoclinic system.[46] Klevstov and his group have worked out in detail the synthesis of simple and mixed rare earth tungstates and one of the important systems is Pr_2O_3-WO_3-LiCl-H_2O, with a concentration of LiCl-20 wt%.[47]–[51] Figure 8.12 shows the TN-diagram of crystallization (N = Pr_2O_3/WO_3). With a decrease in $T < 450$°C and increase > 550°C, the field of crystallization of monocationic tungstates, $PrWO_4 \cdot OH$ and $Pr_2W_2O_9$ occupy relatively lower values of $N \cdot RWO_4(OH)$: hydroxyl wolframates containing almost the entire series of rare earth elements (Pr-Lu) have been obtained by Klevstov and coworkers.[47] The lighter lanthanides crystallize in the aqueous

solutions LiCl, as $LiR(WO_4)_2$, and a similar picture is obtained for KCl, RbCl giving rise to $KR(WO_4)_2$ or $RbR(WO_4)_2$.

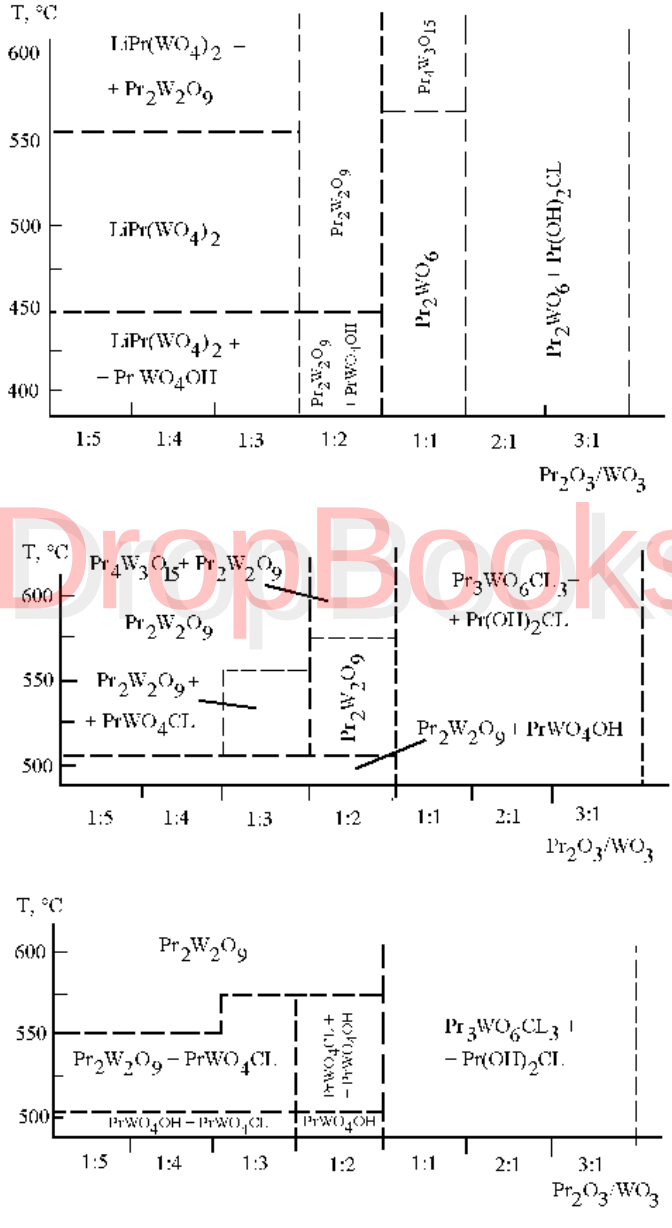

Figure 8.12. TN-diagram of crystallization ($N=Pr_2O_3/WO_3$).[69]

These mixed alkali rare earth tungstates are most important among tungstates in general. Although these tungstates were reported during the late 1950s and 1960s, not much has been studied with reference to their crystal growth and phase relations in the respective systems, and there exists some lacunae in the characterization of alkali rare earth tungstates. The probable reason for this may be the nonavailability of good quality single crystals due to the high temperature of synthesis involved. There are several reports on the synthesis and characterization of alkali rare earth tungstates, but most of them deal with the flux growth and solid state reactions.[46][51]–[53] The crystals are fine grained and poor in quality without a proper morphological development. Similarly, there are quite a few reports on the hydrothermal growth of alkali rare earth tungstates, but the *PT* conditions of synthesis were quite high (T = 700–900°C; P = 2–3 kbar).[41][42] Byrappa and Jain (1996) have reported the hydrothermal growth of $NaLa(WO_4)_2$ crystals under fairly lower *PT* conditions (T = 240°C; P = 80–100 bar), using a suitable mineralizer solution.[54] Carobbi and Tancredi (1928) have studied the system $Ce_2(WO_4)_3$-Na_2WO_4-H_2O at 25°C and this work has formed some basis for the work of Byrappa and Jain (1996) to grow $NaLn(WO4)_2$ (where Ln = La, Ca, Nd) crystals at moderately lower *PT* conditions.[54][55]

On the whole, the growth of alkali rare earth tungstates by the hydrothermal method is quite complicated due to the high temperature of synthesis involved and the lack of solubility data. Moreover, the crystals obtainedby earlier workers were fine-grained or small rounded or subrounded.

A systematic study on the search of a suitable mineralizer has been carried out on the empirical basis. Further, some selected crystal growth experiments have been carried out at lower *PT* conditions using suitable mineralizers. The experiments were carried out using Morey-type autoclaves and teflon liners of 20, 30, 40, and 50 ml capacity. The starting materials such as WO_3 and $La(NO_3)_3$ were taken in desired molar proportions: Na_2O:La_2O_3:WO_3 = 12–18:1:18–23 and placed inside the teflon liner. The alkaline component of the starting materials was taken in the form of a NaOH solution with a definite molarity and this solution acts as a mineralizer. The entire mixture was stirred well until a homogeneous solution was obtained. In addition, several other mineralizers, such as HCl, HCOOH, H_2SO_4, HNO_3, and mixed mineralizers like HCl + HCOOH, HCl + H_2SO_4, and HCOOH + HNO_3, with varying concentrations have been tried. However, the majority of these experiments yielded mainly the crystalline powders and also mixed phases. Therefore, NaOH has been proven to be the most suitable mineralizer for the growth of alkali rare earth tungstates,

whereas the earlier workers had concluded that the chloride solutions were the best for the growth of these tungstates.

The crystallization was carried out in all experiments through spontaneous nucleation by Byrappa and Jain (1996).[54] In order to control the nucleation centers, the temperature of the crystallization reactor was increased very slowly at a rate of 10°C/hr up to 100°C and beyond this at 5°C/hr. The nutrient materials were held at 240°C for a period of three days without any fluctuations in the temperature. From the fourth day onward, temperature fluctuations of ±10°C were introduced periodically in order to reduce the nucleation centers. By this means, the small crystallites that had developed previously dissolved and only the larger crystallites remained. This resulted in the growth of larger crystals (7 mm × 5 mm × 5 mm). The pH of the medium was varied from 7–11, and good quality single crystals were obtained in the pH range 8.4–8.8. The crystals obtained by this method were of good quality, showing high transparency, vitreous luster, and well-developed crystal morphology, with the size varying from 1.0 to 7.0 mm. Table 8.2 gives the experimental conditions of the growth of $NaLa(WO_4)_2$ crystals. The crystals obtained by the earlier workers at higher *PT* conditions were smaller and more equi-dimensional, experimental temperature, T = 240°C; duration = 10 days; pH of the nutrient measured before the experimental run.

DropBooks

Table 8.2. Experimental Conditions For the Growth of $NaLa(WO_4)_2$ Crystals[54]

Sl. No	Nutrient	pH	P	Size (bar)	Remarks (mm)
1.	WO_3:6.0 g $La(NO_3)_3$:0.75 g 4.5 M NaO^{II}:7 ml	7.0	120		White crystalline powder
2.	WO_3:6.0 g $La(NO_3)_3$:0.75 g 4.7 M NaOH:7 ml	7.5	120	2–3	Small, broad, tabular, transparent, rhombohedral, colorless crystals
3.	WO_3:6.0 g $La(NO_3)_3$:0.75 g 5.0 M NaOH:7 ml	8.0	120	3–4	Rhombohedral, colorless crystals
4.	WO_3:6.0 g $La(NO_3)_3$:0.75 g 5.4 M NaOH: 7 ml	8.4	120	4–5	Well-developed, tabular, prismatic, highly transparent, colorless crystals

(Cont'd.)

Table 8.2. *(Cont'd.)*

Sl. No	Nutrient	pH	P	Size (bar)	Remarks (mm)
5.	WO_3:6.0 g $La(NO_3)_3$: 0.75 g 5.4 M NaOH:7 ml	8.4	60		White crystalline powder
6.	WO_3: 6.0 g $La(NO_3)_3$: 0.75 g 5.4 M NaOH: 7 ml	8.4	80	2–3	Thin needlelike crystals
7.	WO_3:6.0 g $La(NO_3)_3$:0.75 g 5.4 M NaOH:7 ml	8.4	100	3–4	Rhombohedral, transparent, colorless crystals
8.	WO_3:6.0 g $La(NO_3)_3$:0.75 g 5.9 M NaOH:7 ml	8.8	120	5–6	Tabular, prismatic, transparent
9.	WO_3:6.0 g $La(NO_3)_3$:0.75 g 6.2 M NaOH:7 ml	9.3	120	6–7	Rod, prismatic subtransparnet, colorless crystals
10.	WO_3:6.0 g $La(NO_3)_3$:0.75 g 6.2 M NaOH:7 ml	9.8	120	4–5	Thin, long, translucent, needlelike crystals
11.	WO_3:6.0 g $La(NO_3)_3$:0.75 g 6.9 M NaOH:7 ml	10.2	120	2–3	Small, thin, translucent, needlelike crystals

The probable reason for the small crystals may be the higher ionic mobility, low viscosity, and higher concentration of solute ions. The crystals obtained by this means were well developed, bigger in size, and of good quality. The experimental conditions are ideal because more controlled diffusion of ions exists at a relatively lower temperature due to high viscosity, high density, and high dielectric constant, and less thermal strain, which leads to well-developed crystals. The crystal morphology varies significantly with a change in the growth parameters.

The formation of $NaLa(WO_4)_2$ takes place under hydrothermal conditions according to the following reactions:

Eq. (10) $2NaOH\ (aq) + WO_3\ (s) \rightarrow Na_2WO_4\ (aq) + H_2O\ (aq)$

Eq. (11) $La(NO_3)_3 + 3NaOH \rightarrow La(OH)_3\,(s) + 3NaNO_3\,(aq)$

Eq. (12) $2La(OH)_3 + 2WO_3\,(s) \rightarrow La_2(WO_4)_3 + 3H_2O$

Eq. (13) $La_2(WO_4)_3 + Na_2WO_4\,(aq) \rightarrow 2NaLa(WO_4)_2$

Eq. (14) $4NaOH(aq) + 2WO_3\,(s) + La(NO_3)_3\,(s) \rightarrow NaLa(WO_4)_2 + 3NaNO_3 + 2H_2O$

The trioxides of tungsten (VI) dissolve in aqueous alkali metal hydroxide to form tungstates and water. These normal tungstates contain the discrete tetrahedral ions WO_4^{2-}. It is not certain that the WO_4^{2-} ions are also tetrahedral in aqueous solution. Tungstate ions polymerize in acid solution to give meta- and paratungstate ions. The degree of polymerization in solution increases as the pH is lowered, and a number of tungstates $M_2O{\cdot}nWO_3M{\cdot}H_2O$, differing in the value of *n*, crystallize from the solution at different pHs. It has been observed that the diffusion coefficient of tungstate ions in aqueous solutions decreases considerably with increasing acidity of the solution, which is probably due to an increase in the polymerization of ions. In all the experiments, pH was measured at the beginning and at the end of the experimental runs and it was found that the system was moderately alkaline, which avoids the possibility of polymerization. Lanthanide ions, in spite of high charges (+3), have low charge densities because of their large size. Therefore, they cannot cause much polarization and, consequently, they do not have much tendency to form complexes. The tendency to form complexes and their stability increase with increasing atomic number. Since ionic size decreases from La^{3+} to Lu^{3+}, the basicity of hydroxides decreases in the same order. Thus, $La(OH)_3$ is the strongest and $Lu(OH)_3$ is the weakest base. $La(OH)_3$ precipitates during the reaction as follows:

Eq. (15) $La(OH)_3 + n - 3 \rightleftharpoons La(OH)_n^{(n-3)}$

and later dissolves in NaOH solution through any one of the earlier quoted reactions. Like La complexes, we can also expect NaLa complexes such as $Na_xLa(OH)_{3-x}$ in the solution. Being a good base, $La(OH)_3$ reacts with WO_3 to form lanthanum tungstates, which in turn dissolves in normal sodium tungstate to form $NaLa(WO_4)_2$ crystals under controlled conditions. In all the previous works on the synthesis of alkali rare earth tungstates, mineralizers such as NH_4Cl and alkali halides were used at very high *PT* conditions, but

DropBooks

in the work of Byrappa and Jain (1996), they have essentially used water and NaOH as mineralizer, with an emphasis on controlling the release of hydration shell water in the system through moderately lower *PT* conditions of synthesis. This permits a considerable reduction in the free energy of the system, leading to the complexation process. Therefore, the use of NaOH in the system and the formation of $La(OH)_3$ in the course of the reaction are quite useful in the complexation process, as it is well-known that hydration shell water experiences less competition from bulk solvent water at moderate temperature. They have also carried out a series of experiments using heavier lanthanides under the same experimental conditions; however, it was found that the solvents used are suitable for the first group of lanthanides (La, Ce, Nd), but not for the other lanthanides. The reason for this may be the decrease in the basicity with an increase in the atomic number. Hence, the synthesis of $NaLn(WO_4)_2$ (where Ln = Pr-Lu) insists on the use of other solvents.

The most common morphological habits observed in $NaLa(WO_4)_2$ crystals are prismatic, rod-shaped, rhombohedral, needle-like, etc. The prism faces dominated over all other faces in the crystals followed by pinacoidal and dome faces. $NaLa(WO_4)_2$ crystals belong to the tetragonal system with scheelite structure type; hence, their morphology is supposed to be simple, at least in the case of single crystals. However, the crystals exhibit simple twinning and pseudo-triclinic symmetry. Figure 8.13 represents the schematic diagrams of $NaLa(WO_4)_2$ crystals. Figures 8.14 and 8.15 show the variation in the growth rate and morphology of $NaLa(WO_4)_2$ crystals with the pH of the medium and internal pressure, respectively. Good quality crystals were obtained in the pH range 8.4–8.8. Figure 8.16 shows the representative photographs of the alkali rare earth tungstates obtained by Byrappa and Jain (1996). The size of the crystals increases with an increase in the pH of the medium, but the quality of the crystals becomes poor and beyond pH 11.5, $NaLa(WO_4)_2$ does not crystallize. The growth rate of $NaLa(WO_4)_2$ crystals was found to increase with an increase in pressure, and good quality crystals were obtained at about 120 bars. The twinning is more in experiments with pH values varying from 8.0 to 9.0. The pH of the mineralizer and the percent fill have a considerable influence on the morphology and growth rate of $NaLa(WO_4)_2$ crystals. With an increase in the pH of the system, the morphology varies from well-developed bulk crystals of pseudo lower symmetry to long needles of even 7 mm long in an experimental run of ten days. Similarly, with an increase in the pressure of the system, the morphology varies from

needles (at lower pressure conditions) to bulk crystals of pseudo-lower symmetry (at moderate pressure conditions); thus, the hydrothermal growth of tungstates, particularly alkali rare earth tungstates, carry a great significance in hydrothermal research.

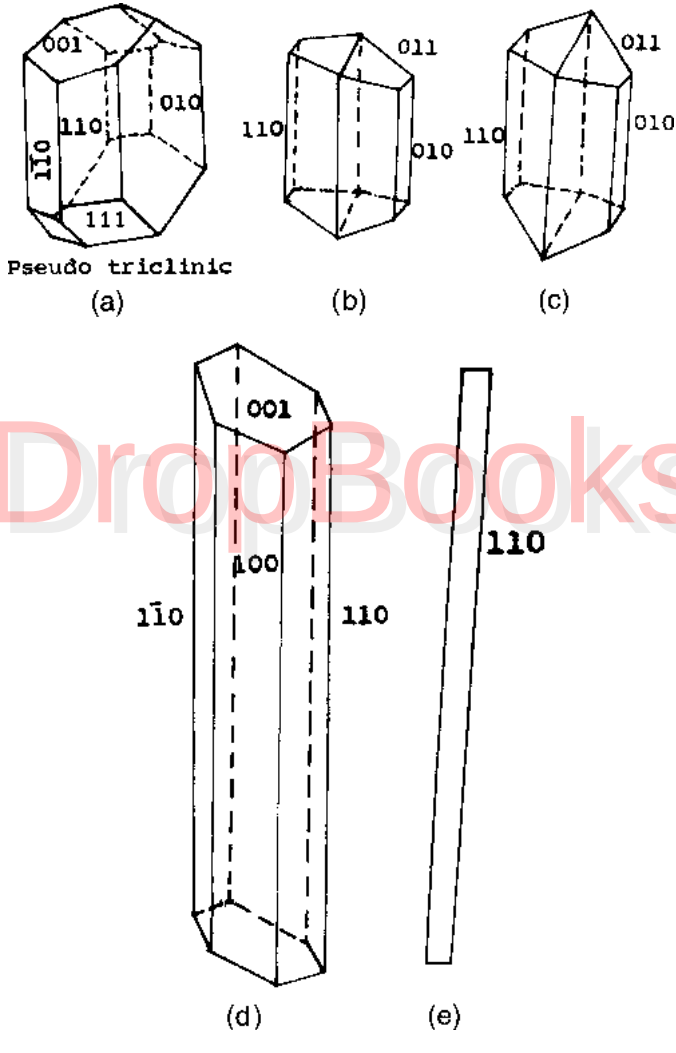

DropBooks

Figure 8.13. Schematic diagrams of $NaLa(WO_4)_2$ crystals.[54]

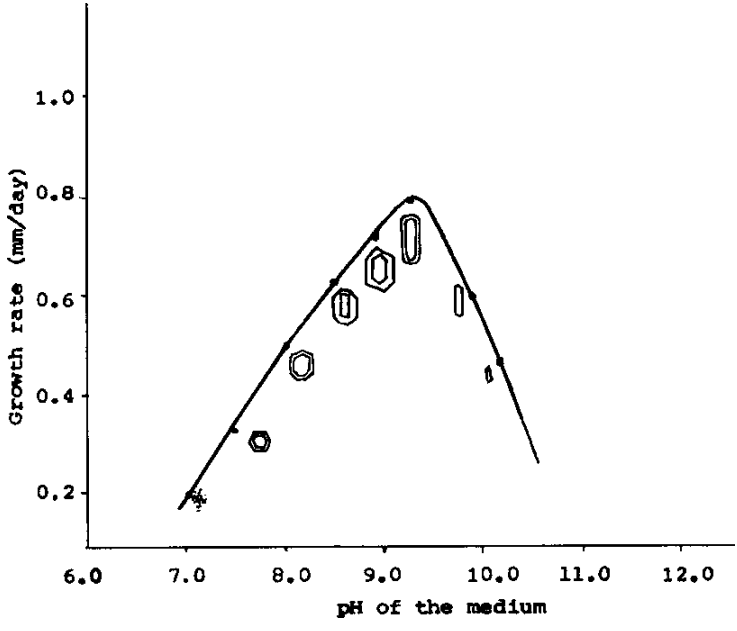

Figure 8.14. Variation in the growth rate and morphology of $NaLa(WO_4)_2$ crystals with the pH.[54]

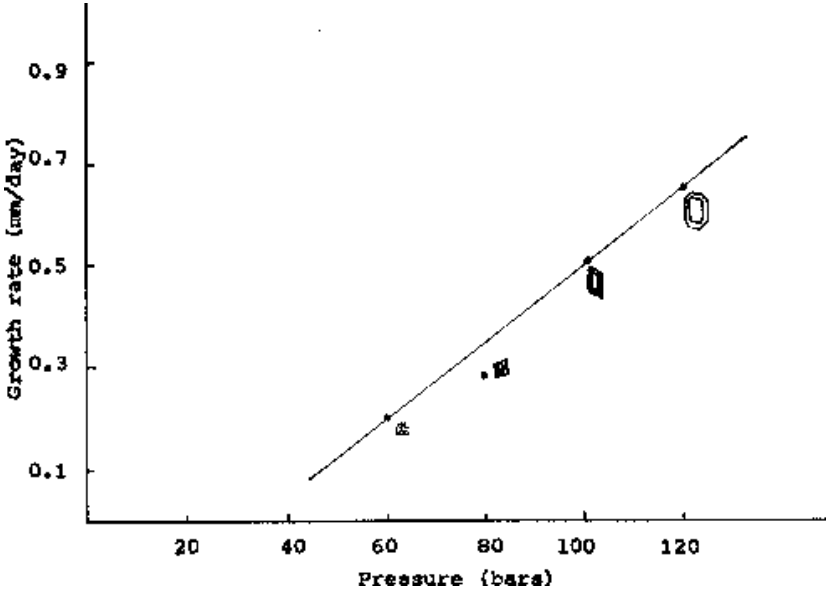

Figure 8.15. Variation in the growth rate and morphology of $NaLa(WO_4)_2$ crystals with internal pressure.[54]

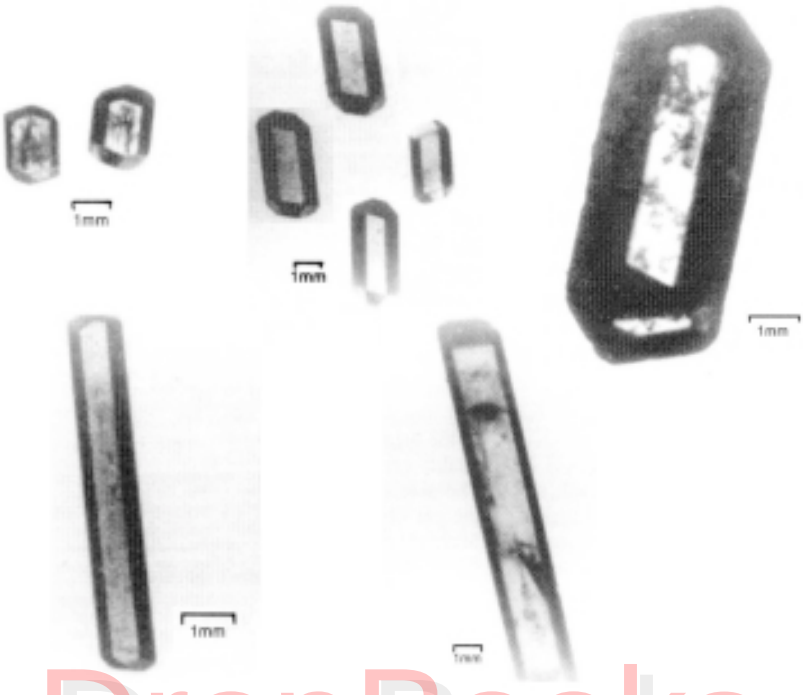

DropBooks

Figure 8.16. Photographs of the alkali rare earth tungstates.[54]

8.8 HYDROTHERMAL SYNTHESIS OF MOLYBDATES

Molybdenum bearing minerals are not many in nature, and the most important mineral is wolfenite, $PbMoO_4$, belonging to the scheelite group. Hence, molybdates are closely related to tungstates in their formation, crystal chemistry, and also physical properties. Several molybdates have been synthesized artificially by various techniques, like melt, solid state, and flux. Their synthesis is closely related to the synthesis of tungstates and hence, several isostructural compounds between tungstates have been obtained. These molybdates show interesting optical, electrical, and magnetic properties. Only a small number of vanadates have been obtained under hydrothermal conditions. In fact, Klevstov and group have worked out the growth technology for molybdates along with tungstates.[41][42] Crystals of $CdMoO_4$ have been obtained in 5–15 wt% NH_4Cl, the nutrient materials are CdO and MoO_3 in stoichiometric ratio.[56] The crystallization was carried out at 350–500°C, ΔT = 10–25°C, in titanium lined autoclaves.

The hydrothermal synthesis of molybdates is carried out usually at high temperature, > 500°C. The most well studied system is R_2O_3-MoO_3-K_2MoO_4-H_2O.[57] Figure 8.17 shows the TN-diagram of crystallization in the system R_2O_3-K_2MoO_4-H_2O. Four major phases crystallize in this system: $RMoO_4$ (OH), R_2MoO_6, $KR(MoO_4)_2$, and $K_5R(MoO_4)_4$.

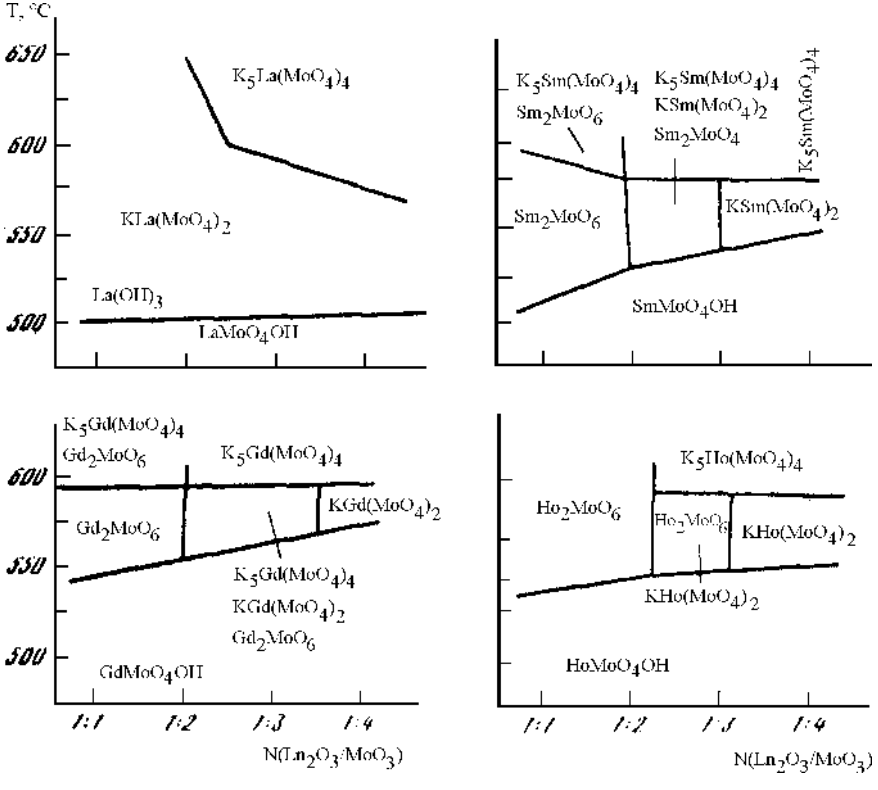

Figure 8.17. TN-diagram of crystallization in the system R_2O_3-K_2MoO_4-H_2O.

Hydroxyl Molybdates, $RMoO_4(OH)$. This has been obtained for La-Eu at temperatures of 450–550°C and pressures of 1200–1400 atm.[57] Rare earth oxides and molybdenum in the molar ratios 1:2, 1:3, 1:4, and 1:5 were taken as the nutrient. Good quality crystals have been obtained in aqueous solutions of LiCl and KCl (20 wt%) with an addition of NH_4Cl (5 wt%). With a rise in the temperature, the crystal output decreases up to 50% at 525°C, and the tabular and needle-like crystals of polyoxides of molybdenum increase.

Oxymolybdates (R_2MoO_6). These are obtained in the ratio R_2O_3/MoO_3 = 1:1, and oxymolybdates with rare earth elements from Pr to Er have been obtained under hydrothermal conditions.[58] The synthesis is carried out at 500–600°C in aqueous solutions of K_2MoO_4 with a concentrations of < 35 wt% and the starting R_2O_3/MoO_3 ratios = 1:1 to 1:2. The oxymolybdates under these conditions crystallize in the low-temperature monoclinic modification isostructural to Nd_2WO_6.[58] Kodama and Ozumi (1980) have obtained Bi_2WO_6 crystals in pure water at T = 300–500°C and P = 500–800 atm.[59] The nutrients Bi_2O_3 and MoO_3 in the ratio 1:1 have been used. Similarly, these authors have obtained Bi_2MoO_6 in Li, Na, K, NH_4 (T = 200–400°C, P = 175–400 atm) chlorides, in KF solution (T = 100–300°C, P = 50–300 atm) and NaF solution (T = 200–400°C, P = 100–420 atm). Several compounds exist in the Bi_2O_3-MoO_3 system because they are efficient catalysts (for instance, for oxidation of unsaturated hydrocarbons). Bi_2MoO_6 is one of the compounds in the system and is found in natural deposits as the mineral koechlinite, which is one of the polymorphs of Bi_2MoO_6. This compound has three polymorphic forms. The γ-form transforms quickly and irreversibly into the high temperature form when it is heated above 600°C. Therefore, the hydrothermal method is very useful for preparing the γ-form. Under hydrothermal conditions, the presence of water vapor enabled reactions between Bi_2O_3 and MoO_3 to occur at much lower temperatures than those required for "dry" conditions. Figure 8.18 shows the photograph of an assembly of γ-Bi_2MoO_6 single crystals obtained in NH_4F solution.

DropBooks

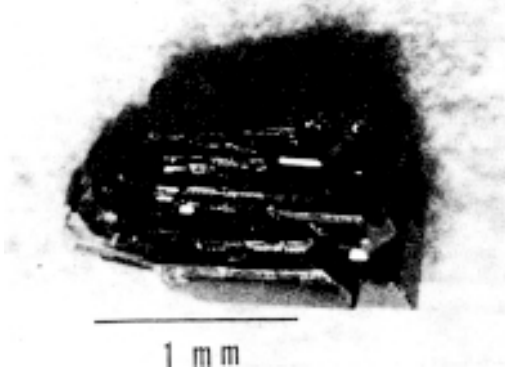

Figure 8.18. Photograph of an assembly of γ- Bi_2MoO_6 single crystals obtained from NH_4F solution.[59]

Several oxymolybdates of 1:3 ratio have been obtained and the prominent ones are $Fe_2(MoO_4)_3$, $In_2(MoO_4)_3$, and $Fe_2(MoO_4)_3$ obtained in 5–10 wt% LiCl solutions at T = 400–500°C and P = 400–1000 atm.

Among the mixed rare earth molybdates, the prominent ones are: $M^+R(MoO_4)_2$ (M^+ = Li, Na, K; R = rare earth elements.[60]–[62] These double molybdates are known for every series of rare earth elements (Ln = La-Lu, Y). They are prepared by crystallization from solution, in the melt, solid-phase synthesis, and by the hydrothermal method. The entire series of compounds are isostructural to the tetragonal scheelite, $CaWO_4$. The experimental conditions are T = 525–600°C, P = 1000–1500 atm. Aqueous solutions of 5 to 50 wt% of K_2MoO_4 were used as solvents and KOH was added to obtain the desired pH of the growth media. The other molybdates are (α-$KBi(MoO_4)_2$, $KY(MoO_4)_2$, $K_5R(MoO_4)_4$, $K_2Pb(MoO_4)_2$, $K_2(K_{.5}R_{.5})(MoO_4)_2$, $LiLa(MoO_4)_2$, and so on.[63] The experimental conditions, like pressure, temperature, and solvent, are the same except for the type and ratio of the starting components which determine the crystallization of other phases.

In recent years, there are several new molybdates synthesized under hydrothermal conditions exhibiting good ionic conductivity and some zeolitic structures. Among them, the copper molybdates are very interesting super-ionic conductors. The $Cu^{1+}_6Mo^{6+}_5O_{18}$ and $Cu^{1+}_4Mo^{6+}_5O_{17}$ have been synthesized by the hydrothermal technique using stoichiometric quantities of cuprous oxide and molybdenum trioxide taken in a gold capsule which is filled with a known quantity of distilled water. The capsule was sealed and held at 3 kb pressure and 500°C temperature for 12 hours, followed by a slow cooling (10°C/hr) to room temperature. Under the microscope, very thin crystals appeared and were reddish-brown in transmitted light.[64][65] Figure 8.19 shows the resistivity data for $Cu_4Mo_5O_{17}$ crystals. The resistivity measurements were made on single crystals using indium contacts soldered on the crystals in a nitrogen atmosphere to avoid oxidation.

Meyer and Haushalter reported many reduced molybdenum phosphates with octahedral-tetrahedral framework.[66] Following this, there is also much interest in molybdates and molybdenum oxides due to their catalytic activity and their capability of forming crystal structures which allow rich intercalation chemistry using secondary and tertiary amines.[67]–[69] These compounds yield microporous structures. The hydrothermal method helps to synthesize molybdates in acidic medium by using various templates as structure-directing units. The structures of $(Mo_xO_y)^{n-}$ can be "tailored"

to a certain degree by altering the size, conformation, and properties of templates and the acidity of the reaction system. This results in a series of chain and layer-type polymeric molybdenum oxides with intercalating cations. Thus, these new molybdates are the most perspective materials which can be obtained only by hydrothermal technique.

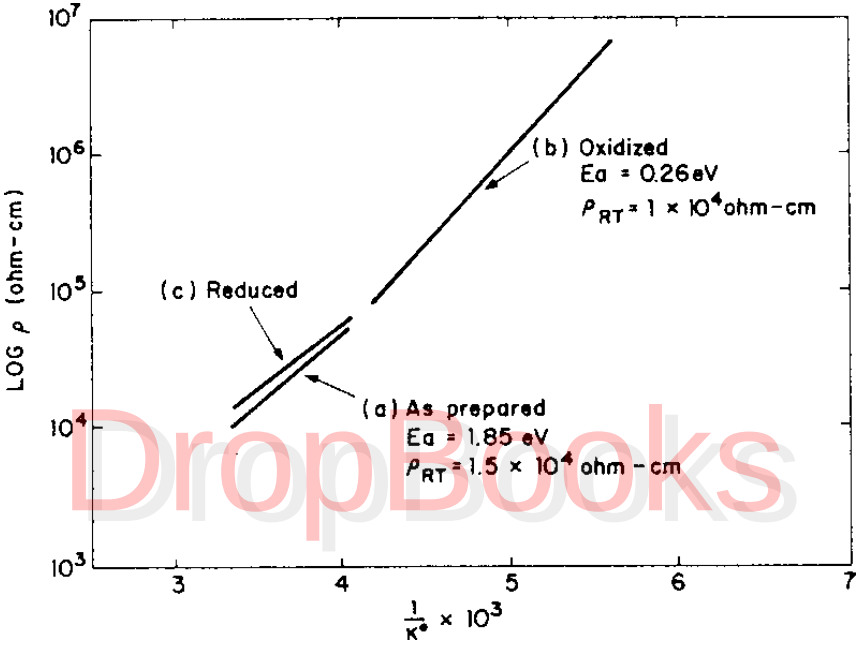

DropBooks

Figure 8.19. Resistivity data for $Cu_4Mo_5O_{17}$.[65] *(Courtesy of the Academic Press, Orlando, Florida.)*

8.9 HYDROTHERMAL SYNTHESIS OF TITANATES

Titanium is one of the most abundant elements in the earth's crust and takes the ninth place in the order of abundance. It can be considered in two parts. The first part is its concentration in only a few mineral structures, like ilmenite, sphene, rutile, and a few others. In the second part, it is an isomorphous substituting cation in a majority of silicates and other complexes in spite of the heterovalency, large difference in the ionic radii,

etc. The presence of Ti^{4+} and Zr^{4+} in the silicates usually leads to the formation of mixed framework structures.

A lot of chemical elements can form the octahedral coordination in crystal structures. Among these compounds it is possible to enlist a rather numerous group of oxides of Ti, Ta, Nb, Zr, and of transitional elements (Cu, Mn, Fe, Cr, Al, etc.). Among these, the titanates are the most important materials, not only because of their structural diversity, but also of their increased technological applications, like electro-optic, laser, superionic, high temperature superconductoring, etc. In contrast to silicates and their analogs, the titanates have octahedral coordination and have layer or framework configurations, but not isolated rings, islands, chains, etc.

8.9.1 Crystal Chemistry of Titanates

In titanates, formally in each $[TiO_6]$ unit, each oxygen atom gets about 4/6 = 0.67 unit from the central cation. Therefore, it is quite certain that during the crystallization of titanates (Ti^{4+}), the oxygen anions should be bonded with additional cations in order to attain the desired local charge balance. However, under surplus concentration of Ti^{4+} in the starting composition, the function of other cations is usually met by Ti^{4+} itself. In the natural systems, titanates usually have Na^+, K^+, Ca^{2+}, Sr^{2+}, Ba^{2+}, and other metals in their composition and the charge balance can be well established in such compounds. In the earth's crust, silicon is more abundant with a higher charge (+4) and lower coordination number (4). Hence, it forms a more common partnership with Ti^{4+} in the earth's crust to form titanosilicates. The other cations which play a major role in the charge compensation in titanium minerals are Zr^{4+}, Fe^{3+}, Fe^{2+}, Mn^{2+}, Mg^{2+}, and also the proton (H^+). Table 8.3 gives the common association of $[TiO_6]^{8-}$ in the structure of oxide compounds. The said formula unit of column 1 of Table 8.3 can be easily obtained directly from the association symbol. For example, the radical formula corresponding to the association 5(1) - 1(2) takes the form $TiO(5/1 + 1/2) = TiO_{5.5}$ or Ti_2O_{11}. It is observed that the sequence of all the Ti-O radicals given in Table 8.3 is made up of homological series with a general formula $[Ti_2O_{12-n}]^{-2(8-n)}$, where n = 0, 1, 2, 3, …8. The most simple titano-oxygen motif is $[TiO_6]^{8-}$ radical with all the six free vertices. Instead of discussing each radical unit given in Table 8.3, only a few selected and most widespread radical groups are discussed here. The most popular among these is the Ti-O framework consisting of the basic structure related to perovskite type $CaTiO_3$.[70] Similarly, it is

Table 8.3 Common Association of $[TiO_6]^{8-}$ In The Structure of Oxide Compounds

Symbol and radical formular	Association character	Structure type
6(1) $(TiO_6)^{8-}$	discrete octahedra	$K_2TiSi_3O_9$, $NaTi_2(PO_4)_3$, $K_2TiSi_6O_{15}$
5(1)-1 (2) $(Ti_2O_{11})^{14-}$	octahedra sharing common vertices	$NaTi_2Al_5O_{12}$, $Ba_4Ti_2PtO_{10}$, $TiTe_3O_8$
4(1) -2(2)- $(TiO_5)^{6-}$	para octahedra sharing common edges, infinite chain of octahedra sharing trans-vertices	Leucosphenite, Neptunite Tinakite
	(a) linear	Pseudobrookite
	(b) zig-zag	Sphene
3(1)- 3(2) $(Ti_2O_9)^{10-}$	para octahedra sharing common faces	Hexagonal modification of $BaTiO_3$
2(1) -4(2) $(TiO_4)^{4-}$	infinite pillars of edge-shared octahedra	
	(a) linear	Rutile
	(b) zigzag layered network of vertices shared octahedra	Brookite
1(1) -5 (2) $(Ti_2O_7)^{6-}$	double layered vertices shared shared octahedra	$Bi_2(NbTi)O_9$, $Bi_3(TaTi)O_9$ $Sr_3Ti_2O_7$
6(2) $(TiO_4)^{4-}$	framework vertices shared octahedra edge shared octahedra, vertices and faces linked octahedra	Ilmenite, Perovskite, pyrochlore $Ca_3Ti_2O_6$ - $ThTi_2O_6$ $CaTi_2O_4$ $BaTiO_3$ hexagonal modification
3(2)-3(3) $(Ti_2O_5)^{2-}$	—	—
6(3) $(TiO_2)^0$ $Ba(Ti_7Mg)O_{16}$	Close packed layered octahedra framework with vertices edges shared octahedra	$TiCl_2$, TiI_2, TiS_2 Rutile, Brookite, anatase
6(4) $(Ti_2O_3)^0$	Framework with vertices, edges and faces shared octahedra	Ti_2O_3 corundum

DropBooks

interesting to consider perovskite type framework in ilmenite, pyrochlore, and spinel types, however, the most important association in the crystal chemistry of titanates is the TiO_2 in three polymorphic modifications, of which the rutile type is the most stable one, with linear columns of octahedra sharing edge. The most complex association is that where each oxygen atom is linked with four Ti^{4+} octahedra and it is considered to be a highly unique structure since it indicates an anomalously high supersaturation of the corresponding oxygen ligands with Ti^{4+}. Such complex structures are formed in $K(NbTi)O_5$, $Na_2Ti_3O_7$, $A_2Ti_6O_{13}$, where A = Na, K, Rb, and similarly $Na_xTi_4O_8$.[71]–[74] Here, it is appropriate to discuss the groups consisting of titanium coordination with five vertices, i.e., tetragonal pyramids and trigonal pyramids. In this case also, it is possible to use the principle of association character. With the help of simple and complex symbols, for Ti-O polyhedra in the discrete form, only tetragonal pyramids have been reported and such structures can be expected in titanates, silicates, germanates, and rare earth titanates, $RTiO_5$ where R = Y, La.[75][76] All the above mentioned different motifs of Ti-O octahedra—either isolated or discrete pairs—are linked with each other to form chains, ribbons, layers, etc., clearly indicating the ability of Ti^{4+} to decrease its coordination number up to five and, thus, giving new motifs corresponding to Pauling's polyhedra. Obviously, intercondensation of Ti-O polyhedra makes a part of their edges and vertices remain free. This is attributed to the higher probability of severely disturbed charge balance, and it becomes important when the Ti-O distances in coordination polyhedra fall from the normal values. Reduction in the coordination number of Ti^{4+} up to 5 can be considered due to the limited manifestation of the tendency of Ti^{4+} ions under the given conditions by giving out one of its ligands.

In summary, the above described crystal chemical elucidation of titanium, particularly Ti octahedra, undergo condensation, their varying associations, abundance of the edge contacts between these polyhedra, an anomalous case of their faces linked, reduction in the coordination number of Ti, the possibility of reaching a complete charge compensation, etc., justify a wide structural diversity, both in natural and synthetic compounds.

In comparison with the other anion forming elements, Ti^{4+} stands close to Si^{4+} in several respects. Probably the main reason for such a closeness is the repulsive forces between the higher valent ions like Ti^{4+}

and, in general, Ti^{4+} can form complexes easily with the group IV elements of the periodic table. Since Ti^{4+} has a higher coordination number, it is not as easy to understand the absence of analogous phase, $TiSiO_4$, in the system TiO_2-SiO_2.[77] Out of thirty-two known titano-silicate compounds in nature, eighteen consist of one or the other groups of titanium octahedra. Under these circumstances, it leads to an unexpected variation in their association, like isolated, infinite motifs of chains and layers, etc. Here it is necessary to emphasize the abundance of Ti octahedra sharing their edges in silicates, making it closer to its neighbor diagonally in the periodic table, i.e., Al^{3+}, which can form tetrahedral and octahedral coordinations with both Al octahedra and Ti octahedra sharing their edges (epidote, kyanite, sillimanite, and andalusite). Such a formal substitution of Al^{3+} in tetrahedra and Ti^{4+} octahedra does not change the charge balance in the silicate structures. Considering the closeness of Al-Si and Ti-Si frameworks, it is necessary to show their principal difference of bonding with different valency and coordination of silicon substitutes.

It is well known that all the variations in the framework silicates are connected with the heterovalent substitution: $Si^{4+} \rightarrow Al^{3+}$. If the framework is made up of pure (SiO_2) then in the isovalent substitution (but not isomorphic) of $Si^{4+} \rightarrow Ti^{4+}$, the Ti^{4+} gets the additional oxygen atoms to form an octahedral coordination.

PropBooks

It is interesting to note that Zr - Hf forms an excellent solid solution because of its unique chemical and crystal chemical closeness, which brings in the neighboring elements, including the lanthanide series. The other elements which can form the isomorphic substitution with Ti^{4+} are Nb^{5+}, Ta^{5+}, Zr^{4+}, Fe^{3+}, and Al^{3+}. All these substitutions are obtained experimentally; however, in nature such a large substitution has not been found, for example, Al^{3+} rarely substitutes for Ti^{4+} in minerals or vice-versa. Here, it is necessary to remember that both Al and Ti show chemically amphoteric behavior which changes their coordination numbers significantly, so also the ionic radii (rTi^{4+} = 0.68 Å, rAl^{3+} = 0.51 Å) plays an important role. Therefore, a part of the Al^{3+}, octahedrally coordinated, can form the isomorphous substitution with octahedrally coordinated Ti^{4+}.

One of the most common schemes observed in the heterovalent substitution of $Ti^{4+} \rightarrow Nb^{5+}$ shows $2Ti^{4+} \rightarrow Nb^{5+} + Fe^{3+}$. There are many such examples for $Ti4+ \rightarrow Nb^{5+}$ in the synthetic compounds like $TiNbO_7$, $Ba6Ti_2Nb_8O_{30}$, and, similarly, $YNbTiO_6$, a symmetric analog of the metamict mineral.[78]–[80] Only in two mineral structures: epistolite,

$Na_2(Nb,Ti)_2Si_2O_9.nH_2O$, and vuonnemite, $Na_4TiNb_2Si_4O_{17}{\cdot}2Na_3PO_4$, has such an isomorphism between Ti^{4+} and Nb^{5+} been reported.

In spite of the isovalent behavior of these Ti^{4+} and Zr^{4+} atoms, their crystal chemical relation is not as close as that of $Ti^{4+} \rightarrow Nb^{4+}$. The main reason is higher ionic radii of Zr^{4+} (0.79 Å) and also the different nature of bonding of Zr-O and Ti-O, particularly the latter, which is appreciably different. Moreover, there is a greater variation in the Ti-O bond distances in the Ti-O octahedra, and also the Ti^{4+} octahedra has a tendency to undergo condensation, and it is well-known that the coordination number of Ti^{4+} in quite a few structures goes down from 6 to 5 and even to 4. In contrast, the Zr-O bond distances do not vary much in the Zr-octahedra, which show no tendency for undergoing condensation. Besides, in a series of oxides (both simple and complex) the Zr^{4+} cations increase their coordination number from 6 to 7 and up to 8.

In recent years, a large number of experiments have been carried out on the isomorphism of various titanium bearing compounds, which have technological applications. $BaTiO_3$, $SrTiO_3$, alkali titanates, $LiNbO_3$, ABO_4 (A = Sb, Bi; B = Nb, Ta, Sb), etc., are the important examples. Alkali titanates with layered structures can form suitable examples for the nonstoichiometry on the guest cations. $KTiNbO_5$ reported by Wadsley (1964) is one such compound, where each sheet $(TiNbO_5)^{n+}$ consists of double zigzag strings of octahedra sharing corners, which suggests the possibility of nonstoichiometry on the K ion sites.[71] Rebbah et al. (1980) have studied the nonstoichiometric $A_{1-x}(Ti_{1-x}M_{1+x})O_5$, (where A = K, Rb, Te, Cs; M = Nb,Ta).[81]

8.9.2 Hydrothermal Synthesis of Selected Titanates

Titanates have great technological applications because of their wide range of structural variations and the possible substitution of Ti^{4+} by various other cations. Here, instead of going into the growth aspects of all the titanates, we discuss only the alkali titanates and rare earth titanates which have some important applications. TiO_2 and alkaline earth titanates are discussed separately in Chs. 9 and 10.

Alkali titanates exhibit layered structures, and the host cations can easily accept the guest cations giving rise to a wide range of nonstoichiometric compounds.[82] All these compounds are very important owing to their ionic conductivity and exchange properties. Usually, the growth of alkali

titanates is carried out by solid state reactions or exchange reactions, flux growth, and melt growth. The structural/stereochemical behavior of the titanium does not favor epitaxial methods. Similarly, the melt technique has not been adapted to the growth of alkali titanates even though this is one of the best techniques for the growth of various titanoniobates. The most popular method for all the titanates, in general, to obtain single crystals is the flux method, because at high temperature these flux agents become highly active and the titanium forms various complexes depending upon the availability of other cations and anions and undergoes condensation.

The alkali titanates could be obtained by reacting carbonates/oxalates of alkali metals with titanium dioxide (anatase) at higher temperatures (usually above 900°C in an inert atmosphere). The introduction of fluoride and sometimes boron containing molten salts leads to the condensation of the titanium octahedra. Also, the crystallization temperature and starting molar ratio of the components play a major role in the preparation of titanates with various degrees of condensation. Although a large variety of alkali titanates have been obtained in the series $A_2O{\cdot}nTiO_2$ ($1 < n < 6$), where A = Li, Na, K, Rb, Cs, Ti, Ag, by by solid state reactions, the member ($n = 5$) has not been obtained.[83]–[85] Keeping this in mind, Byrappa, et al. (1997) made an effort to obtain this member ($n = 5$) of the series by the hydrothermal technique.[86] An attempt to obtain a member ($n = 5$) by the hydrothermal technique was successful. The probable reason might be the stabilities of $Na_2Ti_3O_7$, $Na_2Ti_6O_{13}$ and $K_2Ti_4O_7$ which are higher and they may not allow the formation of other stable phases, although such members might be present during the course of crystallization reactions. Figure 8.20 shows the TN-diagram of crystallization of alkalititanates. The experiments were carried out using Tuttle cold-cone sealed autoclaves provided with platinum liners. The starting materials, such as TiO_2 and NaOH, were taken in desired molar proportions and placed inside the platinum liner. The suitable mineralizer solution with a definite molarity was added into the platinum liner which was sealed later. The platinum liner was later placed inside an autoclave which was kept at $T = 500°C$, and $P = 1$ kbar for a period of three days. Long needle-like crystals of $Na_2Ti_3O_7$ were obtained. The crystals were about 5 to 8 mm long, colorless, and transparent. Such good quality crystals of $Na_2Ti_3O_7$ have not been obtained by the solid state reactions method; the resultant product was mostly a crystalline powder. The experimental conditions of the growth of $Na_2Ti_3O_7$ crystals are given in Table 8.4.

PropBooks

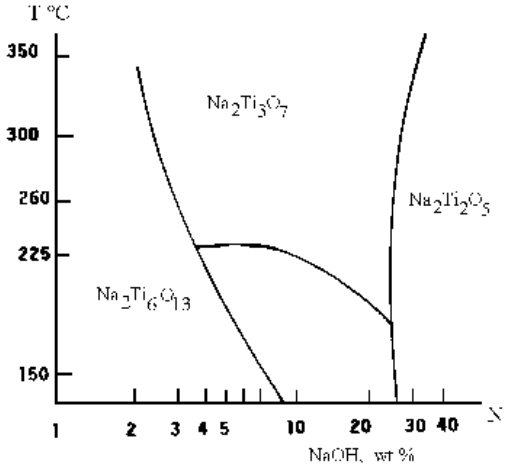

Figure 8.20. TN-diagram of crystallization of alkalititanates.[77]

Table 8.4. Experimental Conditions of the Growth of $Na_2Ti_3O_7$ Crystals

Sl. No.	Nutrient composition	T (°C)	P (Kb)	Duration (days)	Results	Crystal size(mm)	Remarks
1.	NaOH = 5.0g TiO_2 = 2.5g 3MHCOOH = 6ml	500	1	3	$Na_2Ti_3O_7$	10	Long rod like crystals
2.	NaOH = 0.4g TiO_2 = 2.5g 3MHCOOH = 6ml	500	1	3	$Na_2Ti_3O_7$	4	rod like crystals
3.	NaOH = 5.0g TiO_2= 2.5g 2MHCOOH = 6ml	500	1	3	$Na_2Ti_3O_7$	2	small needles
4.	NaOH = 6.0g TiO_2 = 2.5g 3MHCOOH = 6ml	650	1.5	3	$Na_2Ti_3O_7$	1	fine crystals
5.	NaOH= 4.5 g TiO_2= 2.5 g 3MHCOOH = 6ml	650	1	2	$Na_2Ti_3O_7$ + $Na_2Ti_6O_{13}$	< 1	fine crystals
6.	NaOH = 5.0 g TiO_2= 2.5 g 8MHCOOH= 6 ml	500	1	3	$Na_2Ti_3O_7$	< 1	fine crystals
7.	NaOH= 5.0 g TiO_2= 2.5 g 11MHCOOH = 6 ml	500	1	3	—	—	No crystals

(Cont'd.)

Table. 8.4. *(Cont'd.)*

Sl. No.	Nutrient composition	T (°C)	P (Kb)	Duration (days)	Results	Crystal size(mm)	Remarks
8.	NaOH = 5.0 g TiO_2= 2.5 g $4MH_2SO_4$ = 6 ml	550	1	3	$TiOSO_4$ + Rutile	0.2 - 0.4	fine grained
9.	NaOH = 4.0 g TiO_2= 2.5 g $2MHNO_3$= 6 ml	500	1.5	2	$Na_2Ti_3O_7$ + Rutile	0.3	fine grained
10.	NaOH = 6.0 g TiO_2= 2.0 g 3MHCOOH = 6 ml	300	1	3 1/2	$Na_2Ti_3O_7$ + $Na_2Ti_2O_5$ + Rutile	< 0.2	fine grained
11.	NaOH = 6.0 g TiO_2= 2.5 g 3MHCOOH = 6 ml	400	1	3	$Na_2Ti_3O_7$ + $Na_2Ti_2O_5$	< 0.2	fine grained
12.	NaOH = 6.0 g TiO_2= 2.5 g 3MHCOOH = 6 ml	450	1	4	$Na_2Ti_3O_7$	0.3 - 0.5 -	well developed needles
13.	NaOH = 4.0 g TiO_2 = 2.0 g H_2O= 6 ml	400	1	3	Rutile	0.1 - 0.2	fine grained
14.	NaOH = 5.0 g TiO_2= 2.0g H_2O= 6 ml	450	1.5	3	Rutile	0.1	fine grained

DropBooks

The ideal experimental conditions in the growth of $Na_2Ti_3O_7$ crystals are given below:

NaOH	-	5.0 gms
TiO_2	-	2.5 gms
HCOOH	-	6 ml (3 molar)
Temperature	-	600°C
Pressure	-	1 kb
Duration	-	4 days

In experiments with high molarity of HCOOH, the crystal quality was poor, and beyond 10 M HCOOH, the $Na_2Ti_3O_7$ did not crystallize. In the present work, the other mineralizers like HCl, HNO_3, H_2SO_4 and H_2O were tried, but these experiments did not yield good results and instead produced either mixed or other phases. The crystallization of $Na_2Ti_3O_7$ probably takes place through the following reactions:

Eq. (16) $NaOH + HCOOH \rightarrow NaHCOOH + H_2O$

Eq. (17) $5NaHCOO + TiO_2 \rightarrow NaTi(OH)_5 + 2Na_2O + 5CO$

Eq. (18) $Na_2O + HCOOH \rightarrow NaHCOOH + NaOH$

Eq. (19) $5NaOH + TiO_2 \rightarrow NaTi(OH)_5 + 2Na_2O$

Eq. (20) $2NaTi(OH)_5 + TiO_2 \rightarrow Na_2Ti_2O_7 + 5H_2O$

The solubility of $Na_2Ti_3O_7$ was determined under hydrothermal conditions in the HCOOH media with a varying temperature and at a constant pressure of 1 kb. The solubility curve is shown in Fig. 8.21. It is evident from Fig. 8.21 that the hydrothermal synthesis of $Na_2Ti_3O_7$ can be carried out within the temperature range of 350 to 600°C.

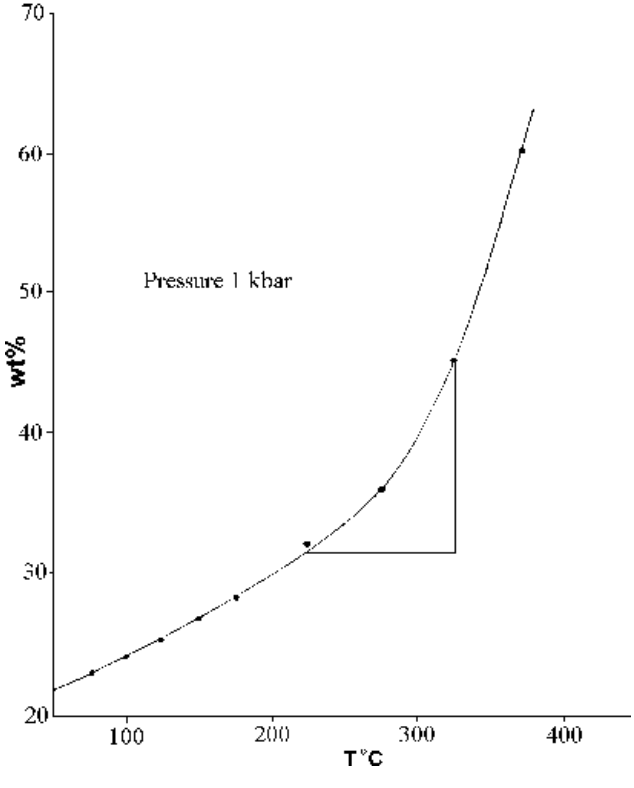

Figure 8.21. The solubility curve of $Na_2Ti_3O_7$.[86]

Besides alkali titanates, trivalent metal titanates, like bismuth titanate, have been studied in great detail owing to their high dielectric permeability. The Bi_2O_3-TiO_2 system has been studied widely, and several phases like $Bi_2Ti_2O_7$, $Bi_2Ti_3O_9$, $Bi_4Ti_3O_{12}$, Bi_8TiO_{14}, $Bi_{12}TiO_{20}$, and $Bi_2Ti_4O_{11}$, are obtained under the varying Bi_2O_3/TiO_2 ratios from 25:1 to 8:1. The solvents consisted of aqueous KF solutions while the initial charge was a mixture of the oxides Bi_2O_3 and TiO_2. The experiments were conducted in the range 450–600°C with a % filling factor 0.5–0.8.

Among these titanates, the Ti sillenite, $Bi_{12}TiO_{20}$, was almost independent of the composition of the initial charge. When the TiO_2 content in the charge was more than 5%, $Bi_4Ti_3O_{12}$ (77.00% Bi_2O_3 and 20.80% TiO_2) began to crystallize together with the Ti selenite. As the TiO_2 content of the charge was increased, the amount of $Bi_4Ti_3O_{12}$ enhanced and this compound became the first predominant and also the only phase over the range 17–25% TiO_2. Due to the temperature gradient in the autoclave, the bismuth titanates crystallize in the upper cooler region. The minimum recrystallization temperatures (500°C) were characteristic of the Ti selenite. The other bismuth titanates required higher temperatures, but sufficiently rapid transfer of all the compounds synthesized occurred at 550–600°C. Figures 8.22*(a)–(c)* show the schematic diagrams of the bismuth titanate crystals.[87] Similarly, Barsukova et al. (1972) have studied the system Bi_2O_3-TiO_2-KF-H_2O under hydrothermal conditions and a part of the phase diagram is shown in Fig. 8.23.[88]

PrintBooks

Muto and Taki (1976) have synthesized potassium lithium hexatitanate $K_2Li_2Ti_6O_{14}$ crystals by the hydrothermal technique using TiO_2 and KOH + LiOH. The compound could be obtained in the following molar ratios: TiO_2:LiOH:KOH = 1.5:1.0:7.5, and concentration of alkali 10N, filling of solutions 35–45%, $T \geq 400$°C, time of run ≥ 70 hrs. The interesting feature is that potassium lithium hexatitanate is not produced through the direct reaction of lithium ion with potassium hexatitanate already formed.[89]

The growth of rare earth titanates has not been reported in literature so far by the hydrothermal method, but there are some scanty reports by the flux method.[90]

Titanates, in general, show interesting physical properties like electrical, nonlinear, dielectric, ferroelectric properties. Figure 8.24 shows the Arrhenius plot $\log \sigma T$ vs $10^3/T$ for $Na_2Ti_3O_7$ crystals.[91] The activation energy calculated from the Arrhenius plot is 1.3 eV. The complex impedance measurements show that $Na_2Ti_3O_7$ represents resonance at

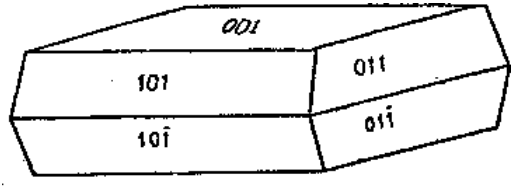

(a)

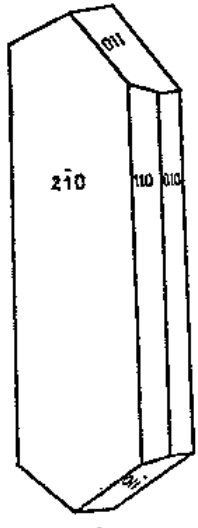

(b)

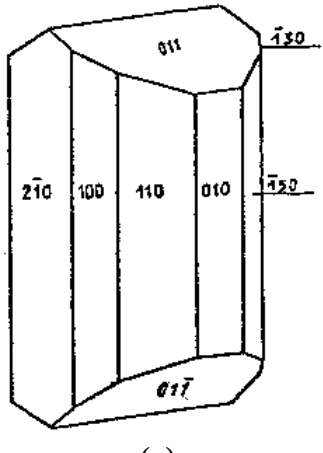

(c)

Figure 8.22. Schematic diagram of the bismuth titanate crystals, (a) crystal of $Bi_4Ti_3O_{12}$, (b) plate-like crystal of $Bi_2Ti_4O_{11}$, and (c) primatic crystal of $Bi_2Ti_4O_{11}$.[87]

about 10 MHz. With a possible modification of the material, it could be used as a dielectric resonator at 10 Hz.

Nonlinear optical properties of Ti-selenite and $Bi_4Ti_3O_{12}$ crystals have been studied in detail and these results have been correlated with other compounds like Ge-and Si-selenites to investigate the effects associated with photoconductivity.

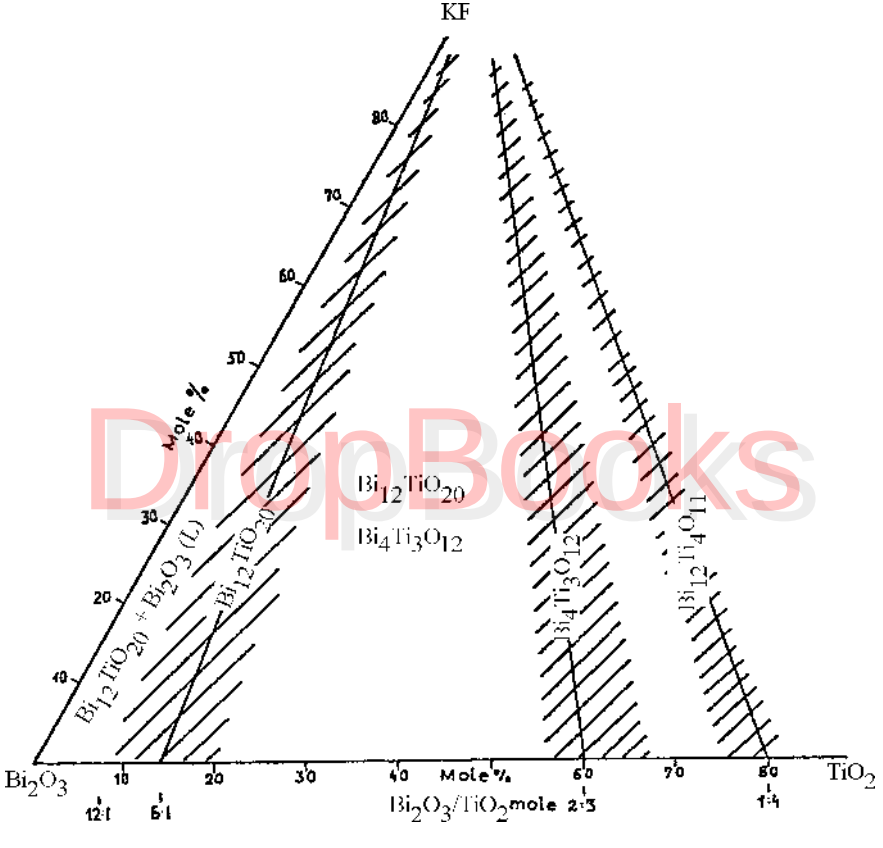

Figure 8.23. Part of the phase diagram of the Bi_2O_3-TiO_2-KF-H_2O system under hydrothermal conditions.[88]

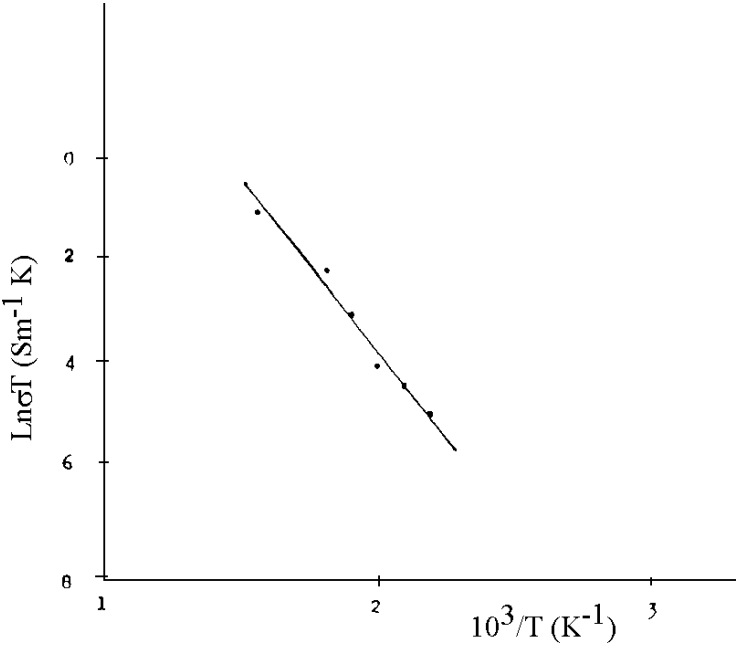

Figure 8.24. Arrhenius plot $\ln\sigma T$ vs $10^3/T$ for $Na_2Ti_3O_7$ crystals.[91]

8.10 HYDROTHERMAL GROWTH OF LITHIUM METAGALLATE CRYSTALS

Lithium metagallate, $LiGaO_2$, is of special interest because of its high electromechanical coupling constant and acoustic Q. The technology of the growth of lithium metagallate has been worked out in detail by Kolb et al. (1971).[92] The $LiGaO_2$ can be obtained by the Czochralskii pulling and flux methods. However, the flux method doesn't result in the growth of large size single crystals, and also the preferential loss of Li_2O at the melting point makes it difficult to control stoichiometry in melt-grown crystals. The initial hydrothermal experiments prompted Marshal and Laudise (1967) to study the hydrothermal solubility of $LiGaO_2$ crystals in NaOH solutions.[93] The experiments have been carried out in platinum-lined Morey type autoclaves using 3.5 M NaOH at T = 360–425°C, ΔT = 5–40°C, percent fill 0.7 to 0.8. Czochralskii grown crystals have been used as seed. The trial experiments at T = 400°C and ΔT = 25°C, percent fill 0.7, show that under these conditions the seed melts. The $LiGaO_2$ nutrient was

hydrothermally synthesized by reacting 5M LiOH and 2.5 M Ga_2O_3 in a short platinum autoclave for 10 days at the dissolving temperature of 390°C, 360°C growth temperature and 76% fill. In addition, the nutrient was made by melting Li_2CO_3 and Ga_2O_3 as a part of Czochralskii-grown crystals or from hydrothermal crystals with a diamond-impregnated wire saw. Growth rates have been measured by determining the increase in seed thickness upon the completion of the experimental run. Figure 8.25 shows the habit of typical hydrothermal $LiGaO_2$ crystals *(a)* grown on a spurious seed, *(b)* grown on (010) seed.

The perfection of hydrothermally grown $LiGaO_2$ was excellent as evidenced by the absence of electrical twinning. The material grown in (001) is virtually free of (OH).

DropBooks

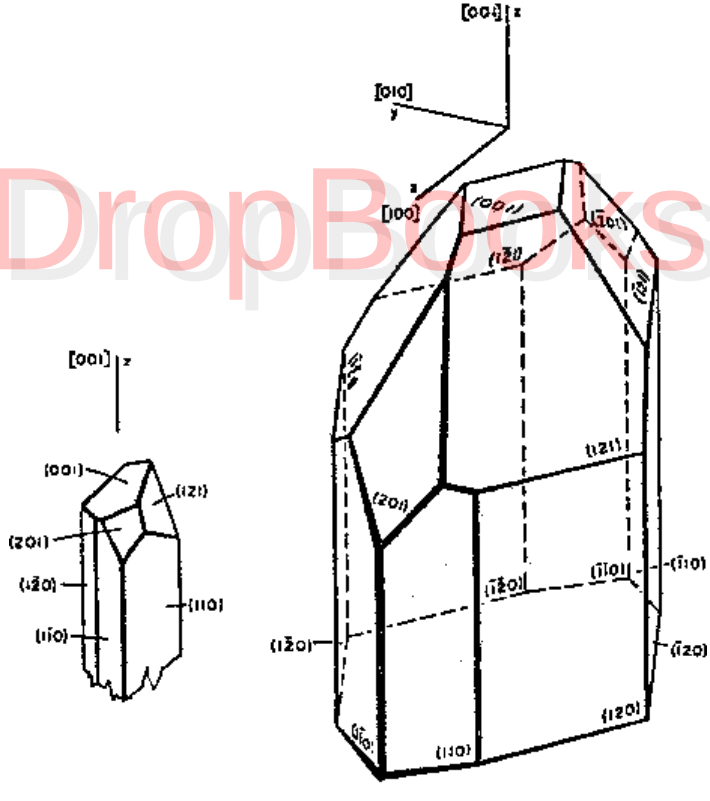

Figure 8.25. Habit of typical hydrothermal $LiGaO_2$ crystals *(a)* grown on a spurious seed, *(b)* grown on (010) seed.[93]

8.11 HYDROTHERMAL SYNTHESIS OF SULPHIDES

The hydrothermal technique has been popularly used for the synthesis of sulphides for the past several decades. The main advantage of this technique is the production of fairly large size single crystals of sulphides. From the literature survey, it is evident that sulphides are next only to silicates and oxides. Similarly, in nature also, sulphides are one of the most abundant minerals whose origin is closely related to hydrothermal—high pressure and temperature. The experimental studies on the growth of sulphides have shown that their crystallization can occur within a large variety of solutions and also strong acid. Thus, the study on the synthesis of sulphide began in the 19th century; however, a systematic study began after the discovery of their technological potential, especially as photo semiconductors and piezoelectric properties. Sulphides can be divided as simple or complex, containing a wide range of elements (uni-, di-, tri-, and tetravalent metals).

The easiest way of obtaining sulphides under hydrothermal conditions is through the following reactions:

Eq. (21) $Me + XS^{-2} + 2H_2O(MeSx + 2OH^- + H_2)$

However, the presence of hydrogen hinders the sulphides formation reaction and hence, the following reaction would be more practical:

Eq. (22) $MeSO_4 + Na_2Sr \rightarrow MeS + Na_2SO_4$

By this exchange reaction one can obtain a variety of sulphides with 100% output.[94]–[97] Latimer (1954) has observed that the monophase synthesis usually occurs through hydrolysis and oxidation of the nutrient with the formation of sulphates:[98]

Eq. (23) $S^{-2} + 4H_2O \leftrightarrow SO_4^{-4} + 4H_2\uparrow$

i.e., with a raise in partial pressure of hydrogen, the sulphate ion becomes unstable leading to the process of hydrolysis:

Eq. (24) $MeS + 5H_2O \leftrightarrow MeO + SO_4^{-4} + 5H_2O$

Eq. (25) $Me_2S_3 + 7H_2O \leftrightarrow Me_2O_3 + SO_4^{-4} + 7H_2 + 2S$

The hydrolysis reaction usually takes place at pH >7.[98]

8.11.1 Hydrothermal Synthesis of Sulphides of Univalent Metals

Simple sulphides of univalent metals, like silver and copper, with 100% output, could be obtained in chloride solutions (1–7 wt%) and lower partial pressure of hydrogen at T = 400–500°C and P = 1000–1500 atm. The growth is usually carried out in titanium-lined autoclaves with a temperature gradient (40–60°C). For the monophase synthesis of the above compounds, the surplus amount of the nutrient is taken. The Cu_2S is abundant in nature as chalcogenides. The other univalent metal sulphides are not common in the literature.

8.11.2 Hydrothermal Synthesis of Divalent Metal Sulphides

Divalent metal sulphides form the largest group of sulphides obtained by the hydrothermal technique. A large number of sulphides like ZnS, CdS, HgS, PbS, MnS, FeS, Fe_3S_4, NiS, CoS, CuS, and so on, have been obtained within a wide range of pH.[94][97][99] Kuznetsov (1990) has studied the solubility and stability fields of these sulphides under hydrothermal conditions in detail.[99] Figure 8.26 shows the solubility of HgS, ZnS, CdS in KOH and NaOH solutions.[99]–[101]

DropBooks

In all cases the dependencies are nonlinear. This means that the composition of complexes is changed with an increase in the solvent concentration. The analysis of above dependencies allows the inference of the reactions responsible for the dissolution of HgS, ZnS and ZnSe, at different solvent concentrations:

Eq. (26) $HgS + HS^- \rightarrow HgS\,(HS)^-$ $C_{NaHS} < 1M$

Eq. (27) $HgS + 2HS^- \rightarrow HgS\,(HS)^{2-}_2$ $C_{NaHS} > 1M$

Eq. (28) $ZnS + OH^- \rightarrow Zn\,(S,OH)^-$ $C_{KOH} \leq 1M$

Eq. (29) $ZnS+3(OH)^- + H_2O \rightarrow Zn\,(OH)^{2-}_4 + HS^-$ $C_{KOH} > 1M$

Eq. (30) $ZnSe + H_2O \rightarrow Zn(H,Se)\,OH°$ $C_{KOH} < 0, 1M$

Eq. (31) $ZnSe + H_2O + OH^- \rightarrow Zn(H,Se)\,(OH)_2^-$ $0.1\,m < C_{KOH} < 0.5\,M$

Eq. (32) $ZnSe + H_2O + 2(OH) \rightarrow Zn(H,Se)\,(OH)_3^{2-}$ $C_{KOH} > 0.5\,M$

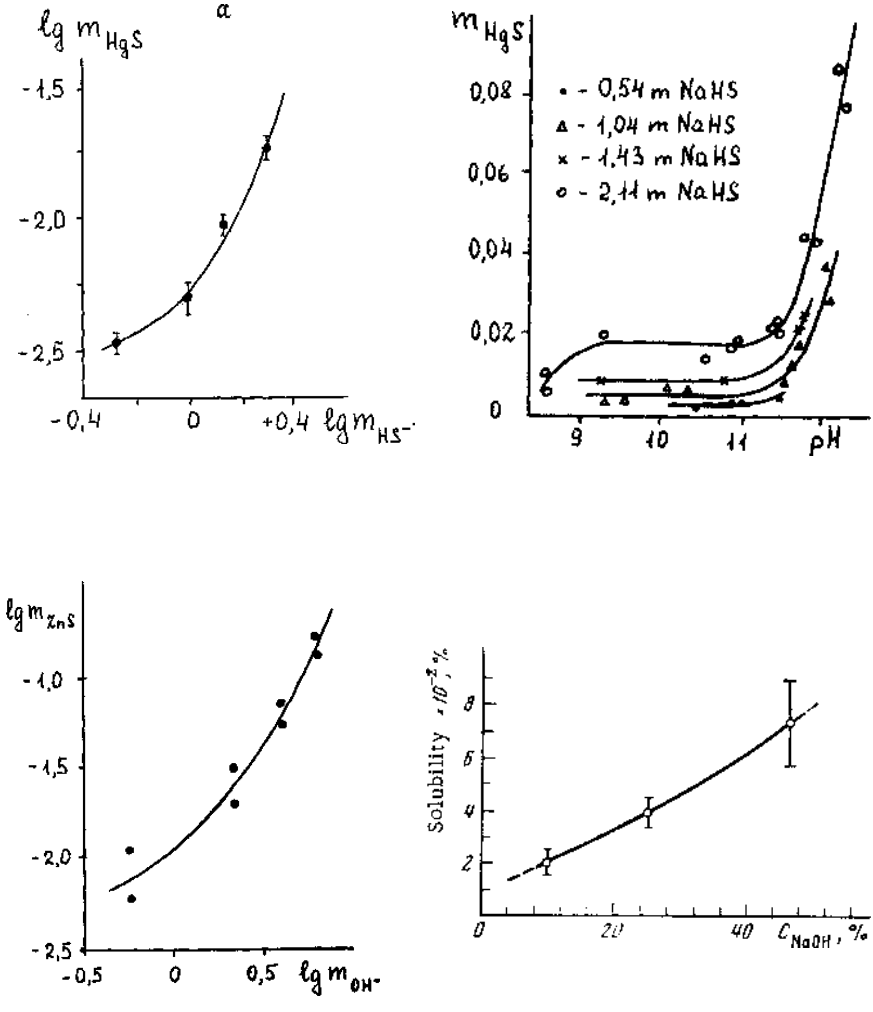

Figures 8.26. Solubility of HgS, ZnS, CdS in KOH and NaOH solutions.[99]

It can be concluded that the dissolution of HgS (in HgS-NaHS-H_2O system) is described by reactions, just as ZnS (in ZnS-KOH-H_2O system) is dissolved by reaction at a low solvent concentration and reaction at a higher one. As a result, the transfer of HgS and ZnS (in low concentrated solutions) takes place in the form of heterocomplexes, and ZnS is transferred in higher concentration solutions by the separated ions ($Zn(OH)_2^{-4}$ and HS^-). These differences are displayed in the kinetics of crystal growth. Figures 8.27*(a)* and *(b)* give examples of the growth rate of HgS and ZnS and its dependence on the solvent concentration.[102][103] From Fig. 8.27*(b)*, one can see that $V_{(III)}$ of ZnS hardly depends on the solvent concentration and remains practically unchanged at C_{KOH} > 20 wt%. The solubility of ZnS under such conditions comes up to ~ 1.5 wt%. The authors associate the unusual situation of ZnS growth with the above specific complex formation in the system ZnS-KOH-H_2O.

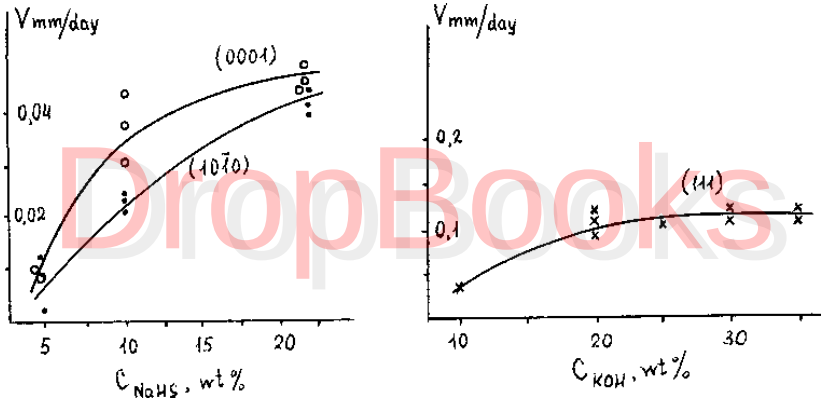

Figure 8.27. Growth rate of HgSd and ZnS and its dependence on the solvent concentration.[102][103]

The interaction of the sulphides with the aqueous solutions can be accompanied by their hydrolysis and redox reactions. In an effort to estimate the stability of the above sulphides under hydrothermal conditions, Kuznetsov (1990) has constructed the theoretical diagrams for Zn-S-H_2O, Cd-S-H_2O, Pb-S-H_2O, Zn-Se-H_2O, Hg-S-H_2O systems with the Eh-pH coordinates at high temperatures.[99] In Fig. 8.28 the upper lines limiting the

stability fields of CdS, correspond to the equilibria of these compounds with the solutions containing the oxidized sulphur; the lowest lines correspond to their equilibria with the solutions, enriched by the reduced forms of the sulphur.

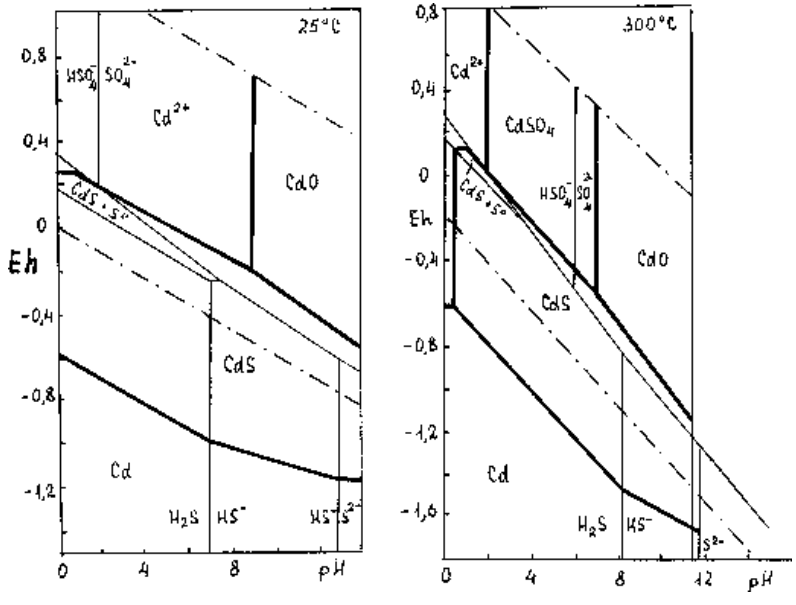

Figure 8.28. Stability fields of CdS.[99]

CdS and ZnS are stable in a wide range of Eh-pH values (from acid to the most alkaline solutions). The fields of the metallic Cd and Zn are located outside the stability field of water, therefore, the "decomposition" reaction of CdS, ZnSe, ZnS can not take place during the usual hydrothermal experiments. Another situation characterizes the Pb-S-H_2O system. Unlike the above sulphides, lead sulphide is unstable at high temperatures in alkaline solutions and the fields of metallic lead appear both at low and high redox potentials.

Among the considered compounds, mercury sulphide has the most narrow field of stability at elevated temperatures which lies inside the water stability field. Moreover, the field of HgS is surrounded by metallic mercury. It means that the insignificant changing of redox potential in the solution can result in the "decomposition" of HgS.

As noted above, the differences in the stability of CdS and ZnS on the one hand, and PbS and HgS on the other hand, are very important for choosing the growth conditions of these substances. It is evident that the stability of CdS and ZnS in a wide range of Eh and pH magnitudes gives the possibility to use various media for its crystallization. In the case of lead sulphide, the growth of crystals in alkaline solutions is only possible in certain interval of Eh values. The narrow field of stability of mercury sulphide makes great demands on growth conditions.

The growth of CdS crystals was realized in acid (H_3PO_4), chlorine (NH_4Cl), and alkaline (KOH, NaOH) solutions. In acid and chloride solutions (H_3PO_4 = 10–30 wt%, NH_4Cl = 1–25 wt%), very intensive transfer of CdS takes place at temperatures above 400°C and spontaneous crystals of about 3–5 mm in size were grown.[101] In alkaline solution, the intensive transfer of the sulphide was observed at higher temperatures (480–500°C), but at lower temperatures partial hydrolysis takes place. At 500°C and KOH, NaOH concentrations of 30–50 wt%, spontaneous CdS crystals reached 10–20 × 0.5–1.0 mm in size.

The intensity of hydrolysis of the sulphides is distinctly inversely proportional to their crystallization. Thus, in KOH solutions, crystallization of CdS takes place stably only at 500°C, and hydrolysis is largely suppressed above 500°C. At 530–535°C, a most intense transfer of the substance from the lower to the upper zone of the autoclave was observed, and circular CdS crystals up to 8–10 mm long are readily formed.

PropBooks

In NaOH solutions, owing to the weaker hydrolysis of CdS and PbS, their crystallization takes place more intensely and at lower temperatures than in KOH solutions. Transfer of considerable amounts of substance takes place, even at 400–450°C. However, as in the case of KOH solutions, maximum transfer of the substance was observed at 500–535°C, when sulphide hydrolysis in NaOH was practically absent.

The properties of crystals obtained in alkaline and acid solutions strongly differ. The hydrothermal method is the only technique to obtain large-size single-crystal cinnabar, HgS. Toudic et al. (1972) obtained large-size HgS crystals using Na_2S solutions at 265°C, considerably below the temperature of the $\alpha \rightarrow \beta$-HgS transition (344°C).[104] These authors have found that, at temperatures above 200°C, cinnabar is unstable in solutions with the high pH values characteristic of Na_2S, hence, it is desirable to crystallize HgS from weak alkaline solutions with lower pH values in which the cinnabar is more stable.

The experiments have been carried out in autoclaves provided with teflon liners. The pressure in these experiments maintained between 100–200 atm, and temperature 230–265°C. The pH is usually maintained at 9–13, ΔT = 28–40°C. The crystals are usually prismatic and often needle-like. The growth rate is nearly 0.1 mm/day in the pinnacoidal face and less than 0.02 mm/day on the prism face. Kuznetsov et al. (1982) have studied in detail the morphological aspects of HgS with reference to the growth conditions.[107]

The sphalerite ZnS crystals grown by different methods differ from one another with reference to the different concentration and, in this respect, the hydrothermal sphalerites are more perfect. The growth of ZnS has been carried out with varying parameters, like temperature, the solvent composition, and pH. The experiments are carried out in autoclaves provided with platinum linings in KOH solutions and the growth temperature varies from 355–400°C; however, the saphalerite crystals of lowest degree of perfection are grown under hydrothermal condition at high temperature (~400°C, Fig. 8.29). Bryatov and Kuzmina (1961) and Ikornikova (1975) have studied the hydrothermal growth of ZnS crystals in acidic chloride solutions.[105][106] When 25 wt% ammonium chloride aqueous solution was used in the experiments, intensive recrystallization of sphalerite takes place at 400°C and ΔT = 2°C. Mininzon et al. (1974) have studied in detail the solubility of sphalerite in phosphoric acid solutions and the morphology of the crystals. It is interesting to note that the solubility of sphalerite is highest in phosphoric acid solutions.[107]

Figure 8.29. Spahalerite crystals grown under hydrothermal conditions.[99]

Greigite, Fe_3S_4, has been synthesized under hydrothermal conditions using Na_2S solution.[108] Mohr's salt solution is mixed with Na_2S solution at room temperature, black particles of iron sulphide precipitates. When they are heated together with the mother solution in a vessel, greigite

(Fe_3S_4, cubic) forms. The optimum heating temperature for preparing greigite depends on the pH of the solution; it is about 180°C for a solution with pH 9 and lowers to 80°C with a decrease in pH. Above these temperatures, greigite particles disappear by decomposition and alternatively, pyrrhotite (Fe_1-XS_1 hexagonal) or pyrite (FeS_2, cubic) forms, depending on the pH of the solution.

8.11.3 Hydrothermal Synthesis of Complex Sulphides

The complex sulphides include compounds containing multiple cations. The difficulties in obtaining these complex sulphides are connected to the existence of a large number of stable phases in these systems; hence, the earliest hydrothermal experiments usually do not cover these complex sulphides. However, in the last few decades much work has been done on the synthesis of these natural analogs of complex sulphides.[109] For obtaining these complex sulphides with 100% output, synthesis through ion exchange reactions is the most useful technique. The more complex the cationic composition, the more difficult it is to fix the stoichiometry of the nutrient material. Under such circumstances, the trial and error experiments are more useful.

DropBooks

8.11.4 Hydrothermal Synthesis of Chalcohalides

The chalcohalides include very complex inorganic compounds in which the sulphide and halogenides simultaneously go as anions in their composition. The interest in these compounds is connected to the photosemiconductor and piezoelectric properties. Hydrothermal synthesis of chalcohalides of type ABC, where A = Sb, Bi; B = S, Se, Te; C = Br, I, have been carried out by several authors.[110]–[113] The principal experimental difficulty arising while studying the conditions of synthesis of the ternary chalcohalides A^{v} B^{vi} C^{vii} under hydrothermal conditions lies in creating conditions that would eliminate the possibility of oxidation or, in other words, it is essential that the original components would have the valence state A^{3+} B^{2-} C^{1-} in the solution. However, a specific value of the redox potential is merely necessary, not a sufficient condition for the synthesis of A^{v} B^{vi} C^{vii}. The probability of the formation of any of these compounds will be determined by the concentration of the original components as well as the pH of the medium, and the presence of a halogen.

Eq. (33) $Sb + 4HI \rightarrow [SbI^{-}_{4}] + 2H_2 \uparrow$

Eq. (34) $2\,[SbI^{-}_{4}] + 4[H_2S] \rightarrow [Sb_2I_2(H_2S)^4{}_{-4}] + 6I$ } pH < 6

Eq. (35) $[Sb_2I_2(H_2S)^4{}_{-4}] \rightarrow 2SbSI + 2H_2S + 2H_2\uparrow$

Eq. (36) $Sb + 4HI \rightarrow [SbI^{-}_{4}] + 2H_2\uparrow$

Eq. (37) $[SbI^{-}_{4}] + 2[HS^{-}] \rightarrow [SbS^{-}_{2}] + 2I + 2HI$ } pH = 7–10

Eq. (38) $Sb + 2[HS^{-}] \rightarrow [SbS^{-}_{2}] + H_2\uparrow$

Eq. (39) $2[SbS^{-}_{2}] + 4[HS^{-}] \rightarrow 2Sb_2S_3 + 2H_2S\uparrow$

Eq. (40) $Sb + 2[HS^{-}] \rightarrow [SbS^{-}_{2}] + H_2\uparrow$

Eq. (41) $2[SbS^{-}_{2}] + 4[HS^{-}] \rightarrow 2Sb_2S_3 + 2H_2S\uparrow$ } pH > 10

Eq. (42) $2[SbS_2] + [S^{2-}] \rightarrow Sb_2S_3 + 2S$

Hence, SbSI will chiefly be formed in solutions with pH < 7. The range of formation of SbSI in solutions with low pH values may be associated with the stability of a hypothetical complex of the $[Sb_2I_2(H_2S)^4{}_{-4}]$ type, which may be formed as a result of an interaction between the two genuinely existing complexes. The $[SbS^{-}_{2}]$ is well-known to be a stable ion interacting with other sulphide complexes; it necessarily leads to the formation of Sb_2S_3. Popolitov and Plakhov (1990) have synthesized $Pb_5S_2I_6$ single crystals in the system Pb-S-I-R-H_2O (R = solvent) under hydrothermal conditions.[112] The experiments were carried out in teflon lined autoclaves at 200–300°C with a temperature gradient of 0.6–1.8°C/cm. Figure 8.30 shows a photograph of $Pb_5S_2I_6$ single crystals.[112] Note that $Pb_5S_2I_6$ belongs to the monoclinic system and the phase transition occurs at 290 ±5°C. Rabenau and Rau (1969) have reported the growth of $Pb_7S_2Br_{10}$ single crystals.[113] The typical experimental conditions are T = 300–450°C, liquid S pressure (2.02–20.2) 107 Pa, ΔT = 0.4–1.6°/cm. Elemental Pb and S, liquid Br_2, $PbBr_2$, and PbS, in various molar ratios were used as starting materials.

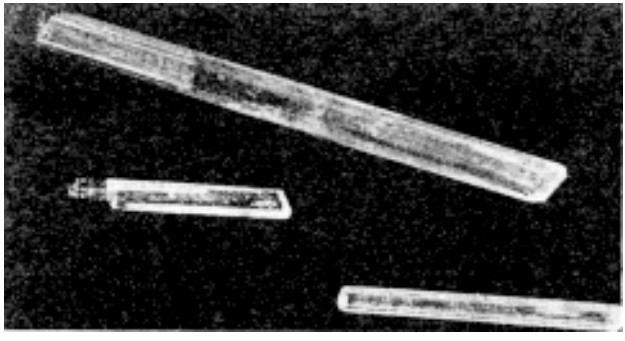

Figure 8.30. Photograph of $Pb_5S_2I_6$ single crystals.[112]

The method of producing arsenic and bismuth sulphohalides differs very little from that producing the corresponding antimony sulphohalides. Above 200°C, the arsenic varieties are characterized by the "igneous" melting of the charge as a result of which a reddish-brown viscous liquid is formed. In experiments at about 300°C, the liquid turns into a vitreous mass on cooling and this is amorphous with reference to x-rays. The important chalcohalides obtained by the hydrothermal technique are SbSI, SIAs, and BiSI.

DropBooks

8.12 HYDROTHERMAL SYNTHESIS OF SELENIDES, TELLURIDES, NIOBATES AND TANTALATES

Selenides and tellurides are popularly grown by two methods: melt and hydrothermal. Although the melt method has been used as the main one for preparing single crystals of selenides and tellurides, some of these belong to the group of minerals which have been deposited in nature under hydrothermal conditions. Among the selenides and tellurides, HgSe, ZnSe, CdSe, HgTe, ZnTe, CdTe, $FeTe_2$, $FeSe_2$, $NiSe_2$, $NiTe_2$, $CoSe_2$, CoTe, Sb_2Se, Bi_2Se_3, Bi_2Te_3, and Sb_2Te_3, are the most popular ones.[99][115]–[117] Their stability range, within a wide interval of pH and Eh values, allows one to use various solutions for crystallization and to investigate the influence of physicochemical conditions on the properties of crystals. In fact, several solutions have been proposed, and the most commonly used ones are the alkaline solutions (5M NaOH, for ZnSe, 1M NaOH or KOH for ZnTe, and 20M NaOH or KOH for CdSe and CdTe).

Polycrystallization HgSe and HgTe or elements in stoichiometric proportions are used as the starting materials. The temperature of growth is 350–380°C, P = 1000 to 2000 atm.[118] Several experiments have been carried out in acid media (HCl and HBr) in vitreous silica ampoules. Rau and Rabenau (1967) have used CO_2 pressure balance gas by pumping CO_2 from a cylinder with a high-pressure intensifier into the autoclave at room temperature.[118] In seeded growth, the temperature gradient was usually 25°C. Figure 8.31 shows the morphology of ZnSe in NaOH and LiOH solutions. The chemical reactions responsible for the crystallization of HgSe and HgTe, for example, can be written as follows:

Eq. (43) $\quad HgSe + 2HCl \rightarrow H_2Se + HgC_{12}$

Eq. (44) $\quad HgTe + 2HCl \rightarrow H_2Te + HgCl_2$

Table 8.5 gives the optimum conditions for the crystallization of HgSe and HgTe.

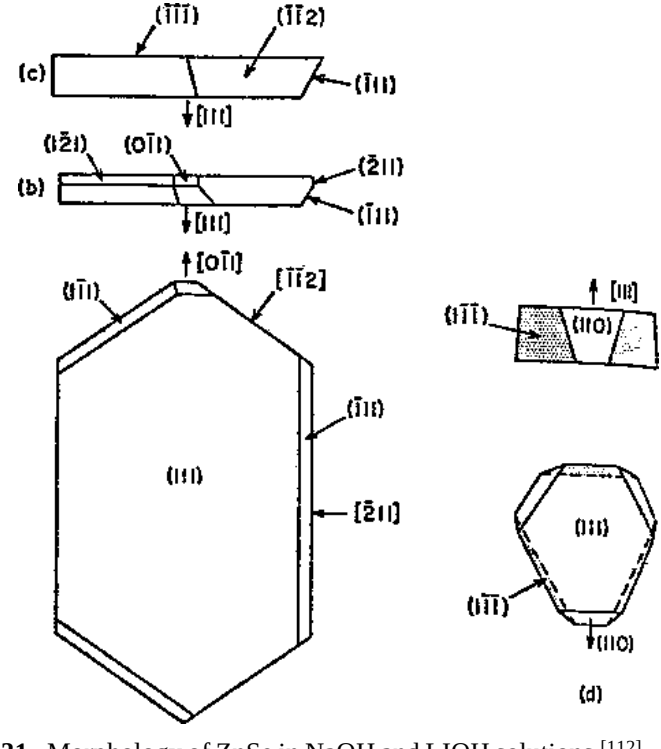

Figure 8.31. Morphology of ZnSe in NaOH and LIOH solutions.[112]

Table 8.5. Optimum Experimental Conditions of Crystallization of HgSe and HgTe[112]

T (°C)	Δ*T* (°C)	Fill (%)	Experimental duration (days)	HCl Concentration (M)	Transport of nutrient (%)
300	100	82.92	7	12	64
316	78	82.92	10	12	82
318	82	83.34	12	12	100
300	50	85.3	6	12	22.5
350	50	80.43	6	12	29

In the hydrothermal synthesis of $FeTe_2$, $FeSe_2$, $NiSe_2$, $NiTe_2$, $CoSe_2$, and $CoTe_2$ crystals, Na_2Se and Na_2Te are used as the nutrient materials. The synthesis of diselenide and ditelluride of Ni and Co is carried out in quartz ampoules, whereas the synthesis of diselenide and ditelluride of iron is carried out in titanium ampoules or liners.

The physical properties of these hydrothermal selenides and tellurides are much superior as they are grown in the controlled atmosphere.

DropBooks

The hydrothermal growth of niobates and tantalates began during the 1960s, at the time when the hydrothermal synthesis of inorganic compounds without natural analogs was extremely popular. The interest in niobates and tantalates is connected to their excellent ferroelectric and piezoelectric properties. In fact, the hydrothermal method is the only perspective method of obtaining the monocrystals of niobates and tantalates. Compared to the majority of the inorganic compounds, these materials have very low solubility. In aqueous solutions, both the elements form the polymeric oxyanions of type $[H_2Nb_6O_{19}]^{6-}$, $[HNb_6O_{19}]^{7-}$, $[Nb_6O_{19}]^{8-}$, $[Ta_6O_{19}]^{6-}$, etc., however, most of these polymeric oxyanions are not stable and, with the variation in pH and with an increase in the growth temperature, they form hydrated pentoxides. These complexes are readily soluble in strong hydrofluoric acid or strong alkaline solutions.[119][120] In weak acidic solutions, the formation of anions like $[NbOF_6]^{3-}$ and $[TaOF_6]^{3-}$ takes place, so that the synthesis of niobates and tantalates is possible, always within limited and narrow boundaries; thus, the synthesis of these compounds is always a challenging one. Marshall and Laudise (1967) have studied the systems K_2O-Ta_2O_5-H_2O and K_2O-Nb_2O_5-H_2O at 400°C and ~ 560 atm.[121] Mixed crystals of $K(Ta, Nb)O_3$ have been grown on a

seed crystal. The rates of growth of the face reached 0.25 mm/day in 15 M KOH at 650°C, ΔT = 40°C, and ~1100 atm.[100] $K(Ta, Nb)O_3$ crystals with dimensions of up to 1 cm were grown. Rare earth orthotantalates, $LnTaO_4$ (Ln = La-Lu) have been obtained at T = 1500°C, $P = 8 \times 10^9$ Pa. These are the high temperature and pressure compounds and exhibit intense polymorphism.[122]–[124]

The discovery of piezo- and ferroelectric properties in the natural mineral stibiotantalite generated a great interest in obtaining a series of synthetic monocrystals of the group ABO_4, where A = Sb, Bi; B = Nb, Ta, Sb^{5+}. Their structures are made up of weakly formed oxygen octahedra and, in the middle of these octahedra, the cations A and B are located. These crystals can be obtained essentially by the hydrothermal technique. Although, some attempts have been made to obtain these crystals by other techniques like flux and melt, good quality crystals are obtained only by the hydrothermal technique.

The hydrothermal growth technology for ABO_4 crystals has been worked out in great detail by Popolitov. Usually, alakaline solutions like MOH, MF, MHF_2, or H_2O_2 (where M = Li, Na, K, Rb, Cs) are used as mineralizers in the hydrothermal growth of these crystals. The growth of these compounds is carried out in the systems A_2O_3-B_2O_5-R-H_2O and ABO_4-R-H_2O (where R = LiF, NaF, KF, RbF, CsF). The crystallization depends upon the growth temperature, temperature gradient, type and concentration of alkali solutions, ratio of the nutrient components, and a series of other parameters.

According to the authors, Nb_2O_5 or Ta_2O_5 exists in the alkaline solutions as hydroxyl complexes like $[Nb_6(OH)_{38}]_{8-}$ or $[Ta_6(OH)_{38}]^{8-}$.[125] They have the following structural form:

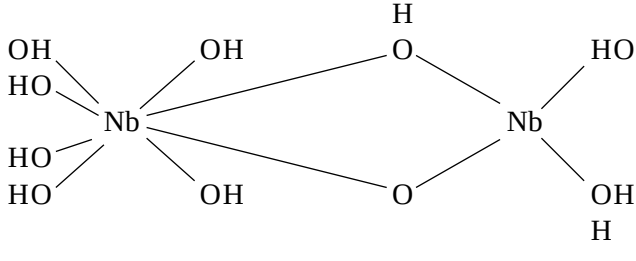

The bonding between the individual atoms of metals in such a structure is obtained through OH-bridging which is necessary for the formation of the polymerized solutions. The entire Nb or Ta is bonded in the above form to develop $SbNbO_4$ or $SbTaO_4$.

The composition of these single crystals shows that under distinct concentrations of aqueous solutions KF, RbF, CsF, there occurs the breaking of valent bonds $Nb(Ta)F_7$. These complexes, in turn, combine with the alkali cations to form $Me_2Nb(Ta)F_7$. The thermal hydration is different for different salts. MeF and the aqueous solutions of KF, RbF, and CsF, consisting of larger cations, are less hydrated. Under higher concentration of aqueous solutions of (K, Rb, Cs)F, the activity of the free ions of F is so high that it forms valent bond with Nb(Ta)-O, resulting in the formation of $Me_2Nb(Ta)F_7$. These studies show that the ability to dissolve the Nb_2O_5 or Ta_2O_5 and Sb_2O_3 increases as follows: LiF → NaF → CsF → RbF → KF; therefore, the crystallization of ABO_4 crystals depends upon the solvent-solute interaction under hydrothermal conditions.

When CO_3 or C_2O_4 is introduced, in the form of potassium carbonate and potassium oxalate, into the mineralizer solutions (aqueous solutions) it was found that the formation of $Nb(Ta)F_7$ becomes very simple and effective because the anions CO_3 and C_2O_4, with their larger size, strongly polarize the Nb(Ta) in the solution. It can be explained through the following reactions:

DropBooks

Eq. (45) $Nb_2O_5 + 15KF + 7H_2O \rightarrow 2(NbF_7)^{2-} + 15K^+ + 12OH^- + 2H^+ + F^-$

Eq. (46) $2[NbF_7]^{2-} + 5[CO_3]^{2-} + H_2O \rightarrow Nb_2(CO_3)_5 + OH^- + H^+ + 14F^-$

Eq. (47) $Nb_2(CO_3)_5 \rightarrow Nb_2O_5$ (solution) $+ 5CO_2$

When KHF_2 mineralizer (5 wt%) was used at T = 530°C and ΔT = 40°C, good single crystals of ABO_4 could be obtained. An increase in the concentration of KHF_2 in the system and change in the molar ratio of Sb_2O_3/Nb_2O_5 lead to the crystallization of intermediatory phases like $K_2SbNb_5O_{15}$. The hydrogen peroxide fulfills the following function: it increases the oxidation potential in the given system, it stabilizes the soluble form of Nb^{5+}, and leads to the transition of less soluble Nb_2O_5 in the solution, consequently, the formation of peroxide complexes takes place.[126]

The growth of $BiNbO_4$ has been carried out in the system Bi_2O_3-Nb_2O_5-H_2O using solvents like KHF_2 and H_2O_2. Figure 8.32*(a)* shows the growth temperature dependence of the crystal output of $BiNbO_4$ and Fig. 8.32*(b)* shows the NC-diagram of fields of crystallization. The hydrothermal crystallization of the ABO_4 crystals can be carried out in an acidic

media, for example, in the system A_2O_3-B_2O_5-H_2SO_4-H_2SO_4-H_2O_2-H_2O within a wide range of concentrations of aqueous solutions and sulphuric acid [$C_{H_2SO_4}$ = 10–15 wt%, C_{H_2O} = 5–6 wt%] and the volume ratio $V_{H_2SO_4}/V_{H_2O}$ = 2.5:1.[127]

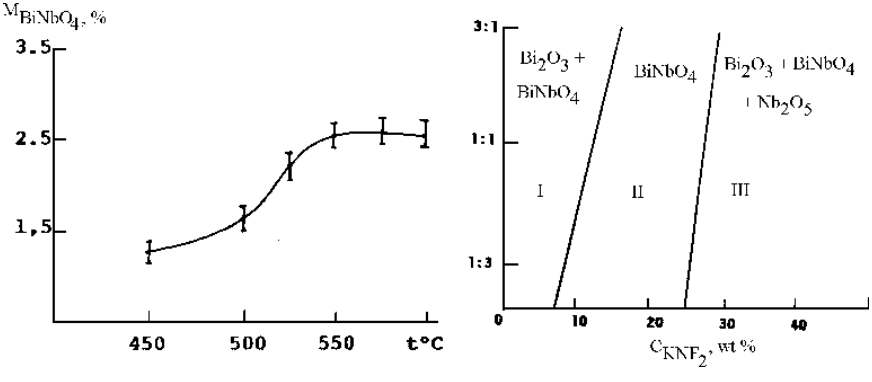

(a) (b)

Figure 8.32. *(a)* Dependence of the growth temperature and crystal output of $BiNbO_4$; and *(b)* the NC-diagram of fields of crystallization of $BiNbO_4$.[127][128]

There are several publications on the hydrothermal growth of Bi and Sb niobates, and tantalates. These compounds strongly decompose at higher temperatures and, hence, the flux or melt techniques are not suitable to grow these compounds; and obviously, the hydrothermal method was found to be the most suitable one.[128]–[130] The synthesis is carried out in two types of solvents: *(i)* in aqueous solutions of alkali metals, LiOH, NaOH, and KOH, *(ii)* in aqueous solutions of alkali fluorides, Li to Cs. The autoclaves used for the synthesis of these bismuth and antimony niobates and tantalates are provided with copper, silver or titanium linings. The growth takes place at T = 450–650°C, and ΔT = 15–30°C. The nutrient materials are the mixtures of Sb_2O_3 and Nb_2O_5 (Ta_2O_5). The analysis of the products of hydrothermal reaction shows that the alkali solutions bring in the reaction $2MeOH + Sb_2O_3 + 2Nb_2O_5 \rightarrow 2SbNbO_4 \downarrow + 2Me\ NbO_3 \downarrow + H_2O$.

Synthesis in strong fluoride solutions KF, RbF, and CsF increases the growth rate, however, further increase in the concentration of F leads to the formation of fluoroniobates and fluorotantalates of alkali metals: Me_2NbF_7 and Me_2TaF_7. Obviously, such concentrated solutions do not give 100% niobates and tantalates of Bi and Sb. It has been found that in aqueous solution of KHF_2, even the formation of complex niobate $K_2SbNb_2O_{15}$ takes place.

Thus, the hydrothermal method is a most valuable tool for the synthesis of a variety of simple and complex niobates and tantalates. However, a complete understanding of the growth technology for these compounds insists on systematic investigations of various aspects of the growth parameters, like temperature, pressure, pH, type of nutrient, and solvent.

8.13 HYDROTHERMAL SYNTHESIS OF ARSENATES

Arsenates are closer to phosphates and vanadates in their mineralogy and crystal chemistry. There are several arsenate minerals occurring in nature, like mimetite, (PbCl) Pb_4 $(AsO_4)_3$, tilasite (MgF) $CaAsO_4$; adelite [(MgOH)$CaAsO_4$], sarkinite [(MnOH) $MnAsO_4$], olivenite [Cu_2(OH) AsO_4], adamite [Zn_2(OH)AsO_4], clinoclasite ($6CuO{\cdot}As_2O_3{\cdot}3H_2O$), soselite $(Ca,Co,Mg)_3$, $As_2O_8{\cdot}2H_2O$, and so on. However, the number of arsenate minerals is much less than the number of vanadates and phosphates. The same is the case with reference to the synthetic analogs, i.e., the number of synthetic arsenates is much less than the number of synthetic phosphates and vanadates. Hence, in comparison with the rich structural chemistry of transition metal phosphates, reports on the arsenates are rare. Although a few arsenates have stoichiometries similar to those of the phosphate analogs, their structures are considerably different. Most of these arsenates adopt new structural types and have stoichiometries not found in the phosphates. The hydrothermal technique helps immensely to obtain new structures among arsenates. Some of the arsenates synthesized belong to the NASICON family ($Na.Zr_2(AsO_4)_3$; $A^{2+}B^{2+}As_2O_7$ (A = Ca, Sr, Ba; B = Cu), both exhibiting superionic properties, $NaNb_2AsO_8$ with nonlinear optical properties, $ABXO_4$ type [A = Mn, Zn, Cu^{2+}, Co^{2+}, Mg^{2+}, etc.; B = (OH); X = As], several complex arsenates showing unique structures related to geolites. In spite of a wide structural diversity, the hydrothermal synthesis of arsenates is not very

PrOOBooks

popular owing to the best known reasons, that arsenic is highly corrosive and highly reaction susceptible. Also, it contaminates the system unless the experiments are carried out at $T < 300°C$ using teflon liners.[132]–[136]

The majority of experiments in recent years have been carried out in stainless steel autoclaves provided with teflon lining. However, the high temperature experiments, like in the case of $NaNb_2AsO_8$, are carried out in sealed gold liners, at $T = 750°C$ and $P = 32{,}000$ psi.

For example, the copper diarsenates ($ACuAs_2O_7$, A = Ca, Sr, Ba) synthesis has been carried out in teflon-lined autoclaves at 230°C for four days, followed by a slow cooling to room temperature at 50°C/hr. The pure phase is obtained by heating a mixture of $Me^{2+}(OH)_2$ (Me^{2+} = Ca, Sr, Ba), CuO, KCl, H_3AsO_4, pyridine and water, in the following molar ratios:

$Ca^{2+} : Cu : As = 1:2:7.5$

$Sr^{2+} : Cu : As = 1:4:15$

$Ba^{2+} : Cu : As = 1:2:7.5$

The crystal chemical study of these $A^{2+}B^{2+}As_2O_7$ compounds shows that the As_2O_7 group is very adaptive to the bonding requirements of other groups in the structure by adjusting the As-O-As bond angle and the torsional angle between the two AsO_4 tetrahedra. The size of the alkali-earth metal cation seems not to play an important a role in deciding the structural types of the arsenates as it does on the corresponding phosphates.

The complex arsenates, like $(Mg,Ni)_2(OH)(AsO_4)$, could be prepared using hydrothermal conditions and starting from the $(Mg_{3-x}Ni_x)(AsO_4)_2.8H_2O$ (X = O, O.5) precursors. The starting compounds were at 180°C in a teflon-lined steel autoclave 90% filled.[132]

Chou and Kanatzidis (1996) have synthesized the novel type of transition and main group metal polychalcogenides, and some of them are inaccessible by traditional solution methods.[137] These authors have used organic counter-ions $R4E^+$ (E = P, R = Ph; E = N, R = alkyl) to synthesize these polychalcoarsenates.

With the recent discovery of several nonlinear optical properties among arsenates, like in KTiOAsO4, there is a growing interest for new NLO materials from the arsenate family.[138] Among these, $NaNb_2AsO_8$ is an important material showing a great promise as second harmonic generator material.[136]

Thus, the growth of complex coordinated compounds like sulphides, selenides, tellurides, and arsenates under hydrothermal conditions, is very important.

REFERENCES

1. Kaminskii, A. A., Verdun, G. R., and Khaidukov, N. M., New CW-laser Crystals with Semiconductor Laser Pumping in Anisotropic Fluorides Containing Nd^{3+} Ions, Obtained by Hydrothermal Method, *Doklady Akad. Nauka, Physika*, 328:181–195 (1993)
2. Demianets, L. N., Hydrothermal Synthesis of New Compounds, in: Hydrothermal Growth of Crystals (K. Byrappa, ed.), *Prog. Crystal Growth Charact.*, 21:299–355 (1990)
3. Bridenbaugh, P. M., Eckert, J. O., Nykolak, G., Thomas, Wilson, W., Demianets, L. N., Riman, R. E., and Laudise, R. A., Hydrothermal Growth and Properties of $KGdF_4$, *J. Crystal Growth*, 144:243–252 (1994)
4. Kaminskii, A. A., Mironov, V. S., Bagaev, S. N., Khaidukov, N. M., Joubert, M. F., Jacquier, B., and Boulon, G., Spectroscopy and Laser Action of Anisotropic Single-Centered $LiKYF_5:Nd^{3+}$ Grown by the Hydrothermal Method, *Phys. Stat. Sol. (a)*, 145:177–195 (1994)
5. Kaminskii, A. A., *Laser Crystals, Their Physics and Properties*, Springer-Verlag, Berlin/Heidelberg/New York/London/Paris/Tokyo (1981, 1990)
6. Weber, M. J., (ed.), *Handbook of Laser Sciences and Technology, Supply, 1*, CRC Press, Boca Raton/Ann Arbor/Boston (1991)
7. Kaminskii, A. A., Sarkisov, S. E., Kurbanov, K. A., Demianets, L. N., and Khaidukov, N. K., *Inorganic Materials*, 23:2049–2054 (Russian) (1987)
8. Kaminskii, A. A. and Khaidukov, N. M., *Phys. Stat. Solidi. (a)*, 129:K65 (1992)
9. Kaminskii, A. A. and Khaidukov, N. M., *Kvantovaya Electronika*, 19:213 (1992)
10. Kaminskii, A. A., Khaidukov, N. M., Koechner, W., and Verdun, H. R., *Phys. Stat. Solidi. (a)*, 132:K105 (1992)
11. Iljushin, L. N., Demianets, L. N., and Sorokin, N. I., in: *Collected Abstracts Internat. Symposium on the System with Fast Ion Transport*, Czechoslovakia, Prague, p. 162 (1985)
12. Yakubovich, O. V., Simonov, M. A., Melnikov, O. K., and Urusov, U. S., *Dokl. Akademy Nauk USSR* (in Russian), 287:126 (1986)
13. Dunin-Barkovskii, R. L., Kolyago, S. S., Pestryakov, E. V., and Razheu, A. M., in: *7th USSR Conference on Crystal Growth, Moscow, Collected Abstracts* (in Russian), 2:166 (Nov. 14–19, 1988)

DropBooks

14. Belov, N. V., Golovastikov, N. I., Ivaschenko, A. N., Kotjuzanskii, B. Ya., Melnikov, O. K., and Filippov, V. I., *Kristallografiya (in Russian),* 27:511 (1982)

15. Matvienko, E. N., Yakubovich, O. V., Simonov, M. A., Ivaschenko, A. N., Melnikov, O. K., and Belov, N. V., *Dokl. Akademii Nauk USSR (in Russian),* 257:105 (1981)

16. Crosnier-Lopez, M. P., Laligand, Y., and Fourquet, J. L., A New Barium Tantalum Oxyfluoride $Ba_3Ta_2F_{12}$, Structural Approach, *Eur. J. Solid State Inorg. Chem.,* 30:155–163 (1993)

17. Ferey, G., Leblanc, M., de Pape, R., Passaret, M., and Bothorel-Razazi, M. P., Cristallisation par voie hydrothermale des Fluorures FeF_3; FeF_3H_2O; $FeF_3.3H_2O$ and NH_4FeF_4, *J. Crystal Growth,* 29:209–211 (1975)

18. Ravez, J. M., Viollet, J., dePape, R., and Hogenmuller, P., *Bull. Soc. Chim. Fr.,* 4:1325 (1967)

19. Leblanc, M., Ferey, G., and dePape, R., Hydrothermal Synthesis of Transition Metal Fluorides in Binary, Ternary, and Quaternary Systems, *Mat. Res. Bull.,* 19:1581–1590 (1984)

20. Belov, N. V., Golovastikov, N. I., Ivashchenko, A. N., Kotyuzhanskii, B. Ya., Mel'nikov, O. K., and Filippov, V. I., Hydrothermal Synthesis Crystal Structure and Magnetic Properties of $Cs_2FeF_5.H_2O$, *Sov. Phys. Crystallogr.,* 27:309–311 (1982)

21. Leblanc, M., Ferey, G., Calage, Y., and de Pape, R., *J. Solid State Chem.,* 53:360 (1984)

22. Verschaeren, W. and Babel, D., *J. Solid State Chem.,* 24:405 (1978)

23. Courbion, G., Jacoboni, C., and dePape, R., *Acta Cryst. B,* 33:405 (1977)

24. Jacoboni, C., *These d'Etat Paris VI* (1976)

25. Mercier, N. and Leblanc, M., Crystal Growth and Structures of Rare Earth Fluorocarbonates: II; Structures of Zhonghuacerite $Ba_2Ce(CO_3)_3F$; Correlations Between Huanghoite, Cebaite, and Zhonghuacerite Type Structures, *Eur. J. Solid State Inorg. Chem.,* 30:207–216 (1993)

26. Mercier, N. and Leblanc, M., A Scandium Fluorocarbonate, $Ba_3Sc(CO_3)F_7$, *Acta Cryst.,* 50:1862–1864 (1994)

27. Mercier, N. and Leblanc, M., A New Rare Earth Fluorocarbonate, $Na_2Eu(CO_3)F_3$, *Acta Cryst.,* 50:1864–1865 (1994)

28. Mercier, N., Taulelle, F., and Leblanc, M., Growth, Structure NMR Characterization of a New Fluorocarbonate $Na_3La_2(CO_3)_4$ F., *Eur. J. Solid State Inorg. Chem.,* 30:609–617 (1993)

29. Mercier, N. and Leblanc, M., Synthesis Characterization and Crystal Structure of a New Copper Fluorocarbonate $KCu(CO_3)F$., *Eur. J. Solid State Inorg. Chem.,* 31:423-430 (1994)

30. Mercier, N. and Leblanc, M., Crystal Growth and Structures of Rare Earth Fluorocarbonates: I. Structures of $BaSm(CO_3)_2$ F and $Ba_3La_2(CO_3)_5F_2$: Revision of the Corresponding Huanghoite and Cebaite Type Structures, *Eur. J. Solid State Inorg. Chem.*, 30:195–205 (1993)

31. Mercier, N. and Leblanc, M., Existence of 3d transition metal fluorocarbonates: Synthesis characterization of $BaM(CO_3)F_2$ (M = Mn, Cu) and Crystal Structure of $BaCu(CO_3)F_2$, *Eur. J. Solid State Inorg. Chem.*, 30:217–225 (1993)

32. Lablanc, M., Fevre-Collin, I., and Ferey, G., The Magnetic Structures of Mn_2PO_4F and Co_2PO_4F at 1.2 K, *J. Magnetism and Magnetic Materials*, 167:71–79 (1997)

33. Loiseau, Th., Calage, Y., Lacorre, P., and Ferey, G., NH_4FePO_4F: Structural Study and Magnetic Properties, *J. Solid State Chem.*, 111:390–396 (1994)

34. Mercier, N. and Leblanc, M., *Eur. J. Sol. State Inorg. Chem.*, 28:727–736 (1991)

35. Crosnier, M. P. and Fourquet, J. L., *Eur. J. Solid State Inorg. Chem.*, 29:199 (1992)

36. Crosnier-Lopez, M. P., Laligand, Y., and Fourquet, J. L., A New Oxyfluoride $Ba_3Ta_2O_2F_{12}$: Structural Approach, *Eur. J. Solid State Inorg. Chem.*, 30:155–163 (1993)

37. Crosnier-Lopez, M. and Fourquet, J. L., Synthesis and Crystal Structure of $Ba_4Nb_2O_3F_{12}$, *Eur. J. Solid State Chem.*, pp. 103–138 (1993)

38. Crosnier-Lopez, M. and Fourquet, J. L., $Ba_3Nb_2O_2F_{12\cdot2}H_2O$: Synthesis and Crystal Structure, *J. Solid State Chem.*, 105:92–99 (1993)

39. Barta, C., Gilar, O., Krcova, E., Lead Halide Crystal Growth., *Chem. Abstr.*, 109:220138K (1988)

40. Nikolskaya, O. K. and Demianets, L. N., Hydrothermal Synthesis of α-PbF_2 Single Crystals, Izvestia Akad. Nauk USSR, *Inorg. Mater.*, 30:1097–1102 (1994)

41. Caruba, R., Baumer, A., Methode d'Obtention de Nin, Raux de Dungstene (Husbnarit, Ferberite et Scheelite), in: *8 Reen Annu. Sci. Terre*, Marseille, p. 1980 (1960)

42. Malyavka, A. G., Lavrinenko, L. I., Seistunova, T. B., and Kolyatkevich, I. R., Investigations of the Influence of Composition Ore Forming Solutions on the Physical Properties of Ferferite, in: Use of Mineralogical Method of Investigations, *Soviet. Alma-Ata*, 2:63–54 (1981)

43. Yastrebova, L. F., Borina, A. F., and Ravich, M. I., Solubility of Molybdate and Wolframite in Aqueous Solutions of Chlorides of Potassium and Sodium at High Temperatures, *J. Inorg. Chem.*, 8:208–217 (1963)

DropBooks

44. Kharchenko, L. Yu., Protasova, V. I., and Gainatutbinova, R. L., Synthesis and X-ray Characteristics of Basic Rare Earth Wolframite Crystals of Yttrium Group., *J. Inorg. Chem.,* 25:851–852 (1980)

45. Kharchenko, L. Yu., Klevstov, P. V., and Solov'eva, L. P., Crystallization Wolframite Chloride, $LnWO_4Cl$ (Ln = Ce, Pr, Nd), *Doklad. Akad. Nauk USSR.,* 176:179 (1967)

46. Oishi, S. and Tate, I., Some Effects of R (R = Li, Na and K) Ions on Crystal Growth of RNd $(WO_4)_2$ Crystals from Ternary Systems Nd_2O_3 - WO_3 - R_2CO_3, *Chem. Letts.,* 1449–1452 (1980)

47. Klevstov, P. V., Kharchenko, L. Yu., Hydrothermal Synthesis of Crystals and Crystallografic Elucidation of Some Double Wolframites of Rare Earth Elements, in: *Crystal Growth,* 7:333–337, Nauka, Moscow (1967)

48. Kharchenko, L. Yu., Klevstov, P. V., Hydrothermal Synthesis in Some Chloride Systems Containing Oxides of Pr and W., *Kristallografia,* 14:1117–1119 (1969)

49. Kharchenko, L. Yu., Polyanskaya, T. M., and Klevstov, P. V., Synthesis and Crystallographic Studies of Oxywolframites $Pr_4W_3O_{15}$ and $Nd_4W_3O_{15}$, Izvestia Akad, Nauk USSR, *Inorg. Mater.,* 6:1720–1722 (1970)

50. Kharchenko, L. Yu. and Klevstov, P. V., Hydrothermal Synthesis of Wolframites Sm, Eu, and Gd, Izvestia Akad, Nauk USSR, *Inorg. Mat.,* 6:594–596 (1970)

51. Klevtsov, P. V., Kozeeva, L. P., and Klevtsova, P. V., Synthesis and Polymorphism of Crystals of Rubidium - Lanthanum Tungstate $RbLa(WO_4)_2$, *Sov. Phys. Crystallogr.,* 21:54–58 (1976)

52. Oishi, S., and Tate, I., *Crystal Growth of Na(La, Nd) $(WO_4)_2$* Solid Solution from High-Temperature Solutions, *Chem. Letts.,* 1227–1228 (1980)

53. Postupaeva, A. G., Petrov, L. L., Nikhtyanova, D. D., and Kharchenko, L. Yu., Morphology of Epitaxial Layers of Double Alkali Rare Earth Tungstates, *Inorg. Mat.,* 28:1191–1196 (1992)

54. Byrappa, K. and Jain, A., Hydrothermal Growth and Characterization of $NaLa(WO_4)_2$ Crystals, *J. Mater. Res.,* 11:2869–2875 (1996)

55. Carobbi, G. and Tancredi, G., *Gass. Chim. Ital.,* 58:45 (1928)

56. Chichagov, A. V., Demianets, L. N., Ilyukhin, V. V., and Belov, N. V., *Synthesis and Structure of Cd-Molybdate, $CdMoO_4$,* 11:686–689 (1966)

57. Protasova, V. I., Kharchenko, L. Yu., and Klevstov, P. V., Hydrothermal Synthesis and Crystallographic Properties Hydroxy Molybdates Rare Earth Elements $LuMoO_4$.OH, Izvestia Akad. Nauk USSR, *Inorg. Mater.,* 9:421–423 (1973)

58. Polyanskaya, T. M., Borisov, S. V., and Belov, N. V., New Modification of Structure Type Scheelite - Crystalline Structure Nd_2WO_6, *Doklady Akad. Nauk USSR,* 193:83–86 (1970)

59. Kodama, H., and Izumi, F., Crystallization of γ - Bi_2MoO_6 Under Hydrothermal Conditions, *J. Cryst. Growth,* 50:515–520 (1980)
60. Kharchenko, L. Yu., Protasova, V. I., and Klevstsov, P. V., Investigation of the Hydrothermal Conditions of Synthesis of Rare Earth Molybdates in Aqueous Solutions of Potassium Molybdate, *J. Inorg. Chem.*, 22:986–990 (1977)
61. Klevstova, P. V., Protasova, V. I., Kharchenko, L. Yu., and Klevstova, R.F., Hydrothermal Synthesis of a New Crystalline Modification of Lithium Lanthanum Molybdate, α-$LiLa(MoO_4)_2$, *Sov. Phys. Crystallogra.*, 18:523–524 (1974)
62. Klevstova, R. F., The Crystal Structure of Lithium Lanthanum Molybdate (α-$LiLa(MoO_4)_2$, S*ov. Phys. Crystallo. Group,* 20:456–458 (1976)
63. Klevstov, P. V., Koz'veva, L. P., and Protasova, V. I., Synthesis and X-Ray Studies of Double Molybdate, $K_5Ln(MoO_4)_4$ Ln = La-Tb, Crystals, *Kristallografia,* 20:57–62 (1975)
64. McCarron, E. M., III, and Calabrese, J. C., Hydrothermal Synthesis and Structure of $Cu^{1+}{}_6\,Mo^{6+}{}_5\,O_{18}$, *J. Solid State Chem.*, 62:64–74 (1986)
65. McCarron, E. M., III, and Calabrese, J. C., Synthesis and Structure of $Cu^{1+}{}_4\,Mo^{6+}{}_5O_{17}$, *J. Solid State Chem.*, 65:215–224 (1986)
66. Meyer, L. A., and Haushalter, R. C., *Inorg. Chem.*, 32:1579–1584 (1993)
67. Guillou, N., and Ferey, G., Hydrothermal Synthesis and Crystal Structure of Anhydrous Ethylene Diamine Trimolybdates $(C_2H_{10}N_2)\,[Mo_3O_{10}]$, *J. Solid State Chem.*, 132:224–227 (1997)
68. Xu, Y., An, Li-H., and Koh, L. L., Investigations into the Engineering of Inorganic/Organic Solids: Hydrothermal Synthesis and Structure Characterization of One-Dimensional Molybdenum Oxide Polymers, *Chem. Mater.*, 8:814–818 (1996)
69. Guo, J., Zavalij, P., and Whittingham, M. S., Hydrothermal Synthesis of a New Molybdate with a Layered Structure $(NMe_4)\,Mo_{4-\delta}\,O_{12}$, *Chem. Mater.*, 6:357–359 (1994)
70. Noray-Szabo, *Naturwissenschaften,* 31:202 (1943)
71. Wadsley, A. D., *Acta Cryst.*, 17:623 (1964)
72. Andersson. S. and Wadsley, A. D., *Acta Chem. Scand.*, 15:663 (1961)
73. Andersson. S. and Wadsley, A. D., A*cta Cryst.*, 15:194 (1962)
74. Andersson. S. and Wadsley, A. D., *Acta Cryst.*, 15:201 (1962)
75. Mumme, W. G. and Wadsley, A. D., *Acta Cryst.*, 24:1327 (1968)
76. Guillen, M. and Bertant, E. F., *Acad. C. R., Sci. Paris Ser.*, 262:962 (1966)
77. Toropov, N. A., Barzakovskii, V. P., Lapin, V. V., and Kursteva, N. N., *Composition Diagrams of Silicate Systems*, Nauka, Moscow (1965)

DeepBooks

78. Wadsley, A. D., *Acta Cryst.*, 14:660 (1961)
79. Jamieson, P. B., and Abrahams, S. C., *Acta Cryst.*, B24:984 (1968)
80. Aleksandrov, V. B., in: *Experimental Investigations in the Field of Mineralogy and Geochemistry of Rare Earth Elements*, Nauka, Moscow, 3–11 (1967)
81. Rebbah, H., DesGardin, G., and Raveau, B., *J. Solid State Chem.*, 31:321 (1980)
82. Andersson, S., *Acta Crystallogr.*, 14:1245 (1961)
83. Anderson, S., and Wadleg, A. D., *Acta. Cryst.*, 14:1245 (1961)
84. Dion, M., Fiffard, Y., and Tournoux, M., *J. Inorg. Nucl. Chem.*, 40:971 (1978)
85. Sanjeev Ravi Raj, B., Ph.D. Thesis, pp. 76–77, Univ. of Mysore, Mysore, India (1996)
86. Byrappa, K., Sanjeeva Ravi Raj, B., Rajeev, V., Kulkarni, A. B., and Clemente, Rafael Rodriguez, Hydrothermal Growth and Characterization of $Na_2Ti_3O_7$, *Indian J. Phys*, 71A:131–142 (1997)
87. Barsukova, M. L., Kuznetsov, V. A., Lobachev, A. N., and Tanakina, T. N., Crystallization of Bismuth Titanates, *Sov. Phys. Crystallogr.*, 17:739–742 (1973)
88. Barsukova, M. L., Kuznetsov, V. A., Lobachev, A. N., and Shaldin, Yu. V., Hydrothermal Crystallization and some Properties of Bismuthtitanates, *J. Crystal Growth*, 13/14:530–534 (1972)
89. Muto, F., and Taki, S., Hydrothermal Synthesis of $K_2Li_2Ti_6O_{14}$ and its Crystal Structure, *Bull. Chem. Soc.*, pp. 77–82, Jpn (1976)
90. Sato, M., and Utsunomiya, T., Crystal Growth and Some Properties of $R_2Ti_2O_7$, *Bull. Tokyo Inst. Technology*, 98:25–35 (1970)
91. Sanjeev Ravi Raj, B., Ph.D. Thesis, University of Mysore, p. 146 (1996)
92. Kolb, E. D., Caporaso, A. J., and Laudise, R. A., The Hydrothermal Growth of Lithium Metagallate, *J. Crystal Growth*, 8:354–358 (1971)
93. Marshall, D. J. and Laudise, R. A., The Hydrothermal Solubility of Lithium Metagallate in NaOH Solutions, *J. Crystal Growth*, 1:88–92 (1967)
94. Cambi, L., and Elli, M., Processi Idrotermali: Sintesi di Solfuri e Solfosali da Ossidi di Metalli e di Metalloidi, per Azione del Solfo e dell'Acqua., *Nota 1 - Chim. e Industr.*, (Ital.), 46:1275–1279 (1964)
95. Cambi, L. and Elli, M., *Processi Idrotermali: Nota 9, Sintesi di Solfuri e Solfosali di Metalli Trivalent, Chim. e Industr.*, (Ital.), 48:944–951 (1966)
96. Cambi, L. and Elli, M., Processi Idrotermali: Sintesi di Solfosali Derivati da Solfuro d'Argentd e Solfuri d'Anti-Monio., *Nota 3 - Chim. e Industr.*, (Ital.) 47:282–290 (1965)

97. Kuznetsov, V. A. and Efremova, E. P., Hydrothermal Synthesis of Sulphides of Divalent Metals, in: *Hydrothermal Synthesis and Growth of Monocrystals*, pp. 78–119, Nauka, Moscow (1982)
98. Latimer, V. M., *Oxidation State of Elements and their Potentials in Aqueous Solutions*, p. 400, Inostrannya Literature, Moscow (1954)
99. Kuznetsov, V. A., The Physical Chemistry of the Hydrothermal Crystal Growth and the Crystallization of Some A_2B_6 Crystals, in: Hydrothermal Growth of Rare Crystals, (K. Byrappa, ed.), *Prog. Crystal Growth and Charact.*, 21:163–193 (1990)
100. Laudise, R. A., Kolb, E. D., and Deneutoille, I. P., *Amer. Miner.*, 50(3/4): 981 (1965)
101. Kotel'nikov, A. R., Kuznetsov, V. A., and Labachev, A. L., Stability and Crystallization of Cds and Pbs in Alkaline High-Temp. Solutions, Izvestiya Akademi Nauk USSR, *Inorg., Mater.*, 12:827–829 (1974)
102. Kuznetsov, V. A. and Kostomarov, D. V., *Krystallography*, 28(1):151 (1983)
103. Efremova, E. P. and Kuznetsov, V. A., *Proc. of the First International Symposium on Hydrothermal Reactions*, p. 317, Tokyo (1982)
104. Toudic, Y., Regreny, A., Passaut, M., Aumont, R., and Bayon, J. F., Nauverau type d'Appareillage Applique la Croissance Hydrothermale de Monocristaux de Cinabare de Grande Dimensions, *J. Crystal Growth*, 13/14:519–523 (1972)
105. Bryatov, L. V. and Kuzmina, I. P., Crystallization of Pb and Zn Sulphides from Aqueous Solutions of Chloride Salts, in: *Crystal Growth*, Vol. 3, Nauka Moscow, pp. 416–420 (1961)
106. Ikornikova, N. Yu., *Hydrothermal Synthesis of Crystals in Chloride System*, Nauka Moscow, p. 227 (1975)
107. Mininzon, Yu. M., Demianets, L. N., and Lobachev, A. N., On the Solubility of Synthetic Sphalerite in Aqueous H_3PO_4 Solution, *Kristallografia*, 19:435–437 (1974)
108. Horiuch, S., Wada, H., and Moori T., Morphology and Imperfection of Hydrothermally Synthesized Greigite (Fe_3S_4), *J. Crystal Growth*, 24/25:624–626 (1974)
109. Voronina, I. P. and Litvin, B. N., *Hydrothermal Synthesis of Inorganic Compounds, Bibliography.*, VINITI, Moscow, p. 188 (1971)
110. Litvin, B. N. and Popolitov, V. I., Hydrothermal Method of Obtaining $A^vB^{vi}C^{vii}$ Compounds, Izvestia Akadem: Nauk USSR, *Inorg. Mater.*, 6:575–576 (1970)
111. Popolitov, V. I., Crystallization of BiSI, *Kristallografia*, 15:1271–1272 (1970)
112. Popolitov, V. I. and Litvin, B. N., Synthesis of Monocrystals of Ternary Chalcohalogenides (AvBviCvii), in: Investigation of Crystallization Processes under Hydrothermal Conditions, *Nauka, Moscow*, pp. 55–68 (1970)

DropBooks

113. Popolitov, V. I. and Lobachev, A. N., Investigation of Processes Crystallization in the system Sb-Se-I-R-H_2O (R = Solution) under Hydrothermal Conditions, Izvestia Akademia, Nauk USSR, *Inorg. Mater.*, 8:1229–1232 (1972)

114. Popolitov, V. I. and Plakhov, G. F., Synthesis of Single-Crystalline Lead Compounds under Hydrothermal Conditions, *Inorg. Mater.*, 27:2618–2623 (1991)

115. Rabenau, A. and Rau, H., *Lead Sulfide Halides and Pb_4 $SeBr_4$, Z., Inorg. Allg. Chem.*, 369:295–305 (1969)

116. Kuznetsov, V. A. and Labochev, A. N., *Hydrothermal Method for the Growth of Crystals, Sov. Physics-Crystallogr.*, 17:775–804 (1973)

117. Litvin, B. N. and Popolitov, V. I., Hydrothermal Synthesis of Inorganic Compounds, *Nauka, Moscow*, pp. 52–59 (1984)

118. Rau, H. and Rabenau, A., Hydrothermal Synthesis von CuS and CuSe in 48%:ger HBr, *Mat. Res. Bull.*, 2:609–614 (1967)

119. Kolb, E. D. and Laudise, R. A., Hydrothermal Crystallization of Zinc Selenide, *J. Crystal Growth*, 7:199–202 (1970)

120. Neumann, G., On the Hydrolysis of Niobates in 3M KCl Medium, *Acta Chem. Scand.*, 18:278–280 (1964)

121. Shternberg, A. A., Lapsker, Ya. E., and Kuznetsov, V. A., Hydrothermal Synthesis of Niobates and Tantalates of Potassium, *Kristallografia*, 12:957–958 (1967)

122. Marshall, D. J., and Laudise, R. A., The Hydrothermal Phase Diagrams K_2O-Nb_2O_5 and K_2O-Ta_2O_5 and the Growth of Single Crystals of $K(Ta,Nb)O_3$, *J. Phys. Chem. Solids Supply*, 1:557–561 (1967)

123. Rooksby, H. P. and White, E. A. D., The Structures of 1:1 Compounds of Rare Earth Oxides with Niobia and Tantala, *Acta Crystallogr.*, 16:888–890 (1963)

124. Stubican, V. S., High Temperature Transitions in Rare Earth Niobates and Tantalates, J. *Am. Ceram. Soc.*, 47:55–58 (1964)

125. Titov, Yu., Sych, A. M., Sokolov, A. N., Kapshuk, A. A., and Yashchuk, V. P., Polymorphism of $NdTaO_4$, *Inorg. Mater.*, 33:60–63 (1997)

126. Popolitov, V. I., Peskin, V. F., and Lobachev, A. N., Investigations of the Conditions of Crystallization of Orthoniobate and Orthotantalate of Antimony, in: *Crystal Growth from High Temperature Aqueous Solutions*, Nauka, Moscow, pp. 217–227 (1977)

127. Popolitov, V. I., Growth of Monocrystals of Orthoniobate of Antimony and their Physical Properties, *Inorg. Mater.*, 26:367–371 (1990)

128. Popolitov, V. I., Growth of $BiNbO_4$ Monocrystals and Some Properties, *Inorg. Mater.*, 26:360–336 (1990)

129. Popolitov, V. I., Lobachev, A. N., and Peskin, V. F., *Antiferroelectrics, Ferroelectrics, and Pyroelectrics of a Stibiotantalite Structure—Ferroelectrics,* 40:9–6 (1982)

130. Popolitov, V. I., Some Physico-Chemical Principles of Crystallization under Hydrothermal Conditions In: *Hydrothermal Synthesis and Growth of Monocrystals*, p. 145, Nauka, Moscow (1982)

131. Leichenko, A. I., Popolitov, V. I., and Peskin, V. F., Dielectric and Ferroelectric Properties of Potassium Antimony Niobate Compounds, *Solid State Physics*, Akademi Nauk USSR, 20:938–941 (1978)

132. Chen, T. C. and Wang, S. L., Synthesis and Structural Study of Copper Diarsenates, *J. Solid State Chemistry,* 121:350–355 (1996)[11]

133. Rojo, M. J., Mesa, J. L., Pizarro, J. L., Lezama, L., Arriortua, M. I., and Rojo, T., Structural and Spectroscopic Study of the $(Mg, Ni)_2$ (OH) (AsO_4) Arsenates, *J. Solid State Chem.,* 132:107–112 (1997)

134. Wang, H. and Pang, W., Hydrothermal Synthesis and Characterization of $NaZr_2(AsO_4)3$, *J. Mater. Chem.,* 3:989 (1993)

135. Effenberger, H. and Miletich, R., $Na_2[Bi_2Cu_3O_4$ $(AsO_4)_2].H_2O$ and $K_2[Bi_2Cu_3O_4(AsO_4)_2].2H_2O$ two related Crystal Structures with Topologically Identical Layers, *Zeit. Kristallogr.,* 210:421–426 (1995)

136. Harrison, W. T. A., Liang, C. S., Nenoff, T. M., and Stucky, G. D., Synthesis and Crystal Structure of $NaNb_2AsO_8$, *J. Solid State Chem.,* 113:367–372 (1994)

137. Chou, J. H. and Kanatzidis, M. G., Hydrothermal Synthesis and Characterization of $(Me_4N)[HgAsSe_3]$, (Et_4N) $[HgAsSe_3]$ Selenoargsenates, *J. Solid State Chem.,* 123:115–122 (1996)

138. Belt, R. F. and Ings, J. B., Hydrothermal Growth of Potassium Titanyl Arsenate (KTA) in Large Autoclaves, *J. Cyrstal Growth,* 128:956–962 (1993)

DropBooks

9

Hydrothermal Synthesis of Native Elements and Simple Oxides

9.1 INTRODUCTION

The hydrothermal technique is very useful for growing crystals of native elements and simple oxides. The native element crystals popularly grown under hydrothermal conditions are gold, silver, platinum, copper, arsenic, cobalt, nickel, tellurium and bismuth related compounds. Similarly, among the hydrothermally produced oxides, zincite, rutile, zirconia, and hafnia are very popular. In fact, the hydrothermal method is the only suitable method for the growth of these compounds for various reasons like high melting point, very low solubility, acid resistance and so on. In this chapter, we describe the hydrothermal synthesis of selected native element crystals.

9.2 HYDROTHERMAL SYNTHESIS OF NATIVE ELEMENTS

The hydrothermal technique is especially suitable for obtaining pure and high quality crystals of elements. The interest in the synthesis of these elements has rejuvenated, particularly after the discovery of noble metals in seafloor hydrothermal mineralization.[1][2] Gold, silver, iridium, palladium, platinum, etc. have been reported in hydrothermal mineralization from two mid-oceanic ridges: Juan de Fuca and Mid-Atlantic at

26°N.[2] The solubilities of noble metals in hydrothermal fluids are highly relevant to the redistribution and possible concentration of these metals by the action of water-rich fluids on magmatic occurrences.

The hydrothermal synthesis of noble metals takes place through two types of reactions:

Eq. (1) $2Me\ (s) + 2\ (OH)^{-}\ (l) \rightarrow 2MeOx\ (l) + H2 \uparrow$

Eq. (2) $2Me\ (s) + 2\ (Hl)\ (l) \rightarrow 2MeL\ (l) + H2 \uparrow$

where L = acid anion (ligand).

The first reaction is characteristic of alkali solutions and the second reaction is characteristic of acids. In both the cases, hydrogen helps in establishing equilibrium. As a result of this, the desired metal crystallizes. If temperature gradient is maintained in the autoclave, the reaction route is determined by the Eh of metals from temperatures. Therefore, in one case, the crystallization of native metal crystals takes place in the hotter zone, and in the other case, in the cooler zone. Thus, the hydrothermal crystallization of metals is possible in both acid and alkali solutions. It is possible to obtain the entire series of metals as single crystals when an oxidizing agent like halogenide is used.[3] The crystallization takes place in quartz ampoules with external control of the CO_2 gas at temperatures 440–600°C and temperature gradients 30–120°C in aqueous solutions of HCl, HI, HBr and the crystals obtained are: Au, Ag, Pt, Co, Ni, Te and As. In this regard, it is appropriate to emphasize the work of Rabenau and Rau (1968) on the hydrothermal synthesis of gold crystals.[4] In aqueous solutions of HI at 500°C, the well-soluble $[AuI_4]^{-}$ complexes are formed, their stability depends upon the temperature, and it falls with destabilization of $[AuI_4]$ complexes and the formation of gold crystals:

Eq. (3) $Au + 4HI \rightarrow [AuI_4]^{-} + 2H_2 \uparrow$

The first attempt of gold crystallization from aqueous solutions was demonstrated by Bujor (1948) under hydrothermal conditions at 390°C and 300 atm and cubic crystals of gold were obtained.[5]

Honma et al. (1991) have studied, in detail, the dissolution and precipitation of gold and silver at 150°C in various strong acid solutions and aqueous NaHS over periods of 60 to 120 days.[6] The alloy $Au_{50}Ag_{50}$ was used as the starting material. For the first time millimeter-sized free-growing enhedral crystals of pure gold were obtained from 6N HCl

DropBooks

solution after 120 days, and no precipitation of either gold or silver was obtained from the sulfuric acid and nitric acid solutions. Small crystals of both electrum ($Au_{71}Ag_{29}$) and argentite were precipitated onto the starting alloy sample after 120 days in 5.2 M aqueous NaHS.[6]

Gold solubility has been studied extensively by several authors in HCl aqueous solution and others.[7]–[12] Seward and his group have done excellent work on the complexing and solubility of gold and other noble metals under hydrothermal conditions, especially in the aqueous sulphide solutions at temperatures between 150 and 500°C and pressure of 500–1500 bar over a wide range of pH.[12]–[14] They have derived stability constants for the complexes AuHS and $Au(HS)^-_2$. It can be used to quantitatively model the transport of gold in natural hydrothermal fluids to understand the mechanisms and conditions of gold deposition. It has been shown that in sulphide solutions at near neutral pH, the complex $Au(HS)^-_2$ is the dominant gold species. The solubility of gold reaches a maximum where pH = pK of H_2S. However, with increasing temperatures, the pK_1 of H_2S shifts towards more alkaline values (Suleimenov and Seward, 1995) and, therefore, the maximum solubility due to this species also shifts to more alkaline pH.[15] In acid-pH, high-temperature solutions, the neutral species AuHS°, therefore, will be the dominant gold transporting species and, although the gold solubility may be 1–2 orders of magnitude lower than the solubility at pH > pK_1 (H_2S), this complex has to be taken in to account when such systems are modeled. The main reason for the decreasing solubility of gold in high-temperature sulphide solutions is the change in pH and/or total reduced sulphur concentration. The effect of temperature on the solubility of gold in sulphide solutions is very strongly related to the total sulphur concentration and the hydrothermal fugacity.

Crystallization of copper, silver, selenium and tellurium in alkaline solutions takes place in aqueous solutions of hydroxides of alkali metals at partial pressure of hydrogen, 0.5–40 atm, water pressure > 600 atm, and temperature 350–550°C. For obtaining fairly large crystals, the experiments are carried out with temperature gradients, and in autoclaves with or without different liners. Glass carbon ampoules are most effective in this respect. In experiments at T < 300°C, Teflon® liners are used. As nutrient, respective metal oxide powders or metal pieces are used.

Popolitov (1969), and Popolitov and Litvin (1970) have studied the systems Sb-Te-I(Br)-H_2O and obtained the crystals of Se and Te. They proposed a simple method of synthesis of Se and Te crystals in aqueous solutions of hydrochloric acid in autoclaves provided with quartz ampoules.[16][17]

The octahedral or more complex form of single crystals of copper have been obtained in the cooler zone of the autoclave containing aqueous solutions of NaOH KOH. In highly concentrated aqueous solutions of hydroxides of alkali metals and at P_{H_2O} > 50 atm, often the plate-like crystals form with (110) faces exhibiting highly vitreous luster, and the crystal size varies from 1–3 mm.[18]

Silver crystallization conditions are very close to those of crystallization of copper. Crystals are usually plate-like and show twinning. The crystal surfaces exhibit metallic luster with a rise in temperature and silver dendrites form, resembling its appearance in nature. The size varies from 0.1 to 0.5 mm.[19]

Selenium crystals have been obtained under hydrothermal conditions by Kolb and Laudise (1971). The crystals are needle-like prismatic with metallic luster, color light-grey. The size of the individual needles or crystals is up to 10–12 mm with a thickness of 0.2–0.3 mm.[20]

Tellurium crystals have been obtained in aqueous NH_4Cl solutions (8–15 wt%) at temperatures 450–550°C, the partial pressure of hydrogen ~ 80 atm and P_{H_2O} 600 atm with a rise in the concentration of the solvent (up to 20 wt%). The skeleton-like forms appear.[21]

DropBooks

Diamond synthesis has become a very important activity. Several research organizations and corporations have taken up diamond synthesis as a challenge in solid state science. Man started using diamond several centuries B.C. At that time, diamond was thought of as a hard glass. When cutting technology was discovered in the 17th century, man began to use diamond as an aristocratic jewel.

Industrial application of diamonds started in the beginning of the 20th century and the first application of diamond was in a grinding wheel. The wheel consisted of diamond powder with metal (or polymer) binder, which can be called a refined material.

In 1955, diamond was produced artificially and the success was closely related to the discovery of high-pressure technology. This technology was later applied to the production of sintered diamond, which can be categorized as a refined artificial material. This technology was also applied to the production of cubic boron nitride (CBN), which is a completely artificial material. The greatest discovery related to diamond was its synthesis from the gas phase for the first time by Deriaguin et al. in 1976, and Matsumoto et al. (1982).[22][23] Although many methods have been reported for diamond synthesis from the gas phase, all methods are

basically modified chemical vapor deposition methods. Diamond made by these methods, therefore, is referred to as CVD diamond. About seventeen years ago, no one could have conceived that diamond would become an electronic material. People considered a diamond mainly as a jewel, but the discovery of diamond synthesis from the gas phase changed that image drastically.

The authors believe that the unique properties of diamond contributed to the enhancement of research on the material, resulting in a wide range of research with hope for new applications.

There are three major processes of diamond synthesis: *i)* high-pressure–high-temperature (HPHT), and *ii)* chemical vapor deposition (CVD), (which are at least 40 and 30 years old respectively), and *iii)* low-pressure solid state source (LPSSS). Bundy et al. (1955) at General Electric Co., announced their success in synthesizing diamond under HPHT conditions.[24] A few tons of industrial diamond abrasive grains are made this way each year in various factories around the world. De Vries (1987) reviewed CVD diamond synthesis in detail.[25] Roy and his group of researchers have worked out the growth technology for diamond using LPSSS method in detail.[26][27] Figure 9.1 shows the schematic diagram comparing three popular methods of diamond synthesis.[27]

It is interesting to note that the nucleation and growth kinetics had won out over thermodynamics. The CVD process represents the field outside the *P-T* stability region for diamond. Figure 9.2 shows the phase diagram for carbon crystalline phases. The equilibrium data for material trapped in inclusions in diamonds indicates final temperatures of 600–800°C and pressures up to 10 MPa.[28]–[30]

De Vries (1990) has argued a case for the possibility of growing diamonds under hydrothermal conditions, and several researchers have presented various attempts.[31][33] Szymanski et al. (1995) have carried out diamond synthesis using relatively low-pressure liquid phase epitaxy on seeds, in an autoclave filled with a specially prepared water solution. Natural diamonds of 0.22 gm and 0.49 were used as seeds. The solution and seeds were subjected to 170 MPa and 400°C for 21 days. A thin irregular (15–14 μm) colorless film of polycrystalline diamond on the natural (111) faces of the seed crystals was obtained (Fig. 9.3). This work shows that hydrothermal synthesis may be an effective way for homo- and heteroepitaxy of diamond as a continuous layer on seed material surfaces of diversified shape and possibly for growth of large diamonds on seeds.

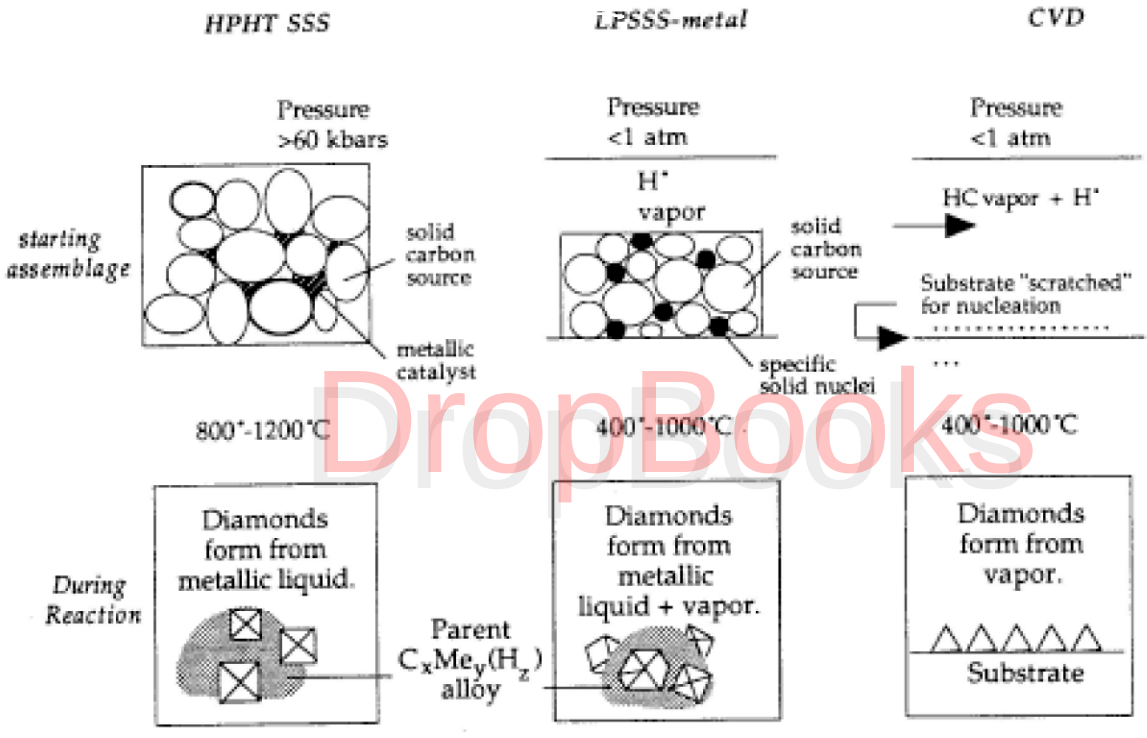

DropBooks

Figure 9.1. Schematic diagram comparing three popular methods of diamond synthesis processes.[27]

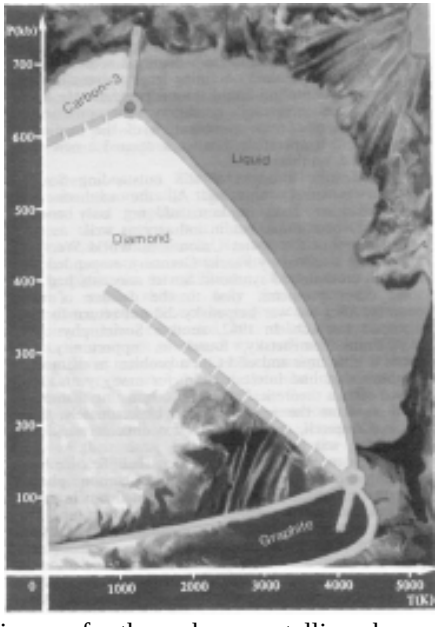

Figure 9.2. Phase diagram for the carbon crystalline phases.

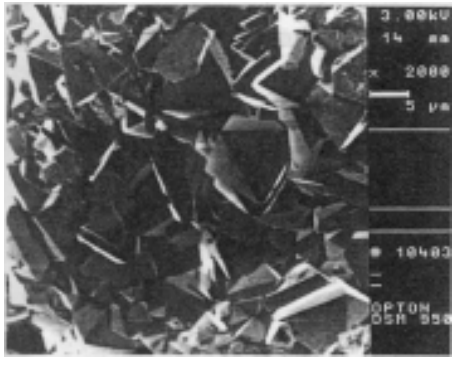

Figure 9.3. Polycrystalline diamond.[28]

Recently, Yamaoka and Akaishi (1999) reported the growth of diamond under HPHT water conditions.[34] The basic principle used by these authors is that carbon reacts with high-temperature water (vapor) producing so called "water gas." It is natural to expect that graphite reacts with water and precipitates as diamond under high-pressure–high-temperature (HPHT) conditions in the thermodynamically stable region of diamond. The authors have used three types of capsules to carry out the diamond synthesis under HPHT conditions: *i)* Ta cylindrical containers,

ii) Mo double capsules, and *iii)* conventional point sealed capsules. The selection of these capsules depends upon the duration of the experiments and the pressure-temperature conditions. Figure 9.4 shows the diamond growth under HPHT conditions. This work shows that graphite reacts with HPHT water and precipitates as diamond in the regions of 1300–2200°C and 5.5–7.7 GPa. The reaction proceeded more rapidly with increasing pressure and temperature.

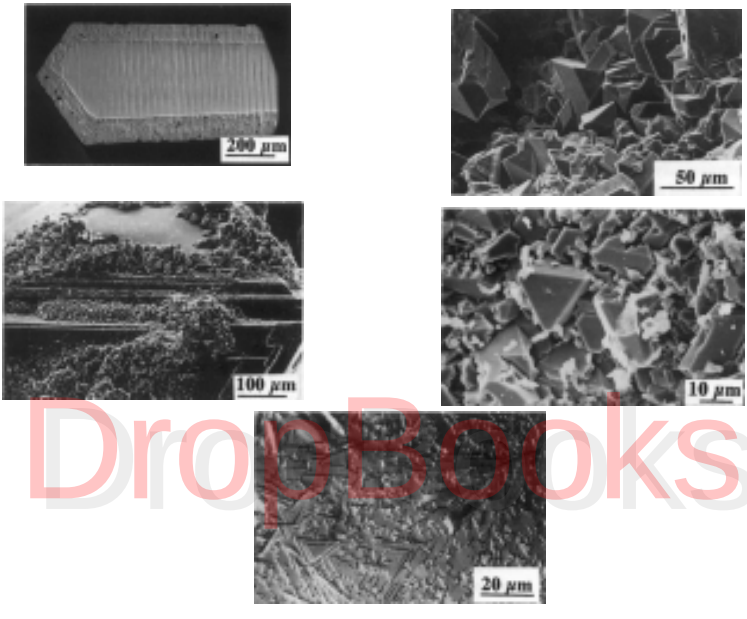

DropBooks

Figure 9.4. Diamond growth under HPHT conditions.[34]

Suito and Onodera (1999) have synthesized diamond using phenolic resins between 1.6 and 4 GPa and cobalt at 10 GPa with calcium carbonate as catalyst-solvents.[35] In this case, the pressure and temperature conditions of diamond synthesis depended upon the pre-firing temperatures. Well-defined single crystals of 0.3–0.7 mm in size were obtained at 4 GPa and 1500°C (Fig. 9.5).

However, the diamond synthesis in the presence of metal powder, molten high molar alkali solution, and water at 800°C and 1.4 kbar pressure range is the most popular technique. The growth rate is quite low. The crystals obtained are usually 5–10 microns in size. Several types of

starting materials have been tried for the synthesis of diamond. The most important aspects are the behavior of carbon under high-pressure–temperature conditions, the presence of a matching substrate, then preferential oxidation of *sp*-bonded C by water. Thermodynamically diamond is stable at temperatures < 800°C. Graphitization of the diamond surface should be prevented. The most important thing is to bring carbon into the high-energy state under hydrothermal conditions and arrest it.

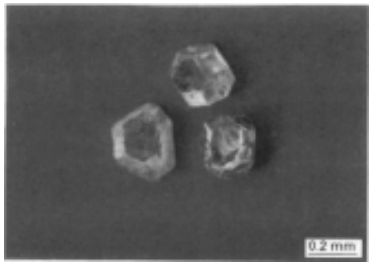

Figure 9.5. Diamond single crystals.[35]

On the whole, the growth of diamond crystals is a challenging task because of the lack of knowledge of the pH of the growth media, halogen problem, very slow growth rates, lack of solubility data, the solvent chemistry, and so on. Therefore, the current situation in diamond synthesis can be compared to that of quartz growth some one hundred years ago. The coming five years will decide the future of diamond research.

In the recent years, carbon nanotubes, particularly the multiwall nanotubes, are becoming materials of great potential in the next generation of electronic nanodevices. Recently, multiwall open-end and closed carbon nanotubes with wall thickness from several to more than 100 carbon layers have been produced by the hydrothermal method by Yoshimura and his team of researchers at Tokyo Institute of Technology, Japan, jointly with the University of Illinois, Chicago, USA, (by Yuri Gagosti) using water-based mixtures in the presence of a catalyst like nickel at 700–800°C under 60–100 MPa pressure. The most significant factor of this work is the use of very low cost materials like polyethylene and water as raw materials. A controlled growth of super-long carbon nanotubes may be possible in autoclaves with temperature gradient. The reader can find more information on carbon nanotubes in the proceedings of the Joint International Symposium on Hydrothermal Reactions and International Conference on Solvothermal Reactions (Joint ISHR & ICSTR) held in Kochi, Japan, during July 25–28, 2000.

9.3 HYDROTHERMAL SYNTHESIS OF HYDROXIDES

The hydrothermal method is popularly used in the synthesis of single crystals of hydroxides of several divalent and trivalent metals. Usually the field of stability is expanded by the presence of surplus water during the transition reaction oxide $\rightleftharpoons$ hydroxide, and temperature of the system. In this regard, the alkali metal hydroxide solutions are more effective. Table 9.1 gives the list of the metal hydroxides obtained by hydrothermal methods, and their experimental conditions.[36] The experimental temperatures and pressures vary from 100 to 600°C and 6 atm to 4000 atm.

Table 9.1. Hydrothermal Experimental Conditions of Synthesis of Hydroxides[36]

Hydroxide	Solvent	*T*°C	*P*, atm
$Be(OH)_2$	H_2O	100–175	4000
$Mg(OH)_2$	3% NaOH	450	600
$Ca(OH)_2$	3% NaOH	550	650
$Cd(OH)_2$	35% NaOH	450	1000
$Mn(OH)_2$	5% NaOH	450	1000
$Co(OH)_2$	1% NaOH	280	3500
$Ni(OH)_2$	1% NaOH	280	3500
$TR(OH_3)$	15% NaOH	350	600
TR = La-Gd			
TR = Dy, Er, Yb	15% NaOH	450	600
$Cr(OH)_3$	3% NaOH	300	1500
$In(OH)_3$	40% NaOH	400	400
$Al(OH)_3$	H_2O	< 150	39
$In(OH)_3$	H_2O	185–275	50–75
$In(OD)_3$	D_2O	180–210	18–50
InOOH	H_2O	325–410	120–800
InOOD	D_2O	360–380	320–400
α-ScOOH	H_2O	162–350	6–170
β-ScOOH	H_2O	350	160
$Y(OH)_3$	H_2O	300	85
CrOOH	H_2O	450	2700
GdOOD	D_2O	600	1400
SmOOH	H_2O	600	1400
$Sr_3Cr_2(OH)_{12}$	H_2O	150–200	

DropBooks

Hydrothermal synthesis of $Mn(OH)_2$, $Cd(OH)_2$, $Co(OH)_2$ and $Ni(OH)_2$ crystals depend upon the partial pressure of hydrogen ($P_{H_2O} > 10$ atm). Some of the hydroxide crystals like $Mg(OH)_2$, $Mn(OH)_2$, $Co(OH)_2$ form fairly large size crystals of 5–10 × 5–10 mm size with a thickness of 0.1 mm. The other hydroxide crystals are small (0.1 mm). The double distilled water is usually used in the synthesis of hydroxides. The temperature gradient method gives single crystals of hydroxides. The oxyhydroxides (MeOOH) often crystallize at relatively higher temperatures. Among these, the polymorphism is very common, and it depends upon the temperature, for example in rare earth hydroxides.[37]

Similar to the alkali solutions in the synthesis of metal hydroxides, acid solutions, particularly chloride solutions, are also used. Thus, in this case, an increase in the concentration of the solution forms hydroxychlorides, often with 100% output. Their synthesis takes place as a result of the substitution of one hydroxyl group with chloride as follows:

Eq. (4) $$Me(OH)_3 + HCl \rightarrow Me(OH)_2Cl + H_2O$$

In this way Demianets and Emelyanova (1969) have obtained hydroxyl-chlorides of neodymium, $Nd(OH)_2Cl$, under hydrothermal conditions using aqueous solutions of NH_4Cl (concentration 7 wt%) at temperatures 450–480°C.[38] At 500°C, rare earth hydroxyl-chlorides, $R(OH)_2Cl$, where R = La, Ce, Pr, Nd, Sm, Gd, have been obtained by Kletsov et al. (1973).[39] Similarly, Carter and Levinson (1969) have obtained hydroxyl-chlorides containing La, Nd, Sm, Gd, Y, and the more complex hydroxyl-chloride of ytterbium, $Yb_3O(OH)_5Cl_2$, using acidic chloride solutions at 1400 atm pressure and 550°C.[40] Under hydrothermal conditions, the chloride group can be replaced by carbonate ions with the formation of hydroxyl carbonate, $R(OH)CO_2$.[41] Similarly, Christensen and Hazeil (1969) have obtained mixed hydroxides of type $MeSn(OH)_6$, where Me = Ca, Mn, Fe, Co, Zn, through the interaction of aqueous solutions of $NaSnO_3$ with chlorides or nitrates of respective metals.[42] Wolski et al. (1997) have obtained $Mn_xFe_{2-2x}(OH)_{6-4x}$ which find numerous applications in technology.[43] For certain *x* values, the initially amorphous mixtures, $Mn_xFe_{2-2x}(OH)_{6-4x}$, are converted into ferrimagnetic species when stored as water suspensions well below 100°C, and the higher the temperature, the shorter the time of transformation. Aqueous solutions of titrated 0.25 M Fe (III) nitrates, mixed together in the desired proportions to give the hydroxide mixtures $Mn_xFe_{2-2x}(OH)_{6-4x}$ in 0.1x intervals,

were treated by constant stirring with 2M NaOH till pH 9.5 was reached, to ensure full M_n^{2+} precipitation and at the same time to avoid oxidation to Mn_3O_4 and β - MgOOH at higher pH. The washed and filtered hydroxides were placed in Teflon® vessels and were stored in the form of water suspensions in autoclaves at 100°C for 24 hours.

Thus, the hydrothermal technique provides unique opportunities for a preparative chemist to obtain a large variety of hydroxides, hydroxyl carbonates, hydroxylchlorides, etc., of various metals.

9.4 HYDROTHERMAL SYNTHESIS OF SELECTED OXIDES

Oxides form one of the largest groups of inorganic compounds both in nature and in the laboratory. The hydrothermal technique is one of the most popular techniques for growing these high-temperature oxides, complex oxides and low-temperature modifications of the oxides. The work on the hydrothermal synthesis of oxides began during the 19th century with quartz in 1845.[44] Followed by this, large-scale research activity began during the 1890s, on corundum and other related high-temperature oxides.[45][46] Today, we find a large number of oxides obtained by the hydrothermal method: TiO_2, ZrO_2, HfO_2, Cu_2O, BeO, Bi_2O_3, In_2O_3, Al_2O_3, ZnO, Fe_2O_3, to mention a few, and a great variety of mixed oxides. Some of these carry great significance as synthetic gemstones, and some as technological materials. Here, we describe the hydrothermal growth of selected oxides of both gemstone and technological grades.

DropBooks

9.4.1 Cu_2O (Cuprite)

The growth of cuprite monocrystals under hydrothermal conditions can be carried out using LiOH, NaOH, KOH in aqueous solutions of alkali ammonium halogenides. Kuzmina and Kaidukov (1977) have worked out a detailed technology of hydrothermal synthesis of cuprite, and the solubility of cuprite can be written as follows:[47]

Eq. (5) $$Cu_2O + (2a - 2)\ OH^- \rightarrow 2CuOa^{(2a-1)-} + (a - 1)\ H_2O$$

The solubility of hemioxide of cuprite under high-pressure-temperature conditions is less stable with respect to supersaturation, and with a slight variation in the temperature gradient, spontaneous crystallization of cuprite takes place such that the growth of cuprite crystals become difficult.

Cuprite crystal growth is carried in autoclaves with copper or silver linings. The growth temperature is 250–450°C, ΔT = 25–75°, %fill 70 to 80%. For chloride solutions, Teflon® liners have been used and the temperature was maintained at T = 300°C and ΔT = 20–45°, and the pH varied from 5.0 to 5.5. The crystals obtained are 4–5 mm in size with ruby-red color having octahedral or often dodecahedral cover.

9.4.2 BeO (Bromelite)

Extremely high toxicity of beryllium makes the crystal growth of beryllium-bearing compounds very difficult. Therefore, the hydrothermal method becomes most useful in this regard. The first attempt to grow bromelite was made by Hartmann (1962).[48] Seeded growth of bromelite was carried out using a 5 mm BeO crystal oriented along [$\bar{1}0\bar{1}0$] and [$\bar{1}0\bar{1}$ 1]. The average growth rate was ~ 0.07 mm/day. The crystallization was carried out at 500–530°C using NaOH solutions.

The autoclaves are usually provided with copper or silver lining though there are several other lining materials. The experimental conditions are as follows:

Mineralizer	-	25wt% NaOH
Nutrient	-	beryllium oxide
Fill %	-	80%
Crystallization temperature	-	450°C
ΔT	-	20–50°C

Under the above conditions, colorless hexagonal crystals of size 3–4 mm with the basic pinacoidal, pyramidal and prismatic forms are formed.

9.4.3 Zinc Oxide

Zinc oxide is well-known as *n*-type semiconductor due to the excess of Zn atoms in the compound. Because of its high electromechanical coupling constant, zinc oxide appears to be the best material for devices utilizing the piezoelectric interaction between acoustic waves and electronic current. Zincite crystals may be grown by different methods: from gas phase (it produces needles of ZnO), from high-temperature

solution using PbF_2 (it produces plate-like crystals), and hydrothermally. It is interesting to note that the properties of crystals grown by the first two methods are technologically unsatisfactory owing to the imperfections in the crystal, and to unsuitable habits. Therefore, the most promising method of producing isometric zinc oxide crystals of good quality is the hydrothermal method.[49] Hence, the process of crystallization represents an important technique for many applications. In this respect, understanding, controlling, and optimizing crystal morphology is of fundamental importance in those fields where an incorrectly defined crystal morphology may have an impact upon a number of important technological applications. Therefore, the hydrothermal technique is found to be the most suitable one for the growth of ZnO crystals. Seeded crystal growth of zincite has been carried out using NaOH and KOH solutions and, similarly, aqueous solutions of chlorides.[50]–[54] The most useful solvent is 2–10M KOH, in which the growth takes place within a wide temperature interval 200–500°C and P = 150–600 atm. Lobachev et al. (1982) have studied the solubility of zincite in detail. The solubility is less dependent upon the temperature when the concentration of the solution is < 3M, but for higher concentrations, it is distinct. Figure 9.6 shows the solubility of zincite in KOH solution. With a raise in the concentration of KOH, the solubility of zincite in KOH solution increases nonlinearly, but with a raise in the concentration of KOH at lower temperature (< 200°C), it becomes linear.

PropBooks

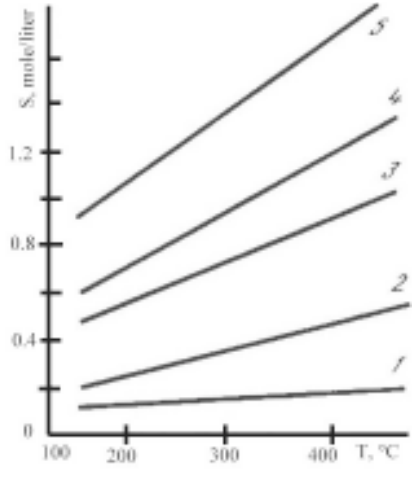

Figure 9.6. Solubility of zincite in KOH solution.[50]

In the growth of zincite, the use of alkalis sometimes leads to the formation of hydrogen arising as a result of the oxidation of the autoclave material. The amount of hydrogen formed depends greatly on the temperature, the concentration of the alkali, and the duration of the experiment. In fact, the dissolution of the crystals, the transport processes, and crystallization in turn, depend greatly on the redox potential of the medium. Sakagami (1990) has obtained zincite crystals of high purity by the hydrothermal method under a partial pressure of oxygen, using platinum-lined autoclaves and ultra-pure reagents.[55] The growth conditions are as follows:

Growth temperature	-	370–400°C
Temperature difference	-	10–15°C
Total pressure	-	700–1000 kg/cm
Partial pressure	-	10–30 kg/cm
Solvent	-	KOH 3.0M + LiOH 1.5M
Oxidizer	-	H_2O_2 0.1M–0.3M
Nutrient	-	ZnO sinter
Lining tube	-	Point (0.3 mm thickness)
Growth run	-	15–20 days/run

Figure 9.7 shows high purity crystals of zincite obtained at a growth rate of 0.2 mm/day in a direction normal to a prismatic face $(1\bar{0}10)$. The degree of coloration depends upon the growth conditions, for example, solutions containing a H_2O_2 oxidizer and without an oxidizer. The author has used the coulometric technique to detect a small deviation in the stoichiometric constituent towards $Zn_{1+x}O$. The concentration of excess Zn in the crystals grown under excess partial pressures of oxygen decreased to the minimum of 0.8 ppm, and their resistivity increased to about 10^8 Ωm. Thus, the composition of the solution in which the zincite crystallizes changes the habit and properties of the developing crystals. In KOH solutions, ZnO crystals or prismatic habit, drawn out sharply along the *'c'* axis, are formed in caustic soda solutions. The crystals are more isometric in LiOH solutions. The growth rate of the monohedral face is very slow, while that of the pyramid face is commensurable with or slightly exceeds that of the prism, and the crystals assume a tabular form. The presence of F^+ ions in the solution increases the growth rate of the monohedral (0001) face. If the solution contains iron, characteristic zincite twins grow along the face of

the monohedron. In aqueous ammonium chloride solutions (1–7 wt%), recrystallization of zincite takes place at 450°C. The crystal habit varies with the concentration of the solution.[56][57] In highly concentrated solutions, hexagonal platelets form. Hence, in order to obtain good crystals of zincite, NaOH and KOH solutions are used. The resistance of zincite crystals grown in alkali solutions containing lithium ions is small: 10^1–10^2 Ωcm. Annealing in air or oxygen increases the resistance of the samples to 10^5–10^8 Ωcm. This is due to the diffusion of the Li ions, and to the motion of the hyper-stoichiometric proportion of zinc to the surface of the crystal faces, with its subsequent oxidation to zinc oxide.

DropBooks

Figure 9.7. High purity crystals of zincite obtained at a growth rate of 0.2 mm/day.[55]

Zincite crystals obtained under hydrothermal conditions are normally activated by Mn^{2+} and Ni^{2+}, which emit red and green radiation. However, the resistance of the crystals remains unchanged. Similarly, the Mn^{2+} and Ni^{2+} ions also have no appreciable effect on the kinetics of the crystallization of zincite.

Wang et al. (1997) has carried out a systematic investigation of zincite crystals and their morphology through a crystal chemical approach to obtain a desirable morphology. Also, they have explained the effects of the additive OH^- on the crystal morphology of ZnO crystallites.[58] ZnO microcrystallites are very important having wide application in ceramics, coatings, and electronic devices. Thus, hydrothermal zincite crystals have great device potential.

9.4.4 Hydrothermal Growth of Corundum

The hydrothermal synthesis of corundum began during the 1890s. Corundum is stable under hydrothermal conditions at $T > 400°C$[59][60] and is soluble in alkali and carbonate solutions. According to Laudise and Parker (1974), corundum shows a lower temperature coefficient of solubility in alkaline solutions and that is the reason for the unsuccessful growth of corundum in these solutions.[61] Although, hydrothermally grown corundum is commercially available at present, as gemstones it has not been reported. The hydrothermal growth of corundum is achieved using a metastable-phase technique because of its very low solubility. Gibbsite ($Al(OH)_3$) is used as a nutrient, α -Al_2O_3 as a seed, and an alkaline solution as a solvent. A more rapid growth rate is obtained in KOH or K_2CO_3 solution than in NaOH or Na_2CO_3 solution. The solubility is lower in KOH or K_2CO_3, but the interaction between the impurity absorbed beforehand onto the crystal surface and K^+ ion existing in the solution, acts as a factor to augment the growth rate. The lower the pH level in the solution, the thicker the growth layer along the *c*-axis. The growth of corundum in extremely low pH 6N HCl has been reported. In this case, the nutrient is dissolved at the lower temperature side and is deposited on the seed crystal at the higher temperature side, because the enthalpy in the α-Al_2O_3-HCl reaction is negative. Isothermal studies of the system Al_2O_3-H_2O have been carried out by many workers and have shown that corundum could be formed from diaspore, boehmite, or gibbsite *in situ* at temperatures > 450°C. The pressure varied from 15,000 to 30,000 psi. Figure 9.8 shows the phase relations in Al_2O_3 systems.[61] Kashkurov et al. (1968) have studied the growth of large corundum crystals at pressures up to 2000 atm and at temperatures up to 550°C in alkali solutions of various concentrations. Crystals weighing up to 1 kg were prepared by the hydrothermal technique, and the imperfect state of these crystals was apparently associated with internal stresses and the mosaic structure of seed crystals which were prepared by Verneuil technique.[62] Rumyanetsev et al. (1972) have shown that among alkali and carbonate solutions, the alkali solutions dissolve corundum and form aluminates.[63]

Eq. (6) $$Al_2O_3 + 2NaOH + 3H_2O \rightarrow 2Na\,[Al\,(OH)_2] + 4OH^-$$

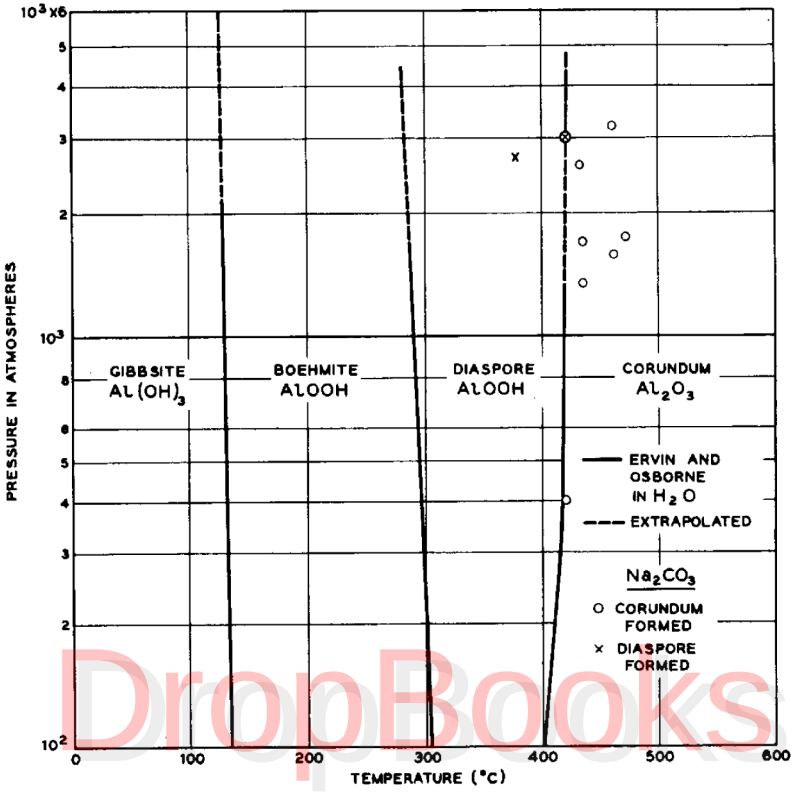

DropBooks

Figure 9.8. Phase relations in Al_2O_3 systems.[61]

In the absence of carbonate ions, CO^{-}_{3}, the aluminate ions are always stable and the reaction becomes irreversible and, at the same time, with the use of carbonate solutions, the reaction becomes reversible. In fact, this is a characteristic feature of lower concentrations of sodium bicarbonate. At higher concentrations of solutions, usually, the heavier phases appear. In aqueous solutions of K_2CO_3 and Pb_2CO_3, the heavy phase does not appear, therefore, the experimenters emphasize the corundum growth in such solutions. Figure 9.9 shows the dependence the of solubility of corundum on temperature; and Fig. 9.10 shows the dependence of the growth rate of different faces on the temperature.[63] With a raise in temperature, the growth rate nonlinearly increases within the temperature interval 400–500°C. Good quality corundum crystals were grown on the seeds oriented along the face (122) and were obtained from the melt. The growth was carried out in 4M K_2CO_3 solution at 480°C,

pressure of 1330 atm, fill 85%, ΔT = 30°C, and colorless and transparent crystals with (211), (311) and (111) faces were obtained. Thomas (1996) has studied the influence of KOH/CO_2 ratio in alkaline-bicarbonate solutions on the growth rate of corundum crystals under hydrothermal conditions. It has been shown that the concentration of CO_2 in the system has a main influence on the growth rate of corundum crystals; as for KOH content in the bicarbonate solutions, it influences growth velocity with only a small concentration of the alkaline component. A mechanism for aluminum transfer with the growth of corundum crystals in the carbonate and bicarbonate solutions has been discussed.[64] The corundum of hydrothermal origin is used both as gemstone and technological material.

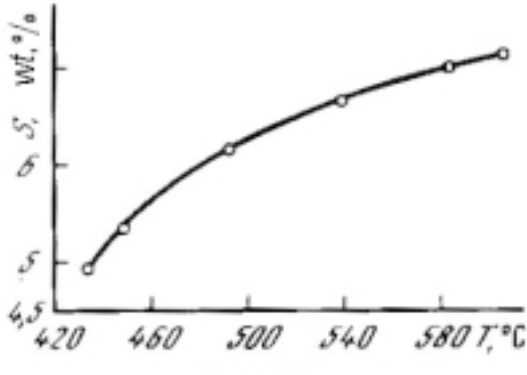

Figure 9.9. Dependence of solubility of corundum.[63]

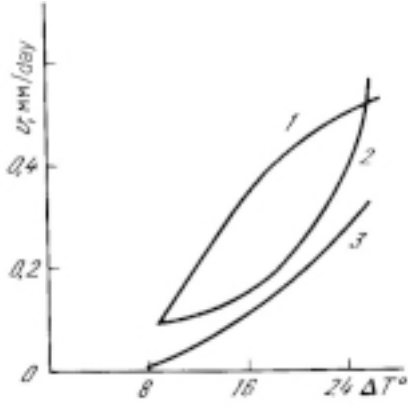

Figure 9.10. Dependence of the growth rate of different faces and the temperature.[63]

The hydrothermal technique is useful for obtaining large crystals of sapphire and ruby. The corundum modifications of Al_2O_3, which are relatively strain free, can be prepared at moderate temperature conditions and without the excessive gradients characteristic of flame fusion and melt techniques. These are the gemstone varieties of corundum and named according to their colors: sapphire blue and ruby red. Probably sapphire is the second material after quartz to be grown in any size by hydrothermal methods. Similarly, large ruby crystals can be grown using carbonate solutions. The solubility of sapphire and ruby is the same as that of corundum and it increases with temperature. Oxides of chromium and iron, when taken in the nutrient along with Na_2CO_3 solution, more strongly influence the crystallization than when taken with K_2CO_3 solution. However, when the concentration of these components in the nutrient is higher than 1.6% in 10% Na_2CO_3 solution, crystals practically do not grow. Kuznetsov and Shternberg (1967) have investigated the crystallization of ruby under hydrothermal conditions by three methods: recrystallization of aluminum oxide in solutions containing chromium; joint recrystallization of Al_2O_3 and Cr_2O_3, which are placed in the autoclave as separate components; and finally, recrystallization of ruby crystals having a given chromic oxide concentration. The last method makes possible uniform and controlled introduction of the impurity into the solution and the growing crystal throughout the experiment.[65] Figure 9.11 shows the growth rate of the $(10\bar{1}1)$ face versus Cr_2O_3 concentration in the initial charge; 10% Na_2CO_3 solution at 550°C, autoclave 60% filled. These authors conclude that in carbonate and bicarbonate solutions, chromic oxide, and aluminum oxide have substantially different solubilities in carbonate solutions and different rates of dissolution. Also, the effect of solution redox potential on the transport of chromic oxide under hydrothermal conditions has been studied by these authors. Monchamp et al. (1967) have carried out very large-scale growth of sapphire and ruby with considerable success.[66][67] Figure 9.12 shows hydrothermally grown ruby crystal.[68] Green crystals containing iron have been grown by carrying out the crystallization in the welded liners directly, and colorless crystals which were essentially pure have been prepared by the use of a silver tube.[67] The overall features are similar to the growth of corundum crystals.

PropBooks

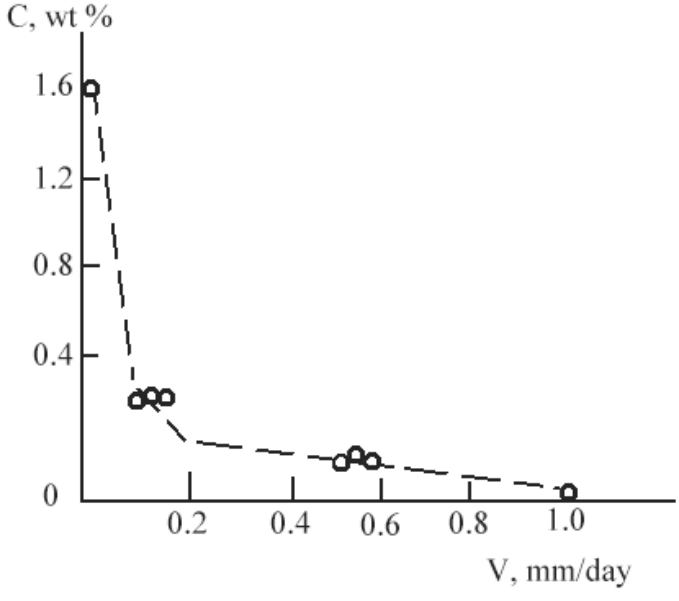

Figure 9.11. Growth rate of $(10\bar{1}1)$ face versus Cr_2O_3 concentration in the initial charge.[65]

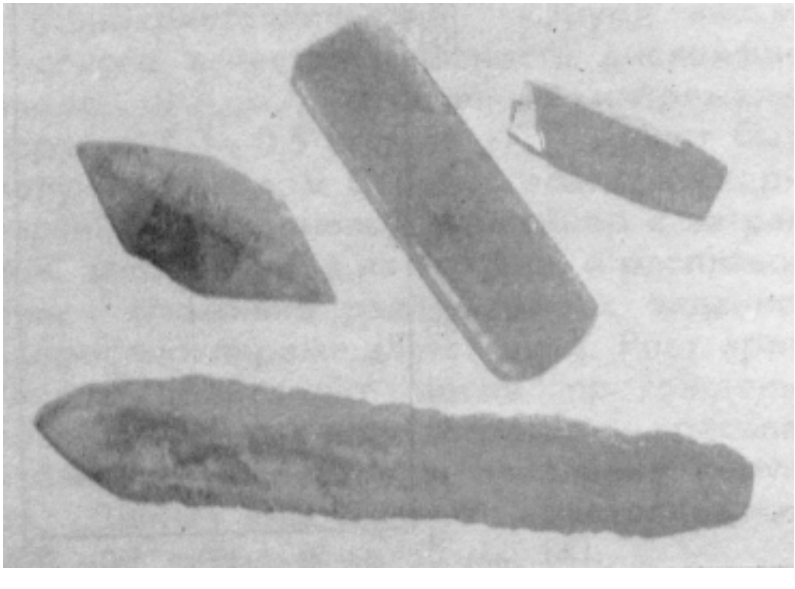

Figure 9.12. Hydrothermally grown ruby crystals.[68] *(Courtesy of V. S. Balitskii.)*

9.4.5 Hydrothermal Growth of Oxides of Ti, Zr and Hf

The oxides of titanium, zirconium, and hafnium belong to a group of chemically stable compounds with high melting points. These properties make them very important technological materials, but at the same time restrict the possibility of growing them in the form of single crystals. Among these three compounds, TiO_2 melts easily (1850°C) and can be grown by direct melting (Verneuil method), but analogous methods have not yet found successful practical application for ZrO_2 and HfO_2, since the melting points are rather high, 2700°C and 2780°C respectively. Hence, Li_2MoO_4, PbF_2, $Na_2B_2O_4$ fluxes are used to grow these crystals, as their high melting points make them difficult to grow directly from the melt. Although the crystallization of rutile by the Verneuil method is frequently employed, the method often yields crystals of a nonstoichiometric nature. Kuznetsov (1973) has reviewed the growth of oxides of titanium subgroup metals in detail.[69] Anikin et al. (1965) have obtained TiO_2 at 550°C and 1000 atm.[70] Subsequently, Harville and Roy (1967) have obtained TiO_2 crystals in H_2SO_4 solutions at 700°C and 1000–4000 atm. However, the growth rate was very low.[71] The commonly used solvents are solutions of alkalis, lithium, potassium, sodium, and ammonium carbonates and bicarbonates, sodium sulfide, lithium, potassium and ammonium chlorides, sulfates (Na_2SO_4, K_2SO_4), borax, boric acid, and fluorides (KF, NaF, NH_4F). The concentrations of the solutions were 5–40%.

DropBooks

TiO_2. Kuznetsov and his group have worked out the growth technology of TiO_2 (rutile phase) under hydrothermal conditions[69][72][73] using 7–10% KF or NaF and 5–10% NH_4F solutions at temperatures over 500–550°C and pressures of 500–800 atm. The amount of material transported increases with increasing temperature of the experiment. Crystals are prismatic with dark-brown or black color. When a small amount of $KClO_3$ is added to the nutrient, crystals become light green in color. Rutile synthesized by the hydrothermal method has properties closer to the natural rutile. In pure water and aqueous solutions of NaOH or Na_2CO_3 at temperatures below 350–400°C, the anatase phase of TiO_2 crystallizes and, at temperatures further down, the brookite phase crystallizes.[73]

A rutile crystal grown by Verneuil method was used as a seed and experiments were carried out at a solubility zone temperature 550–600°C, with respective autoclave filling coefficients of 0.6–0.5 and (T = 20–35°C.[73] Under these conditions the growth rate of the (100) and (110) faces was 0.15–0.21 mm/day in the five-day experiments. Typical conditions for

crystallization were 570°C, autoclave filling coefficient = 0.6, ΔT = 25°C. However, the given directions (100) and (110) are not directions of rapid growth. Judging by the morophology of the spontaneous rutile crystals (they often have a typical long-prismatic form), the growth rate along (001) should be higher.

ZrO_2 (Baddeleyite). Kuznetsov (1973) was the first to synthesize ZrO_2 crystals under hydrothermal conditions using fluoride solutions of NaF, or KF and NH_4F with concentrations 7–10% at temperatures of 520–690°C.[69] In KF solutions, ZrO_2 is transported only at temperatures over 600°C, and small crystals of 0.5 mm size are formed in the upper zone of the autoclave. Below 600°C, all that happens is that the original material is made coarser, and lamellar crystals up to 0.3 mm in size are formed in the lower zone of the autoclave. In NH_4F solution, there occurs an intensive recrystallization of ZrO_2 at relatively low temperatures. However, there are some practical difficulties in the growth of ZrO_2 due to the retrograde solubility in NH_4F solutions. In order to simplify the problem, in a furnace with a horizontal autoclave, a "hot" zone was created at the obturator. By this means, ZrO_2 crystals in the form of thin plates 2.5 × 2.5 × 0.5 mm with (001), (010) and (110) faces were obtained. Increase in the temperature gradient raises the growth rate and the crystals become thicker and form twinning. Growth rate is maximum in the "c" direction, minimum in the "a" direction, and slower in the "b" direction. The growth rate of the (100) face is roughly ten times lower than that of the (001). The basic properties of this synthetic ZrO_2 are closer to the mineral baddeleyite. Figure 9.13 shows a photograph of ZrO_2 crystals grown under hydrothermal conditions.

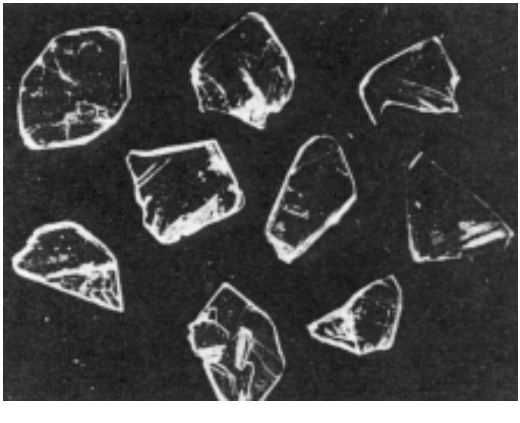

Figure 9.13. ZrO_2 crystals grown under hydrothermal conditions.[69] *(Courtesy of V. A. Kuznetsov.)*

HfO_2. According to Kuznetsov (1968), the growth of HfO_2 does not differ much from that of ZrO_2.[73] The crystallization of HfO_2 takes place at a higher temperature in KF and NaF solutions and at still higher temperatures in NH_4F solution (700°C). Again, the major disadvantage is the higher temperature of crystallization and retrograde solubility. Hence, in this case also, a horizontally disposed autoclave was used by Kuznetsov and his group.[69][73] The autoclave had a transverse baffle in which the orifice area was ~15% of the internal cross sectional area. Crystals up to 2 × 2 × 0.5 mm of HfO_2 (Fig. 9.14) were obtained.

DropBooks

Figure 9.14. HfO_2 crystals.[73] *(Courtesy of V. A. Kuznetsov.)*

9.5 HYDROTHERMAL GROWTH OF TELLURIUM DIOXIDE

Tellurium dioxide has two modifications: tetragonal (paratellurite) and orthorhombic (tellurite).[74][75] Among these two, the paratellurite is of great interest for solid state physicists, because of its valuable piezo-electric and acousto-optical properties. In particular, paratellurite crystals may be used in acousto-optical modulators of light deflectors and delay lines. At present, there are several methods of growing these crystals. The most popular is the Czochralski method but, in this method, the growth temperature is high and there are strong temperature gradients in the growth region.[76] This, together with high vapor pressure of tellurium dioxide, often results in the production of defected and stressed crystals. In addition, the method is rather cumbersome and only about 20% of crystals produced have acceptable quality.

The hydrothermal method of crystallization of paratellurite started almost at the same time as that of the Czochralski method.[74][75] However, the effects of various physical and chemical parameters on the growth of paratellurite crystals were not properly studied. This technology is not advantageous because of its poor reproducibility and poor quality of crystals. The possibility of obtaining spontaneous paratellurite monocrystals from solutions of hydrohalogenic acids was demonstrated in Ref. 64. It was found that the mass crystallization decreases in the following sequence: HCl > HBr > HI > HF, while all other parameters are the same.

The experiments done in platinum lined autoclaves showed that platinum dissolves in hydrohalogenide complexes, hence, the process of dissolution of TeO_2 in the acid deteriorates and goes out of control. Thus, effective usage of hydrothermal technology of paratellurite could not be developed owing to the difficulties in observing and controlling the parameters which determine the crystallization of α-TeO_2 in platinum-lined steel autoclaves.

Popolitov et al. (1975) have studied the solubility of paratellurite in detail in hydrochloric acid, which is an effective solvent for the recrystallization of TeO_2.[77] Figure 9.15 shows the dependence of solubility of tellurium dioxide and HCl concentration measured by titration with sodium hydroxide. The starting material used was monocrystals of paratellurite obtained through spontaneous crystallization from water solutions of HCl.

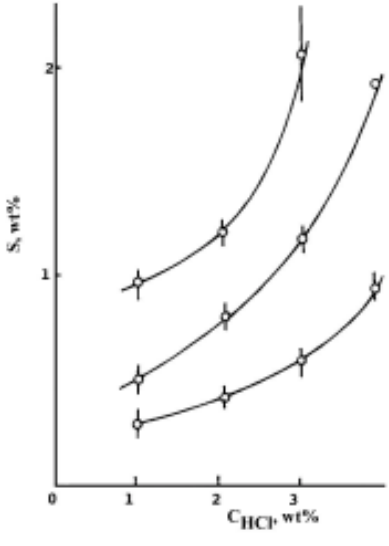

Figure 9.15. Dependence of solubility of tellurium dioxide and HCl concentration.[77]

The hydrothermal growth of monocrystals on seeds is known to include the following stages: dissolution of solid substance, transport of dissolved materials to the growth region, and the growth of seed crystals. To reveal the mechanism of transport, it is of great importance to use the data on solubility of paratelluride in HCl solutions and to consider the possible mechanism of transport from the dissolution region to the growth region in the process of α-TeO_2 growth on the seed.

The synthesis of paratellurite with 100% output occurs in aqueous solutions of nitric acid with concentrations up to 25% at temperatures of 260–340°C and pressures of 50–370 atm.[74] Element tellurium serves as the nutrient, so that the synthesis reaction occurs as follows:

Eq. (7) $$3Te + 4HNO_3 \rightarrow 3TeO_2 \text{ (solid)} + 2H_2O + 4NO \uparrow$$

With further rise in the concentration of aqueous nitric acid solution (>25%), there occurs the oxidation of the tellurium with the formation of crystals of telluric acid:

Eq. (8) $$Te + 6HNO_3 \rightarrow H_2TeO_4 \text{ (solid)} + 6NO_2 + 2H_2O$$

DropBooks

The morphology of paratellurite crystals is very interesting. The crystals grown in hydrochloric acid solutions exhibit more complex forms than the crystals obtained in nitric acid solutions. The paratellurite monocrystals grow in the form of a tetragonal prism (110) and tetragonal dipyramids (101) and (102). The growth forms of tellurium oxychloride monocrystals are pinacoids (001) and (010), rhombic prisms (110) and (130), and rhombic dipyramids (111), (112), (113), and (114). Figure 9.16 shows the habits of *(a)* tellurium dioxide, and *(b)* tellurium oxychloride crystals.

Popolitov and his group have studied, in detail, the kinetics of crystallization of paratellurite under hydrothermal conditions with reference to the mass transport, temperature gradient, solution concentration, growth rate and so on.[77][78] On the basis of the kinetic study of growth conditions for α-TeO_2 crystals, it was found that the growth rate in the homogeneous solution is limited by diffusion mass transport of the dissolved substance towards the growing faces, while in the binary phase, the surface processes are limited. A method for the optimal growth of the uniform α-TeO_2 monocrystals was developed wherein the crystals are grown on seeds and in 3.65 wt% water solution of HCl at 150–200°C.

Acoustic characteristics of α-TeO_2 monocrystals obtained by the hydrothermal method are similar to those of Czochralski grown crystals. A reader can find more information in Ref. 79.

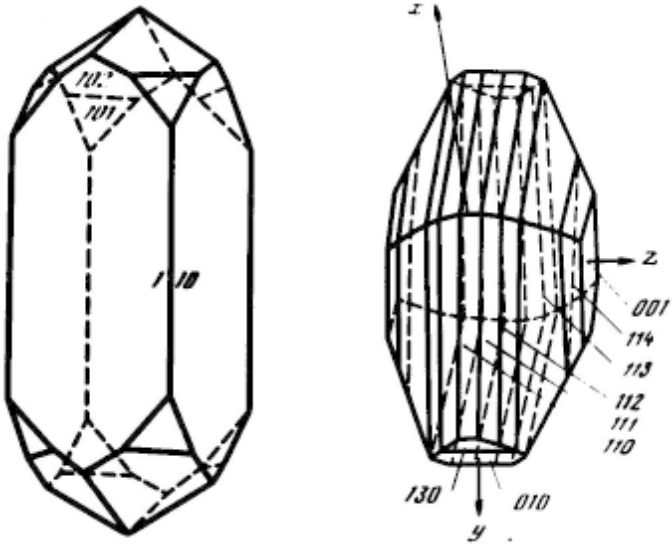

(a) (b)

Figure 9.16. Habits of *(a)* tellurium dioxides and *(b)* tellurium oxychloride crystals.[77]

9.6 HYDROTHERMAL SYNTHESIS OF TiO_2 AND RELATED OXIDE POWDERS

There is a growing interest in the application of oxide semiconductors as catalyst supporters, photocatalysts, oxidation catalysts, and electrocatalysts for carrying out chemical transformations of organic and inorganic compounds.[80]–[82] Fe_3O_4 powders with a spinel structure have potential applications for ferrofluid magnetic refrigeration, bioprocessing, and information storage.[83] Several other oxides like SnO_2 are used as gas sensors,[84] and α-MnO_2 as an adsorbent.[85] Among these especially, TiO_2 is the most important material being studied extensively in the last few years owing to its unique properties. TiO_2 shows maximum light scattering with virtually no absorption. It is non-toxic and chemically

inert. This has been employed extensively in studies of heterogeneous photocatalysis and has been accepted as one of the best photocatalysts for the degradation of environmental contaminants. The process involves the absorption of a photon by TiO_2, leading to the promotion of an electron from the valence band to the conduction band and thus produces an electron hole. The electron in the conduction band is then removed by reacting with O_2 in the outer system. The hole in the valence band can react with OH^- or H_2O species, which are adsorbed on the surface of the TiO_2 to give the hydroxyl radical. This hydroxyl radical initiates the photocatalytic oxidation, a pollution control technology or detoxification technology[86] which destroys the organic chemical contaminants in air, water, and soil. It can be used to treat the polluted water (both surface and ground water, similarly waste and drinking water) and soil. The technique can be used as an industrial pollution management technique for cleaning up gaseous and aqueous waste streams containing organic compounds. The photocatalytic activity of TiO_2 depends upon its crystal structure (anatase, or rutile), surface area, size distribution, porosity, and presence of dopants, surface hydroxyl group density, etc. These factors influence directly on the production of electron-hole pairs, the surface adsorption and desorption process and the redox process.

There are several ways of preparing TiO_2 particles.[87]–[90] The hydrothermal method has many advantages like producing a highly homogeneous crystalline product, which can be obtained directly at relatively lower reaction temperature (<150°C). Its most important feature is that it favors a decrease in agglomeration between particles, narrow particle size distributions, phase homogeneity, and controlled particle morphology. It also offers the uniform composition, purity of the product, monodispersed particles, control over the shape and size of the particles, and so on. The hydrothermal technique has been found to be one of the best techniques to prepare TiO_2 particles of desired size and shape with homogeneity in composition and a high degree of crystallinity. Hence, the authors have carried out the synthesis of TiO_2 under hydrothermal conditions and have used the material in the degradation of organic compounds.

It is well known that several organic pollutants present in industrial waste waters, phenol, nitrophenol isomers and their derivatives, aromatic hydrocarbons, cyanide, sulfites, and so on, have been completely removed by using this TiO_2 based heterogeneous photocatalysis. Several authors have studied in detail the mild hydrothermal synthesis of TiO_2 particles and the influence of various parameters like temperature,

DropBooks

experimental duration, pressure (percentage fill), solvent type, pH, and the starting charge on the resultant product.

The synthesis of TiO_2 is usually carried out in small autoclaves of Morey type, provided with Teflon® liners. The conditions selected for the synthesis of TiO_2 particles are: $T = < 200°C$, $P < 100$ bars. Such pressure-temperature conditions facilitate the use of autoclaves of simple design provided with Teflon® liners. The use of Teflon® liners has helped to obtain pure and homogeneous TiO_2 particles. Though the experimental temperature was low ~ 150°C, TiO_2 particles with a high degree of crystallinity and the desired size and shape could be achieved through a systematic understanding of the hydrothermal chemistry of the media. Here it is appropriate to mention that the size of the titania particles is a most critical factor for the performance of the material in the photocatalytic activity, and the monodispersed nanoparticles are the most suitable ones. It has been shown that the particle size is a crucial factor in the dynamics of the electron/hole recombination process, which offsets the benefits from the ultrahigh surface area of nanocrystalline TiO_2. The dominant e^-/h^+ recombination pathway may be different for TiO_2. Different particle size regimes have been established for improving the photocatalytic efficiencies of different systems.[91]

The starting materials such as that of TiO_2 and the solvent with a definite molarity (1.5 to 4.0 m) were taken in a Teflon® liner. The internal pressure was maintained below 100 bars through percent fill in the liners. The starting mixture was stirred thoroughly to obtain a homogeneous and relatively viscous solution, which was later kept inside an autoclave and heated at 150°C for about 40–48 hours. Several solvents like NaOH, KOH, HCl, HNO_3, HCOOH and H_2SO_4 were treated as mineralizers and it was found that HNO_3 is a better mineralizer for obtaining monodispersed nanoparticles of titania with homogeneous composition under the present experimental conditions.[82] The authors have used different starting charges such as reagent grade anatase, sintered anatase (at about 800 to 900°C for 10 hours), $TiCl_4$ and titanium gel. In each case, the resultant product was TiO_2, however, with different ratios of rutile and anatase depending upon the charge, as confirmed from the x-ray powder diffraction studies. Though the rutile phase was more dominant in the resultant product, the presence of a small amount of anatase persisted except when the experimental temperature was approximately 200°C. When sintered anatase or titanium gel was used as charge, it yielded better results, for example, the resultant

product contained more or less uniformly sized or monodispersed particles with a high degree of crystallinity, and interestingly, the rutile phase was formed as a prominent phase with a better yield. Better results, in this sense, meant good photocatalytic activity because of the monodispersed particles with a high degree of crystallinity. Similarly, the authors have tried $TiCl_4$ as charge, and the resultant product contained both anatase and rutile. The formation of a single phase required the proper selection of pH of the media and crystallization temperature. The present authors have carried out the TiO_2 synthesis within a wide range of pH values of the media. When the pH of the medium was low (pH = 1 to 2) only rutile phase was formed. When the pH was kept even lower, i.e., in the negative range, the product contained a small amount of anatase also. As the pH of the medium was increased, the product contained essentially anatase with very little rutile. Thus, with the addition of KOH or NaOH, the formation of anatase phase was favored. With a further increase in the pH, i.e., beyond twelve, in the present experimental temperature, only an amorphous material was obtained. Raising the temperature results in the formation of alkali titanates. Table 9.2 gives the results of the mild hydrothermal experimental preparation of ultrafine particles of TiO_2. Thus, it is necessary to maintain a proper acidity in the system in order to obtain a homogeneous rutile phase. Similarly, control over the temperature, time, and pH of the medium helps in the preparation of a desired particle size and shape. When the reaction temperature and time were increased, it resulted in the formation of faceted grains of bigger size. Figure 9.17 *a* and *b* shows the representative photographs of TiO_2 particles prepared under hydrothermal conditions. The following experimental conditions were maintained for the preparation of ultrafine rutile particles of TiO_2:

PrabBooks

Nutrient	pre-heated anatase phase or Ti gel
Temperature	150°C
Duration	40 hours
pH	2
Fill %	60%
Mineralizer	1.5 M HCl

Table 9.2. Hydrothermal Experimental Conditions of the Preparation of TiO_2 Ultrafine Particles

Sl. No	Nutrient	Solvent	% Fill	PH	T °C	Time Hours	Remarks
1.	TiO_2 – 2 gm WO_3 – 0.1 gm	1.5M HCl	60	2	150	40	Rutile & anatase ultrafine particles
2.	TiO_2 – 2 gm WO_3 – 0.3 gm	1.5M HNO_3	65	1.8	150	45	Anatase & rutile fine particles
3.	TiO_2 –2 gm WO_3 – 0.3 gm	1.5M HCOOH	60	1.9	160	40	Rutiles & anatase fine particles
4.	TiO_2 –2 gm WO_3 – 0.3 gm	1.5M H_2SO_4	55	2.0	160	40	Rutile & anatase ultrafine particles
5.	TiO_2 –2 gm WO_3 – 0.1 gm	1.5M HCl +1.5M HNO_3	50	1.4	150	48	Anatase & rutile
6.	TiO_2 –2 gm WO_3 – 0.1 gm	1.5M HCl +1.5M HCOOH	60	1.3	160	48	Anatase & rutile
7.	TiO_2 –2 gm WO_3 – 0.3 gm	1.5 HCl + 1.5M H_2SO_4	60	1.2	150	40	Anatase & rutiles particles
8.	TiO_2 –2 gm WO_3 – 0.3 gm NaOH – 1 gm	1.5M HCl	65	2.8	150	40	Rutile & anatase ultrafine particles
9.	TiO_2 –2 gm WO_3 – 0.1 gm NaOH – 2 gm	1.5M HCl	60	3.4	150	48	Rutile & anatase particles
10.	TiO_2 –2 gm WO_3 – 0.1 gm NaOH – 3 gm	1.5M HCl	65	4.2	150	60	$Na_2Ti_6O_{13}$ $Na_2Ti_3O_7$ grains
11.	TiO_2 –2 gm WO_3 – 0.1 gm	2.5M HCl	50	1.2	160	55	Anatase & rutile particles
12.	TiO_2 –2 gm WO_3 – 0.3 gm	4M HCl	55	0.8	150	40	Anatase & rutile
13.	TiO_2 –2 gm WO_3 – 0.3 gm NaOH – 6 gm	1.5M HCl	55	8.1	200	48	$Na_2Ti_3O_7$

(Cont'd.)

Table 9.2. *(Cont'd.)*

Sl. No	Nutrient	Solvent	% Fill	PH	T °C	Time Hours	Remarks
14.	TiO_2 –2 gm WO_3 – 0.3 gm ethanol – 0.1wt%	1.5M HCl	60	2.8	150	40	TiO_2 ultrafine particles with a good yield
15.	TiO_2 –2 gm WO_3 – 0.3 gm urea – 0.1 wt%	1.5M HCl	60	2.7	150	40	TiO_2 ultrafine particles with a good yield
16.	TiO_2 –2 gm WO_3 – 0.3 gm tetrabutyl – ammonium 0.1 wt%	1.5M HCl	60	3.0	150	38	TiO_2 ultrafine particles With a good yield
17.	Titanium gel 2.5gm WO_3 – 1.0 wt%	1.5M HCl	60	2.8	150	46	Ultrafine particles of rutile
18.	Sintered anatase - 2.0 gm WO_3 – 0.3 wt%	1.5M HCl	60	2.2	150	46	Ultrafine particles of rutile

DropBooks

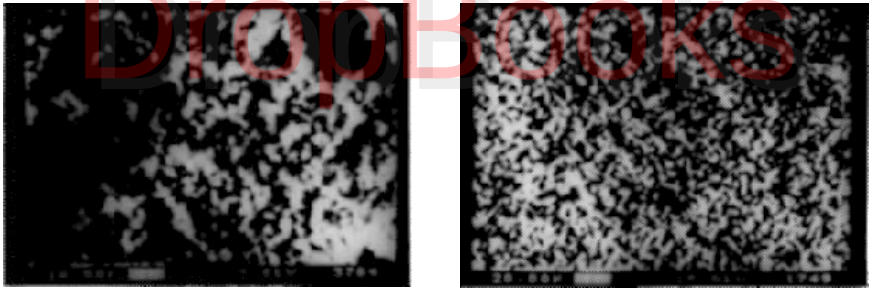

Figure 9.17. Representative photographs of TiO_2 particles.

Qian et al. (1993) have reported the preparation of ultrafine powders of TiO_2 by hydrothermal H_2O_2 oxidation starting from metallic Ti.[90] This can be done in two steps: *i)* oxidation of Ti with an aqueous solution of H_2O_2 and ammonia to form a gel (TiO_2, H_2O), and *ii)* hydrothermal treatment of gel under various conditions. It is expressed as follows:

$$Ti + 3H_2O_2 + 2OH^- \xrightarrow{\text{oxidation}} TiO^{2-}_4 + 4H_2O$$

$$2TiO^{2-}_4 + 2(x+1)H_2O \xrightarrow{\text{heating}} 2TiO_2.\, xH_2O + O_2 + 4OH^-$$

$$TiO_2 \cdot xH_2O \xrightarrow[\text{treatment}]{\text{hydrothermal}} TiO_2 + x\ H_2O$$

It is well known that the photocatalytic activity in TiO_2 increases with the addition of MoO_3, WO_3, or other active element. Therefore, the present authors have introduced WO_3 into the composition of TiO_2 from 5 and 10 wt% by adding the required amount of WO_3 into the nutrient (starting materials) and tested all the samples in the photocatalytic degradation of hydrocarbons. It is to be noted that the introduction of WO_3 up to 10 wt% did not change the homogeneity of the resultant product except for a slight increase in the cell volume. Also, the grain morphology and size did not alter significantly.

In some experiments, the authors have introduced a very small quantity of tetra butyl ammonium hydroxide or ethanol or urea. Addition of these organics enhances the crystallization kinetics greatly and also increases TiO_2 yield. However, the concentration of these organics was maintained at < 0.1 wt% as it alters the size and shape of the particles.

Figure 9.18 shows the TEM micrographs of TiO_2 powder prepared by hydrothermal treatment of gel. Chen et al. (1995) have prepared TiO_2 powders with different morphologies by an oxidation hydrothermal combination method.[89] The effects of carboxymethyl cellulose sodium (CMC), HNO_3, Al^{3+} and K^+ (F^-) additives on the particle shape and crystalline structure are also discussed by these authors. They also studied the crystallization of TiO_2 in great detail, the influence of hydrothermal conditions, pH, reaction temperature, time and mineralizer. Figure 9.19 shows the TEM micrographs of the products with different mineralizers.[80]

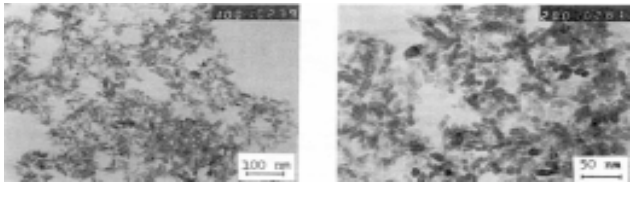

Figure 9.18. TEM micrographs of TiO_2 powder.[89]

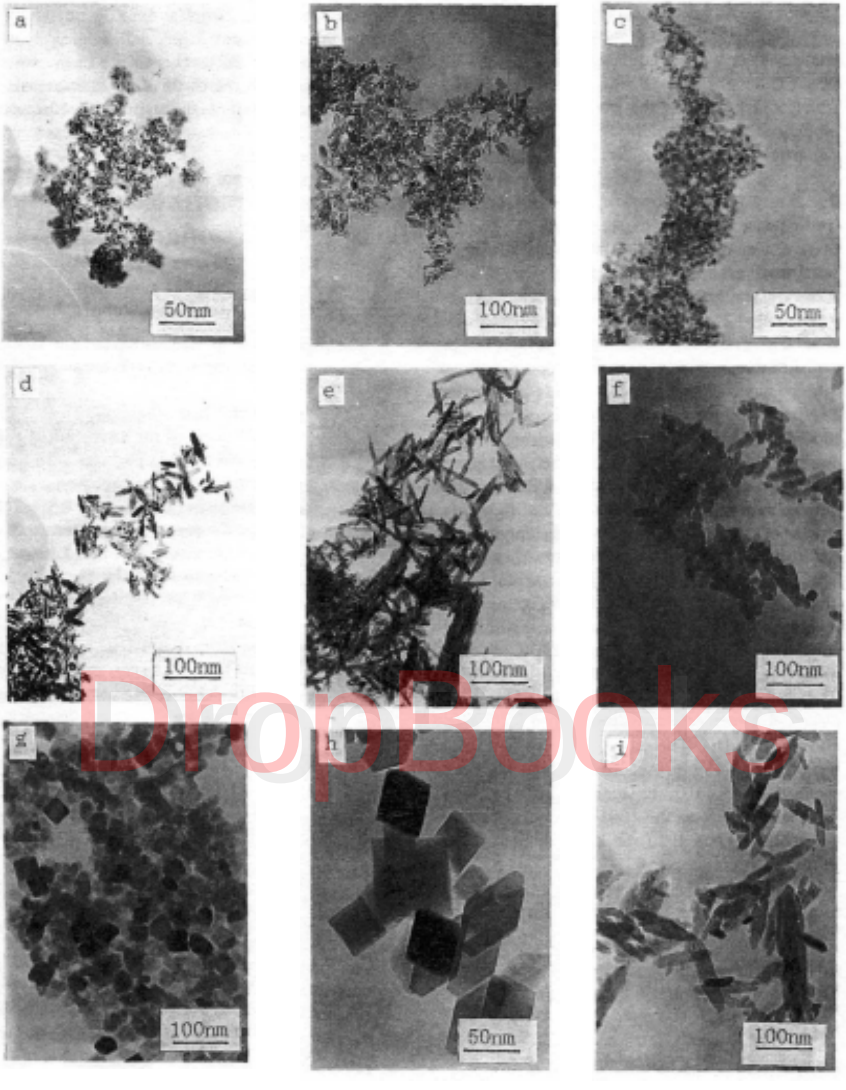

DropBooks

Figure 9.19. TEM micrographs of TiO_2 powder prepared by hydrothermal treatment of Gel: *(a)* in distilled water at 140°C for 12h, *(b)* in distilled water at 200°C for 12h, *(c)* in distilled water with 0.5wt% mineralizer of CMC at 140°C for 12h, *(d)* in 1.0N nitric acid solution at 140°C for 12h, *(e)* in 1.0M nitric solution at 140° for 24h, *(f)* in 1.5N nitric solution at 140°C for 12h, *(g)* in 1.0N nitric acid solution with mineralizer of 0.5wt% KF at 140°C for 12h, *(h)* in 1.0 N nitric acid solution with mineralizer of 0.5wt% KF at 140°C for 12h, and *(i)* in 1.0N nitric acid solution with mineralizer of 0.5wt% Al(NO3)3 at 140°C for 12h.[80] *(Courtesy of the American Chemical Society, Washington, DC.)*

Here, it is impossible to discuss the application of TiO_2 in great detail, because of the enormous amount of literature data available with reference to the photochemical transformations of organic and inorganic compounds, and the catalyst properties, for example, the honeycomb structured porous titania as an odor remover; improving the durability of automotive catalyst; using TiO_2 photocatalyst, the destruction of phenol in water,[93] and degradation of a large variety of trihalomethyl radicals.[94] Similarly, wastewater can also be treated.[95] Byrappa et al. (1999) have studied the photocatalytic degradation of HCCH, and DDT where complete mineralization occurs via the formation of benzophenone derivative Eq. (10).

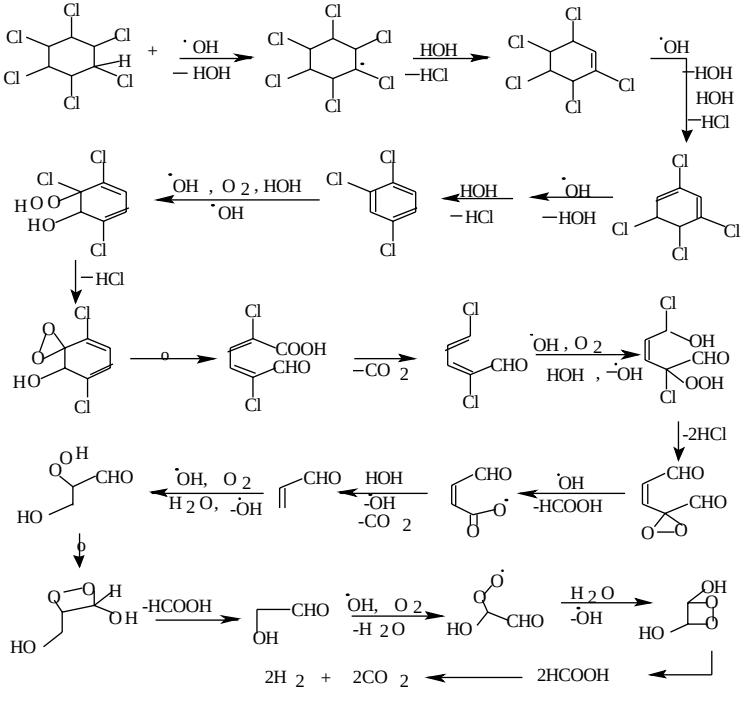

Scheme 1

Eq. (9) $HCCH + 4O_2 + 5H_2O + {}^{\bullet}OH \xrightarrow[\text{-}\dot{O}H]{} 6HCl + 6CO_2 + 4H_2$

Eq. (10) $DDT + 8\ H_2O + 10\ O_2 \quad 14\ O_2 + 8H_2 + 5\ HCl$

In a typical experiment, solution of hexachlorocyclohexane (30 mg) with acetone (20 ml) taken in a flat bottomed flask was treated with 0.1N sodium carbonate (5 ml) and then diluted with distilled water until turbidity persisted. At this junction, one or two drops of acetone were added to clear the solution. To this test solution ~20mg of TiO_2 doped with WO_3 was added and kept in sunlight. Under similar conditions, a blank solution (without TiO_2) was also tested. TLC followed the progress of the reaction. At regular intervals, aliquots of the reaction mixture were removed from both the flasks and extracted into ether separately. It was then spotted on a TLC plate and developed in different solvent systems. The identification of spots was done by keeping the TLC plates in an iodine chamber. It was observed that, as the reaction time increased, the concentration of anthracene decreased and after 2–4 hrs, complete disappearance of HCCH occurred. Similar treatment was given to DDT, which took 5–6 hrs for complete mineralization.

Several authors[96]–[98] have carried out the preparation of magnetite powder. In the pure Fe_2O_3-H_2O system, α-Fe_2O_3 (hematite) is stable up to about 550°C. Above this temperature, up to 710°C, mixtures of α-Fe_2O_3 and Fe_3O_4 are stable. Runs above 710°C yield magnetite (Fe_3O_4) as the only stable phase. Viswanthiah et al. (1980) have conducted experiments in the temperature interval 100–600°C.[95] Traces of magnetite are found to be stable even at temperatures as low as 100°C. From 100 up to 200°C, iron formate ($C_2H_2FeO_4 \cdot 2H_2O$) and hematite (α-Fe_2O_3) are the major phases along with traces of magnetite. HCOOH is used as the mineralizer, and it contributes to the formation of siderite phase also. Further, the liberation of carbon monoxide in the system creates a reducing environment, which promotes the stabilization of Fe_3O_4 rather than of Fe_2O_3. Thus, perfect octahedral crystals of magnetite are formed at 250°C. Figure 9.20 shows hydrothermally grown magnetite crystals, as well as aggregates.

ProBooks

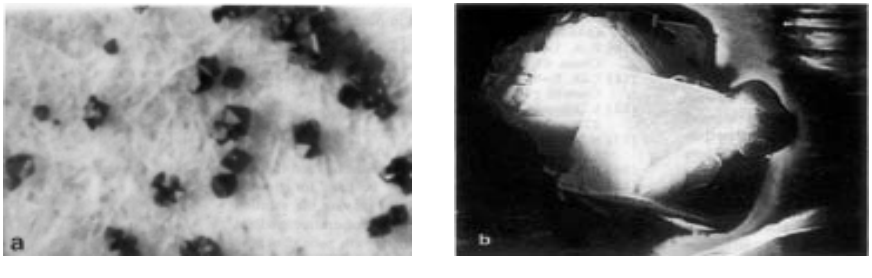

Figure 9.20. Hydrothermally grown magnetite crystals. *(Photo courtesy of Dr. J. A. K. Tareen.)*

Although there are several methods of preparing crystalline iron oxide powders, hydrothermal and sol-gel techniques are supposed to be the most popular ones. Hirano and Somiya (1976) have obtained magnetite crystals under hydrothermal conditions in the presence of hydrogen.[97] The hydrogen for the control of the reduced atmosphere was supplied by the reaction of charged metallic iron with water.[98] The experiments were carried out at 550°C and 1000 kg/cm^2. As the concentration of hydrogen was increased, the (110) faces of magnetite were found to predominate over the (111) faces. The authors have used 10M NaOH as the solvent. No hematite formation was reported. Dendritic magnetite crystals were grown in 5M NH_4Cl solution at 500°C under 1000 kg/cm^2. Figure 9.21 shows the dendritic magnetite crystals grown in 5M NH_4Cl solution in 5.3M mole hydrogen.

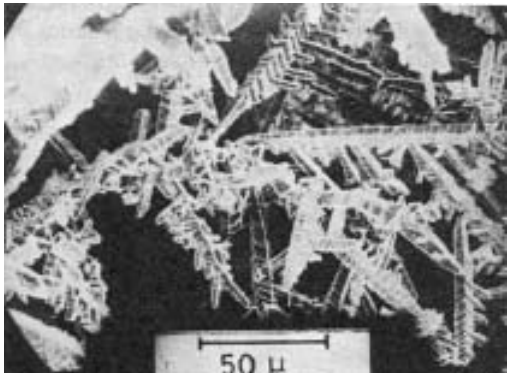

Figure 9.21. Dendrite magnetite crystals grown in 5M NH_4Cl solution 5.3M mole Hydrogen.[98]

Chen and Xu (1998) have prepared Fe_3O_4 particles of nanometer size hydrothermally from iron (II) 2-methoxyethoxides ($Fe(OMOE)_2$), using 2-methoxyethanol (MOE)-water mixed solvent as the medium.[83] As in the TiO_2 preparation, here also the reaction conditions such as solvent, temperature, and time usually have important effects on the resultant products. These authors have shown that the particle size of Fe_3O_4 powders increase with prolonged reaction time.

In recent years, hydrothermal synthesis of magnetite in the presence or absence of organic chelating agents, oxidation of ferrous solutions using KNO_3, and solvothermal methods have become popular.[99][100] The ability to direct the morphology of magnetite particles may be a key

feature in the development of new applications, particularly if other physical, chemical and electronic properties are retained. The formation of iron oxide phases is often influenced by the addition of secondary additives to aqueous systems containing either soluble or insoluble precursors of the iron oxides. There have been quite a few reports dealing with the influence of transition metals on the dissolution-precipitation reactions in which iron oxides can participate under hydrothermal conditions. McGarvey and Owen (1996) have obtained magnetite under hydrothermal conditions at 150°C and 175°C in the presence of hydrazine and copper (II) oxide.[98] In the absence of CuO, octahedral crystals of magnetite corresponding to the literature data are found. In the presence of CuO, magnetite crystals with distorted morphology were prepared[99] in which the crystal faces were absent, leaving a framework structure of corners and edges. (See Fig. 9.22.) Substitution of NiO, ZnO, or Ag_2O produced somewhat different results. Thus copper, as a result of having three accessible oxidation states [Cu(O), Cu^{+1} and Cu^{+2}] and rapid electron transfer between the species, is able to participate in a redox catalytic mechanism involving hydrazine to facilitate the reduction of hematite to magnetite as well as directing its morphology. Uchida et al. (1992) have prepared micaceous iron oxide by the oxidation of iron with pressurized oxygen in concentrated sodium hydroxide solution at elevated temperature.[100] Thus, the preparation of iron oxide under hydrothermal conditions is an attractive field.

PropBooks

There are several other reports in the literature on hydrothermal synthesis of simple oxides like Mn_3O_4, PbO, VO_2, GeO_2, SnO_2, V_2O_3, R_2O_3, In_2O_3, Bi_2O_3, CdO, HgO, and so on.

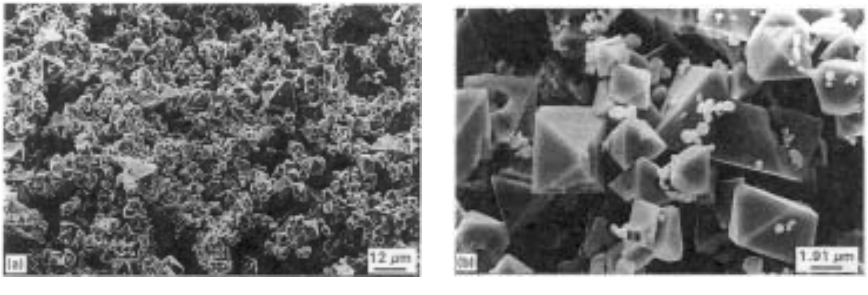

Figure 9.22. Magnetite crystals with distorted morphology.[99]

9.7 HYDROTHERMAL SYNTHESIS OF MIXED OXIDES

Mixed oxides form one of the most important modern materials. The group includes aluminates, garnets, spinel, metal oxides with complex structures, and so on. Especially in the last three to four years, the number of these complex oxides is increasing. Here, we discuss the hydrothermal synthesis of only some important complex oxides.

9.7.1 Hydrothermal Synthesis of Aluminates

The majority of the aluminates form in pure water at elevated temperatures (>500°C) and pressures (>1000 atm). The hydrothermal reaction involving divalent metals takes place through $MeO + Al_2O_3 \rightarrow MeAl_2O_4$.

Since pure water is used in the synthesis of these oxides, their solubility is very low, and to obtain 100% output, it is necessary to maintain the ratio of MeO/Al_2O_3 in the nutrient at 1:1—i.e., to the near stoichiometry. Aluminates crystallize as small crystals of < 0.1 mm. The aqueous solutions of NaOH are preferable in the synthesis, however, crystallization of aluminates of transitional metals (Fe, Co, Ni) takes place with the formation of corresponding oxides. Litvin and Popolitov (1984) have carried out the synthesis of aluminates of Ca, Be, Zn, Fe, Co and Ni under hydrothermal conditions.[101]

For alkaline earth metals (MeO/Al_2O_3 > 2:1) the characteristic feature is the formation of hydrogarnets of type $Me_3Al_2O_6{\cdot}6H_2O$. Crowley (1964) has carried out the synthesis of $Me_3Al_2O_6{\cdot}6H_2O$ in the system $CaO\text{-}Al_2O_3\text{-}H_2O$, at temperatures less than 250°C and partial pressure of water 500–800 atm.[102]–[104] In pure water, 100% output is achieved at MeO/Al_2O_3 ratio in the nutrient equal to 3:1. The stoichiometry of the nutrient may be strongly inclined towards the surplus MeO while synthesizing in the aqueous solutions of NaOH. Moreover, in the synthesis of strontium hydrogarnet, it is shown that the monophase synthesis sharply increases in the highly concentrated solutions as shown in Fig. 9.23 for the system $SrO\text{-}Al_2O_3\text{-}NaOH\text{-}H_2O$ at 500°C.[105] The crystals are either cubic or rhombic dodecahedral in habit. Synthesis takes place at CaO/Al_2O_3 > 5:1 within the temperature interval 300–450°C.[105] Figure 9.24 shows the habit of the calcium aluminate crystals. Similarly, the strontium aluminates form.

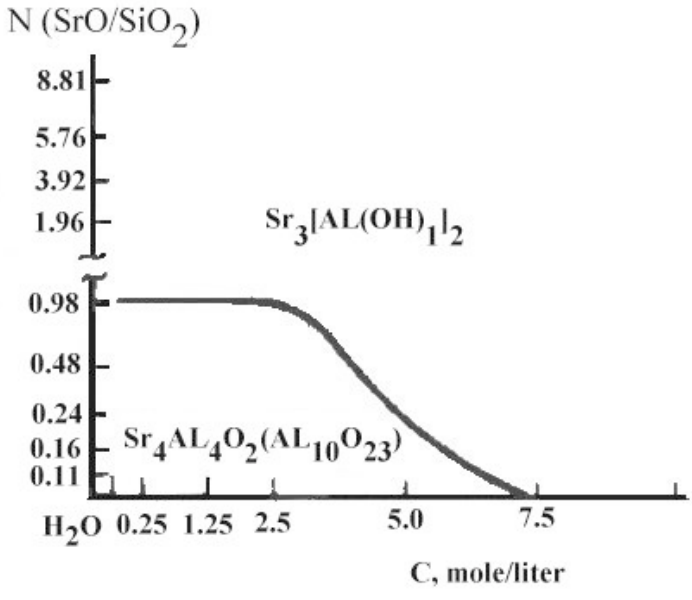

Figure 9.23. Phase diagram for the system SrO-Al_2O_3-NaOH-H_2O at 500°C.[105]

DropBooks

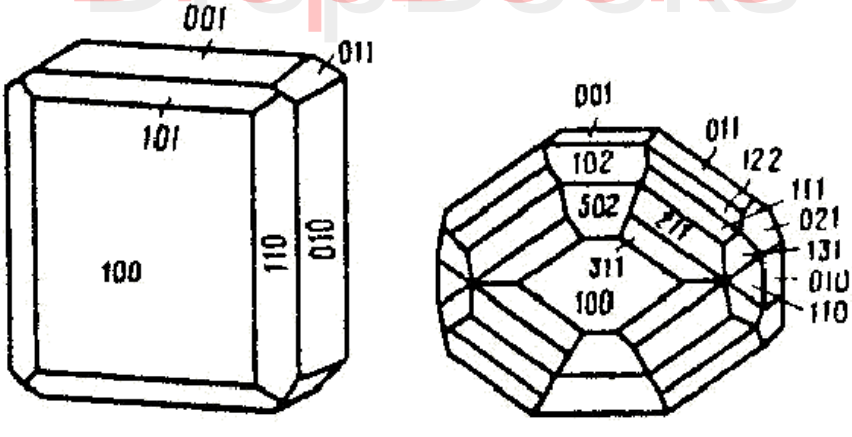

Figure 9.24. Habit of the calcium aluminate crystals.[104]

In weakly concentrated solutions, new phases like $Sr_4Al_{14}O_{25}$, plate-like crystals of aluminates belonging to the rhombohedral symmetry with space group Pmma are obtained.

In the system $Na_2O(K_2O)$-Bi_2O_3-Al_2O_3-H_2O bismuth tetra-aluminate, $Bi_2Al_4O_9$ crystals have been synthesized under hydrothermal conditions.[103] The crystallization occurs at higher concentration of Al_2O_3 in the nutrient in the order of 45–90 wt%. The pure phase occurs only when the molar ratio of Bi_2O_3:Al_2O_3:H_2O = 0.8:0.05:1, and with a rise in concentration of NaOH, the monophase synthesis reduces. This is connected with the structure becoming unstable with the rise in the concentration of NaOH. These crystals belong to the rhombic system with special group Pbam, and the crystals have (110) and (001) forms. However, the size of the crystals is < 1.0 mm.

9.7.2 Hydrothermal Synthesis of Antimonites and Antimonates

Oxides of trivalent antimony belong to the group of antimonates. Among hydrothermally synthesized rare earth penta-antimonites, $R_3Sb_5O_{12}$ and $In_3Sb_5O_{12}$ are the important ones.[106]–[108] Following are the penta-antimonites obtained by hydrothermal technique:

$$In_3Sb_5O_{12},\ La_3Sb_5O_{12},\ Pr_3Sb_5O_{12},\ Tb_3Sb_5O_{12},\ Yb_3Sb_5O_{12}$$

The synthesis of these compounds is usually carried out by the hydrothermal technique within the temperature interval 450–550°C and ΔT = 0.5 to 1.0°C, P = 110–1100 atm.

Variation in the ratio of $R_2O_3(In_2O_3)/Sb_2O_3$ in the nutrient limits the crystallization of the product with the appearance of Sb_2O_3 crystals. Higher concentration of KF or CsF results in formation of K_3RF_6 and both of these phases often reduce the output of penta-antimonites, field.

Penta-antimonite, $In_2Sb_5O_{12}$ forms in the aqueous solutions of KHF_2, KF (45–55wt%) and CsF (20 wt%). The crystals are 1–2 mm in size. The basic forms are hexagonal $(11\bar{2}0)$ and trigonal $(01\bar{1}0)$ prisms, pyramids $(01\bar{1}2)$, $(10\bar{1}1)$, $(02\bar{2}1)$ and $(\bar{1}3\bar{2}\ \bar{1})$. This compound has three polymorphic modifications and two are reversible transformations: trigonal α-form (<140°C), trigonal β-form (140-450°C) and cubic γ-form (>450°C).[107] Figure 9.25 shows the $In_3Sb_5O_{12}$ crystals obtained under hydrothermal conditions.[108] These crystals show interesting piezoelectric and ferroelectric properties.

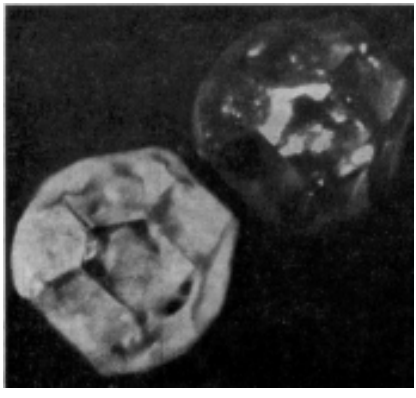

Figure 9.25. $In_3Sb_5O_{12}$ crystals obtained under hydrothermal conditions.[108]

Similarly, $Sc_3Sb_5O_{12}$ crystallizes in the aqueous solutions of KF with concentration up to 60 wt%. The synthesis of scandium penta-antimonite takes place simultaneously with the formation of K_3ScF_6 and attains 70% output in 30% KF solution; In aqueous solutions of CsF with concentrations of 12–60 wt% and Sc_2O_3/Sb_2O_3 ratio > 1:1, $Sc_3Sb_5O_{12}$ crystallizes with 100% output. The morphology of these crystals is similar to that of indium analogue.[108]

Rare earth antimonites with a general formula $R_3Sb_5O_{12}$ (R= La, Pr, Ti and Yb) are the important compounds in this group.[109] It is interesting to note that the lanthanum penta-antimonite crystallization field does not exist and its crystallization in aqueous solutions of KF with concentrations of 5–50 wt% is always accompanied by the related phases. Stefanovich et al. (1982) have studied the phase transformations in these rare earth antimonites in detail.[110] In the presence of an oxidizing agent, trivalent antimony oxidizes up to the pentavalent state forming antimonates and producing $H[Sb(OH)_6]_6$ acid. They are poorly soluble in water. There are several antimonate minerals and among the synthetic varieties, only a few compounds have been obtained: $Na[SbO_3]$, $Na_3Sb_3[Sb_2O_{11}]$ and $Sb[SbO_4]$.[111][112] Figure 9.26 shows *(a)* the field of crystallization of antimonites in the system Na_2O-Sb_2O_3-Sb_2O_5-H_2O, and *(b)* field of synthesis of antimonites. Figure 9.27 shows the field of crystallization of antimony antimonates at *(a)* lower and *(b)* higher oxygen potential.[111] Synthesis is carried out in aqueous solutions in 70% NaOH, 60% KF and 13% KHF_2, at temperature 550°C, with 60–70% fill, and a temperature gradient of 20–35°C. In order to stabilize the pentavalent antimony,

PrepBooks

10–15% H_2O_2 is added. In Sb_2O_5, the rich region (2.5:1) forms $NaSbO_3$; with the change in the oxygen potential in the system, other phases crystallizing in the system are $Sb^{3+}Sb^{5+}O_4$ and $Na_3Sb_3{}^{3+}Sb_2{}^{5+}O_{11}$. In highly concentrated aqueous solution of NaOH (>42%), $Na_3Sb_3{}^{3+}Sb_2{}^{5+}O_{11}$ crystals are formed into prisms up to 5 mm size. In this system, the field of crystallization of $Sb^{3+}Sb^{5+}O_4$ with 100% output doesn't exist. Antimonates can be crystallized in the aqueous KF solutions with concentration 60% and 98% KHF_2 at temperatures of 450–550°C and 60–70% fill.[111] In aqueous KHF_2 solutions, only two phases are formed: Sb_2O_3 and $Sb^{3+}Sb^{5+}O_4$. The antimony antimonates exhibit antiferroelectric properties.

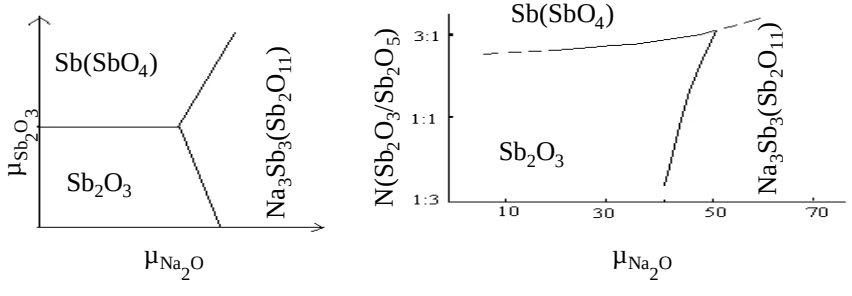

Figure 9.26. *(a)* Field of crystallization of antimonates in the system Na_2O-Sb_2O_3-Sb_2O_5-H_2O and *(b)* field of synthesis of antimonites.

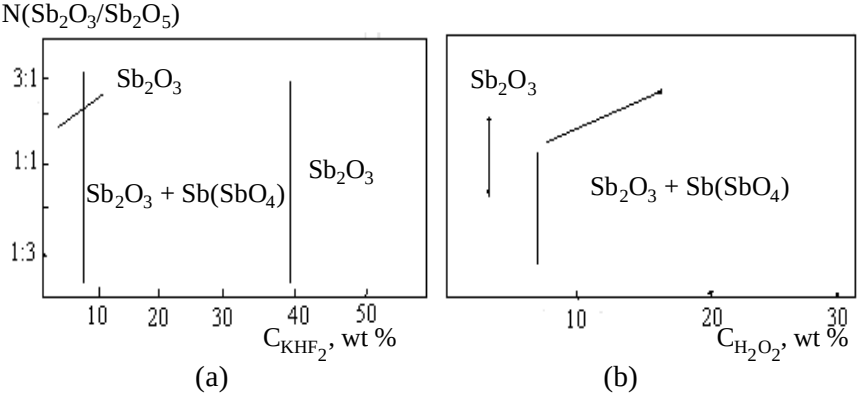

Figure 9.27. Field of crystallization of antimonates at *(a)* lower and *(b)* higher oxygen potentials.[111]

9.7.3 Hydrothermal Synthesis of Garnets

Garnet, $Y_3Al_5O_{12}$, has extensively been used as a host lattice for luminescent ions and as substrates for the epitaxial deposition of magnetic garnets for magnetic bubbles. For these applications, large defect free crystals are requested. Though garnets are ordinarily grown from the flux, the hydrothermal technique is particularly suitable for the preparation of these mixed oxide crystals of high quality and large size. Such growth is easier to control on a seed and it takes place at a lower temperature than the flux growth.[113]–[115]

Yttrium aluminum garnet, $Y_3Al_5O_{12}$, crystallization has been studied in a variety of solvents including $(CO_3)^-$, $(OH)^-$ and halides. Among these, higher temperatures of synthesis are required for growth. Laudise and Kolb (1962); Kolb and Laudise (1975) have studied the phase equilibria of $Y_3Al_5O_{12}$, and $Y_3Fe_5O_{12}$ in the systems Y_2O_3-Al_2O_3-H_2O and Y_2O_3-Fe_2O_3-H_2O respectively.[116][117] Brochier et al. (1972) and Toudic and Passaret (1974) have studied the heteroepitaxial growth of thin $Y_3Fe_{5-x}Ga_xO_{12}$ and $Gd_yY_{3-y}Fe_{5-x}Ga_xO_{12}$ films under hydrothermal conditions using GdGaG as seed plates.[118][119] Similarly, there are several other reports on the hydrothermal epitaxial growth of garnet films.[120]–[123] Figure 9.28 shows the part of the phase diagram Al_2O_3-Y_2O_3-H_2O between 350 and 450°C at a pressure of 25,000 psi, where the K_2CO_3 concentration is constant at 6M. $Gd_3Ga_5O_{12}$ appears to be incongruently saturating in contrast to $Y_3Al_5O_{12}$. Both growth rate and quality were poorer in $(CO_3)^=$ than in $(OH)^-$ at comparable concentrations. Indeed, in 6.0M K_2CO_3, under conditions where growth in $(OH)^-$ was appreciable, seeds grew a negligible amount or dissolved slightly. This is in contrast to Al_2O_3 (corundum) where $(CO_3^=)$, because of the higher coefficient of solubility, gives much larger rates than $(OH)^-$. Thus, $(CO_3^=)$ is preferable to $(OH)^-$. The optimum growth conditions for GdGa are:[117]

Excess Ga_2O_3	:	2-3M
Solvent	:	420°C
Growth temperature	:	80°C
Fill %	:	70–72%
Seed orientation	:	(100) (111)
Growth rate	:	as high as 0.6mm/day flawed; improved quality at rates near 0.25mm/day

DropBooks

These authors have obtained a wide range of garnets using flux grown nutrient:

$Gd_{2.34}Tb_{0.66}Fe_5O_{12}$

$Eu_{1.9}Ga_{1.1}Al_{0.5}Fe_{4.5}O_{12}$

$Er_{2.0}Eu_{1.0}Fe_{4.3}Ga_{0.7}O_{12}$

$Er_{1.0}Eu_{2.0}Fe_{4.3}Ga_{0.7}O_{12}$

$Ca_{1.8}Bi_{1.2}V_{0.9}Fe_{4.1}O_{12}$

$Ca_{2.0}Bi_{0.95}V_{0.95}Fe_{4.05}O_{12}$

In most of the experiments on the hydrothermal growth of garnets, hydrothermal tipping is used to avoid the seed attack during the warm-up stage.

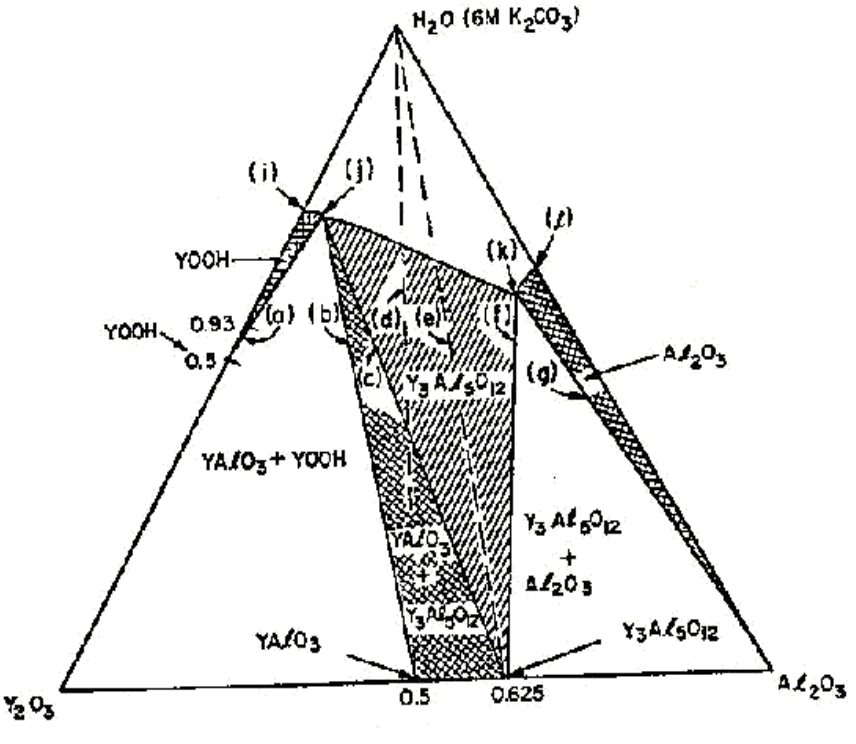

Figure 9.28. Phase diagram Al_2O_3-Y_2O_3-H_2O between 350 and 450°C.[117]

For the epitaxial film growth of $Er_{1.0}Eu_{2.0}Fe_{4.3}Ga_{0.7}O_{12}$ on (110) seeds of $Gd_3Ga_5O_{12}$, the following conditions have been employed by Laudise and Kolb (1975):[116]

Growth temperature	:	330–445°C
ΔT	:	40–80°
Fill %	:	60–65%
Solvent	:	10–20M KOH
Ga_2O_3	:	0.75M

Nijs et al. (1992) have obtained $Mn_3Al_2Si_3O_{12}$ under hydrothermal conditions at temperature 550°C and pressure 2 kb, and in the experimental duration of 14 days.[124] Starting material was $Al_2O_3{\cdot}3SiO_2$ gel, into which ground metallic manganese was added to obtain a fine powder with composition $Al_2O_3{\cdot}3SiO_2{\cdot}3Mn$. This starting material, plus excess water, was taken in a gold capsule which was placed in a Tuttle vessel. After fourteen days, the capsule was opened to get small crystals of manganese garnet. This material shows red luminescence from the Mn^{2+} ions, which is quenched at room temperature due to energy migration to quenching centers.

DropBooks

9.7.4 Hydrothermal Synthesis of Ferrite

Ferrites are important technological materials with great success in the development of magnetic oxide powders with a particle size in the nanometer range.[125] Among them, barium hexaferrite and manganese ferrite are the most important ones. Both could be prepared through solid state sintering, chemical precipitation, melting, and hydrothermal methods.[126]–[130] Of these methods, the hydrothermal method is probably the most attractive one, because the resulting ferrite has a perfect crystal structure with a definite composition and very fine particle size (usually smaller than 1 μm) and is almost a monodispersed crystal. Therefore, the product obtained from hydrothermal synthesis can be used directly for ceramics processes without a calcination step.

Kumazawa et al. (1993) have synthesized barium ferrite fine particles from an aqueous suspension containing goethite and barium hydroxide by the hydrothermal method, and examined systematically the relation between the particle size and the reaction conditions commercially available, and also synthetic goethite particles are used in the

hydrothermal preparation of ferrites.[131] The experimental temperature ranges from 200 to 300°C. Both with and without stirring techniques have been employed under hydrothermal conditions. Alpha-FeOOH is dehydrated to form α-Fe_2O_3. The dehydration rate may increase with increasing outer surface area of the particle. The barium ferrite particle may be formed by the incorporation of barium ion under such conditions that α-FeOH is dehydrated to form α-Fe_2O_3. Similarly, barium hexaferrite particle is formed by dissolution followed by the crystallization. Usually the starting materials in the form of either hydroxides or nitrates of iron and barium, and mineralizer NaOH and water, are taken in the hydrothermal reactor and the slurry mixture is heated to a desired temperature. After the experimental run, the suspension is withdrawn from the reactor, neutralized by a diluted HCl solution and then filtered and washed thoroughly with water. The reaction can be written as follows:

Eq. (11) $$12FeOOH + Be(OH)_2 \rightarrow BaO{\cdot}6Fe_2O_3 + 7H_2O$$

Wang et al. (1991) have studied reaction mechanism of producing barium hexaferrites from α-Fe_2O_3 and $Ba(OH)_2$ under hydrothermal conditions.[132] Wang et al. (1993) have studied the kinetics of the crystallization of barium hexaferrite in detail.[133] The reaction rate of producing barium hexaferrite was highly dependent on the concentrations of $Fe(OH)_4^-$ (aq), $Ba(OH)_2$ and NaOH in the aqueous solution. These authors have found that the reaction should be carried out at a temperature greater than 280°C to obtain the main desired product, $BaO{\cdot}6Fe_2O_3$. A kinetic model, based on the homogenous phase reaction has been built to describe the dissolution of γ-FeOOH (s) and the precipitation of the dissolved γ-FeOOH (s) {or $Fe(OH)_4^-$ (aq)} and $Ba(OH)_2$ in sequence to produce the desired product, $BaO{\cdot}6Fe_2O_3$. The reaction rate at 280°C is expressed as a function of $Fe(OH)_4^-$ (aq) and Ba^{2+} concentration, i.e.

Eq. (12) $$Rp = \frac{0.19\left[Fe(OH)_4^- aq\right]^2\left[Ba^{2+}\right]}{1+8.6\left[Fe(OH)_4^-(aq)\right]}$$

Figure 9.29 shows the effect of alkali concentration on the extent of conversion of the $BaO{\cdot}6Fe_2O_3$: the reaction rate increases with the increase of the concentration of NaOH solution. Higher concentration of

NaOH also results in a higher yield of the production. The maximum yield of $BaO{\cdot}6Fe_2O_3$ achieved is 81% for $[OH]^-$=2N. In case of the nitrate source for the nutrient, the particle size decreased with an increase in alkali molar ratio defined as $[OH^-]/[NO^-_3]$. Particles about 0.1 μm in size were produced at molar ratios above six. As the concentration of NaOH increases, the mean size of the particles decreases. These experimental evidences may support the concept that during hydrothermal treatment at a constant temperature (e.g., 300°C), an increase in the crystallinity of precipitated particles mainly proceeds instead of particle growth driven by Ostwald ripening.

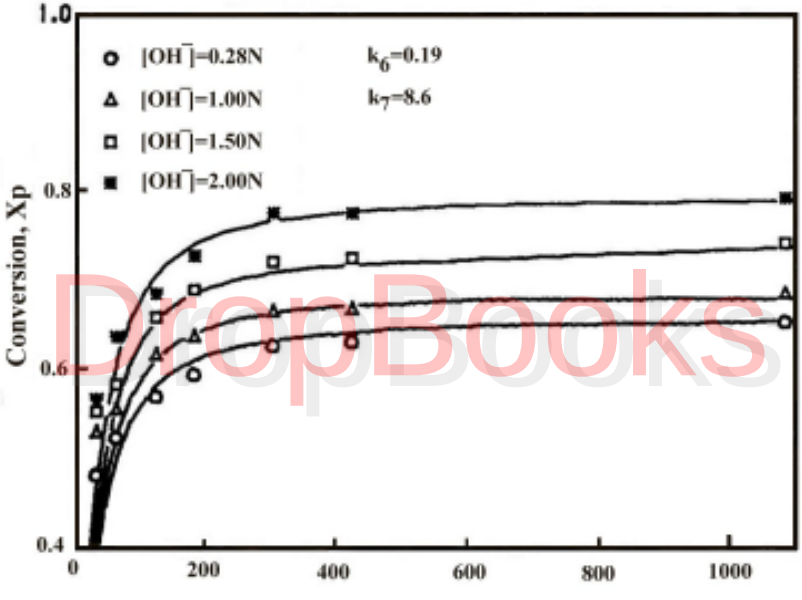

Figure 9.29. Effect of alkali concentration on the conversion of the $Ba0{\cdot}6Fe_2O_3$.[133]

The synthesis of manganese ferrites is carried out in the same way as that of barium hexaferrites. Wolski et al. (1995; 1997) have studied the hydrothermal synthesis and treatment of manganese ferrites in detail.[129][130] The main problem associated with the manganese ferrites is the tendency of manganese to form an enormous number of individuals with various valencies, different $O/_{Mn}$ ratios, and with the vacancies

spread over different positions of the sublattices. Wolski et al. (1997) have studied the hydrothermal treatment of such phases to eliminate the non-magnetic traces from the product and also suggested the probable stages of conversion of $Mn_{0.5}Fe_{1.0}(OH)_4$, for example, up to the product $MnFe_2O_4$, which is a ferri-magnetic spinel.[130]

9.7.5 Hydrothermal Synthesis of Complex Oxides

The mixed/complex oxides represent only a small, but important and diversified part of the entire family of inorganic compounds. Mixed oxides are widely used as superionics, fillers, or pigments in pulp and paper, paint, and ceramic electronic industries, and so on. Most of these mixed or complex oxides have highly complex structures, and are highly heat-resistant and chemically inert. In the recent years, there has been a growing demand for these complex oxides, especially from the manganese family and other related transitional metal families owing to their unique layered structures.[134]–[136] These advanced mixed oxides are those which present specific characteristics in their composition, such as pigments for electronics, or in their morphology, such as nanometer-size particles. The hydrothermal method is potentially superior for low cost production of advanced mixed oxides because complex oxide powders are formed directly. The temperature of synthesis lies between the boiling point of water and its critical temperature (374°C), whereas the pressure can go as high as 15 MPa. The major advantages are the use of inexpensive raw materials such as oxides, hydroxides, chlorides and nitrates, control of growth rate, particle size, stoichiometry, particle shape, elimination of impurities, and so on.

Among these mixed oxides, manganese-bearing mixed oxides are very important as the majority of them show layered structures. Feng et al. (1996) have synthesized birnessite-type lithium manganese oxide, by reacting a $Mn(NO_3)_2$ solution with a mixed solution of H_2O_2 and LiOH at room temperature.[137] This manganese oxide has a layered structure with a single sheet of crystal water and lithium ions between two-dimensional edge-shared MnO_6 octahedral sheets. The interlayer spaces can have Na^+, K^+, and Cs^+. Such manganese oxides can be used as metal ion adsorbents and cathodes for lithium rechargeable batteries.[138][139] Figure 9.30 shows the structure of birnessite-type lithium manganese oxides. The lithium ions may locate between the MnO_6 octahedral sheets, and they can be topotactically exchanged with metal ions.

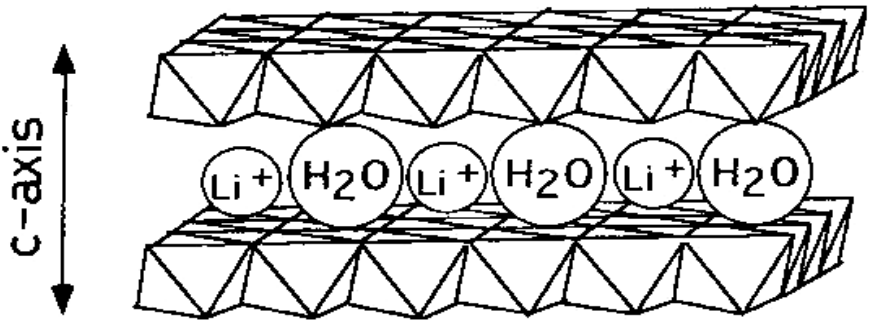

Figure 9.30. Structure of birnessite-type lithium manganese oxides.[137]

Manganese oxides like $LiMn_2O_4$ are of particular interest because they readily intercalate lithium into their structures and are therefore potentially useful as the cathode of lithium batteries. For example, SONY's lithium ion cell uses the very expensive $LiCoO_2$ cathode. Hence, extensive research is currently underway to find promising candidates for cathode materials in lithium secondary batteries to replace the expensive cobalt used in present commercial cells. A manganese oxide that behaved like the layered $LiCoO_2$ would be a prime candidate for this application because of its high free energy of reaction with Li and relatively low cost.[140] The experiments involved reacting potassium permanganate with hydrochloric acid and then hydrothermally treating the reaction mixture. The overall reaction takes place as follows:

DropBooks

Eq. (13) $$KMnO_4 + (1 - x + 2y) / 2H_2O \rightarrow K_2MnO_2 \cdot yH_2O + (1 - x) KOH + (3 + x) / 4O_2$$

Figure 9.31 shows the schematic diagram of layered manganates showing *a)* anlydrous material, and *b)* one water layer and two water layers.

Demazeau et al. (1994) have obtained La_2MnIrO_6 belonging to the perovskite family using a simple approach of ferromagnetic interactions through a 180°C super exchange. The structural and magnetic studies have confirmed the ferromagnetic behavior of such an oxide.[135] Turrillas et al. (1987) have synthesized $Ca_2Pt_3O_8$ under hydrothermal

conditions (T = 528°C, P = 170 MPa).[141] The platinum ternary oxides have potential uses owing to their good ternary catalytic and electrochemical properties, and also semiconductor, insulator and metallic-conductor properties. Schwartz and Prewitt (1984) have studied the structure and properties of a large number of binary and ternary oxides of platinum.[142] Usually KOH and water are used as mineralizers. These platinum compounds/oxides are insoluble in water, nitric acid, hydrochloric acid, or hot aqua-regia, but soluble in hot hydrobromic acid. The most prominent feature of $Ca_2Pt_3O_8$ is that it has three polymorphic modifications (tetragonal, orthorhombic and hexagonal).

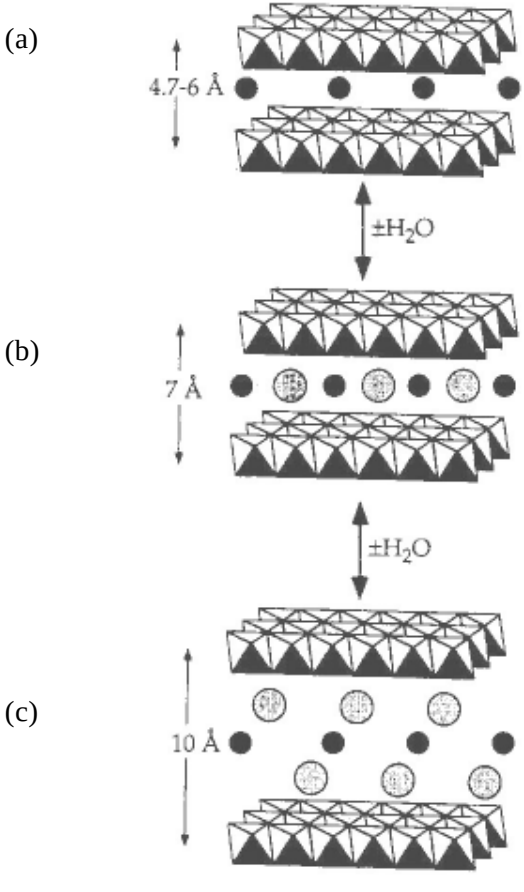

Figure 9.31. Schematic diagram of layered manganates showing *(a)* anhydrous material, *(b)* one water layer, and *(c)* two water layers.[140]

In recent years, there is a growing interest for stabilized yttria, ceria, and zirconia based catalysts, which also act as structural and electronic promoters of heterogeneous catalytic reactions and as oxide ion conducting solid electrolytes in electrochemical cells.[143]–[145] A series of solid solutions based on the perovskite type structure showing the above mentioned physical and chemical properties are being hydrothermally prepared. The prominent members among them are:

$BaZr_{1-x}MxO_{3-x}$ (M = Al, Ga, In; x = 0.20)

$SrZrO_{3-\alpha}$ (M = Al, Ga, In; x = 0.20)

$Ce_{1-x}Pr_xO_{2-\delta}$

$Ce_{1-x}Bi_xO_{2-\delta}$ and so on.[146]–[149]

The preparation of these solid solutions is carried out usually at temperatures of 150 to 250°C under autogeneous pressure. Morey type autoclaves, or other commercially available autoclaves like Parr, or Berghoff autoclaves provided with Teflon® liners are used for the synthesis of these oxides. The pH is maintained usually at higher levels (>10). The commonly used solvents are KOH or NH_4OH. Figure 9.32 shows the SEM photographs of $BaZr_{1-x}MxO_{3-\alpha}$ (M = Al, Ga, In; x = 0.20).

DropBooks

There are several other varieties of mixed oxides synthesized under hydrothermal conditions. Hydrothermal technique is especially suitable for obtaining such unique structures, which are impossible to obtain by other conventional methods.

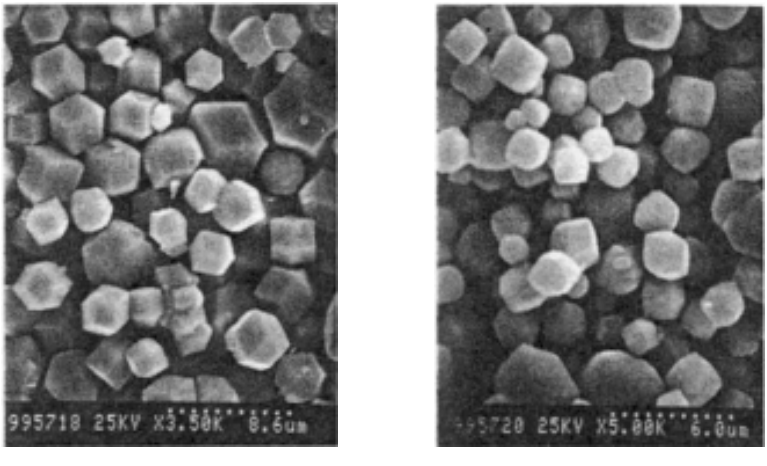

$BaZrO_3$ $BaZr_{0.90}Al_{0.1}O_{3-\alpha}$

Figure 9.32. SEM photographs of $BaZr_{1-x}M_xO_{3-a}$ (M = Al, Ga, In, x = 0.20).[146]

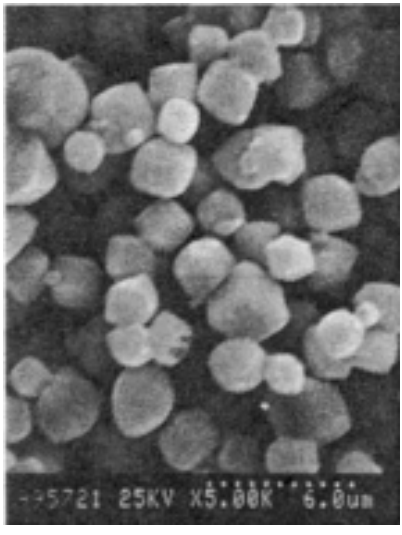

$BaZr_{0.85}Ga_{0.15}O_{3-\alpha}$

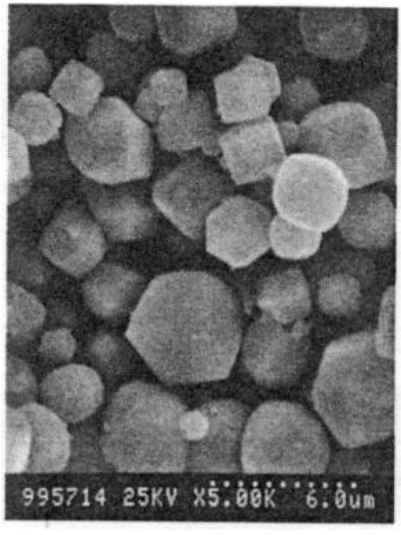

$BaZr_{0.80}In_{0.20}O_{3-\alpha}$

Figure 9.32. *(Cont'd.)*

REFERENCES

1. Crocket, J. H., Noble Metals in Sea-floor Hydrothermal Mineralization From the Juan de Fuca and mid-Atlantic Ridges: A Fractionation of Gold From Platinum Metals in Hydrothermal Fluids, *Can. Miner.,* 28:639–648 (1990)
2. Hannington, M. D., Peter, J. M., and Scott, S. D., Gold in Sea-floor Polymetallic Sulfide Deposits, *Econ. Geol.,* 81:1867–1883 (1986)
3. Rau, H. and Rabenau, A., Hydrothermal Growth of Some Elements, *J. Crystal Growth,* 3/4:417–421 (1968)
4. Rabenau, A. and Rau, H., Hydrothermal Synthesis of Gold, *Naturwissenschaften,* 55:336–339 (1968)
5. Bujor, D. I., Synthetische Versuche uber die Bildung der Golder Zlagerstatten zu Brad in Rumanien, *Ark. Kemi miner. Och. Geol.,* 26A:1–7 (1948)
6. Honma, H., Shikazono, N., and Nakata, M., Hydrothermal Synthesis of Gold, Electrum and Argentite, *Can. Miner.,* 29:217–221 (1991)
7. Ogryzlo, S. P., Hydrothermally Experiments With Gold, *Econ. Geol.,* 30:400–424 (1935)
8. Henley, R. W., Soluble of Gold in Hydrothermal Chloride Solutions, *Chem. Geol.,* 11:73–87 (1973)

9. Glyuk, D. S. and Khlebnikova, A. A., Gold Solubility in Water, HCl, HF and Sodium and Potassium Chloride, Fluoride, Carbonate and Bicarbonate Solutions At A Pressure of 1000 kg / cm^2. *Dokl. Acad. Sci. USSR, Earth Sci. Sect.*, 254:190–194 (1980)
10. Shikazono, N., Selenium Content of Acanthite and The Chemical Environments of Japanese Vein-type Deposits, *Econ. Geol.*, 73:524–533 (1978)
11. Pan, P. and Wood, S. A., The Solubility of Pt and Pd Sulfides and Au Metal in Bisulfide Solutions II. Results at 200–350°C and At Saturated Vapor Pressure, *Mineral. Deposita.*, 29:373–390 (1994)
12. Benning, L. G. and Seward, T. M., Hydro-sulphide Complexing of Au(I) in Hydrothermal Solutions from 150–400°C and 500–1500 bar, *Geochim. Cosmochim. Acta*, 60:1849–1871 (1996)
13. Renders, P. J. and Seward, T. M., The Stability of Hydrosulphido- and Sulphido Complexes of Au (I) and Ag (I) at 25°C. *Geochim. Cosmochim. Acta*, 53: 244–253 (1989)
14. Benning, L. G. and Seward, T. M., Hydrosulphide Complexes of gold (I) At High Pressures and Temperatures: Equilibrium and Kinetics Problems, *Mineral. Mag.*, 58A:75–76 (1994)
15. Suleimenov, O. M. and Seward, T. M., Spectro-photometric Determination of The First Ion: Sat. Constant of Hydrogen Sulphide at High Temperatures, in: Water-Rock Inter Action - 8, (Y. K. Kharaka and O. V. Chudaev, eds.), *Balkema Press, The Netherlands*, pp.113–115 (1995)
16. Popolitov, V. I., Hydrothermal Synthesis of Semiconductor Compounds Group $A^{V}{}_2B^{III}{}_3$ and $A^{V}B^{VI}C^{VII}$, *Ph.D. Thesis, Institute of Crystallography*, Akademy Nauk, USSR (1969)
17. Popolitov, V. I. and Litvin, B. N., Synthesis of Monocrystals of Ternary Chalcohalogenides ($A^{V}B^{VI}C^{VII}$), in: *Investigations of Processes of Crystallization Under Hydrothermal Conditions*, pp. 55–68, Nauka, Moscow (1970)
18. Rabenau, A. and Rau, H., Kristalgróeu en chemische synthese under hydrothermale condities, *Philips Techn. Tijdschr.*, 30:94–101 (1969)
19. Christoph, A., Gorlich, P. and Ludke, U. Synthese *Au- Krist. und Techn.*, 1:563–568 (1966)
20. Kolb, E. D. and Laudise, R. A., Solub. of Se in Na2S, *J. Crystal Growth*, 8:191–196 (1971)
21. Popolitov, V. I., Shapiro, A. Ya., and Plakhov, G. F., Chemical Interaction in Systems Te-R-H_2O (R = HF, HCl, HBr, CH_3COOH, CHOOH, $C_2H_2O_3$) Under High Pressures Temperatures, *J. Phys. Chem.*, 55:1229–1233 (1982)
22. Derjaguin, B. V., Spitsyn, B. V., Bouliov, L. L., Klochkov, A. A., Gorodetsk, A. E., and Smolyanov, A. E., Synthesis of Diamond Crystals on Non-diamond Substrates. *Sov. Phys.*, 21:676–679 (1976)

DropBooks

23. Matsumoto, S., Sato, Y., Kamo, M., and Setaka, N., Vapor Deposition of Diamond Particles From Methane, *J. Appl. Phys.*, 42:L183–L186, Jpn. (1982)

24. Bundy, F. P., Hall, H. T., Strong, H. M., and Wentorf, R. H., Man-made Diamonds. *Nature*, 176:51–54 (1955)

25. De Vries, R. C., Synthesis of Diamond Under Metastable Conditions. *Ann. Rev. Mater. Sci.*, 17:161–187 (1987)

26. Ravichandran, D. and Roy, R., Growth of Diamond on Diamond Substrates in Presence of An Alkali and Metal Under Hydrothermal Conditions, *Mat. Res. Bull.*, 31:1075–1082 (1996)

27. Roy, R., Cherian, K.A., Cheng, J.P., Badzian, A., Langlade, C., Dewan, H. and Drawl, W., Precipitation of Diamond from MexCyHz Solutions at 1 atm, Mat. Res. Innovation., 1:117–129 (1997)

28. Szymanski, A., Abgarowicz, E., Bakon, A., Niedbalska, A., Slalcinski, R., and Sentek, J., Diamond Formed At Low Pressures and Temperatures Through Liquid Phase Hydrothermal Synthesis, *Diamond and Related Material*, 4:234–235 (1995)

29. Chaidarov, A. A., Gafitullina, D. S., and Argunov, K. P., Nuclear-Physical Methods of Diamond Quality Control, *FAN, Taszkent*, pp.115–133 (Russian) (1986)

30. Tauson, W. L. and Abramowicz, M. G., Physicochemical Transformations of Real Crystals in Mineral Formations, *Nauka, Novosibirsk*, p.110 (Russian) (1988)

31. Niedbalska, A. and Szymanski, A., in: Proc. XXV Annual Meeting of European High Pressure Research Group, Potsdam, (Aug. 25–27, 1987)

32. De Vries, R. C., Roy, R., Somiya, S., and Yamada, S., A Review of Liquid Phase Systems Pertinent to Diamond Synthesis, *Trans. Mat. Res. Soc. Jpn.*, 19B:641–647 (1994)

33. Gogotsi, Y. and Yoshimura, M., *Nature*, 367:628 (1994)

34. Yamaoka, S. and Akaishi, M., Growth of Diamond Under HP/HT Water Condition, in: *Proc. 6th NIRIM Int. Symp. Advanced Nat.* (ISAM 99), pp. 1–2, Tsukuba, Jpn. (Feb. 28 – March 3, 1999)

35. Suito, K. and Onodera, A., Synthesis of Diamond Using Phenolic Resin, in: *Proc. 6th NIRIM Int. Symp. Advanced Nat.* (ISAM 99), pp. 7–8, Tsukuba, Jpn. (Feb. 28 – March 3, 1999)

36. Litvin, B.N. and Popolitov, V.I., Hydrothermal Synthesis of Inorganic Compounds, p. 37, Nauka, Moscow (1984)

37. Kolb, E. D., Caporaso, A. Z., and Laudise, R. A., Hydrothermal Crystallization of Some II - VI Compounds, *J. Crystal Growth* , 3/4:422–425 (1968)

38. Demianets, L. N. and Emelyanova, E. N., Crystallization of Hydroxylchloride of Neodymium $Nd(OH)_2O$ Under Hydrothermal Conditions, *Kristallografia*, 14:753–754 (1969)
39. Kletsov, P. V., Lisvnina, T. G., and Kharchenko, L. Yu., Hydrothermal Synthesis and Investigations of Hydroxylchlorides, $Ln_3Cl_2(OH)_5$ and $Ln(OH)_2Cl$, Rare Earth Elements of Yttrium Group, *J. Spec. Chem.* 14:87–91 (1973)
40. Carter, F. L. and Levinson, S., The Hydrothermal Preparation Single Crystal Lattice Parameters, and Decomposition Data for Some Lanthanide Dihydroxy Chlorides and the Related Hydroxy Chloride, $Yb_3O(OH)_5Cl_2$, *Inorg. Chem.*, 8:2788–2791 (1969)
41. Tarren, J. A. K. and Kutty, T. R. N., Hydrothermal Phase Equilibria in Ln_2O_3-H_2O-CO_2 systems, *J. Crystal Growth*, 50:527–532 (1980)
42. Christensen, A. N. and Hazeil, R. G., Hydrothermal Synthesis of Stanats: Structure of $MnSn(OH)_6$. *Acta Chem. Scand.*, 23:1219–1224 (1969)
43. Wolski, W., Wolska, E., Kaczmarek, J., and Piszora, P., Ferrimagnetic Spinels in Hydrothermal and Thermal Treatment of $Mn_xFe_{2-2x}(OH)_{6-4x}$, *J. Thermal Analysis*, 48:247–258 (1997)
44. Schafthaul, Münchener gelehrte Anzeigen, p. 575 (1845), {cited by Bourgeois, L., Reproduction Artificielle des Minerals, Paris, p.80 (1884)}
45. Friedel, G., *Bull. Soc. Min.*, 14:7–10 (1891)
46. Thugutt, S. J., *Z. Anorg. Chem.*, 2:64–107 (1891)
47. Kuzmina, I. P. and Khaidukov, N. M., Crystallization of Copper Oxide Under HydrothermalConditions, in: *Crystal Growth from High Temperature Aqueous Solutions.*, Nauka, Moscow, pp.178–189 (1977)
48. Hartmann, H., Optical Properties of Cu_2O, *Physica Status Solidi*, 2:585–597 (1962)
49. Kuz'mina, I. P., Lobachev, A. N., and Triodina, N. S., Synthesis of Zincite By The Hydrothermal Method, in: *Crystallization Process under Hydrothermal Conditions*, (A. N. Lobachev, ed.) pp. 27–41, Consultants Bureau, New York, (1973)
50. Lobachev, A. N., Kuz'mina, I. P. and Shaldin, Yu. V., Zinc Oxide: Growth and Some Physical Properties; in: *Crystal Growth From High-Temperature Aqueous Solutions*, Nauka, Moscow, pp.158–177 (1977)
51. Nielsen, J. W. and Dearborn, E. E., The Growth of Large Single Crystals of Zinc Oxide, *J. Phys. Chem.* 64:1762–1763 (1960)
52. Laudise, R. A. and Ballman, A. A., Hydrothermal Synthesis of Zinc Oxide and Zinc Sulphide, *J. Phys. Chem.*, 64:688–691 (1960)
53. Lyukina, M. M. and Khaji, V. E., Kinetics of Crystallization of Zincite Under Hydrothermal Conditions, in: *Crystal Growth*, 4:151–156, Nauka, Moscow (1964)

DropBooks

54. Croxall, D. E., Ward R. C., Wallace, C. A., and Kell, R. C., Hydrothermal Growth and Investigation of Highly Doped Zinc Oxide Crystals of High Purity and Perfect, *J. Crystal Growth*, 22:117–124 (1974)

55. Sakagami. N., Hydrothermal Growth and Characterization of ZnO Single Crystals of High Quality, *J. Crystal Growth*, 99:905–909 (1990)

56. Kuz'mina, I. P., Investigation of the Crystallization of Germanates and Zincogermanates of Na and K Under Hydrothermal Conditions, *Ph.D. Thesis., Institute of Crystallography,* Academy Nauk USSR, Moscow (1968)

57. Rykl, D., Bauer, J., Hydrothermal Synthesis von zinkit, *Kristall und Technik*, 3:375–384 (1968)

58. Wang, B. G., Shi, E. W., and Zhong, W. Z., Understanding and Controlling the Morphology of ZnO Crystallites Under Hydrothermal Conditions, *Cryst. Res. Technol.*, 32:659–667 (1997)

59. Barus, R. L., Laudise, R. A., and Shields, R. M., *J. Phys. Chem.* 67:835–840 (1963)

60. Yamaguchi, G., Yanagida, H., and Sojma, S., *Bull. Soc. Chem. Jap.* 35:1789–1791 (1962)

61. Laudise, R. A., *Growth of Single Crystals*, p. 289, Prentice Hall, New Jersey (1970)

62. Kashkurov, K. F., Nikitichev, P. I., Osipov, V. V., Sizova, L. D., and Simonov, A. V., Growth of Large Corundum Crystals By The Hydrothermal Method, *Sov. Phys. Crystallografia*, 12:837– 839 (1968)

63. Rymyanstev, V. N., Ganeev, I. G., and Rez, I. C., SiO_2 in Alkali and Carbonate Solutions, in: *Crystal Growth*, 9:51–54, Nauka, Moscow (1972)

64. Thomas, V. G., On a Mechanism of Substance Transfer Under The Hydrothermal Growth of Corundum Crystals in Bicarbonate Solutions, *Geology and Geophysics*, 37:96–99 (1996)

65. Kuznetsov, V. A. and Shternberg, A. A., Crystallization of Ruby Under Hydrothermal Conditions, *Sov. Phys. - Crystallagrafia*, 12:280–285 (1967)

66. Monchamp, R. R., Puttbach, R. C., and Nielson, J. W., Hydrothermal Growth of Iapphite, *J. Crystal Growth*, 2:178–187 (1968)

67. Laudise, R. A. and Ballman, A. A., Hydrothermal Synthesis of Sapphire, *J. Am. Chem. Soc.*, 80:2655–2657 (1958)

68. Balitskii, V. S. and Lisinstina, E. E., *Synthetic Analog and Imitation of Natural Gemstones*, Nedra, Moscow (1981)

69. Kuznetsov, V. A., Oxides of Titanium Subgroup Metals, *Crystallization Processes under Hydrothermal Conditions.* p.43–55, Consultants Bureau, New York (1973)

70. Anikin, I. N., Naumova, I. A., and Rumyantseva, G. V., *Kristallografiya*, 10:231–235 (1965)

71. Harvill, M. L. and Roy, R., *J. Phys. Chem. Solids, Suppl.,* 1:563–568 (1967)
72. Kuznetsov, V. A. and Panteleev, V. V., Hydrothermal Synthesis of Rutile, *Kristallografia,* 10:445–448 (1965)
73. Kuznetsov, V. A., Crystallization of Titanium, Zirconium and Hafnium Oxides and Some Titanate and Zirconate Compounds Under Hydrothermal Conditions, *J. Crystal Growth,* 3/4:405–410 (1968)
74. Schuilling, R. D. and Vink, B. W., Stability Relation of Some Titanium Minerals (Sphene, Perovskite, Rutile, Anatase), *Geochim. Cosmochim. Acta,* 31:2399–2411 (1967)
75. Popolitov, V. I. and Lobachev, A. N., Crystallization of Paratellurite Under Hydrothermal Conditions, Izv. Akad. Nauk USSR, *Inorgan. Mater.,* 18:960–961 (1972)
76. Kolb, E. D. and Laudise, R. A., The Hydrothermal Crystallization of Paratellurite, α - TeO_2, *Mater. Res. Bull.,* 8:1123–1130 (1973)
77. Zubertz, J., *Krist. und Tech.,* 4:221 (1969)
78. Popolitov, V. I., Kurbanov, Kh. M., Zverkova, O. N., and Zeitlin, M. N., *Dokl. Akad-Nauk Tazhakisthan USSR,* 18:21–24 (1975)
79. Popolitov, V. I., Hydrothermal Growth Under Visual Examination, in: Hydrothermal Growth of Crystals, (K. Byrappa, ed.), *Prog. Crystal Growth Characterization,* 21:255–297 (1990)
80. Cheng, H., Ma, J., Zhao, Z., and Qi, L., Hydrothermal Preparation of Uniform Nanosize Rutile and Anatase Particles, *Chem. Mater.,* 7:663–671 (1995)
81. Ozawa, M. and Kimura, M., Preparation and Characterization of Zirconium Dioxide Catalyst Supports Modified with Rare Earth Elements, *J. Less-Common Metals,* 171:195–212 (1991)
82. Bryappa, K., Lokanath Rai, K. M., and Yoshimura, M., Hydrothermal Preparation of TiO_2 and Photocatalytic Degradation of HCCH and DDT, *Environ. Tech.* (in Press)
83. Chen, D. and Xu, R., Hydrothermal Synthesis and Characterization of Nanocrystallization Fe_3O_4 Powders, *Mat. Res. Bull.,* 33:1015–1021 (1998)
84. Mukhopadhyay, A. K., Mitra, P., Chatterjee, A. P., and Maiti, H. S., A New Method of Preparing Tin Dioxide Thin Film Gas Sensors, *J. Mat. Sci. Letts.* 17:625–627 (1998)
85. Tanaka, Y. and Tsuji, M., New Synthetic Method of Producing *a*-Manganese Oxide for Potassium Selective Adsorbent, *Mat. Res. Bull.,* 29:1183–1191 (1994)
86. Lyons, C. Update: Photocatalytic Oxidation, An Effective and Cost Competitive Process for Destroying Volatile Organic Chemical Pollutants is Now Being Commercialized, *Mat. Tech.,* 10:236–238 (1995)

DropBooks

87. Poniatowski, E. H., Rodriguez-Talavera, R., Heredia, M.de la C., and Canocorona, O., Arroyo-Murillo, R., Crystallization of Nanosized Titania Particles Prepared by the Sol-gel Process, *J. Mater. Res.*, 9:2101–2108 (1994)

88. Lee, W., Gao, Y. M., Dwight, K., and Wold, A., Preparation and Characterization of Titanium (IV) Oxide Photocatalysts, *Mat. Res. Bull.*, 27:685–692 (1992)

89. Chen, Q., Qian, Y., Chen, Z., Zhou, G., and Zhang, Y., Preparation of TiO_2 Powders With Different Morphologies By An Oxidation Hydrothermal Combination Method, *Mater. Letts.*, 22:77–80 (1995)

90. Qian, Y., Chen, Q., Chen, Z., Fan, C., and Zhou, G., Preparation of Ultrafine Powders of TiO_2 by Hydrothermal H_2O_2 Oxidation Starting From Metallic Ti, *J. Mater. Chem.*, 3(2):203–205 (1993)

91. Zhang, Z, Wang, C. C., Zakaria, R., and Ying, J. Y., Role of Particle Size In Nanocrystalline TiO_2-based Photocatalysits, *J. Phys. Chem*, 102:10871–10878 (1998)

92. Matthews, R. W. and Mc Evoy, S. R., Destruction of Phenol in Water with Sun, Sand, and Photocatalysis, *Solar Energy*, 49:507–513 (1992)

93. Choi, W. and Hoffmann, M. R., Novel Photocatalytic Mechanisms For $CHCl_3$, $CHBr_3$, and $CCl_3CO^-_2$ Degradation and The Fate of Photogenerated Trihalomethyl Radicals on TiO_2, *Environ. Sci. Technol.*, 31:89–95 (1997)

94. Anheden, M., Goswami, D. Y., and Svedberg, G., Photocatalytic Treatment of Wastewater From 5 - Fluorouracil Manufacturing, *Trans. ASME* 118:2–8 (1996)

95. Viswanathiah, M. N., Tareen, J. A. K., and Krishnamurthy, K. V., Low Temperature Hydrothermal Synthesis of Magnetite, *J. Crystals Growth*, 49:189–192 (1980)

96. Visalakshi, G., Venkateswaran, G., Kulkreshtha, S. K., and Moorthy, P. N. Compositional Characteristics of Magnetite Synthesized from Aqueous Solutions at Temperatures Up To 523 K, *Mat. Res. Bull.*, 28:829–836 (1993)

97. Hirano, S. and Somiya, S., Hydrothermal Crystal Growth of Magnetite in The Presence of Hydrogen, *J. Crystal Growth*, 35:273–278 (1976)

98. Mc Garvey, G. B. and Owen, D. G., Copper (II) Oxide As A Morphology Directing Agent In The Hydrothermal Crystallization of Magnetite, *J. Mat. Sci.*, 31:49–53 (1996)

99. Okuwaki, A., Synthesis of Several Inorganic Materials Under Hydrothermal Conditions. in: *Proc. Int. Workshop on Soft and Solution Processing for Advanced Inorganic Materials*, (M.Yoshimura, ed.) pp.64–73, Tokyo Inst. of Technology, Tokyo, Jpn. (Feb. 26–27, 1996)

100. Uchida, S., Sato, T., and Okuwaki, A., Preparation of Micaceous Iron Oxide By The Oxidation of Iron With Pressurized Oxygen In Concentrated Sodium Hydroxide Solution At Elevated Temperatures, *J. Mat. Sci.*, 27:1332–1336 (1992)

101. Litvin, B. N. and Popolitov, V. I., *Hydrothermal Synthesis of Inorganic Compounds*, p. 43, Nauka, Moscow (1984)

102. Crowley, M. S., Effect of Starting Materials on Phase Relations in the System, $CaO\text{-}Al_2O_3\text{-}H_2O$, *J. Am. Ceram. Soc.*, 47:144–148 (1964)

103. Nadejdina, T. N., Synthesis and Crystallization Chemical Studies of Sr-Silicates and Their Analogs. *Ph.D. Thesis*, Moscow State University, Moscow (1975)

104. Ponomerev, V. I., Litvin, B. N., and Belov, N. V., Hydrothermal Synthesis of Hydroaluminates of Calcium and Their X-Ray Data, *Izv. Akad. Nauk USSR, Inorg. Mater*. 6:1657–1659 (1970)

105. Nadedjina, T. N., Kuznestov, V. A., Pobedimskaya, E. A., and Belov, N. V., Crystallization of Silicates, Aluminates and Germanates of Strontium Under Hydrothermal Conditions. in: *Crystal Growth for High-Temperature Aqueous Solutions.*, pp. 120–135, Nauka, Moscow (1977)

106. Kurbanov, Kh. M., Hydrothermal Synthesis and Crystal Data of $LuSbO_3$, $PrSbO_3$, $DySbO_3$ Monocrystals, *Kristallografia*, 23:1266–1287 (1978)

107. Buchurin, R.Ch., Hydrothermal Synthesis Antimonites of Trivalent Elements and Their Physico-chemical Properties, *Ph.D. Thesis, Institute of Crystallography*, Akademi Nauk, USSR (1981)

108. Bichurin, R. Ch., Popolitov, V. I., and Stefanovich, S. Yu., Growth and Physico-chemical Propeties of $In_3Sb_5O_{12}$ and $Sc_3Sb_5O_{12}$ Monocrystals, *J. Theor. Phys.*, 7:1292–1295 (1981)

109. Popolitov, V. I. and Bichurin, R. Ch., Hydrothermal Crystallization in the System $Sb_2O_3\text{-}In_2O_3\text{-}R\text{-}H_2O$ (R-Solvent), *Izv. Akad. Nauk, USSR, Inorg. Mater.* 20:1535–1539 (1984)

110. Stefanovich, S. Yu., Bichurin, R. Ch., Popolitov, V. I., and Venevstev, Yu. N., Identification of Phase Transits in Rare Earth Anthimonite Crystals, $Ln_3Sb_5O_{12}$, *J. Solid State Phys.*, 24:616–618 (1982)

111. Popolitov, V.I., Some Physico-chemical Principles Crystallization Under Hydrothermal Conditions. in: *Hydrothermal Synthesis and Growth of Monocrystals*, pp. 119–149, Nauka, Moscow (1982)

112. Popolitov, V. I., Lobachev, A. N., and Steitlin, M. N., Crystallization of Orthoantimonites of Antimony Under Hydrothermal Conditions, in: *Crystal Growth from High Temperature Solutions*, pp.198–216, Nauka, Moscow (1977)

113. Laudise, R. A., *The Growth of Single Crystals*, pp. 291–292, Prentice-Hall, New York (1970)

DropBooks

114. Puttb, R. C., Monchamp, R. R., and Nielsen, J. W., in: *Crystal Growth*, (H. S. Peiser, ed.), p. 569, Pergamon, Oxford (1967)

115. Khattak, C. P. and Wang, F. F .Y., in: *Handbook on the Physics and Chemistry of Rare Earths*, (K. A.Gschneidner Jr. and L. Eyring, Eds.) 3(29): North-Holland, Amsterdam (1979)

116. Laudise, R. A. and Kolb, E. D., *J. Am. Ceram. Soc.*, 45:51–54 (1962)

117. Kolb, E. D. and Laudise, R. A., Phase Equilibria of $Y_3Al_5O_{12}$, Hydrothermal Growth of $Gd_3Ga_5O_{12}$ and Hydrothermal Epitaxy of Magnetic Garnets, *J. Crystal Growth*, 29:29–39 (1975)

118. Brochier, A., Coeure, P., Ferrand, B., Gay, J. C., Joubert, J. C., Mareschal, J., Viguie, J. C., Martin-Binachon, J. C., and Spitz, J., Heteroepitaxie de Couches Minces de Grenat de Feryttrium par Methode de Flux et Synthese Hydrothermale, *J. Crystal Growth*, 13/14:571–575 (1972)

119. Toudic, Y. and Passaret, M., Croissance Parvoie Hydrothermale de Films Ferrimagnetiques., Epitaxies sur des Substrats de GdGaG, *J. Crystal Growth*, 24/25:621–623 (1974)

120. Ferrand, B., Heteroepitaxie par Syntheses Hydrothermale de Films Minces Monocristallins de Grenats Ferrimagnetiques, *High Temp. - High Press.*, 6:619–628 (1974)

121. Ferrand, B., Daval, J., and Joubert, J. C., Heteroepitaxial Growth of Single Crystal Films of YIG on GdGaG Substrates By Hydrothermal Synthesis, *J. Crystal Growth*, 17:312–314 (1972)

122. Ferrand, B., Geynet, J., Challeton, D., Daval, J., and Joubert, J. C., Growth of Epitaxial Substituted Garnet Films by Hydrothermal Synthesis, *Mat. Res. Bull.* 9:495–506 (1974)

123. Van Hout, M. J. G., Verplanke, J. C., and Robertson, J. M., Hydrothermal Synthesis of Single Crystal Thin Films of Magnetic Garnets and Their Analysis, *Mat. Res. Bull.*, 10:125–132 (1975)

124. Nijs, O., Verweij, J. M. W., and Blasse, G., A Divalent Manganese Garnet With Red Luminescence, *Mater. Chem. Phys.*, 30:199–203 (1992)

125. Smit, J. and Wijn, H. P. J., *Ferrites*, p. 194 Wiley, New York (1959)

126. Bye, G. C. and Hooward, C. R., "The Synthesis of Barrium Hexaferrite From Iron Oxide and Barium Carbonate, 1. General Features of the Reaction". *J. Appl. Chem. Biotechnol.*, 21:319–323 (1971)

127. Hibst, H., Hexagonal Ferrites From Melts and Aqueous Solutions Magnetic Recording Materials, *Angew. Chem. Int. Ed. Engl.*, 21:270–275 (1982)

128. Farhat Hadj, M. A. and Jabnert, J. C. Hydrothermal Synthesis and Characterization of The Hexagonal Ferrite Fe-Y, *J. Magnetism and Magnetic Maters.*, 62:353–360 (1986)

129. Wolski, W., Wolska, E., Kaczmarek, J., and Piszora, P., Formation of Manganese Ferrite by Modified Hydrothermal Method. *Phys. Stat. Sola (a)* 152:K19–K22 (1995)

130. Wolski, W., Wolska, E., Kaczmarek, J., and Piszora, P., Ferrimagnetic Spinels in Hydrothermal and Thermal Treatment of $Mn_xFe_{2-2x}(OH)_{6-4x}$, *J. Thermal Analysis*, 48:247–258 (1997)

131. Kumazawa, H., Cho, H. M., and Sada, E., Hydrothermal Synthesis of Barium Ferrite Fine Particles From Goethite, *J. Mat. Sci.*, 28:5247–5250 (1993)

132. Wang, M. L., Shih, Z. W., and Lin, C. H., Preaction Mechanism of Producing Barium Hexaferrites From α-Fe_2O_3 and $Ba(OH)_2$ by Hydrothermal Method, *J. Crystal Growth*, 114:435–445 (1991)

133. Wang, M. L., Shin, Z. W., and Lin, C. H., Kinetic Study of Producing Barium Hexaferrite From Goethite and Barium Hydroxide by Hydrothermal Method., *Chem. Eng. Comm.*, 126:79–95 (1993)

134. Rao, C. N. R., Novel Materials, Materials Design and Synthetic Strategies: Recent Advances and New Directions, *J. Mat. Chem.*, 9:1–14 (1998)

135. Demazeau, G., Siberchicot, B., Matar, S, Gayet, C., and Largeteau, A., New Ferromagnetic Oxides Derived From the Perovskite Structure Prepared Under High Pressures, *High Pressure Research*, 12:337–341 (1994)

136. Cousin, P. and Ross, R. A., Preparation of Mixed Oxides: A Review., *Mater. Sci. Engg.*, A130:119–125 (1990)

137. Feng, Q., Yanagisawa, K., and Yamasaki, N., Synthesis of Birnessite-type Lithium Manganese Oxide, *J. Ceram. Soc. Jpn.*, 104:897–899 (1996)

138. Tsuji, M., Komarneni, S., Tamaura, Y., and Abe, M., *Mat. Res. Bull.*, 27:741–751 (1992)

139. Strobel, P. and Mouget, C., *Mat. Res. Bull.*, 28:93–100 (1993)

140. Chen, R., Zavalij, P., and Whittingham, S., Hydrothermal Synthesis and Characterization of K_xMnO_2. YH_2O, *Chem. Mater.*, 8:1275–1280 (1996)

141. Turrillas, X., Laviron, C., Vincent, H., Pannetier, J., and Joubert, J. C., Synthesis and Characterization of A New Calcium Platinum Oxide: $Ca_2Pt_3O_8$, *J. Solid State Chem.* 67:297–307 (1987)

142. Schwartz, K. B. and Prewitt, C. T., *J. Phys. Chem. Solids*, 45:1–12 (1984)

143. S. P. S. Badwal, (ed.) *Science and Technology of Zirconia Technomic*, Lancaster (1993)

144. Inaba, H. and Tagawa, H. *Solid State Ionics*, 83:1–8 (1996)

145. Shuk, P., Wiemhöfer, H. D., Guth, U, Göpel, W., Greenblatt, M., *Solid State Ionics*, 89:179 (1996)

DropBooks

146. Zheng,W., Liu, C., Yue, Y., and Pang, W., Hydrothermal Synthesis and Characterization of $BaZr_{1-x}MxO_{3-\alpha}$ (M = Al, Ga, In, x 0.20) Series Oxides, *Mat. Letts.*, 30:93–97 (1997)

147. Zheng, W., Pang, W., and Meng, G., Hydrothermal Synthesis of $SrZrO_{3-a}$ (M = Al,Ga,In, x 0.20) Series Oxides, *Solid State Ionics*, 108:37–41 (1998)

148. Shuk, P. and Greenblatt, M., Hydrothermal Synthesis and Properties of Mixed Conductors Based on $Ce_{1-x}Pr_xO_{2-\alpha}$ Solid Solutions, *Solid State Ionics*, 116:217–223 (1999)

149. Dikmen, S., Shuk, P., and Greenblatt, M., Hydrothermal Synthesis and Properties of $Ce_{1-x}Bi_xO_{2-\alpha}$ Solid Solutions, *Solid State Ionics*, 112:299–307 (1998)

10

Hydrothermal Processing of Materials

10.1 INTRODUCTION

DropBooks

The term *processing* is a broad term covering many branches of materials preparation, fabrication, or development. Hydrothermal processing of materials is used in a very broad sense in recent years, and in the 21st century, it will play a vital role in materials science and technology. Hydrothermal processing of materials encompasses processes like synthesis, crystal growth, treatment, fabrication, alteration, hot pressing, recycling, sintering, etc., under hydrothermal conditions. In this chapter, we shall discuss materials processing under hydrothermal conditions dealing with the preparation of ultrafine particles, ceramics, whiskers, composites, thin films, and reinforcement. As the demand for these materials increased, the hydrothermal technique gradually underwent a considerable amount of modification and adaptation. This chapter has been devoted to a rapid progress achieved in the hydrothermal technique to suit modern technological requirements. The technique is especially handy for the preparation of ceramics (PZT, alumina, zirconia, yttria, ceria, and several bioceramics), epitaxial growth of crystalline thin films, composites, and ultrafine particles with a desired shape.

10.2 HYDROTHERMAL PREPARATION OF ADVANCED CERAMICS

In the last twelve years, the science of ceramics has undergone a revolution almost as dramatic as the more familiar ones in electronics. Novel approaches in preparing and processing ceramic solids have been developed, ingenious ways of circumventing the age-old problem of brittleness have been introduced, and new markets have opened up in such areas as electronics, sensors, photonics, orthopaedics, catalysis mixed ionic and electronic conducting ceramics, advanced nitride ceramics, advanced cements, mineralizers, heat engines, functional ceramics related to energy conservation environmental issues and so on.[1][2]

Today's advanced ceramics represent developments well beyond the imagination of even the few far-sighted scientists of twenty-five years ago who first perceived the remarkable potential of ceramic solids and established "ductile' engineering ceramics as a suitable objective for material researchers to pursue. Figure 10.1 shows the interactions of ceramics science with other technical fields.[1] Since 1980 much attention has been paid to hydrothermal processing of fine zirconia, ceria, and titania powders. Several methods were used to prepare fine zirconia hafnia, titania, ceria, PZT particles (powders), under hydrothermal conditions.

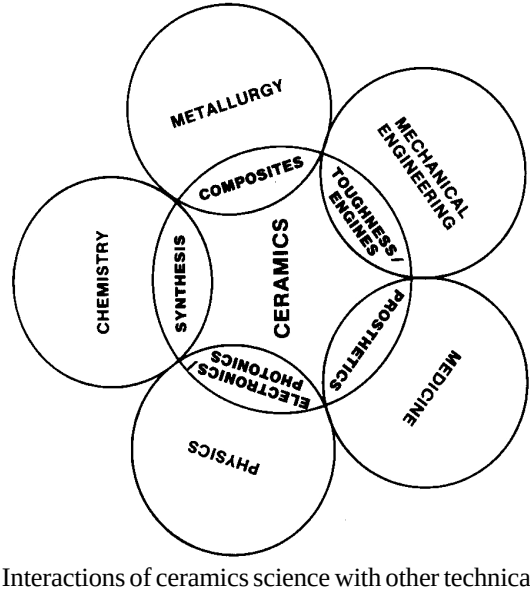

Figure 10.1. Interactions of ceramics science with other technical fields.[1] *(Courtest of the National Academy Press, Washington, DC.)*

Applications of hydrothermal reactions in ceramics include the following aspects: phase equilibria, ultrafine single crystals, ultrafine amorphous, single crystal growth, hydrothermal reaction sintering, hydrothermal sintering, hydrothermal crystallization, dissolving, corrosion, etching, composites (inorganic + organic, inorganic + inorganic), testing, thin films, radioactive waste management, hydrothermal oxidation, hydrothermal decomposition, hydrothermal anodic oxidation, RESA (reactive electrode submerged arc) process, etc. Table 10.1 provides comparison among the popularly adopted techniques of preparation of advanced oxide powder.[3]

Table 10.1. Advanced Oxide Powder Process Comparison (Somiya, S. 1989)

	Conventional	Sol-gel	Coprecip-itation	Hydrothermal
Cost	**Low-moderate**	**High**	**Moderate**	**Moderate**
State of development	Commercial	R & D	Commercial/ demonstration	Demonstration
Compositional control	Poor	Excellent	Good	Good-excellent
Morphology control	**Poor**	**Moderate**	**Moderate**	**Good**
Powder reactivity	Poor	Good	Good	Good
Purity (%)	< 99.5	> 99.9	> 99.5	> 99.5
Calcination step	Yes	Yes	Yes	No
Milling step	**Yes**	**Yes**	**Yes**	**No**

DropBooks

The hydrothermal preparation of very fine powders is an excellent approach to ideal powders. The ideal powder should have the following parameters:

i. Fine powder less than 1μm

ii. Soft or no agglomeration

iii. Narrow particle size distribution

iv. Morphology sphere or equiaxed

v. Chemical composition controllable

vi. Microstructure controllable

vii. Uniformity

viii. Free flowing

ix. Less defects ..... Dense particle

x. Less stress

xi. Reactivity ..... Sinterability

xii. Crystallinity

xiii. Reproducibility

xiv. Process control

The shape of ceramic products obtained under hydrothermal conditions is highly varied and some common hydrothermal products are listed below:

i. Fine Powder (Single crystals or Amorphous)

ii. Fiber

iii. Hydrate ..... Cement

iv. Large single crystal

v. Sintered body

vi. Film

The major advantages of hydrothermal processing of ceramics are as follows:

i. High quality

ii. High purity

iii. High rate of reaction

iv. Dispersion

v. Better shape control

vi. Pollution free

vii. Energy saving

viii. Low temperature operation

ix. Use of large volume of the equipment

x. New products

xi. Better nucleation control and so on

However, there are some disadvantages like equipment—autoclaves which are of complicated design, and the fact that it is expensive; cumbersome operations like assembling and dissembling; the fact that it is impossible to observe the actual process; solubility aspects; and problems related to surface chemistry. Table 10.2 lists some of the salient features of the ceramic synthesis by commonly used techniques.

DropBooks

10.2.1 Hydrothermal Preparation of Simple Oxide Ceramics

Zirconia ceramics are remarkable materials due to their excellent mechanical, electrical, thermal and optical properties.[4][5] Physical and chemical properties associated with these characteristics are closely related to structures and phase changes. Therefore, numerous studies have been undertaken of phase diagrams and structural changes in the zirconia systems.[6]–[8] There are many contradictions and discrepancies, especially around 1000°C. One of the most important steps in solving this problem is the study of *metastable phase diagram*.[9]–[11] Yashima et al. (1996) have studied the problem of diffusionless cubic-tetragonal (*c*-*t*´) phase transition, where *t*´ emphasizes a metastable tetragonal phase.[6] Thus, it can be distinguished from the stable *t*, which is formed diffusionally. Figure 10.2 shows a metastable-stable phase diagram of the ZrO_2 -CeO_2 system that is depicted in a composition temperature field. On cooling from 1650°C, the high-temperature cubic phase (B) transforms without cationic diffusions into a metastable tetragonal phase below the tetragonal-cubic transformation. Such metastable phase boundary is drawn by dashed and dotted lines.[12]

Table.10.2. Ceramics Synthesis (from the works of M. Yoshimura and S. Somiya)

Process	Advantages	Disadvantages	Composites	Particle size
Sol gel(hydrolysis of metal alkoxides), precipitation, coprecipitation	High product purity and homogeneity, crystal symmetry; metastable compounds with unique properties; narrow particle size distribution; lower sintering temperatures	May require calcination, sometimes milling; mixed alkoxides can cause inhomogeneity, non-stoichiometry; sometimes expensive raw materials	Oxides; LAS, mullite, spinel, cordierite	Down to 5 nm 0.1 to 5 μm
Evaporative decomposition solids	Wide range of chemical compositions; single-step process; no seperate calcination or milling required	Hollow aggregates formed; precursor must decompose at low temperatures; excess carbon impurities may require calcination	Oxides, nonoxides, composites, fibers	1 to 20 μm
Hydrothermal processing	High surface area; 99% dense sintered powders; submicron particles with narrow size distribution; simple equipment; continuous; no milling or calcination; short reaction times; lower energy requirements	Requires moderate temperatures/pressures; requires additives (seed crystals), surface treatments	Y_2O_3-PSZ, Eu_2O_3-doped HfO_2 lead-zirconate titanate, other oxides	Down to 8 nm

(Cont'd.)

Table.10.2. *(Cont'd.)*

Process	Advantages	Disadvantages	Composites	Particle size
Rapid expansion of supercritical fluids	Wide range of compositions including amorphous powders and nonequilibrium materials; fast reaction times (10^{-5} sec); lower temperatures than plasma process	Requires high pressures and temperature; corrosive solvents; some agglomeration; machined nozzles to improve morphology	Oxides; (SiO_2, GeO_2, SiO_2-GeO_2) fiber precursors (polycarbosilane); labile, explosive materials	0.01 to 1.3 μm (ceramics) < 0.1 μm fiber, 1 μm particle (polymers)
Reductive dehalogenation of elemental halides	Low temperature, any combination of elemental halides that can be reduced by alkali metals	Crystallization requires higher temperatures; high speed high-shear stirring needed; starting materials can be expensive; reactions are explosive or combustible	Amorphous precursors of TiB_2, SiC, B_4C, and other borides and carbides, SiC/TiC, SiC/TiN	

DropBooks

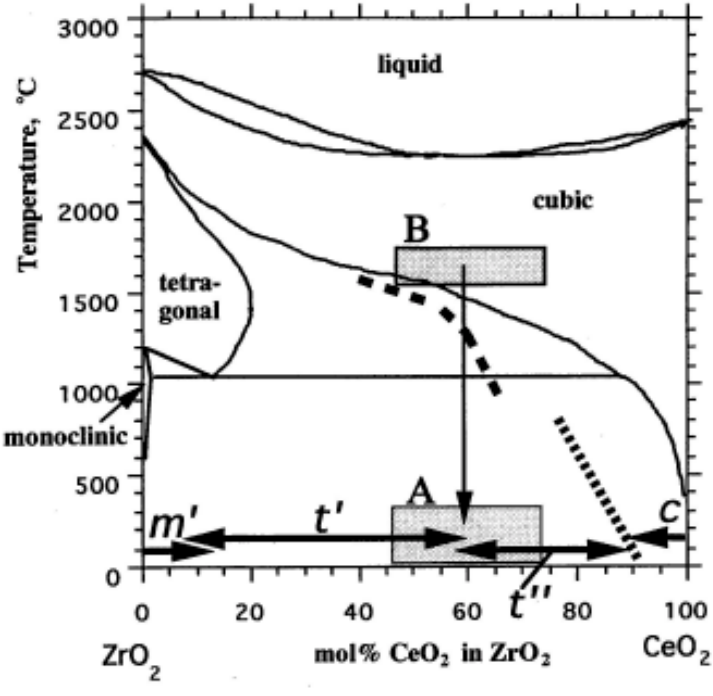

Figure 10.2. Metastable-stable phase diagram of the ZrO_2–CeO_2 system.[12]

Tani et al. (1982) have studied in detail the effect of mineralizers on the crystallization of solid solutions in the system ZrO_2-CeO_2 under hydrothermal conditions.[13] Samples prepared by the coprecipitation method were treated under 100 MPa at 600°C for 2–72 hours using distilled water or a solution of alkaline metal (Li, Na, K) fluorides, chlorides, bromides, carbonates, nitrates, sulfates, or hydroxides, as mineralizers.

Somiya et al. (1990) have given the following flowchart for the hydrothermal homogeneous precipitation method, Fig. 10.3.[14] The autoclaves used were: *i)* Tuttle type; *ii)* 500 cl; *iii)* 1000 ml; *iv)* 5000 ml; *v)* 20,000 ml, etc. The lining metals were Pt, Zr, and Ti.[14] By this means, the authors could obtain very fine powders of ZrO_2 and Y_2O_3-ZrO_2 of size 20 nm, with a narrow size distribution, very high purity, excellent sinterability, less defects and controllable shapes. Hence, hydrothermal processing provides an excellent mean fraction by obtaining controlled shape and size from the ceramic particles.

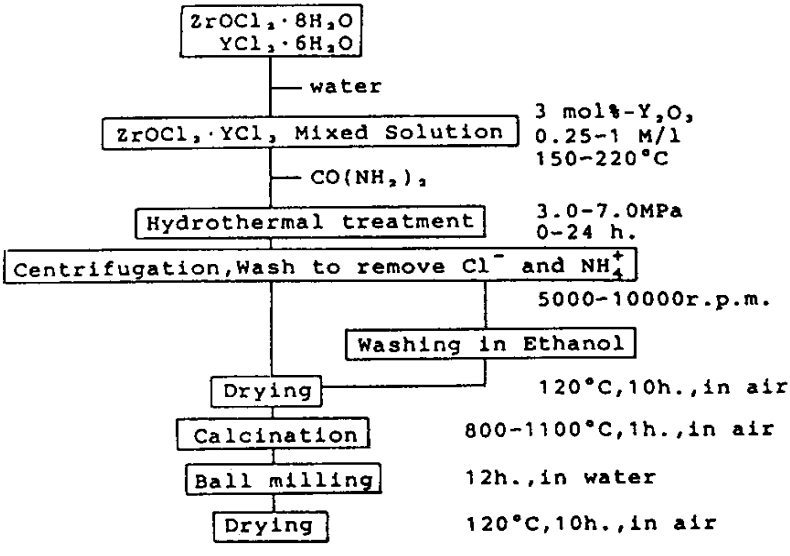

Figure 10.3. Hydrothermal homogeneous precipitation method.[14]

DropBooks

In the hydrothermal oxidation of metals, pulverization and oxidation proceed simultaneously during the reaction with high-temperature, and high-purity water. These phenomena have been applied in the preparation of fine oxide powders (20 to 30 nm) of Fe_3O_4, Cr_2O_3, ZrO_2, HfO_2, Al_2O_3, and others at relatively lower temperatures (400 to 600°C).[15]–[19] Figures 10.4 *(a–d)* show the fine crystals of zirconia and ceria.[20] Figures 10.5 *(a–c)* show the representative photographs of hydrothermally processed ceramic powders.[20]

10.2.2 Hydrothermal Preparation of Perovskite Type of Mixed Oxide Ceramics

Alkaline earth titanates have always appeared in two types of stable phases: the pyrochlore and the perovskite structural. Between these, the high purity, fine perovskite titanates with exact stoichiometry are widely used as ferroelectric materials, owing to their excellent electric, pyroelectric, semiconducting and electro-optic properties. Hydrothermal processing is a very convenient technique for the preparation of various multicomponent oxide materials that have maximum utility in present day

electronics applications.[21]–[23] These multicomponent oxides from electronic ceramic or catalytic applications can be produced by hydrothermal synthesis at moderate temperatures and pressures (>100°C and 0.1 M Pa). The success of hydrothermal synthesis depends on the selection of precursors that are both reactive and cost effective as well as appropriate process condition variables, which include temperature, pH, and reagent concentration.[24] In the last decade, hundreds of publications have appeared in literature devoted to various aspects for preparation of these perovskite type oxides owing to their potential applications in modern technology. However, it is impossible to discuss every aspect of these perovskite types of oxides in this handbook which is devoted to all general aspects of hydrothermal technology.

The general formula for perovskite can be written as ABO_3, and for the solid solution $A(B_xC_{1-x})O_3$, where $0 < x > 1$, A = Ca, Sr, Ba, Pb, and Bi, B = Ti, and C = Zr.

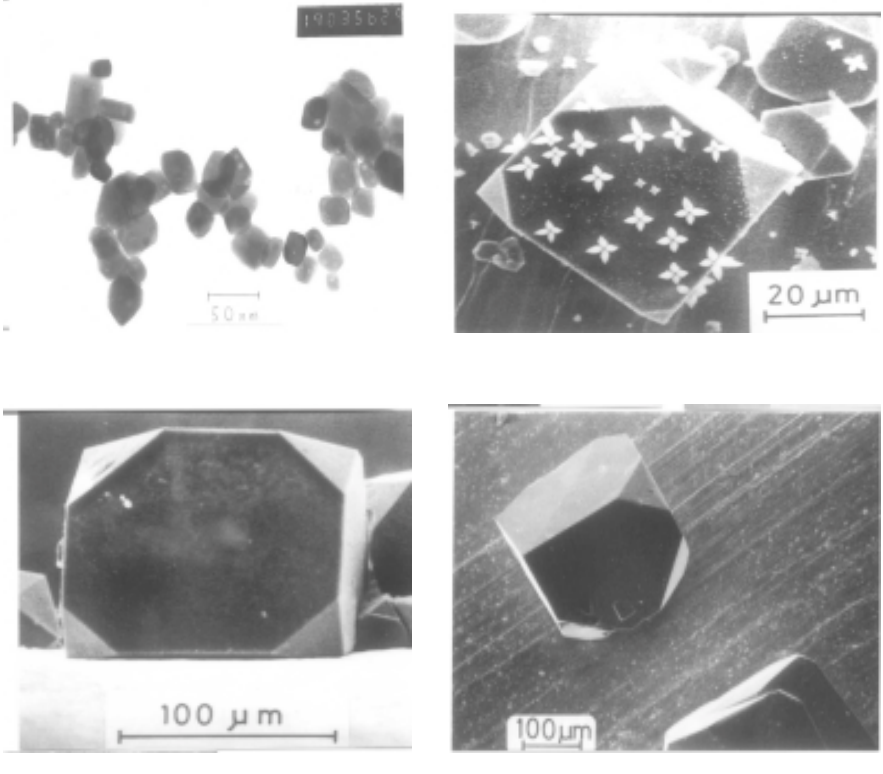

Figure 10.4. Fine crystals of zirconia and ceria. *(Photos by M. Yoshimura.)*

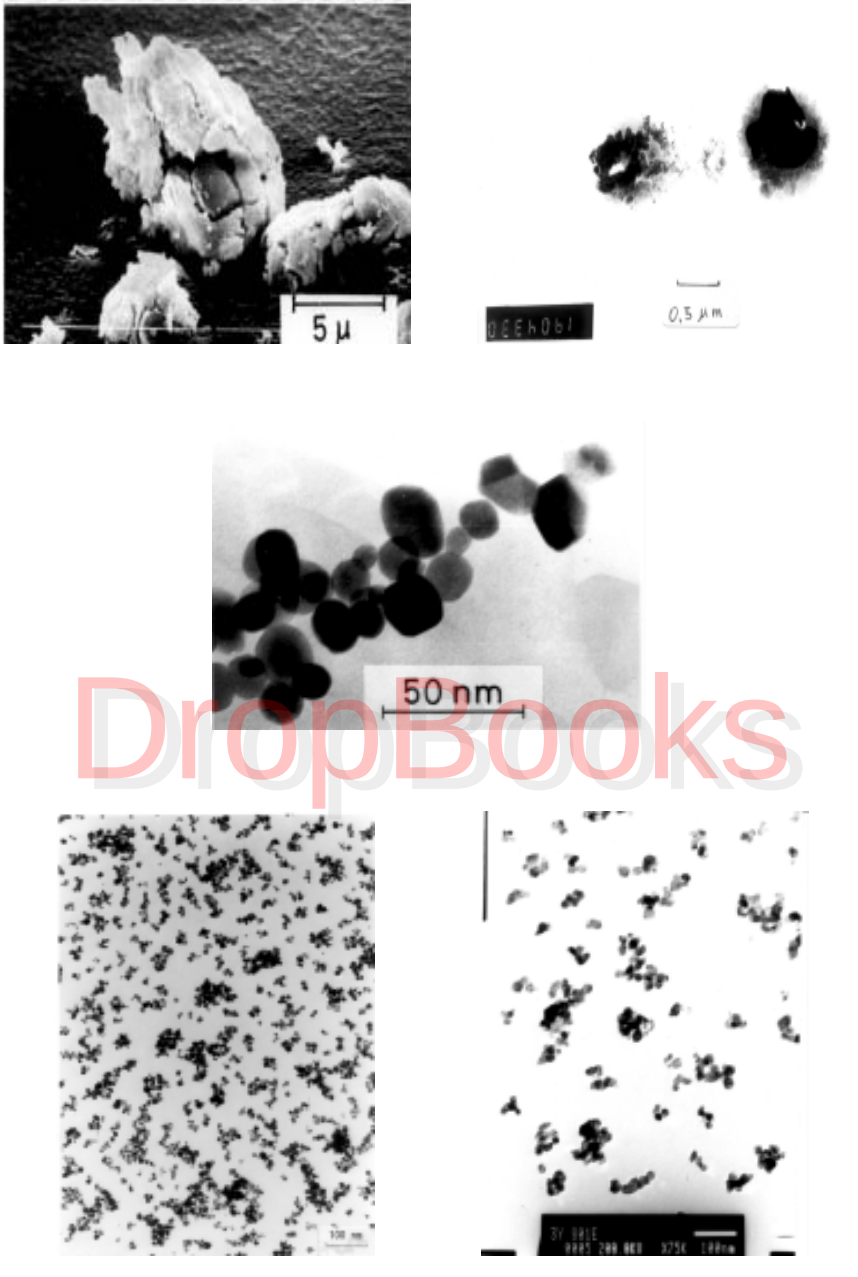

DropBooks

Figure 10.5. Representative photographs of hydrothermally processed ZrO_2 ceramic powders. *(Photos courtesy of S. Somiya.)*

Kutty and Balachandran (1984) have synthesized crystallization of perovskite (x = 0.5) at 573 K starting with crystallization of PbO and mixed Zr-Ti gels, obtained by hydrolyzing $TiOCl_2$ and $ZrOCl_2$ and NH_3 (aq).[25] Beal (1987) obtained perovskite (x = 0.5) at 573 K from mixtures of zirconia-titania gels, crystalline PbO, and various mineralizers.[26] The author found that the purity and morphology of the product depended on the chemical identity of the mineralizers.

Dawson and Swartz (1992) have synthesized several solid solutions ($0 < \times < 1$) from the PZT family using aqueous gels obtained by hydrolyzing $TiCl_4$ and $ZrOCl_2$ in basic solutions.[27] The slurry obtained, along with lead oxide and precursors of other elements (dopants), was hydrothermally treated at 573 K. It was found that the obtained solids had the same metal ion stoichiometry as the feeding material.

Riman and his group have done excellent work on the preparation of these PZT types of ceramics and have studied in detail the thermodynamics and kinetics of these systems.[28]–[30] Also, they have developed a new approach—intelligent engineering—in order to transform hydrothermal synthesis from an empirically based technology to one that revolves around engineering principles. They approached this problem from a multidisciplinary perspective of chemistry, chemical engineering, and physical chemistry, which all embrace principles of thermodynamics and kinetics.[31][32] Thermodynamic principles enable one to determine how to design a reaction to yield phase pure materials. Without this knowledge, it is impossible to distinguish a process that is being controlled by thermodynamics versus kinetics. These authors have studied all the possible reactions that may occur in the hydrothermal medium, more of a typical PZT system, for example, in the Ba-Ti and Pb-Ti systems. Following are the relevant equilibria in the Ba-Ti and Pb-Ti hydrothermal systems:[28]

i. $H_2O = H^+ + OH^-$

ii. $H_2O_{(g)} = H_2O$

iii. $TiO_{2\,(s)} = OH^- - HTiO_3^-$

iv. $Ba(OH)_{2\,(s)} = Ba^{2+} + 2OH^-$

v. $BaOH^+ = Ba^{2+} + OH^-$

vi. $BaTiO_{3(s)} + H_2O = Ba^{2+} + 2OH^- + TiO_{2(s)}$

vii. $Ba(OH)_2 \cdot 8H_2O_{(s)} = Ba^{2+} + 2OH^- + 8H_2O$

viii. $BaO_{(s)} + 2H^+ = Ba^{2+} + H_2O$

ix. $Ba_2TiO_{4(s)} + 2H_2O = 2Ba^{2+} + 4OH^- + TiO_{2(s)}$

x. $CO_{2(g)} = CO_{2(aq)}$

xi. $CO_{2(aq)} + H_2O = H^+ + HCO_3^-$

xii. $HCO_3^- = H^+ + CO_3^{2-}$

xiii. $BaCO_{3(s)} = Ba^{2+} + CO_3^{2-}$

xiv. $BaCO_{3(aq)} = Ba^{2+} + CO_3^{2-}$

xv. $BaHCO_3^+ = Ba^{2+} + HCO_3^-$

xvi. $Ti_4^+ + H_2O = TiOH^{3+} + H^+$

xvii. $TiOH^{3+} + H_2O = Ti(OH)_2^{2+} + H^+$

xviii. $Ti(OH)_2^{2+} + H_2O = Ti(OH)^{3+} + H^+$

xix. $Ti(OH)^{3+} + H_2O = Ti(OH)_{4(aq)} + H^+$

xx. $Ti(OH)_{4(aq)} = TiO_{2(s)} + 2H_2O$

xxi. $PbO_{(s)}^+ H_2O = Pb^{2+} + 2OH^-$

xxii. $PbO_{(aq)}^+ H_2O = PbOH^+ + OH^-$

xxiii. $PbOH^+ = Pb^{2+} + OH^-$

xxiv. $Pb(OH)_{2(s)} = Pb^{2+} + 2OH^-$

xxv. $Pb^{2+} + 2OH^- = H^+ + HPbO_2^-$

xxvi. $Pb_2OH^{3+} + H^+ = 2Pb^{2+} + H_2O$

xxvii. $Pb_3(OH)_4^{2+} = 3Pb^{2+} + 4OH^-$

xxviii. $Pb_4(OH)_4^{4+} = 4Pb^{2+} + 4OH^-$

xxix. $Pb_6(OH)_8^{4+} = 6Pb^{2+} + 8OH^-$

xxx. $PbTiO_{3(s)} + H_2O = Pb^{2+} + 2OH^- + TiO_{2(s)}$

DropBooks

About thirty independent reactions consisting of thirty-one species are shown above.

Aksay et al. (1996) have prepared nanometer sized $BaTiO_3$ particles under hydrothermal conditions by dispersing TiO_2 powders in a concentrated aqueous solution of $Ba(OH)_2$.[33] The TiO_2 particles dissolve in the aqueous $Ba(OH)_2$ solution and lead to the nucleation of nanometer-sized cubic phase $BaTiO_3$ particles. In concentrated solutions, the $BaTiO_3$ particles grow through multiple clustering. These authors have used a similar approach to obtain $BaTiO_3$ films from organo-metallic precursors at 80°C and below. It was found that the grain size of the film depends on the nucleation rate of the $BaTiO_3$ particles.

For the preparation of fine particles of this perovskite type mixed oxide, knowledge of stability diagrams under hydrothermal conditions is very important. The stability diagram shows the regions of reagent concentrations and pH at which various species predominate in the system, Fig. 10.6. Thus, the stability diagrams indicate the optimum synthesis conditions for which desirable products are thermodynamically stable. However, the stability diagrams were considered for a limited number of hydrothermal systems on the assumption that the aqueous solutions were ideal.[34][35] They are especially inaccurate when concentrated electrolyte solutions are utilized or when a multitude of competing reactions occur in a solution, thus making the equilibrium concentrations of various species strongly dependent on activity coefficients. Similarly, the speciation diagrams and yield diagrams help greatly in the hydrothermal synthesis of phase-pure ceramics. Figure 10.7 shows the calculated yield of $PbTiO_3$ in the Pb-Ti-H_2O complexing agent system for various Pb/Ti ratios. A majority of the PZT systems incorporate intolerable amounts of alkaline metals, which are introduced in the form of mineralizers. In recent years, organic mineralizers are being used by a large number of workers. For example, Riman (1996) has found that tetramethylammonium hydroxide [$N(CH_3)_4OH$] is a favorable substitute for alkaline metal hydroxide mineralizers in producing phase-pure PZT.[31] Phase-pure $MeTiO_3$ (Me = Ca, Sr, Ba) can be obtained at input molalities of Ba, Sr, and Ca greater than 7×10^{-5}, 10^{-6} and 5×10^{-5}, respectively. Otherwise, the relative location of the 99.995% yield regions for the three titanates will be similar to the pattern noted for stability diagrams.[23] In concentrated solutions, the consumption of OH^- ions is caused by the following predominant reactions:

Eq. (1) $$Me^{2+} + TiO_2 + 2OH^- = MeTiO_3 + H_2O$$

Thus, 2 molar of OH^- is consumed for the synthesis of 1 molar of $MeTiO_3$, and only a relatively small amount of OH^- is necessary to ensure correct pH for respective alkaline earth. Unlike the synthesis with nitrates, the use of metal hydroxide precursors at high concentrations does not require the addition of a mineralizer because the necessary concentration of OH^- groups is readily provided by the hydroxide precursor. To the contrary, at dilute concentrations identical amounts of mineralizers are needed, irrespective of whether a nitrate or a hydroxide is used as precursor. However, the required mineralizer concentration differs substantially for the three

metals. This may be caused by the strong, specific effects of the chemical identity of cations on activity coefficients due to their high concentration to form alkaline-earth titanates.

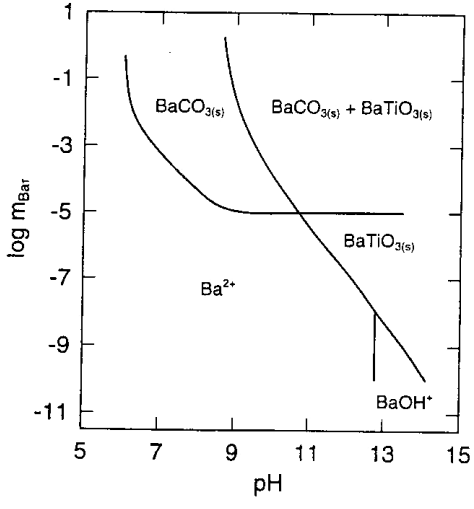

Figure 10.6. Stability diagram for barium titanate system.[31]

DropBooks

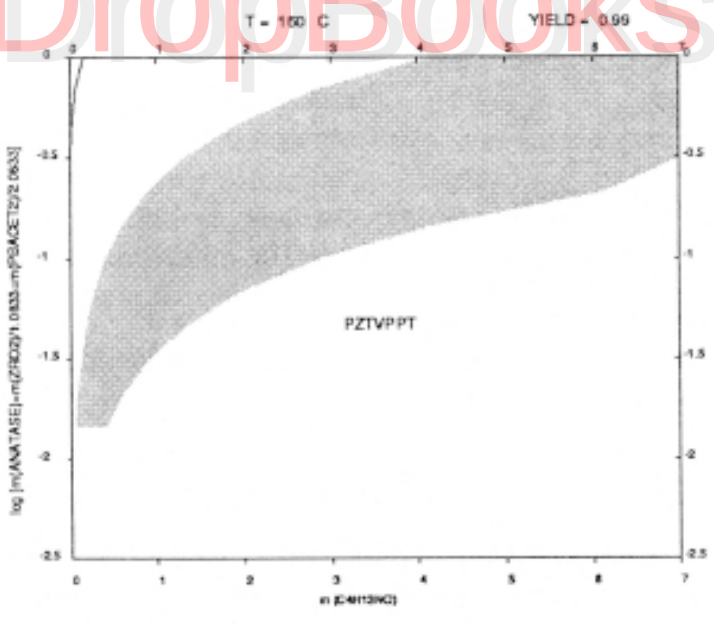

Figure 10.7. Calculated yield of $PbTiO_3$ in the Pb-Ti-H_2O complexing agent system for various Pb/Ti ratios.[31]

Eckert, Jr. et al. (1996) have proposed *in situ* reaction mechanism, and dissolution-precipitation reaction mechanism, Figs. 10.8 and 10.9.[30] As evident from these figures, the *in situ* transformation model assumes that TiO_2 reacts initially with dissolved barium. This produces a continuous layer of $BaTiO_3$ through which additional barium must diffuse in order to continue reaction until the TiO_2 supply is exhausted. The product layer may be either a dense or a porous layer or of monocrystalline or polycrystalline nature. The dissolution-precipitation model involves multiple steps. For an anhydrous TiO_2 precursor, Ti-O bonds must be broken via hydrolytic attack, to form hydroxy-titanium complexes ($Ti(OH)_x^{4-x}$) capable of dissolution and reaction with barium ions or complexes (Ba^{2+} or $BaOH^+$) in solution to precipitate $BaTiO_3$. In contrast, use of a hydrous TiO_2 reactant bypasses some, or most of the hydroxylation steps. $BaTiO_3$ nuclei may either originate at the TiO_2 substrate (heterogeneous nucleation) or form directly in the bulk solution (homogeneous nucleation). When hetereogeneous nucleation occurs, the dissolving TiO_2 particle can be encapsulated, thereby limiting the supply of soluble TiO_2 species available to react with the barium species. As with the *in situ* transformation model, this diffusional barrier serves to slow if not to halt the hydrothermal reaction. Such mechanisms of formation of $BaTiO_3$ can also be applied to other perovskite type titanates. Figure 10.10 shows the perovskite type alkaline-earth titanates prepared under hydrothermal conditions.[23][33] The pH of the medium, precursor and the ratio of Me/Ti play an important role in determining the morphology of these particles.

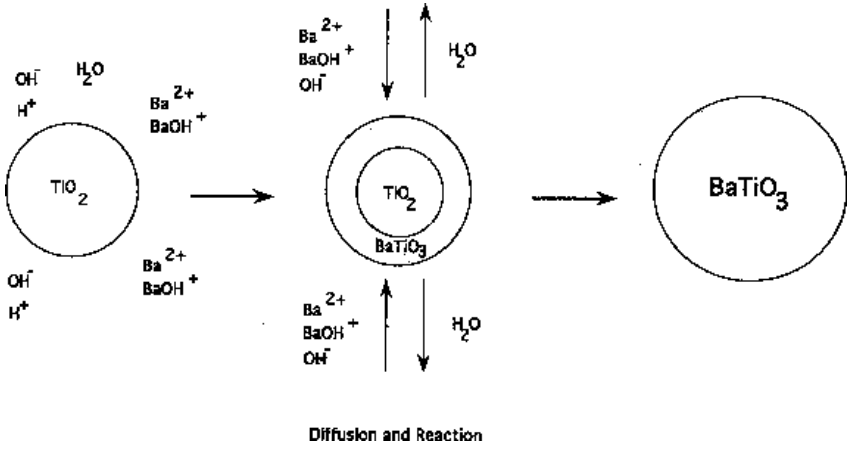

Figure 10.8. *In situ* reaction mechanism.[30]

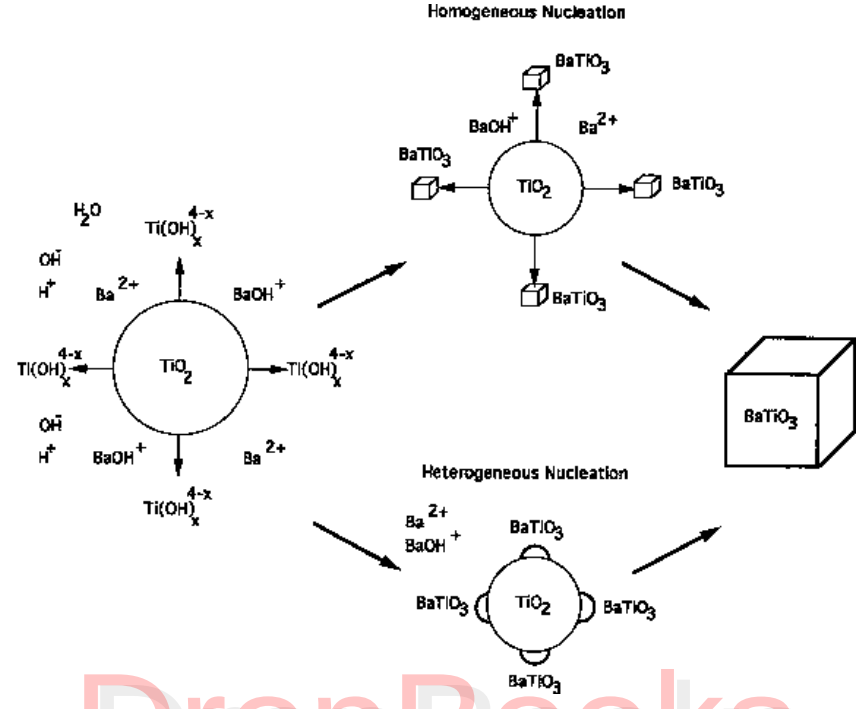

DropBooks

Figure 10.9. Dissolution-precipitation reaction mechanism.[30]

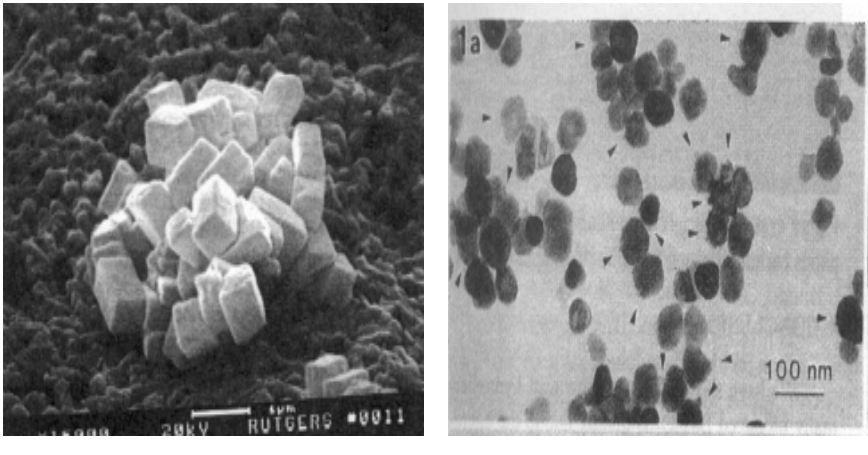

(a) (b)

Figure 10.10. Perovskite type alkaline-earth titanates. *(a)* See Ref. 23 and *(b)* see Ref. 33.

The preparation of alkaline-earth titanates has been carried out using non-aqueous solutions, which come under solvothermal synthesis. This has some advantage, as the solvothermal synthesis might allow the product to be free from foreign atoms because the organic solution, having a low relative permittivity, is free of ionic species. Chen and Xu (1998) have synthesized $PbTiO_3$ powder under solvothermal conditions.[36] The starting materials involved are amorphous xerogels consisting of a mixture of equivalent molar amounts of PbO and TiO_2 (1:1 ratio), prepared by using lead acetylacetate and tetrabutyl titanate. The precursor xerogel was poured into the solvent to form a suspension solution and 30.0 cm^3 of the suspension was fed into a 40 ml capacity stainless steel autoclave with a teflon liner. The required amount of methanol was poured into the autoclave and the autoclave was held at 240°C for 10 to 60 hours. The crystallinity increased with the increasing reaction time.

Although the crystallization of $PbTiO_3$ in alcohol solution required higher temperatures for longer times, the nanometer-sized particles, in comparison with the micrometer-sized ones derived from aqueous solution, exhibited a lower agglomeration due to the organic materials having a lower relative permittivity and a simple mode of size distribution.

Like the hydrothermal process, the formation of $PbTiO_3$ proceeds in alcohol solution by a dissolution-reprecipitation mechanism, in which the dissolution of precursor is the rate controlling stage. In comparison with those in methanol, the reactions in MOE for the syntheses of $PbTiO_3$ powders required higher temperatures or longer time because of MOE having a lower vaporizing pressure and relative permittivity.

Kaiser et al. (1994) have synthesized $BaTiO_3$ powders at a temperature of 175°C and pressures between 0.1 MPa and 1 MPa, starting from $TiO_2.xH_2O$ and $Ba(OH)_2.8H_2O$ in solvents of pure water, 1.5–pentanediol and in different mixtures of both using the lyothermal method.[37] Figure 10.11 shows the schematic preparation route for lyothermal synthesis of $BaTiO_3$.

The authors could control the size and habit of BaTiO3 particles through the viscosity of the solvent and the concentration of the starting materials. The lyothermal method offers a promising means of producing various nanocrystalline materials of alkaline-earth titanates. Table 10.3 lists fine powders synthesized under hydrothermal conditions.

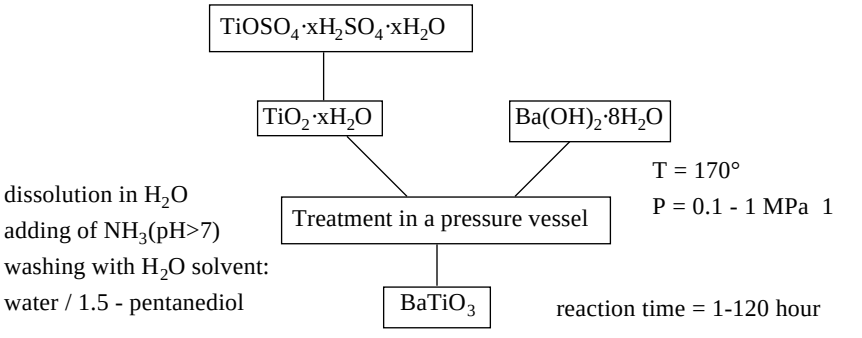

Figure 10.11. Schematic preparation route for lyothermal synthesis of $BaTiO_3$.[37]

Table 10.3. List of Fine Powders Synthesized Under Hydrothermal Conditions *(Courtesy of Prof. S. Somiya)*

AlO-OH	ZrO_2	Al_2O_3	ZrO_2-HfO_2	$BaFe_{12}O_{19}$	Sb_2S_3	Sb	$ZnSiO_4$
FeO-OH	HfO_2	Cr_2O_3	SiO_2-ZrO_2	$CaSiO_3$	CdS	As	$ZrSiO_4$
SiO_2-H_2O	Fe_3O_4	CrO_2	UO_2-ThO_2	$BaTiO_3$	FeS	Bi	$CaCO_3$
Cr_2O_3-H_2O	Fe_2O_3	SiO_2	Al_2O_3-ZrO_2	$BaZrO_3$	MnS	Au	$kTiO_4$
MnO·H_2O	MnO_2	Nb_2O_5	Al_2O_3-TiO_2	$LaCrO_3$	ZnS	Pb	
Mn_3O_4·H_2O	UO_2	TiO_2	Al_2O_3-HfO_2	(La,Sr) CrO_3	Hg		
	FeO	ZnO	NiO-Fe_3O_4	KMF_3	Ni		
	Cu_2O	CoO_3	Y_2O_3-ZrO_2	M=Co,Mn,Fe	Co		
	NiO	MgO	CaO-ZrO_2	$AlPO_4$	Cu		
	CdO	V_2O_3	MgO-ZrO_2	$NdP5O_{14}$	Pt		
	CeO_2	Ta_2O_5	Nb_2O_5-TiO_2	$NdPO_4$	Ag		
		PbO_2	Ta_2O_5-TiO_2	SrF_2-LaF_3	Sm		
			V_2O_5-ZrO_2	YAG	Ga		
				$kNbO_3$	$Na_8[AlSi_4O_4]_6(NO_2)_2$		

Ba-Ferrites	$NiFe_2O_4$	Niobates	$PbZr_xTi_{1-x}O_3$ (0.46 < × < 0.75)
Sr-Ferrite	$ZmFe_2O_4$	Tantalates	$Co_{10}(PO_4)_6(OH)_2$
	$NixZm_{1-x}Fe_2O_4$	Vanadates	Ba Titanate
	$CoFe_2O_4$	Titanate	Pb Titanate
	$Mn_{0.5}Zn_{0.5}Fe_2O_4$		$Rb_2(MoO_3)_3SeO_3$
			$Tl_2(MoO_3)_3SeO_3$
			Na beidellite

DropBooks

In recent years, glycothermal and solvothermal syntheses are being used popularly to prepare fine powders of nitrides, alumina, iron oxide, hexaferrites, and so on.[38]–[41] These methods are very useful in obtaining shaped and sized particles under relatively lower pressure temperature conditions.

10.2.3 Hydrothermal Processing of Bioceramics

Bioceramics represent a broad spectrum of ceramic materials designed for chemical compatibility and optimal mechanical strength with the physiological environment. These materials are used for the repair and reconstruction of diseased or damaged parts of the musculo-skeletal system. Bioceramics may be bioinert (alumina, zirconia), resorbable (tricalcium phosphate), bio-active (hydroxyapatite), bio-active glasses, and glass ceramics, or porous for tissue in-growth (HAp coated metals, alumina). Applications include replacements for hips, knees, teeth, tendons, and ligaments and repair of periodontal disease, maxillofacial reconstruction, augment and stabilization of the jaw bone, spinal fusion, and bone fillers after tumor surgery.[42][43] Table 10.4 gives the types of bioceramics and also the tissue attachment and bioceramic classification.[44] Bioceramics are also widely used in dentistry as restorative materials, gold porcelain crowns, glass-filled ionomer cements, dentures, etc.

High-density, high-purity (>99.5%) Al_2O_3 (α-alumina) was the first bioceramic, widely used for clinical purposes during the 1960s. It is used in total hip prostheses and dental implants because of its combination of excellent corrosion resistance, good bio-compatibility, low friction, high wear resistance, and high strength.[45][46] Other clinical applications of Al_2O_3 include knee prostheses, bone screws, alveolar ridge (jaw bone), and maxillofacial reconstructs, ossicular (middle ear) bone substitutes, Keratoprostheses (Corneal replacements), segmental bone replacements, blade and screw and post-type dental implants.[45][46]

Zirconia (ZrO_2), in tetragonal form, stabilized by either magnesium or yttrium, has also been developed as a medical-grade bioceramic for use in total joint prostheses. The interest in ZrO_2 is derived from its high fracture toughness and tensile strength. These improved properties make it possible to manufacture femoral heads for total hip prostheses that are smaller than the present generation of Al_2O_3 heads. ZrO_2 implants are now used clinically; however, only implant survivability data over a ten year period will establish clinical advantages.[46][47]

Table 10.4. Types of Bioceramic Tissue Attachment and Bioceramic Classification[44]

Type of Attachment	Type of Bioceramic
Dense, nonporous, almost inert ceramics attach by bone growth by cementing the device into the tissue, or by press-fitting into a defect (morphological fixation)	Al_2O_3 ZrO_2
For porous implants, bone ingrowth occurs, which mechanically attaches the bone to the material (biological fixation)	Porous hydroxyapatite Hydroxyapatite-coated porous metals
Surface-reactive ceramics, glasses, and glass-ceramics attach directly by chemical bonding with the bone (bioactive fixation)	Bioactive glasses Bioactive glass-ceramics Dense hydroxyapatite
Resorbable ceramics and glasses in bulk or powder form designed to be slowly replaced by bone	Calcium sulfate (plaster of Paris) Tricalcium phosphate Calcium phosphate salts Bioactive glasses

DropBooks

These materials are prepared by hydrothermal techniques such as hydrothermal sintering, hydrothermal hot pressing and under hot isostatic pressure.

The most significant area of growth for bioceramics, however, involves a more complex material—hydroxyapatite $\{Ca_{10}(PO_4)_6(OH)_2\}$, which is the main mineral constituent of teeth and bones, representing 69% by weight. Hydroxyapatite based bioceramics have been in use in medicine and dentistry for twenty years.[46]–[49] It has the physicochemical advantages of stability, inertness, and biocompatibility. However, its relatively low strength and toughness, produced little interest among researchers searching for bulk structural materials. HAp ceramics do not exhibit any cytoxic effects, and HAp can directly bond to the bone. Unfortunately, due to low reliability, especially in wet environments, the HAp ceramics can not be used for heavy load-bearing applications, like

artificial teeth or bones. Nevertheless, there has been a lot of research aiming to fabricate more mechanically reliable bioactive ceramics including, of course, the HAp materials. Suchanek and Yoshimura (1998) have reviewed in detail the past, present, and future of the HAp-based biomaterials from the point of view of preparation of hard tissue replacement implants.[50] The chemical component of the mineral constituents of teeth and bones is very important in the synthesis of HAp-based biomaterials. The inorganic phases present in the hard tissues contain mostly Ca^{2+} and P, considerable amounts of Na^{+}, Mg^{2+}, K^{+}, also CO^{2-}_{3}, F^{-}, Cl^{-} and H_2O. All these species, if applied in appropriate quantities, should be well tolerated in the implant by the surrounding tissues.

Presently, the HAp-bioceramics are at the pinnacle stage of their development. Powder processing, formation, and densification have been understood quite well, allowing the control of chemical composition and microstructures of both dense and porous HAp ceramics. Any new developments concerning powder preparation/shaping/densification may affect only the price of the products, but are not expected to affect their medical applications, which are restricted due to the nature of HAp.[50]

Several techniques have been used for the preparation of HAp powders.[51]–[54] Two main ways for the preparation of HAp powders are wet methods and solid state reactions. In the case of HAp fabrication, the wet methods can be divided into three groups: precipitation, hydrothermal technique, and hydrolysis of other calcium phosphates. Depending upon the technique, materials with various morphology, stoichiometry, and level of crystallinity, can be obtained. Solid state reactions usually give a stoichiometric and well-crystallized product, but they require relatively high temperatures and long heat-treatment times. Moreover, the sinterability of such powders is usually low. In the case of precipitation, nanometer size crystals can be prepared, and they have the shapes of blades, needles, rods, or equiaxed particles. Their crystallinity and Ca/P ratio depend mainly upon the preparation conditions and are in many cases lower than for well-crystallized stoichiometric hydroxyapatite. The hydrothermal technique usually gives HAp materials with a high degree of crystallinity and with a Ca/P ratio close to the stoichiometric value. Their crystal size is in the range of nanometers to millimeters. Hydrolysis of tricalcium phosphate, monetite, brushite, or octacalcium phosphate, requires low temperatures (usually below 100°C) and results in HAp needles or blades the size of microns. There are also alternative methods of HAp powders preparation, like sol-gel, flux method, electrocrystallization,

spray-pyrolysis, freeze-drying, microwave irradiation, mechano-chemical method, or emulsion processing.[55]–[60]

Many HAp powders can be sintered up to theoretical density, without pressure, at moderate temperatures (1000–1200°C). Processing at higher temperatures may lead to exaggerated grain growth and decomposition of HAp and, subsequently, to strength degradation HP, HIP, or HIP—post-sintering makes it possible to decrease the temperature of the densification process, decrease the grain size, and achieve higher densities. This leads to finer microstructures, higher thermal stability of HAp, and subsequently, better mechanical properties of the prepared HAp ceramics.[50] HAp ceramics, in a porous form, have been widely applied as bone substitutes. Porous HAp exhibits strong bonding to bone. The classical way to fabricate porous HAp ceramics (pore size of 100–600 μm) is through hydrothermal sintering of the HAp powder with appropriate pore-creating additives, like naphthalene, paraffin, hydrogen peroxide, etc., which evolve gases at elevated temperatures. Natural porous materials, like coral skeletons made of $CaCO_3$, can be converted into HAp under hydrothermal conditions (250°C, 24–48 h).[61] Microstructure, undamaged porous HAp structures can also be obtained by HHP.[62][63] This technique allows solidification of HAp powder at 100–300°C, 30 MPa, for 2 hours.

DropBooks

Calcium phosphate bone cements find extensive applications as important biomaterials. These are mixtures of various calcium phosphate powders, such as $CaHPO_4 \cdot 2H_2O$, $Ca_4(PO_4)_2O$, $CaHPO_4$, $Ca_8H_2(PO_4)_6 \cdot 5H_2O$, $Ca(H_2PO_4)2H_2O$, or TCP and water, or another liquid (for example, H_3PO_4 or Na_2HPO_4). The mixture transforms into HAp during setting, forming a porous body, even at 37°C.[64]–[66] The setting time of calcium phosphate cements can be reduced to a few minutes. Similarly, the decay of cements, when in contact with blood, can be prevented. Several types of cements like HAp clays, consisting of HAp granules in a saline solution of calcium alginate, bioactive glass bone cements, HAp-, TCp-, or bioactive glass-reinforced polymeric bone cements, have also been developed.

The advantages of the calcium phosphate bone cements are high biocompatibility, bioactivity, and osteoconductivity. The only serious disadvantage is their relatively poor mechanical strength. Easy shaping of bone cements enables using them to fill bone defects much better than HAp solid blocks, which are difficult to shape, or HAp powders/granules, which are difficult to keep in place. Calcium phosphate bone cements

may, in the future, replace PMMA cements as bone/implant fixation, if their mechanical properties can be improved. Moreover, they can be used as fillings of tooth root canals or as drug-delivery systems.[50][67][68] The hydrothermal method has several advantages in treating these calcium phosphate bone cements and slurries in a simple and effective way.

The future of HAp-based bioceramics lies in HAp-based composites, like HAp-ceramic, HAp-metal, HAp-polymer, HAp-collagen, and so on. However, there remain several unanswered questions related to HAp bioceramics: such as, is it possible to make HAp-based ceramics applicable to heavy-loaded implants?[50] Hydrothermal processing plays a key role in the preparation of bioceramics. A combination of methods, like sol-gel and hydrothermal processing, also help greatly in the development or processing of future bioceramics.

10.2.4 Hydrothermal Preparation of Thin Films

This is one of the fast developing areas in hydrothermal research. The epitaxial growth of thin films under hydrothermal conditions began during the 1970s. The heteroepitaxial growth of single crystal films of YIG on GGG substrates by hydrothermal synthesis has been reported by many workers.[69]–[71] In present day context, the method has been modified and is popularly known as the hydrothermal-electrochemical technique, which is a very convenient method of preparing a wide range of films on substrates, coating of materials, preparation of multi-layered compounds, functionally gradient materials, and so on.[72][73] The method is especially versatile and convenient, because of the lower temperature and pressure conditions involved compared to the conventional hydrothermal technique involving very high-pressure–temperature conditions. Among the compounds obtained through hydrothermal-electrochemical technique, perovskite type alkaline-earth titanates dominate, followed by tungstates, molybdates, and a series of solid solutions of alkaline earth titanates.[74]–[76]

Synthesis of large $PbTiO_3$ single crystals and polycrystallized ceramics is very difficult because it cracks spontaneously when passing through its phase transformation temperature (Tc = 490°C) during cooling. Possible applications in electronic and optical devices have brought much attention to the preparation of pure $PbTiO_3$ film. Most of the films have been fabricated by either *rf* sputtering or chemical vapor deposition. However, these methods have several disadvantages, such

as the stoichiometric change of the film composition and residue of source material, such as $PbCl_2$, in the film. Furthermore, to form ferroelectric $PbTiO_3$ films during or after processing, requires high-temperature treatment, which causes a reaction of the film with the substrate and sometimes leads to cracking and/or peeling of the film. Metal-organic chemical vapor deposition (MOCVD) and sol-gel methods have also been applied to the preparation of $PbTiO_3$ film.[77]–[81]

During processing, high temperatures above 500°C are also needed to remove organics. On the other hand, hydrothermal synthesis has frequently been used in preparing ceramic powders for a variety of applications. It is superior to the other powder preparation methods since high-temperature calcination is not necessary for the synthesis of crystallized ceramic powder. Verification can be supported by the experimental results of hydrothermal synthesis of $PbTiO_3$ powders.

During the 1990s, several authors developed hydrothermal or hydrothermal-electrochemical methods to prepare various double oxides such as $BaTiO_3$ and $SrTiO_3$ crystallized films directly on Ti-metal substrates by taking advantage of the hydrothermal reactions in high-temperature water (200°C).[82]–[90] This method, in general, enables us to synthesize perovskite-type compound ABO_3, on a B-site metal in an aqueous alkaline solution containing A-site elements. It is increasingly being used for the preparations of $BaTiO_3$ film by other groups as well.

ProBooks

In the hydrothermal-electrochemical method, $BaTiO_3$ films are produced on a titanium electrode, which is anodized in the presence of an electrolyte containing $Ba(OH)_2$ under pressurized conditions. Recent results indicate that polycrystalline $BaTiO_3$ films can be prepared at temperatures as low as 55°C, using electrochemical activation in a barium acetate electrolyte in an oxygen atmosphere.[91] This method has been used as a highly versatile one to prepare perovskite films of several materials such as $BaTiO_3$ and $SrTiO_3$,[83]–[85] $CaTiO_3$,[87] $BaFeO_3$,[85] $LiNbO_3$,[85] $BaNbO_3$,[87] $Ba_2Nb_5O_3$,[87] $PbTiO_3$,[76][92] $BaWO_4$,[74] TiO_2,[93] ZnO,[94] and TiO_3,[95] etc.

A closely related technique for film formation is hydrothermal deposition in which perovskite films are produced under similar conditions, but without electrochemical activation. By this technique, $BaTiO_3$,[83][96] $SrTiO_3$,[83] (Ba, Sr) TiO_3 and $BaZrO_3$[96][97] films have been obtained.

The hydrothermal-electrochemical film formation technique is not yet well established and there is not much information on the

electrochemical mechanism involved in the formation of these films. Moreover, there is not a clear understanding of the relationship between the film formation mechanisms for the hydrothermal method and those for the hydrothermal-electrochemical method. Most of the earlier works on $BaTiO_3$ hydrothermal-electrochemical formation has been performed in two-electrode cells, titanium anode and platinum cathode. In such a system, it is not possible to obtain accurate, specific, information on the electrochemical phenomena occurring at the titanium anode as the measured voltage drop on the cell is the result of processes at the anode, cathode, and in the electrolyte.

Kajiyoshi et al. (1995) have described the autoclave designed for hydrothermal-electrochemical treatment/preparation of $ATiO_3$ (A = Ba, Sr) thin films. It has a 3-electrode technique.[89] The electrolytic cell assembled in the autoclave is shown schematically in Fig. 10.12. It accommodates an Ag/AgCl external reference electrode (Toshin Kogyo, Tokyo, Japan),[98] which enables one to measure potentials of electrodes on a thermodynamically meaningful scale, regardless of the electrolysis conditions.[99] The preprocessed Ti substrate and the platinum plate are suspended as the working electrode (anode) and the counter electrode (cathode), respectively, by 0.5 mm diameter wires of the same metal as the respective plates, keeping an interval of 30 mm between them in the electrolytic cell containing 500 ml of the solution. The experiments were carried out at 150°C, an approximate heating rate being 1.5°C/min. The Ti working electrode was polarized potentiostatically from 50°C in the heating region to the end of the 150°C isothermal region, keeping an anodic potential of +12.OV *vs.* Ag/AgCl. The electrolysis current varies characteristically in the heating process and then remains almost constant in the isothermal process. After the experiment, the Ti substrate was washed in distilled water with an ultrasonic cleaner and dried at 120°C. Kajiyoshi et al. (1995) have also studied, in detail, the transport mechanism of film-constituting elements. They propose two models; the first based on the principle of tracer technique: *i)* substitutional transport, *ii)* interstitial transport. The second is the short-circuit path model. The latter one is more appropriate here to describe the mass transport in $ATiO_3$ (A = Ba, Sr). Figure 10.13 illustrates schematically the mass transport and film growth mechanisms of the short-circuit path model. In this model, all the observed results can be explained comprehensively, together with an atom-mixing mechanism accompanied by the dissolution-recrystallization

process. Figure 10.14 shows representative SEM micrographs of a fractured cross section of growth films.[89] All the films have a similar cross-sectional microstructure, regardless of their treatment processes. The advantage thickness of the thin layer is ca. 0.1–0.2 μm.

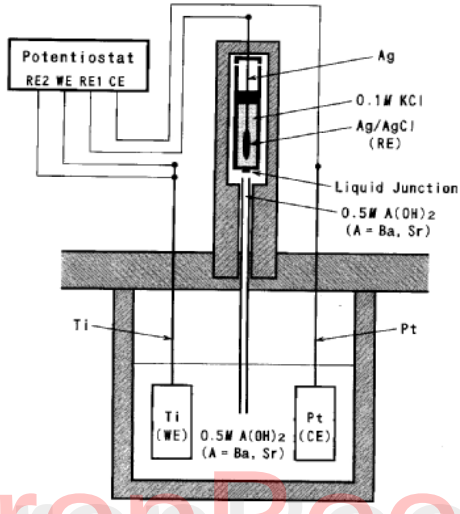

DropBooks

Figure 10.12. Electrolytic cell assembly in the autoclave.[89]

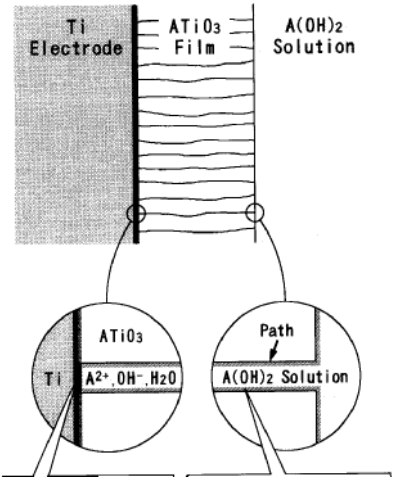

Figure 10.13. Schematic representation of mass transport and the film growth mechanism.[89]

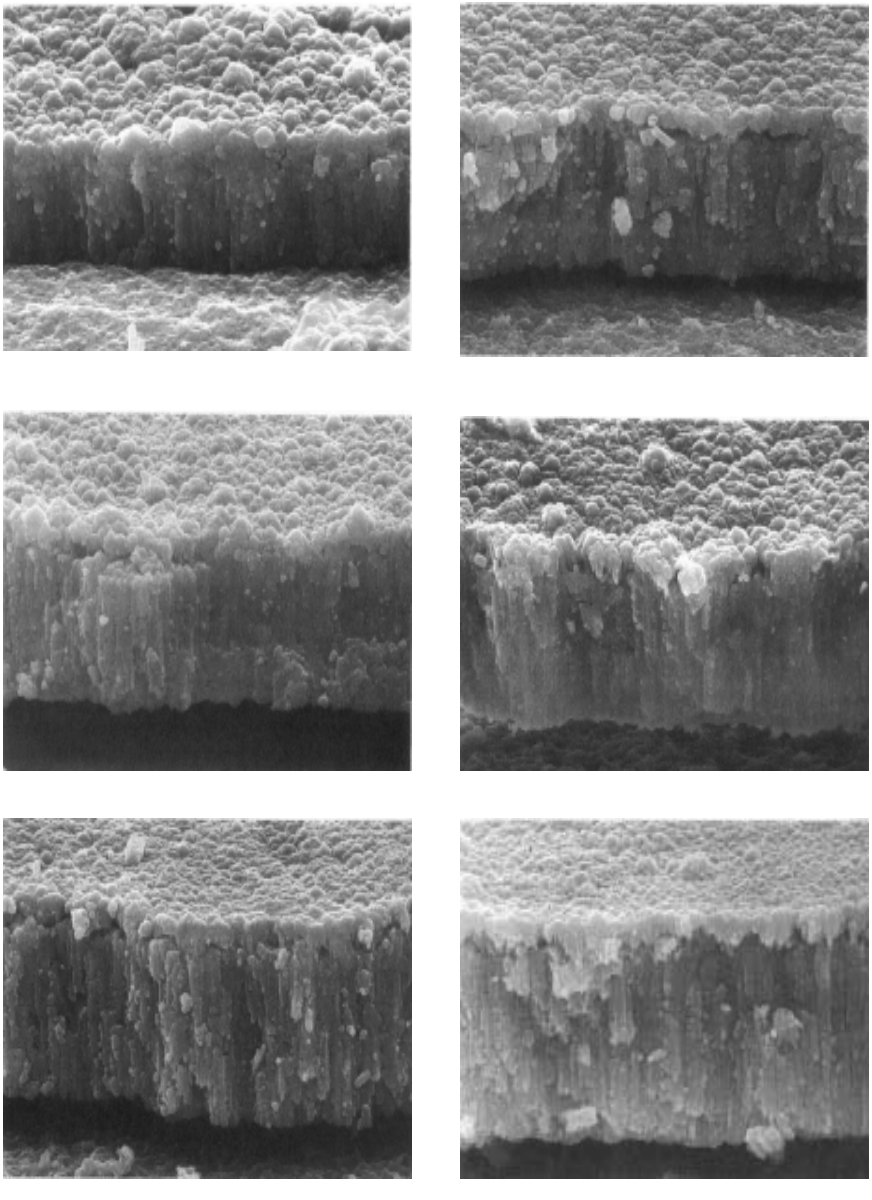

Figure 10.14. Representative SEM micrographs of fractured cross section of growth films. *(Photos by M. Yoshimura.)*

Such studies have been carried out by several other workers on different compounds. For example, Cho and Yoshimura (1997) have studied, in detail, the hydrothermal-electrochemical synthesis of highly crystallized barium tungstate films on tungsten metal substrates at fairly low temperatures.[74] The hydrothermal method did not produce a film because, only discrete $BaWO_4$ particles appeared on the tungsten substrate. The electrolysis experiments were carried out using tungsten substrates as anode (i.e., working electrode) and a platinum substrate as a cathode (i.e. counter electrode). A reference electrode (KCl-saturated Ag/AgCl) was put in a glass tube with a capillary tip close to the working electrode. $Ba(OH)_2$ solutions were made from redistilled water. Figure 10.15 shows the schematic diagram of the autoclave assembly used in the hydrothermal electrochemical method. The authors propose a model that interprets the mechanism for the formation and growth of the amorphous tungsten oxide film. The schematic diagram in Fig. 10.16 illustrates the mass transport and the amorphous film formation during anodic oxidation. Similarly, Fig. 10.17 shows the SEM photographs of sample surfaces prepared by the hydrothermal electrochemical treatments.

DropBooks

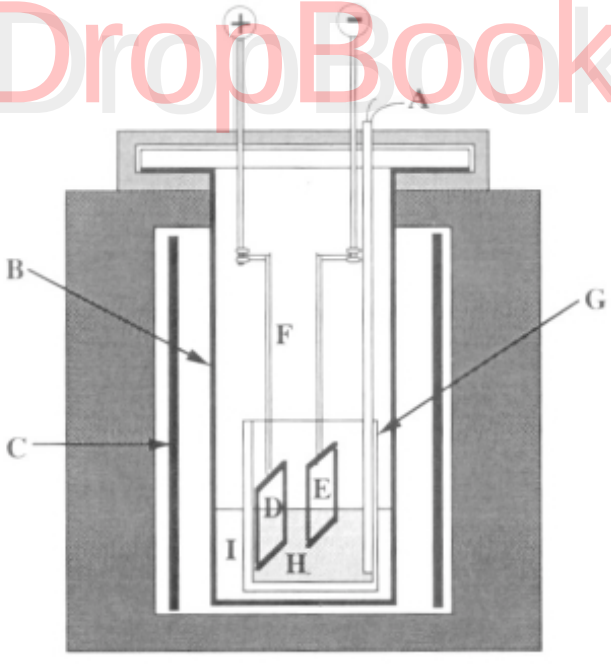

Figure 10.15. Schematic diagram of the autoclave assembly used in the hydrothermal electrochemical method.[74]

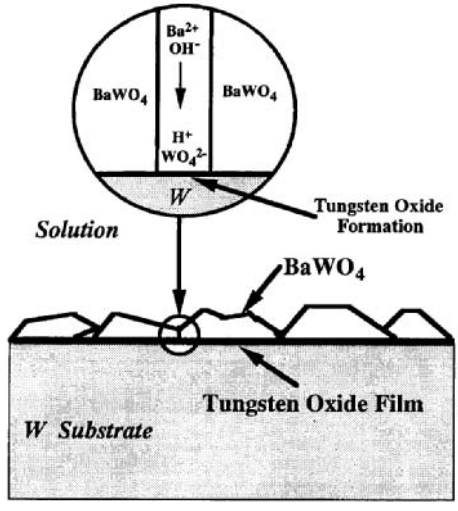

Figure 10.16. Mass transport and the amorphous film formation during anodic oxidation.[74]

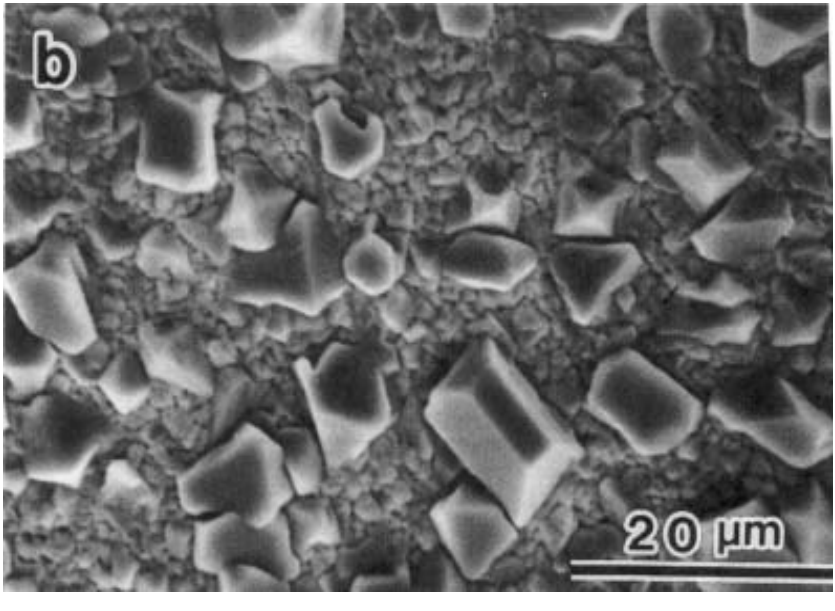

Figure 10.17. SEM photographs of the sample surfaces prepared by the hydrothermal electrochemical treatments. *(Photos by M. Yoshimura.)*

In general, the morphology, grain size, and quality, of the film can be controlled through several parameters, like temperature, pH of the solution at the interface, electrode current density, impurities (dopants), and duration of the experiment. Figure 10.18 *(a–d)* shows the $BaWO_4$ film morphology in 0.01M $Ba(OH)_2$ formed during conduction after *a)* 1 min, *b)* 15 min, *c)* 20 min, *d)* 25 min. The crystallization was characterized by three-dimensional nucleation and growth. Thus, the hydrothermal electrochemical processing/treatment of materials is going to play a pivotal role in futuristic hydrothermal research.

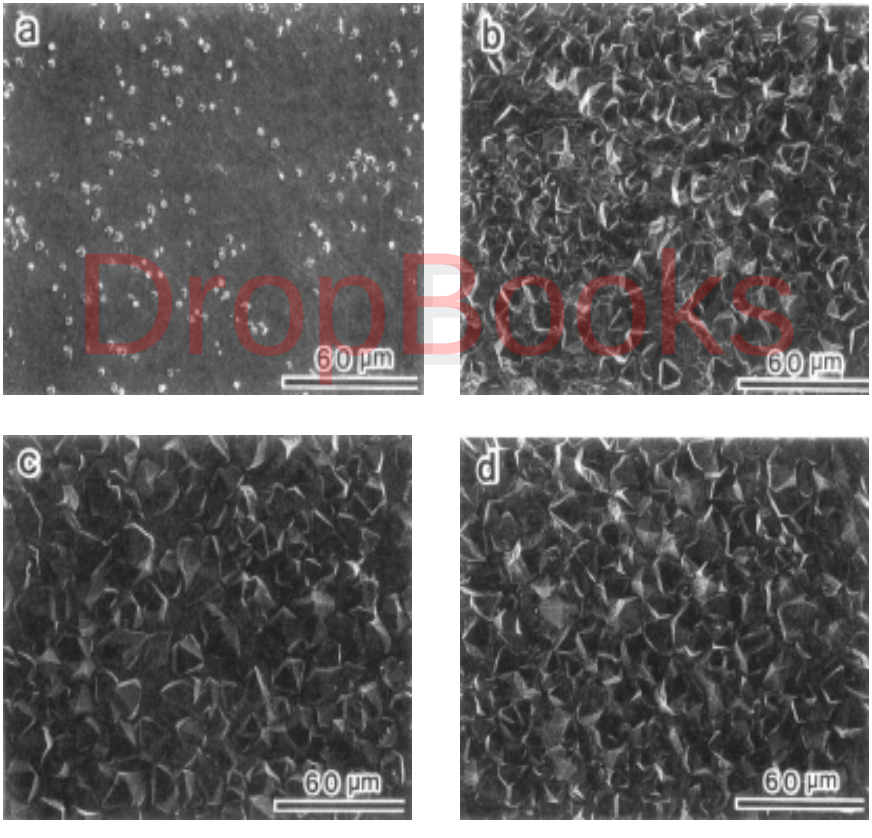

DropBooks

Figure 10.18. $BaWO_4$ film morphology in 0.01M $Ba(OH)_2$ formed during conduction after *(a)* 1 min, *(b)* 15 min, *(c)* 20 min, and *(d)* 25 min. *(Photos by M. Yoshimura.)*

10.2.5 Hydrothermal Processing of Composites

The nature invented composites—wood (cellulose and lignin) and bone (the polymer collagen and the mineral hydroxyapatite)—are specific examples that a composite can, and often does, have much more desirable properties than the individual pure or virgin materials from which it was made. Man-made composites have also been successful, as in the case of the rubber tire, which in its most common modern form is a composite of vulcanized rubber (the synthetic or natural polymer), carbon filler, and steel or polymeric fibers. One reason for interest in other man-made composites is indicated in Fig. 10.19.[100] The high strength-to-weight ratio of composites is more favorable than their ratio of strength to size. The general concept of composite materials has great appeal. It offers the prospect of microstructurally combining various classes of materials, by design, to realize superior sets of properties not obtainable from any of the constituent materials serving alone. Actually, this is an old idea (witness straw in bricks, horsehair in plaster, and reinforcing bars in concrete), but modern engineering requirements have become much more demanding, particularly, with regard to specific strength and stiffness for aerospace, military, and similar critical applications. By 1947, the filament-wound glass composite rocket motor case had been successfully flown, and the associated industrial contractors supported the Navy's decision to use fiberglass motor cases for the Polaris missiles. Since then, composites have served in successive generations of rockets, reducing weight and providing strength and durability.[101] Composites are highly useful in the fabrication of high-performance microelectronic devices consisting of multilayer substrates—multiple layers of ceramic (alumina), metal, and thin-film organic insulators. The fabrication of these substrates is made difficult by a number of problems, prominent among which is that of ensuring adhesion between the different components. These components commonly exhibit widely divergent coefficients of thermal expansion and fundamentally incompatible surface chemistries.

Tailoring the properties of the interface between reinforcing component and matrix is a major application of chemistry in improving the performance of composites. Failure in multilayer fiber-reinforced composite structures often occurs either at the fiber-matrix interface or at the matrix-matrix interface. The surface treatments, now used to modify the surface properties of reinforcing fibers in composites, are largely empirical. In this regard, the hydrothermal method of processing the materials to

obtain composites and multi-layers of ceramics and coating of substrates on other materials is very significant. The literature data available on composites are so vast that it is impossible to discuss each and every material in this chapter. Therefore, we have chosen the most important material, namely hydroxyapatite based composites, owing to their potential applications in modern technology.

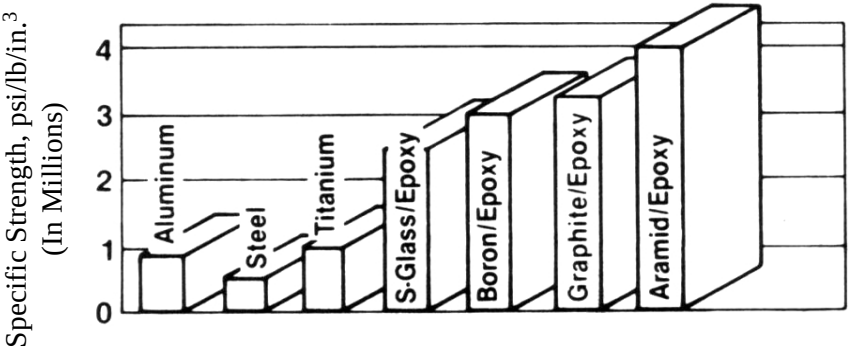

Figure 10.19. Man-made composites.[100] *(Courtesy of the National Academy Press, Washington, DC.)*

DropBooks

Hydrothermal Processing of HAp Coatings and HAp-Based Composites. Industrial application of HAp requires its use in various forms, for example, porous or dense sintered body. Catalytic and chromatographic applications utilize powder HAp. Recently, film HAp has become important as a coating for metal or ceramic bodies, and tiny electronic devices such as sensors.

In order to overcome the inferiority of HAp in mechanical properties, the coating of HAp films has been attempted on bioinert materials of strength and/or toughness, such as polycrystalline alumina (Al_2O_3), zirconia (ZrO_2), titanium metal (Ti), and titanium carbide (TiC). Some methods are reported available to produce thin films of HAp. HAp coatings on Ti plates have been reported to be yielded by electrophoretic deposition.

One of the most important clinical applications of HAp is as a coating on metal implants, such as hip joint prostheses. This concept combines mechanical advantages of metal alloys with an excellent biocompatibility, and bioactivity of HAp. Uncoated metal implants do not

integrate with bone because bioinert materials are encapsulated by dense fibrous tissues which prevent proper distribution of stresses and thereby cause loosening of the implant. In the case of HAp-coated metal, bone tissue integrates itself completely with the implant, even during early functional loading.[50]

HAp coatings provide stable fixation of the implant to bone, and minimize adverse reaction by provision of a biocompatible phase. Moreover, the HAp coatings decrease the release of metal ions from the implant to the body, and shield the metal surface from environmental attack. In the case of porous metal implants, the HAp coating enhances bone in-growth into pores.[102] HAp coatings have been applied to metals like Ti alloys, or Ca-Cr-Mo alloy, to carbon implants, sintered ceramics like ZrO_2 and Al_2O_3, and even to polymers (Pmma).[50] There are various methods to fabricate HAp coatings. The common ones are HIP, spray-painting, oxy-fuel combustion spraying magnetron sputtering, flame spraying, ion-beam deposition, chemical deposition under hydrothermal conditions, electrochemical deposition metal-organic, CVD, and sol-gel. The coating under hydrothermal conditions has been carried out effectively by many workers and all these references are listed by Suchanek and Yoshimura (1998).[50]

Thickness of the HAp coatings is usually in the range of 40–200 μm. With increasing thickness of coating, concentration of metal ions released to the body decreases; the coatings must be thick enough to resist resorbability of HAp, which can be as much as 15–30 μm per year. Fixation to the bone can be improved if the HAp coating has an appropriate porosity, which promotes bone, inter-growth. It has been found that the interface between HAp and the metal, ceramics, or polymers often contain several undesired phases, like phosphides, amorphous phosphates, and so on, which decrease chemical stability and enhance degradation of the coatings.[103] Fujishiro et al. (1995) have carried out a detailed study of the coating of HAp on metal plates using thermal dissociation of calcium-EDTA chelate in phosphate solutions under hydrothermal conditions.[103] Figures 10.20 *(a)* and *(b)* illustrate schematically the mechanism of hydroxyapatite deposition on iron and titanium plates. The mechanism of deposition according to the authors is different in both the cases. Fujishiro et al. (1995) have studied the thermodynamics of the homogeneous precipitation of hydroxyapatite in Ca $(edta)^{2-}$ - NaH_2PO_4 solution.[72] Figure 10.21 shows SEM photographs of hydroxyapatite films formed on the surface of iron plates in various concentrations of Ca $(edta)^{2-}$ - NaH_2PO_4

solutions at pH = 5 and 150°C for four hours.[103] The direct coating of HAp and double coating of HAp on titanium plates have been investigated with varying pH of the NaH_2PO_4 solutions. Depending upon the pH and temperature of deposition, different morphologies of the hydroxyapatite and monetite particles were obtained.[67]

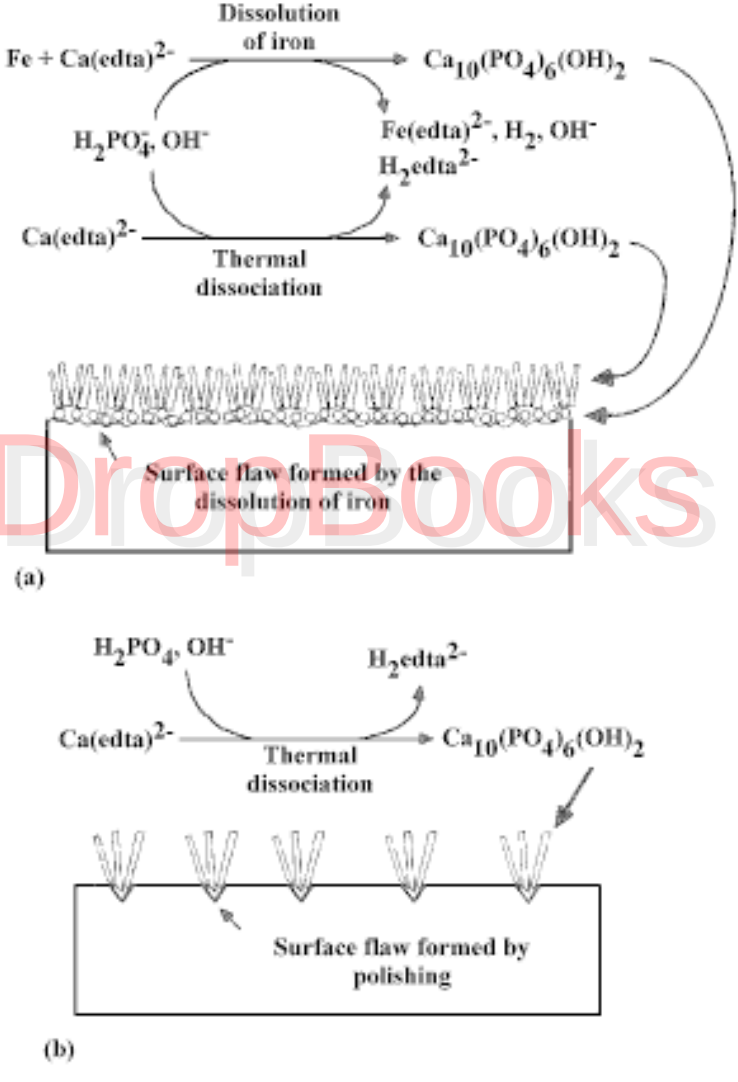

DropBooks

Figure 10.20. Mechanism of hydroxyapatite deposition on iron and titanium plates.[103]

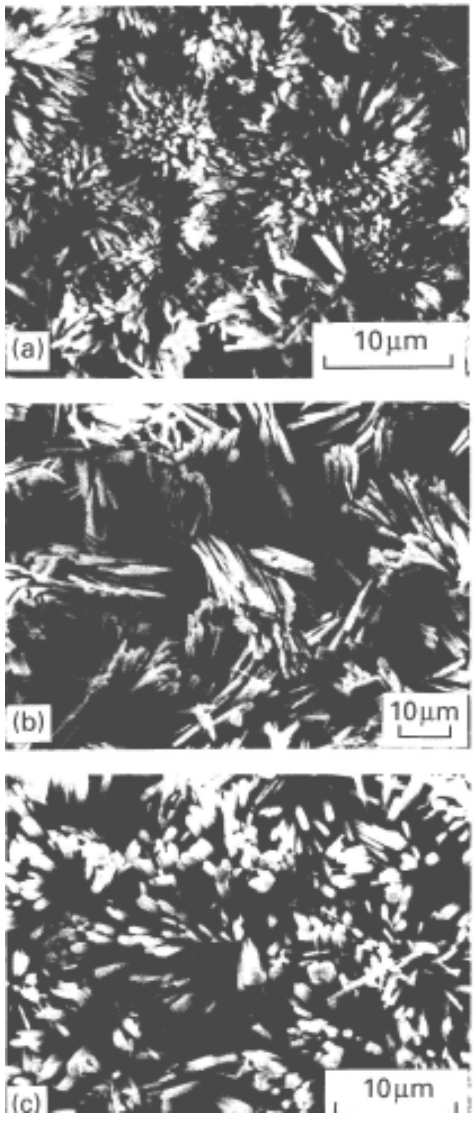

Figure 10.21. SEM photographs of the hydroxyapatite films formed on the surface of the iron plates.[72] *(Courtesy of the Academic Press, Orlando, Florida.)*

Figures 10.22 *(a, b,* and *c)* show SEM photographs of the surfaces of titanium plates coated with hydroxyapatite (experimental conditions 0.05 M $Ca(edta)^{2-}$ - 0.05 M NaH_2PO_4 solution at 160°C for 2 h) at *a)* pH 4, *b)* pH 5, and *c)* pH 6.

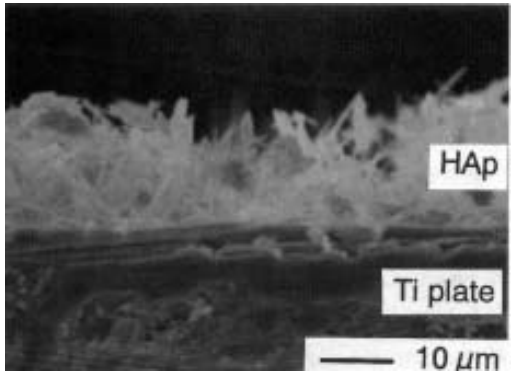

(a)

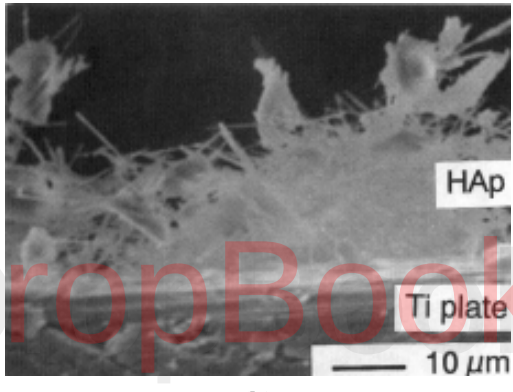

(b)

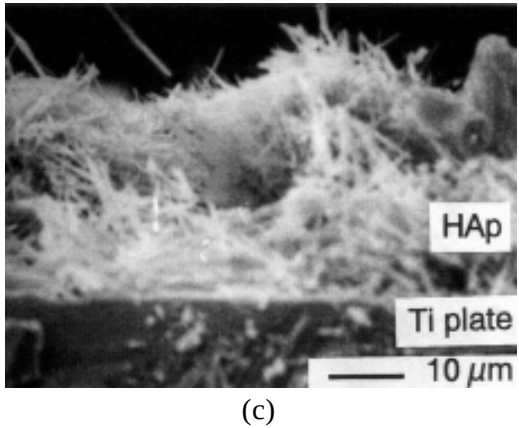

(c)

DropBooks

Figure 10.22. SEM photographs of the surfaces of titanium plates coated with hydroxyapatite at *(a)* pH 4, *(b)* pH 5, and *(c)* pH 6.[67]

Figure 10.23 represents scanning electron micrographs of the surfaces and cross sections of titanium plates after the second coating in 0.05 M Ca $(edta)^{2-}$ - 0.05 M NaH_2PO_4 solution at 160°C for four hours at *a)* pH 6, *b)* pH 9. The first coating was carried out with a solution of the same composition at initial pH 5 and 160°C for two hours.[103]

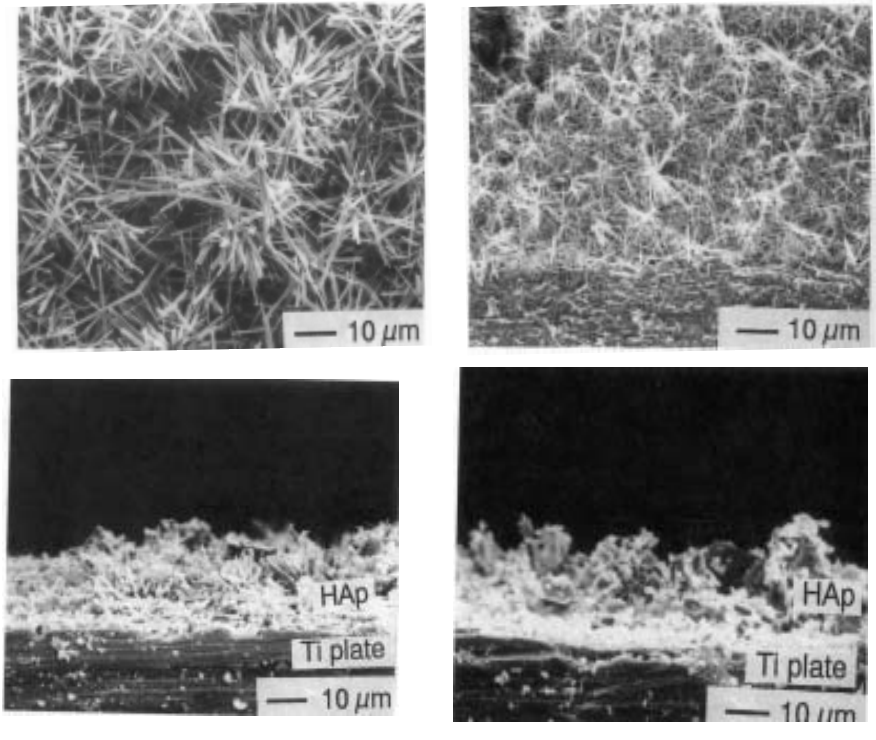

Figure 10.23. Scanning electron micrographs of the surfaces and cross sections of titanium plates.[103]

Thick films of HAp are also attempted for the use of gas sensors. There are several varieties of HAp-based composites like HAp/bioactive glass composites, HAp/polymer composites, HAp/HAp (whiskers), etc. Among the commonly used organics for HAp/polymer composites are phosphorylated cotton fibers, polymeric substrate, polymethyl-methacrylate, poly [bis (sodium carboxylatophenoxy) phosphaze].[103]

A comprehensive study undertaken at the Tokyo Institute of Technology, Japan, under the leadership of Prof. M. Yoshimura, has moved HAp whisker-reinforced HAp (HAw/HA) composites closer to real-world use. Researchers have long eyed HA implants as replacements for natural bone. The two materials share the same chemistry, but the mesostructure of bone gives it two to six times more fracture toughness than HA. This limits current HAp usage to small, unloaded implants and coatings.

HA whisker-reinforced composites might solve the problem. Their production requires hot pressing and/or hot isostatic pressing (HIP) at 1000°C to 1100°C. Even these processes fail to achieve fully dense samples.

Unfortunately, they also give rise to a whole new set of problems. Many sintering additives form tricalcium phosphate, which increases HA biodegradability and reduces implantation lifespan. Others form CaO, a reactive material whose volume changes once inside the body and causes the implant to crumble and fail. In addition, any sintering aid must promote weak binding between the HA whiskers and monolith in order to improve toughness by allowing fibers to pull free under stress.

PropBooks

Researchers selected a very broad range of potential sintering aids that shared the same constituents as hard tissues and bioactive glasses. These were narrowed down by analyzing their phase diagrams and physicochemical properties, then tested in 5 wt% additions to HAw/HA composites. They found that all sodium phosphates improved sinterability without forming tricalcium phosphate or CaO. Beta-$NaCaPO_4$ proved the only sodium phosphate to provide the weak fiber-matrix interface needed for composite toughness.[105]

There are several kinds of HAp/bioactive glass composites. The first one is also called bioactive glass ceramics. In these composites, HAp and/or wollastonite or other crystalline phases crystallize from the glassy matrix during an appropriate heat treatment.[107][111] The bioactive glass-ceramics exhibit strength of 100–200 MPa, $K_{I\,c}$ of 1.0–2.6 MPa, $m^{1/2}$, fracture energy of 6–26 J/m^2, and Weibull modulus of nine. Coefficient of subcritical crack growth (η) is reported to be in the range of 18–33. Bioactive glass ceramics maintain high strength for a longer time than HAp, both under *in vitro* and *in vivo* conditions.[50] HAp/bioactive glass composites can also be prepared by simple sintering of appropriate HAp/bioactive glass powder mixtures. In another approach, small

quantities of bioactive glass are added to HAp ceramics in order to improve densification and/or mechanical properties.

In spite of high bioactivity and high biocompatibility, superior (but still insufficient) mechanical properties of HAp ceramics, the HAp/bioactive glass composites did not find wide applications as bone substitutes.

In contrast with HAp/bioactive glass composites, the HAp/ polymer composites are very interesting. Bonfield and co-workers developed HAp/polyethylene composites. The mechanical properties of the polyethylene-HA composition are similar to those of bone. Implant tests of the poly-ethylene-0.4 volume fraction HA composites demonstrated development of bone bonding between the natural hard tissue and the synthetic implantation. These composites have the advantages of ease of shaping of the implant to meet the patient's needs, the time of surgery, formation of a bioactive bond to hold the implant in place, and mechanical properties that closely match those of the host tissues.[44][112]–[114] HAp/ polyethylene composites exhibit brittle/ductile transition at a HAp volume content of 40-45 %.[115] Their Young's modulus is in the range of 1–8 MPa, which is quite close to the Young's modulus of bone. Unfortunately, HAp/polyethylene composites are not biodegradable.

There are several publications in recent years on the fabrication of HAp/collagen composites, which are similar to bone from the point of view of chemical composition, but do not have such a complex microstructure. The composites can be prepared by mixing HAp with a collagen solution with subsequent hardening by different methods. Suchanek and Yoshimura (1998) have reviewed all the mechanical properties of various HAp/polymer composites.[50] The hydrothermal method of processing of these composites is very useful to achieve the optimum mechanical properties.

10.3 HYDROTHERMAL PROCESSING OF WHISKER CRYSTALS

A whisker is a long filamentary crystal, often containing a single-screw dislocation. A core of the dislocation usually follows the whisker axis. Whiskers are thus single crystals with a very low dislocation density, and are of special interest for studies of the influence of dislocation on

properties. Whiskers have unusually high tensile properties because of their low dislocation density.[116]

The growth of whisker crystallites is not new. In ancient times, the use of fire allowed the development of a ceramic industry. In the heat of pottery kilns (pottery is an older technology, dating from about 15000 BC), the clays transformed so that needle-like crystallites of aluminum silicate mullite could form as a dense crack-free mass in the shapes of vases, lamps, amphoras, and tiles.[117] However, scientific thinking on whiskers began during the 19th century in order to understand their morphology, dislocation density, and other related defects. Vapor growth is one of the favorite techniques for the formation of whiskers, followed by growth from solutions. Whisker crystals are commonly observed in metals and intermetallic alloys. However, interest on whiskers remained purely academic. It was only during the 1990s that interest on whisker growth was rejuvenated, owing to their applications. Therefore, a wide range of whisker crystals has been prepared, even among non-metallic, ceramic, and other inorganic compounds. For many years, inorganic fibers and whiskers have been used mostly as reinforcements in composites and in thermal insulation. Various fibrous materials such as glass, carbon, HAp, SiC, Si_3N_4, Al_2O_3, ZrO_2, etc., have been prepared for such purposes. Among natural fibers, asbestos has been widely used, due to its high tensile strength, chemical stability, and low cost. Unfortunately, its application has a great health risk as it causes many serious diseases, including lung cancer. The toxicity of widely used silicon carbide whiskers is stated to be only slightly lower. The carcinogenic effect of the fibrous materials was restricted to long and thin fibers (diameter < 1μm, length > 10 μm). Many commercially available whiskers and fibers may be safe from this point of view, however, their chemical compositions must also be taken into account. Alumina, zirconia, titania, silicon carbide, and silicon nitride are known as bioinert materials.[44] If the material is toxic, the surrounding tissue dies. If the material is nontoxic and biologically inactive (bioinert), a fibrous tissue of variable thickness forms. If the material is nontoxic and biologically active, an interfacial bond forms. In this respect, HAp is known as the most biocompatible material. It has been used in medicine for many years in the form of small unloaded, implants, powders, and coatings.

Fibrous HAp can be used as insulating agents, packing media for column chromatography, etc. It is a very promising material for preparation of composites. In recent years, because of their excellent

DropBooks

biocompatibility, HAp whiskers are the most studied whiskers. HAp contains non-toxic species, such as Ca, P, OH^-, usually CO^{2-}_3, and, even if some of the crystals have a dangerous shape, they should dissolve in a human body without causing any health problems. It has been reported that different kinds of proteins are absorbed on different planes of HAp crystals. Therefore, if HAp crystals, whose particular planes grow selectively, are obtained, they can separate various kinds of proteins. Nagata et al. (1994) has obtained plate-like HAp crystals synthesized hydrothermally with methanol.[118]

In recent years, several reports concerning the fabrication of HAp fibers and whiskers appeared in literature.[42][51][54][119]–[122] All preparation techniques for HAp whiskers can be divided into two main groups: *i)* the homogenous precipitation method, using urea, and *ii)* the decomposition of chelating agents. The first method utilizes a continuous increase of pH in a solution containing calcium and phosphate ions at a high temperature. In the second case, chelating agents like EDTA, lactic acid, or citric acid, are used. During the heat treatment, which is usually carried out under hydrothermal conditions, Ca-complexes with chelating agents decompose, followed by the precipitation of HAp whiskers.

In the preparation of HAp whiskers by the first method, the resultant product is always contaminated with large quantities of carbonate ions and they have not been verified, as yet, to be single crystals (i.e. whiskers).[42] Yoshimura and co-workers prepared under hydrothermal conditions HAp materials, such as fine needle-like crystals and whiskers. They prepared HAp whiskers of diameters 0.1–5 μm and length 30–100 μm, using decomposition of chelating agents. Christiansen and Riman also adopted a similar procedure to prepare HAp whiskers.[42][120]–[123] The most significant feature of these whiskers is the absence of CO^{2-}_3 species in larger quantities, but their Ca/P molar ratio was in the range of 1.59–1.63, deviating from the stoichiometric value of 1.67.

Suchanek et al. (1995) have obtained several batches of HAp crystals under hydrothermal conditions. Starting chemicals like H_3PO_4, $Ca(OH)_2$, and lactic acid were taken in a teflon beaker, inserted into an autoclave and hydrothermally treated at 200°C for five hours under a pressure of 2 MPa.[120] The molar ratios of lactic acid/Ca and Ca/P were 2.0, 4.0, 6.0, and 1.43, 1.80, 3.00, respectively. Figure 10.24 shows all the steps involved in the experimental procedure concerning the preparation of HAp whiskers.[120] Yoshimura has proposed the mechanism of formation of HAp whiskers under hydrothermal conditions (Fig. 10.25).

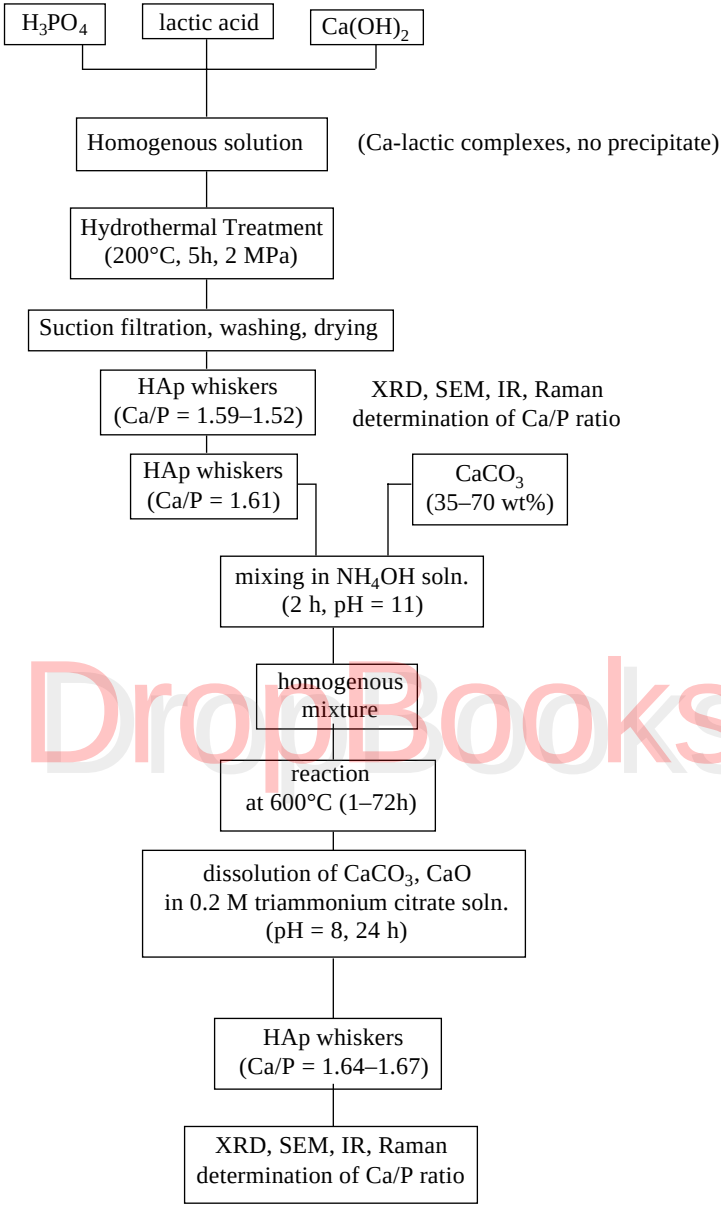

DropBooks

Figure 10.24. Steps involved in the experimental procedure for the preparation of HAp.[120]

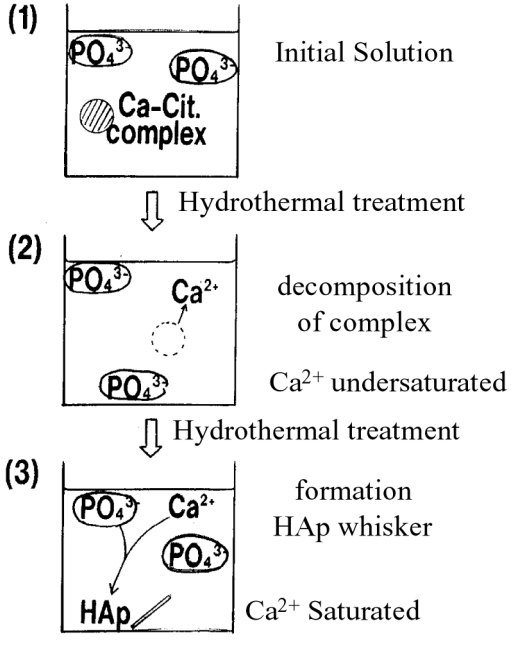

Figure 10.25. HAp whiskers under hydrothermal conditions *(by M. Yoshimura).*[120]

The morphology of HAp crystals was controlled by both the lactic acid/Ca and Ca/P molar ratios in the starting solution. The SEM studies revealed that the crystals were not aggregated and had a shape of hexagonal rods or whiskers, elongated along the c-axis (Figs. 10.26 *a-d*).[120] As shown in Figs. 10.26 (*a* and *b*) the diameter increases with increasing Ca/P molar ratio in the starting solution and is generally larger for high lactic acid/Ca molar ratios. The aspect ratio of HAp crystals is in the range of 5–20. It decreases with increasing Ca/P ratio and is lower in the case of high lactic acid/Ca ratios Figs.10.26 (*c* and *d*). When the lactic acid/Ca and Ca/P starting ratios are low, crystals have shapes of whiskers. While in other cases large elongated grains form.

Distributions of the length and aspect ratio of selected whiskers are shown in Fig. 10.27 *(a* and *b).* In this case, the aspect ratio for the majority of the crystals is in the range of 10–25. Length of the whiskers shows a big scattering, suggesting that some of them might be broken during and/or after the hydrothermal treatments.

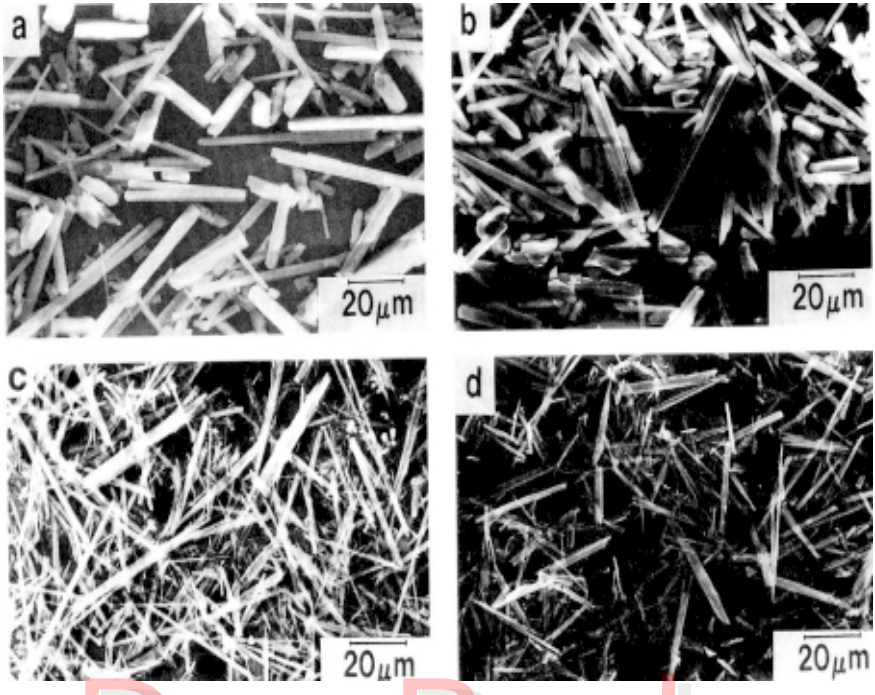

DropBooks

Figure 10.26. SEM photographs of selected HAp crystals. *(Photos courtesy of W. Suchanek.)*

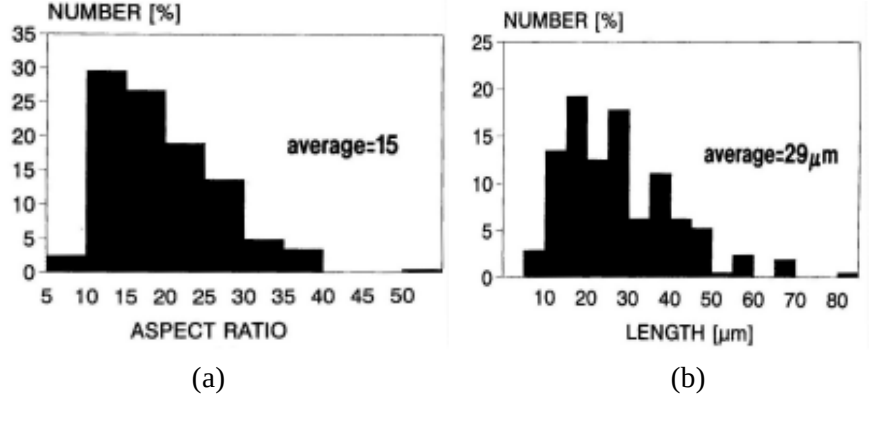

Figure 10.27. Distributions of *(a)* the length and *(b)* the aspect ratio of selected whiskers. *(Courtesy of W. Suchanek.)*

The Ca/P molar ratios of HAp crystals are in the range of 1.59–1.62. Deviation from the stoichiometric value of 1.67 decreases slightly with increasing lactic acid/Ca ratio. It is difficult to explain why whiskers are non-stoichiometric. Several theories have been proposed to explain the phenomenon of non-stoichiometry in HAp. They include adsorbed phosphate species on the surface, presence of additional phases as amorphous calcium phosphate or octacalcium phosphate, and various combinations of lattice defects. This is in agreement with the model involving Ca and OH vacancies and substitution of some phosphate groups by HPO_4^{2-}.

To check the presence of various species of phosphates, carbonates, hydroxides, etc., the IR-spectra are very useful. Absence of any distinct bands in the range of 1400–1500 cm^{-1} indicates that the HAp whiskers do not contain large quantities of carbonate ions.[121] Figure 10.28 shows the IR-spectra of the whiskers with improved stoichiometry (Ca/P molar rations 1.64 and 1.67).

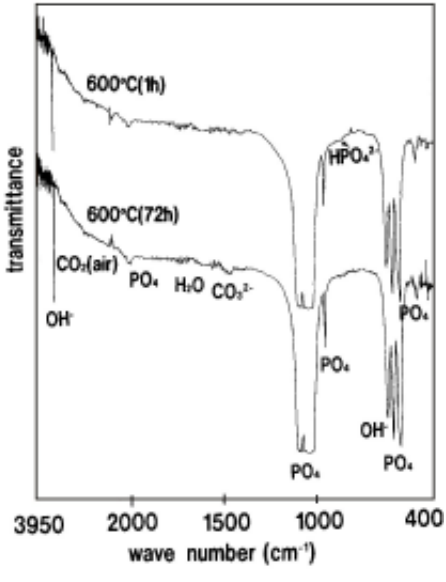

Figure 10.28. IR-spectra of the whiskers which improved stoichometry (Ca/P molar ratios 1.64 and 1.67).[120]

HAp whiskers have the following lattice parameters: a = 9.4317 Å I 0.0007 Å and c = 6.8822 + 0.0012 Å. These values correspond to HAp prepared in aqueous systems. Thus, after a critical evaluation of the

experimental conditions, Yoshimura and co-workers have proposed that in the system $Ca(OH)_2$ - H_3PO_4 - Citric acid, HAp whisker (30 μm length, 0.1–1 μm width) could be synthesized preferentially under the conditions of:

i. lower concentration of Ca^{2+} (0.2 M)

ii. lower Ca/P molar ratio (1.67 for $[Ca^{2+}] = 0.2$ M)

iii. restricted citric acid/Ca molar ratio (1.2–1.31)

iv. higher temperature (180°C) and longer duration (2.75 hr. at 200°C, 220°C)

v. final pH of 3.4–3.8

Suchanek and Yoshimura (1998) have studied the thermal stability and densification of HAp whiskers in great detail.[121]

The HAp whiskers have already been used as a biocompatible reinforcement in the HAp/HAp (whisker) composites Fig. 10.29 *(a).* Consequently, the fracture toughness of pure HAp ceramics has been improved even to the value of 2.0 MPa m, this is the highest value in 25 years. In addition, a variety of microstructurally controlled HAp based composites with improved reliability and high biocompatibility can be prepared using β-rhenenite (β-$NaCaPO_4$), a newly discovered weak interphase material for HAp ceramics (Fig. 10.30). The fibrous HAp can also be used to fabricate porous HAp ceramics or porous HAp/ β- TCP composites as shown in Fig. 10.29 *(b)*. Moreover, the HAp fibrous skeleton should be an appropriate reinforcement for HAp/polymer biodegradable bone substitutes. Thus, HAp whiskers are very important in Materials Science and Technology.

DropBooks

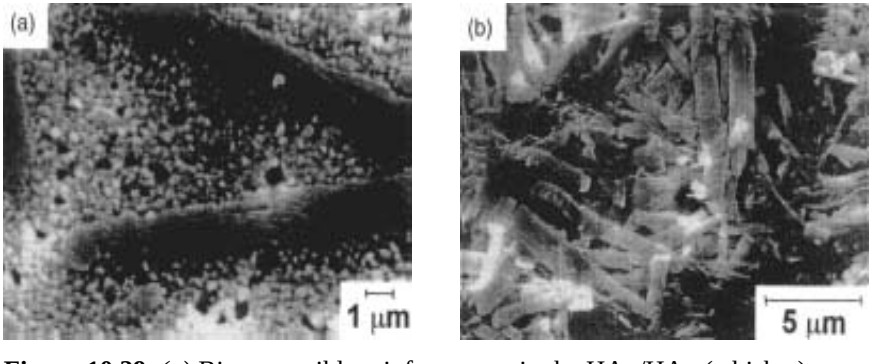

Figure 10.29. *(a)* Biocompatible reinforcement in the HAp/HAp (whisker) composites, and *(b)* HAp whiskers with Ca/p - 1.66. *(Photos courtesy of W. Suchanek.)*

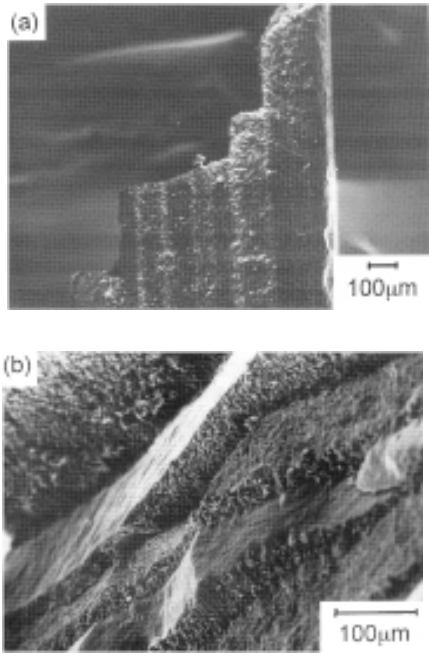

Figure 10.30. SEM images of the fracture surface of the HAp/bioactive glass composite. Notice the crack deflection on the b-$NaCaPO_4$ interphase layers. *(Photos courtesy of W. Suchanek.)*

10.4 RELATED METHODS OF HYDROTHERMAL PROCESSING OF MATERIALS

Modern methods of the hydrothermal processing of materials cover several other processing techniques related to the hydrothermal method. Although, these new methods are not used widely in the routine hydrothermal processing, they have special applications in the processing of some selected technological materials, like hydrothermal transformation alteration, recycling, densification, solidification, strengthening, sintering, and so on. The most commonly used processing techniques are HHP, HIP, hydrothermal sintering, microwave hydrothermal, hydrothermal leaching, hydrothermal decomposition of toxic organic materials, etc. These processes have helped in the processing/treatment of materials, increasing their mechanical properties, enhancing the yield, reaction kinetics, and so on.

10.4.1 Hydrothermal Hot Pressing (HHP) and Hot Isostatic Pressing (HIP)

Hydrothermal hot pressing (HHP) is one of the good processing routes for preparing a ceramic body at relatively low temperatures (below 300°C). Yamasaki and co-workers have used this technique popularly, to process a wide range of materials. The compression of samples under hydrothermal conditions accelerates densification of inorganic materials. This technique is applied to solidify many kinds of materials such as glass, silicate, titania, calcium aluminate-phosphate cement, calcium carbonate, hydroxyapatite sewage sludge, and so on,[123]–[132] and the method is expected to provide energy-effective processing to fabricate new engineering materials. Calcium alumina reacts with phosphate to form strong bonding. Using HHP techniques, the strength of solidified bodies with mixtures of alumina cement or calcium aluminates, sodium phosphates, and silica fume, could be enhanced. Yanagisawa et al. (1993) have solidified three kinds of silica powders, crystalline silica, glass, and gel, using the HHP method.[133] With the addition of an alkaline solution, mixtures of low-quartz and other oxides were densified by this method. Reaction products of the mixtures under alkaline hydrothermal conditions are bonded to quartz grains. The addition of pure water densified silica glass powders containing network-modifying oxides. In this case, a hydrated reaction layer was produced by the reaction of the glass particles. The silica gel (5 g) was placed in the autoclave and compressed at 20 MPa. The autoclave was heated to 300°C at the rate of 2°C/min, while the pressure was kept constant at 20 MPa during HHP. The temperature was kept constant at 300°C for 1 hour and then the autoclave was cooled down to room temperature. The solidified compact was removed from the autoclave and dried at 110°C.

Yanagisawa et al. (1997) have studied the formation of anatase porous ceramics by HHP of amorphous titania spheres prepared by hydrolysis of titanium tetraethoxide.[134] After fine anatase crystals were formed in the original amorphous spheres by HHP, the spherical particles were deformed and fine anatase crystals were flowed into the interstices among the original spheres by compression from outside the autoclave, to form a compact with homogeneous distribution of fine pores. The fine anatase crystals in the compacts were bonded together by dissolution and deposition to form a compact with high mechanical strength. The presence

DropBooks

of water accelerated the crystallization of the starting amorphous titania to anatase, and anatase compacts were produced, even at 100°C.[134]

Yamasaki and his group of researchers have worked out a method to solidify sewage sludge incinerated ash by HHP and investigated superior conditions to solidify ash for producing recycled products. The solidified sample had a high compressive strength of 98 MPa by HHP at T = 300°C, P = 49 MPa, NaOH dosage approximately 6%. The product could be used as building materials, such as tiles and bricks.[135] These authors have also worked out a method of immobilizing and a high-volume reducing technique for low-level radioactive waste from nuclear power plants or reprocessing plants, through the hydrothermal solidification method.[136] It is confirmed through evaluation tests and a full-scale mock-up test that this technique can be adapted to an actual system for spent solvent treatment in commercial reprocessing plants.

HIP allows rapid densification with mineral grain growth and is one of the most effective ceramic densification processes. This method is being popularly employed to process HAp based bioceramics.[137]–[139] Implant materials require not only biocompatibility, but also mechanical strength and porosity to promote the connection with tissues. Therefore, microstructure designing, i.e., grain size, pore size, and porosity, are necessarily tailored in their application to bioceramics. Hydroxyapatite single crystals of about 255 nm × 90 nm in size synthesized hydrothermally at 200°C under 2 MPa for 10 hours, were normally sintered in air for 3 hours. The ceramics obtained were hot-isostatically pressed at temperatures of 900–1100°C under 200 MPa of Ar for 1 hour, without any capsules. This post-sintering brought about densification up to ~100% for the samples. The fully dense ceramics, with a grain size of about 0.54 μm, showed transparency. Furthermore, dense/porous layered hydroxyapatite ceramics could be prepared by the same technique, from the fine crystals and coarse powders with relatively low sinterability. Uematsu et al. (1989) have synthesized hydroxyapatite powder and have formed it into a compact in an aqueous medium using a filter-cake method.[130] The compact was hot isostatically pressed at 700°C to 1000°C and 100 MPa for 2 hours. Fully dense, transparent materials were obtained above 800°C. Both forming and densification methods were found to be important in obtaining transparent materials. Figure 10.31 shows a transparent HAp block obtained through HHP.[137]

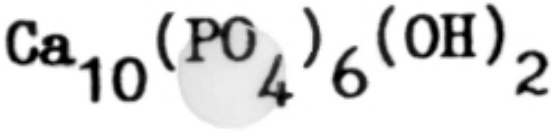

Figure 10.31. Transparent HAp block obtained through HHP. *(Photo by M. Yoshimura.)*

10.4.2 Hydrothermal Reaction Sintering of Processing Materials

Hydrothermal reaction sintering is one of the methods used to produce high-density oxide ceramics. A large variety of oxide ceramics have been processed by this method. Oxide powders were obtained by reactions between solutions or non-aqueous liquid and metals. Hydrothermal reaction sintering is a kind of reaction with hot isostatic processing. The hydrothermal reaction sintering of oxides is as follows:

DropBooks

a) low-temperature sintering – able to make sintered body even if materials have high vapor pressure, decomposition; and/or transit

b) able to make a very fine grain size body

c) able to make high-purity body

d) able to make high-density body

e) able to make uniform microstructures

f) able to save energy due to low-temperature sintering

g) able to control valency

Factors, such as purity, grain size, shape, etc., of starting materials, reaction temperature, pressure, duration time, ratio of metal and water, kinds of salt in solution, and so on, have made hydrothermal reaction sintering unclear. Several ceramic powders have been processed using this technique. The important ceramic materials obtained by this method are magnetite, wüstite, monoclinic ZrO_2, chromia, monoclinic HfO_2, alumina, and so on.[140]–[145]

Figure 10.32 shows the relation between pressure and grain size or relative density hydrothermal reaction sintering of magnetite.[141] Figure 10.33 illustrates the SEM fracture surface of high-density hydrothermal reaction sintered Cr_2O_3 (100 MPa, 1000°C for 3 hours, 0.01 M HNO_3 solution) with a relative density of 99.1%.[142] Table 10.5 gives selected results of hydrothermal reaction sintering of monoclinic ZrO_2 for 3 hr.[141] Yin et al. (1996) have studied the low temperature sintering and mechanical properties of ceria and yttria co-doped zirconia crystallized in supercritical methanol.[146]

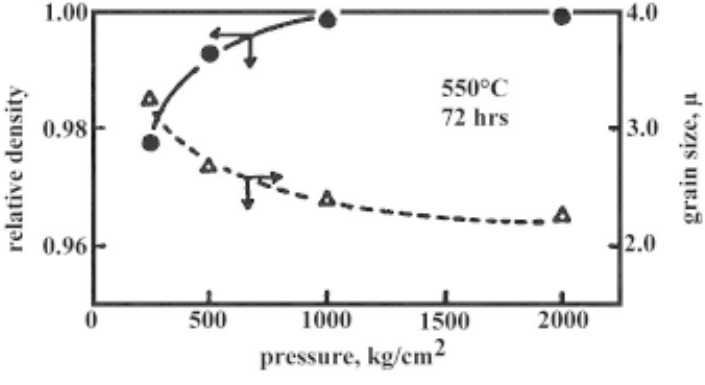

Figure 10.32. Relation between pressure and grain size or relative density hydrothermal reaction sintering of magnetite.[141]

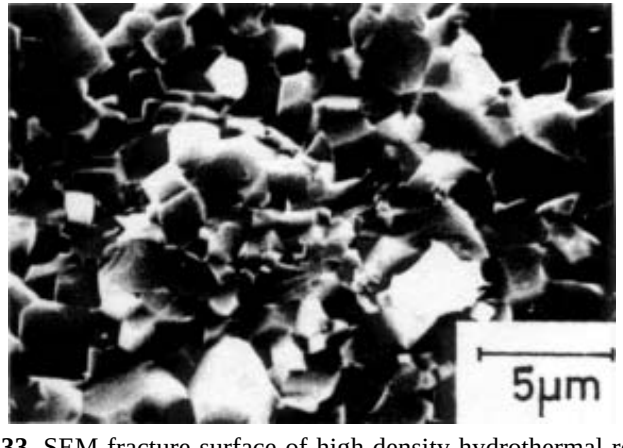

Figure 10.33. SEM fracture surface of high density hydrothermal reaction sintered Cr_2O_3.[142]

Table 10.5. Selected Results of Hydrothermal Reaction Sintering of Monoclinic ZrO_2 for 3 h[141]

Sample No.	H_2O/Zr	Deg. of fill (%)	Temp. (°C)	Pressure (MPa)	Bulk density (g/cm^3)	Relative density (%)	Avg. grain size (μm)
3	1.773	19.3	1000	98	5.85	99.0*	3
5	2.020	15.5	1000	98	5.51	93.2	1
29	2.063	14.8	1000	98	5.17	87.5	0.5
30	2.095	15.0	1000	98	5.38	89.2	0.5
10	2.415	18.4	1000	98	Not sintered		
25	2.038	15.1	1000	196	5.51	93.2	0.3
28	1.985	15.1	1000	294	5.96	100.9	0.1
8	2.012	22.7	1000	490	5.83	98.7	3
7	2.010	20.4	1000	686	5.77	97.7	3
23	2.038	41.2	1000	686	5.70	96.4	
32	2.016	14.8	1000	98	5.68	96.1	2
40	2.142	14.3	1100	98	Not sintered		
41	2.089	14.2	1200	98	Not sintered		
39	2.091	14.1	1000	490	Not sintered		0.5

DropBooks

* With gray skin. Gray fine body, rare case. Capsule leaked slightly.

The preparation and processing of perovskite type titanates is becoming an attractive field owing to their unique electronic properties. However, their electrical properties are closely linked to their microstructural features, such as porosity and grain size.[147] These authors have prepared $BaTiO_3$ powders by the hydrothermal synthesis technique and have fired via a fast sintering process, or so-called zone sintering. During fast sintering, a powder compact undergoes a rapid high-temperature thermal treatment by being brought to a hot zone within a very short time. In this way, the densification process (e.g. lattice diffusion) can be enhanced while limiting the grain growth process (e.g. surface diffusion). With proper control of time and temperature, it can result in a high-density ceramic with a fine grain size. Figure 10.34 shows the typical SEM micrographs of $BaTiO_3$ samples fast-sintered for 5 min at: *a)* 1250°C, *b)* 1300°C, of the fast-sintered samples for 15 min at different temperatures. Table 10.6 and Fig. 10.35 gives density, grain size, and dielectric properties of the sintered $BaTiO_3$ samples.

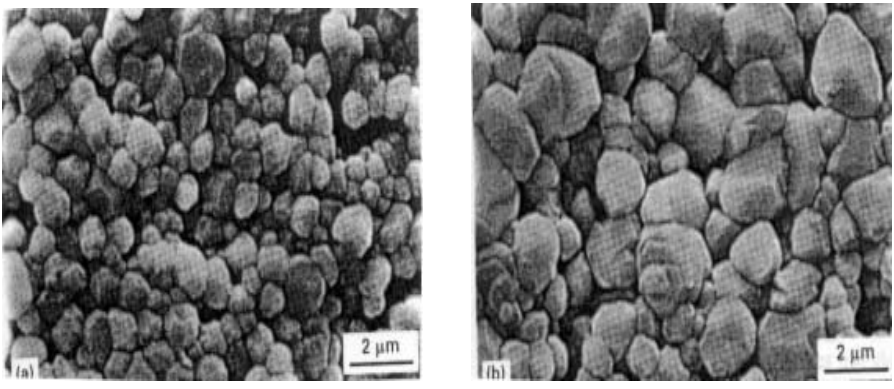

Figure 10.34. SEM fracture surface of high density hydrothermal reaction sintered Cr_2O_3.[147]

Table 10.6. Density, Grain Size, and Dielectric Properties of the Sintered $BaTiO_3$ Samples[147]

Type of sintering	Sintering T°C	k' (30°C)	tan δ (30°C)	Grain Sizes[a] (μm)	Density[b] (g cm^{-1})	T_o (°C)	C ($\times 10^5$ K)
Conventional	1250	2814	0.038	~ 4	5.61 (93)	108	1.8
	1300	2663	0.039	~20	5.63 (93)	109	1.9
	1350	2558	0.037	~28	5.59 (94)	112	2.0
Fast-5 min	1250	3676	0.020	~ 1	5.53 (92)	84	2.1
	1300	3274	0.020	~ 2	5.65 (94)	97	1.7
	1350	2892	0.009	~ 4	5.71 (95)	110	1.8
Fast-15 min	1250	2947	0.009	~ 6	5.76 (96)	111	1.9
	1300	2721	0.006	~12	5.89 (98)	111	2.0

[a] Average grain size determined by taking the mean diagonal values of about 30 grains.

[b] Values in parentheses are the percentage relative densities compared to the theoretical density.

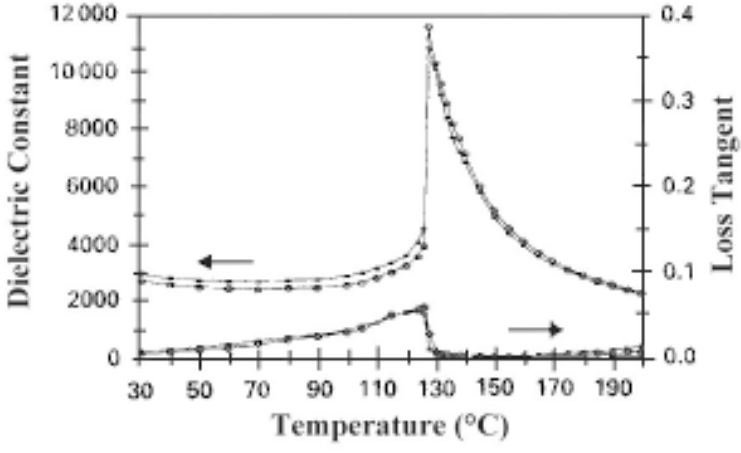

Figure 10.35. Dielectric properties (k' and tan δ) of $BaTiO_3$.[147]

Similarly, sintering effects on hydroxyapatite bioceramics have been studied in detail by several workers.[148][149] Thus, hydrothermal sintering reactions find interesting applications in ceramic processing.

DropBooks

10.4.3 Microwave Hydrothermal Processing

The use of microwaves in solid state materials processing is at least fourteen years old and is presently being employed very widely to process a large variety of inorganic materials.[150]–[152] For the past few years, a number of groups have demonstrated that the kinetics of organic and inorganic chemical synthesis may be significantly accelerated using 2.45 GHz microwaves. The acceleration of chemical reactions by microwave dielectric heating has been demonstrated for organic synthesis,[153][154] organometallic synthesis,[155][156] and preparation of intercalation compounds[157] where organic molecules have been intercalated into inorganic phases. Hydrated inorganic zeolites and other molecular sieves have been synthesized rapidly, using microwaves.[158][159]

Rustom Roy and co-workers, however, were the first to show the rapid synthesis of anhydrous ceramic oxides,[160]–[162] hydroxylated phases,[163][164] metal powders,[163][165] and metal intercalated clays.[166][167] Also, the rapid synthesis of some inorganic phases, such as ZrO_2 and Fe_2O_3, have been reported.[168]–[170] In addition to all the above quoted inorganic phases, microwave-hydrothermal processing is useful in synthesizing

novel phases.[163][171] Komarneni et al. (1996) prepared $BiFeO_3$ and $CsAl_2PO_6$ using microwave-hydrothermal conditions and found an enhancement of kinetics.[172] $BiFeO_3$ has perovskite structure and can be prepared at 194°C under microwave-hydrothermal conditions only. The other phase $CsAl_2PO_6$ is useful in nuclear waste disposal and is accomplished at 138°C under microwave-hydrothermal conditions. Figure 10.36 shows SEM photographs of $BiFeO_3$ powders: *a)* highly crystallized agglomerated $BiFeO_3$ powder prepared by microwave-hydrothermal process at ~ 194°C with a duration of 2 to 3 hours. Figure 10.37 shows SEM photographs of $CsAl_2PO_6$.[172] These results clearly indicate that the use of microwave field catalyzes crystallization of inorganic phases under hydrothermal conditions.

Recently, D'Arrigo et al. have synthesized nanophase ferrites such as $ZnFe_2O_4$, $NiFeO_4$, $MnFe_2O_4$, and $CoFe_2O_4$, under microwave-hydrother-

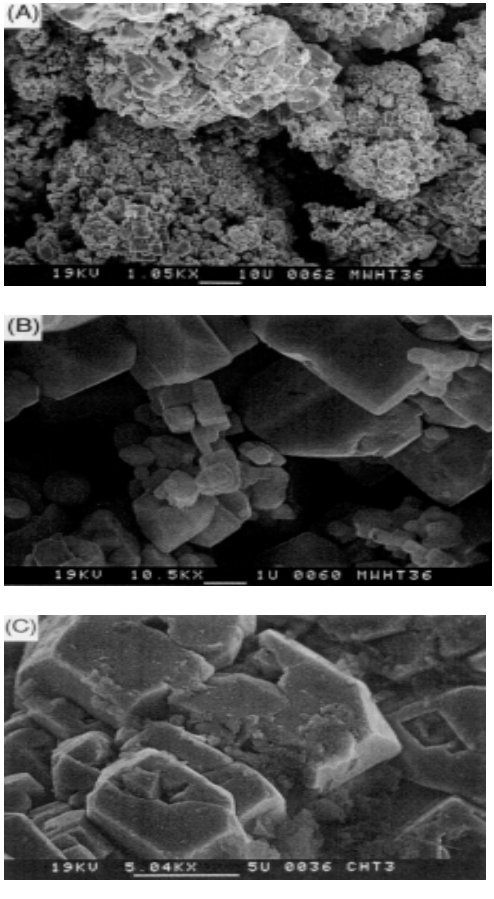

Figure 10.36. SEM photographs of $BiFeO_3$ powders.[172] *(Courtesy of S. Komameni.)*

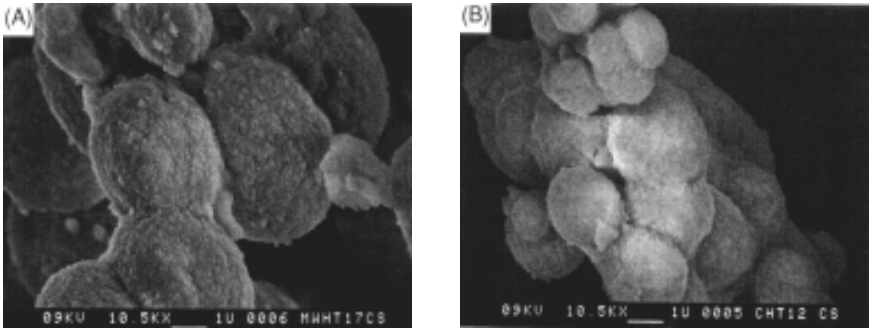

Figure 10.37. SEM photographs of $CsAl_2PO_6$.[172] *(Courtesy of S. Komameni.)*

mal conditions.[173] Nanophase ferrites with high surface areas, in the range of 72–247 m^2/g have been synthesized in a matter of a few minutes at temperatures as low as 164°C. The rapid synthesis of nanophase ferrites via an acceleration of reaction rates under microwave-hydrothermal conditions is expected to lead to savings in energy and the cost of production of these materials.

DropBooks

A majority of the experiments on microwave-hydrothermal processing are done using a commercially available microwave digestion system, MDS-2000, which is designed by the CEM corporation, U.S.A. This system produces a microwave frequency of 2.45 GHz and the maximum pressure is ~ 200 psi.

Komarneni et al. (1993) have carried out the synthesis of $BaTiO_3$, $SrTiO_3$, $Ba_{0.5}Sr_{0.5}TiO_3$, $BaZrO_3$, $SrZrO_3$, $PbZrO_3$, and $Pb(Zr_{0.5}2Ti_{0.48})O_3$, using both conventional and microwave-hydrothermal techniques.[171] Conventional-hydrothermal processing, using $TiO_2 \cdot xH_2O$ gel and $Sr(OH)_2$, usually yields platy, needles, or irregular or sub-rounded agglomerated particles. Whereas, microwave-hydrothermal processing yielda agglomerate-free, narrow particle size (0.1–0.2 μm) distribution with spherical morphology, which is expected to have better sintering properties. Tables 10.7 and 10.8 give XRD analysis of $BaTiO_3$, $SrTiO_3$, $Ba_{0.5}Sr_{0.5}TiO_3$, $BaZrO_3$, $SrZrO_3$, and $PbTiO_3$ powders produced by microwave-hydrothermal and conventional-hydrothermal techniques. Komarneni et al. (1992) had

carried out earlier, similar studies on ceramic powders synthesis (titania, zirconia, iron oxide, chromia, etc.), using both conventional and microwave-hydrothermal conditions, and had obtained similar results. Thus, the crystal size, morphology, and level of agglomeration of the different ceramic oxides can be controlled by parameters such as concentration of the chemical species, pH, time, and temperature. Submicron powders of TiO_2, ZrO_2, Fe_2O_3; KNO_3 and $BaTiO_3$ have been obtained by this means.[160]

Cheng et al. (1997) have studied in detail the microwave processing of tungsten carbide-cobalt composites and ferroic titanates.[174] This helps the sintering of tool bits and related parts with better properties in about 1/10th

Table 10.7. XRD Analysis of $BaTiO_3$, $SrTiO_3$, and $Ba_{0.5}Sr_{0.5}TiO_3$ Produced by the Microwave Hydrothermal Technique[171]

Concentration (M)				*T* °C	Duration (h)	Reaction products in order of abundance as determined by XRD
$Ba(NO_3)_2$	$Sr(NO_3)_2$	$TiCl_4$	KOH			
$BaTiO_3$						
0.35	0	0.33	10	109	2	$BaTiO_3$
0.35	0	0.33	10	194	0.5	$BaTiO_3$, trace $BaCO_3$
0.35	0	0.33	10	194	2	$BaTiO_3$
$SrTiO_3$						
0	0.1334	0.13	10	164	2	$SrTiO_3$
0	0.1334	0.13	10	194	2	$SrTiO_3$
$Ba_{0.5}Sr_{0.5}TiO_3$						
0	0.1334	0.26	10	194	2	$Ba_{0.5}Sr_{0.5}TiO_3$

Table 10.8. XRD Analysis of Titanates Produced by Microwave-Hydrothermal and Conventional-Hydrothermal Techniques[171]

Compound	Concentration (M)			*T* °C	Duration (h)	Reaction products in order of abundance as determined by XRD
$PbTiO_3$	$Pb(NO_3)_2$	$TiCl_4$	KOH			
	Microwave-hydrothermal					
	0.4079	0.4	6	138	0.5	PbO, $PbTiO_3$
	0.4079	0.4	6	138	1.0	PbO, $PbTiO_3$
	0.4079	0.4	6	164	0.5	PbO, $PbTiO_3$
	0.4079	0.4	6	164	1.0	PbO, $PbTiO_3$
	0.3	0.25	2	194	0.5	$PbTiO_3$, PbO
	0.3	0.25	3	194	0.5	$PbTiO_3$, trace PbO
	0.3	0.25	4	194	0.5	$PbTiO_3$, trace PbO
	Conventional-hydrothermal					
	0.4079	0.4	4	195	24	$PbTiO_3$
$BaZrO_3$	$Ba(NO_3)_2$	$Zr(NO_3)_2$	KOH			
	Microwave-hydrothermal					
	0.3113	0.3144	10	194	2	$BaZrO_3$
	0.3113	0.3144	10	130	2	$BaZrO_3$
	Conventional-hydrothermal					
	0.3113	0.3144	10	194	2	$BaZrO_3$
$SrZrO_3$	$SrZrO_3$	$Zr(NO_3)_2$	KOH			
	Microwave-hydrothermal					
	0.3113	0.3113	10	138	0.5	$SrZrO_3$
	0.3113	0.3113	10	138	1	$SrZrO_3$
	0.3113	0.3113	10	164	0.5	$SrZrO_3$
	0.3113	0.3113	10	164	1	$SrZrO_3$
	0.3113	0.3113	10	194	2	$SrZrO_3$
	Conventional-hydrothermal					
	0.3113	0.3113	10	138	24	$SrZrO_3$
	0.3113	0.3113	10	138	24	$SrZrO_3$

DropBooks

the cycle time required by conventional means, and most significantly, it can help in retaining very fine microstructures when starting with very fine powders.

Komarneni et al. (1995) have studied the microwave-hydrothermal processing of metal clusters supported in and/or on montmorillonite.[175] The authors could obtain novel Ag^+, Pt^+- and Pd^+- metal intercalated clays, which may be useful in catalysis. These are prepared by using the combination of microwave-hydrothermal and polyol reduction processes. Fang et al. (1992, 1994) have carried out extensive studies on HAp ceramics using microwave-hydrothermal conditions.[176][177] This not only enhances the reaction kinetics, but also gives better densification and mechanical properties.[178]

The application of microwave-hydrothermal techniques to process modern materials is becoming highly popular and is a rapidly expanding area of research and development. A reader can get more useful information in the reviews of Komarneni (1995) and Ehsani et al. (1994).[175][178]

10.4.4 Hydrothermal Treatment/Recycling/Alteration

This is probably one of the most important areas of research in the field of hydrothermal technology, wherein, the supercritical water (SCW) properties are exploited for effective detoxification and disposal of problematic industrial, nuclear, military, and municipal wastes. In SCW at 450° to 700°C, many organic compounds are rapidly (0.1 to 100s) and efficiently (99.9 to 99.99 + %) oxidized (supercritical water oxidation or SCWO), with their carbon, hydrogen, and nitrogen, almost completely converted to CO_2, H_2O, (mineralization) and N_2. These attributes make SCW an attractive medium for chemical reactions and physical separations, i.e., for hydrothermal processing. Environmental applications include the rapid and efficient destruction of hazardous organic substances, e.g., aqueous wastes, and decontamination and/or separation of inorganic pollutants.[179]–[180] Thus, supercritical water oxidation is an emerging technology for the treatment of aqueous waste streams, so that they can be recycled as process streams and for the ultimate destruction of organic wastes. Recycling of waste plastics, such as polyethylene, polystyrene, polypropylene and polyethyleneterephthalate, radioactive waste, concrete wastes, and so on, have received special attention.[183]–[186] Similarly, the decomposition of chlorocarbons, chlorofluorocarbons, polymers, poly-

mer additives, nitroaromatics, and so on, under higher-pressure temperature conditions, have been well understood.[187]–[189] The conventional method of treating most of these waste materials is oxidation pyrolysis in incinerators, but this method is not effective as to the dechlorination of chlorofluorocarbons, for example, they need high-temperature plasma destruction, requiring large and expensive apparatus, and the reactors are easily corroded by HCl or Cl_2 gas (the decomposed productions). Similarly, reductive decomposition is not a cost-effective method, requiring expensive reductive agents.

Savage and co-researchers have worked out the reaction models for supercritical water oxidation processes in detail, based on molecular dynamics studies of supercritical water, in order to understand better the potential roles of water in influencing elementary chemical reaction rates.[190] The study of hydrogen bonding in supercritical water and its dependence on temperature and density has been carried out by many workers to understand fundamental issues connected with structure dynamics and thermodynamics of pure water.[190]–[193]

Hydrothermal decomposition of organics, or recycling of waste materials is usually carried out in small autoclaves, or Tuttle cold-cone seal autoclaves or batch reactors/flow-reactors, depending on experimental conditions and purpose.

DropBooks

Adschiri et al. (1994) have studied the conversion of lignin, polystyrene, and polyethylene, under supercritical conditions of water and found that polystyrene could be completely decomposed into ethylbenzene, toluene, benzene, styrene, and xylene in 5 min. However, the conversion yield of polyethylene was fairly low, even at a longer reaction time of 2 hours at 35 MPa, 400°C; but, by the addition of oxygen (about 0.013 mol), conversion increased to 60% at the same temperature. The advantages of such conversion are that lesser char and more aldehyde, ketone, and acid production in SCW are observed, as compared to neat pyrolysis reaction.[194]

The above works clearly indicate that a new trend is being set in hydrothermal technology. This technology is going to be the one used in materials processing in the 21st century and it is not only human friendly or environmentally safe, but also economical cost wise. Already, several groups have cropped up all over the world to tackle the existing problems and search for new avenues in materials synthesis and processing under a new concept called green materials, which deals with industrial ecology, environmentally friendly methods, recycling, and so on.

In this regard, hydrothermal technique occupies a unique place because of its pollution free nature as the reactions take place within a closed system. Also, the reactions take place at relatively lower pressure/temperature conditions, which make the technique more popular and easier to operate.

10.5 HYDROTHERMAL TECHNOLOGY FOR THE 21ST CENTURY

Belching smokestacks were viewed as a sign of progress in the 19th century, worldwide, and even now, in some developing countries. Industrialization, indeed, should be viewed as a sign of progress. It leads to higher living standards, greater longevity, and a better quality of life.

Of late, we have begun to understand the implications of pollution and its prevention, of population growth, and increased industrialization in the third world and in the vibrant Pacific Rim economies. By the middle of the 21st century, population will increase by at least by 50% and then probably stabilize as most countries will have relatively high standards of living. Industrial production will probably increase at least five fold as the newly industrialized nations have formed a mainstream.[195]

Modern human society has been sustained both by a remarkable development of advanced materials and by a huge consumption of energy and resources. As we cannot withdraw ourselves from using them now and even in the near future, the wastes of materials, chemicals, energy, and heat would increase markedly to cause environmental problems on the earth (Fig. 10.38).[196] The global environment has great effects on human lives. Far reaching changes in social structure are being forced upon us already by environmental issues such as global warming, desertization, depletion of the ozone layer, acid rain, etc., which stem from two main problems: global scale expansion of the economic activities of industrially advanced nations and population expansion in developing countries. Global environmental problems will lead to great changes in the social structure of the 21st century. These changes will affect not only human life and industrial activity, but will also force significant reforms in fundamental concepts of manufacturing goods.[197] As the earth is almost a closed system with limited biosphere, lithosphere, hydrosphere, and atmosphere (Fig. 10.39), all materials should be cycled, moreover, heat and energy (entropy) loss should be minimized.[196][198] Considering these

specifications, we must search for materials: *1)* which are less hazardous to human life, and preferably compatible with human beings and other living species; and *2)* which have environmentally friendly processing to fabricate, to manipulate, to treat, to reuse, to recycle, and to dispose of those materials. The term *materials cycle* is generally used to designate raw materials synthesis, their fabrication, functional products, and their disposal. It is well known that all materials are extracted from the earth, and then converted into functional products through various means of materials processing, usually involving very high-temperature/energy and cost, which in turn contribute to global warming. These materials may be disposed of on the earth or recycled.[199]

A number of substances with particular compositions, crystal structures, and specified properties, have been investigated in detail by various workers all over the world. However, only a few materials can be considered

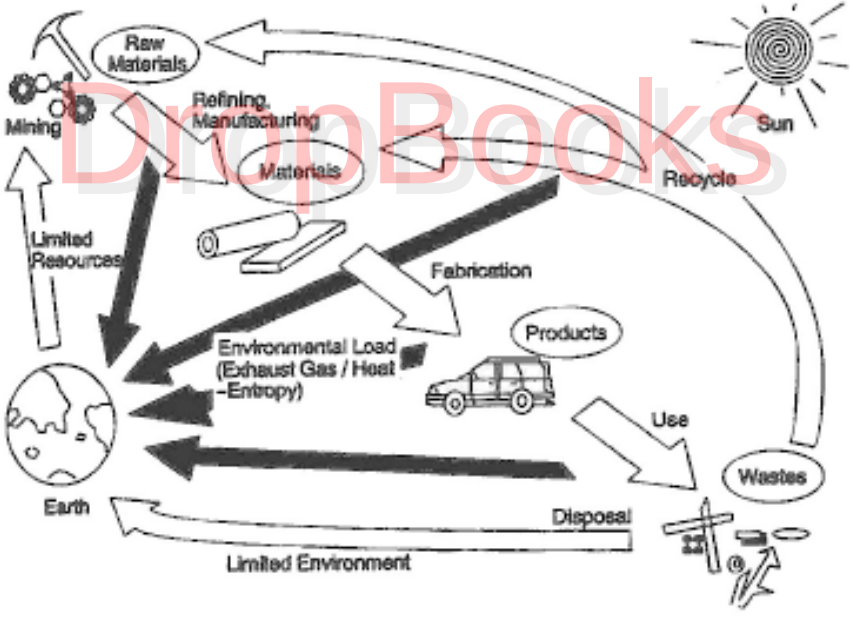

Figure 10.38. Life cycle of artificial materials with environmental/resources on the earth.[196]

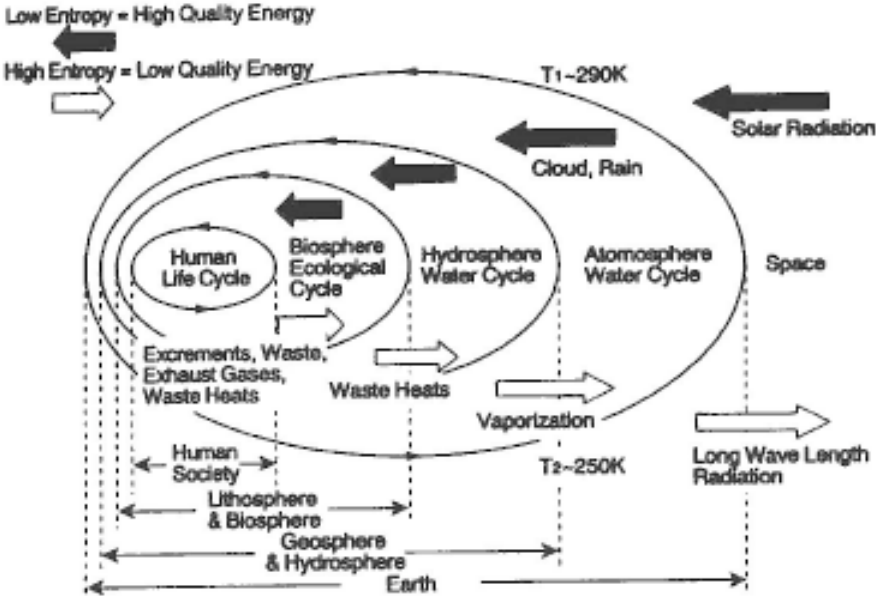

Figure 10.39. Entropy transfer in energy cycle on the earth.[196][198]

as useful materials, because some substances which have desired composition structures and properties cannot be used as they are extremely difficult to give desired shapes or forms (this important point has often been overlooked). Particularly, it is difficult to give desired shapes, forms, and size, to inorganic materials owing to their high brittleness. Organic materials, such as polymers and plastics, or metallic materials can be generally deformed when local stresses (above their yield stresses) are applied to them, but inorganic materials, particularly ceramics, are likely to break due to brittle fracture. Because ceramics have generally been fabricated by a rather special "ceramic processing" which consists of two steps: *1)* synthesis of powders, and *2)* shape-forming by firing/sintering of the powders or melting (in the case of glasses), both the steps usually require high temperatures and consume a lot of energy.

10.5.1 Thermodynamic Principles of Advanced Materials Processing

Processing of advanced materials generally consists of two steps: *1)* synthesis of substances (ceramic, metallic, organic) which have a

particular chemical composition, structure, and properties, and *2)* materials fabrication (i.e., shape-forming by firing/sintering, melting, molding, or casting). Organic materials, like polymers and plastics, or metallic materials can generally be deformed when local stresses (above their yield stresses) are applied to them,[200][201] but ceramics are likely to break due to brittle fracture.[202] The two-steps in "classical" processing usually require high temperatures, thus consuming a lot of energy, particularly in the case of ceramics.[203] More recent processing routes, using a gaseous phase, like CVD, MOCVD, etc.,[204][205] or vacuum systems such as sputtering, MBE, etc.,[204][206] require much more energy than standard high-temperature processing. Generally speaking, all these techniques have resulted in environmental problems because the consumed energies are emitted as exhaust gas(es) or exhaust heat (entropy) except for the part involved in the production. Especially, the vacuum systems seem to be worse because they need continuous pumping to maintain vacuum and their exhaust gas(es) cannot be cycled due to their diluted huge volumes.

The total energy consumption among all the mentioned processing routes should be the lowest in aqueous solution systems, because an excess of energy is necessary to create melts, vapor, gas, or plasma, than to form aqueous solutions at the same temperature (Fig. 1.7).[196] This idea can be demonstrated using an example of $BaTiO_3$, which is one of the most important materials for the electronic industry. Driving force (ΔG) for representative synthesis reactions of the $BaTiO_3$ Eqs. (2), (3), (4), (5), and (6), are 38 kcal/mol, 3685 kcal/mol, 17 kcal/mol, and -14 kcal/mol, respectively, at room temperature.[28][207] Figure 10.40 shows the energy diagram for the formation of $BaTiO_3$ from various precursors.

BrownBooks

Eq. (2) $BaO_{(crystal)} + TiO_{2\ (crystal)} \leftrightarrow BaTiO_{3\ (crystal)}$

Eq. (3) $Ba_{\ (vapor)} + Ti_{\ (vapor)} + 3/2\ O_{2\ (gas)} \leftrightarrow BaTiO_{3\ (crystal)}$

Eq. (4) $Ba^{2+}_{(gas)} + Ti^{4+}_{(gas)} + 3O^{2-}_{(gas)} \leftrightarrow BaTiO_{3\ (crystal)}$

Eq. (5) $TiO_{2\ (crystal)} + Ba^{2+}_{(aq.)} + 2OH^{-}_{(aq.)} \leftrightarrow BaTiO_{3\ (crystal)}$

Eq. (6) $Ba^{2+}_{(aq.)} + Ti(OH)_{4\ (aq.)} - H_2O_{\ (aq.)} - 2H^{+}_{\ (aq.)} \leftrightarrow BaTiO_{3\ (crystal)}$

Because the raw materials of Ba and Ti must be solid oxides or carbonate ores, processing using gas/vapor requires a huge energy expenditure of 727–3685 kcal/mol to make solid $BaTiO_3$ and this energy must be discarded into the environment. On the other hand, as the lattice energy of BaO and TiO_2 is almost equal the hydration (solvation) energy of Ba^{2+}

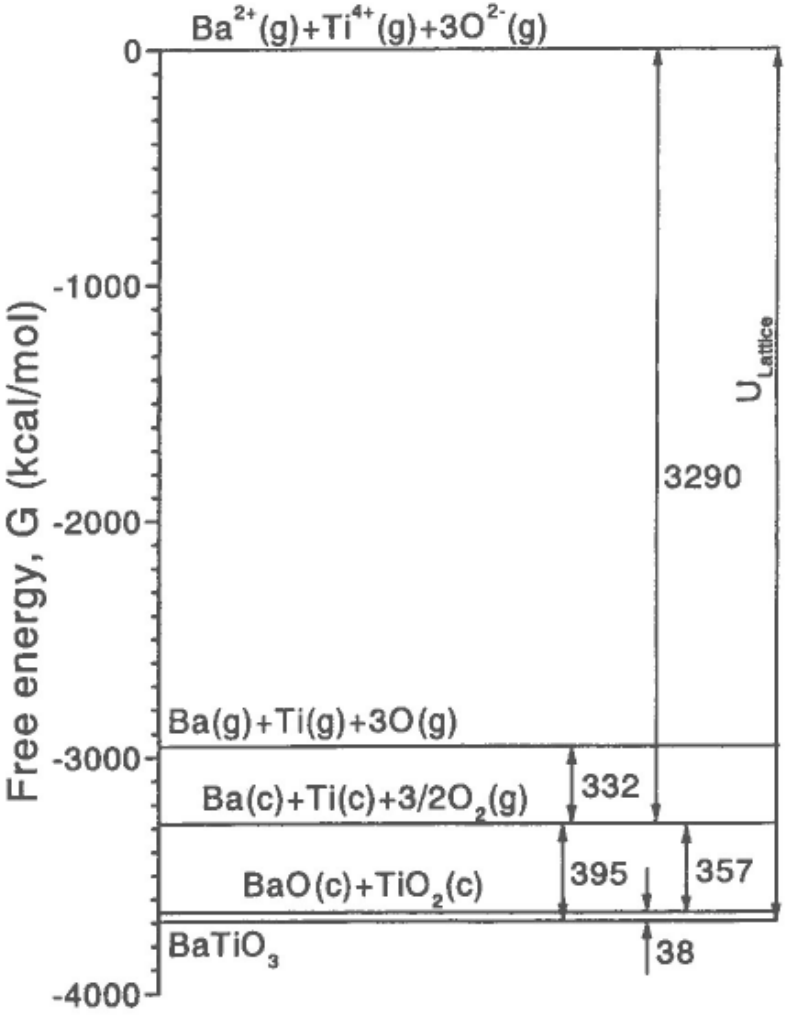

Figure 10.40. Energy diagram for the formation of $BaTiO_3$ from various precursors. *(Courtesy of M. Yoshimura.)*

and Ti^{4+} ions, solution processing consumes very little energy if the synthesis activation energy (ΔG^*) can be overcome. Generally speaking, ΔG^* is inversely proportional to $(\Delta G)^{\eta}$, where ΔG and the activation energy (ΔG^*) are sufficiently provided for reaction to yield crystallization compounds with desired shape/size via several steps, such as diffusion, adsorption, reaction, nucleation, and growth.[208] On the other hand, species in aqueous solutions are hydrated (or chelated by some complexing agents). Thus, they have only a small driving of force (ΔG) for the reaction and rather high activation energies are necessary for reaction to occur by defeating the hydration (chelation) energies of ions. Electro- or electroless-plating for metals is achieved by reducing metal ion(s) electrochemically or chemically. However, in the case of ceramics, anions must be oxidized at the same time as the reduction of cations. Because, some particular activation processes, such as electro-, photo-, sono-, complexo-, organo-, and mechano-activation are required to accelerate kinetics of synthesis of crystallized single/multicomponent ceramic materials from the solution.

Schematic diagram of a *temperature-pressure map* for various kinds of materials processing is shown in Fig. 1.8. Solution processing is located in the pressure temperature range characteristic for conditions of lives on earth. All other processing routes are connected with increasing temperature and/or increasing (or decreasing) pressure; therefore, they are environmentally stressed.

DropBooks

Although environmental problems have been argued from various points of view, ecologically, biologically, technologically, economically, and even politically, the most scientific arrangements, thus universally acceptable, are the thermodynamic ones.

Thus, important subjects of technology in the 21st century are predicted to be the balance of environmental and resource and/or energy problems. This has led to the development of a new concept, related to the processing of advanced materials in the 21st century, namely, industrial ecology—science of sustainability.[209] The first textbook on the subject, written by two AT&T authorities, provides the following definition:

> ..... *Industrial ecology* is the means by which humanity can deliberately and rationally approach and maintain a desirable carrying capacity, when given continued economic, cultural and technological evolution. The concept requires that an industrial system be viewed not in isolation from its surrounding systems, but in concert with them. It is a system's

> view in which one seeks to optimize the total materials cycle, from virgin material, to finished material, to component, to product, to obsolete product, and to ultimate disposal. Factors to be optimized include resources, energy, and capital.[210]

Many believe that implementing industrial ecology will be a principle challenge for business and society in the 21st century. The race is to become the most innovative, most visionary, and most effective company understanding industrial ecology, and implementing design for environment (DFE).

With all of the above discussed aspects in mind, Yoshimura proposed a new concept of materials processing, namely *soft solution processing*, which meets all the demands of materials processing in the 21st century. This soft solution processing for high performance inorganic materials is fast catching on with materials scientists world wide, because it deals with low energy processing using solutions which minimize environmental impact (sometimes called *chimie-douce*), it will be the key to environmental improvement. Temperature for preparation will affect energy consumption and a low temperature leads to "soft processing." A significant example is biological processes that produce magnetite oxides at room temperature.

The solution process also has merit in that some unique inorganic materials can be synthesized only by this process. There are many kinds of processes related to soft solution processing, and the important ones are: soft solution electrochemical process, liquid phase deposition, sol-gel processing, hydrothermal technique, co-precipitation, emulsions, the polymerizable complex method, biomimetic, solvothermal, self-assembly, wet-chemical processing, templating, etc. Development of simple patterning methods with nanometer resolution, acceleration of kinetics of synthesis, framing (deducing) the theoretical approaches to the growth of materials from solutions, and the development of *in situ* observation techniques are some examples of emerging research subjects. One of the most important technological issues of the soft solution processing is its integration with functional device technology, because possibility of fabrication of a variety of materials and microstructures from solutions has been already demonstrated. In these processes, solutions are always used and therefore, many factors, such as pH, concentration, ligand type, temperature, electrode potential, etc., are controlled in order to design advanced materials. Additionally, the technique using the solution flow may be used to synthesize various single phase and multilayered thin films and this is an important step in the application of the soft solution processing in the

technology of the future integrated functional devices. From this point of view, fabrication of the ceramic thin films in the solution flow[211] in the recycled system, below 200°C, is very important. In this connection, a flow-cell for hydrothermal electrochemical synthesis and its applicability to fabricate single phase thin films, as well as multilayered structures in the system $BaTiO_3$-$SrTiO_3$, has been demonstrated by Yoshimura and co-workers.[74]–[76],[82]–[84] The technique using the solution flow under the hydrothermal electrochemical conditions is an important step in the integration of the solution processing with the functional devices technology and may find applications for various single and/or multilayered thin films.

During the 21st century, hydrothermal technology, on the whole, will not just be limited to the crystal growth, or leaching of metals, but it is going to take on a very broad shape, covering several interdisciplinary branches of science. Therefore, it has to be viewed from a different perspective, as it offers several new advantages, like homogeneous precipitation using metal chelates, decomposition of hazardous and/or refractory chemical substances, monomerization of high polymers, like polyethylene or tetraphthalate, and other environmental engineering and chemical engineering issues dealing with recycling of rubbers and plastics instead of burning. Further, the growing interest to enhance the hydrothermal reaction kinetics using microwave, ultrasonic, mechanical, and electrochemical reactions, will be distinct.[212] Also, duration of the experiments is being reduced at least by two orders of magnitude which, in turn, makes the technique more economic. With an ever-increasing demand for composite nanostructures, the hydrothermal technique offers a unique method for the coating of various compounds on metals, polymers, and ceramics, as well as the fabrication of powders or bulk ceramic bodies.

DropBooks

In recent years, activated carbons showing high surface area are specially impregnated with active metals, like Cd, Cu, W, Cr, Mo, etc. Such impregnated activated carbons have additional characteristics, like antibacterial effects, absorb harmful gases in industrial and military applications.[213] The hydrothermal technique is very effective for the impregnation of active metals into activated carbon. Activated carbon impregnated with tungsten metal has been successfully employed for the decomposition of toxic organic compounds, like phenols, nitroarenes, etc.[214][215]

Feng et al. (1998) have employed the hydrothermal soft chemical process for synthesis of tunnel manganese oxides from a layer of manganese oxide.[216]–[218] This process comprises of two steps: *1)* preparation of

a framework precursor with layered structure and insertion of template ions or molecules (structure directing agents) into its interlayer space by a soft chemical reaction and *2)* transformation of the template inserted precursor into a tunnel structure by hydrothermal treatment.

Hydrothermal-solvothermal processing helps greatly in the structure stabilization of several new compounds.[219][220] Natural phyllosilicates are characterized by a low thermal stability due to the presence of $(OH)^-$ groups in the lattice. Through hydrothermal treatment, the replacement of $(OH)^-$ groups by oxygen atoms takes place, and this, in turn, improves the thermal stability of phyllosilicates. Similarly, the replacement of metals can be carried out under hydrothermal conditions to obtain new structures.

Recovery, recycling, decomposition, and treatment processes, under hydrothermal conditions, are going to play a major role in the 21st century.[221]–[225] Figure 10.41 shows the author's imagination—a new generation, complex industry constructed underground which will exhaust no toxic or hazardous wastes.[224] It is an ideal closed system, a combination of waste treatment, energy recovery, and formation of resource. This deals with the recovery process of human waste to energy resource using hydrothermal technology. The authors have decomposed the night soil without any insecticides and deodorizers using the hydrothermal technology. The decomposition of the night soil was defined by a ratio of COD Mn before and after the reaction. The reaction time was just 10 minutes. The decomposition ratio increased with increasing temperature, and oxygen pressure over 2 MPa accelerated the decomposition. Night soil was over 90% decomposed when the reaction temperature of the hydrothermal treatment was at 300°C for 10 minutes. Under these conditions, hydrothermal decomposition of night soil occurred with offensive smelling gas. Figure 10.41 shows the conversion of organic wastes to bioresource and energy. Furthermore, CO_2 gas is not discharged to atmosphere in this system and to change CH_3OH for C1 chemical industry. In the future, a closed system such as this type must be attained in all industrial fields for survival of modern civilization and for earth ecology. To quote an example of such a system, at IAx corp., Japan, a new closed system for the collection of waste, separation, and recycling has been introduced, and achieved a reduction in waste output by 85% without increasing the intake (Fig. 10.42). In order to achieve the objective of a waste zero system, the corporation is working out new technology based on the *closed manufacturing system*.

Soil, solidified hydrothermally, is a new material born from the development of a closed production system.[197] The strength of the hydrothermally processed soil is equal to or greater than that of concrete building materials (flexural strength = 4 to 6 MPa). Its heat capacity is greater than that of wood flooring (1090 k J/m^3, K), tatami (430 k J/m^3, K) and carpet (330 k J/m^3, K). It also exhibits high humidity absorption and desorption ability, similar to wood because of its pore sizes, which are extremely small (10 to 20 nm) when compared to concrete blocks or conventional chinaware. Figure 10.43 shows the influence of earth ceramics on the room temperature and relative humidity (temperature and relative humidity were measured for 1 month in winter).[197] The extremely small pores are the result of the pores in the raw material (soil) itself and the pores that are formed during hydrothermal solidification. This hydrothermally treated soil product, with a trade name *Earth Ceramics*, is being widely used as flooring material in Japan, because of the improved properties compared to the conventional materials (Fig. 10.44). The amount of energy used for air conditioning after the use of soil ceramics was 25% less than that without earth ceramics. Figure 10.45 shows the flexural strength per manufacturing energy (MPa m^3/GJ) for the hydrothermally solidified waste soil (earth ceramics) and other common ceramic products. Similarly, earth ceramics have less allergic problems than vinylon cloth and carpets. Thus, the hydrothermal processing helps greatly in the production of ecofriendly materials, namely ecomaterials or green materials.

DropBooks

REFERENCES

1. Psaras, P. A. and Langford, H. D. (eds.), *Advancing Materials Research*, pp. 225–243, National Academy Press, Washington, D.C. (1987)
2. Sogo, N. and Kato, A. (eds.), *Ceramics: Toward the 21st Century*, Ceramic Society of Jpn., Tokyo (1991)
3. Somiya, S., (ed.), H*ydrothermal Reactions for Materials Science and Engineering: An overview of Research in Japan*, Elsevier Applied Science, (1989)
4. Stickler, D. W. and Carlson, W. G., Electrical Conductivity in the ZrO_2-Rich Region of Several M_2O_3-ZrO_2 Systems, *J. Am. Ceram. Soc.*, 48:286–289 (1965)
5. Green, D. J., Hannink, R. H. J., and Swain, M. V., *Transformation Toughening of Ceramics*, CRS Press, Inc., Boca Raton (1989)

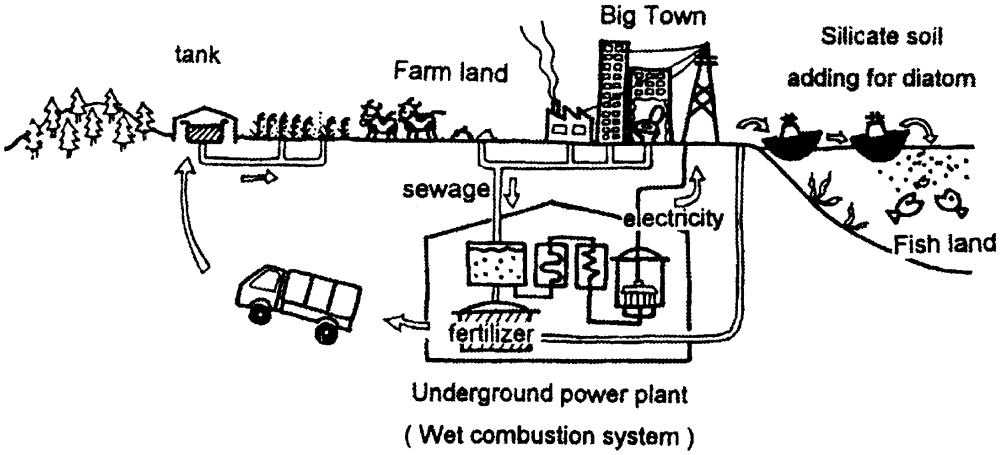

Figure 10.41. Author's imagination—a new generation complex industry, constructed underground and exhausting no toxic or hazardous wastes. *(Courtesy of N. Yoshimura.)*

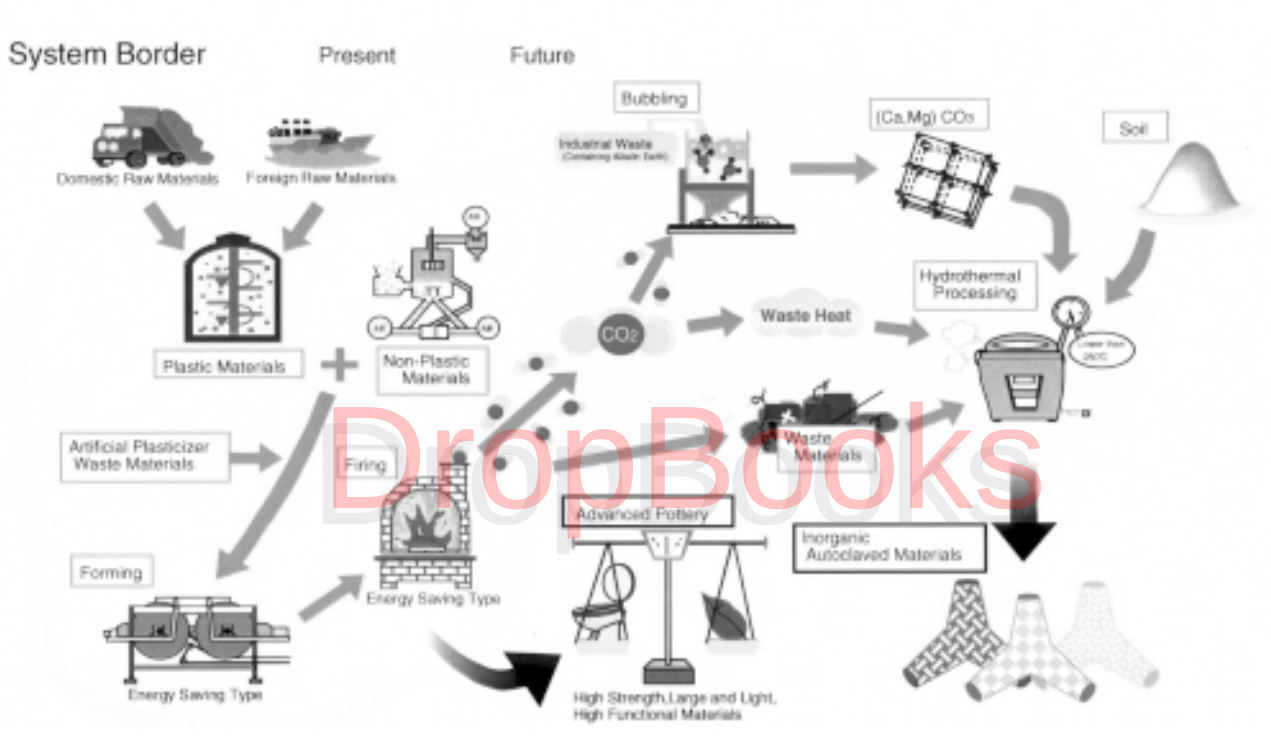

DropBooks

Figure 10.42. Closed manufacturing system. *(Courtesy of E. H. Ishida.)*

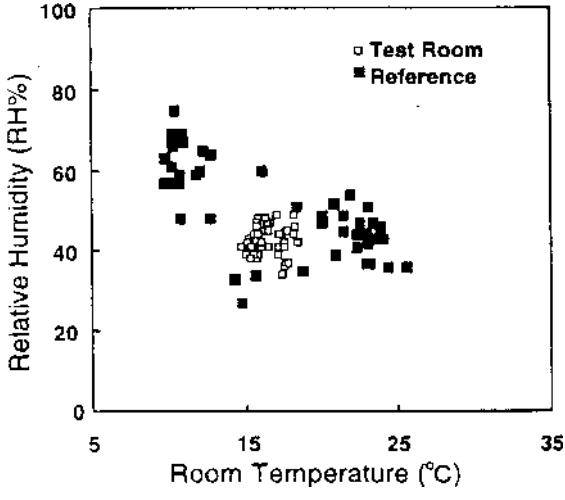

Figure 10.43. Influence of earth ceramics on the room temperature and relative humidity.[197]

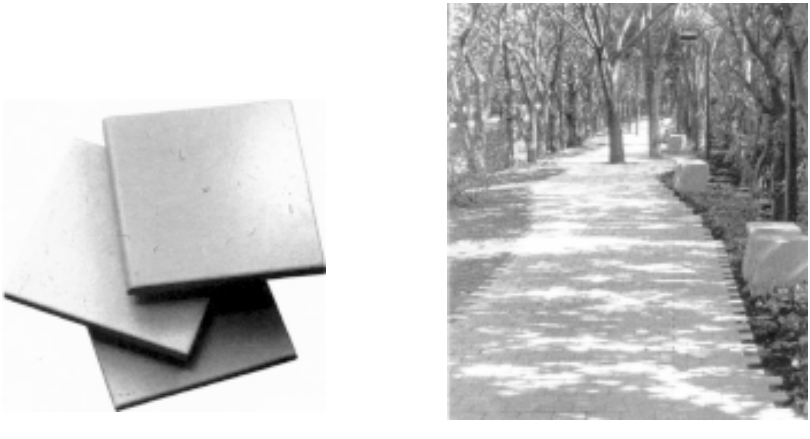

Figure 10.44. Earth ceramics used for floors. *(Photos courtesy of E. H. Ishida.)*

Figure 10.44. *(Cont'd.)*

DropBooks

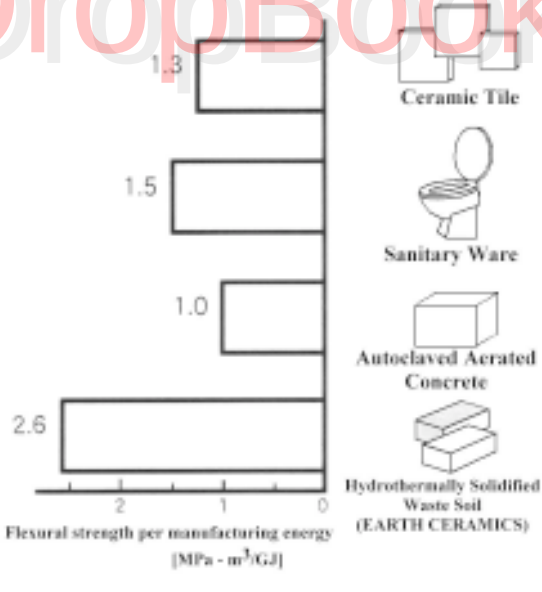

Figure 10.45. Flexural strength per manufacturing energy (MPa m^3/GJ) for the hydrothermally solidified waste soil (earth ceramics) and other common ceramic products.[197]

REFERENCES (continued)

6. Yashima, M., Ishizawa, N., Fujimori, H., Kakiyana, M., and Yoshimura, M., *In-situ* Observation of the Diffusionless Tetragonal Cubic Phase Transition and Metastable Phase Diagram in the ZrO_2-$ScO_{1.5}$ System, *Eur. J. Solid State Inorg. Chem.*, 32:761–770 (1995)
7. Yashima, M., Kakihana, M., and Yoshimura, M., Metastable-Stable Phase Diagrams in the Zirconia-Containing Systems Utilized in Solid-Oxide Fuel Cell Application, *Solid State Ionics*, 86-88:1131–1149 (1996)
8. Thornber, M. R., Bevan, D. J. M., and Summerville, E., Mixed Oxides of the Type MO_2 (fluorite)-M_2O_3 Very Phase Studies in the System ZrO_2-M_2O_3 (M = Sc, Yb, Er, Dy), *J. Solid State Chem.*, 1:545–553 (1970)
9. Yoshimura, M., Phase Stability of Zirconia, *Ceram. Bull.*, 67:1950–1955 (1988)
10. Yashima, M., Sasaki, S., Kakihana, M., Yamaguchi, Y., Arashi, H., and Yoshimura, M., Oxygen-Induced Structural Change of the Tetragonal Phase Around the Tetragonal-Cubic Phase Boundary in ZrO_2-$YO_{1.5}$ Solid Solutions, *Acta crystallogr.*, B 50:663–673 (1994)
11. Yashima, M., Ishizawa, N., and Yoshimura, M., High-Temperature X-Ray Study of the Cubic-Tetragonal Diffusionless Phase Transition in the ZrO_2-$ErO_{1.5}$ System: II, Temperature Dependences of Oxygen Ion Displacement and Lattice Parameter of Compositionally Homogeneous 12 mol% $ErO_{1.5}$ - ZrO_2, *J. Am. Ceram. Soc.*, 76:649–656 (1993)
12. Yashima, M., Ohtake, K., Kakihana, M., Arashi, H., and Yoshimura, M., Determination of Tetragonal-Cubic Phase Boundary of $Zr_{1-x}R_xO_{2-x}$ (R = Nd, Sm, Y, Er and Yb) by Raman Scattering, *J. Phys. Chem. Solids*, 57:17–24 (1996)
13. Tani, E., Yoshimura, M., and Somiya, S. Effect of Mineralizers on the Crystallization of Solid Solutions in the System ZrO_2-CeO_2 Under Hydrothermal Conditions, *Yogyo-Kyokai-Shi*, 90:195–201 (Jpn.) (1982)
14. Somiya, S., Kumaki, T., Hishinuma, K., Nakai, Z., Akiba, T., and Suwa, Y., Hydrothermal Precipitation of ZrO_2 Powder, in: *Hydrothermal Growth of Crystals*, (K. Byrappa, ed.) *Prog. Crystal Growth Charact.*, 21:195–198 (1990)
15. Hirano, S. and Somiya, S., Hydrothermal Crystal Growth of Magnetite in the Presence of Hydrogen, *J. Crystal Growth*, 35:273–278 (1976)
16. Hirano, S. and Somiya, S., Hydrothermal Reaction Sintering of Pure Cr_2O_3, *J. Am. Ceram. Soc.*, 59:534 (1976)
17. Yoshimura, M. and Somiya, S., Fabrication of Dense, Nonstabilized ZrO_2 Ceramics by Hydrothermal Reaction Sintering, *Am. Ceram. Soc. Bull.*, 59:246 (1980)
18. Toraya, H., Yoshimura, M., and Somiya, S., Hydrothermal Oxidation of Hf Metal Chips in the Preparation of Monoclinic HfO_2 Powders, *J. Am. Ceram. Soc.*, 66:148–150 (1983)

Ceram. Soc., 66:148–150 (1983)

19. Yoshimura, M., Kikugawa, S., and Somiya, S., Preparation of Alpha-Alumina Fine Powders by Hydrothermal Oxidation Method, *J. Jpn. Soc. Powder Metall.*, 30:207–210 (1983)
20. Yoshimura, M., Tokyo Inst. of Technology, Jpn., Own work.
21. Riman, R. E., Chemical Precipitation of Ceramic Powders, in: *Colloid Engg.* (R. A., Williams, ed.), pp. 140–167, Buttersworths, New York (1992)
22. Lencka, M. M. and Riman, R. E., Hydrothermal Synthesis of Perovskite Materials: Thermaldynamic Modeling and Experimental Verification, *Ferroelectrics,* 151:159–164 (1994)
23. Lencka, M. M. and Riman, R. E., Thermodynamics of the Hydrothermal Synthesis of Calcium Titanate with Reference to Other Alkaline-Earth Titanates, *Chem. Mater.*, 7:18–25 (1995)
24. Lencka, M. M., Andreko, A., and Riman, R. E., Hydrothermal Precipitation of Lead Zirconate Titanate Solid Solutions: Thermodynamic Modeling and Experimental Synthesis, *J. Am. Ceram, Soc.*, 78:2609–2618 (1995)
25. Kutty,T. R. N. and Balachandran, R., Direct Precipitation of Lead Zirconate Titanate by the Hydrothermal Method, *Mat. Res. Bull.,* 19:1479–1488 (1984)
26. Beal, K. C., Precipitation of Lead Zirconate Titanate Solid Solutions Under Hydrothermal Conditions, in: Advances in Ceramics; Ceramic Powder Science, (G. L. Messing, K. S. Mazdiyasni, J. W. McCauley, and R. A. Haber, eds.), 21:33–41, *American Ceramic Society*, Westerville, OH. (1987)
27. US Patent No. 5112433, Dowson, W. J., and Swartz, S. L., Process for Producing Submicron Ceramic Powders of Perovskite Compounds With Controlled Stoichiometry and Particle Size (May 12, 1992)
28. Lencka, M. M. and Riman, R. E., Thermodynamic Modeling of Hydrothermal Synthesis of Ceramic Powders, *Chem. Mater.*, 5:61–70 (1993)
29. Lencka, M. M. and Riman, R. E., Synthesis of Lead Titanate: Thermodynamic Modeling and Experimental Verification, *J. Am. Ceram., Soc.*, 76:2649–2659 (1993)
30. Eckert, J. O. Jr., Hung-Houston, C. C., Gersten, B. L., Lencka, M. M., and Riman, R. E., Kinetics and Mechanisms of Hydrothermal Synthesis of Barium Titanate, *J. Am. Ceram. Soc.*, 79:2929–2939 (1996)
31. Riman, R. E., Lencka, M. M., Mc Candlish, L. E., Gersten, B. L., Andrenko, A., and Cho, S. B., Intelligent Engineering of Hydrothermal Reactions, in: *Proc. 2nd International Conference Solvothermal Reactions,* pp. 148–151, Takamatsu, Jpn. (Dec. 18–20, 1996)

RapBooks

32. Lencka, M. M. and Riman, R. E., Estimation of Thermochemical Properties for Ceramic Oxides: A Focus on $PbZrO_3$, *Thermochim. Acta.*, 256:193–203 (1995)

33. Aksay, I. A., Chun, C. M., and Lee, T., Mechanism of $BaTiO_3$ Formation by Hydrothermal Reactions, in: *Proc. 2nd International Conference Solvothermal Reactions*, pp. 76–79, Takamatsu, Jpn, (Dec. 18–20, 1996)

34. Adair, J. H., Denkiewicz, R. P., Arriagada, F. J. and Osseo-Asare, K., Ceramic Transactions, Ceramic Powder Science II A; (G. L. Messing, E. R. Fuller Jr., H. Hausner, eds.), 1:135, *American Ceramic Society*, Westerville, OH (1988)

35. Osseo-Asare, K., Arriagada, F. J., and Adair, J. H., Ceramic Transactions, Ceramic Powder Science II A; (G. L. Messing, E. R. Fuller Jr., H. Hausner, eds.), *American Ceramic Society*, 1:47, Westerville, OH (1988)

36. Chen, D. and Xu, R., Solvothermal Synthesis and Charaction of $PbTiO_3$ Powders, *J. Mater. Chem.*, 8:965–968 (1998)

37. Kaiser, A., Berger, A., Sporn, D., and Bertagnolli, H., Lyothermal Synthesis of Nanocrystalline $BaTiO_3$ and TiO_2 - Powders, *Ceramic Processing Science and Technology*, pp. 51–55 (1994)

38. Dubois, T. and Demazeau, G., Preparation of Fe_3O_4 Fine Particles Through a Solvothermal Process, *Mater. Letts.*, 19:38–47 (1994)

39. Demazeau, G., Wang, A., Matar, S., and Cillard, J. D., Solvothermal Synthesis of Nitrides as Fine Particles, *High Pressure Research*, 12:343–346 (1994)

40. Inoue, M., Nishikawa, T., Nakamura, T., and Inui,T. Glycothermal Reaction of Rare Earth Acetate and Iron Acetylacetonate: Formation of Hexagonal $REFeO_3$, *J. Am. Ceram. Soc.*, 80:2157–2160 (1997)

41. Inoue, M., Otsu, H., Komonami, H., Nakamura, T., and Inu, T., Thermal Stability of Phosphorus-Modified Alumina Prepared by the Glycothermal Method, *J. Mat. Sci. Letts.*, 13:787–789 (1994)

42. Christiansen, N. and Riman, R. E., Bioceramics: A Future Through Microstructural and Chemical Design, in: *Proc. 5th Scandinovian Symp. Materials Science, New Materials and Processes*, pp. 209–220 (May 22–23, 1989)

43. Hench, L. L., Bioceramics: From Concept to Clinic, *J. Am. Ceram. Soc.*, 74:1487–1510 (1991)

44. Hench, L. L., Bioceramics, *J. Am. Ceram. Soc.*, 81:1705–1728 (1998)

45. Hubert, F., Bokros, J. C., Hench, L. L., Wilson, J., and Heimke, G., Ceramics in Clinical Applications: Past, Present and Future, in: *High Tech Ceramics*, (P. Vincenzini, ed.), pp. 189–213, Elsevier, Amsterdam (1987)

46. Hench, L. L. and Wilson, J., *An Introduction to Bioceramics*, World Scientific, London, U.K. (1993)

47. Shackelford, J. F., Bioceramics - Current Status and Future Trends, *Mater. Sci. Forum,* 293: 99–106 (1999)

48. Groot, de K., *Bioceramics of Calcium–Phosphate,* CRC Press, Boca Raton, FL. (1983)

49. Yamamuro,T., Hench, L. L., and Wilson, J. (eds.) *Handbook of Bioactive Ceramics, Vol.II., Calcium Phosphate and Hydroxylapatite Ceramics,* CRC Press, Boca Raton, FL. (1990)

50. Suchanek, W. and Yoshimura, M., Processing and Properties of Hydroxyapatite-Based Biomaterials For Use as Hard Tissue Replacement Implant, *J. Mater. Res.,* 13:1–24 (1998)

51. Yoshimura, M. and Suda, H., Hydrothermal Processing of HAp: Past, Present and Future, in: *Hydroxyapatite and Related Compounds,* (P. W. Brown, and B. Constantz, eds.), p. 45, CRC Press, Cleveland, OH and Boca Raton, FL. (1994)

52. Elliott, J. C., Structure and Chemistry of the Apatites and other Calcium Orthophosphates, Elsevier, Amsterdam (1994)

53. Yamashita, K. and Kanazawa, T., Hydroxyapatite, in: *Inorganic Phosphate Materials,* (T. Kanazawa, ed.), Materials Science Monograph 52, p.15, Kodansha and Elsevier (1989)

54. Ioku, K., Yoshimura, M., and Somiya, S., Microstructure-Designed HAp Ceramics From Fine Single Crystals Synthesized Hydrothermally, in: *Bioceramics, Proc. 1st Int. Bioceram. Symp.,* (H. Oonishi, H. Aoki, and K. Sawai, eds.) pp. 62–67, Ishiyaku Euro-America Inc., Tokyo-St. Louis (1989)

55. Takahashi, H., Yashima, M., Kakihana, M., and Yoshimura, M., Synthesis of Stoichiometric (ca/p = 1.67) HAp by a Gel Route From the Aqueous Solution of Citric and Phosphonoacetic Acids, *Eur. J. Solid State Inorg. Chem. "Advanced Materials,"* 32:829–835 (1995)

56. Aoki, H., *Science and Medical Applications of HAp,* JAAS, Tokyo (1991)

57. Inoue, S. and Ono, A., *J. Ceram. Soc. Jpn.* 95:759–760 (Jpn.) (1987)

58. Itatani, K., Takahashi, O., Kishioka, A., and Kinoshita, M., *Gypsum and Lime,* 213:77 (Jpn.) (1988)

59. Aizawa, M., Itatani, K., Howell, F. S., and Kishioka, A., *J. Ceram. Soc. Jpn.,* 103:1214–1216 (1995)

60. Aizawa, M., Itatani, K., Howell, F. S., and Kishioka, A., *J. Ceram. Soc.,* 104:126–128, Jpn. (1995)

61. Roy, D. M. and Linnehan, S. K., *Nature,* 247:220–221 (1974)

62. Ioku, K., Kai, T., and Nishioka, M., in: *Apatite, Proc. 1st Int. Symp. Apatite;* (M. A. H. Aoki, N. Nagai, and T. Tsuji, eds.), 1:131, Takayama Press System Center, Inc. (1992)

DropBooks

63. Ioku, K., Eguchi, Y., and Goto, S., in: *Trans. 12th Symp. on Apatite*, p.29, Nagoya, Jpn, (Dec. 12–13, 1996)

64. Brown, W. E. and Chow, L. C., in: Cements Research Progress-1987, (P. W. Brown, ed.), p. 351, *The American Ceramic Society*, Westerville, OH (1988)

65. Brown, P. W., Martin, R. I., and Tenhuisen, K. S., in: Bioceramics: Materials and Applications, (R. P. Rusin and G. S. Fishman, eds.), *Ceramic Transactions*, 48: 37–46 (1995)

66. US Patent 4,612,053: Brown, W. E. and Chow, L. C., Combinations of Sparingly Soluble Calcium Phosphate in Slurries and Pastes as Mineralizers and Cements (1986)

67. Otsuka, M., Nakahigashi, Y., Matsuda, Y., Fox, J. L., and Higuchi, W. I., *In Vitro* Drug Release Behaviors From Self-Setting Calcium Phosphate Cement Loaded on Bovine Bone, *Apatite*, 2:141–144 (1997)

68. Otsuka, M., Matsuda, Y., Suwa, Y., Fox, J. L., and Higuchi, W. I., A Novel Skeletal Drug Delivery System using Self-Setting Calcium Phosphate Cement 4: Effect of the Mixing Solution Volume on the Drug Release Rate of Heterogeneous Asprin Loaded Cement, *J. Pharm. Sci.*, 83:259–263 (1994)

69. Ferrand, B., Daval, J., and Joubert, J. C., Heteroepitaxial Growth of Single Crystal Films of YIG on GGG Substrates by Hydrothermal Synthesis, *J. Crystal Growth*, 17:312–314 (1972)

70. Ferrand, B., Heteroepitaxie par Syntheses Hydrothermale de Films Minces Monocristallins de Gernats Ferrimagnetiques, *High Temperature - High Pressure*, 6:619–628 (1974)

71. Toudic, Y. and Passareti, M., Croissance par voie Hydrothermale de Films Ferrimagnetiques; Epitaxies sur des Substrats de GGG, *J. Crystal Growth* 24/25:621–623 (1974)

72. Fujishiro, Y., Fujimoto, A., Sato, T., and Okuwaki, A., Coating of HAp on Titanium Plates Using Thermal Dissociation of Calcium-EDTA Chelate Complex in Phosphate Solutions Under Hydrothermal Conditions, *J. Colloid Interface Sci.*, 173:119–127 (1995)

73. Iton, T., Zhang, Q., Abe, M., and Tamaura, Y., Preparation of $CoxFe_{3-x}O_4$ Films in Aqueous Solution at 120–200°C by "Hydrothermal Ferrite Plating," *Jpn. J. Appl. Phys.*, 31:1236–1238 (1992)

74. Cho, W. S. and Yoshimura, M., Hydrothermal; Hydrothermal–Electrochemical and Electrochemical Synthesis of Highly Crystallized Barium Tungstate Films, *Jpn. J. Appl. Phys.*, 36:1216–1222 (1997)

75. Cho, W. S. and Yoshimura, M., Preparation of Highly Crystallized $BaMoO_4$ Film using a Solution Reaction Assisted by Electrochemical Dissolution of Molybdenum, *Solid State Ionics*, 100:143–147 (1997)

76. Cho, W. S. and Yoshimura, M., Hydrothermal Synthesis of Pb TiO_3 Films, *J. Mater. Res.*, 12:833–839 (1997)

77. Xu, J. J., Shaikh A. S., and Vest, R. W., High K $BaTiO_3$ Films From Metal Organic Procursors, *IEEE Trans. Ultrason., Ferroelectr. Frequency Control*, 36:307–312 (1989)

78. Van Buskirk, P. C., Gardiner, R., Kirlin, P. S., and Nutt, S., Reduced Pressure MOCVD of Highly Crystalline $BaTiO_3$ Thin Films, *J. Mater. Res.*, 7: 542–546 (1992)

79. Kamalasanan, M. N., Chandra, S., Joshi, P. C., and Mansingh, A., Structural and Optical Properties of Sol-Gel Processed $BaTiO_3$ Ferroelectric Films, *Appl. Phys. Letts.*, 59:3547–3556 (1991)

80. Fuenzalida, V. M. and Pilleux, M. E., Hydrothermally Grown $BaZrO_3$ Films on Zirconium Metal Microstructure, XPS and AES Depth Profiling, *J. Mater. Res.*, 10: 2749–2755 (1995)

81. Dharmadhikari, V. S. and Grannemann, W. W., AES Study on the Chemical Composition of Ferroelectric $BaTiO_3$ Thin Films rf-sputter Deposited on Silicon, *J. Vac. Sci. Technol.*, A1:483–489 (1983)

82. Hayashi, M., Ishizawa, N., Yoo, S. E., and Yoshimura, M., Preparation of Barium Titanate Thin Film on Titanium Deposited Glass Substrate by the Hydrothermal Electrochemical Method, *J. Ceram. Soc.*, Jpn. 98:930–934 (1990)

83. Ishizawa, N., Banno, H., Hayashi, M., Yoo, S. E., and Yoshimura, M., Preparation of $BaTiO_3$ and $SrTiO_3$ Polycrystallization Thin Films on Flexible Polymer Film Substrate by the Hydrothermal Method, *Jpn. J. Appl. Phys.*, 29:2467–2471 (1990)

84. Yoo, S. E., Hayashi, M., Ishizawa, N., and Yoshimura, M., Preparation of Strontium Titanate Thin Film on Titanium Metal Substrate by the Hydrothermal Electrochemical Method, *J. Am Ceram. Soc.*, 73:2561–2567 (1990)

85. Yoo, S. E., Ishizawa, N., Hayashi, M., and Yoshimura, M., Review on Preparation of Films of Multifunctional Complex Oxide by the Hydrothermal-Electrochemical Method. *Rep. Res. Lab. Eng. Mater.*, 16:39–44, *Tokyo Inst. Technol.* (1991)

86. Basca, R., Ravindranathan, P., and Dougherty, J. P., Electrochemical, Hydrothermal and Electrochemical Hydrothermal Synthesis of Barium Titanate Thin Films on Titanium Substrates, *J. Mater. Res.*, 7:423–428 (1992)

87. Yoshimura, M., Hydrothermal Electrochemical Technique: A New Fabrication Method of Thin Films of Perovskite-Type Oxides, in: *Proc. 95th Annual Meeting of the American. Ceramic Soc.* Cincinnati, OH (April 20, 1993)

88. Pilleux, M. E. and Fuenzalida, V. M., Hydrothermal $BaTiO_3$ Films on

DropBooks

Silicon: Morphological and Chemical Characterization, *J. Appl. Phys.*, 74:4664–4670 (1993)

89. Kajiyoshi, K., Tomono, K., Hamaji, Y., Kasanami, T., and Yoshimura, M., Short-circuit Diffusion of Ba, Sr, and O During $ATiO_3$ (A = Ba, Sr) Thin-Film Grown by the Hydrothermal Electrochemical Method, *J. Am. Ceram. Soc.*, 78:1521–1527 (1995)
90. Kajiyoshi, K., Yoshimura, M., Hamaji, Y., Tomono, K., and Kasanami, T., Growth of (Ba, Sr) TiO_3 Thin Films by the Hydrothermal Electrochemical Method and Effect of Oxygen Evolution on Their Microstructure; *J. Mater. Res.*, 11:169–175 (1996)
91. Bendale, P., Venigalla, S., Ambrose, J. R., Verink, E. D., and Adair, J. H., Preparation of Barium Titanate Films at 55°C by an Electrochemical Method, *J. Am. Ceram. Soc.*, 76:2619–2627 (1993)
92. Ohba, Y., Miyauchi, M., Sakai, E., and Daimon, M., Hydrothermal Synthesis of Lead Zirconate Titanate Thin Films Fabricated by a Continuous-Supply Autoclave, *Jpn. J. Appl. Phys.*, 34:5216–5219 (1995)
93. Chen, Q., Qian, Y., Chen, Z., Wu, W., Chen, Z, Zhou, G., and Zhang, Y., Hydrothermal Epitaxy of Highly Oriented TiO_2 Thin Films on Silicon, *Appl. Phys. Lett.*, 66:1608–1610 (1995)
94. Chen, Q, Qian, Y., Chen, Z., Zhou, G., and Zhang, Y., Hydrothermal Preparation of Highly Oriented Polycrystallization ZnO Thin Films, *Mater. Letts.*, 22:93–95 (1995)
95. Kojiyoshi, K., Tomono, K., Hamaji, Y., and Kasanami, T., Short-Circuit Diffusion of Ba,Sr, and O During $ATiO_3$ (A = Ba, Sr) Thin Film Growth by the Hydrothermal Electrochemical Method, *J. Am. Ceram. Soc.*, 78:1521–1531 (1995)
96. Pilleux, M. E., Grahmann, C. R., Fuenzalida, V. M., and Avila, R., Hydrothermal ABO_3 Ceramic Thin Films, *Appl. Surf. Sci.*, 65/66:283–290 (1993)
97. Fuenzalida, V. M. and Pilleux, M. E., Hydrothermally Grown $BaZrO_3$ Films on Zirconium Metal, Microstructure, XPS and AES Depth Profiling, *J. Mater. Res.*, 10:2749–2754 (1995)
98. Tachibana, K., A New Pressure-Balanced Outer Reference Electrode with Oxidized Zircaloy Tube Container For Corrosion Studies in High-Temperature–High-Pressure Aqueous Solution and Its Application to Obtaining Polarization Curves, *Boshoku Gijutsu*, 34:125–131 (1985)
99. Macdonald, D. D., Scott, A. C., and Wentrcek, P., External Reference Electrodes For Use in High-temperature Aqueous Systems, *J. Electrochem. Soc.*, 126:908–911 (1979)
100. Psaras, P. A. and Langford, H. D., (eds.), *Advancing Materials Research.* p. 274, National Academy Press, Washington, D.C. (1987)

101. Psaras, P. A. and Langford, H. D., (eds.), *Advancing Materials Research.* p. 16, National Academy Press, Washington, D.C.

102. Moroni, A., Caja, V., Egger, E., Pezzuto, V., and Chao, E. Y. In: *Bioceramics, Proc. 5th Int. Symp.Ceramics in Medicine,* (T. Yamamuro, T. Kokubo, and T. Nakamura, eds.), 5:299, Kobunshi Kankokai, Inc. (1992)

103. Fujishiro, Y., Sato, T., and Okuwaki, A., Coating of Hydroxyapatite on Metal Plates Using Thermal Dissociation of Calcium-EDTA Chelate in Phosphate Solutions Under Hydrothermal Conditions, *J. Mater, Sci.: Mater. Med.,* 6:172–176 (1995)

104. Yamashita, K. and Kanazawa, T., Hydroxyapatite, in: Inorganic PhosphateMaterials, (T. Kanazawa, ed.), *Materials Science Monograph 52,* pp. 23-24, Kodansha and Elsevier (1989)

105. Mucalo, M. R., Yokogawa, Y., Toriyama, M., Suzuki, T., Kawamoto, Y., Nagata, F., and Nishizawa, K., Growth of Calcium Phosphate on Phosphorylated Cotton Fibers, *Apatite,* 2:71–73 (1997)

106. Yokogawa, Y., Nagata, F., Toriyama, M., Kawamoto, Y., Suzuki, T., Nishizawa, K., and Mucalo, M. R., HAp Formation on Polymeric Substrate in the Presence of Polyacrylic Acid, *Apatite,* 2:67–70 (1997)

107. Hulbert, S. F. and Dove, J. H., Fatigue Properties of a Polymethylmethacrylate - HAp Composite Bone Cement, *Apatite,* 2:57–60 (1997)

108. Ban, S., Hanaichi, T., and Maruno, S., Microstructure of Electrochemically Deposited Apatite on the HA-G-Ti Composite, *Apatite,* 2L 11–14 (1997)

109. Tenhuisen, K. S., Brown, P. W., Reed, C. S., and Allcock, H. R., Low Temperature Synthesis of a Self-Assembling Composite: HAp-Poly [bis (sodium carboxylatophenoxy) phosphazene], *J. Mater. Sci.: Mater. Med.,* 7:673–682 (1996)

110. HAp Composites Move Closer to Reality, *Bio/Med Technology Alert,* 3(40):4–5 (1997)

111. Höland, W. and Vogel, W., in: An Introduction to Bioceramics, (L. L. Hench, and J. Wilson, eds.), *Adv. Ser. Ceram.* 1:125, World Scientific Publishing Co., Pte. Ltd., London (1993)

112. Höland, W., Rheinberger, V., Frank, M., and Wegner, S., in: Bioceramics, (T. Kokubo, T. Nakamura, and F. Miyaji, eds.), in: *Proc. 9th Int. Symp. Ceramics in Medicine,* p. 445, Otsu, Jpn (1996), Pergamon Press, Oxford, New York (1996)

113. Bonfield, W., Hydroxyapafite-Reinforced Polyethylene as an Analogous Materials for Bone Replacement, in: Bioceramics: Materials Characteristics Versus In Vive Behavior, (P. Ducheyne, and J. Lemons, eds.), *Annals of New York Academy of Science,* pp. 173–177, New York (1988)

DropBooks

114. Bonfield, W., Doyle, C., and Tanner, K. E., In Vivo Evaluation of Hydroxyapatite-Rein forced Polyethylene Composites, in: *Biological and Biological and Biomechanical Performance of Materials,* (P. Christel, A. Meunier, and A. J. C. Lee, eds.), p. 153, Elsevier, New York (1986)

115. Huang, J., Di Silvo, L., Wang, M., Tanner, K. E., and Bonfield, W., In Vitro Mechanical and Biological Assessment of Hydroxyapatite-Reinforced Polyethylene Composite, *J. Mater. Sci. Mater. Med.,* 8:775–779 (1997)

116. Laudise, R. A., *Growth of Single Crystals,* p. 250, Prentice-Hall, Inc., New Jersey (1970)

117. Scheel, H. J., Historical Introduction, in: *Handbook of Crystal Growth,* Vol. 1a:4 (D. T. J. Hurle, ed.) Elsevier Science Publishers B.V., Amsterdam, (1993)

118. Nagata, F., Yokogawa, Y., Toriyama, M., Kawamoto, Y., Suzuki, T., Nishizawa, and Nagae, H., Hydrothermal Synthesis of Plate-Like Hydroxyapatite Crystals, in: Advanced Materials, '93, IIA: Biomaterials, Organic and Intelligent Materials, (H. Aoki, ed.), *Trans. Mat. Res. Soc. Jpn.* Vol.15A, Elsevier Science, B.V. (1994)

119. Fujishiro, Y, Yabuki, H., Kawamura, K., Sato, T., and Okuwaki, A., Preparation of Needle-Like Hydroxyapatite by Homogeneous Precipitation under Hydrothermal Conditions, *J. Chem. Tech. Biotechnol.*, 57:349–353 (1993)

120. Suchanek, W., Suda, H., Yashima, M., Kakihana, M., and Yoshimura, M., Biocompatible Whiskers with Controlled Morphology and Stoichiometry, *J. Mater. Res.*, 10:521–529 (1995)

121. Suchanek, W. and Yoshimura, M., Preparation of Fibrous, Porous Hydroxyapatite Ceramics From Hydroxyapatite Whiskers, *J. Am. Ceram. Soc.*, 81:765–767 (1998)

122. Suchanek, W., Yoshimura, M., Kakihana, M., and Yoshimura, M., β-Rhenanite (β-$NaCaPO_4$) as Weak Interphase for Hydroxyapatite Ceramics, *J. Eur. Ceram. Soc.*, 18:1923–1929 (1998)

123. Suchanek, W., Yashima, M., Kakihana, M., and Yoshimura, M., Hydroxyapatite/Hydroxyapatite Whisker Composites Without Sintering Additives: Mechanical Properties and Microstructural Evolution, *J. Am. Ceram. Soc.*, 80:2805–2813 (1997)

124. Hosoi, K., Hashida, T., Takahashi, H., Yamasaki, N., and Korenaga, T., New Processing Technique for Hydroxyapatite Ceramics by the Hydrothermal Hot-Pressing Method, *J. Am. Ceram. Soc.*, 79:2771–2774 (1996)

125. Hosoi, K., Hashida, T., Takahashi, H., Yamasaki, N., and Korenaga, T., Solidification Behavior of Calcium Carbonate via Aragonite-Calcite Wet Transformation with Hydrothermal Hot Pressing, *J. Mater. Sci.*, 16:382–385 (1997)

126. Hosoi, K., Hashida, T., Takahashi, H., Yamasaki, N., and Korenaga, T., Low Temperature Solidification of Calcium Carbonate Through Vaterite - Calcite Wet Transformation., *J. Mater. Sci. Letts.*, 15:812–814 (1996)

127. Yamasaki, N., Kai, T., Nishioka, M., Yanagisawa, K., and Ioku, K., Porous Hydroxyapatite Ceramics Prepared by Hydrothermal Hot Pressing, *J. Mater. Sci. Letts.*, 9:1150–1151 (1990)

128. Ioku, K., Yanagisawa, K., Kai, T., Yamamoto, K., and Yamasakii, N., Apatite Ceramics, Prepared by Hydrothermal Hot Pressing, in: *Proc. 1st Int. Conf. Solvothermal Reactions*, pp. 118–121, Takamatsu, Jpn. (Dec. 5–7, 1994)

129. Hosoi, K., Korenaga, T., Takahashi, H., Weiping, T., Lei, H., Yanagisawa, K., and Yamasaki, N., Solidification of Carbonate at Low Temperature by HHP Technique, in: *Proc. 1st Int. Conf. Solvothermal Reactions*, pp. 94–97, Takamatsu, Jpn. (Dec. 5–7, 1994)

130. Hosoi, K., Korenaga, T., Hashida, T., Takahashi, H., and Yamasaki, N., Strengthening and Toughening in HHP - Pressed $CaCO_3$ Composite, in: *Proc. 2nd Int. Conf. Solvothermal Reactions*, pp.85–88, Takamatsu, Jpn. (Dec. 18–20, 1996)

131. Sato, K., Hashida, T., Takahasi, H., and Yamasaki, N., Solidification Method for Calcium Aluminate-Phosphate Cement by HHP and Fiber Reinforcement, in: *Proc. 2nd Int. Conf. Solvothermal Reactions*, pp. 89–92, Takamatsu, Jpn. (Dec. 18–20, 1996)

132. Sato, K., Hashida, T., Takahashi, H., and Yamasaki, N., Development of High Strength Calcium Aluminate - Phosphate Cement by Hydrothermal Hot Pressing, *J. Mater. Sci. Letts.*, 16:1464–1468 (1997)

133. Yanagisawa, K., Nishioka, M., Ioku, K., and Yamasaki, N., Densification of Silica Gels by Hydrothermal Hot Pressing, *J. Mater. Sci. Letts.*, 12:1073–1075 (1993)

134. Yanagisawa, K., Ioku, K., and Yamasaki, N., Formation of Anatase Porous Ceramics by HHP of Amorphous Titania Spheres, *J. Am. Ceram. Soc.*, 80:1303–1306 (1997)

135. Ogawa, S., Minamic, S., and Yamasaki, N., Solidification of Sewage Sludge Incinerated Ash by Hydrothermal Hot Pressing, in: *Proc. 1st Int. Conf. Solvothermal Reactions*, pp. 126–129, Takamatsu, Jpn. (Dec. 5–7, 1994)

136. Mori, K., Katakura, M., and Yamasaki, N., Development of Hydrothermal Solidification for Low Level Radioactive Wastes, in: *Proc. 1st Int. Conf. Solvothermal Reactions*, pp. 150–153, Takamatsu, Jpn. (Dec. 5–7,1994)

137. Ioku, K. and Yoshimura, M., Microstructure Designing of Hydroxyapatite Ceramics by HIP Post-Sintering, in: *Hot Isostatic Pressing—Theory and Applications, Proc. 3rd Int. Conf.* (M. Koizumi, ed.) pp. 123–128, Osaka, Jpn. (June 10–14, 1991)

DropBooks

138. Hirota, K., Hasegawa, T., and Monma, H., Densification of Hydroxyapatite by Hot Isostatic Pressing, *Yagyo-Kyokai-Shi*, 90:62–64 (1982)

139. Uematsu, K., Takagi, M., Honda, T., Uchida, N., and Saito, K., Transparent Hydroxyapatite Prepared by Hot Isostatic Processing of Filter Cake, *J. Am. Ceram. Soc.*, 72:1476–1478 (1989)

140. Somiya, S. (ed.) *Advanced Ceramics I.*, pp. 207–243, Elsevier Science Publishers, Amsterdam (1990)

141. Somiya, S. Hydrothermal Reaction Sintering of High-Density Sintered Oxides, in: *Proc. 1st Int. Symp. Hydrothermal Reactions*, pp. 887–903, Jpn. (March 22–26, 1982)

142. Somiya, S., Hydrothermal Reaction Sintering of Oxides, in: *Sintered Metal-Ceramic Composites*, (G. S. Upadhyaya, ed.), pp. 97–105, Elsevier Science Publishers, B. V., Amsterdam (1984)

143. Somiya, S., Hydrothermal Reactions in Inorganic Systems, in: Advanced Materials, 1993, VI/Frontiers in Materials Science and Engineering, (S. Somiya et al., eds.), *Trans. Mat. Res. Soc. Jpn.* 19B:1105–1134 (1994)

144. Toraya, H., Yoshimura, M., and Somiya, S., Densification and Grain Growth in Hydrothermal Reaction Sintering of Hafnia (HfO_2), *Yogyo-Kyokai-Shi*, 91:235–240 (Jpn.) (1983)

145. Pfoff, G. and Feltz, A., Solid State Reactivity and Mechanisms in Oxide Systems. VI. Sintering Behavior of Hematite Prepared by the Hydrothermal Method. *Solid State Ionics.*, 38:25–29 (1990)

146. Yin, S., Fujishiro, Y., Uchida, S., and Sato, T., Low Temperature Sintering and Mechanical Properties of Ceria and Yttria Co-doped Zirconia Crystallized in Supercritical Methanol, in: *Proc. 2nd Int. Conf. Solvothermal Reactions*, pp. 27–30, Takamatsu, Jpn. (Dec. 18–20, 1996)

147. Zhu, W., Wang, C. C., Akbar, S. A., and Asiale, R., Fast-sintering of Hydrothermally Synthesized $BaTiO_3$ Powders and their Dielectric Properties, *J. Mater. Sci.*, 32:4303–4307 (1997)

148. Ruys, A. J., Wei, M., Sorrell, C. C., Dickson, M. R., Brandwood, A., and Milthorpe, B. K., Sintering Effects on the Strength of Hydroxyapatite, *Biomaterials*, 16:409–415 (1995)

149. Suchanek, W., Yashima, M., Kakihana, M., and Yoshimura, M., Hydroxyapatite Ceramics with Selected Sintering Additives, *Bioceramics*, 18:923–933 (1997)

150. Krage, M. K., Microwave Sintering of Ferrites, *Am. Ceram. Soc. Bull.*, 60:1232–1234 (1981)

151. Roy, R., Komarneni, S., and Yang, L. J., Controlled Microwave Heating and Melting of Gels, *J. Am. Ceram. Soc.*, 68:392–395 (1985)

152. Komarneni, S. and Roy, R., Anomalous Microwave Preparation of Mullite Powders, in: *Proc. Mater. Res. Soc. Symp. Microwave Processing of Materials,* (M. H. Brooks, I. J. Chabinsky, and W. H. Sutton, eds.), Vol. 124, *Mater. Res. Soc.*, Pittsburgh, PA (1988)

153. Gedye, R., Smith, F., Westaway, K., Ali, H., Baldisera, L., Laberge, L., and Rousell, J., The Use of Microwave Ovens for Rapid Organic Synthesis, *Tetrahedron Lett.*, 27:279–282 (1986)

154. Gigure, R. J., Bray, T. L., Duncan, S. M., and Majetich, G., Application of Commercial Microwave Ovens to Organic Synthesis, *Tetrahedron Lett.*, 27:4945–4948 (1986)

155. Baghurst, D. R., Mingos, D. M. P., and Watson, M. J., Application of Microwave Dielectric Loss Heating Effects for the Rapid and Convenient Synthesis of Organometallic Compounds, *J. Organomet Chem.*, 368:C43–C45 (1989)

156. Greene, D. L. and Mingos, D. M. P., Application of Microwave Dielectric Loss Heating Effects for the Rapid and Convenient Synthesis of Ruthenium (11) Polypiridine Complexes, *Transition Metals Chemistry*, 16:71–72 (1991)

157. Chatakondu, K., Green, M. L. H., Mingos, D. M. P., and Reynolds, S. M., Application of Microwave Dielectric Loss Heating Effects for the Rapid and Convenient Synthesis of Intercalation Compounds, *J. Chem. Soc., Chem. Commun*, pp. 1515–1517 (1989)

158. US Pat. Application 4778666; Virtuli, V. C., Chu, P., and Dwyer, F. G., *Crystallization Method Using Microwave Radiation* (1988)

159. Arafat, A., Jensen, J. C., Ebaid, A. R., and Van Bekkum, H., Microwave Preparation of Zeolite Y and ZSM-5, *Zeolites*, 13:162–165 (1993)

160. Komarneni, S., Roy, R., and Li, Q.H., Microwave-Hydrothermal Synthesis of Ceramic Powders, *Mater. Res. Bull.*, 27:1393–1405 (1992)

161. Liu, S. F., Abothu, I. R., and Komarneni, S., Barium Titanate Ceramics Prepared From Conventional and Microwave Hydrothermal Powders, *Mat. Letts.*, 38:344–350 (1999)

162. Komarneni, S., Menon, V. C., and Li, Q. H., Synthesis of Ceramic Powders by Novel Microwave-Hydrothermal Processing, in: Ceramic Transactions, Vol. 2, Science, Technology and Commercialization of Powder Synthesis and Shape Forming Processes, (J. J. Kingsley, C. H. Schilling, and J. H. Adair, eds.), pp. 37–46, *Am. Ceramic. Soc.*, Westerville, OH (1995)

163. Komarneni, S., Novel Microwave - Hydrothermal Processing for Synthesis of Ceramic and Metal Powders, in: Novel Techniques in Synthesis and Processing of Advanced Materials, (J. Singh and J. M. Copley, eds.), pp. 103–117, *The Minerals, Metals and Materials Society*, Warrendale, PA (1995)

DropBooks

164. Komarneni, S., Environmentally Benign Microwave-Hydrothermal Processing For Synthesis of Ceramic Powders, in: *Proc. Int. Symp. Environmental Issues of Ceramics,* (H. Yanagida and M. Yoshimura, eds.), pp. 199–206, Ceramic Society of Jpn., Tokyo (1995)

165. Komarneni, S., Pidugu, R., Li, Q. H., and Roy, R., Microwave-Hydrothermal Processing of Metal Powders, *J. Mater. Res.*, 10:1687–1692 (1995)

166. Komarneni, S., Microporous Metal Intercalated Clay Nanocomposites, in: *Ceramic Transactions,* 31:155–168, Porous Materials, (K. Ishizaki, L. Sheppard, S. Okada, T. Hamasaki, and B. Huybrechts, eds.), American Ceramic Society, Westerville, OH (1993)

167. Komarneni, S., Hussein, M. Z., Liu, C., Breval, E., and Malla, P. B., Microwave-Hydrothermal Processing of Metal Clusters Supported In and/or on Montmorillonite, *Eur. J. Solid State Inorg. Chem.*, 32:837–849 (1995)

168. Moon, Y. T., Kim, D. K., and Kim, C. H., Preparation of Monodisperse ZrO_2 by the Microwave Heating of Zirconyl Chloride Solutions, *J. Am. Ceram. Soc.,* 78:1103–1106 (1995)

169. Daichuan, D., Pinjie, H., and Shushan, D., Preparation of Uniform α-Fe_2O_3 Particles by Microwave-Induced Hydrolysis of Ferric Salts, *Mater. Res. Bull.*, 30:531–535 (1995)

170. Daichuan, D., Pinjie, H., and Shushan, D., Preparation of Uniform α - FeO (OH) Colloidal Particles By Hydrolysis of Ferric Salts Under Microwave Irradiation, *Mater. Res. Bull.*, 30:537–541 (1995)

171. Komarneni, S., Li., Q. H., Stefanson, K. M., and Roy, R., Microwave-Hydrothermal Processing For Synthesis of Electroceramic Powders, *J. Mater. Res.*, 8:3176–3183 (1993)

172. Komarneni, S., Menon, V. C., Li, Q. H., Roy, R., and Ainger, F., Microwave-Hydrothermal Processing of $BiFeO_3$ and $CsAl_2PO_6$, *J. Am. Ceram. Soc.*, 79:1409–1412 (1996)

173. D'Arrigo, M. C., Leonelli, C., and Pellacani, G. C., Microwave-Hydrothermal Synthesis of Nanophase Ferrites, *J. Am. Ceram. Soc.*, 81:3041–3043 (1998)

174. Cheng, J. P., Agarwal, D. K., Komarneni, S., Mathis, M., and Roy, R., Microwave Processing of WC-Co Composites and Ferroic Titanates, *Mat. Res. Innovat.*, 1:44–52 (1997)

175. Komarneni, S., Hussein, M. Z., Liu, C., Breval, E., and Malla, P. B., Microwave-Hydrothermal Processing of Metal Clusters Supported In and/or On Montmorillonite, *Eur. J. Solid State Inorg. Chem.*, 32:837–849 (1995)

176. Fang, Yi, Agarwal, D. K., Roy, D. M., and Roy, R., Fabrication of Porous Hydroxyapatite Ceramics by Microwave Processing, *J. Mater. Res.*, 7:490–494 (1992)

177. Fang, Yi, Agarwal, D. K., Roy, D. M., and Roy, R., Microwave Sintering of HAp Ceramics, *J. Mater. Res.*, 9:180–187 (1994)

178. Ehsani, G. N., Ruys, A. J., and Sorrell, C. C., Microwave Sintering of Hydroxyapatite, in: International Ceramic Monographs, Vol.1., (C. C. Sorrell, and A. J. Ruys, eds.), *Proc. Int. Ceram. Conf.*, pp. 714–721 (1994)

179. Shaw, R. W., Brill, T. R., Clifford, A. A., Eckert, C. A., and Franck, E. U., Supercritical Water: A Medium for Chemistry; *Chem. Eng. News*, 69:26–30 (1991)

180. Modell, M., Supercritical Water Oxidation, in: *Standard Handbook of Hazardous Waste Treatment and Disposal*, (H. M. Freeman, eds.), pp. 8.153–8.168, McGraw-Hill, New York (1989)

181. Shanableh, A. and Gloyna, E. F., Supercritical Water Oxidation Waste Waters and Sludges, *Water Sci. Technol.*, 23:389–393 (1991)

182. Peters, W. A., Supercritical Water Technology: Process Systems Research For New Applications, in: *Proc. 2nd Int. Conf. Solvothermal Reactions*, pp. 35–41, Takamatsu, Jpn. (Dec. 18–20, 1996)

183. Yoshioka, T., Hasame, A., Watanabe, S., Shin, S. M., and Okuwaki, A., Determination of Oxalic Acid and Benzene Carboxylic Acids From PVC Materials by Oxygen-Oxidation in NaOH Solutions at Elevated Temperatures, in: *Proc. 2nd Int. Conf. Solvothermal Reactions*, pp. 46–49, Takamatsu, Jpn. (Dec. 18–20, 1996)

184. Smith, R. L., Jr., Atmaji, P., Hakuta, Y., Adschiri, T., and Arai, K., Hydrothermal Crystallization of Metals From Simulated High Level Liquid Waste, in: *Proc. 2nd Int. Conf. Solvothermal Reactions*, pp. 50–53, Takamatsu, Jpn. (Dec. 18–20, 1996)

185. Smith, R. L., Jr., Atmaji, P., Hakuta, Y., Adschiri, T., and Arai, K., Hydrothermal Crystallization of Metals From Simulated High Level Liquid Waste, in: *Proc. 2nd Int. Conf. Solvothermal Reactions*, pp. 42–45, Takamatsu, Jpn. (Dec. 18–20, 1996)

186. Hashida, T. and Takahashi, H., Development of Solvothermal Methods for Recycling Concrete Wastes, in: *Proc. 2nd Int. Conf. Solvothermal Reactions*, pp. 152–155, Takamatsu, Jpn. (Dec. 18–20, 1996)

187. Yamasaki, N. and Yamasaki, Y., Hydrothermal Decomposition of Chlorinated Organic Compounds, in: *Proc. 2nd Int. Conf. Solvothermal Reactions*, pp. 139–142, Takamatsu, Jpn. (Dec. 18–20, 1996)

188. Ross, D. S., Jayaweera, I., and Leif, R., Assisted Hydrothermal Oxidation—A Proposed On-Site Disposal Technology for Halogenated Waste, in: *Proc. 2nd Int. Conf. Solvothermal Reactions*, pp. 144–147, Takamatsu, Jpn. (Dec. 18–20, 1996)

189. Yamasaki, N., Yanagisawa, K., and Fujita, M., Hydrothermal Decompostion of Chlorofluorocarbous; CFC 11 and CFC 113, in: *Proc. 1st Int. Conf. Solvothermal Reactions*, pp.134–141, Takamatsu, Jpn. (Dec. 5–7, 1994)

DropBooks

190. Savage, P. E., Reaction Models for Supercritial Water Oxidation Processes, *Proc. 2nd Int. Conf. Solvothermal Reactions,* pp. 2–4, Takamatsu, Jpn. (Dec. 18–20, 1996)

191. Nakahara, M., Yamaguchi, T., and Ohtaki, H., The Structure of Water and Aqueous Electrolyte Solutions Under Extreme Conditions; *Recent Res. Devel. Phys. Chem.,* 1:17–49 (1997)

192. Ohataki, H., Radnai, T., and Yamaguchi, T., Structure of Water Under Subcritical and Supercritical Conditions Studied by Solution X-ray Diffraction, *Chem. Soc. Rev.,* pp. 41–51 (1997)

193. Nakahara, M., Matubayasi, N., and Wakai, C., NMR Study of Hydrogen Bonds and Water Structure in Super- and Subcritical Conditions, in: *Proc. 2nd Int. Conf. Solvothermal Reactions,* pp. 9–12, Takamatsu, Jpn. (Dec. 18–20, 1996)

194. Adschiri, T., Malaluan, R., Machida, K., Sato, O., and Arai, K., Waste Polymer Conversion to Chemicals in Supercritical Water, in: *Proc. 1st Int. Conf. Solvothermal Reactions,* pp.138–141, Takamatsu, Jpn. (Dec. 5–7, 1994)

195. Laudise, R. A., Green Matls.: Industrial Ecology; In: *Materials Science and Engineering Serving Society,* (S. Somiya, R. P. H. Chang, M. Doyama, and R. Roy, eds.), Elsevier Science B. V., The Netherlands, pp. 23–27 (1998)

196. Yoshimura, M., Importance of Soft Solution Processing For Advanced Inorganic Materials, *J. Mater. Res.,* 13:796–802 (1998)

197. Ishida, E. H., Environmentally Friendly Manufacturing, Processing and Materials, (Personal Communication) (1998)

198. Murota, T., Economy of Entropy and Energy, *Toyo Keizai Shinposha Ltd.,* Tokyo, (in Japanese) (1983)

199. Yoshimura, M., What, Why, and How Soft and Solution Processing for Ceramics?, in: *Proc. World Conf. The Role of Advanced Matle. In Sustainable Development,* pp. 389–397, Seoul, Korea (Sept. 1–6, 1996)

200. Baijal, M. D., *Plastic Polymer Science and Technology,* John Wiley and Sons, New York (1982)

201. Higgins, R. A., *Engineering Metallurgy,* Edward Arnold, London (1993)

202. Kingery, W. D., Bowen, H. K., and Uhlmann, D. R., *Introduction to Ceramics,* John Wiley and Sons, New York (1976)

203. Ring, R. A., *Fundamentals of Ceramic Powder Processing and Synthesis,* Academic Press, San Diego (1996)

204. Ohring, M., *The Materials Sci. of Thin Films,* Academic Press (1992)

205. Morosanu, C. E., *Thin Films by Chemical Vapor Deposition,* Elsevier, Amsterdam (1990)

206. Parker, E. H. C., *The Technology and Physics of Molecular Beam Epitaxy*, Plenum Press, New York (1985)

207. *JANAF Thermochemical Tables*, National Bureau of Standards, American Chemical Society, American Institute of Physics, (1968–1982)

208. Pamplin, B. R., (ed.) *Crystal Growth*, Pergamon Press, Oxford, UK (1980)

209. Jelinski, L. W., Graedal, T. E., Laudise, R. A., McCall, D. W., and Patel, C. K. N., Industrial Ecology: Concepts and Approaches, in: *Proc. Natl. Acad. Sci.*, 89:793–797 (1992)

210. Graedel, T. E. and Allenby, B. R., *Industrial Ecology*, Prentice Hall, Englewood Cliffs, New Jersey (1995)

211. Itoh, T. Hori. S., Abe, M., and Tamaura, Y., *J. Appl. Phys.*, 69:5911 (1991)

212. Roy, R., Accelerating the Kinetics of Low-Temperature Inorganic Syntheses, *J. Solid State Chem.*, 111:11–17 (1994)

213. Marsh, H., Heintz, E. A., and Rodriguez-Reinoso, F., *Introduction to Carbon Technologies*, Publications in Spain, p. 67 (1997)

214. Kasivisweswari, V., Catalytic Decomposition of Phenols using Impregnated Activated Carbon, M. Sc., Dissertation, Univ. of Mysore, India (1999)

215. Muralidhar, Catalytic Decomposition of Nitroarenes using Impregnated Activated Carbon, M. Sc., Dissertation, Univ. of Mysore, India (1999)

216. Feng, Q., Yanagisawa, K., and Yamasaki, N., Synthesis of Manganese Oxides with Tunnel Structure by Hydrothermal Soft Chemical Process, in: *Proc. 2nd Int. Conf. Solvothermal Reactions*, pp. 235–238, Takamatsu, Jpn. (Dec. 18–20, 1996)

217. Feng, Q., Honbu, C., Yanagisawa, K., and Yamasaki, N., Synthesis of Lithiophorite by Hydrothermal Soft Chemical Process, in: *Materials Science and Engineering Serving Society*, (S. Somiya, R. P. H. Chang, M. Doyama, and R. Roy, eds.), pp. 121–124, Elsevier Science B.V., The Netherlands (1998)

218. Feng, Q., Sun, E. H., Yanagisawa, K., and Yamasaki, N., Synthesis of Birnessite-Type Sodium Manganese Oxide and The Behavior Under Hydrothermal Conditions, in: *Materials Science and Engineering Serving Society*, (S. Somiya, R. P. H. Chang, M. Doyama, and R. Roy, eds.) pp. 125–128, Elsevier Science B.V., The Netherlands (1998)

219. Demazeau, G., The Solvothermal Synthesis: A Way To A New Chemistry, in: *Proc. International Workship on Soft and Solution Processing for Advanced Inorganic Materials*, pp. 4–12, Tokyo Institute of Technology, Jpn. (Feb. 22–27, 1996)

220. Demazeau, G., Solvothermal Synthesis: A Way for Stabilizing New Materials, in: *Proc. 2nd Int. Conf. Solvothermal Reactions*, pp. 126–130, Teakamatsu, Jpn. (Dec. 18–20, 1996)

DropBooks

221. Roy, D. M., Concrete, the Gigaphase Ceramic: Its Key Role in Environmentally-Friendly Technology, in: *Materials Science and Engineering Serving Society*, (S. Somiya, R. P. H. Chang, M. Doyama, and R. Roy, eds.), pp. 81–88, Elsevier Science, B. V., The Netherlands (1988)

222. Yamasaki, N., Possibility of Materials Recycling Using Hydrothermal Process, in: *Materials Science and Engineering Serving Society*, (S. Somiya, R. P. H. Chang, M. Doyama, and R. Roy, eds.), pp. 107–112, Elsevier Science, B.V., The Netherlands (1988)

223. Yoshioka, T., Sato, T., and Okuwaki, A., Hydrolysis of Water PET by Sulfuric Acid at 150°C For a Chemical Recycling, *J. Appl. Polymer Sci.*, 52:1353–1355 (1994)

224. Yamasaki, N., Recovery Process of Human Waste to Energy Resource Using Hydrothermal Technology, in: *Proc. World Conf. on the Role of Advanced Materials in Sustainable Development*, pp. 199-205, Seoul, Korea (Sept. 1–6, 1996)

225. Kugimiya, K., Ceramics For The Next Millennium, in: *Materials Science and Engineering Serving Society*, (S. Somiya, R. P. H. Chang, M. Doyama, and R. Roy, eds.), pp. 28–33, Elsevier Science, B. V., The Netherlands (1988)

Acknowledgments

Figure 1.1. Courtesy of the American Geophysical Union, Washington, DC.

Figure 1.4. Courtesy of the American Geophysical Union, Washington, DC.

Figure 1.5. Courtesy of the American Geophysical Union, Washington, DC.

Figure 2.4. Courtesy of the American Chemical Society, Washington, DC.

Figure 2.7. Courtesy of the VEB Deutscher Verlag, Germany.

Figure 3.5. Courtesy of the Elsevier Science Publishers, Oxford, UK.

Figure 3.13. Courtesy of the American Chemical Society, Washington, DC.

Figure 3.16. Courtesy of the Elsevier Science Publishers, Oxford, UK.

Figure 3.17. Courtesy of the Clarendon Press, Oxford, UK.

Figure 3.20a. Courtesy of the Elsevier Science Publishers, Oxford, UK

DropBooks

Figure 3.20b. Courtesy of the American Institute of Physics, Washington, DC.

Figure 3.21. Courtesy of the Elsevier Science Publishers, Oxford, UK.

Figure 3.23. Courtesy of the Kluwer Academic /Plenum Publishers, New York.

Figure 3.24a. Courtesy of the Kluwer Academic /Plenum Publishers, New York.

Figure 3.24b. Courtesy of the American Chemical Society, Washington, DC.

Figure 3.26. Courtesy of the Kluwer Academic /Plenum Publishers, New York.

Figure 3.30. Courtesy of the American Chemical Society, Washington, DC.

Figure 3.31. Courtesy of the American Chemical Society, Washington, DC.

Figure 3.34. Courtesy of the Materials Research Society of Japan.

Figure 3.36. Courtesy of the Kluwer Academic /Plenum Publishers, New York.

Figure 4.4. Courtesy of the Elsevier Science Publishers, Oxford, UK.

Figure 4.10. Courtesy of the American Ceramic Society, Westerville, Ohio.

Figure 5.1. Courtesy of the Akademische Verlagsgesellschaft, Germany.

Figure 5.3. Courtesy of the Wiley Interscience Publications, New York.

Figure 5.8. Courtesy of the Elsevier Science Publishers, Oxford, UK.

Figure 5.9. Courtesy of the American Chemical Society, Washington, DC.

Figure 5.10. Courtesy of the NRC Research Press, Ottawa, Canada.

Figure 5.11. Courtesy of the NRC Research Press, Ottawa, Canada.

Figure 5.13. Courtesy of the American Chemical Society, Washington, DC.

Figure 5.36. Courtesy of the Akademische Verlagsgesellschaft, Germany.

Figure 5.37. Courtesy of the Elsevier Science Publishers, Oxford, UK.

Figure 5.38. Courtesy of the Elsevier Science Publishers, Oxford, UK.

Figure 5.39. Courtesy of the Elsevier Science Publishers, Oxford, UK.

Figure 5.41. Courtesy of the Elsevier Science Publishers, Oxford, UK.

Figure 5.44. Courtesy of the Elsevier Science Publishers, Oxford, UK.

Figure 5.46. Courtesy of the Elsevier Science Publishers, Oxford, UK.

Figure 5.47. Courtesy of the Nippon Seramikkusu Kyokai, Tokyo.

Figure 5.48. Courtesy of the Elsevier Science Publishers, Oxford, UK.

Figure 5.51. Courtesy of the Elsevier Science Publishers, Oxford, UK.

Figure 5.53. Courtesy of the Elsevier Science Publishers, Oxford, UK.

Figure 5.54. Courtesy of the Elsevier Science Publishers, Oxford, UK.

Figure 6.2. Courtesy of the Wiley Interscience Publications, New York.

Table 6.3. Courtesy of the Elsevier Science Publishers, Oxford, UK.

Table 6.4. Courtesy of the Wiley Interscience Publications, New York.

Figure 6.3b. Courtesy of the American Chemical Society, Washington, DC.

DropBooks

Figure 6.6. Courtesy of the American Chemical Society, Washington, DC.

Table 6.10. Courtesy of the Academic Press, London, UK.

Figure 6.11. Courtesy of the Royal Society of Chemistry, Cambridge, UK.

Figure 6.12. Courtesy of the Royal Society of Chemistry, Cambridge, UK.

Figure 6.13. Courtesy of the Royal Society of Chemistry, Cambridge, UK.

Figure 6.14. Courtesy of the Royal Society of Chemistry, Cambridge, UK.

Figure 6.15. Courtesy of the Academic Press, London, UK.

Table 6.16. Courtesy of the Academic Press, London, UK.

Figure 6.28. Courtesy of the American Chemical Society, Washington, DC.

Figure 6.29. Courtesy of the Elsevier Science Publishers, Oxford, UK.

Figure 6.30. Courtesy of the Elsevier Science Publishers, Oxford, UK.

Figure 6.31. Courtesy of the Elsevier Science Publishers, Oxford, UK.

Figure 6.32. Courtesy of the Elsevier Science Publishers, Oxford, UK.

Figure 6.33. Courtesy of the American Chemical Society, Washington, DC.

Figure 6.34. Courtesy of the American Chemical Society, Washington, DC.

Figure 6.35. Courtesy of the American Chemical Society, Washington, DC.

Figure 6.36. Courtesy of the American Chemical Society, Washington, DC.

Figure 6.37. Courtesy of the American Chemical Society, Washington, DC.

Figure 6.38. Courtesy of the Royal Society of Chemistry, Cambridge, UK.

Figure 6.42. Courtesy of the American Chemical Society, Washington, DC.

Figure 6.43. Courtesy of the American Chemical Society, Washington, DC.

Figure 6.44. Courtesy of the American Chemical Society, Washington, DC.

Figure 6.45. Courtesy of the American Chemical Society, Washington, DC.

Figure 6.46. Courtesy of the American Chemical Society, Washington, DC.

Figure 6.48. Courtesy of the Wiley Interscience Publications, New York.

Figure 6.49. Courtesy of the Wiley Interscience Publications, New York.

Figure 7.17. Courtesy of the IUCr.

Figure 7.18. Courtesy of the American Institute of Physics, Washington, DC.

Figure 7.27. Courtesy of the American Institute of Physics, Washington, DC.

Figure 7.28. Courtesy of the Elsevier Science Publishers, Oxford, UK.

Figure 7.30. Courtesy of the Elsevier Science Publishers, Oxford, UK.

Figure 7.32. Courtesy of the Elsevier Science Publishers, Oxford, UK.

Figure 7.38. Courtesy of the Elsevier Science Publishers, Oxford, UK.

Figure 8.1. Courtesy of the Elsevier Science Publishers, Oxford, UK.

Figure 8.2. Courtesy of the Elsevier Science Publishers, Oxford, UK.

DropBooks

Figure 8.3. Courtesy of the Wiley Interscience Publications, New York.

Figure 8.4. Courtesy of the Wiley Interscience Publications, New York.

Figure 8.5. Courtesy of the Springer-Verlag, Germany.

Figure 9.1. Courtesy of the Springer-Verlag, Germany.

Figure 9.3. Courtesy of the Springer-Verlag, Germany.

Figure 9.8. Courtesy of the Prentice Hall Inc. New Jersey, USA.

Figure 9.18. Courtesy of the Elsevier Science Publishers, Oxford, UK.

Figure 9.19. Courtesy of the American Chemical Society, Washington, DC.

Figure 9.21. Courtesy of the Kluwer Academic /Plenum Publishers, New York.

Figure 9.28. Courtesy of the Elsevier Science Publishers, Oxford, UK.

Figure 9.30. Courtesy of the Nippon Seramikkusu Kyokai, Tokyo.

Figure 9.31. Courtesy of the American Chemical Society, Washington, DC.

Figure 9.32. Courtesy of the Elsevier Science Publishers, Oxford, UK.

Table 10.4. Courtesy of the American Ceramic Society, Westerville, Ohio.

Table 10.6. Courtesy of the Kluwer Academic /Plenum Publishers, New York.

Table 10.7. Courtesy of the Materials Research Society, USA.

Table 10.8. Courtesy of the Materials Research Society, USA.

Figure 10.8. Courtesy of the American Ceramic Society, Westerville, Ohio.

Figure 10.9. Courtesy of the American Ceramic Society, Westerville, Ohio.

Figure 10.20. Courtesy of the Kluwer Academic /Plenum Publishers, New York.

Figure 10.23. Courtesy of the Kluwer Academic /Plenum Publishers, New York.

Figure 10.33. Courtesy of the Elsevier Science Publishers, Oxford, UK.

Figure 10.34. Courtesy of the Kluwer Academic /Plenum Publishers, New York.

Figure 10.35. Courtesy of the Kluwer Academic /Plenum Publishers, New York.

DropBooks

Index

Acentric hydrated niobium oxyfluoride 632
Acid solutions 701
Acid-base and Metal-aqua Complexes interactions 544
Acid-base Interactions 543
Acoustic wave stimulation 147
Activated complex theory 173
Activation energy 184, 252
ADC. *See* Analog-to-digital converter
Aging (ripening) period 340
Aging of hydrogel in zeolite synthesis 345
Aging zeolite 342
Alcothermal 8
Alkali aluminosilicates 15
Alkali borates
  morphology 573
Alkali molar ratio 738
Alkali rare earth fluorides 619
Alkali rare earth tungstates 639
Alkali silicates
  hydrothermal synthesis 432
Alkali solutions 701
Alkali titanates 660
  flux method 656
  melt technique 655
Alkali zirconium fluorides 619, 626
Alkaline carbonates 630
Alkaline-earth metals 729
Alkaline-earth titanates 762, 768
  perovskite type 777
  preparation 771
Alkalinity 350
Alkylammonium cations 332
Alkylammonium ions 332
$AlPO_4$. *See* Berlinite
$AlPO_4$ crystals 236
  piezoelectric properties 246
Aluminate ions 708
Alumino-silicates 316
Aluminophosphate hydrates 329
Aluminophosphate zeolites 318, 332, 377, 519
  crystallization 378

Aluminosilicate sodalite 374
single crystals 376
Aluminosilicate-based zeolites 461
Aluminum orthophosphate 231
Aluminum phosphates 248
Ammonium phases
growth 628
Ammonothermal synthesis
autoclave 135
Amphoteric oxides 351
Amygdales
Felspars 315
Analcime 57
Analog-to-digital converter 98
Anatase porous ceramics 802
Anhydrous aluminosilicates 469
Anhydrous ceramic oxides 808
Anionic groups 443
Anionic species 434
Anisotropic single-centered
fluorides 623
Antimonates 731
field of synthesis 732
Apatite 287, 289
crystallochemical stability 291
geochemical stability 291
phase stability 291
Apophyllite 327, 331
Aqueous caustic soda 375
Aqueous media 348
Aqueous systems 179
Arrhenius activation energies 180
Arsenates 419, 680
Arsenic sulfohalides 674
Asymmetric membranes 383
AT cut
piezoelectric characteristics 256
Atlas of Zeolite Structure Types 319
Autoclave
attack 113
design 101
design advances 143
externally heated 116
Grey-Loc sealing 202
laboratory size 202
Morey type 563
proper shielding 149
selection 84, 89
stainless steel 681
AWS 147

Balance system 119
Ball mills 147
Barium ferrite
synthesis 736
Barylite crystals 483
Base metal thermocouples 97
Bastnaesite 630
$BaTiO_3$ particles
nucleation rate 766
BAW 577. *See also* Bulk acoustic
wave
Belt apparatus 117
Berghoff autoclaves 129
Berlinite 223, 224, 225
electric constant 247
high annealing temperature 242
solubility data 125
α-Berlinite
growth rate 235
Berlinite crystals
first successful growth 224
hydrothermal growth 231
important modifications 231
nutrient 231
piezoelectric measurements 224
synthesis 232
Berlinite samples
growth defects 241
Beryl
artificial crystal growth 475
first patent 476
hydrothermal growth 480
Beryllium bearing silicates 483

DropBooks

Bioactive glass ceramics 792
Bioceramics
  area of growth 774
  first used 773
  physicochemical advantages 774
Biohydrothermal research 29
Biomimetic 821
Biron synthetic emerald 479
Bismuth silicates
  fields of crystallization 471
  process of formation 471
Bismuth sulfohalides 674
Boehmite 377
Borate crystals
  hydrothermal growth 576
Borates 572, 573
  properties 591
Boron 14
Bourdon gauge 112
Bowen's Reaction Principle 61
Bridenbaugh 619
Bridgman autoclave 202
Bridgman high-pressure
    autoclave 113
Bridgman technique 577
BSO crystals 471
Building units 323
Bulk acoustic wave 576

$CaCO_3$ 273. *See also* Calcite
Calcite
  optically pure variety 273
  solubility curves 275
Calcite crystals 274
  growth 284
  organic salt solutions 275
Calcite single crystals
  growth 281
  large autoclaves 280
  significant material 273
Calcium phosphate bone cements
  advantages 776
  applications 776
  disadvantages 776
Calculation process
  automation 170
Cancrinites 327, 348
Carbonate ions 427, 708
Catalysts
  stabilized ceria based 742
  stabilized yttria based 742
  stabilized zirconia based 742
Catalytic activity 400
Catalytic monoliths 383
Catalytic oxidation 392
Cavansite 328
Cd system 515
CdS crystals
  growth 670
Ceramic densification processes 803
Ceramic processing 28, 39, 817
Ceramic solids
  preparing and processing 755
Ceramic thin films
  fabrication 822
Ceramics 755, 818
Chabazite 316
Chalcohalides 672
Change in temperature 380
Channel systems 316
Chemical precipitation 736
Chemical properties of HAp 287
Chemical sensors 383
Chemical vapor deposition
    methods 695
Cloverite 401
Co-precipitation 821
Coesite
  structural changes 424
Cold-cone seal 109
  autoclaves 107
Complex arsenates 681
Complex coordinated complexes
  hydrothermal conditions 593

Complex coordinated compounds
growth 681
Complex coordinated crystals
growth 415
hydrothermal synthesis 415
Complex sulphide 672
Composite materials 785
Composites
man-made 785
natural 785
Compositional structural range
Molecular Sieves 328
Computer algorithm
insight 170
Cone closure 106
Cone-in-cone seal 106
Controlling techniques 222
Conventional autoclave designs 101
Copper diarsenates 681
synthesis 681
Copper molybdates 649
Corrosion 41, 85
resistance 89, 94
Corundum
hydrothermal synthesis 707
Corundum crystals
effect of temperature 184
effects of filling and temperature gradient 184
effects of seed orientation 184
hydrothermal conditions 709
Coulometric technique 705
Criolite 627
α-Cristobalite
advantages 211
Crystal
chemical problems 421
chemistry 416
growth 416
seed quality 209
sizes 342, 365
solubility growth rate 235
structure of fluorapatite 291
type 203
Crystal growth 82, 120, 161, 365
3d transition metal fluorocarbonates 629
alkaline earth 629
atomic structure 546
composite gradient method 232
macromorphology 546
melt technique 577
reverse temperature gradient method 233
seeds 234
slow heating method 232
solubility 546
solubility data 565
Crystalline phases 424
Crystallization 692
of aluminates 729
of copper 693
of HfO_2 714
of paratellurite 716
of selenium 693
of silver 693
of tellurium 693
phase diagrams 425
Crystallization kinetics 185
Crystallization of $AlPO_4$ 239
Crystallization of hydrous silicate liquids 62
Crystallization of NiCO3 285
Crystallization of PbTiO3 771
Crystallization of perovskite 765
Crystallization of rhodochrosite crystals 285
Crystallization phase
structure change 432
Crystallization process 162
Crystallization reaction 231
Crystallizing zeolite 339
Crystals 184, 580
hydrothermal growth 161, 182
methodology of growth 164
yttrium orthovanadate 562
Cuprite monocrystals
growth 702

DropBooks

CVD diamond 695
CZ growth
  rate 577
Cz-grown crystals 472
Czochralski technique 562

Darkening of KTP crystals 267
Debye-Hückel theory 178
Defects
  study of 219
Degree of polymerization 642
Degree of silification 457, 491
Dehydrated zeolites 317
Dendritic magnetite crystals 727
Diagenesis process 284
Diamond
  anvil system 117
  crystal growth 699
  hydrothermal conditions 695
Diamond synthesis 694, 698
  capsules 697
  processes 695
Dielectric constant of water 178
Dipyramidal crystals 488
Dissolution in melts 562
Dissolution of berlinite 229
Dissolution of calcite 281
Dissolution-precipitation reaction
    mechanism 769
Dissolution-reprecipitation
    mechanism 771
Ditelluride
  synthesis 676
Dselenide
  synthesis 676
Ductile engineering ceramics 755

Ea. *See* Activation energy
Earliest synthetic zeolites 340
Earth ceramics 824
Ecologically clean technologies 399
Edingtonite 365
Electrical conductance
    measurements 132
Electrolytes
  thermodynamic properties 176
Electrolytic cell pressure 134
Elpasoite
  K_2NaAlF_6 627
Emerald
  hydrothermal synthesis 479
Emulsions 821
Enthalpy 174
Environmental safety 3
Epistolite 654
Equilibria
  hydrothermal phase 620
Equilibrium constant
  enthalpy and entropy 171
Equilibrium during
    crystallization 345
Ethane oxidation 401
EXAFS 179
Experimental petrology 42

Faujasite zeolites 344
Fe_3O_4 particles 727
Felspars 316, 469
  recrystallization 56
Felspathoids 316
Ferrites 736
Ferroic titanates 813
Ferromagnetic interactions 635, 740
Ferromagnets 74
Fibrous HAp 794, 800
Film formation 778
Film-constituting elements
  transport mechanism 779
Filter-cake method 803
Fine powders
  hydrothermal preparations 757
Fluorescence
  lifetime 626

Fluoride ions 401
Fluorides 618, 619
Fluorine 14
Fluorine-bearing systems 15
Fluoroarsenates 619
Fluorocarbonates 619, 633, 634
  hydrothermal synthesis 629
Fluoroniobates 679
Fluorophosphates 619, 633
  hydrothermal synthesis 629, 631
  oxyfluorinated 631
Fluorotantalates 679
Flux 562
  technique 259
Formation of HAp
  hydrothermal reaction 297
Formation of nuclei 359
Formation of spontaneous
    nuclei 282
Framework structure
  mixed 459
Framework structures 320
Fumed silica 335
Furnace windings
  alloys used 97

Gadolinium 621
Gallium orthophosphate 248
Gallium phosphates 248
Galvanostatic electrolysis 134
$GaPO_4$
  dielectric constant 255
  growth rate 254
α-$GaPO_4$
  crystallization processes 250
Garnets 734
  hydrothermal growth 735
Gehlenite 491
Gel aging 344
  at room temperature 345
Geochemical processes and
    phenomena 20
Geoscience
  hydrothermal synthesis 56
Geothermal reactor 17
  merit of cost 18
Germanate system 513
  phase formation 499
Germanates 418, 421, 422, 533
  alkali alumino 516
  alkali gallium 516
  antimony 516
  barium germanate 516
  growth 498
  lead 516
  lithium 517
  neobium 516
  physical properties 516
  structural elucidation 502
  titano 516
Germanium
  natural compounds 498
Gibbs energy minimization 171
Gismondine 328
Glass vessel
  advantages 102
  disadvantages 102
Global environment 815
Glycothermal 8
Gmelinite 380
Gold crystallization
  first attempt 692
Gold solubility 693
Green materials 815
Greigite 671, 672
Grey-loc sealing 74
Growing crystals
  Hydrothermally 622
Grown crystal
  nutrient quality 211
Growth
  berlinite 225
  beryllium 703
  borates 591
  calcite 276, 279, 284

DropBooks

corundum 707
HAp crystals 290
HfO_2 714
KTP 265, 269
otavit 285
α-quartz 202
quartz 89, 215
spherocobaltite 285
Growth kinetics 695
Growth rate 208

HA whisker-reinforced composites 792
Hackmanite 375
Hafrium oxides 712
HAp
ceramics 774, 793
clinical applications 786
coatings 786
film 786
preparation 289
HAp crystals 297
hydrothermal conditions 795
morphology 797
HAp powders 786
preparation techniques 775
HAp single crystals
growth rate measurement 298
preparation 295
HAp whiskers 800
preparation 795
HAp-based bioceramics 777
HAp-based composites 791
HAp-bioceramics 775
HAp/collagen composites
fabrication 793
Helgeson-Kirkham-Flowers equation 21
Hemioxide of cuprite
solubility 702
Heptane 390
Heterogeneous nucleation 769
HHP 802. *See also* Hydrothermal hot pressing
High pressure autoclaves 117
High-pressure technology 694
History of hydrothermal technology 63
History of petrology 61
Homogeneous nucleation 769
HPHT water condition 697
Hydration shell water 643
Hydrogen 89
Hydrogen ions 174
Hydrometallurgy 27, 143
Hydrophilic NaX 398
Hydrophobic silicate 398
Hydrothermal alteration 3
Hydrothermal apparatus 82
Hydrothermal autoclave 59, 84, 132, 140, 149
characteristics 83
commonly used 83
Hydrothermal bomb 59, 133
Hydrothermal cell
stainless steel container 121
teflon lining 121
Hydrothermal chemistry 176
Hydrothermal conditions 777
effects 284
pressure balance 115
stability diagrams 767
Hydrothermal crystal growth 94, 213, 281
advantages 27
Hydrothermal crystallization
processes 129
systematic study 514
Hydrothermal decomposition 3, 801, 814
Hydrothermal dehydration 3
Hydrothermal deposition method 778
Hydrothermal ecosystems 19
Hydrothermal electrochemical reaction 3

Hydrothermal experiments
pressure 97, 99
solutions 173
temperature 97
Hydrothermal extraction 3, 64
Hydrothermal flow reactors 143
Hydrothermal fluids 20
Hydrothermal growth 3, 7, 43, 539
of crystals 74, 166
physical chemistry 161
Hydrothermal hot pressing 40, 284, 774, 802
Hydrothermal KTP
average growth rates 268
Hydrothermal laboratory 111, 149
Hydrothermal leaching 801
Hydrothermal metamorphism 3
Hydrothermal method 166, 289, 290, 332, 538, 700, 718, 736
Hydrothermal mineralizer 9
Hydrothermal ore deposits
conditions of formation 170
Hydrothermal oxidation of metals 762
Hydrothermal phase equilibria 3, 27
Hydrothermal physical chemistry 161
experimental results 176
pioneers in the field 75
understanding of theory 176
Hydrothermal process 754, 771
development 9
Hydrothermal processing of ceramics
advantages 757
disadvantages 758
Hydrothermal reaction
cell 121
in ceramics 756
kinetics 147
sintering 3, 804
Hydrothermal research 60, 101
development 58
development trends 70
first publication 54
future 43
journals 34
key tools 109
research publications 35
reviews and edited books 3
Hydrothermal researchers 66
Hydrothermal sintering 3, 774, 801
Hydrothermal solutions 171
viscosity 177
Hydrothermal synthesis 3, 7, 763, 778
fluorides, sulphides, tungstates, titanates 618
Hydrothermal system 163
black box nature 38
disadvantage 37
important constituent 14
organics 42
Hydrothermal technique 1, 28, 42, 57, 75, 198, 259, 691, 702, 754, 821
adaptability 39
flexibility 39
Hydrothermal technology 60, 74, 82, 161, 813
commercial application 2
early history 53
new trend 814
Hydrothermal treatment 3
Hydrothermal waves 162
Hydrothermal-electrochemical film formation 778
Hydrothermal-electrochemical method 132
Hydrothermal-electrochemical reactions 134
Hydrous aluminosilicates 469
Hydrous silicate melt
boron 14
Hydroxide crystals 701
Hydroxide precursor 767

DropBooks

Hydroxy borate ion
formation 580
Hydroxy polymeric cations 42
Hydroxyapatite 299
field of stablility 291
Hydroxyapatite bioceramics
sintering effects 808
Hydroxyapatite particles
preparation of 185
Hydroxyl molybdates 647

I.B.E. *See* Ion Beam Etching
In situ reaction mechanism 769
Incubation period 359
Incubation time 359
Induction time 350
Industrial chemical etching
process 222
Industrialization 815
Inorganic materials 817
Intrazeolite sulfides 391
Ion beam etching 222
Ion diffusion
synthesis of xonotlite
whiskers 127
Ion solvent interactions
configurational aspects 179
Ionic conductivity 459
Ionization
hydrothermal conditions 178
Iron oxide powders
preparation methods 727
Iron vanadate 572
Isomorphous 400
Isothermal chemical reaction 164
Isothermal zone 97

Kagom lattices 631
Kaolinite 375
Kinetics of crystallization 376
Koechlinite 648

KTA 269. *See also* Potassium
titanyl arsenate
KTA crystals
flux grown 270
ideal morphology 270
ionic conductivity 272
stability 272
$KTiOPO_4$ 256. *See also* Potassium
titanyl phosphate
KTP. *See* $KTiOPO_4$
application 259
conversion efficiency 257
KTP crystals
hydrothermal growth 261
properties 269
structural analogs 272

Lack of solubility data 226
Lanthanide ions 642
Lanthanides 453
Lanthanum coordination
polyhedra 630
Lanthanum series 429
Lanthanum tungstates 642
Large pore zeolites 398
Laser crystals
semiconductor laser pumping 619
Laser fluorides
single-centered 622
Laser Raman 139
Lattice parameter values 272
LBO crystals
solubility curves 583
Lead apatite 287
Lead fluoride 632
Lead sulphide 669
Lead zirconate titanate
morphological control 184
size 184
LiCl solutions 495
Liner
pressure imbalance 93

Liquid phase deposition 821
LISICON 517
Lithium aluminium silicate
system 495
Lithium metagallate 663
Lithium silicates
hydrothermal synthesis 497
Lithium tetraborate 576
Low-temperature inorganic
syntheses 363

Magnetite
hydrothermal synthesis 727
Malachite
kinetic curves 190
solubility 190
synthesis 165
Manganese ferrites
synthesis 738
Marangoni convection 162
Material processing 82
Measuring reaction rates 121
Melt growth method 290
Melt structure 13
Mercury sulphide 669
field of stability 669
Mesoporous materials 354
Metal ammonia solutions 135
Metal intercalated clays 808
Metal powders 808
Metal-aqua complexes
formation 543
Metal-organic chemical vapor
deposition 778
Metastable phases 54
Micas
recrystallization 56
Microautoclave 137
Microcrystallites 207
Microwave dielectric heating 808
Microwave hydrothermal 39,
186, 801
processing 813
technique 810
Microwaves 808
Mineral formation 2
Mineral type structure
Bastnaesite 630
Cebaite Type 630
Huanghoite Type 630
Zhonghuacerite 630
Mineralizer 9, 56, 90, 140,
622, 639
alcoholic solution 187
solutions 177
MOCVD 778. *See also* Metal-
organic chemical vapor
deposition
Modified Bridgman vessels 113
Molar ratio
value 457
Mole number 162
Molecular sieves 317, 318, 394
commercial success 318
films 390
films and membranes 384
Molybdates 649
synthesis 646
Molybdenum 646
Monocapped trigonal prism 632
Monocationic calcium silicates
crystallization 491
Monoclinic BaY_2F_8 crystals 623
Monocrystals
hydrothermal growth 716
Morey autoclaves 106, 147
Morphological features
dependency 236
nutrient composition 236
Morphology 176
advantage 148
Morphology of $AlPO_4$ 236
Multi-centered disordered cubic
crystals 623

DropBooks

Na R-silicates
transition 452
Nanoporous membranes 354
NASICON 521
conductivity 538
stoichiometry 538
structure 533, 538
Native elements crystals
hydrothermal synthesis 691
Natural calcite crystals 281
Natural colored gemstones
sources 480
Natural hydrothermal systems
research 9
Natural quartz
principal source 200
Nepheline 484
crystals 485, 486
Niobates 676, 679
antimony 679
bismuth 679
hydrothermal growth 676
Noble metal thermocouples 97
Noble metals
hydrothermal synthesis 692
two types of reaction 692
Non-centrosymmetric organic
crystals 402
Non-specific solvation 173
Non-tetrahedral cations
properties 420
Nonstoichiometric composition
stability 296
Novel autoclaves 118
designs 101
Nucleation 354, 359, 695
rate 359, 360
Nucleation centers 582
Nucleation theory 360
classical and modern 355

Olivine type motif 504
OLPF. *See* Optical low pass filter
Omega zeolite 352
Opposed anvil system 117
Optical low pass filter 200
Optical second harmonic
generation 402
Optimal energy utilization 3
Organic materials 817
Organic substances 354
Orthophosphates
crystallization 528
Oxidation processes 399
Oxide semiconductors
application 717
Oxides 702
mixed 739
molybdenum 649
Oxyfluorides 619, 633
Oxyfluorinated compounds 631
Oxymolybdates 648

Paratellurite
crystal morphology 716
method of crystallization 715
solubility 715
Parr autoclaves 129
Paulingite 325
Pegmatite crystallization 16
Pendulum Apparatus 120
Penta-antimonites 731, 732
Pentafluorides 621
Pentasils 401
Perovskite oxides 132
crystallization kinetics 184
Perovskite type titanates 806
Phanerostable 54
Phase 166
boundaries 511
diagrams 166
relationships 166
rule 166
tranformations 458
transitions 381

Phase equilibria 291
  data 15
Phillipsite 350
Phosphate anions 522
Phosphate systems
  phase equilibria studies 519
Phosphates 416, 417, 421
  crystal chemistry 418
  hydrothermal synthesis 523
  study 519
  synthesis 520, 533
Phosphoric acid 377
Phosphoro-oxygen anions
  degree of condensation 531
Phosphorus 15
Phosphorus atoms 522
  pentavalent state 418
  trivalent state 418
Phosphorus pentoxide 13
Photo-semiconductors 74
Photorefracting crystal 471
Physical properties of HAp 287
Physico-chemical aspects
  PVT-behavior 83
  solubility 83
Physico-chemical
    considerations 172
Piezo- and ferroelectrics 74
Piezoelectric high frequency
    devices 222
Piezoelectric ultrahigh frequency
    devices 222
Piston cylinder apparatus 117
Plate tectonics theory 19
Platinum lining 90
Polychalcogenides 681
Polycrystalline hydroxyapatite
    disk 298
Polymerizable complex method 821
Polymorphism
  double fluorides 619
Polyphosphates
  crystallization 528
Population balance formalism 360
Porous cyrstalline
    aluminophosphates 334
Potassium carbonate 678
Potassium lithium hexatitanate 660
Potassium niobate crystals
  solubility isochore 119
Potassium oxalate 678
Potassium titanyl arsenate 269
Potassium titanyl phosphate 256
Potassium-zirconium
    heptafluoride 626
Pressure balance arrangement 90
Pressure balancing technique 93
Pressure measurements 99
Pressure of hydrogen 701
Pressure-temperature range 101
Pseudoboehmite 380
PTX diagrams 166
PVT apparatus 121
Pyrochlore structure
  modified 628
Pyrophosphates
  crystallization 546
  morphological habits 546
  morphological variations 553
Pyroxenes
  recrystallization 56
Pyrrhotite 672

Quartz 198
  $\alpha - \beta$ transition 201
  double refraction 200
  hydrothermal growth 207
  single crystal growth 199
  solubility 203
  stability field 454
  structural defects 219
  synthesis large crystals 201
  tuning forks 200
  variety of applications 200
  world's largest producer 70

PropBooks

α-Quartz 199
Quartz autoclaves
  main advantage 105
Quartz crystals
  existence of defects 219
  growth 203, 207
  kinetic studies 203
  parameters 207
  structural defects 208
Quartz glass
  autoclaves 102
  tube liners 92
  tubes 102
Quartz resonators 220

R_2O_3
  high silica concentration 454
Raman spectrascopy 344
Rare earth antimonites 732
Rare earth cation
  radii 521
Rare earth elements 427, 619
  distribution and
    mobility 426, 428
  heavier 503
  high basicity 458
  ionic radii 452
  natural compounds 498
  silicates 436
Rare earth fluorides 619
  unique technological
    applications 626
Rare earth germanates 499
  luminescence properties 517
Rare earth motif 452
Rare earth orthophosphates 532
Rare earth orthovanadates 567
  flux method 568
Rare earth phosphate system
  phase equilibria study 523
  phase formation 524
Rare earth phosphates 521, 531, 555
  anhydrous 531
  formation 522
  growth 528
  hydrothermal synthesis 523
  hydrothermal technique 532
  hydrous 531
  synthesis 520
Rare earth series
  characteristic phase 429
Rare earth silicates 416, 426
  properties 459
  solubility 427
  structural elucidation 502
  synthesis 451
Rare earth titanates
  flux method 660
Rare earth tungstates
  mixed 637
Rare earth vanadates 567
  growth rate 568
Rare-metal transport 14
Reaction cell 121
Reaction kinetics 148, 186
Reaction mixture
  composition 339
Reaction pathway 180
Reaction pressure 140
Reaction time on the
    crystallization 380
Redox reactions 19
Regency emerald 477
Rocking autoclaves
  fixed-volume systems 127
  flexible-cell system 127
Rod mills 147
Role of templates 352
Ruby
  growth 710
  solubility 710

Salts 354
Sapphire
  growth 710
  solubility 710
SAW 577. *See also* Surface acoustic wave
SCW 813
SCWO. *See* Supercritical water oxidation
Second harmonic generation 256
Secondary structural units 323
Seed crystals 365
Seed orientation 264
Seeds
  growth of berlinite 235
Selenides 391, 674
  melt method 674
  physical properties 676
Selenium crystals 694
Self-assembly 821
Shadowgraph technique 162
Shape-selective catalysis 392
SHG. *See* Second harmonic generation
Short-circuit path model 779
Si-O-Si bonding 434
Si-tetrahedra
  bond lengths and angles 416
  stability 421
Si:O phases
  higher pressures 435
  higher temperatures 434
Si:O ratio 435
Silica 335
  autoclaves 188
  precipitated 335
  zeolites 380
Silicate framework
  connectivity decrease 435
Silicate growth
  hydrothermal conditions 467
Silicate melts 13
Silicate structures 420
Silicate technology 415
Silicates 416, 421, 467, 533
  characteristic feature 457
  chemical stability 428
  crystal chemistry 418
  highly condensed 454
Silicates and germanates
  structural comparison 424
Silver liners 94
Single crystals
  growth 183
Sinterability 775
Sintering additives 792
SiO_2
  principal forms 199
  solubility 432
Slow heating method
  major drawback 232
Sodalite 327, 348
  recrystallization 119
  single crystals 374
Sodium orthozincosilicate 489
Sodium zinc germanate
  synthesis 515
Sodium zincosilicates
  synthetic 490
Sodium zirconium silicates 461
  hydrothermally grown crystals 466
Soft solution electrochemical process 821
Soft solution processing 8, 821
Sol-gel method 290
Sol-gel processing 821
Solid catalysts 400
Solid solutions
  crystallization 761
Solid state reaction method 289, 290
Solid state reactions 775
Solid state sintering 736
Solid-phase transformation 336

DropBooks

Solubility 175, 187, 189, 213, 214, 215, 226, 264, 274, 275
apparatus 121
curves for KTP 265
dependence 176
measurement 124
negative coefficient 121
of berlinite 227
of calcite 279
of crystals 186
of α-quartz 215
of quartz 213
of sphalerite 671
of zincite 188
positive coefficient 121
theoretical aspects 186
thermodynamic interpretation 229
thermodynamic principles 174
Solubility of $AlPO_4$ 227
temperature coefficient 231
Solubility of $GaPO_4$ 252
Solubility of HAp 297
Solubility of KTP 264
extensive study 265
Solution-mediated transport 336
Solvated ions 172
Solvation 172
Solvent
dielectric constant 180
Solvothermal 7, 821
synthesis 771
Sonochemical breakdown of liquid phases 147
Sorption properties 392
Sorption uptakes 394
Source materials 335
Spectroscopic properties
rare earth fluorides 623
Sphalerite 671
spontaneous crystallization 119
a-Spodumene 495, 496
Spontaneous nucleation 640
Stability of calcium phosphates 292
Stable complex
formation 542
Steam agitated autoclaves 143
Steel autoclaves 57, 105, 113
Stibiotantalite 677
Stilbite 327
Strecker synthesis 21
Structure-stabilizing agents 352
Submarine hydrothermal systems 19
Submarine hydrothermal vents 21
Substitution
hetervalent 654
Isovalent 654
Substrates
fabrication 785
Sulfide interaction 668
Sulphide aqueous solutions
thermodynamic data 181
Sulphides
synthesis of 665
Supercritical aqueous systems 17
Supercritical water 178, 180
oxidation 813, 814
properties 813
structure and dynamics 180
Superionic phosphates
growth technology 552
hydrothermal crystallization 542
stages of interactions 542
Superionic pyrophosphates 553
Supersaturated solution 165, 359
Surface acoustic wave 576
Sweeping 220, 221
process 221
Synthesis
apatite 287
berlinite 248
calcite 279
chemical composition 338
diselenide 676
ditelluride 676
hydrogel 338
paratellurite 716

scandium penta-antimonite 732
siderite 285
silicates 57, 519
strontium hydrogarnet 729
sulfides 665
TiO_2 718, 719
zeolites 364
Synthesized minerals
hydrothermal method 470
Synthetic emeralds 480
Synthetic Fe^{3+} variety of
elpasoite 627
Synthetic zeolites 318, 328, 335

Tantalates 676
antimony 679
bismuth 679
hydrothermal growth 676
Tectoaluminosilicates 340
Tectosilicates 316
Teflon 282
Teflon liners 93, 719
Teflon ring 105
Tellurides
melt methods 674
physical properties 676
Tellurium crystals 694
Temperature and time 349
Temperature-pressure map 820
Templating 352, 821
Tensile strength 85
Terbium-activated yttrium 621
Ternary system 74
Test-tube bomb 111
Test-tube racks 109
Tetragonal crystals 623
Tetragonal rare earth silicates
field of stability 452
Tetragonal scheelite 649
Tetrahedral complexes
configuration 420
Tetramethylammonium
hydroxide 767
Thermal inversion 225
Thermocouple
calibration 97
measure temperatures 97
Thermodynamics 64, 695
Thin film formation 133
Thin films growth 777
Thomsonite 365
Three-electrode technique 134
TiO_2
application 725
photocatalytic activity 718
Titanates
alkali 655
crystal chemistry 651
crystallization 651
rare earth 655
synthesis 650
technological applications 655
Titanium 650
alloy 85
dioxide 656
elucidation 653
oxides 712
silicates 461
Titanium bearing compounds
isomorphism 655
Titanophosphate zeolites 317
Titanosilicate zeolites 399
Top seeded solution growth 562
Tourmaline 483
Tracer technique 779
Transition metal flourides 633
synthesis 626
Transition metal fluorocarbonates
3d 629
Transitional metal fluorocarbonates
3d 630
Transitional metal silicates 416
Transport and deposition
mechanisms 11
Triangular cationic planes 631
Triisopropylbenzene 398

DropBooks

Trioxides of tungsten 642
Trivalent metal titanates 660
Tungstates 636
Tungsten carbide-cobalt composites 813
Tuttle autoclaves 107, 455
Tuttle cold-cone sealed autoclaves 122
Tuttle cold-seal vessel 111
Tuttle-type closure 109
Twinned 589
Twinning 546, 643

Ultraphosphates
  crystallization 528
Univalent metals
  simple sulfides 666

Vanadates 419
  hydrothermal technique 562
  synthesis 561
Vanadium-oxygen compounds 402
Vanadophosphophosphate zeolites 317
Various shape-selective catalysis 392
Vaterite 273
Veberite
  Na_2MgAlF_7 627
Verneuil method 562, 712
Verneuil technique 707
Versatility of hydrothermal chemistry 348
Vibrational spectroscopic cells 139
Viscosity of water 177
Volatility of water 290
Vuonnemite 655

Water
  as a guest molecule 348
  PVT measurements 178
  temperature - density diagram 180
Wave plate 200
Welded closure 112
Welded liner 113
Wet chemical method 289, 290
Wet chemical processing 821
Whisker 793
  crystallite growth 794
Whiskers of HAp 40
Willemite 488
Wolframites of divalent metals 637
World wide web for zeolites
  Europe 319
  North America 319
Wulfenite 646

X-ray techniques 199
X-ray topography
  horizontal gradient 242

Yield strength 85
Young's modulus of bone 793
Yttrium aluminum garnet 734
Yttrium orthovanadate 562
Yttrium series 429

Zeolite synthesis 332, 336, 351
Zeolites
  applications 391
  as catalysts 392
  chemistry 323
  crystal growth 364
  crystallization 351, 361
  detailed structural classification 323
  formation 327, 331, 335, 349
  genetic types 327

laboratory synthesis 328
lattice 352
minerals 315
nomenclature 325
phase-pure 185
silica composite films 384
structure 316, 319, 324
study of 404
synthesize 331
Zeolitization 331, 335, 352
Zinc oxide 703
Zincite
crystals 706
growth 705
solubility 704
Zincogermanates
hydrothermal growth 515
Zincosilicates
hydrothermal synthesis 486
Zirconia 773
Zirconium germanate
crystallization 511
Zirconium mineral 465
Zirconium oxides 712
Zirconium silicates 461, 466
Zone melting 562

DropBooks